CANCER EVOLUTION: FROM BIOLOGICAL INSIGHTS TO THERAPEUTIC OPPORTUNITIES

EDITED BY: Marco Mina, Lorenzo Gerratana and Andrew Davis
PUBLISHED IN: Frontiers in Oncology, Frontiers in Genetics and Frontiers in Cell and Developmental Biology

frontiers Research Topics

ISSN 1664-8714
ISBN 978-2-83250-008-8
DOI 10.3389/978-2-83250-008-8

About Frontiers

Frontiers is more than just an open-access publisher of scholarly articles: it is a pioneering approach to the world of academia, radically improving the way scholarly research is managed. The grand vision of Frontiers is a world where all people have an equal opportunity to seek, share and generate knowledge. Frontiers provides immediate and permanent online open access to all its publications, but this alone is not enough to realize our grand goals.

Frontiers Journal Series

The Frontiers Journal Series is a multi-tier and interdisciplinary set of open-access, online journals, promising a paradigm shift from the current review, selection and dissemination processes in academic publishing. All Frontiers journals are driven by researchers for researchers; therefore, they constitute a service to the scholarly community. At the same time, the Frontiers Journal Series operates on a revolutionary invention, the tiered publishing system, initially addressing specific communities of scholars, and gradually climbing up to broader public understanding, thus serving the interests of the lay society, too.

Dedication to Quality

Each Frontiers article is a landmark of the highest quality, thanks to genuinely collaborative interactions between authors and review editors, who include some of the world's best academicians. Research must be certified by peers before entering a stream of knowledge that may eventually reach the public - and shape society; therefore, Frontiers only applies the most rigorous and unbiased reviews.
Frontiers revolutionizes research publishing by freely delivering the most outstanding research, evaluated with no bias from both the academic and social point of view. By applying the most advanced information technologies, Frontiers is catapulting scholarly publishing into a new generation.

What are Frontiers Research Topics?

Frontiers Research Topics are very popular trademarks of the Frontiers Journals Series: they are collections of at least ten articles, all centered on a particular subject. With their unique mix of varied contributions from Original Research to Review Articles, Frontiers Research Topics unify the most influential researchers, the latest key findings and historical advances in a hot research area! Find out more on how to host your own Frontiers Research Topic or contribute to one as an author by contacting the Frontiers Editorial Office: frontiersin.org/about/contact

CANCER EVOLUTION: FROM BIOLOGICAL INSIGHTS TO THERAPEUTIC OPPORTUNITIES

Topic Editors:
Marco Mina, HAYA Therapeutics, Switzerland
Lorenzo Gerratana, University of Udine, Italy
Andrew Davis, Washington University in St. Louis, United States

Citation: Mina, M., Gerratana, L., Davis, A., eds. (2022). Cancer Evolution: From Biological Insights to Therapeutic Opportunities. Lausanne: Frontiers Media SA. doi: 10.3389/978-2-83250-008-8

Table of Contents

frontiers | Frontiers in Genetics

TYPE Editorial
PUBLISHED 09 August 2022
DOI 10.3389/fgene.2022.984032

OPEN ACCESS

EDITED AND REVIEWED BY
Heather Cunliffe,
University of Otago, New Zealand

*CORRESPONDENCE
Marco Mina,
marco.mina.85@gmail.com

SPECIALTY SECTION
This article was submitted to Cancer Genetics, a section of the journal Frontiers in Genetics

RECEIVED 01 July 2022
ACCEPTED 12 July 2022
PUBLISHED 09 August 2022

CITATION
Davis AA, Gerratana L and Mina M (2022), Editorial: Cancer evolution: From biological insights to therapeutic opportunities. *Front. Genet.* 13:984032. doi: 10.3389/fgene.2022.984032

Editorial: Cancer evolution: From biological insights to therapeutic opportunities

Andrew A. Davis, Lorenzo Gerratana and Marco Mina*

[1]Washington University in St. Louis, St. Louis, MO, United States, [2]Department of Medical Oncology-CRO Aviano, National Cancer Institute, IRCCS, Aviano, Italy, [3]University of Udine, Udine, Italy, [4]HAYA Therapeutics, Lausanne, Switzerland

KEYWORDS

cancer evolution, biomarker, cancer dynamics, tumor microenevironment, cancer genomics

Editorial on the Research Topic
Cancer Evolution: from biological insights to therapeutic opportunities

At present, cancers are described in both biological and clinical settings with static models that characterize tumors by the phenotypic and genotypic features observed at a given time point. However, cancers are highly dynamic processes that evolve based on specific genomic and epigenomic changes. Such dissonance between the model used to describe tumors and their true nature reverberates all the way from basic biological research to clinical practice. For instance, it is well established that anti-cancer treatments impose selective pressures leading to the emergence of resistant clones (Zheng et al., 2016; O'Leary et al., 2018). This evolutionary process is stochastic and access to better models to analyze and predict mechanisms of resistance is critical.

Historically, the first barrier to the characterization of the evolutionary properties of cancer was the limited amount of available data to accurately reflect tumor heterogeneity, which was traditionally based on a single tissue biopsy (Bertucci et al., 2019; Gerratana et al., 2019; Nguyen et al., 2022). Several factors have changed this paradigm, including the advancement of molecular profiling technologies, the substantial decrease in sequencing costs, and the introduction of multimodal serial sampling in clinical and research settings. Multimodal molecular profiling has pushed research in several directions. On the one hand, profiling of circulating tumor cells (CTC) and cell-free DNA (cfDNA) in peripheral blood samples is paving the way toward non-invasive diagnosis and monitoring of cancer progression (Gerratana et al., 2021). On the other hand, multi-regional sequencing, single cell and spatial transcriptomics, as well as newly emerging epigenomic profiling techniques are leading to a renewed interest in the analysis of genomic, transcriptomic, and epigenetic mechanisms that have previously been understudied (Mina et al., 2017; Mastoraki et al., 2018;

Sanchez-Vega et al., 2018; Penson et al., 2019; Gerratana et al., 2020; Nguyen et al., 2022).

The articles in this research topic address important aspects of cancer evolution, encompassing models associated with a diversity of tumor types including renal cell carcinoma, glioblastoma, breast, colorectal, lung, ovarian, pancreatic and prostate cancer. Our *a priori* expectation when we proposed this research topic was to be confronted by a barrage of works focusing mainly on the genetic aspects of cancer evolution. Looking retrospectively at the collection of accepted manuscripts, however, we were surprised to observe some specific yet unexpected topics recurrently emerging.

Multiple articles within this collection focused on the role of non-coding RNA in cancer, including in particular microRNA (miRNA), circular RNA (circRNA) and long non-coding RNA (lncRNA) (Duică et al.; Gao et al.; Qi et al.; Li et al.; Zheng et al.; Li et al.; Chen et al.; Zhao et al.). Duică et al. presented a review of the role of miRNAs in cancer-relevant processes, focusing on gynecological malignancies (Duică et al.). Another study (Ming Li et al.) evaluated exosomal miRNAs as a mechanism of resistance in small cell lung cancer with particular elevation of exosomal miR-92b-3p that was associated with the PTEN/AKT pathway based on preclinical models (Li et al.). Importantly, this study also included a clinical cohort of 50 patients to help validate the authors' hypothesis that downregulation of this biomarker was associated with better clinical outcomes. Junchen Li et al., instead, focused on the anti-cancer mechanism of andrographolide in patients with luminal-like breast cancer through the inhibition of miR-21-5p (Li et al.). Similarly, Chen et al. investigated the role of circular RNA (circRNAs) in prostate cancer. The authors focused on the regulation, expression, and functional effects of circNOLC1 for *in vitro* and *in vivo* models, proposing circNOLC1 as a potential biomarker and target for prostate cancer treatment.

Multiple studies focused on lncRNAs as well. Gao et al. published a general review on lncRNA mechanisms of action, regulatory functions, and biological relevance in tumor development and progression. In a study by Zhao et al., lncRNAs were compared across primary and recurrent glioblastoma tissue to identify mechanisms that drive poor prognosis, a finding that was validated in preclinical models. The authors identified lncRNA NONHSAT079852.2 as a relevant biomarker in glioblastoma, acting as a sponge of hsa-mir-10401-3p and enhancing HSPA1A expression, and promoting tumor cell proliferation, invasion, and recurrence of glioblastoma (Zhao et al.). Qi et al. evaluated lncRNAs as potential biomarkers to assess heterogeneity in metastasis for colon and rectal cancers. The analysis identified two biomarker lncRNAs, KCNQ1OT1 and SNHG1, associating with cancer initiation and metastatic potential. Interestingly, the authors proposed different mechanisms of actions of these two lncRNAs in colon and rectal cancers (Qi et al.). Finally, Zheng et al. identified a panel of prognosis-associated lncRNAs that were significantly associated with survival in ovarian cancer across multiple independent cohorts, including The Cancer Genome Atlas (TCGA) and Gene Expression Omnibus (GEO). The authors further selected and validated the expression of four lncRNAs *in vitro* on multiple ovarian cancer cell lines (Zheng et al.).

A second theme that was recurrent in our collection is the plasticity of the epithelial-mesenchymal transition (EMT). Within this collection, Zheng et al. published a review on the communication between EMT and cancer stem cells (CSC). While this was once thought to be an unidirectional evolution, more recent studies suggest that this transition is bi-directional, stochastic, and mediated by the tumor microenvironment, ultimately showing how such "hybrid state" or "plasticity" is linked to poor prognosis and resistance. Cui et al. studied the role of ENC1 in accelerating EMT processes in colorectal cancer, whereas the study by Shou et al. reported an inverse relation between tissue inhibitor matrix metalloproteinases 1 (TIMP1) and prognosis in samples from patients with renal cell carcinoma. The study evaluated TIMP1 as a biomarker to enhance metastasis via the EMT signaling pathway. Another study explored EMT-related genes using TCGA and local samples for pancreatic ductal adenocarcinoma (Feng et al.). This study identified a 8-gene signature that impoved prediction compared to clinical variables alone, particularly to assess adjuvant treatment response, such as to immune checkpoint inhibitor therapy. In the future, evaluating therapies that target cells in this "hybrid" EMT state may have specific applications to prevent seeding of metastatic sites.

Finally, it is worth mentioning two reviews on protein condensates and RNA modifications. Lu et al. produced a review of Liquid–liquid Phase Separation (LLPS) and protein/nucleic acid condensates. LLPS are a new paradigm in the study of cellular activities recently coming under more intense research focus. Recent progress has been made to understand the roles of LLPS in cancer. Additionally, Dai et al. published a review on RNA modifications and their role in cancer with a deep discussion on the YTH protein family of m6A readers, summarizing the recent advances in structure and biological function of YTH family proteins, and their roles in human cancer and therapy applications.

This collection of articles highlights promises and challenges of characterizing the dynamic aspects of cancer. They nicely expose the critical need for multi-omics biomarkers to track cancer evolution in both research and clinical settings. Interestingly, we observed an emerging interest towards previously less studied molecular players, such as non-coding RNAs, condensates, and RNA

modifications, both in the context of cancer cells and tumor microenvironment. We anticipate that the use of integrated models based on multiple biomarkers (epigenomics, genomics, transcriptomics, proteomics, and radiomics) will be necessary to capture the complexity of cancer evolution, especially in today's clinical settings dominated by a paradigm shift from monotherapy approaches towards combinations of chemotherapy, immune checkpoint inhibitors and targeted therapies.

Author contributions

AD, LG, and MM participated to the design, creation and redaction of the editorial.

Conflict of interest

The authors declare that the research was conducted in the absence of any commercial or financial relationships that could be construed as a potential conflict of interest.

Publisher's note

References

Bertucci, F., Ng, C. K. Y., Patsouris, A., Droin, N., Piscuoglio, S., Carbuccia, N., et al. (2019). Genomic characterization of metastatic breast cancers. *Nature* 569, 560–564. doi:10.1038/s41586-019-1056-z

Gerratana, L., Basile, D., Franzoni, A., Allegri, L., Viotto, D., Corvaja, C., et al. (2020). Plasma-based longitudinal evaluation of ESR1 epigenetic status in hormone receptor-positive HER2-negative metastatic breast cancer. *Front. Oncol.* 10, 550185. doi:10.3389/fonc.2020.550185

Gerratana, L., Davis, A. A., Shah, A. N., Lin, C., Corvaja, C., Cristofanilli, M., et al. (2019). Emerging role of genomics and cell-free DNA in breast cancer. *Curr. Treat. Options Oncol.* 20, 68. doi:10.1007/s11864-019-0667-9

Gerratana, L., Davis, A. A., Zhang, Q., Basile, D., Rossi, G., Strickland, K., et al. (2021). Longitudinal dynamics of circulating tumor cells and circulating tumor DNA for treatment monitoring in metastatic breast cancer. *JCO Precis. Oncol.* 5, 943–952. doi:10.1200/PO.20.00345

Mastoraki, S., Strati, A., Tzanikou, E., Chimonidou, M., Politaki, E., Voutsina, A., et al. (2018). ESR1 methylation: A liquid biopsy–based epigenetic assay for the follow-up of patients with metastatic breast cancer receiving endocrine treatment. *Clin. Cancer Res.* 24, 1500–1510. doi:10.1158/1078-0432.CCR-17-1181

Mina, M., Raynaud, F., Tavernari, D., Battistello, E., Sungalee, S., Saghafinia, S., et al. (2017). Conditional selection of genomic alterations dictates cancer evolution and oncogenic dependencies. *Cancer Cell* 32, 155–168. e6. doi:10.1016/j.ccell.2017.06.010

Nguyen, B., Fong, C., Luthra, A., Smith, S. A., DiNatale, R. G., Nandakumar, S., et al. (2022). Genomic characterization of metastatic patterns from prospective clinical sequencing of 25, 000 patients. *Cell* 185, 563–575. e11. doi:10.1016/j.cell.2022.01.003

O'Leary, B., Cutts, R. J., Liu, Y., Hrebien, S., Huang, X., Fenwick, K., et al. (2018). The genetic landscape and clonal evolution of breast cancer resistance to palbociclib plus fulvestrant in the PALOMA-3 trial. *Cancer Discov.* 8, 1390–1403. doi:10.1158/2159-8290.CD-18-0264

Penson, A., Camacho, N., Zheng, Y., Varghese, A. M., Al-Ahmadie, H., Razavi, P., et al. (2019). Development of genome-derived tumor type prediction to inform clinical cancer care. *JAMA Oncol.* 6, 84–91. doi:10.1001/jamaoncol.2019.3985

Sanchez-Vega, F., Mina, M., Armenia, J., Chatila, W. K., Luna, A., La, K. C., et al. (2018). Oncogenic signaling pathways in the cancer Genome Atlas. *Cell* 173, 321–337. e10. doi:10.1016/j.cell.2018.03.035

Zheng, D., Ye, X., Zhang, M. Z., Sun, Y., Wang, J. Y., Ni, J., et al. (2016). Plasma EGFR T790M ctDNA status is associated with clinical outcome in advanced NSCLC patients with acquired EGFR-TKI resistance. *Sci. Rep.* 6, 20913. doi:10.1038/srep20913

frontiers in Oncology

REVIEW
published: 23 October 2020
doi: 10.3389/fonc.2020.591181

MiRNAs: A Powerful Tool in Deciphering Gynecological Malignancies

Florentina Duică[1†], Carmen Elena Condrat[1†], Cezara Alina Dănila[1†], Andreea Elena Boboc[1], Mihaela Raluca Radu[1], Junjie Xiao[2], Xinli Li[3], Sanda Maria Creţoiu[4], Nicolae Suciu[1,5,6], Dragoş Creţoiu[1,4] and Dragoş-Valentin Predescu[7]*

[1] Fetal Medicine Excellence Research Center, Alessandrescu-Rusescu National Institute for Mother and Child Health, Bucharest, Romania, [2] Institute of Cardiovascular Sciences, Shanghai University, Shanghai, China, [3] Department of Cardiology, Jiangsu Province Hospital and Nanjing Medical University First Affiliated Hospital, Nanjing, China, [4] Cellular and Molecular Biology and Histology Department, Carol Davila University of Medicine and Pharmacy, Bucharest, Romania, [5] Department of Obstetrics and Gynecology, Polizu Clinical Hospital, Alessandrescu-Rusescu National Institute for Mother and Child Health, Bucharest, Romania, [6] Obstetrics, Gynecology and Neonatology Department, Carol Davila University of Medicine and Pharmacy, Bucharest, Romania, [7] Department of General Surgery, Sf. Maria Clinical Hospital, Carol Davila University of Medicine and Pharmacy, Bucharest, Romania

OPEN ACCESS

Edited by:
Marco Mina,
Sophia Genetics, Switzerland

Reviewed by:
Prashanth N. Suravajhala,
Birla Institute of Scientific Research, India
Chandramani Pathak,
Indian Institute of Advanced Research, India

***Correspondence:**
Sanda Maria Creţoiu
sanda@cretoiu.ro

[†]These authors have contributed equally to this work

Specialty section:
This article was submitted to Cancer Genetics, a section of the journal Frontiers in Oncology

Received: *04 August 2020*
Accepted: *01 October 2020*
Published: *23 October 2020*

Citation:
Duică F, Condrat CE, Dănila CA, Boboc AE, Radu MR, Xiao J, Li X, Creţoiu SM, Suciu N, Creţoiu D and Predescu D-V (2020) MiRNAs: A Powerful Tool in Deciphering Gynecological Malignancies. Front. Oncol. 10:591181. doi: 10.3389/fonc.2020.591181

Accumulated evidence on the clinical roles of microRNAs (miRNAs) in cancer prevention and control has revealed the emergence of new genetic techniques that have improved the understanding of the mechanisms essential for pathology induction and progression. Comprehension of the modifications and individual differences of miRNAs and their interactions in the pathogenesis of gynecological malignancies, together with an understanding of the phenotypic variations have considerably improved the management of the diagnosis and personalized treatment for different forms of cancer. In recent years, miRNAs have emerged as signaling molecules in biological pathways involved in different categories of cancer and it has been demonstrated that these molecules could regulate cancer-relevant processes, our focus being on malignancies of the gynecologic tract. The aim of this paper is to summarize novel research findings in the literature regarding the parts that miRNAs play in cancer-relevant processes, specifically regarding gynecological malignancy, while emphasizing their pivotal role in the disruption of cancer-related signaling pathways.

Keywords: miRNA, gynecology, cancer, signaling molecules, biomarkers, resveratrol

INTRODUCTION

Short nucleotide RNA molecules with a length of 18 to 30 nucleotides, or microRNAs, have first been reported in 1993 (1–4) in studies based on genetic screening in nematodes. These findings have inspired researchers in biomedical sciences to focus on investigating these molecules in various organisms, focusing on their structure and functions. By now, it is well known that approximately 2% of the human genome comprises nearly 20.000–25.000 protein-coding genes, with most of the genome being composed of regions that do not encode but are transcribed into regulatory RNAs

(ncRNAs), introns, and other sequences (4). These RNA sequences bear many functions, including the gene expression regulation of protein-coding genes at transcriptional level through transcript degradation, and at post-transcriptional level by translation suppression (5).

Among non-coding RNAs (ncRNAs), there are two groups of RNAs fulfilling different tasks: some are indispensable for protein synthesis, such as ribosomal RNAs (rRNAs), transfer RNAs (tRNAs), small nuclear RNAs (snRNAs), and small nucleolar RNAs (snoRNAs), while others are involved in regulatory functions, for instance, Piwi-interacting ncRNAs (piRNAs), small interfering RNAs (siRNAs), microRNAs (miRNAs) and long non-coding RNAs (lncRNAs) (6, 7). The two classes of ncRNAs interact both with cellular components, in order to regulate various cellular processes and functions by controlling gene expression, and with each other, thus being consistently co-regulated (8). Depending on the number of specific nucleotides that each class of ncRNAs contains, ncRNAs are divided into lncRNAs, comprised of over 200 nucleotides, and sncRNAs, which are made up of less than 200 nucleotides. Furthermore, based on their functions, they can be divided into housekeeping, which are constitutively expressed RNAs, and regulatory RNAs, which are expressed during specific cell differentiation phases or as an answer to various modifications in the surrounding area (9), as depicted in **Figure 1**. The development of biomolecular techniques and big data analysis has allowed the identification of the functions that these types of RNA fulfill, as well as their interaction with various subcellular components, and their regulation. For instance, lncRNAs interact with miRNAs at specific binding sites, resulting in their mutual regulation and messenger RNA (mRNA) transcript control (10). Furthermore, it has been shown that ncRNAs form interconnected networks that regulate numerous physiological and pathological biological processes, including protein synthesis, gene regulation, chromatin modulation, tumor cell invasion – with multiple studies currently focusing on their roles as either oncogenic or tumor suppressor factors (11–13). These networks also govern the expression of snoRNAs, which can act as precursors for other RNA types such as piRNAs (14).

snoRNAs often originate within the nucleolus, measuring approximately 60–300 nucleotides (nt) in length. snoRNAs are generally encoded within the intronic regions as long non-coding RNAs or can be separately transcribed from the intergenic regions (13). Overall, snoRNAs can be classified into two main groups, namely C/D box snoRNAs (SNORDs), and H/ACA box snoRNAs (SNORAs) (15). snoRNAs contribute to the biogenesis and maturation of rRNA, as well as in the complex interaction between snRNAs, tRNAs, and rRNAs. Individually, SNORAs participate not only in the pseudouridylation process by linkage with SNORDs and the dyskerin nuclear protein (15), but also in the methylation cycle along with fibrillarin proteins (16). However, some snoRNAs lack defined functions, being generally referred to as orphan snoRNAs (17, 18).

While miRNAs are currently considered as the most plentiful circulating ncRNAs in normal and cancer patients,

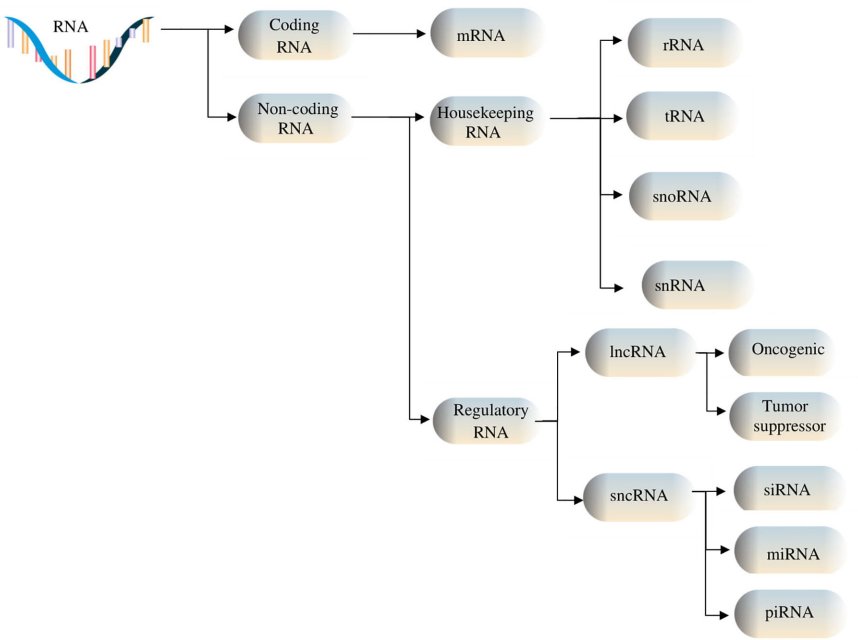

FIGURE 1 | RNA types include coding and non-coding RNAs. Housekeeping ncRNAs are made up of ribosomal (rRNA), transfer (tRNA), small nucleolar RNAs (snoRNAs), and small nuclear (snRNA). Regulatory noncoding RNAs include short ncRNAs (sncRNAs) and long ncRNAs (lncRNAs), the former consisting of microRNAs (miRNAs), small interfering RNAs (siRNAs), and Piwi-associated RNAs (piRNAs), and the latter containing oncogenic and tumor suppressor lncRNAs.

data from an RNA-seq analysis profiling extracellular RNA from both cancer patients and healthy controls has shown that piRNAs amount to almost the same sum (19). Though it has been shown that the synthesis of piRNA does not require the aid of the Dicer enzyme (20), their exact roles are yet to be fully elucidated (21). However, the interaction between miRNAs and piRNAs is known to result in the regulation of gene expression by targeting mRNAs (8).

miRNAs are small non-coding RNA molecules that function as post-transcriptional regulators of gene expressions (5, 22, 23). They are highly important in both physiological and pathological processes in the human body, as well as in cell development and proliferation, tissue differentiation, and programmed cell death (24), while also being involved in maintaining 60 to 70% of the cellular homeostasis (7). miRNAs are abnormally expressed in a multitude of diseases, such as cardiovascular and renal illnesses (25, 26), muscle disorders (27), some types of fibrosis (28, 29), pre-diabetes and diabetes (30, 31), leukemias and hematological malignancies, as well as disorders involving hematopoietic stem cells and stem cell differentiation (32–36). Furthermore, miRNAs have also been revealed to facilitate the maintenance of the blood-brain barrier, thereby mediating central nervous system homeostasis (37–39). Last but perhaps foremost, miRNAs have been extensively studied in a wide variety of malignancies (40, 41). To date, approximately 500–1,000 different mammalian miRNA genes are known (25). A complete list with specific details regarding the nomenclature and annotation of miRNA sequences was founded in the year 2002, later known as the microRNA Registry. Nowadays, the miRbase online instrument can be used, providing information about microRNA sequences from 271 organisms, with 38.589 hairpin precursors and approximately 48.860 mature microRNAs (4, 42).

Cancer cells differ from normal cells mainly due to their ability to divide and grow uncontrollably, as a result of modifications undergone by specific genes. Considerable gene variation and altered pathways have been reported for different types of cancers, which depend on the genetic individuality of the affected organism as well as on epigenetic factors (4). Understanding the mechanisms and signaling pathways by which genes become mutated is therefore essential in order to enhance the chances of establishing personalized therapeutic schemes. To this extent, in the last years, miRNAs have emerged as signaling molecules in a multitude of biological signaling pathways in distinct types of neoplasia, and it has been demonstrated that they can regulate cancer-relevant processes. Due to the capacity of a single miRNA molecule to target hundreds of mRNAs, aberrant miRNA expression can be held responsible for the dysregulation of at least several cancer-related signaling pathways (41).

Gynecological cancers pose an important public health issue, being some of the most frequent cancers among women of all ages (43). Patients are oftentimes diagnosed in late stages not only due to a general lack of awareness and knowledge about cancer but sometimes also because of improper screening and even misdiagnoses (44). In gynecological cancers, several signaling pathways have been identified to be modified, including the transforming growth factor-β (TGF-β)/Smad pathway, G Protein-Coupled Receptors (GPCRs), phosphatidylinositol-3-kinase (PI3K)/Akt, the mechanistic target of rapamycin (mTOR), the mitogen-activated protein kinases (MAPK) and the extracellular signal-regulated kinases (Erk), fibroblast growth factor (FGF), the insulin receptor (IR) and insulin-like growth factor receptor (IGFR), vascular endothelial growth factor (VEGF), Toll-like receptors (TLRs), Wnt/β-catenin, Jak/STAT, the Notch signaling pathway, the nuclear factor kappa B (NF-κB) pathway. Other signaling pathways that are implicated in several pathologies including breast cancer, are related to the nuclear receptor superfamily of ligand-dependent factors such as the estrogen receptor (ER), the retinoic acid-related orphan receptors (ROR α-γ or NR1F1-3), and the orphan receptor TAK1 (TR4 or NR2C2) (45).

In this review, we have summarized the implications and future perspectives regarding the signaling functions of miRNA and their roles in regulating oncogenic processes in breast, ovarian, cervical, vulvar, and endometrial cancer.

MIRNA BIOGENESIS

microRNAs have long been shown to control numerous biological processes, including tumorigenesis, with miRNAs being massively dysregulated in tumor cells (46). While the dysregulation of miRNAs is well documented in a range of diseases, direct causal links in cancer have relatively recently been elucidated. Tumoral cells often associate reduced levels of mature miRNAs as a consequence of genetic loss and epigenetic gene silencing resulting in defects in their synthesis (47).

The biogenesis of microRNAs results from a well-defined conserved processing mechanism, with deviations being associated with several diseases (48, 49). Following experiments on mice, primary miRNAs (pri-miRNAs) represent the basis of creation for miRNAs, which is a process that takes place in two phases, the first one taking place in the nucleus and the second one in the cytoplasm, both being governed by the specialized RNase type III proteins, Drosha and Dicer (**Figure 2**) (50). The fundamental RNA polymerase that is responsible for the transcription of miRNA genes is RNA polymerase II (Pol II). Pol II-dependent miRNA gene expression has a short-term control, in order to enable the synthesis of a specific group of miRNAs per certain conditions and cell types (51–53). pri-miRNA transcripts contain one or more local hairpins that are cleaved by the nuclear RNase III enzyme Drosha and its partner, the DiGeorge syndrome critical region 8 (DGCR8) protein (54, 55) in pre-miRNA sequences made up of almost 80 to 100 nucleotides (56, 57). This step of miRNA biogenesis pathway is localized in the nucleus and requires DGCR8 in order for a large complex, known as the Microprocessor complex, to be formed (56). Following transcription, the pre-miRNA is displaced from the nucleus towards the cytoplasm by Exportin-5 (58, 59). In the cytoplasm, Dicer, a cytoplasmic ribonuclease, cleaves the pre-miRNA into a double incomplete mature miRNA (a miRNA/

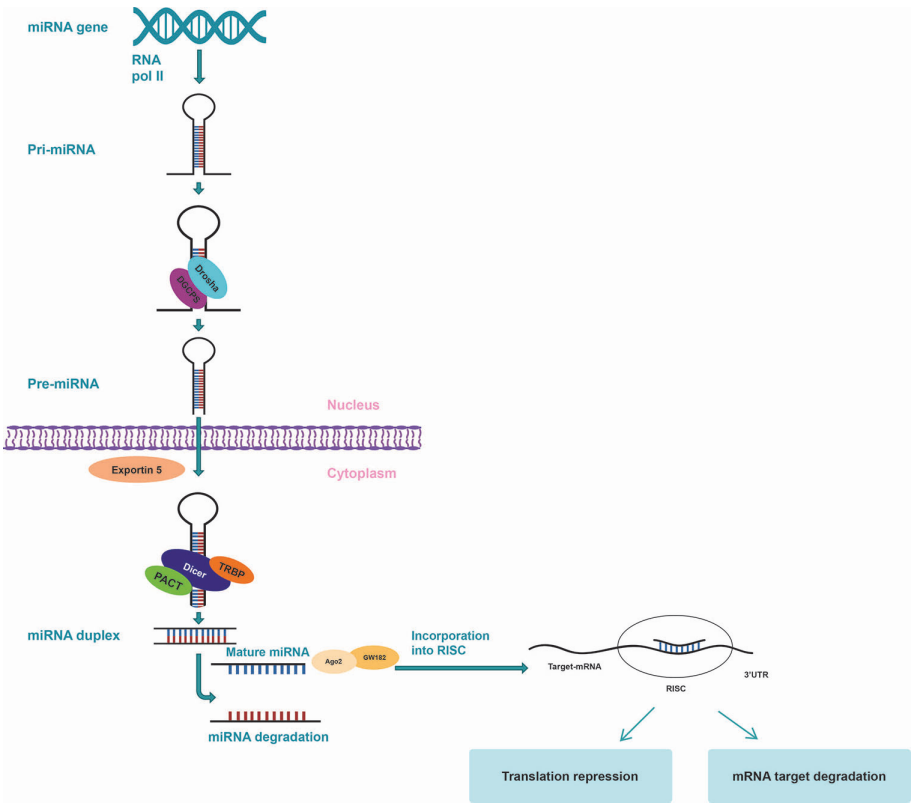

FIGURE 2 | miRNA biogenesis. miRNA gene is transcribed by RNA polymerase II to form a hairpin loop primary transcript (pri-miRNA) which is processed by Drosha/DCGR8 to form pre-miRNA. pre-miRNA is then exported to the cytoplasm by exportin 5, where Dicer cuts off the hairpin loop so as to create a complex that includes the mature miRNA. The mature miRNA is next incorporated into RISC to target the 3'-UTR site of the mRNA to silence expression by cleavage or regression.

miRNA duplex made up of approximately 20 to 22 nucleotides) (24, 60).

Within the cytoplasm, incomplete miRNAs suffer additional modifications in order to become mature miRNAs, being processed by Dicer and RNase III type protein and loaded onto the Argonaute (Ago) protein so as to generate the effector RNA-induced silencing complex (RISC). The mature miRNA duplex is included in RISC, which further coordinates the translation of complementary mRNA and guides it to target miRNA (53, 61). The mature miRNA identifies its correspondent sequences in the 3′ untranslated region (3'-UTR) of their target mRNAs by way of seed region, typically placing nucleotides 2–7 in the miRNA (62, 63). One strand of the produced RNA duplex is subsequently loaded to RISC while the other strand is typically degraded. In some cases, some pre-miRNAs produce mature sequences from both strands that survive and are functional in comparable frequencies (64). Since regulation does not require high complementarity, only one miRNA can target up to hundreds of different mRNAs, leading to the development of aberrant miRNA expression, affecting a multitude of transcripts that have great repercussions on cancer-related signaling pathways. Additionally, miRNAs can trigger downstream signaling pathways by directly binding with Toll-like receptors (TLRs) working as ligands (65–67).

MIRNA AND SIGNALING PATHWAYS IN CANCER

In just a few years, microRNAs have become strongly fixed as key molecular components of the cell in both pathological and normal states (68). The main activity of miRNAs is to lead protein translation by linking to complementary sequences of the 3'-UTR sites of target mRNAs and by negatively regulating mRNA translation (69). The first proof of miRNA involvement in human malignancies was provided by Croce's research group, which aimed to find tumor repressors at chromosome 13q14 site in B-cell chronic lymphocytic leukemia cells (70). This site carries miR-15a and miR-16-1 genes and it has been found to be frequently deleted or downregulated in B-cell chronic lymphocytic leukemia. Both miR-16-1 and miR-15a serve as tumor repressors that promote cell death by suppressing B-cell lymphoma 2 (Bcl-2), an anti-apoptotic protein heavily expressed in malignant non-dividing B cells and other solid malignancies (71, 72).

An abundance of scientific research has lately been published, concerning the function of miRNAs in gynecological malignancies. For instance, miRNAs such as miR-145 have been identified as central players in cervical carcinogenesis, whereas it has been demonstrated that miR-125b, miR-145,

miR-21, and miR-155 have pivotal roles in breast malignancies (73). miR-200 and let-7 have been identified as key modulators in ovarian neoplasms, while miR-185, miR-210, miR-423, let-7c, miR-205, and miR-429 have been associated with oncogenesis, invasion, and metastasis in endometrial carcinomas (74, 75). miRNAs target cell-cycle elements and control various signaling pathways in several physiological and pathological processes, including gynecological malignancies, thus being involved in cell proliferation. Signaling pathways in which miRNAs have been shown to be involved and their target genes have been summarized in **Table 1**.

Toll-like Receptors (TLRs),,, are membrane-bound receptors found on antigen-presenting cells (APCs) and they are members of the group of pattern recognition receptors (PRRs). Some signaling pathways, such as the interferon regulatory factor (IRF), ERKs, NF-κB, MAPKs, c-Jun N-terminal kinases (JNKs), p38, are activated following TLRs stimulation, being involved in the immune response (88).

Transforming growth factor-beta (TGFβ) is part of a large family of growth and differentiation factors that perform multiple functions in embryonic development or act as cytokines in the postnatal period, being divided into two functional groups: TGFβ and the growth/differentiation factor (GDF) group. The key target genes of the TGF-β signaling pathway are the receptor-regulated SMADs (89, 90). In vulvar carcinoma, Yang X et al. have linked the overexpression of miR-590-5p with the downregulation of the target gene TGFβIIR, which induced the appearance of malignant cellular changes and metastasis in sentinel lymph nodes. TGF-β signaling is also involved in other cancers, including breast and endometrial neoplasms (45, 89, 91).

GPCRs contain seven transmembrane regions, making up the largest signaling receptor family. They exert their actions by activating the phosphatidylinositol bisphosphate (PIP2) and cAMP signaling pathways (92). These signaling pathways are involved in different physiological and pathological functions, such as cell proliferation and invasion, being described in numerous cancers, including ovarian and breast cancers (45, 93).

The PI3K/AKT pathway further plays an important role in the survival of tumor cells, metabolism, and growth regulation, with some of the most common mutations in cancer being associated with deviations of this signaling pathway. Its disruption affects both the EGFR/HER family and the mTOR pathway. This signaling pathway is frequently altered in ovarian, cervical, endometrial, and breast cancer (45, 94, 95). For instance, in cervical cancer, miR-21 can increase cell growth via the PI3K/AKT/mTOR signaling pathway, by binding and inhibiting the tumor suppressor PTEN (96). Further on, miR-486, which is substantially downregulated in non-small cell lung cancer, has been demonstrated to alter migration and proliferation via the IGF-1/PI3K/Akt pathway, by targeting IGF1, IGR1R, and p85 (97, 98).

miR-21, on the other hand, promotes cell proliferation, through the Ras/MEK/ERK signaling pathway, which is inhibited by miR-21 targeting the 3'-UTR of RASA1 mRNA in ovarian cancer (99, 100). The MAPK and ERK molecules operate in a signaling cascade defined as the MAPK cascade. MAPK/ERK pathway is downstream of some transmembrane receptors, such

TABLE 1 | miRNA signaling pathways involved in gynecological cancers.

miRNA	Signaling pathway	Target	Target expression	Action	Pathology	Reference
miR-433	MAPK	RAP1A	Overexpression	Cell migration, proliferation, apoptosis	Breast cancer	(76)
miR-99a	mTOR FGFR3	PI3-AKT	Overexpression	Invasion, proliferation, apoptosis	Cervical cancer Breast cancer	(77)
miR-155	AKT	LKB1	Overexpression	Autophagy	Cervical cancer	(78)
miR-21	TNFR1 PI3K/AKT/mTOR RAS/MEK/ERK	Caspase 3 TNF-alpha PTEN RASA1	Overexpression	Apoptosis	Breast cancer Cervical cancer Ovarian cancer	(79)
miR-200 miR-141 miR-200a miR-200b miR-200c	NOTCH TGF-beta	ZEB1 ZEB2 E cadherin EMT	Overexpression	Invasion, metastasis	Ovarian cancer	(80)
Let-7 *miR let-7d-5p	RAS HGMA1	P53	Overexpression	Apoptosis	Ovarian cancer	(81)
miR-34a	p53	HNRNPA1		Cell proliferation	Breast cancer Endometrial cancer	(82)
miR-424	p53	HNRNPA1	Overexpression	Cell proliferation, apoptosis	Breast cancer	(82)
miR-503	p53	HNRNPA1	Overexpression	Cell proliferation, apoptosis	Breast cancer	(82)
miR-142-3p	Bach-1	EMT	Overexpression	Invasion, migration	Breast cancer	(83)
miR-205	ZEB1, ZEB2	EMT PTEN	Overexpression	Apoptosis, cell differentiation, and proliferation	Endometrial cancer	(84)
miR 4712-5p	PTEn/AKT/GSK3beta/cyclin D1	PTEN	Overexpression	Cell invasion, metastasis	Vulvar cancer	(85)
miR-3147	TGF-β/Smad	TGFβ RII EMT	Overexpression	Invasion, cell proliferation, migration	Vulvar cancer	(86)
miR-146a		BRCA1	Overexpression	Cell proliferation	Breast cancer	(87)

ZEB1 and ZEB2 Zinc finger E-box-binding homeobox 1/2 HNRNPA1 Heterogeneous nuclear ribonucleoprotein A1.

as EGFR, FGFR, VEGFR, IGFR, and GPCR, and it is involved in essential functions like development, proliferation, apoptosis, or differentiation of cells in ovarian and endometrial cancer (45, 73, 101).

The Notch signaling pathway is essential in cellular processes and it is activated in response to cell-cell contacts. Notch receptors are transmembrane proteins consisting of a series of different protein molecules. Notch activation is involved in the regulation of gene expression that is implicated in survival, proliferation, and differentiation of cells (102). Through genome-scale sequencing, recent studies have revealed that mutations in the Notch genes could be identified in a broad spectrum of cancers. They further found that resveratrol has an inhibiting action when Notch signaling is oncogenic, while it increases the tumor-suppressive effect when Notch signaling has suppressive tumoral action (45, 103).

CTCF (CCCTC-binding factor) is a zinc-finger protein gene capable of targeting numerous binding sites within the genome, acting both as a transcriptional activator and repressor (104). Furthermore, it can also serve as an insulator, impeding the communication between promoters and enhancers (105). In this manner, and due to its ability to establish inter- and intrachromosomal bonds, CTCF can either up- or down-regulate the expression of a substantial number of target genes, depending on the context, thus fulfilling diverse roles in epigenetic modulation (106). Moreover, when cooperating with chromatin architectural proteins such as cohesin, the resulting complex governs the spatial organization of the genome (107). In addition to these roles, there is an increasing body of evidence suggesting the involvement of CTCF in the regulation of certain miRNAs (106, 108, 109). Specifically, by binding to the CpG sites of miR-375, CTCF manages to silence its expression in estrogen receptor (ER) negative breast cancer cells. As miR-375 is a key driver of cell proliferation, these findings confirm the tumor suppressor role of CTCF in breast cancer (106, 108, 110). Furthermore, silencing of tumor suppressor miR-125b1 in breast cancer due to epigenetic phenomena that result in the methylation of CpG islands preventing CTCF binding, leads to aberrant cell proliferation (108, 109, 111).

miRNAs, BRCA Mutations, and Breast Cancer

Breast cancer is the most common malignancy among women worldwide, with 5 to 10% of patients carrying an inherited predisposition (112). The breast cancer 1 and 2 (BRCA1/2) genes are tumor suppressor genes responsible for the synthesis of proteins involved in damaged DNA repair (113). Mutations in either gene have been associated with significantly increased risk of both breast and ovarian cancer (114), and, to a lesser degree, other types of cancer, including prostate and pancreatic cancer, especially in BRCA2 mutations (115). Specifically, women with germline BRCA1/2 mutations face risks of up to 72 and 69% respectively of having breast cancer by the age of 80 (116, 117). While numerous BRCA genes variants are possible, not all of them carry the same risk, with studies establishing four main pathogenic mutations: single nucleotide mutations (SNPs) resulting in premature termination codons (PTCs) (118), large in-frame deletions or insertions of ≥ 1 exon, transcription regulatory region deletions (114) and certain pathogenic missense variants (119, 120). However, recent whole genome association studies (WGAS) using targeted RNA sequencing have enabled the analysis of multi-exonic ncRNAs in breast cancer samples and, although their functionality has not been revealed yet, they constitute promising leads in better grasping the etiology of breast cancer (121).

The expression of up to thirty miRNA has emerged as having direct consequences on all phases of breast cancer, from formation to progression and propagation (122, 123). Together with the group of miRNAs acting as tumor suppressors that delay or block the potential to cause cancer, there are other oncogene miRNAs (onco-miRNAs) that can cause neoplastic transformation when overexpressed. Breast cancer can be caused by genomic instability as a result of alterations that accumulate in the human genome. One of the processes that can lead to genome instability causing DNA damage is represented by defects in the repair pathway such as double-strand brakes (DSBs), which tend towards cell apoptosis. Considering the crucial role of BRCA1/2 in breast cancer suppression, due to their function in maintaining genome integrity through protein synthesis required for repairing DNA damage, both BRCA genes play parts in apoptosis and the processes of tumor suppression (124, 125). Over 100 miRNAs target the transcription of messenger RNA from the BRCA1 gene. Chang and Sharan have proven that seven miRNAs target BRCA1 (126). miR-146-5p and miR-146a deleting BRCA1 may cause the development of sporadic basal-like and triple-negative breast cancer (127, 128). Negative feedback between BRCA1 miRNA and miR-146a has been described, in which the BRCA1 translation is inhibited by miR-146a and, in turn, miR-146a is up-regulated by BRCA1 (127). Another well-known onco-miRNA is miR-155, which is involved in breast tumor formation and spreading, found more often in inflammation-based cancers and neoplastic transformation caused by inflammation (129). The pathogenesis of breast cancer is influenced by the DNA methylation of miRNA genes, with BRCA1 functionality reduction inducing global hypomethylation. These findings highlight possible treatments of BRCA1-deficient breast tumors that may be developed by targeting miR-155, due to its impact on BRCA1 mutation carriers (126, 130–132).

Several proteins acting as BRCA1/BRCA2 stability regulators have been identified, including the cysteine protease Cathepsin S (CTSS), which reacts on BRCA1 with BRCT domain, initiating the process of proteolytic degradation (133), E3 ubiquitin-protein ligase HERC2, F box protein 44 (FBXO44) and E2 ubiquitin-conjugating enzyme E2T (UBE2T). FBXO44 ubiquitination downregulates the BRCA1 protein (134, 135). BRCA1 expression stabilization is gained through interaction with BARD1 protein and the reduction of proteasome sensitive ubiquitination. The BRCA1 protein level is increased as the proteasomal degradation is prevented by IGF-1 receptor signaling due to AKT-dependent phosphorylation of BRCA1 in

response to estrogen. Recent research performed by Kim et al. has shown that BRCA1 is directly phosphorylated by the Fyn related kinase (Frk/Rak) and, as a result, BRCA1 protein stability is positively regulated (133). Besides protein level regulation, BRCA1 and BRCA2 have been found to participate in a complex regulatory post-transcriptional program. For instance, miR-19a and miR-19b interact with 3'-UTR of BRCA2 mRNA resulting in a simultaneous decrease of protein levels and mRNA of BRCA2. In chronic myeloid leukemia cells, expression of BCR-ABL1 oncoprotein is linked with BRCA1 downregulation. Recent studies revealed that the TIA1 cytotoxic granule-associated RNA-binding protein-like 1 (TIRA) is responsible for BRCA1 downregulation, which disables mRNA translation of BRCA1 by linking to adenylate-uridylate-rich elements (ARE) sites in the 3'-UTR of BRCA1 mRNA. The study also described the complex formed between TIRA, the mRNA binding protein Hu antigen R (HuR), and BRCA1 mRNA (136).

Further on, more recent studies performed by Gorrini and colleagues have demonstrated that BRCA1 deficient cells are protected by estrogen from reactive oxygen species induced death through the activation of PI3K/AKT and NRF2 upregulation (nuclear factor erythroid 2 related factor 2) transcriptional program. In consequence, antioxidant genes are increased (137–139). The results showed that a local upregulated estrogen concentration helps the expansion and survival of BRCA1 mutated breast cancer cells (140). Furthermore, hormone functions are affected by BRCA1 in different ways such as activating Era expression (141), adjusting the level of progesterone receptor (PR) (142, 143), and repression of estrogen-dependent gene transcription (144, 145).

In breast cancer, studies have shown that various signaling pathways are implicated in the proliferation as well as cellular death of malignant cells. For instance, Zhu et al. have shown that one significant role in breast cancer growth is played by the signaling pathway of mTOR (mammalian target of rapamycin) (146), its downregulation by miR-100 and/or miR-125b enabling cellular death and inhibiting the progression of breast cancer (147, 148). Another miRNA, miR-142-3p, belonging to the miR-142 family, might be related to the development of various types of malignancies, especially breast cancer, by targeting various mRNAs, including Bach1, which is highly active in cancerous cells. To this extent, in their study, Liang et al. have found that increased mRNA levels of Bach1 were considerably linked to poor metastasis-free-survival rates (149). Further studies have also indicated that overexpression of miR-142-3p in breast malignancies resulted in the downregulation of Bach-1, making it likely that miR-142-3p could be a target in breast cancer therapy (83, 149, 150).

In previous studies, miR-433 has been found to have acted as an oncogene - for instance, in colorectal cancer, overexpression of miR-433 downregulates MACC1 and leads to cell death, while in hepatocellular carcinoma, it suppresses cell proliferation by targeting HDAC6, PAK4, and GRB2 (151–153). In breast cancer, miR-433 has generally been found to be decreased, while its overexpression has been linked to cell death and inhibition of tumor cell growth and migration. After screening miRNA target genes, T. Zhang et al. predicted Rap1a as a potential target of miR-433, later proceeding with their experiment. Consequently, they found that cells transfected with miR-433 associated decreased Rap1a protein levels along with slightly lowered Rap1a mRNA levels, thus demonstrating that, by targeting the RAP1A gene and subsequently activating the MAPK signaling pathway, miR-433 behaves as a tumor suppressor (76). The MAPK pathway is known to be implicated in tumorigenesis, playing key roles both in the growth and apoptosis of malignant cells (154), however, in breast cancer, the RAP1A/MAPK cascade remains to be further clarified (155).

Past studies have shown miR-99a to take part in the pathology of several cancers, such as non-small lung cell carcinoma, leukemia, and prostate cancer (156–158). Long et al. have later found that miR-99a also plays a significant role in breast neoplasia, where it acts as a regulator of fibroblast growth factor receptor 3 (FGFR3). They proved for the first time that miR-99a directly targeted FGFR3 in breast malignancies and that it could be used as a convenient biomarker for this pathology (77). FGFR3 is also upregulated in various types of tumors, and its abnormal expression could initiate distinct signaling pathways, like the PI3-AKT and the FGFR3 signaling pathways, this way contributing to the development of cancer (159, 160). Several studies have also shown that miR-99a is downregulated in malignant tumors like esophageal carcinoma, head and neck squamous cell carcinoma, cholangiocarcinoma, and also in primary breast tumors compared to normal breast tissue (77). On the other hand, researchers demonstrated that the upregulation of miR-99a in breast cancer inhibits malignant cell proliferation and invasion (77, 161–163), miR-99a working as a tumor suppressor. Further studies are therefore desired before potentially implementing miR-99a as a diagnostic and prognostic biomarker.

In breast cancer, snoRNAs have also been highlighted as having prognostic applicability, including SNORD89 and SNORD46. In this regard, in their thorough NGS analysis, Krishnan et al. have recently found that SNORD89/46 were the most significantly downregulated snoRNAs in breast cancer patients, thus reporting them as prognostic markers for breast cancer (164). Further studies have reported small nucleolar RNA-derived RNA-93 (sdRNA-93), a processed stable form of snoRNA-93, as playing an important role in cell invasiveness in epithelial human breast cancer cell lines. At the same time, sdRNA-93 was significantly higher expressed in Luminal B/HER2+ breast cancer samples when compared to normal breast tissue and other types of breast cancer (165, 166).

Further on, it has been discovered that piR-36712 plays a pivotal role in suppressing breast cancer cell proliferation through the retroprocessed pseudogene of selenoprotein W (SEPW1), SEPW1P, by inhibiting the expression of SEPW1. The expression of both p21 and p53 was inhibited by the mRNA degradation induced by SEPW1. Concurrently, piR-36712 has been found to promote the antineoplastic effect of chemotherapeutic agents (167). A recent study carried out by Fancello and colleagues has found that, in approximately 34% of invasive breast cancer samples, ribosomal alterations were driven

by mutations in the uL18/RPL5 ribosomal protein genes, thus highlighting the suppressor role of RPL5 in breast cancer (168).

Clearly, ncRNAs remain a vast unexplored resource for the better understanding of breast cancer tumorigenesis and metastasis, potentially aiding in the progress of identifying relevant diagnostic and prognostic markers, as well as therapeutic targets.

miRNAs in Ovarian Cancer

Ovarian cancer is the most lethal gynecologic neoplasia, associating a very poor life prognosis. Epithelial ovarian cancers amount to more than 90% of this malignancy, and the 5-year survival rate is just 29% (169). Moreover, ovarian cancer is diagnosed late due to the absence of noticeable symptoms in the early stages, and, when detected, carcinomatosis spread is higher than 60% (170, 171). Biomarkers used today for prediction and prognosis are CA-125 and human epididymis protein 4 (HE4), used along with imaging and screening methods. However, the relatively low sensitivity and specificity of these procedures require the discovery of new, more efficient diagnostic and prognostic methods. To this end, many studies have been performed and more are underway, in order to explore the exact relation between miRNAs and ovarian cancer and to improve current diagnosis, prognosis and treatment methods.

The development of tumors is imposed by the tumor microenvironment. Extracellular matrix molecules regulate cancer invasion and metastasis, and, at the same time, down-regulation of miRNAs controls the spread of the tumor by degrading the extracellular matrix (172, 173). Matrix metalloproteinases are important in tumor aggressiveness and increase cancer metastasis by causing deterioration in the molecules of the extracellular matrix (174). Studies have demonstrated that MMP-9, MMp-3, MMp-7, MMP-2 are involved in tumor aggression in ovarian cancer. An example is that of MMP-7, which is increased in malignant ovarian tissues, where miR-543 is substantially reduced. The explanation resides in the fact that miR-543 decreases MMP-7 transcription by attaching to the 3'-UTRs of MMP-7 mRNA, leading to the reduction of cancer proliferation (175).

The miR-200 group consisting of miR-141, miR-200a, miR-429, miR-200c, and miR-200b, is clustered in chromosome 1 (1p36) and adjusts many cellular functions, including cell death, proliferation, and epithelial-to-mesenchymal transition (EMT). This group decreases the transcriptional suppressors of E-cadherin, ZEB1, and ZEB2, promotes E-cadherin expression, and modulates the conversion of mesenchymal cells into epithelial cells (176, 177). miR-200a can bind to three specific sites within the 3'UTR region of the ZEB1 mRNA, while miR-141 has two potential binding sites in the 3'UTR region of the ZEB2 mRNA. By binding to the ZEB1 and/or ZEB2 mRNAs, these miRNAs mediate the post-transcriptional inhibition of the ZEB1 and ZEB2 gene expression (177, 178). Furthermore, negatively regulated miR-200a in cancer cells inhibits E-cadherin, known invasion, and metastasis suppressor (179). Tumor angiogenesis is another process influenced by the miR-200 family. Studies have shown that new blood vessel development is inhibited by this cluster's influence on the interleukin-8 (IL8) secreted by cancer cells and on chemokine CXCL-1, thus decreasing the spread of tumor cells through blood circulation (180). To this extent, Pecot et al. have implemented several experimental models, demonstrating that tumor-targeted delivery of miRNAs of the miR-200 family leads to a significant decrease in angiogenesis and consecutive tumor cell metastasis, while also promoting vascular normalization (181).

The miRNA let-7 family is another important cluster which has been broadly studied and has a significant function in ovarian cancer growth. It has been demonstrated that, by decreasing the expression of specific proteins like c-Myc, Ras, cyclin 2, and the High Mobility Group AT-Hook 2 (HMGA2) protein, the let-7 group decreases cell proliferation and supports both apoptosis and cell differentiation in various types of cancer. Since the let-7 group is poorly expressed in aggressive ovarian malignancies, it can be concluded that it may decrease the infiltration and spreading of ovarian cancer (81). miR let-7d is known to behave as an oncogene in ovarian malignancies, and its inactivation can lead to the overexpression of Ras, resulting in apoptosis of cancer cells (182, 183). One study performed by Chen Y. et al. found that miR let-7d-5p negatively regulated HGMA1 in ovarian cancer, leading to the obstruction of the p53 signaling pathway, thus suppressing cell proliferation and facilitating programmed cell death (184). Furthermore, in wanting to predict chemotherapy resistance and prognosis of epithelial ovarian cancer, Xiao et al. have performed thorough research focusing on the human let-7 family. They found that let-7e inhibitor had an up-regulatory effect on the mRNAs of target genes regulatory factor X 6 (RFX6), enhancer of zeste 2 (EZH2), caspase 3 (CASP3), and matrix metalloproteinase-9 (MMP9). On the other hand, treatment with let-7e mimics resulted in decreased mRNA levels of poly-ADP-ribose-polymerase 1 (PARP1) and insulin-like growth factor-1 (IGF-1). Further on, they found that ovarian cancer cell lines had an increased sensitivity to cisplatin when associated with overexpression of let-7e, thus confirming the role of poor let-7e expression in platinum resistance in epithelial ovarian cancer (185).

miRNAs in Cervical Cancer

Cervical malignancies pose serious health risks to the female population, associating a poor prognosis with an overall 5 years survival rate amounting to less than 40% (186), thus highlighting the need for new diagnostic methods and targeted treatments. Studies have shown that the abnormal expression of miRNAs contributes to the development of cervical cancer, due to their innate ability to regulate tumor promoter and/or repressors genes (187, 188). To this extent, although limited information regarding cervical tumors is currently available, miR-433 has been demonstrated to be downregulated in cervical tumoral tissues and cell lines, as opposed to normal tissues, its levels reflecting tumor characteristics such as size, stage, and dissemination (189, 190). While the upregulation of miR-433 in cervical cancer inhibits cell proliferation and invasion and promotes cell death, rescue experiments have demonstrated that metadherin (MTDH), an oncogene that facilitates cancer cell migration and metastasis, is a direct target gene of miR-433. In this regard, the overexpression of MTDH has been shown to

reverse the effects of the overexpressed miR-433 in cervical cancer cell lines (191). Employing functional studies, Liang et al. have demonstrated that cervical cancer cell lines treated with miR-433 agomir substantially decreased mRNA levels of MTDH, thus inhibiting tumor cell proliferation and invasion and triggering apoptosis (192). MTDH has also been previously demonstrated to influence the regulation of β-catenin and AKT pathways and, due to its inhibitory effect on these pathways in cervical cancer, it has been validated as a direct target of miR-433 (193, 194).

Additional studies have revealed that miR-21 acts as an oncogene in various malignancies, by regulating several pathways involved in tumor progression (195). In cervical cancer, its overexpression acts as a gene expression inhibitor (196). miR-21 upregulates mRNA and protein expression levels of TNFα (197), which initiates cellular apoptosis by binding and activating the TNFR1 receptor in HeLa cells, thus inhibiting the TNFR1 pathway (198). In contrast, the TNFR2 pathway is increased by miR-21, and cell proliferation is activated by TNFα, which binds TNFR2, upregulating NF-κB, and thus inhibiting Caspase 3 and activating JNK (197). Further on, miR-21 has also been shown to increase cell proliferation via the PI3K/AKT/mTOR signaling pathway, by binding and inhibiting the tumor suppressor PTEN (96, 199). PTEN acts as a negative regulator of this particular signaling cascade, by targeting AKT and therefore modulating cell differentiation, proliferation, and migration (96). Loss of miR-21 leads to considerable upregulation in PTEN mRNA levels, with Chen et al. demonstrating that cells lacking miR-21 display a lesser degree of cisplatin resistance, both in culture and xenograft mouse models (200). Furthermore, miR-21 also promotes cell proliferation through the Ras/MEK/ERK signaling pathway, which is inhibited by miR-21 due to its targeting of the 3'-UTR of RASA1 mRNA (99, 100, 201). However, further investigation is required in order to elucidate other targets of miR-21, as well as their exact implications in cervical malignancy.

miRNAs in Endometrial Cancer

In developed countries, endometrial cancer is the most frequently-occurring gynecological cancer, having to do with increased obesity rates, longer life expectancy, and particular lifestyles in these nations. Globally, it is the second most harmful type of cancer among women, after cervical cancer (202), with the most common type of endometrial cancer being the endometrioid tumor (203, 204). Endometrial cancer is classified into two types: type I - endometrioid endometrial cancer, amounting to 75% of cases, and type II - non-endometrioid, which can have clear-cell or serous histology. Endometrioid cancers more often show mutations in the Kirsten rat sarcoma viral oncogene homolog (KRAS) and Phosphatidylinositol 3-kinase catalytic subunit alpha (PI3KCA) and phosphatase and tensin homolog (PTEN) loss, while non-endometrioid cancers show human epidermal growth factor receptor 2 (HER-2) overexpression and mutations in p53 (205). Phosphoinositide-3-Kinase Regulatory Subunit 1 (PIK3R1) mutations are present in approximately 43% of endometrioid endometrial cancers and about 12% of non-endometrioid endometrial cancers, the mutated PI3KR1 leading to increased activation of the PI3K/AKT signaling pathway (206).

Oncogene expression and aggression factors in endometrial malignancies have been researched in comparison with normal endometrial tissue, and miRNA expression has been found to be significantly different. Moreover, among endometrial cancer types, such as papillary carcinoma and endometrioid carcinoma, miRNA patterns have been demonstrated to vary (207). miRNAs have the ability to link to the associated mRNA targets with or without perfect complementarity, with multiple target genes being simultaneously influenced by a single miRNA, either by means of the same or different cellular signaling pathways. Consequently, delivery of tumor suppressor miRNAs along with silencing of oncogenic miRNAs have been demonstrated to carry the potential to repair aberrations of the related signaling pathways in endometrial cancer (208, 209). For instance, in endometrial cancer, while miR-34b, which is linked to invasion and proliferation, can be overexpressed, along with miR-100, miR-99a, and miR-199b, the tumor-suppressive miR-34a is underexpressed (67, 210). Expressions of specific miRNAs in endometrial cancer cells have been found to be either elevated, such as miR-423, miR-210, miR-185, miR-7, or decreased, like miR-221, miR-let7e, miR-30c, when compared to normal endometrial tissue. To this extent, tumor-suppressor mRNAs have been found to be suppressed by the former miRNAs, thus promoting tumor cell growth, invasion, and metastasis. In turn, tumor suppressor miRNAs such as miR-221, miR-let7e, and miR-30c tend to inhibit oncogenic mRNAs, their lowered levels enabling carcinogenesis (211). Further thorough research conducted by Chung et al. has identified another miRNA cluster that appears to be dysregulated in endometrial cancer. Using low-density arrays, they analyzed the expression of 365 human miRNAs in normal and endometrioid endometrial cancer and identified a cluster of dysregulated miRNAs, including miR-7, miR-194, miR-449b, and miR-204. They also discovered that, by overexpressing miR-204, which is involved in the regulation of Forkhead box C1 (FOXC1), cell migration and the number of invasive cells could be inhibited (212).

In endometrial cancer cells, Dong et al. have identified 23 miRNAs as being dysregulated, mainly as a result of the mutated p53 (213). miR-130b among them, which is decreased in endometrial cancer relative to normal tissues, has the ability to target the key EMT promoter gene ZEB1 and to revert mutant p53-induced EMT/CSC of endometrial cancer cells (213, 214). Furthermore, miR-205 along with the miR-200 family inhibits EMT by regulating the E-cadherin dependent transcription of repressors ZEB1 and ZEB2 (75, 215). Overexpression of miR-200b in adenocarcinoma cells has also been found to inhibit the expression of the tissue inhibitor of metalloproteinase-2 (TIMP2), and increase the matrix metalloproteinase level (MMP), revealing the implication of miR-200b in endometrial cancer metastasis (216). EMT plays an important role in promoting chemoresistance and tumor cell invasion, with

cancer biology studies and genetic evidence showing that the PI3K/AKT signaling pathway is the main mechanism controlling EMT features, despite its effects on cancer cell survival and proliferation (217). During EMT, adhesive and polarizing capabilities of the epithelial cells are lost, therefore gaining invasive and migratory behaviors which promote cancer invasion and metastatic spread. Judging by the suppressive action of miR-205 on EMT, some studies have suggested that high levels of miR-205 can be regarded as a marker of early-stage cancer, thus leading to an improved prognosis (218, 219).

Further on, the overexpression of miR-21 in endometrial cancer tissues and downregulation of PTEN through linking to 3'UTR of PTEN mRNA has been shown to promote cell proliferation (220). Similarly, decreased expression of PTEN associated with an increased expression of miR-205 in endometrial cancer has been linked to smaller overall patient survival rates, suggesting the link between miR-205 and the 3'-UTR of PTEN mRNA in endometrial cancer cells (84). Additional research has indicated that the transfection of endometrial cancer cells with miR-183 resulted in PTEN protein expression reduction. However, it is yet to be clear if miR-183 can suppress 3'-UTR of PTEN mRNA in endometrial cancer cells (84, 221).

Endometrial cancer proliferation has also been revealed to be promoted by the abnormal regulation of the Notch pathway (222). The Notch signaling cascade is initiated by the interactions between specific ligands and receptors, and Guo and colleagues have demonstrated that, by repressing Notch signaling, the tumor suppressor lncRNA human maternally expressed gene 3 (MEG3) inhibits cell proliferation in endometrial carcinoma (223). The initiation of the Notch signaling pathway is triggered by the ligand-receptor interaction, followed by the intramembranous proteolytic cleavage of the Notch receptors, which ensures the delivery of an active form of the Notch intracellular domain (NICD). NICD shows positive regulation of target genes such as the hes family bHLH transcription factor 1 (HES1), by acting as a transcriptional activator following nuclear translocation. HES1 has a particular effect on cell proliferation, by acting as a transcriptional repressor that negatively regulates genes such as the cyclin-dependent kinase inhibitor p27Kip1 (224). The Notch signaling pathway is also thought to be involved in the interaction between miR-184 and cell division cycle 25 A (CDC25A) protein. By examining the CDC25A mRNA sequence and identifying an optimal binding site for miR-184, Chen et al. have recently found that miR-184 overexpression significantly reduced CDC25A protein levels, thus hindering endometrial carcinoma cell growth and invasion. Conversely, they have also highlighted that downregulation of Notch receptors (NOTCH 1,2,3,4) and target gene HES1 induced by miR-184 can be overturned by the overexpression of CDC25A (225).

miRNAs in Vulvar Cancer

Vaginal and vulvar carcinomas are rather rare diseases, adding up to 4% of gynecological cancers worldwide (226). According to the Centers for Disease Control and Prevention, approximately 5% of US females with genital tract malignancies are diagnosed with vulvar and vaginal neoplasm (227). The management of vulvar neoplasia is highly dependent on early diagnosis, clinical, and pathological degree of the tumoral process at the time of detection and on the emergence of loco-regional lymph node metastases (228). Therefore, the identification and detection of specific miRNAs for this type of cancer may help better address this public health concern and patients' needs. Some types of miRNA molecules make up specific profiles for vulvar carcinoma, with some authors proposing them as biomarkers for both early diagnostics and therapeutic signaling targets in personalized treatments (229). However, so far only a few suitable references regarding microRNAs expressed in vulvar cancerous lesions, especially vulvar squamous cell carcinoma, have been reported (230).

There are two different pathways by which vulvar cancers develop. Squamous cells leading to vulvar squamous cell carcinomas (VSCC) amount to about 80% of all vulvar malignant tumors (230, 231). Most of these tumors, especially among young women, are linked to high-risk human papillomavirus (hrHPV) infections (231, 232) and are associated with other risk factors such as immunosuppression and smoking (233). Other types of carcinomas may appear in the context of chronic inflammatory skin diseases such as lichen sclerosus (LS) or may constitute differentiated vulvar intraepithelial malignancies, basal cell carcinomas, malignant melanomas, Paget disease or Bartholin gland carcinoma (232, 234). Genetic and epigenetic changes in vulvar lesions were reported in quite a few studies, where vulvar intraepithelial neoplasia (VIN) and VSCCs were correlated with HPV infection. Some of these studies have identified p53 as an altered signaling pathway, where NOTCH1 mutations were often detected (235, 236). Some studies have reported somatic mutations in higher range regarding HPV-negative tumors compared to HPV-positive tumors, where mutations of TP53 were detected (237). The number of genetic changes, however, also depends on the cancer stage, increasing the number of dysregulated signaling pathways and the altered signaling molecules, thus elevating the grade of dysplasia (235). Other studies reported different altered signaling processes related to VSCC. For instance, in VSCC it has been shown that miR−3147 regulates the Smad4 pathway by repressing mRNAs of Bax, Bim, p21, and PAI-1 genes, thus increasing both migration and invasion (86), while miR−590−5p promotes malignant cellular processes by upregulating the target gene TGFβRII (228). The extensive roles of miRNAs in vulvar carcinoma have also been recently investigated by Yang et al., who suggested that miR −4712−5p may promote carcinogenesis by targeting PTEN and could facilitate VSCC growth and invasion through the alteration of the PTEN/Akt/p−GSK3β/cyclin D1 signaling pathway (231).

Further on, the expression of miRNA molecules involved in vulvar carcinomas has also been explored by Yang and colleagues, so as to elucidate their mechanism of action in correlation with the expression levels of transforming growth factor-β (TGF-β) and Smad pathway factors (228). They found

that 157 miRNA molecules were expressed in a significantly altered manner in this type of carcinoma. They concluded that while some miRNA molecules like miR-590-5p, miR-182-5p and miR-183-5p were upregulated, others were downregulated, especially miR-603, miR-103a-3p, and miR-107. Overexpression of miR-590-5p was found to induce decreased mRNA and protein levels of TGFβIIR, thus altering the TGF-β/Smad signaling pathway, and therefore facilitating the generation of malignant cellular changes along with sentinel lymph node metastasis (228). Further on, Zalewski et al. have recently conducted a study aimed at researching the expression levels of several miRNAs in plasma of patients harboring the same type of lesions: vulvar intraepithelial neoplasia and vulvar carcinoma. Six microRNAs (hsa-miR-425-5p, hsa-miR-191-5p, hsa-miR93-5p, hsa-miR-423-5p, hsa-miR-103a-3p and hsa-miR-16-5p) were analyzed. Of these, hsa-miR-93-5p and hsa-miR-425-5p were the most appropriate genes that could be used as internal controls for quantitative miRNA expression in these kind of rare gynecological malignancies (226).

RESVERATROL: THE MIRNA CONTROLLING COMPOUND

Inflammation is a non-specific immune response of the human body to a tissue injury, toxic compounds, damaged cells, irritant molecules or allergens. Inflammation is associated with both healing and destruction of the tissue from the surrounding area. In response to inflammation, the immune system coordinates a large variety of mediators. The hallmark of inflammation is the recruitment of the leukocytes in the peripheral zone of the tissue (238, 239). There are two pathways that connect inflammation with cancer: the intrinsic pathway, based on genetic alterations that induce neoplasia and inflammation, and the extrinsic pathway, which increases cancer risk by inflammatory conditions (240). Several miRNAs have been shown to play a part in both cancer and inflammation, with the most investigated being miR-21, miR-125b, and miR-155. For instance, miR-155, which is elevated in lymphomas and human leukemias, is known to be involved in erythropoiesis and myelopoiesis, B-cell maturation, Th1 differentiation, gene conversion, IgG1 production, B- and T-cell homeostasis and in the overall regulation of the immune response (91).

Found in grapes and berries, resveratrol is a natural polyphenolic antioxidant. Recent studies have shown that resveratrol has properties in cancer and cardiovascular prevention. It was first shown that resveratrol can inhibit tumor promotion and progression in skin cancer studied on mice (241, 242). Resveratrol 4-hydroxystyryl and m-hydroxyquinone moieties seem to be significant due to their inhibitory properties concerning various enzymes, such as cyclooxygenases and lipoxygenases that produce pro-inflammatory factors starting from arachidonic acid and protein kinases (243). Resveratrol is a pleiotropic element known to target a series of proteins in patients diagnosed with ovarian cancer, particularly HES1 and NOTCH2 in CAOV-3 and OVCAR-3 cells. Resveratrol has been shown to downregulate WNT2 in CAOV3 cells and the nuclear cumulation of B-catenin was reduced. Furthermore, resveratrol notably reduced OVCAR-3 cell nuclear cumulation of STAT3. Despite the evidence about resveratrol targeting multi-proteins, it is necessary to determine the particular features of the mechanism involved in the signaling pathways of this interwoven network (244).

The effect on NOTCH signaling of resveratrol is known to be context-dependent. Resveratrol has an inhibiting effect when NOTCH signaling is oncogenic. However, resveratrol is potentiating the tumor-suppressive action when NOTCH signaling has suppressive tumoral action. c-Myc (oncogenic transcription factor), an mRNA protein, was repressed by resveratrol in treated breast cancer cells. In consequence, c-Myc decrease resulted in the diminishing of miR-17 and pri-miR-17-92, whilst c-Myc overexpression significantly increased miR-17 and pri-miR-17-92 (245).

Studies have shown that this antioxidant also impedes the proliferation of MDA-MB-231-luc-D3H2LN breast cancer cells and the attention was directed to miRNA analysis, being revealed that resveratrol generates the expression of miR-141 and miR-200c within these cells (82, 246, 247). Besides, various genes and biological signaling pathways were regulated by resveratrol. One example is the p53 pathway which, once activated by resveratrol, leads to cell death with the implication of miRNAs. Several miRNAs like miR-34a, miR-424, and miR-503 can impede breast cancer development being downregulated by resveratrol through the p53 pathway, thus inhibiting HNRNPA1, whose expression is connected with cancer spread (248, 249). The effects of resveratrol on miRNAs invariably prove to be essential due to its anti-cancer, anti-inflammation, and anti-metastatic properties. miR-663, miR-155, and miR-21 are implicated in the regulation of native immunity, cell proliferation, tumor development, and metastasis apparition, which suggests that the capacity of resveratrol to behave as an anti-proliferation, anti-tumor, and anti-inflammatory agent at the same time arises from its ability to promote the expression of endogenous miRNAs, thus having the capacity to globally affect the cell proteome (91).

CONCLUSIONS AND FUTURE PERSPECTIVES

Due to their high incidence and mortality rate worldwide, gynecological cancers have become a global public health problem. In this review article, while summarizing the findings in the literature regarding the roles of miRNAs in cancer-relevant processes, specifically in the context of gynecological cancers, we have also focused on implications of miRNA signaling pathways and their role in regulating oncogenic processes in breast, ovarian, cervical, vulvar and endometrial cancer.

miRNAs have arisen as signaling molecules in virtually all biological pathways in different forms of cancer, including gynecological neoplasia, and it has been proven that these molecules could regulate various processes involved in

tumorigenesis. Considering the ability of a single miRNA to target hundreds of mRNAs, expressions of aberrant miRNA are liable for the deregulation of signaling pathways that control cancer-associated processes. Understanding the mechanism by which these changes within intercellular and intracellular signaling pathways occur represents a challenge for the survival of women who are detected with advanced and/or recurrent gynecological malignancies. As the important functions of miRNAs in gynecological cancer are being deciphered, their potential use as prognostic and/or diagnostic markers is evidenced by a long list of studies. Therapeutic strategies involving the reintroduction of lost miRNAs in cancer or inhibition of oncogenic miRNAs are steadily being developed. Various signaling pathways have been identified and described to be modified in gynecological cancers. The occurrence of oncogenic mutations may result in overexpression of the affected genes or in the production of mutated proteins whose activity is downregulated. Such proteins could be involved in signaling pathways that are implicated in many physiological cellular processes, like inflammatory cytokine production, proliferation, senescence and apoptosis, metastasis, and drug resistance

miRNAs such as miR-145, have been identified as central players in cervical carcinogenesis, whereas it has been demonstrated that miR-125b, miR-145, miR-21, and miR-155 have pivotal roles in breast neoplasia. miR-200 and let-7 have been described as key modulators in ovarian malignancies and miR-185, miR-210, miR-423, let-7c, miR-205, and miR-429 have been associated with oncogenesis, invasion, and metastasis in endometrial carcinoma. Resveratrol, on the other hand, has the capacity to behave as an anti-proliferation, anti-tumor, and anti-inflammatory agent at the same time, due to its expression on the endogenous miRNAs, having the capacity to globally affect the cell proteome.

In this review article, we have summarized new research findings regarding the importance that miRNAs have in cancer-relevant processes, specifically concerning the gynecological field, and about their significant role in the disruption of cancer-related signaling pathways, so as to improve the overall medical management of gynecological malignancies.

AUTHOR CONTRIBUTIONS

Conceptualization: FD, CC, CD, EB. Methodology: SC, JX, DC. Investigation: NS, MR. Resources, NS, D-VP. Writing—original draft preparation: FD, CC, CD, EB. Writing—review and editing: JX, XL, DC. Supervision: XL, SC, D-VP. Funding acquisition: NS, D-VP. All authors contributed to the article and approved the submitted version.

FUNDING

This work was supported by grants of the Romanian Ministry of Research and Innovation, CCCDI-UEFISCDI, project number PN-III-P1-1.2-PCCDI- 2017-0833/68/2018 and PN-III-P1-1.2-PCCDI-2017-0820/67/2018 within PNCDI III.

REFERENCES

1. Lee SY, Dutta A. MicroRNAs in cancer. *Annu Rev Phatol* (2009) 4:199–227. doi: 10.1146/annurev.phatol.4.110807.092222
2. Bo B, Zang T, Jiang Y, Cui H, Miao P. Triple Signal Amplification Strategy for Ultrasensitive Determination of miRNA Based on Duplex Specific Nuclease and Bridge DNA–Gold Nanoparticles. *Anal Chem* (2018) 90:2395–400. doi: 10.1021/acs.analchem.7b05447
3. Cretoiu D, Xu J, Xiao J, Suciu N, Cretoiu SM. Circulating MicroRNAs as Potential Molecular Biomarkers in Pathophysiological Evolution of Pregnancy. *Hindawi Publishing Corporation Dis Markers* (2016) 2016:1–7. doi: 10.1155/2016/3851054
4. Ilaria C, Varano G, Simioni C, Laface I, Milani D, Rimondi E, et al. miRNAs as Influencers of Cell–Cell Communication in Tumor Microenvironment. *Cells* (2020) 9:220. doi: 10.3390/cells9010220
5. Schmidt MF. Drug Target miRNA: Methods and Protocols. *Methods Mol Biol* (2017) 1517:3–22. doi: 10.1007/978-1-4939-6563-2_1
6. Humphries B, Wang Z, Yang C. MicroRNA Regulation of Epigenetic Modifiers in Breast Cancer. *Cancers* (2019) 11:897. doi: 10.3390/cancers11070897
7. Ghosh A, Ekka MK, Tawani A, Kumar A, Chakraborty D, Maiti S. Restoration of miRNA-149 expression by TmPyP4 induced unfolding of quadruplex within its precursor. *Biochemistry* (2019) 58(6):1–35. doi: 10.1021/acs.biochem.8b00880
8. Yamamura S, Imai-Sumida M, Tanaka Y, Dahiya R. Interaction and cross-talk between non-coding RNAs. *Cell Mol Life Sci* (2018) 75:467–84. doi: 10.1007/s00018-017-2626-6
9. Gusic M, Prokisch H. ncRNAs: New Players in Mitochondrial Health and Disease? *Front Genet* (2020) 11:95. doi: 10.3389/fgene.2020.00095
10. López-Urrutia E, Bustamante Montes LP, Ladrón de Guevara Cervantes D, Pérez-Plasencia C, Campos-Parra AD. Crosstalk Between Long Non-coding RNAs, Micro-RNAs and mRNAs: Deciphering Molecular Mechanisms of Master Regulators in Cancer. *Front Oncol* (2019) 9:669. doi: 10.3389/fonc.2019.00669
11. West JA, Davis CP, Sunwoo H, Simon MD, Sadreyev RI, Wang PI, et al. The long noncoding RNAs NEAT1 and MALAT1 bind active chromatin sites. *Mol Cell* (2014) 55:791–802. doi: 10.1016/j.molcel.2014.07.012
12. Pavet V, Portal MM, Moulin JC, Herbrecht R, Gronemeyer H. Towards novel paradigms for cancer therapy. *Oncogene* (2011) 30:1–20. doi: 10.1038/onc.2010.460
13. Zhang P, Wu W, Chen Q, Chen M. Non-Coding RNAs and their Integrated Networks. *J Integr Bioinf* (2019) 16(3):20190027. doi: 10.1515/jib-2019-0027
14. Jorge NAN, Wajnberg G, Ferreira C, Carvalho BDS, Passetti F. snoRNA and piRNA expression levels modified by tobacco use in women with lung adenocarcinoma. *PLoS One* (2017) 12(8):e0183410. doi: 10.1371/journal.pone.0183410
15. Martens-Uzunova ES, Olvedy M, Jenster G. Beyond microRNA–novel RNAs derived from small non-coding RNA and their implication in cancer. *Cancer Lett* (2013) 340:201–11. doi: 10.1016/j.canlet.2012.11.058
16. Bratkovič T, Božič J, Rogelj B. Functional diversity of small nucleolar RNAs. *Nucleic Acids Res* (2020) 48:1627–51. doi: 10.1093/nar/gkz1140
17. Weinstein LB, Steitz JA. Guided tours: from precursor snoRNA to functional snoRNP. *Curr Opin Cell Biol* (1999) 11:378–84. doi: 10.1016/s0955-0674(99)80053-2
18. Filipowicz W, Pogacić V. Biogenesis of small nucleolar ribonucleoproteins. *Curr Opin Cell Biol* (2002) 14:319–27. doi: 10.1016/s0955-0674(02)00334-4
19. Yuan T, Huang X, Woodcock M, Du M, Dittmar R, Wang Y, et al. Plasma extracellular RNA profiles in healthy and cancer patients. *Sci Rep* (2016) 6:19413. doi: 10.1038/srep19413

20. Meister G. Argonaute proteins: functional insights and emerging roles. *Nat Rev Genet* (2013) 14:447–59. doi: 10.1038/nrg3462
21. Siomi MC, Sato K, Pezic D, Aravin AA. PIWI-interacting small RNAs: the vanguard of genome defence. *Nat Rev Mol Cell Biol* (2011) 12:246–58. doi: 10.1038/nrm3089
22. Ø Ulf Andersson Vang editor. *miRNA Biogenesis: Methods and Protocols, Methods in Molecular Biology*. (2018) 1823:1–9. doi: 10.1007/978-1-4939-8624-8_1. Springer-Verlag New York, © Springer Science+Business Media, LLC, part of Springer Nature.
23. Guescini M, Guidolin D, Luciana V, Casadei L, Gioacchini A, Tibollo P, et al. C2C12 myoblasts release micro-vesicles containing mtDNA and proteins involved in signal transduction. *Exp Cell Res* (2010) 316:1977–84. doi: 10.1016/j.yexcr.2010.04.006
24. Bartel DP. MicroRNAs: genomics, biogenesis, mechanism and function. *Cell.* (2004) 116:281–97. doi: 10.1016/S0092-8674(04)00045-5
25. Thum T, Catalucci D, Bauersachs J. MicroRNAs: novel regulators in cardiac development and disease. *Cardiovasc Res* (2008) 79:562–70. doi: 10.1093/cvr/cvn137
26. Kriegel AJ, Liu Y, Fang Y, Ding H, Liang M. The miR29 family: genomics, cell biology, and relevance to renal and cardiovascular injury. *Physiol Genomics* (2012) 44, 4:237–44. doi: 10.1152/physiolgenomics.00141.2011
27. Eisenberg I, Eran A, Nishino I, Moggio M, Lamperti C, Amato AA, et al. Distinctive patterns of microRNA expression in primary muscular disorders. *Proc Natl Acad Sci U S A* (2007) 104:107016–17021. doi: 10.1073/pnas.0708115104
28. Roderburg C, Urban GW, Bettermann K, Vucur M, Zimmermann H, Schmidt S, et al. Micro-RNA profiling reveals a role for miR-29 in human and murine liver fibrosis. *Hepatology* (2011) 53:209–18. doi: 10.1002/hep.23922
29. Cushing L, Kuang P, Lü J. The role of miR-29 in pulmonary fibrosis. *Biochem Cell Biol* (2015) 93:109–18. doi: 10.1139/bcb-2014-0095
30. Kong L, Zhu J, Han W, Jiang X, Xu M, Zhao Y, et al. Significance of serum microRNAs in pre-diabetes and newly diagnosed type 2 diabetes: a clinical study. *Acta Diabetol* (2011) 48, 1:61–9. doi: 10.1007/s00592-010-0226-0
31. Prieto DMM, Markert UR. MicroRNAs in pregnancy. *J Reproduct Immun* (2011) 88, 2:106–11. doi: 10.1016/j.jri.2011.01.004
32. Santanam U, Zanesi N, Efanov A, Costineana S, Palamarchuka A, Hagana JP, et al. Chronic lymphocytic leukemia modeled in mouse by targeted miR-29 expression. *Proc Natl Acad Sci* (2010) 107, 27:12210–5. doi: 10.1073/pnas.1007186107
33. Han YC, Park CY, Bhagat C, Zhang J, Wang Y, Fan JB, et al. MicroRNA-29a induces aberrant self-renewal capacity in hematopoietic progenitors, biased myeloid development, and acute myeloid leukemia. *J Exp Med* (2010) 207, 3:475–89. doi: 10.1084/jem.20090831
34. Trino S, Lamorte ID, Caivano A, Laurenzana I, Tagliaferri D, Falco G, et al. MicroRNAs as New Biomarkers for Diagnosis and Prognosis, and as Potential Therapeutic Targets in Acute Myeloid Leukemia. *Int J Mol Sci* (2018) 19, 460:1–25. doi: 10.3390/ijms19020460
35. Rodenand C, Lu J. MicroRNAs in Control of Stem Cells in Normal and Malignant Hematopoiesis. *Curr Stem Cell Rep* (2016) 2(3):183–96. doi: 10.1007/s40778-016-0057-1
36. Heinrich EM, Dimmeler S. Micro-RNAs and stem cells: control of pluripotency, reprogramming, and lineage commitment. *Circ Res* (2012) 110:1014–22. doi: 10.1161/CIRCRESAHA.111.243394
37. Shioya M, Obayashi S, Tabunokietal H. Aberrant microRNA expression in the brains of neurodegenerative diseases: MiR29a decreased in Alzheimer disease brains targets neurone navigator3. *Neuropath Appl Neurobiol* (2010) 36, 4:320–30. doi: 10.1111/j.1365-2990.2010.01076.x
38. Pereira PA, Tomás JF, Queiroz JA, Figueiras AR, Sousa F. Recombinant pre-miR-29b for Alzheimer's disease therapeutics. *Sci Rep* (2016) 6:19946. doi: 10.1038/srep19946
39. Maa F, Zhanga X, Yina KJ. ABSTRACT, MicroRNAs in central nervous system diseases: A prospective role in regulating blood-brain barrier integrity. *Exp Neurol* (2019) 323:113094. doi: 10.1016/j.expneurol.2019.113094
40. Huang Y, Yang S, Zhang J, Tan L, Jiang F, Li N, et al. MicroRNAs as promising biomarkers for diagnosing human cancer. *Cancer Invest* (2010) 28:670–1. doi: 10.3109/07357901003631064
41. Jasson MD, Lund AH. Micro-RNA and cancer. *Molec Oncol* (2012) 6:590–610. doi: 10.1016/j.molonc.2012.09.006
42. Kozomara A, Birgaoanu M, Griffiths-Jones S. miRBase: from microRNA sequences to function. *Nucleic Acids Res* (2019) 47:D155–62. doi: 10.1093/nar/gky1141
43. Maheshwari A, Kumar N, Mahantshetty U. Gynecological cancers: A summary of published Indian data. *South Asian J Cancer* (2016) 5:112–20. doi: 10.4103/2278-330X.187575
44. Esserman LJ, Thompson IM, Reid B, Nelson P, Ransohoff DF, Welch HG, et al. Addressing overdiagnosis and overtreatment in cancer: a prescription for change. *Lancet Oncol* (2014) 15:e234–42. doi: 10.1016/S1470-2045(13)70598-9
45. Azarov I, Liu C, Reynolds H, Tsekouras Z, Lee JS, Gladwin MT, et al. Mechanisms of slower nitric oxide uptake by red blood cells and other hemoglobin-containing vesicles. *J Biol Chem* (2011) 286:33567–79. doi: 10.1074/jbc.M111.228650
46. Peng Y, Croce CM. The role of MicroRNAs in human cancer. *Signal transduction Targeted Ther* (2016) 1:15004–4. doi: 10.1038/sigtrans.2015.4
47. Jansson MD, Lund AH. MicroRNA and cancer. *Mol Oncol* (2012) 6:590–610. doi: 10.1016/j.molonc.2012.09.006
48. Krol J, Loedige I, Filipowicz W. The widespread regulation of microRNA biogenesis, function and decay. *Nat Rev Genet* (2010) 11(9):597–610. doi: 10.1038/nrg2843
49. Yayan J. Emerging families of biomarkers for coronary artery disease: inflammatory mediators. *Vasc Health Risk Manage* (2013) 9:435–56. doi: 10.2147/vhrm.S45704
50. Salem ESB, Fan GC. Pathological Effects of Exosomes in Mediating Diabetic Cardiomyopathy. *Adv Exp Med Biol* (2017) 998:113–38. doi: 10.1007/978-981-10-4397-0_8
51. Zheng D, Ma J, Yu Y, Li M, Ni R, Wang G, et al. Silencing of miR-195 reduces diabetic cardiomyopathy in C57BL/6 mice. *Diabetologia* (2015) 58:1949–58. doi: 10.1007/s00125-015-3622-8
52. Vrijsen KR, Maring JA, Chamuleau SA, Verhage V, Mol EA, Deddens JC, et al. Exosomes from Cardiomyocyte Progenitor Cells and Mesenchymal Stem Cells Stimulate Angiogenesis Via EMMPRIN. *Advanced Healthcare Mater* (2016) 5:2555–65. doi: 10.1002/adhm.201600308
53. Tauro BJ, Greening DW, Mathias RA, Ji H, Mathivanan S, Scott AM, et al. Comparison of ultracentrifugation, density gradient separation, and immunoaffinity capture methods for isolating human colon cancer cell line LIM1863-derived exosomes. *Methods (San Diego Calif.)* (2012) 56:293–304. doi: 10.1016/j.ymeth.2012.01.002
54. Todorova D, Simoncini S, Lacroix R, Sabatier F, Dignat-George F. Extracellular Vesicles in Angiogenesis. *Circ Res* (2017) 120:1658–73. doi: 10.1161/circresaha.117.309681
55. Thum T, Galuppo P, Wolf C, Fiedler J, Kneitz S, van Laake LW, et al. MicroRNAs in the human heart: a clue to fetal gene reprogramming in heart failure. *Circulation* (2007) 116:258–67. doi: 10.1161/circulationaha.107.687947
56. Teng X, Chen L, Chen W, Yang J, Yang Z, Shen Z. Mesenchymal Stem Cell-Derived Exosomes Improve the Microenvironment of Infarcted Myocardium Contributing to Angiogenesis and Anti-Inflammation. *Cell Physiol Biochem* (2015) 37:2415–24. doi: 10.1159/000438594
57. Zhang Y, Chopp M, Liu XS, Katakowski M, Wang X, Tian X, et al. Exosomes Derived from Mesenchymal Stromal Cells Promote Axonal Growth of Cortical Neurons. *Mol Neurobiol* (2017) 54:2659–73. doi: 10.1007/s12035-016-9851-0
58. van Rooij E, Liu N, Olson EN. MicroRNAs flex their muscles. *Trends Genet* (2008) 24:159–66. doi: 10.1016/j.tig.2008.01.007
59. Schotten U, Ausma J, Stellbrink C, Sabatschus I, Vogel M, Frechen D, et al. Cellular mechanisms of depressed atrial contractility in patients with chronic atrial fibrillation. *Circulation* (2001) 103:691–8. doi: 10.1161/01.CIR.103.5.691
60. Sahoo S, Klychko E, Thorne T, Misener S, Schultz KM, Millay M, et al. Exosomes from human CD34(+) stem cells mediate their proangiogenic paracrine activity. *Circ Res* (2011) 109:724–8. doi: 10.1161/circresaha.111.253286
61. Tian C, Gao L, Zimmerman MC, Zucker IH. Myocardial infarction-induced microRNA-enriched exosomes contribute to cardiac Nrf2 dysregulation in

chronic heart failure. *Am J Physiol Heart Circ Physiol* (2018) 314:H928–h939. doi: 10.1152/ajpheart.00602.2017
62. Wang X, Chen Y, Zhao Z, Meng Q, Yu Y, Sun J, et al. Engineered Exosomes With Ischemic Myocardium-Targeting Peptide for Targeted Therapy in Myocardial Infarction. *J Am Heart Assoc* (2018) 7:e008737. doi: 10.1161/jaha.118.008737
63. Mott JL, Kobayashi S, Bronk SF, Gores GJ. mir-29 regulates Mcl-1 protein expression and apoptosis. *Oncogene* (2007) 26(42):6133–40. doi: 10.1038/sj.onc.1210436
64. Turchinovich A, Weiz L, Langheinz A, Burwinkel B. Characterization of extracellular circulating microRNA. *Nucleic Acids Res* (2011) 39:7223–33. doi: 10.1093/nar/gkr254
65. Borchert GM, Lanier W, Davidson BL. RNA polymerase III transcribes human microRNAs. *Nat Struct Mol Biol* (2006) 13(12):1097–101. doi: 10.1038/nsmb1167
66. Lee Y, Kim M, Han J, Yeom KH, Lee S, Baek SH, et al. MicroRNA genes are transcribed by RNA polymerase II. *EMBO J* (2004) 23(20):4051–60. doi: 10.1038/sj.emboj.7600385
67. Macfarlane LA, Murphy PR. MicroRNA: Biogenesis, Function and Role in Cancer. *Curr Genomics* (2010) 11:537–61. doi: 10.2174/138920210793175895
68. Ebert MS, Sharp PA. Roles for microRNAs in conferring robustness to biological processes. *Cell* (2012) 149(3):515–24. doi: 10.1016/j.cell.2012.04.005
69. Griffiths-Jones S, Saini HK, van Dongen S, Enright AJ. miRBase: tools for microRNA genomics. *Nucleic Acids Res* (2008) 36(Database issue):D154–8. doi: 10.1093/nar/gkm952
70. Calin GA, Dumitru CD, Shimizu M, Bichi R, Zupo S, Noch E, et al. Frequent deletions and down-regulation of micro- RNA genes miR15 and miR16 at 13q14 in chronic lymphocytic leukemia. *Proc Natl Acad Sci U S A* (2002) 99 (24):15524–9. doi: 10.1073/pnas.242606799
71. Cimmino A, Calin GA, Fabbri M, Iorio M, Ferracin M, Shimizu M, et al. miR-15 and miR-16 induce apoptosis by targeting BCL2. *Proc Natl Acad Sci U S A* (2005) 102(39):13944–9. doi: 10.1073/pnas.0506654102
72. Calin GA, Cimmino A, Fabbri M, Ferracin M, Wojcik SE, Shimizu M, et al. MiR-15a and miR-16-1 cluster functions in human leukemia. *Proc Natl Acad Sci U S A* (2008) 105(13):5166–71. doi: 10.1073/pnas.0800121105
73. Wang X, Tang S, Le SY, Lu R, Rader J, Meyers C, et al. Aberrant expression of oncogenic and tumor-suppressive microRNAs in cervical cancer is required for cancer cell growth. *PLoS One* (2008) 3(7):e2557. doi: 10.1371/journal.pone.0002557
74. Boren T, Xiong Y, Hakam A, Wenham R, Apte S, Wei Z, et al. MicroRNAs and their target messenger RNAs associated with endometrial carcinogenesis. *Gynecol Oncol* (2008) 110(2):206–15. doi: 10.1016/j.ygyno.2008.03.023
75. Wu W, Lin Z, Zhuang Z, Liang X. Expression profile of mammalian microRNAs in endometrioid adenocarcinoma. *Eur J Cancer Prev* (2009) 18:50–5. doi: 10.1097/CEJ.0b013e328305a07a
76. Zhang T, Jiang K, Zhu X, Zhao G, Wu H, Deng G, et al. miR-433 inhibits breast cancer cell growth via the MAPK signaling pathway by targeting Rap1a. *Int J Biol Sci* (2018) 14:622–32. doi: 10.7150/ijbs.24223
77. Long X, Shi Y, Ye P, Guo J, Zhou Q, Tang Y. MicroRNA-99a Suppresses Breast Cancer Progression by Targeting FGFR3. *Front Oncol* (2020) 9:1473. doi: 10.3389/fonc.2019.01473
78. Lao G, Liu P, Wu Q, Zhang W, Liu Y, Yang L, et al. Mir-155 promotes cervical cancer cell proliferation through suppression of its target gene LKB1. *Tumor Biol* (2014) 35:11933–8. doi: 10.1007/s13277-014-2479-7
79. Buscaglia LEB, Li Y. Apoptosis and the target genes of microRNA-21. *Chin J Cancer* (2011) 30:371–80. doi: 10.5732/cjc.011.10132
80. Chen Y, Zhang L. Members of the microRNA-200 family are promising therapeutic targets in cancer. *Exp Ther Med* (2017) 14:10–7. doi: 10.3892/etm.2017.4488
81. Chirshev E, Oberg KC, Ioffe YJ, Unternaehrer JJ. Let-7 as biomarker, prognostic indicator, and therapy for precision medicine in cancer. *Clin Transl Med* (2019) 8:24–4. doi: 10.1186/s40169-019-0240-y
82. Otsuka K, Yamamoto Y, Ochiya T. Regulatory role of resveratrol, a microRNA-controlling compound, in HNRNPA1 expression, which is associated with poor prognosis in breast cancer. *Oncotarget* (2018) 9:24718–30. doi: 10.18632/oncotarget.25339
83. Mansoori B, Mohammadi A, Ghasabi M, Shirjang S, Dehghan R, Montazeri V, et al. miR-142-3p as tumor suppressor miRNA in the regulation of tumorigenicity, invasion and migration of human breast cancer by targeting Bach-1 expression. *J Cell Physiol* (2019) 234:9816–25. doi: 10.1002/jcp.27670
84. Karaayvaz M, Zhang C, Liang S, Shroyer KR, Ju J. Prognostic significance of miR-205 in endometrial cancer. *PLoS One* (2012) 7:e35158–8. doi: 10.1371/journal.pone.0035158
85. Yang S, Zhao Y, Wang L, Liu C, Lu Y, Fang Z, et al. MicroRNA−4712−5p promotes proliferation of the vulvar squamous cell carcinoma cell line A431 by targeting PTEN through the AKT/cyclin D1 signaling pathways. *Oncol Rep* (2019) 42:1689–98. doi: 10.3892/or.2019.7320
86. Yang X-H, Guo F. miR−3147 serves as an oncomiR in vulvar squamous cell cancer via Smad4 suppression. *Mol Med Rep* (2018) 17:6397–404. doi: 10.3892/mmr.2018.8697
87. Gao W, Hua J, Jia Z, Ding J, Han Z, Dong Y, et al. Expression of miR-146a-5p in breast cancer and its role in proliferation of breast cancer cells. *Oncol Lett* (2018) 15:9884–8. doi: 10.3892/ol.2018.8589
88. Balta N, Dumitru IF, Stoian G, Petec G, Dinischiotu A. Influence of isoproterenol-induced cardiac hypertrophy on oxydative myocardial stress. *Romanian J Physiol Physiol Sci* (1995) 32:149–54.
89. Dubin R, Li Y, H Ix J, G Shlipak M, Whooley M, Peralta C. Associations of Pentraxin-3 with Cardiovascular Events, Incident Heart Failure and Mortality Among Persons with Coronary Heart Disease: Data from the Heart and Soul Study. *Am Heart J* (2012) 163:274–9. doi: 10.1016/j.ahj.2011.11.007
90. Ailawadi S, Wang X, Gu H, Fan GC. Pathologic function and therapeutic potential of exosomes in cardiovascular disease. *Biochim Biophys Acta* (2015) 1852:1–11. doi: 10.1016/j.bbadis.2014.10.008
91. Tili E, Michaille JJ. Resveratrol, MicroRNAs, Inflammation, and Cancer. *J Nucleic Acids* (2011) 2011:102431. doi: 10.4061/2011/102431
92. Predescu DV, Cretoiu SM, Cretoiu D, Pavelescu LA, Suciu N, Radu BM, et al. Protein-Coupled Receptors (GPCRs)-Mediated Calcium Signaling in Ovarian Cancer: Focus on GPCRs activated by Neurotransmitters and Inflammation-Associated Molecules. *Int J Mol Sci* (2019) 20(22):5568. doi: 10.3390/ijms20225568
93. Agouni A, Lagrue-Lak-Hal AH, Ducluzeau PH, Mostefai HA, Draunet-Busson C, Leftheriotis G, et al. Endothelial dysfunction caused by circulating microparticles from patients with metabolic syndrome. *Am J Pathol* (2008) 173:1210–9. doi: 10.2353/ajpath.2008.080228
94. Admyre C, Johansson SM, Qazi KR, Filen JJ, Lahesmaa R, Norman M, et al. Exosomes with immune modulatory features are present in human breast milk. *J Immunol* (2007) 179:1969–78. doi: 10.4049/jimmunol.179.3.1969
95. Bang C, Batkai S, Dangwal S, Gupta SK, Foinquinos A, Holzmann A, et al. Cardiac fibroblast-derived microRNA passenger strand-enriched exosomes mediate cardiomyocyte hypertrophy. *J Clin Invest* (2014) 124:2136–46. doi: 10.1172/jci70577
96. Hu SL, Chang AC, Huang CC, Tsai CH, Lin CC, Tang CH. Myostatin promotes interleukin-1β expression in rheumatoid arthritis synovial fibroblasts through inhibition of miR-21-5. *Front Immunol* (2017) 8:1747. doi: 10.3389/fimmu.2017.01747
97. Peng Y, Daia Y, Hitchcockb C, Yangc X, Kassisd E, Luoa Z, et al. Insulin growth factor signaling is regulated by microRNA-486, an underexpressed microRNA in lung cancer. *Proc Natl Acad Sci U S A* (2013) 110(37):15043–8. doi: 10.1073/pnas.1307107110
98. Lima RT, Busacca S, Almeida G, Gaudino G, Fennell D, Vasconcelor MH, et al. MicroRNA regulation of core apoptosis pathways in cancer. *Eur J Cancer* (2011) 47(2):163–74. doi: 10.1016/j.ejca.2010.11.005
99. Zhang L, Zhan X, Yan D, Wang Z. Circulating MicroRNA-21 is involved in lymph node metastasis in cervical cancer by targeting RASA1. *J Gynecol Cancer* (2016) 26:810–6. doi: 10.1097/IGC.0000000000000694
100. Tidyan WE, Rauen KA. he RASopathies: Developmental Syndromes of Ras/MAPK pathways dysregulation. *Curr Opin Genet Dev* (2009) 19:230–6. doi: 10.1016/j.gde.2009.04.001
101. Balaj L, Lessard R, Dai L, Cho YJ, Pomeroy SL, Breakefield XO, et al. Tumour microvesicles contain retrotransposon elements and amplified oncogene sequences. *Nat Commun* (2011) 2:180. doi: 10.1038/ncomms1180

102. Barbu MG, Condrat CE, Thompson DC, Bugnar OL, Cretoiu D, Toader OD, et al. MicroRNA Involvement in Signaling Pathways During Viral Infection. *Front Cell Dev Biol* (2020) 8:143. doi: 10.3389/fcell.2020.00143
103. Azevedo LC, Janiszewski M, Pontieri V, Pedro Mde A, Bassi E, Tucci PJ, et al. Platelet-derived exosomes from septic shock patients induce myocardial dysfunction. *Crit Care (Lond Engl)* (2007) 11:R120. doi: 10.1186/cc6176
104. Holwerda SJB, de Laat W. CTCF: the protein, the binding partners, the binding sites and their chromatin loops. *Philos Trans R Soc London Ser B Biol Sci* (2013) 368:20120369. doi: 10.1098/rstb.2012.0369
105. Kim S, Yu N-K, Kaang B-K. CTCF as a multifunctional protein in genome regulation and gene expression. *Exp Mol Med* (2015) 47:e166–6. doi: 10.1038/emm.2015.33
106. Oh S, Oh C, Yoo KH. Functional roles of CTCF in breast cancer. *BMB Rep* (2017) 50:445–53. doi: 10.5483/bmbrep.2017.50.9.108
107. Ramani V, Shendure J, Duan Z. Understanding Spatial Genome Organization: Methods and Insights. *Genomics Proteomics Bioinf* (2016) 14:7–20. doi: 10.1016/j.gpb.2016.01.002
108. Saito Y, Saito H. Role of CTCF in the regulation of microRNA expression. *Front Genet* (2012) 3:186. doi: 10.3389/fgene.2012.00186
109. Soto-Reyes E, González-Barrios R, Cisneros-Soberanis F, Herrera-Goepfert R, Pérez V, Cantú D, et al. Disruption of CTCF at the miR-125b1 locus in gynecological cancers. *BMC Cancer* (2012) 12:40. doi: 10.1186/1471-2407-12-40
110. de Souza Rocha Simonini P, Breiling A, Gupta N, Malekpour M, Youns M, Omranipour R, et al. Epigenetically deregulated microRNA-375 is involved in a positive feedback loop with estrogen receptor alpha in breast cancer cells. *Cancer Res* (2010) 70:9175–84. doi: 10.1158/0008-5472.can-10-1318
111. Jiang F, Liu T, He Y, Yan Q, Chen X, Wang H, et al. MiR-125b promotes proliferation and migration of type II endometrial carcinoma cells through targeting TP53INP1 tumor suppressor in vitro and in vivo. *BMC Cancer* (2011) 11:425. doi: 10.1186/1471-2407-11-425
112. Apostolou P, Fostira F. Hereditary breast cancer: the era of new susceptibility genes. *BioMed Res Int* (2013) 2013:747318–8. doi: 10.1155/2013/747318
113. Yoshida K, Miki Y. Role of BRCA1 and BRCA2 as regulators of DNA repair, transcription, and cell cycle in response to DNA damage. *Cancer Sci* (2004) 95:866–71. doi: 10.1111/j.1349-7006.2004.tb02195.x
114. Rebbeck TR, Mitra N, Wan F, Sinilnikova OM, Healey S, McGuffog L, et al. Association of type and location of BRCA1 and BRCA2 mutations with risk of breast and ovarian cancer. *JAMA* (2015) 313:1347–61. doi: 10.1001/jama.2014.5985
115. Petrucelli N, Daly MB, Pal T. BRCA1- and BRCA2-Associated Hereditary Breast and Ovarian Cancer. In: MP Adam, HH Ardinger, RA Pagon, SE Wallace, LJH Bean, K Stephens and A Amemiya, editors. *GeneReviews(®)*. Seattle: University of Washington (1993). Copyright © 1993-2020, University of Washington, Seattle. GeneReviews is a registered trademark of the University of Washington, Seattle. All rights reserved.: Seattle (WA).
116. Kuchenbaecker KB, Hopper JL, Barnes DR, Phillips KA, Mooij TM, Roos-Blom MJ, et al. Risks of Breast, Ovarian, and Contralateral Breast Cancer for BRCA1 and BRCA2 Mutation Carriers. *JAMA* (2017) 317:2402–16. doi: 10.1001/jama.2017.7112
117. Kotsopoulos J. BRCA Mutations and Breast Cancer Prevention. *Cancers* (2018) 10:524. doi: 10.3390/cancers10120524
118. Claes K, Poppe B, Machackova E, Coene I, Foretova L, De Paepe A, et al. Differentiating pathogenic mutations from polymorphic alterations in the splice sites of BRCA1 and BRCA2. *Genes Chromosomes Cancer* (2003) 37:314–20. doi: 10.1002/gcc.10221
119. Chenevix-Trench G, Healey S, Lakhani S, Waring P, Cummings M, Brinkworth R, et al. Genetic and histopathologic evaluation of BRCA1 and BRCA2 DNA sequence variants of unknown clinical significance. *Cancer Res* (2006) 66:2019–27. doi: 10.1158/0008-5472.can-05-3546
120. Goldgar DE, Easton DF, Deffenbaugh AM, Monteiro AN, Tavtigian SV, Couch FJ. Integrated evaluation of DNA sequence variants of unknown clinical significance: application to BRCA1 and BRCA2. *Am J Hum Genet* (2004) 75:535–44. doi: 10.1086/424388
121. Moradi Marjaneh M, Beesley J, O'Mara TA, Mukhopadhyay P, Koufariotis LT, Kazakoff S, et al. Non-coding RNAs underlie genetic predisposition to breast cancer. *Genome Biol* (2020) 21(1):7. doi: 10.1186/s13059-019-1876-z
122. Bertoli G, Cava C, Castiglioni I. MicroRNAs: New Biomarkers for Diagnosis, Prognosis, Therapy Prediction and Therapeutic Tools for Breast Cancer. *Theranostics* (2015) 5(10):1122–43. doi: 10.7150/thno.11543
123. Tang J, Ahmad A, Sarkar FH. The role of microRNAs in breast cancer migration, invasion and metastasis. *Int J Mol Sci* (2012) 13(10):13414–37. doi: 10.3390/ijms131013414
124. Murphy CG, Moynahan ME. BRCA gene structure and function in tumor suppression: a repair-centric perspective. *Cancer J* (2010) 16(1):39–47. doi: 10.1097/PPO.0b013e3181cf0204
125. Shaver TM, et al. Diverse, Biologically Relevant, and Targetable Gene Rearrangements in Triple-Negative Breast Cancer and Other Malignancies. *Cancer Res* (2016) 76(16):4850–60. doi: 10.1158/0008-5472.CAN-16-0058
126. Chang S, Sharan SK. Epigenetic control of an oncogenic microRNA, miR-155, by BRCA1. *Oncotarget* (2012) 3:5–6. doi: 10.18632/oncotarget.433
127. Garcia AI, Buisson M, Bertrand P, Rimokh R, Rouleau E, Lopez BS, et al. Down-regulation of BRCA1 expression by miR-146a and miR-146b-5p in triple negative sporadic breast cancers. *EMBO Mol Med* (2011) 3:279–90. doi: 10.1002/emmm.201100136
128. Tanic M, et al. Integration of BRCA1-mediated miRNA and mRNA profiles reveals microRNA regulation of TRAF2 and NFkappaB pathway. *Breast Cancer Res Treat* (2012) 134(1):41–51. doi: 10.1007/s10549-011-1905-4
129. Tili E, Croce CM, Michaille JJ. miR-155: on the crosstalk between inflammation and cancer. *Int Rev Immunol* (2009) 28:264–84. doi: 10.1080/08830180903093796
130. Lehmann U. Aberrant DNA methylation of microRNA genes in human breast cancer - a critical appraisal. *Cell Tissue Res* (2014) 356(3):657–64. doi: 10.1007/s00441-014-1793-0
131. Chang S, Wang RH, Akagi K, Kim KA, Martin B, Cavallone L, et al. Tumor suppressor BRCA1 epigenetically controls oncogenic microRNA-155. *Nat Med* (2011) 17(10):1275–82. doi: 10.1038/nm.2459
132. Shukla V, Coumoul X, Lahusen T, Wang RH, Xu X, Vassilopoulos A, et al. BRCA1 affects global DNA methylation through regulation of DNMT1. *Cell Res* (2010) 20(11):1201–15. doi: 10.1038/cr.2010.128
133. Kim S, Jin H, Seo H-R, Lee HJ, Lee Y-S. Regulating BRCA1 protein stability by cathepsin S-mediated ubiquitin degradation. *Cell Death Differ* (2019) 26:812–25. doi: 10.1038/s41418-018-0153-0
134. Wu W, Sato K, Koike A, Nishikawa H, Koizumi H, Venkitaraman AR, et al. HERC2 is an E3 ligase that targets BRCA1 for degradation. *Cancer Res* (2010) 70:6384–92. doi: 10.1158/0008-5472.Can-10-1304
135. Lu Y, Li J, Cheng D, Parameswaran B, Zhang S, Jiang Z, et al. The F-box protein FBXO44 mediates BRCA1 ubiquitination and degradation. *J Biol Chem* (2012) 287:41014–22. doi: 10.1074/jbc.M112.407106
136. Gorodetska I, Kozeretska I, Dubrovska A. BRCA Genes: The Role in Genome Stability, Cancer Stemness and Therapy Resistance. *J Cancer* (2019) 10:2109–27. doi: 10.7150/jca.30410
137. Ouchi T, Monteiro AN, August A, Aaronson SA, Hanafusa H. BRCA1 regulates p53-dependent gene expression. *Proc Natl Acad Sci U S A* (1998) 95:2302–6. doi: 10.1073/pnas.95.5.2302
138. Gorrini C, Baniasadi PS, Harris IS, Silvester J, Inoue S, Snow B, et al. BRCA1 interacts with Nrf2 to regulate antioxidant signaling and cell survival. *J Exp Med* (2013) 210:1529–44. doi: 10.1084/jem.20121337
139. Gorrini C, Gang BP, Bassi C, Wakeham A, Baniasadi SP, Hao Z, et al. Estrogen controls the survival of BRCA1-deficient cells via a PI3K-NRF2-regulated pathway. *Proc Natl Acad Sci U S A* (2014) 111:4472–7. doi: 10.1073/pnas.1324136111
140. Lee EY, Abbondante S. Tissue-specific tumor suppression by BRCA1. *Proc Natl Acad Sci U S A* (2014) 111:4353–4. doi: 10.1073/pnas.1403033111
141. Hosey AM, Gorski JJ, Murray MM, Quinn JE, Chung WY, Stewart GE, et al. Molecular basis for estrogen receptor alpha deficiency in BRCA1-linked breast cancer. *J Natl Cancer Inst* (2007) 99:1683–94. doi: 10.1093/jnci/djm207
142. Ma Y, Katiyar P, Jones LP, Fan S, Zhang Y, Furth PA, et al. The breast cancer susceptibility gene BRCA1 regulates progesterone receptor signaling in mammary epithelial cells. *Mol Endocrinol* (2006) 20:14–34. doi: 10.1210/me.2004-0488
143. Wang S, Li Y, Hsu PH, Lee SY, Kim Y, Lee EY. Progesterone receptor A stability is mediated by glycogen synthase kinase-3beta in the Brca1-deficient

mammary gland. *J Biol Chem* (2013) 288:26265–74. doi: 10.1074/jbc.M113.476556
144. Fan S, Ma YX, Wang C, Yuan RQ, Meng Q, Wang JA, et al. Role of direct interaction in BRCA1 inhibition of estrogen receptor activity. *Oncogene* (2001) 20:77–87. doi: 10.1038/sj.onc.1204073
145. Zheng L, Annab LA, Afshari CA, Lee WH, Boyer TG. BRCA1 mediates ligand-independent transcriptional repression of the estrogen receptor. *Proc Natl Acad Sci U S A* (2001) 98:9587–92. doi: 10.1073/pnas.171174298
146. Zhu M, Wang M, Yang F, Tian Y, Cai J, Yang H, et al. ir-155-5p inhibition promotes the transition of bone marrow mesenchymal stem cells to gastric cancer tissue derived MSC-like cells via NF-kappaB p65 activation. *Oncotarget* (2016). 7:16567–80. doi: 10.18632/oncotarget.7767
147. Wang Y, Zeng G, Jiang Y. The Emerging Roles of miR-125b in Cancers. *Cancer Manag Res* (2020) 12:1079–88. doi: 10.2147/CMAR.S232388
148. Zhang B, Zhao R, He Y, Fu X, Fu L, Zhu Z, et al. MicroRNA 100 sensitizes luminal A breast cancer cells to paclitaxel treatment in part by targeting mTOR. *Oncotarget* (2016) 7:5702–14. doi: 10.18632/oncotarget.6790
149. Liang Y, Wu H, Lei R, Chong R, Wei Y, Lu X, et al. Transcriptional network analysis identifies BACH1 as a master regulator of breast cancer bone metastasis. *J Biol Chem* (2012) M112:392332.jbc. doi: 10.1074/jbc.M112.392332
150. Davudian S, Mansoori B, Shajari N, Mohammadi A, Baradaran B. BACH1, the masterregulator gene: A novel candidate target for cancer therapy. *Gene* (2016) 588(1):30–7. doi: 10.1016/j.gene.2016.04.040
151. van der Pol E, Hoekstra AG, Sturk A, Otto C, van Leeuwen TG, Nieuwland R. Optical and non-optical methods for detection and characterization of microparticles and exosomes. *J Thromb Haemost* (2010) 8:2596–607. doi: 10.1111/j.1538-7836.2010.04074.x
152. Xin H, Li Y, Cui Y, Yang JJ, Zhang ZG, Chopp M. Systemic administration of exosomes released from mesenchymal stromal cells promote functional recovery and neurovascular plasticity after stroke in rats. *J Cereb Blood Flow Metab* (2013) 33:1711–5. doi: 10.1038/jcbfm.2013.152
153. Zhong Z, Hou J, Zhang Q, Zhong W, Li B, Li C, et al. Circulating microRNA expression profiling and bioinformatics analysis of dysregulated microRNAs of patients with coronary artery disease. *Medicine* (2018) 97:e11428. doi: 10.1097/md.0000000000011428
154. Xu B, Zhang Y, Du XF, Li J, Zi HX, Bu JW, et al. Neurons secrete miR-132-containing exosomes to regulate brain vascular integrity. *Cell Res* (2017) 27:882–97. doi: 10.1038/cr.2017.62
155. Zhang Y, Chopp M, Zhang ZG, Katakowski M, Xin H, Qu C, et al. Systemic administration of cell-free exosomes generated by human bone marrow derived mesenchymal stem cells cultured under 2D and 3D conditions improves functional recovery in rats after traumatic brain injury. *Neurochem Int* (2017) 111:69–81. doi: 10.1016/j.neuint.2016.08.003
156. Tian Y, Liu Y, Wang T, Zhou N, Kong J, Chen L, et al. A microRNA-Hippo pathway that promotes cardiomyocyte proliferation and cardiac regeneration in mice. *Sci Trans Med* (2015) 7:279ra238. doi: 10.1126/scitranslmed.3010841
157. Schubert S, Weyrich AS, Rowley JW. A tour through the transcriptional landscape of platelets. *Bloods* (2014) 124:493–502. doi: 10.1182/blood-2014-04-512756
158. Zhang Y, Chopp M, Meng Y, Katakowski M, Xin H, Mahmood A, et al. Effect of exosomes derived from multipluripotent mesenchymal stromal cells on functional recovery and neurovascular plasticity in rats after traumatic brain injury. *J Neurosurg* (2015) 122:856–67. doi: 10.3171/2014.11.Jns14770
159. Wubbolts R, Leckie RS, Veenhuizen PT, Schwarzmann G, Mobius W, Hoernschemeyer J, et al. Proteomic and biochemical analyses of human B cell-derived exosomes. Potential implications for their function and multivesicular body formation. *J Biol Chem* (2003) 278:10963–72. doi: 10.1074/jbc.M207550200
160. Sygitowicz G, Tomaniak M, Blaszczyk O, Koltowski L, Filipiak KJ, Sitkiewicz D. Circulating microribonucleic acids miR-1, miR-21 and miR-208a in patients with symptomatic heart failure: Preliminary results. *Arch Cardiovasc Dis* (2015) 108:634–42. doi: 10.1016/j.acvd.2015.07.003
161. Yeo RW, Lai RC, Zhang B, Tan SS, Yin Y, Teh BJ, et al. Mesenchymal stem cell: an efficient mass producer of exosomes for drug delivery. *Advanced Drug Deliv Rev* (2013) 65:336–41. doi: 10.1016/j.addr.2012.07.001
162. Yellon DM, Davidson SM. Exosomes: nanoparticles involved in cardioprotection? *Circ Res* (2014) 114:325–32. doi: 10.1161/circresaha.113.300636
163. Wang X, Gu H, Huang W, Peng J, Li Y, Yang L, et al. Hsp20-Mediated Activation of Exosome Biogenesis in Cardiomyocytes Improves Cardiac Function and Angiogenesis in Diabetic Mice. *Diabetes* (2016) 65:3111–28. doi: 10.2337/db15-1563
164. Krishnan P, Ghosh S, Wang B, Heyns M, Graham K, Mackey JR, et al. Profiling of Small Nucleolar RNAs by Next Generation Sequencing: Potential New Players for Breast Cancer Prognosis. *PLoS One* (2016) 11:e0162622–e0162622. doi: 10.1371/journal.pone.0162622
165. Bastide A, David A. The ribosome, (slow) beating heart of cancer (stem) cell. *Oncogenesis* (2018) 7(4):34. doi: 10.1038/s41389-018-0044-8
166. Patterson DG, Roberts JT, King VM, Houserova D, Barnhill EC, Crucello A, et al. Human snoRNA-93 is processed into a microRNA-like RNA that promotes breast cancer cell invasion. *NPJ Breast Cancer* (2017) 3:25. doi: 10.1038/s41523-017-0032-8
167. Wu X, Pan Y, Fang Y, Zhang J, Xie M, Yang F, et al. The Biogenesis and Functions of piRNAs in Human Diseases. *Mol Ther Nucleic Acids* (2020) 21:108–20. doi: 10.1016/j.omtn.2020.05.023
168. Fancello L, Kampen KR, Hofman IJF, Verbeeck J, De Keersmaecker K. The ribosomal protein gene RPL5 is a haploinsufficient tumor suppressor in multiple cancer types. *Oncotarget* (2017) 8:14462–78. doi: 10.18632/oncotarget.14895
169. American Cancer Society. *Cancer facts & figures* . Available at: https://www.cancer.org/con-tent/dam/cancer-org/research/cancer-facts-and-statistics/annual-cancer-facts-and-figures/2018/cancer-facts-and-figures-2018.pdf (Accessed June 10, 2018).
170. Xiong X, Zhang J, Hua X, Cao W, Qin S, Dai L, et al. FBP1 promotes ovarian cancer development through the acceleration of cell cycle transition and metastasis. *Oncol Lett* (2018) 16:1682–8. doi: 10.3892/ol.2018.8872
171. Lengyel E. Ovarian cancer development and metastasis. *Am J Pathol* (2010) 177:1053–64. doi: 10.2353/ajpath.2010.100105
172. Januchowski R, Zawierucha P, Rucinski M, Zabel M. Microarray-based detection and expression analysis of extracellular matrix proteins in drugresistant ovarian cancer cell lines. *Oncol Rep* (2014) 32:1981–90. doi: 10.3892/or.2014.3468
173. Meng X, Zhao Y, Wang J, Gao Z, Geng Q, Liu X. Regulatory roles of miRNA-758 and matrix extracellular phosphoglycoprotein in cervical cancer. *Exp Ther Med* (2017) 14:2789–94. doi: 10.3892/etm.2017.4887
174. Luo Z, Wang Q, Lau WB, Lau B, Xu L, Zhao L, et al. Tumor microenvironment: The culprit for ovarian cancer metastasis? *Cancer Lett* (2016) 377:174–82. doi: 10.1016/j.canlet.2016.04.038
175. Song N, Liu H, Ma X, Zhang S. Placental growth factor promotes metastases of ovarian cancer through MiR-543-regulated MMP7. *Cell Physiol Biochem* (2015) 37:1104–12. doi: 10.1159/000430235
176. Korpal M, Kang Y. The emerging role of miR-200 family of microRNAs in epithelial-mesenchymal transition and cancer metastasis. *RNA Biol* (2008) 5:115–9. doi: 10.4161/rna.5.3.6558
177. Bendoraite A, Knouf EC, Garg KS, Parkin RK, Kroh EM. O'Briant, K.C. et al. Regulation of miR-200 family microRNAs and ZEB transcription factors in ovarian cancer: Evidence supporting a mesothelial-to-epithelial transition. *Gynecol Oncol* (2010) 116:117–25. doi: 10.1016/j.ygyno.2009.08.009
178. Chen S-N, Chang R, Lin L-T, Chern C-U, Tsai H-W, Wen Z-H, et al. MicroRNA in Ovarian Cancer: Biology, Pathogenesis, and Therapeutic Opportunities. *Int J Environ Res Public Health* (2019) 16:1510. doi: 10.3390/ijerph16091510
179. Jeanes A, Gottardi CJ, Yap AS. Cadherins and cancer: how does cadherin dysfunction promote tumor progression? *Oncogene* (2008) 27:6920–9. doi: 10.1038/onc.2008.343
180. Braga EA, Fridman MV, Kushlinskii NE. Molecular Mechanisms of Ovarian Carcinoma Metastasis: Key Genes and Regulatory MicroRNAs. *Biochemistry* (2017) 82:529–41. doi: 10.1134/S0006297917050017
181. Pecot CV, Rupaimoole R, Yang D, Akbani R, Ivan C, Lu C, et al. Tumour angiogenesis regulation by the miR-200 family. *Nat Commun* (2013) 4:2427. doi: 10.1038/ncomms3427
182. Shotan A, Widerhorn J, Hurst A, Elkayam U. Risks of angiotensin-converting enzyme inhibition during pregnancy: experimental and clinical

evidence, potential mechanisms, and recommendations for use. *Am J Med* (1994) 96:451–6. doi: 10.1016/0002-9343(94)90172-4
183. Song YH, Shao L, Zhang Y, Zhou J, Liu B, Pan X, et al. Exosomes Derived from Embryonic Stem Cells as Potential Treatment for Cardiovascular Diseases. *Adv Exp Med Biol* (2017) 998:187–206. doi: 10.1007/978-981-10-4397-0_13
184. Srikanthan S, Li W, Silverstein RL, McIntyre TM. Exosome poly-ubiquitin inhibits platelet activation, downregulates CD36 and inhibits pro-atherothombotic cellular functions. *J Thromb Haemost* (2014) 12:1906–17. doi: 10.1111/jth.12712
185. Xiao M, Cai J, Cai L, Jia J, Xie L, Zhu Y, et al. Let-7e sensitizes epithelial ovarian cancer to cisplatin through repressing DNA double strand break repair. *J Ovarian Res* (2017) 10(1):24. doi: 10.1186/s13048-017-0321-8
186. Dai S, Lu Y, Long Y, Lai Y, Du P, Ding N, et al. Prognostic value of microRNAs in cervical carcinoma: A systematic review and meta-analysis. *Oncotarget* (2016) 7:35369–78. doi: 10.18632/oncotarget.9294
187. Hu X, Schwarz JK, Lewis JSJr, Huettner PC, Rader JS, Deasy JO, et al. A microRNA expression signature for cervical cancer prognosis. *Cancer Res* (2010) 70:1441–8. doi: 10.1158/0008-5472.CAN-09-3289
188. Kerscher EA, Slack FJ. Oncomirs- microRNAs with a role in cancer. *Nat Rev Cancer* (2006) 6:259–69. doi: 10.1038/nrc1840
189. Sun S, Wang X, Xu X, Di H, Du J, Xu B, et al. Mir-433-3p suppresses cell growth and enhances chemosensitivity by targeting CREB in human glioma. *Oncotarget* (2017) 8:5057–68. doi: 10.18632/oncotarget.13789
190. Liang T, Guo Q, Li L, Cheng Y, Ren C, Zhang G. MicroRNA -433 inhibits migration and invasion of ovarian cancer cells via targeting Notch1. *Neoplasma* (2016) 63:696–704. doi: 10.4149/neo_2016_506
191. Changyan L, Jie D, Yuebo Y, Liuzhi D, Xiaomao Li. MicroRNA-433 inhibits cervical cancer progression by directly targeting methaderin to regulate the AKT and β-catenin signaling pathways. *Oncol Rep* (2017) 38(6):3693–49. doi: 10.3892/or.2017.6049
192. Liang C, Ding J, Yang Y, Deng L, Li X. MicroRNA-433 inhibits cervical cancer progression by directly targeting metadherin to regulate the AKT and β-catenin signalling pathways. *Oncol Rep* (2017) 38:3639–49. doi: 10.3892/or.2017.6049
193. Li WF, Dai H, Ou Q, Zuo GQ, Liu CA. Overexpression of microRNA-30-1-5p inhibits liver cancer cell proliferation and induces apoptosis by targeting MTDH/PTEN/AKT pathway. *Tumor Biol* (2016) 37:5885–95. doi: 10.1007/s13277-015-4456-1
194. Shen X, Si Y, Yag Z, Wang Q, Yuan J, Zhang X. MicroRNA 542-3p suppressed cell growth of gastric cancer cells via targeting oncogene astrocyte-elevated gene-1. *Med Oncol* (2015) 32:361. doi: 10.1007/s12032-014-0361-5
195. Feng Y-H, Tsao C-J. Emerging role of microRNA-21 in cancer. *BioMed Rep* (2016) 5:395–402. doi: 10.3892/br.2016.747
196. Wen Q, Liu Y, Lyu H, Xu X, Wu Q, Liu N, et al. Long noncoding RNA GAS5, which acts as a tumor suppressor via micriRNA 21, regulates cisplatin resistance expression in cervical cancer. *Int J Gynecol Cancer* (2017) 27:1096–108. doi: 10.1097/IGC.0000000000001028
197. Xu L, Xu Q, Li X, Zhang X. MicroRNA-21 regulates the proliferation and apoptosis of cervical cancer cells via tumor necrosis factor-α. *Mol Med Rep* (2017) 16:4659–63. doi: 10.3892/mmr.2017.7143
198. Micheau O, Tschopp J. Induction of TNF receptor I mediated apoptosis via two sequential signaling complexes. *Cless* (2003) 114:181–90. doi: 10.1016/S0092-8674(03)00521-X
199. Song L, Liu S, Zhang L, Yao H, Gao F, Xu D, et al. MiR-21 modulates radiosensitivity of cervical cancer through inhibiting autophagy via the PTEN/Akt/HIF-1α feedback loop and the Akt-mTOR signaling pathway. *Tumour Biol J Int Soc Oncodevelopmental Biol Med* (2016) 37:12161–8. doi: 10.1007/s13277-016-5073-3
200. Chen B, Chen X, Wu X, Wang X, Wang Y, Lin TY, et al. Disruption of microRNA-21 by TALEN leads to diminished cell transformation and increased expression of cell-environment interaction genes. *Cancer Lett* (2015) 356:506–16. doi: 10.1016/j.canlet.2014.09.034
201. Tidyman WE, Rauen KA. The RASopathies: developmental syndromes of Ras/MAPK pathway dysregulation. *Curr Opin Genet Dev* (2009) 19:230–6. doi: 10.1016/j.gde.2009.04.001
202. Varughese J, Richman S. Cancer care inequity for women in resource-poor countries. *Rev Obstet Fynecol* (2010) 3:122–32.
203. Wilczynski M, Danielska J, Dzieniecka M, Szymanska B, Wojciechowski M, Malinowski A. Prognostic and Clinical Significance of miRNA-205 in Endometrioid Endometrial Cancer. *PLoS One* (2016) 11:e0164687. doi: 10.1371/journal.pone.0164687
204. Ferlay J, Soerjomataram I, Dikshit R, Eser S, Mathers C, Rebelo M, et al. Cancer incidence and mortality worldwide: sources, methods and major patterns in GLOBOCAN 2012. *Int J Cancer* (2015) 136:E359–86. doi: 10.1002/ijc.29210
205. Acharya S, Hensley ML, Montag AC, Fleming GF. Rare uterine cancers. *Lancet Oncol* (2005) 6:961–71. doi: 10.1016/s1470-2045(05)70463-0
206. Urick ME, Rudd ML, Godwin AK, Sgroi D, Merino M, Bell DW. PIK3R1 (p85α) is somatically mutated at high frequency in primary endometrial cancer. *Cancer Res* (2011) 71:4061–7. doi: 10.1158/0008-5472.CAN-11-0549
207. Chan E, Prado DE, Weidhaas JB. Cancer microRNAs: from subtype profiling to predictors of response to therapy. *Trends Mol Med* (2011) 17:235–43. doi: 10.1016/j.molmed.2011.01.008
208. Hiroki E, Akahira J-I, Suzuki F, Nagase S, Ito K, Sasano H, et al. Changes in microRNA expression levels correlate with clinicopathological features and prognoses in endometrial serous adenocarcinomas. *Cancer Sci* (2009) 101:241–9. doi: 10.1111/j.1349-7006.2009.01385.x
209. Dong P, Konno Y, Watari H, Hosaka M, Noguchi M, Sakuragi N. The impact of microRNA-mediated PI3K/AKT signaling on epithelial-mesenchymal transition and cancer stemness in endometrial cancer. *J Transl Med* (2014) 12:231. doi: 10.1186/s12967-014-0231-0
210. Pillai RS. MicroRNA function: multiple mechanisms for a tiny RNA? *RNA* (2005) 11:1753–61. doi: 10.1261/rna.2248605
211. Yanokura M, Banno K, Iida M, Irie H, Umene K, Masuda K, et al. MicroRNAS in endometrial cancer: recent advances and potential clinical applications. *EXCLI J* (2015) 14:190–8. doi: 10.17179/excli2014-590
212. Chung TK, Lau TS, Cheung TH, Yim SF, Lo KW, Siu NS, et al. Dysregulation of microRNA-204 mediates migration and invasion of endometrial cancer by regulating FOXC1. *Int J Cancer* (2012) 130:1036–45. doi: 10.1002/ijc.26060
213. Dong P, Karaayvaz M, Jia N, Kaneuchi M, Hamada J, Watari H, et al. Mutant p53 gain-of-function induces epithelial-mesenchymal transition through modulation of the miR-130b-ZEB1 axis. *Oncogene* (2013) 32:3286–95. doi: 10.1038/onc.2012.334
214. Dong P, Kaneuchi M, Watari H, Sudo S, Sakuragi N. MicroRNA-106b modulates epithelial-mesenchymal transition by targeting TWIST1 in invasive endometrial cancer cell lines. *Mol Carcinog* (2014) 53:349–59. doi: 10.1002/mc.21983
215. Gregory PA, Bert AG, Paterson EL, Barry SC, Tsykin A, Farshid G, et al. The miR-200 family and miR-205 regulate epithelial to mesenchymal transition by targeting ZEB1 and SIP1. *Nat Cell Biol* (2008) 10:593–601. doi: 10.1038/ncb1722
216. Huang Y, Yang N. MicroRNA-20a-5p inhibits epithelial to mesenchymal transition and invasion of endometrial cancer cells by targeting STAT3. *Int J Clin Exp Pathol* (2018) 11:5715–24.
217. Larue L, Bellacosa A. Epithelial–mesenchymal transition in development and cancer: role of phosphatidylinositol 3′ kinase/AKT pathways. *Oncogene* (2005) 24:7443–54. doi: 10.1038/sj.onc.1209091
218. Orang AV, Safaralizadeh R, Hosseinpour Feizi MA. Insights into the diverse roles of miR-205 in human cancers. *Asian Pac J Cancer Prev* (2014) 15:577–83. doi: 10.7314/apjcp.2014.15.2.577
219. Guarino M, Rubino B, Ballabio G. The role of epithelial-mesenchymal transition in cancer pathology. *Pathology* (2007) 39:305–18. doi: 10.1080/00313020701329914
220. Qin X, Yan L, Zhao X, Li C, Fu Y. microRNA-21 overexpression contributes to cell proliferation by targeting PTEN in endometrioid endometrial cancer. *Oncol Lett* (2012) 4:1290–6. doi: 10.3892/ol.2012.896
221. Cohn DE, Fabbri M, Valeri N, Alder H, Ivanov I, Liu C-G, et al. Comprehensive miRNA profiling of surgically staged endometrial cancer. *Am J Obstet Gynecol* (2010) 202:656.e651–8. doi: 10.1016/j.ajog.2010.02.051
222. Wei Y, Zhang Z, Liao H, Wu L, Wu X, Zhou D, et al. Nuclear estrogen receptor-mediated Notch signaling and GPR30-mediated PI3K/AKT signaling in the regulation of endometrial cancer cell proliferation. *Oncol Rep* (2012) 27:504–10. doi: 10.3892/or.2011.1536
223. Guo Q, Qian Z, Yan D, Li L, Huang L. LncRNA-MEG3 inhibits cell proliferation of endometrial carcinoma by repressing Notch signaling.

BioMed Pharmacother (2016) 82:589–94. doi: 10.1016/j.biopha.2016.02.049
224. Murata K, Hattori M, Hirai N, Shinozuka Y, Hirata H, Kageyama R, et al. Hes1 directly controls cell proliferation through the transcriptional repression of p27Kip1. *Mol Cell Biol* (2005) 25:4262–71. doi: 10.1128/MCB.25.10.4262-4271.2005
225. Chen Z, Zhu Y, Fan X, Liu Y, Feng Q. Decreased expression of miR-184 restrains the growth and invasion of endometrial carcinoma cells through CDC25A-dependent Notch signaling pathway. *Am J Trans Res* (2019) 11:755–64.
226. Zalewski K, Misiek M, Kowalik A, Bakuła-Zalewska E, Kopczyn´ski J, Zielin´ska A, et al. Normalizers for microRNA quantification in plasma of patients with vulvar intraepithelial neoplasia lesions and vulvar carcinoma. *Tumor Biol* (2017), 39(11):1010428317717140. doi: 10.1177/1010428317717140
227. PDQ Cancer Genetics Editorial Board. Cancer Genetics Overview (PDQ®): Health Professional Version. 2020 Jul 24. In: PDQ Cancer Information Summaries [Internet]. Bethesda (MD): National Cancer Institute (US); 2002.
228. Yang X, Wu X. miRNA expression profile of vulvar squamous cell carcinoma and identification of the oncogenic role of miR 590 5p. *Oncol Rep* (2016) 35:398–408. doi: 10.3892/or.2015.4344
229. Liolios T, Kastora SL, Colombo G. MicroRNAs in Female Malignancies. *Cancer Inf* (2019) 18:1–9. doi: 10.1177/1176935119828746. 1176935119828746.
230. Taylor DD, Zacharias W, Gercel-Taylor C. Exosome isolation for proteomic analyses and RNA profiling. *Methods Mol Biol (Clifton N.J.)* (2011) 728:235–46. doi: 10.1007/978-1-61779-068-3_15
231. Szczepanski MJ, Szajnik M, Welsh A, Whiteside TL, Boyiadzis M. Blast-derived microvesicles in sera from patients with acute myeloid leukemia suppress natural killer cell function via membrane-associated transforming growth factor-beta1. *Haematologica* (2011) 96:1302–9. doi: 10.3324/haematol.2010.039743
232. Satoh M, Minami Y, Takahashi Y, Tabuchi T, Nakamura M. Expression of microRNA-208 is associated with adverse clinical outcomes in human dilated cardiomyopathy. *J Cardiac Failure* (2010) 16:404–10. doi: 10.1016/j.cardfail.2010.01.002
233. Simpson JR, Mathivanan S. Extracellular Microvesicles: The Need for Internationally Recognised Nomenclature and Stringent Purification Criteria. *J Proteomics Bioinform* (2012) 5:ii–ii. doi: 10.4172/jpb.10000e10
234. Williams A, Syed S, VelangiS, Ganesan R. New Directions in Vulvar Cancer Pathology. *Curr Oncol Rep* (2019) 21:88. doi: 10.1007/s11912-019-0833-z
235. Schneider HG, Lam L, Lokuge A, Krum H, Naughton M, De Villiers Smit P, et al. B-Type Natriuretic Peptide Testing, Clinical Outcomes, and Health Services Use in Emergency Department Patients With Dyspnea A Randomized Trial. *Ann Inter Med* (2009) 150:365–71. doi: 10.7326/0003-4819-150-6-200903170-00004
236. Abels ER, Breakefield XO. Introduction to Extracellular Vesicles: Biogenesis, RNA Cargo Selection, Content, Release, and Uptake. *Cell Mol Neurobiol* (2016) 36:301–12. doi: 10.1007/s10571-016-0366-z
237. Choschzick M, Hantaredja W, Tennstedt P, Gieseking F, Wölber L, Simon R. Role of TP53 mutations in vulvar carcinomas. *Int J Gynecol Pathol* (2011) 30:497–504. doi: 10.1097/PGP.0b013e3182184c7a
238. Medzhitov R. Origin and physiological roles of inflammation. *Nature* (2008) 454(7203):428–35. doi: 10.1038/nature07201
239. Charo IF, Ransohoff RM. The many roles of chemokines and chemokine receptors in inflammation. *N Engl J Med* (2006) 354(6):610–21. doi: 10.1056/NEJMra052723
240. Allavena P, Garlanda C, Borrello MG, Sica A, Mantovani A. Pathways connecting inflammation and cancer. *Curr Opin Genet Dev* (2008) 18:3–10. doi: 10.1016/j.gde.2008.01.003
241. Bishayee A. Cancer prevention and treatment with resveratrol: from rodent studies to clinical trials. *Cancer Prev Res (Phila)* (2009) 2(5):409–18. doi: 10.1158/1940-6207.CAPR-08-0160
242. Athar M, et al. Resveratrol: a review of preclinical studies for human cancer prevention. *Toxicol Appl Pharmacol* (2007) 224(3):274–83. doi: 10.1016/j.taap.2006.12.025
243. Pirola L, Frojdo S. Resveratrol: one molecule, many targets. *IUBMB Life* (2008) 60:323–32. doi: 10.1002/iub.47
244. Farooqi A, Gohar Khalid S, Ahmad A. Regulation of Cell Signaling Pathways and miRNAs by Resveratrol in Different Cancers. *Int J Mol Sci* (2018) 19 (3):652. doi: 10.3390/ijms19030652
245. Pan J, Shen J, Si W, Du C, Chen D, Xu L, et al. Resveratrol promotes MICA/B expression and natural killer cell lysis of breast cancer cells by suppressing c-Myc/miR-17 pathway. *Oncotarget* (2017) 8:65743–58. doi: 10.18632/oncotarget.19445
246. Vislovukh A, Kratassiouk G, Porto E, Gralievska N, Beldiman C, Pinna G, et al. Proto-oncogenic isoform A2 of eukaryotic translation elongation factor eEF1 is a target of miR-663 and miR-744. *Br J Cancer* (2013) 108:2304–11. doi: 10.1038/bjc.2013.243
247. Hagwara K, Kosaka N, Yoshioka Y, Takahashi RU, Takeshita F, Ochiya T. Stilbene derivates promote Ago2-depedent tumour-suppressive microRNA activity. *Sci Rep* (2012) 2:3:314. doi: 10.1038/srep00314
248. Caporali A, Emanueli C. MicroRNA-503 and the extended microRNA-16 family in angiogenesis. *Trends Cardiovasc Med* (2011) 21:162–6. doi: 10.1016/j.tcm.2012.05.003
249. Schmeier S, MacPherson CR, Essack M, Kaur M, Schaefer U, Suzuki H, et al. Deciphering the transcriptional circuitry of microRNA genes expressed during human monocytic differentiation. *BMC Genomics* (2009) 10:595. doi: 10.1186/1471-2164-10-595

Conflict of Interest: The authors declare that the research was conducted in the absence of any commercial or financial relationships that could be construed as a potential conflict of interest.

frontiers in Oncology

ORIGINAL RESEARCH
published: 29 October 2020
doi: 10.3389/fonc.2020.588557

Intratumor Heterogeneity of MYO18A and FBXW7 Variants Impact the Clinical Outcome of Stage III Colorectal Cancer

*Peng-Chan Lin[1,2,3], Yu-Min Yeh[1,2], Bo-Wen Lin[4], Shao-Chieh Lin[4], Ren-Hao Chan[4], Po-Chuan Chen[4] and Meng-Ru Shen[5,6,7]**

[1] Department of Oncology, National Cheng Kung University Hospital, College of Medicine, National Cheng Kung University, Tainan, Taiwan, [2] Department of Internal Medicine, National Cheng Kung University Hospital, College of Medicine, National Cheng Kung University, Tainan, Taiwan, [3] Department of Computer Science and Information Engineering, College of Electrical Engineering and Computer Science, National Cheng Kung University, Tainan, Taiwan, [4] Department of Surgery, National Cheng Kung University Hospital, College of Medicine, National Cheng Kung University, Tainan, Taiwan, [5] Graduate Institute of Clinical Medicine, National Cheng Kung University Hospital, College of Medicine, National Cheng Kung University, Tainan, Taiwan, [6] Department of Obstetrics and Gynecology, National Cheng Kung University Hospital, College of Medicine, National Cheng Kung University, Tainan, Taiwan, [7] Department of Pharmacology, National Cheng Kung University Hospital, College of Medicine, National Cheng Kung University, Tainan, Taiwan

Many studies failed to demonstrate benefit from the addition of targeted agents to current standard adjuvant FOLFOX chemotherapy in stage III colorectal cancer (CRC) patients. Intratumor heterogeneity may foster the resistant subclones and leads to cancer recurrence. Here, we built a cancer evolution model and applied machine learning analysis to identify potential therapeutic targets. Among 78 CRC cases, whole-genome (WGS) and deep targeted sequencing data generated from paired blood and primary tumor were used for phylogenetic tree reconstruction. Genetic alterations in the PI3K/AKT, and RTK oncogenic signaling pathways were commonly detected in founding clones. The dominant subclones frequently exhibited dysregulations in the TP53, FBXW7/NOTCH1 tumor suppression, and DNA repair pathways. Fourteen genetic mutations were simultaneously selected by random forest and LASSO methods. The logistic regression model had better accuracy (79%), precision (70%), and recall (65%) and area under the curve (AUC) (82%) for cancer recurrence prediction. Three genes, including MYO18A in the founding clone, FBXW7, and ATM in the dominant subclone, affected the prognosis were selected simultaneously by different feature sets. The *in vitro* studies, HCT-116 cells transfected with MYO18A siRNA demonstrated a significant reduction in cell migration activity by 20–40%. These results indicate that MYO18A plays a crucial role in the migration of human CRC cells. The cancer evolution model revealed the critical mutations in the founding and dominant subclones. They can be used to predict clinical outcomes and the development of novel therapeutic targets for stage III CRC.

Keywords: colorectal cancer, whole-genome sequencing, targeted gene sequencing, tumor evolution, intratumor heterogeneity

OPEN ACCESS

Edited by:
Lorenzo Gerratana, University of Udine, Italy

Reviewed by:
Elena Ongaro, Centro di Riferimento Oncologico di Aviano (IRCCS), Italy
Zhenhua Xu, Children's National Hospital, United States

***Correspondence:**
Meng-Ru Shen
mrshen@mail.ncku.edu.tw

Specialty section:
This article was submitted to Cancer Genetics, a section of the journal Frontiers in Oncology

Received: *29 July 2020*
Accepted: *05 October 2020*
Published: *29 October 2020*

Citation:
Lin P-C, Yeh Y-M, Lin B-W, Lin S-C, Chan R-H, Chen P-C and Shen M-R (2020) Intratumor Heterogeneity of MYO18A and FBXW7 Variants Impact the Clinical Outcome of Stage III Colorectal Cancer. Front. Oncol. 10:588557. doi: 10.3389/fonc.2020.588557

INTRODUCTION

Colorectal cancer (CRC) is the most commonly diagnosed gastrointestinal cancer and is also one of the leading causes of cancer-related death worldwide (1). Although adjuvant FOLFOX (5-fluorouracil, leucovorin, and oxaliplatin) chemotherapy benefits stage III CRC patients, recurrence develops in 30–35% of patients (2). Many studies have tried to assess the addition of targeted therapy, including bevacizumab and cetuximab, to FOLFOX in the adjuvant treatment of stage III CRC. However, no significant improvement in survival was noted. A considerable challenge of recurrent stage III CRC is identifying the critical genetic mutations responsible for tumor metastasis and delivering effective therapeutic strategies (3, 4). CRC is a highly heterogeneous disease that differs in clinical presentations, molecular characteristics, and responses to treatment and survival. Intratumor heterogeneity is defined as the distinct morphological and phenotypic differences within a tumor (5). Hence, building the genome evolution model underlying the mechanism of tumor carcinogenesis and biological pathways and identifying genetic markers to predict cancer recurrence is crucial to accelerate and facilitate the development of CRC treatment targets.

Cancer cells accumulate somatic alterations over time. Most cancers arise from a single clone with acquired genetic variability, and tumor progression and metastasis result from the sequential selection of more aggressive subclones (6). Cancer evolves dynamically as clonal expansions. Recent genomic studies have demonstrated that cancer relapse or metastasis is associated with the addition of new mutations and clonal evolution (7). Intratumor heterogeneity may foster tumor evolution and adaptation and hinder the biomarker development of personalized-medicine strategies that depend on results from single tumor-biopsy samples (7). The most common technology used for the molecular characterization of tumor heterogeneity is the high-throughput DNA sequencing of bulk samples. There is a significant acceleration in the use of next-generating sequencing (NGS) to approach tumor heterogeneity and evolution for precision medicine (8, 9). By using advances in bioinformatics and artificial intelligence, determining the essence of key genetic mutations in cancer evolution has recently become possible. From the evolutionary models, we can identify the "oncogenic addiction or driver" mutations that provide a fitness advantage to cancer targets against neutral "passenger" mutations.

In this study, we aimed to develop a genome evolution model by analyzing tumor heterogeneity and discovering actionable mutational targets. We first developed a cancer evolution model for the development of new agents in tumor heterogeneity and the generation of novel and more effective therapies by analyzing somatic mutations and tumor heterogeneity. Second, we established a model predicting cancer recurrence and survival and identified therapeutic driver mutation targets *via* robust optimization in machine learning. Finally, we used the causal inference model and biological methods to validate the potential cancer evolution targets. The results further described early mutation changes that predict tumors progress to stage III carcinomas and showed that statistical inference predicts that the subclone-related pathogenic mutations are acquired when the cancer is progressing. Here, we defined a broad time window of opportunity for early detection to prevent recurrence and death in advanced colorectal cancer patients. A fine-resolution view of this clonal architecture provides insight into tumor heterogeneity, evolution, and treatment response, all of which may have clinical implications.

MATERIALS AND METHODS

Study Population

A total of 78 CRC cancer patients were recruited for the study from National Cheng Kung University Hospital (NCKUH) between January 2014 and January 2019. All CRC patients were pathological stage III and received standard surgical resection followed by adjuvant chemotherapy with the regimen of mFOLFOX6 (5-fluorouracil, leucovorin, and oxaliplatin). Clinical information was obtained from medical records. Tumor tissues and blood samples were collected at the time of enrollment. This study was approved by the Institutional Review Board of NCKUH (A-ER-103-395 and A-ER-104-153) and conducted under the Declaration of Helsinki. All participants provided written informed consent.

Germline Whole-Genome Sequencing

Whole blood was collected for genomic DNA extraction. Genomic DNA was quantified with a Qubit fluorescence assay (Thermo Fisher Scientific) and sheared with an S2 instrument (Covaris). Library preparation was carried out using the TruSeq DNA PCR-Free HT Kit (Illumina). Individual DNA libraries were measured by 2100 Bioanalyzer (Agilent) qPCR and Qubit (Thermo Fisher Scientific). Normalized DNA libraries were combined into five-sample pools per flow cell in all eight lanes and clustered on a cBot instrument (Illumina) with Paired-End Cluster Kit V4 (Illumina). All flow cells were sequenced on the HiSeq2500 sequencer (Illumina) using the SBS Kit V4 chemistry (Illumina). FastQC was used to check read quality, and the resulting reads were aligned to the hg19 reference genome with the BWA-MEM algorithm (10). Single nucleotide variants (SNVs) and indel identification and genotyping were performed across all samples simultaneously using standard hard filtering parameters or variant quality score recalibration according to GATK Best Practices recommendations. WGS was presented with a minimum, median coverage of 30X.

Targeted Tumor Sequencing by Cancer Panel

A total of 78 formalin-fixed paraffin-embedded primary tumor samples were collected for histologic assessment followed by the extraction of nucleic acids. The histologic evaluation was performed by pathologists, who determined the percentage of

tumors and adequacy for sequencing. Tumor deep targeted sequencing was performed by Oncomine Comprehensive Assays (OCA) version 1 (Thermo Fisher Scientific) (11). OCA v1 was designed to detect 143 drug targets, including 73 hotspot genes, 49 focal copy number variation (CNV) gains, 26 genes for full coding region sequencing (CDS), and 22 fusion driver genes. (druggable) The Ion PGM Sequencing 200 Kit v.2 was used with the Ion PGM sequencer (Thermo Fisher Scientific) according to the manufacturer's instructions. All samples were analyzed using the Torrent Suite Software 5.0.4, aligning all reads to the hg19 reference genome, and variant calling was performed running the Torrent Variant Caller plugin version 5.0.4.0. We used the ANNOVAR tool to annotate variants and filter out indels not reported in the 1000 Genomes Project, the Single Nucleotide Polymorphism Database (dbSNP), and the Exome Aggregation Consortium (ExAc) (12).

Cancer Evolution Model Construction

The somatic mutation calling was performed by comparing the sequencing data generated by OCA v1 and germline genetic variants by WGS. Somatic SNVs were obtained by DeepSNV (13). DeepSNV (a beta-binomial model and a likelihood ratio test) is a tool that can detect subclonal SNVs with frequencies higher than 10^{-4} with higher sensitivity and specificity. The tumor subclones were identified, and clusters were identified using SciClone (14), a Bayesian clustering method. ClonEvol was used to establish the evolution tree in cancer (15).

Statistical Analysis

Chi-square tests, Fisher's exact tests, and unpaired t-tests were used to assess the differences between groups. Kaplan–Meier curves were used to evaluate disease-free survival, and the log-rank test was used to compare the differences between groups. Disease-free survival was defined as the time between surgery and recurrence of cancer. A P value < 0.05 was considered statistically significant.

Pathway Analysis

Signaling pathways for frequently mutated genes detected in founding clones and dominant subclones were enriched by using Reactome (http://www.reactome.org) (16). Significance was derived from over-representation analysis built in Reactome.

Machine Learning Analysis

Feature Selection

The machine learning model includes logistic regression (LR), least absolute shrinkage and selection operator (LASSO) method, and random forest. The LASSO method is a regression model that penalizes the absolute size of the coefficients, causing some regression coefficients to shrink to zero. The penalization, or constraint, allows the LASSO method to estimate a model while simultaneously performing automatic variable selection (17). The random forest (RF) model consists of an ensemble of classification trees, where each classifier was built from different independent and identically distributed bootstrap samples from a training set. Each classifier casts a vote for the most popular class. Odds ratio (OD) measures the strength of the association between two types, and hazard ratio (HR) is the ratio of the hazard rates corresponding to the conditions described by two levels of an explanatory variable in survival analysis. LASSO method was done by R package glmnet, Random forest was done by R package randomForest, the odds ratio was done by R package fmsb, and the hazard ratio was done by R package survival and survminer.

Classifier Model

The support vector machine (SVM) (18) is a state-of-the-art classification method referred to as black-box processes. Random forest (RF) (19) is an "off-the-shelf" widely used machine learning method that shows competitive prediction performance. XGBoost (20) is an optimized implementation of gradient boosting (GBM). The advantages of the classifier include less prone to overfitting due to the strong inner regularization scheme, easy to implement parallelization and scalability. C5.0 is a machine learning method based on decision trees, which is also referred to as white box processes and is known for interpretability (21). Logistic regression is used to describe data and to explain the relationship between one dependent binary variable and one or more nominal, ordinal, interval, or ratio-level independent variables (22, 23). Finally, we performed ten-fold cross-validation on our dataset to evaluate the efficiency of the models using the caret packages in R with default parameters (24). SVM, XGBoost, and C5.0 were done by R package e1071, xgboost, and C50.

Migration Assay

For the migration assay, placed on a cell culture surface, the ibidi Culture-Insert 2 Well (ibidi GmbH, Planegg, Germany) provides two cell cultureservoirs, each separated by a 500 μm wall. Cells were plated at 80,000 cells per well and allowed to attach overnight. On the following day, culture inserts were removed, and light microscopy images were acquired. Cells were maintained under standard culture conditions while migrating toward the cell-free gap area. For HCT-116, HT-29, and DLD-1 cells, images were acquired every 24 hours later. Images were analyzed using ImageJ software.

RESULTS

Identification of Cancer Driver Mutations by Conventional Approaches

The discovery of somatic mutations that drive cancer progression is essential for therapeutic strategies. Following the protocol shown in **Supplementary Figure 1A**, we used conventional statistical methods such as odds ratio (OD) and hazard ratio (HR) to evaluate the clinical impact of somatic mutations in a cohort of 78 stage III CRC patients. The median follow-up duration of this cohort was 31.2 months. Among these patients, 33% (26/78) had recurrent disease, and 67% (52/78) remained disease-free. Of all patients, the distribution of gender

was the same. The median age of these patients was 58 years old. The prevalent primary tumor site was left colon (80.8%). There was no significant difference between recurrence and tumor characteristics, such as tumor site, tumor invasion stage (T), and nodal stage (N) (**Supplementary Table 1**). A total of 30 mutated genes were identified. There was no genetic variant significantly associated with recurrence in these CRC patients by odds ratio. The hazard ratio (**Supplementary Figure 1B**) of four mutated genes, including *MTOR*, *BAP1*, *TSC1*, and *NOTCH1*, showed a correlation with worse progression-free survival [$p < 0.05$ and hazard ratio (HR) =10.5–76.5]. However, these four genetic variants were rare and were found only in 1.3% (1/78) of these CRC patients (**Supplementary Figure 1C**). Targeting these rare mutations does not seem to provide significant improvements in the clinical outcome of stage III CRC. These data imply the limitation of the conventional approach of the analytic sequencing method.

Targeting Intratumor Heterogeneity by Cancer Evolution Model

Evolutionary dynamic models have been studied to elucidate the process of tumorigenesis and discover the driver somatic mutations for the development of potential therapeutic strategies (25). Accordingly, we built clonal evolution models and applied statistics and machine learning algorithms to identify disease-related driver mutations. As shown in

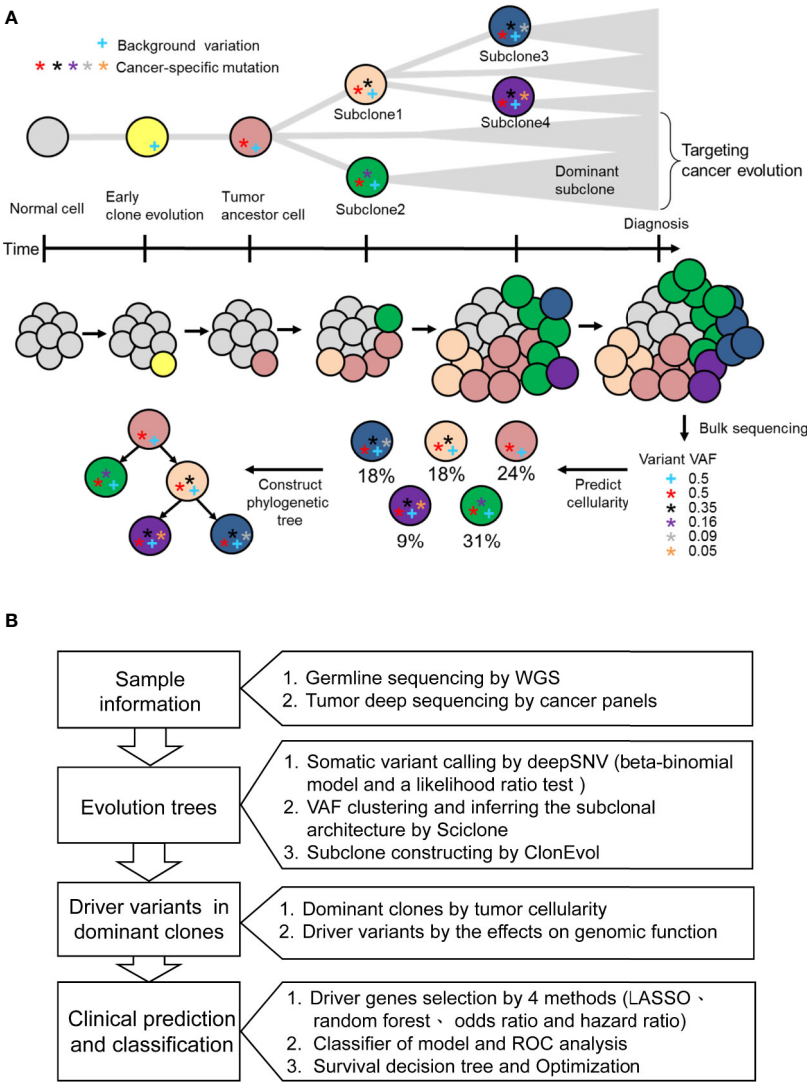

FIGURE 1 | The concept of cancer evolution and study design. **(A)** The cancer evolution model depicts the accumulation of cancer-specific mutations and clonal expansion during tumor formation. The data of VAF generated from deep sequencing of tumor tissues could be used to predict the cellularity and construct the phylogenetic tree. The blue cross indicates the background variation. Stars with different colors represent mutations that develop during cancer evolution. **(B)** Based on the concept of cancer evolution, the research design is proposed to identify driver mutations with crucial clinical impact.

Figure 1A, normal cells accumulate background variations (blue cross) and many cancer-specific mutations (stars) over a prolonged clinically latent period to become cancers. Multiple subclones could be found within single cancer tissue. Theoretically, the background variation and driver mutation (red star) are present in the ancestor cell and all the subclones. During cancer evolution, additional mutations occur subsequently in different subclones, which give rise to intratumoral heterogeneity. Deep targeted-gene sequencing of bulky tumor tissue provides useful information on variant allele frequency (VAF), which could be used to predict cellularity and construct phylogenetic trees. Therefore, we used the targeted-gene sequencing data of 78 stage III CRCs to reconstruct the tumor evolution. The WGS data from paired normal blood samples were used to filter germline variants (**Figure 1B**). After the somatic variant calling by DeepSNV (13), SciClone (14) was applied for analyzing the distribution of purity-scaled variant allele fractions, and ClonEvol (15) was used to reconstruct the phylogenetic tree. We determined the dominant clone according to the predicted cellularity. After that, the potential candidate driver mutations in ancestor and dominant clones could be identified. We applied machine learning models to predict the risk of cancer recurrence by using different genetic variant feature selection strategies and classifiers. By this pipeline, we could identify the critical driver genetic variants that could be potential drug targeting clonal variants and involved in cancer survival stratification (**Figure 1B**).

Phylogenetic Tree Reconstruction From the Clonal Evolution Model

A clinical example is shown in **Figure 2**. This case was a 40-year-old man with stage III CRC at initial diagnosis. He received standard surgical resection followed by adjuvant chemotherapy with mFOLFOX6. Recurrence was detected by computed tomography (CT) scan 15.4 months after surgery. WGS and deep targeted-gene sequencing were performed on paired normal and tumor samples, respectively. **Figure 2A** displays the allele frequency of the detected variants in tumor and germline tissues and indicates the levels of significance of the deepSNV test. Using the *VHL* gene as an example, the dots above the diagonal line represented the variants that were called as true variants rather than sequencing errors by the deepSNV algorithm. A total of 307 somatic SNVs were detected in this case. When SciClone was used to perform the clustering, 307 SNVs clustered into four groups (**Figure 2C**). The mean VAF values of clusters 1 to 4 are 36.5, 22.1, 11.2, and 4.2%. Besides, the mean posterior probabilities of clusters 1 to 4 are 93.5, 83, 95, and 99%. **Figure 2D** shows the kernel density plots of VAF under two copy number estimations. The model did not perfectly fit the original distribution because the mean probability of cluster 2 was 83%. **Figure 2E** shows the scatter plot of each cluster's SNV

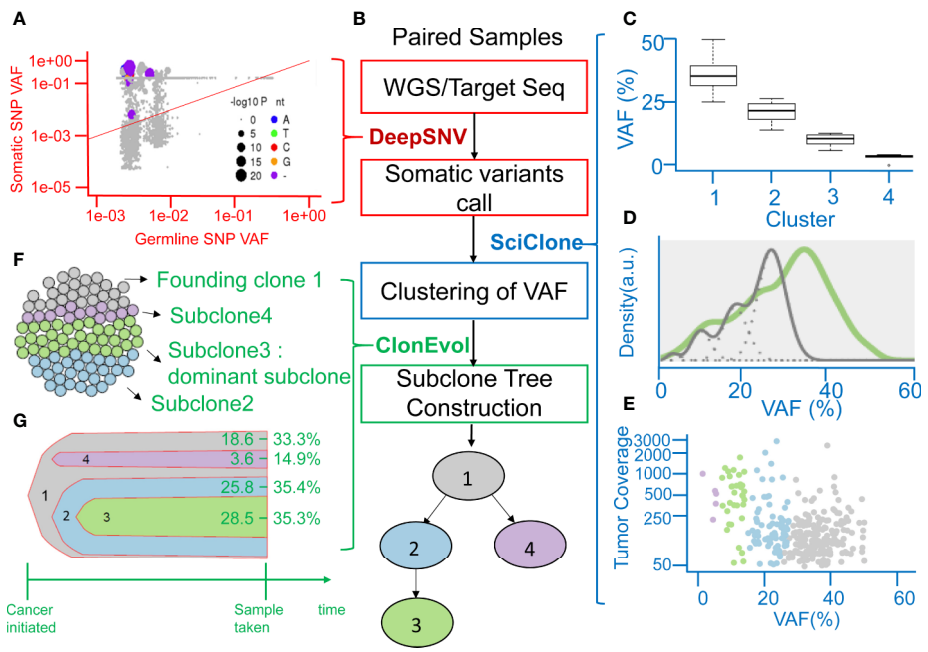

FIGURE 2 | Representation of analyzing clonal evolution in a CRC patient as an example. **(A)** Scatter plot showing the variant allele frequencies (VAFs) of the example *VHL* gene in tumor and normal tissues and the levels of significance of the deepSNV test. **(B)** The flow chart showing the utility of various algorithms for calling of SNV, clustering of VAFs, and analysis of clonal relationships from the sequencing data of paired normal-tumor samples. **(C)** Inferring subclones according to the clustering of VAFs by SciClone. **(D)** Kernel density estimation (KDE) of VAFs. The distribution of mutations occurring in colon cancer patients. The gray line represents the mutations detected in the founding clone, and the green line represents driver mutations in the dominant subclone. **(E)** The read depth versus VAF plot showing the read depth of 4 clusters of genes under the assumption of neutral copy number (copy number = 2). **(F)** Sphere of cells demonstrating the founding clone and clonal subpopulations of the CRC tumor sample by CloneEvol. **(G)** Bell plot showing clonal dynamics during tumor formation.

coverage and VAF. The SNVs with coverage less than 50x were filtered out in this study because the low coverage would lead to biased estimation. **Figures 2F, G** demonstrate the cancer cellularity prediction and the most likely evolutionary tree of the primary tumor *via* ClonEvol. In this case, the gray color was the founding clone with cellularity ranging from 18.6–33.3%, the green color was the dominant subclone ranging from 28.5–35.3%, the blue color was subclone two ranging from 25.8–35.4%, and the purple color was subclone four ranging from 3.6–14.9%. Finally, the phylogenetic tree was constructed (**Figure 2B**).

Sequential Oncogenic and Tumor Suppression Genetic Alterations in Cancer Evolution

By using the study protocol shown in **Figure 1B**, we identified possible driver mutations in the founding clone and dominant subclone for each cancer patient. Among 78 CRC patients, 66 and 49 genetic variants with high or moderate protein impact were detected in founding and dominant subclones, respectively. Several variants were frequently detected in the founding clones of these 78 CRCs, including the *ABL1*, *MYO18A*, and *ATM* mutations (**Figure 3A**). Approximately 78.2, 73.1, and 64.1% of patients harbored the *ABL1*, *MYO18A*, and *ATM* mutations, respectively, in their founding clone. In contrast, the most commonly detected mutations in the dominant subclones of these CRCs were *BRCA1*, *BRCA2*, *TET2*, *APC*, *VHL*, *MSH2*, *TP53*, *PIK3CA*, and *FBXW7* mutations, accounting for 79.5, 93.6, 64.1, 55.1, 53.8, 41, 30.8, 32, and 21.8%, respectively. Driver genes can be classified into distinct signaling pathways that control cell survival, cell fate, and genome maintenance (26). Accordingly, we analyzed the dysregulated signaling pathways in founding clones and dominant subclones. As shown in **Figure 3B**, the signaling pathways involved were significantly different between the founding clones and dominant subclones. Alterations in the *PI3K*/*AKT*, *RAF*/*MAP*, and RTK signaling pathways were commonly detected in founding clones. By contrast, the dominant subclones frequently exhibited dysregulations in the *TP53*, *FBXW7*/*NOTCH1*, and DNA repair pathways. These results implied that cancer cells accumulated different somatic mutations during cancer evolution. Oncogenic alterations in signaling pathways controlling cell proliferation and survival, such as the *PI3K*/*AKT* and *MAPK* pathways, occurred at the early stage of cancer formation (27, 28). Mutations involving the tumor suppressors and DNA repair pathways became more important during evolution.

Optimizing the Selection of Clonal Mutations by Recurrence Status

To investigate the clinical significance of mutations detected in the founding clone and dominant subclones, we used different feature selection techniques to identify the important mutations associated with the recurrence of CRC patients. Top 30 mutations were selected by Gini importance using the random forest (RF). The *FBXW7* and *MYO18A* mutations were the variables with the highest importance among these CRC patients. LASSO was performed to select mutated genes with nonzero coefficients, and 23 mutations (LASSO23) were selected. By calculating the odds ratio (OD) and hazard ratio (HR), we identified 8 (OD8) and 25 (HR25) genes, respectively, that were significantly associated with recurrence in this CRC cohort ($p < 0.05$). The above results were shown in **Supplementary Table 2**.

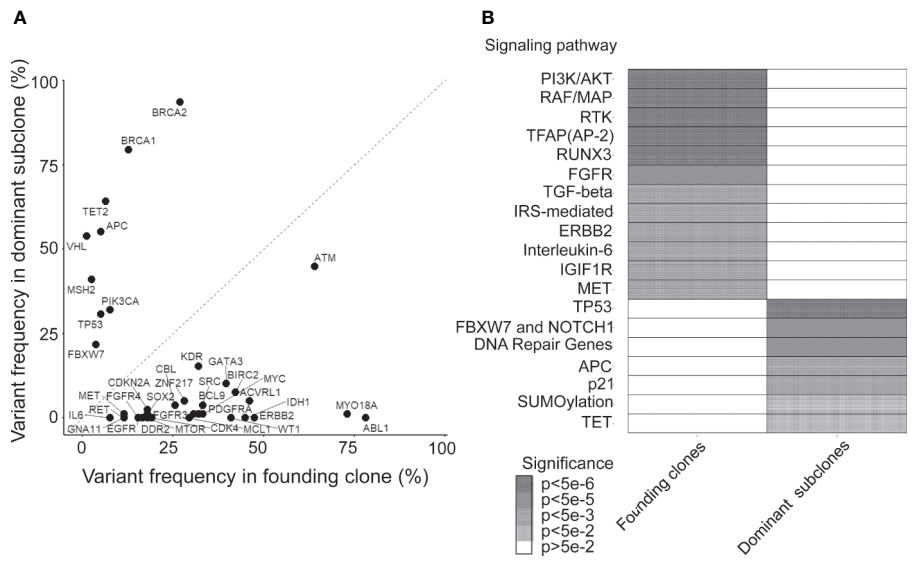

FIGURE 3 | Mutated genes and relevant pathways in the founding clone and dominant subclones. **(A)** Percentage of patients who harbor each mutated gene was occurring in founding clones or dominant subclones of their primary tumors. A gene under the dashed diagonal indicates that mutation frequently occurs in the founding clone than the dominant subclone of these patients. **(B)** Heatmap showing oncogenic pathways enriched by mutated genes frequently occurring in founding clones and dominant subclones, respectively. Color density represents the significance of enrichment derived by Reactome.

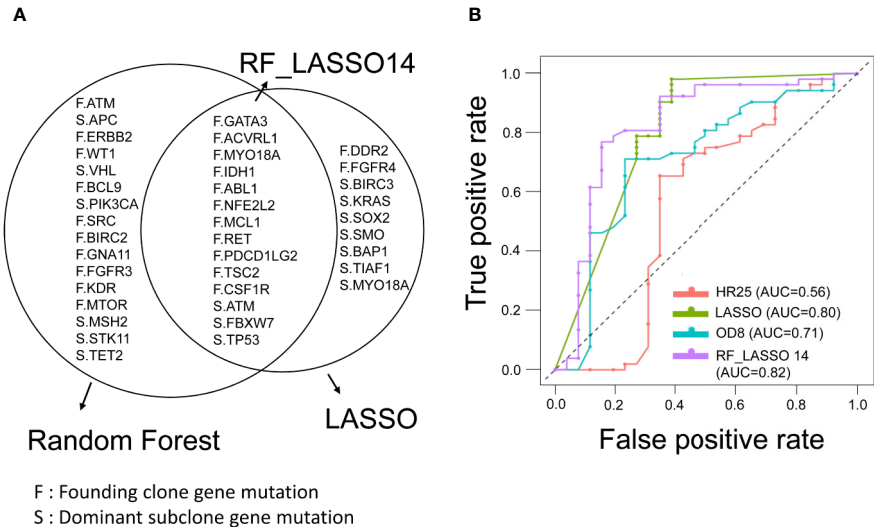

FIGURE 4 | Feature selection of founding clone and dominant subclone genes and prediction model for CRC recurrence. **(A)** Venn diagram showing overlapping genes selected by the random forest (RF) and LASSO models. RF_LASSO14 indicates a group of 14 overlapping genes. F represents the founding clone gene mutation, and S represents the dominant subclone gene mutation. **(B)** Receiver operating characteristic (ROC) curves of gene sets selected by different statistical and machine learning models for prediction of recurrence in stage III CRCs. The area under the curve of ROC corresponding to each gene set was shown. RF_LASSO14, 14 genes simultaneously selected by random forest and LASSO; OD8, eight genes selected by odds ratio; HR25, 25 genes selected by hazard ratio.

Fourteen genes were simultaneously selected by random forest and LASSO, including *GATA3*, *ACVRL1*, *MYO18A*, *IDH1*, *ABL1*, *NFE2L2*, *MCL1*, *RET*, *PDCD1LG2*, *TSC2*, *CSF1R*, *ATM*, *FBXW7*, and *TP53*. RF_LASSO14 was named for this 14-gene set (**Figure 4A**). We analyzed the correlation between disease-free survival (DFS) and the mutation status of 14 genes selected by both the random forest and lasso. Among these 14 genes, mutations of *CSF1R*, *PDCD1LG2*, *FBXW7*, *TSC2*, and *NFE2L2* gene were significantly associated with shorter DFS. In contrast, *MYO18A* mutation was associated with better DFS. No association between the DFS and the mutation status of the other eight genes was observed (**Supplementary Table 3**). The heatmap of these 14 mutated genes is shown in **Supplementary Figure 2**. For robust optimization, we input the gene groups identified by four different feature sets into five classifier models, including support vector machine (SVM), C5.0, random forest, logistic regression, and XGBoost (gradient boosting), to predict and classify the cancer recurrence. The recall value of 10-fold cross-validation for SVM, C5.0, RF, LR, and XGBoost were 0.615, 0.346, 0.384, 0.654, and 0.461, respectively. The accuracy for SVM, C5.0, RF, LR, and XGBoost were 0.756, 0.615, 0.756, 0.795, and 0.744, respectively. The logistic regression model had the best performance with the highest recall value and better accuracy. The results were shown in **Supplementary Figure 3**. The receiver operating characteristic (ROC) curve analysis confirmed that the RF_LASSO14 gene set had better accuracy (79%), precision (70%), and recall (65%) and area under the curve (AUC) (82%) in the logistic regression model (**Figure 4B**). To emphasize the importance of cancer evolution, we compared the performance between the models with or without intratumor heterogeneity. We operated the bootstrapping process 5000 times and selected background genetic mutations as features by lasso methods and built the same logistic regression classifier to calculate the probability of accuracy over 0.795. Consequently, the probability of a conventional model with better accuracy than the evolution model was only 4.54%, which proved that our model was quite meaningful.

Survival Stratification by Three Genetic Variants *via* the Decision Tree Model

Currently, the "one size fits all" approach is still used for adjuvant treatment of stage III CRC patients. FOLFOX6 chemotherapy is the gold standard regimen without considering genomic alterations. In this CRC cohort, all patients were pathological stage III and received standard surgical resection followed by adjuvant FOLFOX6 chemotherapy. The 5-year DFS was approximately 70% (**Figure 5A**). The decision tree, a nonparametric supervised learning method, was used to analyze the predictive value of the mutations identified in the founding clone and dominant to further subclassify these stage III CRC patients and identify potential treatment strategies subclone. As shown in **Figure 5B**, three mutations, including the *MYO18A* mutation in the founding clone and *FBXW7* and the *ATM* mutation in the dominant subclone, could be used to stratify these 78 CRC patients into four subgroups that had different clinical outcomes. Group 1 (G1) was the patient without the *MYO18A* mutation in the founding clone (F.MYO18A), and this group of patients had the worst DFS (**Figure 5C**). Patients harboring the *MYO18A* mutation could be further categorized into groups 2, 3, and 4 according to the

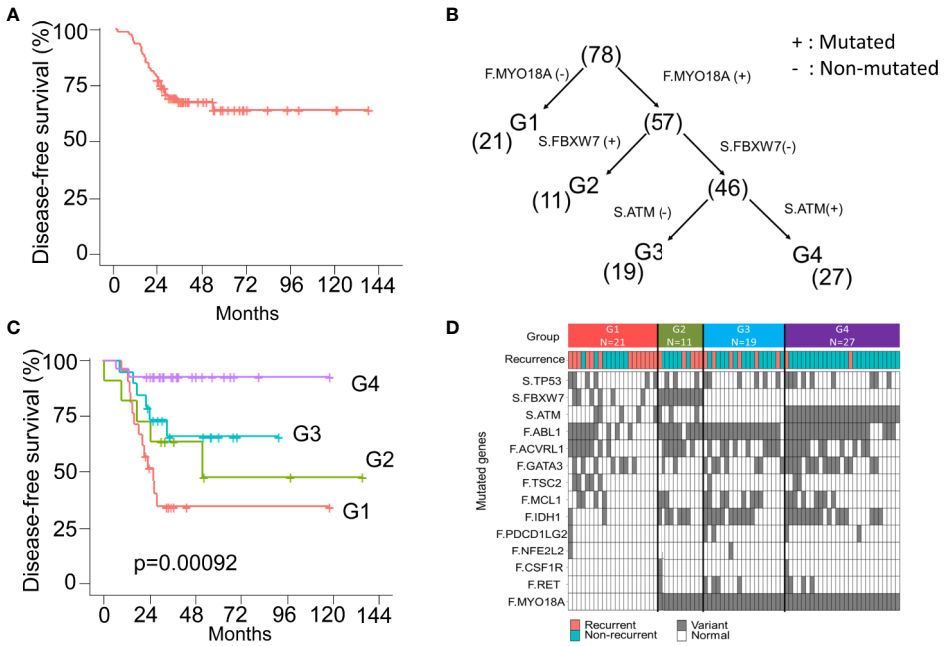

FIGURE 5 | The model of survival decision tree (CRC) **(A)** The Kaplan-Meier curve of disease-free survival (DFS) for 78 stage III CRC patients. **(B)** CRC patients are grouped into four subgroups according to the mutation status of the *MYO18A* gene in the founding clone (F) MYO18A) and *FBXW7* and *ATM* genes in the dominant subclone (S. FBXW7 and S.ATM). Parentheses indicate the number of patients in each group. **(C)** The Kaplan-Meier curves of DFS stratified by group (1–4) and compared with the log-rank test. **(D)** Summary of the mutations and clinical outcome in 4 subgroups of CRC patients. The colored rectangles indicate the detection of recurrent disease or not. The gray and white rectangles indicate the gene with and without the mutation.

dominant subclone's mutation status of *FBXW7* and *ATM*. Patients in group 2 (G2) had *FBXW7* mutations (S.FBXW7), and patients in group 4 (G4) had *ATM* mutations in the dominant subclone (S.ATM). Patients in group 4 had the best outcome, followed by groups 3 and 2. The mutated genes in the founding and dominant subclones detected in these four subgroups of patients are shown in **Figure 5D**. Targeting these relevant mutations in founding and dominant subclones might provide benefits for stage III CRC patients, especially groups 1 and 2. Since *MYO18A*, *FBXW7*, and *ATM* mutations (**Supplementary Figure 5**) have a considerable impact on clinical outcomes, these mutations might be potential therapeutic targets. *MYO18A* mutation was detected in 50 and 84.6% of patients with and without recurrence. In contrast, the percentage of *FBXW7* mutations in patients with or without recurrence was 38.5 and 13.5%, respectively. When analyzed by the Chi-Square test, the distributions of *MYO18A* and *FBXW7* mutations are significantly different in these two groups of patients ($p = 0.002$ and 0.019) (**Supplementary Table 1**). Several clinical and pathological factors, as shown in the **Supplementary Table 4**, were also considered when analyzing the prognostic impact of *MYO18A* and *FBXW7* mutations. We analyzed these factors through univariate and multivariate Cox proportional hazards model. The results showed *MYO18A*, and *FBXW7* mutations are significantly associated with the clinical outcome when univariate analysis. The outcome was not affected by age, gender, primary tumor location, the depth of tumor invasion, and the number of lymph node metastasis. In multivariate analysis, both the *MYO18A* and *FBXW7* mutations were still the independent prognostic factors (**Supplementary Table 4**).

Examining the Biological Role of MYO18A *In Vitro*

MYO18A is a gene encoding a unique myosin involved in intracellular transport processes and cell motilities (29). Therefore, we assessed whether *MYO18A* has a role in CRC cell invasion or migration. Specific siRNA targeting *MYO18A* was transfected into human CRC cancer cells, and the impact on cell migration was determined by gap closure assay. As shown in **Figure 6A**, *MYO18A* siRNA significantly reduced the level of *MYO18A* protein after 48 hours of transfection. Compared to cells treated with scrambled siRNA, HCT-116 cells transfected with *MYO18A* siRNA demonstrated a significant reduction in cell migration activity by 20 to 40% (**Figures 6B, C**). Reduced migration was also observed in *MYO18A* siRNA-treated HT-29 and DLD-1 cells. These results indicate that *MYO18A* plays an essential role in the migration of human CRC cells.

DISCUSSION

With the advances of NGS technologies and machine learning in cancer biology, targeting cancer evolution has become more feasible. Here, we demonstrate using a genomic-machine

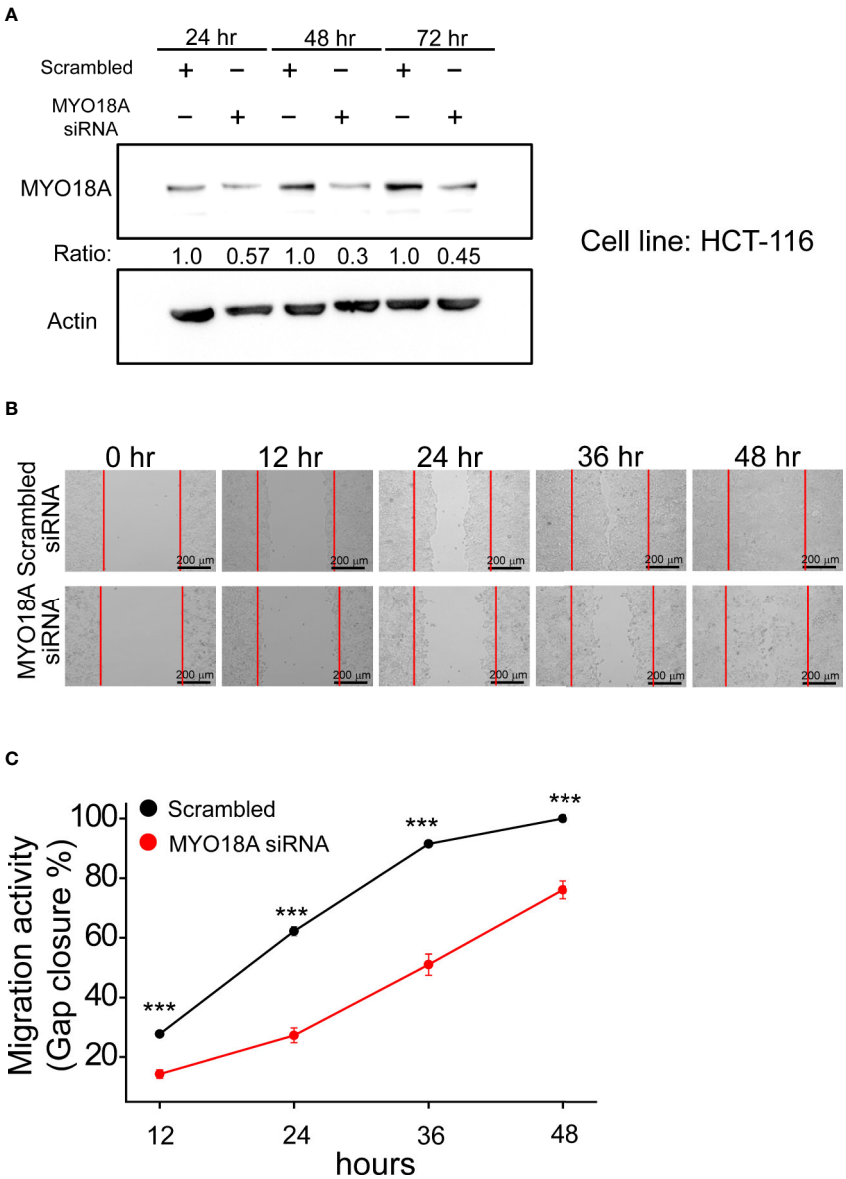

FIGURE 6 | Depletion of MYO18A by siRNA suppressed cell migration in human CRC cells. **(A)** HCT-116 cells were transfected with either scrambled or *MYO18A* siRNA. Cells were harvested 24, 48, and 72 hours after transfection, and western blotting was used to determine the effect on MYO18A protein expression. Representative images **(B)** and quantitative analysis **(C)** of gap closure assay in HCT-116 cells. Forty-eight hours after the transfection of siRNA, the gap was created and monitored with a microscope every 12 hours. The red dotted lines indicate where the migration began. The total gap area created at 0 hours and gap closure areas at the indicated time points were quantified by ImageJ software. The migration activity, which was determined by the percentage of gap closure area, was compared between cells transfected with the scramble and *MYO18A* siRNA. Each value represents the mean +/- SEM from at least three independent experiments in each group. ***p < 0.01.

learning model for recurrence-risk prediction and identification of potential therapeutic targets for CRC. Importantly, we designed different treatment strategies for different risk subgroups of CRC patients. Our results highlight the following important points: (i) The sequential oncogenic and tumor suppression genetic alterations were found during tumor evolution. (ii) We identified a fourteen genes panel that could predict the risk of recurrence in stage III CRC. (iii) Three genes, including *MYO18A* in the founding clone, *FBXW7*, and *ATM* in the dominant subclone, affected the prognosis. (iv) MYO18A plays an important role in the migration of human CRC cells. These findings suggest that the integration of genomic data and cancer evolution models provides insights into disease biology. These results could be applied for the recurrence-risk classification of stage III CRC and the development of novel therapeutic strategies.

The ability to predict the future behavior of individual cancers is crucial for precision cancer medicine. Considering that traditional methods might hinder the efficacy of rare somatic selection, we established a more comprehensive pipeline by the cancer evolution model for treatment strategy analysis. First, we selected rare somatic mutations that were not detected by traditional methods. To target intratumor heterogeneity and cancer evolution somatic mutations to overcome chemotherapy resistance, we used the evolution model. We supposed that founding clone and dominant clones (the most estimated prevalence) are the significant events for cancer recurrence, which was confirmed by the probability of random two subclone sampling (**Supplementary Figure 5**). Finally, for robust optimization, the different machine learning algorithms and statistical methods were selected for cancer recurrence-risk prediction and survival stratification models.

In the CRC multistage progression model, the adenoma-carcinoma sequence refers to a stepwise pattern of mutational activation of oncogenes and inactivation of tumor suppressor genes. In our cancer evolution model, we provide information about genetic changes in cancer-driving metastasis. In the early stages, mutations in the oncogenic pathway, such as the receptor kinase signaling (RTK) pathway, the fibroblast growth factor receptor (FGFR) signaling pathway, and the transforming growth factor-beta (TGFB) signaling pathway, appear to be the first step. Second, mutations in *TP53*, *FBXW7*, and *APC* may play a role in cancer evolution. Sequential oncogenic and tumor suppression genetic alterations were consistent with the hypothesis of cancer two-hit theory.

Classification and decision systems in data analysis are mostly based on accuracy. In our study, we trade off accuracy, precision, and recall for useful optimization in a multiple machine learning model. We selected the 14 genetic variants for cancer recurrence prediction. The variant distribution and frequency in cancer patients with or without recurrence are shown in **Figure 4**. There are 11 genetic variants in the funding clone and three genetic variants in the dominant subclone. This study implies a robust optimization cancer panel for recurrence prediction. We have developed a genomic-machine learning model and pipeline software for CRC recurrence-risk prediction.

Figure 5A shows the 5-year DFS of this CRC cohort. The 5-year disease-free survival rate is approximately 70%, which has reached the benchmark of a worldwide standard. In addition to modeling for recurrence prediction, we need to improve care survival by different treatment strategies. Using the three machine learning models, we can classify the CRC subgroup by three genetic variants. Group 1 and group 2 have a poor prognosis. The progression-free survival of Group 4 was better than that of group 3. This successful study identified associations between three genetic markers and survival subgroup and recurrence status. The uniqueness of this study is that the evolution model shows the clinical impact on stage III colorectal cancer by the machine learning method utilizing the comprehensive clinical and genomic information. However, the major limitation of this study is the small sample size. It is too early to make a strong conclusion at this stage in terms of the case number.

MYO18A and *FBXW7* intratumor heterogeneity variants are potential targets in the cancer evolution model. *MYO18A* is an unconventional myosin that has been implicated in multiple cellular processes. *MYO18A* has been involved as a cancer driver. Overexpression of *MYO18A* was observed in metastatic prostate cancer cell lines in a previous study (29, 30). Migration assay of various cancer cell lines also revealed that *MYO18A*-depleted cells had decreased cell motility (31, 32). By analyzing the clinical data, we found that patients without *MYO18A* mutation in the founding clone (F. MYO18A) had the worst DFS (**Figures 5B, C**). Moreover, the *in vitro* study showed knockdown of *MY018A* by siRNA caused a reduction in cell migration activity by 20–40% (**Figure 6**). These results imply that *MYO18A* is a potential tumor driver for cancer cell migration. The alteration of *MYO18A* was common in the founding clone (**Figure 3**). To conclude, the alteration of *MY018A* is a gain-of-function or loss-of-function mutation; further *in vitro* and *in vivo* investigations are needed to study the impact of *MYO18A* mutations on cell survival, proliferation, or angiogenesis. *FBXW7* is a critical tumor suppressor involved in the ubiquitin-proteasome system in human cancer. It has been demonstrated that metastatic CRC patients with *FBXW7* missense mutations show shorter overall survival compared with patients with wild-type *FBXW7* (33). The results are consistent with our data showing poor prognosis survival in the G1 and G2 groups.

In conclusion, this study highlights the importance of a cancer evolution model in the development of new therapeutic strategies. The integration of genomics and machine learning could provide an opportunity to identify new targets for cancers.

DATA AVAILABILITY STATEMENT

The datasets presented in this study can be found in online repositories. The names of the repository/repositories and accession number(s) can be found below: NCBI BioProject (Accessions: PRJNA655796/PRJNA662159).

ETHICS STATEMENT

This study was approved by the institutional review board of NCKUH (A-ER-103-395 and A-ER-104-153) and conducted under the Declaration of Helsinki. All participants provided written informed consent.

AUTHOR CONTRIBUTIONS

Conception and study design: P-CL and M-RS. Development of methodology: P-CL, Y-MY, and M-RS. Acquisition of data: Y-MY, B-WL, S-CL, and P-CC. Statistical and computational analysis: P-CL, Y-MY, and M-RS. Writing, review, and/or revision of the manuscript: P-CL, Y-MY, B-WL, S-CL, R-HC, P-CC, and M-RS. Study supervision: M-RS. All authors contributed to the article and approved the submitted version.

FUNDING

This work was supported by the Ministry of Science and Technology (MOST 104-2320-B-006-015-MY3, MOST 107-2319-B-006-001 and MOST 108-2319-B-006-001 to M-RS), National Health Research Institutes (NHRI-108A1-CACO-02181811), the Ministry of Health Welfare (MOHW107-TDU-B-211-114018, MOHW108-TDU-B-211-124018), National Cheng Kung University and National Cheng Kung University Hospital, Taiwan.

ACKNOWLEDGMENTS

The authors gratefully acknowledge the significant contribution of Kimforest LTD Taiwan and CC Pan for the bioinformatics support.

SUPPLEMENTARY MATERIAL

The Supplementary Material for this article can be found online at: https://www.frontiersin.org/articles/10.3389/fonc.2020.588557/full#supplementary-material

REFERENCES

1. Siegel R, DeSantis C, Virgo K, Stein K, Mariotto A, Smith T, et al. Erratum: Cancer treatment and survivor statistics, 2012.*CA Cancer J Clin* (2012) 62 (4):220–41. doi: 10.3322/caac.21149
2. Kuebler JP, Wieand HS, O'Connell MJ, Smith RE, Colangelo LH, Yothers G, et al. Oxaliplatin combined with weekly bolus fluorouracil and leucovorin as surgical adjuvant chemotherapy for stage II and III colon cancer: Results from NSABP C-07. *J Clin Oncol* (2007) 25(16):2198–204. doi: 10.1200/JCO.2006.08.2974
3. Meric-Bernstam F, Brusco L, Kopetz S, Davies M, Routbort MJ, Piha-Paul SA, et al. 1 Feasibility of large-scale genomic testing to facilitate enrollment on genomically-matched clinical trials. *J Clin Oncol* (2015) 33(25):2753–62. doi: 10.1200/JCO.2014.60.4165
4. Le Tourneau C,, Delord J-P,, Gonçalves A,, Gavoille C,, Dubot C,, Isambert N,, et al. Molecularly targeted therapy based on tumour molecular profiling versus conventional therapy for advanced cancer (SHIVA): A multicentre, open-label, proof-of-concept, randomised, controlled phase 2 trial. *Lancet Oncol* (2015) 16(13):1324–34. doi: 10.1016/S1470-2045(15)00188-6
5. Marusyk A, Polyak K. Tumor heterogeneity: Causes and consequences. *Biochim Biophys Acta Rev Cancer* (2010) 1805(1):105–17. doi: 10.1016/j.bbcan.2009.11.002
6. Nowell PC. The clonal evolution of tumor cell populations. *Science* (1976) 194 (4260):23–8. doi: 10.1126/science.959840
7. Ding L, Ley TJ, Larson DE, Miller CA, Koboldt DC, Welch JS, et al. Clonal evolution in relapsed acute myeloid leukaemia revealed by whole-genome sequencing. *Nature* (2012) 481(7382):506–10. doi: 10.1038/nature10738
8. Gerlinger M, Rowan AJ, Horswell S, Larkin J, Endesfelder D, Gronroos E, et al. Intratumor heterogeneity and branched evolution revealed by multiregion sequencing. *N Engl J Med* (2012) 366(10):883–92. doi: 10.1056/NEJMoa1113205
9. Nik-Zainal S, VanLoo P, Wedge DC, Alexandrov LB, Greenman CD, Lau KW, et al. The life history of 21 breast cancers. *Cell* (2012) 149(5):994–1007. doi: 10.1016/j.cell.2012.04.023
10. Li H. [Heng Li - Compares BWA to other long read aligners like CUSHAW2] Aligning sequence reads, clone sequences and assembly contigs with BWA-MEM. *ArXiv* (2013) 1303.3997. doi: 10.6084/M9.FIGSHARE.963153.V1
11. Hovelson DH, McDaniel AS, Cani AK, Johnson B, Rhodes K, Williams PD, et al. Development and Validation of a Scalable Next-Generation Sequencing System for Assessing Relevant Somatic Variants in Solid Tumors. *Neoplasia* (2015) 17(4):385–99. doi: 10.1016/j.neo.2015.03.004
12. Wang K, Li M, Hakonarson H. ANNOVAR: Functional annotation of genetic variants from high-throughput sequencing data. *Nucleic Acids Res* (2010) 38 (16):e164. doi: 10.1093/nar/gkq603
13. Gerstung M, Beisel C, Rechsteiner M, Wild P, Schraml P, Moch H, et al. Reliable detection of subclonal single-nucleotide variants in tumour cell populations. *Nat Commun* (2012) 3:811. doi: 10.1038/ncomms1814
14. Miller CA, White BS, Dees ND, Griffith M, Welch JS, Griffith OL, et al. SciClone: Inferring Clonal Architecture and Tracking the Spatial and Temporal Patterns of Tumor Evolution. *PloS Comput Biol* (2014) 10(8): e1003665. doi: 10.1371/journal.pcbi.1003665
15. Dang HX, White BS, Foltz SM, Miller CA, Luo J, Fields RC, et al. ClonEvol: Clonal ordering and visualization in cancer sequencing. *Ann Oncol* (2017) 28 (12):3076–82. doi: 10.1093/annonc/mdx517
16. Croft D, Mundo AF, Haw R, Milacic M, Weiser J, Wu G, et al. The Reactome pathway knowledgebase. *Nucleic Acids Res* (2014) 42:D472–7. doi: 10.1093/nar/gkt1102
17. Tibshirani R. Regression Shrinkage and Selection Via the Lasso. *J R Stat Soc Ser B* (1996) 58:267–88. doi: 10.1111/j.2517-6161.1996.tb02080.x
18. Meyer D, Dimitriadou E, Hornik K, Weingessel A, Leisch F. Misc functions of the Department of Statistics (e1071), TU Wien. *R Packag Version 1.6-2* (2014).
19. Liaw A, Wiener M. Classification and Regression by random. *Forest R News* (2002) 2(3):18–22.
20. Chen T, Guestrin C. XGBoost: A scalable tree boosting system. *Proc ACM SIGKDD Int Conf Knowledge Discovery Data Min* (2016) 785–94. doi: 10.1145/2939672.2939785
21. Strobl C, Malley J, Tutz G. An Introduction to Recursive Partitioning: Rationale, Application, and Characteristics of Classification and Regression Trees, Bagging, and Random Forests. *Psychol Methods* (2009) 14:323–48. doi: 10.1037/a0016973
22. R Development Core Team R. *R: A Language and Environment for Statistical Computing* (2011). doi: 10.1007/978-3-540-74686-7
23. Hosmer DW, Lemeshow S, Sturdivant RX. *Applied Logistic Regression*, *3rd ed.* (2013). doi: 10.1002/9781118548387
24. Kuhn M. Building predictive models in R using the caret package. *J Stat Software* (2008) 28:1–26. doi: 10.18637/jss.v028.i05
25. Amirouchene-Angelozzi N, Swanton C, Bardelli A. Tumor evolution as a therapeutic target. *Cancer Discovery* (2017) 7:805–17. doi: 10.1158/2159-8290.CD-17-0343
26. Vogelstein B, Papadopoulos N, Velculescu VE, Zhou S, Diaz LA, Kinzler KW. Cancer genome landscapes. *Science* (2013) 340:1546–58. doi: 10.1126/science.1235122
27. Juric D, Castel P, Griffith M, Griffith OL, Won HH, Ellis H, et al. Convergent loss of PTEN leads to clinical resistance to a PI(3)Kα inhibitor. *Nature* (2015) 518:240–4. doi: 10.1038/nature13948
28. Rübben A, Araujo A. Cancer heterogeneity: Converting a limitation into a source of biologic information. *J Transl Med* (2017) 15. doi: 10.1186/s12967-017-1290-9
29. Buschman MD, Field SJ. MYO18A: An unusual myosin. *Adv Biol Regul* (2018) 67:84–92. doi: 10.1016/j.jbior.2017.09.005
30. Makowska KAA, Hughes REE, White KJJ, Wells CMM, Peckham M. Specific Myosins Control Actin Organization, Cell Morphology, and Migration in Prostate Cancer Cells. *Cell Rep* (2015) 13:2118–25. doi: 10.1016/j.celrep.2015.11.012
31. Hsu RM, Tsai MH, Hsieh YJ, Lyu PC, Yu JS. Identification of MYO18A as a novel interacting partner of the PAK2/βPIX/GIT1 complex and its potential function in modulating epithelial cell migration. *Mol Biol Cell* (2010) 21:287–301. doi: 10.1091/mbc.E09-03-0232
32. Xing M, Peterman MC, Davis RL, Oegema K, Shiau AK, Field SJ. GOLPH3 drives cell migration by promoting Golgi reorientation and directional trafficking to the leading edge. *Mol Biol Cell* (2016) 27:3828–40. doi: 10.1091/mbc.E16-01-0005
33. Korphaisarn K, Morris VK, Overman MJ, Fogelman DR, Kee BK, Raghav KPS, et al. FBXW7 missense mutation: A novel negative prognostic factor in metastatic colorectal adenocarcinoma. *Oncotarget* (2017) 8:39268–79. doi: 10.18632/oncotarget.16848

Conflict of Interest: The authors declare that the research was conducted in the absence of any commercial or financial relationships that could be construed as a potential conflict of interest.

frontiers in Oncology

ORIGINAL RESEARCH
published: 30 October 2020
doi: 10.3389/fonc.2020.535985

Biomarker Discovery for the Carcinogenic Heterogeneity Between Colon and Rectal Cancers Based on lncRNA-Associated ceRNA Network Analysis

Xin Qi[1,2†], *Yuxin Lin*[2,3†], *Xingyun Liu*[2,4], *Jiajia Chen*[1] *and Bairong Shen*[4*]

[1] School of Chemistry and Life Sciences, Suzhou University of Science and Technology, Suzhou, China, [2] Center for Systems Biology, Soochow University, Suzhou, China, [3] Department of Urology, The First Affiliated Hospital of Soochow University, Suzhou, China, [4] Institutes for Systems Genetics, West China Hospital, Sichuan University, Chengdu, China

Background: Colorectal cancer (CRC) is one of the leading causes of cancer death worldwide. Emerging evidence has revealed that risk factors and metastatic patterns differ greatly between colon and rectal cancers. However, the molecular mechanism underlying their pathogenic differences remains unclear. Therefore, we here aimed to identify non-coding RNA biomarkers based on lncRNA-associated ceRNA network (LceNET) to elucidate the carcinogenic heterogeneity between colon and rectal cancers.

Methods: A global LceNET in human was constructed by employing experimental evidence-based miRNA-mRNA and miRNA-lncRNA interactions. Then, four context-specific ceRNA networks related to cancer initiation and metastasis were extracted by mapping differentially expressed lncRNAs, miRNAs and mRNAs to the global LceNET. Notably, a novel network-based bioinformatics model was proposed and applied to identify lncRNA/miRNA biomarkers and critical ceRNA triplets for understanding the carcinogenic heterogeneity between colon and rectal cancers. Moreover, the identified biomarkers were further validated by their diagnostic/prognostic performance, expression pattern and correlation analysis.

Results: Based on network modeling, lncRNA KCNQ1OT1 (AUC>0.85) and SNHG1 (AUC>0.94) were unveiled as common diagnostic biomarkers for the initiation and metastasis of colon and rectal cancers. qRT-PCR analysis uncovered that these lncRNAs had significantly higher expression level in CRC cell lines with high metastatic potential. In particular, KCNQ1OT1 and SNHG1 function in colon and rectal cancers *via* different ceRNA mechanisms. For example, KCNQ1OT1/miR-484/ANKRD36 axis was involved in the initiation of colon cancer, while KCNQ1OT1/miR-181a-5p/PCGF2 axis was implicated in the metastasis of rectal cancer; the SNHG1/miR-484/ORC6 axis played a role in colon cancer, while SNHG1/miR-423-5p/EZH2 and SNHG1/let-7b-5p/ATP6V1F axes participated in the initiation and metastasis of rectal cancer, respectively. In these ceRNA triplets, miR-484, miR-181a-5p, miR-423-5p and let-7b-5p were identified as

OPEN ACCESS

Edited by:
Marco Mina,
Sophia Genetics, Switzerland

Reviewed by:
Jiheng Xu,
New York University, United States
Yongsheng Kevin Li,
Hainan Medical University, China

****Correspondence:***
Bairong Shen
bairong.shen@scu.edu.cn

[†]These authors have contributed equally to this work

Specialty section:
This article was submitted to Cancer Genetics, a section of the journal Frontiers in Oncology

Received: *19 February 2020*
Accepted: *05 October 2020*
Published: *30 October 2020*

Citation:
Qi X, Lin Y, Liu X, Chen J and Shen B (2020) Biomarker Discovery for the Carcinogenic Heterogeneity Between Colon and Rectal Cancers Based on lncRNA-Associated ceRNA Network Analysis. Front. Oncol. 10:535985. doi: 10.3389/fonc.2020.535985

miRNA biomarkers with excellent distinguishing ability between normal and tumor tissues, and ANKRD36, PCGF2, EZH2 and ATP6V1F were closely related to the prognosis of corresponding cancer.

Conclusion: The landscape of lncRNA-associated ceRNA network not only facilitates the exploration of non-coding RNA biomarkers, but also provides deep insights into the oncogenetic heterogeneity between colon and rectal cancers, thereby contributing to the optimization of diagnostic and therapeutic strategies of CRC.

Keywords: cancer heterogeneity, lncRNA biomarker, miRNA biomarker, ceRNA network, colon and rectal cancers, initiation and metastasis

INTRODUCTION

Colorectal cancer (CRC) is one of the most commonly diagnosed malignant tumors with high prevalence and mortality rates worldwide. Tumor progression and distant metastasis are the major lethal factors for CRC patients, leading to 5-year survival rate less than 10% (1). Moreover, anatomical distinction between colon cancer and rectal cancer was closely related to patient morbidity, risk factor, therapeutic strategies, and especially may have an impact on prognosis (2–4). Therefore, systematically illuminating the molecular mechanisms and discovering predictive biomarkers specific respectively to colon and rectal cancers are in urgent need for the diagnosis and treatment of CRC.

Recent advances in high-throughput sequencing technology have uncovered that there is a tremendous number of RNAs without protein-coding potential, defined as non-coding RNAs (ncRNAs) (5). For example, microRNAs (miRNAs) are a class of well-characterized ncRNAs that post-transcriptionally regulate target gene expression through complementary pairing (6–8); long non-coding RNAs (lncRNAs) are a class of recently discovered ncRNAs longer than 200 nucleotides with emerging roles in diverse cancer-related processes, e.g., proliferation, invasion, metastasis, and metabolism (9, 10). Owing to the huge potential in regulating gene expression, considerable effort has been made to decode how ncRNAs exert functions in cancer-related biological processes. Salmena etal. (11) proposed a ceRNA (competing endogenous RNA) hypothesis, which states that RNA transcripts sharing common miRNA response elements (MREs), e.g. lncRNAs, pseudogenes, circular RNAs and competing mRNAs, can compete for miRNA binding and thereby reciprocally modulate each other's expression. Increasing evidence has supported that miRNA-mediated ceRNA crosstalk is widely involved in the pathogenesis of multiple cancers (12), representing a novel layer of post-transcriptional gene regulation. Notably, mounting evidence has demonstrated that lncRNAs could act as oncogenic or tumor-suppressive genes in the initiation and progression of CRC through a ceRNA mechanism. For example, lncRNA SNHG7 was found to be significantly over-expressed in CRC. It accelerates tumor proliferation and metastasis by serving as a miR-216b-mediated ceRNA of GALNT1 (13). Thus, lncRNAs represent promising diagnostic biomarkers and therapeutic targets for CRC, thereby becoming the research hotspot among the ceRNA family.

As the perturbation of pivotal RNA abundance in the ceRNA network could lead to cancer initiation and/or progression, a growing number of researchers have made great effort to identify the lncRNA biomarkers in specific cancer *via* constructing lncRNA-associated ceRNA network (LceNET) (14, 15). Notably, the lnCeDB database providing a collection of human lncRNAs that potentially function as ceRNA was built in 2014 (16). However, it has not been updated continuously, resulting in inconsistency of lncRNA ID version between lnCeDB and TCGA database, which is a widely utilized pool of high-throughput cancer datasets. Those facts revealed that, optimizing the method of constructing ceRNA network and systematically evaluating lncRNA biomarkers that act as ceRNA are urgently needed to explore the molecular distinction in the pathogenesis of cancers.

In this study, we focused on comparatively decoding molecular mechanism underlying the initiation and metastasis of colon and rectal cancers through a ceRNA network manner. To facilitate the investigation of context-specific ceRNA crosstalk, we firstly constructed a global LceNET in human and applied a computational approach to identify lncRNA/miRNA biomarkers through constructing LceNETs implicated in the initiation and metastasis of colon and rectal cancers. Moreover, key lncRNA-miRNA-mRNA interactions associated with pathogenesis were identified in colon and rectal cancers, respectively. The pipeline of the present study was shown in **Figure 1**. Thus, systematically identifying and comparing lncRNA biomarkers acting as ceRNAs, could contribute to elucidate the similarities and differences of the molecular mechanisms between colon and rectal cancers, thereby providing valuable clues for CRC therapy.

MATERIALS AND METHODS

TCGA Data Collection

To explore ceRNA biomarkers associated with colorectal carcinogenesis, the level 3 RNA-Seq gene expression data, miRNA-seq data and clinical data of 459 colon cancer patients and 171 rectal cancer patients were retrieved from TCGA-COAD and TCGA-READ database (up to March 26, 2019),

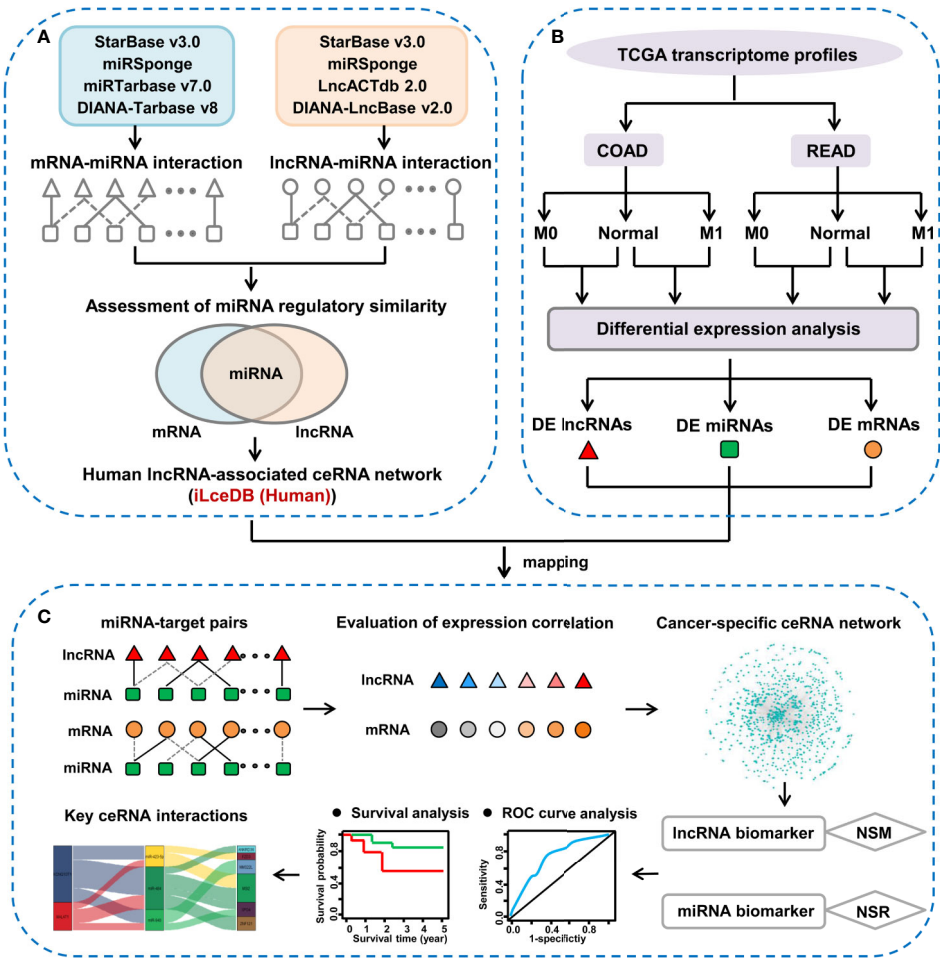

FIGURE 1 | The integrative pipeline for ceRNA network construction and characterization. **(A)** Construction of lncRNA-associated ceRNA network in human. **(B)** Identification of lncRNAs, miRNAs and mRNAs with differential expression pattern between colon/rectal cancers and corresponding normal tissues. **(C)** Discovery of key ceRNA interactions based on context-specific LceNET network.

respectively. According to the tumor-node-metastasis (TNM) staging system of colorectal cancer, patients were divided into without distant metastasis (M0) or with distant metastasis (M1) subgroups. As adenocarcinoma is the most common histotype accounting for 90% of CRC cases (17), only adenocarcinoma cases with matched RNA-seq and miRNA-seq data were retained for subsequent analyses. The sample number of each group was shown in the **Supplementary Figure 1**. The study was performed according to the TCGA guidelines.

Construction of the Global LceNET in Human

Based on "ceRNA hypothesis" (11), the lncRNA-associated competing triplets consist of miRNA-lncRNA and miRNA-mRNA interactions sharing at least one common miRNA. Therefore, identifying miRNA-target interactions is a prerequisite to recognize lncRNA-related ceRNA triplet. Accordingly, the global lncRNA-associated ceRNA network in human was constructed by the following two steps.

First, high-confidence miRNA-target interactions supported by low-/high-throughput experiments were collected and integrated. The experimentally verified miRNA-mRNA pairs were downloaded from starBase v3.0 (18), DIANA-Tarbase v8 (19), miRTarbase (v7.0) (20) and miRSponge (21) databases, while the experimentally validated miRNA-lncRNA pairs were extracted from starBase v3.0 (18), LncACTdb2.0 (22), DIANA-LncBase Experimental v.2 (23) and miRSponge (21) databases. Importantly, considering the unprecedented utility of TCGA database for data mining across cancers, lncRNAs were converted to be consistent with the annotation file of TCGA dataset (GENCODE v22). By integrating the interactions among above corresponding databases and removing redundant relationships, 718,708 miRNA-mRNA pairs and 29,373 miRNA-lncRNA pairs were finally obtained.

Second, to further identify competing lncRNA-mRNA interactions, a hypergeometric test was performed to evaluate the significance of shared common miRNAs between each lncRNA-mRNA pairs. The *P* was calculated as follows:

$$P = 1 - \sum_{i=0}^{x-1} \frac{\binom{N_{lnc}}{i}\binom{N_T - N_{lnc}}{N_{mRNA} - i}}{\binom{N_T}{N_{mRNA}}}$$

where N_T represents the total number of miRNAs in human genome, N_{lnc} and N_{mRNA} represent the total number of miRNAs that regulate lncRNA and mRNA, respectively, and x is the number of miRNAs shared by lncRNA and mRNA. The P was subject to Benjamini-Hochberg correction. The lncRNA-mRNA competing pairs with adj.P<0.01 were selected as significant pairs. Finally, 20,888,725 lncRNA-miRNA-mRNA pairs were selected as ceRNA interactions.

Identification of Differentially Expressed lncRNAs, miRNAs, and mRNAs

To keep consistent with gene annotations in TCGA, lncRNAs and mRNAs in RNA-Seq expression data were firstly identified and annotated by using GENCODE database (v22) (24), respectively. Meanwhile, the accession number of miRNAs in miRNA-Seq data were converted into miRNA official symbol referring to miRBase database (v21) (25). RNAs which cannot be converted into gene symbol were excluded. Then, the count data were analyzed using edgeR package (26) to identify differentially expressed lncRNAs, mRNAs and miRNAs between normal and M0/M1 tissues. lncRNAs/mRNAs/miRNAs that sufficiently expressed (count per million (CPM) > 1) in at least 80% samples were kept in the differential expression analysis. Then, the lncRNAs/mRNAs/miRNAs were considered significantly differentially expressed based on the following criteria: $|\log_2$ (fold change)| >=1 and false discovery rate (FDR) <0.05.

Reconstruction of Context-Specific ceRNA Networks for Cancer Initiation and Metastasis

Based on "ceRNA hypothesis", a two-step approach was employed to build context-specific LceNETs. First, the differentially expressed lncRNAs, miRNAs and mRNAs in each group were separately mapped to the global lncRNA-associated ceRNA network to extract context-specific ceRNA networks. Second, expression correlation between lncRNA and mRNA in a candidate ceRNA triplet was evaluated by Pearson correlation coefficient using matched expression profiles. lncRNA-mRNA pairs with R>0.5 and P<0.05 were selected as significantly positively correlated interactions, which were then used to construct LceNETs visualized by Cytoscape (v3.6.1) (27). Hub nodes were defined as the top 5% of highest degree nodes in the context-specific LceNET.

KEGG Pathway Enrichment Analysis of Differentially Expressed mRNAs

To investigate the function of the identified differentially expressed mRNAs, KEGG pathway enrichment analysis was performed using "ClusterProfiler" package (28) in R. Adjusted P < 0.05 (Benjamini-Hochberg method) was used as the cut-off for selecting statistically significant KEGG terms. The top five pathways were shown by Circos plots using "GOplot" (29) and "ggplot2" packages in R.

Bioinformatics Model for lncRNA/miRNA Biomarker Screening

As reported previously, the strength of competitive interaction between lncRNA and mRNA is closely related to the number of common miRNAs shared by two RNA molecules (30). Accordingly, in this study a novel bioinformatics model was applied to screen candidate lncRNA and miRNA biomarkers for colon and rectal cancer. In the model, the NSM measurement was defined to detect the ability of a lncRNA in competitively binding miRNAs in the context-specific ceRNA network. lncRNAs with significantly higher NSM value (P<0.05, Wilcoxon signed-rank test) in initiation or metastasis-associated LceNETs were recognized as lncRNA biomarkers. As highlighted in our previous research, the regulatory power of a miRNA can be evaluated by NSR parameter, *i.e.*, the number of single-line regulated-RNAs, since the single-line regulatory site is vulnerable in the network (8). Evidences indicated that miRNAs with high NSR values are likely to be biomarkers (31). Here, we applied NSR in lncRNA-miRNA-mRNA triple network to identify key miRNAs. Those miRNAs with significantly higher NSR value (NSR > average of NSRs and P<0.05, Wilcoxon signed-rank test) in initiation or metastasis-associated ceRNA network were recognized as miRNA biomarkers. In the next step, key lncRNA-miRNA-mRNA triplet biomarkers were screened by assessing each component's function as follows: 1) lncRNA and miRNA were the identified biomarker, respectively; 2) mRNAs were reported as tumor-associated genes (TAGs) or related to the prognosis of colon/rectal cancer. The lncRNA-miRNA-mRNA interactions were visualized by "ggalluvial" package in R.

ROC Curve Analysis

To evaluate the sensitivity and specificity of the identified lncRNA and miRNA biomarkers for distinguishing between normal and cancer tissues, ROC curve analyses were conducted and the AUC were calculated using the 'ROCR' package (32) in R.

Survival Analysis

To assess the prognostic value of lncRNA/miRNA biomarkers and key mRNAs, patients were divided into high-expression and low-expression groups using the criteria from OncoLnc (http://www.oncolnc.org/) (33). Then, Kaplan-Meier survival analyses were carried out to evaluate the differences in OS times between high-expression and low-expression groups using the "survival" and "survminer" packages in R, and the log-rank test was employed to calculate the statistical significance of the KM survival curves (P < 0.05).

Cell Lines and Culture Condition

CRC cell lines HCT116, SW480, HT29, Lovo and SW620 were obtained from the laboratory of professor Yufeng Xie at the First Affiliated Hospital of Soochow University, and human normal

colon mucosal epithelial cell line NCM 460 was purchased from the cell bank of Chinese Academy of Sciences. Cells were cultured in RPMI-1640 medium (HyClone) supplemented with 10% fetal bovine serum (Gibco) at 37°C with 5% CO_2.

Quantitative Real-Time Polymerase Chain Reaction (qRT-PCR)

Total RNA was isolated from cultured cells using miRNeasy Mini Kit (Qiagen, Germany) and converted into complementary DNA using 5× All-In-One RT MasterMix (abm, Canada). qRT-PCR was performed in triplicate for each sample using BrightGreen 2× qPCR MasterMix (abm, Canada) and a LightCycler 96 Real-Time PCR detection system (Roche, USA) according to the manufacturer's instructions. For qRT-PCR, KCNQ1OT1 primers (Sangon Biotech, China) were: 5'-TGCAGAAGACA GGACACTGG-3' (sense) and 5'-CTTTGGTGGGAAA GGACAGA-3' (antisense); SNHG1 primers (Sangon Biotech, China) were: 5'-GCCAGCACCTTCTCTCTAAAGC-3' (sense) and 5'- GTCCTCCAAGACAGATTCCATTTT-3' (antisense); GAPDH primers (Sangon Biotech, China) were: 5'-GCATC CTGGGCTACACTG-3' (sense) and 5'-TGGTCGTTGA GGGCAAT-3' (antisense). The $2^{-\triangle\triangle Ct}$ method was used to calculate the relative gene expression levels of KCNQ1OT1 and SNHG1, which were normalized to the corresponding *GAPDH* mRNA levels.

RESULTS

Construction of the Global lncRNA-Associated ceRNA Network (LceNET) in Human

To facilitate exploring lncRNA-associated competing interactions in cancers, we employed a computational method to uncover genome-wide ceRNA cross-talk in human. Notably, factors including the experiment-supported miRNA-target pairs, the consistency of lncRNA names between ceRNA network and TCGA database, and the miRNA regulatory similarity were considered (see the *Materials and Methods* section). Based on the identified ceRNA interaction triplets, the global LceNET composed by 3,102 lncRNAs, 1,085 miRNAs and 16,490 mRNAs was constructed in human.

Characterization of Differentially Expressed RNAs in Colon and Rectal Cancers

To systematically elucidate the molecular distinction in the carcinogenesis of colon and rectal cancers, patient samples were divided into without distant metastasis (M0) and with distant metastasis (M1) subgroups from TCGA-COAD and TCGA-READ databases, respectively. We then explored the differential expression profiles of lncRNAs, miRNAs and mRNAs in the four comparable groups, including M0 vs. normal in colon cancer (colon M0/N), M1 vs. normal in colon cancer (colon M1/N), M0 vs. normal in rectal cancer (rectal M0/N) and M1 vs. normal in rectal cancer (rectal M1/N). The number of differentially expressed RNAs (DERNAs) in each comparable group was shown in **Supplementary Table 1-3**. Notably, 271 lncRNAs, 198 miRNAs and 980 mRNAs were identified as common DERNAs in all of the four comparable groups (**Figure 2A**).

To gain insights into the different biological features implicated with colon and rectal carcinogenesis, functional enrichment analysis was respectively performed for differentially expressed mRNAs (DEmRNAs) identified in the above four comparable groups. As shown in **Figures 2B, C**, DEmRNAs identified in colon M0/N and M1/N groups were significantly enriched in diverse critical biological pathways, e.g. "cell cycle", "protein digestion and absorption", "p53 signaling pathway" and "PPAR signaling pathway", revealing their essential roles in tumorigenesis of colon cancer. Comparatively, DEmRNAs in rectal M0/N and M1/N groups were primarily implicated in the well-characterized colorectal cancer-associated pathways including "cGMP-PKG signaling pathway", "proteoglycans in cancer", and "vascular smooth muscle contraction" (**Figures 2D, E**). For example, PKG is a promising therapeutic target for metastatic colorectal cancer (34); activating cGMP-PKG signaling pathway could suppress tumor growth by inhibiting Wnt/β-Catenin signaling in colon cancer (35). Notably, DEmRNAs in rectal M0/N and M1/N groups were also significantly enriched in "oxytocin signaling pathway" (**Figures 2D, E**), which exhibits emerging potential links with cancer, but has not been demonstrated to be associated with colorectal cancer previously.

Dynamical Competitive Interactions Between lncRNAs and mRNAs During the Initiation and Metastasis of Colon and Rectal Cancers

As ceRNA network tightly links the roles of miRNAs with that of coding and non-coding RNAs sharing common MREs, investigating miRNA-mediated ceRNA crosstalk can contribute to elucidate their biological functions in carcinogenesis. Therefore, we set out to establish context-specific LceNETs by extracting lncRNA-miRNA-mRNA interactions through mapping DERNAs from colon M0/N, colon M1/N, rectal M0/N and rectal M1/N groups into the global human LceNETs, respectively.

Based on the ceRNA theory, ceRNA triplets consisting of positively correlated lncRNA-mRNA competing pairs were selected. As shown in **Figure 3A**, most of the ceRNA nodes in each LceNET were interconnected and they could cross-talk with each other through shared miRNAs, indicating complex and robust regulatory relationship. Thus, perturbation in key ceRNA interactions may affect the stability of the entire LceNETs. Notably, the sizes of LceNETs associated with metastasis (LceNETs_colon_M1/N and LceNETs_rectal_M1/N) were relatively larger than that implicated with occurrence (LceNETs_colon_M0/N and LceNETs_rectal_M0/N), indicating the complexity of tumor metastasis. In particular, 350 ceRNA interactions were shared by the four networks, suggesting that certain lncRNAs and mRNAs tend to serve as

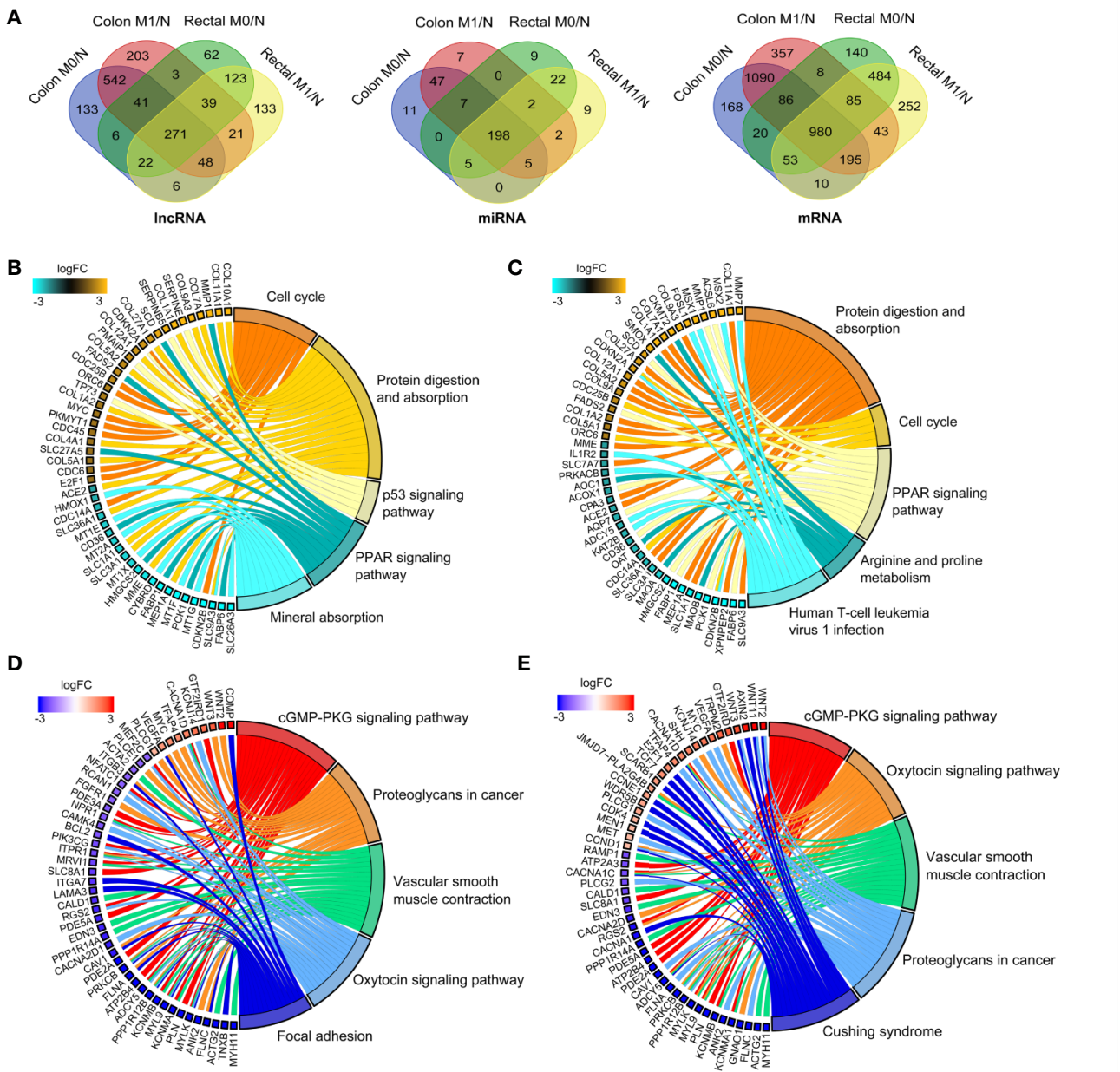

FIGURE 2 | Global landscape of differentially expressed RNAs in colon and rectal cancers. **(A)** Venn diagrams showing the overlapping differentially expressed lncRNAs (left), miRNAs (middle) and mRNAs (right) among colon M0/N, colon M1/N, rectal M0/N and rectal M1/N groups. **(B-E)** The top five significantly enriched KEGG pathways and related genes in colon M0/N **(B)**, colon M1/N **(C)**, rectal M0/N **(D)** and rectal M1/N **(E)** groups, respectively. M0 represents patients without distant metastasis; M1 represents patients with distant metastasis; N represents normal paracancerous tissue.

common ceRNAs that regulate the occurrence and metastasis of colon cancer as well as that of rectal cancer (**Supplementary Figure 2**). Besides, it has been shown that various lncRNAs such as MIR22HG and LINC01600 play an important role in colorectal cancer (36, 37). Here, we found that MIR22HG could serve as a ceRNA by sponging miR-25-3p or miR-425-5p in the occurrence and metastasis processes of rectal cancer rather than colon cancer, suggesting its distinct roles in the two cancer types.

Next, topological analysis showed that the degree distribution of nodes in the four LceNETs closely followed a power law distribution with $R^2 > 0.87$ (**Figure 3B**), indicating LceNETs were scale-free networks rather than randomly connected networks. As hub nodes with top degree in biological network tend to possess critical function, we investigated the lncRNAs acting as hub nodes in the four LceNETs, respectively. As shown in **Supplementary Table 4**, KCNQ1OT1 and SNHG1 possessed hub nodes properties in all of the four context-specific ceRNA

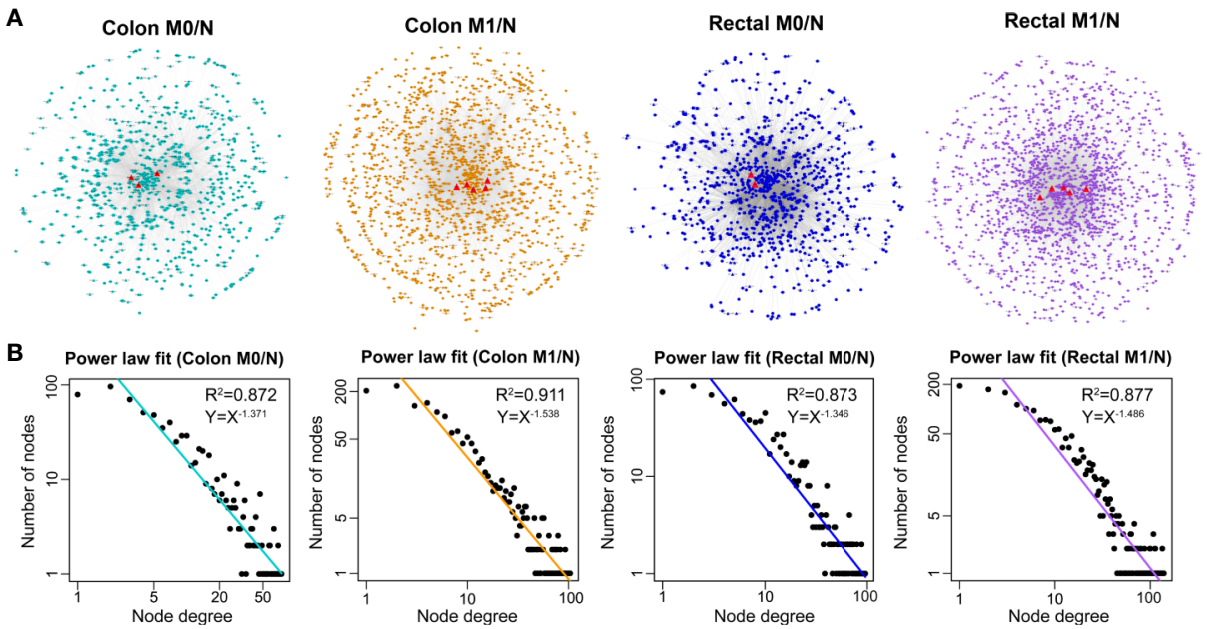

FIGURE 3 | The global view **(A)** and node degree distribution **(B)** of the four context-specific LceNETs. The identified lncRNA biomarkers were highlighted by red triangle. M0 represents patients without distant metastasis; M1 represents patients with distant metastasis; N represents paracancerous normal tissue.

networks, implying significant potential in regulating colorectal carcinogenesis.

Diagnostic and Prognostic Significance of LceNET-Driven lncRNA Biomarkers Implicated in the Carcinogenesis of Colon and Rectal Cancers

Cancer is a complicated disease with perturbation of various molecular interactions; hence, identifying biomarkers based on systems-guided ceRNA network is urgently needed to provide more reliable and effective signatures for cancer diagnosis and treatment. Here, a computational approach, in which the potential of lncRNA acting as a ceRNA was evaluated by the number of shared miRNAs (NSM), was developed to explore lncRNA biomarkers involved in the initiation and metastasis of colon and rectal cancers based on context-specific LceNETs. As shown in **Figure 4A**, lncRNA biomarkers possessed significantly higher NSM values compared with all lncRNAs in the corresponding context-specific LceNETs. Furthermore, the sensitivity and specificity of lncRNA biomarkers in diagnosing cancer patients without or with distant metastasis were evaluated by receiver operating characteristic (ROC) curve analyses. As shown in **Figures 4B, C**, area under curve (AUC) values of lncRNA biomarkers ranged from 0.75 to 0.97 in distinguishing normal and tumor without distant metastasis, and were more than 0.82 in distinguishing normal and tumor with distant metastasis, revealing superior diagnostic performance.

Notably, lncRNA KCNQ1OT1 and SNHG1 were identified as common biomarkers in colon M0/N, colon M1/N, rectal M0/N and rectal M1/N groups, indicating their critical roles in the carcinogenesis of both colon and rectal cancers; lncRNA MALAT1 was recognized as biomarkers in colon M0/N and colon M1/N groups, suggesting its specific functions in diagnosing colon cancer rather than rectal cancer. Furthermore, lncRNA ZFAS1 was characterized as specific biomarkers in colon M1/N and rectal M1/N groups, indicating it can be used to identify CRC patients with distant metastasis (**Table 1**). To further investigate lncRNA biomarkers playing important roles in cancer prognosis, Kaplan-Meier survival analysis of colon or rectal patients with relatively high or low expression levels of those biomarker were performed, respectively. Strikingly, MALAT1 and KCNQ1OT1 were significantly associated with overall survival (OS) times of colon cancer patients (**Figure 4D**), while lncRNA biomarkers identified in rectal M0/N or M1/N groups were not related to patients prognosis, suggesting they may participate in the regulation of prognosis through other mechanisms.

As lncRNAs KCNQ1OT1 and SNHG1 exhibited high potential in diagnosing patients with colon cancer or rectal cancer, we further validated their experimental gene expression pattern and diagnostic performance *via* published GEO datasets including GSE21510, GSE23878, and GSE9348. Notably, both of KCNQ1OT1 and SNHG1 were significantly up-regulated in tumor tissues (**Figures 5A, B**) and possessed excellent ability in distinguishing colorectal cancer patients (**Figure 5C**). Consistently, the expression levels of KCNQ1OT1 and SNHG1 were significantly higher in CRC cell lines than that in the normal colonic epithelial cell line NCM460 (**Figure 5E**). Moreover, both of the results from CCLE (Cancer Cell Line Encyclopedia) database and qRT-PCR analysis showed that KCNQ1OT1 and SNHG1 had significantly higher expression

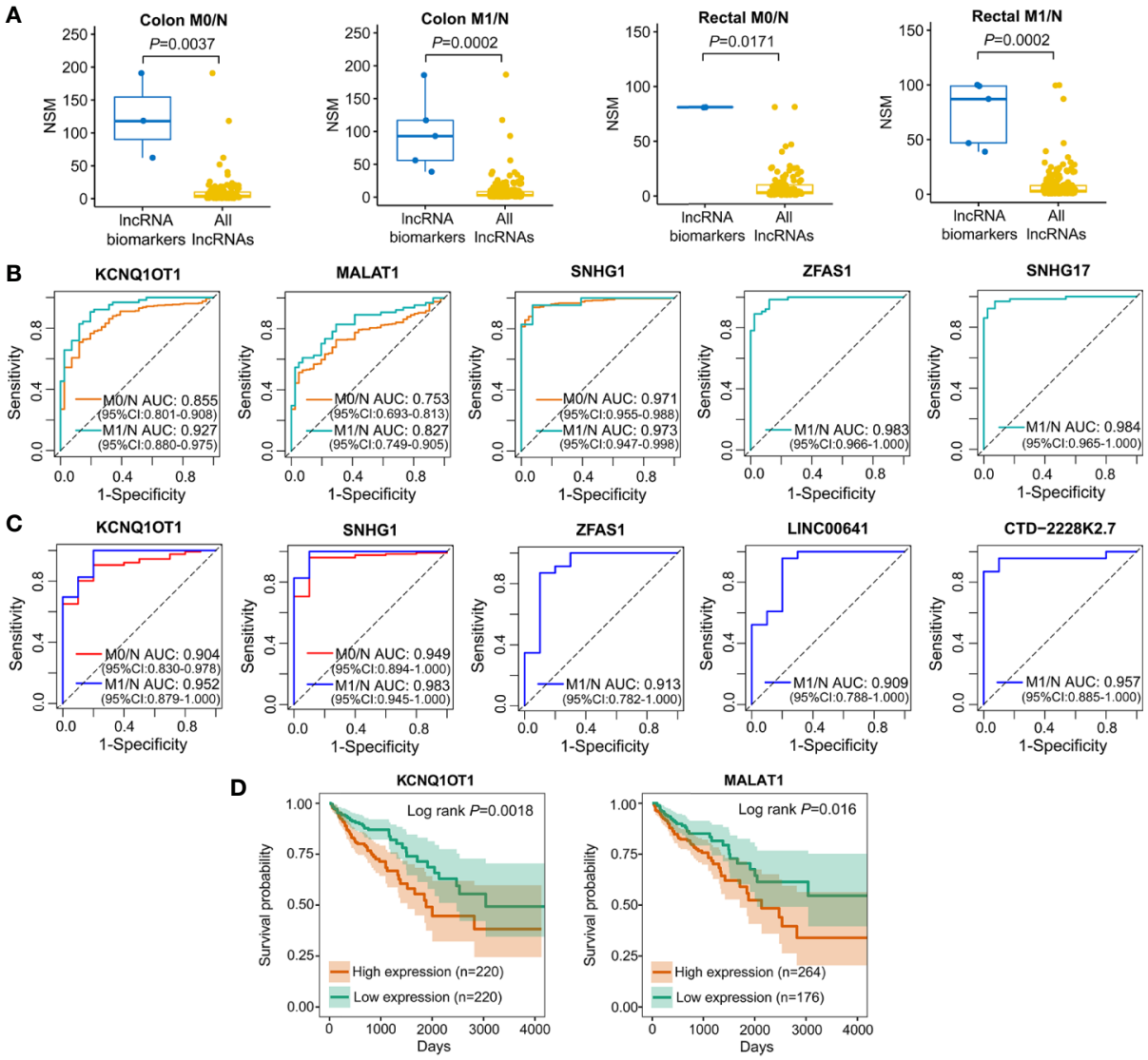

FIGURE 4 | Characterization of lncRNA biomarkers in the initiation and metastasis of colon and rectal cancers. **(A)** NSM distribution of the identified lncRNA biomarkers and all lncRNAs in context-specific ceRNA network. Statistical significance was calculated using the Wilcoxon rank-sum test. **(B, C)** ROC curve analysis was carried out to evaluate the predictive role of lncRNA biomarkers for colon cancer **(B)** and rectal cancer **(C)** in TCGA datasets. **(D)** Kaplan-Meier survival analysis of lncRNA biomarkers that significantly associated with overall survival in colon cancer (n=440) by OncoLnc.

level in CRC cell lines with high metastatic potential (e.g. SW620) than that with low metastatic potential (e.g. SW480) (**Figures 5D, E**), implying their roles in promoting CRC metastasis.

Characterization of miRNA Biomarkers Identified in LceNETs Indicating the Carcinogenesis of Colon and Rectal Cancers

Increasing evidence has demonstrated that multiple miRNAs can be used as biomarkers to guide decision on cancer diagnosis and therapy. We employed single-regulatory theory that consider single-line regulated miRNA-target interactions as the vulnerable structure for biological networks, to identify miRNA biomarkers in ceRNA triplet networks for the first time (**Supplementary Table 5**). As shown in **Figure 6A**, miRNA biomarkers possessed significantly higher number of single-line regulation (NSR) values compared with all miRNAs in the corresponding context-specific LceNETs ($P < 0.05$, Wilcoxon rank sum test). Strikingly, miR-27a-3p, miR-24-3p and miR-19b-3p were identified in all of colon M0/N, colon M1/N, rectal M0/N and rectal M1/N groups (**Supplementary Figure 3**), indicating their widely predictive roles in diagnosing colon and rectal cancers.

The different expression level of miRNA biomarkers between tumor and normal tissues could be clearly observed from the

TABLE 1 | lncRNA biomarkers involved in the carcinogenesis of colon and/or rectal cancers.

Groups	lncRNA biomarker
Colon M0/N	MALAT1, KCNQ1OT1 and SNHG1
Colon M1/N	MALAT1, KCNQ1OT1, SNHG1, ZFAS1 and SNHG17
Rectal M0/N	KCNQ1OT1 and SNHG1
Rectal M1/N	KCNQ1OT1, CTD-2228K2.7, SNHG1, ZFAS1 and LINC00641

heatmaps (**Figure 6B**). Moreover, their excellent distinguishing ability between normal and tumor without or with distant metastasis was validated by ROC curve analysis with all of their AUC values were over 0.95 (**Figures 6C, D**). Unexpectedly, the miRNA biomarkers in neither colon cancer nor rectal cancers were not associated with clinical outcome, suggesting their indirect roles in affecting patient prognosis.

Key lncRNA-miRNA-mRNA Interactions With Oncogenic Roles Across Colon and Rectal Cancers

To further elucidate the molecular distinction between colon cancer and rectal cancer, key lncRNA-associated competing triplets involved in cancer initiation and metastasis were identified *via* screening interactomes composed by lncRNA and miRNA biomarkers. As miRNA negatively regulate target gene expression, only the triplets in which miRNA and its lncRNA/mRNA target with opposite expression pattern were retained (**Figure 7A**). Importantly, in the identified ceRNA triplets, ANKRD36, FKBP14, PPRC1, and NAB1 were closely related to the prognosis of colon cancer patients (**Figure 7B**), while PCGF2 and ATP6V1F was tightly linked to the prognosis of rectal cancer patients (**Figure 7C**), suggesting that lncRNA biomarker may contribute to CRC occurrence and metastasis by regulating prognosis-related gene expression *via* ceRNA mechanism.

As shown in **Figure 7A**, lncRNA KCNQ1OT1 and SNHG1 may contribute to the progression of colon and rectal cancers through distinct mechanisms. For example, KCNQ1OT1/miR-484/ANKRD36, KCNQ1OT1/miR-181a-5p/FKBP14 or COL12A1, KCNQ1OT1/miR-132-3p/OGT, and KCNQ1OT1/miR-181a-5p/PCGF2 regulatory axes were respectively identified in colon M0/N, colon M1/N, rectal M0/N and rectal M1/N groups. Similarly, SNHG1/miR-484/ORC6 was discovered in both of colon M0/N and colon M1/N groups, while SNHG1/

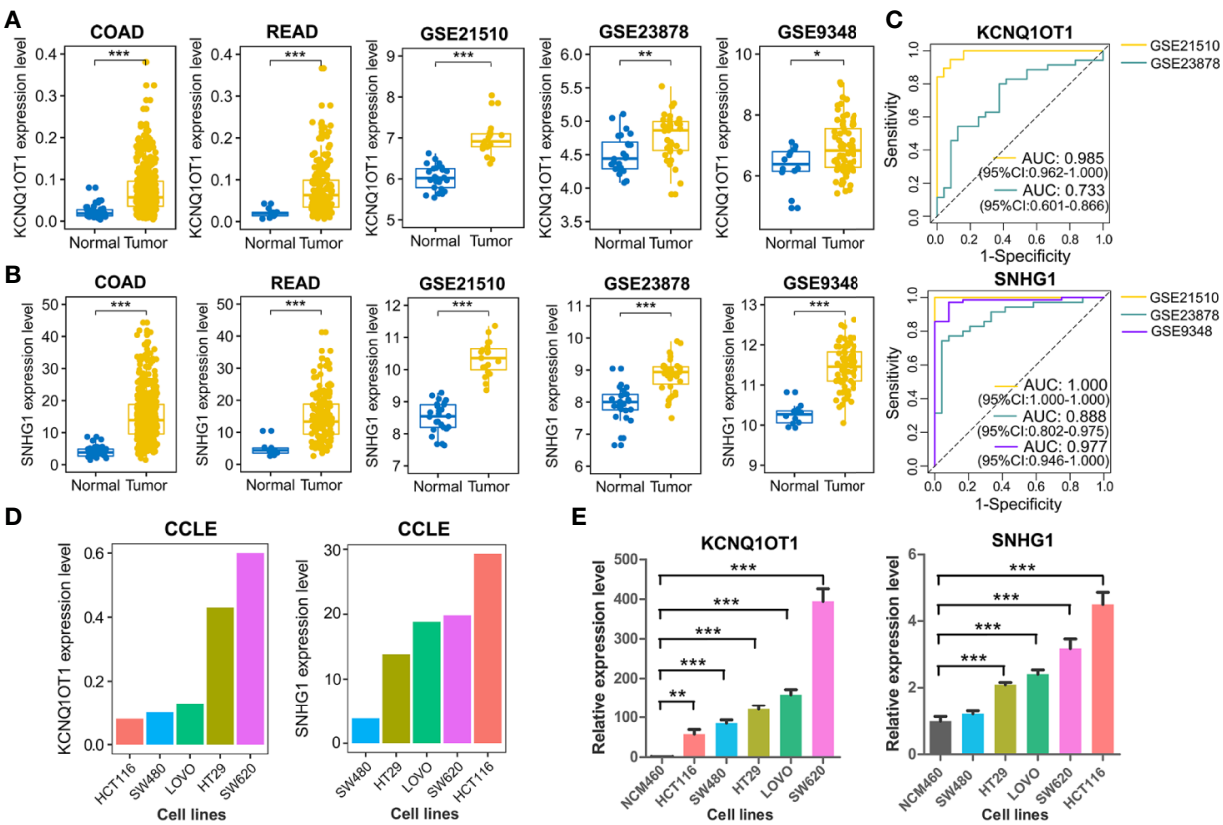

FIGURE 5 | Validation of common lncRNA biomarkers by assessing their expression pattern and diagnostic performance. **(A)** Boxplots showing the expression level of lncRNA KCNQ1OT1 between tumor and normal tissues from TCGA and GEO datasets. **(B)** Boxplots showing the expression level of lncRNA SNHG1 between tumor and normal tissues from TCGA and GEO datasets. **(C)** ROC curve analysis was employed to evaluate the predictive role of KCNQ1OT1 and SNHG1 in GEO datasets. **(D)** Relative expression level of KCNQ1OT1 and SNHG1 in CRC cell lines was detected in the CCLE database. **(E)** Relative expression level of KCNQ1OT1 and SNHG1 in CRC cell lines was determined by qRT-PCR. $^{*}P < 0.05$, $^{**}P < 0.01$, $^{***}P < 0.001$.

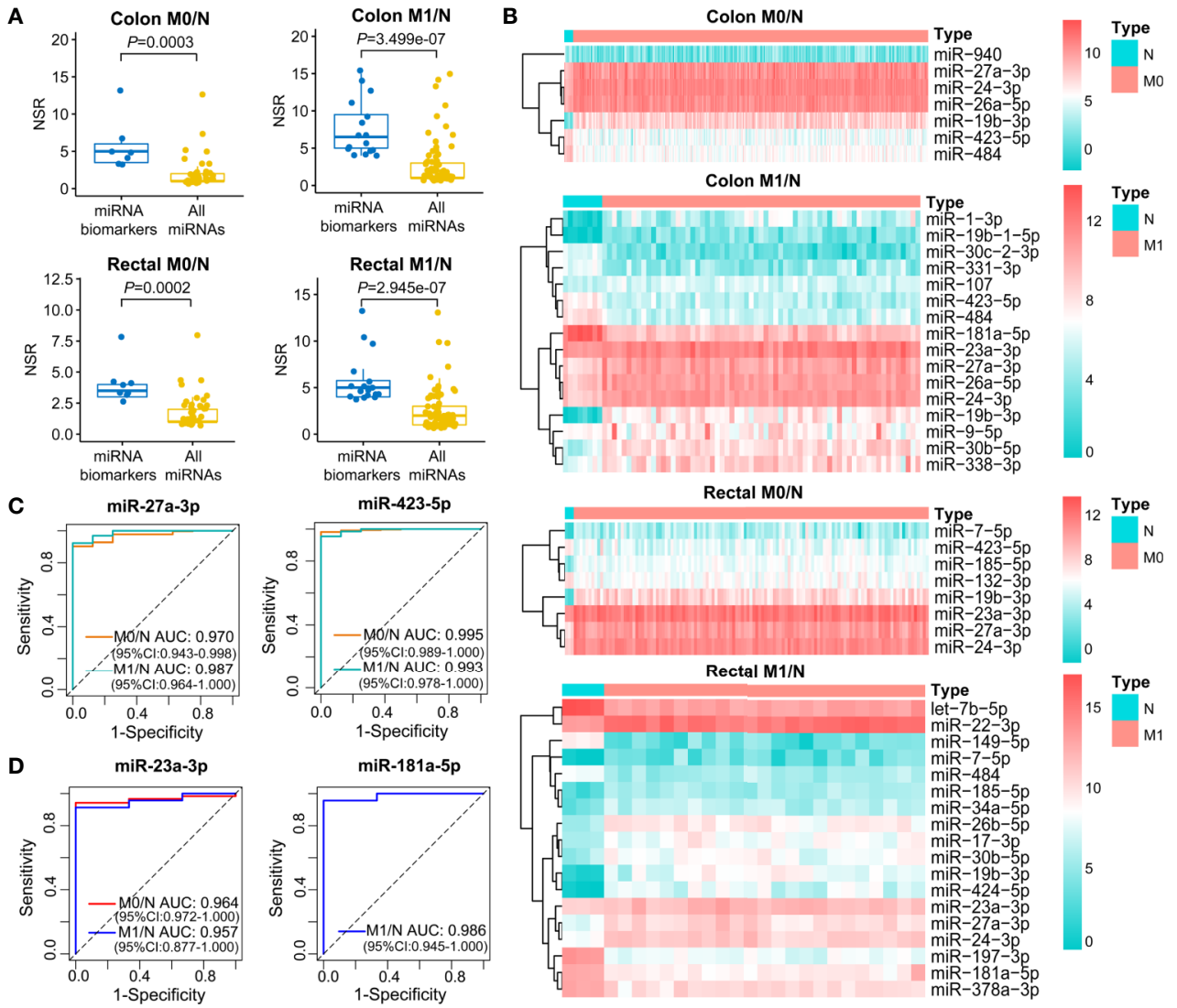

FIGURE 6 | Characterization of miRNA biomarkers in the initiation and metastasis of colon and rectal cancers. **(A)** NSR distribution of the identified miRNA biomarkers and all miRNAs in context-specific ceRNA network. Statistical significance was calculated using the Wilcoxon rank-sum test. **(B)** Heatmap of the expression level of miRNA biomarkers between colon/rectal cancer and normal tissues. M0 represents patients without distant metastasis; M1 represents patients with distant metastasis; N represents paracancerous normal tissue. **(C, D)** ROC curve revealed the clinical role of representative miRNA biomarkers in the screening of colon cancer **(C)** and rectal cancer **(D)**.

miR-423-5p/EZH2 and SNHG1/let-7b-5p/ATP6V1F were identified in rectal M0/N and rectal M1/N groups, respectively. Furthermore, the correlation between lncRNAs and representative target mRNAs in the identified ceRNA triplets were examined. As expected, KCNQ1OT1 strongly correlated with ANKRD36, FKBP14, OGT, and PCGF2, and SNHG1 strongly correlated with ORC6, ORC6, EZH2, and ATP6V1F in colon M0/N, colon M1/N, rectal M0/N, and rectal M1/N groups, respectively (**Figure 8A**). By analyzing the significantly enriched KEGG pathways, we found that COL12A1 and PCGF2 regulated by KCNQ1OT1, were closely involved in "Protein digestion and absorption" and "axon guidance" pathways, respectively. Comparatively, ORC6 and ATP6V1F were enriched in "cell cycle" and "Peroxisome" pathways, respectively. Based on the above results, we proposed the possible regulatory mechanisms of KCNQ1OT1 and SNHG1 acting as ceRNA in colon cancer and rectal cancer (**Figures 8B, C**).

DISCUSSION

As reported, the dysregulated lncRNAs could contribute to tumor initiation and progression through a ceRNA mechanism

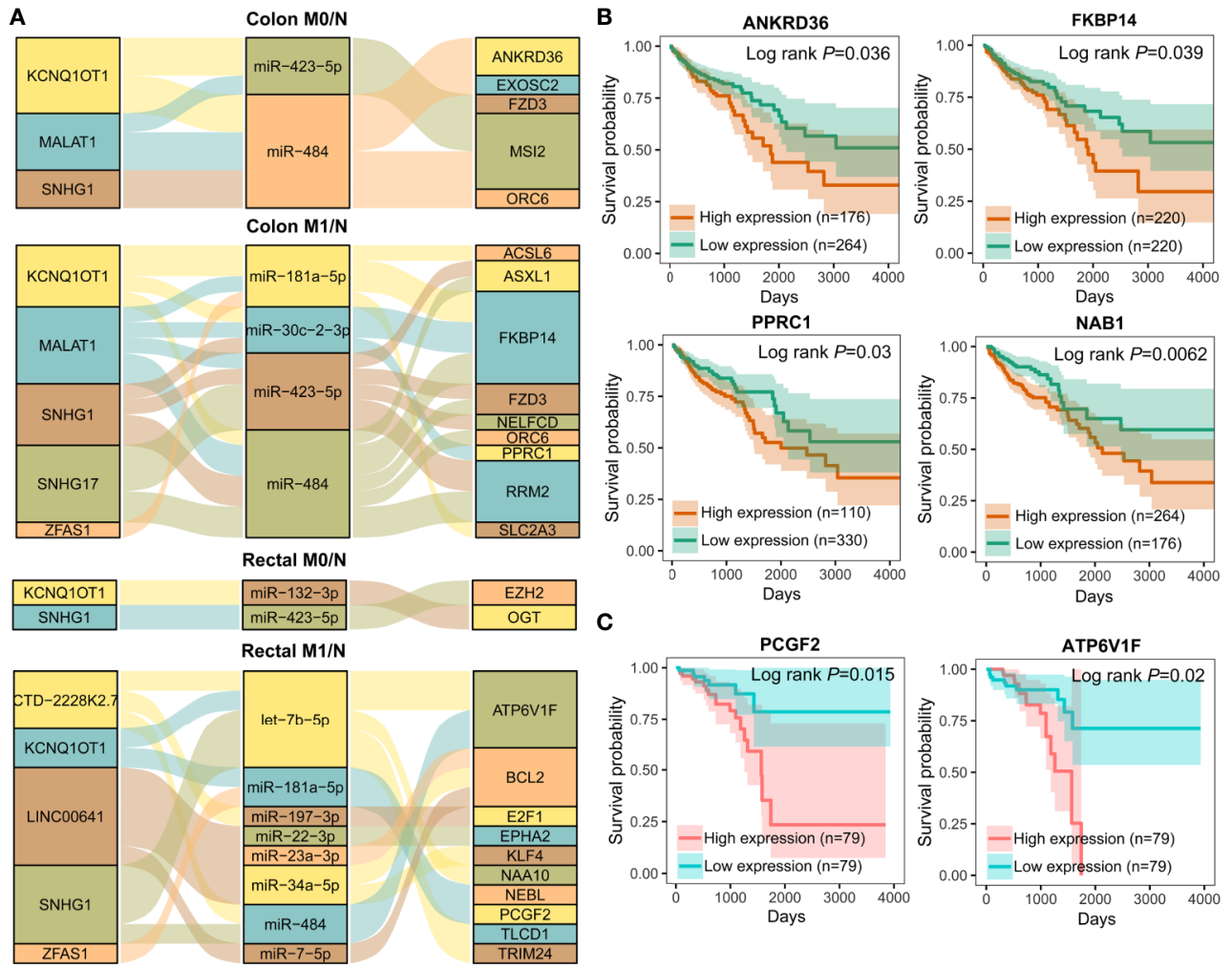

FIGURE 7 | Important lncRNA-miRNA-mRNA interactions composed by lncRNA and miRNA biomarkers and prognostic value of target mRNAs. **(A)** Sankey diagram showing the representative lncRNA-miRNA-mRNA regulatory axes involving lncRNA and miRNA biomarkers. **(B, C)** Kaplan-Meier analysis for overall survival of colon cancer (n=440) **(B)** and rectal cancer (n=158) **(C)** patients according to representative mRNAs expression level by OncoLnc.

by competitively sponging shared miRNAs with their target genes (38, 39). Recently, researchers tend to investigate lncRNA biomarkers in various cancers based on ceRNA network, which mainly include two steps: 1) identifying differentially expressed lncRNAs/miRNAs/mRNAs; 2) discovering miRNA-mRNA and miRNA-lncRNA pairs composed by differentially expressed lncRNAs/miRNAs/mRNAs *via* computational algorithms or experimental methods. For example, Gao et al. (40) unveiled lncRNA, miRNA and mRNA prognostic biomarkers associated with invasive breast cancer; Zhang G. et al. (41) identified new panel biomarkers indicating the occurrence and recurrence of myocardial infarction. We herein initially constructed a global LceNET in human and collected miRNA-mRNA and miRNA-lncRNA interactions verified by experimental methods, e.g. luciferase reporter assay, HITS-CLIP and PAR-CLIP, from the most commonly used databases. Then a novel computational model was developed and applied to uncover lncRNA biomarkers based on context-specific LceNET by considering their miRNA binding ability.

Furthermore, efforts have been made to comparatively investigate the heterogeneity in cancer-related pathways between colon and rectal cancer. Strikingly, DEmRNAs identified in colon cancer were significantly enriched in pathways, e.g. "cell cycle" (42), "protein digestion and absorption" (43), "p53 signaling pathway" (44) and "PPAR signaling pathway" (45), while DEmRNAs in rectal cancers were closely implicated in the pathways including "cGMP-PKG signaling pathway" (46), "proteoglycans in cancer" (47), and "vascular smooth muscle contraction" (48) and "oxytocin signaling pathway" (**Figures 2B–E**), indicating distinct oncogenic mechanisms of colon and rectal cancers. Especially, among those top enriched pathways, "oxytocin signaling pathway" is newly deciphered to be associated with colorectal cancer.

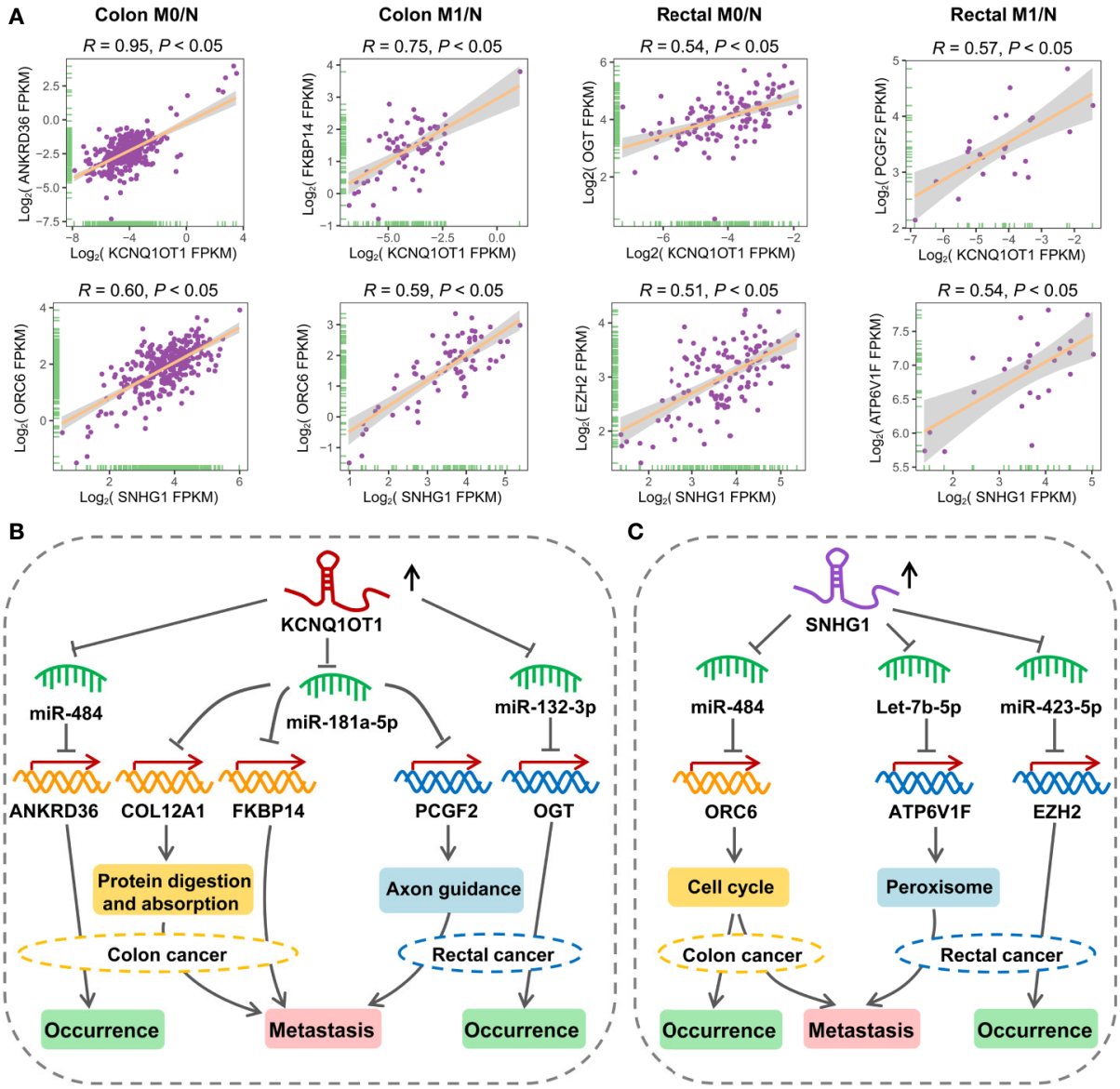

FIGURE 8 | Putative regulatory mechanisms of KCNQ1OT1 and SNHG1 underlying the initiation and metastasis of colon and rectal cancers. **(A)** Expression correlation of KCNQ1OT1 and its ceRNAs analyzed by Pearson correlation coefficient. We use the non-log scale for calculation and use the log-scale axis for visualization. **(B)** Expression correlation of SNHG1 and its ceRNAs analyzed by Pearson correlation coefficient. We use the non-log scale for calculation and use the log-scale axis for visualization. **(C)** Distinct mechanism of KCNQ1OT1 and SNHG1 in the processes of initiation and metastasis of colon and rectal cancers.

Based on our computational model, KCNQ1OT1 and SNHG1 possessing hub nodes properties in all of the four context-specific ceRNA networks, were identified as shared lncRNA biomarkers in colon and rectal cancer, revealing their critical role in colorectal carcinogenesis. Consistently, both of KCNQ1OT1 and SNHG1 have been demonstrated as oncogenes through ceRNA mechanisms in CRC. For example, KCNQ1OT1 has been reported to promote drug resistance of CRC cells by sponging miR-34a (49) or miR-760 (50), and contribute to cell proliferation, migration and EMT formation in CRC through regulating miR-217/ZEB1 axis (51); SNHG1 could act as decoy of miR-137 (52), miR-497 (53), miR-195-5p (53), miR-154-5p (54) and miR-145 (55) to weaken their suppressive effect on target genes, thereby facilitating colorectal tumorigenesis.

As an interesting result, we found that KCNQ1OT1 and SNHG1 could regulate the initiation and metastasis of colon and rectal cancers through distinct ceRNA regulatory axes, which have not been reported in previous studies. As shown in the proposed mechanism, KCNQ1OT1 may regulate the initiation of colon cancer by sponging miR-484 to derepress its inhibiting effect on ANKRD36 that related to prognosis, accelerate the initiation of rectal cancer by acting as a miR-132-3p-mediated ceRNA of OGT,

while promote the metastasis of colon and rectal cancers through miR-181a-5p-mediated ceRNA regulatory relationship (**Figure 8B**). In addition, SNHG1 exhibited potentials in regulating the initiation and metastasis of colon cancer *via* cell cycle signaling pathway by working as a miR-484-mediated ceRNA of ORC6. Comparatively, SNHG1 was found to promote initiation and metastasis of rectal cancer through regulating let-7b-5p/ATP6V1F and miR-423-5p/EZH2 axes, respectively (**Figure 8C**). Especially, serum miR-423-5p and miR-484 have been proven as diagnostic biomarkers for CRC (56). Taken together, these results have shown distinct mechanism between colon and rectal cancers in terms of initiation and metastasis.

Although SNHG1 or KCNQ1OT1 has been reported to be significantly correlated with the prognosis of colon cancer (57–61), the regulatory mechanism of SNHG1 or KCNQ1OT1 underlying the pathogenic differences between colon cancer and rectal cancer has not been well explored. Hence, our findings provide insights into the oncogenetic heterogeneity between colon and rectal cancers. In addition, MALAT1, ZFAS1 and SNHG17 have been identified as diagnostic biomarker specific to colon cancer, the metastasis of colon and rectal cancer, and the metastasis of colon cancer, respectively, therefore the tumor/stage-specific roles of MALAT1, ZFAS1 and SNHG17 in colon and rectal cancers need further investigation.

CONCLUSION

In summary, we constructed context-specific LceNETs that reveal distinct mechanisms underlying the initiation and metastasis between colon and rectal cancer. A novel computational model was proposed and applied for lncRNA biomarker identification, which will greatly facilitate systematic investigation of LceNETs in various human cancers. Moreover, we found that different pathways, lncRNA biomarkers and miRNA biomarkers were closely involved in the tumorigenesis between colon and rectal cancer. Especially, the KCNQ1OT1 and SNHG1 were unveiled as common lncRNA biomarkers with critical roles in the initiation and metastasis of colon and rectal cancers *via* distinct ceRNA mechanisms.

DATA AVAILABILITY STATEMENT

Publicly available datasets were analyzed in this study. This data can be found here: http://cancergenome.nih.gov/, https://www.ncbi.nlm.nih.gov/geo/.

AUTHOR CONTRIBUTIONS

BS and XQ designed the research. YL developed the computational method. XQ and XL collected the data and performed the computational and experimental analyses. XQ, YL, XL, JC, and BS drafted and revised the manuscript. BS supervised and coordinated the research. All authors contributed to the article and approved the submitted version.

FUNDING

This work was supported by National Natural Science Foundation of China (Grant Nos. 31900490, 31770903, and 31670851), Jiangsu Planned Projects for Postdoctoral Research Funds (2018K173C), China Postdoctoral Science Foundation (2019M651938) and the Natural Science Foundation of the Jiangsu Higher Education Institutions of China (19KJB180027).

ACKNOWLEDGMENTS

The authors gratefully thank Prof. Yufeng Xie at Department of Oncology, The First Affiliated Hospital of Soochow University for providing experimental ground.

SUPPLEMENTARY MATERIAL

The Supplementary Material for this article can be found online at: https://www.frontiersin.org/articles/10.3389/fonc.2020.535985/full#supplementary-material

REFERENCES

1. Stein U, Schlag PM. Clinical, biological, and molecular aspects of metastasis in colorectal cancer. *Recent Results Cancer Res* (2007) 176:61–80. doi: 10.1007/978-3-540-46091-6_7
2. Wei EK, Giovannucci E, Wu K, Rosner B, Fuchs CS, Willett WC, et al. Comparison of risk factors for colon and rectal cancer. *Int J Cancer* (2004) 108 (3):433–42. doi: 10.1002/ijc.11540
3. Riihimaki M, Hemminki A, Sundquist J, Hemminki K. Patterns of metastasis in colon and rectal cancer. *Sci Rep* (2016) 6:29765. doi: 10.1038/srep29765
4. Buchwald P, Hall C, Davidson C, Dixon L, Dobbs B, Robinson B, et al. Improved survival for rectal cancer compared to colon cancer: the four cohort study. *ANZ J Surg* (2018) 88(3):E114–7. doi: 10.1111/ans.13730
5. Djebali S, Davis CA, Merkel A, Dobin A, Lassmann T, Mortazavi A, et al. Landscape of transcription in human cells. *Nature* (2012) 489(7414):101–8. doi: 10.1038/nature11233
6. Chen J, Zhang D, Zhang W, Tang Y, Yan W, Guo L, et al. Clear cell renal cell carcinoma associated microRNA expression signatures identified by an integrated bioinformatics analysis. *J Transl Med* (2013) 11:169. doi: 10.1186/1479-5876-11-169
7. Zhang W, Zang J, Jing X, Sun Z, Yan W, Yang D, et al. Identification of candidate miRNA biomarkers from miRNA regulatory network with application to prostate cancer. *J Transl Med* (2014) 12:66. doi: 10.1186/1479-5876-12-66
8. Lin Y, Wu W, Sun Z, Shen L, Shen B. MiRNA-BD: an evidence-based bioinformatics model and software tool for microRNA biomarker discovery. *RNA Biol* (2018b) 15(8):1093–105. doi: 10.1080/15476286.2018.1502590
9. Cui W, Qian Y, Zhou X, Lin Y, Jiang J, Chen J, et al. Discovery and characterization of long intergenic non-coding RNAs (lincRNA) module biomarkers in prostate cancer: an integrative analysis of RNA-Seq data. *BMC Genomics* (2015) 16(Suppl 7):S3. doi: 10.1186/1471-2164-16-s7-s3
10. Chen J, Miao Z, Xue B, Shan Y, Weng G, Shen B. Long Non-coding RNAs in Urologic Malignancies: Functional Roles and Clinical Translation. *J Cancer* (2016) 7(13):1842–55. doi: 10.7150/jca.15876

11. Salmena L, Poliseno L, Tay Y, Kats L, Pandolfi PP. A ceRNA hypothesis: the Rosetta Stone of a hidden RNA language? *Cell* (2011) 146(3):353–8. doi: 10.1016/j.cell.2011.07.014
12. Qi X, Lin Y, Chen J, Shen B. Decoding competing endogenous RNA networks for cancer biomarker discovery. *Brief Bioinform* (2020) 21(2):441–57. doi: 10.1093/bib/bbz006
13. Shan Y, Ma J, Pan Y, Hu J, Liu B, Jia L. LncRNA SNHG7 sponges miR-216b to promote proliferation and liver metastasis of colorectal cancer through upregulating GALNT1. *Cell Death Dis* (2018) 9(7):722. doi: 10.1038/s41419-018-0759-7
14. Xu J, Li Y, Lu J, Pan T, Ding N, Wang Z, et al. The mRNA related ceRNA–ceRNA landscape and significance across 20 major cancer types. *Nucleic Acids Res* (2015) 43(17):8169–82. doi: 10.1093/nar/gkv853
15. Li Y, Li L, Wang Z, Pan T, Sahni N, Jin X, et al. LncMAP: Pan-cancer atlas of long noncoding RNA-mediated transcriptional network perturbations. *Nucleic Acids Res* (2018) 46(3):1113–23. doi: 10.1093/nar/gkx1311
16. Das S, Ghosal S, Sen R, Chakrabarti J. lnCeDB: database of human long noncoding RNA acting as competing endogenous RNA. *PloS One* (2014) 9(6): e98965. doi: 10.1371/journal.pone.0098965
17. Munro MJ, Wickremesekera SK, Peng L, Tan ST, Itinteang T. Cancer stem cells in colorectal cancer: a review. *J Clin Pathol* (2018) 71(2):110–6. doi: 10.1136/jclinpath-2017-204739
18. Li JH, Liu S, Zhou H, Qu LH, Yang JH. starBase v2.0: decoding miRNA-ceRNA, miRNA-ncRNA and protein-RNA interaction networks from large-scale CLIP-Seq data. *Nucleic Acids Res* (2014) 42(Database issue):D92–97. doi: 10.1093/nar/gkt1248
19. Karagkouni D, Paraskevopoulou MD, Chatzopoulos S, Vlachos IS, Tastsoglou S, Kanellos I, et al. DIANA-TarBase v8: a decade-long collection of experimentally supported miRNA-gene interactions. *Nucleic Acids Res* (2018) 46(D1):D239–45. doi: 10.1093/nar/gkx1141
20. Huang HY, Lin YC, Li J, Huang KY, Shrestha S, Hong HC, et al. miRTarBase 2020: updates to the experimentally validated microRNA-target interaction database. *Nucleic Acids Res* (2020) 48(D1):D148–54. doi: 10.1093/nar/gkz896
21. Wang P, Zhi H, Zhang Y, Liu Y, Zhang J, Gao Y, et al. miRSponge: a manually curated database for experimentally supported miRNA sponges and ceRNAs. *Database (Oxford)* (2015) 2015. doi: 10.1093/database/bav098
22. Wang P, Li X, Gao Y, Guo Q, Wang Y, Fang Y, et al. LncACTdb 2.0: an updated database of experimentally supported ceRNA interactions curated from low- and high-throughput experiments. *Nucleic Acids Res* (2019) 47 (D1):D121–7. doi: 10.1093/nar/gky1144
23. Paraskevopoulou MD, Vlachos IS, Karagkouni D, Georgakilas G, Kanellos I, Vergoulis T, et al. DIANA-LncBase v2: indexing microRNA targets on non-coding transcripts. *Nucleic Acids Res* (2016) 44(D1):D231–238. doi: 10.1093/nar/gkv1270
24. Frankish A, Diekhans M, Ferreira AM, Johnson R, Jungreis I, Loveland J, et al. GENCODE reference annotation for the human and mouse genomes. *Nucleic Acids Res* (2019) 47(D1):D766–73. doi: 10.1093/nar/gky955
25. Kozomara A, Birgaoanu M, Griffiths-Jones S. miRBase: from microRNA sequences to function. *Nucleic Acids Res* (2019) 47(D1):D155–62. doi: 10.1093/nar/gky1141
26. Nikolayeva O, Robinson MD. edgeR for differential RNA-seq and ChIP-seq analysis: an application to stem cell biology. *Methods Mol Biol* (2014) 1150:45–79. doi: 10.1007/978-1-4939-0512-6_3
27. Kohl M, Wiese S, Warscheid B. Cytoscape: software for visualization and analysis of biological networks. *Methods Mol Biol* (2011) 696:291–303. doi: 10.1007/978-1-60761-987-1_18
28. Yu G. clusterProfiler: universal enrichment tool for functional and comparative study. *bioRxiv* (2018) 256784. doi: 10.1101/256784
29. Walter W, Sanchez-Cabo F, Ricote M. GOplot: an R package for visually combining expression data with functional analysis. *Bioinformatics* (2015) 31 (17):2912–4. doi: 10.1093/bioinformatics/btv300
30. Karreth FA, Pandolfi PP. ceRNA cross-talk in cancer: when ce-bling rivalries go awry. *Cancer Discovery* (2013) 3(10):1113–21. doi: 10.1158/2159-8290.CD-13-0202
31. Lin Y, Chen F, Shen L, Tang X, Du C, Sun Z, et al. Biomarker microRNAs for prostate cancer metastasis: screened with a network vulnerability analysis model. *J Transl Med* (2018a) 16(1):134. doi: 10.1186/s12967-018-1506-7
32. Sing T, Sander O, Beerenwinkel N, Lengauer T. ROCR: visualizing classifier performance in R. *Bioinformatics* (2005) 21(20):3940–1. doi: 10.1093/bioinformatics/bti623
33. Anaya J. OncoLnc: linking TCGA survival data to mRNAs, miRNAs, and lncRNAs. *PeerJ Comput Sci* (2016) 2:e67. doi: 10.7717/peerj-cs.67
34. Browning DD. Protein kinase G as a therapeutic target for the treatment of metastatic colorectal cancer. *Expert Opin Ther Targets* (2008) 12(3):367–76. doi: 10.1517/14728222.12.3.367
35. Li N, Xi Y, Tinsley HN, Gurpinar E, Gary BD, Zhu B, et al. Sulindac selectively inhibits colon tumor cell growth by activating the cGMP/PKG pathway to suppress Wnt/beta-catenin signaling. *Mol Cancer Ther* (2013) 12(9):1848–59. doi: 10.1158/1535-7163.MCT-13-0048
36. Xu J, Shao T, Song M, Xie Y, Zhou J, Yin J, et al. MIR22HG acts as a tumor suppressor via TGFβ/SMAD signaling and facilitates immunotherapy in colorectal cancer. *Mol Cancer* (2020) 19(1):1–15. doi: 10.1186/s12943-020-01174-w
37. Zhang J, Li S, Zhang L, Xu J, Song M, Shao T, et al. RBP EIF2S2 Promotes Tumorigenesis and Progression by Regulating MYC-Mediated Inhibition via FHIT-Related Enhancers. *Mol Ther* (2020) 28(4):1105–18. doi: 10.1016/j.ymthe.2020.02.004
38. Wang Y, Hou J, He D, Sun M, Zhang P, Yu Y, et al. The Emerging Function and Mechanism of ceRNAs in Cancer. *Trends Genet* (2016) 32(4):211–24. doi: 10.1016/j.tig.2016.02.001
39. Fan CN, Ma L, Liu N. Systematic analysis of lncRNA-miRNA-mRNA competing endogenous RNA network identifies four-lncRNA signature as a prognostic biomarker for breast cancer. *J Transl Med* (2018) 16(1):264. doi: 10.1186/s12967-018-1640-2
40. Gao C, Li H, Zhuang J, Zhang H, Wang K, Yang J, et al. The construction and analysis of ceRNA networks in invasive breast cancer: a study based on The Cancer Genome Atlas. *Cancer Manage Res* (2019) 11:1–11. doi: 10.2147/CMAR.S182521
41. Zhang G, Sun H, Zhang Y, Zhao H, Fan W, Li J, et al. Characterization of dysregulated lncRNA-mRNA network based on ceRNA hypothesis to reveal the occurrence and recurrence of myocardial infarction. *Cell Death Discovery* (2018) 4:35. doi: 10.1038/s41420-018-0036-7
42. Wang L, Zhao Z, Feng W, Ye Z, Dai W, Zhang C, et al. Long non-coding RNA TUG1 promotes colorectal cancer metastasis via EMT pathway. *Oncotarget* (2016) 7(32):51713–9. doi: 10.18632/oncotarget.10563
43. Xu C, Sun L, Jiang C, Zhou H, Gu L, Liu Y, et al. SPP1, analyzed by bioinformatics methods, promotes the metastasis in colorectal cancer by activating EMT pathway. *Biomed Pharmacother* (2017) 91:1167–77. doi: 10.1016/j.biopha.2017.05.056
44. Slattery ML, Mullany LE, Wolff RK, Sakoda LC, Samowitz WS, Herrick JS. The p53-signaling pathway and colorectal cancer: Interactions between downstream p53 target genes and miRNAs. *Genomics* (2019) 111(4):762–71. doi: 10.1016/j.ygeno.2018.05.006
45. Zhang X, Yao J, Shi H, Gao B, Zhang L. LncRNA TINCR/microRNA-107/CD36 regulates cell proliferation and apoptosis in colorectal cancer via PPAR signaling pathway based on bioinformatics analysis. *Biol Chem* (2019) 400 (5):663–75. doi: 10.1515/hsz-2018-0236
46. Lee K, Lindsey AS, Li N, Gary B, Andrews J, Keeton AB, et al. β-catenin nuclear translocation in colorectal cancer cells is suppressed by PDE10A inhibition, cGMP elevation, and activation of PKG. *Oncotarget* (2016) 7 (5):5353. doi: 10.18632/oncotarget.6705
47. Suhovskih AV, Aidagulova SV, Kashuba VI, Grigorieva EV. Proteoglycans as potential microenvironmental biomarkers for colon cancer. *Cell Tissue Res* (2015) 361(3):833–44. doi: 10.1007/s00441-015-2141-8
48. Xi W, Liu Y, Sun X, Shan J, Yi L, Zhang T. Bioinformatics analysis of RNA-seq data revealed critical genes in colon adenocarcinoma. *Eur Rev Med Pharmacol Sci* (2017) 21(13):3012–20.
49. Li Y, Li C, Li D, Yang L, Jin J, Zhang B. lncRNA KCNQ1OT1 enhances the chemoresistance of oxaliplatin in colon cancer by targeting the miR-34a/ATG4B pathway. *Onco Targets Ther* (2019) 12:2649–60. doi: 10.2147/OTT.S188054
50. Xian D, Zhao Y. LncRNA KCNQ1OT1 enhanced the methotrexate resistance of colorectal cancer cells by regulating miR-760/PPP1R1B via the cAMP signalling pathway. *J Cell Mol Med* (2019) 23(6):3808–23. doi: 10.1111/jcmm.14071
51. Bian Y, Gao G, Zhang Q, Qian H, Yu L, Yao N, et al. KCNQ1OT1/miR-217/ZEB1 feedback loop facilitates cell migration and epithelial-mesenchymal

transition in colorectal cancer. *Cancer Biol Ther* (2019) 20(6):886–96. doi: 10.1080/15384047.2019.1579959
52. Fu Y, Yin Y, Peng S, Yang G, Yu Y, Guo C, et al. Small nucleolar RNA host gene 1 promotes development and progression of colorectal cancer through negative regulation of miR-137. *Mol Carcinog* (2019) 58(11):2104–17. doi: 10.1002/mc.23101
53. Bai J, Xu J, Zhao J, Zhang R. lncRNA SNHG1 cooperated with miR-497/miR-195-5p to modify epithelial-mesenchymal transition underlying colorectal cancer exacerbation. *J Cell Physiol* (2020) 235(2):1453–68. doi: 10.1002/jcp.29065
54. Xu M, Chen X, Lin K, Zeng K, Liu X, Pan B, et al. The long noncoding RNA SNHG1 regulates colorectal cancer cell growth through interactions with EZH2 and miR-154-5p. *Mol Cancer* (2018) 17(1):141. doi: 10.1186/s12943-018-0894-x
55. Tian T, Qiu R, Qiu X. SNHG1 promotes cell proliferation by acting as a sponge of miR-145 in colorectal cancer. *Oncotarget* (2018) 9(2):2128–39. doi: 10.18632/oncotarget.23255
56. Lu X, Lu J. The significance of detection of serum miR-423-5p and miR-484 for diagnosis of colorectal cancer. *Clin Lab* (2015) 61(1-2):187–90. doi: 10.7754/Clin.Lab.2014.140625
57. Yang H, Wang S, Kang Y-J, Wang C, Xu Y, Zhang Y, et al. Long non-coding RNA SNHG1 predicts a poor prognosis and promotes colon cancer tumorigenesis. *Oncol Rep* (2018) 40(1):261–71. doi: 10.3892/or.2018.6412
58. Zhang Z, Qian W, Wang S, Ji D, Wang Q, Li J, et al. Analysis of lncRNA-associated ceRNA network reveals potential lncRNA biomarkers in human colon adenocarcinoma. *Cell Physiol Biochem* (2018) 49(5):1778–91. doi: 10.1159/000493623
59. Wang W-J, Li H-T, Yu J-P, Han X-P, Xu Z-P, Li Y-M, et al. A competing endogenous RNA network reveals novel potential lncRNA, miRNA, and mRNA biomarkers in the prognosis of human colon adenocarcinoma. *J Surg Res* (2019) 235:22–33. doi: 10.1016/j.jss.2018.09.053
60. Zhang K, Yan J, Yi B, Rui Y, Hu H. High KCNQ1OT1 expression might independently predict shorter survival of colon adenocarcinoma. *Future Oncol* (2019) 15(10):1085–95. doi: 10.2217/fon-2018-0499
61. Poursheikhani A, Abbaszadegan MR, Nokhandani N, Kerachian MA. Integration analysis of long non-coding RNA (lncRNA) role in tumorigenesis of colon adenocarcinoma. *BMC Med Genomics* (2020) 13 (1):1–16. doi: 10.1186/s12920-020-00757-2

Conflict of Interest: The authors declare that the research was conducted in the absence of any commercial or financial relationships that could be construed as a potential conflict of interest.

frontiers in Cell and Developmental Biology

ORIGINAL RESEARCH
published: 26 November 2020
doi: 10.3389/fcell.2020.602174

A Prognostic Model for Colon Cancer Patients Based on Eight Signature Autophagy Genes

*Jiasheng Xu[1,2], Siqi Dai[1,2], Ying Yuan[2,3], Qian Xiao[1,2] and Kefeng Ding[1,2]**

[1] Department of Colorectal Surgery and Oncology, Key Laboratory of Cancer Prevention and Intervention, Ministry of Education, The Second Affiliated Hospital, Zhejiang University School of Medicine, Hangzhou, China, [2] Zhejiang University Cancer Center, Hangzhou, China, [3] Department of Medical Oncology, The Second Affiliated Hospital, Zhejiang University School of Medicine, Hangzhou, China

Objective: To screen key autophagy genes in colon cancer and construct an autophagy gene model to predict the prognosis of patients with colon cancer.

Methods: The colon cancer data from the TCGA were downloaded as the training set, data chip of GSE17536 as the validation set. The differential genes of the training set were obtained and were analyzed for enrichment and protein network. Acquire autophagy genes from Human Autophagy Database www.autophagy.lu/project.html. Autophagy genes in differentially expressed genes were extracted using R-packages limma. Using LASSO/Cox regression analysis combined with clinical information to construct the autophagy gene risk scoring model and divide the samples into high and low risk groups according to the risk value. The Nomogram assessment model was used to predict patient outcomes. CIBERSORT was used to calculate the infiltration of immune cells in the samples and study the relationship between high and low risk groups and immune checkpoints.

Results: Nine hundred seventy-six differentially expressed genes were screened from training set, including five hundred sixty-eight up-regulated genes and four hundred eight down regulated genes. These differentially expressed genes were mainly involved: the regulation of membrane potential, neuroactive ligand-receptor interaction. We identified eight autophagy genes *CTSD*, *ULK3*, *CDKN2A*, *NRG1*, *ATG4B*, *ULK1*, *DAPK1*, and *SERPINA1* as key prognostic genes and constructed the model after extracting the differential autophagy genes in the training set. Survival analysis showed significant differences in sample survival time after grouping according to the model. Nomogram assessment showed that the model had high reliability for predicting the survival of patients with colon cancer in the 1, 3, 5 years. In the high-risk group, the infiltration degrees of nine types of immune cells are different and the samples can be well distinguished according to these nine types of immune cells. Immunological checkpoint correlation results showed that the expression levels of *CTLA4*, *IDO1*, *LAG3*, *PDL1*, *and TIGIT* increased in high-risk groups.

OPEN ACCESS

Edited by:
Andrew Davis, Washington University in St. Louis, United States

Reviewed by:
Moacyr Rêgo, Federal University of Pernambuco, Brazil
Talib Hassan Ali, Thi Qar University, Iraq

***Correspondence:**
Kefeng Ding
dingkefeng@zju.edu.cn

Specialty section:
This article was submitted to Molecular and Cellular Oncology, a section of the journal Frontiers in Cell and Developmental Biology

Received: *02 September 2020*
Accepted: *28 October 2020*
Published: *26 November 2020*

Citation:
Xu J, Dai S, Yuan Y, Xiao Q and Ding K (2020) A Prognostic Model for Colon Cancer Patients Based on Eight Signature Autophagy Genes. Front. Cell Dev. Biol. 8:602174. doi: 10.3389/fcell.2020.602174

Conclusion: The prognosis prediction model based on autophagy gene has a good evaluation effect on the prognosis of colon cancer patients. Eight key autophagy genes can be used as prognostic markers for colon cancer.

Keywords: colon cancer, autophagy genes, prognostic model, TCGA, prognostic markers

INTRODUCTION

Colon cancer (carcinoma of colon) is a common malignant tumor in the gastrointestinal tract (Fearon and Vogelstein, 1990; Jemal et al., 2011). Its morbidity and mortality are only second to gastric cancer, esophageal cancer and primary liver cancer in malignant tumors of the digestive system (Meyerhardt and Mayer, 2005). Recent studies have shown that autophagy is involved in the occurrence and development of malignant tumors, neurodegenerative diseases, tissue fibrosis, cardiovascular diseases and immune diseases (Eskelinen, 2011). Depending on how the intracellular substrate is degraded and transported to the lysosomal cavity (Fulda and Kogel, 2015), autophagy can be divided into three types: macroautophagy, microautophagy, and chaperone-mediate autophgy.

Because of the prevalence of giant autophagy, in most cases giant autophagy is commonly referred to autophagy and is the most detailed form of autophagy being currently studied. Macroautophagy cannot only degrade macromolecules and organelles to protect cells, but also induce cell death mediated by autophagy, which is the main mechanism regulating the degradation of proteins and organelles in eukaryotic cells (Kondo et al., 2005; Maiuri et al., 2007; Martinet and De Meyer, 2009). In some tumors, autophagy can inhibit the growth of tumor cells and activate programmed cell death. In addition, autophagy can also regulate the occurrence and development of tumors through multiple mechanisms and signaling pathways, so that cells can survive under stress conditions. Therefore, the effects of autophagy on tumors are not unilateral or harmful, and their specific types of cancer should be differentiated (Mizushima, 2007; Cheng et al., 2013). Many key molecules related to autophagy have been extensively studied. It has been found that the process is highly conserved in yeast and human beings. A series of homologs of autophagy related genes in yeast have been widely found in mammals. Several core autophagy related factors play roles in two ubiquitination systems which are necessary for autophagy formation.

Although the autophagy response has been shown to be related to the occurrence and development of various tumors, the key genes affecting the prognosis of colon cancer patients in the autophagy response have yet to be confirmed. In this paper, we used machine learning methods to analyze the expression of 210 autophagy genes in 433 colon cancer patients and their prognostic value in colon cancer patients. In order to establish an accurate and reliable prognostic model for colon cancer patients, we constructed a prognostic model by using autophagy genes with significant prognostic relevance, and validated the model with external colon cancer datasets.

Abbreviations: COAD, Colon cancer; RMA, Multi-Array Average; PPI, Protein–protein interaction; MCC, Maximum neighborhood component; ROC, Receiver operating characteristic; HPA, Human Protein Atlas; HR, Hazard ratio.

MATERIALS AND METHODS

Ethics Approval Statement

No animals or humans were involved in this study. This study was carried out in accordance with the Declaration of Helsinki.

Research Object

We downloaded the expression profile data and corresponding clinical information mRNA colon cancer (COAD) patients in The Cancer Genome Atlas (tcga)[1] database, after excluding patients with incomplete information, 433 patients had complete survival information. In addition, we also downloaded the dataset numbered GSE17536 in the Gene Expression Omnibus (GEO database)[2] database, the dataset contained 177 colon cancer patients, and 177 patients contained complete survival information. The samples were analyzed using Affymetrix Human Genome U133 Plus 2.0 Array platform to obtain data. Two hundred ten autophagy genes were collected in www.autophagy.lu/project.html, autophagy genes are detailed in **Supplementary Table S1**.

Differential Gene Analysis

The differential expression gene analysis was based on the limma (PMID: 25605792) function package of R language (version3.5.2, the same below). The absolute values of differential expression multiples (Log2FC) of logarithmic transformation > 1 and FDR ≤ 0.05 were used as criteria to screen differentially expressed genes.

Functional Enrichment Analysis

For the differentially expressed genes, we used the "clusterProfiler" (PMID: 22455463) function package in R to carry out the enrichment analysis of GO (including Biological Process, Molecular Function and Cellular Component) and KEGG Pathway enrichment analysis (DAVID[3] online website can also be used to finish the same enrichment analysis). We thought the corresponding entries were significantly enriched at < 0.05.

Protein–Protein Interaction (PPI) Networks

The STRING database is a database for analyzing and predicting protein functional connectivity and protein interactions. We

[1]https://tcga-data.nci.nih.gov/tcga/

[2]https://www.ncbi.nlm.nih.gov/geo/

[3]https://david.ncifcrf.gov/

used STRING (PMID: 30476243)[4] to analyze the functional relationship and protein interaction of proteins, and used cytoHubba plug-in in Cytoscape (PMID: 14597658) (version 3.7.2) software to screen the key genes in PPI networks.

LASSO Cox Regression Analysis

Based on the expression values of 210 autophagy genes, single factor Cox regression analysis was performed for colon cancer samples, autophagy genes significantly associated with colon cancer prognosis were screened with $P < 0.05$ as a threshold. Then LASSO Cox regression analysis with R package glmnet (PMID: 20808728) was used to further identify autophagy genes related to the prognosis of colon cancer, and the Risk Score of each sample was calculated using the screened autophagy genes through the following formula.

Risk score = $\sum_{i=1}^{n} \mathrm{Coef_i} * \mathrm{x}_i$,

Coefi is the risk coefficient of each factor calculated by the LASSO-Cox model, Xi is the expression value of each factor and in this study, the expression value of mRNA is used. Then the optimal cutoff value of the Risk score was determined by R package survival, survminer, and bilateral test, patients were divided into Low Risk and High Risk groups according to the cutoff values.

Survival Analysis

R language survival package and survminer package were used to estimate the overall survival rate of different groups based on the Kaplan-Meier method. R language survival ROC package (PMID: 10877287) plot time dependent subject work characteristics (ROC) curves. The multivariate Cox regression model was used to analyze whether Risk Score could independently predict the survival of patients with colon cancer independently of other factors.

The Proportion of Immune Cell Infiltration and the Calculation of Tumor Purity

We used software CIBERSORT (PMID: 25822800) to calculate the relative proportions of 22 immune cells in each cancer sample. CICERSORT software is based on the gene expression matrix. CICERSORT software can use the deconvolution algorithm to characterize the composition of immune infiltrating cells using the preset 547 barcode genes based on gene expression matrix. The proportion of all estimated immune cell types in each sample was equal to 1. Using the R language estimate function package (PMID: 24113773) to calculate the tumor purity of each cancer sample.

Establishment of Nomogram Prognosis Prediction Model

Nomogram is widely used to predict the prognosis of cancer. In order to predict the survival probability of patients in 1, 3, and 5 years, to predict patient survival probability for 1, 3, and 5 years, we established nomogram, and plotted nomogram calibration curves based on all independent prognostic factors determined by multivariate Cox regression analysis using the R language rms package to observe the relationship between the predicted probability and the actual incidence.

Expression Verification of Prognosis-Related Genes

Verification of gene expression of the selected autophagy genes related to prognosis.

The Human Protein Atlas (HPA)[5] was used to validate the expression of autophagy genes related to prognosis in colon cancer tumor tissues and normal tissues, and to compare whether the expression differences were consistent with the results of previous analysis.

Statistical Analysis

Kaplan-Meier method was used to estimate the overall survival rate of different groups, and log-rank was used to test the significance of the difference between different groups. The difference of infiltration of immune cells in different groups was compared by using Wilcoxon signed rank sum test, and $P < 0.05$ was used as a significant threshold. Statistical analysis was made using R software, with version number v3.5.2.

Ethical Approval and Consent to Participate

No animals or humans were involved in this study. This study was carried out in accordance with the Declaration of Helsinki.

RESULTS

Analysis of Differentially Expressed Genes

In the TCGA dataset, we obtained 976 differentially expressed genes in cancer samples relative to the samples from the cancer samples, including 568 up-regulated genes and 408 down regulated genes (**Figure 1A**). The difference in the expression of differentially expressed genes between cancer and paracancerous samples was more obvious (**Figure 1B**).

Go and KEGG Enrichment Analysis Results

Through GO and KEGG enrichment analysis, we found that 976 differentially expressed genes were significantly enriched in GO term, such as regulation of membrane potential, and the top 10 most significant differentially expressed genes GO terms were shown in **Figures 1C,D**, detailed results of the GO enrichment analysis were shown in **Supplementary Table S1**. The 976 differentially expressed genes were significantly enriched in Neuroactive ligand-receptor interaction and other KEGG Pathway, among the most significant of the first 20 pathways were shown in the detailed results of the **Figures 1E,F**, KEGG enrichment analysis in **Supplementary Table S2**.

[4]https://string-db.org/,version 11.0

[5]http://www.proteinatlas.org/

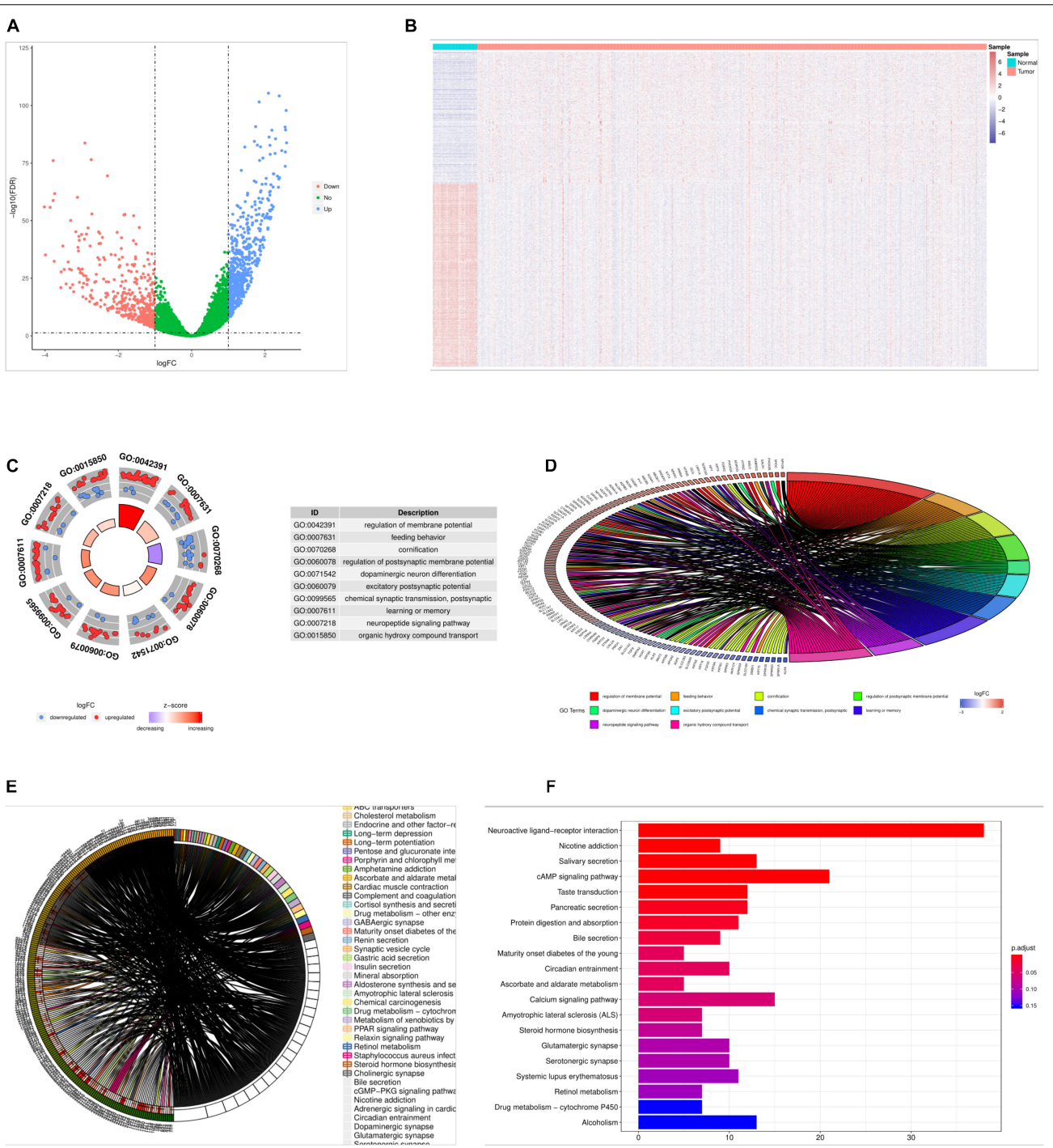

ID	Description
GO:0042391	regulation of membrane potential
GO:0007631	feeding behavior
GO:0070268	cornification
GO:0060078	regulation of postsynaptic membrane potential
GO:0071542	dopaminergic neuron differentiation
GO:0060079	excitatory postsynaptic potential
GO:0099565	chemical synaptic transmission, postsynaptic
GO:0007611	learning or memory
GO:0007218	neuropeptide signaling pathway
GO:0015850	organic hydroxy compound transport

FIGURE 1 | Results of differential gene analysis. **(A)** volcano plot of differentially expressed genes, the horizontal axis is the differential expression multiple (Log2FC), the longitudinal axis is—log10(fdr), the blue point is the up-regulated gene, and the red point is the down-regulated gene. **(B)** The heat map of the differentially expressed genes, the horizontal axis is the sample, the longitudinal axis is the different genes, the red indicates the high expression of the gene, and the blue indicates the low expression of the gene. **(C)** Circle graph of the top 10 GO terms with the most enriched genes. **(D)** Enriched the first 10 GO term and chord graphs with the largest number of genes, the right semicircle represented 10 GO term, the left semicircle represented the genes enriched in these 10 GO term. **(E)** Chord diagram of the main KEGG signaling pathway for gene enrichment. **(F)** Top 20 KEGG pathway, with the largest number of enriched genes, the horizontal axis of the map indicated the number of genes enriched, and the longitudinal axis indicated the names of each species.

PPI Network Construction and Screening Results of Key Genes

We used STRING database to construct PPI networks for 976 differentially expressed genes, a threshold of minimum required interaction score > 0.4 was used to screen interaction pairs, PPI network had 634 nodes and 2,999 sides in **Figure 2A**. A node represented a gene, and the edges represent the interrelationships between them. Then we used Cytoscape software to analyze the whole PPI network. MCC algorithm was used to score each node in the network, and the top 100 genes were selected from large to small. The 100 genes were shown in detail in **Supplementary Table S3**. The deeper the color is, the higher the importance of nodes is (**Figures 2B,C**).

Construction and Validation of a Prognostic Model

Using TCGA data sets, 210 autophagy gene expression values were used as continuous variables to conduct univariate Cox regression analysis, and Hazard ratio (HR) of each gene was calculated. $P < 0.05$ was selected as the threshold for screening. Finally, 11 genes were obtained, and the HR value of two genes was less than 1. There were nine genes with a HR value greater than 1 which were risk genes that were unfavorable to prognosis (**Figure 3A**). After that, we screened the 11 autophagy genes by LASSO Cox regression analysis. The optimal number of genes was determined to be 8 (minimum **Figure 3B**, lambda value) according to the lambda values corresponding to the number of different genes in the LASSO Cox analysis. The eight genes were *CTSD*, *ULK3*, *CDKN2A*, *NRG1*, *ATG4B*, *ULK1*, *DAPK1*, and *SERPINA1*.

Based on the expression of each gene and the regression coefficient of LASSO Cox regression analysis, a risk score model for predicting the survival of patients was established. Risk Score = (Express Value of *CTSD**0.08810216)+(Express Value of *ULK3**0.06755919)+(Express Value of *CDKN2A**0.08355253)+(Express Value of *NRG1**-0.11920988)+(Express Value of *ATG4B**0.07071560)+(Express

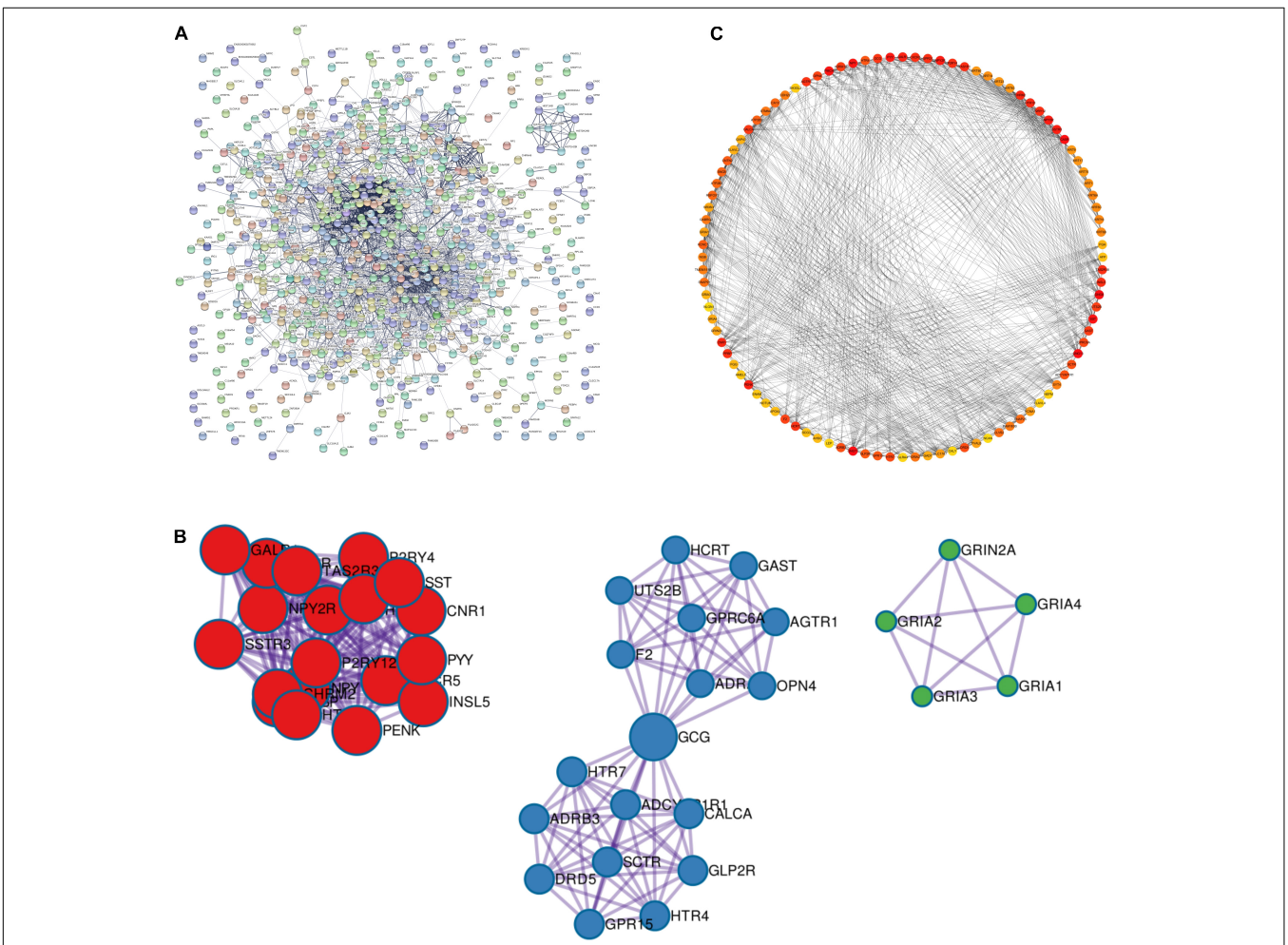

FIGURE 2 | PPI network build results. **(A)** PPI network diagram, every dot in the network represents a node, the more lines connected to the dot, the larger the degree representing this node. It means that the gene on this node may be more important in the network structure. **(B)** The three main clustering modules in the PPI network. **(C)** MCC degree higher top 100 genes in the network screened by the algorithm, the darker the red color indicates the higher the degree.

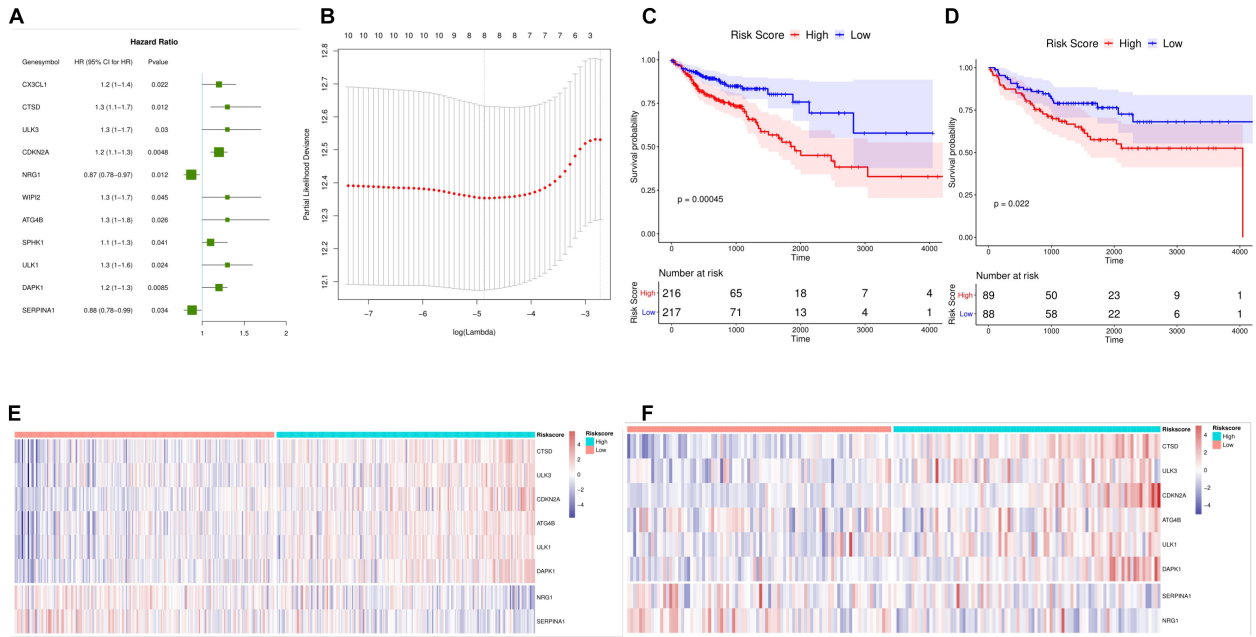

FIGURE 3 | Establishment of a prognostic model for colon cancer. **(A)** Forest maps of 15 autophagy genes significantly associated with colon cancer prognosis. HR Hazard ratio, 95%CI 95% confidence interval. **(B)** LASSO Figure in the regression model to determine the tuning parameter lambda. the horizontal axis is log (lambda), and the longitudinal axis is the partial likelihood deviation value (partial likelihood Deviance). the corresponding Lambda value at the minimum of this value is the best, that is, the best Lambda value after taking the Log below the dotted line, and the number of variables corresponding above. **(C)** Survival curve Kaplan Meier TCGA data set, the horizontal axis is time, the longitudinal axis is survival, and different colors represent different groups. *P*-values are based on log-rank tests. **(D)** Kaplan Meier survival curve and time dependent ROC curve of (GEO) datasets. **(E,F)** Heat maps of mRNA expression of eight selected genes in high and low risk score samples of TCGA and GEO datasets. The horizontal axis is the sample, the longitudinal axis is the gene, the red represents the high expression, the blue represents the low expression, and the heat map shows the category of the sample with different colors above.

Value of *ULK1**0.01917531)+ (Express Value of *DAPK1**0.12813474)+ (Express Value of *SERPINA1**-0.15361284). We calculated the risk score for each patient and divided the samples of TCGA dataset and GEO validation set into high-risk and low-risk groups according to the median. Survival analysis revealed that in TCGA and GEO datasets, High risk colon cancer samples showed poorer overall survival (**Figures 3C,D**) than those with low risk. At the same time, we found that there was a significant difference in the expression of the eight genes between the high-risk groups (**Figures 3E,F**). Overall, the results showed that the risk score (Risk Score) calculated using the evaluation model constructed by *CTSD, ULK3, CDKN2A, NRG1, ATG4B, ULK1, DAPK1,* and *SERPINA1* could better predict the prognosis of colon cancer patients.

Risk Score Is an Independent Prognostic Marker for Colon Cancer

We included four factors including age, TNMStage, gender, and Risk Score to conduct a multivariate Cox regression analysis to determine whether the risk score was an independent prognostic indicator. Results were shown in **Figure 4A**. Risk Score, TNMStage, and age were found to remain significantly associated with overall survival, with a higher risk of death in samples with a high risk score, which was a poor prognostic factor (*HR* = 2.8, 95% CI :1.864-4.19, $P < 0.001$).

To further explore the prognostic value of Risk Score in colon cancer specimens with different clinicopathological factors, including age, TNM Stage and sex, we regrouped the patients with colon cancer according to these factors and analyzed the survival of Kaplan-Meier. Stage I, Stage II, Stage III, and Stage IV samples were found (**Figures 4B,C**); ≤68 and 68 (**Figures 4D,E**); male and female samples (**Figures 4F,G**); The overall survival rates of the high-risk group were significantly lower than those of the low risk group. These results indicated that Risk Score could be used as an independent indicator to predict the prognosis of patients with colon cancer.

The Nomogram Model Can Better Predict the Prognosis and Survival of Patients

We used the three independent prognostic factors of age, TNMStage and Risk Score to construct the nomogram model (**Figure 5A**). For each patient, three lines were drawn up to determine the Points. The sum of these Points was located on the "Total Points" axis, and then drew a line down from the Total Points axis to determine the probability that colon cancer patients will survive for 1, 3, and 5 years. The corrected curve in the calibration map was closer to the ideal curve (45 degree line with a slope of 1 at the origin of the coordinate axis) which indicated that the

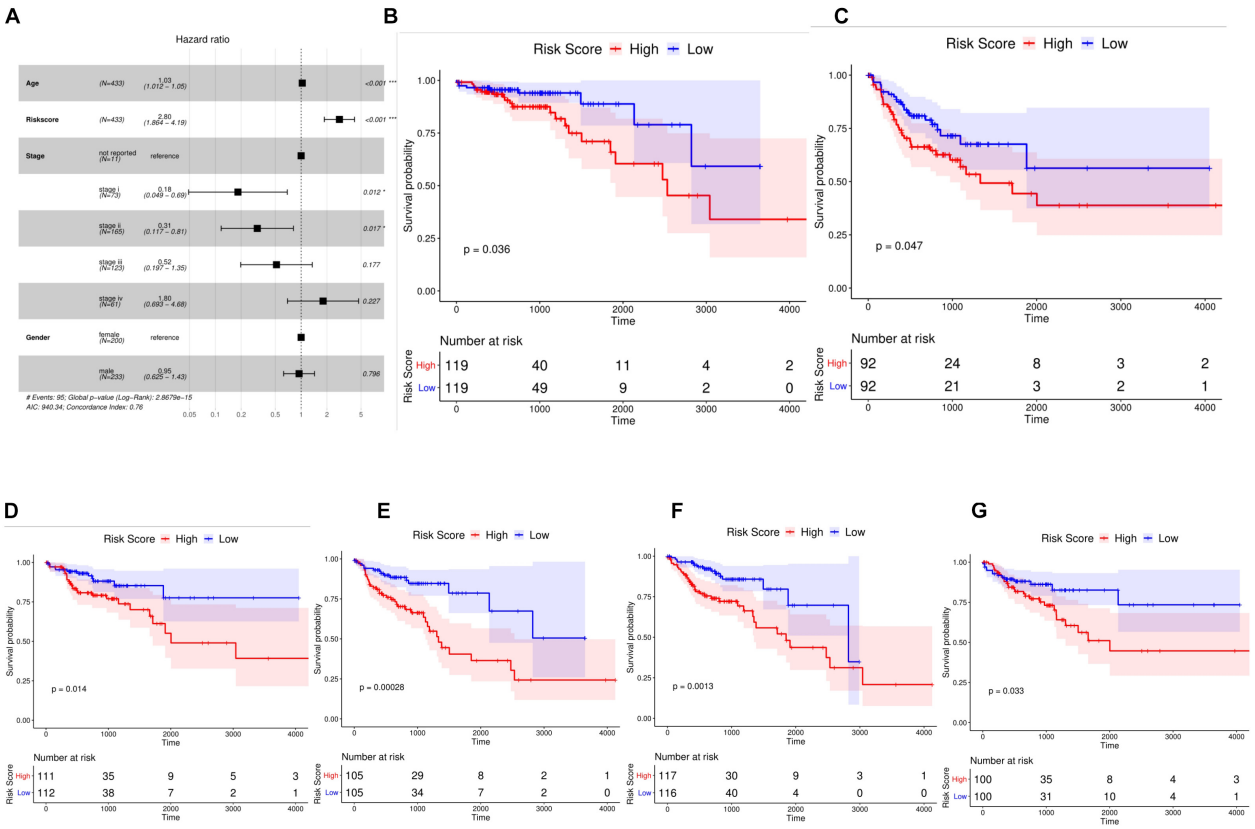

FIGURE 4 | Risk score was independent prognostic marker for colon cancer. **(A)** Multivariate Cox regression analysis of forest plots. Compared with reference samples, samples with Hazard ratio greater than 1 had higher risk of death. Samples with Hazard ratio less than 1 had a lower risk of death. **(B,C)** Kaplan Meier survival curves of colon cancer samples with different Stage stages. **(D,E)** Kaplan Meier survival curves of colon cancer samples from different age groups. **(F,G)** Kaplan survival curves of colon cancer samples from different sexes.

prediction was in good agreement with the actual results (**Figures 5B–D**).

Immune Status of Colorectal Cancer Patients With High and Low Risk Group

We used CIBERSORT method combined with LM22 feature matrix to estimate the immune infiltration differences between 22 immune cells in colorectal cancer patients with high and low risk groups. **Figure 6A** summarized the results of immune cell infiltration in 433 colon cancer patients. The changes in the proportion of tumor infiltrating immune cells in different patients may represent the intrinsic characteristics of individual differences. The correlation between the infiltration ratios of different types of immune cells is relatively weak (**Figure 6B**). There was a significant difference in the proportion of nine kinds of immune cells in Macrophages between the high risk group and the low risk group (**Figure 6C**). The PCA analysis showed that the samples could be divided into high-risk group and low-risk group (**Figure 7A**) according to the clustering of these nine different immune cells, indicating that the content difference of immune cells may be the potential cause of the risk of sample height and height.

Relationship Between Riskscore and Immunological Checkpoint Genes

The expression of immune checkpoints has become a biomarker for colon cancer patients to choose immunotherapy. We analyzed the correlation between patient risk score and key immune checkpoints (CTLA4, PDL1, LAG3, TIGIT, IDO1, TDO2), and found that the risk score was correlated with them (**Figure 7B**). Moreover, the six immunoassay checkpoints were in addition to TDO2, the other five immunocheck points had significant difference in the expression of high risk colon cancer patients (**Figure 7C**), and the expression level of high risk colon cancer group was significantly higher than that of low risk colon cancer group ($P < 0.05$).

Immunohistochemical Verification of Prognostic Genes

The data verification results of the HPA database indicated that the expression of ULK1 in cancer and adjacent tissues had not been detected in the database, and the expression of the remaining seven genes in cancer and adjacent tissues could be verified. Among them, NRG1 gene was not significantly

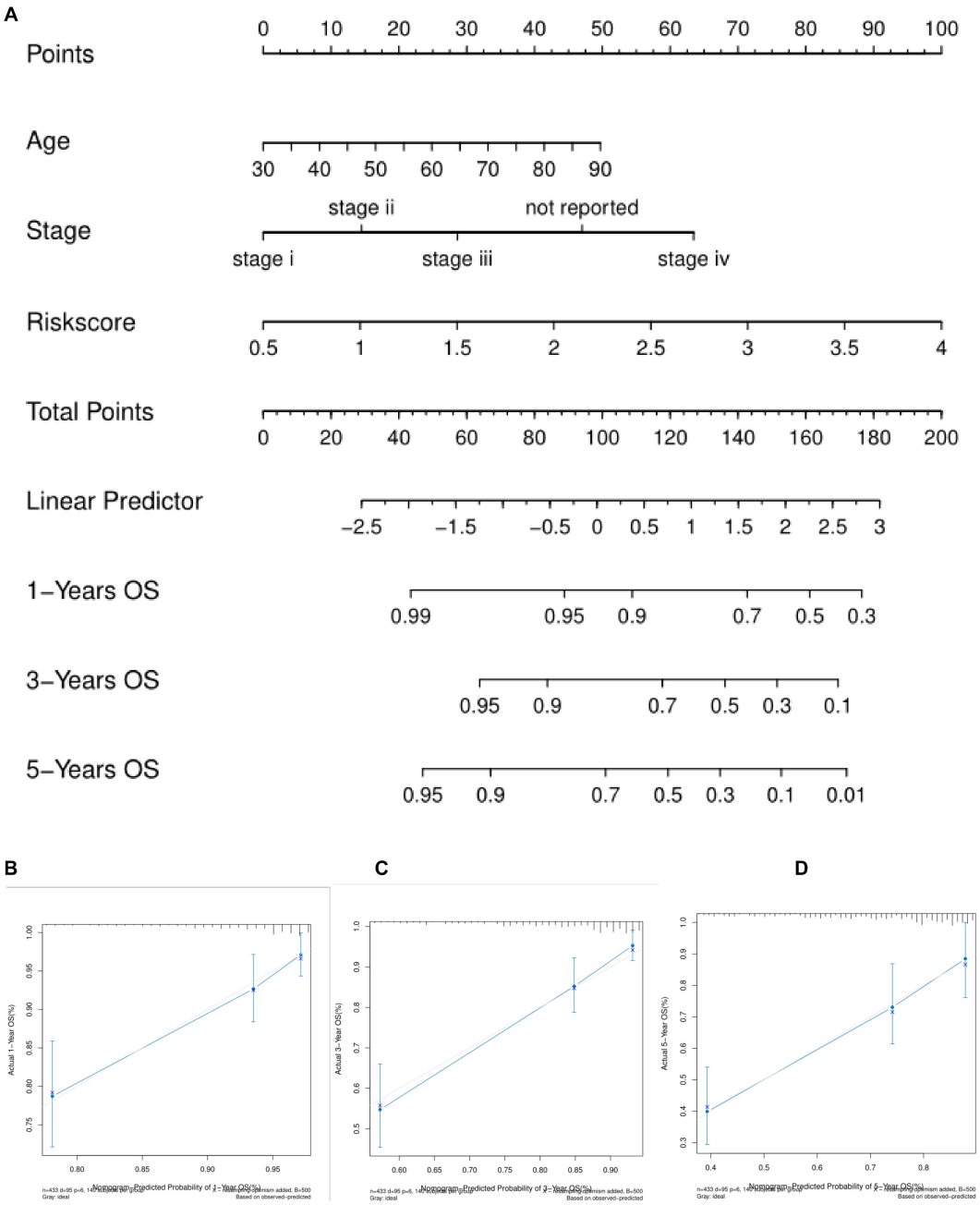

FIGURE 5 | Nomogram predicts the survival of patients with colon cancer. **(A)** Nomogram to predict the probability of 1, 3, and 5 years OS in colon cancer patients. **(B–D)** Normative curve for predicting the probability of 1, 3, and 5 years OS colon cancer patients. the X axis represents nomogram predicted survival and the Y axis represents the actual survival.

expressed in tumor and normal tissues, and there was no significant difference in expression. Compared with normal tissues, the expressions of *CTSD, ULK3, CDKN2A, ATG4B, and DAPK1* in tumor tissues were significantly up-regulated, and the expression of *SERPINA1* in tumor tissues was significantly down-regulated; the verification results were basically consistent with the research analysis results (**Figure 8**).

DISCUSSION

Colon cancer is one of the main malignant tumors of the gastrointestinal tract, around 600 thousand people die of colon cancer every year (American Cancer Society, 2017; Siegel et al., 2017; Bray et al., 2018). With the improvement of surgical method and follow-up treatment, the 5 year survival rate of colon cancer in developed countries is close to 65% (Miller et al., 2016).

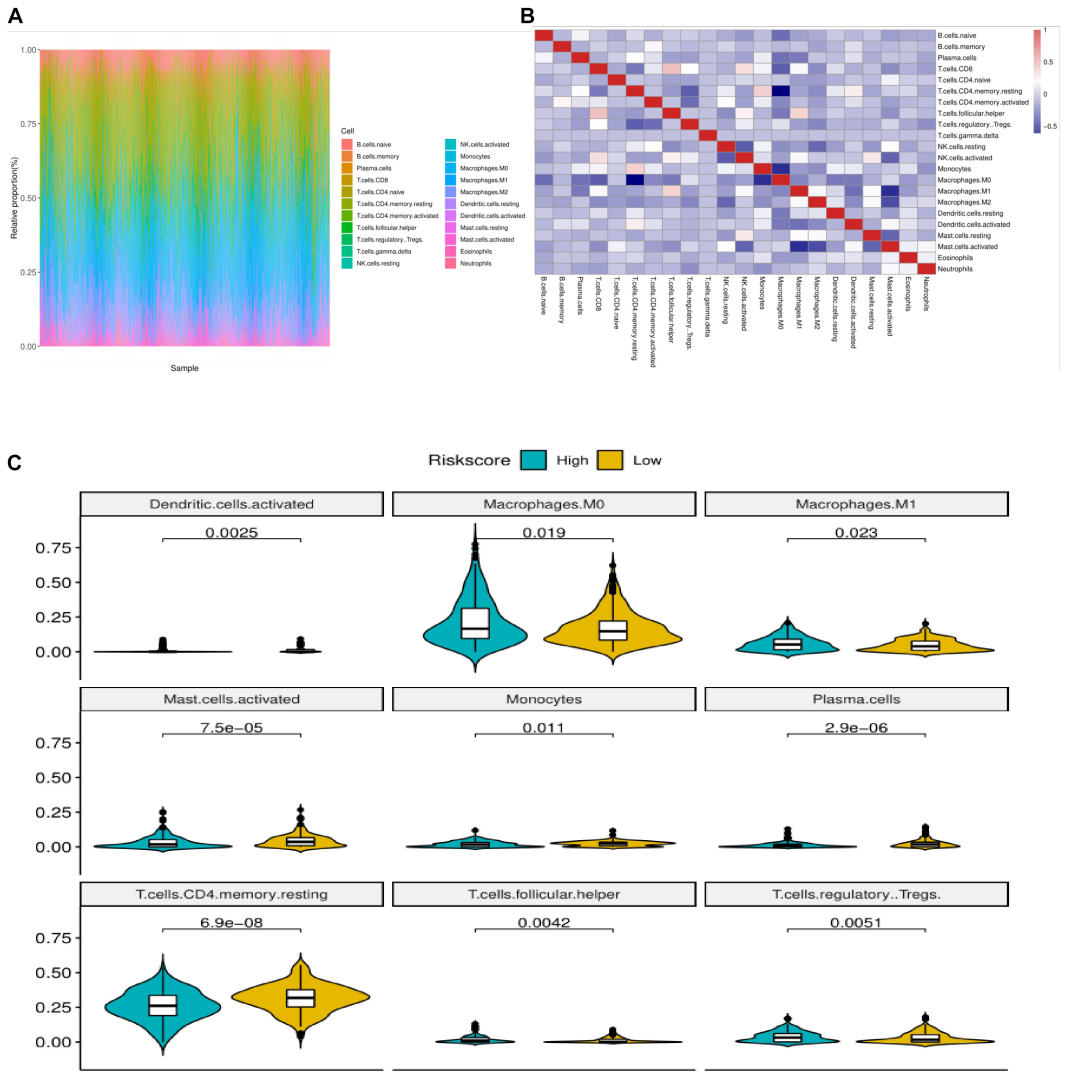

FIGURE 6 | Correlation analysis of immune infiltration in colon cancer patients with high and low risk groups. **(A)** Relative proportion of immune infiltrating cells in all patients. **(B)** Correlation matrix of 22 immune cell proportions. Red represents positive correlation. Blue is negative correlation. The deeper the color is, the greater the correlation. **(C)** The violin diagram of immune cells with significant difference in high and low risk group, the horizontal axis is high and low risk group, the longitudinal axis is the relative infiltration ratio of immune cells, and the *p*-value is calculated by wilcoxn method.

However, for patients with cancer penetrating the intestinal wall or distant metastasis, their mortality is very high (Misale et al., 2012; Edwards et al., 2014; Fang et al., 2017). Therefore, it is urgent to find some new therapeutic targets which are closed to the prognosis of the patient.

In recent years, autophagy has been found to be closely related to the occurrence and development of tumors and the prognosis of cancer patients (Kroemer et al., 2010; Mizushima and Komatsu, 2011). Autophagy is very important for physiological processes such as cell development, differentiation, tissue remodeling and so on, and is very important for maintaining cell homeostasis (Kroemer and Levine, 2008; Li et al., 2010; Bhardwaj et al., 2018). Current studies have indicated that ABHD5, PFKFB3, oxaliplatin, for example, can play an antitumor role by regulating autophagy. However, a comprehensive study of the correlation between autophagy defects and metabolic dysfunction in colon cancer and its close relationship as well as functional interdependence in tumorigenesis have not been conducted (Kumar et al., 2012; Yan et al., 2014). At present, there are no studies that specifically analyze which genes in autophagy genes have an impact on the prognosis of colon cancer patients and what are the related biological response processes. It is of great significance to find which autophagy genes that play an important role in the development of the colon cancer and the prognosis of the patient. We used machine learning methods to analyze the data of a large number of colon cancer patients, constructed a prognostic evaluation model of colon cancer patients based on autophagy genes and verified the efficiency of the model using external data sets; using immunohistochemistry to verify the prognosis-related autophagy

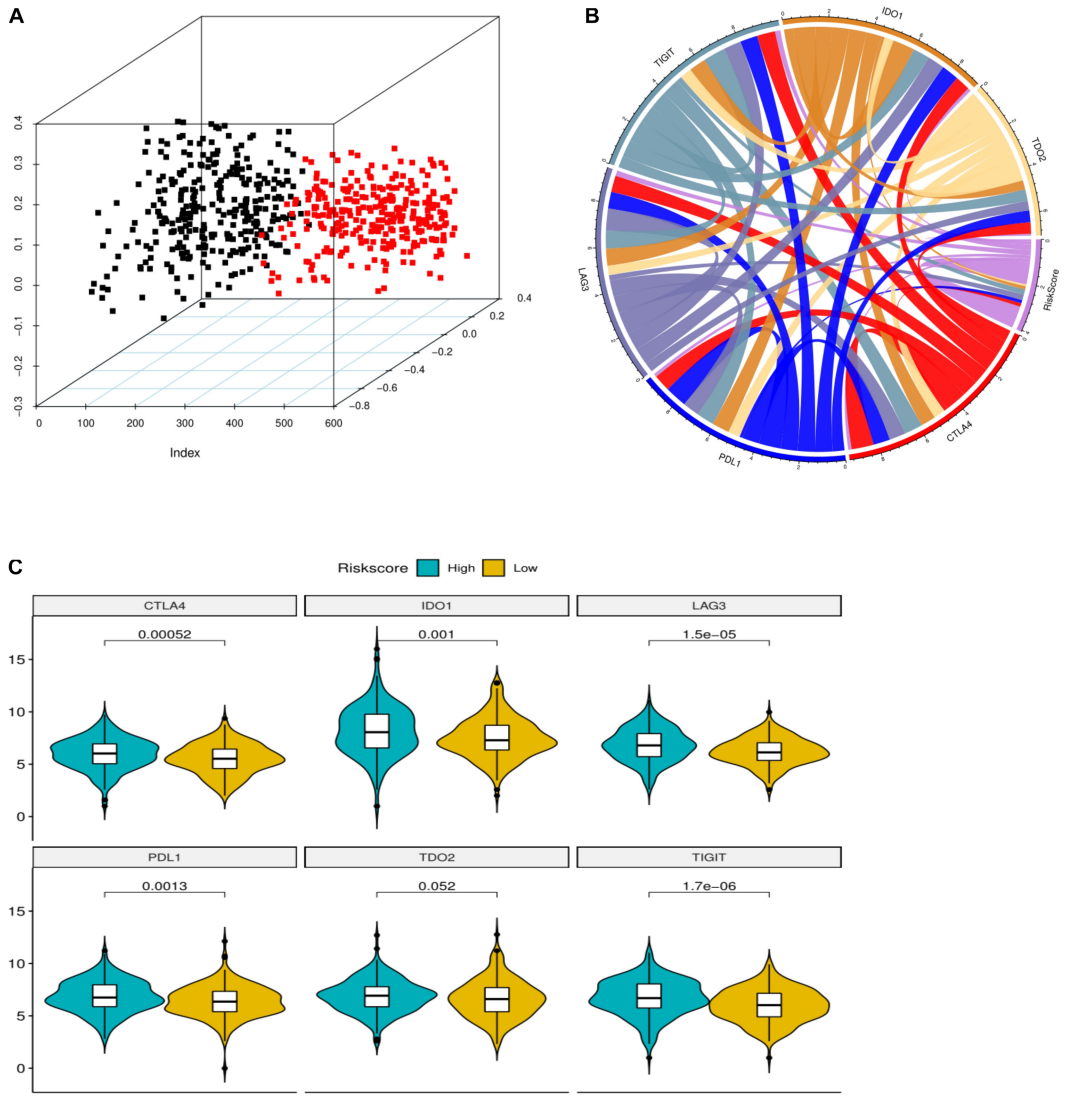

FIGURE 7 | (A) PCA three dimensional clustering diagram. Different color points represented different types of samples. **(B)** Correlation chord maps (Chord diagram) of risk scores with six prominent immune checkpoint expression, the more connections between them represent the stronger correlation between them. **(C)**The immune checkpoint violin diagram with significant difference in expression in high and low risk groups. Different colors represent high and low risk groups. The longitudinal axis is the expression amount. The *p*-value is calculated by wilcoxon method.

genes. In this study, we used colon cancer samples from TCGA as training group, GSE17536 as validation group, eight key prognostic autophagy genes in colon cancer were screened and identified, they were modeled by differential analysis, PPI network construction, COX single factor analysis, and LASSO Cox regression analysis. We used machine learning methods to analyze the data of a large number of colon cancer patients, constructed the prognostic evaluation model of colon cancer patients based on autophagy genes and verified the efficiency of the model using external data sets. Immunohistochemistry was used to verify the prognosis-related autophagy genes. Our results suggested that the constructed model can well distinguish colon cancer patients and predict prognosis, thereby helping to develop individualized treatment options based on patients' risk.

We identified a group of ARGs that predict the prognosis of colon cancer patients. Most of these genes have been reported in previous studies to be closely related to the prognosis of colon cancer or other malignancies. Lu et al. (2017); Shen et al. (2017), and Yan et al. (2019) reported that *CTSD* promotes the proliferation, migration, invasion and metastasis of hepatocellular carcinoma cells. Goruppi et al. (2017) reported that *ULK3* links two main signaling pathways involved in cancer-associated fibroblasts conversion of several tumor types and is an attractive target for stroma-focused anti-cancer intervention. *CDKN2A* inhibition combined with TAE therapy can promote tumor cell necrosis in hepatocellular carcinoma rats (Gade et al., 2017). The phosphorylation of *ATG4B* at Ser34 promoted the Warburg effect and the decrease of oxygen consumption

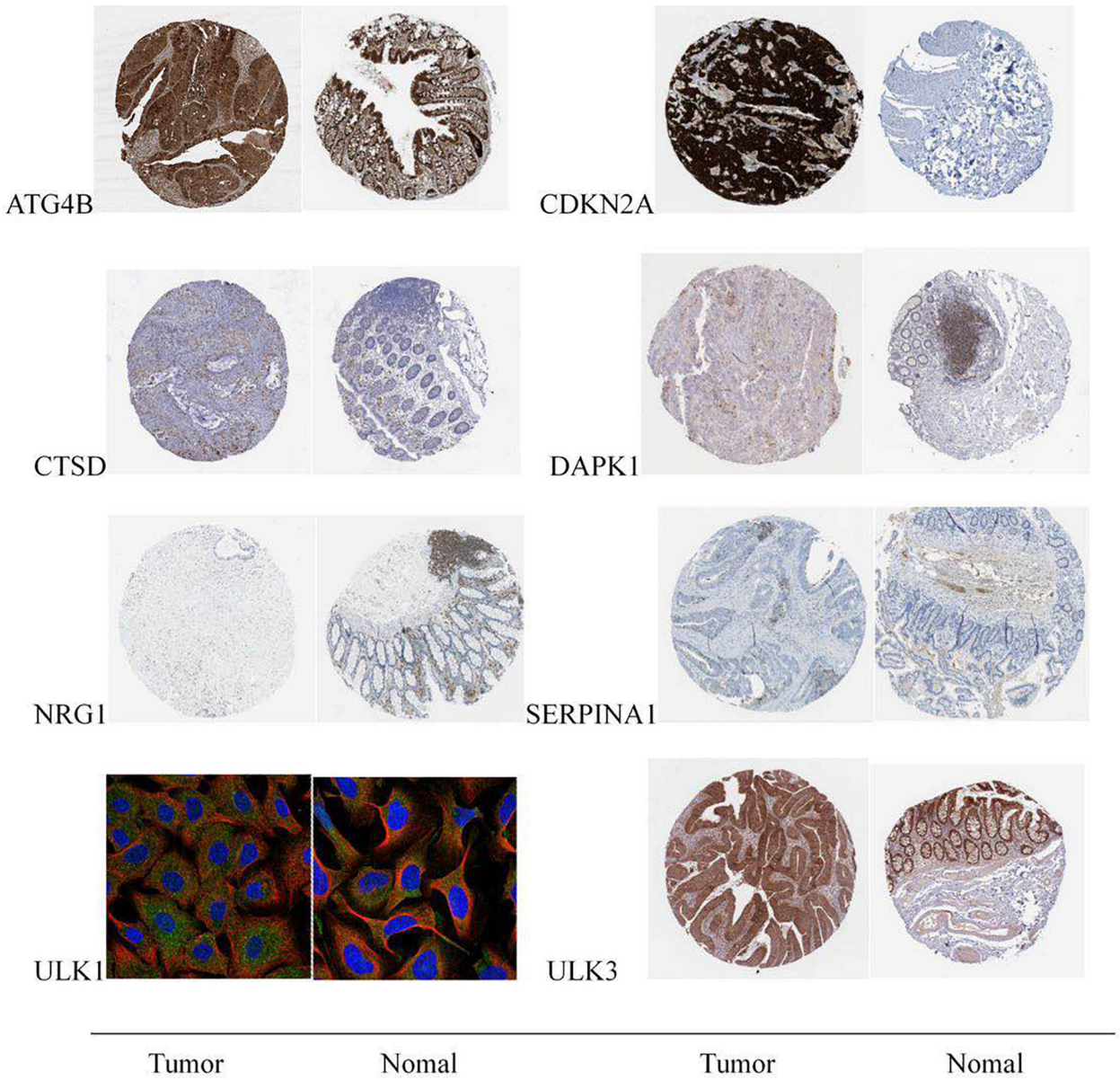

FIGURE 8 | Expression of eight prognostic-related autophagy genes in colon cancer tumor tissues and normal tissues.

in hepatocellular carcinoma cells (Ni et al., 2018). It can also alleviate intestinal inflammatory reaction and intestinal epithelial apoptosis through autophagy pathway (Li et al., 2018), while *ULK1* is the key gene of autophagy. Liu et al. (2019) reported that blocking *AMPK/ULK1*-dependent autophagy promoted apoptosis and initiated autophagy simultaneously, and suppressed colon cancer growth. The increased expression of *DAPK1* in cholangiocarcinoma promotes the apoptosis of cholangiocarcinoma cells and alleviates the autophagy induced by cholangiocarcinoma cells (Thongchot et al., 2018). The constructed model can well distinguish colon cancer patients and predict prognosis, thereby helping to develop individualized treatment options based on patient risk.

The aim of this study is to construct a model composed of prognostic autophagy genes which can well distinguish colon cancer patients and predict prognosis. The model we constructed included *CTSD, ULK3, CDKN2A, NRG1, ATG4B, ULK1, DAPK1*, and *SERPINA1* these eight genes. Among them, *CTSD, ULK3, CDKN2A, ATG4B, ULK1, DAPK1* are beneficial genes that are benefit to prognosis. *NRG1* and *SERPINA1* are dangerous genes that are not conducive to prognosis (**Figure 3A**). We performed a multivariate Cox regression analysis and Risk Score, the results showed that the survival time of the high-risk group was significantly lower than that of the low risk group (**Figures 4D–G**). This shows that our model can be used as an independent prognostic factor for colon cancer patients. According to the

nomogram model, the survival rate of colon cancer patients is consistent with the actual situation. This indicates that the constructed model can well distinguish colon cancer patients and predict prognosis. The results of immune cell infiltration in colon cancer samples showed that there was a significant difference in the infiltration ratio and other nine immune cells in high and low risk groups (**Figure 6C**). PCA results showed that the samples can be well differentiated according to these nine immune cells (**Figure 7A**). This indicates that the autophagy gene may affect the tumor cells by affecting the immune cells. The immune checkpoint correlation study of the samples grouped according to the model found that the expression of *CTLA4*, *PDL1*, *LAG3*, *TIGIT*, *IDO1* in the high risk group was significantly higher than that in the low risk group (**Figure 7C**). It is suggested that the poor prognosis of patients with high risk colon cancer may be due to immunosuppressive microenvironment. According to our research, the models constructed from these eight autophagy genes can well predict the prognosis of patients with colon cancer. We think these eight genes are biomarkers for predicting the prognosis of colon cancer patients, and may become new research targets for colon cancer patients. Our research identified the autophagy genes associated with prognosis and provided a new method for evaluating the prognosis of colon cancer patients. However, there are still some limitations in our study. The prognostic model still needs to be further validated in other independent large sample cohorts to ensure the reliability of our model. Functional experiments are needed to further reveal the possible mechanisms for predicting the role of autophagy genes.

CONCLUSION

We constructed an autophagy gene model closely related to the prognosis of colon cancer patients by analyzing the samples from patients with colon cancer. The model contains eight autophagy genes, including *CTSD*, *ULK3*, *CDKN2A*, *NRG1*, *ATG4B*, *ULK1*, *DAPK1*, and *SERPINA1*. These eight genes are closely related to the autophagy process of tumor development and development. We think that the models constructed from these eight genes can predict the prognosis of colon cancer patients well. And these eight genes may become biological targets regulating cell autophagy and treating colon cancer patients.

DATA AVAILABILITY STATEMENT

The datasets generated for this study can be found in the online repositories. The names of the repository/repositories and accession number(s) can be found in the article/**Supplementary Material**.

AUTHOR CONTRIBUTIONS

JX: research design and drafting the manuscript. SD: experiment implementation. YY: literature search and experiment implementation. QX: help modify articles and collate references. KD: review and revision of the manuscript and writing guidance. All authors contributed to the article and approved the submitted version.

FUNDING

The authors' research was supported by the research fund of the National Key R&D Program of China (2017YFC0908200), the Key Technology Research and Development Program of Zhejiang Province (No. 2017C03017), Project of the regional diagnosis and treatment center of the Health Planning Committee (No. JBZX-201903), and National Natural Science Foundation of China (No. 81772545).

SUPPLEMENTARY MATERIAL

The Supplementary Material for this article can be found online at: https://www.frontiersin.org/articles/10.3389/fcell.2020.602174/full#supplementary-material

REFERENCES

American Cancer Society (2017). *Cancer Facts & Figures*. Atlanta, GA: American Cancer Society.

Bhardwaj, M., Cho, H. J., Paul, S., Jakhar, R., Khan, I., Lee, S. J., et al. (2018). Vitexin induces apoptosis by suppressing autophagy in multi-drug resistant colorectal cancer cells. *Oncotarget* 9, 3278–3291. doi: 10.18632/oncotarget.22890

Bray, F., Ferlay, J., Soerjomataram, I., Siegel, R. L., Torre, L. A., and Jemal, A. (2018). Global cancer statistics 2018: GLOBOCAN estimates of incidence and mortality worldwide for 36 cancers in 185 countries. *CA Cancer J. Clin.* 68, 394–424. doi: 10.3322/caac.21492

Cheng, Y., Ren, X., Hait, W. N., and Yang, J. M. (2013). Therapeutic targeting of autophagy in disease: biology and pharmacology. *Pharmacol. Rev.* 65, 1162–1197. doi: 10.1124/pr.112.007120

Edwards, B. K., Noone, A. M., Mariotto, A. B., Simard, E. P., Boscoe, F. P., Henley, S. J., et al. (2014). Annual Report to the Nation on the status of cancer, 1975-2010, featuring prevalence of comorbidity and impact on survival among persons with lung, colorectal, breast, or prostate cancer. *Cancer* 120, 1290–1314. doi: 10.1002/cncr.28509

Eskelinen, E. L. (2011). The dual role of autophagy in cancer. *Curr. Opin. Pharmacol.* 11, 294–300. doi: 10.1016/j.coph.2011.03.009

Fang, C., Fan, C., Wang, C., Huang, Q., Meng, W., Yu, Y., et al. (2017). Prognostic value of CD133+ CD54+ CD44+ circulating tumor cells in colorectal cancer with liver metastasis. *Cancer Med.* 6, 2850–2857. doi: 10.1002/cam4.1241

Fearon, E. R., and Vogelstein, B. (1990). A genetic model for colorectal tumorigenesis. *Cell* 61, 759–767. doi: 10.1016/0092-8674(90)90186-I

Fulda, S., and Kogel, D. (2015). Cell death by autophagy: emerging molecular mechanisms and implications for cancer therapy. *Oncogene* 34, 5105–5113. doi: 10.1038/onc.2014.458

Gade, T. P. F., Tucker, E., Nakazawa, M. S., Stephen, J. H., Waihay, W., and Bryan, K. (2017). Ischemia induces quiescence and autophagy dependence in hepatocellular carcinoma. *Radiology* 283, 702–710. doi: 10.1148/radiol.2017160728

Goruppi, S., Procopio, M. G., Jo, S., Clocchiatti, A., Neel, V., and Dotto, G. P. (2017). The ULK3 kinase is critical for convergent control of cancer-associated fibroblast activation by CSL and GLI. *Cell Rep.* 20, 2468–2479. doi: 10.1016/j.celrep.2017.08.048

Jemal, A., Bray, F., Center, M. M., Ferlay, J., Ward, E., and Forman, D. (2011). Global cancer statistics. *CA Cancer J. Clin.* 61, 69–90. doi: 10.3322/caac.20107

Kondo, Y., Kanzawa, T., Sawaya, R., and Kondo, S. (2005). The role of autophagy in cancer development and response to therapy. *Nat. Rev. Cancer* 5, 726–734. doi: 10.1038/nrc1692

Kroemer, G., and Levine, B. (2008). Autophagic cell death: the story of a misnomer. *Nat. Rev. Mol. Cell Boil.* 9, 1004–1010. doi: 10.1038/nrm2529

Kroemer, G., Marino, G., and Levine, B. (2010). Autophagy and the integrated stress response. *Mol. Cell.* 40, 280–293. doi: 10.1016/j.molcel.2010.09.023

Kumar, P., Zhang, D.-M., Degenhardt, K., and Chen, Z.-S. (2012). Autophagy and transporter-based multi-drug resistance. *Cells* 1, 558–575. doi: 10.3390/cells1030558

Li, J., Hou, N., Faried, A., Tsutsumi, S., and Kuwano, H. (2010). Inhibition of autophagy augments 5-fluorouracil chemotherapy in human colon cancer in vitro and in vivo model. *Eur. J. Cancer* 46, 1900–1909. doi: 10.1016/j.ejca.2010.02.021

Li, Z., Wang, G., Feng, D., Guo, Z., Yang, L., and Xue, S. (2018). Targeting the miR-665-3p-ATG4B-autophagy axis relieves inflammation and apoptosis in intestinal ischemia/reperfusion. *Cell Death Dis.* 9:483. doi: 10.1038/s41419-018-0518-9

Liu, J., Long, S., Wang, H., Nannan, L., Chuchu, Z., and Lingling, Z. (2019). Blocking AMPK/ULK1-dependent autophagy promoted apoptosis and suppressed colon cancer growth. *Cancer Cell Int.* 19:336. doi: 10.1186/s12935-019-1054-0

Lu, W.-Q., Hu, Y.-Y., Lin, X.-P., and Fan, W. (2017). Knockdown of PKM2 and GLS1 expression can significantly reverse oxaliplatin-resistance in colorectal cancer cells. *Oncotarget* 8, 44171–44185. doi: 10.18632/oncotarget.17396

Maiuri, M. C., Zalckvar, E., Kimchi, A., and Kroemer, G. (2007). Self-eating and self-killing: crosstalk between autophagy and apoptosis. *Nat. Rev. Mol. Cell Biol.* 8, 741–752. doi: 10.1038/nrm2239

Martinet, W., and De Meyer, G. R. (2009). Autophagy in atherosclerosis: a cell survival and death phenomenon with therapeutic potential. *Circ. Res.* 104, 304–317. doi: 10.1161/circresaha.108.188318

Meyerhardt, J. A., and Mayer, R. J. (2005). Systemic therapy for colorectal cancer. *N. Engl. J. Med.* 352, 476–487. doi: 10.1056/NEJMra040958

Miller, K. D., Siegel, R. L., Lin, C. C., Mariotto, A. B., Kramer, J. L., Rowland, J. H., et al. (2016). Cancer treatment and survivorship statistics. *CA Cancer J. Clin.* 2016, 271–289. doi: 10.3322/caac.21349

Misale, S., Yaeger, R., Hobor, S., Scala, E., Janakiraman, M., Liska, D., et al. (2012). Emergence of KRAS mutations and acquired resistance to anti-EGFR therapy in colorectal cancer. *Nature* 486, 532–536. doi: 10.1038/nature11156

Mizushima, N. (2007). Autophagy: process and function. *Genes Dev.* 21, 2861–2873. doi: 10.1101/gad.1599207

Mizushima, N., and Komatsu, M. (2011). Autophagy: renovation of cells and tissues. *Cell* 147, 728–741. doi: 10.1016/j.cell.2011.10.026

Ni, Z., He, J., Wu, Y., Hu, C., Dai, X., Yan, X., et al. (2018). AKT-mediated phosphorylation of ATG4B impairs mitochondrial activity and enhances the Warburg effect in hepatocellular carcinoma cells. *Autophagy* 14, 685–701. doi: 10.1080/15548627.2017.1407887

Shen, S., Gong, J., Yang, Y., Si, Q., Lifan, H., and Sha, S. (2017). Molecular mechanism of C-reaction protein in promoting migration and invasion of hepatocellular carcinoma cells in vitro. *Int. J. Oncol.* [Epub ahead of print]. doi: 10.3892/ijo.2017.3911

Siegel, R. L., Miller, K. D., Fedewa, S. A., Ahnen, D. J., Meester, R. G. S., Barzi, A., et al. (2017). Colorectal cancer statistics. *CA Cancer J. Clin.* 2017, 177–193. doi: 10.3322/caac.21395

Thongchot, S., Vidoni, C., Ferraresi, A., Watcharin, L., and Puangrat, Y. (2018). Dihydroartemisinin induces apoptosis and autophagy-dependent cell death in cholangiocarcinoma through a DAPK1-BECLIN1 pathway. *Mol. Carcinog.* 57, 1735–1750. doi: 10.1002/mc.22893

Yan, S., Yang, X., Chen, T., Xi, Z., and Jiang, X. (2014). The PPARgamma agonist Troglitazone induces autophagy, apoptosis and necroptosis in bladder cancer cells. *Cancer Gene Ther.* 21, 188–193. doi: 10.1038/cgt.2014.16

Yan, S., Zhou, N., Zhang, D., Zhang, K., Zheng, W., and Bao, Y. (2019). PFKFB3 inhibition attenuates oxaliplatin-induced autophagy and enhances its cytotoxicity in colon cancer cells. *Int. J. Mol. Sci.* 20:5415. doi: 10.3390/ijms20215415

Conflict of Interest: The authors declare that the research was conducted in the absence of any commercial or financial relationships that could be construed as a potential conflict of interest.

frontiers in Oncology

REVIEW
published: 18 December 2020
doi: 10.3389/fonc.2020.598817

Long Non-Coding RNAs: The Regulatory Mechanisms, Research Strategies, and Future Directions in Cancers

Na Gao[1], Yueheng Li[1], Jing Li[1], Zhengfan Gao[1], Zhenzhen Yang[1,2], Yong Li[1,3], Hongtao Liu[4] and Tianli Fan[1]**

[1] Department of Pharmacology, School of Basic Medicine, Zhengzhou University, Zhengzhou, China, [2] Translational Medicine Research Center, People's Hospital of Zhengzhou, Zhengzhou, China, [3] Faculty of Medicine, St George and Sutherland Clinical School, St George Hospital, The University of New South Wales (UNSW) Sydney, Kensington, NSW, Australia, [4] Laboratory for Cell Biology, College of Life Sciences of Zhengzhou University, Zhengzhou, China

OPEN ACCESS

Edited by:
Lorenzo Gerratana,
University of Udine, Italy

Reviewed by:
Anup Kumar Singh,
Beckman Research Institute, City of Hope, United States
Young-Jun Jeon,
Sungkyunkwan University, South Korea

***Correspondence:**
Hongtao Liu
liuht@zzu.edu.cn
Tianli Fan
fantianli@zzu.edu.cn

Specialty section:
This article was submitted to Molecular and Cellular Oncology, a section of the journal Frontiers in Oncology

Received: 25 August 2020
Accepted: 18 November 2020
Published: 18 December 2020

Citation:
Gao N, Li Y, Li J, Gao Z, Yang Z, Li Y, Liu H and Fan T (2020) Long Non-Coding RNAs: The Regulatory Mechanisms, Research Strategies, and Future Directions in Cancers. Front. Oncol. 10:598817. doi: 10.3389/fonc.2020.598817

The development and application of whole genome sequencing technology has greatly broadened our horizons on the capabilities of long non-coding RNAs (lncRNAs). LncRNAs are more than 200 nucleotides in length and lack protein-coding potential. Increasing evidence indicates that lncRNAs exert an irreplaceable role in tumor initiation, progression, as well as metastasis, and are novel molecular biomarkers for diagnosis and prognosis of cancer patients. Furthermore, lncRNAs and the pathways they influence might represent promising therapeutic targets for a number of tumors. Here, we discuss the recent advances in understanding of the specific regulatory mechanisms of lncRNAs. We focused on the signal, decoy, guide, and scaffold functions of lncRNAs at the epigenetic, transcription, and post-transcription levels in cancer cells. Additionally, we summarize the research strategies used to investigate the roles of lncRNAs in tumors, including lncRNAs screening, lncRNAs characteristic analyses, functional studies, and molecular mechanisms of lncRNAs. This review will provide a short but comprehensive description of the lncRNA functions in tumor development and progression, thus accelerating the clinical implementation of lncRNAs as tumor biomarkers and therapeutic targets.

Keywords: long non-coding RNA, mechanism of action, research strategies, therapeutic targets, cancer

INTRODUCTION

Cancer is a complex disease associated with multiple genetic mutations. Over the past few decades, oncogenes such as Src and Ras have been discovered, and the functions of their encoded proteins have been elucidated. While cancer awareness is gradually increasing worldwide, the current focus is still concentrated on the DNA sequence responsible for the abnormal protein synthesis. With the widespread application of next-generation sequencing (NGS) technology, a large number of non-coding genes have been identified and found to be strongly associated with tumor development and progression. Therefore, it is of paramount importance to understand the underlying mechanism through which non-coding genes influence the tumorigenic process.

In 1961, the central position of RNA in the flow of genetic information was revealed (1) and in the following 50 years, the emergence of whole-genome sequencing technology has greatly accelerated our understanding of both coding and non-coding RNAs (ncRNAs) (2, 3). Many regulatory RNAs harboring various sizes have been discovered (4), especially long non-coding RNAs (lncRNAs) (5). LncRNAs are a class of RNA molecules comprised of more than 200 nucleotides, which do not encode proteins. LncRNAs were originally thought to be by-products transcribed by RNA polymerase II and have no biological function; however, with the development of high-throughput sequencing technology, an increasing number of lncRNAs have been annotated, and their functions of lncRNAs in tumorigenesiss and tumor progression have been gradually elucidated. Previous studies showed that lncRNAs are involved in the regulation of cell survival, growth (6–10), invasion, and metastasis (11), maintenance of stemness (12, 13), as well as tumor angiogenesis (14). These studies highlight the essential role of lncRNAs in cancer development and progression, as well as their potential as novel therapeutic targets for multiple tumors.

LncRNAs are structurally similar to mRNAs and are also generated through DNA transcription (15). Based on the chromosomal position of the lncRNAs, they are divided into antisense lncRNAs, intronic lncRNAs, divergent lncRNAs, intergenic lncRNAs, promoter-associated lncRNAs, transcription start site-associated lncRNAs, and enhancer RNAs (eRNAs) (16–20). Interestingly, the number of lncRNAs far exceeds the number of protein-coding genes (21). Numerous lncRNAs are abnormally expressed in specific cancer types (22) and participate in a variety of complex biological processes by interacting with proteins, DNA, as well as RNAs (23–26). However, the specific mechanisms of abnormally expressed lncRNAs in cancer cells remain unclear. There are still many outstanding questions that need to be explored. For example, what are the specific modes of action of lncRNAs? How dose the location of lncRNAs in the nucleus or cytoplasm affect their mechanism of action? How can the research strategies of lncRNAs in cancer cells be explored?

Here, we describe the specific regulatory mechanisms of lncRNAs, mainly focusing on their signal, decoy, guide, and scaffold functions in cancer cells. The lncRNAs in the nucleus are mainly involved in epigenetic and transcriptional regulation while the lncRNAs in the cytoplasm are often involved in post-transcriptional regulation, thus regulating the mRNA stability, protein translation and the competitive endogenous RNA (ceRNA) network. In addition, the research strategies used to identify the roles of lncRNAs in tumors are summarized, including lncRNA screening, lncRNA characteristic analyses, functional studies and molecular mechanisms of lncRNAs. The current review will provide a comprehensive description of the lncRNA functions and novel insights into their underlying molecular mechanisms.

THE MECHANISMS OF ACTION OF LNCRNAS IN CANCER

The lncRNA mechanisms of action can be divided into four categories: signal, decoy, guide, and scaffold (19, 27–29) (**Figure 1**).

LncRNAs as Signal Molecules

As signal molecules, lncRNAs are often considered to regulate the transcription of downstream genes. Previous studies have demonstrated that lncRNAs are specifically transcribed and they influence certain signaling pathways under different stimulation conditions. The transcribed lncRNAs act by themselves or in combination with certein proteins (such as transcription factors) to mediate the transcription of downstream genes. Huarte et al. showed that p53-induced lncRNA-p21 interacted with nuclear heterogeneous ribonucleoprotein-K to inhibit the expression of downstream genes in the p53 signaling pathway (10). LncRNA

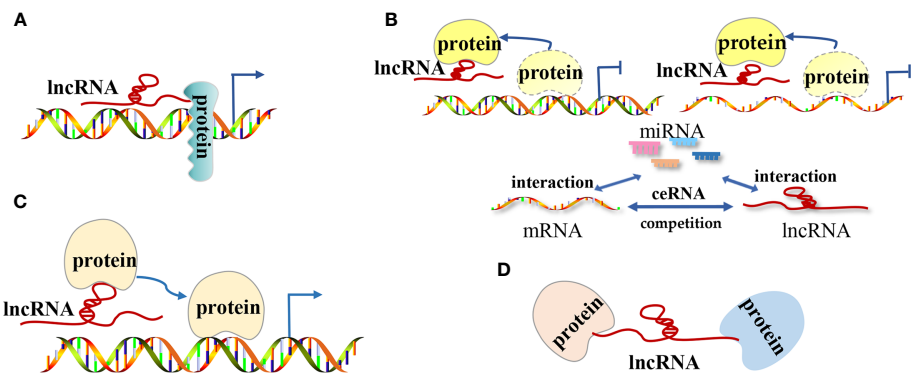

FIGURE 1 | The modes of action of long non-coding RNAs (lncRNAs) in tumors. **(A)** LncRNAs as signal molecules can be used alone or combined with some proteins(such as transcription factors) to mediate the transcription of downstream genes; **(B)** LncRNAs as decoy molecules bind to some functional protein molecules to block the protein molecules from regulating DNA and mRNA molecules or bind to miRNA molecules competitively with mRNA molecules to block the inhibitory effect of miRNA on mRNA molecules; **(C)** LncRNAs as guide molecules carries some functional protein molecules and locates them in the target area to perform functions; **(D)** LncRNAs as a scaffold molecule guide related different types of macromolecular complexes to assemble in the target area to work together.

PANDA, which is activated by the interaction between p53 and cyclin-dependent kinase inhibitor 1A (CDKN1A, p21) in the presence of DNA damage, prevents the expression of apoptosis-related genes by interacting with the nuclear transcription factor Y subunit α (NF-YA) to prolong the survival time of tumor cells (30). Nevertheless, the use of RNA for transcriptional regulation is homeostatically advantageous due to its capacity to influence protein as a rapid response to external factors that interact with the body.

LncRNAs as Decoy Molecules

LncRNA commonly act as a decoy molecule by blocking a certain molecular pathway. After lncRNA is transcribed, it directly binds to some protein molecules such as chromosome folding proteins or transcription regulators and impairs the function of that protein. LncRNAs directly bind to transcription regulators to block the function of transcription factors, further suppressing the downstream gene transcription. For instance, DNA damage-induced lncRNA PANDA directly binds to the nuclear transcription factor NF-YA and impairs its function, thus preventing the expression of apoptosis-related genes and ultimately inhibiting the NF-YA-dependent apoptosis pathways (30). Furthermore, lncRNAs can interact with certain proteins in order to hinder the proteins' capacity to regulate mRNA expression. For example, the lncRNA MALAT1 located in the nucleus regulates the phosphorylation status of serine/arginine (SR) by binding to the SR splicing factors that regulate the variable splicing of pre-mRNA (31).

LncRNAs can also affect the expression of target genes by sponging miRNAs. In certain tumor cells and specific tissues, lncRNAs directly bind to the miRNA molecules and prevent them binding to the target mRNAs, thus upregulating of the expression of the target genes. In prostate cancer, lncRNA PCAT-1 acts as a sponge for absorbs miR-3667-3p and reduce its inhibitory effect on c-Myc mRNA, which promotes the proliferation and migration of the tumor (32).

LncRNAs as Guide Molecules

LncRNAs can act as guiding molecules by aiding specific protein in reaching their target location and exerting their biological functions. As guiding molecules, lncRNAs are often interacting with transcription factors, which are located on a specific DNA sequence and regulate gene transcription. Numerous studies showed that lncRNAs can regulate gene transcription through cis regulation, thus regulating the transcription of adjacent mRNAs. Wang et al. found that lncTCF7 can recruit the SWI/SNF complex to the TCF7 promoter and regulate the expression of TCF7. This process can trigger the activation of the Wnt signaling pathway, and ultimately promote the self-renewal of liver cancer stem cells and the proliferation of cancer cells (33). Nevertheless, lncRNAs can also regulate gene expression through trans regulation, which is characterized by lncRNAs' capacity to regulate the transcription of remote mRNAs. For instance, lncRNA HOTAIR interacts with the polycomb repressive complex 2 (PRC2) and induces the relocation of PRC2 complex throughout the genome, thus promoting histone methylation modifications in several target genes (34). Tsai et al. showed that the two ends of the lncRNA HOTAIR interact with two different histone modification complexes (35). The 5′-domain of lncRNA HOTAIR binds to the PRC2 complex (methylation effect), while the 3′-domain binds to the LSD1/CoREST/REST complex (demethylation effect). Thus, these two complexes allow heterogeneous histone modification enzyme assembly. Lastly, the assembled histone modification enzymes localize to different gene regions and regulate the histone methylation patterns of several genes, thereby regulating the transcription of several target genes.

LncRNAs as Scaffold Molecules

LncRNA can act as a "central platform" and facilitate the interaction of numerous molecules and protein. Furthermore, the scaffold properties of lncRNAs enable the assembly of different types of macromolecular complexes, thus promoting the convergence and integration of information among different signaling pathways (20, 36). One of the most important scaffold lncRNAs is the X-inactive specific transcript (Xist) RNA, which has a length of 17kb and is encoded by the X chromosome to be suppressed in females. Xist recruits the polycomb repressive complex 1 (PRC1) and PRC2 complexes, which suppress the gene expression of one X chromosome in females, thus having a dose compensation role in mammals (37, 38). Emerging evidence also confirmed that Xist RNA is associated with cancer (39). For instance, Xist acts as an oncogene in non-small cell lung cancer by recruiting EZH2 to the epigenetically repressed kruppel-like factor 2 gene (KLF2) (40). In addition to Xist, there are other lncRNAs that have scaffold regulation functions. LncRNA HOTAIR promotes the recruitment and interaction between lysine (K)-specific demethylase 1A (LSD1) and hepatitis B X-interacting protein (HBXIP), thus mediating the activation of transcription factor c-Myc, along with transcription activation of Cyclin A, elF4E, and LDHA (41). LncRNA INK4 is an antisense transcription product of cyclin-dependent kinase inhibitor 2B (CDKN2B, p15 INK4b), which can act as a scaffold for PRC1 and PRC2 complexes and result in the silencing of the tumor suppressor gene cyclin-dependent kinase inhibitor 2A (CDKN2A, p16 INK4a) (42). As a scaffold molecule, lncRNA CCAT1 was shown to bind two distinct epigenetic modification complexes [5'-domain of CCAT1 binds PRC2, while 3'-domain binds the suppressor of variegation 3-9 homolog 1 (SUV39H1)], thus regulating the histone methylation pattern of the sprouty RTK signaling antagonist 4 (SPRY4) promoter, and ultimately promoting the proliferation and metastasis of esophageal squamous cell carcinoma (ESCC) (43).

LNCRNAS REGULATE TUMOR PROGRESSION AT THREE DIFFERENT LEVELS

Accumulating evidence shows that lncRNAs play different roles in the nucleus and cytoplasm. In the nucleus, lncRNAs regulate the epigenome by recruiting chromatin remodeling complexes as well as chromatin modification complexes. Furthermore,

lncRNAs act as transcriptional regulators by themselves or by recruiting transcription factors and are involved in the process of pre-mRNA alternative splicing. Nevertheless, numerous studies indicated that there are a large number of lncRNAs in the cytoplasm, which are involved in post-transcriptional regulation processes such as the mRNAs stability, mRNAs translation, protein stability, and "ceRNA" network (44, 45) (**Figure 2**). Overall, lncRNAs can regulate the gene expression at epigenetic, transcriptional and post-transcriptional level.

LncRNAs Participate in Epigenetic Regulation of Genes

Some lncRNAs manipulate gene expression by recruiting chromatin remodeling complexes and chromatin modification complexes to specific sites and influence the chromosome structure, histone modification status, and DNA methylation status (46, 47).

A recent report indicated that lncRNAs are associated with chromatin remodeling (48), and lncRNAs can recruit chromatin remodeling complexes, change chromatin structure, and regulate oncogene expression. Tang et al. demonstrated that after the interaction of lncRNAs with the chromatin remodeling complex switching defective/sucrose non-fermenting (SWI/SNF), the ATP hydrolysis energy was used to change the chromatin structure and regulate gene transcription, ultimately resulting in oncogene expression changes (49). It has been reported that lncRNA HOTAIR interacts with SMARCB1 and ARID1, which are subunits of the chromatin remodeling complex SWI/SNF and change the chromatin structure as well as promote the transcription of the SNAIL gene, ultimately promoting kidney cancer progression (50).

LncRNA-mediated changes in histone status are associated with H3K4me3, H3K9me2, and H3K27me3 modifications of the promoter region. These histone modifications change the chromatin structure and alter the expression of the underlying genes (51). The lncRNA HOTAIR transcribed by the HOXC gene cluster is one of most common lncRNAs that influence gene expression through histone modifications. The lncRNA HOTAIR can recruit the chromatin modification complex and locate it to the target gene region, thuschanging the chromatin state and regulating the transcription of several target genes (34, 35). In addition to lncRNA HOTAIR, there are other lncRNAs that recruit histone modification complexes to modify histone epigenetic patterns. for instance, lncRNA INK4 can act as a scaffold molecule, which promotes the interaction between PRC1 and PRC2 complexes, leading to histone modifications and silencing of the CDKN2A gene (42). LncRNA CCAT1 binds to PCR2 and SUV39H1 in order to regulate the histone methylation of the SPRY4 promoter region, thus promoting the proliferation and metastasis of ESCC (43). Furthermore, lncRNA HOXA11-AS binds to EZH2 to promote histone methylation of the p21 promoter region, thus inhibiting the transcription of the tumor suppressor gene p21 (52).

While lncRNAs can aid the localization of DNA methylases or demethylases to a specific target gene promoter, the DNA methylation is a dynamic and reversible process. Arab et al.

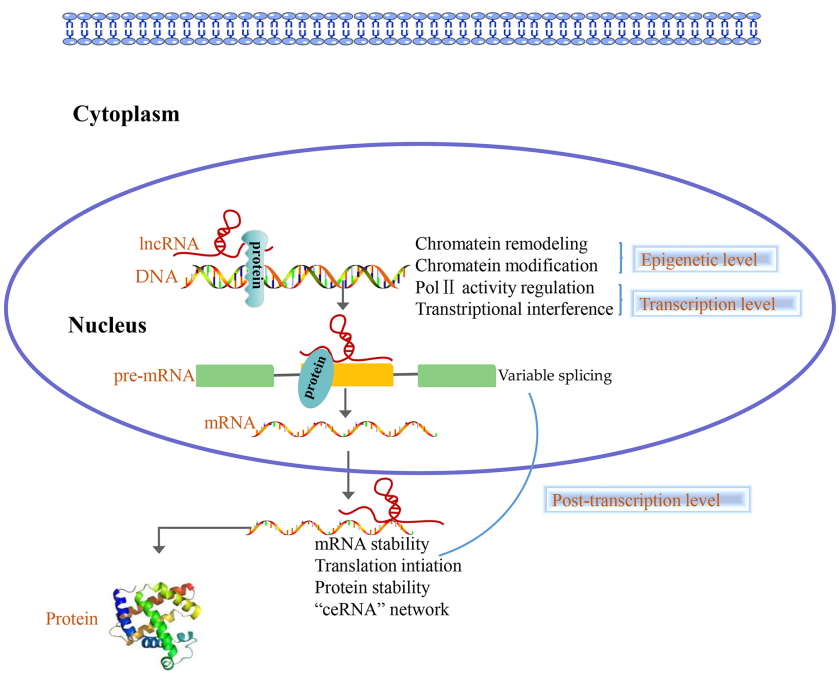

FIGURE 2 | Long non-coding RNAs (LncRNAs) function at three levels. In the nucleus, lncRNAs control the epigenetic state of genes, participate in transcriptional regulation and are involved in the process of pre-mRNA alternative splicing. In the cytoplasm, lncRNAs are involved in post-transcriptional regulation such as the mRNAs stability, mRNAs translation, protein stability and "ceRNA" network.

showed that after lncRNA TARID binds to growth arrest and DNA-damage-inducible, alpha (GADD45A, with demethylation), the 5-methylcytosine on the TCF21 promoter (tumor suppressor) was demethylated, thereby mediating the transcriptional activation of TCF21 (53).

LncRNAs Are Involved in Gene Transcriptional Regulation

In eukaryotic cells, transcription factors bind to DNA and control the transcription, localization, and stability of the RNA transcribed. Some lncRNAs that act as ligands often interact with transcription factors to form complexes and control gene transcription (54). LncRNAs regulate genetic transcription through cis and trans regulation. LncRNAs regulate the transcription expression of nearby mRNAs through cis regulation. To reveal if lncRNAs use cis regulation to influence gene transcription, first, we must observe the expression of nearby mRNAs following knockdown or overexpression of lncRNAs to confirm if there is a correlation between lncRNA and nearby mRNA levels. Next, we would have to determine whether the lncRNA recruits some proteins or protein complexes, which are attached to the promoter region of the target genes to achieve regulatory functions. For instance, Wang et al. found that lncTCF7 recruited SWI/SNF complex to the TCF7 promoter to regulate the expression of TCF7, thereby mediating the activation of the Wnt signaling pathway, and ultimately promoting the self-renewal of liver CSCs and tumor proliferation (33). However, if the expression of nearby functional genes does not change after lncRNAs are knocked down or overexpressed, lncRNAs are considered to regulate the transcription of genes through the trans mode of action. To reveal if lncRNAs use trans regulation to influence gene transcription, first, we should screen the proteins that might bind to the lncRNAs through experiments and bioinformatics, identify the potential target mRNAs, and analyze the correlation between the expression of lncRNAs and the target genes. Ultimately, we would have to prove that the lncRNA and its associated proteins bind to the target gene promoter region to regulate its transcription. Li et al. showed that lncRNA AGAP2-AS1 recruited EZH2 and LSD1 to the promoter regions of KLF2 and large tumor suppressor 2 (LATS2), thus, inhibiting the transcription of KLF2 as well as LATS2 and promoting the non-small cell lung cancer progression (55). Certain lncRNAs act as transcription factors themselves. Ketab et al. discovered that lncRNA GAS5 folds into a DNA-like structure that binds to the glucocorticoid receptor (GR), and inhibits GR transcription activity. Finally, lncRNA GAS5 can reduce the production of red blood cells, platelets, and white blood cells, which was associated with to a poorer prognosis for acute myeloid leukemia (56).

LncRNAs Control Gene Expression by Post-Transcriptional Level

In addition to the two regulatory mechanisms aforementioned, lncRNAs are involved in post-transcriptional regulation, including alternative splicing of pre-mRNA, stabilization of mRNA, and translation and stabilization of proteins (57–59). Most lncRNAs involved in the post-transcriptional regulation of mRNAs are antisense lncRNAs. In the pre-mRNA variable splicing regulation process, antisense lncRNAs act by themselves or combined with splicing factors to control the pre-mRNA splicing process. For instance, lnc-Spry1 binds to U2 small nuclear ribonucleoprotein auxiliary factor 65kD splicing factor, and influences the variable splicing process of fibroblast growth factor receptor pre-mRNA related to the epithelial-mesenchymal transition (EMT) (60). Furthermore, lncRNAs can regulate mRNA stability. For instance, the lncRNA PXN-AS1 can be expressed as the PXN-AS1-L (large) or PXN-AS1-S (small) transcript. Compared to PXN-AS1-S, PXN-AS1-Lhas an extra exon. Due to the presence of the exon 4 sequence, PXN-AS1-L binds to the 3'UTR region of the Paxillin (PXN) mRNA, which impairs the binding of miRNA-24 to the PXN mRNA and reduces its degradation (61). LncRNAs also regulate protein translation. For instance, lncRNA GAS5 recruits the translation initiation factor eIF4E and allows it to bind to the c-Myc mRNA, thus inhibiting c-Myc protein translation and ultimately downregulating the c-Myc expression (62). LncRNA MT1JP directly binds to cytotoxic granule-associated RNA binding protein-like 1 (TIAR) to enhance the translation process of p53 mRNA, thereby up-regulating p53 expression (63). LncRNAs also regulate protein stability. For example, lncRNA UPAT interacts with ubiquitin-like with PHD and RING finger domains 1 (UHRF1) protein to ensure its stability by interfering with its ubiquitination process (64).

LncRNAs often affect the expression of their target genes by interacting with miRNAs, which are the main post-transcriptional regulation factors. In some tumor cells and specific tissues, some lncRNAs carrying "seed sequences" of certain miRNAs bind to miRNAs and act like sponges, thereby preventing miRNAs from binding to their target mRNAs (65–67). Qu et al. showed that lncARSR promotes the expression of Anexelekto and cellular-mesenchymal to epithelial transition factor in renal cancer cells through competitive binding to miR-34/miR-449, thereby increasing the resistance to sunitinib (68). Jia et al. revealed that lncRNA H19 acts as a sponge for miR-29a, thus upregulating angiogenesis factor vasohibin 2 and promoting angiogenesis of glioma and other biological processes of endothelial cells associated with glioma (69). Zhang et al. showed that lncRNA CCAT1 promoted the expression of the transcription factor homeobox gene B1 by sponging miR-7 from the cytoplasm, thereby promoting the proliferation and metastasis of ESCC (43).

In summary, it has been found that lncRNAs regulate gene expression at following three levels by interfering with the epigenome and by regulating the transcriptional as well as post-transcriptional processes of the targeted genes.

RESEARCH STRATEGIES OF LNCRNAS IN TUMOR

With the development of high-throughput sequencing technology, an increasing number of lncRNAs are annotated;

however, the function of most lncRNAs in tumors remains unclear. Since the field of lncRNAs remains broadly unknown, its exploration is of paramount importance. Previous studies showed that the function of lncRNAs in tumors can be investigated using lncRNA screening, lncRNA characteristic analyses, functional studies and lncRNA molecular mechanisms analyses (**Figure 3**).

Screening of lncRNAs

Under the premise of guaranteeing at least three samples, differentially expressed lncRNAs can be screened using high-throughput sequencing technologies such as NGS (70). Various tissues, whole blood, cells, plasma, serum, and exosomes can be used to screen the differentially expressed lncRNAs according to the purpose of the experiment. High-throughput sequencing technology is sensitive enough to detect rare transcripts that have only a few copies and can also detect unknown genes and new transcripts with a wide detection range. However, its high costs will limit its widespread application in different laboratories (71).

The lncRNAs of interest were also obtained from databases such as the TCGA database, a multi-omics database related to tumors, which includes DNA-Sep, RNA-Sep, protein-Sep, and other omics data (72).

Following lncRNA screening, qRT-PCR/northern blot were used to reduce the number of candidate lncRNAs and verify their expression in clinical specimens and cell lines. Furthermore, the correlation between the lncRNA expression and clinical indicators would be determined, thus identifying the importance of the candidate lncRNAs in clinical diagnosis and treatment.

Characteristic Analysis of lncRNAs

The mostly explored characteristics of lncRNAs include coding potential, location information on the genome, secondary structure, correlation with disease, full-length analysis, and cell localization, which can be determined through bioinformatical analysis. NONCODE, LncBook, LncRNAdb v2.0, and LncRNADisease are some softwares that can be used to obtain a provide comprehensive annotations of lncRNAs (73–77).

Rapid-amplification of cDNA ends (RACE) is a method that can provide the full length of the lncRNAs by extending and amplifying the two ends of a known cDNA fragment based on PCR technology (78–80). Before constructing an overexpression plasmid, researchers often clone the full-length candidate lncRNA and identify its sequence through 5'-RACE and 3'-RACE (81).

Understanding the cellular localization of lncRNAs helps us to understand their potential molecular mechanisms. Fluorescence *in situ* hybridization (FISH) is a method often used to identify the cellular localization of the candidate lncRNAs. The principle is that the foreign nucleic acid containing radioactive labels (3H, 32P, 35S, 125I) or non-radioactive labels [biotin, digoxin, horseradish peroxidase, fluorescein (FITC, rhodamine)] is complementary paired with the DNA or RNA to be tested on tissues, cells or chromosomes to form a specific nucleic acid hybrid molecule (82, 83). In addition to FISH localization, certain prediction software such as

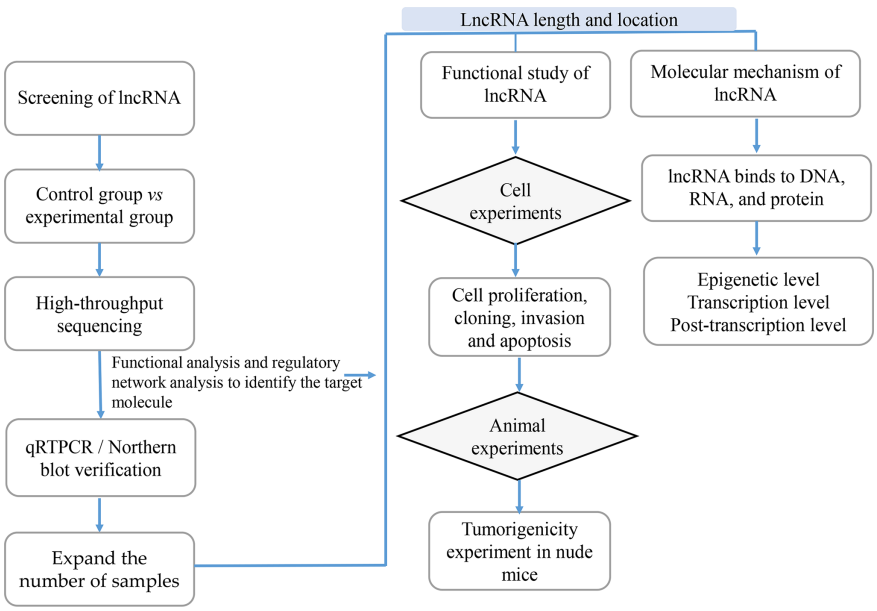

FIGURE 3 | The Research Strategies of Long Non-Coding RNAs (lncRNAs) in Tumors. In order to study lncRNAs, high-throughput sequencing technology or high-throughput data in the database are usually used to screen out candidate lncRNAs, while qRTPCR and Northern/blot technologies are used for verification; then RACE and FISH technologies are used to determine the full length and location of lncRNAs; the functional research of lncRNAs is usually verified from *in vitro* experiments including cell proliferation, cloning, invasion and apoptosis, and *in vivo* experiments mainly including tumor-bearing experiments in nude mice; the research on the mechanism of lncRNAs is usually carried out at the epigenetic level, transcription level and post-transcriptional level according to their cellular location.

LncATLAS (84) can predict the cellular localization of lncRNAs; however, the predictive data need to be verified experimentally.

The Functional Study of lncRNAs

Before exploring the specific lncRNAs' molecular mechanisms of action, their functions should be elucidated. The functions of lncRNAs are often verified through *in vitro* and *in vivo* experiments.

In vitro experiments: Following overexpression or knock down of certain lncRNAs, their role in tumor progression is analyzed by measuring the changes in biological behaviors, phenotype, EMT markers, stem cell markers, and drug sensitivity. *In vivo* experiments: First, a lentiviral expression vector capable to knock down or overexpress a specific lncRNA is constructed. Next, the virus is transfected into cells, which are first screened for resistance, and then analyzed using qRT-PCR to detect the knockdown or overexpression levels of the candidate lncRNAs. Finally, the stably transfected cell strains that were screened are inoculated into the backs of nude mice, and the tumorigenicity of the candidate lncRNAs is verified using the nude mouse tumorigenic model or other animal models (85).

The Molecular Mechanism of lncRNAs

If the lncRNAs are localized in the nucleus, they are considered to play regulatory roles at the chromatin and transcription levels, while the lncRNAs are localized in the cytoplasm, are considered to play regulatory role at the post-transcriptional level.

LncRNAs Affect the Expression of Downstream Genes by Mediating Chromatin Remodeling and Chromatin Modification

LncRNAs regulate chromatin remodeling, DNA methylation, and histone modification by DNA methylase and histone modification enzymes. The cat RAPID database can evaluate the protein-RNA binding tendency through the contribution of secondary structure, hydrogen bonding and van der Waals forces, thus it can provide an accurate prediction of the protein-lncRNA binding ability (86). The use of databases plays an auxiliary role in studying the interactions of lncRNAs with DNA methylases and histone modification enzymes. Generally, the epigenetic mechanisms of lncRNAs are confirmed through the following four aspects: (1) Confirmation of expression correlation. Following knock down or overexpression of lncRNAs, qRT-PCR, northern blot, and western blot should be used to observe whether the expression of the target mRNAs, histone modification enzymes and DNA methylases are affected; (2) Dissection of the chromatin status of the target genes. Following knock down or overexpression of lncRNAs, DNA-FISH experiments should be used to observe the effect of lncRNAs on the chromatin state of the target genes (87–89); (3) LncRNAs role in histone modification. Following knock down or overexpression of lncRNAs, chromatin immunoprecipitation (ChIP) (90, 91) and chromatin isolation by RNA purification (ChIRP) (92) experiments should be used to analyze the effect of lncRNAs on histone modification. The RNA-pull down and RNA immunoprecipitation (RIP) (92) experiments can provide information regarding the binding ability of lncRNAs to the histone modification enzyme; (4) The role of lncRNAs in the regulation of DNA methylation modification. Following knock down or overexpression of lncRNAs, methylation-specific PCR (MSP) and bisulfite sequencing PCR (BSP) (93, 94) experiments should be used to investigate the effects of lncRNAs on DNA methylation modification.

LncRNAs Can Regulate the Transcription of Target Genes Alone or in Combination With Transcription Factors

Whether lncRNAs regulate gene transcription through the cis or trans action mode depends on its relative position tothe target genes. Numerous databases provide valuable information regarding the combination of lncRNAs and transcription factors. For example, the ChIPBase v2.0 database integrates the binding sites of lncRNAs and transcription factors identified using the ChIP-Seq method (95). Generally, the influence of lncRNAs on transcriptional regulation of target genes was explored using the following processes: (1) Confirmation of expression correlation. Following knock down or overexpression of lncRNAs, qRT-PCR should be used to investigate the changes in target mRNA expression; (2) Whether lncRNAs recruit transcription regulators. Following lncRNA knock down or overexpression, RNA-pull down/RIP should be used to explore the binding ability of lncRNA and RNA-binding proteins; (3) Whether lncRNAs regulate the transcription of target genes: After lncRNA is knocked down or overexpressed, ChIP and ChIRP experiments should be used to analyze the regulation of lncRNAs on target gene transcription.

LncRNA as a ceRNA

The ceRNA network is one of main methods through which lncRNAs exert post-transcriptional regulation in the cytoplasm. Previous studies have shown that lncRNAs can competitively bind to miRNAs and affect the miRNA' function on the target genes. The core experiments usually performed to prove the functions of ceRNA are: (1) Use of bioinformatics to predict the possible "ceRNA" networks. There are many databases that can predict possible "ceRNA" networks, such as Starbase (96), LncACTdb 2.0 (97), LncBase Predicted v2 (98), TargetScan (99), which contains all kinds of ceRNA regulatory relationships including miRNA-mRNA, miRNA-lncRNA, miRNA-circRNA and miRNA-ceRNA; (2) Confirmation of expression correlation. Following knock down or overexpression lncRNA, the changes in miRNA should be investigated; (3) Verifying the interaction of lncRNA, miRNA, and mRNA. Luciferase reporters should be used to confirm the interactions between lncRNAs, miRNAs, and mRNAs (100, 101).

In conclusion, the use of bioinformatics to predict the functions of lncRNAs is favored over the traditional, time-consuming, and expensive experimental methods. For the lncRNA field, it is essential to establish a variety of databases meant to help researchers identify and name their newly discovered lncRNAs. The already established databases for lncRNA are listed in (**Table 1**).

CONCLUSIONS

The role of lncRNAs has become one ofmain focus for fundamental and clinical tumor studies. Given the increasing pool of evidence regarding the role of lncRNAs in tumor development and progression, here we summarized the four main models of action through which lncRNAs influence tumor progression (as a signal, decoy, guide, or scaffold molecule). The lncRNAs in the nucleus are often involved in chromatin remodeling and modification, transcriptional regulation, and alternative splicing of pre-mRNA, while the lncRNAs in the cytoplasm are often involved in the stability of mRNAs, protein translation, and the ceRNA network (102). Based on previous studies, we also propose the specific research strategies through which the lncRNA functions can be investigated (lncRNA screening, lncRNA characteristic analyses, functional studies, and molecular mechanisms of lncRNAs).

Meanwhile, these findings raise further questions. For example: what is the mechanism that causes the abnormal expression of lncRNAs in tumors? Many upstream regulatory mechanisms of lncRNAs have not been elucidated. A potential new direction for future research would be to investigate the upstream regulatory factors of lncRNAs. According to previous literature, the expression of lncRNAs may be regulated by histone status, DNA methylation patterns, transcription factors, and post-transcriptional regulation. For example, the activation mechanism of lncRNA CCAT1, which can promote the proliferation and metastasis of ESCC, is represented by the acetylation of histone H3K27 (43). Moreover, the high expression of lncRNA H19 is due to the decreased methylation level of the CpG islands in the promoter region (103). Additionally, the high expression of lnc01503, which can promote the progression of ESCC, is due to the capacity of the transcription factor to bind to the promoter region (104). Lastly, the interaction between IGF2BP1 and the lncRNA HULC reduces the stability of lncRNA HULC and decreases its expression (105). Numerous types of lncRNAs have been classified according to their position relative to the genome. Regardless of their similarities, their mechanism of action is not exactly the same. The effects of eRNAs on the formation and stabilization of the chromatin loop between the enhancer and the promoter and their capacity to regulate the expression of some target genes at close and long distances became highly investigated recently (106, 107). Notably, previous studies have reported that eRNAs are a subclass of lncRNAs that play a critical role in cancer development (108). For example, HPSE eRNA promotes cancer progression by interfering with the chromatin looping and regulating the hnRNPU/p300/EGR1/HPSE axis (109). Based on the vast number of eRNAs and their expression regulation to some target genes without distance and cell type limitation, eRNAs may become potential targets for the diagnosis and treatment of human cancers (110, 111). Liquid biopsies based on exosome contents represent a potential direction for future molecular diagnosis as well as evaluation of chemotherapy effects and cancer prognosis, which have great application values for early detection of disease (112–118). Recent studies have shown that some lncRNAs can be encapsulated in exosomes, and exosomes can be used as a medium to transmit lncRNAs among tumor cells, thereby regulating the occurrence and development of tumors (119–123) (**Figure 4**). For example, lncARSR delivered *via* exosomes can promote sunitinib resistance as a competitive endogenous RNA in renal cancer (68). Furthermore, lncRNA PART1 delivered *via* exosomes can induce gefitinib resistance as a competitive endogenous RNA in ESCC (124). Lastly, chimeric RNA GOLM1-NAA35 from salivary exosomes might represent a potential biomarker for esophageal cancer (125). This would allow us to understand specific pathological conditions in cancer patients through the detection of specific lncRNAs encapsulated by exosomes (126). A previous study showed that engineered exosomes with phospholipid bilayer structures can be used to load certain anti-tumor drugs, therapeutic miRNAs, or proteins and target tumor cells (127).

In conclusion, the lncRNAs field is highly investigated due to their potential key role in cancer development and progression. A comprehensive understanding of lncRNAs in cancer signaling will stimulate new directions for future research, diagnosis, and therapies (128). LncRNAs are of great significance for the early

TABLE 1 | Databases related to long non-coding RNA (lncRNA) research.

Database	Internet site	Function	Literatures
TCGA	https://www.cancer.gov/about-nci/organization/ccg/research/structural-genomics/tcga	Preliminary screening of lncRNA	(72)
NONCODE	http://www.noncode.org	Comprehensive annotation of lncRNA	(73–74)
LncBook	http://bigd.big.ac.cn/lncbook/index	Comprehensive annotation of lncRNA	(74–75)
lncRNAdb v2.0	http://lncrnadb.org	Comprehensive annotation of lncRNA	(76)
LncRNADisease	http://www.cuilab.cn/lncrnadisease	The relationship between lncRNA and disease	(77)
lncATLAS	http://lncatlas.crg.eu/	The cell localization of lncRNA	(84)
cat RAPID	http://service.tartaglialab.com/page/catrapid_group	Predict the combination of lncRNA and protein	(86)
ChIPBase v2.0	http://rna.sysu.edu.cn/chipbase/	Identify transcription factor binding sites mediated by lncRNA	(95)
Starbase	http://starbase.sysu.edu.cn/tutorialAPI.php	ceRNA	(96)
LncACTdb 2.0	http://www.bio-bigdata.net/LncACTdb/index.html	ceRNA	(97)
LncBase Predicted v2	http://carolina.imis.athena-innovation.gr/diana_tools/web/index.php?r=lncbasev2/index-predicted	ceRNA	(98)
TargetScan	http://www.targetscan.org/vert_72/	ceRNA	(99)

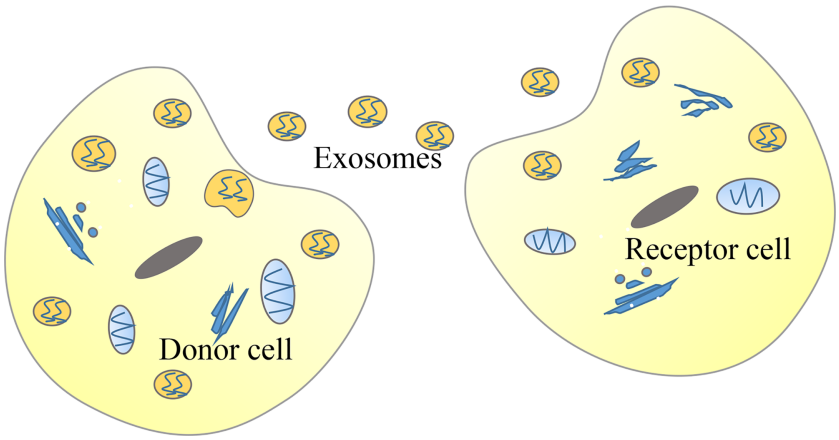

FIGURE 4 | Tumor cells can deliver long non-coding RNAs (lncRNAs) through exosomes. In cancer, donor cells can deliver exosomes-encapsulated lncRNAs to recipient cells so that lncRNAs function in recipient cells.

diagnosis of cancer patients due to their abnormal expression changes as the cancer progresses. For example, the lncRNA prostate cancer antigen 3, which has been studied for early diagnosis, is a prostate-specific lncRNA, which can be detected with high specificity and sensitivity (129). Loewen et al. discussed the potential of lncRNA HOTAIR in the diagnosis and treatment of lung cancer (130). In addation, lncRNAs also serve as promising therapeutic targets. Given their divers modes of action, lncRNAs can be targeted using multiple approaches: (1) Regulate lncRNA genes through spatial blockade of promoters or the use of genome editing technology; (2) Regulate lncRNA levels through siRNAs; (3) Prevent lncRNAs from exerting their effect by inhibiting the interaction between RNAs and proteins or prevent the formation of secondary structures (131, 132). Recently, an increasing number of researchers considered lncRNAs as potential therapeutic targets for cancer. For example, Shin et al. discussed the feasibility of lncRNA BC200 as a cancer therapeutic target (133). Liu et al. investigated whether lncRNA PANDAR is a powerful diagnostic and therapeutic marker for patients with gastric cancer (134). The effective application of lncRNAs as potential targets for diagnosis and therapy has broad prospects for future cancer treatment. However, there are still numerous limitations for the use of lncRNAs as potential therapeutic targets and biomarker development. Nevertheless, with the rapid development of biochemical toolkits and technological breakthroughs for lncRNA research, an increasing number of lncRNAs are being discovered. However, the increasing rate of discovery of new lncRNAs presents challenges to their definition and annotation, which requires more comprehensive transcriptome analyses and transcription assembly. In addition, the functional characterization of lncRNAs is still challenging, mainly due to the complexity and diversity of their association with cancer cell functions. Overall, elucidating the mechanism of abnormal expression of lncRNAs and the downstream mechanism of lncRNAs in tumors would allow us to better understand lncRNAs and provide novel tumor markers for clinical diagnosis and prognostic evaluation of tumors.

AUTHOR CONTRIBUTIONS

NG, YHL, JL, ZG, and ZY wrote the manuscript, which TF, HL, and YL revised. All authors contributed to the article and approved the submitted version.

FUNDING

This work was supported by the Key Scientific Research Projects of Colleges and Universities in Henan Province (No.20A310021 TF).

REFERENCES

1. JACOB F, MONOD J. Genetic regulatory mechanisms in the synthesis of proteins. *J Mol Biol* (1961) 3:318–56. doi: 10.1016/S0022-2836(61)80072-7
2. Bertone P, Stolc V, Royce TE, Rozowsky JS, Urban AE, Zhu X, et al. Global identification of human transcribed sequences with genome tiling arrays. *Science* (2004) 306(5705):2242–6. doi: 10.1126/science.1103388
3. Carninci P, Kasukawa T, Katayama S, Gough J, Frith MC, Maeda N, et al. The transcriptional landscape of the mammalian genome. *Sci (New York NY)* (2005) 309(5740):1559. doi: 10.1126/science.1112014
4. Amaral PP, Dinger ME, Mercer TR, Mattick JS. The eukaryotic genome as an RNA machine. *Science* (2008) 319(5871):1787–9. doi: 10.1126/science.1155472
5. Ponting CP, Oliver PL, Reik W. Evolution and functions of long noncoding RNAs. *Cell* (2009) 136(4):629–41. doi: 10.1016/j.cell.2009.02.006
6. Kim T, Cui R, Jeon YJ, Lee JH, Lee JH, Sim H, et al. Long-range interaction and correlation between MYC enhancer and oncogenic long noncoding RNA CARLo-5. *Proc Natl Acad Sci U S A* (2014) 111(11):4173–8. doi: 10.1073/pnas.1400350111
7. Hung CL, Wang LY, Yu YL, Chen HW, Srivastava S, Petrovics G, et al. A long noncoding RNA connects c-Myc to tumor metabolism. *Proc Natl Acad Sci U S A* (2014) 111(52):18697–702. doi: 10.1073/pnas.1415669112

8. Leveille N, Melo CA, Rooijers K, Diaz-Lagares A, Melo SA, Korkmaz G, et al. Genome-wide profiling of p53-regulated enhancer RNAs uncovers a subset of enhancers controlled by a lncRNA. *Nat Commun* (2015) 6:6520. doi: 10.1038/ncomms7520
9. Dimitrova N, Zamudio JR, Jong RM, Soukup D, Resnick R, Sarma K, et al. LincRNA-p21 activates p21 in cis to promote Polycomb target gene expression and to enforce the G1/S checkpoint. *Mol Cell* (2014) 54 (5):777–90. doi: 10.1016/j.molcel.2014.04.025
10. Huarte M, Guttman M, Feldser D, Garber M, Koziol MJ, Kenzelmann-Broz D, et al. A large intergenic noncoding RNA induced by p53 mediates global gene repression in the p53 response. *Cell* (2010) 142(3):409–19. doi: 10.1016/j.cell.2010.06.040
11. Prensner JR, Zhao S, Erho N, Schipper M, Iyer MK, Dhanasekaran SM, et al. RNA biomarkers associated with metastatic progression in prostate cancer: a multi-institutional high-throughput analysis of SChLAP1. *Lancet Oncol* (2014) 15(13):1469–80. doi: 10.1016/S1470-2045(14)71113-1
12. Kretz M, Siprashvili Z, Chu C, Webster DE, Zehnder A, Qu K, et al. Control of somatic tissue differentiation by the long non-coding RNA TINCR. *Nature* (2013) 493(7431):231–5. doi: 10.1038/nature11661
13. Pandey GK, Mitra S, Subhash S, Hertwig F, Kanduri M, Mishra K, et al. The risk-associated long noncoding RNA NBAT-1 controls neuroblastoma progression by regulating cell proliferation and neuronal differentiation. *Cancer Cell* (2014) 26(5):722–37. doi: 10.1016/j.ccell.2014.09.014
14. Lu Z, Xiao Z, Liu F, Cui M, Li W, Yang Z, et al. Long non-coding RNA HULC promotes tumor angiogenesis in liver cancer by up-regulating sphingosine kinase 1 (SPHK1). *Oncotarget* (2016) 7(1):241–54. doi: 10.18632/oncotarget.6280
15. Zhang H, Chen Z, Wang X, Huang Z, He Z, Chen Y. Long non-coding RNA: a new player in cancer. *J Hematol Oncol* (2013) 6:37. doi: 10.1186/1756-8722-6-37
16. Ma L, Bajic VB, Zhang Z. On the classification of long non-coding RNAs. *RNA Biol* (2013) 10(6):925–33. doi: 10.4161/rna.24604
17. Isin M, Dalay N. LncRNAs and neoplasia. *Clin Chim Acta* (2015) 444:280–8. doi: 10.1016/j.cca.2015.02.046
18. Hombach S, Kretz M. Non-coding RNAs: Classification, Biology and Functioning. *Adv Exp Med Biol* (2016) 937:3–17. doi: 10.1007/978-3-319-42059-2_1
19. Balas MM, Johnson AM. Exploring the mechanisms behind long noncoding RNAs and cancer. *Noncoding RNA Res* (2018) 3(3):108–17. doi: 10.1016/j.ncrna.2018.03.001
20. Wu R, Su Y, Wu H, Dai Y, Zhao M, Lu Q. Characters, functions and clinical perspectives of long non-coding RNAs. *Mol Genet Genomics* (2016) 291 (3):1013–33. doi: 10.1007/s00438-016-1179-y
21. Derrien T, Johnson R, Bussotti G, Tanzer A, Djebali S, Tilgner H, et al. The GENCODE v7 catalog of human long noncoding RNAs: analysis of their gene structure, evolution, and expression. *Genome Res* (2012) 22(9):1775–89. doi: 10.1101/gr.132159.111
22. Iyer MK, Niknafs YS, Malik R, Singhal U, Sahu A, Hosono Y, et al. The landscape of long noncoding RNAs in the human transcriptome. *Nat Genet* (2015) 47(3):199–208. doi: 10.1038/ng.3192
23. Rinn JL, Chang HY. Genome regulation by long noncoding RNAs. *Annu Rev Biochem* (2012) 81:145–66. doi: 10.1146/annurev-biochem-051410-092902
24. Schmitt AM, Chang HY. Long Noncoding RNAs in Cancer Pathways. *Cancer Cell* (2016) 29(4):452–63. doi: 10.1016/j.ccell.2016.03.010
25. Quinn JJ, Chang HY. Unique features of long non-coding RNA biogenesis and function. *Nat Rev Genet* (2016) 17(1):47–62. doi: 10.1038/nrg.2015.10
26. Rao A, Rajkumar T, Mani S. Perspectives of long non-coding RNAs in cancer. *Mol Biol Rep* (2017) 44(2):203–18. doi: 10.1007/s11033-017-4103-6
27. Wang KC, Chang HY. Molecular mechanisms of long noncoding RNAs. *Mol Cell* (2011) 43(6):904–14. doi: 10.1016/j.molcel.2011.08.018
28. Bolha L, Ravnik-Glavac M, Glavac D. Long Noncoding RNAs as Biomarkers in Cancer. *Dis Markers* (2017) 2017:7243968. doi: 10.1155/2017/7243968
29. Maruyama R, Suzuki H. Long noncoding RNA involvement in cancer. *BMB Rep* (2012) 45(11):604–11. doi: 10.5483/BMBRep.2012.45.11.227
30. Hung T, Wang Y, Lin MF, Koegel AK, Kotake Y, Grant GD, et al. Extensive and coordinated transcription of noncoding RNAs within cell-cycle promoters. *Nat Genet* (2011) 43(7):621–9. doi: 10.1038/ng.848
31. Tripathi V, Ellis JD, Shen Z, Song DY, Pan Q, Watt AT, et al. The nuclear-retained noncoding RNA MALAT1 regulates alternative splicing by modulating SR splicing factor phosphorylation. *Mol Cell* (2010) 39 (6):925–38. doi: 10.1016/j.molcel.2010.08.011
32. Prensner JR, Chen W, Han S, Iyer MK, Cao Q, Kothari V, et al. The long non-coding RNA PCAT-1 promotes prostate cancer cell proliferation through cMyc. *Neoplasia* (2014) 16(11):900–8. doi: 10.1016/j.neo.2014.09.001
33. Wang Y, He L, Du Y, Zhu P, Huang G, Luo J, et al. The long noncoding RNA lncTCF7 promotes self-renewal of human liver cancer stem cells through activation of Wnt signaling. *Cell Stem Cell* (2015) 16(4):413–25. doi: 10.1016/j.stem.2015.03.003
34. Gupta RA, Shah N, Wang KC, Kim J, Horlings HM, Wong DJ, et al. Long non-coding RNA HOTAIR reprograms chromatin state to promote cancer metastasis. *Nature* (2010) 464(7291):1071–6. doi: 10.1038/nature08975
35. Tsai MC, Manor O, Wan Y, Mosammaparast N, Wang JK, Lan F, et al. Long noncoding RNA as modular scaffold of histone modification complexes. *Science* (2010) 329(5992):689–93. doi: 10.1126/science.1192002
36. Spitale RC, Tsai MC, Chang HY. RNA templating the epigenome: long noncoding RNAs as molecular scaffolds. *Epigenetics-US* (2011) 6(5):539–43. doi: 10.4161/epi.6.5.15221
37. Colognori D, Sunwoo H, Kriz AJ, Wang CY, Lee JT. Xist Deletional Analysis Reveals an Interdependency between Xist RNA and Polycomb Complexes for Spreading along the Inactive X. *Mol Cell* (2019) 74(1):101–17. doi: 10.1016/j.molcel.2019.01.015
38. Bousard A, Raposo AC, Zylicz JJ, Picard C, Pires VB, Qi Y, et al. The role of Xist-mediated Polycomb recruitment in the initiation of X-chromosome inactivation. *EMBO Rep* (2019) 20(10):e48019. doi: 10.15252/embr.201948019
39. Weakley SM, Wang H, Yao Q, Chen C. Expression and function of a large non-coding RNA gene XIST in human cancer. *World J Surg* (2011) 35 (8):1751–6. doi: 10.1007/s00268-010-0951-0
40. Fang J, Sun CC, Gong C. Long noncoding RNA XIST acts as an oncogene in non-small cell lung cancer by epigenetically repressing KLF2 expression. *Biochem Biophys Res Commun* (2016) 478(2):811–7. doi: 10.1016/j.bbrc.2016.08.030
41. Li Y, Wang Z, Shi H, Li H, Li L, Fang R, et al. HBXIP and LSD1 Scaffolded by lncRNA Hotair Mediate Transcriptional Activation by c-Myc. *Cancer Res* (2016) 76(2):293–304. doi: 10.1158/0008-5472.CAN-14-3607
42. Meseure D, Vacher S, Alsibai KD, Nicolas A, Chemlali W, Caly M, et al. Expression of ANRIL-Polycomb Complexes-CDKN2A/B/ARF Genes in Breast Tumors: Identification of a Two-Gene (EZH2/CBX7) Signature with Independent Prognostic Value. *Mol Cancer Res* (2016) 14(7):623–33. doi: 10.1158/1541-7786.MCR-15-0418
43. Zhang E, Han L, Yin D, He X, Hong L, Si X, et al. H3K27 acetylation activated-long non-coding RNA CCAT1 affects cell proliferation and migration by regulating SPRY4 and HOXB13 expression in esophageal squamous cell carcinoma. *Nucleic Acids Res* (2017) 45(6):3086–101. doi: 10.1093/nar/gkw1247
44. Li L, Song X. The Working Modules of Long Noncoding RNAs in Cancer Cells. *Adv Exp Med Biol* (2016) 927:49–67. doi: 10.1007/978-981-10-1498-7_2
45. Yang G, Lu X, Yuan L. LncRNA: a link between RNA and cancer. *Biochim Biophys Acta* (2014) 1839(11):1097–109. doi: 10.1016/j.bbagrm.2014.08.012
46. Morlando M, Fatica A. Alteration of Epigenetic Regulation by Long Noncoding RNAs in Cancer. *Int J Mol Sci* (2018) 19(2):570. doi: 10.3390/ijms19020570
47. Beckedorff FC, Amaral MS, Deocesano-Pereira C, Verjovski-Almeida S. Long non-coding RNAs and their implications in cancer epigenetics. *Biosci Rep* (2013) 33(4):e61. doi: 10.1042/BSR20130054
48. Han P, Chang CP. Long non-coding RNA and chromatin remodeling. *RNA Biol* (2015) 12(10):1094–8. doi: 10.1080/15476286.2015.1063770
49. Tang Y, Wang J, Lian Y, Fan C, Zhang P, Wu Y, et al. Linking long non-coding RNAs and SWI/SNF complexes to chromatin remodeling in cancer. *Mol Cancer* (2017) 16(1):42. doi: 10.1186/s12943-017-0612-0
50. Imai-Sumida M, Dasgupta P, Kulkarni P, Shiina M, Hashimoto Y, Shahryari V, et al. Genistein Represses HOTAIR/Chromatin Remodeling Pathways to Suppress Kidney Cancer. *Cell Physiol Biochem* (2020) 54(1):53–70. doi: 10.33594/000000205

51. Joh RI, Palmieri CM, Hill IT, Motamedi M. Regulation of histone methylation by noncoding RNAs. *Biochim Biophys Acta* (2014) 1839 (12):1385–94. doi: 10.1016/j.bbagrm.2014.06.006
52. Liu Z, Chen Z, Fan R, Jiang B, Chen X, Chen Q, et al. Over-expressed long noncoding RNA HOXA11-AS promotes cell cycle progression and metastasis in gastric cancer. *Mol Cancer* (2017) 16(1):82. doi: 10.1186/s12943-017-0651-6
53. Arab K, Park YJ, Lindroth AM, Schafer A, Oakes C, Weichenhan D, et al. Long noncoding RNA TARID directs demethylation and activation of the tumor suppressor TCF21 via GADD45A. *Mol Cell* (2014) 55(4):604–14. doi: 10.1016/j.molcel.2014.06.031
54. Kurokawa R. Long noncoding RNA as a regulator for transcription. *Prog Mol Subcell Biol* (2011) 51:29–41. doi: 10.1007/978-3-642-16502-3_2
55. Li W, Sun M, Zang C, Ma P, He J, Zhang M, et al. Upregulated long non-coding RNA AGAP2-AS1 represses LATS2 and KLF2 expression through interacting with EZH2 and LSD1 in non-small-cell lung cancer cells. *Cell Death Dis* (2016) 7:e2225. doi: 10.1038/cddis.2016.126
56. Ketab F, Gharesouran J, Ghafouri-Fard S, Dastar S, Mazraeh SA, Hosseinzadeh H, et al. Dual biomarkers long non-coding RNA GAS5 and its target, NR3C1, contribute to acute myeloid leukemia. *Exp Mol Pathol* (2020) 114:104399. doi: 10.1016/j.yexmp.2020.104399
57. Shi X, Sun M, Wu Y, Yao Y, Liu H, Wu G, et al. Post-transcriptional regulation of long noncoding RNAs in cancer. *Tumour Biol* (2015) 36 (2):503–13. doi: 10.1007/s13277-015-3106-y
58. Yoon JH, Abdelmohsen K, Gorospe M. Posttranscriptional gene regulation by long noncoding RNA. *J Mol Biol* (2013) 425(19):3723–30. doi: 10.1016/j.jmb.2012.11.024
59. He RZ, Luo DX, Mo YY. Emerging roles of lncRNAs in the post-transcriptional regulation in cancer. *Genes Dis* (2019) 6(1):6–15. doi: 10.1016/j.gendis.2019.01.003
60. Rodriguez-Mateo C, Torres B, Gutierrez G, Pintor-Toro JA. Downregulation of Lnc-Spry1 mediates TGF-beta-induced epithelial-mesenchymal transition by transcriptional and posttranscriptional regulatory mechanisms. *Cell Death Differ* (2017) 24(5):785–97. doi: 10.1038/cdd.2017.9
61. Yuan JH, Liu XN, Wang TT, Pan W, Tao QF, Zhou WP, et al. The MBNL3 splicing factor promotes hepatocellular carcinoma by increasing PXN expression through the alternative splicing of lncRNA-PXN-AS1. *Nat Cell Biol* (2017) 19(7):820–32. doi: 10.1038/ncb3538
62. Hu G, Lou Z, Gupta M. The long non-coding RNA GAS5 cooperates with the eukaryotic translation initiation factor 4E to regulate c-Myc translation. *PloS One* (2014) 9(9):e107016. doi: 10.1371/journal.pone.0107016
63. Liu L, Yue H, Liu Q, Yuan J, Li J, Wei G, et al. LncRNA MT1JP functions as a tumor suppressor by interacting with TIAR to modulate the p53 pathway. *Oncotarget* (2016) 7(13):15787–800. doi: 10.18632/oncotarget.7487
64. Taniue K, Kurimoto A, Sugimasa H, Nasu E, Takeda Y, Iwasaki K, et al. Long noncoding RNA UPAT promotes colon tumorigenesis by inhibiting degradation of UHRF1. *Proc Natl Acad Sci U S A* (2016) 113(5):1273–8. doi: 10.1073/pnas.1500992113
65. Salmena L, Poliseno L, Tay Y, Kats L, Pandolfi PP. A ceRNA hypothesis: the Rosetta Stone of a hidden RNA language? *Cell* (2011) 146(3):353–8. doi: 10.1016/j.cell.2011.07.014
66. Qi X, Zhang DH, Wu N, Xiao JH, Wang X, Ma W. ceRNA in cancer: possible functions and clinical implications. *J Med Genet* (2015) 52(10):710–8. doi: 10.1136/jmedgenet-2015-103334
67. Yang C, Wu D, Gao L, Liu X, Jin Y, Wang D, et al. Competing endogenous RNA networks in human cancer: hypothesis, validation, and perspectives. *Oncotarget* (2016) 7(12):13479–90. doi: 10.18632/oncotarget.7266
68. Qu L, Ding J, Chen C, Wu ZJ, Liu B, Gao Y, et al. Exosome-Transmitted lncARSR Promotes Sunitinib Resistance in Renal Cancer by Acting as a Competing Endogenous RNA. *Cancer Cell* (2016) 29(5):653–68. doi: 10.1016/j.ccell.2016.03.004
69. Jia P, Cai H, Liu X, Chen J, Ma J, Wang P, et al. Long non-coding RNA H19 regulates glioma angiogenesis and the biological behavior of glioma-associated endothelial cells by inhibiting microRNA-29a. *Cancer Lett* (2016) 381(2):359–69. doi: 10.1016/j.canlet.2016.08.009
70. Hardwick SA, Joglekar A, Flicek P, Frankish A, Tilgner HU. Getting the Entire Message: Progress in Isoform Sequencing. *Front Genet* (2019) 10:709. doi: 10.3389/fgene.2019.00709
71. Lim B, Lin Y, Navin N. Advancing Cancer Research and Medicine with Single-Cell Genomics. *Cancer Cell* (2020) 37(4):456–70. doi: 10.1016/j.ccell.2020.03.008
72. Tomczak K, Czerwinska P, Wiznerowicz M. The Cancer Genome Atlas (TCGA): an immeasurable source of knowledge. *Contemp Oncol (Pozn)* (2015) 19(1A):A68–77. doi: 10.5114/wo.2014.47136
73. Xiyuan L, Dechao B, Liang S, Yang W, Shuangsang F, Hui L, et al. Using the NONCODE Database Resource. *Curr Protoc Bioinf* (2017) 58:12–6. doi: 10.1002/cpbi.25
74. Zhang Z, Zhao W, Xiao J, Bao Y, He S, Zhang G, et al. Database Resources of the National Genomics Data Center in 2020*Nucleic Acids Res* (2020) 48(D1): D24–33. doi: 10.1093/nar/gkz913
75. Ma L, Cao J, Liu L, Du Q, Li Z, Zou D, et al. LncBook: a curated knowledgebase of human long non-coding RNAs. *Nucleic Acids Res* (2019) 47(D1):D128–34. doi: 10.1093/nar/gky960
76. Quek XC, Thomson DW, Maag JL, Bartonicek N, Signal B, Clark MB, et al. lncRNAdb v2.0: expanding the reference database for functional long noncoding RNAs. *Nucleic Acids Res* (2015) 43(Database issue):D168–73. doi: 10.1093/nar/gku988
77. Bao Z, Yang Z, Huang Z, Zhou Y, Cui Q, Dong D. LncRNADisease 2.0: an updated database of long non-coding RNA-associated diseases. *Nucleic Acids Res* (2019) 47(D1):D1034–7. doi: 10.1093/nar/gky905
78. Freeman LA. Cloning full-length transcripts and transcript variants using 5' and 3' RACE. *Methods Mol Biol* (2013) 1027:3–17. doi: 10.1007/978-1-60327-369-5_1
79. Vizzini A. 5' and 3' RACE Method to Obtain Full-Length 5' and 3' Ends of Ciona robusta Macrophage Migration Inhibitory Factors Mif1 and Mif2 cDNA. *Methods Mol Biol* (2020) 2080:223–35. doi: 10.1007/978-1-4939-9936-1_20
80. Liu F, Zheng K, Chen HC, Liu ZF. Capping-RACE: a simple, accurate, and sensitive 5' RACE method for use in prokaryotes. *Nucleic Acids Res* (2018) 46 (21):e129. doi: 10.1093/nar/gky739
81. Lagarde J, Uszczynska-Ratajczak B, Santoyo-Lopez J, Gonzalez JM, Tapanari E, Mudge JM, et al. Extension of human lncRNA transcripts by RACE coupled with long-read high-throughput sequencing (RACE-Seq). *Nat Commun* (2016) 7:12339. doi: 10.1038/ncomms12339
82. Rodriguez-Mateos P, Azevedo NF, Almeida C, Pamme N. FISH and chips: a review of microfluidic platforms for FISH analysis. *Med Microbiol Immunol* (2020) 209(3):373–91. doi: 10.1007/s00430-019-00654-1
83. Ratan ZA, Zaman SB, Mehta V, Haidere MF, Runa NJ, Akter N. Application of Fluorescence In Situ Hybridization (FISH) Technique for the Detection of Genetic Aberration in Medical Science. *Cureus* (2017) 9(6):e1325. doi: 10.7759/cureus.1325
84. Mas-Ponte D, Carlevaro-Fita J, Palumbo E, Hermoso PT, Guigo R, Johnson R. LncATLAS database for subcellular localization of long noncoding RNAs. *RNA* (2017) 23(7):1080–7. doi: 10.1261/rna.060814.117
85. Luo ML. Methods to Study Long Noncoding RNA Biology in Cancer. *Adv Exp Med Biol* (2016) 927:69–107. doi: 10.1007/978-981-10-1498-7_3
86. Agostini F, Zanzoni A, Klus P, Marchese D, Cirillo D, Tartaglia GG. catRAPID omics: a web server for large-scale prediction of protein-RNA interactions. *Bioinformatics* (2013) 29(22):2928–30. doi: 10.1093/bioinformatics/btt495
87. Gelali E, Girelli G, Matsumoto M, Wernersson E, Custodio J, Mota A, et al. iFISH is a publically available resource enabling versatile DNA FISH to study genome architecture. *Nat Commun* (2019) 10(1):1636. doi: 10.1038/s41467-019-09616-w
88. Fields BD, Nguyen SC, Nir G, Kennedy S. A multiplexed DNA FISH strategy for assessing genome architecture in Caenorhabditis elegans. *Elife* (2019) 8: e42823. doi: 10.7554/eLife.42823
89. Giorgetti L, Heard E. Closing the loop: 3C versus DNA FISH. *Genome Biol* (2016) 17(1):215. doi: 10.1186/s13059-016-1081-2
90. Nakato R, Sakata T. Methods for ChIP-seq analysis: A practical workflow and advanced applications. *Methods* (2020) S1046-2023(20)30059–1. doi: 10.1016/j.ymeth.2020.03.005
91. Muhammad II, Kong SL, Akmar AS, Munusamy U. RNA-seq and ChIP-seq as Complementary Approaches for Comprehension of Plant Transcriptional Regulatory Mechanism. *Int J Mol Sci* (2019) 21(1):167. doi: 10.3390/ijms21010167

92. Cao M, Zhao J, Hu G. Genome-wide methods for investigating long noncoding RNAs. *BioMed Pharmacother* (2019) 111:395–401. doi: 10.1016/j.biopha.2018.12.078
93. Hernandez HG, Tse MY, Pang SC, Arboleda H, Forero DA. Optimizing methodologies for PCR-based DNA methylation analysis. *Biotechniques* (2013) 55(4):181–97. doi: 10.2144/000114087
94. Li LC. Designing PCR primer for DNA methylation mapping. *Methods Mol Biol* (2007) 402:371–84. doi: 10.1007/978-1-59745-528-2_19
95. Zhou KR, Liu S, Sun WJ, Zheng LL, Zhou H, Yang JH, et al. ChIPBase v2.0: decoding transcriptional regulatory networks of non-coding RNAs and protein-coding genes from ChIP-seq data. *Nucleic Acids Res* (2017) 45 (D1):D43–50. doi: 10.1093/nar/gkw965
96. Yang JH, Li JH, Shao P, Zhou H, Chen YQ, Qu LH. starBase: a database for exploring microRNA-mRNA interaction maps from Argonaute CLIP-Seq and Degradome-Seq data. *Nucleic Acids Res* (2011) 39(Database issue): D202–9. doi: 10.1093/nar/gkq1056
97. Wang P, Li X, Gao Y, Guo Q, Wang Y, Fang Y, et al. LncACTdb 2.0: an updated database of experimentally supported ceRNA interactions curated from low- and high-throughput experiments. *Nucleic Acids Res* (2019) 47 (D1):D121–7. doi: 10.1093/nar/gky1144
98. Paraskevopoulou MD, Vlachos IS, Karagkouni D, Georgakilas G, Kanellos I, Vergoulis T, et al. DIANA-LncBase v2: indexing microRNA targets on non-coding transcripts. *Nucleic Acids Res* (2016) 44(D1):D231–8. doi: 10.1093/nar/gkv1270
99. Shi Y, Yang F, Wei S, Xu G. Identification of Key Genes Affecting Results of Hyperthermia in Osteosarcoma Based on Integrative ChIP-Seq/TargetScan Analysis. *Med Sci Monit* (2017) 23:2042–8. doi: 10.12659/MSM.901191
100. Zhang Y, Wang F, Chen G, He R, Yang L. LncRNA MALAT1 promotes osteoarthritis by modulating miR-150-5p/AKT3 axis. *Cell Biosci* (2019) 9:54. doi: 10.1186/s13578-019-0302-2
101. Zhou Z, Zhu Y, Gao G, Zhang Y. Long noncoding RNA SNHG16 targets miR-146a-5p/CCL5 to regulate LPS-induced WI-38 cell apoptosis and inflammation in acute pneumonia. *Life Sci* (2019) 228:189–97. doi: 10.1016/j.lfs.2019.05.008
102. Batista PJ, Chang HY. Long noncoding RNAs: cellular address codes in development and disease. *Cell* (2013) 152(6):1298–307. doi: 10.1016/j.cell.2013.02.012
103. Hadji F, Boulanger MC, Guay SP, Gaudreault N, Amellah S, Mkannez G, et al. Altered DNA Methylation of Long Noncoding RNA H19 in Calcific Aortic Valve Disease Promotes Mineralization by Silencing NOTCH1. *Circulation* (2016) 134(23):1848–62. doi: 10.1161/CIRCULATIONAHA.116.023116
104. Xie JJ, Jiang YY, Jiang Y, Li CQ, Lim MC, An O, et al. Super-Enhancer-Driven Long Non-Coding RNA LINC01503, Regulated by TP63, Is Over-Expressed and Oncogenic in Squamous Cell Carcinoma. *Gastroenterology* (2018) 154(8):2137–51. doi: 10.1053/j.gastro.2018.02.018
105. Hammerle M, Gutschner T, Uckelmann H, Ozgur S, Fiskin E, Gross M, et al. Posttranscriptional destabilization of the liver-specific long noncoding RNA HULC by the IGF2 mRNA-binding protein 1 (IGF2BP1). *Hepatology* (2013) 58(5):1703–12. doi: 10.1002/hep.26537
106. Lam MT, Li W, Rosenfeld MG, Glass CK. Enhancer RNAs and regulated transcriptional programs. *Trends Biochem Sci* (2014) 39(4):170–82. doi: 10.1016/j.tibs.2014.02.007
107. Kim TK, Hemberg M, Gray JM. Enhancer RNAs: a class of long noncoding RNAs synthesized at enhancers. *Cold Spring Harb Perspect Biol* (2015) 7(1): a18622. doi: 10.1101/cshperspect.a018622
108. Liu Y, Ding M, Gao Q, He A, Liu Y, Mei H. Current Advances on the Important Roles of Enhancer RNAs in Gene Regulation and Cancer. *BioMed Res Int* (2018) 2018:2405351. doi: 10.1155/2018/2405351
109. Jiao W, Chen Y, Song H, Li D, Mei H, Yang F, et al. HPSE enhancer RNA promotes cancer progression through driving chromatin looping and regulating hnRNPU/p300/EGR1/HPSE axis. *Oncogene* (2018) 37(20):2728–45. doi: 10.1038/s41388-018-0128-0
110. Leveille N, Melo CA, Agami R. Enhancer-associated RNAs as therapeutic targets. *Expert Opin Biol Ther* (2015) 15(5):723–34. doi: 10.1517/14712598.2015.1029452
111. Zaiou M. Circular RNAs as Potential Biomarkers and Therapeutic Targets for Metabolic Diseases. *Adv Exp Med Biol* (2019) 1134:177–91. doi: 10.1007/978-3-030-12668-1_10
112. Royo F, Zuniga-Garcia P, Torrano V, Loizaga A, Sanchez-Mosquera P, Ugalde-Olano A, et al. Transcriptomic profiling of urine extracellular vesicles reveals alterations of CDH3 in prostate cancer. *Oncotarget* (2016) 7(6):6835–46. doi: 10.18632/oncotarget.6899
113. Hornick NI, Huan J, Doron B, Goloviznina NA, Lapidus J, Chang BH, et al. Serum Exosome MicroRNA as a Minimally-Invasive Early Biomarker of AML. *Sci Rep* (2015) 5:11295. doi: 10.1038/srep11295
114. Sohn W, Kim J, Kang SH, Yang SR, Cho JY, Cho HC, et al. Serum exosomal microRNAs as novel biomarkers for hepatocellular carcinoma. *Exp Mol Med* (2015) 47:e184. doi: 10.1038/emm.2015.68
115. Momen-Heravi F, Saha B, Kodys K, Catalano D, Satishchandran A, Szabo G. Increased number of circulating exosomes and their microRNA cargos are potential novel biomarkers in alcoholic hepatitis. *J Transl Med* (2015) 13:261. doi: 10.1186/s12967-015-0623-9
116. Quinn JF, Patel T, Wong D, Das S, Freedman JE, Laurent LC, et al. Extracellular RNAs: development as biomarkers of human disease. *J Extracell Vesicles* (2015) 4:27495. doi: 10.3402/jev.v4.27495
117. Ben-Dov IZ, Whalen VM, Goilav B, Max KE, Tuschl T. Cell and Microvesicle Urine microRNA Deep Sequencing Profiles from Healthy Individuals: Observations with Potential Impact on Biomarker Studies. *PloS One* (2016) 11(1):e147249. doi: 10.1371/journal.pone.0147249
118. Long JD, Sullivan TB, Humphrey J, Logvinenko T, Summerhayes KA, Kozinn S, et al. A non-invasive miRNA based assay to detect bladder cancer in cell-free urine. *Am J Transl Res* (2015) 7(11):2500–9.
119. Fan Q, Yang L, Zhang X, Peng X, Wei S, Su D, et al. The emerging role of exosome-derived non-coding RNAs in cancer biology. *Cancer Lett* (2018) 414:107–15. doi: 10.1016/j.canlet.2017.10.040
120. Sun Z, Yang S, Zhou Q, Wang G, Song J, Li Z, et al. Emerging role of exosome-derived long non-coding RNAs in tumor microenvironment. *Mol Cancer* (2018) 17(1):82. doi: 10.1186/s12943-018-0831-z
121. Jiang N, Pan J, Fang S, Zhou C, Han Y, Chen J, et al. Liquid biopsy: Circulating exosomal long noncoding RNAs in cancer. *Clin Chim Acta* (2019) 495:331–7. doi: 10.1016/j.cca.2019.04.082
122. Zhao W, Liu Y, Zhang C, Duan C. Multiple Roles of Exosomal Long Noncoding RNAs in Cancers. *BioMed Res Int* (2019) 2019:1460572. doi: 10.1155/2019/1460572
123. Wang M, Zhou L, Yu F, Zhang Y, Li P, Wang K. The functional roles of exosomal long non-coding RNAs in cancer. *Cell Mol Life Sci* (2019) 76 (11):2059–76. doi: 10.1007/s00018-019-03018-3
124. Kang M, Ren M, Li Y, Fu Y, Deng M, Li C. Exosome-mediated transfer of lncRNA PART1 induces gefitinib resistance in esophageal squamous cell carcinoma via functioning as a competing endogenous RNA. *J Exp Clin Cancer Res* (2018) 37(1):171. doi: 10.1186/s13046-018-0845-9
125. Lin Y, Dong H, Deng W, Lin W, Li K, Xiong X, et al. Evaluation of Salivary Exosomal Chimeric GOLM1-NAA35 RNA as a Potential Biomarker in Esophageal Carcinoma. *Clin Cancer Res* (2019) 25(10):3035–45. doi: 10.1158/1078-0432.CCR-18-3169
126. Jia Y, Chen Y, Wang Q, Jayasinghe U, Luo X, Wei Q, et al. Exosome: emerging biomarker in breast cancer. *Oncotarget* (2017) 8(25):41717–33. doi: 10.18632/oncotarget.16684
127. Gilligan KE, Dwyer RM. Engineering Exosomes for Cancer Therapy. *Int J Mol Sci* (2017) 18(6):1122. doi: 10.3390/ijms18061122
128. Lin C, Yang L. Long Noncoding RNA in Cancer: Wiring Signaling Circuitry. *Trends Cell Biol* (2018) 28(4):287–301. doi: 10.1016/j.tcb.2017.11.008
129. Filella X, Foj L, Mila M, Auge JM, Molina R, Jimenez W. PCA3 in the detection and management of early prostate cancer. *Tumour Biol* (2013) 34 (3):1337–47. doi: 10.1007/s13277-013-0739-6
130. Loewen G, Jayawickramarajah J, Zhuo Y, Shan B. Functions of lncRNA HOTAIR in lung cancer. *J Hematol Oncol* (2014) 7:90. doi: 10.1186/s13045-014-0090-4
131. Arun G, Diermeier SD, Spector DL. Therapeutic Targeting of Long Non-Coding RNAs in Cancer. *Trends Mol Med* (2018) 24(3):257–77. doi: 10.1016/j.molmed.2018.01.001

132. Chandra GS, Nandan TY. Potential of long non-coding RNAs in cancer patients: From biomarkers to therapeutic targets. *Int J Cancer* (2017) 140 (9):1955–67. doi: 10.1002/ijc.30546
133. Shin H, Kim Y, Kim M, Lee Y. BC200 RNA: An Emerging Therapeutic Target and Diagnostic Marker for Human Cancer. *Mol Cells* (2018) 41 (12):993–9. doi: 10.14348/molcells.2018.0425
134. Liu J, Ben Q, Lu E, He X, Yang X, Ma J, et al. Long noncoding RNA PANDAR blocks CDKN1A gene transcription by competitive interaction with p53 protein in gastric cancer. *Cell Death Dis* (2018) 9(2):168. doi: 10.1038/s41419-017-0246-6

Conflict of Interest: The authors declare that the research was conducted in the absence of any commercial or financial relationships that could be construed as a potential conflict of interest.

frontiers in Cell and Developmental Biology

ORIGINAL RESEARCH
published: 08 January 2021
doi: 10.3389/fcell.2020.624764

Circular RNA CircNOLC1, Upregulated by NF-KappaB, Promotes the Progression of Prostate Cancer via miR-647/PAQR4 Axis

Wenbin Chen[1], Shengren Cen[1], Xumin Zhou[1], Taowei Yang[1], Kaihui Wu[1], Libin Zou[1], Junqi Luo[1], Chuanyin Li[1], Daojun Lv[2]* and Xiangming Mao[1]**

[1] Department of Urology, Zhujiang Hospital, Southern Medical University, Guangzhou, China, [2] Guangdong Key Laboratory of Urology, Department of Urology, The First Affiliated Hospital of Guangzhou Medical University, Guangzhou, China

OPEN ACCESS

Edited by:
Lorenzo Gerratana,
University of Udine, Italy

Reviewed by:
Francesca Benedetti,
University of Maryland, United States
Avisek Majumder,
University of California,
San Francisco, United States

***Correspondence:**
Chuanyin Li
li-chuanyin@163.com
Daojun Lv
15914336377@163.com
Xiangming Mao
mxm@smu.edu.cn

Specialty section:
This article was submitted to Molecular and Cellular Oncology, a section of the journal Frontiers in Cell and Developmental Biology

Received: 01 November 2020
Accepted: 14 December 2020
Published: 08 January 2021

Citation:
Chen W, Cen S, Zhou X, Yang T, Wu K, Zou L, Luo J, Li C, Lv D and Mao X (2021) Circular RNA CircNOLC1, Upregulated by NF-KappaB, Promotes the Progression of Prostate Cancer via miR-647/PAQR4 Axis. Front. Cell Dev. Biol. 8:624764. doi: 10.3389/fcell.2020.624764

Background: CircRNAs recently have shown critical roles in tumor biology. However, their roles in prostate cancer (PCa) remains largely unclear.

Methods: CircRNA microarrays were performed in immortal prostate cell line RWPE1 and PCa cell lines as DU145, PC3, LNCaP, C4-2, and 22RV1. Combined with upregulated circRNAs in PCa tissues, circNOLC1 expression was validated in PCa cells and tissues *via* qRT-PCR and FISH. Sanger sequencing, actinomycin D, gDNA, and cDNA, RNase R assays were used to assess the circular characteristics of circNOLC1. CCK-8, colony formation, transwell migration assays, and mice xenograft models were conducted to evaluate the functions of PCa cells after circNOLC1 knockdown and overexpression. RNA pulldown, luciferase reporter assay, FISH (fluorescence *in situ* hybridization), and CHIP were utilized to illustrate the further mechanisms of circNOLC1.

Results: Our research indicated that circNOLC1 was overexpressed in PCa cells and tissues, and circNOLC1 was more stable than linear NOLC1 mRNA. CircNOLC1 promoted PCa cells proliferation and migration *in vitro* and *vivo*. Additionally, we found that circNOLC1 could upregulate PAQR4 expression by sponging miR-647, leading to the activation of PI3K/Akt pathway. Moreover, NF-kappaB was identified to bind to the NOLC1 promoter sites and upregulated both NOLC1 and circNOLC1 expression.

Conclusion: CircNOLC1, elevated by transcription factor NF-kappaB, promotes PCa progression *via* a miR-647/PAQR4 axis, and circNOLC1 is a potential biomarker and target for PCa treatment.

Keywords: circRNAs, prostate cancer, miR-647, PAQR4, NF-kappaB, progression

Abbreviations: circRNAs, circular RNAs; PCa, prostate cancer; qRT-PCR, quantitative real-time polymerase chain reaction; ceRNA, competing endogenous RNA; IHC, immunohistochemistry; NC, negative control; siRNA, small interfering RNA.

INTRODUCTION

Prostate cancer (PCa) is currently the first and second leading cause of new diagnosis and mortality, accounting for 21% of all new cancer cases and 10% of all death cases in men (Siegel et al., 2020). Although primary tumors frequently can be cured through androgen deprivation therapy (Berger et al., 2011), many patients exhibited poor prognosis due to tumor metastasis (Wang et al., 2018). Therefore, further researches are needed to explore the novel diagnostic and therapeutic biomarkers and reveal the detailed underlying mechanisms in PCa progression.

Circular RNA (CircRNA), a novel type of non-coding RNA, is formed by covalently closed loop structures without free terminal ends (Chen, 2020). Due to their special property, circRNAs show higher stability and stronger resistance to ribonuclease R degradation than linear RNAs (Chen and Yang, 2015). Owing to the progression of advanced high-throughput sequencing, various circRNAs were discovered to exhibit abnormal expression in cancers (Chen et al., 2019b; Vo et al., 2019). Recent reports revealed that circRNAs exert their biological functions mainly relying on the miRNA sponging (Hansen et al., 2011, 2013). Besides, circRNAs could also play a role in interacting with RNA binding proteins (RBPs) (Liu et al., 2020). In PCa, circRNAs, such as, circ_0007494 and circFMN2, have been recognized to function as competing endogenous RNAs (ceRNAs) to relieve the inhibition of miRNA targets (Shan et al., 2020; Zhang et al., 2020). CircAR3 was identified to show high expression levels in the plasma of PCa patients, which may serve as a novel PCa biomarker (Luo et al., 2019). These findings revealed the significant roles of circRNAs in PCa. However, there are still plenty of circRNAs involved in the PCa have not been identified.

In this study, circRNA microarray in five common PCa cells combined with the published microarray data for PCa tissues, we identified 22 different circRNAs. Subsequently, circNOLC1 (circBase ID: has_circ_0000257) were chosen for further study to explore its role in the PCa proliferation and progression by using a series of *in vitro* assays and *in vivo* mouse model. Finally, the underlying mechanism of circNOLC1 were also evaluated. In summary, our works revealed that circNOLC1 could act as a oncogene in the progression of PCa, and may provide a novel target for the diagnosis and treatment of PCa.

MATERIALS AND METHODS

Clinical Specimens

Eighty prostate tissues and sixteen adjacent tissues were obtained from patients who underwent radical prostatectomy (RP) at Zhujiang Hospital of Southern Medical University from 2016 to 2018, and then the paraffin specimens were constructed as a tissue microarray (TMA). The clinical details of patients were collected from the medical records. All experimental procedures were approved by the Ethics Committee of the Southern Medical University Zhujiang Hospital. The median age of the enrolled patients was 67.5 years and average age was 65.1 (range: 20–97 years). Clinical TNM staging and Gleason scores of patient specimens were based on the American Joint Committee on Cancer (AJCC) Eighth Edition (2017) and the 2016 World Health Organization (WHO) classification of genitourinary tumors. The detailed clinicopathological information of all samples was presented in **Supplementary Table 1**.

CircRNA Microarrays

Arraystar Human circRNA Array v2 (Kangcheng Biotech, Shanghai, China) was applied to analysis circRNA microarray. Total RNA from each sample was quantified with the NanoDrop ND-1000. Sample preparation and microarray hybridization were performed as outlined in the standard protocols stipulated by Arraystar, as described previously (Chen et al., 2019a). Normalized Intensity of each group (averaged normalized intensities of replicate samples, log2 transformed) were analyzed by paired *t*-test (*P*: 0.05). Quantile normalization and subsequent data processing was performed through the R 4.0.2 software limma package. Differentially expressed circRNAs were identified via Fold Change filtering. Hierarchical Clustering was used to perform the distinguishable circRNAs expression pattern among the samples.

Bioinformatics Analysis

The circRNA-miRNA interactome was drawn by circBank[1] and circinteractome[2]. Overlapping candidates were considered as putative miRNA targets. Two algorithms (TargetScan and miRpathDB) were used to predict the potential miRNAs targeting the 3'-UTR of PAQR4. Data from The Cancer Genome Atlas (TCGA) was analyzed by Starbase 2.0[3].

Cell Culture and Transfection

DU145, PC3, C4-2, LNCaP, 22RV1 (PCa cell lines), RWPE1 (normal prostate epithelial cell line), and HEK-293T cells were obtained from Cell Bank of Chinese Academy of Sciences, grown with RPMI-1640 medium (Gibco, United States) supplemented with 10% FBS (Gibco, United States) and incubated at 37℃ in 5% CO_2. Small interfering RNAs (siRNAs) of circNOLC1 and NF-kappaB, and miR-647 inhibitor or mimics were purchased from RiboBio Company (Guangzhou, China). Lentivirus vectors (GeneChem Bio-Medical Biotechnology, Shanghai, China) were utilized to establish cell lines stably overexpressing circNOLC1, and the transfected cells were selected in puromycin (2 μg/ml) for 1 week. All the target sequences were shown in **Supplementary Table 2**.

Cellular Fraction and RNA Isolation

Nuclear and Cytoplasmic Extraction Reagents (No. 78833, Thermo Fisher Scientific, United States) were used to separate nuclear and cytoplasm of cultured cells following the manufacturer's protocol. And RNA extraction was described as followed.

[1]http://www.circbank.cn/

[2]https://circinteractome.nia.nih.gov/

[3]starbase.sysu.edu.cn/

RNA Extraction and RT-qPCR

Total RNA was obtained from cells with TRIzol (Invitrogen, United States), while the cDNA was reverse-transcribed via utilizing PrimeScript RT reagent Kit (TaKaRa) following the manufacturer's instructions. The genome DNA was isolated by special extraction kit (DP304, TIANGEN, China). SYBR Green PCR Master Mix (TaKaRa) and Applied Bio-systems 7500 Fast Real-Time RCR System (Applied Biosystems, United States) were used for RT-qPCR analysis. Data were acquired from three independent experiments and normalized to GAPDH. All the primers were shown in **Supplementary Table 2**.

Actinomycin D and RNase R Treatment Assay

To compare the stability of linear RNA and circRNA, Actinomycin D (MedChemExpress, China) was added into medium to block RNA transcription and the solvent dimethyl sulfoxide (DMSO; Sigma) was applied as a negative control. Cells were treated with actinomycin D or DMSO in a final concentration of 1 μg/mL for 0, 4, 8, 12, and 24 h, and then the RNA was extracted for RT-qPCR detection, using 18S as an internal reference. For RNase R treatment, 2 mg total RNA was incubated for 15 min at 37°C with or without 3 U/mg RNase R (No. R0301, Geneseed, China), and followed by RT-qPCR analysis.

Fluorescence *in situ* Hybridization (FISH) Analysis

CircNOLC1 and miR-647 were captured by Cy3-labeled probes (RiboBio, Guangzhou, China) and Alexa 488-labeled probes (FOCOFISH, Guangzhou, China). FISH experiment was conducted using Fluorescent *in situ* Hybridization Kit (No. C10910, RiboBio, Guangzhou, China), according to the official guidelines. DAPI was utilized to stain the nuclei. Subsequently, circNOLC1 and miR-647 were observed through a confocal microscope (LSM 880 with Airyscan, Carl Zeiss, Germany).

Cell Proliferation Measurement

Cell proliferation was measured by CCK-8 kit (CK-04, Dojindo). 2,000 PCa cells were planted into 96-well plates. Then medium with 10%CCK-8 was added into each well, and incubated for 2 h. Subsequently, the absorbance values at 450 nm were detected by a microplate reader (EXL800, BioTek Instruments).

Colony Formation Assay

PCa cells were seeded into 6-well plates and cultured with complete medium for 2 weeks. The formed cells were fixed with 4% paraformaldehyde for 10 min and stained with Giemsa (Baso Diagnostics Inc, Zhu Hai, China) for 5 min. Each experiment was performed with three replicates.

Transwell Migration Assays

Cell migration assay was performed using transwell inserts (8 mm pores; Corning, NY, United States) in 24-well plates. PCa cells (5×10^4) were resuspended in 300 μl serum-free medium and seeded into the upper chamber of the insert. Subsequently, the lower chamber was filled with 500 μl complete medium. After 24 h, the cells were fixed with 4% paraformaldehyde for 10 min and stained with Giemsa (Baso Diagnostics Inc, Zhu Hai, China). Five randomly selected fields were photographed using an invert microscope at 200× magnification. The cell numbers of each image were counted by Image J software. Experiments were performed in triplicate.

Western Blot

Cells were lysed in RIPA lysis buffer (#KGP250, KeyGEN BioTECH, Nanjing, China), following the manufacturer's instructions. Equal amounts of proteins were separated in 10% SDS-PAGE gels and transferred to PVDF membranes (Millipore, Germany). The membranes were then blocked for 1 h with 5% no fat milk and incubated overnight at 4°C with the following primary antibodies: EMT marker (#9782, Cell signaling, United States), anti-PAQR4 (#13401-1-AP, Proteintech), anti-β-actin (#60008-1-Ig, Proteintech). Subsequently, the membranes were immersed in the anti-rabbit or anti-mouse secondary antibodies (#7074S or #7076S, Cell signaling, United States) for 1.5 h at room temperature. Enhanced chemiluminescence (ECL) kit (Pierce Biotechnology, Rockford, IL, United States) was used to detect and visualize the protein.

RNA-Pulldown

CircRNA pulldown assay was carried out using Pierce™ Magnetic RNA-Protein Pull-Down Kit (No: 20164, Thermo Fisher Scientific, United States), all procedures were followed as manufacturer's instructions. Then the final RNA was extracted by TRIzol (Invitrogen, United States) and analyzed by RT-qPCR.

Dual-Luciferase Reporter Assay

The sequences of circNOLC1 and its mutant types without miR-647 binding sites were designed and packaged into pEZX-MT06 vector (GeneCopoeia, Guangzhou, China), termed as circNOLC1-WT and circNOLC1-MUT. The miRNA mimics were purchased from RiboBio Company (Guangzhou, China). HEK-293T cells (5×10^5) were seeded into each well of a 12-well plate for 24 h. Then, a mixture of luciferase reporter vectors and miRNA mimics was transfected into cells. The relative luciferase activity was measured utilizing Luc-Pair™ Duo-Luciferase HS Assay Kit (GeneCopoeia, China). Each group was confirmed in triplicate.

Xenograft Model

All experimental animal procedures were authorized by the Animal Care and Use Committee of Southern Medical University and Specific Pathogen Free (SPF) conditions were used to raise animals. BALB/c nude mice were obtained from the Animal Center of Southern Medical University, Guangzhou, China. A total of 2×10^6 du145 cells stably transfected with circNOCL1 or Vector were subcutaneously injected into the mice axillae ($n = 6$ per group). Tumor volume was measured every 4–5 days and volumes were calculated using the formula: length × width^2 × 0.5.

Immunohistochemistry Analysis

Detection of Ki-67 and CD31 was performed on 3 μm thick paraffin sections with the indicated antibodies. Briefly, sections were incubated with primary antibodies Ki-67 (1:250, ab15580, Abcam, United States) or CD31 (ZM-0044, Zhong Shan Jin Qiao, Beijing, China) antibodies at 4°C overnight. Subsequently, Horseradish peroxidase (HRP)-conjugated secondary antibodies (dilution 1:250, Beyotime, Shanghai, China) were further incubated at 37°C for 30 min. Finally, the sections were stained with 3,3'-diaminobenzidine (DAB, ZLI-9018, Zhong Shan Jin Qiao, Beijing, China) for 5 min and examined with a microscope.

CHIP Assay

CHIP assay was performed using SimpleChIP® Plus Enzymatic Chromatin IP Kit (#9005, Cell Signaling Technology, United States), according to the manufacturer's protocols. Anti-NF-kappaB antibody for CHIP was obtained from Cell Signaling Technology (#8242). The detailed binding sites between the promoter sites of NOLC1 and NF-kappaB were predicted by *Consite*[4], as: GGGAAGTCCC. The specific primers for binding sites were shown in **Supplementary Table 2**. And the following analysis was detected by RT-qPCR. Experiments were performed in triplicate.

Statistical Analysis

All statistical analysis was performed using GraphPad Prism 8 (GraphPad Software, United States). The data were presented as mean ± *SD*. Two-tailed Student's *t*-test or ANOVA was conducted to analyze the significance between variables. The relation between circNOLC1 expression and clinicopathological properties was analyzed using a χ^2 test. $P < 0.05$ was considered as statistically significant.

RESULTS

Upregulation and Characterization of CircNOLC1 in PCa

To investigate the differential expressed circRNAs in PCa, we performed a microarray of the PCa cell lines, DU145, PC3, LNCaP, C4-2, and 22RV1 cells (**Supplementary Figure 1A**). We found 22 circRNAs both upregulated in five PCa cells and a microarray dataset that contains five pairs of high-grade and low-grade PCa (**Figures 1A–C**). The expression levels of top five upregulated circRNAs in PCa cells and normal prostate cell were validated via qRT-PCR (**Figure 1D** and **Supplementary Figures 1B–E**), circNOLC1 (hsa_circ_0000257) displayed the greatest increase and was chosen for further study. Next, we verified the expression of circNOLC1 in 79 Prostate adenocarcinoma tissues and 16 normal prostate tissues by FISH assays (**Figure 1E** and **Table 1**). These findings demonstrated that circNOLC1 is upregulated in PCa cells and tissues.

CircNOLC1 is generated by head-to-tail splicing of NOLC1 exon 2–5 and contains 487 nucleotides (**Figure 1F**, left panel, upper). Sanger sequencing was used to confirm the putative circNOLC1 junction (**Figure 1F**, right panel, lower). Besides, we amplified circNOLC1 and NOLC1 from cDNA and gDNA utilizing divergent and convergent primers, which showed that circNOLC1 only exist in the cDNA (**Figure 1G**). Actinomycin D assay demonstrated that circNOLC1 was more stable compared with linear NOLC1 (**Figure 1H**). Moreover, RNase R assays exhibited that the linear mRNA NOLC1 was digested, while circNOLC1 not (**Figure 1I**). We also isolated the cytoplasmic and nuclear RNA in DU145 and C4-2 cells, which demonstrated that circNOLC1 was expressed equally in cytoplasm and nuclear (**Figure 1J**). These results illustrated the circular characteristics of circNOLC1.

CircNOLC1 Promotes PCa Proliferation and Migration *in vitro*

To discover the function of circNOL1 in PCa, we randomly chose DU145 and C4-2 cell lines for silencing, PC3 and C4-2 for overexpression. We constructed three siRNAs targeting circNOLC1 to silence its expression. Finally, si-circ#02 exhibited the highest silencing efficiency measured by qRT-PCR and was chosen for the following experiments (**Figure 2A**, left). Meanwhile, we established stably overexpressed circNOLC1 in PC3 and C4-2 cells via utilizing lentiviral vectors, and the circNOLC1 overexpression cells exhibited a great increased level of circNOLC1 (**Figure 2A**, right). However, the NOLC1 mRNA level was not affected by circNOLC1 expression (**Supplementary Figures 2A,B**). CCK-8 and colony formation assays exhibited that the cell proliferation ability was restrained after circNOLC1 knockdown, while the overexpression of circNOLC1 showed the opposite results (**Figures 2B–D**). Transwell migration assays demonstrated that circNOLC1 downregulation significantly decreased PCa cells migration, while circNOLC1 overexpression revealed the opposite effects (**Figure 2E**). Meanwhile, western blots exhibited that loss of circNOLC1 significantly decreased E-cadherin expression and increased Vimentin level, while gain of circNOLC1 showed the opposite results (**Figure 2F**). Besides, CCK-8 and Transwell migration assays revealed that knockdown of NOLC1 also suppressed the growth and migration of PCa cells (**Supplementary Figures 2C–E**). These results revealed that circNOLC1 promotes PCa progression *in vitro*.

CircNOLC1 Acted as a miR-647 Sponge in PCa Cells

Plenty of reports have revealed that circRNAs mainly function as miRNA sponges in various cancers (Hansen et al., 2013; Zheng et al., 2016). To figure out how circNOLC1 play a role in PCa, we predicted the potential miRNA targets of circNOLC1 using three databases (including miRanda, TargetScan, and CircInteractome). We chose eight miRNAs overlapped in the three databases for further study (**Figure 3A**). To verify the interaction between circNOLC1 and miRNAs, circRNA pulldown assay was performed in DU145 cells via designed circNOLC1 probe. The observation showed that circNOLC1, miR-647 and miR-326 were significantly enriched (**Figure 3B**). Besides,

[4]http://consite.genereg.net/

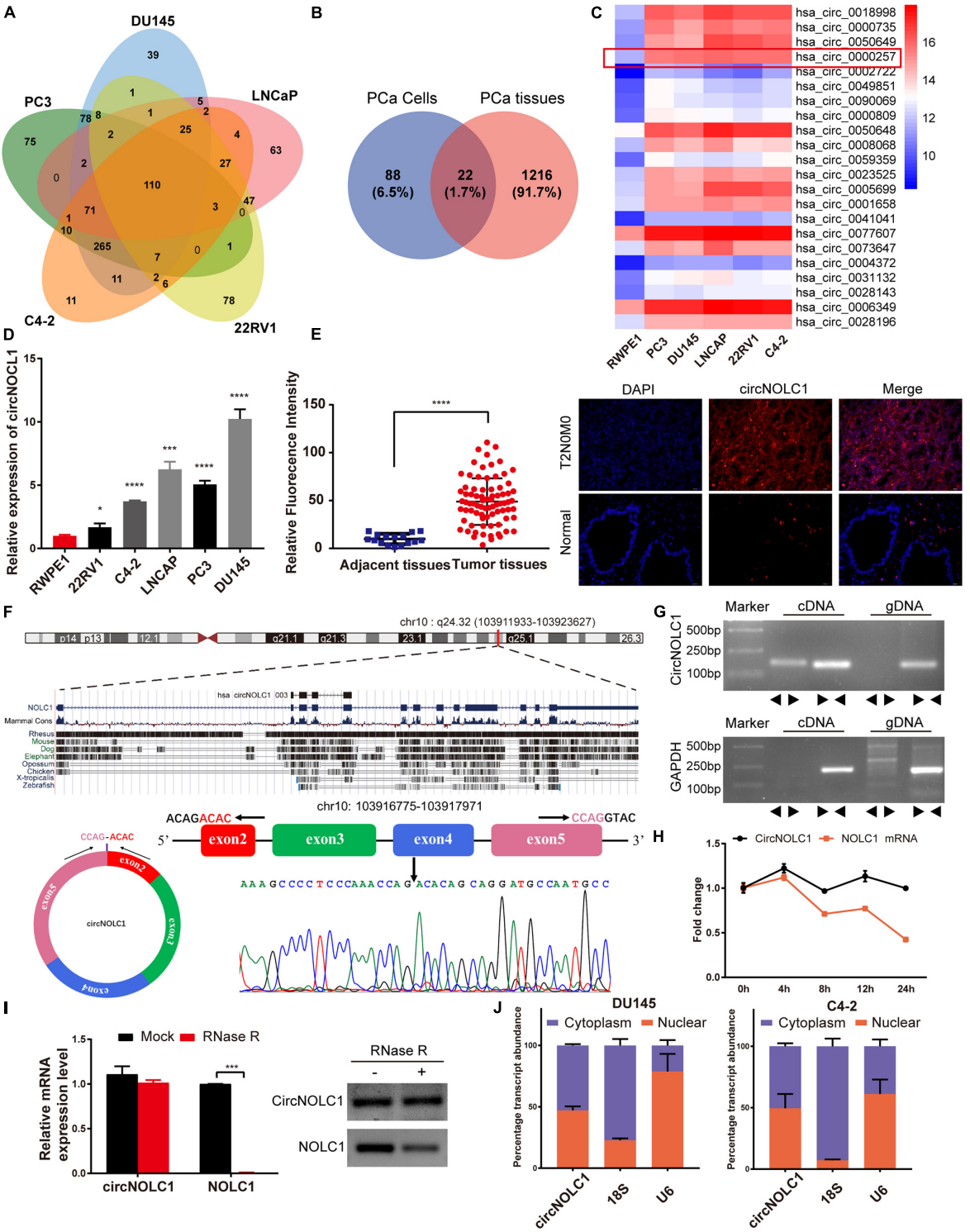

FIGURE 1 | Screening and characterization of circNOLC1 in PCa. **(A,B)** Schematic illustration demonstrates that 22 circRNAs were commonly upregulated in PCa cells and tissues. **(C)** The heatmap showing upregulated circRNA expression profiles between PCa cells and normal prostate cells. **(D)** Expression of circNOLC1 in five PCa cells and normal prostate cells. **(E)** Relative Fluorescence Intensity of each tissues and representative images of FISH analysis of circNOLC1 in normal and PCa tissues. Scale bar = 50 μm. **(F)** Sketch map for circNOLC1 and sanger sequencing confirming the back splicing site of circNOLC1. **(G)** The existence of circNOLC1 was validated by qRT-PCR and Gel electrophoresis. Divergent primers could amplify circNOLC1 in cDNA but not gDNA. GAPDH was used as negative control. **(H,I)** Actinomycin D treatment and RNase R to confirm the circular characteristics of circNOLC1. **(J)** Cellular localization of circNOLC1 in DU145 and C4-2 cells. Nuclear and cytoplasmic fraction was separated followed by RNA extraction. circNOLC1, U6 and 18S levels were analyzed by qRT-PCR. $^{*}p < 0.05$, $^{***}p < 0.001$, $^{****}p < 0.0001$.

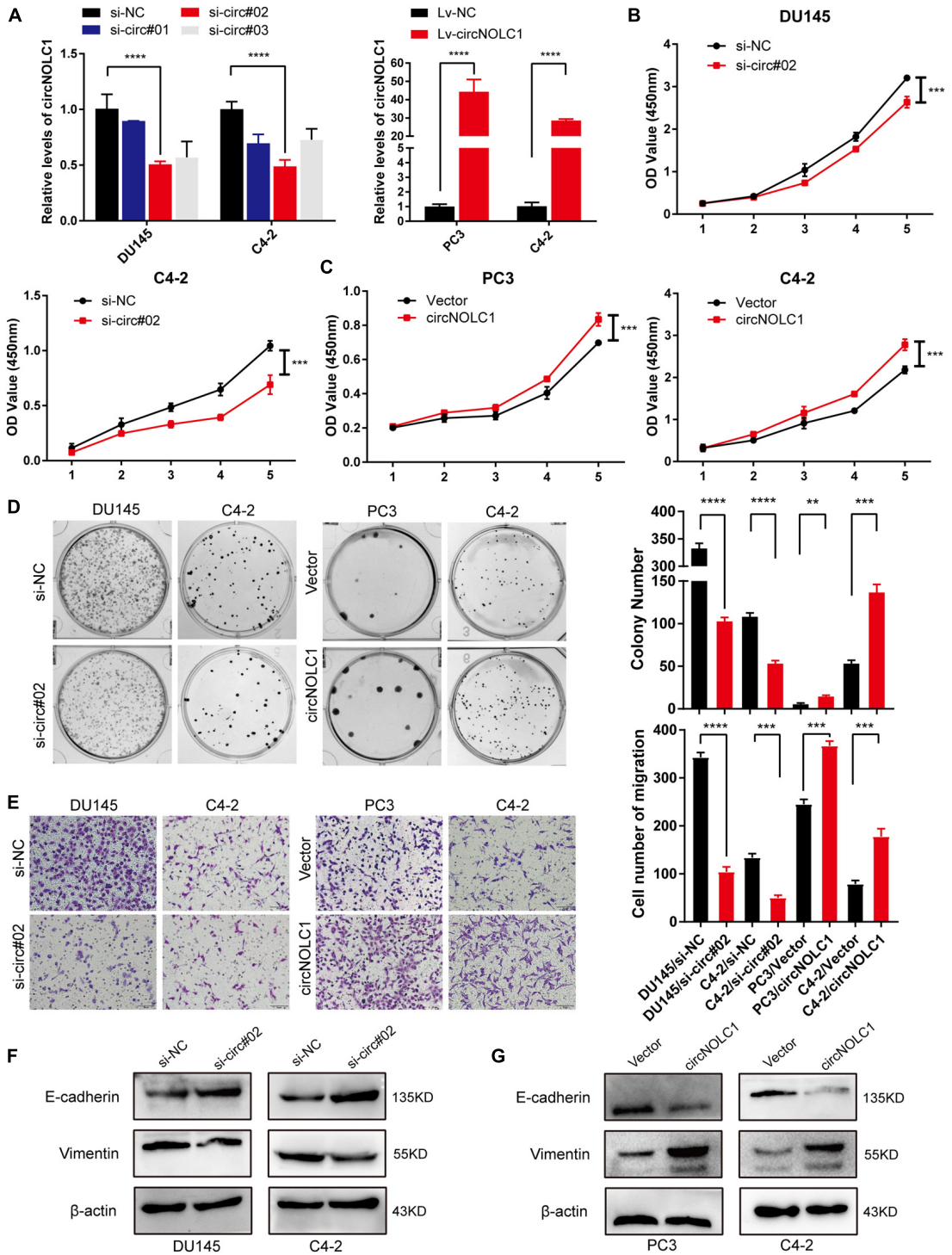

FIGURE 2 | CircNOLC1 promotes cell growth and migration in PCa cells. **(A)** RT-qPCR was performed to confirm the inhibiting efficiency of three siRNAs targeting circNOLC1 in DU145 and C4-2 cells and the overexpression of circNOLC1 vector in PC3 and C4-2 cells. **(B–D)** CCK8 and colony formation assays were utilized to evaluate the proliferation of PCa cells after knockdown and overexpression of circNOLC1. **(E)** Transwell migration assay was conducted to assess the cell migration ability in circNOLC1-silenced and circNOLC1-overexpressed PCa cells. **(F,G)** The influence of circNOLC1 on the protein expression of Vimentin and E-cadherin were measured by western blot. $^{**}p < 0.01$, $^{***}p < 0.001$, $^{****}p < 0.0001$.

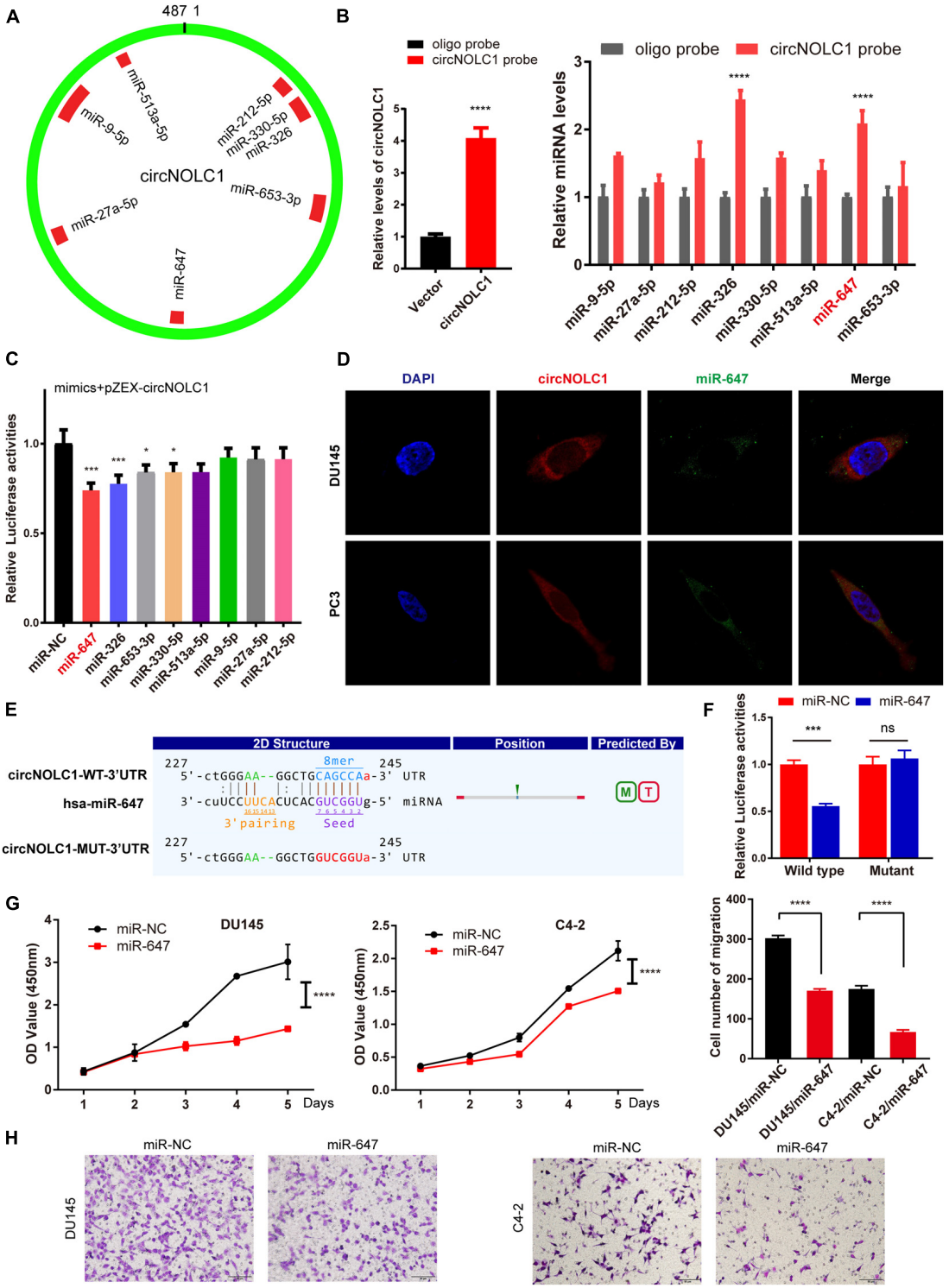

FIGURE 3 | CircNOLC1 acts as a sponge of miR-647. **(A)** Schematic illustration exhibiting the potential circNOLC1 targeting miRNAs, predicted by miRanda, Targetscan, and CircInteractome. **(B)** RNA-Pulldown was performed in DU145 cells using circNOLC1 and negative control probes. **(C)** Effects of nine predicted miRNAs and a negative control on the luciferase activity of circNOLC1, as determined by luciferase reporter assay. **(D)** Colocalization between circNOLC1 and miR-647 was observed using RNA-FISH in DU145 and PC3 cells. The nuclei were stained with DAPI. Scale bar = 40 μm. **(E)** Schematic illustration exhibiting the potential binding sites between circNOLC1 and miR-647, predicted by Targetscan. **(F)** The luciferase activity of pEZX-circNOLC1 in HEK-293 T cells subsequently co-transfected with miR-647. **(G,H)** CCK8 assays and transwell assays were utilized to detect the proliferation and migration of PCa cells after overexpression of miR-647. $^{*}p < 0.05$, $^{***}p < 0.001$, $^{****}p < 0.0001$.

Luciferase-circNOLC1 reporters were transfected into HEK-293T cells along with miRNA mimics or negative controls, which indicated that miR-647 significantly reduced luciferase activity, compared to miR-NC (**Figure 3C**). Next, RNA-FISH was utilized to confirm the localization of circNOLC1 and miR-647 in DU145 and PC3 cells. Notably, circNOLC1 and miR-647 were mainly co-localized in the cytoplasm of PCa cells (**Figure 3D**). Moreover, luciferase reporter assays were constructed in DU145 cells by transfected with luciferase reporter vectors (including the wild type or mutant sequence targeted by miR-647). The luciferase activity was obviously decreased in cells co-transfected with the miR-647 mimics and the wild-type sequence, when compared with the mutant sequence (**Figures 3E,F**). Taken together, we provided evidences that circNOLC1 could directly bind to miR-647 in PCa cells.

CircNOLC1 Upregulates PAQR4 Expression Through Sponging miR-647

Due to previous reports, miR-647 could retard tumor progression via inhibiting downstream oncogenes (Ye et al., 2017; Qin et al., 2020). We subsequently discovered that overexpression of miR-647 promoted PCa cells proliferation and migration, which indicated that miR-647 act as a tumor inhibitor role in

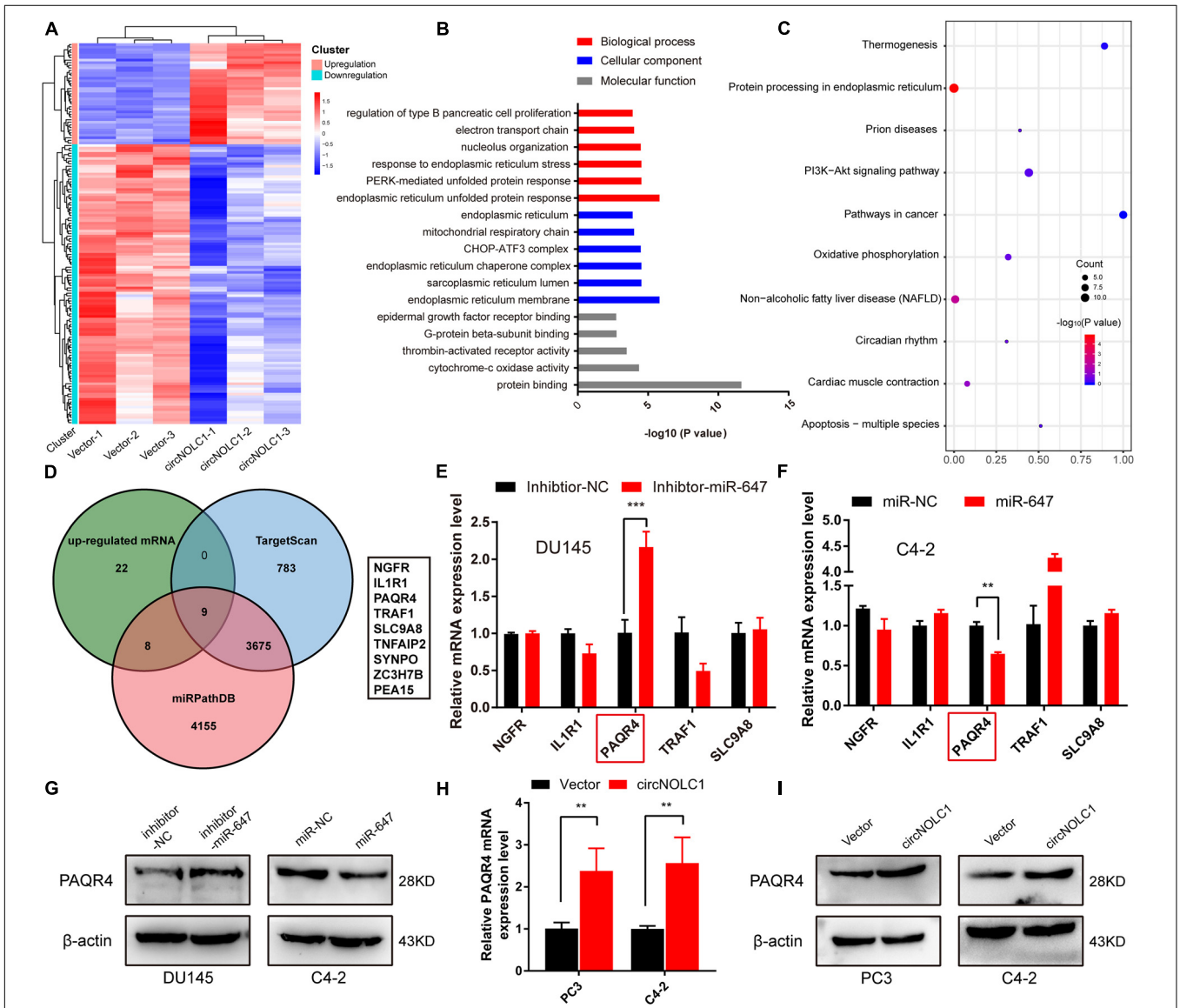

FIGURE 4 | CircNOLC1 upregulates the PAQR4 level through sponging miR-647. **(A)** The heatmap of differentially expressed mRNAs in PC3 cells transfected with Vector or circNOLC1. Each sample was mixed with three replicates. **(B,C)** GO and KEGG analyses of DEGs in PC3 cells. **(D)** Venn diagram illustrating overlapping of miR-647 targeting mRNAs and upregulated mRNAs in PC3 cells. **(E,F)** The mRNA expressions of NGFR, IL1R1, PAQR4, TRAF1, and SLC9A8 were measured via RT-qPCR. **(G)** Relative PAQR4 protein levels in PCa cells transfected with miR-647 inhibitor or mimics. **(H,I)** PAQR4 mRNA and protein expression in circNOLC1 overexpression PCa cells. $^{**}p < 0.01$; $^{***}p < 0.001$.

PCa (**Figures 3G,H**). Therefore, we assumed that circNOCL1 drove tumor development by avoiding downregulation of these oncogenes induced by miR-647. We performed RNA-seq in PC3-circNOLC1 and PC3-Vector cells, and discovered that 39 genes were upregulated and 108 genes were downregulated in PC3-circNOLC1 cells compared with PC3-Vector cells (**Figure 4A**). GO analysis showed the mainly enriching GO terms (**Figure 4B**), KEGG analysis were mainly enriched in Pathways in cancer, PI3K-Akt signaling pathway, and apoptosis (**Figure 4C**). Next, TargetScan and miRPathDB were utilized to predict the downstream targets of miR-647, nine overlapped genes were obtained from the 39 upregulated and miR-647 targets genes (**Figure 4D**). We picked up the top five upregulated genes for further studies, as NGFG, IL1R1, PAQR4, TRAF1, and SLC9A8. Then, we, respectively, transfected miR-647 inhibitor and mimics into DU145 and C4-2 cells. The five chosen genes mRNA levels were verified by qRT-PCR, and the results exhibited that PAQR4 mRNA level was remarkably increased after miR-647 knockdown and decreased after miR-647 overexpression (**Figures 4E,F**). Meanwhile, PAQR4 protein level showed the same expression change with mRNA (**Figure 4G**). Moreover, PAQR4 mRNA and protein levels were significantly upregulated in circNOLC1 overexpression PCa cells (**Figure 4H**).

NF-KappaB Is an Upstream TF of NOLC1 in PCa Cells

Previous studies showed that the expression of circRNA was tightly associated with its linear mRNA. To investigate the abnormal expression of circNOLC1 in PCa, we analyzed the bioinformation of NOLC1 in PCa from TCGA database. We found that NOLC1 was upregulated in PCa and the promoter methlation level of NOLC1 showed no difference between the primary tumor and normal group (**Figures 5A,B**). We then predicted the potential TFs of NOLC1 by *Consite*, and found that NF-kappaB scores ranked the most (**Figure 5C**). NF-kappaB was obviously correlated with NOLC1 expression (**Figure 5D**). Moreover, we confirmed the direct binding between NF-kappaB and NOLC1 promoter sites via CHIP assay (**Figure 5E**). NOLC1 expression levels were notably decreased due to the reduction of NF-kappaB, while circNOLC1 exhibited the same trend (**Figure 5F**). These results revealed that NF-kappaB could regulate the expression of NOLC1, thus leading to a downregulation of circNOLC1.

CircNOLC1 Promotes PCa Tumor Growth *in vivo*

To investigate the functions of circNOLC1 *in vivo*, DU145 cells transfected with vector and circNOLC1 were subcutaneously injected in nude mice. Tumor volumes were measured 5 days followed injection. The mice were euthanized 4 weeks after injection, the subcutaneous tumor tissues were separated, and the weight and volume of isolated tumors were measured. As the results showed, overexpression of circNOLC1 remarkably increased tumors growth *in vivo* (**Figures 6A–C**). The histopathological features of the isolated tumor tissues were revealed by H&E staining (**Figure 6D**). Besides, the expression of Ki-67 antigen in circNOLC1-overexpression xenografts tumors was significantly increased, which was detected

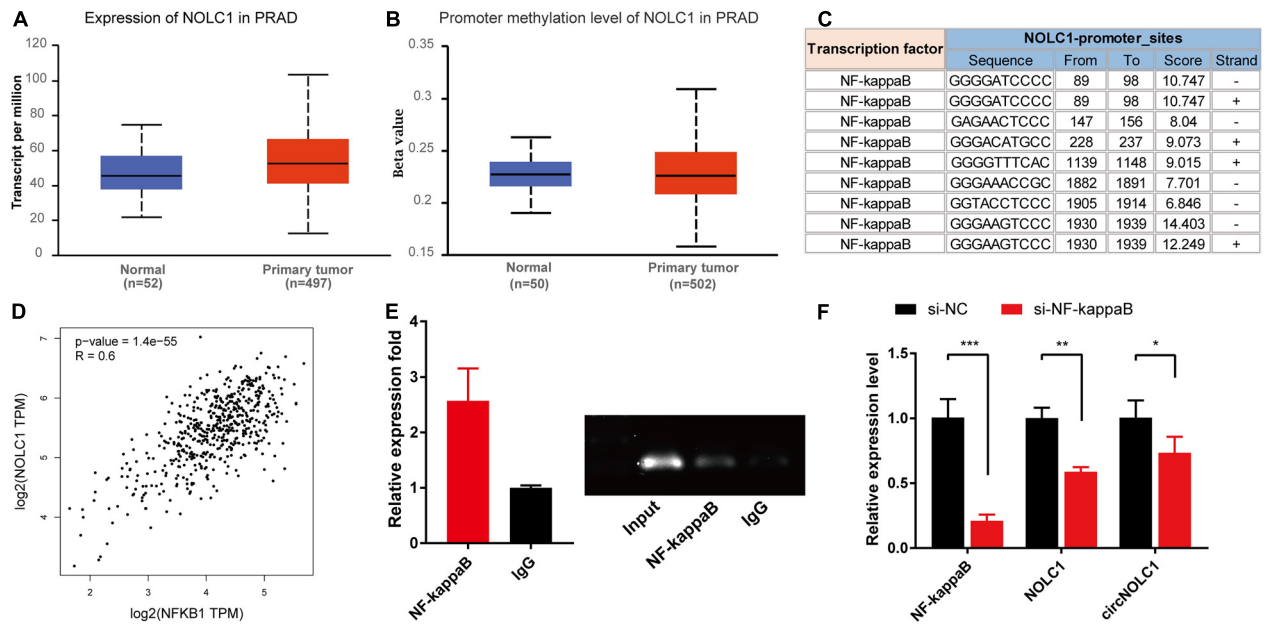

Transcription factor	NOLC1-promoter_sites				
	Sequence	From	To	Score	Strand
NF-kappaB	GGGGATCCCC	89	98	10.747	-
NF-kappaB	GGGGATCCCC	89	98	10.747	+
NF-kappaB	GAGAACTCCC	147	156	8.04	-
NF-kappaB	GGGACATGCC	228	237	9.073	+
NF-kappaB	GGGGTTTCAC	1139	1148	9.015	+
NF-kappaB	GGGAAACCGC	1882	1891	7.701	-
NF-kappaB	GGTACCTCCC	1905	1914	6.846	-
NF-kappaB	GGGAAGTCCC	1930	1939	14.403	-
NF-kappaB	GGGAAGTCCC	1930	1939	12.249	+

FIGURE 5 | NF-kappaB is an upstream transcription factor of NOLC1 in PCa cells. **(A,B)** The expression and promoter methylation level of NOLC1 in PCa via TCGA database. **(C)** Potential binding sites between NF-kappaB and NOLC1 promoter sites was predicted by CONSITE. **(D)** The relationship between NF-kappaB and NOLC1 expression levels in TCGA, analyzed by GEPIA. **(E)** ChIP-PCR validated the direct binding site of NF-kappaB to the NOLC1 promoter. **(F)** NF-kappaB, NOLC1, and circNOLC1 mRNA levels after NF-kappaB knockdown in DU145 cells, measured by RT-qPCR. $^{*}p < 0.05$, $^{**}p < 0.01$, $^{***}p < 0.001$.

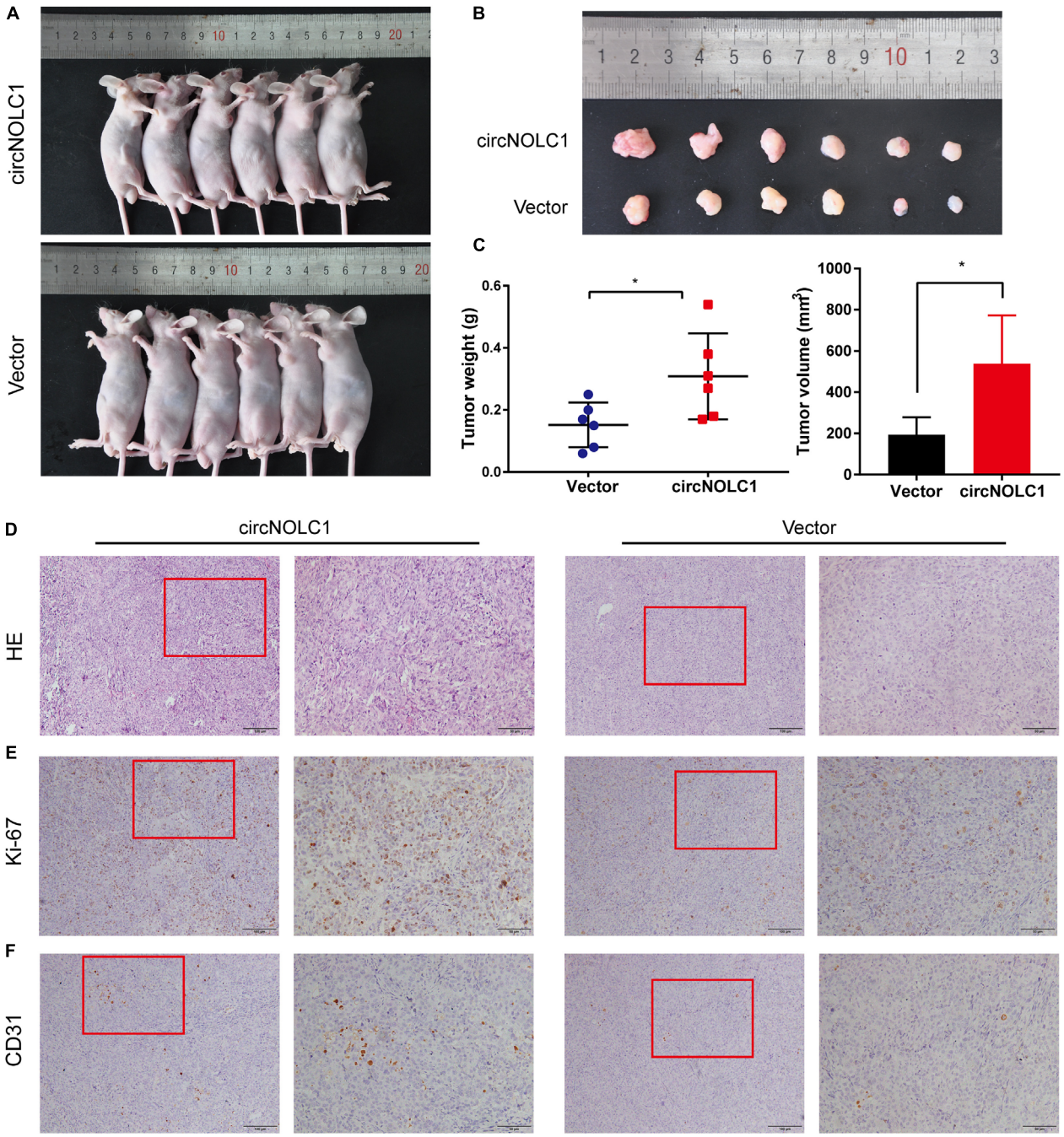

FIGURE 6 | CircNOLC1 promotes the growth of PCa cells *in vivo*. **(A,B)** Images of subcutaneous xenograft tumors derived from DU145 cells transfected with vector and circNOLC1. **(C)** Tumor weights and volume of DU145 cells were shown. **(D)** H&E staining of xenograft tumors. **(E,F)** Ki-67 and CD31 expression in xenograft tumors were detected by IHC. *$p < 0.05$.

by IHC (**Figure 6E**). Moreover, IHC results of the tumor tissues also revealed that CD31 expression was higher in circNOLC1-overexpression tumor compared to the vector, which indicated that circNOLC1 promoted tumor angiogenesis *in vivo* (**Figure 6F**). These results demonstrated that circNOLC1 overexpression drove PCa tumor growth *in vivo*.

DISCUSSION

Recent studies have shown non-coding RNAs play a growing role in PCa (Martens-Uzunova et al., 2014; Hua et al., 2019). CircRNAs, a novel non-coding circular RNAs, were once considered as junks of the transcription product. Due to the

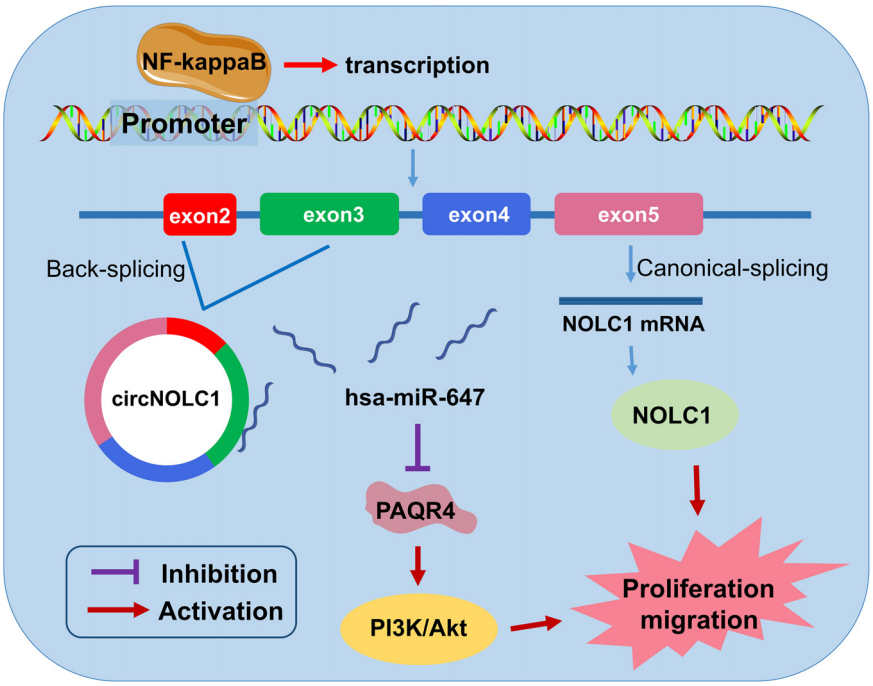

FIGURE 7 | The biological function and mechanism of circNOLC1 in PCa. Schematic diagram exhibiting the biological function and mechanism of circNOLC1 in PCa.

TABLE 1 | Expression of circNOLC1 in normal prostate tissues and prostate cancer tissues (n = 79).

	Group	*N*	CircNOLC1		χ^2	*p*-values
			Low	High		
Type	Normal	16	16	0	46.039	< 0.001
	Adenocarcinoma	79	12	67		
Age	≤ 69	41	6	35	0.036	0.849
	> 69	38	5	33		
Clinical stage	I–II	35	2	33	1.059	0.303
	III–IV	22	3	19		
Primary tumor	T1–T2	35	2	33	1.059	0.303
	T3–T4	22	3	19		
Gleason score	≤ 6	13	2	11	0.0004	> 0.9999
	≥ 7	66	10	56		

CircNOLC1 expression was determined by FISH; p-value is from χ^2-test. A remarkably increasing frequency of positive expression of circNOLC1 was detected in prostate cancer specimens compared to normal prostate tissues ($P < 0.001$, χ^2-test).

development of NGS, numerous circRNAs were explored and participated in the biological functions of tumor development, especially in PCa (Chen et al., 2019b; Yang et al., 2019). For instance, circMBOAT2 sponged miR-1271-5p to promote PCa progression (Shi et al., 2020); circSMAD2 restrained miR-9 to govern PCa migration (Han et al., 2019); circFMN2 accelerated PCa tumorigenesis via a miR-1238/LHX2 axis (Shan et al., 2020). Therefore, it is of great clinical value to identify potential early biomarkers for diagnosis and prognosis.

Here, circRNA microarrays were established in five PCa cells as DU145, PC3, LNCaP, C4-2, 22RV1, compared with immortalized normal prostatic epithelium (RWPE1). We discovered 110 upregulated circRNAs both in five PCa cells, and 22 were overlapped overexpressing in PCa tissues. Among them, top five upregulated circRNAs were chosen for further validation, and circNOLC1 was significantly elevated in PCa cells and tissues. Meanwhile, circNOLC1 exhibited stronger stability than its linear mRNA. Through *in vivo* and *in vitro* experiments, circNOLC1 was confirmed to induce cell proliferation and migration, which indicated that it may act as an oncogene in PCa.

Nucleolar and coiled-body phosphoprotein 1 (NOLC1), the host gene of circNOLC1, was firstly discovered as a nuclear localization signal binding protein, which functions as a chaperone that shuttles between the nucleolus and cytoplasm

(Meier and Blobel, 1990, 1992). Previous researches have illustrated that NOLC1 is overexpressed in nasopharyngeal carcinomas and regulate tumorigenesis by working with TP53 (Hwang et al., 2009). Besides, NOLC1 exhibited a low expression in hepatocellular carcinoma tissues and overexpression of NOLC1 inhibited hepatocellular carcinoma cells proliferation (Duan et al., 2013; Yuan et al., 2017). Interestingly, a recent study of mass spectrometry-based proteomics have revealed that NOLC1 is significantly increased in PCa samples and cell lines (Kwon et al., 2020). Our studies demonstrated that NOLC1 could promote PCa cells proliferation and migration, however, the detailed mechanisms of its oncogenic roles still needed to be fully investigated.

Previous studies indicated that circRNAs exert their functions by various biological processes, such as miRNA sponges, protein-binding, and transcriptional and translational regulation (Kristensen et al., 2019). The ceRNA mechanism suggested that circRNAs competitively bind to miRNA to relieve the suppression on miRNA targeting genes (Zhong et al., 2018). Deng et al. (2020) indicated that circRHOBTB3 suppress gastric cancer growth by sponging miR-654-3p; Li et al. (2018) revealed that circITGA7 act as a ceRNA of miR-370-3p to inhibit RAS pathway, thus restraining CRC development. Here, our results indicated that circNOLC1 were co-localized mainly in the cytoplasm of PCa cells which implied that it may act as a ceRNA. Thus, we screened and validated the interaction between circNOLC1 and miRNAs by circRNA pulldown and dual-luciferase reporter assay, results demonstrated that circNOLC1 function as a sponge of miR-647. Meanwhile, miR-647 was identified as a tumor inhibitor in glioma and gastric cancer (Ye et al., 2017; Qin et al., 2020). Whereas, its role in PCa remains unclear. We identified that miR-647 act as a tumor inhibitor in PCa. Through the overlap of miR-647 target prediction and RNA-seq in PC-3 cells with overexpression of circNOLC1, we acquired nine potential miR-647 target genes. Then, top five candidate target mRNAs were validated the *via* knockdown and overexpression of miR-647, and PAQR4 was confirmed to be the most likely downstream target gene. Further immunoblot validated that PAQR4 was negatively regulated by miR-647. These findings supported that circNOLC1 sponges with miR-647 promoted PCa progression *via* upregulating PAQR4 expression.

Progestin and adipoQ receptor family member 4 (PAQR4) was reported to be high expression in PCa cells and tissues, and significantly improve PCa malignant phenotype by activating PI3K/Akt pathway (Ye et al., 2020). Besides, Zhang et al. (2018) demonstrated that PAQR4 exert its oncogenic role in breast cancer through inhibiting CDK4 degradation. Moreover, PAQR4 promoted cell growth, metastasis, and chemoresistance in non-small-cell lung cancer (Wu and Liu, 2019; Xu et al., 2020). Combing to our KEGG results of RNA-seq in circNOLC1 overexpression, we assumed that circNOLC1 activates PI3K/Akt pathway in PCa *via* a miR-647/PAQR4 axis.

The mechanism of circRNAs biogenesis is a remarkably complicated process (Ma et al., 2020). Previous studies indicated that the reverse complementary sequences, like Alu sequences, may facilitate back-splicing by closing up the flanking introns together. Besides, m6A-enriched sites were easier to generate back-splicing as reported (Tang et al., 2020). Therefore, further experiments are needed to investigate the biogenesis of circRNAs. Here, we found that NOLC1 is also upregulated in PCa tissues using TCGA database, which is validated by a previous research (Kwon et al., 2020). We then illustrated that NF-kappaB could positively regulate linear NOLC1 mRNA and circNOLC1 expression in PCa. Previous study also exhibited that NOLC1 could be positively regulated by NF-kappaB and CREB (Gao et al., 2011). Through these results, we demonstrated that NF-kappaB could also regulate the expression of circRNAs, which gives a new insight in circRNAs biogenesis.

CONCLUSION

In summary, we discovered a novel circRNA (circNOLC1) remarkably upregulated in PCa cells and tissues. Our results indicated that circNOLC1 participate in the malignant progression in PCa, mainly by sponging miR-647 to upregulate PAQR4 expression, thus activating the PI3K/Akt pathway. Also, NOLC1 and circNOLC1 can be regulated by NF-kappaB via binding to NOLC1 promoter sites. Our studies suggested that circNOLC1/PAQR4 axis could serve as a novel biomarker and therapeutic target for PCa (**Figure 7**).

DATA AVAILABILITY STATEMENT

The raw data supporting the conclusions of this article will be made available by the authors, without undue reservation.

ETHICS STATEMENT

The studies involving human participants were reviewed and approved by the ethics committee of Zhujiang Hospital, Southern Medical University. The patients/participants provided their written informed consent to participate in this study. The animal study was reviewed and approved by the ethics committee of Zhujiang Hospital, Southern Medical University. Written informed consent was obtained from the individual(s) for the publication of any potentially identifiable images or data included in this article.

AUTHOR CONTRIBUTIONS

XM, DL, and CL conceived and designed the study. WC and SC carried out the experiments. TY, KW, and LZ collected and analyzed the clinical data. JL and XZ analyzed and interpreted the data. WC and DL wrote the manuscript. XM and DL executed the

funding acquisition. All authors have reviewed and approved the final version of the manuscript.

FUNDING

This work was supported by the National Natural Science Foundation of China (No. 81773277), the Science and Technology Program of Guangzhou (No. 201803010014), the China Postdoctoral Science Foundation funded project (No. 2019M662865), the Guangdong Basic and Applied Basic Research Foundation (No. 2019A1515110033), Distinguished Young Talents in Higher Education Foundation of Guangdong Province (No. 2019KQNCX115), and achievement cultivation and clinical transformation application cultivation projects of The First Affiliated Hospital of Guangzhou Medical University (No. ZH201908).

SUPPLEMENTARY MATERIAL

The Supplementary Material for this article can be found online at: https://www.frontiersin.org/articles/10.3389/fcell.2020.624764/full#supplementary-material

Supplementary Figure 1 | Screening of circRNAs in PCa cells. **(A)** Heatmap of all differentially expressed circRNAs between PC3, DU145, C4-2, 22RV1, LNCaP, and RWPE1 cells. Red and green strips represent high and low expression, respectively. **(B–D)** Expression of hsa_circ_0018998, hsa_circ_0000735, hsa_circ_0050649, and hsa_circ_0002722 in five PCa cells and normal prostate cells.

Supplementary Figure 2 | Knockdown of NOLC1 inhibits PCa cells proliferation and migration. **(A,B)** NOLC1 mRNA expression after knockdown circNOLC1 in DU145, C4-2, PC3. **(C)** RT-qPCR was performed to confirm the silencing efficiency of three siRNAs targeting NOLC1 in DU145 cells. **(D)** CCK8 was applied to exam the proliferation of DU145 cells after silencing the NOLC1. **(E)** Transwell migration assay was conducted to assess the cell migration ability in NOLC1-silenced DU145 cells.

REFERENCES

Berger, M. F., Lawrence, M. S., Demichelis, F., Drier, Y., Cibulskis, K., Sivachenko, A. Y., et al. (2011). The genomic complexity of primary human prostate cancer. *Nature* 470, 214–220. doi: 10.1038/nature09744

Chen, L. J., Nan, A., Zhang, N., Jia, Y. Y., Li, X., Ling, Y. H., et al. (2019a). Circular RNA 100146 functions as an oncogene through direct binding to miR-361-3p and miR-615-5p in non-small cell lung cancer. *Mol. Cancer* 18:13. doi: 10.1186/s12943-019-0943-0

Chen, L. L. (2020). The expanding regulatory mechanisms and cellular functions of circular RNAs. *Nat Rev Mol Cell Biol* 21, 475–490. doi: 10.1038/s41580-020-0243-y

Chen, L.-L., and Yang, L. (2015). Regulation of circRNA biogenesis. *RNA Biol.* 12, 381–388. doi: 10.1080/15476286.2015.1020271

Chen, S., Huang, V., Xu, X., Livingstone, J., Soares, F., Jeon, J., et al. (2019b). Widespread and functional RNA circularization in localized prostate cancer. *Cell* 176:e822. doi: 10.1016/j.cell.2019.01.025

Deng, G., Mou, T., He, J., Chen, D., Lv, D., Liu, H., et al. (2020). Circular RNA circRHOBTB3 acts as a sponge for miR-654-3p inhibiting gastric cancer growth. *J. Exp. Clin. Cancer Res.* 39:1. doi: 10.1186/s13046-019-1487-2

Duan, X., Zhang, J., Liu, S., Zhang, M., Wang, Q., and Cheng, J. (2013). Methylation of nucleolar and coiled-body phosphoprotein 1 is associated with the mechanism of tumorigenesis in hepatocellular carcinoma. *Oncol. Rep.* 30, 2220–2228. doi: 10.3892/or.2013.2676

Gao, X., Wang, Q., Li, W., Yang, B., Song, H., Ju, W., et al. (2011). Identification of nucleolar and coiled-body phosphoprotein 1 (NOLC1) minimal promoter regulated by NF-κB and CREB. *BMB Rep.* 44, 70–75. doi: 10.5483/BMBRep.2011.44.1.70

Han, N., Ding, L., Wei, X., Fan, L., and Yu, L. (2019). circSMAD2 governs migration and epithelial-mesenchymal transition by inhibiting microRNA-9. *J. Cell Biochem.* 2019:29638. doi: 10.1002/jcb.29638

Hansen, T. B., Jensen, T. I., Clausen, B. H., Bramsen, J. B., Finsen, B., Damgaard, C. K., et al. (2013). Natural RNA circles function as efficient microRNA sponges. *Nature* 495, 384–388. doi: 10.1038/nature11993

Hansen, T. B., Wiklund, E. D., Bramsen, J. B., Villadsen, S. B., Statham, A. L., Clark, S. J., et al. (2011). miRNA-dependent gene silencing involving Ago2-mediated cleavage of a circular antisense RNA. *EMBO J.* 30, 4414–4422. doi: 10.1038/emboj.2011.359

Hua, J. T., Chen, S., and He, H. H. (2019). Landscape of noncoding RNA in prostate cancer. *Trends Genet.* 35, 840–851. doi: 10.1016/j.tig.2019.08.004

Hwang, Y.-C., Lu, T.-Y., Huang, D.-Y., Kuo, Y.-S., Kao, C.-F., Yeh, N.-H., et al. (2009). NOLC1, an enhancer of nasopharyngeal carcinoma progression, is essential for TP53 to regulate MDM2 expression. *Am. J. Pathol.* 175, 342–354. doi: 10.2353/ajpath.2009.080931

Kristensen, L. S., Andersen, M. S., Stagsted, L. V. W., Ebbesen, K. K., Hansen, T. B., and Kjems, J. (2019). The biogenesis, biology and characterization of circular RNAs. *Nat. Rev. Genet.* 20, 675–691. doi: 10.1038/s41576-019-0158-7

Kwon, O. K., Ha, Y.-S., Na, A.-Y., Chun, S. Y., Kwon, T. G., Lee, J. N., et al. (2020). Identification of novel prognosis and prediction markers in advanced prostate cancer tissues based on quantitative proteomics. *Cancer Genom. Proteomics* 17, 195–208. doi: 10.21873/cgp.20180

Li, X., Wang, J., Zhang, C., Lin, C., Zhang, J., Zhang, W., et al. (2018). Circular RNA circITGA7 inhibits colorectal cancer growth and metastasis by modulating the Ras pathway and upregulating transcription of its host gene ITGA7. *J. Pathol.* 246, 166–179. doi: 10.1002/path.5125

Liu, X., Shen, S., Zhu, L., Su, R., Zheng, J., Ruan, X., et al. (2020). SRSF10 inhibits biogenesis of circ-ATXN1 to regulate glioma angiogenesis via miR-526b-3p/MMP2 pathway. *J. Exp. Clin. Cancer Res.* 39:121. doi: 10.1186/s13046-020-01625-8

Luo, J., Li, Y., Zheng, W., Xie, N., Shi, Y., Long, Z., et al. (2019). Characterization of a Prostate- and prostate cancer-specific circular RNA encoded by the androgen receptor gene. *Mol. Ther. Nucleic Acids* 18, 916–926. doi: 10.1016/j.omtn.2019.10.015

Ma, S., Kong, S., Wang, F., and Ju, S. (2020). CircRNAs: biogenesis, functions, and role in drug-resistant Tumours. *Mol. Cancer* 19:119. doi: 10.1186/s12943-020-01231-4

Martens-Uzunova, E. S., Böttcher, R., Croce, C. M., Jenster, G., Visakorpi, T., and Calin, G. A. (2014). Long noncoding RNA in prostate, bladder, and kidney cancer. *Eur. Urol.* 65, 1140–1151. doi: 10.1016/j.eururo.2013.12.003

Meier, U. T., and Blobel, G. (1990). A nuclear localization signal binding protein in the nucleolus. *J. Cell Biol.* 111(6 Pt 1), 2235–2245. doi: 10.1083/jcb.111.6.2235

Meier, U. T., and Blobel, G. (1992). Nopp140 shuttles on tracks between nucleolus and cytoplasm. *Cell* 70, 127–138. doi: 10.1016/0092-8674(92)90539-o

Qin, K., Tian, G., Chen, G., Zhou, D., and Tang, K. (2020). miR-647 inhibits glioma cell proliferation, colony formation and invasion by regulating HOXA9. *J. Gene. Med.* 22:e3153. doi: 10.1002/jgm.3153

Shan, G., Shao, B., Liu, Q., Zeng, Y., Fu, C., Chen, A., et al. (2020a). circFMN2 Sponges miR-1238 to promote the expression of LIM-homeobox gene 2 in prostate cancer cells. *Mol. Ther. Nucleic Acids* 21, 133–146. doi: 10.1016/j.omtn.2020.05.008

Shi, J., Liu, C., Chen, C., Guo, K., Tang, Z., Luo, Y., et al. (2020). Circular RNA circMBOAT2 promotes prostate cancer progression via a miR-1271-5p/mTOR axis. *Aging* 12, 13255–13280. doi: 10.18632/aging.103432

Siegel, R. L., Miller, K. D., and Jemal, A. (2020). Cancer statistics, 2020. *CA. Cancer J. Clin.* 70, 7–30. doi: 10.3322/caac.21590

Tang, C., Xie, Y., Yu, T., Liu, N., Wang, Z., Woolsey, R. J., et al. (2020). m(6)A-dependent biogenesis of circular RNAs in male germ cells. *Cell Res.* 30, 211–228. doi: 10.1038/s41422-020-0279-8

Vo, J. N., Cieslik, M., Zhang, Y., Shukla, S., Xiao, L., Zhang, Y., et al. (2019). The landscape of circular RNA in cancer. *Cell* 176, 869–881. doi: 10.1016/j.cell.2018.12.021

Wang, G., Zhao, D., Spring, D. J., and DePinho, R. A. (2018). Genetics and biology of prostate cancer. *Genes Dev.* 32, 1105–1140. doi: 10.1101/gad.315739.118

Wu, B., and Liu, R. (2019). PAQR4 promotes cell proliferation and metastasis through the CDK4-pRB-E2F1 pathway in non-small-cell lung cancer. *Onco. Targets Ther.* 12, 3625–3633. doi: 10.2147/ott.S181432

Xu, P., Jiang, L., Yang, Y., Wu, M., Liu, B., Shi, Y., et al. (2020). PAQR4 promotes chemoresistance in non-small cell lung cancer through inhibiting Nrf2 protein degradation. *Theranostics* 10, 3767–3778. doi: 10.7150/thno.43142

Yang, Z., Qu, C. B., Zhang, Y., Zhang, W. F., Wang, D. D., Gao, C. C., et al. (2019). Dysregulation of p53-RBM25-mediated circAMOTL1L biogenesis contributes to prostate cancer progression through the circAMOTL1L-miR-193a-5p-Pcdha pathway. *Oncogene* 38, 2516–2532. doi: 10.1038/s41388-018-0602-8

Ye, G., Huang, K., Yu, J., Zhao, L., Zhu, X., Yang, Q., et al. (2017). MicroRNA-647 Targets SRF-MYH9 axis to suppress invasion and metastasis of gastric cancer. *Theranostics* 7, 3338–3353. doi: 10.7150/thno.20512

Ye, J., Gao, M., Guo, X., Zhang, H., and Jiang, F. (2020). Breviscapine suppresses the growth and metastasis of prostate cancer through regulating PAQR4-mediated PI3K/Akt pathway. *Biomed. Pharmacothr.* 127:110223. doi: 10.1016/j.biopha.2020.110223

Yuan, F., Zhang, Y., Ma, L., Cheng, Q., Li, G., and Tong, T. (2017). Enhanced NOLC1 promotes cell senescence and represses hepatocellular carcinoma cell proliferation by disturbing the organization of nucleolus. *Aging cell* 16, 726–737. doi: 10.1111/acel.12602

Zhang, H., Han, R., Ling, Z. Q., Zhang, F., Hou, Y., You, X., et al. (2018). PAQR4 has a tumorigenic effect in human breast cancers in association with reduced CDK4 degradation. *Carcinogenesis* 39, 439–446. doi: 10.1093/carcin/bgx143

Zhang, S., Zhang, X., Chen, G., Zheng, X., Zhu, X., and Shan, L. (2020). Hsa_circ_0007494 suppresses prostate cancer progression via miR-616/PTEN axis. *Exper. Cell Res.* 395:112233. doi: 10.1016/j.yexcr.2020.112233

Zheng, Q. P., Bao, C. Y., Guo, W. J., Li, S. Y., Chen, J., Chen, B., et al. (2016). Circular RNA profiling reveals an abundant circHIPK3 that regulates cell growth by sponging multiple miRNAs. *Nat. Commun.* 7:11215.

Zhong, Y., Du, Y., Yang, X., Mo, Y., Fan, C., Xiong, F., et al. (2018). Circular RNAs function as ceRNAs to regulate and control human cancer progression. *Mol. Cancer* 17:79. doi: 10.1186/s12943-018-0827-8

Conflict of Interest: The authors declare that the research was conducted in the absence of any commercial or financial relationships that could be construed as a potential conflict of interest.

frontiers in Oncology

ORIGINAL RESEARCH
published: 29 January 2021
doi: 10.3389/fonc.2020.583533

Searching for a Putative Mechanism of RIZ2 Tumor-Promoting Function in Cancer Models

Monica Rienzo[1†], Anna Sorrentino[2†], Erika Di Zazzo[2,3†], Marzia Di Donato[2], Vincenzo Carafa[2], Maria Michela Marino[2], Caterina De Rosa[2], Patrizia Gazzerro[4], Gabriella Castoria[2], Lucia Altucci[2], Amelia Casamassimi[2] and Ciro Abbondanza[2*]*

[1] Department of Environmental, Biological, and Pharmaceutical Sciences and Technologies, University of Campania "Luigi Vanvitelli", Caserta, Italy, [2] Department of Precision Medicine, University of Campania "Luigi Vanvitelli", Naples, Italy, [3] Department of Medicine and Health Sciences "V. Tiberio", University of Molise, Campobasso, Italy, [4] Department of Pharmacy, University of Salerno, Fisciano, Italy

OPEN ACCESS

Edited by:
Andrew Davis,
Washington University in St. Louis, United States

Reviewed by:
Federico Pio Fabrizio,
IRCCS Casa Sollievo della Sofferenza Ospedale di San Pio da Pietrelcina, Italy
Lorenzo Gerratana,
University of Udine, Italy

***Correspondence:**
Ciro Abbondanza
ciro.abbondanza@unicampania.it
Amelia Casamassimi
amelia.casamassimi@unicampania.it

[†]These authors have contributed equally to this work

Specialty section:
This article was submitted to Molecular and Cellular Oncology, a section of the journal Frontiers in Oncology

Received: 15 July 2020
Accepted: 08 December 2020
Published: 29 January 2021

Citation:
Rienzo M, Sorrentino A, Di Zazzo E, Di Donato M, Carafa V, Marino MM, De Rosa C, Gazzerro P, Castoria G, Altucci L, Casamassimi A and Abbondanza C (2021) Searching for a Putative Mechanism of RIZ2 Tumor-Promoting Function in Cancer Models. Front. Oncol. 10:583533. doi: 10.3389/fonc.2020.583533

Positive Regulatory Domain (PRDM) gene family members commonly express two main molecular variants, the PR-*plus* isoform usually acting as tumor suppressor and the PR-*minus* one functioning as oncogene. Accordingly, PRDM2/RIZ encodes for RIZ1 (PR-*plus*) and RIZ2 (PR-*minus*). In human cancers, genetic or epigenetic modifications induce RIZ1 silencing with an expression level imbalance in favor of RIZ2 that could be relevant for tumorigenesis. Additionally, in estrogen target cells and tissues, estradiol increases RIZ2 expression level with concurrent increase of cell proliferation and survival. Several attempts to study RIZ2 function in HeLa or MCF-7 cells by its over-expression were unsuccessful. Thus, we over-expressed RIZ2 in HEK-293 cells, which are both RIZ1 and RIZ2 positive but unresponsive to estrogens. The forced RIZ2 expression increased cell viability and growth, prompted the G2-to-M phase transition and organoids formation. Accordingly, microarray analysis revealed that RIZ2 regulates several genes involved in mitosis. Consistently, RIZ silencing in both estrogen-responsive MCF-7 and -unresponsive MDA-MB-231 cells induced a reduction of cell proliferation and an increase of apoptosis rate. Our findings add novel insights on the putative RIZ2 tumor-promoting functions, although additional attempts are warranted to depict the underlying molecular mechanism.

Keywords: *PRDM2*, RIZ2 overexpression, microarray, cell proliferation, apoptosis, 3D models

INTRODUCTION

PR/SET Domain 2 (PRDM2) or Retinoblastoma Interacting Zinc finger (RIZ) protein is a member of the Positive Regulatory Domain (PRDM) gene family, which encodes for 19 different transcription factors in humans (1–3). All PRDM family members share an evolutionary conserved N-terminal domain, known as PR domain (PRDI-BF1-RIZ1 homologous), structurally and functionally similar to the SET domain (Su(var)3-9, Enhancer-of-zeste and Trithorax) (4–7). PR domain is followed by a variable number of Zinc finger domains towards the C-terminus, potentially mediating sequence-specific nucleic acid binding, protein-protein interactions or

functioning in nuclear import (4–7). PRDMs are involved in epigenetic regulation of gene expression by acting as histone methyltransferases (HMTs) or by recruiting chromatin modifying enzymes (3, 5). Importantly, PRDM proteins function by tethering transcription factors to target gene promoters or by recognition of specific DNA consensus sequences *via* the Zinc-finger domains (6, 7). Of note, PRDM proteins contribute to many developmental processes, driving cell proliferation, differentiation, and maturation events by specifying cell fate choice or maintaining cell specialization through transduction of several cell signals (3, 4, 6).

Common feature of *PRDM* genes is the expression of two main molecular variants, generated by alternative splicing or alternative use of different promoters and differing for the presence or absence of the PR domain (3, 6, 7). The PRDM variants show an opposite, bivalent "yin-yang" behavior with the PR-*plus* isoform usually acting as a tumor suppressor, and the PR-*minus* one functioning as an oncogene (3, 7). Of note, the expression level imbalance between the two isoforms in favor of the PR-*minus* is often observed in many human malignancies being attributed to inactivating mutations or silencing of the complete form and/or increased expression of the PR-*minus* form (3, 6–8).

Specifically, *PRDM2* encodes for two main protein forms, known as RIZ1 or PRDM2a, containing the PR domain, and RIZ2 or PRDM2b lacking this domain (**Supplementary Figure S1**). RIZ2 transcript is generated by an internal TATA-less promoter localized at the 5' boundary of *PRDM2* coding exon 5 (3, 9). Both RIZ1 and RIZ2 are widely expressed in normal tissues in a similar ratio. However, the imbalance in their expression level could represent an important cause of malignancies (10, 11). Genetic evidences from tumor samples and cancer cell lines indicated that RIZ1 is a putative tumor suppressor gene commonly deleted (10), inactivated by point-mutations, especially those affecting its HMT activity (12–14), downregulated or silenced by DNA methylation of its promoter CpG island (13, 15–20). Altogether, these studies indicated that the PR domain through its HMT activity could play an important role in mediating RIZ1 tumor suppressor functions (14, 21). Furthermore, frameshift mutations of microsatellite repeats within the *PRDM2* coding region are frequently observed in colorectal, gastric, endometrial, and pancreatic cancers. Most of these mutations lead to a truncated protein at the C-terminal region containing the PR-binding motif, which is pivotal for RIZ1 folding, dimerization/oligomerization, and its PR domain-specific functions (12, 13, 22, 23). In addition, a microsatellite locus in *PRDM2* gene is frequently mutated in colorectal cancer implying its role as a driver mutation (24, 25). Of note, frameshift mutations in the *PRDM2* A (9) track have been observed in melanomas and nevi (26), as well as in leukemia cells (27).

PRDM2a/RIZ1 is also a component of the double-strand break (DSB) repair complex, which is essential for ensuring accurate repair outcome and genomic integrity maintenance (3, 8). Basically, RIZ1 cooperates with the macrohistone variant mH2A1.2 to direct the choice between the antagonistic DSB repair mediators, BRCA1 and 53BP1. The mH2A1/RIZ1 module enables a dynamic switch in chromatin conformation through H3K9me2 mediated by RIZ1. Then, a homologous recombination and repair through BRCA1 follows (28). Otherwise, the possible role of RIZ2 in this context has not been investigated so far.

Several studies have investigated the RIZ1 tumor suppressor functions. RIZ1 exerts growth inhibition and anti-cancer activities (29–33) and its ectopic expression induces cell growth arrest and apoptosis in a variety of cancer cells (15, 34, 35). In addition, RIZ1 mediates the estradiol proliferative effect in MCF-7 cell line, as a specific effector of estrogen action downstream of the hormone-receptor interaction. RIZ1, through its HMT activity, maintains gene-specific gatekeeper functions that prevent unliganded ER from binding to its target gene promoters and causing constitutive gene activation in the absence of stimulating signals. Upon estrogen-ER bound, RIZ1 become a coactivator able to induce the optimal estrogen response in female reproductive tissues (36, 37). Besides, RIZ1 silencing prompts cell proliferation (38, 39). Moreover, RIZ1 is expressed in normal prostate epithelial cells and is downregulated in cancer, with a switch of its sub-cellular localization from the nucleus to the cytoplasm upon cancer grade progression (40).

Likely, as a result of a positive selection related to RIZ2 promoting effects on proliferation, RIZ2 is always expressed in cancer cells (11, 15).

We have previously suggested that the Zinc-finger domains could be responsible for the oncogenic activity of RIZ2. MCF-7 cells expressing an Enhanced Green Fluorescent Protein (EGFP) fusion protein containing three of the eight putative Zinc-finger motifs common to both RIZ1 and RIZ2 showed a higher growth rate, being less sensitive to anti-estrogens growth inhibitory effect and expressing higher levels of cyclins D1 and A (41). We also demonstrated that RIZ2 is an ERα target gene, since an estrogen-responsive element (ERE) within the RIZ promoter 2 is regulated in a ligand-specific manner by ERα. Upon estradiol treatment a RIZ2 expression level increase was observed at both RNA and protein expression levels. The pattern of ERα binding, histone H4 acetylation, and histone H3 cyclical methylation of lysine 9 was comparable to other estrogen-regulated promoters. Association of topoisomerase IIβ with the RIZ promoter 2 confirmed the transcriptional activation induced by estrogens. This ligand-specific regulation induced the preferential transcription of exon 9a and a subsequent reduction in the amount of transcripts with exons 9b and 10, which determine different polyadenylation sites (11, 42).

The presence of transcripts with different UTRs suggests that a possible post-transcriptional control through miRNAs may occur. For instance, estradiol could modulate RIZ2/RIZ1 ratio also through various miRNAs that control estradiol response in breast cancer cells (43); interestingly, some of these target consensus sequences could be recognized in the exon 9 of PRDM2 gene by bioinformatics analysis (http://mirdb.org/cgi-bin/search.cgi). However, to date a mechanism involving PRDM2 regulation by these miRNAs can only be hypothesized.

Furthermore, microarray analysis revealed PRDM2 as a target of the miR-17-92 cluster in human cholangiocarcinoma cells (44).

Despite several findings suggest that RIZ gene products are related to proliferation and apoptosis control with an opposite function, the molecular mechanisms and the involved cellular pathways through which RIZ2 displays oncogenic functions stay quite unclear.

Thus, the present study points to elucidate the putative mechanisms of the tumor-promoting function of RIZ2 isoform, through the investigation of its effects on regulated genes and enriched pathways by microarray analysis. Moreover, the biological consequences of RIZ2 overexpression in HEK-293 cells have been explored through some functional studies.

MATERIALS AND METHODS

Cell Culture and Transfection

HEK-293, MCF-7, and MDA-MB-231 cells were grown and propagated as described elsewhere (11, 45).

MCF-7 and MDA-MB-231 cells were made quiescent as described (46), using phenol red-free Dulbecco's modified Eagle Medium (DMEM) supplemented with 3% charcoal-dextran-stripped fetal bovine serum (FCS), 1 nM cortisol, and 10 ng/ml insulin.

HEK-293 were maintained at 37°C with 5% CO_2 in humidified atmosphere in DMEM high glucose supplemented with 10% FCS, 1% Non-Essential Amino Acid (NEAA), and antibiotics (100 U/ml penicillin, 100 mg/ml streptomycin).

Cells were transfected with siRNAs and plasmid DNAs using Lipofectamine™ 2000 Reagent in OptiMem I Reduced Serum Medium (Life Technologies, Carlsbad, CA, USA) for 6 h, following the manufacturer's instructions. After removal of reaction mixtures, MCF-7 and MDA-MB-231 cells were cultured for an additional 60 h in phenol red-free DMEM with 5% charcoal-dextran-stripped fetal bovine serum, 1 nM cortisol, 10 ng/ml insulin. For HEK-293 stable clones, selection was performed by addition of 0.8 mg/ml Geneticin G418 (Sigma-Aldrich). Positive colonies were selected by manual picking. At least two clones for each transfection were selected and characterized. Transfection was also verified by fluorescent microscopy analysis.

RNA Interference (RNAi), Plasmids, and Constructs

The siRNA duplex (Dharmacon Research, Lafayette, CO, USA) designed for silencing of both RIZ gene products (siRNA-total) covered the region coding for aa 333–340 of RIZ1 protein or aa 132–139 of RIZ2 protein (sense 5'-GACUGCUCAGAGGU AACAC-3'). For each experiment, at least two concentrations of siRNA-total (35 and 50 nM) were transfected in the presence of an excess of tRNA (Ambion Inc., Austin, USA). An equal concentration of SilencerR Negative Control #1 siRNA (Ambion Inc.) was used as negative control. The efficiency of transfection was measured by labeling siRNA-total with equimolar amounts of fluorescein ULSR (Fermentas Inc., Hanover, MD, USA), according to manufacturer's instruction, and expressed as the average of the percentage of fluorescent cells in each microscope field (five fields). Data derived from experiments with transfection efficiency greater than 55%. Experiments with differences >20% in transfection efficiency among different experimental points were discarded.

The pEGFP-C1 vector was purchased from Clontech (Palo Alto, CA, USA) and was used to clone in the BamH1 site, the sequence of RIZ2 open reading frame (NM_015866.4) (41). The primers used to amplify RIZ2 coding sequence with Bam H1 site restriction were as follows: RIZ2F (forward) (5'-AAGGATCC AGAGATTCTGCAGAATGGT-3') and RIZ2R (reverse) (5'-AAGGATCCTACAGGAAGTTCCTGAAG-3'). A 4.42 kb RIZ2 fragment were recovered and ligated by T4 DNA Ligase (Promega, Madison, WI, USA). Recombinant plasmids were identified by restriction enzyme fragment analysis. In order to verify the correct orientation of the inserts and the integrity of the open reading frames, positive recombinant plasmids were directly sequenced with an ABI Prism Dye Terminator sequencing kit and analyzed on an ABI PRISM automated sequencer (Applied Biosystems) (47). The resultant plasmid expressing RIZ2, designated pEGFP_hRIZ2, was in frame with the EGFP coding sequence, with no intervening in-frame stop codons. Plasmids for transfection were prepared with Plasmid Midi Kit (Qiagen Inc, Valencia, CA, USA), according to manufacturer's instructions. The EGFP expressed in the vectors was used to measure transfection efficiency (an average >80% of HEK-293 cells were transfected). For RIZ truncated C-terminal, the forward primer (5'-AAGGATCCCTGCAGACAC CCTCCCTTT-3') was employed instead of RIZ2F, which was utilized in transient transfection experiment.

RNA Extraction, Quantitative and Semi-Quantitative Reverse Transcriptase Polymerase Chain Reaction (RT-PCR)

Total RNAs were extracted from cells using Trizol solution (Thermofisher), according to the manufacturer's instructions. RNA samples were then treated with RNase-free DNase-I (Boehringer Mannheim, Indianapolis, IN, USA). The integrity and quantity of RNAs were assessed by denaturing agarose gel electrophoresis and by spectrophotometry analysis. Then, 500 ng total RNA was reverse transcribed with SuperScript III (Thermofisher); 1 µl of the reverse-transcriptase reaction was used as a template in a PCR reaction as previously described (39). The amplification products were also analyzed by agarose gel electrophoresis. *GAPDH* was used as housekeeping control gene. Quantitative RT-PCR analysis was performed using the SYBR Green PCR Master Mix (Applied Biosystems, Foster City, CA, USA), 160 nM of each primer and about 50ng of cDNA (RNA equivalent) as template in an iCycler thermocycler (Bio-Rad Laboratories Inc., Hercules, CA, USA). PCR condition were 95°C for 4 min followed by 51 cycles of 20 s at 95°C, 45 s at 60°C, and 45 s at 70°C. RIZ1 transcript amplification was performed with the following primers: 118F (5'-CTG GAT CCA CCC GGA TTG GTG TCT GGG-3') and 438R (5'- TCG GAT CCA GGG TTG TCT TCC CCA TTG TAC C-3'). Primers 649F (5'-CTG GAT

CCT CAG CCT CAG CAC TTG AGC AG-3') and 975R (5'-TCG GAT CCT GTT TTT GGT TCC TCT AAT AAA TCT TC-3') were used for analysis of all RIZ transcripts (34, 39). All reactions were carried out at least in triplicate for every cDNA template and the melting curves were analyzed to verify the specificity of reaction. The relative gene expression was calculated using the $2^{\Delta\Delta Ct}$ method (48). *GAPDH* was used as a housekeeping gene for normalization. Differences between two experimental groups were analyzed by the Student's t-test. Differences between means were considered significant at $P < 0.05$ (47, 49).

Western Blot Assay and Densitometric Analysis

Electrophoresis and Western blot analysis were performed as described elsewhere (38) with mouse monoclonal antibodies to green fluorescent protein (GFP) from Roche (Roche, Mannheim, Germany) and mouse monoclonal antibody RZ2413 (1 mg/ml) to a synthetic peptide at residues 960–972 containing RIZ nuclear receptor box protein (41).

Western blot analysis of total cell extract of interfered MCF-7 and MDA-MB-231 were revealed with commercial polyclonal antibodies to RIZ1 protein (aa 6-22) or with commercial antibodies to human Cyclin B1, and histone H1.1 (Abcam Ltd., Cambridge, UK).

Immunofluorescence and Cytoskeleton Analysis

HEK 293-pEGFP and HEK 293-pEGFP_hRIZ2 were plated on gelatin-coated coverslips. After 24 h, cells on coverslips were fixed in 4% paraformaldehyde and permeabilized using diluted (0,2% in PBS) Triton-X100 at room temperature. Nuclei were stained with 1 µg/ml Hoechst 33258 (Sigma). Cytoskeleton analysis was performed by Texas red-labeled phalloidin (Sigma-Aldrich), as reported elsewhere (50). Fields were analyzed with a DMBL Leica fluorescence microscope equipped with HCX PL Fluotar 100 × oil objective. Representative images from three independent experiments were captured using a DC480 camera (Leica) and acquired by Application Suite (Leica) software (50).

Cell Cycle Analysis

HEK 293-pEGFP and HEK 293-pEGFP_hRIZ2 cells (2×10^5 cells/well) were seeded into six-well plates. After 24 h, cells were harvested, centrifuged at 1,200 rpm for 5 min, and resuspended in 500 µl of cell cycle buffer solution (0.1% sodium citrate, 0.1% NP-40, RNase A, and 50 mg/ml Propidium Iodide -PI in PBS 1X). The results were acquired on fluorescence-activated cell sorting- FACS Calibur (BD Biosciences). Each experiment was performed in biological triplicates and values expressed as mean ± standard deviation. Mitotic blockade was obtained through cell treatment with 100 ng/ml nocodazole for 18 h (Sigma-Aldrich Co.). Cell distribution in the G1, S, and G2/M phases of the cell cycle was calculated from the resulting DNA histogram with BD CellQuest software.

Cell cycle distribution of PI-labeled MCF-7 and MDA-MB-231 cells was obtained by FACS analyses at 40 h from transfection with reported concentrations of siRNA-total.

Clonogenic Assay

HEK 293-pEGFP and HEK 293-pEGFP_hRIZ2 cells (3×10^2) were seeded into six-well plates and cultured at 37°C for ~10 days until cells have formed sufficiently large clones (at least 50 cells). Fresh media were supplied every 3 days. Clones were counted after 30 min fixing with a mixture of 6% glutaraldehyde and 0.5% crystal violet (51). The stained colonies were photographed and the number colonies with sizes ≥1 mm were counted using the ImageJ software (National Institutes of Health, USA) and expressed as mean ± S.E.M. Each assay was performed in at least three independent experiments in triplicate.

HEK 293 Cell Viability

HEK 293-pEGFP and HEK 293-pEGFP_hRIZ2 cells (5×10^3 cells/well) were seeded into 96-well plates. Cell viability was assessed by the 3-(4,5-dimethylthiazol-2-yl)-2,5-biphenyltetrazolium bromide (MTT) assay (Sigma-Aldrich Co.) at 0, 24, 48, and 72 h, as previously described (52). Absorbance was measured at 570 nm wavelength and at 690 nm for background subtraction. To estimate cell number through absorbance of solution, the regression lines of OD570-690nm values on serial dilutions of HEK293 cells, both pEGFP_RIZ2 and control cells was generated (53).

MCF-7 and MDA-MB-231 Cell Number

MCF-7 and MDA-MB-231 cells were counted by the method of optical microscopy in the Bürker chamber. Cells interfered with two different siRNA concentrations (35 and 50 nM) were compared with untreated cells.

Miniaturized 3D Cultures in Extracellular Matrix (ECM)

Miniaturized 3D cultures in Matrigel were performed as reported (54). Briefly, cell suspension containing 3×10^4 cells was mixed with 200 µl of Matrigel Growth Factor Reduced (GFR) Basement Membrane Matrix (BD Biosciences) for each well and the embedding method was used to establish organoids (55). The mixture was seeded in 24-well plate and allowed to solidify for 45 min at 37°C, before the addition of 400 µl organoid plating medium to each well. Organoid plating medium was made using DMEM/F12 medium, containing 10% FBS, penicillin (100 U/ml), streptomycin (100 U/ml), diluted GlutaMAX 100X, 10 mM Hepes, 1M nicotinamide, 500 mM N-acetylcysteine, and 10 µM Y-27632 (Millipore, Burlington, MA, USA). After 3 days, when the organoid structure was visible, the organoid-plating medium was replaced with a similar medium without N-acetylcysteine and Y-27632. The medium was changed every 3 days. Different fields were analyzed using DMIRB Leica (Leica) microscope equipped with HCL PX Fluotar 40× and 63× objectives (Leica). At the indicated times, phase-contrast and immunofluorescence microscopy images were acquired using a DFC 450C camera (Leica). Images are representative of three independent experiments, each performed in duplicate. The relative organoid size (area) was calculated using the Application Suite Software and expressed as a fold increase over the organoid area calculated at 3th day.

Human Gene Expression Microarrays

Agilent Technologies SurePrint Gene Expression Microarrays (Agilent Techologies, Santa Clara, CA, USA) were used to profile gene expression of RNA samples. Samples were processed according to Agilent Two-color Microarray Based Gene Expression Analysis (Low Input Quick Amp Labeling Kit protocol) by Agilent Spike-In Kit, according to the manufacturer's instructions. The Agilent Two-Color Microarray-based Gene Expression Analysis uses Cyanine 3- and Cyanine 5-labeled targets to measure gene expression in experimental and control samples. Equal amounts of Cyanine 3-labeled (control samples) and Cyanine 5-labeled (experimental samples) cRNA from samples were simultaneously co-hybridized onto the arrayed oligonucleotides on the same Agilent 44k Whole Human Genome chip (Agilent Technologies, 4 × 44k format) slide at 65°C for 17 h using an Agilent Gene Expression Hybridization Kit in Agilent's SureHyb Hybridization Chambers (G2545A). The hybridized microarrays were washed according to manufacturer's instructions, and then scanned by Agilent Feature Extraction software (10.5, Protocol GE2_105_Dec08).

Array Data Analysis

Data were analyzed *via* the R packages Limma and Hdaarray, both available in R. Specifically, Limma is an R package for the analysis of gene expression microarray data, especially the use of linear models for analyzing designed experiments and the assessment of differential expression (56). Limma allows to analyze comparisons between many RNA targets simultaneously in arbitrary complicated designed experiments. Empirical Bayesian methods are used to provide stable results even when the number of arrays is small. Expression intensities were at first background corrected. Then, they were normalized so that the intensities or log-ratios have similar distributions across a set of arrays. A regularized version of the T-test was then applied (57). A FRD correction for multiplicity was applied.

GO Functional and Pathway Analyses

GO analysis is a commonly applied method for the functional annotation of large-scale expression data. The KEGG pathways database is a comprehensive and recognized database with a wide range of biochemical pathways, linking genomic information with higher-order functional information. Gene ontology and pathway analysis were carried out using Database for Annotation, Visualization, and Integrated Discovery (DAVID) v.6.7 and Reactome [(58–60); https://david.ncifcrf.gov/; https://reactome.org/]. The list of DEGs with a more stringent level of $P < 0.01$ was used to limit the input to DAVID to achieve meaningful overrepresented data. From the obtained output, GO FAT terms were used instead of GO ALL, because the FAT category filters out the very broad GO terms based on a measured specificity of each term to yield more specific terms. Using these data, differences in biological processes (BP), molecular function (MF), cellular component (CC) were detected. Significant enrichment was considered when enriched gene count ≥2, and p value <0.05. Pathways with a $P < 0.05$ were considered.

Statistical Analysis

Results are reported as mean ± Standard Deviation (SD). Three independent experiments in triplicates ($n \geq 9$) were performed. Differences between experimental groups were analyzed by the Student's t-test. All statistical analyses have been performed using JMP Software purchased by Statistical Discovery SAS Institute. Finally, differences between means were considered significant at $^{*}p < 0.05$ and particularly significant at $^{**}p < 0.01$.

RESULTS

RIZ2 Overexpression in HEK-293 Cell Line

In order to investigate the RIZ2 oncogenic mechanisms of action together with the pathways impacted, RIZ2 was overexpressed in the normal human embryonic kidney HEK-293 cell line, both RIZ1 and RIZ2 positive and unresponsive to estrogens. To this purpose, we transfected HEK-293 cells with a plasmid encoding for RIZ2 in frame with EGFP (pEGFP_hRIZ2) and with the E-GFP empty vector (pEGFP). In this way, the balance between RIZ1 and RIZ2 was modified in favor to RIZ2, reproducing a condition often observed in cancer (3, 8). Quantitative assay of the RIZ2 transcript was unfeasible because of the extensive similarity between the two gene products, RIZ1 and RIZ2. The RIZ2 overexpression was verified after transfection by qRT-PCR of reverse-transcribed total cellular RNA, using two sets of primers: 118F/438R and 649F/975R recognizing sequences on exons 3 and 5 (exclusive of RIZ1) or on exon 8 (common to both RIZ1 and RIZ2 and indicated as RIZtot) respectively in both transient (data not shown) and stable transfected cells (**Figure S1** and **Figure 1A**) (34, 39). qRT-PCR analysis revealed a highly significant increase of RIZ2 expression levels with a decrease in RIZ1 expression levels compared to control cells suggesting a putative mechanism of transcription autoregulation. RIZ2 protein expression level was evaluated by Western blot analysis with the monoclonal antibody RZ2413 (41) recognizing the residues 960–972 of the proline rich domain (aa sequence 952–1,052) common to RIZ1 and RIZ2 forms in transient (**Figures 1B, C**) and stable transfected (**Figure 1D**) cells. A RIZ2 overexpression was revealed in transiently transfected cells (**Figure 1C**). Western blot analysis of RIZ gene products in pEGFP-hRIZ2 stable transfected cells, revealed a band of 162kDa corresponding to the predictable MW from the primary sequence of RIZ2 (http://www.ensembl.org/index.html) that is weaker than observed in transient transfection (**Figure 1D**). Additionally, the WB analysis showed specific immunoreactive bands migrating at 110–90 kDa, likely resulting from processing events, as previously reported (11) (**Figures 1C, D**). Altogether, both qRT-PCR and Western blot analysis confirmed RIZ2 overexpression. As expected, fluorescence microscopy analysis revealed that RIZ2 was predominantly localized in the nucleus (**Figure 1E**). Furthermore, HEK-293 cells overexpressing RIZ2 showed an increased content of thickened F-actin on the periphery of the cells with pronounced membrane protrusions, such as filopodia and lamellipodia (**Figure 1E**). These findings indicate that RIZ2 overexpression induces cytoskeleton changes.

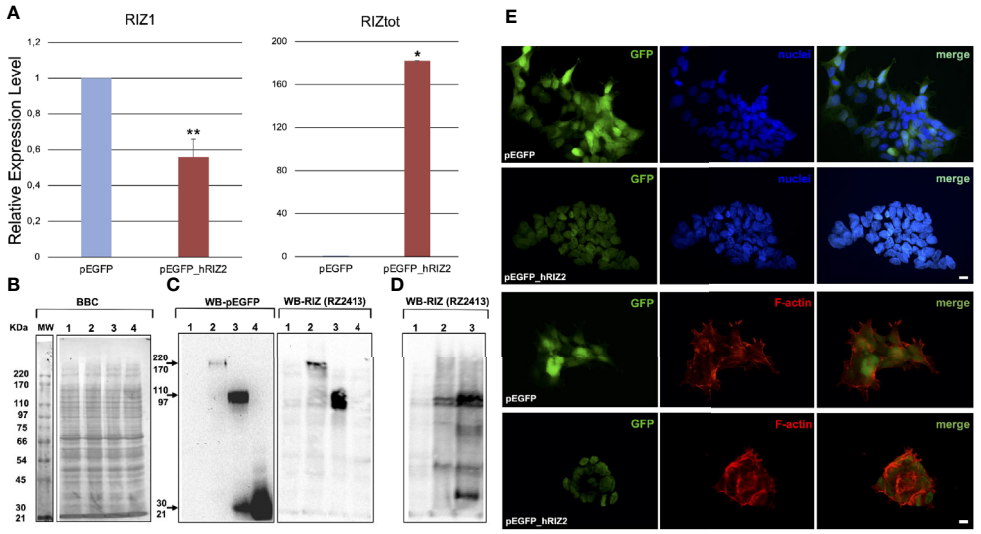

FIGURE 1 | *RIZ2 overexpression in HEK-293 cell line.* **(A)** Histograms represent the relative expression level of RIZ1 and RIZtot by qRT-PCR analysis using two sets of primers: 118F/438R recognizing sequences on exons 3 and 5 (exclusive of RIZ1) and 649F/975R recognizing a C-terminal region common to both RIZ1 and RIZ2 and indicated as RIZtot. The relative expression level is indicated as fold changes from HEK 293-pEGFP cells. Data were obtained from three independent experiments and expressed as mean ± SD. **p < 0.01 and *p < 0.0005 for RIZ1 or RIZtot *versus* control. **(B)** A representative Coomassie brilliant blue (BBC) stained gel. **(C, D)** Representative western blot analyses of total cell lysates from HEK-293 cells transiently **(C)** or stable **(D)** transfected with pEGFP or pEGFP_hRIZ2. Antibodies against RIZ (RZ2413) and EGFP were used in western blotting analysis. Sample 1, empty vector; sample 2, HEK 293-pEGFP_hRIZ2; sample 3, pEGFP-hRIZaa923-COOH; sample 4, pEGFP). **(E)** Immunofluorescence analysis of GFP (left panel) and F-actin (lower section, middle panel) in HEK 293-pEGFP and HEK 293-pEGFP_hRIZ2. Nuclei are stained in blue (upper section, middle panel). Merged images are shown in the right panels. The images shown are representative of three independent experiments. Images were captured using a DC480 camera (Leica) and acquired by Application Suite (Leica) software.

Gene Ontology and Pathway Enrichment Analyses

In order to evaluate the effects of RIZ2 overexpression on gene expression, a pilot expression study was performed through microarrays analysis. We compared the differential gene expression between HEK-293 cells overexpressing RIZ2 (pEGFP_hRIZ2) *versus* control cells transfected with the E-GFP empty vector (pEGFP). The obtained data have been deposited in NCBI's Gene Expression Omnibus (61) and are accessible through GEO Series accession number GSE150031 (https://www.ncbi.nlm.nih.gov/geo/query/acc.cgi?acc=GSE150031). Differentially expressed genes (DEGs) were initially selected on the basis of an adjusted P-value <0.05 (2520 DEGs). Given the huge number of DEGs obtained, a more stringent level of $P < 0.01$ was applied to generate the list of differentially expressed probe sets used for functional categorization through gene ontology (GO) overrepresentation analysis (595 DEGs). A total of 595 DEGs were identified in pEGFP-hRIZ2 cells compared to control cells, including 292 downregulated (49.1%) and 303 upregulated (50.9%).

The GO analysis was performed through DAVID online tool and allowed classifying DEGs into three categories, including the biological process, the cellular component, and the molecular function (**Figure 2A**; **Tables S1–S3**) (https://david.ncifcrf.gov/). As shown in **Table S1**, in the biological process category DEGs were enriched in different GO function such as in macromolecular complex assembly, cell cycle, mRNA processing, RNA splicing, macromolecule catabolic process, intracellular transport, RNA processing (**Table S1**). In the cellular component category, the identified DEGs were significantly associated with intracellular organelle lumen, non-membrane-bounded organelle, membrane-enclosed lumen, organelle lumen, nuclear lumen, mitochondrion, cytosol, nucleoplasm, and organelle membrane (**Table S2**). For the molecular function category, enrichment of DEGs was revealed in RNA binding, structural molecule activity, transcription cofactor activity, nucleotide binding (**Table S3**).

DEGs functional and signaling pathway enrichment was performed using online websites of KEGG pathway in DAVID online tool (https://david.ncifcrf.gov/). The upregulated genes mainly enriched in oxidative phosphorylation (p = 5.9E-4) and cell cycle (p = 2.3E-3) whereas the downregulated genes mainly enriched in spliceosome signaling pathways (p = 1.1E-2) (**Table S4**). Additionally, DEGs were analyzed using the "Reactome" website in order to study and visualize pathway overrepresentation (enrichment) and representation of expression data viewed as an overlay on "reactome" pathways (https://reactome.org/). In this case, pathway analysis using this database, revealed cell cycle, metabolism, gene expression (transcription), and protein localization as significantly enriched pathways. In particular, several DEGs (i.e. *CCNB2*, *CDKNC2*, *CDC26*, *PSMD10*) were overrepresented in cell cycle, mitotic phase (R-HSA-69278) hypothesizing a possible role of RIZ2 during cell cycle progression (**Figure 2B**).

Supplementary Figure S2 shows the top SP-PIR keywords of enriched DEGs. Many DEGs were associated with phosphoprotein

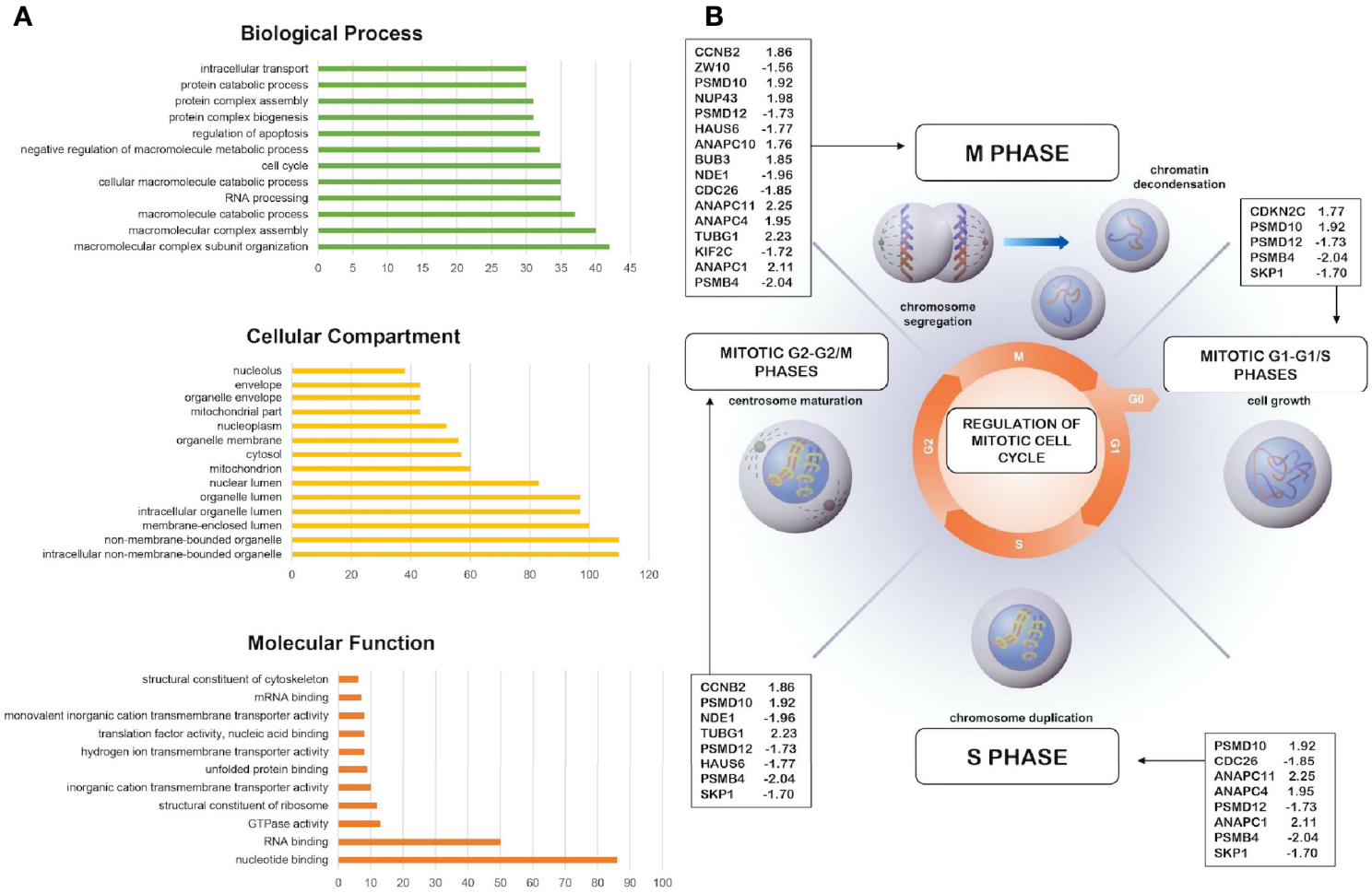

FIGURE 2 | *Bioinformatics analysis of the differentially expressed genes and pathway analysis.* **(A)** More representative Gene Ontology enrichment of differentially expressed genes (DEGs) in cellular component, molecular function, and biological process. Count: number of genes related to the enriched GO. **(B)** Overrepresentation and enrichment analysis of DEGs in cell cycle, mitotic phase (R-HSA-69278). The fold change value of indicated genes are reported.

(46.1%; p = 2.1E-9), alternative splicing (40.7%; p = 5.7E-3), nucleus (29.8%; p = 4.3E-8), acetylation (26.4%; p = 5.5E-20, and cytoplasm (20.2%; p = 3.2E-3) (**Table S4**).

Effects of RIZ2 Overexpression on HEK-293 Cell Viability and Cell Cycle Progression

In order to investigate the role of RIZ2 in the control of cell viability and survival, colorimetric MTT assay was performed in HEK-293 cells stable transfected with pEGFP_hRIZ2 or with pEGFP control vector after 24, 48, and 72 h. The number of HEK 293-pEGFP_hRIZ2 cells at 24, 48, and 72 h was greater than HEK 293-pEGFP (**Figure 3A**). As shown in **Figure 3B**, RIZ2 overexpressing cells exhibited a significant increase in cell viability, as compared with the control cells at 48 and 72 h.

The biological effect of RIZ2 overexpression on cell cycle progression was evaluated through FACS analysis using HEK-293 stable overexpressing pEGFP_hRIZ2 or pEGFP vectors. pEGFP_hRIZ2 clones showed a decrease of cell percentages in G1 and G2/M phases (G1, 38,79 *vs* 47,73%; G2/M 12,10 *vs* 20,54%) as well as an increase of cell percentages in S phase (49,12 *vs* 31,73%; **Figure 3C**), as compared to the control cells. To better discriminate the observed effects, cells were synchronized with nocodazole treatment for 16 h (**Supplementary Figure S3**). Three hours after nocodazole release, cells were recovered, and cell cycle analysis was done. After synchronization, FACS analysis confirmed the decrease of cells in G2 phase (25,52 *vs* 34,45%) and the increase of cells in S phase (44,21 *vs* 31,20%). No significant effects were observed in G1 phase. Altogether, these data indicate that RIZ2 could promote the G2-to-M phase transition.

To deeper assess the role of RIZ2 in tumorigenesis, we also analyzed the ability of HEK-293 cells stable overexpressing pEGFP_hRIZ2 or the pEGFP control vector to form colonies. To this purpose, HEK-293 stable transfected cells were seeded at low density in six-well plates. Ten days later colonies were counted, and their cellularity was evaluated by phase-contrast microscopy. Overexpression of RIZ2 induced the formation of a markedly higher number of colonies than the control cells (**$P < 0.0001$ *versus* empty vector; *$P < 0.001$ *versus* empty vector) (**Figure 3D**).

In summary, these data suggest that RIZ2 may exert a promoting role in cell cycle progression and tumor formation.

RIZ2 Overexpression Increases HEK-293 3D-Organoid Growth

3D cell culture systems are mini organ-like structures capable of self-renewal and self-organization, which closely recapitulate the *in vivo* microenvironment as well as the molecular and genetic signature of tissues or organs of origin (62).

To develop cell culture models resuming cancer tissues and to reproduce the complex *in vivo* architecture, 3D organoids were established. Phase-contrast and immunofluorescence images at 3 days revealed a 3D structure in both pEGFP (**Figure 4A**) and pEGFP overexpressing RIZ2 HEK-293 cells (**Figure 4B**) cultured in Matrigel. Both cell types generated roundish and well-differentiated organoids. Changes in dimension and structure of organoids were then monitored for additional 15 days. Phase-contrast and immunofluorescence microscopy images at 10th day were captured and shown (**Figures 4A, B**). Quantification of data was also done, and the graphs in **Figures 4C, D** show that pEGFP organoid size was increased by about 2- and 2,5-fold after 10 and 15 days, respectively. Interestingly, we observed a significant ($p < 0.05$) increase (about 7,5- and 9-fold at 10 and 15 days, respectively) in the size of pEGFP hRIZ2-derived organoids (**Figures 4C, D**).

In conclusion, these findings demonstrate for the first time a role for RIZ2 in the growth of HEK293-derived organoids.

RIZ Silencing in MCF-7 and MDA-MB-231 Cell Lines

Based on our findings on the dual role of PRDM2 products in the control of cell proliferation and survival in MCF-7 cell line (39), we aimed at clarifying whether the effects previously observed in MCF-7 cells are merely due to RIZ1 silencing or the resulting imbalance in favor of RIZ2.

To this purpose, a RIZtot mRNA interference experiment was set up in MCF-7 and MDA-MB-231 breast cancer cell lines with a siRNA spanning a sequence coding for a region common to both RIZ1 and RIZ2 gene products (aa 333–340 of RIZ1 protein or aa 132–139 of RIZ2 protein), indicated as siRNA-total (see also **Figure S1**). The siRNA was designed taking into account the principles able to ensure efficiency and specificity of target gene knockdown (63–65). Specifically, the selected siRNA-total sequence is near to the ATG initiation codon for the RIZ2 protein and not able to efficaciously interfere the RIZ1 product, whose ATG start codon is localized at about 1,000 nucleotides upstream (65). Thus, siRNA-total interference resulted much more efficient towards RIZ2 than RIZ1 transcripts. Different concentrations of siRNA-total (20, 25, 35, and 50 nM) were initially used. MCF-7 and MDA-MB-231 cells are ERα- positive and negative respectively, with the first expressing both RIZ1 and RIZ2, while the latter expressing very low levels of RIZ1 but substantial levels of RIZ2 (11) (**Figures 5A, B**, and **Supplementary Figure S4**). Transfection of MCF-7 cells with the various concentrations of siRNA-total produced an increase in the amounts of total transcripts, as evidenced from the analysis of the RT-PCR amplified fragments with primers complementary to sequences common to RIZ1 and RIZ2, including exon 8 (**Figure 5A**). The analysis of the same RNAs with primers complementary to a RIZ1-specific sequence including exons 3, 4, and 5, showed also an increase of the RIZ1-specific amplicon in the cells treated with the different concentrations of siRNA-total (**Figure 5A**). These findings suggest that RIZ1 transcript is upregulated in RIZtot MCF-7 interfered cells. Thus, this silencing modified the balance between RIZ1 and RIZ2 in favor to RIZ1, suggesting that the ratio between RIZ1 and RIZ2 is pivotal and the two molecular variants regulate each other (**Figure 5C**). Besides, transfection of MDA-MB-231 cells, expressing very low level of RIZ1, with increasing concentrations of the same siRNAs produced a decrease in the amount of total RIZ products and a concomitant decrease in RIZ1 expression level (**Figures 5B, D**).

We next analyzed the effect of the imbalance of RIZ2/RIZ1 ratio on cell viability. For this purpose, we used 35 and 50 nM of siRNA-total to silence RIZ2 in both cell lines. RIZtot silencing produced a

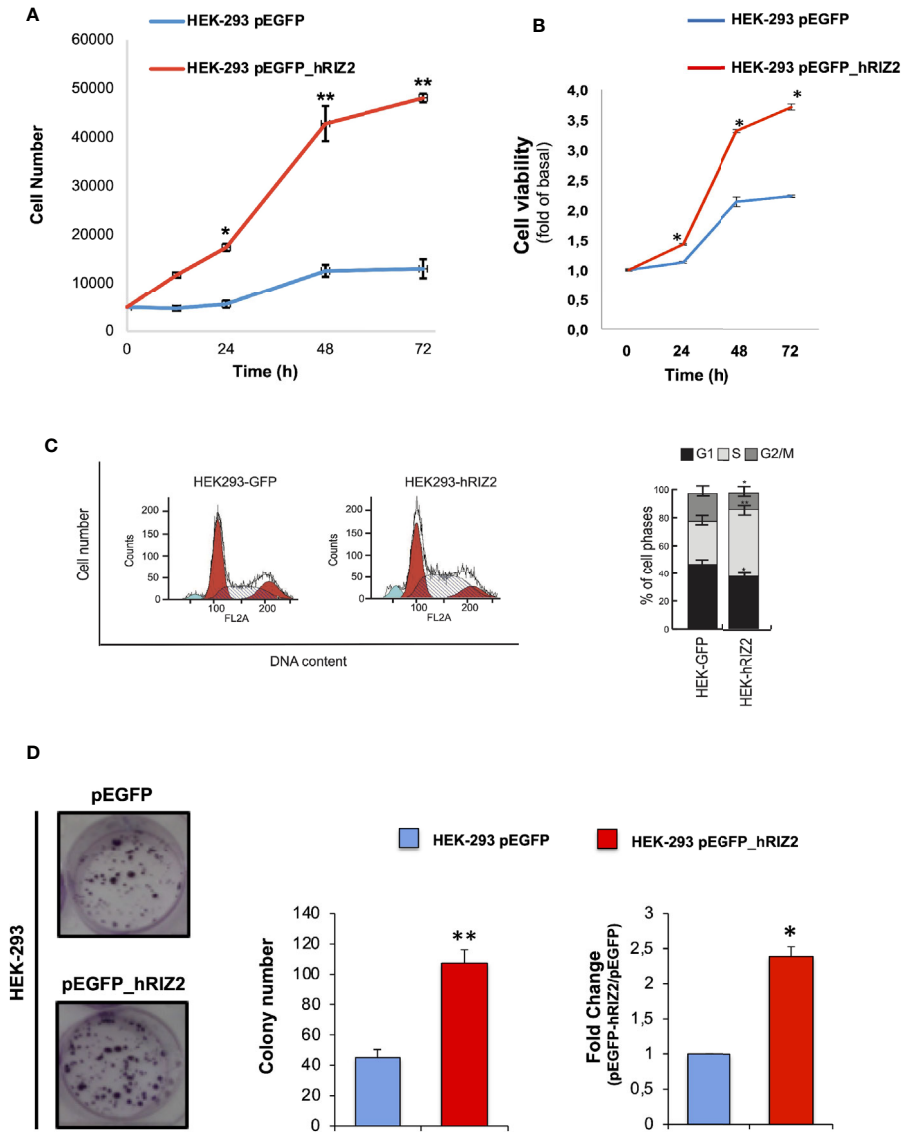

FIGURE 3 | *Effects of RIZ2 overexpression on HEK-293 cell Viability and cell cycle progression* **(A, B)** Effect of RIZ2 overexpression on HEK-293 cell viability by MTT assay. **(A)** HEK-293 cells stable transfected with pEGFP_hRIZ2 or with pEGFP alone, as control, were cultured for 24, 48, and 72 h. Graph represents the extrapolated cell number at the different time points. **(B)** HEK-293 cells stable transfected with pEGFP_hRIZ2 or with pEGFP alone, as control, were cultured for 24, 48, and 72 h. Graph represents the cell viability, expressed as fold increase over the basal. Three independent experiments were done. Means and standard error of the means (SEMs) are shown. *p < 0.005 for the indicated experimental points *vs.* the corresponding untreated control. **(C)** Effects of pEGFP_hRIZ2 overexpression on HEK293 cell cycle regulation. Histogram Plots of cell cycle distribution (left) and cell cycle analysis (right) are illustrated. Graphs show the mean of at least three independent experiments with error bars indicating standard deviation. Values are mean ± standard deviation (SD) of biological triplicates. ****p-value ≤ 0.0001, ***p-value ≤ 0.001, **p-value ≤ 0.01, *p-value ≤ 0.05, ns p-value > 0.05 *vs.* pEGFP control cells. **(D)** Representative image of clonogenic assay. Ten days after seeding, clones were counted, and their cellularity was evaluated by phase contrast microscopy. The histogram represents the average number of colonies of at least three independent experiments, each performed in triplicate (**$P < 0.0001$ *vs.* empty vector); on the right the fold change in colony number formation between pEGFP_hRIZ2 cells and pEGFP control cells (*$P < 0.001$ *vs.* empty vector).

significant decrease of MCF-7 and MDA-MB-231 cell numbers, as compared to control cells (**Figures 5E, F**). Additionally, cell cycle analysis indicated an increase of SubG1 phase in interfered cells over the control, suggesting an increase of the cells undergoing apoptosis especially when we used siRNA-total 50 nM; besides, a reduction of S-G2 was detected (**Figures 5G, H**).

We then analyzed also the protein levels of RIZ1 (**Figures 5I–L**). Results observed by RT-PCR analysis were confirmed by western blot technique. In MCF-7 cells, a sharp increase in the RIZ1 expression level was observed at the different concentrations of siRNA used (**Figures 5I–L**). In MDA-MB-231, instead, RIZtot silencing reduced the RIZ1 expression level. In this context,

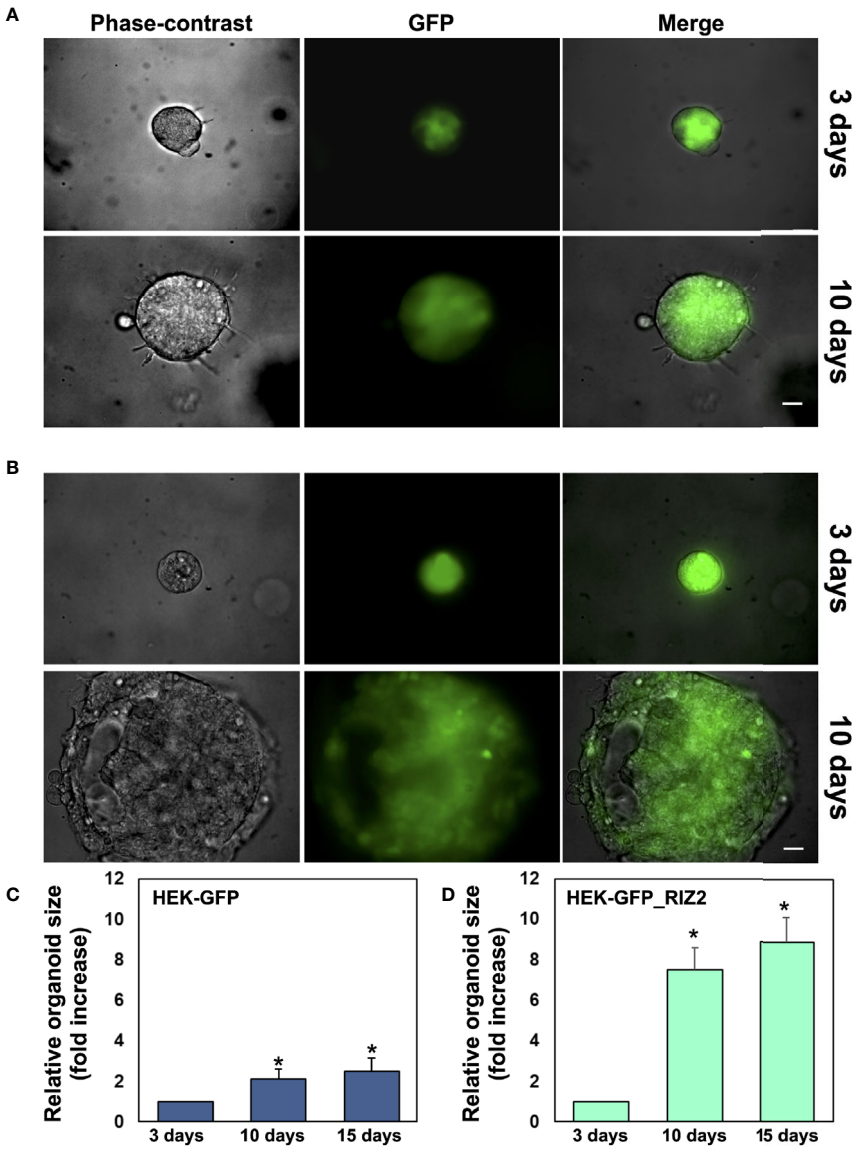

FIGURE 4 | *RIZ2 overexpression Increases HEK-293 3D-Organoid Growth.* In **(A)** HEK-293 cells stable transfected with pEGFP were used in miniaturized 3D cultures in extracellular matrix (ECM). In **(B)** HEK-293 cells stable transfected with pEGFP_hRIZ2 were used in miniaturized 3D cultures in ECM. In **(A, B)**, at the indicated times, phase-contrast- (left panels), immunofluorescence- (middle panels), and merged (right panels) microscopy images were captured using DMIRB Leica (Leica) microscope equipped with C-Plan 40× objective (Leica) and acquired using a DFC 450C camera (Leica). Scale bar, 100 μ. Images are representative of three independent experiments, each performed in duplicate. **(C, D)** Graphs represent the relative organoid size (area), which was calculated using the Application Suite Software and expressed as a relative fold increase over the organoid area calculated at 3th day. Means and standard error of the means (SEMs) are shown. *$p < 0.05$ for the indicated pEGFP_hRIZ2 HEK-293 cells *vs.* the corresponding pEGFP HEK-293 control cells.

a reduction of cyclin B1 expression level was shown in both siRNA transfected cell lines (**Figures 5I–L**).

DISCUSSION

PRDM2, a member of the PRDM family, is involved in the proliferation and apoptosis control and acts in the transcriptional regulation of genes encoding for proteins implicated in development, cell cycle progression and cell adhesion. Several evidences have suggested that an imbalance in the expression levels of *PRDM2* main proteins, RIZ1 and RIZ2, could be relevant for neoplastic transformation (3, 8, 10). However, the underlying molecular mechanisms and the related cellular pathways are still unclear. RIZ1 functions have been extensively investigated (21, 36). In many reports, genetic evidence from tumor samples and cancer cell lines indicates that RIZ1 is a putative tumor suppressor gene (3). In addition, its ectopic expression is able to induce cell growth

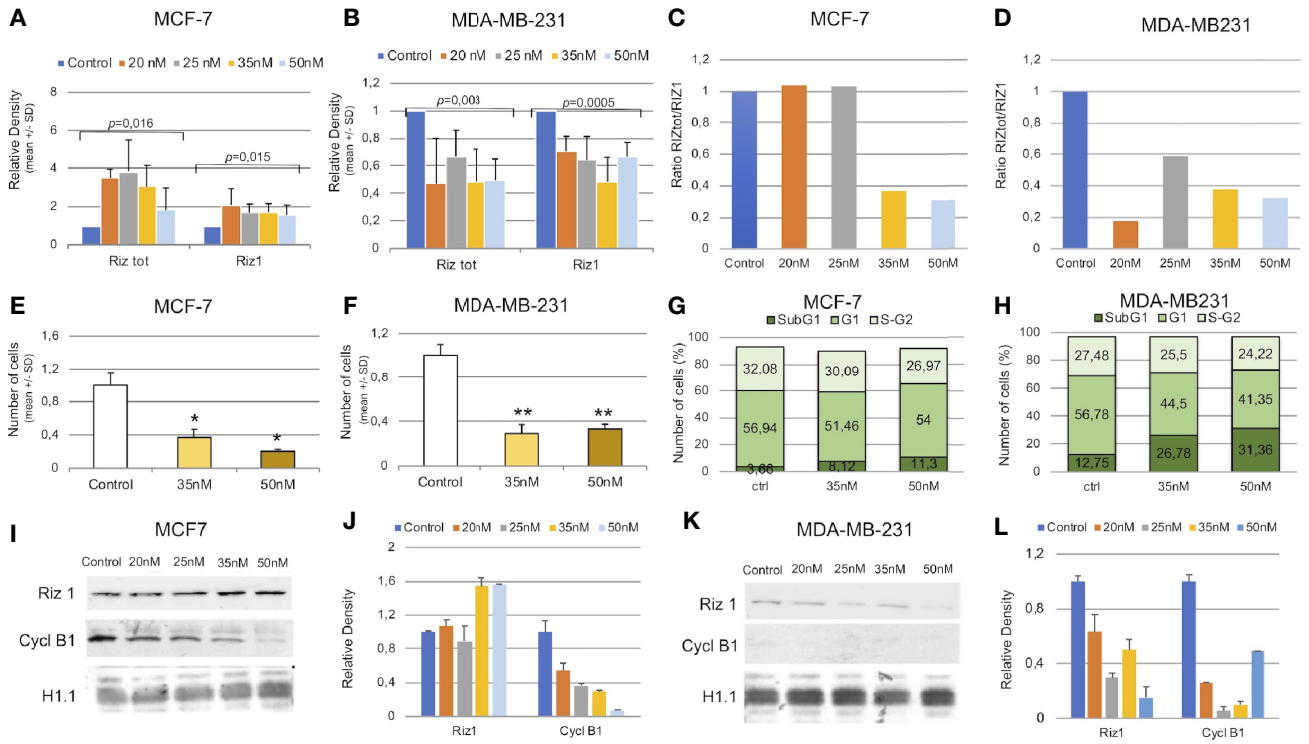

FIGURE 5 | *RIZ2 silencing in MCF-7 and MDA-MB-231 cell line.* **(A, B)** Relative expression by semi-quantitative RT-PCR of RIZtot transcripts in cells interfered with different concentrations of siRNA-total (20, 25, 35, and 50 nM). **(C, D)** Histograms representing the variation of RIZ2/RIZ1 ratio are shown. **(E, F)** Cell counts in cells interfered with two different concentrations (35 and 50 nM) compared with untreated cells (*p < 0.05 and **p < 0.01). **(G, H)** Cell cycle distribution of PI-labeled cells by FACS analyses at 40 h from transfection with reported concentrations of siRNA-total. **(I–L)** Representative Western blot analysis of total interfered cell extracts with the indicated antibodies and the relative densitometry analysis.

blockade and apoptosis in a variety of cancer cell lines (15, 33). Genetic or epigenetic modifications of the PRDM2/RIZ gene observed in human cancers lead to silencing of RIZ1 expression (12, 16, 22, 66), while, in contrast, they do not affect RIZ2 expression level. These findings suggest a positive selection for RIZ2 expression that could be related to its promotion of cell proliferation (15). Over the past decades, few studies have focused on RIZ2 biological activity. The main experimental pitfalls are related to the sequence identity of RIZ2 and RIZ1. Firstly, RT-PCR analysis is not able to evaluate the RIZ2 expression level but only the sum of RIZ1 and RIZ2 expression levels. Finally, the commonly used and commercially available antibodies raised against the common C-terminal domain do not enable the unique identification of RIZ2. As such, the inability to specifically detect RIZ2 has obviously hindered the study of its functional roles. In addition, in accordance with previously published experiments, pEGFP_hRIZ2 stable transfected HEK-293 cells showed a weaker RIZ2 specific product expression, than observed in transient transfection, accompanied by processed proteins of ≅110–90 kDa, which have a similar MW to the main product of a plasmid construct with RIZ insert starting from aa 923 to the carboxylic terminal aa 1682 (RIZ isoform 2) and bands with a lower mass. Similarly, Western blotting analysis of nuclear fraction revealed this band pattern that increased in estradiol time course MCF-7 treatment (11). To overcome these challenges, there is the need to discover peculiar features of RIZ2 and develop new methods for its identification. In the present study, we explored for the first time the role of RIZ2 by its forced expression in HEK-293 cells, which express equal amount of RIZ1 and RIZ2 proteins. Interestingly, this ectopic expression was able to increase cell viability and had a growth-prompting effect. Additionally, the forced expression of RIZ2 caused the deregulation of several genes involved in mitosis, including the overexpression of genes coding for Cyclin B and for some subunits of the Anaphase-Promoting Complex/Cyclosome (APC/C), which are often dysregulated during tumorigenesis (67). Accordingly, cell cycle analysis showed that RIZ2 could facilitate the G2-to-M phase transition. Altogether, these findings suggest that the imbalance in the amount of *PRDM2* products in favor of RIZ2 modifies the expression pattern of PRDM2 target genes involved in the promotion of cell division. Moreover, our data indicated also that RIZ2 over-expression induced the increase in the size of organoids. Organoid culture is largely accepted to study stem cells, organ development and patient-specific diseases (62). Noteworthy, the role of RIZ2 on organoid growth has not been reported so far. Additionally, in our study, we set up, for the first time, specific conditions to perform organoid culture of HEK 293 cells. We found that organoids were formed after 3-days of culture in Matrigel and that RIZ2 overexpression significantly enhanced their growth already after 10 days of culture

if compared with pEGFP HEK293-derived organoids, used as controls. Provided that 3D models recapitulate more reliably the features of human cancers, these data address useful information about the role of RIZ2 in tumorigenesis that might be transferred to clinical practice and drug screening. In these cells, RIZ2 increase was also accompanied by a concomitant decrease of RIZ1 transcription. Thus, RIZ2 could exert also its oncogenic functions by impairing other mechanisms involving the methyltransferase activity of RIZ1, such as DSB repair (3, 28).

Our previous investigation demonstrated that RIZ1 is able to negatively control breast cancer cell proliferation, confirming its role as tumor suppressor gene. In addition, it is well known that in estrogen-responsive cells and target tissues, estradiol is able to modulate the expression of RIZ isoforms by inducing a change in the balance of their intracellular concentrations (38). Indeed, selective RIZ1 silencing increased the number of MCF-7 cells undergoing cell division with an effect on the growth rate similar to the estradiol outcome (39). Therefore, this set of experiments did not reveal if the observed effect on cell proliferation was merely due to RIZ1 silencing or to the imbalance in favor of RIZ2. Here, the RIZtot silencing in MCF-7 cells and the consequent reduction of RIZ2/RIZ1 ratio determined a reduction of cell proliferation and an increase of cells number undergoing apoptosis, suggesting that the previously observed behavior was related to the imbalance in favor of RIZ2. MCF-7 cells are estrogen-responsive and express both RIZ1 and RIZ2. Moreover, RIZ2 silencing produced similar effects also in MDA-MB-231 cells, which express RIZ1 at very low levels and are unresponsive to estradiol. In this context, we observed a sharp decrease of cell number, with a concomitant change in cell cycle distribution.

Overall, these findings add new insights to the understanding of the putative mechanism of the tumor-promoting function of RIZ2. The presented results indicate that RIZ2 exerts a tumor-promoting function, most likely through the transcriptional regulation of genes involved in cell cycle progression. Although several candidate genes have been extrapolated by our microarray studies, the detailed genes still need to be confirmed by further analyses on stable clones. Our results strongly suggest that RIZ2 is a promising candidate oncogene in cancer development; however, additional attempts to discover cell partners interacting with RIZ2 are warranted to elucidate how the deregulation of RIZ2 prompts cell growth, survival, and organoid formation. Indeed, most of these proteins are still undefined. Progresses in mass spectrometry instrumentation and computational tools allow the identification of high-confidence interaction proteomes of numerous biologically relevant protein groups refining our knowledge of protein interaction networks and functions (68). In this context, a whole transcriptome analysis through next-generation sequencing technologies, accompanied by proteomic studies may be useful to define all the RIZ2 target genes, thus obtaining a landscape of genes and pathways involved in its tumor-promoting action (69). Thus, the study of transcriptome and RIZ2 interaction proteome could represent a crucial step to elucidate molecular bases of its function. Besides, the integration of genomic and proteomic analyses could be relevant to solve additional open questions in this topic. As mentioned, an altered ratio of RIZ2/RIZ1 isoforms could be determined also through DNA methylation of RIZ1 promoter CpG island; in this scenario, we could hypothesize that this methylation event might interfere with the binding of CCTC-binding factor (CTCF). The functions of this transcription factor are related to the recognition and binding of a preferentially unmethylated CpG-rich consensus sequence within several genomic sites, with a strong correlation between its global occupancy and DNA methylation (68, 70, 71). Although previous studies showed that CTCF binding could regulate DNA methylation, recently it has been indicated that also DNA methylation can direct CTCF binding (72, 73). Interestingly, chromatin immunoprecipitation sequencing (ChIP-seq) data suggested that CTCF might bind also the PRDM2 promoter (70). Thus, this method could be applied also to determine the degree to which CTCF occupancy could be actively inhibited *via* DNA methylation. Finally, CTCF could also function as interaction partner of RIZ1 and/or RIZ2 proteins, as previously demonstrated for Prdm5 in mouse embryonic stem cells by high-throughput technologies (74).

Although this study is still preliminary and no clinical-derived samples were analyzed, our results could have a clinical significance. Indeed, we have shown that RIZ2 overexpression caused the deregulation of several genes involved in mitosis. Significantly, many of these genes are deregulated in cancer and/or have been suggested as potential cancer therapeutic targets (67). For instance, based on the Cancer Genome Atlas data, *CCNB2* is upregulated in advanced tumor stage and correlates with poor prognosis in breast cancer (75); also, *PSMD10* is upregulated in various cancers and the use of agents directed against its protein product gankyrin has been recently indicated as a promising cancer therapeutic and preventive strategy (76). Likewise, aberrant increases of APC10 and APC11 proteins, which are two subunits of the APC/C encoded by *ANAPC10* and *ANAPC11* genes, have been recently evidenced in non-small cell lung and colorectal cancer tissues (77, 78); interestingly, inhibitors of APC/C activity are currently under investigation (67).

In summary, this study provides evidence that RIZ2 overexpression fosters viability, cell cycle progression, and organoid formation. Taken together, our findings indicate that RIZ2 upregulation may contribute to tumor promotion, supporting the hypothetical oncogenic role of this PRDM2 protein isoform. Further investigations are required to explore the RIZ2 molecular mechanisms of action in cancer and discover cell partners interacting with RIZ2. Understanding the RIZ2 functions and interacting partners would provide new hints in the discovery of diagnostic and therapeutic strategies in human cancers. Obviously, studies analyzing the overexpression of RIZ2 isoform in tumor specimens are needed; furthermore, integrated analysis would be also useful to elucidate its impact on the deregulation of genes involved in mitosis.

DATA AVAILABILITY STATEMENT

The datasets presented in this study can be found in online repositories. The names of the repository/repositories and accession number(s) can be found below: https://www.ncbi.nlm.nih.gov/geo/, GSE150031.

AUTHOR CONTRIBUTIONS

CA, PG, MR, EDZ, and AC conceived the study. AS, CR, MMM, EDZ, MDD, VC, and MR performed the experiments. MR, MDD, VC, EDZ, PG, AC, and CA analyzed the data. AS, MMM, and MR performed bioinformatics analyses. MR, EDZ, MDD, and VC prepared the figures. EDZ, CA, MR, and AC wrote the original manuscript draft. LA, GC, PG, AC, and CA reviewed and edited the paper. All authors contributed to the article and approved the submitted version.

FUNDING

This work was supported by University of Campania "Luigi Vanvitelli," VALERE program to GC (ID 263), CA, and VC (ID 342); Italian Ministry of University and Scientific Research (P.R.I.N. 2017EKMFTN_002) to GC. MDD was supported by a fellowship of 'Fondazione Umberto Veronesi' (FUV Post-doctoral fellowship 2020, until 09/2020) and iCURE Project (B21C17000030007- Regione Campania) from 10/2020.

ACKNOWLEDGMENTS

We thank Dr. Luisa Cutillo (University of Naples "Parthenope") for assistance in analyzing microarrays.

SUPPLEMENTARY MATERIAL

The Supplementary Material for this article can be found online at: https://www.frontiersin.org/articles/10.3389/fonc.2020.583533/full#supplementary-material

REFERENCES

1. Fumasoni I, Meani N, Rambaldi D, Scafetta G, Alcalay M, Ciccarelli FD. Family expansion and gene rearrangements contributed to the functional specialization of PRDM genes in vertebrates. *BMC Evol Biol* (2007) 7:187. doi: 10.1186/1471-2148-7-187
2. Clifton MK, Westman BJ, Thong SY, O'Connell MR, Webster MW, Shepherd NE, et al. The identification and structure of an N-terminal PR domain show that FOG1 is a member of the PRDM family of proteins. *PloS One* (2014) 9: e106011. doi: 10.1371/journal.pone.0106011
3. Sorrentino A, Rienzo M, Ciccodicola A, Casamassimi A, Abbondanza C. Human PRDM2: Structure, function and pathophysiology. *Biochim Biophys Acta Gene Regul Mech* (2018) 1861:657–71. doi: 10.1016/j.bbagrm.2018.06.002
4. Hohenauer T, Moore AW. The Prdm family: expanding roles in stem cells and development. *Development* (2012) 139:2267–82. doi: 10.1242/dev.070110
5. Fog CK, Galli GG, Lund AH. PRDM proteins: Important players in differentiation and disease. *BioEssays* (2012) 34:50–60. doi: 10.1002/bies.201100107
6. Di Zazzo E, De Rosa C, Abbondanza C, Moncharmont B. PRDM Proteins: Molecular Mechanisms in Signal Transduction and Transcriptional Regulation. *Biology (Basel)* (2013) 2:107–41. doi: 10.3390/biology2010107
7. Mzoughi S, Tan YX, Low D, Guccione E. The role of PRDMs in cancer: One family, two sides. *Curr Opin Genet Dev* (2016) 36:83–91. doi: 10.1016/j.gde.2016.03.009
8. Casamassimi A, Rienzo M, Di Zazzo E, Sorrentino A, Fiore D, Proto MC, et al. Multifaceted Role of PRDM Proteins in Human Cancer. *Int J Mol Sci* (2020) 21(7):2648. doi: 10.3390/ijms21072648
9. Liu L, Shao G, Steele-Perkins G, Huang S. The retinoblastoma interacting zinc finger gene RIZ produces a PR domain-lacking product through an internal promoter. *J Biol Chem* (1997) 272:2984–91. doi: 10.1074/jbc.272.5.2984
10. Huang S. The retinoblastoma protein-interacting zinc finger gene RIZ in 1p36-linked cancers. *Front Biosci* (1999) 4:D528–32. doi: 10.2741/huang
11. Abbondanza C, De Rosa C, D'Arcangelo A, Pacifico M, Spizuoco C, Piluso G, et al. Identification of a functional estrogen-responsive enhancer element in the promoter 2 of PRDM2 gene in breast cancer cell lines. *J Cell Physiol* (2012) 227:964–75. doi: 10.1002/jcp.22803
12. Piao Z, Fang W, Malkhosyan S, Kim H, Horii A, Perucho M, et al. Frequent frameshift mutations of RIZ in sporadic gastrointestinal and endometrial carcinomas with microsatellite instability. *Cancer Res* (2000) 60:4701–4.
13. Jiang GL, Huang S. Adenovirus expressing RIZ1 in tumor suppressor gene therapy of microsatellite-unstable colorectal cancers. *Cancer Res* (2001) 61:1796–8.
14. Kim KC, Geng L, Huang S. Inactivation of a histone methyltransferase by mutations in human cancers. *Cancer Res* (2003) 63:7619–23.
15. He L, Yu JX, Liu L, Buyse IM, Wang MS, Yang QC, et al. RIZ1, but not the alternative RIZ2 product of the same gene, is underexpressed in breast cancer, and forced RIZ1 expression causes G2-M cell cycle arrest and/or apoptosis. *Cancer Res* (1998) 58:4238–44.
16. Du Y, Carling T, Fang W, Piao Z, Sheu JC, Huang S. Hypermethylation in human cancers of the RIZ1 tumor suppressor gene, a member of a histone/protein methyltransferase superfamily. *Cancer Res* (2001) 61:8094–9.
17. Chang HW, Chan A, Kwong DL, Wei WI, Sham JS, Yuen AP. Detection of hypermethylated RIZ1 gene in primary tumor, mouth, and throat rinsing fluid, nasopharyngeal swab, and peripheral blood of nasopharyngeal carcinoma patient. *Clin Cancer Res* (2003) 9:1033–8.
18. Zhang C, Li J, Huang T, Duan S, Dai D, Jiang D, et al. Meta-analysis of DNA methylation biomarkers in hepatocellular carcinoma. *Oncotarget* (2016) 7:81255–67. doi: 10.18632/oncotarget.13221
19. Zhao Z, Hu Y, Shen X, Lao Y, Zhang L, Qiu X, et al. HBx represses RIZ1 expression by DNA methyltransferase 1 involvement in decreased miR-152 in hepatocellular carcinoma. *Oncol Rep* (2017) 37:2811–8. doi: 10.3892/or.2017.5518
20. Xue Y, Chen R, Du W, Yang F, Wei X. RIZ1 and histone methylation status in pituitary adenomas. *Tumour Biol* (2017) 39:1010428317711794. doi: 10.1177/1010428317711794
21. Steele-Perkins G, Fang W, Yang XH, Van Gele M, Carling T, Gu J, et al. Tumor formation and inactivation of RIZ1, an Rb-binding member of a nuclear protein methyltransferase superfamily. *Genes Dev* (2001) 15:2250–62. doi: 10.1101/gad.870101
22. Sakurada K, Furukawa T, Kato Y, Kayama T, Huang S, Horii A. RIZ, the retinoblastoma protein interacting zinc finger gene, is mutated in genetically unstable cancers of the pancreas, stomach, and colorectum. *Genes Chromosomes Cancer* (2001) 30:207–11. doi: 10.1002/1098-2264(2000)9999:9999<::AID-GCC1080>3.0.CO;2-V
23. Chadwick RB, Jiang GL, Bennington GA, Yuan B, Johnson CK, Stevens MW, et al. Candidate tumor suppressor RIZ is frequently involved in colorectal carcinogenesis. *Proc Natl Acad Sci USA* (2000) 97:2662–7. doi: 10.1073/pnas.040579497
24. Maruvka YE, Mouw KW, Karlic R, Parasuraman P, Kamburov AP, Haradhvala NJ, et al. Analysis of somatic microsatellite indels identifies driver events in human tumors. *Nat Biotechnol* (2017) 35:951–9. doi: 10.1038/nbt.3966
25. Pandzic T, Rendo V, Lim J, Larsson C, Larsson J, Stoimenov I, et al. Somatic PRDM2 c.4467delA mutations in colorectal cancers control histone methylation and tumor growth. *Oncotarget* (2017) 8:98646–59. doi: 10.18632/oncotarget.21713
26. Poetsch M, Dittberner T, Woenckhaus C. Frameshift mutations of RIZ, but no point mutations in RIZ1 exons in malignant melanomas with deletions in 1p36. *Oncogene* (2002) 21:3038–42. doi: 10.1038/sj.onc.1205457

27. Sasaki O, Meguro K, Tohmiya Y, Funato T, Shibahara S, Sasaki T. Nucleotide alteration of retinoblastoma protein-interacting zinc finger gene, RIZ, in human leukemia. *Tohoku J Exp Med* (2002) 196:193–201. doi: 10.1620/tjem.196.193
28. Khurana S, Kruhlak MJ, Kim J, Tran AD, Liu J, Nyswaner K, et al. A macrohistone variant links dynamic chromatin compaction to BRCA1-dependent genome maintenance. *Cell Rep* (2014) 8:1049–62. doi: 10.1016/j.celrep.2014.07.024
29. Jiang G, Liu L, Buyse IM, Simon D, Huang S. Decreased RIZ1 expression but not RIZ2 in hepatoma and suppression of hepatoma tumorigenicity by RIZ1. *Int J Cancer* (1999) 83:541–6. doi: 10.1002/(sici)1097-0215(19991112)83:4<541::aid-ijc17>3.0.co;2-f
30. Sun W, Qiao L, Liu Q, Chen L, Ling B, Sammynaiken R, et al. Anticancer activity of the PR domain of tumor suppressor RIZ1. *Int J Med Sci* (2011) 8:161–7. doi: 10.7150/ijms.8.161
31. Liu ZY, Wang JY, Liu HH, Ma XM, Wang CL, Zhang XP, et al. Retinoblastoma protein-interacting zinc-finger gene 1 (RIZ1) dysregulation in human malignant meningiomas. *Oncogene* (2013) 32:1216–22. doi: 10.1038/onc.2012.155
32. Ding MH, Wang Z, Jiang L, Fu HL, Gao J, Lin XB, et al. The transducible TAT-RIZ1-PR protein exerts histone methyltransferase activity and tumor-suppressive functions in human malignant meningiomas. *Biomaterials* (2015) 56:165–78. doi: 10.1016/j.biomaterials.2015.03.058
33. Yang S, Liu T, Cheng H, Wang Z, Feng Y, Yan J, et al. Decreased Expression of Retinoblastoma Protein-Interacting Zinc-Finger Gene 1 Is Correlated With Poor Survival and Aggressiveness of Cervical Cancer Patients. *Front Oncol* (2019) 9:1396. doi: 10.3389/fonc.2019.01396
34. Gazzerro P, Bontempo P, Schiavone EM, Abbondanza C, Moncharmont B, Armetta I, et al. Differentiation of myeloid cell lines correlates with a selective expression of RIZ protein. *Mol Med* (2001) 7:552–60. doi: 10.1007/BF03401861
35. Zhang C, Zhu Q, He H, Jiang L, Qiang Q, Hu L, et al. RIZ1: A potential tumor suppressor in glioma. *BMC Cancer* (2015) 15:990. doi: 10.1186/s12885-015-2023-1
36. Carling T, Kim KC, Yang XH, Gu J, Zhang XK, Huang S. A histone methyltransferase is required for maximal response to female sex hormones. *Mol Cell Biol* (2004) 24:7032–42. doi: 10.1128/MCB.24.16.7032-7042.2004
37. Garcia-Bassets I, Kwon YS, Telese F, Prefontaine GG, Hutt KR, Cheng CS, et al. Histone methylation-dependent mechanisms impose ligand dependency for gene activation by nuclear receptors. *Cell* (2007) 128:505–18. doi: 10.1016/j.cell.2006.12.038
38. Abbondanza C, Medici N, Nigro V, Rossi V, Gallo L, Piluso G, et al. The retinoblastoma-interacting zinc-finger protein RIZ is a downstream effector of estrogen action. *Proc Natl Acad Sci USA* (2000) 97:3130–5. doi: 10.1073/pnas.050015697
39. Gazzerro P, Abbondanza C, D'Arcangelo A, Rossi M, Medici N, Moncharmont B, et al. Modulation of RIZ gene expression is associated to estradiol control of MCF-7 breast cancer cell proliferation. *Exp Cell Res* (2006) 312:340–9. doi: 10.1016/j.yexcr.2005.11.002
40. Rossi V, Staibano S, Abbondanza C, Pasquali D, De Rosa C, Mascolo M, et al. Expression of RIZ1 protein (Retinoblastoma-interacting zinc-finger protein 1) in prostate cancer epithelial cells changes with cancer grade progression and is modulated in vitro by DHT and E2. *J Cell Physiol* (2009) 221:771–7. doi: 10.1002/jcp.21920
41. Rossi M, Abbondanza C, D'Arcangelo A, Gazzerro P, Medici N, Moncharmont B, et al. The Zn-finger domain of RIZ protein promotes MCF-7 cell proliferation. *Cancer Lett* (2004) 215:229–37. doi: 10.1016/j.canlet.2004.05.014
42. Abbondanza C, De Rosa C, Ombra MN, Aceto F, Medici N, Altucci L, et al. Highlighting chromosome loops in DNA-picked chromatin (DPC). *Epigenetics* (2011) 6:979–86. doi: 10.4161/epi.6.8.16060
43. Bhat-Nakshatri P, Wang G, Collins NR, Thomson MJ, Geistlinger TR, Carroll JS, et al. Estradiol-regulated microRNAs control estradiol response in breast cancer cells. *Nucleic Acids Res* (2009) 37:4850–61. doi: 10.1093/nar/gkp500
44. Zhu H, Han C, Lu D, Wu T. miR-17-92 cluster promotes cholangiocarcinoma growth: evidence for PTEN as downstream target and IL-6/Stat3 as upstream activator. *Am J Pathol* (2014) 184:2828–39. doi: 10.1016/j.ajpath.2014.06.024
45. Messina S, Frati L, Leonetti C, Zuchegna C, Di Zazzo E, Calogero A, et al. Dual-specificity phosphatase DUSP6 has tumor-promoting properties in human glioblastomas. *Oncogene* (2011) 30:3813–20. doi: 10.1038/onc.2011.99
46. Castoria G, Barone MV, Di Domenico M, Bilancio A, Ametrano D, Migliaccio A, et al. Non-transcriptional action of oestradiol and progestin triggers DNA synthesis. *EMBO J* (1999) 18:2500–10. doi: 10.1093/emboj/18.9.2500
47. Rienzo M, Nagel J, Casamassimi A, Giovane A, Dietzel S, Napoli C. Mediator subunits: gene expression pattern, a novel transcript identification and nuclear localization in human endothelial progenitor cells. *Biochim Biophys Acta* (2010) 1799:487–95. doi: 10.1016/j.bbagrm.2010.05.001
48. Pfaffl MW. A new mathematical model for relative quantification in real-time RT-PCR. *Nucleic Acids Res* (2001) 29:e45. doi: 10.1093/nar/29.9.e45
49. Rienzo M, Schiano C, Casamassimi A, Grimaldi V, Infante T, Napoli C. Identification of valid reference housekeeping genes for gene expression analysis in tumor neovascularization studies. *Clin Transl Oncol* (2013) 15:211–8. doi: 10.1007/s12094-012-0904-1
50. Giovannelli P, Di Donato M, Auricchio F, Castoria G, Migliaccio A. Androgens Induce Invasiveness of Triple Negative Breast Cancer Cells Through AR/Src/PI3-K Complex Assembly. *Sci Rep* (2019) 9:4490. doi: 10.1038/s41598-019-41016-4
51. Donini CF, Di Zazzo E, Zuchegna C, Di Domenico M, D'Inzeo S, Nicolussi A, et al. The p85α regulatory subunit of PI3K mediates cAMP-PKA and retinoic acid biological effects on MCF7 cell growth and migration. *Int J Oncol* (2012) 40:1627–35. doi: 10.1155/2014/565839
52. Di Zazzo E, Feola A, Zuchegna C, Romano A, Donini CF, Bartollino S, et al. The p85 regulatory subunit of PI3K mediates cAMP-PKA and insulin biological effects on MCF-7 cell growth and motility. *Sci World J* (2014) 2014:565839. doi: 10.1155/2014/565839
53. Nga NTH, Ngoc TTB, Trinh NTM, Thuoc TL, Thao DTP. Optimization and application of MTT assay in determining density of suspension cells. *Anal Biochem* (2020) 610:113937. doi: 10.1016/j.ab.2020.113937
54. Di Donato M, Cernera G, Migliaccio A, Castoria G. Nerve Growth Factor Induces Proliferation and Aggressiveness In Prostate Cancer Cells. *Cancers (Basel)* (2019) 11:784. doi: 10.3390/cancers11060784
55. Chua CW, Shibata M, Lei M, Toivanen R, Barlow LJ, Bergren SK, et al. Single luminal epithelial progenitors can generate prostate organoids in culture. *Nat Cell Biol* (2014) 16:951. doi: 10.1038/ncb3047
56. Ritchie ME, Phipson B, Wu D, Hu Y, Law CW, Shi W, et al. limma powers differential expression analyses for RNA-sequencing and microarray studies. *Nucleic Acids Res* (2015) 43:e47. doi: 10.1093/nar/gkv007
57. Baldi P, Long AD. A Bayesian framework for the analysis of microarray expression data: regularized t -test and statistical inferences of gene changes. *Bioinformatics* (2001) 17:509–19. doi: 10.1093/bioinformatics/17.6.509
58. Huang DW, Sherman BT, Lempicki RA. Bioinformatics enrichment tools: paths toward the comprehensive functional analysis of large gene lists. *Nucleic Acids Res* (2009) 37:1–13. doi: 10.1093/nar/gkn923
59. Huang DW, Sherman BT, Lempicki RA. Systematic and integrative analysis of large gene lists using DAVID bioinformatics resources. *Nat Protoc* (2009) 4:44–57. doi: 10.1038/nprot.2008.211
60. Fabregat A, Jupe S, Matthews L, Sidiropoulos K, Gillespie M, Garapati P, et al. The Reactome Pathway Knowledgebase. *Nucleic Acids Res* (2018) 46(D1):D649–55. doi: 10.1093/nar/gkx1132
61. Edgar R, Domrachev M, Lash AE. Gene Expression Omnibus: NCBI gene expression and hybridization array data repository. *Nucleic Acids Res* (2002) 30:207–10. doi: 10.1093/nar/30.1.207
62. Gjorevski N, Sachs N, Manfrin A, Giger S, Bragina ME, Ordóñez-Morán P, et al. Designer matrices for intestinal stem cell and organoid culture. *Nature* (2016) 539:560–4. doi: 10.1038/nature20168
63. Medema RH. Optimizing RNA interference for application in mammalian cells. *Biochem J* (2004) 380:593–603. doi: 10.1042/BJ20040260
64. Elbashir SM, Harborth J, Lendeckel W, Yalcin A, Weber K, Tuschl T. Duplexes of 21-nucleotide RNAs mediate RNA interference in cultured mammalian cells. *Nature* (2001) 411:494–8. doi: 10.1371/journal.pone.0048057
65. Filhol O, Ciais D, Lajaunie C, Charbonnier P, Foveau N, Vert JP, et al. DSIR: assessing the design of highly potent siRNA by testing a set of cancer-relevant target genes. *PloS One* (2012) 7:e48057. doi: 10.1371/journal.pone.0048057

66. Lal G, Padmanabha L, Smith BJ, Nicholson RM, Howe JR, O'Dorisio MS, et al. RIZ1 is epigenetically inactivated by promoter hypermethylation in thyroid carcinoma. *Cancer* (2006) 107:2752–9. doi: 10.1002/cncr.22325
67. Schrock MS, Stromberg BR, Scarberry L, Summers MK. APC/C ubiquitin ligase: functions and mechanisms in tumorigenesis. *Semin Cancer Biol* (2020) 67:80–91. doi: 10.1016/j.semcancer.2020.03.001
68. Marino MM, Rega C, Russo R, Valletta M, Gentile MT, Esposito S, et al. Interactome mapping defines BRG1, a component of the SWI/SNF chromatin remodeling complex, as a new partner of the transcriptional regulator CTCF. *J Biol Chem* (2019) 294:861–73. doi: 10.1074/jbc.RA118.004882
69. Casamassimi A, Federico A, Rienzo M, Esposito S, Ciccodicola A. Transcriptome Profiling in Human Diseases: New Advances and Perspectives. *Int J Mol Sci* (2017) 18:E1652. doi: 10.3390/ijms18081652
70. Cuddapah S, Jothi R, Schones DE, Roh TY, Cui K, Zhao K. Global analysis of the insulator binding protein CTCF in chromatin barrier regions reveals demarcation of active and repressive domains. *Genome Res* (2009) 19:24–32. doi: 10.1101/gr.082800.108
71. Wang H, Maurano MT, Qu H, Varley KE, Gertz J, Pauli F, et al. Widespread plasticity in CTCF occupancy linked to DNA methylation. *Genome Res* (2012) 22:1680–8. doi: 10.1101/gr.136101.111
72. Stadler MB, Murr R, Burger L, Ivanek R, Lienert F, Schöler A, et al. DNA-binding factors shape the mouse methylome at distal regulatory regions. *Nature* (2011) 480:490–5. doi: 10.1038/nature10716
73. Wiehle L, Thorn GJ, Raddatz G, Clarkson CT, Rippe K, Lyko F, et al. DNA (de)methylation in embryonic stem cells controls CTCF-dependent chromatin boundaries. *Genome Res* (2019) 29:750–61. doi: 10.1101/gr.239707.118
74. Galli GG, Carrara M, Francavilla C, de Lichtenberg KH, Olsen JV, Calogero RA, et al. Genomic and proteomic analyses of Prdm5 reveal interactions with insulator binding proteins in embryonic stem cells. *Mol Cell Biol* (2013) 33:4504–16. doi: 10.1128/MCB.00545-13
75. Tang J, Kong D, Cui Q, Wang K, Zhang D, Gong Y, et al. Prognostic Genes of Breast Cancer Identified by Gene Co-expression Network Analysis. *Front Oncol* (2018) 8:374. doi: 10.3389/fonc.2018.00374
76. Fujita J, Sakurai T. The Oncoprotein Gankyrin/PSMD10 as a Target of Cancer Therapy. *Adv Exp Med Biol* (2019) 1164:63–71. doi: 10.1007/978-3-030-22254-3_5
77. Wang Y, Han T, Gan M, Guo M, Xie C, Jin J, et al. A novel function of anaphase promoting complex subunit 10 in tumor progression in non-small cell lung cancer. *Cell Cycle* (2019) 18:1019–32. doi: 10.1080/15384101.2019.1609830
78. Drouet Y, Treilleux I, Viari A, Léon S, Devouassoux-Shisheboran M, Voirin N, et al. Integrated analysis highlights APC11 protein expression as a likely new independent predictive marker for colorectal cancer. *Sci Rep* (2018) 8:7386. doi: 10.1038/s41598-018-25631-1

Conflict of Interest: The authors declare that the research was conducted in the absence of any commercial or financial relationships that could be construed as a potential conflict of interest.

frontiers in Cell and Developmental Biology

ORIGINAL RESEARCH
published: 01 February 2021
doi: 10.3389/fcell.2021.620883

Temozolomide Treatment Induces HMGB1 to Promote the Formation of Glioma Stem Cells via the TLR2/NEAT1/Wnt Pathway in Glioblastoma

Xiang-Yu Gao[1,2†], Jian Zang[1†], Min-Hua Zheng[3†], Yu-Fei Zhang[1†], Kang-Yi Yue[1,2], Xiu-Li Cao[3], Yuan Cao[1,2], Xin-Xin Li[4], Hua Han[1], Xiao-Fan Jiang[2*] and Liang Liang[1*]*

[1] State Key Laboratory of Cancer Biology, Department of Biochemistry and Molecular Biology, Fourth Military Medical University, Xi'an, China, [2] Department of Neurosurgery, Xijing Hospital, Fourth Military Medical University, Xi'an, China, [3] Department of Medical Genetics and Developmental Biology, Fourth Military Medical University, Xi'an, China, [4] Institute of Medical Research, Northwestern Polytechnical University, Xi'an, China

Formation of glioma stem cells (GSCs) is considered as one of the main reasons of temozolomide (TMZ) resistance in glioma patients. Recent studies have shown that tumor microenvironment-derived signals could promote GSCs formation. But the critical molecule and underlying mechanism for GSCs formation after TMZ treatment is not entirely identified. Our study showed that TMZ treatment promoted GSCs formation by glioma cells; TMZ treatment of biopsy-derived glioblastoma multiforme cells upregulated HMGB1; HMGB1 altered gene expression profile of glioma cells with respect to mRNA, lncRNA and miRNA. Furthermore, our results showed that TMZ-induced HMGB1 increased the formation of GSCs and when HMGB1 was downregulated, TMZ-mediated GSCs formation was attenuated. Finally, we showed that the effect of HMGB1 on glioma cells was mediated by TLR2, which activated Wnt/β-catenin signaling to promote GSCs. Mechanistically, we found that HMGB1 upregulated NEAT1, which was responsible for Wnt/β-catenin activation. In conclusion, TMZ treatment upregulates HMGB1, which promotes the formation of GSCs via the TLR2/NEAT1/Wnt pathway. Blocking HMGB1-mediated GSCs formation could serve as a potential therapeutic target for preventing TMZ resistance in GBM patients.

Keywords: high mobility group box 1, glioma stem cell, TLR2, Wnt, NEAT1, temozolomide

OPEN ACCESS

Edited by:
Marco Mina,
Sophia Genetics, Switzerland

Reviewed by:
Anup Kumar Singh,
City of Hope, United States
Gabriele Multhoff,
Technical University of Munich, Germany

****Correspondence:***
Liang Liang
lliang2@fmmu.edu.cn
Xiao-Fan Jiang
jiangxf@fmmu.edu.cn
Hua Han
huahan_biochem8796@163.com

† These authors have contributed equally to this work

Specialty section:
This article was submitted to Molecular and Cellular Oncology, a section of the journal Frontiers in Cell and Developmental Biology

Received: *24 October 2020*
Accepted: *08 January 2021*
Published: *01 February 2021*

Citation:
Gao X-Y, Zang J, Zheng M-H, Zhang Y-F, Yue K-Y, Cao X-L, Cao Y, Li X-X, Han H, Jiang X-F and Liang L (2021) Temozolomide Treatment Induces HMGB1 to Promote the Formation of Glioma Stem Cells via the TLR2/NEAT1/Wnt Pathway in Glioblastoma. Front. Cell Dev. Biol. 9:620883. doi: 10.3389/fcell.2021.620883

INTRODUCTION

Glioblastoma multiforme (GBM) is the most common primary brain tumor with the average survival of only about 15 months in patients receiving appropriate treatment (Stupp et al., 2005, 2009). The recognized treatment at present is surgical resection followed by adjuvant therapies such as radiotherapy and chemotherapy (Stupp et al., 2005). Temozolomide (TMZ) is one of the few medicines with a proven efficiency against GBM by inducing tumor cell death via methylating DNA (Ma et al., 2016). However, TMZ treatment also results in drug resistance, contributing

to unsatisfactory prognosis for glioma patients. The mechanism of TMZ resistance reported so far is related to the heterogeneity of glioma cells, upregulation of O6-methylguanine DNA methyltransferase (MGMT), DNA repair, and signal transducer and activator of transcription 3 (STAT3) (Pajonk et al., 2010; Happold et al., 2012; Kohsaka et al., 2012).

Cancer stem-like cells (CSCs) are cancer cells that possess certain degree of stemness, including the ability to self-renew, proliferate, differentiate into more "mature" tumor cells with differentiated properties, and initiate tumorigenic process at high efficiency (Clarke, 2005; Batlle and Clevers, 2017). An important characteristic of CSCs is resistance to radiotherapy and chemotherapy (Olivares-Urbano et al., 2020; Sun et al., 2020; Walcher et al., 2020). Multiple studies have confirmed the existence of CSCs, or glioma stem cells (GSCs), in GBM (Lathia et al., 2015; Hira et al., 2018; Ma et al., 2018). GSCs constitute a rare cell subpopulation with stem cell characteristics in GBM, which are highly similar to neural stem cells (Ignatova et al., 2002; Singh et al., 2003). There is a consensus that GSCs are the main cause of tumor recurrence after chemotherapy with TMZ (Jiapaer et al., 2018). In addition, studies have reported that metabolites and cytokines secreted by tumor cells can regulate the tumor-initiating ability of GSCs and thus mediate resistance to TMZ (Calabrese et al., 2007; Li et al., 2009). However, the potential mechanism of GSCs formation and resistance to TMZ remains to be elucidated.

At present, the origin of CSCs is not yet fully understood. Recent studies have shown that tumor microenvironment (TME), which is composed of immune cells, perivascular cells, fibroblasts and factors secreted by these cells, can provide extracellular signals for the generation and maintenance of CSCs (Dzobo et al., 2020). It was recently reported that chemotherapy could cause immunogenic cell death (ICD) of tumor cells, which release damage-associated molecular patterns (DAMPs) into TME (Inoue and Tani, 2014). Secreted DAMPs as a result of ICD include high-mobility group box 1 (HMGB1), adenosine triphosphate (ATP), heat-shock proteins and calreticulin. HMGB1 is a highly conserved protein and expressed in many cell types (Sims et al., 2010). In the extracellular environment, HMGB1 can exert various biological functions by binding to high-affinity receptors including Toll-like receptor (TLR) 2, TLR4, TLR9, and the receptor for advanced glycation end-products (RAGE) (Angelopoulou et al., 2016). Additionally, HMGB1 derived from tumor cells or TME could promote the CSCs phenotype in lung, colon, pancreatic cancer cells (Zhao et al., 2017; Qian et al., 2019; Zhang et al., 2019). HMGB1 has also been reported to be upregulated in GBM and played a significant role in proliferation, apoptosis, migration, and invasion of GBM (Wang X. et al., 2015; Angelopoulou et al., 2016). Our recent study has shown that HMGB1 could promote the GSCs phenotype. However, the biological effects of HMGB1 on GSCs have not been studied in detail. In this study, we show that TMZ treatment upregulates HMGB1 in GBM cells *in vitro*. HMGB1 mediates the effect of TMZ in inducing the formation of GSCs via TLR2/NEAT1/Wnt/β-catenin signaling, thus might promote the resistance to TMZ in GBM patients.

MATERIALS AND METHODS

Culture of Biopsy-Derived GBM Cells

Culture of biopsy-derived GBM cells has been described previously (Zang et al., 2020). Tumor tissues were collected from GBM patients accepting neurosurgery at Xijing Hospital, with signed informed consent and approved by the Ethics Committee of Xijing Hospital for use of human samples. Tumor tissues were dispersed and cultured in Dulbecco's modified Eagle's medium (DMEM)/F12 (1:1) (Invitrogen, Carlsbad, CA) supplemented with 10% fetal bovine serum (FBS, Invitrogen) and 1% penicillin–streptomycin solution. Cells were cultured for three passages and then frozen for further use. To culture GSCs, GBM cells were seeded in low adhesion plates (Corning Inc., Corning, NY) and cultured under the neurosphere condition in DMEM/F12 with 20 ng/mL epidermal growth factor (EGF, Peprotech, Rocky Hill, NJ), 10 ng/mL basic fibroblast growth factor (bFGF, Peprotech), B27 (1:50, Invitrogen), N2 (1:100, Invitrogen) and 1% penicillin–streptomycin solution for 7 days, and the number and size of tumor spheres were quantified. For re-plating, spheres were dispersed by Accutase (Invitrogen), counted, and cultured as above for 7 days. For differentiation, spheres were dissociated by Accutase into single cells and cultured in DMEM/F12 median supplemented with 10% FBS for 5 days. Cells were treated with TMZ (300 μM, MedChem Express, Monmouth Junction, NJ) for 48 h. In other cases, cells were treated with recombinant human HMGB1 (rhHMGB1, R&D Systems, Minneapolis, MN) at different concentrations (0, 200, 400, 600, 800, 1,000 ng/ml) for 48 h.

Transfection of Cells With siRNA

siRNA against targeted genes and negative control siRNA (siCtrl) were designed and synthesized by RiboBio (Guangzhou, China). GBM cells were transfected with 10 nM of siRNA using Lipofectamine 2000 (Life Technologies) following the manufacturer's protocol. Cells were re-plated for tumor sphere assay 48 h after the transfection, or for RNA and protein extraction. The sequences of the siRNA used are listed as followed: HMGB1-siRNA1, 5′- GAGGCCUCCUUCGGCCUUC and 5′- GAAGGCCGAAGGAGGCCUC; HMGB1-siRNA2, 5′-GUUGGUUCUAGCGCAGUUU and 5′- AAACUGCGCUAGAACCAAC; TLR2-siRNA1, 5′-GCCCUCUCUACAAACUUUATT and 5′-UAAAGUUUGUAGAGAGGGCTT; TLR2-siRNA2, 5′-GCCUUGACCUGUCCAACAATT and 5′-UUGUUGGACAGGUCAAGGCTT; β-catenin-siRNA1, 5′- GACUACCAGUUGUGGUUAA and 5′- UUAACCACAACUGGUAGUC; β-catenin-siRNA2, 5′- GAUGGACAGUAUGCAAUGA and 5′-UCAUUGCAUAC; NEAT1-siRNA1, 5′- CGUCAGACUUGCAUACGCA and 5′- UGCGUAUGCAAGUCUGACG; NEAT1-siRNA2, 5′- GACCACUUAAGACGAGAUU and 5′- AAUCUCGUCUUAAGUGGUC.

Immunofluorescence

Cells were fixed in 4% paraformaldehyde (PFA) for 10 min and blocked with 1% bovine serum albumin (BSA) for 30 min. Rabbit anti-HMGB1 (1:500, Abcam, Cambridge, UK), mouse anti-MAP2 (1:1,000, Sigma, St. Louis, MO), rabbit anti-GFAP

(1:500, Sigma) and mouse anti-O4 (1:100, Sigma) were used as primary antibodies. Secondary antibodies included Cy2-conjugated donkey anti-mouse (1:500) and Cy2-conjugated donkey anti-rabbit (1:500, Jackson ImmunoResearch, West Grove, PA). Samples were examined under a fluorescence microscope (FV-100, Olympus, Japan).

Flow Cytometry

Primary GBM cells were isolated and incubated with a PE anti-human CD133 (1:50, Biolegend, San Diego, CA) for 30 min at 4°C in dark. Then cells were analyzed by FACS using a FACS CaliburTM flow cytometer (BD Immunocytometry Systems, USA). Dead cells were excluded by propidium iodide (PI) staining. The acquired data were analyzed with FlowJo vX.0.6 software (Tree Star Inc., Ashland, OR).

Enzyme-Linked Immunosorbent Assay (ELISA)

HMGB1 in culture supernatants was determined with an ELISA kit (Chondrex, Redmond, WA) according to the manufacturer's instructions.

RNA-Sequencing (RNA-seq)

RNA-seq and data analyses were provided by commercial services (Gene Denovo Biotechnology, Guangzhou, China). RNA was extracted using the Trizol reagent (Thermo Fisher, Waltham, MA) and rRNA was removed. RNA samples were fragmented into appropriate short fragments, followed by reverse transcription with random hexamers, and second-strand cDNA synthesis. The cDNA fragments were purified with QiaQuick PCR extraction kit (Qiagen, Duesseldorf, Germany), end-repaired, and ligated to adapters. The uracil-N-glycosylase (UNG) was used to degrade the second-strand cDNA. The digested products were size-selected by agarose gel electrophoresis, PCR-amplified, and sequenced on Illumina HiSeq 3000 platform. Raw data of RNA-seq reported in this paper have been deposited in the Genome Sequence Archive in BIG Data Center (Beijing) under the accession number CRA003319, which is publicly accessible at https://bigd.big.ac.cn/gsa/.

For miRNA sequencing, RNA fragments of 18–30 nucleotides in length were enriched by polyacrylamide gel electrophoresis (PAGE). After adding 3' and 5' adapters, samples were subjected to RT-PCR, and PCR products with 140–160 bp size were enriched to generate a cDNA library and sequenced using Illumina Xten. Data analysis was performed using the OmicShare tools at www.omicshare.com/tools. The raw miRNA sequencing data generated from this study have been deposited in NCBI GEO (https://www.ncbi.nlm.nih.gov/geo) under the accession number GSE163504.

Bioinformatics

mRNA expression data of GBM were downloaded from The Cancer Genome Atlas (TCGA, $n = 162$, http://xena.ucsc.edu/getting-started/) and the Chinese Glioma Genome Atlas (CGGA, $n = 388$, http://www.cgga.org.cn) databases. Statistical analyses were performed using Pearson's correlation analysis. Gene set enrichment analysis (GSEA) was performed using GSEA v2.0 software (Broad Institute of MIT, MIT).

Quantitative Reverse Transcription-Polymerase Chain Reaction (qRT-PCR)

Total RNA was extracted using the TRIzol reagent. For mRNA analysis, cDNA was synthesized from 2 μg total RNA using PrimeScrip RT reagent kit (TaKaRa Biotechnology, Dalian, China). Quantitative PCR was performed on Applied Biosystems 7500 Real-time PCR system using a SYBR Premix Ex Taq Kit (Takara), with β-actin as a reference control. Primers are listed in **Supplementary Table 1**.

Western Blotting

Cells were lysed using the radio immunoprecipitation assay (RIPA) buffer (Beyotime, Shanghai, China) containing 10 mM phenylmethanesulfonyl fluoride (PMSF). Protein samples were separated by sodium dodecyl sulfate-12% polyacrylamide gel (SDS-PAGE) electrophoresis, and electro-transferred onto polyvinyl difluoride (PVDF) membranes (Millipore, Billerica, MA). Membranes were blocked with 5% skim milk for 1 h, and incubated with primary antibody at 4°C overnight followed by secondary antibody for 1 h at room temperature. Membranes were developed with enhanced chemiluminescence (ECL, Thermo Fisher) and detected using ChemiDoc Touch Imaging System (BioRad). Antibodies included β-actin (1:2,000, Santa Cruz Biotechnology), HMGB1 (1:1,000, Abcam), CD133 (1:1,000, Abcam), SOX2 (1:1,000, Abcam), OCT4 (1:1,000, Abcam), NANOG (1:1,000, Abcam), TLR2 (1:1,000, CST, Boston, MA), p-GSK-3β (1:1,000, CST), β-catenin (1:1,000, CST), c-MYC (1:1,000, SAB), HRP-conjugated goat anti-rabbit IgG (Genshare, Xian, China) and HRP-conjugated goat anti-mouse IgG (Genshare).

Subcutaneous Patient-Derived GBM Xenograft Model

All experiments involving mice were approved by the Animal Experiment Administration Committee of the Fourth Military Medical University. 5×10^6 patient-derived GBM cells suspended in 100 μL PBS were inoculated subcutaneously into the right forelimb interior root of BABL/c-A nude mice (female) at 4 weeks of age. About 7–8 days after cell implantation, the mice bearing tumor around 50 mm^3 were randomly divided into a control group, glycyrrhizin group, TMZ group or TMZ + glycyrrhizin group. Mice in the control group received equivalent drug vehicle (dimethyl sulfoxide, DMSO), mice in glycyrrhizin group received 10 mg/kg glycyrrhizin (SelleckChem, Houston TX, USA) five times per week for 2 weeks (intraperitioneal injection, i.p.), mice in TMZ group received 5 mg/kg TMZ five times per week for 3 weeks (i.p.), and mice in TMZ + glycyrrhizin group received 10 mg/kg glycyrrhizin five times per week for 2 weeks and also 5 mg/kg TMZ five times per week for 3 weeks (i.p.). Tumor volume was measured every 3 days with a caliper and calculated using the formula tumor volume (mm^3) = (length

$\times$ width^2) /2. About 24 days after the first treatment, all mice were euthanized and the tumor were carefully removed, weighed.

Statistics

All the statistical analyses were performed with Graph Pad Prism 7.0 software. The unpaired and two-tailed Student's *t*-test was used to determine the statistical significance between groups. All data were shown as the mean ± standard error of mean (SEM). $P < 0.05$ was considered statistically significant.

RESULTS

TMZ Treatment Promote GSCs Formation in Culture

To assess the effects of TMZ on GBM cells, biopsy-derived GBM cells were treated with TMZ (300 μM) for 48 h, followed by culturing in ultra-low adhesion plates under the neurosphere condition for 7 days. The result showed that TMZ treatment could promote the formation of tumor spheres in terms of sphere number and size (**Figure 1A**). The results of flow cytometry experiment showed that the surface expression level of CD133 in GBM cells was increased after TMZ treatment (**Figure 1B**). Analyses of qRT-PCR and western blotting showed that TMZ treatment increased the expression of CD133, SOX2, OCT4, and NANOG (**Figures 1C,D**), suggesting that TMZ treatment promotes GSCs formation in GBM cells.

TMZ Upregulates HMGB1 in GBM Cells

HMGB1, a well-known DAMP released by damaged cells, is reported to upregulate pluripotency-related genes in GBM cells (Zang et al., 2020). We then asked whether TMZ treatment could promote the expression of HMGB1. qRT-PCR and western blotting showed that TMZ upregulated HMGB1 in GBM cells at both mRNA and protein levels (**Figures 2A,B**). While most HMGB1 located in nuclei as visualized by immunofluorescence (**Supplementary Figure 1A**). The release of HMGB1 protein was significantly increased in the culture supernatants after TMZ treatment (**Figure 2C**). These results suggested that TMZ treatment induced GBM cell-derived HMGB1 in TME.

To explore the effect of HMGB1 on GBM cells, we compared transcriptomes of GBM cells treated with rhHMGB1 (800 ng/ml, 48 h) with the control (PBS-treated) by RNA-seq. Our result showed that HMGB1 treatment did not lead to dramatically transcriptional changes in GBM cells, as suggested by the principal component analysis (PCA) (**Supplementary Figure 1B**). However, a total of 115 upregulated and 104 downregulated encoding genes were still detected in GBM cells treated with HMGB1 (**Figure 2D**). Gene pathway enrichment analysis displayed pathways that are potentially activated by HMGB1 (**Figure 2E**), some of which have been demonstrated in experiments reported previously (Lin et al., 2016; Meng et al., 2018; Xu et al., 2019). We also identified 107 upregulated and 114 downregulated lncRNAs, as well as a group of differentially expressed miRNAs in GBM cells after HMGB1 treatment (**Figures 2F,G**). These results suggested that GBM cells are targets of TME-derived HMGB1.

HMGB1 Promotes the Formation of GSCs

GSEA analysis showed that HMGB1 upregulated pluripotency-related genes in GBM cells (**Supplementary Figures 1C,D**), consistent with previously reports (Zang et al., 2020). We then cultured GBM cells with different concentrations of HMGB1, and determined the formation of tumor spheres under the neural sphere culture condition. The result showed that the number and size of tumor spheres increased proportionally with increasing HMGB1 concentrations (**Figure 3A**; **Supplementary Figure 1E**). Re-plating assay showed that the number and the size of tumor spheres increased consistently in different passages (**Figure 3A**; **Supplementary Figure 1E**). To confirm the stemness of tumor spheres derived from GBM cells stimulated by HMGB1, we cultured dispersed tumor spheres adherently in the presence of serum. The result of immunofluorescence showed that these tumor spheres were able to differentiate into MAP2$^+$ neurons, O4$^+$ oligodendrocytes and GFAP$^+$ astrocytes (**Figure 3B**). In addition, qRT-PCR and western blotting showed that the expression of GSCs marker CD133 and pluripotency factors including SOX2, OCT4 and NANOG were upregulated proportionally in GBM cells treated with increasing HMGB1 concentrations (**Figures 3C,D**). Analysis of GBM data from TCGA and CGGA databases showed that HMGB1 expression was positively correlated with CD133, SOX2 and OCT4 expression (**Supplementary Figure 2A**). These results indicated HMGB1 promotes GSCs formation in cultured GBM cells.

TMZ Promote GSCs Formation by Upregulating HMGB1

We then asked whether TMZ treatment could promote GSCs formation by upregulating HMGB1. We transfected GBM cells with HMGB1 or Ctrl siRNAs (**Supplementary Figures 2B,C**), and collected culture supernatants. GBM cells were cultured with supernatants derived from siCtrl- or siHMGB1-transfected GBM cells in the presence of TMZ for 48 h. The results of qRT-PCR and western blotting showed that supernatant from siCtrl-transfected GBM cells could promote the expression of CD133, SOX2, OCT4, and NANOG, compared to siHMGB1-transfected GBM cells (**Figures 4A,B**). The *in vivo* effect of TMZ induced HMGB1 was further explored by xenograft GBM models in nude mice. Glycyrrhizin, a direct HMGB1 inhibitor (Mollica et al., 2007), and TMZ were injected in nude mice with tumors as described above. Compared with the control group, TMZ group had much smaller tumor volume since day 18 after first treatment and this difference became more obvious over time. Average tumor volume of the TMZ + glycyrrhizin group was strikingly smaller than TMZ group since day 21 (**Figure 4C**). Consistent with alternation in tumor volume, the average tumor weights at the end of vivo experiment in TMZ group were much smaller than that of the control group and greatly larger than that of TMZ + glycyrrhizin group (**Figure 4D**). The data of vivo experiment indicated that the combination of TMZ and glycyrrhizin exerted a much stronger growth-inhibitory effect on patient-derived GBM xenograft models. In addition, we analyzed the published sequencing data of glioblastoma treated with TMZ and compared them

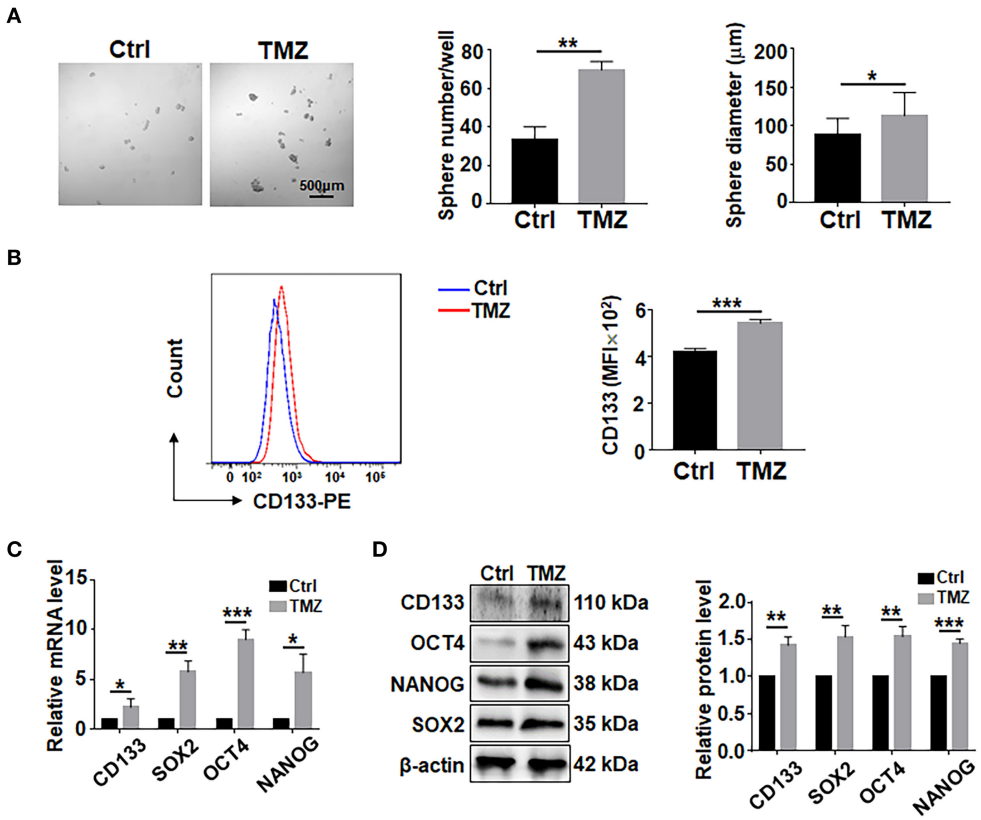

FIGURE 1 | TMZ treatment promote GSCs formation in culture. **(A)** Primary GBM cells were treated with TMZ for 48 h, and then cultured under the neurosphere condition for 7 days and photographed. Number and diameter of spheres on day 7 were quantified. Cell not treated with TMZ were used as controls. **(B)** Primary GBM cells treated with TMZ for 48 h were analyed by flow cytometry for CD133 ($n = 3$), MFI, mean fluorescence intensity. **(C)** Expression of stemness-related factors in primary glioma cells after TMZ stimulation was determined by qRT-PCR ($n = 3$). **(D)** Expression of stemness-related factors in primary glioma cells after TMZ stimulation was determined by western blot ($n = 3$). Data are represented as mean ± SEM, $^{*}P < 0.05$; $^{**}P < 0.01$; $^{***}P < 0.001$.

with our sequencing data (Chen et al., 2017; Li et al., 2018; Huang K. et al., 2019; Guo et al., 2020). We found that there were 35 protein-coding genes and 9 miRNAs (miR-23, miR-34, miR-106, miR-142, miR-148, miR-580, miR-590, miR-652 and miR-4454) in the two sets of sequencing data that exhibited similar alterations (**Supplementary Figure 3A**). Furthermore, 11 out of the top 50 signaling pathways displayed overlapping activity in the two sets of data as the shown KEGG analysis (**Supplementary Figure 3B**). These results were consistent with that glioblastoma cells released HMGB1 into extracellular space after TMZ treatment and HMGB1 in TME could increase the formation of GSCs.

TLR2 Mediates HMGB1-Induced GSCs Formation

To investigate signaling pathways mediating HMGB1-induced GSCs formation. TLR2, TLR4, TLR9, and RAGE are the most common receptors of HMGB1 and have been identified in GBM cells (Angelopoulou et al., 2016). Because HMGB1 has been shown to exhibit autocrine activity, we examined the effect of HMGB1 on the expression of different receptors in GBM cells. qRT-PCR analyses showed that TLR2, TLR4, TLR9 and RAGE were accumulated in GBM cells treated with HMGB1 at a concentration of 800 ng/ml, and the expression of TLR2 increased most remarkably (**Figure 5A**). Consistently, the protein level of TLR2 was upregulated when GBM cells were treated with HMGB1 (**Figure 5B**). In addition, in gene expression profiling of GBM reported in TCGA and CGGA databases, higher levels of TLR2 correlated with a decrease in median survival of GBM patients and TLR2 was positively correlated with the expression of CD133, SOX2 and OCT4 (**Supplementary Figures 4A,B**), consistent with previous studies (Chen et al., 2019). We therefore focused our study on TLR2 and siRNAs targeting TLR2 were synthesized. Then we stimulated GBM cells, which were transfected with TLR2 siRNAs, by HMGB1. The results indicated that the mRNA and protein levels of CD133, SOX2, OCT4, and NANOG were downregulated when TLR2 was knocked down (**Figures 5C–E**). Consistently, the number and the size of tumor spheres decreased significantly by TLR2 siRNAs compared with the negative control (**Figure 5F**). Our data suggested that HMGB1 might promote GSCs formation via TLR2.

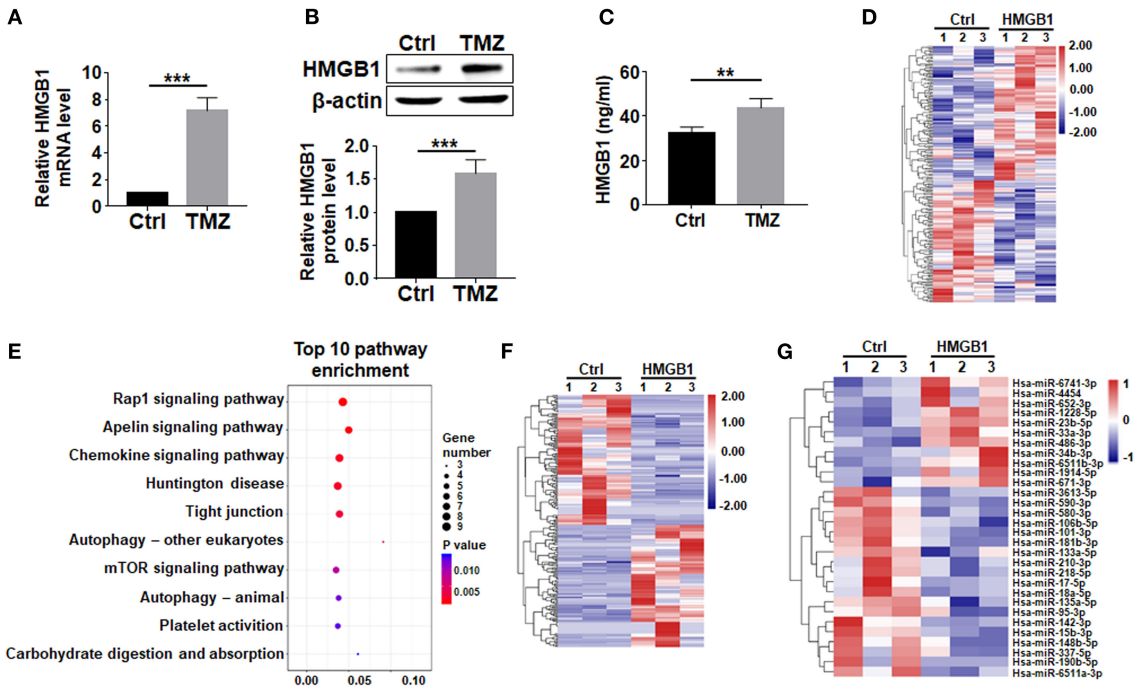

FIGURE 2 | TMZ upregulates HMGB1 in GBM cells. **(A)** Expression of HMGB1 in glioma cells from a single GBM biopsy after TMZ stimulation was determined by qRT-PCR ($n = 5$). **(B)** Expression of HMGB1 in glioma cells from a single GBM biopsy after TMZ stimulation was determined by western blot ($n = 5$). **(C)** ELISA-based analysis of the HMGB1 concentration in the culture supernatants of glioma cells from a single GBM biopsy at 48 h ($n = 5$). **(D)** Heatmap of mRNA-seq analysis from a single GBM biopsy (GBM cells treated with 800 ng/ml rhHMGB1, $n = 3$; control GBM cells, $n = 3$). Two hundred and nineteen genes were identified with a cut-off of >1.2-fold for gene expression change and $p < 0.05$. **(E)** KEGG analysis was performed to identify differential pathway enrichment. **(F)** Heatmap of lncRNA-seq analysis from a single GBM biopsy (GBM cells treated with 800 ng/ml rhHMGB1, $n = 3$; control GBM cells, $n = 3$). Two hundred and twenty-one lncRNAs were identified with a cut-off of >1.2-fold for gene expression change and $p < 0.05$. **(G)** Heatmap of miRNA-seq analysis from a single GBM biopsy (GBM cells treated with 800 ng/ml rhHMGB1, $n = 3$; control GBM cells, $n = 3$). Thirty hsa-miRNAs were identified with a cut-off of >1.2-fold for gene expression change and $p < 0.05$. Data are represented as mean ± SEM, $^*P < 0.05$; $^{**}P < 0.01$; $^{***}P < 0.001$.

HMGB1 Promotes GSCs Formation via Wnt/β-Catenin Downstream to TLR2

To explore the potential pathway downstream to HMGB1-TLR2, we compared transcriptomes of GBM cells treated with HMGB1 and PBS. Bioinformatic analyses showed that several important molecules in the Wnt pathway were up-regulated, suggesting that Wnt/β-catenin pathway, which plays an important role in the regulation of stemness and tumorigenicity of GSCs (Gong and Huang, 2012), might be activated (**Figure 6A**). We then knocked down TLR2 in GBM cells in the presence of HMGB1, and determined the expression of Wnt/β-catenin signaling-related molecules by qRT-PCR and western blotting. The results confirmed that the expression of β-catenin, c-Myc, p-GSK-3β and LEF1 were upregulated in GBM cells in presence of HMGB1, and silencing TLR2 by siRNAs could attenuate this effect (**Figures 6B,C**), suggesting that HMGB1 activated Wnt signaling via TLR2. To further explore the role of Wnt/β-catenin signaling pathway in formation of GSCs in HMGB1-treated GBM cells, we synthesized siRNAs targeting β-catenin and transfected GBM cells stimulated by HMGB1. Analyses of qRT-PCR and western blotting showed that the expression of CD133, SOX2, OCT4 and NANOG were down-regulated by β-catenin siRNAs in the presence of HMGB1 (**Figures 6D,E**). Consistently, the number and the size of tumor spheres were attenuated significantly by β-catenin siRNAs compared with the negative control (**Figure 6F**). These results suggested that HMGB1-TLR2 promote GSCs formation by activating the Wnt/β-catenin signaling pathway.

LncRNA NEAT1 Is Required for the Formation of HMGB1 Induced GSCs

Comparison of transcriptomes of GBM cells treated with HMGB1 and PBS showed that the expression of NEAT1, a lncRNA reportedly playing important roles in GSCs (Gong et al., 2016; Yang et al., 2017; Lulli et al., 2020), was significantly upregulated (**Figure 7A**). qRT-PCR confirmed the proportional upregulation of NEAT1 in the presence of increasing concentrations of HMGB1 (**Figure 7B**). Silencing TLR2 by siRNA reduced the expression of NEAT1 in the presence of HMGB1 (**Figure 7C**). To confirm a potential role of NEAT1 in HMGB1-induced GSCs, we synthesized siRNA targeting NEAT1. The results showed that silencing NEAT1 by siRNAs reduced the mRNA and protein levels of CD133, SOX2, OCT4 and NANOG (**Figures 7D,E**). The number and size of tumor spheres decreased also upon NEAT1 knockdown (**Figure 7F**). We conclude that NEAT1 is required for HMGB1-induced GSCs formation. In addition, silencing NEAT1 by siRNA abrogated upregulation of

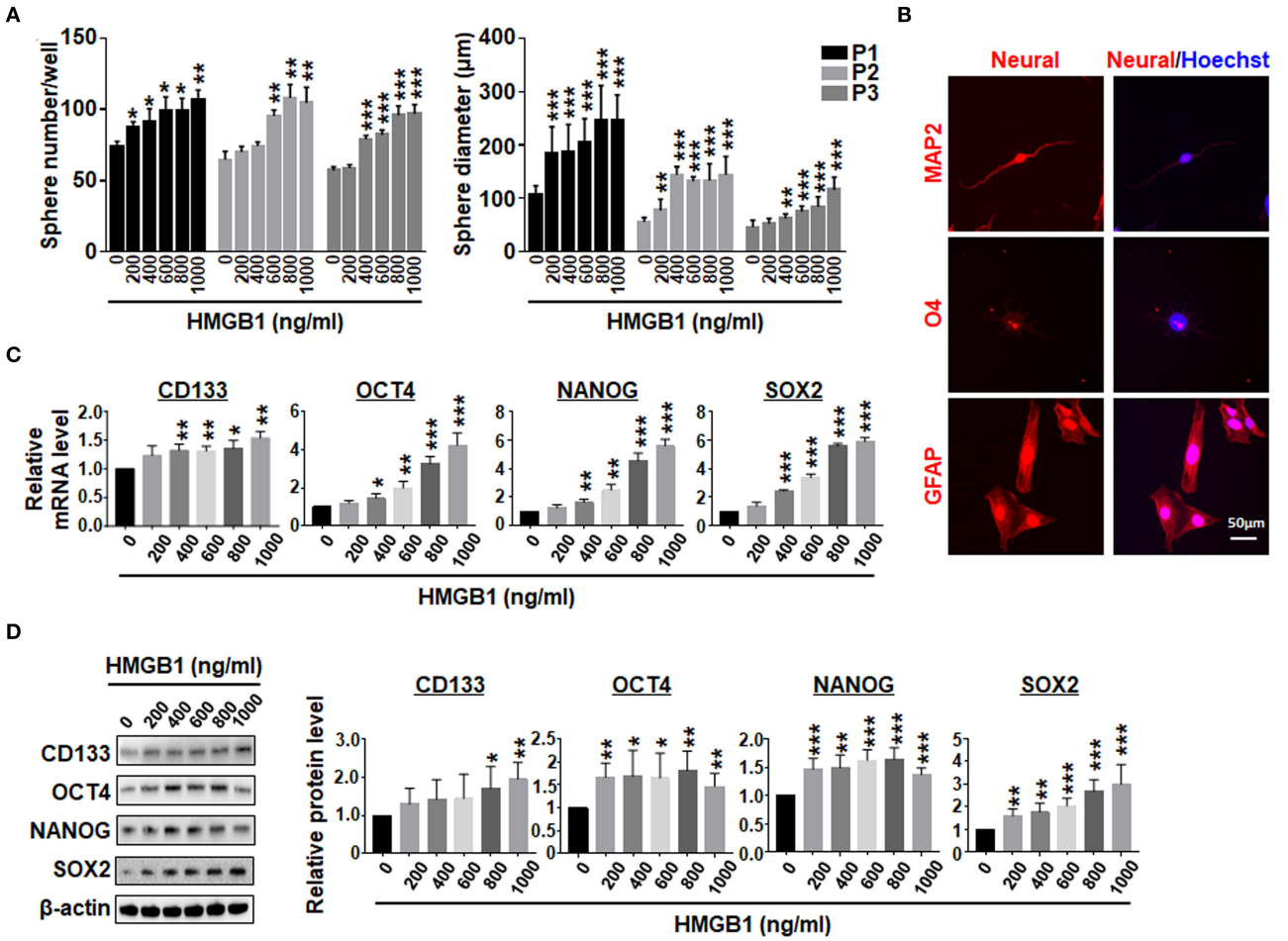

FIGURE 3 | HMGB1 promotes the formation of GSCs. **(A)** Primary GBM cells were cultured under the neurosphere condition with different concentration of HMGB1 for 7 days (P1). The tumor spheres were re-plated every 7 days for another 2 passages (P2, 3). Number and diameter of tumor spheres on day 7 were quantified. **(B)** Tumor spheres derived from HMGB1-induced or control primary glioma cells were subjected to differentiation culture for 7 days. The expression of markers of neurons (MAP-2), oligodendrocytes (O4) and astrocytes (GFAP) were determined by immunofluorescence, and counter-stained with Hoechst. **(C)** Expression of stemness-related factors in primary glioma cells treated with different concentration of HMGB1 was determined by qRT-PCR ($n = 3$). **(D)** Expression of stemness-related factors in primary glioma cells treated with different concentration of HMGB1 was determined by western blot ($n = 5$). Data are represented as mean ± SEM, $^*P < 0.05$; $^{**}P < 0.01$; $^{***}P < 0.001$.

β-catenin, c-Myc, p-GSK-3β and LEF1, as shown by qRT-PCR and western blotting, respectively (**Figures 7G,H**). Therefore, NEAT1 is downstream to TLR2 and activates Wnt/β-catenin in GBM cells to promote GSCs formation.

DISCUSSION

CSCs or tumor-initiating cells are considered as drivers of tumor growth and relapse, and are often identified in heterogeneous, aggressive and therapy-resistant tumors (Walcher et al., 2020). Although the mechanisms of CSCs for tumor growth, recurrence, and drug resistance have been well documented, the origin of CSCs is not entirely clear. One opinion suggests that CSCs can be generated under the pressure of chemotherapy and changes in TME, in other words, CSCs could originate from non-CSC tumor cells (De Angelis et al., 2019). GBM is the most common malignant tumor in the brain and there have been many reports demonstrating the existence of GSCs in GBM (Varghese et al., 2008). In the current study, we show that GBM-derived HMGB1 promote the formation of GSCs from patient-derived GBM cells treated with TMZ. Chemotherapy could cause ICD of tumor cells that release DAMPs into TME. DAMPs induced by ICD include heat shock protein 70 (HSP70), calreticulin, ATP and HMGB1 (Garg et al., 2015). TMZ could elevate the secretion of HSP70, calreticulin, ATP and HMGB1 in TME (Liikanen et al., 2013; Pasi et al., 2014). It has been reported that HSP70 and calreticulin are beneficial for glioma patients, while ATP could serve as a critical signaling molecule supporting glioblastoma growth (Jantaratnotai et al., 2009; Muth et al., 2016). Our results showed that TMZ could up-regulate the expression of HMGB1 in primary GBM cells and promote the release of HMGB1 into TME after TMZ treatment. Previous

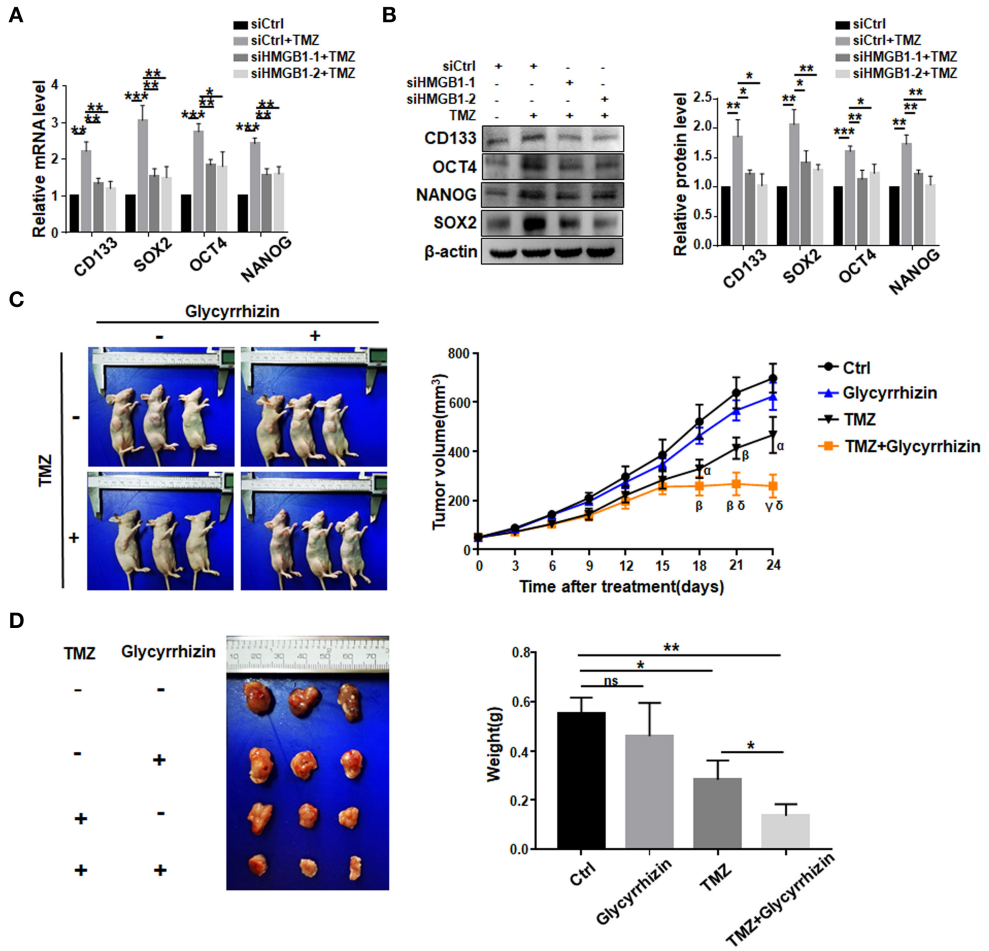

FIGURE 4 | TMZ promote GSCs formation by upregulating HMGB1. **(A,B)** qRT-PCR and western blot analysis of the expression level of stemness-related factors in primary GBM cells co-cultured with supertanant from the following cells: Ctrl siRNA; Ctrl siRNA + TMZ (300 μM); HMGB1 siRNA + TMZ (300 μM). **(C)** Images of subcutaneously xenograft glioma models in nude mice at day 24 after first treatment. Vivo tumor volume was measured every 3 days and the same day collected data were compared among groups. $\alpha < 0.05$, $\beta < 0.01$, $\gamma < 0.001$, compared to control group; $\delta < 0.05$, compared to TMZ group. **(D)** Images of glioma tumors taken from the mice of each group and the weight of the tumor is measured at day 24 after first treatment. Data are represented as mean ± SEM, $^{*}P < 0.05$; $^{**}P < 0.01$; $^{***}P < 0.001$.

studies have suggested that extracellular HMGB1 could enhance and maintain the stemness of CSCs in breast cancer, colorectal cancer and pancreatic cancer (Zhao et al., 2017; Qian et al., 2019; Zhang et al., 2019). Our study demonstrated for the pivotal role of HMGB1 in promoting GSCs formation in patient-derived primary glioma cells upon TMZ treatment. In addition, we analyzed the published sequencing data of glioblastoma treated with TMZ and compared them with our sequencing data (Chen et al., 2017; Li et al., 2018; Huang K. et al., 2019; Guo et al., 2020). We found that 35 protein-coding genes and nine miRNAs exhibited similar alterations in the two sets of sequencing data. Furthermore, 11 out of the top 50 signaling pathways displayed overlapping activity in the two sets of data as the shown KEGG analysis. These results further confirmed that glioblastoma cells released HMGB1 into extracellular space after TMZ treatment and HMGB1 in TME could increase the formation of GSCs. Serum HMGB1 level is quite low in glioma patients untreated or treated with TMZ (Liikanen et al., 2013; Kluckova et al., 2020), in contrast with HMGB1 in culture in our experiments. However, serum HMGB1 level could not represent HMGB1 in TME. It has been reported that HMGB1 expression was significantly higher in TME than in adjacent non-tumor tissues (Cheng et al., 2018). Referring to other published literatures (varying between 150 and 2,000 ng/ml. For instance, Zhao et al., 2017; Chen et al., 2019), we examined the effect of different concentrations of HMGB1 on GSCs, and used 800 ng/ml in most of our experiments, because with this concentration, HMGB1 induced significant stemness in glioma cells. To examine the role of HMGB1 *in vivo*, we established subcutaneous GBM xenograft models with patient-derived GBM cells, and observed the effect of glycyrrhizin, a HMGB1 inhibitor, on tumor growth. The results showed that glycyrrhizin reinforced the growth-inhibitory effect of TMZ on xenograft GBM, suggesting that HMGB1 plays an important role in promoting GBM growth in the presence of TMZ. Briefly, our

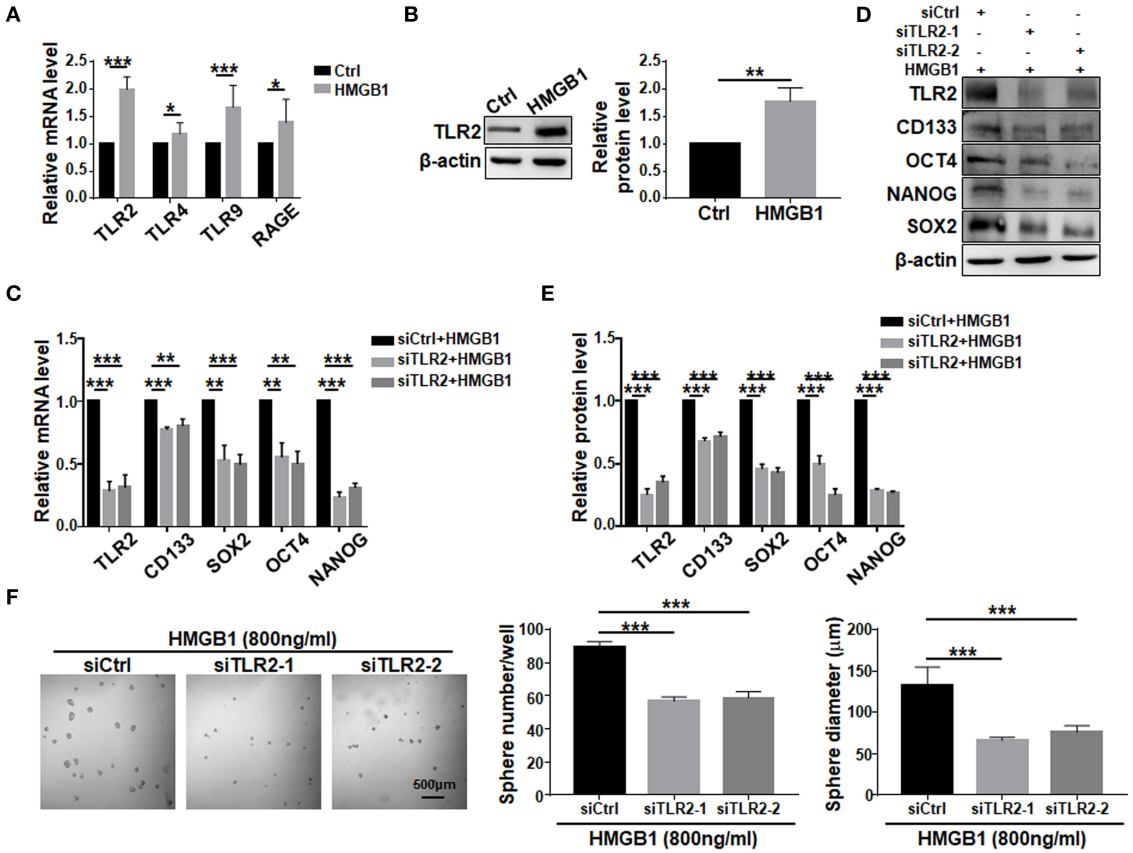

FIGURE 5 | TLR2 is required for HMGB1-induced GSCs formation. **(A)** Expression of TLR2, TLR4, TLR9, RAGE in primary glioma cells after HMGB1 stimulation (800 ng/ml) was determined by qRT-PCR ($n = 3$). **(B)** Expression of TLR2 in primary glioma cells after HMGB1 stimulation (800 ng/ml) was determined by western blot ($n = 3$). **(C)** qRT-PCR analyses of the levels of CD133, OCT4, SOX2, and NANOG in TLR2 knockdown primary GBM cells treated with 800 ng/ml rhHMGB1 ($n = 3$). **(D,E)** Western blot analyses of the levels of CD133, OCT4, SOX2, and NANOG in TLR2 knockdown primary GBM cells treated with 800 ng/ml rhHMGB1 ($n = 3$). **(F)** Primary glioma cells were treated with HMGB1 (800 ng/ml) and transfected with siRNAs to TLR2, and then cultured under the neurosphere condition for 7 d. Number and diameter of tumor spheres on day 7 were quantified. Data are represented as mean ± SEM, $^{*}P < 0.05$; $^{**}P < 0.01$; $^{***}P < 0.001$.

observations possess clinical significance, because recurrence of glioma after TMZ treatment has always been an urgent challenge in clinical treatment of GBM patients.

Currently, the clinical use of TMZ is 150–200 mg/mm^2. In *in vitro* experiment, considering drug absorption and metabolism, we could not directly use the *in vivo* dosage. The TMZ dosage we used in our experiments was the one that induces glioblastoma cell death in dose- and time-dependent manners *in vitro* (Chen et al., 2017; Huang W. et al., 2019). Glycyrrhizin, a direct HMGB1 inhibitor, reportedly could exert inhibitory effects on the proliferation of human glioblastoma U251 cell line (Li et al., 2014). Glycyrrhizin has been tested in the treatment of various diseases, such as psoriasis and vitiligo (Yu et al., 2017; Li et al., 2019), but not in the glioma. Our *in vivo* result showed that glycyrrhizin reinforced the growth-inhibitory effect of TMZ on xenograft GBM. Our study provided a significant research basis for performing further investigation on glycyrrhizin in glioma therapy and combining TMZ and glycyrrhizin might be considered as a future therapeutic strategy.

After being released into TME, HMGB1 needs to interact with its high-affinity receptors to elicit its biological functions. TLR2, TLR4, TLR9, and RAGE have been identified as the most common receptors for HMGB1 on cell surface in different cancer models and patients (Angelopoulou et al., 2016; Qian et al., 2019; Zhang et al., 2019). The effects of activating TLR2 on glioma cells are complicated and sometimes contradictory. Wang et al. reported that activation of TLR2 promotes tumor invasion by upregulating MMPs in glioma stem cells (Wang F. et al., 2015). Another study by Curtin et al. indicated that TLR2 activation could promote glioma regression (Curtin et al., 2009). According to our findings, TLR2 functions as the major receptor responsible for HMGB1-mediated GSCs formation in patient-derived GBM cells. TLR2 has been demonstrated to affect cancer cell behaviors by activating several downstream signaling pathways, including NF-kB, PI3K/Akt and Wnt/β-catenin pathways (Liu et al., 2018; Chen et al., 2019). Our results have shown that TLR2 participates in GSCs formation most likely via Wnt/β-catenin signaling, which is a classic pathway regulating

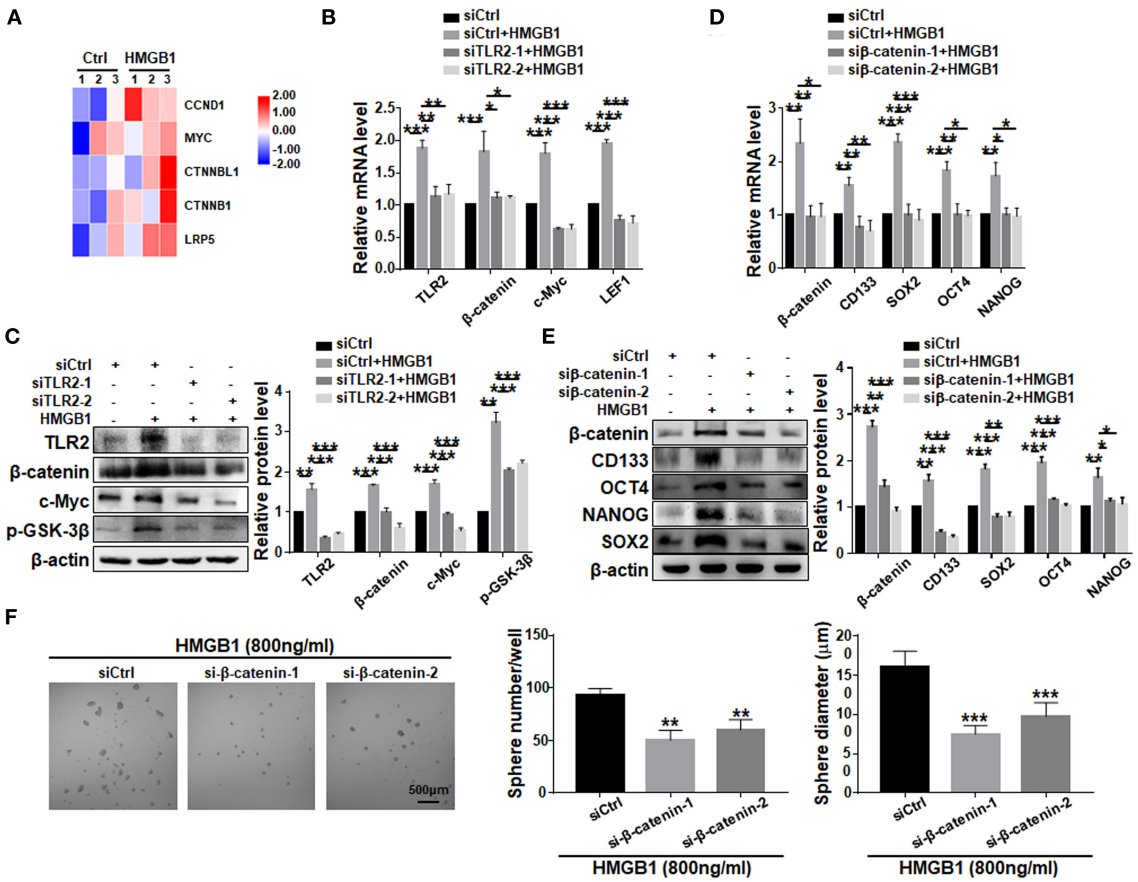

FIGURE 6 | HMGB1 promotes GSCs formation via the Wnt/β-catenin pathway downstream to TLR2. **(A)** Patient derived GBM cells treated with HMGB1 (800 ng/ml) and control GBM cells were subjected to RNA-seq. The expression of Wnt-associated genes is shown by a heatmap. **(B)** qRT-PCR analyses of the levels of TLR2, β-catenin, c-Myc and LEF1 in TLR2 knockdown primary GBM cells treated with 800 ng/ml rhHMGB1 ($n = 3$). **(C)** Western blot analyses of the levels of TLR2, β-catenin, c-Myc and p-GSK-3β in TLR2 knockdown primary GBM cells treated with 800 ng/ml rhHMGB1 ($n = 3$). **(D,E)** qRT-PCR and western blot analyses of the levels of β-catenin, CD133, OCT4, SOX2, and NANOG in β-catenin knockdown primary GBM cells treated with 800 ng/ml rhHMGB1 ($n = 3$). **(F)** Primary glioma cells were treated with HMGB1 (800 ng/ml) and transfected with siRNAs to β-catenin, and then cultured under the neurosphere condition for 7 d. Number and diameter of tumor spheres on day 7 were quantified. Data are represented as mean ± SEM, $^*P < 0.05$; $^{**}P < 0.01$; $^{***}P < 0.001$.

the pluripotency of stem cells and determines the fate of cell differentiation during development.

The nuclear paraspeckle assembly transcript 1 (NEAT1) is a long non-coding RNA, and is often highly expressed in human tumors with different origins. Clinical studies have shown that patients with high NEAT1 expression have a poor prognosis (Pan et al., 2015; Chen et al., 2016; Han et al., 2018). NEAT1 drives the occurrence and development of tumors by regulating genes associated with tumor cell growth, migration, invasion, stem-like phenotypes, and chemotherapeutic and radiological resistance. These characteristics indicate that NEAT1 has the potential to be a new diagnostic biomarker and therapeutic target (Dong et al., 2018). Additionally, NEAT1 is reported to be overexpressed in GSCs, and silencing the expression of NEAT1 in GSCs could weaken their capacity of proliferation, invasion and migration (Yang et al., 2017). In lung cancer cell lines, down-regulation of NEAT1 could decrease the expression of stemness-related factors, including CD133, CD44, SOX2, OCT4 and NANOG (Jiang et al., 2018). In our study, we have shown that NEAT1 is upregulated in GBM cells after HMGB1 stimulation, and knocking down NEAT1 could abrogate HMGB1-induced upregulation of stemness-related factors and GSCs formation. Mechanistically, some TME-derived signals, such as hypoxia, and activation of STAT3 and NF-κB induced by EGFR signaling could promote NEAT1 expression (Choudhry et al., 2015; Chen et al., 2018). In addition, Chen et al. reported that NEAT1 overexpression could induce the activity of the Wnt/β-catenin signaling to mediate tumorigenesis and progression in GBM (Chen et al., 2018). Consistently, our data have shown that upregulation of NEAT1 in GSCs in the presence of HMGB1 could be attributed to TLR2 activation, and NEAT1 could activate Wnt/β-catenin signaling to promote GSCs formation (**Supplementary Figure 4C**).

In conclusion, we have found that patient-derived GBM cells release HMGB1 into extracellular space after TMZ treatment, and HMGB1 in TME could increase the formation of GSCs,

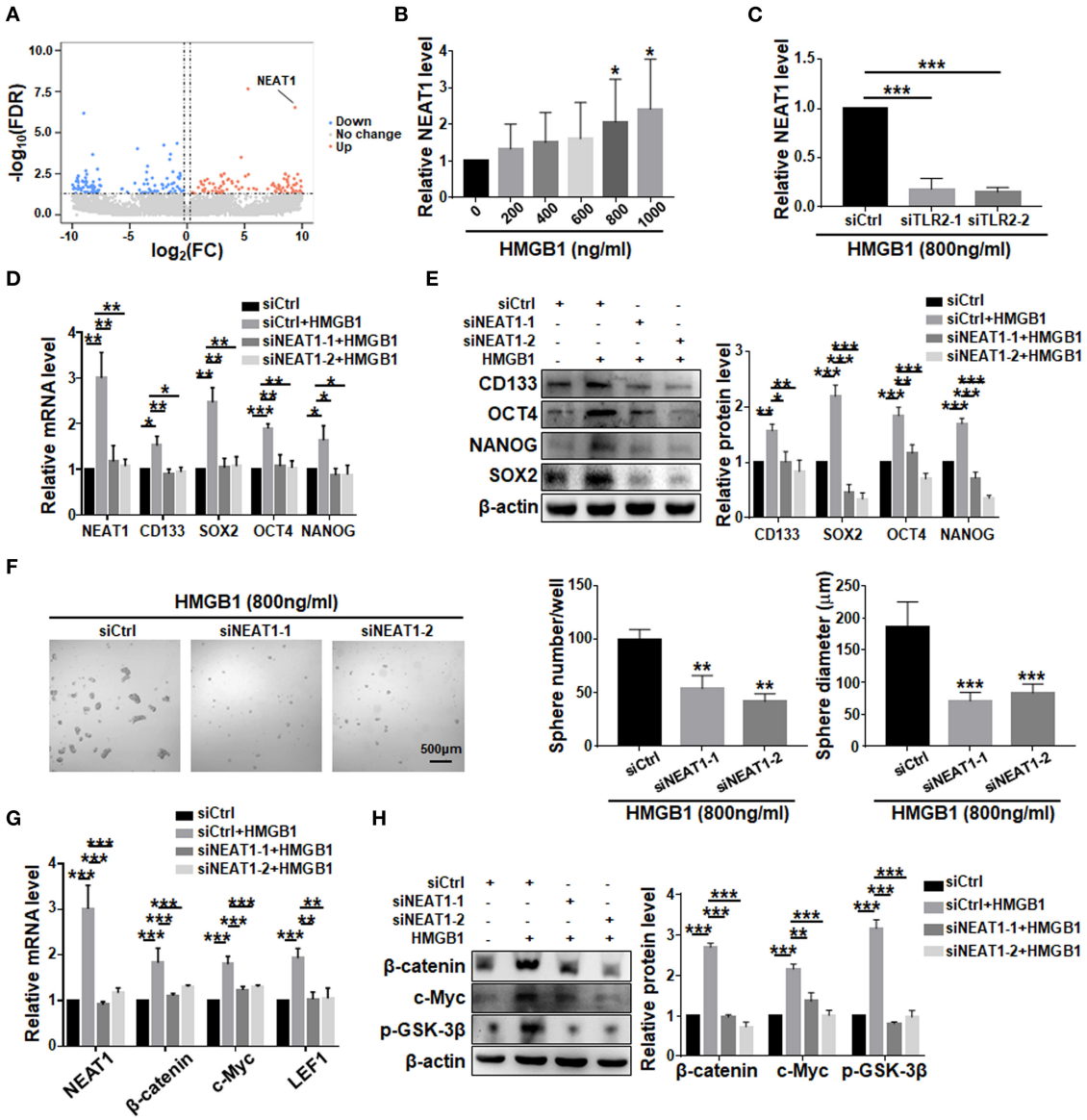

FIGURE 7 | LncRNA NEAT1 is required for the formation of HMGB1 induced GSCs. **(A)** Patient derived GBM cells treated with HMGB1 (800 ng/ml) and control GBM cells were subjected to lncRNA-seq. The expression level is shown by a heatmap. **(B)** Expression of NEAT1 in primary glioma cells treated with different concentration of HMGB1 was determined by qRT-PCR ($n = 6$). **(C)** qRT-PCR analyses of the levels of NEAT1 in TLR2 knockdown primary GBM cells treated with 800 ng/ml rhHMGB1 ($n = 3$). **(D,E)** qRT-PCR and western blot analyses of the levels of NEAT1, CD133, SOX2, OCT4 and NANOG in NEAT1 knockdown primary GBM cells treated with 800 ng/ml rhHMGB1. **(F)** Primary glioma cells were treated with HMGB1 (800 ng/ml) and transfected with siRNAs to NEAT1, and then cultured under the neurosphere condition for 7 d. Number and diameter of tumor spheres on day 7 were quantified. **(G)** qRT-PCR analyses of the levels of NEAT1, β-catenin, c-Myc and LEF1 in NEAT1 knockdown primary GBM cells treated with 800 ng/ml rhHMGB1 ($n = 3$). **(H)** Western blot analyses of the levels of β-catenin, c-Myc and p-GSK-3β in NEAT1 knockdown primary GBM cells treated with 800 ng/ml rhHMGB1 ($n = 3$). Data are represented as mean ± SEM, $^{*}P < 0.05$; $^{**}P < 0.01$; $^{***}P < 0.001$.

which further induce TMZ resistance. Mechanistically, HMGB1 upregulates lncRNA NEAT1, which is downstream to TLR2 and plays pivotal roles in GSCs formation likely by activating Wnt/β-catenin signaling. Our results provide a new potential strategy to overcome TMZ resistance in GBM patients. Combining TMZ and an HMGB1 inhibitor may be considered as a future therapeutic strategy.

DATA AVAILABILITY STATEMENT

The datasets presented in this study can be found in online repositories. The names of the repository/repositories and accession number(s) can be found in the article/**Supplementary Material**.

ETHICS STATEMENT

The studies involving human participants were reviewed and approved by Ethics Committee of Xijing Hospital. The patients/participants provided their written informed consent to participate in this study. The animal study was reviewed and approved by Ethics Committee of Xijing Hospital.

AUTHOR CONTRIBUTIONS

X-YG performed the experiments and wrote the manuscript. JZ, M-HZ, Y-FZ, and K-YY collected the data. HH, X-FJ, and LL designed the project. YC, X-XL, and X-LC analyzed the data. LL, X-XL, and HH revised the manuscript. All authors contributed to the article and approved the submitted version.

FUNDING

This study was supported by grants from the National Natural Science Foundation of China (31101054, 31730041, 81871023, 31671523). The experiments were fulfilled at the Postgraduate Innovative Research Center of the Fourth Military Medical University.

SUPPLEMENTARY MATERIAL

The Supplementary Material for this article can be found online at: https://www.frontiersin.org/articles/10.3389/fcell.2021.620883/full#supplementary-material

REFERENCES

Angelopoulou, E., Piperi, C., Adamopoulos, C., and Papavassiliou, A. (2016). Pivotal role of high-mobility group box 1 (HMGB1) signaling pathways in glioma development and progression. *J. Mol. Med.* 94, 867–874. doi: 10.1007/s00109-016-1435-y

Batlle, E., and Clevers, H. (2017). Cancer stem cells revisited. *Nat. Med.* 23, 1124–1134. doi: 10.1038/nm.4409

Calabrese, C., Poppleton, H., Kocak, M., Hogg, T., Fuller, C., Hamner, B., et al. (2007). A perivascular niche for brain tumor stem cells. *Cancer Cell* 11, 69–82. doi: 10.1016/j.ccr.2006.11.020

Chen, P., Shen, W., Shih, C., Ho, K., Cheng, C., Lin, C., et al. (2017). The CHAC1-inhibited Notch3 pathway is involved in temozolomide-induced glioma cytotoxicity. *Neuropharmacology* 116, 300–314. doi: 10.1016/j.neuropharm.2016.12.011

Chen, Q., Cai, J., Wang, Q., Wang, Y., Liu, M., Yang, J., et al. (2018). NEAT1Long noncoding RNA, regulated by the EGFR pathway, contributes to glioblastoma progression through the WNT/-catenin pathway by scaffolding EZH2. *Clin. Cancer Res.* 24, 684–695. doi: 10.1158/1078-0432.CCR-17-0605

Chen, X., Cheng, F., Liu, Y., Zhang, L., Song, L., Cai, X., et al. (2019). Toll-like receptor 2 and Toll-like receptor 4 exhibit distinct regulation of cancer cell stemness mediated by cell death-induced high-mobility group box 1. *EBioMedicine* 40, 135–150. doi: 10.1016/j.ebiom.2018.12.016

Chen, Z., Zhang, Z., Xie, B., and Zhang, H. (2016). Clinical significance of up-regulated lncRNA NEAT1 in prognosis of ovarian cancer. *Eur. Rev. Med. Pharmacol. Sci.* 20, 3373–3377.

Cheng, P., Ma, Y., Gao, Z., and Duan, L. (2018). High mobility group box 1 (HMGB1) predicts invasion and poor prognosis of glioblastoma multiforme via activating AKT signaling in an autocrine pathway. *Med. Sci. Monit.* 24, 8916–8924. doi: 10.12659/MSM.912104

Choudhry, H., Albukhari, A., Morotti, M., Haider, S., Moralli, D., Smythies, J., et al. (2015). Tumor hypoxia induces nuclear paraspeckle formation through HIF-2α dependent transcriptional activation of NEAT1 leading to cancer cell survival. *Oncogene* 34, 4482–4490. doi: 10.1038/onc.2014.378

Clarke, M. (2005). Self-renewal and solid-tumor stem cells. *Biol. Blood Marrow Transplant.* 11, 14–16. doi: 10.1016/j.bbmt.2004.11.011

Curtin, J., Liu, N., Candolfi, M., Xiong, W., Assi, H., Yagiz, K., et al. (2009). HMGB1 mediates endogenous TLR2 activation and brain tumor regression. *PLoS Med.* 6:10. doi: 10.1371/journal.pmed.1000010

De Angelis, M., Francescangeli, F., La Torre, F., and Zeuner, A. (2019). Stem cell plasticity and dormancy in the development of cancer therapy resistance. *Front. Oncol.* 9:626. doi: 10.3389/fonc.2019.00626

Dong, P., Xiong, Y., Yue, J., Hanley, S., Kobayashi, N., Todo, Y., et al. (2018). Long non-coding RNA NEAT1: a novel target for diagnosis and therapy in human tumors. *Front. Genet.* 9:471. doi: 10.3389/fgene.2018.00471

Dzobo, K., Senthebane, D., Ganz, C., Thomford, N., Wonkam, A., and Dandara, C. (2020). Advances in therapeutic targeting of cancer stem cells within the tumor microenvironment: an updated review. *Cells* 9:1896. doi: 10.3390/cells9081896

Garg, A., Galluzzi, L., Apetoh, L., Baert, T., Birge, R., Bravo-San Pedro, J., et al. (2015). Molecular and translational classifications of DAMPs in immunogenic cell death. *Front. Immunol.* 6:588. doi: 10.3389/fimmu.2015.00588

Gong, A., and Huang, S. (2012). FoxM1 and Wnt/β-catenin signaling in glioma stem cells. *Cancer Res.* 72, 5658–5662. doi: 10.1158/0008-5472.CAN-12-0953

Gong, W., Zheng, J., Liu, X., Ma, J., Liu, Y., and Xue, Y. (2016). Knockdown of NEAT1 restrained the malignant progression of glioma stem cells by activating microRNA let-7e. *Oncotarget* 7, 62208–62223. doi: 10.18632/oncotarget.11403

Guo, X., Luo, Z., Xia, T., Wu, L., Shi, Y., and Li, Y. (2020). Identification of miRNA signature associated with BMP2 and chemosensitivity of TMZ in glioblastoma stem-like cells. *Genes Dis.* 7, 424–439. doi: 10.1016/j.gendis.2019.09.002

Han, D., Wang, J., and Cheng, G. (2018). LncRNA NEAT1 enhances the radio-resistance of cervical cancer via miR-193b-3p/CCND1 axis. *Oncotarget* 9, 2395–2409. doi: 10.18632/oncotarget.23416

Happold, C., Roth, P., Wick, W., Schmidt, N., Florea, A., Silginer, M., et al. (2012). Distinct molecular mechanisms of acquired resistance to temozolomide in glioblastoma cells. *J. Neurochem.* 122, 444–455. doi: 10.1111/j.1471-4159.2012.07781.x

Hira, V., Aderetti, D., and van Noorden, C. (2018). Glioma stem cell niches in human glioblastoma are periarteriolar. *J. Histochem. Cytochem.* 66, 349–358. doi: 10.1369/0022155417752676

Huang, K., Liu, X., Li, Y., Wang, Q., Zhou, J., Wang, Y., et al. (2019). Genome-wide CRISPR-Cas9 screening identifies NF-κB/E2F6 responsible for EGFRvIII-associated temozolomide resistance in glioblastoma. *Adv. Sci.* 6:1900782. doi: 10.1002/advs.201900782

Huang, W., Zhong, Z., Luo, C., Xiao, Y., Li, L., Zhang, X., et al. (2019). The miR-26a/AP-2α/Nanog signaling axis mediates stem cell self-renewal and temozolomide resistance in glioma. *Theranostics* 9, 5497–5516. doi: 10.7150/thno.33800

Ignatova, T., Kukekov, V., Laywell, E., Suslov, O., Vrionis, F., and Steindler, D. (2002). Human cortical glial tumors contain neural stem-like cells expressing astroglial and neuronal markers *in vitro*. *Glia* 39, 193–206. doi: 10.1002/glia.10094

Inoue, H., and Tani, K. (2014). Multimodal immunogenic cancer cell death as a consequence of anticancer cytotoxic treatments. *Cell Death Differ.* 21, 39–49. doi: 10.1038/cdd.2013.84

Jantaratnotai, N., Choi, H., and McLarnon, J. (2009). ATP stimulates chemokine production via a store-operated calcium entry pathway in C6 glioma cells. *BMC Cancer* 9:442. doi: 10.1186/1471-2407-9-442

Jiang, P., Chen, A., Wu, X., Zhou, M., Ul Haq, I., Mariyam, Z., et al. (2018). NEAT1 acts as an inducer of cancer stem cell-like phenotypes in NSCLC by inhibiting EGCG-upregulated CTR1. *J. Cell. Physiol.* 233, 4852–4863. doi: 10.1002/jcp.26288

Jiapaer, S., Furuta, T., Tanaka, S., Kitabayashi, T., and Nakada, M. (2018). Potential strategies overcoming the temozolomide resistance for glioblastoma. *Neurol. Med. Chir.* 58, 405–421. doi: 10.2176/nmc.ra.2018-0141

Kluckova, K., Kozak, J., Szaboova, K., Rychly, B., Svajdler, M., Suchankova, M., et al. (2020). TREM-1 and TREM-2 expression on blood monocytes could help predict survival in high-grade glioma patients. *Mediat. Inflamm.* 2020:1798147. doi: 10.1155/2020/1798147

Kohsaka, S., Wang, L., Yachi, K., Mahabir, R., Narita, T., Itoh, T., et al. (2012). STAT3 inhibition overcomes temozolomide resistance in glioblastoma by downregulating MGMT expression. *Mol. Cancer Ther.* 11, 1289–1299. doi: 10.1158/1535-7163.MCT-11-0801

Lathia, J., Mack, S., Mulkearns-Hubert, E., Valentim, C., and Rich, J. (2015). Cancer stem cells in glioblastoma. *Genes Dev.* 29, 1203–1217. doi: 10.1101/gad.261982.115

Li, L., Ma, Q., and Li, H. (2019). Effect of vitiligo treatment using compound glycyrrhizin combined with fractional carbon dioxide laser and topical triamcinolone acetonide on serum interleukin-17 and tissue growth factor-levels. *J. Int. Med. Res.* 47, 5623–5631. doi: 10.1177/0300060519871382

Li, S., Zhu, J., Cao, L., Sun, Q., Liu, H., Li, W., et al. (2014). Growth inhibitory *in vitro* effects of glycyrrhizic acid in U251 glioblastoma cell line. *Neurol. Sci.* 35, 1115–1120. doi: 10.1007/s10072-014-1661-4

Li, Y., Liu, Y., Ren, J., Deng, S., Yi, G., Guo, M., et al. (2018). miR-1268a regulates ABCC1 expression to mediate temozolomide resistance in glioblastoma. *J. Neuro Oncol.* 138, 499–508. doi: 10.1007/s11060-018-2835-3

Li, Z., Bao, S., Wu, Q., Wang, H., Eyler, C., Sathornsumetee, S., et al. (2009). Hypoxia-inducible factors regulate tumorigenic capacity of glioma stem cells. *Cancer Cell* 15, 501–513. doi: 10.1016/j.ccr.2009.03.018

Liikanen, I., Ahtiainen, L., Hirvinen, M., Bramante, S., Cerullo, V., Nokisalmi, P., et al. (2013). Oncolytic adenovirus with temozolomide induces autophagy and antitumor immune responses in cancer patients. *Mol. Ther.* 21, 1212–1223. doi: 10.1038/mt.2013.51

Lin, F., Xue, D., Xie, T., and Pan, Z. (2016). HMGB1 promotes cellular chemokine synthesis and potentiates mesenchymal stromal cell migration via Rap1 activation. *Mol. Med. Rep.* 14, 1283–1289. doi: 10.3892/mmr.2016.5398

Liu, Y., Ji, C., Li, S., Yan, F., Gu, Q., Balic, J., et al. (2018). Toll-like receptor 2 stimulation promotes colorectal cancer cell growth via PI3K/Akt and NF-κB signaling pathways. *Int. Immunopharmacol.* 59, 375–383. doi: 10.1016/j.intimp.2018.04.033

Lulli, V., Buccarelli, M., Ilari, R., Castellani, G., De Dominicis, C., Di Giamberardino, A., et al. (2020). Mir-370-3p impairs glioblastoma stem-like cell malignancy regulating a complex interplay between HMGA2/HIF1A and the oncogenic long non-coding RNA (lncRNA) NEAT1. *Int. J. Mol. Sci.* 21:3610. doi: 10.3390/ijms21103610

Ma, Q., Long, W., Xing, C., Chu, J., Luo, M., Wang, H., et al. (2018). Cancer stem cells and immunosuppressive microenvironment in glioma. *Front. Immunol.* 9:2924. doi: 10.3389/fimmu.2018.02924

Ma, W., Li, N., An, Y., Zhou, C., Bo, C., and Zhang, G. (2016). Effects of temozolomide and radiotherapy on brain metastatic tumor: a systematic review and meta-analysis. *World Neurosurg.* 92, 197–205. doi: 10.1016/j.wneu.2016.04.011

Meng, L., Li, L., Lu, S., Li, K., Su, Z., Wang, Y., et al. (2018). The protective effect of dexmedetomidine on LPS-induced acute lung injury through the HMGB1-mediated TLR4/NF-κB and PI3K/Akt/mTOR pathways. *Mol. Immunol.* 94, 7–17. doi: 10.1016/j.molimm.2017.12.008

Mollica, L., De Marchis, F., Spitaleri, A., Dallacosta, C., Pennacchini, D., Zamai, M., et al. (2007). Glycyrrhizin binds to high-mobility group box 1 protein and inhibits its cytokine activities. *Chem. Biol.* 14, 431–441. doi: 10.1016/j.chembiol.2007.03.007

Muth, C., Rubner, Y., Semrau, S., Rühle, P., Frey, B., Strnad, A., et al. (2016). Primary glioblastoma multiforme tumors and recurrence: comparative analysis of the danger signals HMGB1, HSP70, and calreticulin. *Strahlenther. Onkol.* 192, 146–155. doi: 10.1007/s00066-015-0926-z

Olivares-Urbano, M., Griñán-Lisón, C., Marchal, J., and Núñez, M. (2020). CSC radioresistance: a therapeutic challenge to improve radiotherapy effectiveness in cancer. *Cells* 9:1651. doi: 10.3390/cells9071651

Pajonk, F., Vlashi, E., and McBride, W. (2010). Radiation resistance of cancer stem cells: the 4 R's of radiobiology revisited. *Stem Cells.* 28, 639–648. doi: 10.1002/stem.318

Pan, L., Zhong, T., Tang, R., Li, P., Dang, Y., Huang, S., et al. (2015). Upregulation and clinicopathological significance of long non-coding NEAT1 RNA in NSCLC tissues. *Asian Pac. J. Cancer Prev.* 16, 2851–2855. doi: 10.7314/APJCP.2015.16.7.2851

Pasi, F., Paolini, A., Nano, R., Di Liberto, R., and Capelli, E. (2014). Effects of single or combined treatments with radiation and chemotherapy on survival and danger signals expression in glioblastoma cell lines. *BioMed Res. Int.* 2014:453497. doi: 10.1155/2014/453497

Qian, F., Xiao, J., Gai, L., and Zhu, J. (2019). HMGB1-RAGE signaling facilitates Ras-dependent Yap1 expression to drive colorectal cancer stemness and development. *Mol. Carcinog.* 58, 500–510. doi: 10.1002/mc.22944

Sims, G., Rowe, D., Rietdijk, S., Herbst, R., and Coyle, A. (2010). HMGB1 and RAGE in inflammation and cancer. *Ann. Rev. Immunol.* 28, 367–388. doi: 10.1146/annurev.immunol.021908.132603

Singh, S., Clarke, I., Terasaki, M., Bonn, V., Hawkins, C., Squire, J., et al. (2003). Identification of a cancer stem cell in human brain tumors. *Cancer Res.* 63, 5821–5828. doi: 10.1002/cncr.11592

Stupp, R., Hegi, M., Mason, W., van den Bent, M., Taphoorn, M., Janzer, R., et al. (2009). Effects of radiotherapy with concomitant and adjuvant temozolomide versus radiotherapy alone on survival in glioblastoma in a randomised phase III study: 5-year analysis of the EORTC-NCIC trial. *Lancet Oncol.* 10, 459–466. doi: 10.1016/S1470-2045(09)70025-7

Stupp, R., Mason, W., van den Bent, M., Weller, M., Fisher, B., Taphoorn, M., et al. (2005). Radiotherapy plus concomitant and adjuvant temozolomide for glioblastoma. *New Engl. J. Med.* 352, 987–996. doi: 10.1056/NEJMoa043330

Sun, X., Lv, X., Yan, Y., Zhao, Y., Ma, R., He, M., et al. (2020). Hypoxia-mediated cancer stem cell resistance and targeted therapy. *Biomed. Pharmacother.* 130:110623. doi: 10.1016/j.biopha.2020.110623

Varghese, M., Olstorn, H., Sandberg, C., Vik-Mo, E., Noordhuis, P., Nistér, M., et al. (2008). A comparison between stem cells from the adult human brain and from brain tumors. *Neurosurgery* 63, 1022–1033; discussion 1033-1024. doi: 10.1227/01.NEU.0000335792.85142.B0

Walcher, L., Kistenmacher, A., Suo, H., Kitte, R., Dluczek, S., Strau,ß, A., et al. (2020). Cancer stem cells-origins and biomarkers: perspectives for targeted personalized therapies. *Front. Immunol.* 11:1280. doi: 10.3389/fimmu.2020.01280

Wang, F., Zhang, P., Yang, L., Yu, X., Ye, X., Yang, J., et al. (2015). Activation of toll-like receptor 2 promotes invasion by upregulating MMPs in glioma stem cells. *Am. J. Transl. Res.* 7, 607–615.

Wang, X., Zhou, S., Fu, X., Zhang, Y., Liang, B., Shou, J., et al. (2015). Clinical and prognostic significance of high-mobility group box-1 in human gliomas. *Exp. Ther. Med.* 9, 513–518. doi: 10.3892/etm.2014.2089

Xu, T., Jiang, L., and Wang, Z. (2019). The progression of HMGB1-induced autophagy in cancer biology. *OncoTargets Ther.* 12, 365–377. doi: 10.2147/OTT.S185876

Yang, X., Xiao, Z., Du, X., Huang, L., and Du, G. (2017). Silencing of the long non-coding RNA NEAT1 suppresses glioma stem-like properties through modulation of the miR-107/CDK6 pathway. *Oncol. Rep.* 37, 555–562. doi: 10.3892/or.2016.5266

Yu, J., Zhang, C., Coyle, M., Du, Y., Zhang, A., Guo, X., et al. (2017). Compound glycyrrhizin plus conventional therapy for psoriasis vulgaris: a systematic review and meta-analysis of randomized controlled trials. *Curr. Med. Res. Opin.* 33, 279–287. doi: 10.1080/03007995.2016.1254605

Zang, J., Zheng, M., Cao, X., Zhang, Y., Zhang, Y., Gao, X., et al. (2020). Adenovirus infection promotes the formation of glioma stem cells from glioblastoma cells through the TLR9/NEAT1/STAT3 pathway. *Cell Comm. Signal.* 18:135. doi: 10.1186/s12964-020-00598-7

Zhang, L., Shi, H., Chen, H., Gong, A., Liu, Y., Song, L., et al. (2019). Dedifferentiation process driven by radiotherapy-induced HMGB1/TLR2/YAP/HIF-1α signaling enhances pancreatic cancer stemness. *Cell Death Dis.* 10:724. doi: 10.1038/s41419-019-1956-8

Zhao, X., Lin, Y., Jiang, J., Tang, Z., Yang, S., Lu, L., et al. (2017). High-mobility group box 1 released by autophagic cancer-associated fibroblasts maintains the stemness of luminal breast cancer cells. *J. Pathol.* 243, 376–389. doi: 10.1002/path.4958

Conflict of Interest: The authors declare that the research was conducted in the absence of any commercial or financial relationships that could be construed as a potential conflict of interest.

frontiers in Oncology

ORIGINAL RESEARCH
published: 22 February 2021
doi: 10.3389/fonc.2020.600762

MLK3 Is Associated With Poor Prognosis in Patients With Glioblastomas and Actin Cytoskeleton Remodeling in Glioblastoma Cells

Yan Zhu[1,2], *Jin-Min Sun*[1,2,3], *Zi-Chen Sun*[1], *Feng-Jiao Chen*[1], *Yong-Ping Wu*[3] *and Xiao-Yu Hou*[1,2*]

[1] *Jiangsu Key Laboratory of Brain Disease Bioinformation, Research Center for Biochemistry and Molecular Biology, Xuzhou Medical University, Xuzhou, China,* [2] *State Key Laboratory of Natural Medicines, School of Life Science and Technology, China Pharmaceutical University, Nanjing, China,* [3] *Laboratory of Clinical and Experimental Pathology, Department of Pathology, Xuzhou Medical University, Xuzhou, China*

OPEN ACCESS

Edited by:
Lorenzo Gerratana, University of Udine, Italy

Reviewed by:
Leticia Veras Costa Lotufo, University of São Paulo, Brazil
Omar Torres-Quesada, University of Innsbruck, Austria

***Correspondence:**
Xiao-Yu Hou
xyhou@cpu.edu.cn

Specialty section:
This article was submitted to Molecular and Cellular Oncology, a section of the journal Frontiers in Oncology

Received: *31 August 2020*
Accepted: *30 December 2020*
Published: *22 February 2021*

Citation:
Zhu Y, Sun J-M, Sun Z-C, Chen F-J, Wu Y-P and Hou X-Y (2021) MLK3 Is Associated With Poor Prognosis in Patients With Glioblastomas and Actin Cytoskeleton Remodeling in Glioblastoma Cells. Front. Oncol. 10:600762. doi: 10.3389/fonc.2020.600762

Mixed lineage kinase 3 (MLK3) has been implicated in human melanoma and breast cancers. However, the clinical significance of MLK3 in human gliomas and the underlying cellular and molecular mechanisms remain unclear. We found that MLK3 proteins were highly expressed in high-grade human glioma specimens and especially prevalent in primary and recurrent glioblastoma multiforme (GBM). High levels of MLK3 mRNA were correlated with poor prognosis in patients with isocitrate dehydrogenase (*IDH*)-wild-type (wt) gliomas. Furthermore, genetic ablation of MLK3 significantly suppressed the migration and invasion abilities of GBM cells and disrupted actin cytoskeleton organization. Importantly, MLK3 directly bound to epidermal growth factor receptor kinase substrate 8 (EPS8) and regulated the cellular location of EPS8, which is essential for actin cytoskeleton rearrangement. Overall, these findings provide evidence that MLK3 upregulation predicts progression and poor prognosis in human *IDH*-wt gliomas and suggest that MLK3 promotes the migration and invasion of GBM cells by remodeling the actin cytoskeleton *via* MLK3-EPS8 signaling.

Keywords: actin cytoskeleton remodeling, epidermal growth factor receptor kinase substrate 8 (EPS8), glioblastoma prognosis, glioma progression, isocitrate dehydrogenase (IDH), mixed lineage kinase 3 (MLK3), primary and recurrent glioblastoma multiforme (GBM)

INTRODUCTION

Gliomas, one of the most prevalent forms of primary brain tumors, are classified into four grades (grade I–IV) in line with the World Health Organization (WHO) 2016 classification criteria (1). Glioblastoma multiforme (GBM) is a malignant grade IV tumor with poor prognosis. According to the statistics, the 3-year overall survival of patients with GBM is approximately 12% (2). Tumor invasion and immune evasion account for the main causes of recurrence and death in patients with

GBM. Therefore, understanding the underlying cellular and molecular events may provide promising molecular markers for GBM diagnosis, prognosis, and targeted therapy.

Mixed lineage kinase 3 (MLK3), also known as mitogen-activated protein kinase kinase kinase 11 (MAP3K11) and Src-homology 3 (SH3) domain-containing proline-rich kinase (SPRK), is a member of the serine/threonine protein kinase family encoded by the *MAP3K11* gene in humans (3). MLK3 is involved in human melanoma and breast cancers (4–6). High levels of MLK3 mRNA are found in metastatic primary malignant melanoma tissues (4). Breast tumors express a comparable level of MLK3 proteins, whereas MLK3 kinase activity is profoundly reduced and inversely correlated with tumor grades in human epidermal growth factor receptor (EGFR) 2-positive breast cancer tissues (5, 6). In diverse human cancer cell lines, MLK3 is involved in multiple cellular processes, including proliferation, proapoptosis, migration, and invasion (4–11). MLK3-JNK signaling has been reported to be related to EGFR activation-driven migration and invasion of GBM cell line (10). However, the pathophysiological function of MLK3 in the progression and prognosis of human gliomas remains unknown, and how MLK3 promotes the development of gliomas has not been well understood.

Cancer cell migration and invasion involves integrated complexes and is a dynamic process that requires actin cytoskeletal rearrangement to change the cell shape and generate the driving force for cell movement. A group of regulatory molecules are involved in cytoskeletal remodeling, including EGFR kinase substrate 8 (EPS8) (12–15). EPS8 is responsible for actin cytoskeleton formation and facilitates the migratory and invasive capacities of GBM cells (16). Furthermore, recent findings implicate that actin cytoskeleton remodeling drives cancer cell resistance to antitumor immunity (17). Altogether, elucidating the roles of MLK3 in actin cytoskeleton regulation is essential for understanding glioma progression and invasion.

In this study, we examined the expression of MLK3 in human glioma tissue specimens. Additionally, we determined the correlation between MLK3 protein and mRNA levels and glioma progression and poorer prognosis in patients with GBM. Furthermore, we investigated whether and how MLK3 is involved in GBM cell migration, invasion, and actin cytoskeletal remodeling. Our data provide evidence that MLK3 is a valuable biomarker for predicting the prognosis and towards targeted therapy of GBM.

METHODS

Human Tissue Analysis

Glioma tissues (WHO grade I, n = 6; grade II, n = 23; grade III, n = 20; and grade IV, n = 48) were obtained from the Department of Pathology of the Affiliated Hospital of Xuzhou Medical University between 2016 and 2017. All samples were identified by pathologists according to the 2016 WHO classification criteria.

Publicly available RNA-seq data of gliomas were collected from the Freije dataset (https://www.oncomine.org) and the CGGA database (https://www.cgga.org.cn). The Freije dataset includes 81 glioma tissues (WHO grade III, n = 24 and grade IV, n = 57), and the Chinese Glioma Genome Atlas (CGGA) dataset includes 325 glioma tissues. After incomplete data (grade, overall survival, isocitrate dehydrogenase (*IDH*) mutation status, 1p/19q codeletion status, O^6-methylguanine-DNA methyltransferase (*MGMT*) promoter methylation status) were deleted, 286 glioma tissues in the CGGA dataset (WHO grade II, n = 86; grade III, n = 68; and grade IV, n = 132) were used to analyze overall survival and the levels of MLK3, EGFR, MAPK8, MAPK9, MAPK10, and EPS8 mRNA. The median levels of various mRNA in glioma samples were chosen as the respective cut-off points.

Antibodies and Plasmids

Rabbit polyclonal anti-MLK3 (#sc-536) and mouse monoclonal anti-EPS8 (#sc-390257) antibodies were obtained from Santa Cruz Biotechnology. Mouse monoclonal anti-GAPDH (glyceraldehyde phosphate dehydrogenase) (#60004-1-Ig) antibody and rabbit polyclonal anti-vinculin antibody (#26520-1-AP) were obtained from Proteintech. Mouse monoclonal anti-Myc (#05-419) and rabbit polyclonal anti-GST (glutathione S-transferase) (#06-332) antibodies were obtained from Millipore. Horseradish peroxidase-conjugated goat anti-mouse IgG (#A28177) and goat anti-rabbit IgG (#31460), goat anti-mouse IgG-Alexa Fluor 488 (#A-11029), and goat anti-rabbit IgG-Alexa Fluor 594 (#A11037) were obtained from Invitrogen. Phalloidin (#PHDR1) was obtained from Cytoskeleton.

Full-length human MLK3 cDNA (puc19-hMAP3K11, #HG11067-U) was obtained from Sino Biological Inc. and subcloned into pcDNA3.1-Myc plasmids. EPS8 cDNA was amplified from human HEB cells and cloned into the pcDNA3.1-His plasmids. Human cDNA coding for MLK3 (1–104 aa) and MLK3 (632–847 aa) were amplified and cloned into pGEX-4T-1 plasmids. All recombinant plasmids were identified by sequencing.

Immunohistochemical Staining

Paraffin-embedded glioma tissue sections were deparaffinized and hydrated using xylene and graded alcohols. Antigen retrieval was performed with high pressure for 3 min. The tissues were blocked with 3% bovine serum albumin for 20 min at room temperature. Primary antibodies were incubated overnight at 4°C. Then, biotinylated secondary antibodies were incubated for 30 min at room temperature. The staining was carried out using an ABC reagent kit (VECTASTAIN) and a 3,3-diaminobenzidine peroxidase substrate reagent kit (Vector, #SK-4100). The nuclei were treated with hematoxylin staining, and the sections were mounted on glass slides. Images were acquired with Nikon microscopy. The evaluation of MLK3 staining was as previously described (18). According to staining intensity and area, MLK3 staining was categorized into scores 0–12. The median level of MLK3 (score 6) as the cut-off point, the samples were divided into low/high expression of MLK3 groups.

Cell Culture and Transfection

The human GBM cell lines U87, U118, U251, U343, and T98G were maintained in Dulbecco's modification of Eagle's medium (DMEM, Gibco, #12000-014) supplemented with 10% fetal bovine serum (FBS). Cells were grown at 37°C and 5% CO_2. All cell lines were authenticated through short tandem repeat DNA fingerprinting from Cell Bank/Stem Cell Bank, The Committee of Type Culture Collection of Chinese Academy of Sciences (Shanghai, China) in August 2018. Plasmid transfections were carried out with Lipofectamine 3000 (Invitrogen, #L3000-015).

Knockout of the *MAP3K11* Gene

The knockout of the *MAP3K11* gene was performed by the CRISPR/Cas9 system. The special guide (sg) RNA1 sequence (5'-CACTGGGCTCGTAGTCGAAC-3') and sgRNA2 sequence (5'-TTGAGTCCTCCAGACGTCGG-3') targeting exons 1 and 7, respectively, were cloned into pSpCas9 (BB)-2A-Puro (PX459) vector. PX459 recombinants vector were transfected into U118 and U251 cells. Single cell colonies were screened with 0.75 μg/ml puromycin and identified by sequencing and western blot assays. The fragments of genomic DNA were amplified with forward primer F1 (5'-AAAAAGACCCAACCGGAGT-3') and reverse primers R1 (5'-CAGCCTTGAGGGCAATGAT-3') and R2 (5'-AGAGCAACCAGGGCAGGAC-3'). The PCR products were sequenced.

Transwell Migration and Invasion Assays

Cells were treated with serum-free DMEM for 14 h. Then, cells (5×10^4) were suspended in serum-free DMEM and added to the upper chamber of a 24-well transwell plate (Corning, #3422). For the invasion assay, the upper chambers were precoated with a Matrigel Basement Membrane Matrix (BD Biosciences, #356234). DMEM supplemented with 10% FBS was added to the lower chambers. The cells were cultured at 37°C for 10 h ~ 24 h. The chambers were washed with phosphate-buffered saline (PBS), fixed with 4% paraformaldehyde for 20 min and washed with PBS. The cells on the upper surface of the membrane were removed with a cotton swab. The cells on the bottom surface were stained with Giemsa staining.

Immunofluorescence Analysis

Cells were plated on glass slides, washed with PBS, fixed with 4% paraformaldehyde for 10 min at 4°C, permeabilized with Triton X-100 (0.2%) for 15 min at room temperature, and blocked with 10% normal goat serum for 2 h at room temperature. Primary antibodies were incubated overnight at 4°C. The fluorescent secondary antibodies were incubated for 2 h at room temperature. The nuclei were stained with 4-6-diamidino-2-phenylindole (DAPI) (Sigma, #D8417). Coverslips were mounted on the glass slides, and images were taken with confocal microscopy.

Immunoblot Analysis

Cell total protein was separated by 10% sodium dodecyl sulfate polyacrylamide gel electrophoresis (SDS-PAGE) and transferred to nitrocellulose membranes. After blocking with 3% bovine serum albumin for 2 h, the membranes were incubated with the primary antibody overnight, followed by horseradish peroxidase-conjugated secondary antibody for 1 h at 4°C. The specific proteins were detected by enhanced chemiluminescence reagent. The band intensity was quantified with ImageJ software.

Immunoprecipitation (IP)

U251 cells were transfected with pcDNA3.1-Myc-MLK3 and pcDNA3.1-His-EPS8 plasmids for 24 h, and protein lysates were obtained. IP assay of MLK3-EPS8 interaction was performed with anti-EPS8, anti-MLK3 or anti-Myc antibodies as previously described (19).

GST Pull-Down Assay

GST-fused MLK3 (1–104 aa) and MLK3 (632–847 aa) proteins were expressed in BL21 cells and purified with the Pierce™ GST Protein Interaction Pull-Down Kit (Thermo, #21516) according to the manufacturer's instructions. The purified proteins were incubated with the protein lysates from pcDNA3.1-EPS8-transfected HEK293 cells for 2 h at 4°C. The beads were washed and boiled in loading buffer for the immunoblot assay.

Statistical Analysis

All data are presented as the mean ± standard deviation (SD). Statistical analyses were performed using GraphPad Prism 7.0 software. Pearson correlation analysis and chi-square (X^2) tests were conducted to detect correlations. The Kaplan-Meier method was applied to assess overall survival. For parametric data, two-tailed Student's *t*-tests and one-way ANOVA were used to examine differences. For non-parametric data, a two-sided Mann-Whitney test was used. $P < 0.05$ was considered statistically significant.

RESULTS

Mixed Lineage Kinase 3 Is Highly Expressed in High-Grade Human Glioma Specimens

First, 97 clinical glioma tissue specimens were analyzed with immunohistochemistry (IHC) to determine the protein expression and subcellular distribution of MLK3. As shown in **Figures 1A, B**, the expression levels of MLK3 protein were higher in glioma tissues than in para-tumor tissues. Clearly, MLK3 proteins were mainly localized in the cytoplasm of glioma cells. Next, we assessed the correlation between MLK3 levels and clinicopathological characteristics (tumor size and WHO grade). IHC analysis showed that the levels of MLK3 protein were closely correlated with age and tumor grade (**Table 1**). MLK3 staining was weaker in low-grade glioma tissues (grade I and II) than in high-grade glioma tissues (grade III and IV) (**Figures 1A, C**). In addition, there was significant variation of MLK3 levels among patients within the same grade gliomas (**Figure 1D**). The percentage of high MLK3 level cases increased with the grade of glioma.

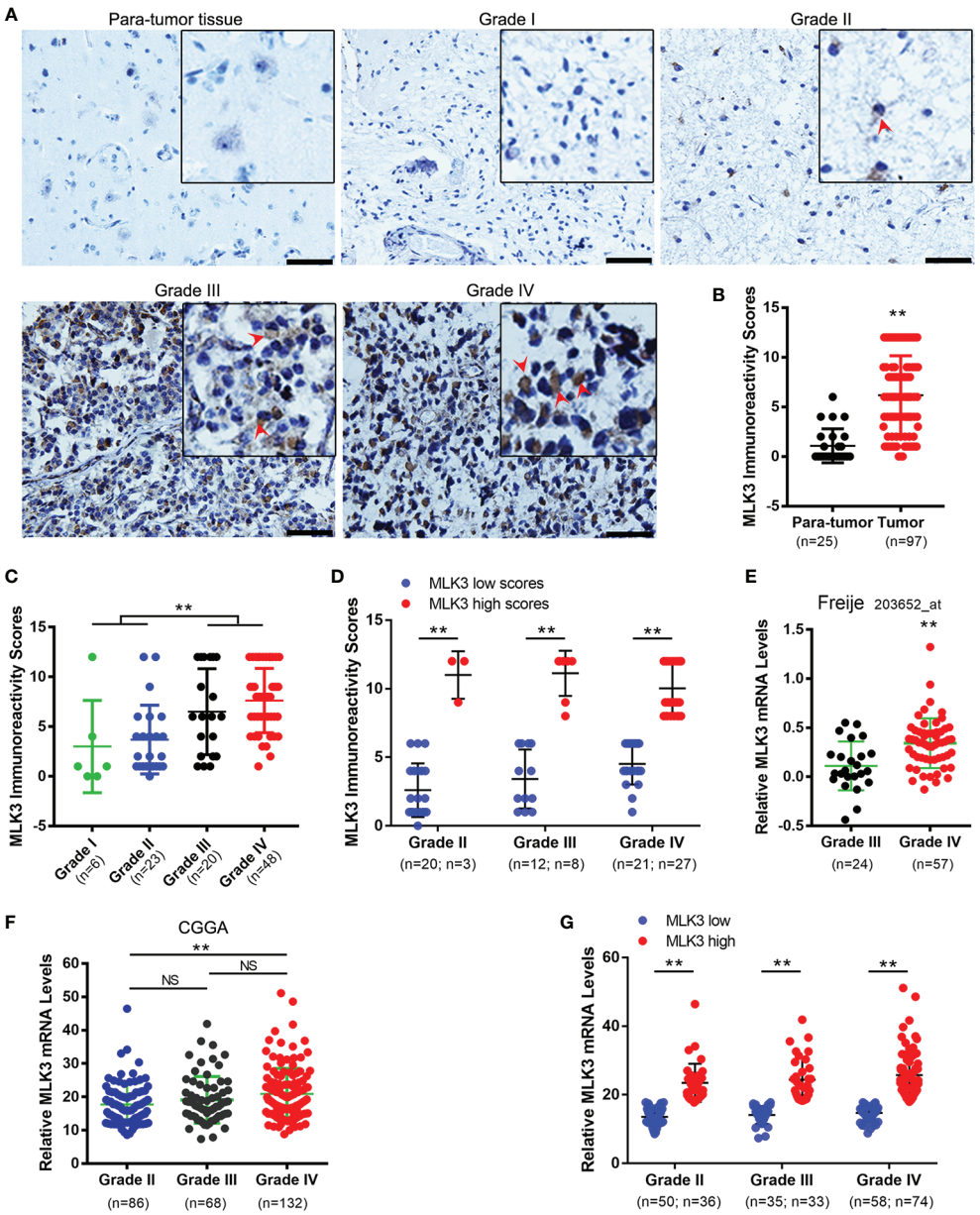

FIGURE 1 | MLK3 is highly expressed in high-grade human glioma specimens. **(A–C)** MLK3 protein levels are upregulated in high-grade gliomas. **(A)** Representative immunohistochemistry IHC images of MLK3 in human glioma tissues. Scale bars, 50 μm. **(B)** MLK3 expression in para-tumor tissues (n = 25) and glioma tissues (n = 97). **(C)** Comparison of MLK3 expression between low-grade (grade I and II, n = 29) and high-grade (grade III and IV, n = 68) glioma tissues. Mann-Whitney *U* test. $^{**}P < 0.01$. **(D)** The variation of MLK3 levels in the same grade gliomas. Mann-Whitney *U* test, $^{**}P < 0.01$. **(E, F)** MLK3 mRNA levels are upregulated in high-grade gliomas. mRNA sequencing-based glioma datasets from Oncomine database **(E)** and the CGGA database **(F)** were analyzed by two-tailed Student's *t*-tests and one-way ANOVA. NS, not significant. $^{**}P < 0.01$. **(G)** The variation of MLK3 mRNA levels in the same grade gliomas. Two-tailed Student's *t*-tests, $^{**}P < 0.01$.

Next, we explored MLK3 mRNA levels in glioma tissues by using RNA sequencing (RNA-seq) data from the Chinese Glioma Genome Atlas (CGGA) database and the Freije dataset from the Oncomine database. The results showed that the levels of MLK3 mRNA were significantly increased in high-grade gliomas (grade IV) and closely associated with the progression of gliomas (**Figures 1E, F**). MLK3 mRNA levels showed significant variation within the same grade (**Figure 1G**), which is consistent with the results of IHC analysis.

These findings suggest that MLK3 is significantly upregulated in high-grade human glioma tissues and positively associated with a malignant phenotype.

TABLE 1 | MLK3 staining and clinicopathological characteristics of 97 glioma patients.

Variables		Number	MLK3 expression		X^2 value	*P* value
			High (%)	Low (%)		
Age	≤50	44	20 (45.5)	24 (54.5)	4.149	0.042*
	>50	53	35 (66.0)	18 (34.0)		
Gender	Male	60	36 (60.0)	24 (40.0)	0.697	0.404
	Female	37	19 (51.4)	18 (48.6)		
Tumor size	<5 cm	31	17 (54.8)	14 (45.2)	0.000	1.000
	≥5 cm	31	17 (54.8)	14 (45.2)		
WHO grade	Low (I+II)	29	7 (24.1)	22 (75.9)	17.867	0.000**
	High(III+IV)	68	48 (70.6)	20 (29.4)		

*$P < 0.05$, **$P < 0.01$.

High Mixed Lineage Kinase 3 Levels Are Prevalent in Isocitrate Dehydrogenase Gene-Wild-Type Glioblastoma Multiforme and Correlated With the Poor Prognosis of Patients

The detection of several molecular markers, including *IDH1* mutation, 1p/19q codeletion, *MGMT* promoter methylation status, and *EGFR* amplification has been applied with clinical diagnoses of gliomas (1). We analyzed the correlation between MLK3 levels and the status of these biomarkers by using CGGA data and IHC analysis. The results revealed that the expression of MLK3 mRNA in human gliomas was correlated with *IDH* status but not 1p/19q codeletion and *MGMT* promoter methylation status. While it was negatively related to EGFR mRNA levels (**Table 2**). We also analyzed the correlation between MLK3 levels and downstream regulators. The results showed that MLK3 mRNA in human gliomas was negatively related to MAPK8, MAPK9, and MAPK10 (**Table 2**). Additionally, MLK3 was highly expressed in *IDH*-wt gliomas and especially prevalent in *IDH*-wt GBM (59/95) (**Figure 2A**). In *IDH*-wt GBM, high levels of MLK3 frequently occurred in primary GBM (43/71), recurrent GBM (9/15) and secondary GBM (7/9) (**Figure 2B**). The results of the IHC analysis confirmed that the MLK3 protein was abundantly expressed in *IDH*-wt GBM (24/33) (**Figure 2C**) and are in accordance with the results of the bioinformatics analysis.

We further studied the correlation between MLK3 expression and the overall survival of patients with gliomas by bioinformatics analysis. The Kaplan-Meier analysis showed that high levels of MLK3 were associated with the poor prognosis of patients (**Figure 2D**). Glioma patients with the *IDH*-mutant (mut) phenotype had a better prognosis than patients with the *IDH*-wt phenotype. Remarkably, in *IDH*-wt gliomas, patients with comparatively lower levels of MLK3 had a higher overall survival rate than patients with high levels of MLK3 (**Figure 2E**). By contrast, there was no difference in the overall survival of *IDH*-mut patients with either high or low levels of MLK3 (**Figure 2E**).

These data suggest that MLK3 upregulation predicts poorer prognosis in *IDH*-wt gliomas.

Mixed Lineage Kinase 3 Promotes Glioblastoma Multiforme Cell Migration and Invasion and Is Required for Actin Cytoskeleton Rearrangement

To assess the roles of MLK3 in the biological behaviors of glioma cells, we first detected the protein levels of MLK3 in high-migration glioma cell lines (U87, U118, and U251) and low-migration glioma cell lines (U343 and T98G) 48 h after serum starvation (**Figure 3A**).

TABLE 2 | Relationship between MLK3 mRNA expression and clinicopathologic variables of patients with gliomas.

Variables		Number	MLK3 expression		X^2 value	*P* value
			High (%)	Low (%)		
IDH	Wildtype	136	79 (58.1)	57 (41.9)	6.785	0.009**
	Mutation	150	64 (42.7)	86 (57.3)		
1p/19q codeletion	Codel	57	24 (42.1)	33 (57.9)	1.775	0.183
	Non-codel	229	119 (52.0)	110 (48.0)		
***MGMT* promoter**	Methylated	147	73 (49.7)	74 (50.3)	0.014	0.906
	Unmethylated	139	70 (50.4)	69 (49.6)		
EGFR	High	143	58 (40.6)	85 (59.4)	10.196	0.001**
	Low	143	85 (59.4)	58 (40.6)		
MAPK8	High	143	45 (31.5)	98 (68.5)	39.287	0.000**
	Low	143	98 (68.5)	45 (31.5)		
MAPK9	High	143	53 (37.1)	90 (62.9)	19.147	0.000**
	Low	143	90 (62.9)	53 (37.1)		
MAPK10	High	143	56 (39.2)	87 (60.8)	13.441	0.000**
	Low	143	87 (60.8)	56 (39.2)		

** $P < 0.01$.

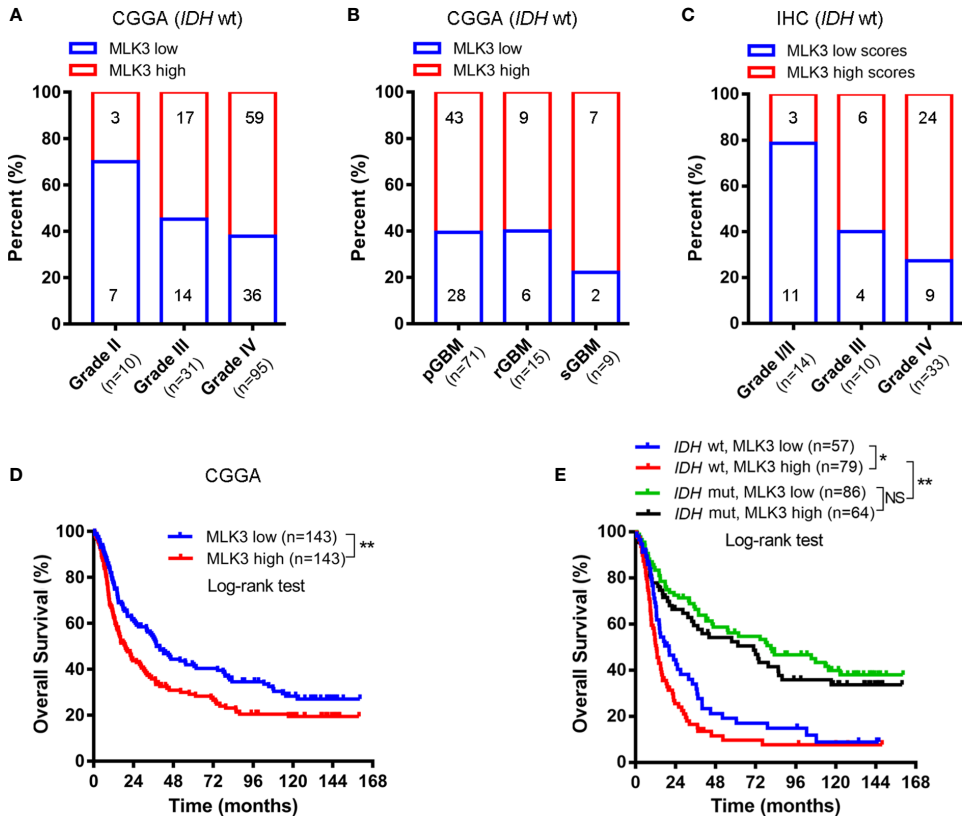

FIGURE 2 | High MLK3 levels are correlated with poor prognosis in patients with *IDH*-wt GBM. **(A, B)** High levels of MLK3 mRNA are prevalent in *IDH*-wt GBM. The frequencies of high MLK3 mRNA levels in *IDH*-wt gliomas (n = 136), primary GBM (n = 71), recurrent GBM (n = 15), and secondary GBM (n = 9) were analyzed. The data were derived from the CGGA dataset. The median level of MLK3 mRNA in glioma samples was chosen as the cut-off point. pGBM, primary GBM; rGBM, recurrent GBM; sGBM, secondary GBM. **(C)** MLK3 abundantly expressed in *IDH*-wt GBM. The percent of high MLK3 protein levels in *IDH*-wt gliomas (n = 57) was investigated. The data were obtained from IHC analysis. **(D, E)** High levels of MLK3 mRNA are associated with the poor prognosis of patients. Kaplan-Meier survival analyses for MLK3 mRNA expression (n = 286) **(D)** and MLK3 mRNA expression and *IDH* gene status (n = 286) **(E)**. The data were derived from the CGGA dataset. Log-rank test. NS, not significant. $^{*}P < 0.05$, $^{**}P < 0.01$.

MLK3 was highly expressed in U87, U118, and U251 cells, implying that MLK3 could be related to the migration and invasion of GBM cells. To evaluate the roles of MLK3 in the migration and invasion of GBM cells, we generated *MAP3K11* gene knockout U251 and U118 cells by the CRISPR/Cas9 system. Positive clones (U251 ko, U118 ko-1, and U118 ko-2) were confirmed by sequencing and immunoblot analysis (**Supplementary Figure S1**, **Figures 3B, C**). The loss of MLK3 robustly restrained cell migration in U251 and U118 cells compared to wt cells (**Figures 3D, E**). The Matrigel assay showed that MLK3 ablation evidently suppressed U251 and U118 cell invasion (**Figures 3F, G**). The above results suggest that MLK3 is required for the migration and invasion of GBM cells *in vitro*.

Next, the MLK3 kinase inhibitors CEP-701 was used to test the roles of MLK3 activity in the regulation of GBM cell migration and invasion. Immunoblot analysis showed that CEP-701 effectively inhibited the activity of MLK3 (**Supplementary Figure S2A**). A wound healing assay showed that CEP-701 (at the appropriate concentration) significantly inhibited the wound closure of U87, U251, and T98G cells in comparison to vehicle-treated cells (**Supplementary Figures S2B–D**). Transwell assays showed that CEP-701 (400 nM) markedly suppressed the migration of U251 and U87 cells (**Supplementary Figures S2E, F**). The Matrigel assay revealed that the invasion ability of U251 and U87 cells was remarkably reduced after treatment with CEP-701 (400 nM) (**Supplementary Figures S2G, H**).

Actin cytoskeleton remodeling is a vital event in cell migration and invasion. To clarify the role of MLK3 in actin cytoskeleton organization, F-actin and vinculin (for focal adhesion) staining were carried out to identify changes in the actin cytoskeleton. The results showed that MLK3 ablation in U251 and U118 cells resulted in marked changes of the actin cytoskeleton, and actin based "mass-like structures" appeared on the edge of cells (**Figures 3H, I**). MLK3 ablation increased stress fibers in U251 cells (**Figure 3H**), while the distribution of vinculin obviously decreased on the edge of U251 ko and U118 ko cells (**Figures 3H, I**). More interestingly, the altered cell morphology and more filamentous protuberances were observed by ectopic expression of MLK3 in T98G cells (**Supplementary**

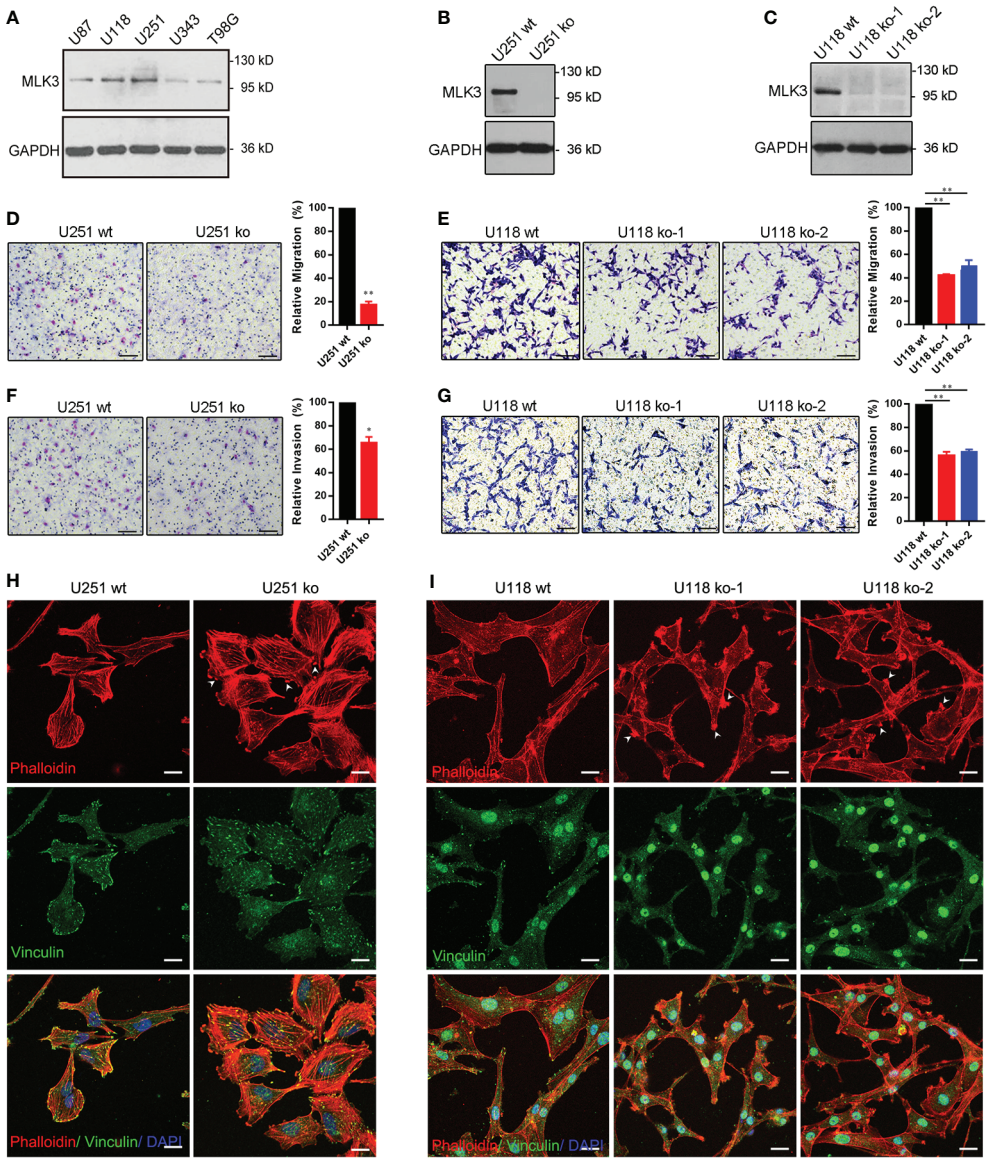

FIGURE 3 | MLK3 deficiency attenuates glioblastoma multiforme (GBM) cell migration and invasion and disrupts actin cytoskeleton rearrangement. **(A)** MLK3 proteins are overexpressed in highly migrating GBM cells. Cells were treated with serum-free DMEM for 48 h. Immunoblot analysis of MLK3 levels in several GBM cell lines. GAPDH was used as a loading control. **(B, C)** Immunoblot assay of the *MAP3K11* gene knockout in U251 **(B)** and U118 **(C)** cells. GAPDH was used as a loading control. **(D–G)** Transwell assay of GBM cell migration and invasion in *MAP3K11* gene knockout U251 **(D, F)** and U118 **(E, G)** cells. Two-tailed Student's *t*-test. Scale bars, 100 μm; n = 3; $^{**}P < 0.01$. **(H, I)** The loss of MLK3 disrupts actin cytoskeleton rearrangement. The results shown are representative of at least three independent cultures. Phalloidin was used to label F-actin (red), anti-vinculin antibody was used to stain focal adhesion structure (green), and DAPI was used to stain nuclei (blue). White arrows indicate the actin based "mass-like structures." Scale bars, 20 μm.

Figure S3). These findings indicate that MLK3 contributes to actin cytoskeleton remodeling.

Mixed Lineage Kinase 3 Directly Binds to Epidermal Growth Factor Receptor Kinase Substrate 8

Previous studies have indicated that EPS8 controls actin cytoskeleton reorganization (20, 21). To elucidate the molecular mechanism underlying MLK3-mediated cell migration and invasion, we identified the molecular interactions of MLK3 and EPS8. Co-IP analysis showed that overexpressed (**Figure 4A**) and endogenous MLK3 (**Figure 4B**) interacted with EPS8 in U251 cells. Furthermore, *in vitro* GST pull-down analysis showed that the c-terminal domain of MLK3 (1–104 aa) and the proline-rich domain (PRD) of MLK3 (632–847 aa) directly bound to EPS8 (**Figure 4D**). In addition, MLK3

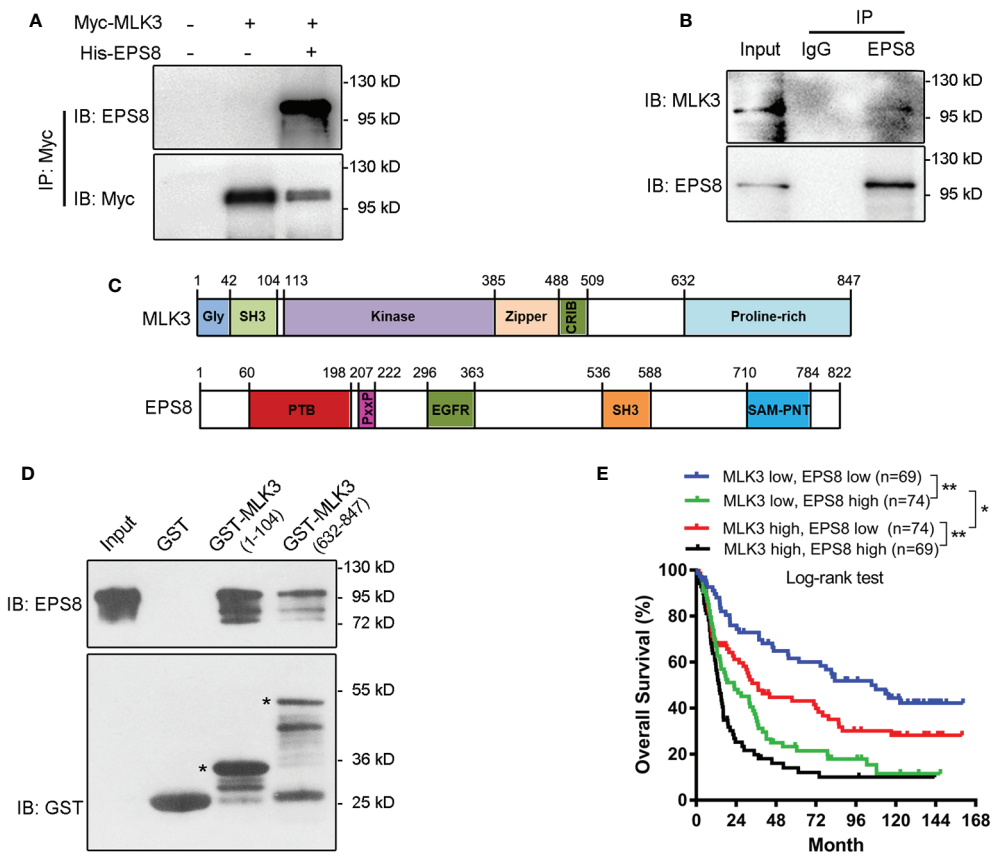

FIGURE 4 | MLK3 directly binds with EPS8. The results shown are representative of at least three independent experiments. **(A, B)** Overexpressed and endogenous MLK3 binds to EPS8 in U251 cells. U251 cells were cotransfected with pcDNA3.1-Myc-MLK3 and pcDNA3.1-His-EPS8 plasmids for 24 h, with the pcDNA3.1 plasmid as a control. The lysates were immunoprecipitated using anti-Myc **(A)**, anti-EPS8 **(B)** or control IgG, EPS8, or MLK3 was detected with an immunoblot assay. **(C)** The molecular structure of MLK3 and EPS8. **(D)** AAs 1–104 and 632–847 of MLK3 directly bound to EPS8 *in vitro*. GST-tagged MLK3 segments were expressed in BL21 cells. The purified proteins were incubated with the protein lysates from pcDNA3.1-EPS8-transfected HEK293 cells. The proteins were immunoblotted with indicated antibodies. * the target protein. **(E)** The expression of MLK3 and EPS8 predicts the overall survival of patients. The data were derived from the CGGA dataset (n = 286). Kaplan-Meier survival analyses for MLK3 and EPS8 mRNA levels. Log-rank test. $^{*}P < 0.05$, $^{**}P < 0.01$.

cooperates with EPS8 and affects the overall survival of patients with gliomas. Bioinformatics analysis showed that high levels of MLK3 and EPS8 in gliomas are correlated with a significantly worse overall survival in patients (**Figure 4E**). These results suggest that MLK3-EPS8 signaling may be involved in the development of gliomas.

Mixed Lineage Kinase 3 Regulates the Localization of Epidermal Growth Factor Receptor Kinase Substrate 8

To further explore the mechanisms of MLK3-mediated actin cytoskeleton remodeling, we examined the localization and expression of EPS8 in MLK3-depleted U118 and U251 cells. Immunoblot assays showed that EPS8 was upregulated in MLK3-depleted U118 and U251 cells (**Figures 5A, B**). Additionally, the immunofluorescence assay results showed that the subcellular localization of EPS8 was disrupted in MLK3-ablated cells, and mass-like structures were assembled on the cell edges (**Figures 5C, D**). These data suggest that MLK3 is critical for actin cytoskeleton rearrangement by regulating EPS8 localization in GBM cells.

DISCUSSION

GBMs are devastating malignancies with highly migratory and invasive behavior. Despite advancements in clinical diagnosis and treatment, recurrence remains universal, and available salvage strategies are rare. Therefore, identifying special molecular markers for the early diagnosis, prognosis evaluation, and targeted therapy of GBM is of great significance. Our findings provide the first evidence that MLK3 upregulation plays an essential role in tumor progression and correlates with an unfavorable overall survival in patients with *IDH*-wt GBM. MLK3 may serve as a valuable diagnostic and prognostic marker and may be a promising therapeutic target for GBM therapy.

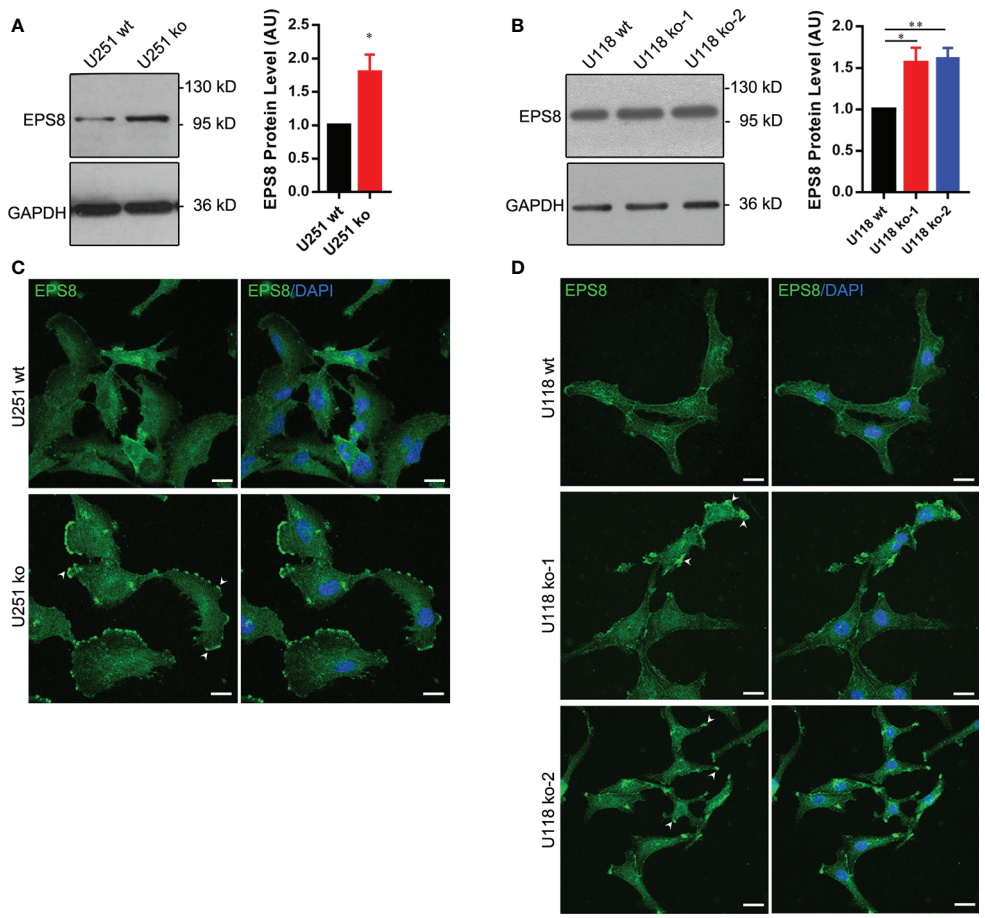

FIGURE 5 | MLK3 regulates the localization of EPS8 in U251 and U118 cells. **(A, B)** The *MAP3K11* gene knockout increases the expression of EPS8 in U251 **(A)** and U118 **(B)** cells. Relative levels of MLK3 were normalized to U251 wt or U118 wt groups. GAPDH was used as a loading control. Two-tailed Student's *t*-test. n = 3, $^{*}P < 0.05$, $^{**}P < 0.01$. AU, arbitrary unit. **(C, D)** The *MAP3K11* gene knockout alters the location of EPS8 in U251 **(C)** and U118 **(D)** cells. The results shown are representative of at least three independent cultures. EPS8 (green); DAPI-stained nuclei (blue). Scale bars, 20 μm.

To date, patients with *IDH*-wt gliomas exhibit the poorest outcomes, and few targeted agents are therapeutically effective for *IDH*-wt gliomas. The present study provides evidence that MLK3 might be required for the evaluation of prognosis and targeted therapy of *IDH*-wt gliomas. Previous studies indicated that the *IDH* and *IDH2* mutations are more frequent in grade II–III gliomas and secondary GBMs (22–24). Approximately 80% of secondary GBMs have somatic mutations in *IDH*, which are absent in primary GBM (25). Patients with *IDH* mutations have a better prognosis, which is consistent with our findings. An increase in R (-)-2-hydroxyglutarate in gliomas harboring *IDH* mutations has been found to prevent the association of MLK3 with Cdc42 and further inhibit the activity of MLK3, which may be one of the reasons for the better prognosis in patients with *IDH*-mut gliomas (26, 27). More notably, our findings showed that *IDH*-mut gliomas present with low levels of MLK3, suggesting that mutant *IDH* not only blocks MLK3 activity but also reduces MLK3 expression. Although there is no correlation between the MLK3 levels and overall survival of patients with *IDH*-mut gliomas, high levels of MLK3 are positively correlated with poor prognosis in *IDH*-wt gliomas. Therefore, the prognosis of patients with *IDH*-wt gliomas can be reasonably evaluated by MLK3. In addition, this study demonstrated that MLK3 cooperates with EPS8, which might aid in prognosis prediction for patients with gliomas.

MLK3 appears to function as an oncogene to promote cell migration and invasion through the MLK3/JNK pathway in human breast and gastric cancer cells (7, 8, 10), the MLK3/FRA-1/MMP-1 axis in human triple-negative breast cancer cells (28), or MLK3/ERK signaling in ovarian and colorectal cancer cells (9, 11). Here, our data showed that MLK3 is responsible for the migration and invasion abilities of GBM cells *via* MLK3/EPS8 signaling. MLK3 has been reported to contribute to EGF-induced GBM cell migration and invasion (10). Here, we found that MLK3 mRNA levels in human gliomas was negatively related to EGFR and MAPK8, MAPK9, MAPK10 mRNAs levels, and MLK3 downregulation reduces GBM cell migration and invasion without EGF induction, suggesting that the MLK3 regulation of cell migration and invasion is EGF signaling-independent.

Cell migration is a multipurpose process (29, 30) and drives the progression of cancer (31, 32). The alteration of the actin cytoskeleton is critical in the process of cell migration and generates the forces that push cell migration. MLK3 silencing enhances stress fibers in breast cancer cells (33). In this study, we confirmed that genetic depletion of MLK3 disturbs actin cytoskeleton organization. However, the molecular mechanisms underlying actin cytoskeleton remodeling remain unclear. Previous studies showed that EPS8 directly binds to actin and blocks actin prolongation by its effector domain (648–821 aa) *via* its capping activity to activate Rac signaling (34, 35). Therefore, the accurate localization of EPS8 is essential and contributes to actin rearrangement. In this study, we found that MLK3 interacts with EPS8 and controls the localization of EPS8. Following the loss of MLK3 in U118 and U251 cells, EPS8 expression was apparently increased, and its location was disarranged, which resulted in a number of mass-like structures on the cell edge. We verified that the regions of MLK3 (1–104 aa) with an SH3 domain and MLK3 (632–847 aa) containing PRD directly bind with EPS8. Targeting the two domains of MLK3 could be used as a valuable strategy for developing drugs for glioma therapy. Taken together, our results confirmed a novel mechanism by which MLK3 promotes cell migration and invasion *via* MLK3/EPS8 signaling.

The actin cytoskeleton is a dynamic cell structure that is attributed to diverse cellular processes, including cell morphogenesis, membrane trafficking, cell division, and immune response (17, 36–38). In addition, actin cytoskeleton dynamic remodeling has emerged as a critical event for glioma invasion. Therefore, controlling the change in actin is a feasible approach for glioma therapy. Currently, immunological therapies are crucial strategies for glioma therapy. Thus, tumor cells that escape from immunological surveillance are a barrier to effective immunotherapies. A study confirmed that the alteration of actin dynamics in tumor cells facilitates immune evasion (17). It would be interesting to ascertain whether MLK3 is involved in immune evasion of gliomas by regulating actin dynamics.

In summary, our findings have illustrated that as an oncogene, MLK3 may be a crucial regulator of the progression of gliomas and is associated with poor prognosis. As a consequence, the deletion of MLK3 in GBM cells decrease the capacity for cell migration and invasion and disrupt actin cytoskeleton remodeling. Furthermore, we provided a novel mechanism by which MLK3 facilitates glioma cell migration by regulating actin skeleton remodeling *via* MLK3/EPS8 signaling. Therefore, MLK3 is a potential target for therapy.

DATA AVAILABILITY STATEMENT

The original contributions presented in the study are included in the article/**Supplementary Material**, further inquiries can be directed to the corresponding author.

ETHICS STATEMENT

In this study, human glioma tissue samples were approved for use by the Ethics Committee of the Affiliated Hospital of Xuzhou Medical University (No. XYFY2018-KL056-01). All samples were obtained and analyzed previously by pathologists according to the 2016 WHO classification criteria. Written informed consent has been provided by the participants' legal guardian/next of kin prior to the surgery. For re-use of these samples in this study, written informed consent was not required in accordance with the national legislation and the institutional requirements.

AUTHOR CONTRIBUTIONS

YZ and X-YH designed the study. J-MS and Y-PW designed and performed the staining and scoring protocols for the human glioma tissues. YZ and Z-CS performed the cellular and molecular experiments and analyzed the data. F-JC assisted with the gene knockout by CRISPR/Cas9, and YZ and X-YH wrote the manuscript. All authors contributed to the article and approved the submitted version.

FUNDING

This work was supported by grants from the National Natural Science Foundation of China (81473185, 81673418), the Natural Science Foundation of the Jiangsu Higher Education Institutions of China (18KJA310007), a project funded by the Priority Academic Program Development of Jiangsu Higher Education Institutions (PAPD), and a project funded by the Jiangsu 333 Program (BRA2018059).

SUPPLEMENTARY MATERIAL

The Supplementary Material for this article can be found online at: https://www.frontiersin.org/articles/10.3389/fonc.2020.600762/full#supplementary-material

REFERENCES

1. Banan R, Hartmann C. The new WHO 2016 classification of brain tumors-what neurosurgeons need to know. *Acta Neurochir (Wien)* (2017) 159:403–18. doi: 10.1007/s00701-016-3062-3
2. Jovčevska I, Kočevar N, Komel R. Glioma and glioblastoma - how much do we (not) know? *Mol Clin Oncol* (2013) 1:935–41. doi: 10.3892/mco.2013.172
3. Gallo KA, Mark MR, Scadden DT, Wang Z, Gu Q, Godowski PJ. Identification and characterization of SPRK, a novel src-homology 3 domain-containing proline-rich kinase with serine/threonine kinase activity. *J Biol Chem* (1994) 269:15092–00. doi: 10.1016/S0021-9258(17)36578-X
4. Zhang J, Lu L, Xiong Y, Qin W, Zhang Y, Qian Y, et al. MLK3 promotes melanoma proliferation and invasion and is a target of microRNA-125b. *Clin Exp Dermatol* (2014) 39:376–84. doi: 10.1111/ced.12286

5. Rangasamy V, Mishra R, Mehrotra S, Sondarva G, Ray RS, Rao A, et al. Estrogen suppresses MLK3-mediated apoptosis sensitivity in ER^+ breast cancer cells. *Cancer Res* (2010) 70:1731–40. doi: 10.1158/0008-5472.CAN-09-3492
6. Das S, Sondarva G, Viswakarma N, Nair RS, Osipo C, Tzivion G, et al. Human epidermal growth factor receptor 2 (HER2) impedes MLK3 kinase activity to support breast cancer cell survival. *J Biol Chem* (2015) 290:21705–12. doi: 10.1074/jbc.M115.655563
7. Chen J, Miller EM, Gallo KA. MLK3 is critical for breast cancer cell migration and promotes a malignant phenotype in mammary epithelial cells. *Oncogene* (2010) 29:4399–11. doi: 10.1038/onc.2010.198
8. Mishra P, Senthivinayagam S, Rangasamy V, Sondarva G, Rana B. Mixed lineage kinase-3/JNK1 axis promotes migration of human gastric cancer cells following gastrin stimulation. *Mol Endocrinol* (2010) 24:598–607. doi: 10.1210/me.2009-0387
9. Zhan Y, Abi Saab WF, Modi N, Stewart AM, Liu J, Chadee DN. Mixed lineage kinase 3 is required for matrix metalloproteinase expression and invasion in ovarian cancer cells. *Exp Cell Res* (2012) 318:1641–48. doi: 10.1016/j.yexcr.2012.05.002
10. Misek SA, Chen J, Schroeder L, Rattanasinchai C, Sample A, Sarkaria JN, et al. EGFR signals through a DOCK180-MLK3 axis to drive glioblastoma cell invasion. *Mol Cancer Res* (2017) 15:1085–95. doi: 10.1158/1541-7786.MCR-16-0318
11. Schroyer AL, Stimes NW, Abi Saab WF, Chadee DN. MLK3 phosphorylation by ERK1/2 is required for oxidative stress-induced invasion of colorectal cancer cells. *Oncogene* (2018) 37:1031–40. doi: 10.1038/onc.2017.396
12. Werner A, Disanza A, Reifenberger N, Habeck G, Becker J, Calabrese M, et al. SCFFbxw5 mediates transient degradation of actin remodeller Eps8 to allow proper mitotic progression. *Nat Cell Biol* (2013) 15:179–88. doi: 10.1038/ncb2661
13. Skau CT, Fischer RS, Gurel P, Thiam HR, Tubbs A, Baird MA, et al. FMN2 makes perinuclear actin to protect nuclei during confined migration and promote metastasis. *Cell* (2016) 167:1571–85.e18. doi: 10.1016/j.cell.2016.10.023
14. Haffner MC, Esopi DM, Chaux A, Gürel M, Ghosh S, Vaghasia AM, et al. AIM1 is an actin-binding protein that suppresses cell migration and micrometastatic dissemination. *Nat Commun* (2017) 8:142. doi: 10.1038/s41467-017-00084-8
15. Kazazian K, Go C, Wu H, Brashavitskaya O, Xu R, Dennis JW, et al. Plk4 promotes cancer invasion and metastasis through Arp2/3 complex regulation of the actin cytoskeleton. *Cancer Res* (2017) 77:434–47. doi: 10.1158/0008-5472.CAN-16-2060
16. Cattaneo MG, Cappellini E, Vicentini LM. Silencing of Eps8 blocks migration and invasion in human glioblastoma cell lines. *Exp Cell Res* (2012) 318:1901–12. doi: 10.1016/j.yexcr.2012.05.010
17. Al Absi A, Wurzer H, Guerin C, Hoffmann C, Moreau F, Mao X, et al. Actin cytoskeleton remodeling drives breast cancer cell escape from natural killer-mediated cytotoxicity. *Cancer Res* (2018) 78:5631–43. doi: 10.1158/0008-5472.CAN-18-0441
18. Tao Y, Shen C, Luo S, Traoré W, Marchetto S, Santoni MJ, et al. Role of Erbin in ErbB2-dependent breast tumor growth. *Proc Natl Acad Sci U S A* (2014) 111:E4429–38. doi: 10.1073/pnas.1407139111
19. Du CP, Wang M, Geng C, Hu B, Meng L, Xu Y, et al. Activity-induced SUMOylation of neuronal nitric oxide synthase is associated with plasticity of synaptic transmission and extracellular signal-regulated kinase 1/2 signaling. *Antioxid Redox Sign* (2020) 32:18–34. doi: 10.1089/ars.2018.7669
20. Disanza A, Carlier MF, Stradal TE, Didry D, Frittoli E, Confalonieri S, et al. Eps8 controls actin-based motility by capping the barbed ends of actin filaments. *Nat Cell Biol* (2004) 6:1180–88. doi: 10.1038/ncb1199
21. Disanza A, Mantoani S, Hertzog M, Gerboth S, Frittoli E, Steffen A, et al. Regulation of cell shape by Cdc42 is mediated by the synergic actin-bundling activity of the Eps8-IRSp53 complex. *Nat Cell Biol* (2006) 8:1337–47. doi: 10.1038/ncb1502
22. Yan H, Parsons DW, Jin G, McLendon R, Rasheed BA, Yuan W. et al. IDH1 and IDH2 mutations in gliomas. *N Engl J Med* (2009) 360:765–73. doi: 10.1056/NEJMoa0808710
23. Hartmann C, Meyer J, Balss J, Capper D, Mueller W, Christians A, et al. Type and frequency of IDH1 and IDH2 mutations are related to astrocytic and oligodendroglial differentiation and age: a study of 1,010 diffuse gliomas. *Acta Neuropathol* (2009) 118:469–74. doi: 10.1007/s00401-009-0561-9
24. Sonoda Y, Kumabe T, Nakamura T, Saito R, Kanamori M, Yamashita Y, et al. Analysis of IDH1 and IDH2 mutations in Japanese glioma patients. *Cancer Sci* (2009) 100:1996–98. doi: 10.1111/j.1349-7006.2009.01270.x
25. Parsons DW, Jones S, Zhang X, Lin JC, Leary RJ, Angenendt P. et al. An integrated genomic analysis of human glioblastoma multiforme. *Science* (2008) 321:1807–12. doi: 10.1126/science.1164382
26. Dang L, White DW, Gross S, Bennett BD, Bittinger MA, Driggers EM, et al. Cancer-associated IDH1 mutations produce 2-hydroxyglutarate. *Nature* (2009) 462:739–44. doi: 10.1038/nature08617
27. Jiang B, Zhang J, Xia J, Zhao W, Wu Y, Shi M, et al. IDH1 mutation promotes tumorigenesis by inhibiting JNK activation and apoptosis induced by serum starvation. *Cell Rep* (2017) 19:389–400. doi: 10.1016/j.celrep.2017.03.053
28. Rattanasinchai C, Llewellyn BJ, Conrad SE, Gallo KA. MLK3 regulates FRA-1 and MMPs to drive invasion and transendothelial migration in triple-negative breast cancer cells. *Oncogenesis* (2017) 6:e345. doi: 10.1038/oncsis.2017.44
29. Te Boekhorst V, Preziosi L, Friedl P. Plasticity of cell migration in vivo and in silico. *Annu Rev Cell Dev Biol* (2016) 32:491–526. doi: 10.1146/annurev-cellbio-111315-125201
30. van Helvert S, Storm C, Friedl P. Mechanoreciprocity in cell migration. *Nat Cell Biol* (2018) 20:8–20. doi: 10.1038/s41556-017-0012-0
31. Ridley AJ, Schwartz MA, Burridge K, Firtel RA, Ginsberg MH, Borisy G, et al. Cell migration: integrating signals from front to back. *Science* (2003) 302:1704–09. doi: 10.1126/science.1092053
32. Friedl P, Gilmour D. Collective cell migration in morphogenesis, regeneration and cancer. *Nat Rev Mol Cell Biol* (2009) 10:445–57. doi: 10.1038/nrm2720
33. Chen J, Gallo KA. MLK3 regulates paxillin phosphorylation in chemokine-mediated breast cancer cell migration and invasion to drive metastasis. *Cancer Res* (2012) 72:4130–40. doi: 10.1158/0008-5472.CAN-12-0655
34. Scita G, Tenca P, Areces LB, Tocchetti A, Frittoli E, Giardina G. et al. An effector region in Eps8 is responsible for the activation of the Ra c-specific GEF activity of Sos-1 and for the proper localization of the Rac-based actin-polymerizing machine. *J Cell Biol* (2001) 154:1031–44. doi: 10.1083/jcb.200103146
35. Hertzog M, Milanesi F, Hazelwood L, Disanza A, Liu H, Perlade E, et al. Molecular basis for the dual function of Eps8 on actin dynamics: bundling and capping. *PLoS Biol* (2010) 8:e1000387. doi: 10.1371/journal.pbio.1000387
36. Pollard TD, Cooper JA. Actin, a central player in cell shape and movement. *Science* (2009) 326:1208–12. doi: 10.1126/science.1175862
37. Gurel PS, Hatch AL, Higgs HN. Connecting the cytoskeleton to the endoplasmic reticulum and Golgi. *Curr Biol* (2014) 24:R660–72. doi: 10.1016/j.cub.2014.05.033
38. Heng YW, Koh CG. Actin cytoskeleton dynamics and the cell division cycle. *Int J Biochem Cell B* (2010) 42:1622–33. doi: 10.1016/j.biocel.2010.04.007

Conflict of Interest: The authors declare that the research was conducted in the absence of any commercial or financial relationships that could be construed as a potential conflict of interest.

frontiers in Oncology

ORIGINAL RESEARCH
published: 24 February 2021
doi: 10.3389/fonc.2020.623048

TIPE Regulates DcR3 Expression and Function by Activating the PI3K/AKT Signaling Pathway in CRC

Mengya Zhong[1,2†], Xingfeng Qiu[3†], Yu Liu[3,4], Yan Yang[1], Lei Gu[5], Chenxi Wang[1], Huiyu Chen[1], Zhongchen Liu[5], Jiayin Miao[6*] and Guohong Zhuang[1,7*]*

[1] Cancer Research Center, School of Medicine, Xiamen University, Xiamen, China, [2] Department of Hematology, The First Affiliated Hospital of Xiamen University and Institute of Hematology, School of Medicine, Xiamen University, Xiamen, China, [3] Department of Gastrointestinal Surgery, Zhongshan Hospital, Xiamen University, Xiamen, China, [4] General Surgery Center of Bazhong Central Hospital, Bazhong, China, [5] Department of Gastrointestinal Surgery, Shanghai Tenth People's Hospital Affiliated to Tongji University, Shanghai, China, [6] Department of Neurology, Zhongshan Hospital, Xiamen University, Xiamen, China, [7] Organ Transplantation Institute of Xiamen University, Fujian Provincial Key Laboratory of Organ and Tissue Regeneration, School of Medicine, Xiamen University, Xiamen, China

OPEN ACCESS

Edited by:
Andrew Davis, Washington University in St. Louis, United States

Reviewed by:
Jun Peng, Fujian University of Traditional Chinese Medicine, China
Napoleon Navarro-Tito, Autonomous University of Guerrero, Mexico

***Correspondence:**
Zhongchen Liu
13860184888@163.com
Jiayin Miao
miaojiayin2006@163.com
Guohong Zhuang
zhgh@xmu.edu.cn

[†]These authors have contributed equally to this work

Specialty section:
This article was submitted to Molecular and Cellular Oncology, a section of the journal Frontiers in Oncology

Received: *31 October 2020*
Accepted: *23 December 2020*
Published: *24 February 2021*

Citation:
Zhong M, Qiu X, Liu Y, Yang Y, Gu L, Wang C, Chen H, Liu Z, Miao J and Zhuang G (2021) TIPE Regulates DcR3 Expression and Function by Activating the PI3K/AKT Signaling Pathway in CRC. Front. Oncol. 10:623048. doi: 10.3389/fonc.2020.623048

Tumor necrosis factor-induced protein-8 (TIPE) is highly expressed in colorectal cancer (CRC). Decoy receptor 3 (DcR3) is a soluble secreted protein that can antagonize Fas ligand (FasL)-induced apoptosis and promote tumorigenesis. It remains unclear whether TIPE can regulate DcR3 expression. In this study, we examined this question by analyzing the relationship between these factors in CRC. Bioinformatics and tissue microarrays were used to determine the expression of TIPE and DcR3 and their correlation in CRC. The expression of TIPE and DcR3 in colon cancer cells was detected. Plasma samples were collected from CRC patients, and DcR3 secretion was measured. Then, dual-luciferase reporter gene analysis was performed to assess the interaction between TIPE and DcR3. We exogenously altered TIPE expression and analyzed its function and influence on DcR3 secretion. Lipopolysaccharide (LPS) was used to stimulate TIPE-overexpressing HCT116 cells, and alterations in signaling pathways were detected. Additionally, inhibitors were used to confirm molecular mechanisms. We found that TIPE and DcR3 were highly expressed in CRC patients and that their expression levels were positively correlated. DcR3 was highly expressed in the plasma of cancer patients. We confirmed that TIPE and DcR3 were highly expressed in HCT116 cells. TIPE overexpression enhanced the transcriptional activity of the DcR3 promoter. TIPE activated the PI3K/AKT signaling pathway to regulate the expression of DcR3, thereby promoting cell proliferation and migration and inhibiting apoptosis. In summary, TIPE and DcR3 are highly expressed in CRC, and both proteins are associated with poor prognosis. TIPE regulates DcR3 expression by activating the PI3K/AKT signaling pathway in CRC, thus promoting cell proliferation and migration and inhibiting apoptosis. These findings may have clinical significance and promise for applications in the treatment or prognostication of CRC.

Keywords: colorectal cancer, cell proliferation, migration, apoptosis, PI3K/AKT signaling pathway

INTRODUCTION

Colorectal cancer (CRC) kills nearly 2 million people each year, making it the fourth deadliest cancer worldwide behind lung, liver and stomach cancers (1). According to The Global Cancer Observatory (GLOBOCAN) 2018 data (http://gco.iarc.fr), CRC is currently the most common malignant tumor in China, ranking first in prevalence and second in incidence. Surgery, chemotherapy, radiotherapy and molecular targeted therapy are the most commonly used treatments for CRC, but the survival rate remains low (2). Patients with advanced CRC who receive radiation therapy and chemotherapy experience serious adverse reactions. Therefore, the development of new, effective treatment strategies is urgently needed. Currently, researchers are devoted to elucidating the molecular mechanism of the occurrence and development of CRC (3).

Tumor necrosis factor-induced protein-8 (TNFAIP8/TIPE; also called SCC-S2, MDC-3.13, GG2-1, and NDED) was the first identified protein in the TIPE family and is closely associated with tumors and inflammation (4). As an antiapoptotic and carcinogenic molecule, TIPE promotes the growth, proliferation and migration of cancer cells (5). The activation of TNF-α and NF-κB in the inflammatory environment can induce TIPE expression (6). A large number of studies have revealed that TIPE is highly expressed in various tumors, and high TIPE expression is related to clinical parameters and metastasis (7–9). TIPE has been reported to be overexpressed in colon cancer and to regulate cell proliferation (10). The latest research shows that TIPE can promote tumor proliferation and invasion by activating Wnt signaling and inhibiting Hippo signaling in CRC cells (11). Our previous studies showed that TIPE promotes angiogenesis in CRC by regulating VEGFR2 expression.

Decoy receptor 3 (DcR3) is a member of the tumor necrosis factor receptor superfamily (TNFRSF). DcR3 cDNA encodes the 300-amino acid (aa) protein, which contains four cysteine-rich repeats of TNFRSF. Unlike most members of the TNFRSF, DcR3 is a soluble secreted protein lacking transmembrane sequences and can be detected in serum and cell culture media (12). DcR3 binds and neutralizes three members of the tumor necrosis factor superfamily (TNFSF): Fas ligand (FasL) (13), TNF-like molecule 1A (TL1A) (14), and herpes virus entry mediator L (LIGHT) (15). By binding these ligands, DcR3 can inhibit apoptosis, induce angiogenesis and modulate immune cell function. Additionally, DcR3 is almost undetectable in most individuals with noninflammatory diseases and cancers. The expression level of DcR3 protein is related to tumorigenesis and metastasis (16). Earlier studies confirmed that DcR3 is a predictor of 5-fluorouracil (5-FU)-based adjuvant chemotherapy responses in CRC patients (17). Later, Yu et al. confirmed that DcR3 has the potential to regulate the growth and metastasis of SW480 colon cancer cells (18). Zong et al. found that the overexpression of DcR3 in CRC increases the risk of malignancy (19). These findings suggest that DcR3 is a potential therapeutic target in CRC.

Our previous studies demonstrated that TIPE is highly expressed in stage III gastric cancer and positively correlated with DcR3 and ERK1/2 (20). However, it is unclear whether TIPE can regulate the expression of DcR3; both of these factors can act as antiapoptotic molecules to antagonize cell apoptosis and promote cell proliferation and metastasis. In this study, with bioinformatic methods, we first detected high TIPE and DcR3 expression in CRC and found a positive correlation between the expression of these two proteins. In addition, we collected plasma samples from CRC patients diagnosed at the Department of Gastrointestinal Surgery at Zhongshan Hospital of Xiamen University, and high DcR3 expression was detected in the plasma. Dual-luciferase reporter gene analysis showed that TIPE overexpression enhanced the transcriptional activity of the DcR3 promoter. Exogenous changes in the expression of TIPE in HCT116 cells also altered the expression of DcR3. *In vitro* functional experiments indicated that TIPE plays a vital role in the proliferation, migration and apoptosis of CRC cells. Interestingly, when we stimulated TIPE-overexpressing HCT116 cells with LPS, we found that the expression of phosphorylated AKT, P105, and P65 was upregulated compared to that in control cells. After using the PI3K inhibitor LY294002 to suppress upstream PI3K expression, the abovementioned molecular phosphorylation was downregulated. Finally, these data combined with tissue microarray data demonstrated that TIPE and DcR3 were highly expressed in CRC and associated with poor prognosis. Our study revealed that TIPE regulated DcR3 expression by activating the PI3K/AKT signaling pathway in CRC, thereby promoting cell proliferation and metastasis and inhibiting apoptosis.

MATERIALS AND METHODS

Cell Culture

The CRC cell lines HCT116, and SW620 and human embryonic kidney (HEK) 293T cells were obtained from the Anti-cancer Center of Xiamen University (Xiamen, Fujian). All cell lines were cultured in Dulbecco's modified Eagle's medium (DMEM, Gibco, CA, USA) supplemented with 10% fetal bovine serum (FBS, Gibco), 100 units/ml penicillin and 100 mg/ml streptomycin (Invitrogen, Carlsbad, CA, USA) and in a humidified environment containing 5% CO_2 at 37°C.

Cell Transfection

The lentiviral vector and the control vector (TIPE/PLNX2) encoding TIPE were donated by the School of Life Sciences, Xiamen University. We used 293T and HCT116 cells in the logarithmic growth phase to perform experiments. The day before transfection, 1×10^6 cells were seeded into 6-well plates, and 2 ml serum-free medium was added to each well. According to the manufacturer's instructions, 6 μl Lipofectamine 2000 (Invitrogen, Carlsbad, CA, USA) and 2 μg plasmid DNA were separately added to 250 μl Opti-MEM I serum-free medium (Sigma-Aldrich, St. Louis, USA) and incubated for 5 min, and then the two solutions were mixed and incubated at room temperature for 20 min. The mixture was added to the cells for transient transfection for 36 h. In all experiments, real-time quantitative PCR (qRT-PCR) and Western blot analysis showed

that the transfection efficiency of the cells was > 60%. TIPE-overexpressing cells and the corresponding control cells were cultured for subsequent experiments.

Cell Proliferation

According to the manufacturer's instructions, cell proliferation activity was measured using a Cell Counting Kit-8 (CCK-8; TransGen Biotech, Beijing, China). Cells were seeded into 96-well plates (Corning Inc., NY, USA) in triplicate at an initial density of 4,000–7,000 cells per well and cultured in a 37°C, 5% CO2 incubator for 24 h. On the second day, CCK-8 reagent (10% of the total volume of medium) was added to each well, and the cells were cultured in the incubator for another 4 h. Finally, a Bio-Rad microplate reader (California, USA) was used to measure the absorbance at 450 nm at each indicated time point.

Wound Healing Assay

In a six-well plate, lines were evenly drawn across the wells every 0.5–1 cm, with a total of three lines in each well. Transfected HCT116 cells (approximately 5×10^5 cells per well) were added and cultured overnight. The next day, a 20-μl pipette tip was used to make a scratch as close to perpendicular to the horizontal line on the back as possible. Then, the cells were washed three times with preheated phosphate-buffered saline (PBS; Solarbio, Beijing, China) to detached cells, and 2 ml serum-free DMEM was added to each well. The cells were placed in a 37°C, 5% CO2 incubator, and measurements were taken after 0, 12, 24, and 36 h. ImageJ (NIH, MD, USA) was used to measure the scratch area. The experiment was repeated three times for each group of cells.

Transwell Assay

HCT116 cells transfected with TIPE overexpression plasmids or TIPE interference plasmids (experimental group) and HCT116 cells transfected with PLNCX-2 empty vector plasmids (control group) were cultured in 6-well plates (5×10^5 cells/ml) for 24 h, and then the cell medium was changed to serum-free DMEM. Cells were starved for 24 h. The two groups of cells were detached from the plates and counted, and a 2×10^5 cell suspension was placed into a Transwell chamber. In addition, 500 μl of medium containing 15% FBS was added to the lower chamber, and the cells were cultured for 24 h. The Transwell chamber was removed, and the medium was discarded. The cells were washed three times with prechilled PBS, fixed with 4% paraformaldehyde for 20 min, and stained with 0.1% crystal violet for 15 min. Nonmigrated cells were gently removed from the top of the membrane with cotton swabs, and then the remaining invaded cells were observed and counted in 5 fields under a microscope at 100-fold magnification.

Enzyme-Linked Immunosorbent Assay

Plasma from patients diagnosed with CRC was obtained from the Department of Gastrointestinal Surgery, Zhongshan Hospital Affiliated to Xiamen University. All aspects of the study were approved by the medical ethics committee of Zhongshan Hospital, Xiamen University. All registered patients provided written informed consent, and the use of patient samples in the study was approved by the Institutional Review Board of the Tumor Tissue Bank of Zhongshan Hospital, Xiamen University. Cell culture supernatant was obtained after cultivating cells for 24 h. Changes in DcR3 levels in cell supernatants and plasma were measured using an ELISA kit (R&D Systems, Minnesota, USA). Test samples and standards were added to a 96-well plate coated with the capture antibody, incubated at room temperature for 2 h and removed. The wells were washed with a series of buffers. Then, a biotin anti-human DCR3 antibody was added and incubated at room temperature for 1 h. The plate was washed three times, and an avidin-peroxidase complex was added and allowed to react for 30 min. After washing, tetramethyl benzidine (TMB) color solution was added, and the mixture was incubated at room temperature for 30 min in the dark. Finally, TMB stop solution was added, and the color in the wells changed. We determined the optical density (OD) value at 450 nm and calculated the corresponding concentration according to the absorbance value of the sample on the standard curve.

Dual-Luciferase Reporter Gene Assay

The medium was removed from the cells, and the cells were washed with PBS. The wash solution was removed after washing. Then, 50 μl Report Lysis Buffer (Promega, Madison, Wisconsin, USA) was added to each well, the culture plate was gently shaken at room temperature for 15 min, the cells were scraped off the petri dish, and the sample was centrifuged at 16,000 g and placed at 4°C for 30 s. LARII (100 μl) was added to the test tube in advance, the program for the fluorescence luminometer was set, and the lysate was transferred to the test tube. Cell lysates containing an equal amount of protein (10–20 μg) were placed into the wells of an opaque black 96-well microtitration plate, 5 μl of luciferase substrate (Promega) was added, and firefly luciferase activity was detected on a Packard apparatus. Then, 100 μl Stop&Glo Reagent was added to the test tube to detect Renilla luciferase activity. Both firefly and Renilla luciferase activities were quantified according to the manufacturer's instructions using the dual-luciferase reporter system (Promega).

Western Blot Analysis

Cells were lysed with RIPA buffer (Sigma-Aldrich) at 4°C for 1 h with 1% protease inhibitor mixture and 1% phenylmethanesulfonyl fluoride (Gold Biotechnology, USA). The tricarboxylic acid (TCA) precipitation method was used to collect the supernatant of the culture medium to extract DcR3 protein. After centrifugation at 12,000 rpm for 10 min at 4°C, the supernatant was collected. The protein standard curve was developed by the BCA method, and protein concentrations of the samples were determined (Bio-Rad, Hercules, CA). The samples were mixed with sodium dodecyl sulfate (SDS) loading buffer, heated at 100°C for 10 min, and centrifuged at 12,000 rpm for 5 min. Then, an equal amount of protein (10–40 μg) was separated by electrophoresis on a 12% SDS gel, transferred to a PVDF membrane (Millipore, Billerica, MA, USA) and blocked with 5% skim milk powder. The membranes were washed and incubated at 4°C overnight with the following specific primary antibodies: rabbit monoclonal antibodies against TIPE (1:1,000; Abcam, MA, USA), PI3K, P-PI3K (1:1,000; Abcam, MA, USA), and P-AKT (1:2,000; Cell Signaling, MA, USA); a mouse

monoclonal antibody against AKT (1:2,000; Cell Signaling, MA, USA); and rabbit polyclonal antibodies against DcR3 (1:1,000; Affinity Biosciences, Jiangsu, China), P105, P-P105, P65, P-P65 (1:500; Affinity Biosciences, Jiangsu, China), and β-actin (1:5,000; Proteintech, Suite, USA). The next day, immunoblotting was performed using the corresponding HRP-binding secondary antibody, followed by the visual detection of the protein bands using a hypersensitive enhance chemiluminescence (ECL) kit (NCM Biotech, Suzhou, China) and a Bio-Rad ChemiDoc XRS + detection system (Bio-Rad, Hercules, CA).

Real-Time Quantitative PCR

Total RNA was extracted from cells using TRIzol reagent (TransGen Biotech, Beijing). One microgram of RNA was reverse transcribed into cDNA using a cDNA Synthesis SuperMix kit (TransGen Biotech, Beijing). TransStart Top Green qPCR SuperMix (TransGen Biotech, Beijing) was used for real-time PCR, and data collection was performed on a Bio-Rad Biosystems 7500 instrument using SYBR Green (Bio-Rad, Hercules, CA). The sequences of the forward and reverse primers are as follows:

β-actin -F: 5'-AGCGAGCATCCCCCAAAGTT-3,
β-actin-R: 5'-GGGCACGAAGGCTCATCATT-3;
TIPE-F: 5'-TTCAGGCCTCCCTCTT-TAACAATC-3,
TIPE-R: 5'-CGTTCGTGGCAGGGGTTATT-3;
DCR3-F: 5'-GCCGCTACTGCAACGTCCTC-3,
DCR3-R: 5'-GGCTGGCACTGCGTGTTCTG-3.

Relative gene expression levels were normalized to β-actin as a control.

Flow Cytometry

The apoptosis of HCT116 cells in different treatment groups was examined by flow cytometry. Cells were seeded into six-well plates at a density of 1×10^5 per well and incubated for 24 h. After transfection for 36 h, sFasL (100 ng/ml) was added to some groups for 24 h. The cells were then harvested, washed twice with fluorescence-activated cell sorting (FACS) wash buffer (PBS containing 1% FBS), and centrifuged at 1,000 g for 5 min. To assess cell cycle progression, 1 ml PBS was added to fully resuspend single cells, and 3 ml prechilled absolute ethanol was slowly added while gently swirling. After reaching a final concentration of 75%, cells were fixed at 4°C for 4 h. Then, the cells were washed twice with FACS wash buffer, and 500 μl propidium iodide (PI) working solution (Meilunbio, Dalian, China) was added to each cell sample; the samples were gently mixed to completely resuspend the cell pellet and then incubated at 37°C for 30 min in the dark. After staining, a CytoFlex S flow cytometer (Beckman Coulter, CA, USA) was used to analyze cell fluorescence, and FlowJo software (Stanford University, USA) was used for analysis. The cell cycle distribution is shown as the percentage of cells in G0/G1, S, G2, and M phase based on PI staining. The percentage of apoptotic cells with sub-G1 (<G1) DNA content was determined. These experiments were performed with at least three biological replicates.

Tissue Microarray and Immunohistochemistry

Normal tissue and CRC tissue microarrays (CRC-1402) were obtained from Wuhan Servicebio Biotechnology Company (Wuhan, China). The paraffin-embedded microarray was dewaxed in an oven at 65°C overnight, dehydrated and rehydrated with xylene and a series of concentration gradients of ethanol, and subjected to heat-induced antigen recovery in a pressure cooker with a sodium citrate antigen repair solution (Maixin, Fuzhou, China) for 15 min. The samples were then blocked at room temperature with endogenous peroxidase blockers for 15 min, washed with PBST three times and incubated overnight at 4°C with anti-TIPE antibodies (1:50, Abcam, Suite Cambridge, USA) and DCR3 antibodies (1:50, BioLegend, London, United Kingdom). On the next day, the samples were washed with PBST three times, and a biotin-labeled secondary antibody was added and incubated for 30 min at room temperature. The sections were visualized with the diaminobenzidine method and then counterstained with hematoxylin. Finally, Image-Pro Plus 6.0 (Media Cybernetics, Inc., MD, USA) was used to analyze the immunohistochemical staining density and average optical (AO) density. For the negative control of the staining process, the primary antibody was omitted, while all other experimental conditions remained the same.

Statistical Methods

Statistical Package for the Social Sciences 21.0 (SPSS 21.0), GraphPad Prism 6 and Excel were used to analyze all the results. A t-test was used for comparisons between two groups, one-way ANOVA was used for comparisons among more than two groups, and the Bonferroni method was used for comparisons between groups and within groups. Differences with $p<0.05$ were considered statistically significant (* $p<0.05$; ** $p<0.01$; *** $p<0.001$; and **** $p<0.0001$).

RESULTS

Tumor Necrosis Factor-Induced Protein-8 and Decoy Receptor 3 Are Highly Expressed and Positively Correlated in Patients with Colorectal Cancer

To investigate the role of TIPE and DcR3 in human CRC, we first analyzed the available datasets of CRC patients in the Cancer Genome Atlas (TCGA) database, and the differential expression of TIPE and DcR3 in CRC tissues and adjacent tissues was randomly validated with Gene Expression Profiling Interactive Analysis (GEPIA; http://gepia.cancer-pku.cn/index.html). The bioinformatics results showed that TIPE and DcR3 expression was significantly increased in CRC tissues compared to adjacent tissues at the mRNA level (the red area represents the tumor),

and the difference in DcR3 expression was significant (**Figures 1A, B**). In addition, to build on our previous literature review, we further searched the Oncomine dataset (Gaspar) to evaluate the relationship between TIPE and DcR3, and linear correlation analysis results confirmed that the expression of TIPE and DcR3 was positively correlated (**Figure 1C**). These results suggested that TIPE and DcR3 are highly expressed in CRC and may play a vital role in the tumorigenesis and development of CRC.

To further investigate the function of TIPE and DcR3 in CRC, we continued to examine the association between their expression and clinical factors in the UALCAN (http://ualcan.path.uab.edu/index.html) database. The results confirmed that as the tumor stage gradually increased, the mRNA expression level of DcR3 increased compared with that in normal tissues (**Figure 1D**). Conversely, the expression level of TIPE decreased (**Figure 1E**) as the tumor stage increased, which may be related to the difference in tumor subtypes. In addition, we used the same dataset (GSE17536) from the Gene Expression Omnibus (GEO) database to analyze the relationship between TIPE and DcR3 and the survival of CRC patients. As shown in **Figures 1F, G**, higher expression levels of TIPE and DcR3 were associated with worse survival rates in patients, indicating that high expression levels of TIPE and DcR3 are associated with poor prognosis. This further supported that TIPE and DcR3 play a vital role in the tumorigenesis and development of CRC.

To determine whether the increase in TIPE and DcR3 expression was associated with clinical features, we collected GSE17536 data and analyzed correlations between TIPE and DcR3 expression and the sex, age, tumor grade, stage, total survival and disease-free survival of CRC patients. No significant

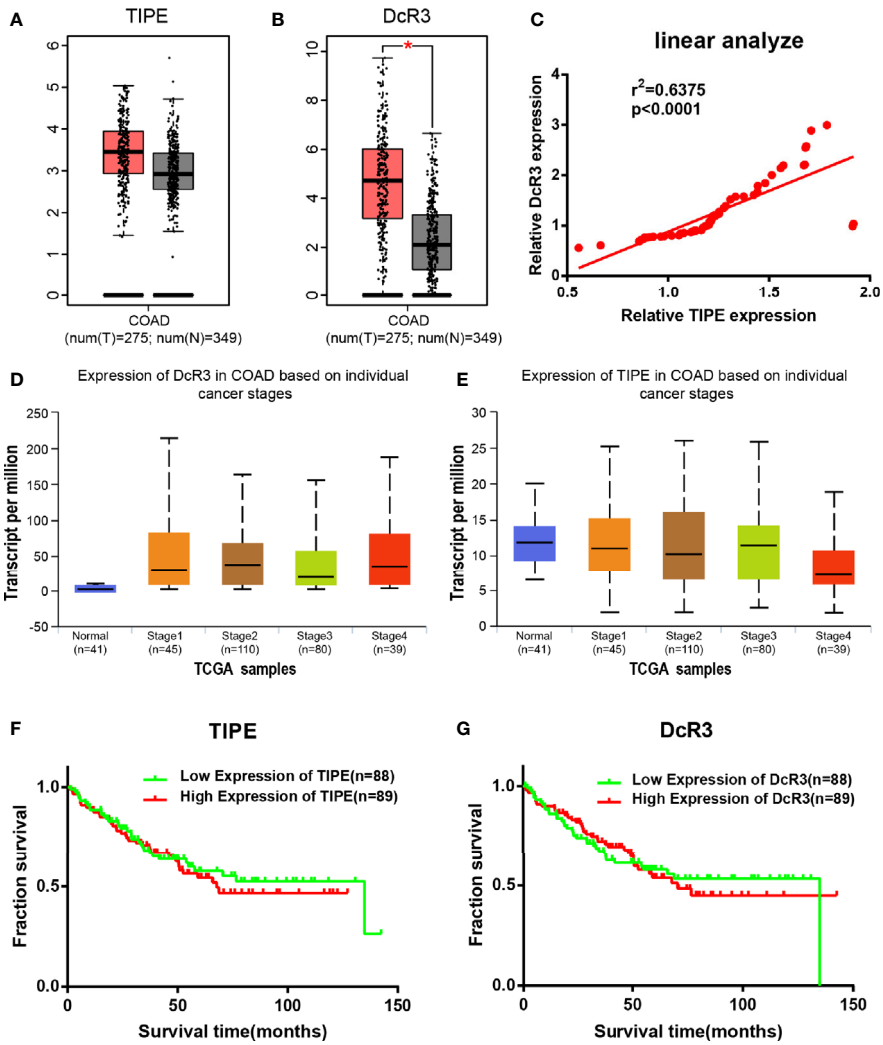

FIGURE 1 | Tumor necrosis factor-induced protein-8 (TIPE) and DcR3 are highly expressed and positively correlated in colorectal cancer (CRC) patients. Box plots showing **(A)** TIPE and **(B)** DcR3 mRNA upregulation in CRC samples relative to normal samples (data downloaded from GEPIA). **(C)** The linear analysis relationship between TIPE and DcR3 showed that the proteins were positively correlated. **(D)** Relative DcR3 mRNA expression in UALCAN datasets, which included 41 normal samples and 274 samples with different stages of colorectal cancer. **(E)** Detection of relative TIPE mRNA expression in the same database. Kaplan-Meier curves for the overall survival of 177 CRC patients stratified by **(F)** TIPE and **(G)** DcR3 expression. *$p < 0.05$.

correlations were observed in these analyses ($p > 0.05$) (**Supplementary Tables 1**, **2**).

The Expression of Tumor Necrosis Factor-Induced Protein-8 and Decoy Receptor 3 Is Increased in Colorectal Cancer

To verify the relationship between TIPE and DcR3 in CRC, we first selected two colon cancer cell lines, HCT116, and SW620, which are commonly used in experiments, and evaluated the expression of TIPE and DcR3 by qRT-PCR and Western blot analysis. As shown in **Figures 2A, B**, all cell lines expressed TIPE. DcR3 was low expressed in SW620 cells, and the mRNA and protein levels of TIPE and DcR3 were higher in HCT116 cells. In addition, we also collected plasma samples from patients with CRC and healthy individuals (the control group) and determined the DcR3 level in the plasma with ELISA. Plasma samples from cancer patients had significantly higher levels of DcR3 than those from the control group (**Figure 2C**). These results demonstrate that TIPE and DcR3 were highly expressed in CRC and that their protein expression patterns were consistent with their mRNA expression patterns.

DcR3 is generally difficult to detect because it lacks a transmembrane sequence, and DcR3 is a soluble protein. However, our results combined with the previous linear correlation analysis results of bioinformatics data demonstrated that TIPE was highly expressed in stage III gastric cancer and

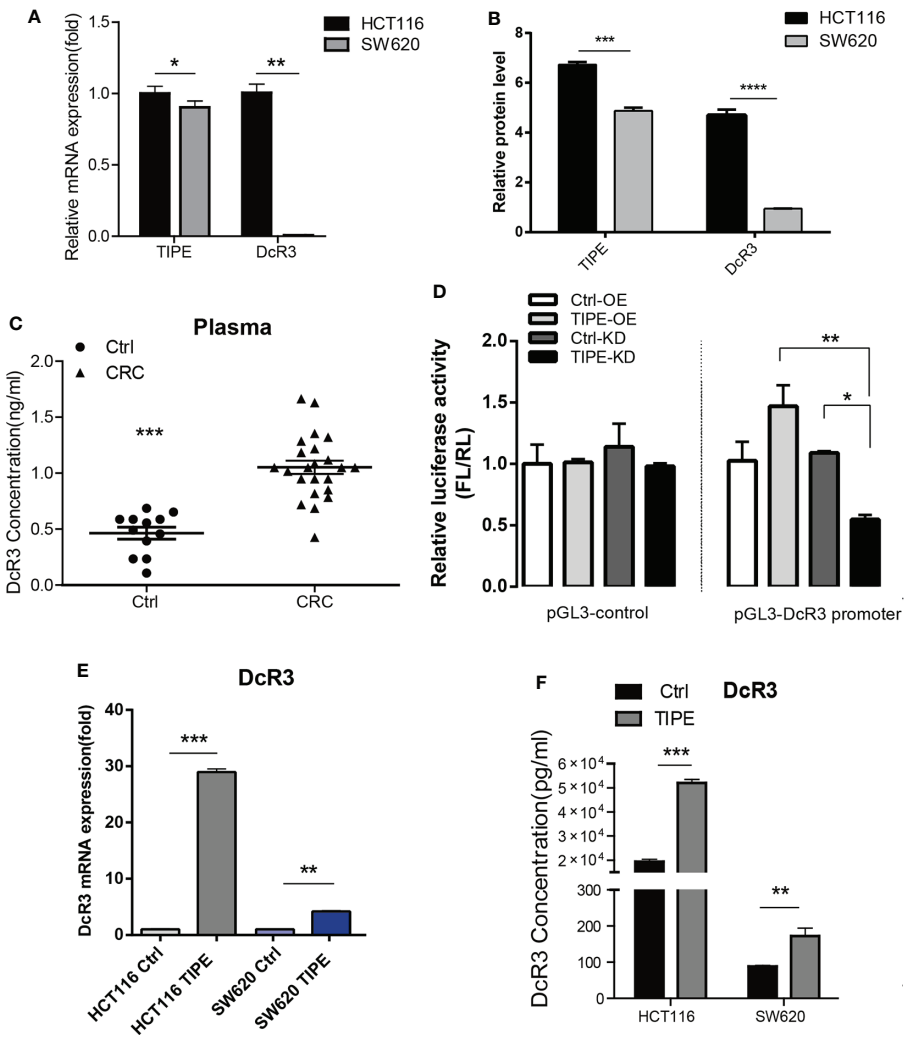

FIGURE 2 | Tumor necrosis factor-induced protein-8 (TIPE) can upregulate DcR3 expression and positively regulate DcR3 transcription. **(A)** Comparison of TIPE and DcR3 mRNA expression in HCT116, and SW620 cells. TIPE and DcR3 mRNA expression was quantified by qRT-PCR and normalized in HCT116 cells. **(B)** Expression of TIPE and DcR3 in HCT116, and SW620 cells based on Western blot assays. **(C)** ELISA analysis and statistical analysis of DcR3 in a group of patients with CRC (n = 8) and healthy individuals (n = 4). **(D)** The relative luciferase activity of the DcR3 promoter was detected after TIPE overexpression and TIPE knockdown. **(E)** qRT-PCR assay of relative mRNA expression levels of DcR3 in two colon cancer cells based in TIPE overexpression or control cells. **(F)** DcR3 protein expression was detected by ELISA in supernatants of HCT116, and SW620 cells. TIPE promoted DcR3 secretion compared with that in the control group. ns, not significant, $^{*}p < 0.05$, $^{**}p < 0.01$, $^{***}p < 0.001$.

positively correlated with DcR3 and ERK1/2 expression. We hypothesized that there may be a regulatory relationship between TIPE and DcR3. Through dual-luciferase reporter gene assays, we found that overexpressing TIPE enhanced the transcriptional activity of the DcR3 promoter, whereas knocking down TIPE expression reduced the transcriptional activity of DcR3 (**Figure 2D**). We then overexpressed TIPE in two cell lines and examined whether the expression of DcR3 was altered. When the expression of TIPE increased (Supplementary **Figure 1A**), the expression of DcR3 also significantly increased compared with that in the control group (**Figures 2E, F**). In summary, these results suggested that TIPE positively regulated DcR3 transcription and that TIPE overexpression upregulated DcR3 expression.

Tumor Necrosis Factor-Induced Protein-8 Affects Proliferation and Apoptosis by Regulating Decoy Receptor 3 Expression

Based on the above findings, we next explored whether TIPE can affect the function of DcR3. Due to the low expression level of DcR3 and detection difficulty, we selected HCT116, which had higher expression level of DcR3 after the overexpression of TIPE, as the target cell line for our subsequent experiments. CCK-8 assays showed that cell growth declined after knocking down TIPE, while overexpressing TIPE reversed this phenomenon and promoted the proliferation of HCT116 cells. With the increase in cell number and culture time, the differences became more apparent, and they were significant compared with those in the control group ($p<0.001$) (**Figures 3A, B**). These results suggest that TIPE overexpression promoted the proliferation of colon cancer cells.

Resistance to apoptosis is considered a reason for cancer treatment failure. We first used a PI staining solution to detect apoptotic cells under normal conditions, and there was no difference in the number of sub-G1 cells between the normal group (control group) and the TIPE control group (vector group) in HCT116 cells. Subsequently, we found that the sub-G1 population was larger in the TIPE knockdown group, whereas the sub-G1 population was smaller after the overexpression of TIPE in HCT116 cells (**Figure 3C**). Statistical analysis revealed significant differences among the shTIPE group, TIPE group and control group (**Figure 3D**). Numerous studies have shown that the DcR3 protein acts as a decoy receptor, neutralizing FasL-mediated apoptosis signals. Therefore, we further exposed the cells in the above groups to sFasL (100 ng/ml) for 24 h and then detected cell apoptosis. We discovered that the sub-G1 population decreased in the TIPE-overexpressing group, while the sub-G1 and apoptotic cell populations increased in the TIPE knockout group (**Figure 3C**). Further statistical analysis confirmed that the TIPE overexpression and knockdown groups were significantly different from the control group in terms of apoptosis rates ($p<0.001$), and the TIPE overexpression group and the TIPE knockout group were also significantly different ($p<0.001$) (**Figure 3D**). Meanwhile, we also detected the secretion of DcR3 in different groups with ELISA, and the results showed that as TIPE expression increased, DcR3 also increased, and vice versa (**Supplementary Figure 1B**). These results further confirmed that the overexpression of TIPE upregulated DcR3 secretion and blocked the cytotoxic effect of FasL in HCT116 cells.

Tumor Necrosis Factor-Induced Protein-8 Overexpression Enhances the Migration of Colon Cancer Cells

Since both proliferation and migration are important in tumor growth and metastasis, we further verified the effect of TIPE on the migration ability of HCT116 cells. Through a wound healing assay, we found that compared with the control group, the TIPE overexpression group showed stronger wound healing ability, especially after 24 h, while TIPE knockdown had the opposite effect (**Figure 4A**). We also performed statistical analysis of the scratch area. As shown in **Figure 4B**, the area of the TIPE knockdown group was significantly smaller than that of the control group, while the healing rate of the TIPE overexpression group significantly increased at 24 h compared with that of the control group ($p<0.01$). All these results indicated that TIPE enhanced the migration ability of colon cancer cells.

We used a Transwell assay to further evaluate the effect of TIPE on the motility of HCT116 cells. After 24 h of culture, we found that the number of adherent cells on the lower side of the Transwell chamber significantly increased in the TIPE overexpression group compared with that in the control group, while TIPE knockdown had the opposite effect (**Figure 4C**). These results again illustrate that TIPE promotes the migration of the colon cancer cell line HCT116. Statistical analysis further confirmed that there were significant differences among the three groups in terms of cell migration (**Figure 4D**). We also extracted proteins from three groups of cells and verified the effect of TIPE overexpression with Western blot analysis (**Supplementary Figure 1C**). The cell supernatant was collected, and the secretion of DcR3 was further detected with ELISA. The expression of DcR3 was increased in the TIPE overexpression group but decreased in the TIPE knockdown group (**Supplementary Figure 1D**). These results all demonstrated that TIPE overexpression promotes DcR3 secretion and cell migration.

Tumor Necrosis Factor-Induced Protein-8 Regulates Decoy Receptor 3 Expression by Activating the Phosphatidylinositol 3-Kinase/AKT Signaling Pathway in Colorectal Cancer

To confirm the importance of the PI3K signaling pathway in regulating DcR3 expression in CRC after changes in TIPE expression, we stimulated the HCT116 colon cancer cell line with LPS. Through Western blot analysis, we found that in response to LPS, the expression levels of total PI3K, AKT, P105, and P65 did not change, but the phosphorylation levels of AKT, P105, and P65 increased in a time-dependent manner in response to LPS stimulation in the TIPE overexpression group compared to those in the control group (**Figure 5A**). To further

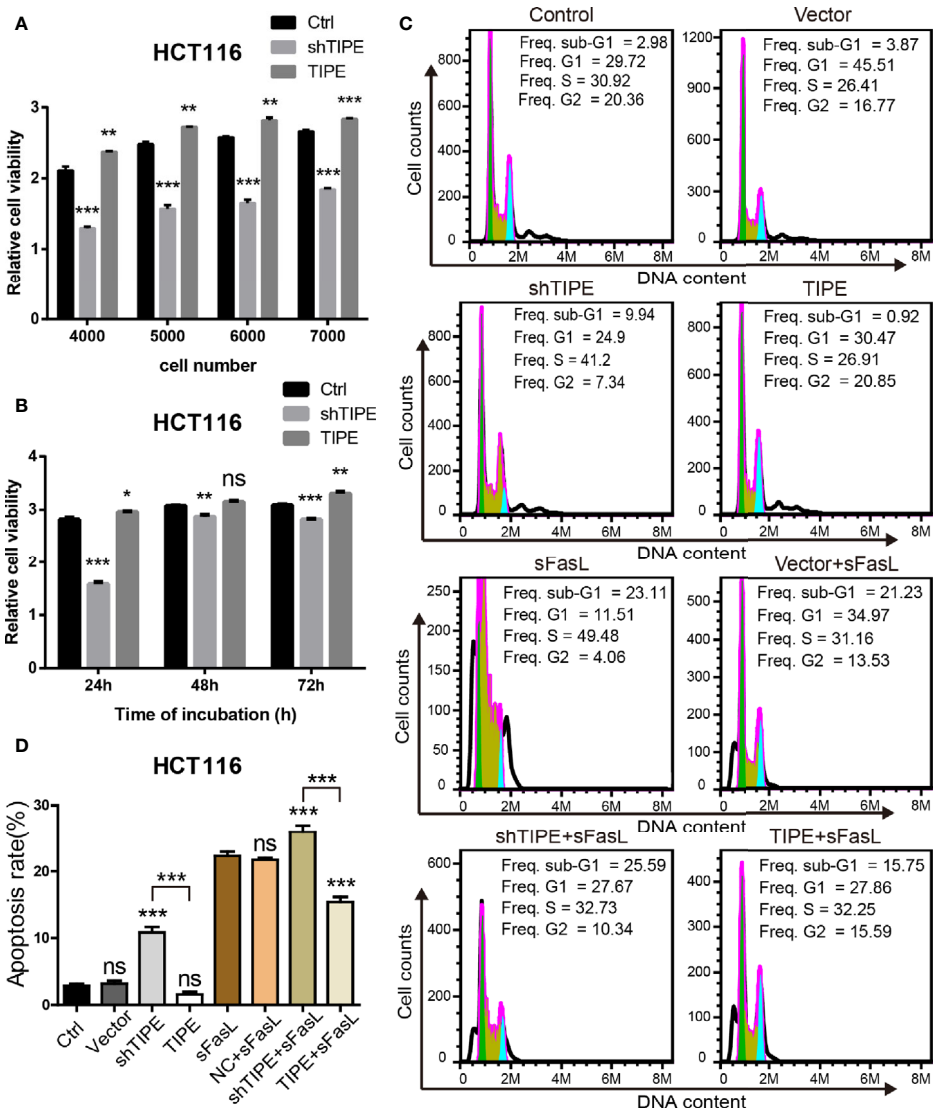

FIGURE 3 | Alteration in tumor necrosis factor-induced protein-8 (TIPE) expression regulates cell proliferation and apoptosis in HCT116 cells. **(A)** TIPE was overexpressed or knocked down in HCT116 cells, and cell proliferation was measured by CCK-8 assays. **(B)** Cell proliferation assays of HCT116 cells transfected with TIPE and shTIPE after 24, 48, and 72 h of incubation. **(C)** HCT116 cells were transfected with TIPE or shTIPE for 24 (h) sFasL (100 ng/ml) was added for another 24 h, and the cells were fixed and stained with PI to analyze the DNA content with a CytoFlex S flow cytometer. The cell cycle phase (sub-G1, G1, S, and G2) is indicated. The sub-G1 phase is indicative of apoptosis. The experiment was performed three times with similar results. **(D)** Statistical analysis was used to assess the apoptosis rate of HCT116 cells after changes in TIPE,expression and sFasL treatment. ns, not significant, $^{*}p < 0.05$, $^{**}p < 0.01$, $^{***}p < 0.001$.

examine the role of the PI3K/AKT signaling pathway in DcR3 expression, we pretreated LPS-stimulated cells with the PI3K inhibitor LY294002, Rac GTPase inhibitor NSC23766, MEK inhibitor U0126 or IκBα/NF-κB inhibitor BAY 11-7082. The results showed that compared with the DMSO group, the two groups treated with the PI3K inhibitor LY294002 or NF-κB inhibitor BAY 11-7082 had significantly decreased expression of DcR3 at the mRNA and protein levels (**Figures 5B, C**).

Then, to examine the activation of AKT and downstream NF-κB, TIPE-overexpressing HCT116 cells stimulated with LPS were further treated with the PI3K inhibitor LY294002. Although the change in phosphorylation levels after LPS stimulation was not obvious, the phosphorylation levels of PI3K, AKT, P105, and P65 in the TIPE overexpression group decreased after the PI3K inhibitor LY294002 was added and were significantly different from those in the group without inhibitor treatment (**Figure 5D**). Collectively, these results confirm that TIPE regulates DcR3 secretion by activating the PI3K/AKT signaling pathway in CRC.

Clinical Value of Tumor Necrosis Factor-Induced Protein-8 and Decoy Receptor 3 in Colorectal Cancer

To investigate the clinical value of and relationship between TIPE and DcR3 expression in CRC samples, we evaluated their

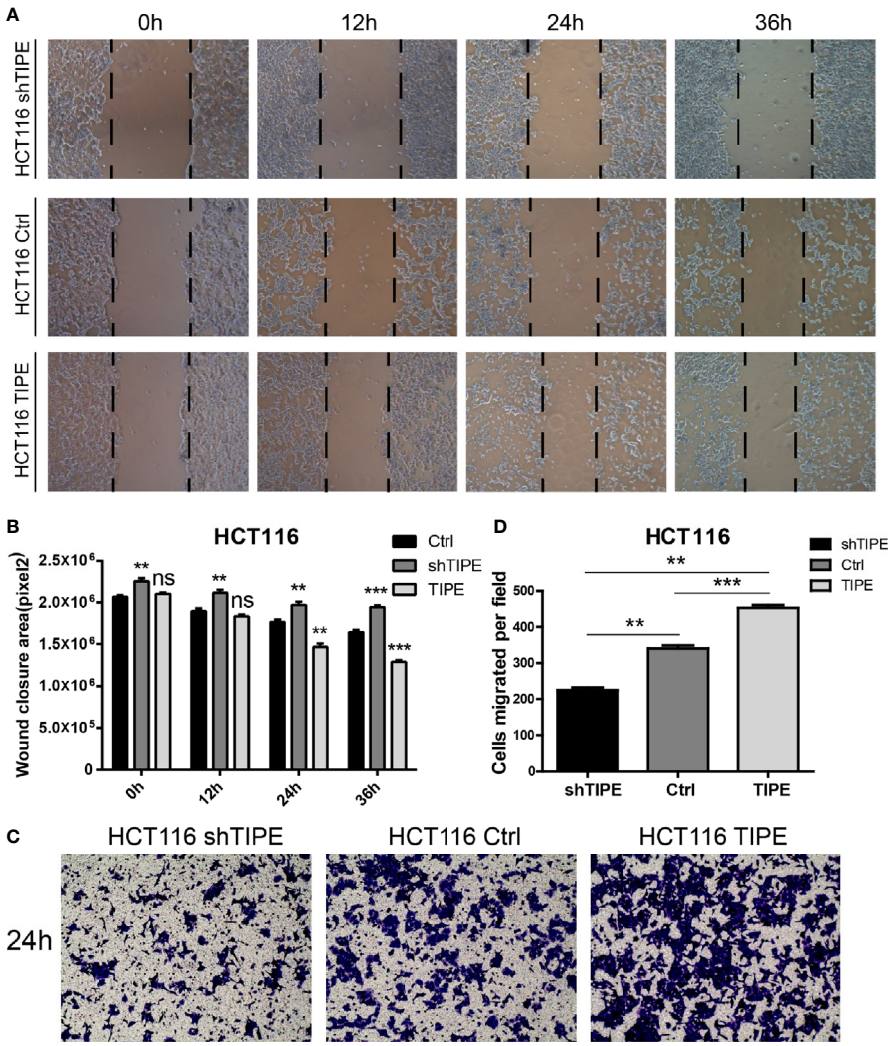

FIGURE 4 | Changes in the expression of tumor necrosis factor-induced protein-8 (TIPE) affect cell migration. **(A)** After 12, 24, and 36 h incubation, in vitro wound healing assays with TIPE or shTIPE transfected HCT116 cells were performed to evaluate cell migration. **(B)** Histograms indicated the size of the wound healing area, and representative statistical results are shown. **(C)** Based on a Transwell assay, cell migration was significantly enhanced after transfection with TIPE in HCT116 cells but decreased after transfection with shTIPE. Quantitative analysis of three independent experiments is shown in **(D)**; ns, not significant, $^{**}p < 0.01$, $^{***}p < 0.001$.

expression at the protein level with immunohistochemistry. We used 35 pairs of CRC cancer tissues and corresponding adjacent tissues. Through tissue microarray analysis, we found that in the 35 pairs of samples, 24 adjacent cancer tissues were negative for TIPE expression, while the cytoplasm of tumor cells in CRC tissues showed very strong positive staining (**Figure 6A**). DcR3 staining showed that there was high expression in 22 cases (**Figure 6A**). The analysis of tumor stages showed that the expression of TIPE was increased in advanced tumors (**Figure 6B**), while the expression of DcR3 was increased in early tumors (**Figure 6C**). In addition, TIPE expression was associated with tumor size ($p<0.05$), stage of disease progression ($p<0.05$), and distant metastasis ($p<0.05$), while DcR3 expression was only associated with distant metastasis ($p<0.05$). We analyzed the survival time according to the expression of TIPE and DcR3. As the expression of TIPE and DcR3 increased, the survival time of patients decreased, but there was no significant difference (**Supplementary Figure 1E, 1F**). These results support that TIPE and DcR3 are highly expressed in CRC samples, suggesting that TIPE and DcR3 are elevated and act as oncogenes in CRC and that TIPE expression is positively correlated with CRC metastasis and poor prognosis in patients.

DISCUSSION

CRC is the fourth most common malignant tumor worldwide, and it has become a global threat to human life (1). Although

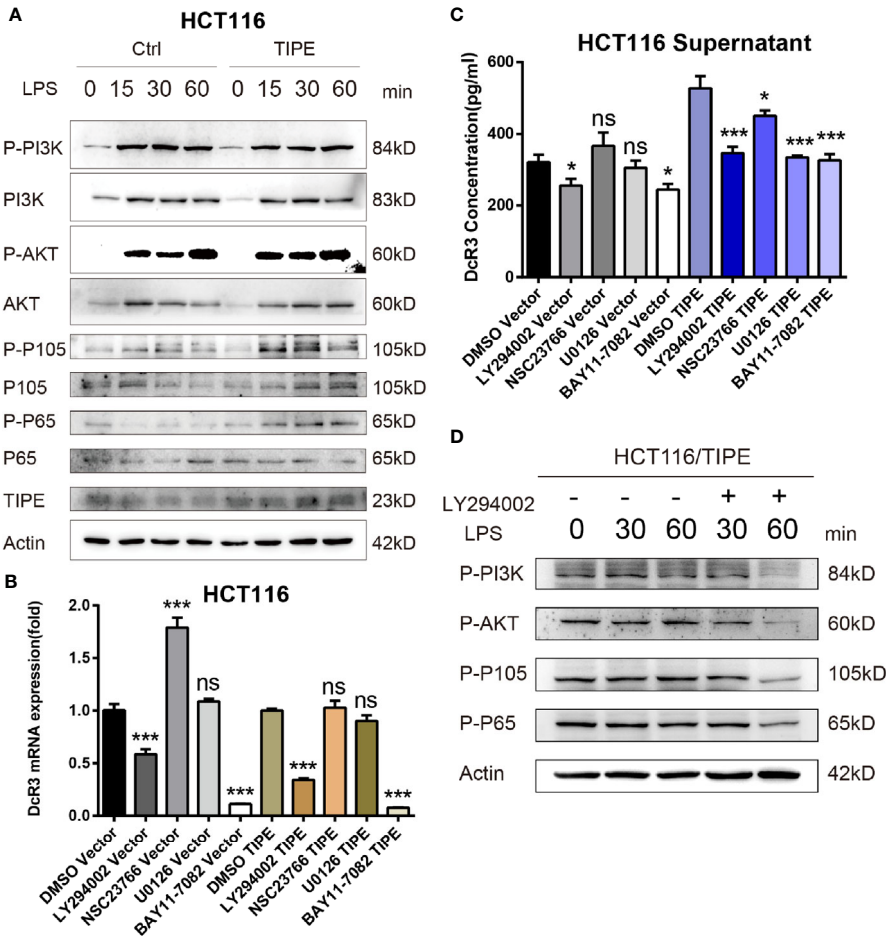

FIGURE 5 | Tumor necrosis factor-induced protein-8 (TIPE)-mediated activation of the PI3K/Akt pathway is involved in the modulation of DcR3 levels in HCT116 cells. **(A)** HCT116 cells were transfected with TIPE or an empty vector (control) for 24 h with lipopolysaccharide (LPS) stimulation for the indicated time (0, 15, 30, and 60 min). Cells were harvested, and whole-cell extracts were prepared for Western blot analysis of the indicated proteins. The blots shown are representative of those obtained in three separate experiments. **(B)** HCT116 cells were cultured in 6-well plates and transfected with TIPE or an empty vector (control) for 24 h, then qRT-PCR assays were performed to measure the relative DcR3 mRNA expression of HCT116 cells after treatment with LY294002 (50 μM), NSC23766, U0126, and BAY 11-7082. Expression was normalized to that in the control cells. **(C)** The culture medium was collected, and DcR3 protein levels were measured by ELISA. **(D)** HCT116 cells were transfected with tumor necrosis factor-induced protein-8 (TIPE) after treatment with lipopolysaccharide (LPS) for the indicated time (0, 30, and 60 min), and Western blot analysis of whole-cell lysates was performed to examine the indicated proteins in HCT116 cells after treatment with or without LY294002 (50 μM). ns, not significant, $^{*}p < 0.05$, $^{***}p < 0.001$.

extensive studies have been performed that focus on CRC, the detailed molecular events that occur during disease development are still unclear. More research is needed to elucidate CRC pathogenesis.

Inflammation is very closely related to the occurrence of tumors, and many factors involved in inflammation and the tumor microenvironment interact with each other to promote the occurrence and development of tumors. TIPE was the first member of the TNFAIP8 family to be identified (4). The TNFα (21) and NF-κB (22) pathways can induce the expression of TIPE, and TIPE plays an important role in inflammation and tumors (23). Numerous studies have revealed that TIPE is overexpressed in various tumors and that its overexpression is associated with clinical parameters and metastasis. In non-small-cell lung cancer (NSCLC), the expression of TIPE is downregulated *via* a decrease in EGFR levels and an increase in SNX (a key regulator of EGFR transporters) levels, which further inhibits ECL- and IGF-1-stimulated NSCLC cell migration (5). In gastric cancer patients, increased TIPE expression in tumor tissue is related to lymph node metastasis, tumor-node-metastasis (TNM) stage, and poor prognosis (24). In addition, the TIPE genotype was found to be linked to hematological malignancies, including diffuse large B-cell lymphoma (25), acute myelogenous leukemia (26), and multiple myeloma (27). TIPE is overexpressed in colon cancer and regulates cell proliferation (10). Recent studies

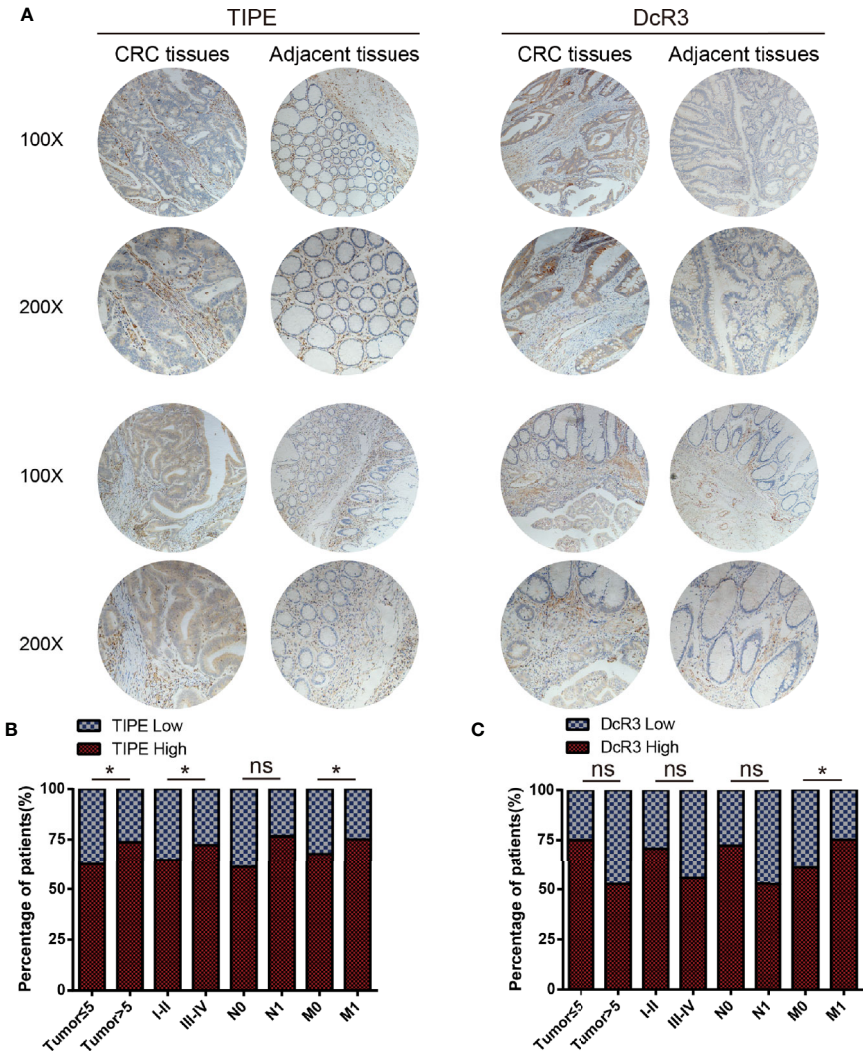

FIGURE 6 | Tumor necrosis factor-induced protein-8 (TIPE) and DcR3 are upregulated in human colorectal cancer (CRC) and positively correlated with CRC metastasis. **(A)** Representative immunohistochemical detection of TIPE (left panel) or DcR3 (right panel) in tissue microarrays of CRC tissues and adjacent tissues. **(B)** Percentage of patients with high and low TIPE expression according to the following clinical parameters: tumor size (cm), tumor stage (I–II and III–IV), lymph node status (N0 or N1), and metastasis status (M0 or M1). **(C)** The percentage of patients with different expression levels of DcR3 according to different clinical parameters. ns, not significant, $^*p < 0.05$.

have shown that TIPE promotes the growth and metastasis of MDA-MB-435 breast cancer cells by enhancing the expression of VEGFR2, MMP1 and MMP9 (8). Yang et al. confirmed that TIPE can promote tumor proliferation and invasion by activating Wnt signaling and inhibiting Hippo signaling in CRC (11). Our previous studies showed that TIPE was highly expressed in stage III gastric cancer and was positively correlated with DcR3 and ERK1/2 (20). Our study also found that TIPE is highly expressed in CRC, confirming that TIPE promotes angiogenesis in CRC by regulating the expression of VEGFR2. Our results revealed that TIPE regulates DcR3 expression, inhibits apoptosis, and promotes cell proliferation and metastasis.

DcR3, a member of the TNFRSF, can block apoptosis mediated by FasL, LIGHT and TL1A (28, 29). Studies have found that DcR3 is expressed at low levels in some normal tissues and in serum but overexpressed in many malignant tumors (16, 30). The serum DcR3 level in ovarian cancer is associated with tumor invasion and the number of tumor blood vessels, and the serum DcR3 level of patients is significantly decreased after tumor resection (31). Previous studies found that DcR3 mRNA levels are high in colon cancer tumors and the CRC cell lines SW480 and SW1116 (13). Our previous results showed that DcR3 is highly expressed in gastric cancer cell lines and surgically resected gastric cancer tissues. BGC823 cells were used to establish a tumor model in nude mice, and the expression of

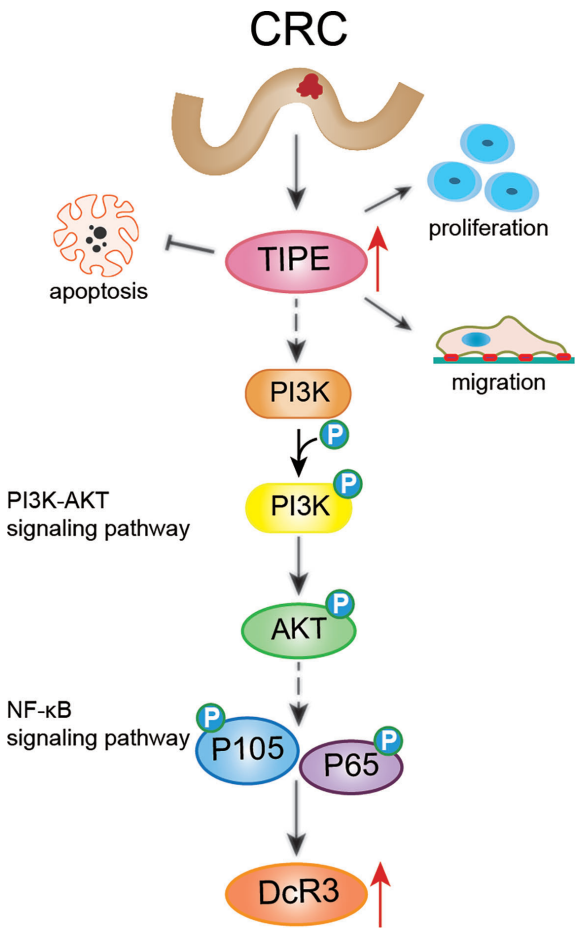

FIGURE 7 | Schematic diagram representing that TIPE regulates DcR3 expression and function by activating the PI3K/AKT signaling pathway in CRC. The solid line indicates direct regulation, the dashed line indicates indirect influence.

DcR3 at the inoculation site was increased during tumor development (32). Studies have confirmed that DcR3 is a predictor of 5-FU-based adjuvant chemotherapy responses in CRC (17). Yu et al. discovered that DcR3 has the potential to regulate the growth and metastasis of SW480 colon cancer cells (18). Zong et al. found that the overexpression of DcR3 in CRC can increase the risk of malignancy (19). These results suggest that DcR3 plays an antiapoptotic and proliferative role in intestinal inflammation and CRC.

In this study, we investigated the expression of TIPE and DcR3 in CRC and analyzed their correlation and relationship with CRC prognosis. We also explored the possible mechanisms by which TIPE regulates DcR3 expression. First, by searching the databases, we found that TIPE and DcR3 were highly expressed and positively correlated in CRC patients. We also collected plasma samples from CRC patients diagnosed by the Department of Gastrointestinal Surgery, Zhongshan Hospital of Xiamen University and detected significantly elevated DcR3 expression in these samples compared to control samples. Through *in vitro* cell experiments, we confirmed that TIPE and DcR3 were highly expressed in two colon cancer cell lines and that the expression levels were higher in the HCT116 cell line. Then, we overexpressed TIPE in all colon cancer cell lines and found that increased TIPE expression significantly upregulated the mRNA and protein levels of DcR3. Finally, a dual-luciferase reporter gene assay showed that the overexpression of TIPE enhanced the transcriptional activity of the DcR3 promoter.

Studies have shown that TIPE family members are the only known transfer proteins for the lipid second messengers phosphatidylinositol 4,5-diphosphate (PIP2) and phosphatidylinositol 3,4,5-triphosphate (PIP3) (33). These proteins act by regulating phosphatidylinositol 3-kinase (PI3K) and downstream mediators, such as AKT, Rac1, GSK3, ERK1/2, NF-κB, to trigger inflammation and tumorigenesis. It is widely accepted that the PI3K/AKT signaling pathway plays a crucial role in many human cancers (34). To confirm the importance of the PI3K/AKT signaling pathway in regulating DcR3 expression in CRC after changes in TIPE, we stimulated TIPE-overexpressing HCT116 colon cancer cells with LPS and found increased phosphorylation levels of AKT, P105, and p65 and NF-κB activation. Treatment with the PI3K inhibitor LY294002 significantly inhibited the phosphorylation of PI3K, AKT, P105, and P65 and decreased the expression of DcR3. These results provided preliminarily confirmation that TIPE regulates the expression of DcR3 through the PI3K/AKT signaling pathway (**Figure 7**). Functional experiments showed that the increased expression of TIPE not only upregulated the expression of DCR3 but also significantly enhanced the proliferation and migration ability of HCT116 cells and reduced FasL-induced apoptosis. Our results demonstrate that in the occurrence and development of CRC, TIPE can regulate the secretion of DcR3 and play a synergistic role in promoting tumor growth and migration. DcR3 is a soluble protein that is easy to detect, and it is associated with the occurrence, development and prognosis of tumors, so it can be used as a biomarker during tumor diagnosis and treatment response evaluation. Through tissue microarray analysis, we observed that TIPE and DcR3 act as oncogenes and have increased expression in CRC compared to normal controls. In addition, the expression of TIPE is positively correlated with CRC metastasis and poor prognosis in patients.

CONCLUSIONS

In summary, this study revealed that TIPE and DcR3 are highly expressed in CRC and are associated with poor prognosis in patients. Furthermore, TIPE may regulate the expression of DcR3 by activating the PI3K/AKT signaling pathway in CRC, thereby promoting cell proliferation and migration and inhibiting apoptosis (**Figure 7**). Therefore, it is of great clinical significance to elucidate the pathogenesis and prognosis of CRC.

DATA AVAILABILITY STATEMENT

The datasets presented in this study can be found in online repositories. The names of the repository/repositories and accession number(s) can be found in the article/**Supplementary Material**.

ETHICS STATEMENT

The studies involving human participants were reviewed and approved by the medical ethics committee of Zhongshan Hospital, Xiamen University. The patients/participants provided their written informed consent to participate in this study.

AUTHOR CONTRIBUTIONS

MZ, XQ, and GZ designed the study. MZ and YL collated the data and designed and developed the database. MZ, XQ, YY, LG, and CW conducted the experiments. MZ, YY, and HC analyzed the results. JM, ZL, and GZ provided the critical reagents. MZ and HC wrote the paper. JM, ZL, and GZ edited the manuscript and provided critical comments. All authors contributed to the article and approved the submitted version.

FUNDING

This study was supported by the National Natural Science Foundation (No. 81272720 and No. 81400984), the Natural Science Foundation of Fujian Province (No. 2018J01138 and No. 2014D009), the National Health and Family Planning Commission Scientific Research Foundation-Health, the Education Cooperation Foundation (WKJ2016-2-17), and the Fujian Province Health project of Innovative Medical Talents Training and Medical Innovation Project (2017-CXB-22).

SUPPLEMENTARY MATERIAL

The Supplementary Material for this article can be found online at: https://www.frontiersin.org/articles/10.3389/fonc.2020.623048/full#supplementary-material

Supplementary Figure 1 | (A) qRT-PCR assaying relative mRNA expression levels of TIPE in two colon cancer cells (TIPE-overexpressing or control cells). **(B)** HCT116 cells were transfected with TIPE or shTIPE for 24 h. sFasL (100 ng/ml) was added for another 24 h, the culture medium was collected, and DcR3 levels were measured with ELISA. **(C)** Expression of TIPE in HCT116 cells transfected with TIPE, shTIPE or a control as measured by Western blot assays. **(D)** The culture medium of HCT116 cells transfected with TIPE, shTIPE or a control were collected, and DcR3 levels were measured by ELISA. **(E)** Different expressions of TIPE affected overall survival. **(F)** Compared with patients with low DcR3 levels, patients with high DcR3 levels had a higher probability of recurrence and worse overall survival. ns, not significant, $^{*}p < 0.05$, $^{**}p < 0.01$, $^{***}p < 0.001$.

REFERENCES

1. Gu MJ, Huang QC, Bao CZ, Li YJ, Li XQ, Ye D, et al. Attributable causes of colorectal cancer in China. *BMC Cancer* (2018) 18:38. doi: 10.1186/s12885-017-3968-z
2. Kuipers EJ, Grady WM, Lieberman D, Seufferlein T, Sung JJ, Boelens PG, et al. Colorectal cancer. *Nat Rev Dis Primers* (2015) 1:15065. doi: 10.1038/nrdp.2015.65
3. Markowitz SD, Bertagnolli MM. Molecular origins of cancer: Molecular basis of colorectal cancer. *New Engl J Med* (2009) 361:2449–60. doi: 10.1056/NEJMra0804588
4. Patel S, Wang FH, Whiteside TL, Kasid U. Identification of seven differentially displayed transcripts in human primary and matched metastatic head and neck squamous cell carcinoma cell lines: implications in metastasis and/or radiation response. *Oral Oncol* (1997) 33:197–203. doi: 10.1016/s0964-1955(96)00065-6
5. Day TF, Kallakury BVS, Ross JS, Voronel O, Vaidya S, Sheehan CE, et al. Dual Targeting of EGFR and IGF1R in the TNFAIP8 Knockdown Non-Small Cell Lung Cancer Cells. *Mol Cancer Res MCR* (2019) 17:1207–19. doi: 10.1158/1541-7786.Mcr-18-0731
6. You Z, Ouyang H, Lopatin D, Polver PJ, Wang CY. Nuclear factor-kappa B-inducible death effector domain-containing protein suppresses tumor necrosis factor-mediated apoptosis by inhibiting caspase-8 activity. *J Biol Chem* (2001) 276:26398–404. doi: 10.1074/jbc.M102464200
7. Shi TY, Cheng X, Yu KD, Sun MH, Shao ZM, Wang MY, et al. Functional variants in TNFAIP8 associated with cervical cancer susceptibility and clinical outcomes. *Carcinogenesis* (2013) 34:770–8. doi: 10.1093/carcin/bgt001
8. Zhang C, Chakravarty D, Sakabe I, Mewani RR, Boudreau HE, Kumar D, et al. Role of SCC-S2 in experimental metastasis and modulation of VEGFR-2, MMP-1, and MMP-9 expression. *Mol Ther J Am Soc Gene Ther* (2006) 13:947–55. doi: 10.1016/j.ymthe.2005.11.020
9. Liu T, Gao H, Chen X, Lou G, Gu L, Yang M, et al. TNFAIP8 as a predictor of metastasis and a novel prognostic biomarker in patients with epithelial ovarian cancer. *Br J Cancer* (2013) 109:1685–92. doi: 10.1038/bjc.2013.501
10. Miao Z, Zhao T, Wang Z, Xu Y, Song Y, Wu J, et al. SCC-S2 is overexpressed in colon cancers and regulates cell proliferation. *Tumour Biol J Int Soc Oncodevel Biol Med* (2012) 33:2099–106. doi: 10.1007/s13277-012-0469-1
11. Yang C, Xu W, Meng X, Zhou S, Zhang M, Cui D. SCC-S2 Facilitates Tumor Proliferation and Invasion via Activating Wnt Signaling and Depressing Hippo Signaling in Colorectal Cancer Cells and Predicts Poor Prognosis of Patients. *J Histochem Cytochem Off J Histochem Soc* (2019) 67:65–75. doi: 10.1369/0022155418799957
12. Lin WW, Hsieh SL. Decoy receptor 3: a pleiotropic immunomodulator and biomarker for inflammatory diseases, autoimmune diseases and cancer. *Biochem Pharmacol* (2011) 81:838–47. doi: 10.1016/j.bcp.2011.01.011
13. Pitti RM, Marsters SA, Lawrence DA, Roy M, Kischkel FC, Dowd P, et al. Genomic amplification of a decoy receptor for Fas ligand in lung and colon cancer. *Nature* (1998) 396:699–703. doi: 10.1038/25387
14. Migone TS, Zhang J, Luo X, Zhuang L, Chen C, Hu B, et al. TL1A is a TNF-like ligand for DR3 and TR6/DcR3 and functions as a T cell costimulator. *Immunity* (2002) 16:479–92. doi: 10.1016/s1074-7613(02)00283-2
15. Yu KY, Kwon B, Ni J, Zhai Y, Ebner R, Kwon BS. A newly identified member of tumor necrosis factor receptor superfamily (TR6) suppresses LIGHT-mediated apoptosis. *J Biol Chem* (1999) 274:13733–6. doi: 10.1074/jbc.274.20.13733
16. Hsieh SL, Lin WW. Decoy receptor 3: an endogenous immunomodulator in cancer growth and inflammatory reactions. *J Biomed Sci* (2017) 24:39. doi: 10.1186/s12929-017-0347-7
17. Mild G, Bachmann F, Boulay JL, Glatz K, Laffer U, Lowy A, et al. DCR3 locus is a predictive marker for 5-fluorouracil-based adjuvant chemotherapy in colorectal cancer. *Int J Cancer* (2002) 102:254–7. doi: 10.1002/ijc.10711
18. Yu W, Xu YC, Tao Y, He P, Li Y, Wu T, et al. DcR3 regulates the growth and metastatic potential of SW480 colon cancer cells. *Oncol Rep* (2013) 30:2741–8. doi: 10.3892/or.2013.2769
19. Zong L, Chen P, Wang DX. Death decoy receptor overexpression and increased malignancy risk in colorectal cancer. *World J Gastroenterol* (2014) 20:4440–5. doi: 10.3748/wjg.v20.i15.4440

20. Hu R, Liu W, Qiu X, Lin Z, Xie Y, Hong X, et al. Expression of tumor necrosis factor-alpha-induced protein 8 in stage III gastric cancer and the correlation with DcR3 and ERK1/2. *Oncol Lett* (2016) 11:1835–40. doi: 10.3892/ol.2016.4133
21. Horrevoets AJ, Fontijn RD, van Zonneveld AJ, de Vries CJ, ten Cate JW, Pannekoek H. Vascular endothelial genes that are responsive to tumor necrosis factor-alpha in vitro are expressed in atherosclerotic lesions, including inhibitor of apoptosis protein-1, stannin, and two novel genes. *Blood* (1999) 93:3418–31. doi: 10.1182/blood.v93.10.3418.410k23_3418_3431
22. Day TF, Mewani RR, Starr J, Li X, Chakravarty D, Ressom H, et al. Transcriptome and Proteome Analyses of TNFAIP8 Knockdown Cancer Cells Reveal New Insights into Molecular Determinants of Cell Survival and Tumor Progression. *Methods Mol Biol (Clifton NJ)* (2017) 1513:83–100. doi: 10.1007/978-1-4939-6539-7_7
23. Kumar D, Whiteside TL, Kasid U. Identification of a novel tumor necrosis factor-alpha-inducible gene, SCC-S2, containing the consensus sequence of a death effector domain of fas-associated death domain-like interleukin- 1beta-converting enzyme-inhibitory protein. *J Biol Chem* (2000) 275:2973–8. doi: 10.1074/jbc.275.4.2973
24. Chen L, Yang X, Yang X, Fan K, Xiao P, Zhang J, et al. Association between the expression levels of tumor necrosis factor-alpha-induced protein 8 and the prognosis of patients with gastric adenocarcinoma. *Exp Ther Med* (2016) 12:238–44. doi: 10.3892/etm.2016.3327
25. Zhao S, Dong X, Shen W, Ye Z, Xiang R. Machine learning-based classification of diffuse large B-cell lymphoma patients by eight gene expression profiles. *Cancer Med* (2016) 5:837–52. doi: 10.1002/cam4.650
26. Eisele L, Klein-Hitpass L, Chatzimanolis N, Opalka B, Boes T, Seeber S, et al. Differential expression of drug-resistance-related genes between sensitive and resistant blasts in acute myeloid leukemia. *Acta Haematol* (2007) 117:8–15. doi: 10.1159/000096854
27. Wang MC, Liu SX, Liu PB. Gene expression profile of multiple myeloma cell line treated by realgar. *J Exp Clin Cancer Res CR* (2006) 25:243–9. doi: 10.1007/s11596-007-0606-z
28. Macher-Goeppinger S, Aulmann S, Wagener N, Funke B, Tagscherer KE, Haferkamp A, et al. Decoy receptor 3 is a prognostic factor in renal cell cancer. *Neoplasia (New York NY)* (2008) 10:1049–56. doi: 10.1593/neo.08626
29. Tu HF, Liu CJ, Liu SY, Chen YP, Yu EH, Lin SC, et al. Serum decoy receptor 3 level: a predictive marker for nodal metastasis and survival among oral cavity cancer patients. *Head Neck* (2011) 33:396–402. doi: 10.1002/hed.21467
30. Wu Y, Han B, Sheng H, Lin M, Moore PA, Zhang J, et al. Clinical significance of detecting elevated serum DcR3/TR6/M68 in malignant tumor patients. *Int J Cancer* (2003) 105:724–32. doi: 10.1002/ijc.11138
31. Bradford L, Ziebarth A, Felder M, Connor J, Harter J. Association of ascites and serum decoy receptor 3 (DCR3) levels with tumor infiltrating lymphocytes (TILS) and tumor vessels counts in epithelial ovarian cancer (EOC). *J Gynecol Oncol* (2009) 116:598. doi: 10.1016/j.ygyno.2009.10.033
32. Li W, Zhang C, Chen C, Zhuang G. Correlation between expression of DcR3 on tumor cells and sensitivity to FasL. *Cell Mol Immunol* (2007) 4:455–60. doi: 10.1007/s00262-007-0299-y
33. Goldsmith JR, Fayngerts S, Chen YH. Regulation of inflammation and tumorigenesis by the TIPE family of phospholipid transfer proteins. *Cell Mol Immunol* (2017) 14:482–7. doi: 10.1038/cmi.2017.4
34. Lien EC, Dibble CC, Toker A. PI3K signaling in cancer: beyond AKT. *Curr Opin Cell Biol* (2017) 45:62–71. doi: 10.1016/j.ceb.2017.02.007

Conflict of Interest: The authors declare that the research was conducted in the absence of any commercial or financial relationships that could be construed as a potential conflict of interest.

frontiers in Genetics

ORIGINAL RESEARCH
published: 08 March 2021
doi: 10.3389/fgene.2021.638244

Dicer1 Promotes Colon Cancer Cell Invasion and Migration Through Modulation of tRF-20-MEJB5Y13 Expression Under Hypoxia

Na Luan[1,2†], Yali Mu[1,2†], Jiayi Mu[2], Yiquan Chen[1,2], Xun Ye[1,2], Qin Zhou[1,2], Miaorong Xu[2], Qun Deng[2], Yeting Hu[2], Zhe Tang[3,4] and Jianwei Wang[1,2*]*

[1] Department of Colorectal Surgery, 4th Affiliated Hospital, Zhejiang University School of Medicine, Hangzhou, China, [2] Key Laboratory of Cancer Prevention and Intervention, Ministry of Education, Department of Colorectal Surgery and Oncology, 2nd Affiliated Hospital, Zhejiang University School of Medicine, Hangzhou, China, [3] Department of Surgery, 4th Affiliated Hospital, Zhejiang University School of Medicine, Hangzhou, China, [4] Department of Surgery, 2nd Affiliated Hospital, Zhejiang University School of Medicine, Hangzhou, China

OPEN ACCESS

Edited by:
Marco Mina,
Sophia Genetics, Switzerland

Reviewed by:
Adam J. Dupuy,
The University of Iowa, United States
Arsheed A. Ganaie,
University of Minnesota Twin Cities, United States

***Correspondence:**
Jianwei Wang
sypzju@zju.edu.cn
Zhe Tang
8xi@zju.edu.cn

[†] These authors have contributed equally to this work

Specialty section:
This article was submitted to Cancer Genetics, a section of the journal Frontiers in Genetics

Received: 05 December 2020
Accepted: 15 February 2021
Published: 08 March 2021

Citation:
Luan N, Mu Y, Mu J, Chen Y, Ye X, Zhou Q, Xu M, Deng Q, Hu Y, Tang Z and Wang J (2021) Dicer1 Promotes Colon Cancer Cell Invasion and Migration Through Modulation of tRF-20-MEJB5Y13 Expression Under Hypoxia. Front. Genet. 12:638244. doi: 10.3389/fgene.2021.638244

Hypoxia plays a key role in colorectal cancer (CRC) metastasis, but its underlying mechanism remains largely unknown. Dicer1, an RNase, has been considered as a tumor regulator in many tumors. However, whether Dicer1 affects CRC progression under hypoxia remains uncertain. In this study, we found that Dicer1 expression was induced by hypoxia in CRC cells and it mediates hypoxia-induced CRC cell progression. Furthermore, we found that the expression of tRF-20-MEJB5Y13, a small non-coding RNA derived from tRNA, was increased under hypoxic conditions, and its upregulation by Dicer1 resulted in hypoxia-induced CRC cell invasion and migration. These results advance the current understanding of the role of Dicer1 in regulating hypoxia signals and provide a new pathway for the development of therapeutic interventions for inhibiting cancer progression.

Keywords: colorectal cancer, Dicer, tRNA-derived fragments, epithelial-to-mesenchymal transition, hypoxia

INTRODUCTION

Colorectal cancer (CRC) is one of the most common causes of cancer-related deaths worldwide, which poses serious threats to public health, and its morbidity and mortality rates are increasing annually. Approximately 1.2 million new cases are reported annually, accounting for 10–15% of all malignant tumors, and it ranks third with respect to morbidity and mortality among malignant tumors (Miller et al., 2019). However, many clinical CRCs show micrometastasis of the tumor before surgery, which in itself is a complex and continuous process regulated by multiple factors and steps (Crotti et al., 2017). Therefore, studying the underlying mechanism of colon cancer invasion and migration is essential for establishing targeted intervention strategies to improve survival.

Tumor cells are characterized by uncontrolled cell proliferation, resistance to apoptosis, and metabolic shift to anaerobic glycolysis (Warburg effect). As the tumor cells continue to proliferate and the tumor volume increases, high demand for oxygen is created and this oxygen demand of the cells cannot be satisfied by the blood supply, which limits the use of oxygen by the cells, thereby resulting in hypoxic conditions for tumor cells (Catalano et al., 2013; Sormendi and Wielockx, 2018). Hypoxia, oxidative stress, and acidosis in the tumor microenvironment trigger extracellular

matrix remodeling and stimulate adjacent stromal cells (such as fibroblasts) and immune cells (such as lymphocytes and macrophages) to induce angiogenesis, thereby promoting tumor invasion and migration ultimately (Roma-Rodrigues et al., 2019).

Recent studies have shown that Dicer1 required for transfer RNA-derived fragments (tRF) biogenesis is associated with the development of cancer (Karube et al., 2005; Chiosea et al., 2006, 2007; Flavin et al., 2008; Merritt et al., 2008; Grelier et al., 2009). Currently, several studies have shown that the expression level and mode of action of Dicer1 may vary depending on the type of tumor, but the regulatory mechanism of these genes remains unclear. Additionally, recent studies on CRC have demonstrated that high expression of Dicer1 mRNA and protein is associated with poor survival, and this effect is independent of any clinical parameters of patients with CRC, including sex and age (Chiosea et al., 2006). Interestingly, Dicer1 downregulation was statistically correlated with tumor progression, tumor grade, and lymph node metastasis (Faggad et al., 2012). However, the relationship between Dicer1 and tumor invasion and migration and their underlying mechanisms are unclear.

tRF belongs to the short non-coding RNA family present in most organisms, and can be processed by Dicer (Cole et al., 2009) and RNase (Lee et al., 2009) under stress conditions such as hypoxia. Dicer is a ribonuclease, which is generally considered to be the cause of mature miRNA biogenesis. A study suggests that Dicer can cleave tRNA from the 3′-end of tRNA to produce tRF (tRF-3) (Haussecker et al., 2010). Contrastingly, a recent study demonstrated that certain tRF-3 series can be produced independently of the Dicer enzyme (Kuscu et al., 2018). Dicer can also cleave the D arm of mature tRNA in cancer cells to produce tRF-5 (Cole et al., 2009). As hypoxia is the main stress condition encountered by the cells during cancer progression, tRF expression induced under hypoxia may affect metastasis (Goodarzi et al., 2015). Huang et al. (2017) identified a human-specific tRF/miR fragment, tRF/miR-1280, which could inhibit Notch/Gata and miR-200b signal transduction through direct interaction with JAG2 3′-untranslated region, thereby suppressing colon cancer cell proliferation and metastasis. Zhang et al. (2019) found that tRF-03357 might promote the proliferation, invasion and migration of SK-OV-3 cells.

Our aim was to explore whether hypoxia microenvironment affects Dicer1 expression in CRC cells and to investigate the relationship between changes in Dicer1 expression and epithelial-to-mesenchymal transition (EMT) in CRC. Finally, we identified a novel mechanism that links hypoxia with upregulated Dicer1 expression and specific tRF expression associated with EMT in CRC.

Abbreviations: CRC, Colorectal cancer; tRFs, tRNA-derived fragments; EMT, Epithelial-to-mesenchymal; RT-qPCR, Reverse transcription quantitative polymerase chain reaction; PVDF, Polyvinylidene fluoride; CST, Cell Signaling Technology; MTT, 3-(4,5-Dimethylthiazol-2-yl)-2,5-diphenyltetrazolium bromide.

MATERIALS AND METHODS

Cell Culture

The human CRC cell lines SW480 and RKO were obtained from the American Type Culture Collection. Cells were cultured in Dulbecco's modified Eagle medium (Gibco, USA) supplemented with 10% fetal bovine serum (BI, USA) and 100 IU/mL penicillin. All cells were incubated in a CO_2 constant temperature incubator (37°C, 21% O_2, and 5% CO_2) (Thermo Fisher Scientific, Rockford, IL, USA) for normal oxygen culture or in a hypoxic incubator (37°C, 1% O_2, and 5% CO_2) for hypoxic culture for 24 h.

Plasmid Construction and Cell Transfection

To construct the Dicer1 expression plasmid, the synthetic Dicer1 gene encoding the coding sequences was inserted into the pcDNA3.1 vector, and puromycin resistance gene and green fluorescent protein tag were added simultaneously. Lipofectamine 2000 was used to transfect RKO and SW480 cells with Dicer1 overexpression plasmid. tRF-20-MEJB5Y13 mimics and negative control mimics were purchased from (GenePharma Shanghai, China). For each dish of cells, 2 μL of Lipo 2000 was added to 48 μL of Opti-MEM and mixed. The plasmid preparation solution was added to the Lipo 2000 preparation solution in an equal volume and incubated for 20 min. After 2 h of transfection, the cells were harvested for further experiments.

RNA Sequencing

Total RNA was extracted with Trizol (Invitrogen, Carlsbad, CA, USA). RNA integrity was analyzed with Agilent 2100 Bioanalyzer (Agilent Technologies, Santa Clara, CA, USA). Qubit RNA detection kit deteced RNA concentration in the Qubit Fluorometer (Invitrogen, Carlsbad, USA). The total RNA samples used in subsequent experiments all meet the following requirements: RNA integrity number (RIN) 7.0, 28S:18S ratio 1.5. The sequencing library was generated and sequenced by Boao Biotechnology (Beijing, China). The total dose of each sample is 5μg RNA. Briefly, ribosomal RNA (rRNA) was removed using the Ribose Zero Magnetic Kit (epicenter technologies, Madison, WI, USA). To remove linear RNA, total RNA was digested with RNase R (Epicenter Technologies, Madison, WI, USA). The NEBNext Ultra RNA Library Preparation Kit from Illumina (Nebraska, USA) was used to construct a sequencing library according to the manufacturer's protocol. In NEBNext first-strand synthesis reaction buffer (5x), RNA is fragmented into fragments of approximately 300 base pairs (bp) in length. The RNA fragment was synthesized by reverse transcriptase and random hexamer primers to synthesize the first strand cDNA, and the second strand cDNA was synthesized with 10x dUTP Mix in the second strand synthesis reaction buffer. The end of the cDNA fragment undergoes an end repair process, which involves adding a single a base and then connecting the adaptor. After connecting the Illumina sequencing adapter, the second strand of cDNA was digested with user enzyme (NEB, USA) to construct a strand-specific library. In order to amplify the library DNA, the library was purified and PCR enriched. Then, these libraries were certified by Agilent 2100 and quantified using the KAPA Library

TABLE 1 | Primer sequences for qRT-PCR.

Gene	Primer Sequence (5′-3′)
Primer Sequence (5′-3′)	F: GTCGTGCCGTATTGGTAGTT
	R: CTGCTGTCGCTCATATGGTT
tRF-20-MEJB5Y13	F: AGGTATTCGCACT
	R: CGGATCAGAAGATT
U6	F: CTCGCTTCGGCAGCACA
	R: AACGCTTCACGAATTTGCGT

Quantification kit (KAPA Biosystems, South Africa). Finally, the library was sequenced with paired ends on an Illumina HiSeq sequencer (Illumina, San Diego, CA, USA). The read length of the paired ends was 150 bp.

Reverse Transcription Quantitative Polymerase Chain Reaction

The cells (transfected cell lines including RKO and SW480) were collected in a 1.5 mL RNase-free eppendorf tube, and 500 μL TRIzol reagent was added to ensure that the cells were fully lysed. After RNA extraction and concentration determination, cDNA was reverse transcribed using a cDNA Synthesis Kit (Thermo Fisher Scientific). RT-qPCR amplifications were performed with the SYBR Green qPCR Master Mix (ABI) by using the ABI 7300 real-time PCR detection system. Detailed information including forward primers and reverse primers of specific tRFs and Dicer1 were designed and synthesized (**Table 1**).

Western Blot Assay

The transfected cells were collected in an eppendorf tube, and RIPA buffer (Sigma-Aldrich, Shanghai, China) was added to the lysate containing proteinase inhibitors depending on the density of cells. After quantitative analysis, the proteins were separated using sodium dodecyl sulfate-polyacrylamide gel vertical electrophoresis. The proteins were then transferred onto polyvinylidene fluoride (PVDF) membranes (Millipore, USA). The PVDF membranes were at the anode and the gel was at the cathode electrode, and the apparatus was then immersed in the electrophoresis tank. Subsequently, the PVDF membranes were immersed in a blocking solution containing 5% skimmed milk powder and sealed at room temperature for 2 h. Thereafter, the blocked PVDF membranes were removed, immersed in 1 × phosphate-buffered saline solution with Tween 20, washed 3 times on a shaker, diluted with primary antibody solution, and incubated at 4°C overnight. The following primary antibodies were used: anti-N-cadherin [1:1000, Cell Signaling Technology (CST), USA], anti-vimentin (1:1000, CST, USA), anti-ZEB1 (1:1000, CST, USA), anti-MMP7 (1:1000, CST, USA), anti-Slug (1:1000, CST, USA), and anti-SSnail (1:1000, CST, USA). Subsequently, the membranes were probed with goat anti-rabbit IgG antibody (1:3000, Sigma-Aldrich, Japan). The proteins were then visualized with enhanced chemiluminescence western blot detection reagents (Bio-Rad, Cal, USA) and exposed to the chemical photosensitive mode.

Transwell Assay

Cell migration and invasion assays were conducted using 24-well Transwell® chambers (Costar, USA). Serum-free medium was added to each well in order to adjust the densities of RKO and SW480 cells to 1.6×10^5 cells/mL before seeding the cells in the upper chamber, whereas 500 μL of fetal bovine serum-supplemented medium was added to the lower layer, and then the chamber was incubated in a 37°C, 5% CO_2, saturated humidity incubator for 2 h or overnight. For invasion experiments, it is necessary to pre-lay 20 μL of Matrigel mixture (the ratio of Matrigel and Dulbecco's modified Eagle medium was 1: 1) on the upper layer of the chamber in advance and incubate it at 37°C for 30 min until the glue solidifies. Matrigel needs to be melted into a liquid state beforehand, and it is not necessary to add matrigel for migration experiments. After culturing the cells at 37°C for 24 h, the cells were fixed with methanol for 20 min, washed with phosphate buffered saline 3 times, and stained with crystal violet. The cell number was visually counted in 3–5 random fields by using an inverted fluorescence microscope (Leica DMI3000B).

3-(4,5-Dimethylthiazol-2-yl)-2,5-Diphenyltetrazolium Bromide (MTT) Assay

MTT assay was performed to measure the proliferation of CRC cells. The transfected cells were cultured in 96-well-plates, and 96-well-flat bottom plates were incubated at 3°C for 24, 48, 72, and 96 h. Thereafter, 50 μL MTT solution (Sigma-Aldrich, St. Louis, MO) was added to the cells after the incubation, and the plates were then incubated for 4 h in a cell culture incubator under dark conditions to form formazan. Subsequently, 150 μL of dimethyl sulfoxide was added to each well. The density of cells in each well was measured by taking the absorbance at a wavelength of 570 nm.

Statistical Analysis

All data are expressed as mean ± standard deviation. Data analysis was performed using GraphPad Prism 7 and SPSS 22.0 (version 22.0; IBM SPSS, Armonk, NY, USA) statistical softwares. All experiments were repeated 3 times. Statistical comparisons for significance were performed using the Wilcoxon signed-rank test for paired samples. Differences between groups were analyzed statistically using the paired Student's *t*-test. $P < 0.05$ were considered statistically significant.

RESULTS

Hypoxia Inhibits Tumor Growth but Promotes Cell Invasion and Migration

Cell proliferation in the hypoxia group was decreased as compared to that in the control group (**Figure 1A**). However, the transwell assays showed that the number of migrated and invaded cells was significantly increased in the hypoxic groups in RKO and SW480 cells (**Figure 1B**).

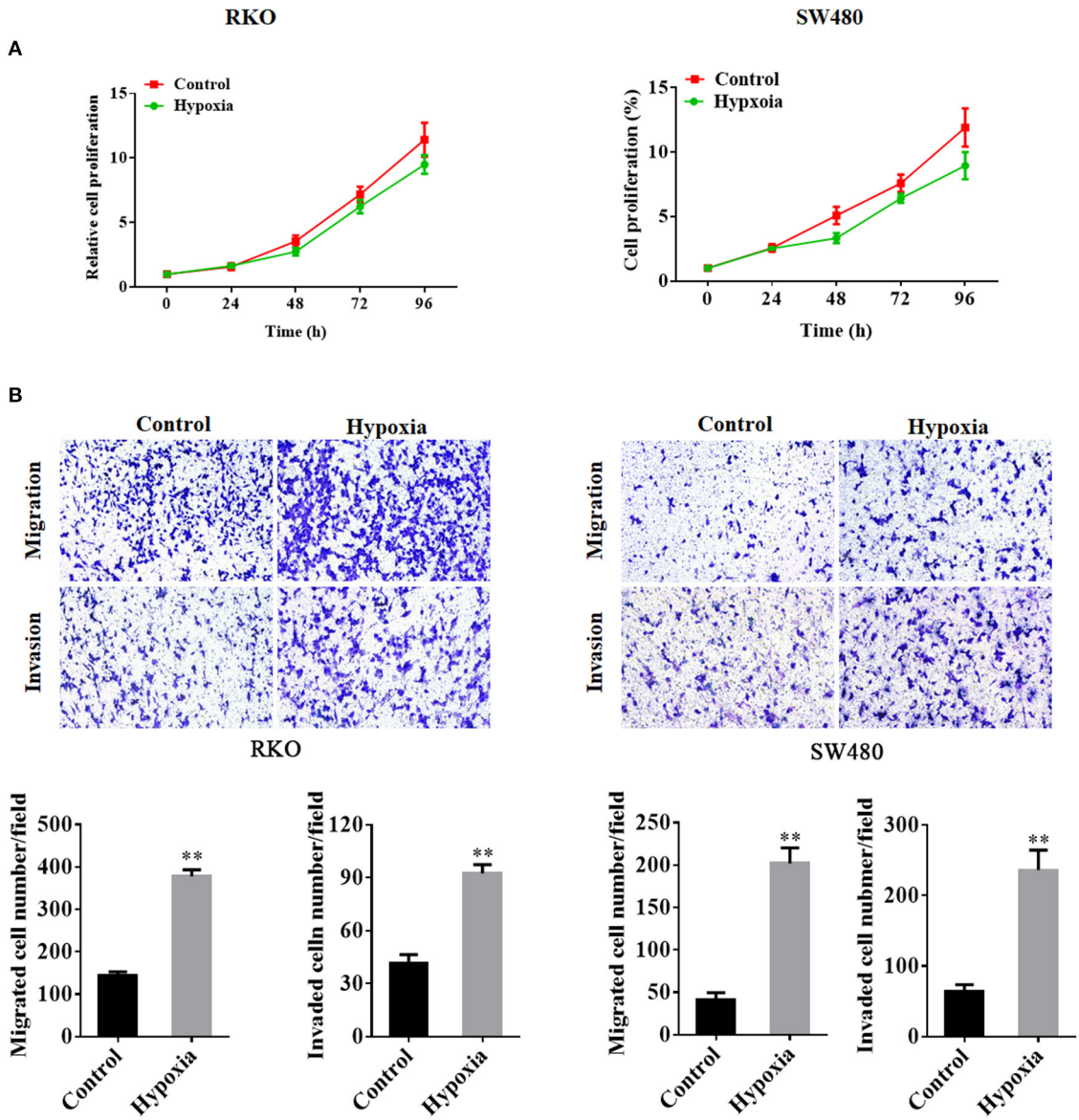

FIGURE 1 | Colorectal cancer cell proliferation, migration, and invasion under nomoxic and hypoxic conditions. The MTT proliferation assay was performed to determine cell proliferation **(A)**. Transwell assays were performed to detect the migration and invasion of RKO cells and SW480 cells under normoxic or hypoxic conditions **(B)**. $^{**}P < 0.01$. The assays were repeated at least 3 times. MTT, 3-(4,5-dimethylthiazol-2-yl)-2,5-diphenyltetrazolium bromide.

Dicer1 Was Upregulated in CRC Cells Under Hypoxic Conditions

The relationship between Dicer and cancer prognosis has been observed in many human cancers. However, whether Dicer plays a functional role in the mechanism of CRC progression under hypoxic conditions and whether they are associated with tRFs remains to be elucidated. To test our hypothesis, we performed high-throughput sequencing to identify changes in the expression of Dicer1 and tRFs. Next, we successfully sequenced small RNAs from CRC cells under hypoxic conditions. GO terms listed can be clustered into three groups: (I) biological process, (II) molecular function, and (III) cellular component, describing detailed biological processes in their respective levels (**Figure 2A**). Enrichment analysis of the KEGG signaling pathway suggested that RNA degradation, RNA transport and Splisome were significantly enriched in the signaling pathways (**Figure 2B**). According to the sequencing results, the number of genes with significant differences in expression were identified. Among them, 888 genes were significantly upregulated and 3,168 genes were significantly downregulated under hypoxic conditions (**Figure 2C**). The expression of 3 RNases involved in tRNA cleavage were found to be increased. Notably, the

expression of the RNase Dicer, which plays an important role in the biological process of tRFs, varied significantly between the two groups (**Figure 2D**). The expression of Dicer1, which increased significantly under hypoxic conditions, was further evaluated using RT-qPCR analysis. RT-qPCR results showed that Dicer1 mRNA expression levels were significantly upregulated in RKO and SW480 cells under hypoxic conditions (**Figures 2E,F**). The data showed that RT-qPCR results were consistent with the expression patterns identified through high-throughput sequencing.

Dicer1 Overexpression Promotes CRC Cell Invasion and Migration

The expression of Dicer1, which increased significantly under hypoxic conditions, was further evaluated through western blot assays. The results showed that Dicer1 protein expression was significantly upregulated in RKO and SW480 cells under hypoxic conditions (**Figure 3A**). Furthermore, RKO and SW480 cells were used for subsequent studies. After transfecting Dicer1 overexpression plasmid in RKO and SW480 cells with Lipofectamine 2000, the transfection efficiency was estimated using RT-qPCR and western blot assays. The mRNA and protein expression of Dicer1 in the transfected group were evidently higher than those in the negative control group (**Figure 3B**). Next, the MTT assay was performed to study the effects of Dicer1 on CRC cell proliferation. The MTT assay results suggested that Dicer1 upregulation significantly decreased the proliferation of RKO and SW480 cells (**Figure 3C**). Furthermore, we performed transwell assays to investigate whether Dicer1 overexpression could influence CRC cell invasion and migration. The assay results showed that Dicer1 upregulation evidently promoted RKO and SW480 cell invasion and migration in the transfected groups as compared to the negative control groups (**Figure 3D**). Taken together, these findings indicate that Dicer1 plays a critical role during CRC development.

Dicer1 Overexpression in CRC Cells Increases the Expression of Cell Invasion and Migration Markers

We found that Dicer1 overexpression promotes CRC cell invasion and migration. Thereafter, we investigated whether upregulated Dicer1 expression could affect the mRNA and protein expression of oncogenic and EMT-related markers in RKO and SW480 cell lines. The results showed that both the mRNA and protein expression of MMP7 and EMT-related markers, including E-cadherin, N-cadherin, vimentin, ZEB1, Slug, and Snail were upregulated after Dicer1 transfection (**Figures 4A–D**). Therefore, the overexpression of these markers indicates an increased potential for cell invasion, migration, and metastasis following Dicer1 overexpression. Taken together, our results suggest that increasing Dicer1 expression markedly increased the expression of a broad range of tumor progression markers.

Dicer1 Facilitated CRC Cell Migration and Invasion Through tRF-20-MEJB5Y13

When the expression of small RNAs in CRC cells under hypoxic conditions were compared with the control group, the expression of 14 tRFs was found to significantly vary between the two groups. High-throughput sequencing data revealed that tRF-20-MEJB5Y13 expression was significantly upregulated in CRC cells under hypoxic conditions (**Figure 5A**). The expression of tRF-20-MEJB5Y13, which increased significantly under hypoxic conditions, was further evaluated using RT-qPCR analysis. Additionally, PCR analysis suggested that tRF-20-MEJB5Y13 expression was consistent with the high-throughput sequencing data obtained for CRC cell lines under hypoxic conditions (**Figure 5B**). Several assays were performed to further confirm our hypothesis that Dicer1 promotes CRC cell invasion and migration through its cleavage product, tRFs, under hypoxic conditions. tRF-20-MEJB5Y13 expression was significantly upregulated with Dicer1 overexpression, thereby suggesting that the expression of Dicer1 and tRF-20-MEJB5Y13 was positively correlated, and Dicer1 may act through tRF-20-MEJB5Y13 (**Figure 5C**). Next, we further explored the effect of tRF-20-MEJB5Y13 on the progression of CRC cells. RT-qPCR analysis results revealed that tRF-20-MEJB5Y13 expression was significantly upregulated after transfecting the cells with tRF-20-MEJB5Y13 mimics (**Figure 5C**). Furthermore, transwell assay results indicated that tRF-20-MEJB5Y13 overexpression in RKO and SW480 cells enhanced cell migration and invasion, respectively (**Figure 5D**), thereby suggesting that tRF-20-MEJB5Y13 might play a critical role in promoting CRC cell migration and invasion.

To confirm the influence of Dicer1 on the biological function of CRC and that it acts through tRF-20-MEJB5Y13, we stably overexpressed Dicer1 and inhibited tRF-20-MEJB5Y13 expression (**Figure 6A**). MTT assays were used to detect the effects upon combination of Dicer1 and tRF-20-MEJB5Y13 on proliferation of CRC cells. The results indicated that tRF-20-MEJB5Y13 could prompt cells proliferation, which partially covered up the inhibiting effects of Dicer1 (**Figure 6B**). Transwell assays were performed to detect the effect of Dicer1 combined with tRF-20-MEJB5Y13 on CRC cell invasion and migration. Therefore, the results show that Dicer1 overexpression can significantly promote CRC cell invasion and migration, and this effect is partially eliminated by suppressing tRF-20-MEJB5Y13 expression (**Figure 6C**).

DISCUSSION

Dicer1 is a ribonuclease, a key enzyme necessary for the biogenesis of non-coding RNA such as microRNA, tRFs, and small interfering RNAs, and is essential for mammalian development and cell differentiation (Grelier et al., 2009). In the present study, we confirmed that CRC cell invasion and migration were increased under hypoxic conditions. Our results showed that Dicer1 expression under hypoxic conditions in colon cancer cells was upregulated. Moreover, the results suggested that Dicer1 enhances the invasion and migration ability of CRC cells.

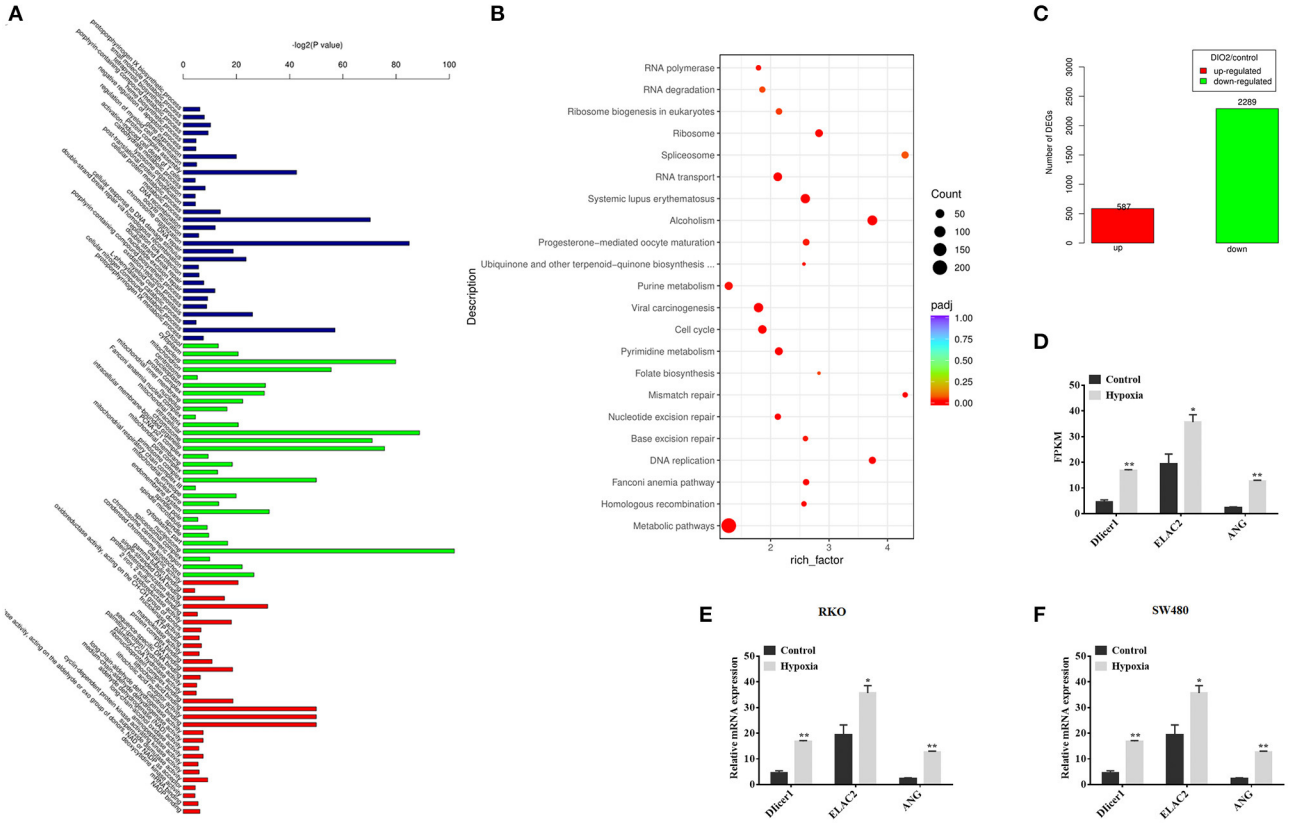

FIGURE 2 | Dicer1 upregulation in colorectal cancer cells under hypoxic conditions. GO terms listed can be clustered into three groups: (I) biological process, (II) molecular function, and (III) cellular component, describing detailed biological processes in their respective levels **(A)**. Apart from the GO terms, Bulb map of KEGG analysis was found to be effective for identifying different genes expressed under hypoxic and normoxic conditions. Rich factor represented the enrichment degree of differentially expressed genes. Y axis showed the name of enriched pathways. The area of each node represented the number of the differentially enriched host genes. The *p*-value was represented by a color scale. The statistical significance increased from purple (relatively lower significance) to orange (relatively higher significance) **(B)**. Sequencing analysis results showed significant differences of gene expression **(C)**. High-throughput sequencing was performed to detect the expression of RNases, which plays an important role in the biological process of tRFs, between the two groups **(D)**. The RT-qPCR assay results verify the expression of Dicer1 in RKO and SW480 cells **(E,F)**. $^{*}P < 0.05$, $^{**}P < 0.01$. The assays were repeated more than 3 times. NC, negative control; GO, Gene Ontology; KEGG, Kyoto Encyclopedia of Genes and Genomes; tRF, transfer RNA-derived fragments; RT-qPCR, reverse transcription quantitative polymerase chain reaction.

More importantly, we found that Dicer1 mediated EMT through tRF-20-MEJB5Y13, a key mechanism that promotes CRC cell invasion and migration.

Rapid proliferation of cancer cells as well as structural and functional defects in tumor blood vessels results in hypoxic conditions within solid tumors (Gilkes et al., 2014). Hypoxia, a characteristic of the tumor microenvironment and a common feature of solid tumors, has been associated with an increased risk of tumor metastasis and poor prognosis (Hiraga, 2018). Our study verified that hypoxic conditions inhibit the growth of CRC cells. We speculate that hypoxia may cause tumor cells to initiate apoptosis or cell necrosis. It is known that the genes *bnip3*, Bcl-2/adenovirus EIB 19 kDa-interacting protein 3, and *bnip3L* (bnip3-like), whose products are members of the Bcl-2 homology 3-only protein family of cell death factors, are highly expressed in hypoxia. Furthermore, a large amount of data shows that hypoxia promotes the invasion potential of tumor cells. Hypoxia-inducible factor activation is associated with the loss of E-Cadherin, a component of the meeting point of believers that acts as an inhibitor of invasion and migration (Sullivan and Graham, 2007). Interestingly, TWIST1 regulates EMT and is induced under hypoxia (Yang et al., 2006). In addition, cells that survive acidosis not only proliferate, but also become more aggressive and invasive (Walenta and Mueller-Klieser, 2004). This effect is partly through the activation of hypoxia-inducible factor-UPD regulatory proteins involved in matrix remodeling, such as Lysyl oxidase (Petrella et al., 2005), and metalloproteinases that disrupt extracellular matrix interactions (Pouyssegur et al., 2006).

To explore the specific mechanism of increased invasion and migration ability of CRC cells under hypoxic conditions, we analyzed and compared the expression of different genes between the test and the control groups. KEGG analysis results revealed that the RNA degradation and spliceosome pathways were enriched in CRC cells. Hence, in this study, we examined the differences in Dicer1 expression between hypoxic and normoxic conditions in CRC cells to explore whether Dicer1 expressional changes are related to CRC progression. High-throughput sequencing and RT-qPCR analyses conducted on CRC cell lines

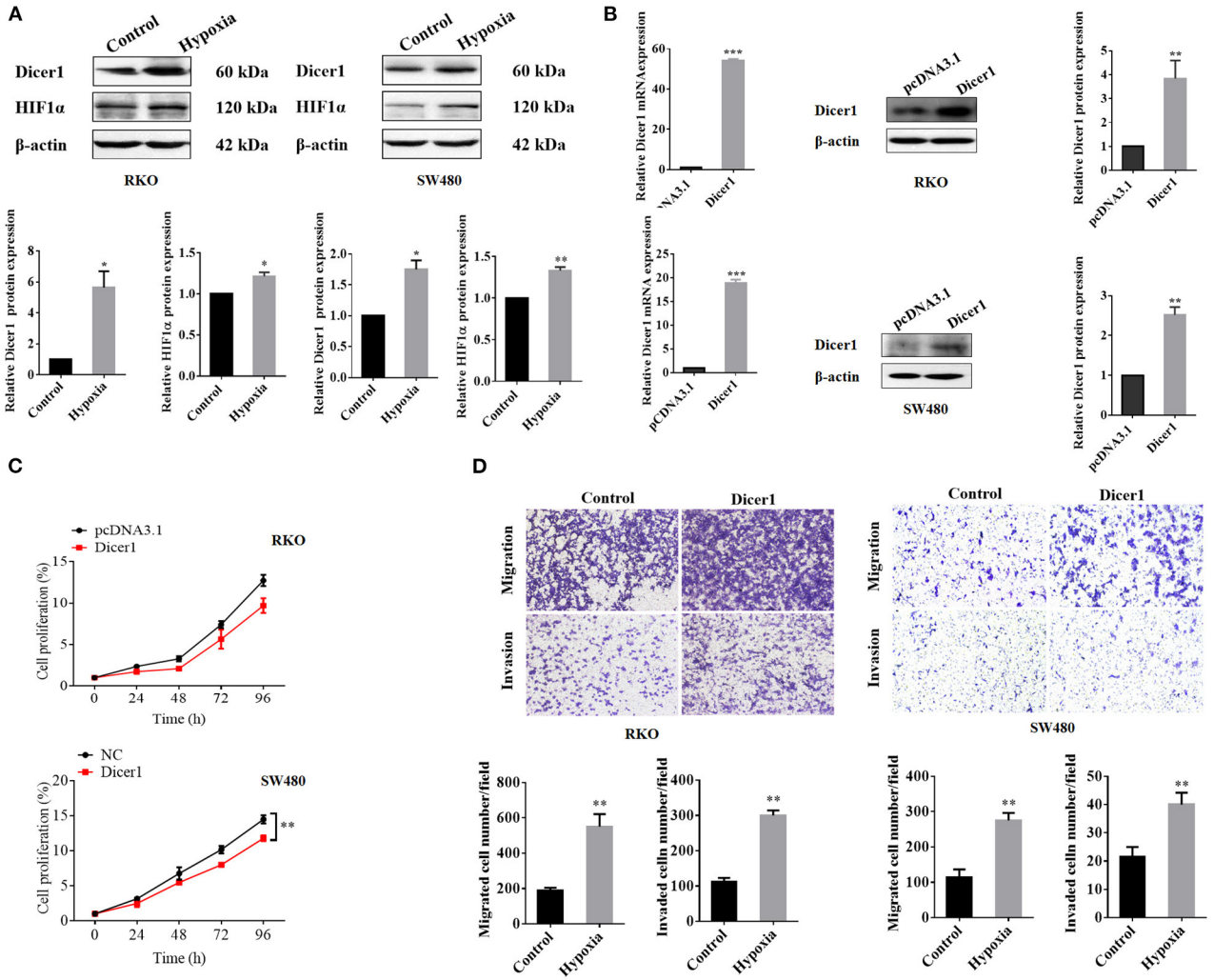

FIGURE 3 | Upregulation of Dicer1 expression affects the proliferation, invasion, and migration of colorectal cancer cells. Dicer1 and HIF1α expression under hypoxic conditions was further evaluated using western blot assays **(A)**. We transfected the Dicer1 overexpression plasmid into RKO and SW480 cells and detected its transfection efficiency using RT-qPCR and western blot assays **(B)**. MTT test results showed the proliferation of RKO and SW480 cells **(C)**. Transwell assays showed that Dicer1 overexpression could promote RKO and SW480 cell invasion and migration **(D)**. $^{*}P < 0.05$, $^{**}P < 0.01$, and $^{***}P < 0.001$. The assays were repeated more than 3 times. NC, negative control; RT-qPCR, reverse transcription quantitative polymerase chain reaction; MTT, 3-(4,5-dimethylthiazol-2-yl)-2,5-diphenyltetrazolium bromide.

cultured under normoxia and hypoxia demonstrated that Dicer1 expression is upregulated under hypoxic conditions. However, Lai et al. found that hypoxia-inducible factor 1α (HIF1α) induced the proteolysis of Dicer1 in the CRC cell line HCT116 (Lai et al., 2018). While presumably other pathways or regulatory mechanisms that lead to the increased expression of Dicer1 under hypoxic conditions, since Dicer1 is a specific nuclease that produces tRFs from tRNA cleavage under hypoxia (Shen et al., 2018). Although Dicer1 displays different expression patterns in different cancers, our data suggest that Dicer1 expression under hypoxic conditions in colon cancer cells was upregulated and it may affect CRC cells and tumor microenvironment.

Several studies have been carried out on different types of cancer to clarify the role of Dicer1 in carcinogenesis and its impact on prognosis. In the present study, proliferation assays showed that Dicer1 transfection inhibited the proliferation of two CRC cell lines. Our transwell assay results suggested that upregulated Dicer1 expression promotes CRC cell invasion and migration. Our results were consistent with the results reported for prostate adenocarcinoma, which suggested that Dicer1 expression was upregulated and affected tumor invasion characteristics (Chiosea et al., 2006). Consistently, a study investigating the expression of ribonuclease Dicer in CRC cell lines reported that Phase III Dicer mRNA expression was significantly higher than that in the Phase II, thereby suggesting that Dicer may play a key role in the development of a more invasive form of tumor (Papachristou et al., 2011). In ovarian cancer, Dicer expression correlates with

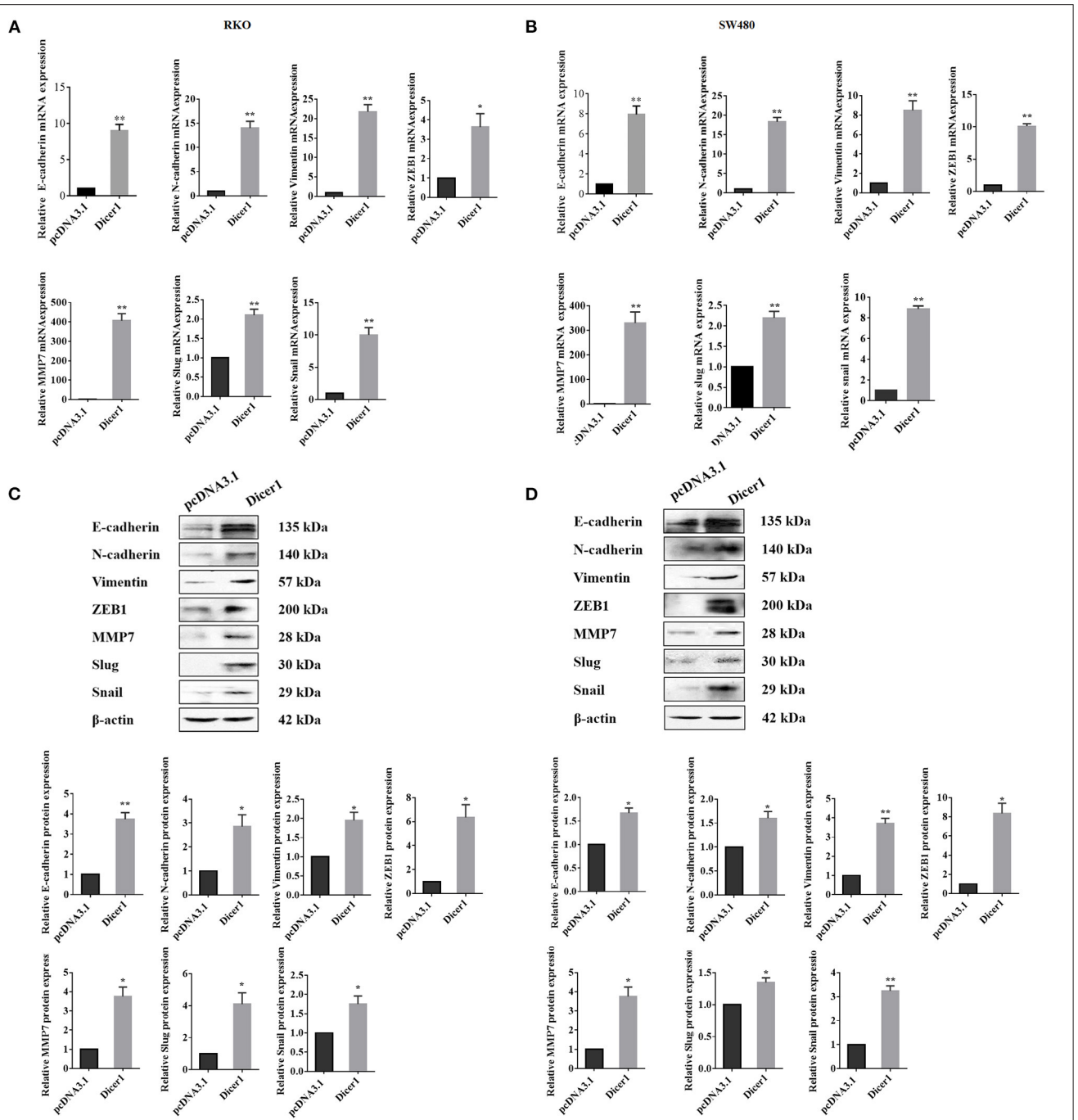

FIGURE 4 | Increased Dicer1 expression in colorectal cancer cell lines promotes the expression of various carcinogenic markers, including EMT-related markers. Comparison of the mRNA expression of indicated markers in RKO and SW480 cells between the control and Dicer-overexpressing groups based on RT-qPCR analysis **(A,B)**. Western blot assays were performed for analyzing the expression of E-cadherin, N-Cadherin, Vimentin, ZEB1, MMP7, Slug, and Snail **(C,D)**. $^{*}P < 0.05$, $^{**}P < 0.01$. The assays were repeated more than 3 times. RKO and SW480, human colorectal cancer cells; NC, Negative control; EMT, epithelial-to-mesenchymal transition; RT-qPCR, reverse transcription quantitative polymerase chain reaction.

lymph node metastasis status, and its high expression denotes lymph node metastasis (Flavin et al., 2008). However, on the contrary, in breast cancer cell lines, low Dicer expression was found in cells with mesenchymal phenotypes and metastatic bone derivatives, thereby indicating that downregulated Dicer expression may be related to tumor metastasis (Grelier et al., 2009). Moreover, Dicer has a tumor-suppressing effect on lung adenocarcinoma and ovarian cancer cells (Chiosea et al.,

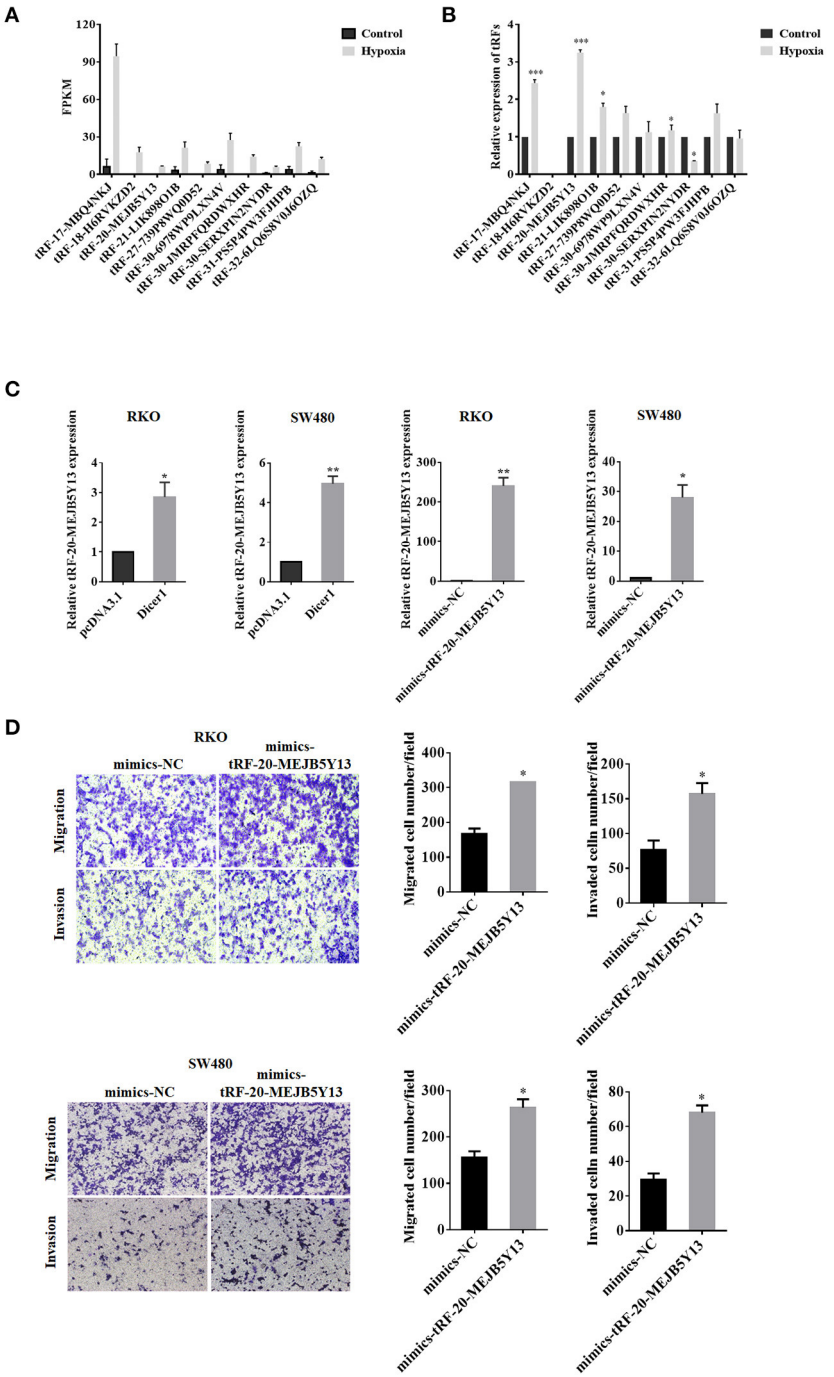

FIGURE 5 | Dicer1 promotes the invasion and migration of CRC through tRF-20-MEJB5Y13. High-throughput sequencing and RT-qPCR analyses showed significant differences in the expression of 14 tRFs **(A,B)**. RT-qPCR assay was performed to explore whether tRF-20-MEJB5Y13 expression was related to Dicer1 overexpression and to detect the transfection of tRF-20-MEJB5Y13 mimics **(C)**. Transwell assays were performed to evaluate CRC cell migration and invasion with tRF-20-MEJB5Y13 overexpression **(D)**. $^{*}P < 0.05$, $^{**}P < 0.01$. The assays were repeated more than 3 times. CRC, colorectal cancer; RT-qPCR, reverse transcription quantitative polymerase chain reaction; tRF, transfer RNA-derived fragments.

2007; Merritt et al., 2008). Although Dicer plays different roles in the progression of cancer in different solid tumors, our study found that upregulated Dicer1 expression is associated with CRC cell invasion and migration. Therefore, Dicer1 overexpression may be a powerful independent predictor of poor CRC prognosis.

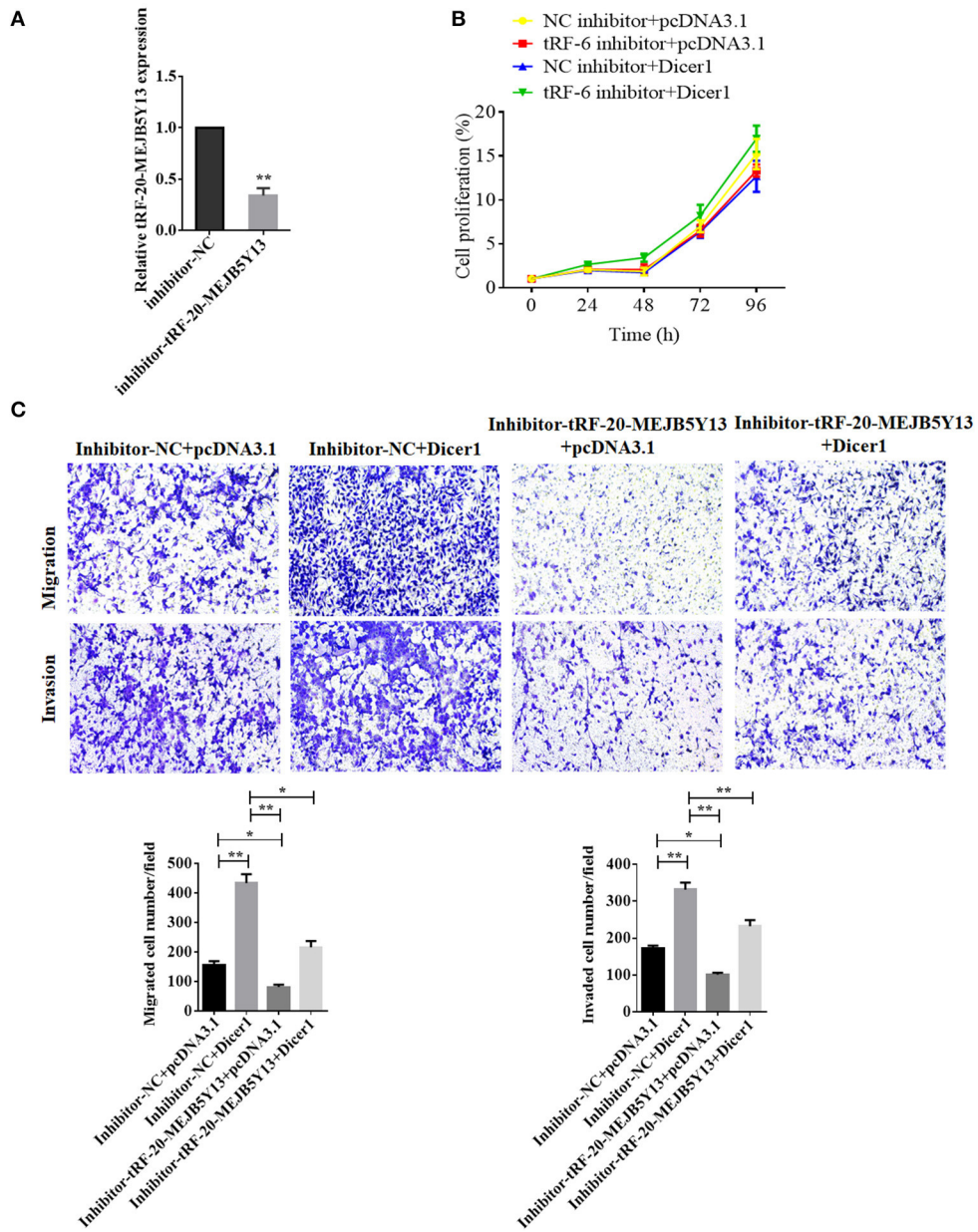

FIGURE 6 | RT-qPCR assay was performed to detect the transfection of tRF-20-MEJB5Y13 inhibitor **(A)**. MTT assays were performed to explore CRC cell proliferation after the co-transfection of both Dicer1 mimics and tRF-20-MEJB5Y13 inhibitor **(B)**. Transwell assays were performed to evaluate the common effects of Dicer1 overexpression and tRF-20-MEJB5Y13 knockdown on CRC cell invasion and migration **(C)**. $^{*}P < 0.05$, $^{**}P < 0.01$. The assays were repeated more than 3 times. CRC, colorectal cancer; RT-qPCR, reverse transcription quantitative polymerase chain reaction; MTT, 3-(4,5-dimethylthiazol-2-yl)-2,5-diphenyltetrazolium bromide.

Next, we explored the mechanism through which Dicer1 promotes CRC cell invasion and migration. The most common mechanism for enhancing the motility of cancer cells is EMT, which liberates tumor cells from adhesion, thereby allowing them to migrate and invade. In our study, we confirmed that Dicer1 overexpression induced the expression of EMT-related molecules, namely E-cadherin, N-cadherin, vimentin, ZEB1, MMP7, Slug, and Snail. This suggests that the elevated expression of Dicer1 in CRC cells contributes to multiple carcinogenic characteristics, including cell migration and invasion.

Notably, Dicer1 is the core component of the tRF regulatory network. Therefore, several studies have aimed to explore the significant role of ribonuclease in cancer pathology. In the present study, high-throughput sequencing and bioinformatics analysis results revealed significant differences in the expression of 14 tRFs under hypoxic conditions (named from database

MINTbase). Retrospective verification results of RT-qPCR experiments showed that the expression of tRF (tRF-20-MEJB5Y13) in the differentially expressed tRFs was significantly upregulated with the most significant differences in their expression, which was consistent with that of the sequencing results. Recently, it was reported that the expression of a series of tRFs is altered in cancer tissues, and they are related to the development of cancer (Chen et al., 2019). Huang et al. found that tRF/miR-1280 expression was decreased in tumor tissues as tRF/miR-1280 overexpression reduces cell proliferation and colony formation (Huang et al., 2017). In our study, we explored the specific role and regulatory mechanism of tRF-20-MEJB5Y13 in the EMT in CRC. Functional assays verified that tRF-20-M0NK5Y93 overexpression can facilitate the acquisition of a variety of oncogenic characteristics, including cell invasion and migration, which supported the hypothesis that tRF-20-MEJB5Y13 functions as a tumor-suppressive molecule *in vitro*. These findings demonstrate that tRF-20-MEJB5Y13 exerts its effects on CRC progression by promoting the metastatic activity of CRC cells.

Finally, our results showed that tRF-20-MEJB5Y13 knockdown could inhibit the stimulatory effect of Dicer1 overexpression on CRC cell migration and invasion. Thus, our results suggest that Dicer1 plays a key role in CRC progression by regulating tRF-20-MEJB5Y13 expression under hypoxic conditions. Currently, we have reasons to believe that Dicer1 acts as a nuclease to produce tRF-20-MEJB5Y13 from pre-tRNAs and mature tRNAs, thereby promoting CRC cell invasion and migration. However, there are other reasons why high Dicer1 expression makes CRC cells more invasive. Dicer performs additional functions that may lead to malignant transformation. Recently, studies have shown that Dicer1 is essential for maintaining the methylation of CpG promoter islands in CRC cell lines (Ting et al., 2008). As we know, over-methylation and under-methylation of several genes in CRC are common phenomena, and Dicer can promote or at least maintain these carcinogenic events (Samowitz and Ogino, 2008). Therefore, this may partly explain the contradiction between the findings of colorectal cancer and other cancers.

CONCLUSION

In this study, we found that Dicer1 expression can be induced by hypoxia in CRC cells, and it promotes hypoxia-induced CRC cell metastasis. Additionally, we found that the expression of tRF-20-MEJB5Y13, a small ncRNA, was increased under hypoxic conditions, and its upregulation by Dicer1 resulted in hypoxia-induced CRC cell progression. Therefore, further studies need to be performed to establish Dicer1 as a potential tumor metastasis molecule, thereby further developing it as a novel biological marker for tumor development diagnosis or as a new avenue for new drugs, which offers an innovative strategy for inhibiting tumor metastasis that has broad application prospects in cancer advances.

DATA AVAILABILITY STATEMENT

The original contributions presented in the study are included in the article/**Supplementary Material**, further inquiries can be directed to the corresponding author/s.

AUTHOR CONTRIBUTIONS

JW and ZT provided the idea and designed the framework of the study. NL, YM, and JW conceived and designed the experiments. NL, YM, JM, XY, QZ, and MX performed the experiments. NL, QD, YH, and JW analyzed the bioinformatics data. NL wrote the draft. YH, ZT, and JW revised the manuscript. All authors have read and approved the final manuscript.

FUNDING

This study was financially supported by the grants provided from the National Natural Science Foundation of China (Grant Nos. 81672364, 81871917, and 81802750).

SUPPLEMENTARY MATERIAL

The Supplementary Material for this article can be found online at: https://www.frontiersin.org/articles/10.3389/fgene.2021.638244/full#supplementary-material

REFERENCES

Catalano, V., Turdo, A., Di Franco, S., Dieli, F., Todaro, M., and Stassi, G. (2013). Tumor and its microenvironment: a synergistic interplay. *Semi. Cancer Biol.* 23, 522–532. doi: 10.1016/j.semcancer.2013.08.007

Chen, H., Xu, Z., and Liu, D. (2019). Small non-coding RNA and colorectal cancer. *J. Cell. Mol. Med.* 23, 3050–3057. doi: 10.1111/jcmm.14209

Chiosea, S., Jelezcova, E., Chandran, U., Acquafondata, M., McHale, T., Sobol, R. W., et al. (2006). Up-regulation of dicer, a component of the MicroRNA machinery, in prostate adenocarcinoma. *Am. J. Pathol.* 169, 1812–1820. doi: 10.2353/ajpath.2006.060480

Chiosea, S., Jelezcova, E., Chandran, U., Luo, J., Mantha, G., Sobol, R. W., et al. (2007). Overexpression of dicer in precursor lesions of lung adenocarcinoma. *Cancer Res.* 67, 2345–2350. doi: 10.1158/0008-5472.CAN-06-3533

Cole, C., Sobala, A., Lu, C., Thatcher, S. R., Bowman, A., Brown, J. W., et al. (2009). Filtering of deep sequencing data reveals the existence of abundant dicer-dependent small RNAs derived from tRNAs. *RNA* 15, 2147–2160. doi: 10.1261/rna.1738409

Crotti, S., Piccoli, M., Rizzolio, F., Giordano, A., Nitti, D., and Agostini, M. (2017). Extracellular matrix and colorectal cancer: how surrounding microenvironment affects cancer cell behavior? *J. Cell Physiol.* 232, 967–975. doi: 10.1002/jcp.25658

Faggad, A., Kasajima, A., Weichert, W., Stenzinger, A., Elwali, N. E., Dietel, M., et al. (2012). Down-regulation of the microRNA processing enzyme dicer is a prognostic factor in human colorectal cancer. *Histopathology* 61, 552–561. doi: 10.1111/j.1365-2559.2011.04110.x

Flavin, R. J., Smyth, P. C., Finn, S. P., Laios, A., O'Toole, S. A., Barrett, C., et al. (2008). Altered eIF6 and dicer expression is associated with clinicopathological

features in ovarian serous carcinoma patients. *Mod. Pathol.* 21, 676–684. doi: 10.1038/modpathol.2008.33

Gilkes, D. M., Semenza, G. L., and Wirtz, D. (2014). Hypoxia and the extracellular matrix: drivers of tumour metastasis. *Nat. Rev. Cancer* 14, 430–439. doi: 10.1038/nrc3726

Goodarzi, H., Liu, X., Nguyen, H. C., Zhang, S., Fish, L., and Tavazoie, S. F. (2015). Endogenous tRNA-derived fragments suppress breast cancer progression via YBX1 displacement. *Cell* 161, 790–802. doi: 10.1016/j.cell.2015.02.053

Grelier, G., Voirin, N., Ay, A. S., Cox, D. G., Chabaud, S., Treilleux, I., et al. (2009). Prognostic value of Dicer expression in human breast cancers and association with the mesenchymal phenotype. *Br. J. Cancer.* 101, 673–683. doi: 10.1038/sj.bjc.6605193

Haussecker, D., Huang, Y., Lau, A., Parameswaran, P., Fire, A. Z., and Kay, M. A. (2010). Human tRNA-derived small RNAs in the global regulation of RNA silencing. *RNA* 16, 673–695. doi: 10.1261/rna.2000810

Hiraga, T. (2018). Hypoxic microenvironment and metastatic bone disease. *Int. J. Mol. Sci.* 19:3523. doi: 10.3390/ijms19113523

Huang, B., Yang, H., Cheng, X., Wang, D., Fu, S., Shen, W., et al. (2017). tRF/miR-1280 suppresses stem cell-like cells and metastasis in colorectal cancer. *Cancer Res.* 77, 3194–3206. doi: 10.1158/0008-5472.CAN-16-3146

Karube, Y., Tanaka, H., Osada, H., Tomida, S., Tatematsu, Y., Yanagisawa, K., et al. (2005). Reduced expression of dicer associated with poor prognosis in lung cancer patients. *Cancer Sci.* 96, 111–115. doi: 10.1111/j.1349-7006.2005.00015.x

Kuscu, C., Kumar, P., Kiran, M., Su, Z., Malik, A., and Dutta, A. (2018). tRNA fragments (tRFs) guide ago to regulate gene expression post-transcriptionally in a Dicer-independent manner. *RNA* 24, 1093–1105. doi: 10.1261/rna.066126.118

Lai, H. H., Li, J. N., Wang, M. Y., Huang, H. Y., Croce, C. M., Sun, H. L., et al. (2018). HIF-1alpha promotes autophagic proteolysis of dicer and enhances tumor metastasis. *J. Clin. Invest.* 128, 625–643. doi: 10.1172/JCI89212

Lee, Y. S., Shibata, Y., Malhotra, A., and Dutta, A. (2009). A novel class of small RNAs: tRNA-derived RNA fragments (tRFs). *Genes Dev.* 23, 2639–2649. doi: 10.1101/gad.1837609

Merritt, W. M., Lin, Y. G., Han, L. Y., Kamat, A. A., Spannuth, W. A., Schmandt, R., et al. (2008). Dicer, drosha, and outcomes in patients with ovarian cancer. *N. Engl. J. Med.* 359, 2641–2650. doi: 10.1056/NEJMoa0803785

Miller, K. D., Nogueira, L., Mariotto, A. B., Rowland, J. H., Yabroff, K. R., Alfano, C. M., et al. (2019). Cancer treatment and survivorship statistics, 2019. *CA Cancer J. Clin.* 69, 363–385. doi: 10.3322/caac.21565

Papachristou, D. J., Korpetinou, A., Giannopoulou, E., Antonacopoulou, A. G., Papadaki, H., Grivas, P., et al. (2011). Expression of the ribonucleases drosha, dicer, and Ago2 in colorectal carcinomas. *Virchows Arch.* 459, 431–440. doi: 10.1007/s00428-011-1119-5

Petrella, B. L., Lohi, J., and Brinckerhoff, C. E. (2005). Identification of membrane type-1 matrix metalloproteinase as a target of hypoxia-inducible factor-2 alpha in von Hippel-Lindau renal cell carcinoma. *Oncogene* 24, 1043–1052. doi: 10.1038/sj.onc.1208305

Pouyssegur, J., Dayan, F., and Mazure, N. M. (2006). Hypoxia signalling in cancer and approaches to enforce tumour regression. *Nature* 441, 437–443. doi: 10.1038/nature04871

Roma-Rodrigues, C., Mendes, R., Baptista, P. V., and Fernandes, A. R. (2019). Targeting tumor microenvironment for cancer therapy. *Int. J. Mol. Sci.* 20:840. doi: 10.3390/ijms20040840

Samowitz, W. S., and Ogino, S. (2008). DNA methylation in breast and colorectal cancers. *Mod. Pathol.* 21:1054; author reply 1054–1055. doi: 10.1038/modpathol.2008.21

Shen, Y., Yu, X., Zhu, L., Li, T., Yan, Z., and Guo, J. (2018). Transfer RNA-derived fragments and tRNA halves: biogenesis, biological functions and their roles in diseases. *J. Mol. Med.* 96, 1167–1176. doi: 10.1007/s00109-018-1693-y

Sormendi, S., and Wielockx, B. (2018). Hypoxia pathway proteins as central mediators of metabolism in the tumor cells and their microenvironment. *Front. Immunol.* 9:40. doi: 10.3389/fimmu.2018.00040

Sullivan, R., and Graham, C. H. (2007). Hypoxia-driven selection of the metastatic phenotype. *Cancer Metastasis Rev.* 26, 319–331. doi: 10.1007/s10555-007-9062-2

Ting, A. H., Suzuki, H., Cope, L., Schuebel, K. E., Lee, B. H., Toyota, M., et al. (2008). A requirement for DICER to maintain full promoter CpG island hypermethylation in human cancer cells. *Cancer Res.* 68, 2570–2575. doi: 10.1158/0008-5472.CAN-07-6405

Walenta, S., and Mueller-Klieser, W. F. (2004). Lactate: mirror and motor of tumor malignancy. *Semin. Radiat. Oncol.* 14, 267–274. doi: 10.1016/j.semradonc.2004.04.004

Yang, J., Mani, S. A., and Weinberg, R. A. (2006). Exploring a new twist on tumor metastasis. *Cancer Res.* 66, 4549–4552. doi: 10.1158/0008-5472.CAN-05-3850

Zhang, M., Li, F., Wang, J., He, W., Li, Y., Li, H., et al. (2019). tRNA-derived fragment tRF-03357 promotes cell proliferation, migration and invasion in high-grade serous ovarian cancer. *Onco. Targets Ther.* 12, 6371–6383. doi: 10.2147/OTT.S206861

Conflict of Interest: The authors declare that the research was conducted in the absence of any commercial or financial relationships that could be construed as a potential conflict of interest.

frontiers in Cell and Developmental Biology

ORIGINAL RESEARCH
published: 16 March 2021
doi: 10.3389/fcell.2021.616887

ENC1 Facilitates Colorectal Carcinoma Tumorigenesis and Metastasis via JAK2/STAT5/AKT Axis-Mediated Epithelial Mesenchymal Transition and Stemness

*Ying Cui[1], Jiani Yang[2], Yibing Bai[2], QingWei Li[2], Yuanfei Yao[2], Chao Liu[2], Feng Wu[3], Jingchun Zhang[2] and Yanqiao Zhang[2]**

[1] Department of Radiation Oncology, Harbin Medical University Cancer Hospital, Harbin, China, [2] Department of Gastrointestinal Medical Oncology, Harbin Medical University Cancer Hospital, Harbin, China, [3] Department of Gastroenterology, The First Affiliated Hospital of Harbin Medical University, Harbin, China

OPEN ACCESS

Edited by:
Marco Mina,
Sophia Genetics, Switzerland

Reviewed by:
Qing Chun Zhao,
Shenyang Pharmaceutical University, China
Priyanka Gupta,
University of Alabama at Birmingham, United States

***Correspondence:**
Yanqiao Zhang
yanqiaozhang@ems.hrbmu.edu.cn

Specialty section:
This article was submitted to Molecular and Cellular Oncology, a section of the journal Frontiers in Cell and Developmental Biology

Received: 13 October 2020
Accepted: 05 February 2021
Published: 16 March 2021

Citation:
Cui Y, Yang J, Bai Y, Li QW, Yao Y, Liu C, Wu F, Zhang J and Zhang Y (2021) ENC1 Facilitates Colorectal Carcinoma Tumorigenesis and Metastasis via JAK2/STAT5/AKT Axis-Mediated Epithelial Mesenchymal Transition and Stemness. Front. Cell Dev. Biol. 9:616887. doi: 10.3389/fcell.2021.616887

Ectodermal neural cortex 1 (ENC1) is an actin-binding protein and has been known to be upregulated in several cancers, but the molecular mechanisms through which it contributes to the pathology of CRC have largely been elusive. We utilized data mining and validated the aberrant expression of ENC1, following which phenotypic traits of malignancy were assessed *in vitro*. Ruxolitinib was used as a surrogate to compare the effects of ENC1 expression and silencing on the JAK-STAT-AKT pathway. *In vivo* models were employed to confirm the *in vitro* observations. Computation analysis, strengthened by *in situ* and *in vitro* data, confirmed the overexpression of ENC1 in CRC and predicted a poor prognosis, while enhanced cell proliferation, invasion, migration, EMT, and stemness were associated with ENC1 overexpression. Silencing of ENC1 downregulated the phenotypes. Additionally, silencing of ENC1 significantly reduced the activation of JAK2 and consequent activation of STAT5 and AKT comparable to ruxolitinib inhibition of JAK2. Silencing of ENC1 resulted in lesser tumor volumes and fewer numbers of tumors, *in vivo*. These data suggest that ENC1 induces CRC through the JAK2-STAT5-AKT axis. ENC1 is a suitable diagnostic marker for CRC detection, and ENC1 targeting therapies may suppress CRC progression.

Keywords: colorectal carcinoma, CRC, ENC1, epithelial mesenchymal transition, stemness

INTRODUCTION

A recently concluded longitudinal study undertaken in 195 countries over a period of 27 years (1990–2017) is an in-depth analysis of incidence, mortality, disability, and associated risk factors in Colorectal Cancer Collaborators (CRC) (2019). The study found that CRC is the third most deadly and fourth most found cancer in the world, preceded by lung, liver, and stomach cancer. During the period of the study, there was a consistent increase in the age-standardized incidence rate, and the

findings are concurrent with the recent GLOBOCAN database, estimating about 1,800,977 incident cases and a million deaths due to CRC (Bray et al., 2018). These figures are attributed to higher CRC screening and are indicative of a decline or stabilization. However, several countries have been reporting CRC occurrence in individuals under 50 years of age identified with western diet and lifestyle (The Lancet Gastroenterology Hepatology, 2019; Hofseth et al., 2020).

Colorectal cancer is etiologically a heterogeneous disease arising through three major pathways–the traditional adenoma–carcinoma sequence, the serrated pathway, and the inflammatory pathway (Keum and Giovannucci, 2019). A stepwise accumulation of such genetic mutations and/or epigenetic changes is known to contribute to the occurrence of sporadic CRC (Long et al., 2017; Nguyen and Duong, 2018; De Palma et al., 2019). The most implicated molecular pathways in CRC progression are EGFR/MAPK, Notch, PI3K, TGF-β, and Wnt signaling pathways, given the significance of these pathways to critical cellular processes. Further, the cross talk between these pathways in CRC progression has also been discussed (Koveitypour et al., 2019).

The roles of several genes such as EGFR, RAS, RAF, Notch-1, Jagged-1, PIK3CA, PTEN, TGFBR2, TGFBR1, SMADs, AXIN, and CTNNB1 have been assessed and linked to the abovementioned pathways. While reviewing the literature, we identified that several of these genes serve as biomarkers of CRC progression and bear a prognostic value (Garcia-Bilbao et al., 2012). ENC1 is one such gene also found to be overexpressed in primary colon cancers (Garcia-Bilbao et al., 2012; Uddin et al., 2019).

Upregulation of ENC1 has also been recorded in medulloblastoma, prostate, glioblastomas, and astrocytomas, indicating that the gene may have an oncogenic potential if inappropriately expressed (Hammarsund et al., 2004). Expression of ENC1 correlates with the transcriptional activity of the β-catenin/Tcf4 complex and p53 or p53-regulated factors explaining the aberrant expression of ENC1 in CRC (Fujita et al., 2001). However, the molecular role of ENC1 in CRC progression and its role in pathway cross talk remain less explored.

In the current study using a combinatorial approach of *in vitro* and *in vivo* models, we report that ENC1 expression in CRC is associated with increased cellular proliferation, migration, invasion, and tumor growth, and this was likely mediated through the JAK2-STAT5-AKT axis. Through our study, we have elaborated the potential role of ENC1 in primary CRC.

MATERIALS AND METHODS

Data Mining and the Gene Set Enrichment Analysis (GSEA)

The Oncomine database[1] and GEPIA database[2] were utilized to assess the mRNA expression status of ENC1 in CRC. From TCGA, we downloaded the gene expression profile data of CRC tissues for a large cohort of CRC patients (n = 469) and compared them with normal colon samples (n = 41) using bioinformatic tools.

CRC-related RNA-seq data were retrieved from the TCGA database portal[3] for pathway and function analyses. GSEA software[4] was applied to calculate enrichment levels. ENC1 expression values were used as the phenotype.

Tissue Microarrays and Tissue Specimens

The CRC TMAs (HColA180Su17) consisted of 100 primary CRC specimens and 78 matched peritumoral tissues containing complete clinicopathological information and long-term follow-up data which were commercially procured from Shanghai Outdo Biotech Co., Ltd (Shanghai, China).

Twenty-four pairs of snap-frozen CRC specimens and adjacent normal tissues used for quantitative real-time PCR (qRT-PCR) were obtained from the Department of Colorectal Cancer Surgery, the Second Affiliated Hospital of Harbin Medical University, between September 2018 and February 2019. Twelve paired CRC samples were randomly selected for western blotting analysis. Selected patients had only undergone colectomy without neoadjuvant therapy. Pre-approval for the study was sought from the Institutional Review Board of Harbin Medical University.

Cell Lines and Cell Culture

The human colorectal cancer cell lines HT29, LOVO, DLD-1, SW620, HCT116, SW480, RKO, and normal colorectal cells NCM460 were commercially procured from the ATCC (United States). As per the manufacturer's instructions, HT29, DLD-1, HCT116, and NCM460 were cultured in RPMI-1640 medium (Gibco, United States) while LOVO was grown in F-12K medium (Gibco, United States) and RKO was in MEM (Gibco, United States), respectively. All cell lines were maintained in a humidified atmosphere with 5% CO_2 at 37°C. SW620 and SW480 were incubated in Leibovitz's L-15 medium (Gibco, United States). Uniform, 10% FBS (ScienCell, United States) supplementation without antibiotic was maintained for all cells in the abovementioned medium. All experiments were performed with mycoplasma-free cells. Moreover, all cell lines have been authenticated using STR profiling within the last 3 years.

Ectopic ENC1 Overexpression and Knockdown of Colorectal Cancer Cells

HT29/HCT116 cells were transiently transfected with plasmid pcDNA3.1 vector as a negative control and full-length pLVX-ENC1-HA (Umibio, Shanghai, China) for ectopic overexpression of ENC1. The transfections were performed by Lipofectamine 2000 (Invitrogen, United States) as per the manufacturer's protocol. After 48 h of transfection, the following series of experiments were undertaken.

To establish stable ENC1-knockdown cells, HT29/HCT116 cells were infected with lentivirus containing two different

[1]https://www.oncomine.org/

[2]http://gepia.cancer-pku.cn/

[3]https://cancergenome.nih.gov/

[4]http://www.broadinstitute.org/gsea

shRNAs targeting ENC1 (GeneChem, Shanghai, China). The virus was added to cells cultured in the RPMI-1640 medium at an MOI of approximately 10 with 8 μg/ml polybrene. At 48 h post infection, puromycin (2 μg/mL) was added for an additional 10–14 days to select stable cells. The sequences of shRNA were as follows:

shRNA-negative control: 5′-TTCTCCGAACGTGTCACGT-3′;
ENC1-shRNA1: 5′-CCATCCACCCAGAAGTCTT-3′;
ENC1-shRNA2: 5′-GCTGATTCCTACTGCATTT-3′.

Western Blotting

Total proteins were extracted from human tissue samples or cultured cells using RIPA buffer (Solarbio, Beijing, China) containing commercially procured protease and phosphatase inhibitor cocktails (Roche, Mannheim, Germany). The total protein concentration was determined using a BCA kit (Beyotime, shanghai, China). Further, proteins were separated using a 10% SDS-PAGE and then transferred onto PVDF membranes (Merck, Darmstadt, Germany). Upon transfer, membranes were blocked using five percent skimmed milk solution in PBS/Tween-20 for an hour. The membranes were incubated overnight at 4°C with a diluted solution of primary antibodies followed by washing and re-incubation with a horseradish peroxidase (HRP)-conjugated secondary antibody (Zsbio, China) for 1 h at room temperature. The following commercial antibody preparations were used: antibodies for ENC1, E-cadherin, N-cadherin, Vimentin, Snail, CD44, and CD133 were purchased from the Proteintech Group (Wuhan, China); antibodies for p-JAK2 (Tyr1007/1008), JAK2, p-STAT5 (Tyr694), STAT5, p-AKT (Ser473), AKT, and SOX2 were obtained from Cell Signaling Technology (CST, United States); and antibodies for GAPDH (internal controls) were procured from Zsbio, China.

qRT-PCR

Total RNA was extracted by TRIzol reagent (Thermo Fisher Scientific, United States), and reverse transcription reactions were performed with a ReverTra Ace qPCR RT Master Mix (TOYOBO, Japan). PCR amplification was performed using a SYBR Green Master Mix (Roche, Mannheim, Germany) on an ABI 7500 Fast Real-time PCR Detection System (Applied Biosystems, Foster City, CA, United States). The $2^{-\Delta\Delta Ct}$ or ΔCt method was selected to calculate relative mRNA expression levels. GAPDH was utilized as the endogenous control to normalize the relative expression levels of target genes. The specific primer sequences used are listed as follows: ENC1-F: 5′-GCAGTAGGAATCAGCGAGTA-3′; ENC1-R: 5′-CCAAGGTGGGAGATGTGA-3′; GAPDH-F: 5′-CATGTTCGTCATGGGTGTGAA-3′; GAPDH-R: 5′-GGCATGGACTGTGGTCATGAG-3′.

Immunohistochemistry (IHC)

For TMA IHC staining, the TMAs were deparaffinized in xylene and rehydrated using graded alcohol after heating at 63°C for an hour, and the DAKO automatic immunohistochemical pretreatment system (Autostainer Link 48, Dako North America, Inc., United States) was used for antigen retrieval. For mouse tumor tissues, all samples were fixed in formalin and paraffin embedded. Briefly, the slides were deparaffinized with xylene and rehydrated using graded ethanol and citric acid under high temperature and pressure was used for antigen retrieval. Then, the TMAs or mouse tissue slices were incubated with the rabbit primary anti-ENC1 (1:150 for TMAs, 1:50 for mouse tumor tissues, ProteinTech, China) and Ki-67 (1:150 for mouse tumor tissues, Zsbio, China) overnight at 4°C. This was followed by goat anti-rabbit IgG secondary antibody for 30 min at room temperature. After washing with PBS, DAB was used for the color reaction and specimens were counterstained with hematoxylin finally.

The immunoreactions were evaluated by two independent researchers blinded to the clinicopathologic information. The staining intensity was categorized as follows: 0 (no staining), 1 (weak), 2 (moderate), and 3 (strong). The positive rate of stained cells was classified as follows: 0 (no positive cells), 1 (<25%), 2 (25–50%), 3 (51–75%), and 4 (76–100%). The immunoreactivity score was calculated by tissue staining intensity multiplied by positive rate of stained cells (range: 0 to 12). Score > 8 was considered as high expression level and ≤8 as low expression level.

Cell Proliferation Assay

Cancer cells lines (3×10^3 cells per well) were inoculated into 96-well plates in triplicate and incubated at 37°C for 24, 48, 72, and 96 h. CCK-8 reagents (Dojindo, Kumamoto, Japan) with a ratio of 10 μl solution per 100 μl medium were added to each well. Cell viability was measured at the indicated time points, and the absorbance was read at 450 nm under a fluorescence microplate reader.

Colony Formation Assay

Thousand cells were seeded on the 6-well culture plates with a 10% FBS-containing medium and incubated. After 7 to 14 days, large colonies (>100 cells/per colony) were fixed and stained by methanol and crystal violet for 30 min and counted manually.

Wound-Healing Assay

Cells were cultured until about 90% confluence in a 6-well plate, then the monolayers were wounded using a 20-μl plastic pipette tip. 0 and 24 h later, cells migrated into the wounded area were photographed. The analysis of wound area was conducted by ImageJ software.

Transwell Migration and Invasion Assays

For the migration and invasion assays, a total of 5×10^5 cells were seeded in the upper chambers of a transwell plate (Corning, United States) or a Matrigel (BD BioCoat, San Jose, CA, United States)-precoated transwell plate in 200 μl of serum-free medium. The bottom chambers contained 600 μl of RPMI-1640 medium with 20% FBS. After the cells were incubated at 37°C for 48 h, the bottom chambers were fixed by 4% methanol and stained with 1% crystal violet. Before staining, the non-migratory

or non-invasive cells on the top surface were gently removed using a cotton swab. Then, cells were randomly counted and photographed with a microscope in at least three fields.

Immunofluorescence Staining

Cells were seeded in 24-well plates and transfected with plasmids vector and ENC1 until about 95% confluence. After washing thrice with PBS, cells were fixed with 4% paraformaldehyde, permeabilized with 0.2% Triton X-100 (Solarbio, Beijing, China) for 20 min, and blocked with 5% bovine serum albumin for half an hour. The cells were then incubated with primary antibodies against E-cadherin, N-cadherin, and Vimentin (1:100, ProteinTech, China), overnight at 4°C, followed by incubation with corresponding fluorescence-labeled secondary antibodies (1:200, Zsbio, China) at room temperature for 1 h. The nuclei were stained with 4′-6-diamidino-2-phenylindole (DAPI; Beyotime, shanghai, China) for 15 min. Fluoroscent microscope-guided imaging was undertaken.

Sphere Formation Assay

A total of 3×10^3 cancer cells were plated in ultra-low-attachment 6-well culture plates (Corning, United States) containing DMEM/F-12 (Gibco, United States) supplemented with B-27 supplement (Gibco, United States), 20 ng/ml human EGF (PeproTech, Israel), and 20 ng/ml human FGF (PeproTech, Israel). After 10 to 14 days of incubation at 37°C, the tumor stem spheres were imaged and the number of spheres $\geq$50 μm was counted under a light microscope.

Flow Cytometry Analysis

The concentration of cancer cells was adjusted to 1×10^6/ml. The cells were washed three times with ice-cold PBS and incubated with FITC-labeled mouse anti-human CD44 antibody (BD Biosciences, 560977) for 30 min in the dark and then analyzed using a flow cytometer instrument (BD Biosciences).

In vivo Studies

All mice used in studies were BALB/c nude mice (4–5 weeks old, female) purchased from Vital River Laboratory (Beijing, China), were maintained under a constant temperature and humidity under pathogen-free conditions with a 12-h light–dark cycle, and received free access to food and water. For the xenograft mouse model, HCT116 cells transfected with ENC1 shRNA-1 and Ctrl-shRNA (5×10^6, suspended in 100 μl of PBS) were inoculated into the left dorsal flank of mice that randomized into two groups ($n = 6$). The tumor volumes were measured using calipers every 4 days and calculated using the equation: (length $\times$ width^2)/2. After the last measurement of tumor volume, the mice were humanely sacrificed by carbon dioxide asphyxiation, cervical dislocation was performed subsequently to ensure death, then tumor tissues were removed and used for subsequent assays.

For the lung metastasis mouse model, mice (2 mice/group) were given intravenous tail vein injections of 5×10^6 HCT116 cells (ENC1 shRNA-1, Ctrl-shRNA). About 10 weeks later, the mice were euthanized (the method was administered as above), and lungs were harvested and imaged. The lung tissue was collected in paraformaldehyde for further H&E staining and IHC analysis. All animal studies were taken at the animal laboratory of the Second Affiliated Hospital of Harbin Medical University and approved by the Ethics Committee for Animal Experimentation of Harbin Medical University.

Statistical Analysis

All data from at least three independent experiments were presented as the mean ± SD. GraphPad Prism 7.0 statistical software (GraphPad, San Diego, CA, United States) and SigmaPlot 14.0 (Systat Software, San Jose, CA, United States) were used for the two-tailed Student's *t*-test, Wilcoxon matched-pair test, analysis of variance (ANOVA), Tukey's post test, and chi-square test, when appropriate. The Kaplan–Meier method was used to draw survival curves, and the log-rank was performed for statistical analysis. Univariate and multivariate survival analyses were conducted using a Cox proportional hazard regression model. Values of $P < 0.05$ were considered statistically significant (*), $P < 0.01$ was considered more statistically significant (**), and $P < 0.001$ was considered the most statistically significant (***).

RESULTS

High ENC1 Expression in CRC Correlates With Poor Prognosis

To investigate the relationship between ENC1 expression and clinical significance in CRC, we first utilized data mining from public databases to analyze the ENC1 expression status. Based on the Oncomine database, the result showed significantly increased ENC1 mRNA expression patterns in 21 CRC datasets (**Figure 1A**). Following which, differential expression of ENC1 between CRC and normal colon tissues was analyzed through published files. We downloaded the gene expression profile data of CRC from TCGA which contains 469 CRC tissues and 41 adjacent normal colon tissues. Heat map and Violin plot exhibited the ENC1 expression which was markedly upregulated in CRC contrasted with normal colon tissues (**Figures 1B,C**). Meanwhile, data from GEPIA corroborated with those from the TCGA cohort substantiating enhanced ENC1 expression in CRC tissues ($n = 275$) in comparison to normal tissues ($n = 41$) (**Figure 1D**).

To further confirm the results from computation analysis, we examined the mRNA expression levels of ENC1 in 24 paired CRC patients using qRT-PCR. We found that ENC1 was significantly overexpressed in 20/24 (83.3%) of CRC samples (**Figures 1E,F**). Moreover, the increased ENC1 protein expression was detected in 12 pairs of CRCs compared with normal tissues by Western blotting (**Figure 1G**). Based on CRC TMAs, 100 CRC patients were tested by IHC. **Figure 1H** shows representative ENC1 images of immunostaining from patients in different clinical stages. Cytoplasmic ENC1 immunoreactivity was higher in tumors than in matched adjacent normal tissues. Additionally, box plots illustrated that the IHC score of ENC1 was upregulated in CRC samples. Findings from our cohort were identical to findings from other public databases.

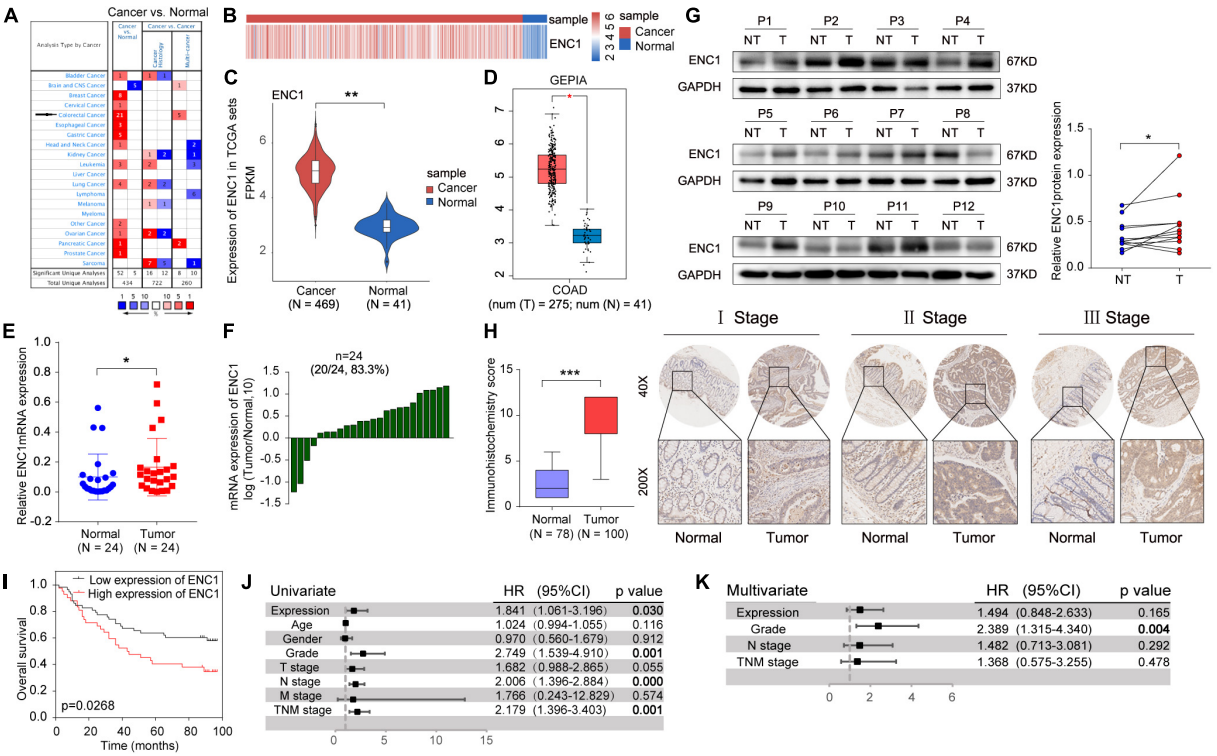

FIGURE 1 | ENC1 expression is often upregulated in CRC and associated with poor clinical outcomes. **(A)** The ENC1 mRNA expression levels in CRC and other cancers from the Oncomine cohort. The threshold was selected with the following parameters: p-value of 1E-4, fold change of 2, and gene rank of top 10%. **(B,C)** Heat map and Violin plot presented the upregulated expression of ENC1 between CRC (n = 469) and normal colon tissues (n = 41) by bioinformatics analysis from TCGA. Unpaired t-test, ** $P < 0.01$. **(D)** ENC1 expression was overexpressed in CRC (n = 275) compared with normal colon tissues (n = 41) by box plot in the GEPIA database. *$P < 0.05$. **(E)** The ENC1 mRNA expression in 24 paired CRC patients quantified from qRT-PCR. Wilcoxon matched-pair test, *$P < 0.05$. **(F)** Log10-fold change was used to show the differential mRNA expression of ENC1 between CRC and normal tissues. **(G)** The ENC1 protein expression was detected by Western blotting in 12 pairs of CRC tissues (T) and adjacent normal tissues (NT). The scatter plot revealed the relevant density of ENC1 protein expression. **(H)** IHC analysis of ENC1 expression in CRC TMAs. Representative stage images were shown (upper: magnification × 40, scale bar = 500 μm; lower: magnification × 200, scale bar = 100 μm). Box plot described the IHC score of ENC1 in 100 CRC tissues (IHC score: 9.17 ± 2.719) and 78 matched peritumoral tissues (IHC score: 2.397 ± 1.59). Mean ± SD, unpaired t-test, ***$P < 0.001$. **(I)** Kaplan–Meier's overall survival curve showed that the patients with a higher expression level of ENC1 have a shorter survival period. **(J)** Univariate and **(K)** multivariate Cox proportional hazard analyses were conducted to evaluate the HR of ENC1 for overall survival in CRC.

The relationship between ENC1 expression and clinicopathologic characteristics was also explored. The clinicopathological features in 100 CRC patients with informative IHC data are categorized in **Table 1**, including age, gender, grade, T stage, N stage, M stage, and TNM stage. Based on the staining score, the results revealed that higher ENC1 expression was positively associated with T stage (P = 0.020). Additionally, Kaplan–Meier's overall survival analysis described that the patients with higher ENC1 expression level associated with poorer survival in CRC (p = 0.0268; **Figure 1I**). Furthermore, univariate COX proportional hazard analysis demonstrated that high levels of ENC1, Grade, N stage, and TNM stage were significantly associated with worse survival of CRC patients (**Figure 1J**). Multivariate Cox proportional hazard analysis indicated that Grade (P = 0.004) was an independent prognostic factor for poor survival of CRC patients (**Figure 1K**). By univariate Cox model analysis, we found that the increased level of ENC1 in CRC was a risk factor of prognosis, but further multivariate analysis implicated that this risk factor bore statistical significance. The above findings are suggestive that ENC1 is upregulated and may serve as a considerable prognostic indicator for CRC patients.

ENC1 Overexpression or Knockdown Affects Cell Proliferation, Migration, and Invasion of CRC *in vitro*

To excavate the underlying biological behaviors of ENC1 in CRC, we evaluated endogenous ENC1 expression levels in seven CRC cell lines (HT29, LOVO, DLD-1, SW620, HCT116, SW480, and RKO) compared with the human normal colonic epithelial cell line (NCM460) by western blotting and qRT-PCR. The protein and mRNA expression patterns of ENC1 were significantly higher in five CRC cell lines (HT29, LOVO, DLD-1, HCT116, and SW480) than normal (**Figures 2A,B**). HT29/HCT116 was selected for both gain of function and loss of function simultaneously in subsequent experiments because of their moderate levels of expression.

TABLE 1 | Correlation between ENC1 expression and clinicopathological features in 100 CRC patients.

	Variables	ENC1 expression		Total	χ^2	*p* value
		Low	High			
Age (year)					0.134	0.714
	≤65	27	18	45		
	>65	31	24	55		
Gender					0.164	0.685
	Female	28	22	50		
	Male	30	20	50		
Grade					1.588	0.208
	I/II	51	33	84		
	III/IV	7	9	16		
T stage					5.429	**0.020**
	T1/T2/T3	51	29	80		
	T4	7	13	20		
N stage					0.066	0.797
	N0	36	25	61		
	N1/N2	22	17	39		
M stage					1.395	0.238
	M0	58	41	99		
	M1	0	1	1		
TNM stage					0.066	0.797
	I/II	36	25	61		
	III/IV	22	17	39		

The bold value is statistically significant ($p < 0.05$).

Furthermore, we identified functions between low and high ENC1 expressions on TCGA by GSEA, and GO-REGULATION-OF-DENDRITIC-CELL-DIFFERENTIATION (cell differentiation) was enriched in the ENC1 high group (**Supplementary Figure 1A**; $P = 0.06679$). Although the result was not statistically significant, it is deemed to represent a trend. Next, to verify this hypothesis, we performed a series of experiments to evaluate whether the suggested signatures may be involved *in vitro*. We ectopically overexpressed ENC1 to gain of function and used two ENC1-targeting shRNAs (shRNA1 and shRNA2) to loss of function in HT29/HCT116 cells. ENC1 protein expression levels were significantly increased in ENC1 overexpression and decreased in ENC1 knockdown CRC cells as assessed by Western blotting (**Figures 2C,D** and **Supplementary Figures 1B,C**). CCK-8 and colony formation assays revealed that overexpression of ENC1 significantly accelerated the CRC cell proliferation (**Figure 2E**) and colony formation ability (**Figure 2G**). In contrast, after the silencing of ENC1, growth, and colony formation numbers of cells were attenuated (**Figures 2F,H**). Furthermore, we investigated the impact of ENC1 on cell migratory and invasive properties in HT29/HCT116. Wound-healing assay reflected that overexpression of ENC1 resulted in faster closing of scratch wounds whereas ENC1 depletion resulted in delayed wound closure (**Figures 2I,J**). As shown in **Figure 2K**, migration and invasion abilities were also confirmed through migration and Matrigel invasion assays in an ENC1-overexpressing cell population. Contrarily reduced cell motility and invasive capability were observed in the ENC1-silenced cell type (**Figure 2L**). The results from these analyses illustrated that ENC1 modulates CRC cell tumorigenesis and progression *in vitro*.

ENC1 Accelerates the EMT Process and Maintains Stemness Phenotypes of CRC

Deciphered using the framework developed previously, it has been widely known that EMT and cancer stemness are closely related to the tumor progression and metastasis in various types of cancer cells (Pang et al., 2017; Matsuyama et al., 2019; Park et al., 2019a; Wu et al., 2020). Thus, we speculated that ENC1 might be involved in the EMT process and stemness in CRC cells. To evidence our speculation, immunofluorescence staining, sphere formation assay, and flow cytometry analysis of CD44, well-known EMT, and stemness-related markers by Western blotting were further determined. First, the overexpression or knockdown efficiency of ENC1 in HT29/HCT116 cells was validated by qRT-PCR (**Figures 3A,B**). Next, to confirm EMT, immunofluorescence staining assay reflected that ENC1 overexpression induced a weaker E-cadherin (epithelial marker) and stronger Vimentin (mesenchymal marker) expression in HT29 cells (**Figure 3C**), while ENC1 silencing reversed the phenotype (**Figure 3D**). The changes of representative EMT markers (E-cadherin, N-cadherin, Vimentin, and Snail) were verified through western blotting subsequently. As illustrated in **Figure 3E**, overexpression of ENC1 led to increased levels of N-cadherin, Vimentin, and Snail but lessened the levels of E-cadherin in HT29/HCT116. Expectedly, the observations were reversed upon ENC1 silencing (**Figure 3F**).

To confirm the impact on stemness of HT29/HCT116 cells, we examined tumor sphere-forming ability that directly correlated with cancer stemness. More and larger spheres formed in ENC1-overexpressed cells (**Figure 3G**), while fewer and less spheres were seen in ENC1-silenced cells (**Figure 3H**) compared with controls in CRC. We also assessed the cell surface marker CD44 expression levels using flow cytometry. As shown in **Figure 3I**, the ectopic expression of ENC1 upregulated the proportion of CD-44-positive cells in HT29/HCT116. Finally, we assessed the effect of ENC1 on sentinel markers associated with stemness, including CD44, CD133, and SOX2 in CRC cells by western blotting. We observed conspicuous increased protein levels of CD44, CD133, and SOX2 by ENC1 overexpression (**Figure 3J**) and declined protein level by ENC1 knockdown (**Figure 3K**). Taken together, data implicated that there is a positive correlation and regulation of ENC1 in EMT progress and maintenance of stemness.

ENC1 Knockdown Eliminates Xenograft Tumor Growth and Lung Metastasis *in vivo*

In addition to validate above findings *in vivo*, we constructed mouse xenograft and lung metastasis models. The mouse xenograft model was established to prove whether silenced ENC1 could retard tumor growth *in vivo*. After subcutaneous injection with HCT116-ENC1 shRNA-1 and HCT116-Ctrl-shRNA into

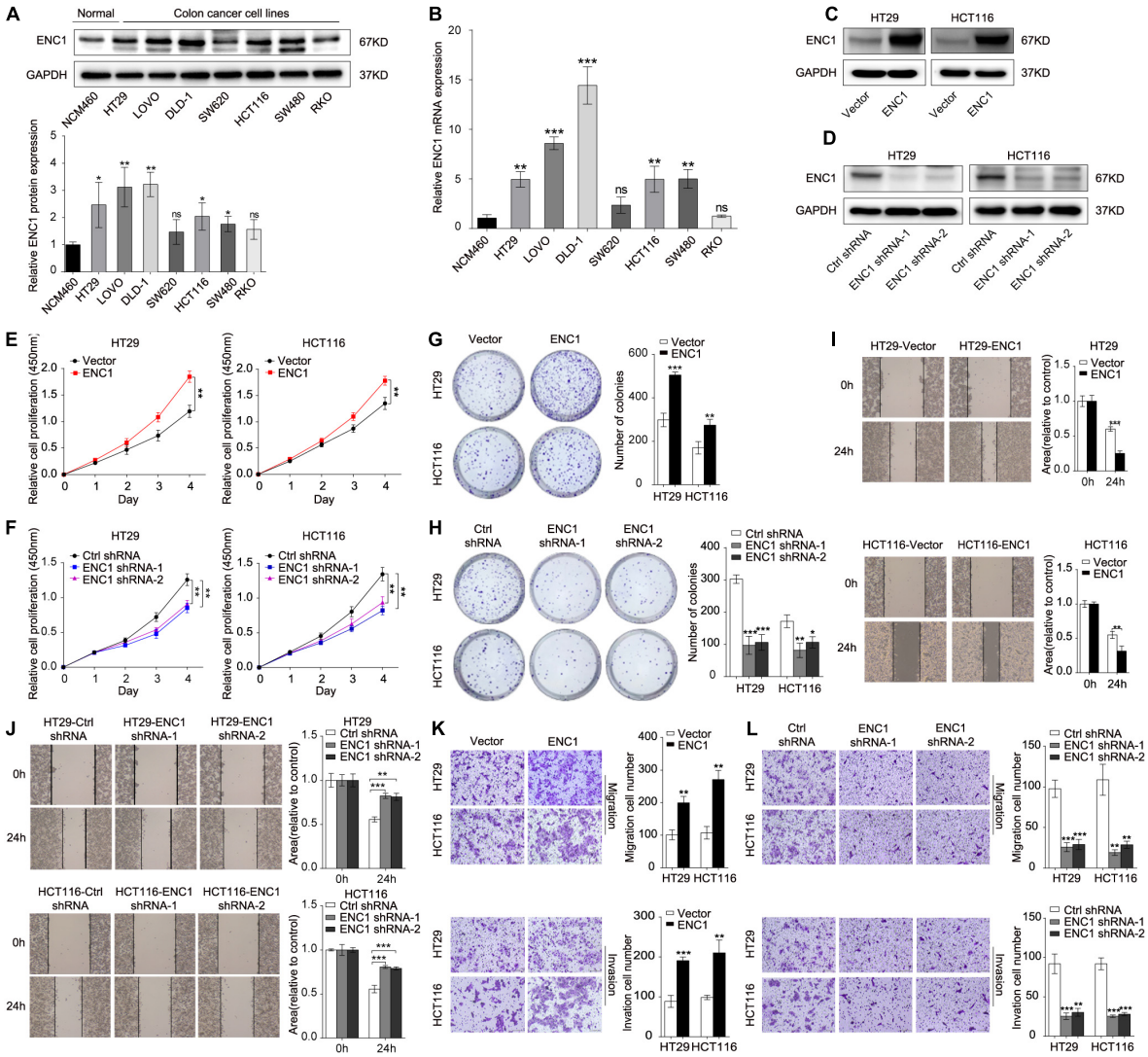

FIGURE 2 | ENC1 regulates proliferation, migration, and invasion of CRC cells. **(A)** Endogenous ENC1 protein expression status was tested in human normal colonic epithelial cells (NCM460) and CRC cells (HT29, LOVO, DLD-1, SW620, HCT116, SW480, and RKO) by Western blotting. **(B)** Endogenous ENC1 mRNA expression status was compared between NCM460 and CRC cells by qRT-PCR. Western blot analysis of ENC1 protein expression levels in ENC1 overexpression **(C)** and ENC1 knockdown **(D)** CRC cells HT29/HCT116. **(E,F)** CCK-8 and **(G,H)** colony formation assays were performed to assess cell proliferation in CRC cells with ENC1 overexpression or knockdown. Wound-healing assay was used to detect cell migration ability in ENC1 overexpression **(I)** and ENC1 knockdown **(J)** CRC cells. Transwell assays showed the effect of ENC1 overexpression **(K)** and ENC1 knockdown **(L)** on CRC cell migration and invasion (left: representative images; right: quantitative analyses). Results are presented as the mean ± SD of three independent experiments. $^{*}P < 0.05$, $^{**}P < 0.01$, and $^{***}P < 0.001$.

the left dorsal flank of nude mice, tumor volume was monitored by a caliper for 6 weeks. When the mouse tumor size in the ENC1 shRNA-1 group was significantly less than the Ctrl-shRNA group, xenograft tumors were isolated and imaged (**Figure 4A**). The changes in tumor growth were plotted on a tumor growth curve which showed that mouse tumor size decreased in the ENC1 shRNA-1 group (**Figure 4B**). Additionally, H&E staining results identified tumor morphological characteristics and IHC showed reduced the expression of ENC-1 and Ki-67 in the Ctrl-shRNA group in comparison to xenograft tumor groups (**Figure 4C**). Western blotting (**Figure 4D**) and qRT-PCR (**Figure 4E**) verified ENC1 protein and mRNA expression being downregulated in the ENC1 shRNA-1 xenograft tumor group.

In order to verify whether tumors of lung metastasis were restricted by ENC1 shRNA-1 *in vivo*, mice were given intravenous tail vein injections of HCT116-ENC1 shRNA-1 and HCT116-Ctrl-shRNA, respectively. Ten weeks after injection, the mice were sacrificed and lungs were imaged. As represented in **Figure 4F**, the mice injected with HCT116-ENC1 shRNA-1 cells formed fewer nodules on the lung surfaces than mice injected with HCT116-Ctrl-shRNA cells. Metastatic nodules on the surfaces of mice lungs were confirmed by H&E staining, whereas the expression level of ENC1 in the nodules was

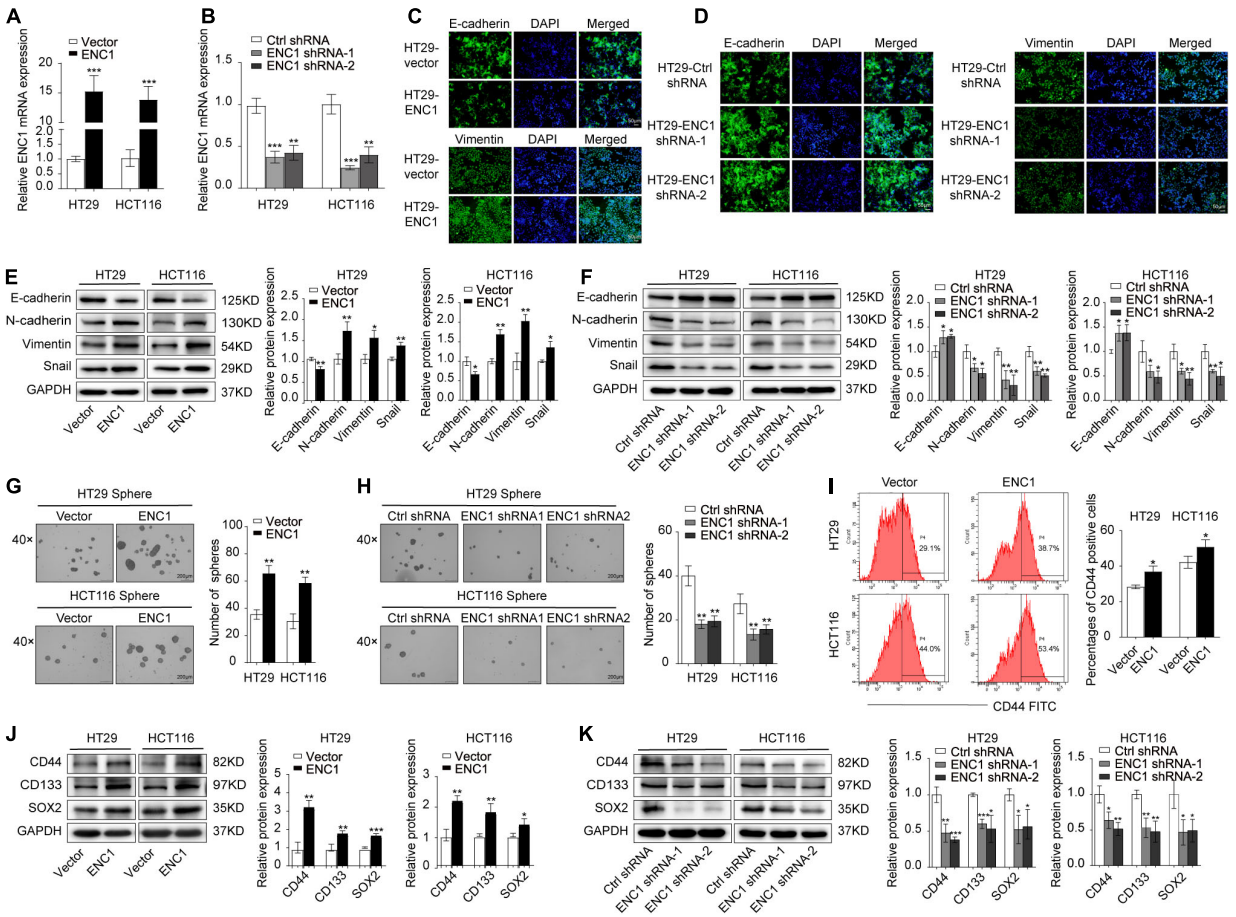

FIGURE 3 | ENC1 overexpression induces EMT and maintains stemness of CRC. **(A,B)** The ENC1 overexpression or knockdown efficiency was assessed in ENC1-overexpression and ENC1-knockdown HT29/HCT116 cells by qRT-PCR. **(C,D)** Immunofluorescence staining of E-cadherin and Vimentin expression in overexpressed or silenced HT29 (magnification × 20, scale bar = 50 μm), and the cell nuclei were stained with DAPI in blue. **(E,F)** EMT markers of E-cadherin, N-cadherin, Vimentin, and Snail protein expression levels in ENC1-overexpression and ENC1-knockdown CRC cells were detected by Western blotting. Representative images of sphere formation and sphere number analysis were displayed (magnification × 40, scale bar = 200 μm) in HT29/HCT116 after ENC1 overexpression **(G)** and ENC1 knockdown **(H)**. **(I)** Flow cytometry analysis of CD44-positive cells in the indicated groups of cells. **(J,K)** Western blotting analysis of stemness markers (CD44, CD133, and SOX2) expression in ENC1-overexpression and ENC1-knockdown CRC cells. Results are presented as the mean ± SD of three independent experiments. $^{*}P < 0.05$, $^{**}P < 0.01$, and $^{***}P < 0.001$.

also verified by IHC staining (**Figure 4G**), thus concluding that ENC1 knockdown restrains xenograft tumor growth and lung metastasis.

ENC1 Modulates the JAK2/STAT5/AKT Axis in CRC

To dissect the potential molecular mechanisms mediated by ENC1 in CRC tumorigenesis and progression, we performed GSEA for pathway enrichment in the TCGA CRC database to identify biological pathways between low and high ENC1 expressions. **Figure 5A** shows the most significantly and positively enriched pathways of the top five with a high ENC1 expression phenotype, and the STAT5-related pathway (PID_IL2_STAT5_PATHWAY) indicated the most meaningful association with ENC1 (ES = 0.686374, NES = 1.536346, $P = 0.025794$) (**Figure 5B**). As has been previously established, abnormal activation of JAK2/STAT5 signaling led to cell proliferation, differentiation, and other biological processes in human cancers (Gu et al., 2013; Jiang et al., 2019; Wang et al., 2020). Thus, we focused to assess the effects of ENC1 on JAK2/STAT5 signaling. Aiming to confirm the functional gene signatures, we detected the effects of ENC1 on the protein levels of JAK2/STAT5 signaling target genes by Western blotting. We found that the phosphorylation levels of JAK2, STAT5, and AKT increased in ENC1-overexpressed CRC cells (**Figure 5C**) but decreased in ENC1-silenced CRC cells (**Figure 5D**). However, no considerable changes were observed in total JAK2, STAT5, and AKT protein levels from different panels (**Figures 5C,D**).

Ruxolitinib is a selective JAK1 and JAK2 inhibitor that targets JAK/STAT-associated signaling, exhibiting an effective clinical treatment of myelofibrosis adopted by FDA (Chang et al., 2019), which was used to confirm the effect of ENC1 on activation of the JAK2/STAT5/AKT axis in CRC cells. HT29/HCT116 cells after

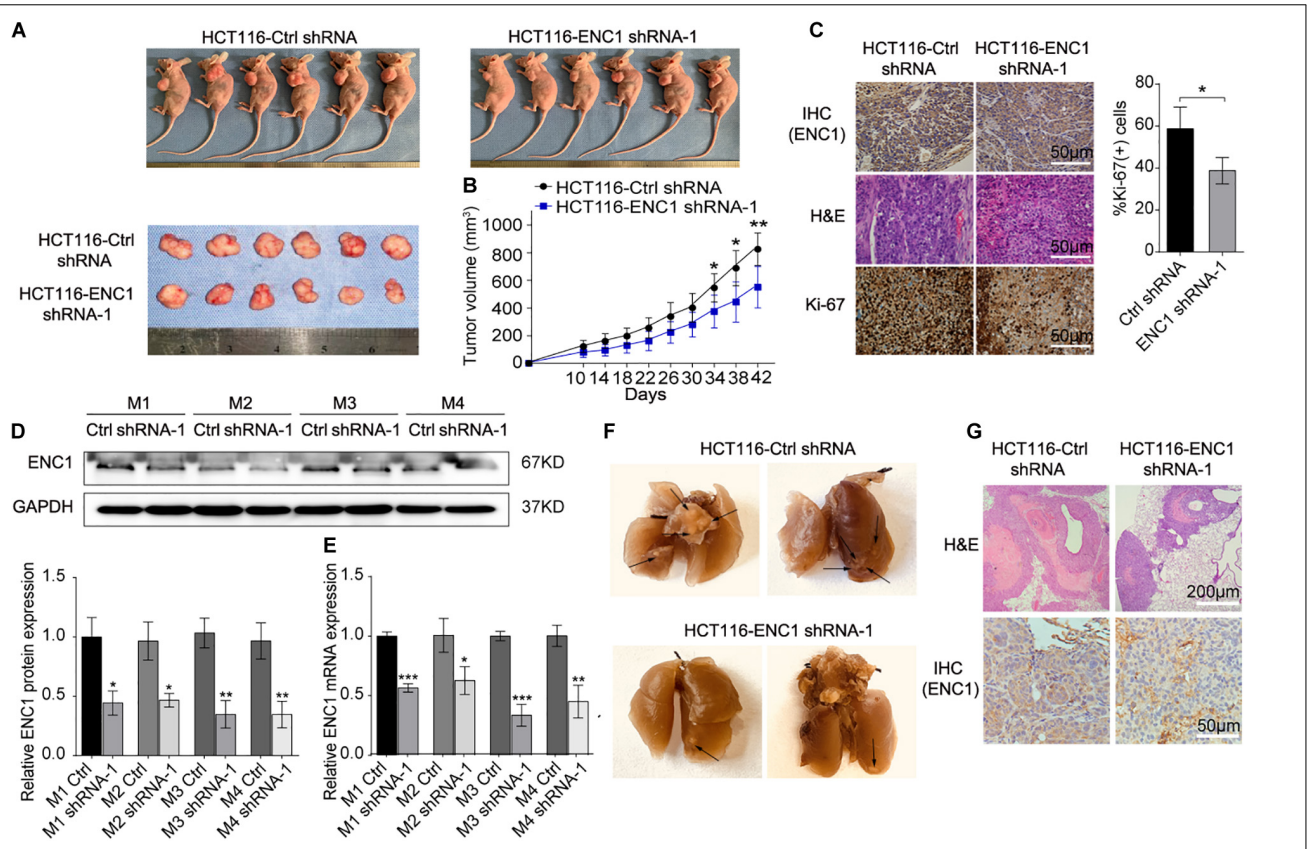

FIGURE 4 | *In vivo*, downregulation of ENC1 inhibits xenograft tumor growth and lung metastasis. **(A)** Images of xenograft tumors from six BALB/c nude mice at 42 days after subcutaneously inoculated with HCT116-Ctrl shRNA and HCT116-ENC1 shRNA-1 cells. **(B)** The growth of xenograft tumors was measured by tumor volume every 4 days and tumor growth curves were plotted between the comparison in two groups ($n = 6$). **(C)** Representative images of IHC and H&E staining show that ENC1 silencing downregulated the expression of ENC1 and Ki-67 in xenograft tumors (magnification × 400, scale bar = 50 μm). The protein and mRNA levels of ENC1 were also analyzed in xenograft tumor tissues by Western blotting **(D)** and qRT-PCR **(E)**, respectively. **(F)** Representative images of metastatic lungs in the HCT116-Ctrl shRNA (left) group and HCT116-ENC1 shRNA-1 (right) group. Black arrows indicated the metastatic pulmonary nodules. **(G)** H&E staining (upper panel: magnification × 100, scale bar = 200 μm) and IHC staining with ENC1 (lower panel: magnification × 400, scale bar = 50 μm) were performed on section of metastatic pulmonary nodules. Results are presented as the mean ± SD of three independent experiments. Student's *t* test was applied for statistical analysis in two-group comparison: $^{*}P < 0.05$, $^{**}P < 0.01$, and $^{***}P < 0.001$.

transfection with ENC1 and empty vector were treated with a concentration of 25 μM ruxolitinib for 24 h which prevented the release of activated JAK2. Predictably, the upregulated expression levels of phosphorylated JAK2, STAT5, and AKT induced by ENC1 overexpression effectively reversed with ruxolitinib treatment. However, ruxolitinib suppressed ENC1-induced JAK2 release and STAT5 and AKT expression but did not affect ENC1 expression and total JAK2, STAT5, and AKT protein levels in HT29/HCT116 cells (**Figure 5E**). We thus present the significance of ENC1 in activating the JAK2/STAT5/AKT axis.

ENC1 Promotes CRC Cell Tumorigenesis, Progression, EMT, and Stemness Through Activating the JAK2/STAT5/AKT Axis

To further clarify the oncogenic effects of ENC1 on JAK2/STAT5/AKT axis activation in tumorigenesis and metastasis properties of CRC, CCK-8, and colony formation assays were first examined to assess the cell proliferation with or without ruxolitinib treatment. As shown in **Figures 6A,B**, ruxolitinib treatment weakened the proliferation and colony formation ability of ENC1-overexpressed CRC cells and less inhibition were observed in cells without ectopic expression. Transwell assays revealed that the enhanced effects of ENC1 on HT29/HCT116 cell motility and invasiveness capability were also alleviated with ruxolitinib treatment (**Figure 6C**).

Additionally, we assessed the role of the ENC1-activated JAK2/STAT5/AKT axis in EMT and stemness. Sphere formation assay was undertaken, and EMT and stemness-related markers were assessed by Western blotting. Notably, ruxolitinib could restrict tumor-sphere formation caused by ENC1 overexpression (**Figure 6E**). EMT markers (E-cadherin, N-cadherin, Vimentin, and Snail) along with stemness markers (CD44, CD133, and SOX2) were significantly less pronounced, indicating that ruxolitinib mediated the disruption of ENC1 effects in CRC cells (**Figures 6D,F**). Briefly, blockage of JAK2/STAT5 signaling could effectively prevent

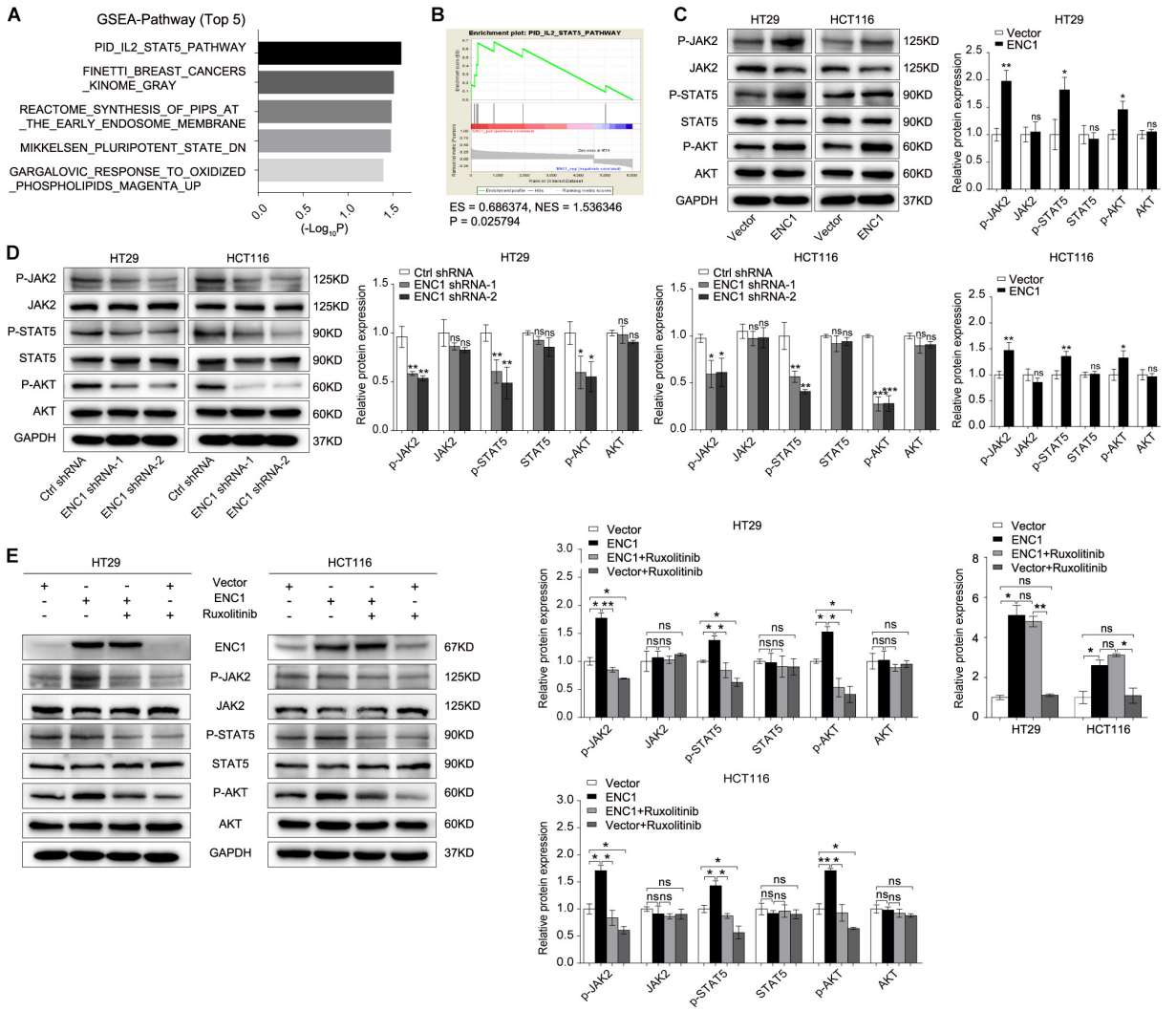

FIGURE 5 | ENC1 activates JAK2/STAT5/AKT signaling in CRC. **(A)** Top five significantly and positively enriched pathways with high ENC1 expression by GSEA. **(B)** ENC1 expression positively correlated with STAT5-activated gene signatures (PID_IL2_STAT5_PATHWAY). **(C,D)** Western blotting analysis of JAK2/STAT5 signaling key members (p-JAK2, p-STAT5, p-AKT, JAK2, STAT5, and AKT) in HT29/HCT116 after ENC1 overexpression and ENC1 knockdown. **(E)** ENC1-overexpressed HT29/HCT116 were treated with JAK1/2 inhibitor ruxolitinib. After being treated for 24 h, as indicated, p-JAK2, p-STAT5, p-AKT, JAK2, STAT5, and AKT expression levels were detected by western blotting. Results are presented as the mean ± SD of three independent experiments. $^{*}P < 0.05$, $^{**}P < 0.01$, and $^{***}P < 0.001$.

CRC cell tumorigenesis, progression, EMT, and stemness mediated by ENC1.

DISCUSSION

Western lifestyles and diet have been identified as substantial risks to the development and progression of colorectal cancer (CRC), the burden of which is faced most by low- and middle-income countries. The global estimates for cancers worldwide report an increasing trend of both incidence and mortality in countries of the Baltic, Russia, and China (Bray et al., 2018). While early and more effective screening is helpful in reducing the burden of CRC, early onset of the disease and changing molecular paradigms present a challenge to diagnosis and existing successful therapies.

A common focus in cancer disease diagnosis is a search for robust molecular markers that would facilitate both diagnosis and prognosis. Similar approaches have been applied to CRC, and the utility of several genes and microRNAs with strong upregulation in CRC has been explored (Garcia-Bilbao et al., 2012; Pellino et al., 2018; Alves Martins et al., 2019). One such candidate gene with limited exploration in CRC biology is ENC1 (Garcia-Bilbao et al., 2012). ENC1 encodes for an actin-associated protein. The expression of ENC1 was found high during gastrulation in the neuroectodermal region of the epiblast and later in the nervous system. Normally, it has been ascribed to have roles in neuronal

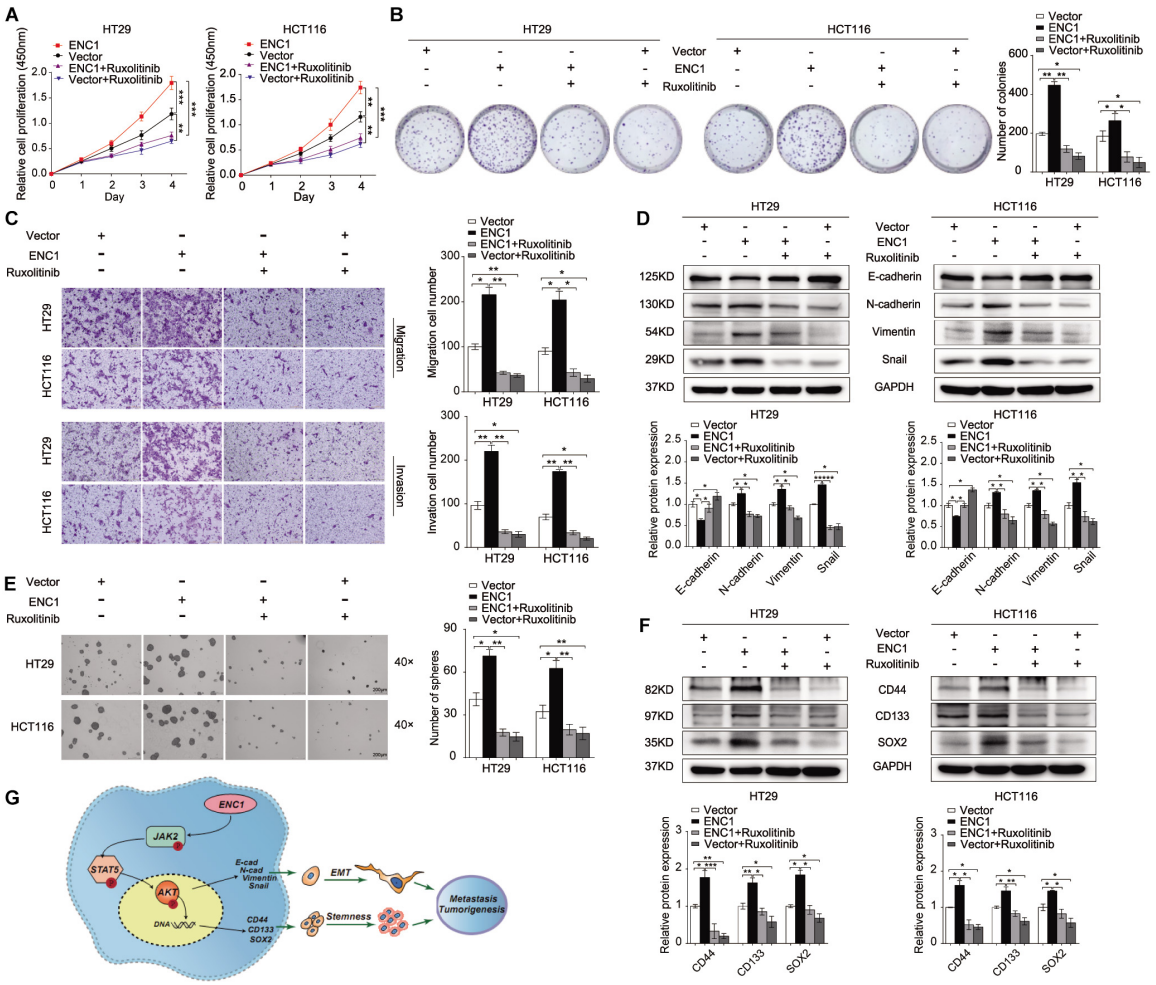

FIGURE 6 | ENC1 accelerates cell proliferation, migration, invasion, EMT, and stemness through activating JAK2/STAT5/AKT signaling in CRC. Cell proliferation was assessed by CCK8 assay **(A)** and colony formation assay **(B)** in ENC1-overexpression CRC cells treated with ruxolitinib. **(C)** Effects of ruxolitinib treatment on ENC1-overexpressed HT29/HCT116 cell motility and invasiveness capability were detected by Transwell assay. **(D)** Western blotting showed the protein changes of EMT markers between ENC1-overexpressed cells with and without ruxolitinib treatment. **(E)** Effect of ruxolitinib in tumor spheres caused by ENC1 overexpression in contrast with no treatment. **(F)** The expression of stemness markers (CD44, CD133, SOX2) were detected by Western blotting in ENC1-overexpressed CRC cells treated with ruxolitinib. **(G)** Schematic diagram of ENC1 promotes CRC tumorigenesis and metastasis via the JAK2/STAT5/AKT axis mediated EMT and stemness. Results are presented as the mean ± SD of three independent experiments. $^{*}P < 0.05$, $^{**}P < 0.01$, and $^{***}P < 0.001$.

and adipocyte differentiation; however, the aberrant expression of ENC1 has been reported in human brain tumors including glioblastoma and astrocytoma (Kim et al., 2000). Further, ENC1 dysregulation and associated malignancies have been confirmed in cancers of prostrate (Lapointe et al., 2004), ovarian (Fan et al., 2019), pancreatic (Ross et al., 2000), and colon (Fujita et al., 2001). While some studies have a cause–effect link, some identify the molecular mechanisms that drive the activation of ENC1 (Kim et al., 2000; Fujita et al., 2001). Very few studies identify the pathway downstream of ENC1 and its contribution to transformation. Our study is the preliminary demonstration of a detailed analysis of pathways downstream of ENC1 contributing to malignancy in a CRC model. The study is a triage presenting data from computational, *in vitro*, and *in vivo* experimental analyses. By a comparison of various databases, we compared the expression profile of ENC1 across CRC and normal patients. This computational analysis was validated with CRC tissues and normal adjacent samples using qRT-PCR and western blotting methods. We also investigated the correlation between ENC1 expression and clinical outcomes by IHC data, high expression of ENC1 related to advanced T stage, and unfavorable clinical outcomes in patients with CRC. The expression was further confirmed in CRC cell lines, and analysis is further carried out using HT29 and HCT 116 confirming the phenotypic malignancy traits of increased cell proliferation, migration, invasion, EMT, sphere formation, and stemness. ENC1 induced EMT, stemness, and other prognostic features described above, and its association with clinical prognosis, to the best of our knowledge, has not been discussed previously. Thus, the study is a significant advancement contributing to the advancement of understanding of CRC

at a molecular level and utilizing the phenotypic changes for prognostic implications.

Further, we hypothesized that these individual phenotypic traits may have a common master regulator activated by ENC1, which in turn would regulate the multiple pathways at transcriptional and translational levels. The role of the JAK-STAT pathway in EMT and stemness has been discussed (Jin, 2020). For instance, single-cell cultures of cells derived from myxoid liposarcoma expressed different amounts of canonical JAK-STAT transcripts (Dolatabadi et al., 2019). Similar studies exploring the roles of JAK-STAT signaling and induction of EMT and cancer stemness have been demonstrated for hematopoietic cancers (Wingelhofer et al., 2018), oral squamous cell carcinoma (Chen et al., 2020), and colon cancers (Park et al., 2019b), among others. The role of EMT effectors (Snail, Slug among others) on EMT core regulators (Vimentin, E-cadherin, and N-cadherin) through modulation of various signaling pathways and epigenetic regulation of EMT effectors has been discussed previously (Vu and Datta, 2017; Huang et al., 2020). However, the role of ENC1 as a modulator of EMT effectors and stemness via the JAK-STAT pathway has not been reported previously.

Our GSEA analysis on the TCGA database indicated that a high expression of ENC1 was associated with the JAK2-STAT5-AKT axis, thereby supporting our hypothesis. While, the expression of ENC1 positively correlated with JAK2-STAT5 and AKT, the activation of JAK2 via STAT5 remains elusive. Since JAK2 activation can result from ligation of several homo- and hetero-dimeric pairs of signaling receptors, belonging to class I and II cytokine receptor families, we thus propose two alternative mechanisms of activation of JAK 2 in CRC via the ENC1 pathway. (1) ENC1 is an actin-binding protein like Src homology 2 (SH2) domain-containing adapter protein SH2B1β which is known to bind to JAK2 and potentiate its activation in response to other proteins such as growth hormone or leptin (Rider and Diakonova, 2011). (2) Evidence has also been mounting for several non-canonical methods of JAK activation wherein a subset of receptors exists in a pre-dimerized state and conformational shifts in the transmembrane domain result in JAK activation (Ferrao et al., 2018). It is also likely that ENC1 through alternative pathways leads to activation of cytokines and/or growth hormones which canonically activate the JAK-STAT pathway. However, the hypothesis tests bearing.

In conclusion, our study is the first report demonstrating the downstream ENC1-JAK2-STAT5-AKT axis and its implications on CRC progression and metastasis. It is also a demonstration of how ENC1 activation may not only contribute to the adenomatous carcinoma and the immunological pathway through the JAK-STAT pathway. The study is a novel proposition with silencing of ENC1, not only significantly reducing the malignant phenotype but also showing a therapeutic reduction in tumor numbers and volumes *in vivo*.

The utility of ENC1 as a diagnostic, prognostic, or even plausible therapeutic target is proposed. A complete understanding of the suitability and feasibility of the proposed work may benefit resource strengthening and allocation at a global scale.

DATA AVAILABILITY STATEMENT

The datasets presented in this study can be found in online repositories. The names of the repository/repositories and accession number(s) can be found in the article/ **Supplementary Material**.

ETHICS STATEMENT

The studies involving human participants were reviewed and approved by Committees for the Institutional Review Board of Harbin Medical University, China. The patients/participants provided their written informed consent to participate in this study. The animal study was reviewed and approved by Committees for the Institutional Review Board of Harbin Medical University, China. Written informed consent was obtained from the owners for the participation of their animals in this study.

AUTHOR CONTRIBUTIONS

YC conceived and performed the experiments, analyzed the data, and wrote the manuscript. JY and YB carried out the experiments and analyzed the data. QL, FW, and JZ were involved in the implementation of the study. YZ and YY guided the study and corrected the manuscript. CL participated in the project guidance. All authors contributed to the article and approved the submitted version.

FUNDING

This work was supported by the National Natural Science Foundation of China (NSFC) (Grant Nos. 81672428, 81872427, and 81703000), Applied Technology Research and Development Program of Heilongjiang Province (No. GA19C002), NN10 Excellent Discipline Construction Program (No. Hepatobiliary and Pancreatic Tumor 2017), and Fundamental Research Funds for the Provincial Universities of Heilongjiang Province.

ACKNOWLEDGMENTS

YC would particularly like to thank her great mentors YZ, her coworkers, and her family members for their support and understanding. YC would also like to thank her friends Prof. Haihai Liang, Xinlei Li, Shangwei Ning, Tong Li, Qin Wang, Lu Zhang, and Xiuxiu Wang for their help during the experiments.

SUPPLEMENTARY MATERIAL

The Supplementary Material for this article can be found online at: https://www.frontiersin.org/articles/10.3389/fcell.2021.616887/full#supplementary-material

REFERENCES

Alves Martins, B. A., de Bulhoes, G. F., Cavalcanti, I. N., Martins, M. M., de Oliveira, P. G., and Martins, A. M. A. (2019). Biomarkers in colorectal cancer: the role of translational proteomics research. *Front. Oncol.* 9: 1284. doi: 10.3389/fonc.2019.01284

Bray, F., Ferlay, J., Soerjomataram, I., Siegel, R. L., Torre, L. A., and Jemal, A. (2018). Global cancer statistics 2018: GLOBOCAN estimates of incidence and mortality worldwide for 36 cancers in 185 countries. *CA Cancer J. Clin.* 68, 394–424. doi: 10.3322/caac.21492

Chang, W.-M., Chang, Y.-C., Yang, Y.-C., Lin, S.-K., Chang, P. M.-H., and Hsiao, M. (2019). AKR1C1 controls cisplatin-resistance in head and neck squamous cell carcinoma through cross-talk with the STAT1/3 signaling pathway. *J. Exp. Clin. Cancer Res.* 38:245. doi: 10.1186/s13046-019-1256-2

Chen, Y., Shao, Z., Jiang, E., Zhou, X., Wang, L., Wang, H., et al. (2020). CCL21/CCR7 interaction promotes EMT and enhances the stemness of OSCC via a JAK2/STAT3 sig naling pathway. *J. Cell Physiol.* 235, 5995–6009. doi: 10.1002/jcp.29525

Colorectal Cancer Collaborators (CRC) (2019). The global, regional, and national burden of colorectal cancer and its attributable risk factors in 195 countries and territories, 1990-2017: a systematic analysis for the Global Burden of Disease Study 2017. *Lancet Gastroenterol. Hepatol.* 4, 913–933. doi: 10.1016/S2468-1253(19)30345-0

De Palma, F. D. E., D'Argenio, V., Pol, J., Kroemer, G., Maiuri, M. C., and Salvatore, F. (2019). The molecular hallmarks of the serrated pathway in colorectal cancer. *Cancers (Basel)* 11:1017. doi: 10.3390/cancers11071017

Dolatabadi, S., Jonasson, E., Linden, M., Fereydouni, B., Backsten, K., Nilsson, M., et al. (2019). JAK-STAT signalling controls cancer stem cell properties including chemotherapy resistance in myxoid liposarcoma. *Int. J. Cancer* 145, 435–449. doi: 10.1002/ijc.32123

Fan, S., Wang, Y., Sheng, N., Xie, Y., Lu, J., Zhang, Z., et al. (2019). Low expression of ENC1 predicts a favorable prognosis in patients with ovarian cancer. *J. Cell Biochem.* 120, 861–871. doi: 10.1002/jcb.27447

Ferrao, R. D., Wallweber, H. J., and Lupardus, P. J. (2018). Receptor-mediated dimerization of JAK2 FERM domains is required for JAK2 activation. *Elife* 7:e38089. doi: 10.7554/eLife.38089

Fujita, M., Furukawa, Y., Tsunoda, T., Tanaka, T., Ogawa, M., and Nakamura, Y. (2001). Up-regulation of the ectodermal-neural cortex 1 (ENC1) gene, a downstream target of the beta-catenin/T-cell factor complex, in colorectal carcinomas. *Cancer Res.* 61, 7722–7726.

Garcia-Bilbao, A., Armananzas, R., Ispizua, Z., Calvo, B., Alonso-Varona, A., Inza, I., et al. (2012). Identification of a biomarker panel for colorectal cancer diagnosis. *BMC Cancer* 12:43. doi: 10.1186/1471-2407-12-43

Gu, L., Liao, Z., Hoang, D. T., Dagvadorj, A., Gupta, S., Blackmon, S., et al. (2013). Pharmacologic inhibition of Jak2-Stat5 signaling By Jak2 inhibitor AZD1480 potently suppresses growth of both primary and castrate-resistant prostate cancer. *Clin. Cancer Res.* 19, 5658–5674. doi: 10.1158/1078-0432.CCR-13-0422

Hammarsund, M., Lerner, M., Zhu, C., Merup, M., Jansson, M., Gahrton, G., et al. (2004). Disruption of a novel ectodermal neural cortex 1 antisense gene, ENC-1AS and identification of ENC-1 overexpression in hairy cell leukemia. *Hum. Mol. Genet.* 13, 2925–2936. doi: 10.1093/hmg/ddh315

Hofseth, L. J., Hebert, J. R., Chanda, A., Chen, H., Love, B. L., Pena, M. M., et al. (2020). Early-onset colorectal cancer: initial clues and current views. *Nat. Rev. Gastroenterol. Hepatol.* 17, 352–364. doi: 10.1038/s41575-019-0253-4

Huang, K., Gao, N., Bian, D., Zhai, Q., Yang, P., Li, M., et al. (2020). Correlation between FAK and EGF-Induced EMT in Colorectal Cancer Cells. *J. Oncol.* 2020:5428920. doi: 10.1155/2020/5428920

Jiang, L., Zhao, X. H., Mao, Y. L., Wang, J. F., Zheng, H. J., and You, Q. S. (2019). Long non-coding RNA RP11-468E2.5 curtails colorectal cancer cell proliferation and stimulates apoptosis via the JAK/STAT signaling pathway by targeting STAT5 and STAT6. *J. Exp. Clin. Cancer Res.* 38:465. doi: 10.1186/s13046-019-1428-0

Jin, W. (2020). Role of JAK/STAT3 signaling in the regulation of metastasis, the transition of cancer stem cells, and chemoresistance of cancer by epithelial-mesenchymal transition. *Cells* 9:217. doi: 10.3390/cells9010217

Keum, N., and Giovannucci, E. (2019). Global burden of colorectal cancer: emerging trends, risk factors and prevention strategies. *Nat. Rev. Gastroenterol. Hepatol.* 16, 713–732. doi: 10.1038/s41575-019-0189-8

Kim, T. A., Ota, S., Jiang, S., Pasztor, L. M., White, R. A., and Avraham, S. (2000). Genomic organization, chromosomal localization and regulation of expression of the neuronal nuclear matrix protein NRP/B in human brain tumors. *Gene* 255, 105–116. doi: 10.1016/s0378-1119(00)00297-3

Koveitypour, Z., Panahi, F., Vakilian, M., Peymani, M., Seyed Forootan, F., Nasr Esfahani, M. H., et al. (2019). Signaling pathways involved in colorectal cancer progression. *Cell Biosci.* 9:97. doi: 10.1186/s13578-019-0361-4

Lapointe, J., Li, C., Higgins, J. P., van de Rijn, M., Bair, E., Montgomery, K., et al. (2004). Gene expression profiling identifies clinically relevant subtypes of prostate cancer. *Proc. Natl. Acad. Sci. U.S.A.* 101, 811–816. doi: 10.1073/pnas.0304146101

Long, A. G., Lundsmith, E. T., and Hamilton, K. E. (2017). Inflammation and colorectal cancer. *Curr. Colorectal. Cancer Rep.* 13, 341–351. doi: 10.1007/s11888-017-0373-6

Matsuyama, T., Ishikawa, T., Takahashi, N., Yamada, Y., Yasuno, M., Kawano, T., et al. (2019). Transcriptomic expression profiling identifies ITGBL1, an epithelial to mesenchymal transition (EMT)-associated gene, is a promising recurrence prediction biomarker in colorectal cancer. *Mol. Cancer* 18:19. doi: 10.1186/s12943-019-0945-y

Nguyen, H. T., and Duong, H. Q. (2018). The molecular characteristics of colorectal cancer: implications for diagnosis and therapy. *Oncol. Lett.* 16, 9–18. doi: 10.3892/ol.2018.8679

Pang, B., Wu, N., Guan, R., Pang, L., Li, X., Li, S., et al. (2017). Overexpression of RCC2 enhances cell motility and promotes tumor metastasis in lung adenocarcinoma by inducing epithelial-mesenchymal transition. *Clin. Cancer Res.* 23, 5598–5610. doi: 10.1158/1078-0432.CCR-16-2909

Park, S. Y., Kim, J. Y., Choi, J. H., Kim, J. H., Lee, C. J., Singh, P., et al. (2019a). Inhibition of LEF1-Mediated DCLK1 by niclosamide attenuates colorectal cancer stemness. *Clin. Cancer Res.* 25, 1415–1429. doi: 10.1158/1078-0432.CCR-18-1232

Park, S. Y., Lee, C. J., Choi, J. H., Kim, J. H., Kim, J. W., Kim, J. Y., et al. (2019b). The JAK2/STAT3/CCND2 Axis promotes colorectal cancer stem cell persistence and radioresistance. *J. Exp. Clin. Cancer Res.* 38:399. doi: 10.1186/s13046-019-1405-7

Pellino, G., Gallo, G., Pallante, P., Capasso, R., De Stefano, A., Maretto, I., et al. (2018). Noninvasive biomarkers of colorectal cancer: role in diagnosis and personalised treatment perspectives. *Gastroenterol. Res. Pract.* 2018:2397863. doi: 10.1155/2018/2397863

Rider, L., and Diakonova, M. (2011). Adapter protein SH2B1beta binds filamin A to regulate prolactin-dependent cytoskeletal reorganization and cell motility. *Mol. Endocrinol.* 25, 1231–1243. doi: 10.1210/me.2011-0056

Ross, D. T., Scherf, U., Eisen, M. B., Perou, C. M., Rees, C., Spellman, P., et al. (2000). Systematic variation in gene expression patterns in human cancer cell lines. *Nat. Genet.* 24, 227–235. doi: 10.1038/73432

The Lancet Gastroenterology Hepatology (2019). The shifting epidemiology of colorectal cancer. *Lancet Gastroenterol. Hepatol.* 4:489. doi: 10.1016/S2468-1253(19)30150-5

Uddin, M. N., Li, M., and Wang, X. (2019). Identification of transcriptional signatures of colon tumor stroma by a meta-analysis. *J. Oncol.* 2019:8752862. doi: 10.1155/2019/8752862

Vu, T., and Datta, P. K. (2017). Regulation of EMT in colorectal cancer: a culprit in metastasis. *Cancers (Basel)* 9:171. doi: 10.3390/cancers9120171

Wang, M., Chen, L., Chen, Y., Wei, R., Guo, Q., Zhu, S., et al. (2020). Intracellular matrix Gla protein promotes tumor progression by activating JAK2/STAT5 signaling in gastric cancer. *Mol. Oncol.* 14, 1045–1058. doi: 10.1002/1878-0261.12652

Wingelhofer, B., Neubauer, H. A., Valent, P., Han, X., Constantinescu, S. N., Gunning, P. T., et al. (2018). Implications of STAT3 and STAT5 signaling on gene regulation and chromatin remodeling in hematopoietic cancer. *Leukemia* 32, 1713–1726. doi: 10.1038/s41375-018-0117-x

Wu, C., Ding, H., Wang, S., Li, Y., Liu, S.-B., Wang, X., et al. (2020). DAXX inhibits cancer stemness and epithelial–mesenchymal transition in gastric cancer. *Br. J. Cancer* 122, 1477–1485. doi: 10.1038/s41416-020-0800-3

Conflict of Interest: The authors declare that the research was conducted in the absence of any commercial or financial relationships that could be construed as a potential conflict of interest.

frontiers in Genetics

ORIGINAL RESEARCH
published: 17 March 2021
doi: 10.3389/fgene.2021.637887

Systematic Characterization of Expression Profiles and Prognostic Values of the Eight Subunits of the Chaperonin TRiC in Breast Cancer

Wen-Xiu Xu†, Wei Song†, Meng-Ping Jiang, Su-Jin Yang, Jian Zhang, Dan-Dan Wang* and Jin-Hai Tang**

Department of General Surgery, The First Affiliated Hospital of Nanjing Medical University, Nanjing, China

OPEN ACCESS

Edited by:
Andrew Davis, Washington University in St. Louis, United States

Reviewed by:
Annette R. Khaled, University of Central Florida, United States
Oksana Sergeeva, École Polytechnique Fédérale de Lausanne, Switzerland

***Correspondence:**
Jin-Hai Tang
jhtang@njmu.edu.cn
Dan-Dan Wang
dandanw92@njmu.edu.cn
Jian Zhang
dr_jianzhang@njmu.edu.cn

†*These authors have contributed equally to this work*

Specialty section:
This article was submitted to Cancer Genetics, a section of the journal Frontiers in Genetics

Received: *04 December 2020*
Accepted: *22 February 2021*
Published: *17 March 2021*

Citation:
Xu W-X, Song W, Jiang M-P, Yang S-J, Zhang J, Wang D-D and Tang J-H (2021) Systematic Characterization of Expression Profiles and Prognostic Values of the Eight Subunits of the Chaperonin TRiC in Breast Cancer. Front. Genet. 12:637887. doi: 10.3389/fgene.2021.637887

Background: Chaperonin-containing TCP-1 (TRiC or CCT) was demonstrated to be involved in oncogenesis of cancers carcinogenesis and development of various malignancies. Increasing experimental evidence indicated that dysregulation of TRiC was implicated in the tumor progression of breast cancer (BCa). However, few definitive studies have addressed the diverse expression patterns and prognostic values of eight TRiC subunits. Thus, we aimed to investigate the clinical significance of TRiC subunit expression and prognostic values for their possible implications in diagnosis and treatment of BCa.

Methods: Based on updated public resources and comprehensive bioinformatics analysis, we used some online databases (e.g., UALCAN, GEPIA, cBioPortal, TIMER, BC-GenExMiner, metascape, and GeneMANIA) to comprehensively explore the expression levels and the prognostic effects of eight TRiC subunits in patients with BCa.

Results: The transcriptional levels of most subunits of the Chaperonin TRiC (CCT2, CCT3, CCT4, CCT5, CCT6A, and CCT7) were significantly elevated compared with normal breast tissues, whereas TCP1, CCT4, and CCT6B were lower in BCa tissues than in normal tissues. Besides, copy-number alterations (CNA) of eight TRiC subunits positively regulated their mRNA expressions. Furthermore, high mRNA expression of TCP1/CCT2/CCT4/CCT5/CCT6A/CCT7/CCT8 was significantly associated with poor overall survival (OS) in BCa patients. The eight subunits of the chaperonin TRiC was related to tumor purity and immune infiltration levels of BCa. Co-expression analysis showed CCT6B was negatively associated with other subunits of TRiC and other subunits of TRiC were positively correlated with each other. Additionally, TRiC and their interactive proteins were correlated with positive regulation of biological process, localization, and biological regulation.

Conclusion: This study systematically illustrated the expression profiles and distinct prognostic values of chaperonin TRiC in BCa, providing insights for further investigation of subunits of the chaperonin TRiC as novel therapeutic targets and potential prognostic biomarkers in BCa.

Keywords: bioinformatic analysis, breast cancer, gene expression, eight subunits of the chaperonin TRiC, prognosis

INTRODUCTION

Breast cancer (BCa) ranks first in terms of morbidity and is the second leading cause of mortality among all female's cancers globally, and 276,480 new cancer cases and 42,170 cancer deaths are expected in United States in 2020 according to the estimation by the American Cancer Society (Siegel et al., 2020). Surgery and chemotherapy are curative treatments in early-stage BCa patients. However, a considerable proportion of BCa patients are not diagnosed or treated until they reach an advanced stage, resulting in a poor prognosis (Zheng et al., 2018). In such circumstances, identification of novel biomarkers, and treatment targets are needed to better delineate patient outcomes and individualize patient management in BCa.

Chaperonins are molecules that mediates nascent polypeptide chains folding and include two groups, group I and group II. Heat shock protein 60 (HSP60) or bacteria GroEL belongs to group I, and CCT [chaperonin-containing t-complex polypeptide 1 (TCP-1) or TRiC] belongs to group II. The eukaryotic cytoplasmic CCT complexes are assembled into two symmetry rings, each of which consists of eight paralogous but distinct subunits, denoted TCP1, CCT2, CCT3, CCT4, CCT5, CCT6A, CCT6B, CCT7, and CCT8 (or CCTα, CCTβ, CCTγ, CCTδ, CCTε, CCTζ-1, CCTζ-2, CCTη, and CCTθ) (Shimon et al., 2008; Amit et al., 2010). TRiC, also known as CCT, is essential for cell viability and has been shown to assist the folding of cytoskeletal proteins (tubulins and actins) and other proteins related to carcinogenesis, such as p53, STAT3 (Signal transducer and activator of transcription 3) in an ATP-dependent fashion (Amit et al., 2010; Trinidad et al., 2013; Kasembeli et al., 2014; Gestaut et al., 2019). Under such circumstances, elevated expression of TRiC subunits may lead to upregulation of these oncogenic proteins, concomitantly resulting in carcinogenesis. Except for CCT6B, other TRiC subunits, TCP1, CCT2, CCT3, CCT4, CCT5, CCT6A, CCT7, and CCT8 exhibit approximately 30% identity. Intriguingly, CCT6B is the most special one among different TRiC subunits, and is expressed only in testis, which may play a specific role in helping the biosynthesis of particular testicular proteins (Kubota et al., 1997).

In the current research, the subunits of CCT have been shown to be critical for the development and progression of BCa (Guest et al., 2015). Intriguingly, we investigated and found aberrant expressions of the TRiC subunits in BCa, including significantly elevated expressions of TCP1, CCT2, CCT3, CCT4, CCT5, CCT6A, CCT7, and CCT8 as well as decreased expression of CCT6B, which were determinants of growth and overall survival (OS) in BCa. Our results demonstrated a role for the TRiC subunits, suggesting that the role of the entire complex potentially could be explored as a functional macrocosm in BCa.

MATERIALS AND METHODS

UALCAN Database Analysis

UALCAN web-portal[1] is an interactive and effective platform based on level 3 RNA-seq and clinical information from The Cancer Genome Atlas (TCGA) project (Chandrashekar et al., 2017). It can be utilized to analyze relative transcriptional levels of target genes between cancerous and paired normal tissues. In the current study, we explored the relative expression of eight subunits of the chaperonin TRiC between BCa and paracancerous tissues and compared the expression differences among different molecular subtypes based on UALCAN database. All the BCa cases publicly available on UALCAN were included in our research.

cBioPortal Database Analysis

cBioPortal[2] is a user-friendly, comprehensive website resource and provides visualization, analysis, and download of large-scale cancer genomics datasets (Wu et al., 2019). In our study, we analyzed the genetic alterations of TRiC, which contained genomic profiles counted on mutations and putative copy-number alterations (CNA) from GISTIC. Breast Invasive Carcinoma (TCGA, Cell 2015) was selected for further analysis of TRiC, and tumor samples included in our research contained total 817 BCa samples. OncoPrint was constructed in cBioPortal to directly reflect all types of changes in eight subunits of the chaperonin TRiC gene amplification, deep deletion, mRNA upregulation, and mRNA downregulation in patients with BCa. Furthermore, we downloaded the data of putative CNAs and mRNA expression *z*-scores to evaluate the association between various CNAs and transcriptional levels of chaperonin TRiC.

GEPIA Database Analysis

The Gene Expression Profiling Interactive Analysis (GEPIA) database[3], a newly developed web server for analyzing the of RNA sequencing data based on 9,736 tumors and 8,587 normal samples from TCGA and GTEx projects. It provides key interactive and customizable functions including differential expression analysis, correlation analysis, profiling plotting, similar gene detection, patient survival analysis, and dimensionality reduction analysis (Tang et al., 2017). The Survival Analysis module on GEPIA was applied to estimate the correlation between TRiC expression and survival information of BCa patients. The prognostic values of chaperonin TRiC (TCP1, CCT2, CCT3, CCT4, CCT5, CCT6A, CCT6B, CCT7, and CCT8) at mRNA level were analyzed using all BCa samples available in GEPIA. The patients' cohorts were split at the median expression of each subunit of the chaperonin TRiC mRNA level. Hazard ratio (HR) and log-rank *P*-value were calculated and displayed online. Meanwhile, the relationship between the expression level of chaperonin TRiC and gene markers of tumor-infiltrating immune cells

[1]http://ualcan.path.uab.edu/

[2]www.cbioportal.org/

[3]http://gepia.cancer-pku.cn/

(TIICs) was also explored in GEPIA. These markers were used to characterize immune cells, including CD8+ T cell, T cell (general), B cell, Tfh, M1, M2, and TAM (tumor-associated macrophages) in BCa.

TIMER Database Analysis

Tumor Immune Estimation Resource database (TIMER[4]) includes more than 10,000 samples across 32 cancer types from TCGA, which is an easy-to-operate online tool established for systematically analyzing the abundance of immune infiltration (Li et al., 2016, 2017). In our research, we mainly explored the correlation of TRiC expression with the abundance of all six immune infiltration fluids in BCa, including B cells, CD4+ T cells, CD8+ T cells, neutrophils, macrophages, and dendritic cells (DCs).

BC-GenExMiner Database Analysis

Breast cancer Gene-Expression Miner (bc-GenExMiner v4.5)[5], a mining tool of annotated genomics data, provides biologists with prognostic analysis and may be conducted on cohorts split by estrogen receptor (ER), nodal (N), or molecular subtype status (Jézéquel et al., 2012). This online tool also allowed Pearson correlation analysis of eight subunits of the chaperonin TRiC in BCa.

Protein–Protein Interaction and Functional Enrichment Analysis

GeneMANIA[6]is a user-friendly online tool that can be adopted to derive hypotheses based on gene functions (Warde-Farley et al., 2010). It generated a list of genes with similar functions and constructed an interactive functional-association network to elucidate relationships between genes and datasets. In our study, this database was applied to construct a PPI network for eight subunits of the chaperonin TRiC to evaluate their functions. Metascape[7] provides a flexible web interface for systematic and comprehensive functional annotation and analysis to aid investigators identify the biological meaning behind an extensive list of genes (Zhou et al., 2019). In this study, we used it to perform enrichment analysis of eight subunits of the chaperonin TRiC and their identified co-expression genes.

Statistical Analysis

The differential mRNA expression of TRiC in BCa tissues from the UALCAN database was analyzed by Student's *t*-test and normalized as transcripts per million reads (TPM). Survival curves were generated and compared by log-rank test. The correlation analysis was evaluated in the GEPIA database using Spearman's correlation analysis. Differences were considered statistically significant when P-values were and/or equal to 0.05.

[4]https://cistrome.shinyapps.io/timer/

[5]http://bcgenex.centregauducheau.fr

[6]http://www.genemania.org

[7]http://metascape.org

RESULTS

Transcriptional Levels of the Eight Subunits of TRiC in BCa

To explore the exact expression profiles of TRiC in BCa patients, we compared their differential transcriptional levels between BCa and normal samples by using UALCAN database. The findings revealed that the expression of five genes was higher in BCa samples than in normal control samples. As shown in **Figure 1**, the mRNA expression levels of CCT2 (**Figure 1B**, $P < 0.001$), CCT3 (**Figure 1C**, $P < 0.001$), CCT5 (**Figure 1F**, $P < 0.001$), CCT6A (**Figure 1E**, $P < 0.001$), CCT7 (**Figure 1H**, $P < 0.001$), and CCT8 (**Figure 1I**, $P < 0.001$) was significantly upregulated in BCa tissues compared with paracancerous tissues. Besides, the transcriptional level of TCP1 (**Figure 1A**, $P < 0.001$), CCT4 (**Figure 1D**, $P < 0.001$) and CCT6B (**Figure 1G**, $P < 0.001$) was significantly downregulated in BCa tissues compared with paracancerous tissues. Further, when sorting the patients by subgroups, all subunits of the chaperonin TRiC were still significantly up-regulated in different molecular subtypes compared with paracancerous samples, except for CCT6B, which was down-regulated BCa patients (**Figure 2G**). Additionally, the highest expression levels of TCP1, CCT3, CCT4, CCT5, and CCT7 were observed in triple-negative BCa tissues (**Figures 2A,C–E,H**). CCT6A and CCT8 was enriched in HER2-positive BCa tissues (**Figures 2F,I**), and CCT2 was enriched in luminal BCa tissues (**Figure 2B**).

Genetic Alterations of the Eight Subunits of TRiC in BCa Samples

Next, the genetic alterations of TRiC in BCa patients were explored based on TCGA database and cBioPortal online tool. The frequencies of mutations of the eight subunits of TRiC genes in breast invasive carcinoma were assessed using cBioPortal database. DNA copy number amplifications, mutations, and deep deletion were the main genetic mutations of BCa (**Figure 3A**). As shown in **Figure 2B**, the percentages of genetic variations in the eight subunits of TRiC among BCa patients varied from 0.7 to 9% for individual genes (TCP1, 1.3%; CCT2, 3%; CCT3, 9%; CCT4, 1%; CCT5, 2.1%, CCT6A, 1.6%; CC6B, 2.5%, CCT7, 0.7%, and CCT8, 1.6%, respectively). CCT2, CCT3, and CCT6B were ranked as the top three of the eight members. DNA CNA are most common genetic alterations which are involved in carcinogenesis through modulating cancer-related gene expression (Thomas et al., 2015; Choi et al., 2017). The eight subunits of TRiC were dysregulated in BCa tissues, we further hypothesized that DNA CNA might modulate their transcriptional levels. As shown in **Figure 3**, low amplification rate of the eight subunits of TRiC was observed in BCa patients. However, although copy gain (gain and amplification) of eight subunits of TRiC was not frequent, it was still linked with significant upregulated eight subunits of TRiC mRNA levels compared with the copy-loss (deep deletion and shallow deletion) and copy-neutral (diploid) patients (**Figures 3C–K**). To sum up, these results indicated that eight subunits of TRiC mRNA expressions were modulated by their DNA CNA.

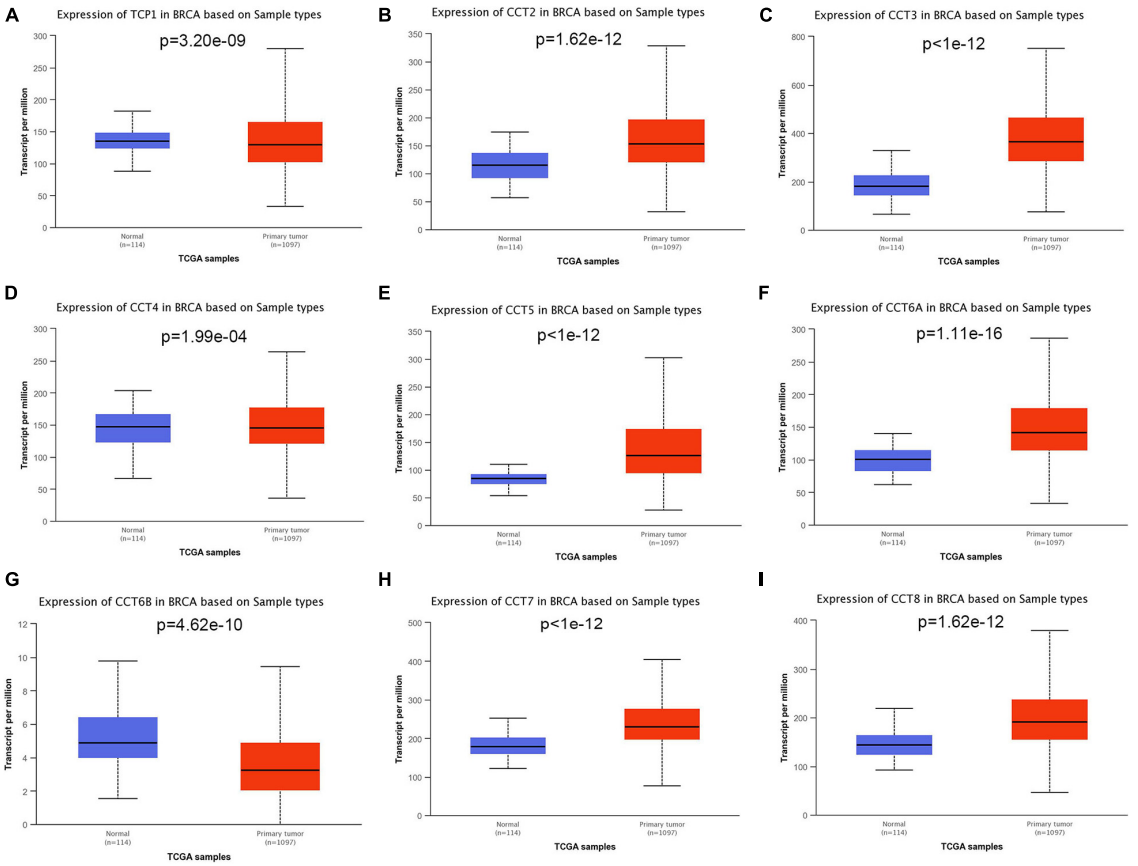

FIGURE 1 | Boxplot showed relative expression of eight subunits of the chaperonin TRiC in BCa primary tumor and in corresponding normal tissues based on UACLAN database. **(A)** TCP1, **(B)** CCT2, **(C)** CCT3, **(D)** CCT4, **(E)** CCT5, **(F)** CCT6A, **(G)** CCT6B, **(H)** CCT7, and **(I)** CCT8.

Prognostic Values of TRiC mRNA Expression in All BCa Samples

Further, we employed GEPIA database to analyze the associations between TRiC mRNA expression and prognosis of BCa patients. As shown in **Figure 4**, high mRNA expression of TCP1 (HR = 1.9, $P < 0.001$), CCT2 (HR = 1.4, $P = 0.034$), CCT4 (HR = 1.6, $P = 0.0041$), CCT5 (HR = 1.5, $P = 0.0089$), CCT6A (HR = 1.5, $P = 0.014$), CCT7 (HR = 1.6, $P = 0.0056$), and CCT8 (HR = 1.7, $P = 0.002$) were significantly associated with poor OS of BCa patients. However, other subunits of TRiC mRNA expression showed a null correlation with prognosis of BCa patients. Overall, our findings above implied that mRNA expressions of TCP1, CCT2, CCT4, CCT5, CCT6A, CCT7, and CCT8 were remarkably correlated with BCa patients' OS, which might be identified as promising biomarkers to predict the survival of BCa patients.

Relationships Between TRiC Expression and Immune Infiltration

Immune cells in the TME can affect patient survival, and the prognosis of patients with BCa is closely related to the infiltration of immune cells (Shen et al., 2020). The above findings indicated a prognostic role of TRiC in BCa. Hence, it would be meaningful to explore the association between immune infiltration and TRiC expression. We determined whether TRiC expression was correlated with the immune infiltration level in different cancers by calculating the coefficient of TRiC expression and immune infiltration level in BCa in TIMER. As distinctly shown in **Figure 5**, the results revealed that TRiC expression had positive correlations with tumor purity and CD8+ T cells except CCT6B. CCT2 was positively associated with macrophage, while CCT3 was negatively associated with macrophage. Furthermore, TCP1, CCT2, CCT4, CCT5, CCT6A, and CCT8 were positively associated with neutrophil, B cell and DC, while CCT6B was negatively associated with DC. These results showed the eight subunits of the chaperonin TRiC was related to tumor purity and immune infiltration levels of BCa by TIMER analysis.

Relationships Between TriC Expression and Immune Markers

Accumulating evidence showed that the interaction between cancer cells and the tumor microenvironment, specifically the immune microenvironment, was also believed to be a vital factor and involved in the tumor progression and therapy (Hirsch et al., 2017). So as to further explore the potential relationships between TRiC and infiltrating immune cells, we examined the correlations between eight subunits of TRiC and

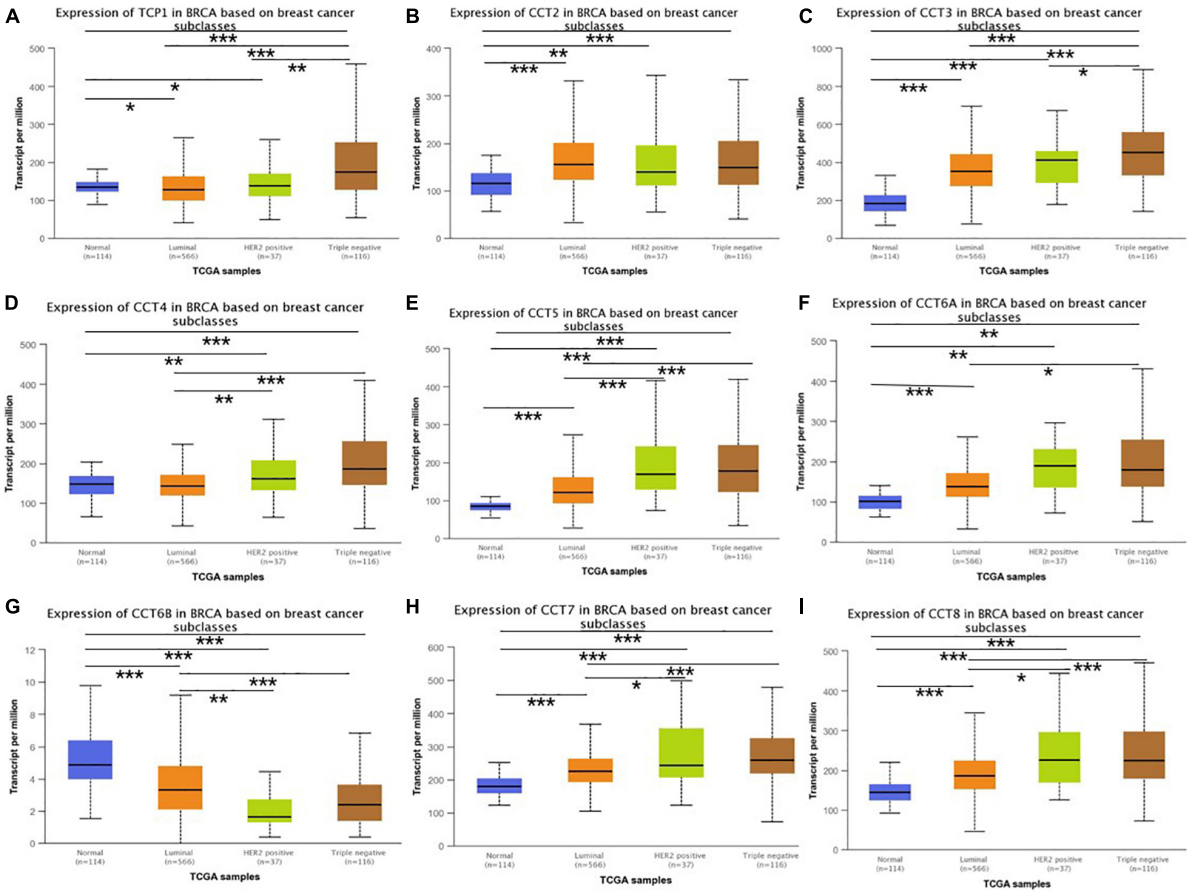

FIGURE 2 | Boxplot showed relative expression of eight subunits of the chaperonin TRiC in BCa patients with different molecular subtypes and in normal individuals based on UACLAN database. **(A)** TCP1, **(B)** CCT2, **(C)** CCT3, **(D)** CCT4, **(E)** CCT5, **(F)** CCT6A, **(G)** CCT6B, **(H)** CCT7, and **(I)** CCT8. *$p < 0.05$; **$p < 0.01$; ***$p < 0.001$.

several immune cell markers in GEPIA. Immune genes were selected from ImmPort database[8] (Zalocusky et al., 2018). These markers were used to characterize immune cells, including CD8A, CD8B, CD3D, CD3E, CD2, CD19, CD79A, BCL6, NOS2, ROS, ARG1, MRC1, HLA-G, CD80, and CD86 in BCa (**Table 1**). Most subunits of TRiC were positively correlated with CD8+ T cell markers (CD8A and CD8B) in breast normal tissues. Hence, these results confirmed our speculation that TRiC expression in BCa was correlated with gene markers of immune cells in different manners, which can help explain the differences in patient survival.

Enrichment Analysis of Protein–Protein Interaction of TriC

As shown in **Figure 6A**, it revealed a significant negative correlation between CCT6B and other subunits of TRiC. Furthermore, other subunits of TRiC were correlated to a significant degree. A network of eight subunits of TRiC and 20 proteins that significantly interacted with TRiC was constructed using GeneMANIA. The results revealed that BBS12, MKKS, BBS10, HSPD1, SPHK1, PFDN2, PFDN6, PIKFYVE, PFDN5, PFDN1, PFDN4, PDCL3, VBP1, USP9X, ACTB, TRIM28, PPP4C, EHD2, and GSPT2 were closely associated with eight subunits of TRiC (**Figure 6B**). Next, a PPI enrichment analysis, was then used to explore the relationships among these genes in BCa. The functions of these genes were next explored through GO analyses (**Figures 6C,D**). GO analyses allow assessment of the biological process, molecular function, and cellular component annotations of genes of interest. These 29 genes were primarily enriched for regulation of cellular process, positive regulation of biological process, localization, biological regulation, cellular component organization or biogenesis, metabolic process, reproductive process, and regulation of biological process.

DISCUSSION

Chaperonin-containing TCP-1, a multi-subunit complex and encoded by eight distinct genes, folds various proteins that essential for cancer development, and is expressed in diverse

[8]https://immport.niaid.nih.gov

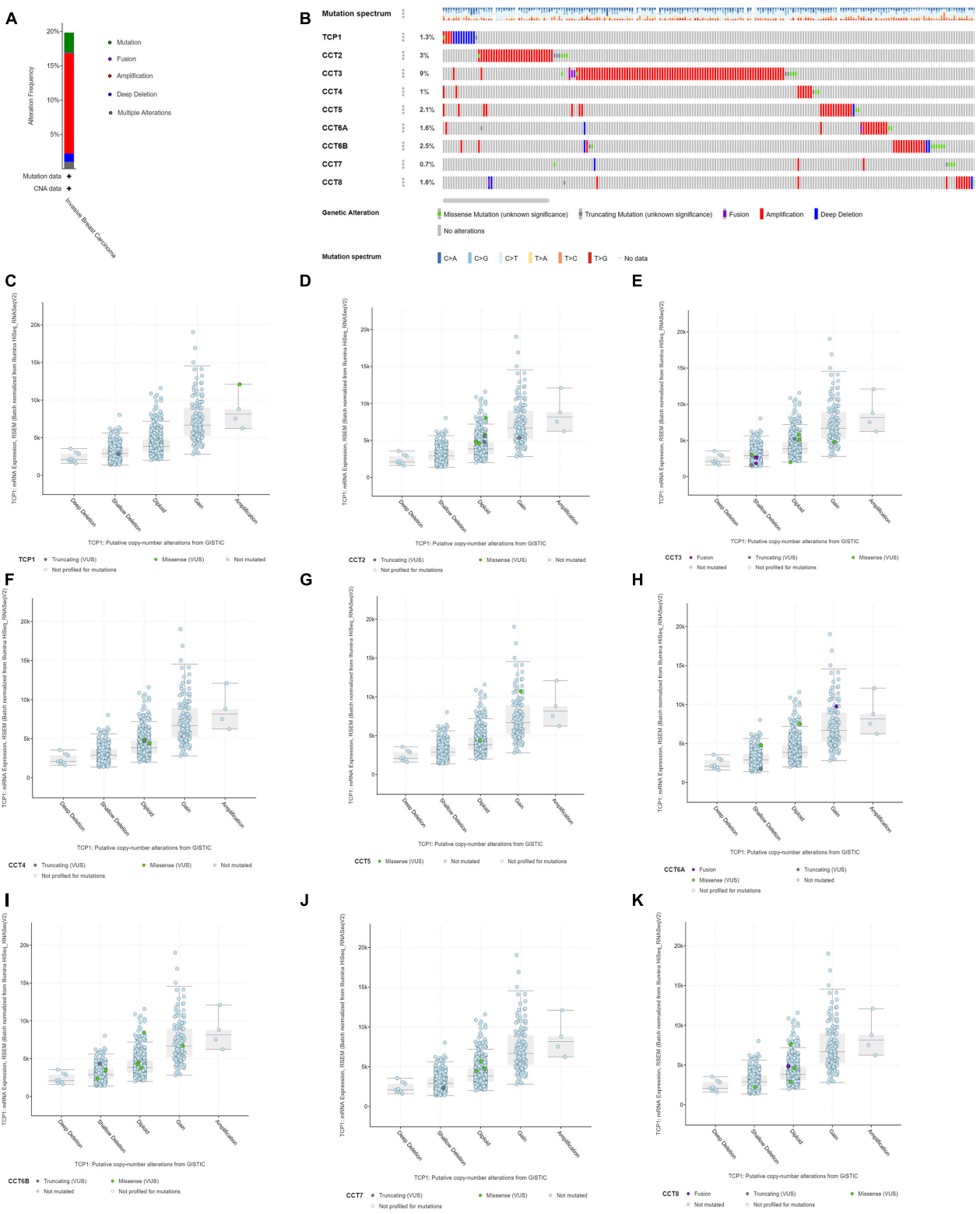

FIGURE 3 | Genetic mutation analysis of eight subunits of the chaperonin TRiC in BCa (cBioPortal). **(A)** Types of mutations and their proportions contained in BCa. **(B)** OncoPrint visual summary of genetic alteration on a query of eight subunits of the chaperonin TRiC in BCa. TCP1, CCT2, CCT3, CCT4, CCT5, CCT6A, CCT6B, CCT7, and CCT8 mutation rates were 1.3, 3, 9, 1, 2.1, 1.6, 2.5, 0.7, and 1.6%, respectively. **(C–K)** Copy gain (gain and amplification) of TRiC was linked with significant upregulated TRiC mRNA levels compared with the copy-loss (deep deletion and shallow deletion) and copy-neutral (diploid) patients **(C)** TCP1, **(D)** CCT2, **(E)** CCT3, **(F)** CCT4, **(G)** CCT5, **(H)** CCT6A, **(I)** CCT6B, **(J)** CCT7, and **(K)** CCT8.

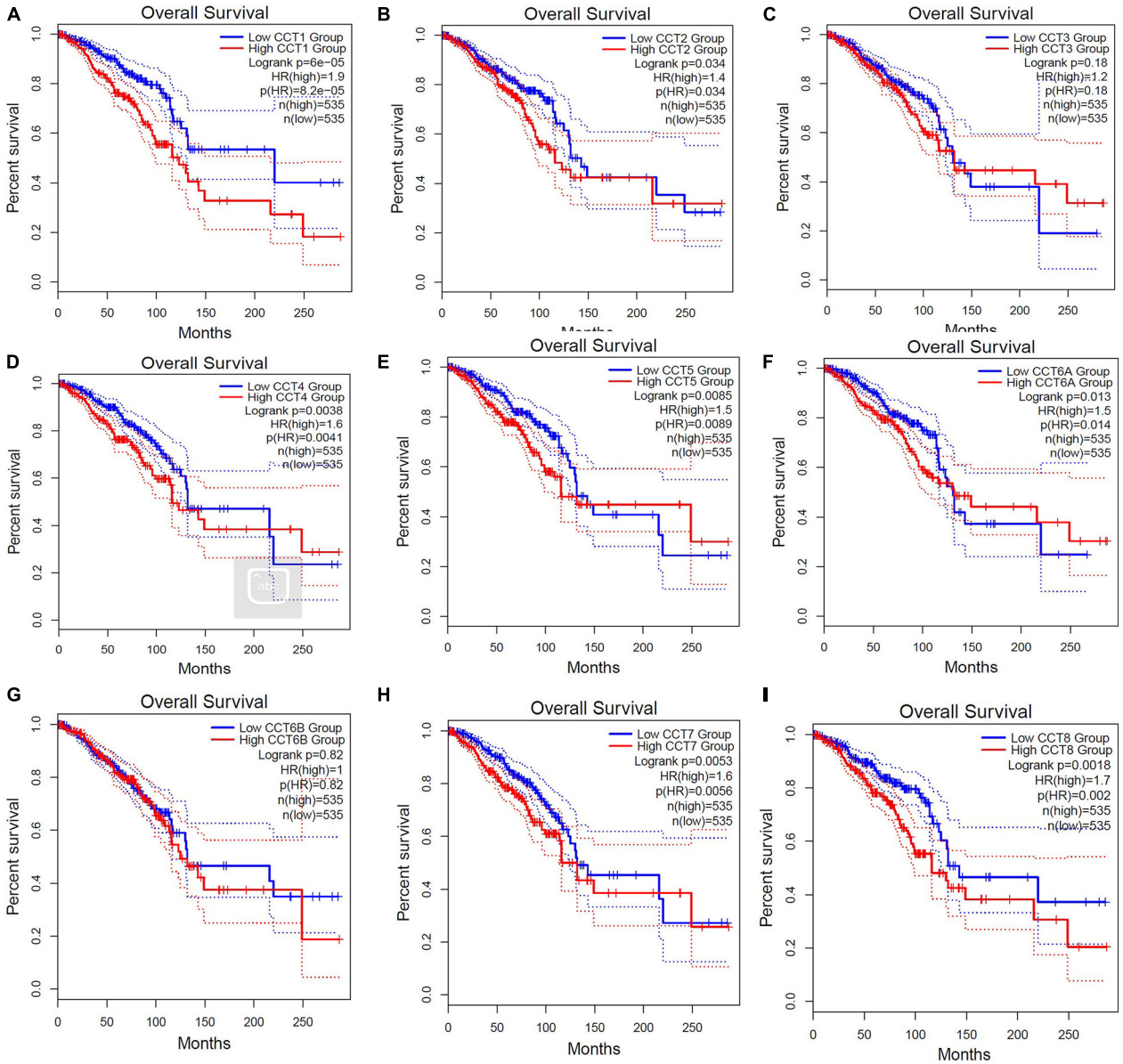

FIGURE 4 | Elevated expressions of eight subunits of the chaperonin TRiC were associated with poor clinical outcomes (OS). Prognostic value of mRNA level of TRiC in BCa patients **(A)** TCP1, **(B)** CCT2, **(C)** CCT3, **(D)** CCT4, **(E)** CCT5, **(F)** CCT6A, **(G)** CCT6B, **(H)** CCT7, and **(I)** CCT8.

cancers and can serve as a viable therapeutic target (Showalter et al., 2020). Previous studies reported that the expression levels of different CCT subunits were upregulated in various cancers, such as CCT2 in prostate, breast, and lung cancers (Guest et al., 2015; Bassiouni et al., 2016; Carr et al., 2017), CCT3 in hepatocellular carcinoma (HCC) (Qian et al., 2016), and CCT8 in HCC and glioblastoma (Huang et al., 2014; Qiu et al., 2015). CCT2 played a pivotal role in clinical tubulin-binding agent-resistant or CCT2-overexpressing cancers, and targeting the β-tubulin/CCT2 complex might provide these cancers with a novel chemotherapeutic strategy (Lin et al., 2009). These pathways proceeded through activating mitogen-activated protein kinases (MAPKs) at the onset of β-tubulin/CCT2 complex disruption (Liu et al., 2017). Besides, targeting the complex also induced apoptosis and inhibited migration and invasion of metastatic human lung adenocarcinoma (Liu et al., 2020). CCT2 was a vital determinant of survival in CRC (colorectal cancer) patients and could regulate the folding of Gli-1, a Hedgehog signaling factor in relation to hypoxia (Park et al., 2020). CCT3 functioned as a trigger of YAP and TFCP2 to affect tumorigenesis and served as a potential biomarker in liver cancer (Liu et al., 2019). Furthermore, CCT3 was closely related to the proliferation and migration of BCa and papillary thyroid carcinoma (PTC) (Shi et al., 2018; Xu et al., 2020). The correlation between the

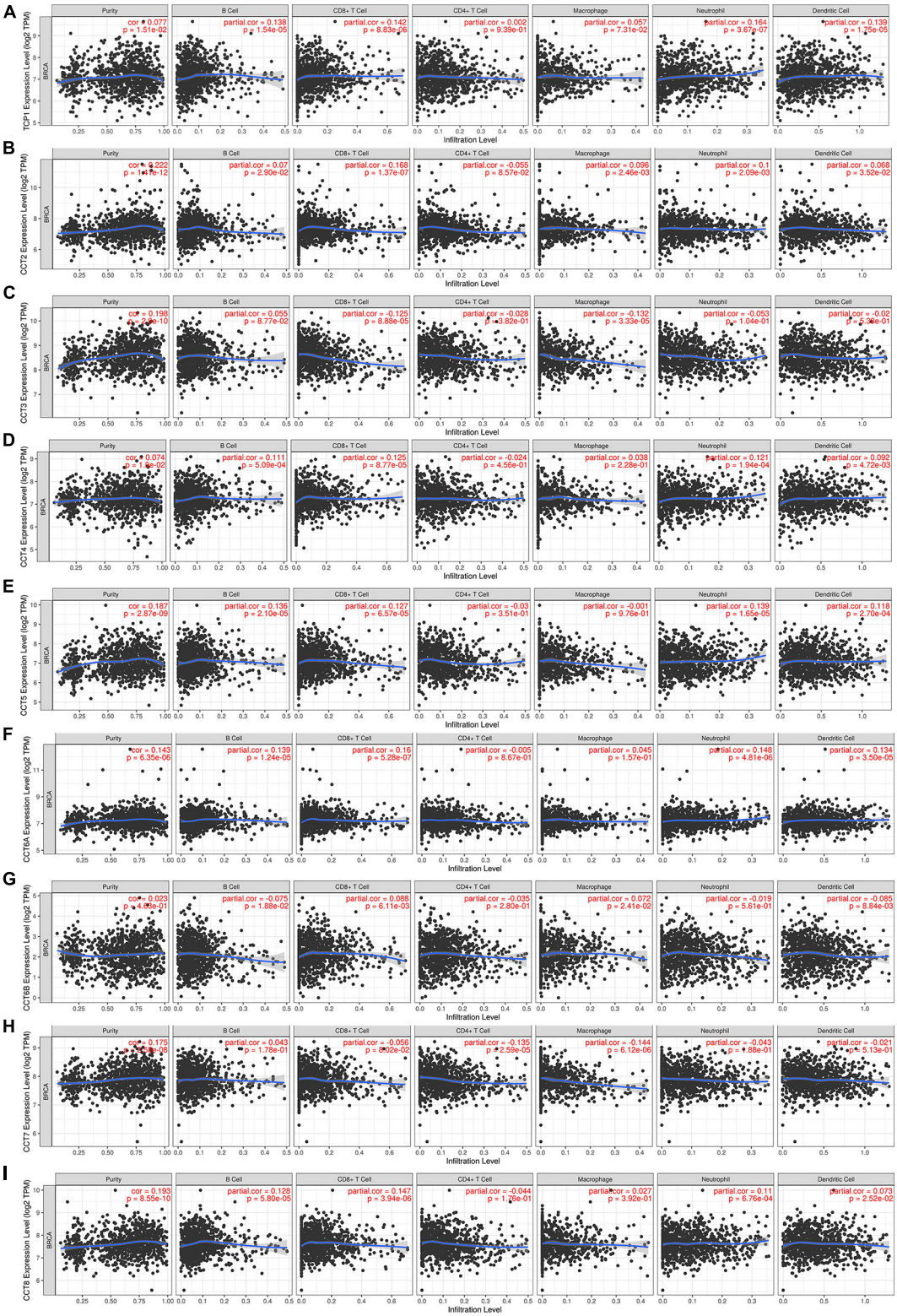

FIGURE 5 | Correlation of eight subunits of the chaperonin TRiC with immune infiltration level in BCa. **(A)** TCP1 expression had significant positive correlations with infiltrating levels of CD4+ T cells. **(B)** CCT2 expression had significant correlations with infiltrating levels of CD4+ T cells, macrophages, neutrophils, and dendritic cells in GC. **(C)** CCT3 expression was significantly related to infiltrating levels of CD4+ T cells and macrophages in GC but no significant correlation with infiltrating level of B cells. **(D)** CCT4 expression had significant positive correlations with infiltrating levels of CD4+ T cells and macrophages in GC. **(E)** CCT5, **(F)** CCT6A, **(G)** CCT6B, **(H)** CCT7, and **(I)** CCT8.

TABLE 1 | Correlation analysis between TRiC and genes markers of immune cells in GEPIA.

Description			CD8+ T cell		T cell (general)			B cell		Tfh	M1		M2		TAM		
Gene markers			CD8A	CD8B	CD3D	CD3E	CD2	CD19	CD79A	BCL6	NOS2	ROS	ARG1	MRC1	HLA-G	CD80	CD86
TCP1	Tumor	*R*	−0.039	0.014	−0.092	−0.072	−0.017	−0.088	−0.1	−0.078	0.024	0.12	−0.031	0.019	−0.0011	0.17	0.11
		P	0.19	0.64	*	0.018	0.59	*	**	0.01	0.43	***	0.3	0.52	0.97	***	***
	Normal	*R*	0.43	0.38	0.17	0.19	0.27	−0.016	0.038	−0.057	0.15	−0.14	0.3	−0.13	−0.035	0.18	0.022
		P	***	***	0.066	0.046	*	0.87	0.69	0.55	0.11	0.14	*	0.16	0.72	0.056	0.82
CCT2	Tumor	*R*	−0.058	−0.05	−0.1	−0.09	−0.069	−0.082	−0.1	−0.032	−0.025	0.015	−0.019	−0.019	−0.028	0.011	−0.031
		P	0.056	0.1	**	*	0.022	*	**	0.29	0.4	0.63	0.53	0.54	0.35	0.72	0.31
	Normal	*R*	0.42	0.37	0.21	0.19	0.22	0.022	0.09	−0.17	0.061	−0.12	0.27	−0.23	0.0058	0.22	−0.0071
		P	***	***	0.023	0.041	0.02	0.81	0.34	0.067	0.52	0.21	*	0.016	0.95	0.019	0.94
CCT3	Tumor	*R*	−0.11	0.056	−0.15	−0.15	−0.11	−0.15	−0.19	−0.074	0.018	−0.0019	0.0033	−0.06	0.043	0.081	−0.04
		P	**	0.064	***	***	**	***	***	0.015	0.56	0.95	0.91	0.048	0.16	*	0.18
	Normal	*R*	0.45	0.53	0.32	0.3	0.3	0.09	0.18	−0.29	0.072	−0.13	0.27	−0.46	0.15	0.19	−0.17
		P	***	***	**	**	*	0.35	0.061	*	0.45	0.19	*	***	0.11	0.049	0.07
CCT4	Tumor	*R*	−0.041	0.056	−0.082	−0.084	−0.028	−0.1	−0.12	−0.15	0.054	0.085	−0.037	0.026	0.02	0.15	0.067
		P	0.17	0.064	*	*	0.35	**	***	***	0.075	*	0.22	0.39	0.5	***	0.027
	Normal	*R*	0.5	0.53	0.26	0.31	0.32	−0.0042	0.095	−0.31	0.051	−0.13	0.3	−0.45	−0.0014	0.067	0.19
		P	***	***	*	*	**	0.96	0.32	***	0.59	0.17	*	***	0.89	0.48	0.043
CCT5	Tumor	*R*	−0.031	0.036	−0.094	−0.079	−0.031	−0.088	−0.11	−0.041	0.053	0.062	−0.014	−0.014	0.15	0.19	0.095
		P	0.31	0.23	*	*	0.31	*	**	0.18	0.079	0.041	0.64	0.65	***	***	*
	Normal	*R*	0.27	0.22	0.17	0.17	0.18	0.09	0.11	−0.012	0.0042	0.05	0.12	0.052	0.14	0.29	0.19
		P	*	0.019	0.066	0.081	0.058	0.35	0.25	0.9	0.96	0.6	0.19	0.58	0.15	*	0.043
CCT6A	Tumor	*R*	−0.033	−0.0098	−0.032	−0.031	−0.012	−0.039	−0.044	−0.063	0.0036	0.0076	−0.0088	−0.012	−0.0018	0.038	0.036
		P	0.28	0.75	0.29	0.3	0.7	0.2	0.15	0.037	0.9	0.8	0.77	0.7	0.95	0.21	0.24
	Normal	*R*	0.54	0.49	0.37	0.37	0.4	0.11	0.16	−0.36	−0.052	0.05	0.23	−0.28	0.092	0.27	0.096
		P	***	***	***	***	***	0.24	0.086	***	0.58	0.6	0.014	*	0.33	*	0.31
CCT6B	Tumor	*R*	−0.096	−0.099	−0.14	−0.12	−0.12	0.0011	−0.13	0.12	−0.011	−0.027	−0.01	0.0068	−0.03	−0.079	−0.068
		P	*	*	***	***	***	−0.099	***	***	0.72	0.38	0.73	0.82	0.33	*	0.025
	Normal	*R*	0.39	0.4	0.17	0.18	0.18	0.021	0.31	−0.22	0.24	−0.18	0.26	−0.41	0.01	0.082	−0.15
		P	***	***	0.069	0.054	0.054	0.83	0.097	0.019	0.012	0.064	*	***	0.92	0.39	0.11
CCT7	Tumor	*R*	−0.11	−0.026	−0.14	−0.15	−0.12	−0.14	−0.17	−0.2	0.063	0.052	−0.0082	−0.045	0.012	0.044	−0.083
		P	**	0.39	***	***	***	***	***	***	0.038	0.09	0.79	0.14	0.7	0.15	*
	Normal	*R*	0.28	0.39	0.18	0.16	0.15	−0.037	0.03	−0.4	0.012	−0.078	0.15	−0.35	0.11	0.03	−0.13
		P	*	***	0.053	0.091	0.12	0.7	0.75	***	0.9	0.41	0.11	***	0.26	0.75	0.16
CCT8	Tumor	*R*	−0.084	−0.055	−0.13	−0.11	−0.062	−0.12	−0.15	−0.081	0.012	0.069	0.0017	0.0034	−0.0033	0.11	0.059
		P	*	0.069	***	**	0.042	***	***	*	0.68	0.024	0.96	0.91	0.91	***	0.054
	Normal	*R*	0.54	$2.1e-07$	0.34	0.35	0.4	0.13	0.18	−0.17	0.056	−0.15	0.36	−0.35	0.076	0.22	−0.059
		P	***	0.47	**	**	***	0.17	0.055	0.07	0.56	0.11	***	***	0.43	0.022	0.54

*Tfh, follicular helper T cell; TAM, tumor-correlated macrophage; R, R-value of Spearman's correlation; P, P-value of Spearman's correlation. *P < 0.01; **P < 0.001; ***P < 0.0001.*

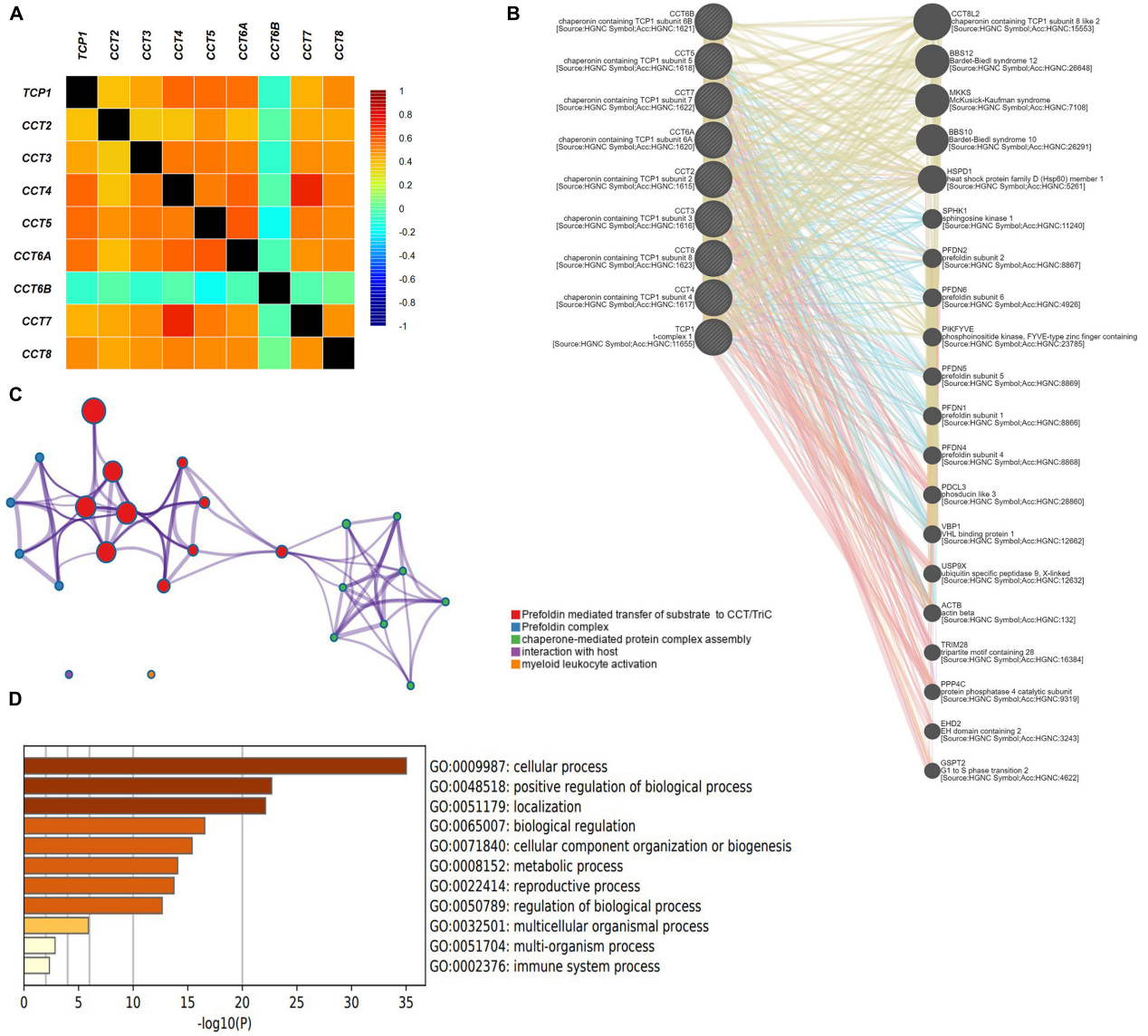

FIGURE 6 | Enrichment analysis **(A)** Pearson correlation analysis of eight subunits of the chaperonin TRiC. **(B)** Protein–protein interaction network among eight subunits of the chaperonin TRiC in the GeneMANIA dataset. **(C)** Interactive network of the top five enriched terms colored by cluster ID. Each color represents one enrichment pathway. **(D)** Heatmap of enriched terms regarding Gene Ontology biological processes across eight subunits of the chaperonin TRiC and its co-expressed genes constructed by Metascape.

aberrant overexpression of CCT3 and the poor prognosis of HCC patients has been shown, as has the depletion of CCT3 sensitized HCC cells to chemotherapy (Zhang et al., 2016). MALAT-1 enhanced cell motility of lung adenocarcinoma by downregulating CCT4 (Tano et al., 2010). CCT5 was a tumor associated antigen of non-small cell lung cancer (NSCLC) (Gao et al., 2017). CCT6A sustained the oncogenic arm of TGF-β signaling and functioned as a potent promoter of TGF-β-induced metastasis of NSCLC cells, blocking SMAD2-SMAD4 interaction (Ying et al., 2017). Increased CCT8 expression was associated with poor prognosis and cisplatin resistance by regulating α-actin and β-tubulin in ESCC (Yang et al., 2018). Compared with the controls, the glioma cells expressing CCT8-siRNA exhibited a significantly decreased proliferation and invasion capacity (Qiu et al., 2015). Another study defined CCT8 as an oncogene and demonstrated its function of participating in HCC cell proliferation by facilitating S-phase entry (Huang et al., 2014). Overexpression of CCT8 could promote the proliferation, accelerate the G1/S transition and reverse cell adhesion-mediated drug resistance (CAM-DR) phenotype in B-cell non-Hodgkin's lymphoma (Yin et al., 2016). Tumor infiltrates consist of a heterogeneous population of immune cells frequently dominated by T cells but also containing B cells, macrophages, NK cells, DCs,

and neutrophils, which play vital roles in anti-tumor immunity (Garaud et al., 2019). Tumor-infiltrating lymphocytes (TILs) and tumor-infiltrating B-cells (TIL-B) are crucial determinants of favorable outcomes in patients with BCa (Garaud et al., 2019; Byrne et al., 2020). Immunotherapy using immune cells-based vaccination is a promising approach to eliminate tumor cells (Sabado et al., 2017).

Here, we explored the role and prognostic value of the full chaperonin TRiC in BCa by studying the altered expression of each of its subunits in the context of this disease. Furthermore, we also found that the chaperonin TRiC subunits can act as mediators only in certain states, such as when associated with ATP. Chaperonin TRiC was thus a viable target for therapeutic intervention in cancer due to its function as a critical protein-folding complex. Overall, our research preliminarily but systematically characterized the expression profiles of eight subunits of TRiC in BCa and revealed that the detection of the TRiC expression status of BCa patients might be promising and valuable biomarkers for early diagnosis, immunotherapy, and prognostic assessment.

CONCLUSION

In summary, our results indicated that subunits of TRiC displayed varying degrees of abnormal expressions, and CCT2, CCT3, CCT5, CCT6A, CCT7, and CCT8 were significantly upregulated in BCa patients and their upregulation was positively correlated with BCa tumor stage. Based on the above findings, it was expected that TRiC could act as potential prognostic biomarkers and therapeutic targets for BCa. Our research contributed to a better understanding of the pathogenesis of BCa and might assist in the development of more effective targeted drugs for BCa. However, further relevant experimental studies were needed to validate our findings and to promote clinical application of TRiC as prognostic or therapeutic targets in BCa, owing to limited sample sizes and differences found among databases.

DATA AVAILABILITY STATEMENT

The original contributions presented in the study are included in the article/supplementary material, further inquiries can be directed to the corresponding author/s.

AUTHOR CONTRIBUTIONS

W-XX and WS conceived and designed this study. W-XX, WS, M-PJ, and S-JY acquired and downloaded the data. W-XX, WS, D-DW, and JZ analyzed the data. W-XX, WS, D-DW, JZ, and J-HT helped discuss the results. W-XX drafted the manuscript. All authors revised and reviewed this work, and gave their final approval of this manuscript.

FUNDING

This research was supported by the National Key Research and Development Program of China (No. 2016YFC0905900), National Natural Science Foundation of China (No. 81872365), and Jiangsu Provincial Key Research Development Program (No. BE2019731).

REFERENCES

Amit, M., Weisberg, S. J., McCormack, E. A., Feldmesser, E., Kaganovich, D., Willison, K. R., et al. (2010). Equivalent mutations in the eight subunits of the chaperonin CCT produce dramatically different cellular and gene expression phenotypes. *J. Mol. Biol.* 401, 532–543. doi: 10.1016/j.jmb.2010.06.037

Bassiouni, R., Nemec, K. N., Iketani, A., Flores, O., Showalter, A., Khaled, A. S., et al. (2016). Chaperonin containing TCP-1 protein level in breast cancer cells predicts therapeutic application of a cytotoxic peptide. *Clin. Cancer Res.* 22, 4366–4379. doi: 10.1158/1078-0432.Ccr-15-2502

Byrne, A., Savas, P., Sant, S., Li, R., Virassamy, B., Luen, S. J., et al. (2020). Tissue-resident memory T cells in breast cancer control and immunotherapy responses. *Nat. Rev. Clin. Oncol.* 17, 341–348. doi: 10.1038/s41571-020-0333-y

Carr, A. C., Khaled, A. S., Bassiouni, R., Flores, O., Nierenberg, D., Bhatti, H., et al. (2017). Targeting chaperonin containing TCP1 (CCT) as a molecular therapeutic for small cell lung cancer. *Oncotarget* 8, 110273–110288. doi: 10.18632/oncotarget.22681

Chandrashekar, D. S., Bashel, B., Balasubramanya, S. A. H., Creighton, C. J., Ponce-Rodriguez, I., Chakravarthi, B., et al. (2017). UALCAN: a portal for facilitating tumor subgroup gene expression and survival analyses. *Neoplasia* 19, 649–658. doi: 10.1016/j.neo.2017.05.002

Choi, W., Ochoa, A., McConkey, D. J., Aine, M., Kim, W. Y., Real, F. X., et al. (2017). Genetic alterations in the molecular subtypes of bladder cancer: illustration in the cancer genome atlas dataset. *Eur. Urol.* 72, 354–365. doi: 10.1016/j.eururo.2017.03.010

Gao, H., Zheng, M., Sun, S., Wang, H., Yue, Z., Zhu, Y., et al. (2017). Chaperonin containing TCP1 subunit 5 is a tumor associated antigen of non-small cell lung cancer. *Oncotarget* 8, 64170–64179. doi: 10.18632/oncotarget.19369

Garaud, S., Buisseret, L., Solinas, C., Naveaux, C., Lodewyckx, J. N., Boisson, A., et al. (2019). Tumor infiltrating B-cells signal functional humoral immune responses in breast cancer. *JCI Insight* 5:e129641. doi: 10.1172/jci.insight.129641

Gestaut, D., Roh, S. H., Ma, B., Pintilie, G., Joachimiak, L. A., Leitner, A., et al. (2019). The chaperonin TRiC/CCT associates with prefoldin through a conserved electrostatic interface essential for cellular proteostasis. *Cell* 177, 751–765.e15. doi: 10.1016/j.cell.2019.03.012

Guest, S. T., Kratche, Z. R., Bollig-Fischer, A., Haddad, R., and Ethier, S. P. (2015). Two members of the TRiC chaperonin complex, CCT2 and TCP1 are essential for survival of breast cancer cells and are linked to driving oncogenes. *Exp. Cell Res.* 332, 223–235. doi: 10.1016/j.yexcr.2015.02.005

Hirsch, F. R., Scagliotti, G. V., Mulshine, J. L., Kwon, R., Curran, W. J. Jr., and Wu, Y. L. (2017). Lung cancer: current therapies and new targeted treatments. *Lancet* 389, 299–311. doi: 10.1016/s0140-6736(16)30958-8

Huang, X., Wang, X., Cheng, C., Cai, J., He, S., Wang, H., et al. (2014). Chaperonin containing TCP1, subunit 8 (CCT8) is upregulated in hepatocellular carcinoma and promotes HCC proliferation. *Apmis* 122, 1070–1079. doi: 10.1111/apm.12258

Jézéquel, P., Campone, M., Gouraud, W., Guérin-Charbonnel, C., Leux, C., Ricolleau, G., et al. (2012). bc-GenExMiner: an easy-to-use online platform for gene prognostic analyses in breast cancer. *Breast Cancer Res. Treat.* 131, 765–775. doi: 10.1007/s10549-011-1457-7

Kasembeli, M., Lau, W. C., Roh, S. H., Eckols, T. K., Frydman, J., Chiu, W., et al. (2014). Modulation of STAT3 folding and function by TRiC/CCT chaperonin. *PLoS Biol.* 12:e1001844. doi: 10.1371/journal.pbio.1001844

Kubota, H., Hynes, G. M., Kerr, S. M., and Willison, K. R. (1997). Tissue-specific subunit of the mouse cytosolic chaperonin-containing TCP-1. *FEBS Lett*. 402, 53–56. doi: 10.1016/s0014-5793(96)01501-3

Li, B., Severson, E., Pignon, J. C., Zhao, H., Li, T., Novak, J., et al. (2016). Comprehensive analyses of tumor immunity: implications for cancer immunotherapy. *Genome Biol*. 17:174. doi: 10.1186/s13059-016-1028-7

Li, T., Fan, J., Wang, B., Traugh, N., Chen, Q., Liu, J. S., et al. (2017). TIMER: a web server for comprehensive analysis of tumor-infiltrating immune cells. *Cancer Res*. 77, e108–e110. doi: 10.1158/0008-5472.Can-17-0307

Lin, Y. F., Tsai, W. P., Liu, H. G., and Liang, P. H. (2009). Intracellular beta-tubulin/chaperonin containing TCP1-beta complex serves as a novel chemotherapeutic target against drug-resistant tumors. *Cancer Res*. 69, 6879–6888. doi: 10.1158/0008-5472.Can-08-4700

Liu, Y., Zhang, X., Lin, J., Chen, Y., Qiao, Y., Guo, S., et al. (2019). CCT3 acts upstream of YAP and TFCP2 as a potential target and tumour biomarker in liver cancer. *Cell Death Dis*. 10:644. doi: 10.1038/s41419-019-1894-5

Liu, Y. J., Chang, Y. J., Kuo, Y. T., and Liang, P. H. (2020). Targeting β-tubulin/CCT-β complex induces apoptosis and suppresses migration and invasion of highly metastatic lung adenocarcinoma. *Carcinogenesis* 41, 699–710. doi: 10.1093/carcin/bgz137

Liu, Y. J., Kumar, V., Lin, Y. F., and Liang, P. H. (2017). Disrupting CCT-β:β-tubulin selectively kills CCT-β overexpressed cancer cells through MAPKs activation. *Cell Death Dis*. 8:e3052. doi: 10.1038/cddis.2017.425

Park, S. H., Jeong, S., Kim, B. R., Jeong, Y. A., Kim, J. L., Na, Y. J., et al. (2020). Activating CCT2 triggers Gli-1 activation during hypoxic condition in colorectal cancer. *Oncogene* 39, 136–150. doi: 10.1038/s41388-019-0972-6

Qian, E. N., Han, S. Y., Ding, S. Z., and Lv, X. (2016). Expression and diagnostic value of CCT3 and IQGAP3 in hepatocellular carcinoma. *Cancer Cell Int*. 16:55. doi: 10.1186/s12935-016-0332-3

Qiu, X., He, X., Huang, Q., Liu, X., Sun, G., Guo, J., et al. (2015). Overexpression of CCT8 and its significance for tumor cell proliferation, migration and invasion in glioma. *Pathol. Res. Pract*. 211, 717–725. doi: 10.1016/j.prp.2015.04.012

Sabado, R. L., Balan, S., and Bhardwaj, N. (2017). Dendritic cell-based immunotherapy. *Cell Res*. 27, 74–95. doi: 10.1038/cr.2016.157

Shen, Y., Peng, X., and Shen, C. (2020). Identification and validation of immune-related lncRNA prognostic signature for breast cancer. *Genomics* 112, 2640–2646. doi: 10.1016/j.ygeno.2020.02.015

Shi, X., Cheng, S., and Wang, W. (2018). Suppression of CCT3 inhibits malignant proliferation of human papillary thyroid carcinoma cell. *Oncol. Lett*. 15, 9202–9208. doi: 10.3892/ol.2018.8496

Shimon, L., Hynes, G. M., McCormack, E. A., Willison, K. R., and Horovitz, A. (2008). ATP-induced allostery in the eukaryotic chaperonin CCT is abolished by the mutation G345D in CCT4 that renders yeast temperature-sensitive for growth. *J. Mol. Biol*. 377, 469–477. doi: 10.1016/j.jmb.2008.01.011

Showalter, A. E., Martini, A. C., Nierenberg, D., Hosang, K., Fahmi, N. A., and Gopalan, P. (2020). Investigating chaperonin-containing TCP-1 subunit 2 as an essential component of the chaperonin complex for tumorigenesis. *Sci. Rep*. 10:798. doi: 10.1038/s41598-020-57602-w

Siegel, R. L., Miller, K. D., and Jemal, A. (2020). Cancer statistics, 2020. *CA Cancer J. Clin*. 70, 7–30. doi: 10.3322/caac.21590

Tang, Z., Li, C., Kang, B., Gao, G., Li, C., and Zhang, Z. (2017). GEPIA: a web server for cancer and normal gene expression profiling and interactive analyses. *Nucleic Acids Res*. 45, W98–W102. doi: 10.1093/nar/gkx247

Tano, K., Mizuno, R., Okada, T., Rakwal, R., Shibato, J., Masuo, Y., et al. (2010). MALAT-1 enhances cell motility of lung adenocarcinoma cells by influencing the expression of motility-related genes. *FEBS Lett*. 584, 4575–4580. doi: 10.1016/j.febslet.2010.10.008

Thomas, L. E., Winston, J., Rad, E., Mort, M., Dodd, K. M., Tee, A. R., et al. (2015). Evaluation of copy number variation and gene expression in neurofibromatosis type-1-associated malignant peripheral nerve sheath tumours. *Hum. Genomics* 9:3. doi: 10.1186/s40246-015-0025-3

Trinidad, A. G., Muller, P. A., Cuellar, J., Klejnot, M., Nobis, M., Valpuesta, J. M., et al. (2013). Interaction of p53 with the CCT complex promotes protein folding and wild-type p53 activity. *Mol. Cell* 50, 805–817. doi: 10.1016/j.molcel.2013.05.002

Warde-Farley, D., Donaldson, S. L., Comes, O., Zuberi, K., Badrawi, R., Chao, P., et al. (2010). The GeneMANIA prediction server: biological network integration for gene prioritization and predicting gene function. *Nucleic Acids Res*. 38, W214–W220. doi: 10.1093/nar/gkq537

Wu, P., Heins, Z. J., Muller, J. T., Katsnelson, L., de Bruijn, I., Abeshouse, A. A., et al. (2019). Integration and analysis of CPTAC proteomics data in the context of cancer genomics in the cBioPortal. *Mol. Cell. Proteomics* 18, 1893–1898. doi: 10.1074/mcp.TIR119.001673

Xu, G., Bu, S., Wang, X., Zhang, H., and Ge, H. (2020). Suppression of CCT3 inhibits the proliferation and migration in breast cancer cells. *Cancer Cell Int*. 20:218. doi: 10.1186/s12935-020-01314-8

Yang, X., Ren, H., Shao, Y., Sun, Y., Zhang, L., Li, H., et al. (2018). Chaperonin-containing T-complex protein 1 subunit 8 promotes cell migration and invasion in human esophageal squamous cell carcinoma by regulating α-actin and β-tubulin expression. *Int. J. Oncol*. 52, 2021–2030. doi: 10.3892/ijo.2018.4335

Yin, H., Miao, X., Wu, Y., Wei, Y., Zong, G., Yang, S., et al. (2016). The role of the chaperonin containing t-complex polypeptide 1, subunit 8 (CCT8) in B-cell non-Hodgkin's lymphoma. *Leuk. Res*. 45, 59–67. doi: 10.1016/j.leukres.2016.04.010

Ying, Z., Tian, H., Li, Y., Lian, R., Li, W., Wu, S., et al. (2017). CCT6A suppresses SMAD2 and promotes prometastatic TGF-β signaling. *J. Clin. Invest*. 127, 1725–1740. doi: 10.1172/jci90439

Zalocusky, K. A., Kan, M. J., Hu, Z., Dunn, P., Thomson, E., Wiser, J., et al. (2018). The 10,000 immunomes project: building a resource for human immunology. *Cell Rep*. 25, 513–522.e3. doi: 10.1016/j.celrep.2018.09.021

Zhang, Y., Wang, Y., Wei, Y., Wu, J., Zhang, P., Shen, S., et al. (2016). Molecular chaperone CCT3 supports proper mitotic progression and cell proliferation in hepatocellular carcinoma cells. *Cancer Lett*. 372, 101–109. doi: 10.1016/j.canlet.2015.12.029

Zheng, Y., Walsh, T., Gulsuner, S., Casadei, S., Lee, M. K., Ogundiran, T. O., et al. (2018). Inherited breast cancer in nigerian women. *J. Clin. Oncol*. 36, 2820–2825. doi: 10.1200/JCO.2018.78.3977

Zhou, Y., Zhou, B., Pache, L., Chang, M., Khodabakhshi, A. H., Tanaseichuk, O., et al. (2019). Metascape provides a biologist-oriented resource for the analysis of systems-level datasets. *Nat. Commun*. 10:1523. doi: 10.1038/s41467-019-09234-6

Conflict of Interest: The authors declare that the research was conducted in the absence of any commercial or financial relationships that could be construed as a potential conflict of interest.

frontiers in Cell and Developmental Biology

ORIGINAL RESEARCH
published: 25 March 2021
doi: 10.3389/fcell.2021.638174

3-Deoxysappanchalcone Inhibits Skin Cancer Proliferation by Regulating T-Lymphokine-Activated Killer Cell-Originated Protein Kinase *in vitro* and *in vivo*

Xiaorong Fu[1,2†], Ran Zhao[1,2†], Goo Yoon[3†], Jung-Hyun Shim[2,3], Bu Young Choi[4], Fanxiang Yin[1,2,5], Beibei Xu[1,2], Kyle Vaughn Laster[2], Kangdong Liu[1,2], Zigang Dong[1,2] and Mee-Hyun Lee[1,2,6*]*

[1] Department of Pathophysiology, School of Basic Medical Sciences, College of Medicine, Zhengzhou University, Zhengzhou, China, [2] China-US (Henan) Hormel Cancer Institute, Zhengzhou, China, [3] Department of Pharmacy, College of Pharmacy, Mokpo National University, Muan, South Korea, [4] Department of Pharmaceutical Science and Engineering, School of Convergence Bioscience and Technology, Seowon University, Cheongju, South Korea, [5] Department of Translational Medicine Center, The First Affiliated Hospital of Zhengzhou University, Zhengzhou, China, [6] College of Korean Medicine, Dongshin University, Naju, South Korea

OPEN ACCESS

Edited by:
Lorenzo Gerratana,
University of Udine, Italy

Reviewed by:
Feng Zhu,
Huazhong University of Science and Technology, China
Cheoljung Lee,
Catholic University of Korea, South Korea

***Correspondence:**
Zigang Dong
zgdong@hci-cn.org
Mee-Hyun Lee
mhyun_lee@hanmail.net

[†] These authors have contributed equally to this work

Specialty section:
This article was submitted to Molecular and Cellular Oncology, a section of the journal Frontiers in Cell and Developmental Biology

Received: 05 December 2020
Accepted: 16 February 2021
Published: 25 March 2021

Citation:
Fu X, Zhao R, Yoon G, Shim J-H, Choi BY, Yin F, Xu B, Laster KV, Liu K, Dong Z and Lee M-H (2021) 3-Deoxysappanchalcone Inhibits Skin Cancer Proliferation by Regulating T-Lymphokine-Activated Killer Cell-Originated Protein Kinase in vitro and in vivo. Front. Cell Dev. Biol. 9:638174. doi: 10.3389/fcell.2021.638174

Background: Skin cancer is one of the most commonly diagnosed cancers worldwide. The 5-year survival rate of the most aggressive late-stage skin cancer ranges between 20 and 30%. Thus, the discovery and investigation of novel target therapeutic agents that can effectively treat skin cancer is of the utmost importance. The T-lymphokine-activated killer cell-originated protein kinase (TOPK), which belongs to the serine-threonine kinase class of the mitogen-activated protein kinase kinase (MAPKK) family, is highly expressed and activated in skin cancer. The present study investigates the role of 3-deoxysappanchalcone (3-DSC), a plant-derived functional TOPK inhibitor, in suppressing skin cancer cell growth.

Purpose: In the context of skin cancer prevention and therapy, we clarify the effect and mechanism of 3-DSC on different types of skin cancer and solar-simulated light (SSL)-induced skin hyperplasia.

Methods: In an *in vitro* study, western blotting and *in vitro* kinase assays were utilized to determine the protein expression of TOPK and its activity, respectively. Pull-down assay with 3-DSC and TOPK (wild-type and T42A/N172 mutation) was performed to confirm the direct interaction between T42A/N172 amino acid sites of TOPK and 3-DSC. Cell proliferation and anchorage-independent cell growth assays were utilized to determine the effect of 3-DSC on cell growth. In an *in vivo* study, the thickness of skin and tumor size were measured in the acute SSL-induced inflammation mouse model or SK-MEL-2 cell-derived xenografts mouse model treated with 3-DSC. Immunohistochemistry analysis of tumors isolated from SK-MEL-2 cell-derived xenografts was performed to determine whether cell-based results observed upon 3-DSC treatment could be recapitulated *in vivo*.

Results: 3-DSC is able to inhibit cell proliferation in skin cancer cells in an anchorage-dependent and anchorage-independent manner by regulation of TOPK and its related signaling pathway *in vitro*. We also found that application of 3-DSC reduced acute SSL-induced murine skin hyperplasia. Additionally, we observed that 3-DSC decreased SK-MEL-2 cell-derived xenograft tumor growth through attenuating phosphorylation of TOPK and its downstream effectors including ERK, RSK, and c-Jun.

Conclusions: Our results suggest that 3-DSC may function in a chemopreventive and chemotherapeutic capacity by protecting against UV-induced skin hyperplasia and inhibiting tumor cell growth by attenuating TOPK signaling, respectively.

Keywords: skin cancer, solar sinulated light, T-LAK cell-originated protein kinase, 3-deoxysappanchalcone, cancer growth, skin hyperplasia

INTRODUCTION

Skin cancer is one of the most commonly diagnosed cancers worldwide and poses a huge financial burden to society (Linares et al., 2015). Skin cancer can be classified as basal cell carcinoma (BCC), squamous cell carcinoma (SCC), or melanoma. Excess solar ultraviolet (SUV) radiation is the dominant risk factor for skin cancer (Ratushny et al., 2012; Gao et al., 2017). It has been suggested that acute solar-simulated light (SSL) irradiation enhances T-lymphokine-activated killer cell-originated protein kinase (TOPK) expression and induces inflammation in SKH1 mice dorsal skin (Xue et al., 2017; Roh et al., 2018). Therefore, targeting TOPK may be a promising strategy for skin cancer prevention and treatment (Gao et al., 2017; Roh et al., 2018).

TOPK, a serine-threonine kinase, is a member of the mitogen-activated protein kinase kinase (MAPKK) family (Dougherty et al., 2005) and exists at the same hierarchical level of MEK in the MAPK signaling axis. Mutations in the MAPK signaling cascade are pronounced in many types of cancer (Braicu et al., 2019). Previous research has established that TOPK can induce cancer cell proliferation and is highly expressed in numerous types of cancer including lung adenocarcinoma (Lei et al., 2013), ovarian cancer (Ikeda et al., 2016), gastric carcinoma (Ohashi et al., 2017), breast cancer (Park et al., 2006), nasopharyngeal carcinoma (Wang et al., 2016), and colon cancer (Zhu et al., 2007). TOPK regulates a wide range of tumor processes such as tumor growth, invasion (Lee et al., 2020), development (Hu et al., 2010), and resistance (Herbert et al., 2018). As a MAPKK member in MAPK signal pathway, TOPK inhibitors may be utilized to treat MEK-resistant patients or in the form of target combination therapy. Until now, there have been no clinical trials to investigate the therapeutic potential of TOPK inhibitors. As such, active investigation of TOPK inhibitors may provide a means of reducing cancer growth across many different types of cancer. To date, the efficacy of several TOPK inhibitors have been investigated *in vitro* and *in vivo*. However, variable degrees of cytotoxicity have been observed, which may clinically translate to diminished patient quality of life. Therefore, there is an unmet need for TOPK inhibitors with minimal toxicity.

In the present manuscript, we characterize the role 3-deoxysappanchalcone (3-DSC), a natural compound derived from *Caesalpinia sappan* L., which plays as a novel TOPK inhibitor in skin carcinogenesis and cancer. We report that 3-DSC effectively inhibited skin cancer cell growth by directly attenuating TOPK signaling *in vitro*. Additionally, an *in vivo* study showed that 3-DSC reduced SSL-induced skin hyperplasia and tumor growth in a SK-MEL-2 cell-derived xenograft mouse model. Our observations suggest that 3-DSC functions as an effective anti-cancer prophylactic and chemotherapeutic reagent that may be used to clinically treat skin cancer.

MATERIALS AND METHODS

Reagents

3-DSC (purity $\geq$ 95%, $C_{16}H_{14}O_4$, CAS No. 112408-67-0), a natural compound isolated from the plant of *Caesalpinia sappan* L. (Leguminosae), was purchased from ChemFaces (Wuhan, Hubei, China). Active TOPK kinase (100 ng, Cat#T14-10G), kinase dilution buffer (Cat#K01-09-20), and 10 mM ATP (Cat#A50-09) were purchased from SignalChem Biotech Inc. (Richmond, BC, Canada). Recombinant human myelin basic protein (MBP) (Cat#M42-51N) was purchased from Sigma-Aldrich (St. Louis, MO, United States). Matrigel was purchased from Corning (Tewksbury, MA, United States). Protease inhibitor cocktail (100X, HY-K0010) and phosphatase inhibitor cocktail II (100X, HY-K0022) were purchased from MedChemExpress (Monmouth Junction, NJ, United States). Antibodies to detect rabbit anti-cleaved PARP (1:1,000, Cat#5625), rabbit anti-PARP (1:1,000, Cat#9542), rabbit anti-caspase 3 (1:1,000, Cat#9662), rabbit anti-caspase 7 (1:1,000, Cat#9492), rabbit anti-cleaved caspase 3 (1:1,000,Cat#9664), rabbit anti-cleaved caspase 7 (Asp 198, 1:1,000, Cat#8438), rabbit anti-cyclin B1 (1:1,000, Cat#12231), rabbit anti-phosphorylated ERK (Thr202/Tyr204) (1:1,000, Cat#4370), rabbit anti-phosphorylated TOPK (Thr9) (1:1,000, Cat#4941), rabbit anti-phosphorylated c-Jun (Ser63) (1:1,000, Cat#2361), rabbit anti-phosphorylated p90RSK (Ser380) (1:1,000, Cat#11989), rabbit anti-ERK1/2 (p44/p42 MAPK) (1:1,000, Cat#4695), rabbit anti-TOPK (1:1,000, Cat#4942), rabbit anti-c-Jun (1:1,000, Cat#9165), and rabbit anti-RSK2 (1:1,000, Cat#5528) were purchased from Cell Signaling Technology (Beverly, MA, United States). Antibodies to detect mouse anti-phosphoserine (1:1,000, Cat#ab9332), rabbit anti-phosphothreonine (1:1,000,

Cat#ab9337), and rabbit anti-Ki67 (1:200, Cat#ab16667) were purchased from Abcam Inc. (Cambridge, United Kingdom). Xfect Transfection Reagent was purchased from TaKaRa Biomedical Technology Beijing Co., Ltd. (Beijing, China).

Cell Lines and Cell Culture

Skin normal cell JB6 CI 41-5a (JB6); HaCaT cells; Normal Human Dermal Fibroblasts (NHDF); and skin cancer cell lines SK-MEL-2, SK-MEL-28, A375, and A431 were purchased from American Type Culture Collection (ATCC, Manassas, VA, United States). Cells were cultured in Minimum Essential Medium (MEM)/Earle's Balanced Salt Solution (EBSS) (SK-MEL-2), MEM (SK-MEL-28), and Dulbecco's Modified Eagle's medium (DMEM) (A375 and A431) supplemented with 10% fetal bovine serum and penicillin/streptomycin (1×). Normal skin cell line JB6, HaCaT, and NHDF were cultured in MEM and DMEM medium supplemented with 5 or 10% fetal bovine serum and penicillin/streptomycin (1×). All the cells used in this study were authenticated through STR profiling and maintained at 37℃ in a 5% CO_2 humidified incubator.

Western Blot Analysis

Cells were rinsed with phosphate-buffered saline (PBS) before being scraped and lysed in radioimmunoprecipitation assay (RIPA) buffer supplemented with protease inhibitor cocktail and phosphatase inhibitor cocktail II. After centrifugation at 14,000 rpm for 15 min, the supernatant fractions were harvested as the total cellular protein extracts. The protein concentration was determined using a protein assay kit (Solarbio Life Science, Beijing, China). The total cellular protein extracts were separated by sodium dodecyl sulfate polyacrylamide gel electrophoresis (SDS-PAGE) and transferred to polyvinylidene fluoride membranes in 20 mM Tris–HCl (pH 8.0), 150 mM glycine, and 20% (*v*/*v*) methanol. Membranes were blocked with 5% nonfat dry milk in 1xPBS containing 0.05% Tween-20 (PBS-T) and incubated with antibodies against p-TOPK, TOPK, p-ERK1/2, ERK1/2, p-RSK2, RSK2, p-c-Jun, total c-Jun, PARP, caspase 3, caspase 7, cleaved PARP, cleaved caspase 3, cleaved caspase 7, or β-actin at 4℃, overnight. Blots were washed three times with 1xPBS-T buffer, followed by incubation with the appropriate horseradish peroxidase-linked immunoglobulin G (IgG). The specific proteins in the blots were visualized using an enhanced chemiluminescence detection reagent and the Amersham Imager 600 (GE Healthcare life Science, Pittsburgh, PA, United States).

The Cancer Genome Atlas Database Analysis

Gene expression and patient clinical data of The Cancer Genome Atlas-Skin Cutaneous Melanoma (TCGA-SKCM) cohort was downloaded using TCGA GDAC Firehose [Broad Institute TCGA Data Analysis Center (2016): Firehose 2016/01/28, Broad Institute of MIT and Harvard; doi: 10.7908/C11G0KM9). RNA-seq data detailing TOPK expression in normal skin samples unexposed to sun were downloaded from the GTEx database. RSEM values were transformed to transcript per million (TPM) values by multiplying scaled estimates by 1E7. TOPK gene expression was plotted in TPM units with respect to features such as tumor stage, patient age, race, weight, etc., by cross-querying clinical data. Statistical significance ($p < 0.05$) of gene expression was assessed using a Wilcoxon rank-sum test. Whisker charts illustrating the median, upper, and lower quantiles of TPM expression values were generated using Mathematica 12.

In vitro Kinase Assay

Active TOPK kinase (100 ng), recombinant human myelin basic protein (MBP substrate, 200 ng), kinase assay buffer, and 100 μM ATP were incubated at 30℃ for 30 min in the presence or absence of 3-DSC. To stop the reaction, 5 μl of 6μ loading buffer was then added. The protein mixture was loaded into a 12% SDS-PAGE gel and run as a western blot to quantify p-serine/threonine (1:1,000) expression.

In vitro Pull-Down Assay

Skin cancer cells, A431, A375, SK-MEL-2, and SK-MEL-28, were cultured in complete growth medium until an optimal confluence of 70% was obtained. Cells were rinsed with PBS before being scraped and lysed in RIPA buffer. The individual cell lysates were incubated with Sepharose 4B beads or 3-DSC-Sepharose 4B beads in reaction buffer (50 mM Tris–HCl, pH 7.5, 5 mM EDTA, 150 mM NaCl, 1 mM DTT, 0.01% NP-40, 0.2 mM PMSF, and 20× protease inhibitor). After incubation with gentle rocking overnight at 4°C, the beads were washed three times with washing buffer (50 mM Tris–HCl, pH 7.5, 5 mM EDTA, 150 mM NaCl, 1 mM DTT, 0.01% NP-40, and 0.2 mM PMSF), and binding was visualized by western blotting against TOPK antibody. For the ATP competitive binding assay, active TOPK was incubated with 3-DSC-Sepharose 4B beads and vehicle, 10, 100, or 1,000 μM ATP, following the procedure described above for the binding assay.

Construction and Expression of TOPK Wild Type and Mutants

pcDNA4.1-HisC-TOPK encoding recombinant plasmid was used to construct TOPK-T42A by site mutagenesis with Hieff MutTM Site-Directed Mutagenesis Kit (Yeasen Biotech Co., Ltd, Shanghai, China). The forward primer of TOPK T42A used was as follows: 5′-TTGGCTTTGGTGCTGGGGTA-3′. The reverse primer of TOPK T42A used was as follows: 5′-GCAAGATGGTTATGAAGGCAGG-3′. Annealing temperature was tested to be 57°C. Then, TOPK-T42A or *pcDNA4.1-HisC-TOPK* was applied to get TOPK N172A + T42A or TOPK N172A by overlap PCR assay. The primer sequences here were as follows:

TOPK-N172A-forward-1: 5′-TTGAATTCATGGAAGGGATCAGTAATT TCAAG-3′;
TOPK-N172A-reverse-1: 5′- AAATCGCCTTTAATTACAACAGCTGAAGAC-3′;
TOPK-N172A-forward-2: 5′-CTTCATGGAGACATAAAGTCTTCAGCTGTTGT-3′;
TOPK-N172A-reverse-2: 5′-TTGCGGCCGCCTAGACATCTGTTTCCAGAGC-3′.

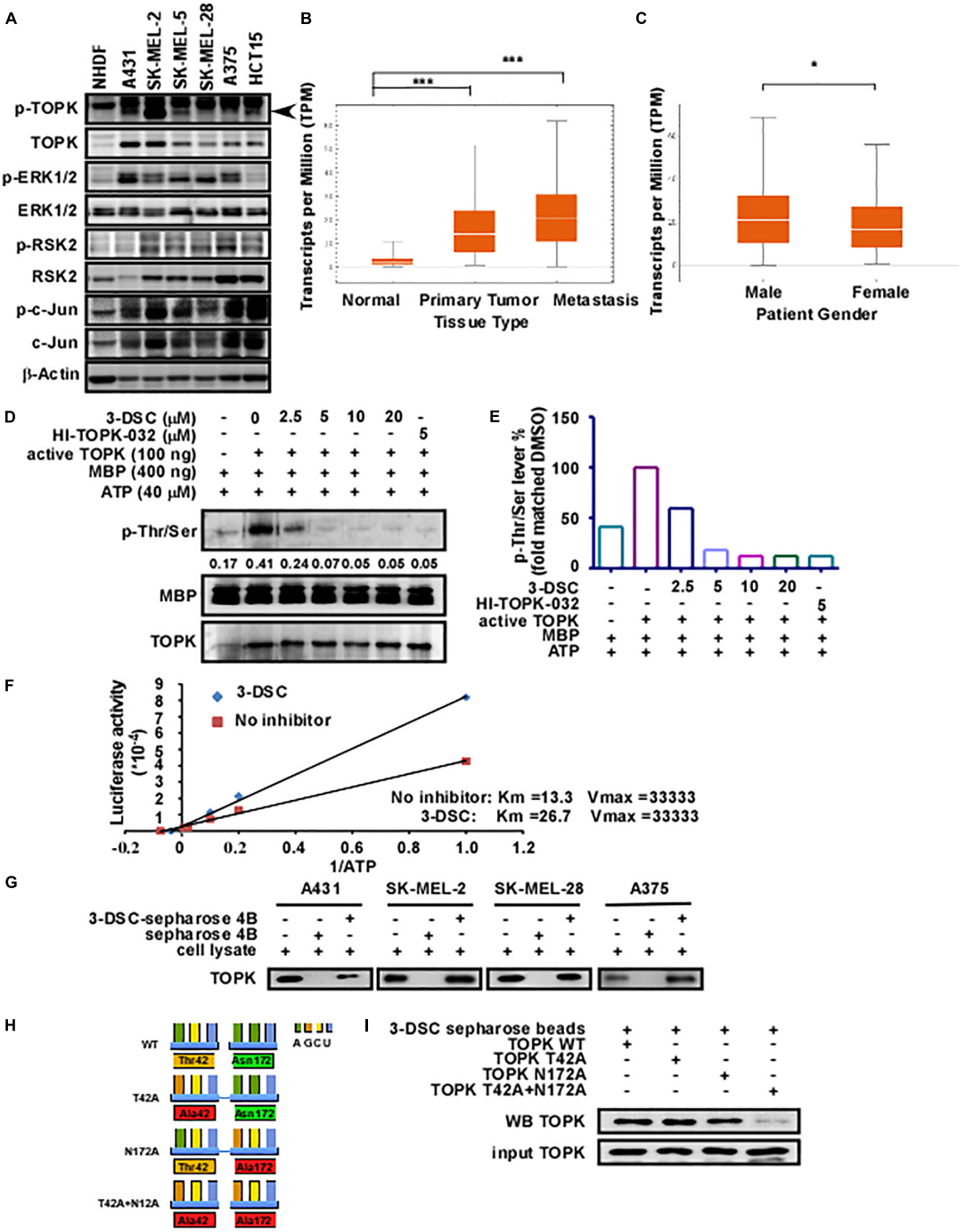

FIGURE 1 | 3-Deoxysappanchalcone (3-DSC) inhibits T-LAK cell-originated protein kinase (TOPK) kinase activity by binding to Thr42 and Asn172. **(A)** The protein expression levels of TOPK and its downstream protein effectors in Normal Human Dermal Fibroblast (NHDF) and skin cancer cell lines (A431, SK-MEL2, SK-MEL-28, and A375) and colon cancer cell line HCT15 (positive control). **(B,C)** The expression levels of TOPK dependent on the tumor type (primary melanoma patients, metastatic melanoma patient, and normal person) or gender from The Cancer Genome Atlas-Skin Cutaneous Melanoma (TCGA-SKCM) cohort database. TOPK transcript expression was analyzed according to tissue type according to transcript per million (TPM) units. **(D)** Effect of 3-DSC on TOPK phosphorylation. Kinase assay was performed with active TOPK (100 ng), 3-DSC (2.5, 5, 10, or 20 μM), HI-TOPK-032 (5 μM), myelin basic protein (MBP) (400 ng), and ATP (40 μM). MBP is the substrate of TOPK kinase; p-Thr/Ser levels are an indicator of TOPK activity. The band intensity of p-Thr/Ser is significantly reduced when the assay was performed with inclusion of 2.5 μM 3-DSC. **(E)** Band quantification results of **(D)**. **(F)** Kinetic analysis of 3-DSC whether competing ATP with TOPK substrate. Km and Vm values of TOPK enzyme incubated with or without 3-DSC. **(G)** Binding affinity of 3-DSC to TOPK was assessed in four skin cancer cells. 3-DSC-Sepharose 4B or Sepharose 4B were incubated with cell lysates. Protein was then eluted from the beads and separated by SDS-PAGE. **(H)** Diagram illustrating the mutation of residues previously predicted to be important in facilitating the interaction between TOPK and 3-DSC. TOPK was mutated at the T42A, N172A, and T42A residues based upon computer docking analysis. **(I)** *In vitro* pull-down assay with TOPK WT, TOPK T42A, TOPK N172A, and TOPK T42A + N172A. Double mutation significantly attenuated binding of 3-DSC with TOPK. $^{*}p < 0.05$, $^{***}p < 0.001$.

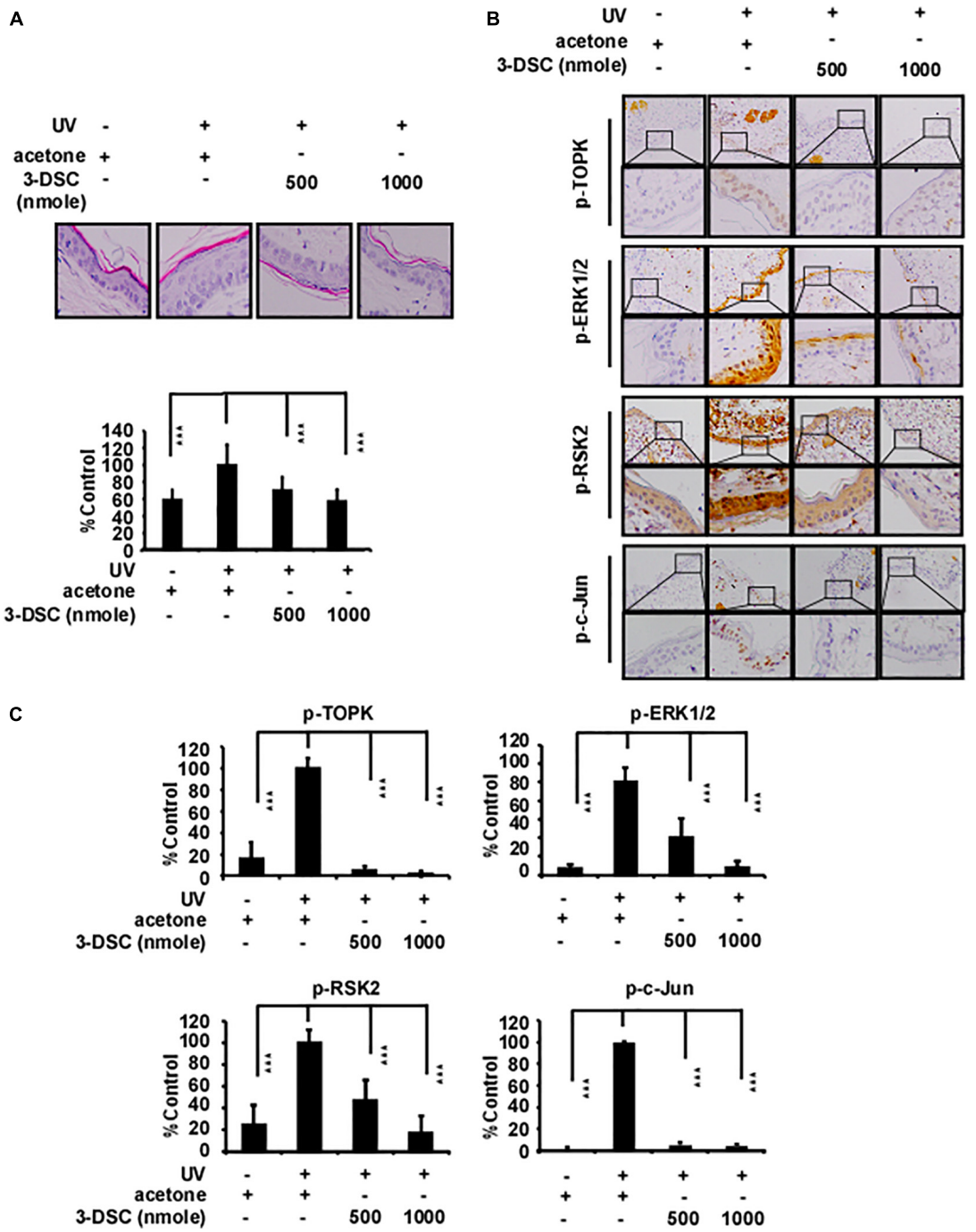

FIGURE 2 | 3-DSC decreases skin epidermal thickening caused by solar ultraviolet (SUV) exposure by targeting TOPK. **(A)** Representative hematoxylin and eosin (H&E) staining results of mice dorsal skin treated with or without 3-DSC prior to SUV exposure. Each group consisted of 8–10 mice. Tissue thickness was measured using a microscope ruler. Data are shown as mean ± SD values. **(B)** Protein expressions of p-TOPK, p-ERK, p-RSK, and p-c-Jun were detected by immunohistochemical (IHC) analysis. **(C)** Quantification of the IHC results in panel **(B)**. Data are shown as mean ± SD values. ***$p < 0.001$.

Annealing temperature here was 54°C. The recombinant plasmids were transformed to *E. coli* DH5μ and colonies were sent to analyze the sequences. TOPK-T42A, TOPK-N172A, and TOPK-T42A-N172A plasmids were extracted by AxyPrep^{TM} Plasmid Midiprep Kit (Corning, Tewksbury, MA, United States). TOPK wild-type or mutants were transfected to HEK-293T cells by Xfect^{TM} Transfection Reagent, and cells were rinsed with PBS before being scraped and lysed in RIPA buffer and incubated with antibodies against p-TOPK, TOPK, p-ERK1/2, ERK1/2, p-RSK2, RSK2, p-c-Jun, total c-Jun, or β-actin.

Acute SSL Exposure to 3-DSC-Treated Mouse

Five–six weeks SKH1 male mice were maintained under specific pathogen-free (SPF) conditions. Mice with similar body weight (18–20 g) were divided into four groups as follows: (1) acetone (vehicle), (2) acetone + SSL, (3) 500 nmol 3-DSC + SSL, and (4) 1,000 nmol 3-DSC + SSL. Acetone or 3-DSC were topically applied onto the dorsal skin of SKH1 mice. One hour later, 149 kJ/m^2 UVA and 7.2 kJ/m^2 SSL were applied to the dorsal skin of the mice. After treatment, 24 h later, the irradiated dorsal skin tissue (about 2 cm^2) was harvested. Hematoxylin and eosin (H&E) staining and immunohistochemistry were performed on the tissues using p-PBK/TOPK (Thr9), p-ERK1/2 (Thr202/Tyr204), p-c-Jun (Ser63), and p-p90RSK (Ser380) antibodies.

Cell Proliferation Assay

The cells (A431, A375, SK-MEL-2, and SK-MEL-28) were seeded (2×10^3 cells per well for) in 96-well plates and incubated for 24 h and then treated with different doses of 3-DSC or vehicle. After incubation for 24, 48, 72, or 96 h, cell proliferation was measured by MTT assay.

Anchorage-Independent Cell Transformation Assay

The normal cells (JB6 CI 41-5a or HaCaT) or the skin cancer cells (A431, A375, SK-MEL-2, and SK-MEL-28) suspended in complete Basal Medium Eagle growth medium were seeded (8,000 cells/well) into 0.3% agar with or without epidermal growth factor (EGF) (10 ng/ml) and 3-DSC (0, 5, 10, and 20 μM) over a base layer of 0.6% agar containing the same concentration of EGF and 3-DSC. The cultures were maintained at 37°C in a 5% CO_2 incubator for 3 weeks. Colonies were visualized using an inverted microscope and counted using the Image−Pro Plus software (v.6) program (Media Cybernetics, Rockville, MD, United States).

Knock-Down of TOPK Expression

Each viral vector and packaging vectors (pMD2G, psPAX2, and shTOPK#1 and 2) were transfected using the Xfect Transfection Reagent into Lenti-X-293T cells. The viral particles were harvested by filtration using a 0.22-μm filter and then stored at −20°C. The cultured SK-MEL-2 and A375 skin cancer cells were infected with virus particles and 8 μg/ml polybrene (Millipore, Billerica, MA, United States, Cat#TR-1003) for 24 h. Then, the cells were selected with puromycin for 24 h, and the selected cells were used for anchorage-independent cell growth assay and western blot analysis.

Cell Cycle and Apoptosis Analysis

The cells (2×10^5 cells) were seeded in 60-mm dishes and treated with 0, 5, 10, or 20 μM 3-DSC for 48 h. For cell cycle analysis, the cells were fixed in 70% ethanol and stored at −20°C for 24 h. After staining with annexin-V for apoptosis or propidium iodide for cell cycle assessment, the cells were analyzed using a BD FACSCalibur Flow Cytometer (BD Biosciences, San Jose, CA, United States).

Cell-Derived Xenograft Mouse Model

All animal experiments were approved by the Ethics Committee of China-US (Henan) Hormel Cancer Institute. Nu/Nu mice (5–6 weeks old) were maintained under standard SPF mice room. We injected 5×10^6 SK-MEL-2 cells per mouse into near the right hind leg for inducing cell-derived xenograft tumors. After 1 week, the cell-derived xenograft (CDX) tumor's average size growth was measured to 100 mm^3, and the tumors were randomly separated into three groups (vehicle, 10, or 20 mg/kg; 10 mice each group). Then mice were treated with 3-DSC (10 or 20 mg/kg) or vehicle by intraperitoneal injection every day throughout the whole experiment. Mice were euthanized after 43 days; the tumor, blood, spleen, and the liver were collected.

Immunohistochemical Analysis

Tumors were collected from the mice and fixed, and paraffin-embedded sections (3 μm) were prepared for hematoxylin and eosin (H&E) staining and immunohistochemical (IHC) analysis. After antigen unmasking, the sections were blocked with 5% goat serum and incubated at 4°C overnight with antibodies Ki-67 (1:200), p-TOPK (1:200), p-ERK1/2 (1:100), p-RSK (1:100), and p-c-Jun (1:100). After incubation with a rabbit secondary antibody, DAB (3,3-diaminobenzidine) staining was used following the manufacturer's instructions to visualize the protein targets. Sectioned tissues were counterstained with hematoxylin, dehydrated through a graded series of alcohol into xylene, and mounted under glass coverslips. Images were obtained using Olympus Imaging BX43 (Southborough, MA, United States). The fluorescence intensity was quantified using Image-Pro Plus software (version 6.0).

Statistical Analysis

All other quantitative results are expressed as mean values ± SD. Data was analyzed by one-way ANOVA or Student's t test. A value of $p < 0.05$, $p < 0.001$ was indicated as "*", "***" for statistical significance.

RESULTS

3-DSC Inhibited TOPK Kinase Activity by Binding at the Sites of Thr42 and Asn172

PBK/TOPK is highly expressed in several types of cancer including lung adenocarcinoma (Xiao et al., 2019), ovarian cancer (Ikeda et al., 2016), gastric carcinoma (Ohashi et al., 2017), breast cancer (Park et al., 2006), nasopharyngeal carcinoma (Wang et al., 2016), and colon cancer (Zhu et al., 2007). To determine protein expression levels of TOPK in the context of skin cancer, we quantified protein expression in several skin cancer lines by western blot. Our results showed that TOPK was highly expressed in skin cancer cells relative to the normal human dermal fibroblast cell line, with the HCT-15 colon cancer cell line serving as a positive control (**Figure 1A**). We next queried the

SKCM cohort of the TCGA database to determine whether TOPK expression is associated with patient features and cancer staging. As RNA-seq data from normal skin samples is under-represented within the TCGA-SKCM cohort, we supplemented the TCGA data with RNA-seq data from the GTEx database detailing TOPK expression in normal skin that was unexposed to sunlight. The results confirm that TOPK is significantly over-expressed in primary and metastatic melanoma tumors compared to normal tissues. The results also show that TOPK expression is significantly increased in the case of metastatic melanoma compared to that in primary tumors (**Figure 1B**). Additionally, there appear to be gender-specific differences in the expression of TOPK in tumor tissues, with the TOPK profile in tumors derived from male patients exhibiting increased expression (**Figure 1C**). We observed that transcript expression does not appreciably change across race (**Supplementary Figure 1A**), age (**Supplementary Figure 1B**), and stage (**Supplementary Figure 1C**). Thus, based upon the aforementioned observations, we hypothesized that TOPK could play a role in the establishment or maintenance of skin cancer and that inhibition of TOPK may be useful in treating skin cancer. We recently reported that 3-DSC could suppress cell growth by directly binding to TOPK in colon cancer (Zhao et al., 2019). As TOPK is over-expressed in skin cancer, we sought to determine whether we could achieve comparable targeting efficacy in different types of skin cancer. Thus, we measured the effect of 3-DSC on TOPK activity by performing kinase assay using lysates derived from skin cancer cells (**Figures 1D,E**) and ATP competitive kinase assays with an increasing Km value from 13.3 to 26.7 (**Figure 1F**). The results indicate that 3-DSC inhibited TOPK activity in an ATP-competitive manner (**Figures 1D–F**). *In vitro* pull-down results showed that 3-DSC could directly bind with TOPK in different skin cancer cell lines (**Figure 1G**). Our previous work utilized a computer docking model to predict that 3-DSC binds with TOPK at the Thr42 and Asn172 residues. However, this prediction was not experimentally validated. Therefore, we established TOPK plasmid constructs harboring mutations at the predicted binding sites, denoted as TOPK T42A, TOPK N172A, and TOPK T42A + N172A (**Figure 1H**), to verify the computer model predictions by pull-down assay. Our results suggest that the prediction made by the computer docking model was valid, as the TOPK double mutant (T42A + N172A) greatly reduced binding affinity between 3-DSC and TOPK (**Figure 1I**).

3-DSC Decreased Skin Epidermal Thickness Caused by SSL Exposure

Actinic keratosis (AK) is characterized by accretive atypical keratinocytes, which results in abnormally thickened skin. AK is a precursor to cutaneous squamous cell carcinoma (cSCC) (Ratushny et al., 2012). Acute solar ultraviolet (SUV), a major contributor to the emergence of AK, increases TOPK protein levels in human skin tissue (Roh et al., 2018). Therefore, we investigated if 3-DSC can be utilized to prevent skin thickening through targeting TOPK. We applied two doses of 3-DSC onto SKH1 hairless mice before administering SSL and harvesting tissue for H&E staining and IHC analysis. We observed that application of 3-DSC decreased epidermal thickening in addition to decreasing TOPK, ERK, RSK, and c-Jun protein phosphorylation levels (**Figures 2A–C**). This finding strongly suggests that 3-DSC may possess chemoprevention potential with respect to SSL-induced damage by directly attenuating TOPK and its downstream effectors.

3-DSC Inhibited Skin Cancer Cell Proliferation

To determine the toxicity of 3-DSC, we performed an MTT assay over a concentration gradient of 3-DSC ranging between 0 and 20 μM using NHDF cells. The results indicated that 3-DSC showed minimal toxicity in NHDF cells at the tested concentrations (**Supplementary Figure 2A**). Based on the results of the toxicity assay, we then treated A431, SK-MEL-2, SK-MEL-28, and A375 skin cancer cell lines with 3-DSC over a range of 0–20 μM. After incubating for 24, 48, 72, or 96 h, cell viability was analyzed by microplate reader. The MTT results indicated that 3-DSC began to significantly inhibit skin cancer cell proliferation at the concentration of 10 and 20 μM in these four cell lines (**Figure 3A**). To provide additional evidence supporting the inhibitory potential of 3-DSC in skin cancer cells, we performed a soft agar assay using skin cancer cells (A431, SK-MEL-2, SK-MEL-28, and A375) to determine whether cell growth is affected upon treatment with 3-DSC (**Figure 3B**). Our results illustrated that 3-DSC was able to affect anchorage-independent cell growth in A431, SK-MEL-2, SK-MEL-28, and A375 cells starting at a concentration of 10 μM. EGF is known to activate MAPK/ERK signaling (Pan et al., 2018). Thus, we performed an anchorage-independent cell transformation assay to test whether treatment of 3-DSC could affect the colony formation potential of normal skin cells cultured in the presence of EGF. Our results indicated that 3-DSC was effective in significantly inhibiting EGF-induced cell transformation at a concentration of 5 μM (**Figures 3C,D**). To give more evidence of the role of TOPK in proliferation of skin cancer, we established TOPK knock-down skin cancer cells from the TOPK highly expressing SK-MEL-2 and A375 cell lines. The results indicated that TOPK knock-down inhibited anchorage-independent colonies growth of skin cancer cells. We confirmed that treatment of SK-MEL2 and A375 TOPK knock-down cells with 3-DSC failed to inhibit anchorage-independent cell growth (**Figures 3E,F**).

3-DSC Induced Skin Cancer Cell Cycle Arrest at G2/M Phase and Cell Apoptosis

The results above suggest that 3-DSC treatment induces cell growth inhibition *in vitro*. However, the inhibition that we observed could be due to cell cycle perturbations, induction of cell apoptosis, or a combination of both. Thus, we first sought to determine whether 3-DSC treatment affects cell cycle dynamics in skin cancer cells. We applied 3-DSC to skin cancer cells before performing cell flow cytometry and western blotting using G2/M phase marker cyclin B1 (**Figures 4A,B**). The results indicated that 3-DSC induced cell cycle arrest at G2/M phase at a concentration of 20 μM. The western blot results verified that protein levels of the G2/M phase marker, cyclin B1, decreased at 20 μM.

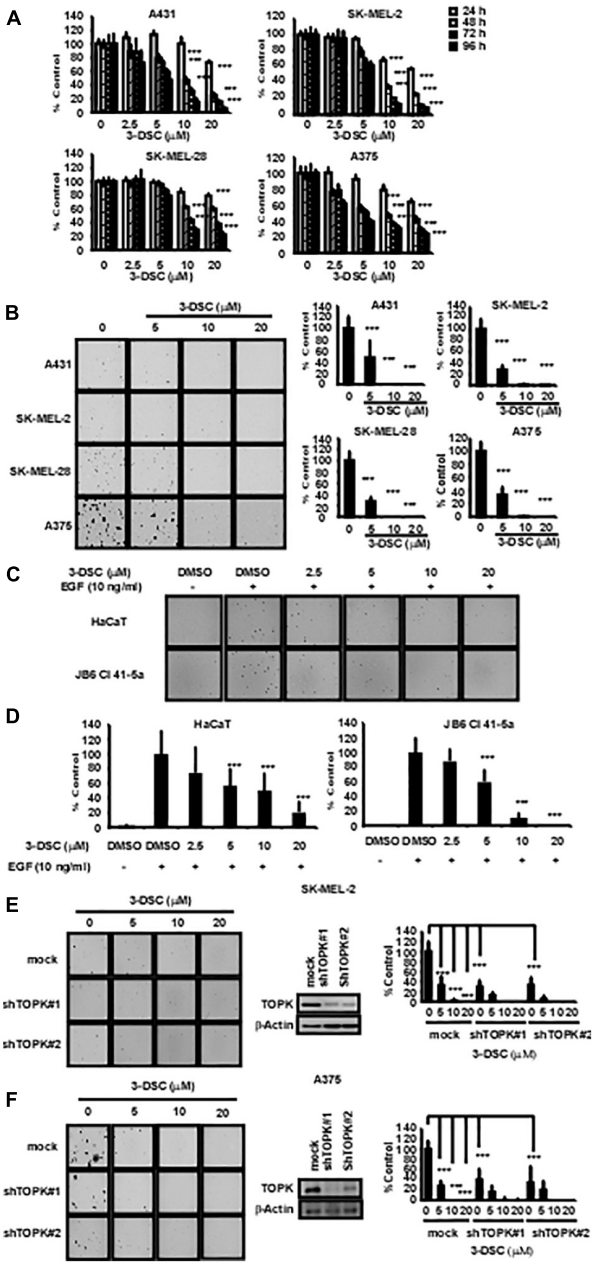

FIGURE 3 | 3-DSC inhibits anchorage-dependent and independent growth in skin cancer cell lines. **(A)** The inhibition effects of different concentrations of 3-DSC in cell proliferation of A431, SK-MEL-2, SK-MEL-28, and A375 cells. Skin cancer cells were incubated with 3-DSC for 24, 48, 72, and 96 h and growth was detected by MTT assay. Data shown as mean ± SD values. **(B)** Representative images of anchorage-independent soft agar growth assay using skin cancer cell lines incubated with various concentrations of 3-DSC. **(C)** Representative images showing the effect of 3-DSC on anchorage-independent growth of EGF-induced transformation of normal skin cells. **(D)** Quantification of colony numbers shown in panel **(C)**. Data are shown as mean ± SD values. **(E)** SK-MEL-2 cell anchorage-independent colony growth after knocking down TOPK and treating with various concentrations of 3-DSC. Colony number is quantified in the right side of the panel. **(F)** A375 cell anchorage-independent colony growth after knocking down TOPK and treating with various concentrations of 3-DSC. Colony number is quantified in the right side of the panel. ***$p < 0.001$.

To assess whether 3-DSC contributes to cell death in addition to growth inhibition in skin cancer cells, we next performed a cell apoptosis assay. A431, SK-MEL-2, and A375 cells were incubated with or without 3-DSC for 24 h before being harvested and examined by cell flow cytometry. The results indicated a significant increase in the percentage of PI and annexin-V-positive cells (dead or apoptotic cells) in the 3-DSC-treated group relative to the untreated control cells (**Figure 4C**). Additionally, we detected apoptosis protein markers, cleaved PARP, cleaved caspase-3, cleaved caspase-7, caspase 3, and caspase 7 in 3-DSC-treated and untreated cells using western blot. The results showed that the cell apoptosis markers, cleaved-PARP, cleaved-caspase 3, and cleaved-caspase 7, were significantly increased upon treatment of skin cancer cells with 3-DSC in a dose-dependent manner (**Figure 4D**).

3-DSC Inhibited TOPK Signaling Pathway

To determine the effect of 3-DSC on TOPK signaling in the context of skin cancer, we incubated SK-MEL2 and A375 cells over the concentration of 3-DSC ranging between 0 and 20 μM for 2 h before harvesting cell lysates to measure the protein level of TOPK and its downstream effectors by western blot. The results revealed that 3-DSC decreased the level of p-TOPK in a dose-dependent manner. Consequently, levels of downstream p-ERK, p-RSK, and p-c-Jun protein were also decreased due to attenuated p-TOPK (**Figure 5A**). To further confirm whether the inhibitory effect of 3-DSC is due to modulation of TOPK activity, we over-expressed TOPK in HEK-293T cell by transfection of the *pcDNA4.1HisC-TOPK* plasmid. The western blot results indicated that we successfully induced TOPK over-expression (**Figure 5B**). We then performed a soft agar assay using the HEK-293T cell line over-expressing TOPK in the presence or absence of 3-DSC. The results showed that over-expression of TOPK promoted proliferation in untreated HEK-293T cells; however, TOPK-induced proliferation of the HEK293T cells was reduced upon treatment with 3-DSC (**Figures 5C,D**). Thus, we concluded that 3-DSC inhibited skin cancer cell growth by reducing p-TOPK expression and the downstream effectors of TOPK.

3-DSC Inhibited Skin Cancer Cell-Derived Xenograft Growth

To determine the toxicity of 3-DSC *in vivo*, we treated Nu/Nu mice via abdominal injection with 3-DSC (20 or 40 mg/kg) or vehicle alone and measured body weight every day for 43 days. Mice were then euthanized and the liver and spleen were collected and weighed. The body, liver, and spleen weight indicated no significant toxicity of 3-DSC to mice at the administered concentrations (**Supplementary Figures 2B,C**). To determine whether the inhibitory effect of 3-DSC observed *in vitro* could be recapitulated *in vivo*, we applied 3-DSC to a CDX mice model. Mice were weighed (**Figure 6A**) and the tumor size (length × width × height × 0.52) was measured twice a week (**Figure 6B**). Results indicated that body weight steadily increased over the duration of the experiment. The tumor size indicated 3-DSC significantly reduced SK-MEL-2 CDX tumor growth (**Figures 6C,D**). We also performed IHC

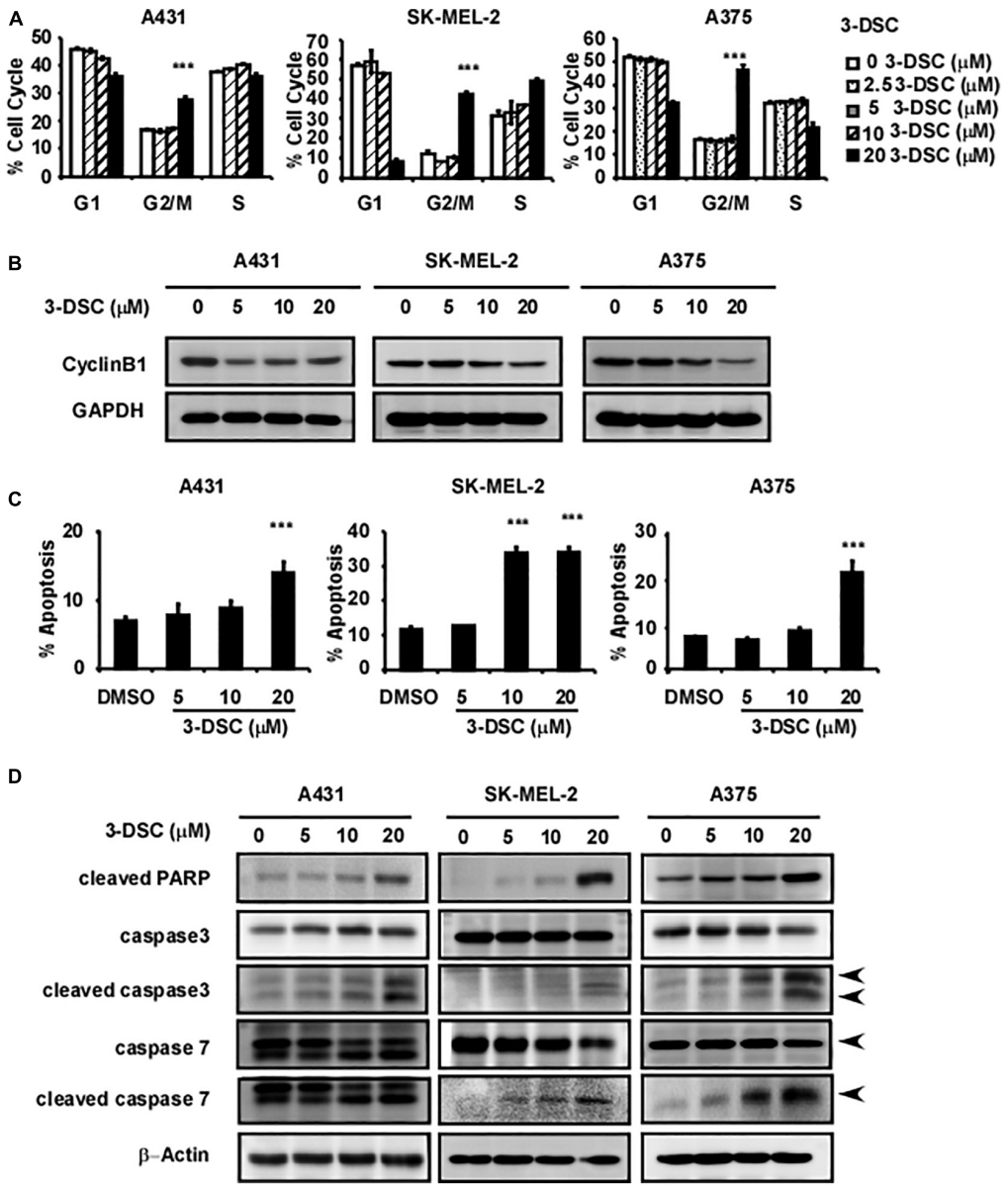

FIGURE 4 | 3-DSC induces arrest at G2/M phase and cell apoptosis in skin cancer cells. **(A)** Effect of 3-DSC to skin cancer cells' cell cycle. **(B)** G2/M phase marker cyclin B1 protein expression level in skin cancer cell lines after treatment with 3-DSC at various concentrations. **(C)** 3-DSC induces apoptosis in skin cancer cell lines. Skin cancer cells were incubated with various concentrations of 3-DSC for 48 h and analyzed for apoptosis markers indicating pre/late apoptosis by flow cytometry. Data are shown as mean ± SD values. **(D)** Cell apoptosis marker cleaved PARP/cleaved caspase 3/cleaved caspase 7/PARP/caspase 3/caspase 7 expression after 3-DSC treatment. 3-DSC treatment increased cleaved PARP/cleaved caspase 3/cleaved caspase 7 protein expression in a dose-dependent manner. ***$p < 0.001$.

analysis on the tumor tissues to assess if the administered concentrations of 3-DSC were effective in attenuating TOPK signaling at the protein level *in vivo*. Indeed, the results indicated a significant decrease in the levels of p-TOPK, p-ERK, p-RSK, and p-c-Jun proteins (**Figures 6E,F**). Based upon our experimental results, we suggest that 3-DSC is able to prevent SUV damage to skin, inhibit skin cancer growth *in vitro* and *in vivo*, and induce apoptosis and cell cycle arrest at G2/M phase by attenuating TOPK activity through direct physical interaction.

DISCUSSION

Solar ultraviolet (sUV) irradiation as a major environmental carcinogen is the main risk factor that causes inflammation and skin cancer (Roh et al., 2018). Acute solar-simulated light was also found to rapidly activate PI3K/AKT/mTOR and MAPK signaling pathways in human tissues (Bermudez et al., 2015). As an anti-cancer target (Park et al., 2006; Alachkar et al., 2015; Ikeda et al., 2016; Ohashi et al., 2017) and upstream MAPK family member (Abe et al., 2000), TOPK may be potentially

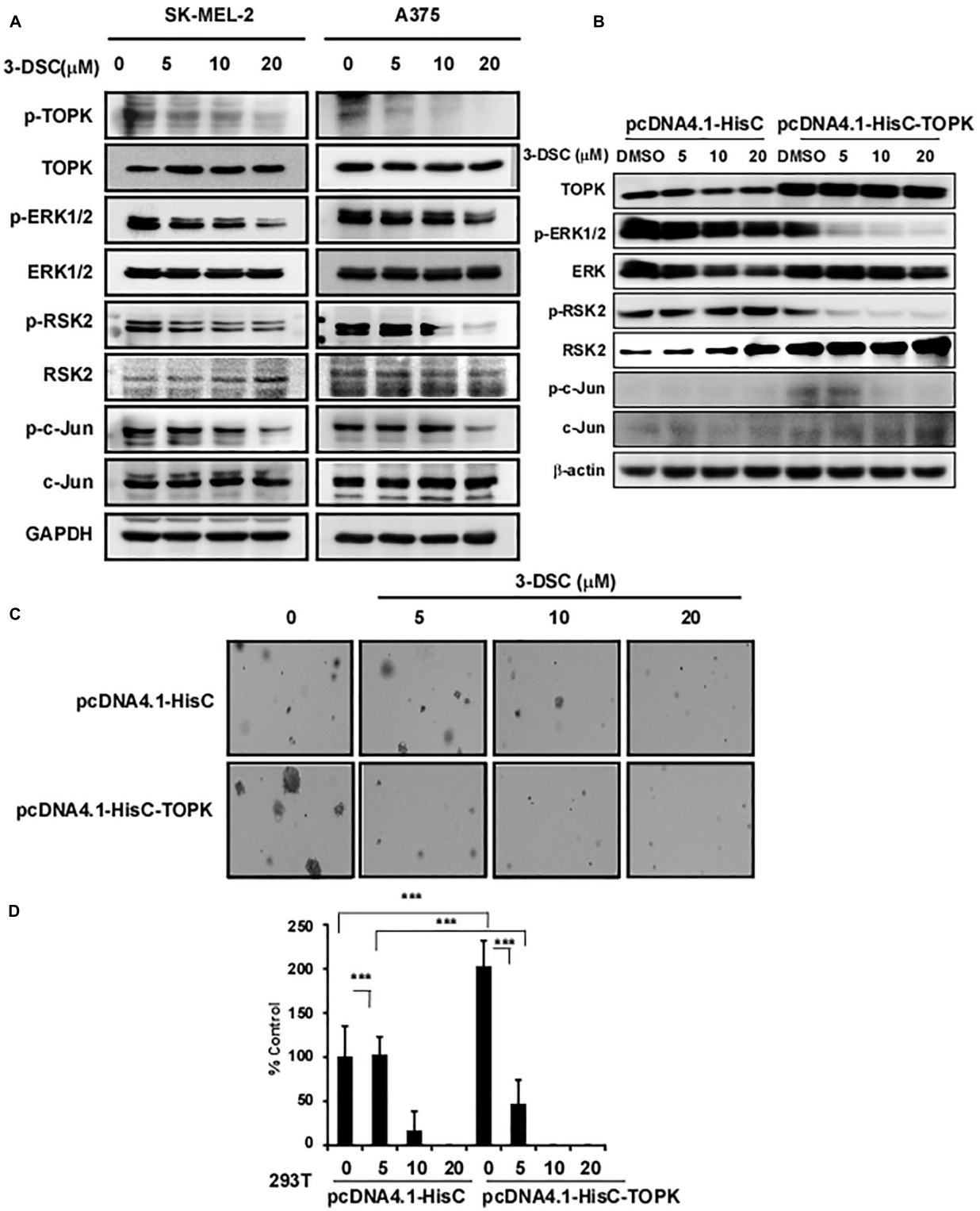

FIGURE 5 | 3-DSC inhibited TOPK signaling pathway in skin cancer cell lines. **(A)** p-TOPK, TOPK, and downstream effector protein expression after 3-DSC treatment. SK-MEL-2 and A375 cells were incubated with a culture medium with FBS and 3-DSC (5, 10, or 20 μM) or without 3-DSC for 2 h, and cell lysates were harvested before analysis by western blot. **(B)** TOPK was overexpressed in HEK-293T cells using pcDNA4.1-HisC (control) and pcDNA4.1-HisC-TOPK before cells were treated with or without 3-DSC at various concentrations. **(C)** Effect of 3-DSC on anchorage-independent growth in HEK-293T cells expressing *pcDNA4.1-HisC* and *pcDNA4.1-HisC-TOPK*. TOPK over-expression increased colony number and size. **(D)** Quantification of colony number in panel **(C)**. Data are shown as mean ± SD values. ***$p < 0.001$.

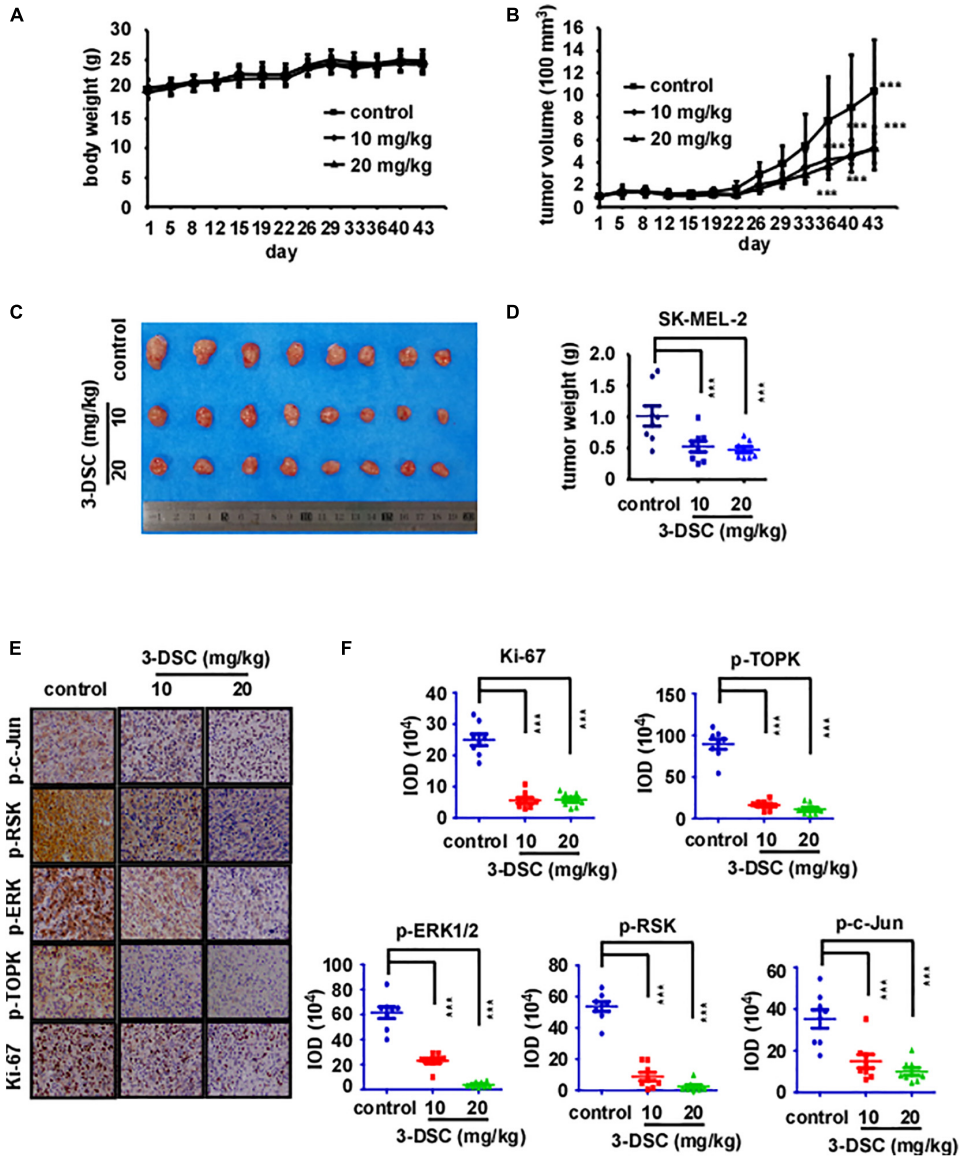

FIGURE 6 | 3-DSC inhibited skin cancer cell-derived xenograft (CDX) growth by attenuating TOPK expression. **(A)** Bodyweight of three groups of CDX mice over the duration of 43 days. Body weight was measured twice a week. **(B)** Tumor volume of three groups CDX mice over the duration of the experiment. Tumor size was measured twice a week. **(C)** Photograph showing tumors excised from control and 3-DSC-treated groups after euthanasia. **(D)** Quantification of tumor weight in panel **(C)**. Data are shown as mean ± SD values. **(E)** IHC results of CDX tumor tissues (Ki-67/p-TOPK/p-ERK/p-RSK/p-c-Jun) derived from control and 3-DSC-treated groups. **(F)** Quantification of IHC results shown in panel **(E)**. Data are shown as mean ± SD values. ***$p < 0.001$.

relevant for treating UV-induced skin cancer (Gao et al., 2017). TOPK and p-TOPK were highly expressed in skin cancer cell lines (**Figure 1A**) and in metastatic melanoma tumors compared with primary melanoma tumors according to GTEx and TCGA patient samples (**Figure 1B**). Independent cohort data presented within the Gene Expression Omnibus (GEO) database provide further evidence of heightened TOPK expression in cancer (Liu et al., 2019). In esophageal squamous cell carcinoma, TOPK was positively correlated with tumor metastasis (Seol et al., 2017; Zykova et al., 2017; Ma et al., 2019) by activating Src/GSK3β/STAT3 signaling pathway (Jiang et al., 2019). TOPK expression was also correlated with p53 expression (Hu et al., 2010; Lei et al., 2015) and cancer patients' prognosis (Ikeda et al., 2016; Ohashi et al., 2016; Pirovano et al., 2017; Hayashi et al., 2018; Koh et al., 2018; Su et al., 2018; Xu and Xu, 2019; Zhang et al., 2019). These observations indicate that TOPK may show promise as a potential target for skin cancer treatment. Indeed, upon knocking down TOPK in SK-MEL-2 and A375 cell lines (**Figures 3E,F**), we showed that anchorage-dependent colony formation was inhibited.

According to our previous study, 3-DSC could bind with TOPK and inhibit colon cancer growth (Zhao et al., 2019).

As targeting TOPK may be a strategy for the treatment of skin cancer, we performed experiments to verify the effect of 3-DSC on skin cancer. Kinase assay results showed a significant inhibitory effect of 3-DSC on TOPK kinase at 5 μM (**Figures 1D,E**) and the KD value of 3-DSC to TOPK was increased from 13.3 to 26.7 in the TOPK enzyme kinetics assay (**Figure 1F**). Moreover, the specific binding sites between 3-DSC and TOPK were Thr42 and Asn172 (**Figures 1G–I**), and these all suggested that the kinase activity of TOPK has been suppressed by 3-DSC (**Figures 1A–I**). 3-DSC showed a significant inhibitory effect in the cell proliferation of skin cancer cell lines (**Figures 3A,B**), which was also supported by cell cycle assay (**Figures 4A,B**) and apoptosis assay (**Figures 4C,D**). 3-DSC inhibited the phosphorylation of ERK/RSK/c-Jun, which are the downstream of TOPK (**Figures 5A–D**; Li et al., 2016).

Furthermore, targeting TOPK has been a strategy to prevent solar-related inflammation (Xue et al., 2017), and 3-DSC showed anti-inflammatory effects in previous research (Kim et al., 2014). In our study, we also found that 3-DSC prevented skin thickening, which was induced by acute SSL (**Figure 2**). Cell line−derived xenograft (CDX) models created by implanting cancer cell lines into immunodeficient mice have contributed largely to the development of cancer drug therapies (Lin et al., 2018). HI-TOPK-032, one of the TOPK inhibitors, was shown to inhibit tumor growth by nearly 50% in a HCT116 colon cancer cell-derived xenograft mouse model at a dose of 10 mg/kg (Kim et al., 2012). We are the first researchers to investigate the effect of 3-DSC *in vivo* by SK-MEL2 cell-derived xenograft mouse model. We confirmed its inhibitory effect via IHC, whereby we observed a significant reduction in Ki-67 and TOPK/ERK/RSK/c-Jun signaling protein expression (**Figures 6E,F**). Another TOPK inhibitor, acetylshikonin, was observed to inhibit tumor growth in colon cancer patient−derived xenograft (PDX) models compared with vehicle group at a dose of 120 mg/kg (Zhao et al., 2020). Whereas the inhibitory effect of 3-DSC to tumors is 50% with no significant changes to body, liver, and spleen weight, other TOPK inhibitors, such as OTS514 and OTS964, induced hematopoietic toxicity as reported in an *in vivo* study (Matsuo et al., 2014; Nakamura et al., 2015). The present study revealed that 3-DSC showed no obvious effect on the weight of liver and spleen.

In conclusion, as 3-DSC prevents SUV-induced damage, inhibits skin cancer *in vitro* and *in vivo*, and shows minimal side effects when administered at a high dosage, this compound could be considered a viable therapeutic option for the treatment of skin cancer and as a skin cancer therapeutic in further clinical research. The compound could potentially be used in pre-cancer stages or applied topically after extensive UV exposure with more efficiency and less side effect.

DATA AVAILABILITY STATEMENT

The original contributions presented in the study are included in the article/**Supplementary Material**, further inquiries can be directed to the corresponding author/s.

ETHICS STATEMENT

The animal study was reviewed and approved by the Ethics Committee of China-US (Henan) Hormel Cancer Institute.

AUTHOR CONTRIBUTIONS

XF, RZ, and GY were involved in study concept and design, acquisition of data, analysis and interpretation of data, and drafting of the manuscript. XF, RZ, GY, FY, BX, and KVL performed the experiments. J-HS, KL, and BC provided material support. XF, RZ, M-HL, and ZD wrote the manuscript. ZD and M-HL had supervision of the whole study. All authors read and approved the final manuscript.

FUNDING

This work was supported by grant funding from the National Natural Science Foundation of China (NSFC81672767 and NSFC81972839), the Key Program of Henan Province, China (grant no. 161100510300), the Scientific and Technological Project in Henan Province (no. 212102310882) and the Henan Provincial Government, China.

ACKNOWLEDGMENTS

We wish to thank Ran Yang, Shen Yang, and Fangfang Liu in the China-US (Henan) Hormel Cancer Institute for supporting the experiments.

SUPPLEMENTARY MATERIAL

The Supplementary Material for this article can be found online at: https://www.frontiersin.org/articles/10.3389/fcell.2021.638174/full#supplementary-material

Supplementary Figure 1 | TOPK expression does not appreciably change across race, age, and stage. **(A)** RNA-seq data detailing TOPK transcript expression in tumors derived from Asian and Caucasian patients. **(B)** RNA-seq data detailing TOPK transcript expression in patient-derived tumor tissues was analyzed according to patient age. **(C)** RNA-seq data detailing TOPK transcript expression in patient-derived tumor tissues was analyzed according to tumor stage.

Supplementary Figure 2 | 3-DSC showed no toxicity in NFDH cells or mice. **(A)** Effect of 3-DSC in Normal Human Dermal Fibroblasts. NHDF cells were treated various concentrations of 3-DSC and cell growth was determined by MTT assay. **(B)** Influence of 3-DSC to mice body weight. Three mice per group were treated with 3-DSC (20 or 40 mg/kg) or vehicle solution and weighed once per day over 2 weeks. **(C)** Spleen and liver weight and photograph of control and 3-DSC-treated groups over the duration of 2 weeks for the toxicity experiment. No significance was observed between control and experiment groups. **(D)** Spleen and liver weight of control and 3-DSC-treated groups in 3-DSC CDX experiment. No significance was observed between control and experiment groups.

REFERENCES

Abe, Y., Matsumoto, S., Kito, K., and Ueda, N. (2000). Cloning and expression of a novel MAPKK-like protein kinase, lymphokine-activated killer T-cell-originated protein kinase, specifically expressed in the testis and activated lymphoid cells. *J. Biol. Chem.* 275, 21525–21531. doi: 10.1074/jbc.m909629199

Alachkar, H., Mutonga, M., Malnassy, G., Park, J.-H., Fulton, N., Woods, A., et al. (2015). T-LAK cell-originated protein kinase presents a novel therapeutic target in FLT3-ITD mutated acute myeloid leukemia. *Oncotarget* 6, 33410–33425. doi: 10.18632/oncotarget.5418

Bermudez, Y., Stratton, S. P., Curiel-Lewandrowski, C., Warneke, J., Hu, C., Bowden, G. T., et al. (2015). Activation of the PI3K/Akt/mTOR and MAPK signaling pathways in response to acute solar-simulated light exposure of human skin. *Cancer Prev. Res. (Phila)* 8, 720–728. doi: 10.1158/1940-6207.capr-14-0407

Braicu, C., Buse, M., Busuioc, C., Drula, R., Gulei, D., Raduly, L., et al. (2019). A comprehensive review on MAPK: a promising therapeutic target in cancer. *Cancers (Basel)* 11:1618. doi: 10.3390/cancers11101618

Dougherty, J. D., Garcia, A. D. R., Nakano, I., Livingstone, M., Norris, B., Polakiewicz, R., et al. (2005). PBK/TOPK, a proliferating neural progenitor-specific mitogen-activated protein kinase kinase. *J. Neurosci.* 25, 10773–10785. doi: 10.1523/jneurosci.3207-05.2005

Gao, G., Zhang, T., Wang, Q., Reddy, K., Chen, H., Yao, K., et al. (2017). ADA-07 suppresses solar ultraviolet-induced skin carcinogenesis by directly inhibiting TOPK. *Mol. Cancer Ther.* 16, 1843–1854. doi: 10.1158/1535-7163.mct-17-0212

Hayashi, T., Hayakawa, Y., Koh, M., Tomita, T., Nagai, S., Kashiwazaki, D., et al. (2018). Impact of a novel biomarker, T-LAK cell-originating protein kinase (TOPK) expression on outcome in malignant glioma. *Neuropathol. J. Jpn. Soc. Neuropathol.* 38, 144–153. doi: 10.1111/neup.12446

Herbert, K. J., Ashton, T. M., Prevo, R., Pirovano, G., and Higgins, G. S. (2018). T-LAK cell-originated protein kinase (TOPK): an emerging target for cancer-specific therapeutics. *Cell Death Dis.* 9, 1089–1089.

Hu, F., Gartenhaus, R. B., Eichberg, D., Liu, Z., Fang, H. B., and Rapoport, A. P. (2010). PBK/TOPK interacts with the DBD domain of tumor suppressor p53 and modulates expression of transcriptional targets including p21. *Oncogene* 29, 5464–5474. doi: 10.1038/onc.2010.275

Ikeda, Y., Park, J.-H., Miyamoto, T., Takamatsu, N., Kato, T., Iwasa, A., et al. (2016). T-LAK cell-originated protein kinase (TOPK) as a prognostic factor and a potential therapeutic target in ovarian cancer. *Clin. Cancer Res. J. Am. Assoc. Cancer Res.* 22, 6110–6117. doi: 10.1158/1078-0432.ccr-16-0207

Jiang, Y., Zhang, J., Zhao, J., Li, Z., Chen, H., Qiao, Y., et al. (2019). TOPK promotes metastasis of esophageal squamous cell carcinoma by activating the Src/GSK3β/STAT3 signaling pathway via γ-catenin. *BMC Cancer* 19:1264. doi: 10.1186/s12885-019-6453-z

Kim, D. J., Li, Y., Reddy, K., Lee, M.-H., Kim, M. O., Cho, Y.-Y., et al. (2012). Novel TOPK inhibitor HI-TOPK-032 effectively suppresses colon cancer growth. *Cancer Res.* 72, 3060–3068. doi: 10.1158/0008-5472.can-11-3851

Kim, J. H., Choo, Y. Y., Tae, N., Min, B. S., and Lee, J. H. (2014). The anti-inflammatory effect of 3-deoxysappanchalcone is mediated by inducing heme oxygenase-1 via activating the AKT/mTOR pathway in murine macrophages. *Int. Immunopharmacol.* 22, 420–426. doi: 10.1016/j.intimp.2014.07.025

Koh, M., Hayakawa, Y., Akai, T., Hayashi, T., Tomita, T., Nagai, S., et al. (2018). Novel biomarker, phosphorylated T-LAK cell-originated protein kinase (p-TOPK) can predict outcome in primary central nervous system lymphoma. *Neuropathol. J. Jpn. Soc. Neuropathol.* 38, 228–236. doi: 10.1111/neup.12463

Lee, Y.-J., Park, J.-H., and Oh, S.-M. (2020). TOPK promotes epithelial-mesenchymal transition and invasion of breast cancer cells through upregulation of TBX3 in TGF-β1/Smad signaling. *Biochem. Biophys. Res. Commun.* 522, 270–277. doi: 10.1016/j.bbrc.2019.11.104

Lei, B., Liu, S., Qi, W., Zhao, Y., Li, Y., Lin, N., et al. (2013). PBK/TOPK expression in non-small-cell lung cancer: its correlation and prognostic significance with Ki67 and p53 expression. *Histopathology* 63, 696–703.

Lei, B., Qi, W., Zhao, Y., Li, Y., Liu, S., Xu, X., et al. (2015). PBK/TOPK expression correlates with mutant p53 and affects patients' prognosis and cell proliferation and viability in lung adenocarcinoma. *Hum. Pathol.* 46, 217–224. doi: 10.1016/j.humpath.2014.07.026

Li, Y., Yang, Z., Li, W., Xu, S., Wang, T., Wang, T., et al. (2016). TOPK promotes lung cancer resistance to EGFR tyrosine kinase inhibitors by phosphorylating and activating c-Jun. *Oncotarget* 7, 6748–6764. doi: 10.18632/oncotarget.6826

Lin, S., Huang, G., Cheng, L., Li, Z., Xiao, Y., Deng, Q., et al. (2018). Establishment of peripheral blood mononuclear cell-derived humanized lung cancer mouse models for studying efficacy of PD-L1/PD-1 targeted immunotherapy. *MAbs* 10, 1301–1311. doi: 10.1080/19420862.2018.1518948

Linares, M. A., Zakaria, A., and Nizran, P. (2015). Skin Cancer. *Prim. Care* 42, 645–659.

Liu, H., Chen, D., Liu, P., Xu, S., Lin, X., and Zeng, R. (2019). Secondary analysis of existing microarray data reveals potential gene drivers of cutaneous squamous cell carcinoma. *J. Cell Physiol.* 234, 15270–15278. doi: 10.1002/jcp.28172

Ma, H., Li, Y., Wang, X., Wu, H., Qi, G., Li, R., et al. (2019). PBK, targeted by EVI1, promotes metastasis and confers cisplatin resistance through inducing autophagy in high-grade serous ovarian carcinoma. *Cell Death Dis.* 10, 166–181.

Matsuo, Y., Park, J. H., Miyamoto, T., Yamamoto, S., Hisada, S., Alachkar, H., et al. (2014). TOPK inhibitor induces complete tumor regression in xenograft models of human cancer through inhibition of cytokinesis. *Sci. Trans. Med.* 6:259ra145. doi: 10.1126/scitranslmed.3010277

Nakamura, Y., Matsuo, Y., Hisada, S., Ahmed, F., Huntley, R., Sajjadi-Hashemi, Z., et al. (2015). Tricyclic compounds and PBK inhibitors containing the same. US-9453025-B2

Ohashi, T., Komatsu, S., Ichikawa, D., Miyamae, M., Okajima, W., Imamura, T., et al. (2016). Overexpression of PBK/TOPK contributes to tumor development and poor outcome of esophageal squamous cell carcinoma. *Anticancer. Res.* 36, 6457–6466. doi: 10.21873/anticanres.11244

Ohashi, T., Komatsu, S., Ichikawa, D., Miyamae, M., Okajima, W., Imamura, T., et al. (2017). Overexpression of PBK/TOPK relates to tumour malignant potential and poor outcome of gastric carcinoma. *Br. J. Cancer* 116, 218–226. doi: 10.1038/bjc.2016.394

Pan, M., Schinke, H., Luxenburger, E., Kranz, G., Shakhtour, J., Libl, D., et al. (2018). EpCAM ectodomain EpEX is a ligand of EGFR that counteracts EGF-mediated epithelial-mesenchymal transition through modulation of phospho-ERK1/2 in head and neck cancers. *PLoS Biol.* 169:e2006624. doi: 10.1371/journal.pbio.2006624

Park, J.-H., Lin, M.-L., Nishidate, T., Nakamura, Y., and Katagiri, T. (2006). PDZ-binding kinase/T-LAK cell-originated protein kinase, a putative cancer/testis antigen with an oncogenic activity in breast cancer. *Cancer Res.* 66, 9186–9195. doi: 10.1158/0008-5472.can-06-1601

Pirovano, G., Ashton, T. M., Herbert, K. J., Bryant, R. J., Verrill, C. L., Cerundolo, L., et al. (2017). TOPK modulates tumour-specific radiosensitivity and correlates with recurrence after prostate radiotherapy. *Br. J. Cancer* 117, 503–512. doi: 10.1038/bjc.2017.197

Ratushny, V., Gober, M. D., Hick, R., Ridky, T. W., and Seykora, J. T. (2012). From keratinocyte to cancer: the pathogenesis and modeling of cutaneous squamous cell carcinoma. *J. Clin. Invest.* 122, 464–472. doi: 10.1172/jci57415

Roh, E., Lee, M. H., Zykova, T. A., Zhu, F., Nadas, J., Kim, H. G., et al. (2018). Targeting PRPK and TOPK for skin cancer prevention and therapy. *Oncogene* 37, 5633–5647. doi: 10.1038/s41388-018-0350-9

Seol, M.-A., Park, J.-H., Jeong, J. H., Lyu, J., Han, S. Y., and Oh, S.-M. (2017). Role of TOPK in lipopolysaccharide-induced breast cancer cell migration and invasion. *Oncotarget* 8, 40190–40203. doi: 10.18632/oncotarget.15360

Su, T.-C., Chen, C.-Y., Tsai, W.-C., Hsu, H.-T., Yen, H.-H., Sung, W.-W., et al. (2018). Cytoplasmic, nuclear, and total PBK/TOPK expression is associated with prognosis in colorectal cancer patients: a retrospective analysis based on immunohistochemistry stain of tissue microarrays. *PLoS One* 13:e0204866. doi: 10.1371/journal.pone.0204866

Wang, M.-Y., Lin, Z.-R., Cao, Y., Zheng, L.-S., Peng, L.-X., Sun, R., et al. (2016). PDZ binding kinase (PBK) is a theranostic target for nasopharyngeal carcinoma: driving tumor growth via ROS signaling and correlating with patient survival. *Oncotarget* 7, 26604–26616. doi: 10.18632/oncotarget.8445

Xiao, J., Wang, F., Lu, H., Xu, S., Zou, L., Tian, Q., et al. (2019). Targeting the COX2/MET/TOPK signaling axis induces apoptosis in gefitinib-resistant NSCLC cells. *Cell Death Dis.* 10, 777–789.

Xu, M., and Xu, S. (2019). PBK/TOPK overexpression and survival in solid tumors: a PRISMA-compliant meta-analysis. *Medicine* 98, e14766. doi: 10.1097/md.0000000000014766

Xue, P., Wang, Y., Zeng, F., Xiu, R., Chen, J., Guo, J., et al. (2017). Paeonol suppresses solar ultraviolet-induced skin inflammation by targeting T-LAK cell-originated protein kinase. *Oncotarget* 8, 27093–27104. doi: 10.18632/oncotarget.15636

Zhang, Y., Yang, X., Wang, R., and Zhang, X. (2019). Prognostic value of PDZ-binding kinase/T-LAK cell-originated protein kinase (PBK/TOPK) in patients with cancer. *J. Cancer* 10, 131–137. doi: 10.7150/jca.28216

Zhao, R., Choi, B. Y., Wei, L., Fredimoses, M., Yin, F., Fu, X., et al. (2020). Acetylshikonin suppressed growth of colorectal tumour tissue and cells by inhibiting the intracellular kinase, T-lymphokine-activated killer cell-originated protein kinase. *Br. J. Pharmacol.* 17710, 2303–2319. doi: 10.1111/bph.14981

Zhao, R., Huang, H., Choi, B. Y., Liu, X., Zhang, M., Zhou, S., et al. (2019). Cell growth inhibition by 3-deoxysappanchalcone is mediated by directly targeting the TOPK signaling pathway in colon cancer. *Phytomedicine* 61, 152813–152828. doi: 10.1016/j.phymed.2018.12.036

Zhu, F., Zykova, T. A., Kang, B. S., Wang, Z., Ebeling, M. C., Abe, Y., et al. (2007). Bidirectional signals transduced by TOPK-ERK interaction increase tumorigenesis of HCT116 colorectal cancer cells. *Gastroenterology* 133, 219–231. doi: 10.1053/j.gastro.2007.04.048

Zykova, T. A., Zhu, F., Wang, L., Li, H., Bai, R., Lim, D. Y., et al. (2017). The T-LAK cell-originated protein kinase signal pathway promotes colorectal cancer metastasis. *EBioMedicine* 18, 73–82. doi: 10.1016/j.ebiom.2017.04.003

Conflict of Interest: The authors declare that the research was conducted in the absence of any commercial or financial relationships that could be construed as a potential conflict of interest.

frontiers in Oncology

ORIGINAL RESEARCH
published: 13 April 2021
doi: 10.3389/fonc.2021.644895

Unique Profile of Driver Gene Mutations in Patients With Non-Small-Cell Lung Cancer in Qujing City, Yunnan Province, Southwest China

Yongchun Zhou[1†], Feng Ge[2†], Yaxi Du[1], Quan Li[1], Jingjing Cai[1], Xin Liu[1], Yinjin Guo[1], Zhenghai Shen[3], Lincan Duan[4], Zhan Huang[5], Fei Yao[5], Changbin Zhu[5], Hutao Shi[6] and Yunchao Huang[7*]*

[1] Molecular Diagnosis Sub Center of Yunnan Cancer Center, Yunnan Cancer Molecular Diagnosis Center, The Third Affiliated Hospital of Kunming Medical University (Yunnan Tumor Hospital), Kunming, China, [2] Yunnan Provincial Key Laboratory of Panax notoginseng, Faculty of Life Science and Technology, Kunming University of Science and Technology, Kunming, China, [3] Cancer Center Office, The Third Affiliated Hospital of Kunming Medical University (Yunnan Tumor Hospital), Kunming, China, [4] Department of Thoracic Surgery II, The Third Affiliated Hospital of Kunming Medical University (Yunnan Tumor Hospital), Kunming, China, [5] Department of Medical Affairs, Amoy Diagnostics Co., Ltd., Xiamen, China, [6] Imaging Department, Kunming Tongren Hospital, Kunming, China, [7] Department of Thoracic Surgery I, The Third Affiliated Hospital of Kunming Medical University (Yunnan Tumor Hospital), Kunming, China

Objective: Qujing City, Yunnan Province, China, has a high incidence of lung cancer and related mortality. The etiology of NSCLC in Qujing area and distribution of associated molecular aberrations has not been fully elucidated. This study aimed to reveal the profile of driver gene mutations in patients with non-small-cell lung cancer (NSCLC) in Qujing and explore their relationships with clinicopathological characteristics.

Methods: In this study, the mutation profiles of NSCLC driver genes, including *EGFR, ALK, ROS1, KRAS, BRAF, RET, MET, HER2, NRAS*, and *PIK3CA*, were investigated in patients with NSCLC from Qujing and compared with those from other regions in Yunnan Province. The associations between molecular mutations and clinicopathological characteristics were further analyzed.

Results: A distinct profile of driver gene mutations was discovered in patients with NSCLC from Qujing. Interestingly, a higher proportion of *EGFR* compound mutations, including G719X + S768I (19.65% vs 3.38%, P < 0.0001) and G719X + L861Q (21.10% vs 2.82%, P < 0.0001), was observed in patients with NSCLC in Qujing compared with patients in non-Qujing area, besides significantly different distributions of *EGFR* (46.01% vs. 51.07%, *P* = 0.0125), *ALK* (3.17% vs. 6.97%, *P* = 0.0012), *ROS1* (0.5% vs. 2.02%, *P* = 0.0113), and *KRAS* (23.02% vs. 7.85%, *P* < 0.0001). Further, *EGFR* compound mutations were more likely associated with the occupation of patients (living/working in rural areas, e.g., farmers). Moreover, *KRAS* G12C was the dominant subtype (51.11% vs 25.00%, *P* = 0.0275) among patients with NSCLC having *KRAS* mutations in Qujing.

OPEN ACCESS

Edited by:
Andrew Davis, Washington University in St. Louis, United States

Reviewed by:
Xuefei Li, Shanghai Pulmonary Hospital, China
Renato Franco, University of Campania Luigi Vanvitelli, Italy

***Correspondence:**
Hutao Shi
shi_hutao1105@163.com
Yunchao Huang
hycyn2008@163.com

[†]These authors have contributed equally to this work

Specialty section:
This article was submitted to Molecular and Cellular Oncology, a section of the journal Frontiers in Oncology

Received: *22 December 2020*
Accepted: *18 March 2021*
Published: *13 April 2021*

Citation:
Zhou Y, Ge F, Du Y, Li Q, Cai J, Liu X, Guo Y, Shen Z, Duan L, Huang Z, Yao F, Zhu C, Shi H and Huang Y (2021) Unique Profile of Driver Gene Mutations in Patients With Non-Small-Cell Lung Cancer in Qujing City, Yunnan Province, Southwest China. Front. Oncol. 11:644895. doi: 10.3389/fonc.2021.644895

Conclusions: Patients with NSCLC in Qujing displayed a unique profile of driver gene mutations, especially a higher prevalence of *EGFR* compound mutations and dominant *KRAS* G12C subtype, in this study, indicating a peculiar etiology of NSCLC in Qujing. Therefore, a different paradigm of therapeutic strategy might need to be considered for patients with NSCLC in Qujing.

Keywords: *ALK*, *EGFR*, *KRAS*, *ROS1*, mutation profile, non-small-cell lung cancer, Qujing

INTRODUCTION

Lung cancer has been the most common cancer globally for more than two decades (1). Every year, 1.8 million people are diagnosed with lung cancer and 1.6 million die of the disease (2). In China, lung cancer has the highest mortality and modality. Qujing City, located in Southwest China, is an area with an extremely high incidence of lung cancer, especially in Xuanwei County (3, 4). Previous studies showed several exposures contributing to a higher incidence of non-small-cell lung cancer (NSCLC), including the use of smoky coal in unvented stoves (5), tobacco smoking (6), food contamination (7), and arsenic and radon among tin miners (8) in this area. These external exposures might lead to a distinct profile of genetic alterations contributing to the occurrence and development of NSCLC. Studies with limited sample size indicated that patients with NSCLC in Xuanwei County had lower *EGFR* and *ALK* mutation rates and a higher rate of *KRAS* mutations (9–11). A higher proportion of *EGFR* exons 18 and 20 co-mutations were also reported (12). In recent years, the discovery of lung cancer driver genes has opened the door to individualized treatment of lung cancer and made the molecular typing of lung cancer more refined (13). Therefore, understanding the real-world driver gene mutation characteristics of patients with NSCLC in the Qujing area is of great importance in unrevealing the genetic etiology and optimizing therapeutic regimens for patients in this region. In this study, 2672 patients with NSCLC from Yunnan Province, including 946 patients from Qujing City, were retrospectively examined. The mutation statuses of lung cancer driver genes *EGFR*, *ALK*, *ROS1*, *KRAS*, *BRAF*, *RET*, *MET*, *HER2*, *NRAS*, and *PIK3CA* were detected. Also, the mutational characteristics of these driver genes were analyzed. A specific profile of mutations in these driver genes was revealed in patients from this region, which might lead to the development of more effective targeted therapeutic interventions for this disease.

MATERIALS AND METHODS

Patients

A total of 2672 patients with pathologically diagnosed NSCLC from various regions, including Qujing in Yunnan Province, who visited Yunnan Cancer Hospital between January 2016 and September 2019 were retrospectively recruited (**Figure 1**). This study was conducted with approval from the Institutional Review Board of Yunnan Cancer Hospital. Informed consent was waived because of the retrospective nature of this study, and the de-sensitized clinical data were collected.

Samples and Mutation Detection

Formalin-fixed paraffin-embedded (FFPE) tumor tissues, or fine-needle aspiration and/or core needle biopsies, were used to detect mutations in at least one of the following genes, *EGFR*, *ALK*, *ROS1*, *KRAS*, *BRAF*, *RET*, *MET*, *HER2*, *NRAS*, and *PIK3CA*. Genomic DNA and total RNA were extracted from FFPE samples using the AmoyDx FFPE DNA/RNA extraction kit (Amoy Diagnostics, Xiamen, China) following the manufacturer's protocols. For other types of samples, an AmoyDx Tissue DNA/RNA extraction kit (Amoy Diagnostics) was used. An Amplification Refractory Mutation System Polymerase Chain Reaction (ARMS-PCR) and a Mutation Detection Kit (Amoy Diagnostics) were used to detect the mutations in driver genes (n = 2146). The other 526 specimens were captured using commercially available panels and subjected to next-generation sequencing (NGS) following manufacturer's protocols (**Table 1** and **Supplementary Table 1**).

Statistical Analysis

SPSS23.0 (SPSS version 23.0 for Windows, IBM Inc., IL, USA) was used to analyze the relationship between gene mutations and clinicopathological characteristics with the help of χ^2 test, Fisher's exact test, or binary logistic regression. The two-sided significance level was set at P <0.05.

RESULTS

Clinicopathological Characteristics of Patients With NSCLC in Qujing and Non-Qujing Regions

Among the 2146 patients with NSCLC tested by ARMS-PCR, 758 (35.25%) were from Qujing and 1384 (64.75%) were non-Qujing patients. Regional information was not available for the remaining four patients. The clinicopathological characteristics, including sex, age at diagnosis, smoking history, staging, histopathology, family history, ethnic, lesion site, and metastasis, are listed in **Table 1**. No difference in baseline characteristics was found between these two patient groups.

Abbreviation: EGFR, Epidermal growth factor receptor; ALK, Anaplastic lymphoma kinase; ROS1, Proto-oncogene receptor tyrosine kinase; KRAS, Kirsten rat sarcoma 2 viral oncogene homolog; BRAF, V-raf murine sarcoma viral oncogene homolog B; RET, Ret Proto-Oncogene; MET, MET proto-oncogene receptor tyrosine kinase; HER2, Epidermal growth factor receptor 2; NRAS, Neuroblastoma RAS viral oncogene homolog; PIK3CA, Phosphatidylinositol-4,5-Bisphosphate 3-Kinase Catalytic Subunit Alpha.

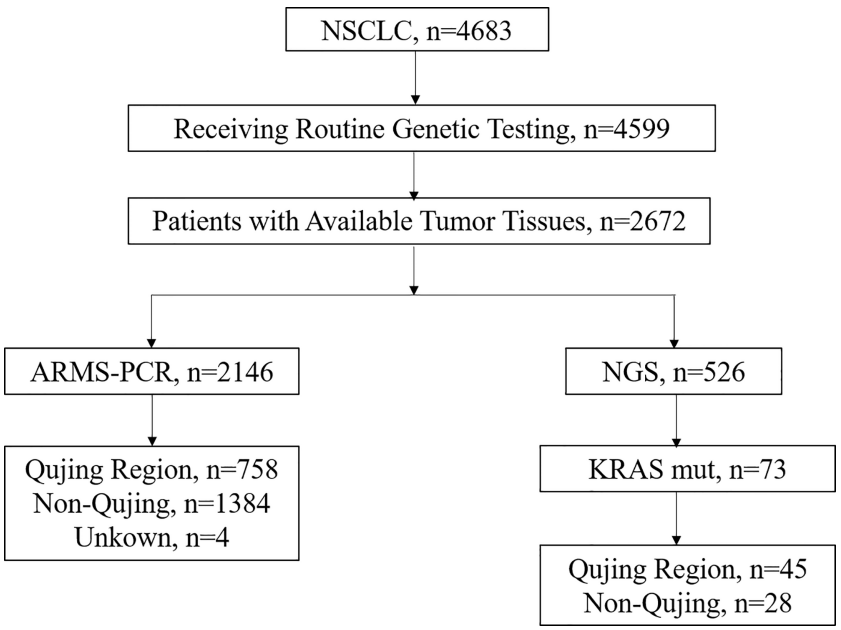

FIGURE 1 | Flowchart of participant selection in this study.

TABLE 1 | Characteristics of patients with NSCLC from Qujing and non-Qujing areas.

Characteristic	All patients (n=2142)	Region		*P-value*
		Qujing (n=758)	Non-Qujing (n=1384)	
Gender				
Male	1026 (47.90%)	357 (47.10%)	669 (48.34%)	
Female	1116 (52.10%)	401 (52.90%)	715 (51.66%)	0.3901
Age				
Median (range)		53 (17-92)	55 (24-89)	
≤40	109 (5.09%)	42 (5.54%)	67 (4.84%)	
>40	2033 (94.91%)	716 (94.46%)	1317 (95.16%)	0.481
Histopathology				
Adenocarcinoma	1978 (92.34%)	726 (95.78%)	1252 (90.46%)	
Squamous carcinoma	157 (7.33%)	32 (4.22%)	125 (9.03%)	<0.001
Unknown (NSCLC)	7 (0.33%)	0	7 (0.51%)	
Smoking history				
Yes	672 (31.37%)	251 (33.11%)	421 (30.42%)	
No	1454 (67.88%)	504 (66.49%)	950 (68.64%)	0.2285
Unknown	16 (0.75%)	3 (0.40%)	13 (0.94%)	
Family history				
Yes	187 (8.73%)	96 (12.66%)	91 (6.58%)	
No	1954 (91.22%)	661 (87.20%)	1293 (93.42%)	<0.001
Unknown	1 (0.05%)	1 (0.13%)	0	
Staging				
I-IIIa	988 (46.13%)	411 (54.22%)	577 (41.69%)	
IIIb-IV	976 (45.56%)	345 (45.51%)	631 (45.59%)	0.0044
Unknown	251 (11.72%)	75 (9.89%)	176 (12.72%)	
Lesion site				
Left	769 (35.90%)	229 (30.21%)	540 (39.02%)	
Right	1255 (58.59%)	446 (58.84%)	809 (58.45%)	0.0076
Unknown	48 (2.24%)	13 (1.72%)	35 (2.53%)	
Occupation				
Farmer	1005 (46.92%)	460 (60.39%)	545 (39.38%)	
Non-farmer/Unknown	1137 (53.08)	298 (39.31%)	592 (42.77%)	<0.001

The clinicopathological characteristics of other 526 specimens tested using NGS are shown in **Supplementary Table 2**.

Mutational Status of Driver Genes in Patients With NSCLC in Qujing

Among 2142 patients with NSCLC, 1978 were diagnosed with lung adenocarcinoma (92.34%) and 157 had lung squamous carcinoma (7.33%). The landscape of driver mutations in patients with NSCLC from Qujing, non-Qujing, Yunan (non-Qujing), and non-Yunnan regions displayed a region-specific mutational profile (**Figure 2**). Especially, the prevalence of *EGFR* (46.01% vs 51.07%, $P = 0.0125$), *ALK* (3.17%% vs 6.97%%, $P = 0.0012$), and *ROS1* (0.5% vs 2.02%, $P = 0.0113$) was significantly lower in patients from Qujing than in those from non-Qujing regions. On the contrary, the *KRAS* mutation rate was significantly higher in patients with NSCLC in Qujing compared with non-Qujing patients (23.0214% vs 7.85%, $P < 0.0001$) (**Figures 3**, **4A**, and **5A**). Similar results were also obtained in patients with lung adenocarcinoma (**Supplementary Figure 1**). In addition, fewer patients with NSCLC in Qujing had co-mutations of these 10 driver genes compared with those from non-Qujing areas (**Supplementary Figure 2**). Among 526 specimens tested using NGS, the prevalence of *ALK* and *KRAS* mutations in NSCLC patients from Qujing and non-Qujing areas was as similar as the results by ARMS-PCR (**Supplementary Table 3**).

Relationship Between Clinical Characteristics and *EGFR*, *ALK/ROS1*, and *KRAS* Mutation Statuses in Patients With NSCLC in Qujing

Further, the relationship between *EGFR*, *KRAS*, and *ALK/ROS1* mutation statuses and clinical characteristics in patients with NSCLC in Qujing was analyzed. *EGFR* mutations were more common in female patients with adenocarcinoma, nonsmoker patients with NSCLC ($P < 0.0001$), and patients aged more than 40 years ($P = 0.0196$). *ALK/ROS1* fusions occurred more in patients younger than 40 years old ($P = 0.0002$). However, *KRAS* mutations were more frequent in men ($P = 0.0066$) and smokers ($P = 0.0084$) (**Table 2** and **Supplementary Table 4**).

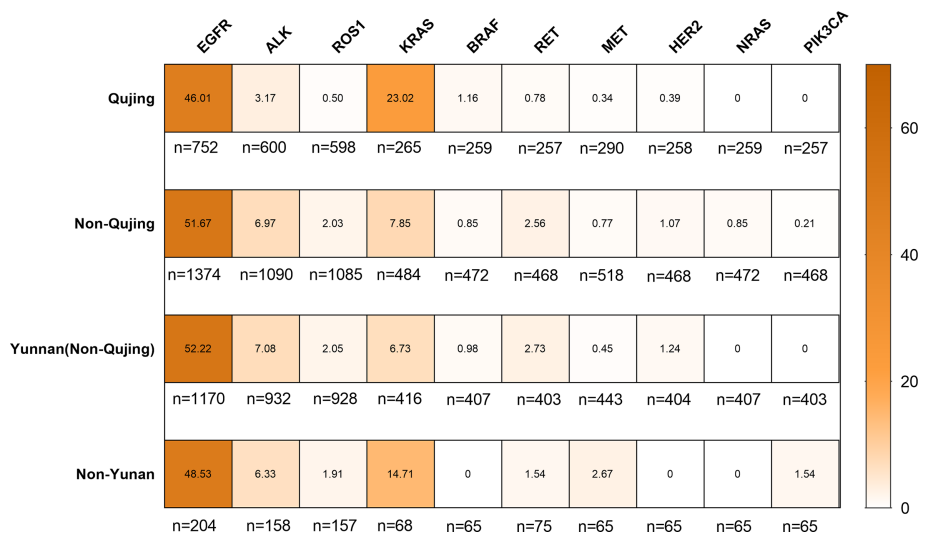

FIGURE 2 | Mutation frequencies of 10 lung cancer driver genes in patients with NSCLC according to the regions in Yunnan Province.

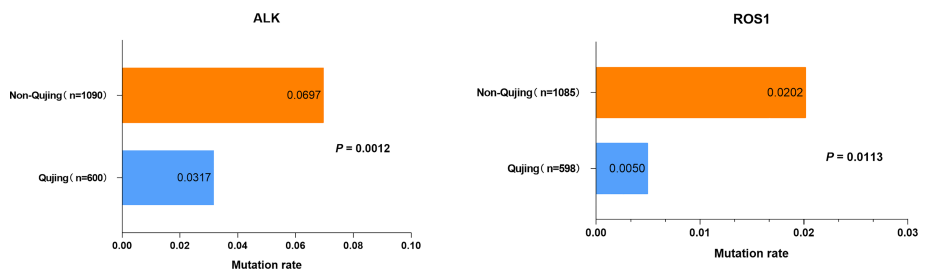

FIGURE 3 | Mutation frequencies of *ALK* and *ROS1* in patients with NSCLC from Qujing and non-Qujing regions.

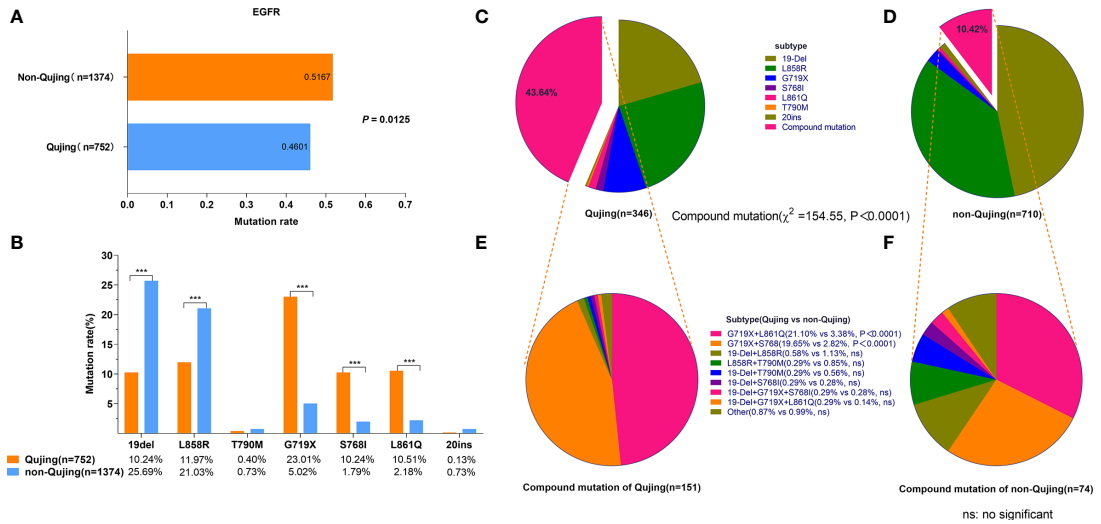

FIGURE 4 | Frequencies of *EGFR* mutations, *EGFR* subtypes, and compound mutations in patients with NSCLC from Qujing and non-Qujing areas. **(A)** the prevalence of *EGFR* mutation in Qujing patients was compared with non-Qujing patients. **(B)** the point mutation frequencies of G719X, S768I, and L861Q were higher in Qujing patients, and the point mutation of 19Del and L858R were lower in Qujing patients. **(C, D)** the distribution of *EGFR* mutation subtypes in Qujing and non-Qujing patients. **(E, F)** the distribution of *EGFR* compound mutation subtypes in Qujing and non-Qujing patients.

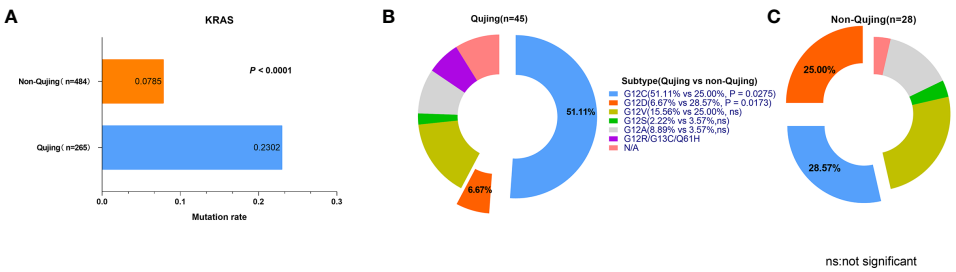

FIGURE 5 | Profile of *KRAS* mutation and subtypes in patients with NSCLC from Qujing and non-Qujing areas. **(A)** the prevalence of *KRAS* mutation in Qujing patients was compared with non-Qujing patients. **(B, C)** the distribution of KRAS mutation subtypes in Qujing and non-Qujing patients.

Distribution of *EGFR* Mutation Subtypes in Patients With NSCLC in Qujing

The mutation frequencies of G719X (23.01% vs 5.02%, $P < 0.0001$), S768I (10.24% vs 1.79%, $P < 0.0001$), and L861Q point mutations (10.51% vs 2.18%, $P < 0.0001$) were significantly higher, while the prevalence of 19Del (10.24% vs 25.69%, $P < 0.0001$) and L858R point mutations (11.97% vs 21.03%, $P < 0.0001$) was significantly lower in patients with NSCLC from Qujing compared with those from non-Qujing areas (**Figure 4B**). In addition, a significantly higher proportion of *EGFR* compound mutations were detected (43.35% vs 10.12%, $P < 0.0001$, for all *EGFR* mutations) (**Figures 4C, D**), and the proportion of *EGFR* G719X + L861Q (21.10% vs 3.38%, $P < 0.0001$) and *EGFR* G719X + S768I (19.65% vs 2.82%, $P < 0.0001$) subtypes was significantly higher in patients with NSCLC from Qujing (**Figures 4E, F**). The multivariate analysis showed that the occupation of patients (living/working in the rural area, e.g., farmers) (odds ratio, 1.923; 95% confidence interval, 1.179–3.137) was independently associated with an increased rate of *EGFR* compound mutations (**Table 3**).

Mutational Profile of *KRAS* Subtypes in Patients With NSCLC From Qujing

A total of 73 patients harbored *KRAS* mutations (13.88%) among 526 patients receiving NGS testing, including 45 patients from Qujing and 28 patients from non-Qujing areas. The mutation frequency of *KRAS* G12C was significantly higher in patients with NSCLC from Qujing than in those from non-Qujing areas (51.11% vs 25.00%, $P = 0.0275$). However, the frequency of *KRAS* G12D was significantly lower in patients with NSCLC from Qujing than in those from non-Qujing areas (6.17% vs 28.57%, $P = 0.0173$) (**Figures 5B, C**).

TABLE 2 | Relationship between clinical characteristics and *EGFR, ALK/ROS1*, and *KRAS* mutations in patients with NSCLC from Qujing.

Characteristics	EGFR				ALK/ROS1				KRAS			
	Mut	WT	χ2	*p*	Mut	WT	χ2	*p*	Mut	WT	χ2	*p*
Gender												
Male	120	235			13	269			39	90		
Female	226	171	40.34	<0.0001	9	307	1.305	0.2532	22	114	7.381	0.0066
Age												
≤40	12	30			5	27			4	7		
>40	334	376	5.446	0.0196	17	549	13.62	0.0002	57	197	1.153	0.2829
Histopathology												
AD	343	374			21	554			59	196		
SCC	3	29	18.23	<0.0001	1	22		0.5847	2	8	0.05345	0.8172
Smoking history												
Yes	74	176			9	184			26	51		
No	272	227	40.58	<0.0001	12	391	1.091	0.2963	35	152	6.953	0.0084
Family history												
Yes	45	50			4	76			10	34		
No	301	335	5.67E-05	0.994	18	500	0.4549	0.5	51	170	0.0025	0.9599
Ethnic												
Han	333	339			22	559			60	196		
Non-Han	13	7	1.854	0.1734	0	17		1*	1	8		0.6892*
***Staging**												
I-IIIa	196	213			10	328			40	127		
IIIb-IV	116	153	1.504	0.22	9	189	0.9196	0.3376	18	51	0.1201	0.729
Lesion site												
Left	138	158			9	217			26	73		
Right	204	239	0.023	0.8786	13	354	0.07582	0.783	34	129	1.019	0.3128
Occupation												
Farmer	214	242			10	341			35	112		
Non farmer/unknown	132	164	0.394	0.5302	12	235	1.652	0.1987	26	92	0.1165	0.7329

*AD, adenocarcinoma; SCC, squamous cell carcinoma; *Fisher exact test.*

TABLE 3 | Multivariate logistic regression analysis of correlations between baseline characteristics and *EGFR* compound mutations in patients with NSCLC from Qujing.

Characteristics	Exp(B)	EXP(B) 95% CI		*P-value*
		upper	lower	
Sex (Male vs Female*)	0.986	0.499	1.948	0.969
Age	0.993	0.967	1.020	0.628
Occupation (Farmer vs non-Farmer*)	1.923	1.179	3.137	0.009
Race (Han vs non-Han*)	1.313	0.368	4.690	0.675
Smoking (Yes vs No*)	1.145	0.519	2.527	0.738
Family history (Yes vs No*)	1.223	0.622	2.403	0.560
Lesion (Left vs Right*)	0.991	0.621	1.581	0.969
Stage (I-IIIa vs IIIb-IV*)	0.779	0.484	1.255	0.305
Histopathology (AD vs SCC*)	1.502	0.121	18.679	0.752

**reference variable.*

DISCUSSION

Lung cancer in Qujing City (including Xuanwei County), Yunnan, has four remarkable features: higher incidence, higher mortality, adenocarcinoma as the main histological type, and similar incidence in men and women (5). However, the mutation status of lung cancer driver genes has not been thoroughly investigated among the populations in this region due to the lack of a large-sized study cohort.

Previous studies suggested that lung cancer in the Qujing area had unique epidemiological characteristics due to severe air pollution and the toxicology of indoor coal-fired particles (4, 14–16). This area had more female patients with lung cancer, indicating the presence of strong carcinogens in the body, which had different effects on men and women (17). This study showed that patients with NSCLC in Qujing had a unique driver gene mutation profile and significant differences in *EGFR* and *KRAS* mutation frequencies between men and women. The characteristics of gene mutations associated with patients with lung cancer in Qujing have been identified. However, the underlying molecular mechanisms of lung cancer in Qujing are complex and still not fully understood. On the contrary, a number of animal and *in vitro* studies showed that alveolar macrophages loaded with

carbon particles from smoke led to an increased risk of respiratory tract infections. They also showed that the pathways involved in lung carcinogenesis induced by indoor coal-fired particles and that induced by tobacco smoke might be identical (18–20). However, no evidence directly demonstrated that abnormal driver gene profile was the cause of the high incidence of lung cancer in this region. Therefore, the molecular mechanism underlying the high incidence of lung cancer in the Qujing population remains to be further explored.

This study was based on the analysis of multi-gene mutations in a large number of patients in Qujing compared with patients from other regions in Yunnan Province. In the present study, a distinct profile of driver gene mutations was found in patients with NSCLC from the Qujing area. Except the differential distribution of *EGFR*, *ALK*, *ROS1*, and *KRAS* mutations, *EGFR* compound mutations as well as *KRAS* G12C and G12D also displayed a "Qujing"-specific spectrum in this study. Previous findings and the findings of this study suggested that the prevalence of common driver mutations in patients with NSCLC from Qujing was different from that in patients from other regions of China, but similar to that in Western populations (9, 10, 21–23). However, further studies are required to validate the findings.

The *EGFR* mutation rate in patients with lung cancer from Xuanwei is still controversial. Wei et al. reported that 57% (51/90) and 43% (73/168) of patients with lung cancer from Xuanwei and non-Xuanwei regions carried *EGFR* mutations, respectively (24). Hosgood et al. showed that the incidence of *EGFR* mutation was 35% in female patients (never smokers) with lung cancer in Xuanwei (9). The present study found that the *EGFR* mutation rate was 46.01% in patients with NSCLC from Qujing, which was lower than that reported by Wei et al., but higher than that reported by Hosgood et al. This inconsistency in results might be due to the differences in population selection. On the one hand, Qujing City includes Xuanwei and other counties in its administrative area, and therefore this study included patients who were not in Xuanwei but belonged to Qujing City. On the other hand, the patients were not selected according to specific clinical characteristics.

The most commonly known type of *EGFR* mutation is 19Del (accounting for ~45% of *EGFR* mutations), followed by L858R (accounting for ~40% of *EGFR* mutations). The remaining ~10% of *EGFR* mutations are defined as uncommon mutations, including exon 20 insertions (20ins), T790M, G719X, L861X, and S768I (25). However, the mutation frequencies of 19Del (20.52%) and L858R (24.28%) in patients with NSCLC from Qujing were lower than those reported in the literature. In addition, a higher proportion of *EGFR* G719X + L861Q (21.10%) and G719X + S768I (19.65%) mutation subtypes were found in patients with NSCLC from Qujing. Interestingly, *EGFR* compound mutations were more likely associated with epidemiological issues (living/working in the rural area, e.g., farmers). People who used to live or work in the rural areas of Qujing might have a higher chance of being exposed, for example, to coal-fired flue gas (4, 10). However, further large-scale investigations are warranted to confirm the correlation between *EGFR* compound mutations in NSCLC and environmental exposures in this region.

NSCLC with the coexistence of multiple *EGFR* mutations may have a unique oncogenic mechanism that may reflect the efficacy of EGFR-specific tyrosine kinase inhibitors. ERBB2 phosphorylation was markedly reduced in cells expressing L861Q plus G719X compared with lung cancer cells expressing L861Q alone. The viability assays revealed that lung cancer cells expressing L861Q + G719A showed decreased sensitivity (8- to 58-fold reduction) to EGFR-specific inhibitors, erlotinib and osimertinib, compared with cells expressing L861Q alone, but pan-ERBB inhibitors exerted superior growth-inhibitory effects on cells expressing compound L861Q/G719X mutations (26). Similarly, the cells co-expressing G719X and S768I also showed a good response to afatinib, a pan-ERBB inhibitor (27). In this study, a higher proportion of *EGFR* compound mutations were detected in patients with NSCLC from Qujing. Therefore, pan-ERBB inhibitors exerted superior tumor-growth-inhibitory effects in these patients compared with EGFR-specific inhibitors. Further clinical data should be collected to confirm these cell research based findings.

KRAS is the second most common driver gene in lung cancer, and the frequency of *KRAS* mutation is lower in Chinese patients than in Western populations. However, the mutation frequency of *KRAS* in Qujing (including Xuanwei) was inconsistent (6.3%–29.2%) in previous reports due to the limited number of patients (9–11, 28, 29). In this study based on a large number of patients with NSCLC, the frequency of *KRAS* mutation was significantly higher in patients with NSCLC from Qujing than in those from non-Qujing regions (23.02% vs 7.85%). Targeting KRAS protein has been one of the toughest challenges in cancer treatment research. A specific mutation known as *KRAS* G12C is a major driver of tumor growth, occurring broadly across solid-tumor indications. *KRAS* G12C mutation is found in about 13% of patients with NSCLC in the United States (30), and approximately 32.3% of patients with NSCLC in China (31). In this study, *KRAS* G12C was also the main mutant subtype of *KRAS* in patients with NSCLC from Qujing (51.11%). With the development of drugs inhibiting *KRAS* G12C, this study suggested that patients with *KRAS* G12C mutations in Qujing might benefit from targeted therapy, such as AMG510 (32).

In general, previous studies based on patients with lung cancer from Xuanwei/Qujing showed that a higher proportion of *EGFR* compound mutations and *KRAS* mutations were observed, although *EGFR* mutation rate in patients with lung cancer patients from Xuanwei was still controversial (9–12, 24, 28, 29, 33–35) (**Table 4**). The cause of these specific genetic changes remains unclear. However, the main findings were as follows: people using smoky coal had an up to 30-fold higher risk of lung cancer compared with those using smokeless coal and wood (4); lung cancer patients with coal exposure history in Xuanwei had a higher *KRAS* mutation rate (11, 33) (**Table 4**); and the occupation of patients (living/working in the rural area, e.g., farmers) was independently associated with an increased rate of *EGFR* compound mutations in this study. These findings suggested that environmental exposure might be an important reason for the specific mutation spectrum in this area. Hence, further large-scale investigations are warranted to confirm the

TABLE 4 | *EGFR* and *KRAS* mutation characteristics in patients with lung cancer from Xuanwei/Qujing in previous studies.

Study	Gene	Patients	n	Mutation rate
Hosgood 3rd, et al. (9)	EGFR	NSCLC, female, non-smoking	40	35%
	KRAS	NSCLC, female non-smoking	40	15%
Ma et al. (34)	EGFR	NSCLC	119	EGFR: 39.45% G719X+S768I: 22.69% G719X+L861Q: 0.8%
	KRAS	NSCLC	119	23.53%
DeMarini et al. (29)	KRAS	Lung tumors, female, non-smoking, smoky exposure,	24	29.2%
Keohavong et al. (10)	KRAS	No evidence of lung cancer from XuanWei County	92	2.2%
Keohavong et al. (11)	KRAS	Lung cancer	41	22.9%
Yu et al. (33)	EGFR	NSCLC, smoky coal exposure	79	37.97%
	KRAS	NSCLC, smoky coal exposure	79	29.11%
Chen et al. (24)	EGFR	NSCLC patients	90	EGFR: 57% G719X+S768I: 25.56% G719X+L861Q: 1.0%
Yang et al. (28)	EGFR	NSCLC patients	63	55.6% G719X+S768I: 17.1%
	KRAS	NSCLC patients	63	6.3%
Zhou et al. (12)	EGFR	NSCLC patients	447	EGFR: 34.9% G719X+S768I: 4.5% G719X+L861Q: 0.6%
Zhou et al. (35)	EGFR	NSCLC patients	212	EGFR: 30.1%

correlation between the driver gene profile of patients with lung cancer and the environmental exposure in this region.

On the other hand, some studies showed that patients with *EGFR* mutations in Xuanwei had a poor prognosis after receiving EGFR-TKI treatment. This might be due to the high incidence of rare *EGFR* mutations in this area (12, 36). These studies also found that the incidence of uncommon *EGFR* mutations and *EGFR* compound mutations was high in patients with NSCLC from Qujing. Therefore, the information on the significance of these mutations in targeted treatment deserves further investigation due to the high incidence of NSCLC with the so-called uncommon *EGFR* mutations in the Qujing population. On the contrary, chemotherapy is usually less effective in patients with NSCLC having *KRAS* mutations (37). Many novel treatment strategies have been developed, including targeting downstream signaling pathways (38), directly targeting KRAS (39), and using immunotherapy (40). Of these, immunotherapy may be one of the most promising treatment strategies for patients with NSCLC having *KRAS* mutations. Thus, we hope that these treatment strategies will bring clinical benefits to patients with lung cancer having *KRAS* mutations in Qujing in the future.

The incidence of lung cancer in the Qujing City of China is very high, and the related mortality is also high. Therefore, a comprehensive understanding of the molecular characteristics of patients with lung cancer in this region may provide the basis for a precise diagnosis and treatment. A major strength of this study was the large number of patients with NSCLC included to estimate the prevalence of common actionable genomic alterations (involving *EGFR*, *ALK*, *ROS1*, *KRAS*, *BRAF*, *RET*, *MET*, *HER2*, *NRAS*, and *PIK3CA*) in Qujing. These estimates can serve as a reference for future research. However, this study also had several limitations. First, it was a retrospective analysis and included only a single institution. Second, not all patients underwent the same molecular testing. Furthermore, the data on the treatment and prognosis of these patients were not collected, and therefore whether these patients could benefit from targeted therapy was unclear.

CONCLUSION

In conclusion, this study displayed a unique profile of driver gene mutations in patients with NSCLC in Qujing. More patients with NSCLC in Qujing harbored *EGFR* G719X + S768I and *EGFR* G719X + L861Q compound mutations, besides 19DEL and L858R. Also, patients with NSCLC in Qujing had a higher proportion of *KRAS* (G12C) mutations. Therefore, these findings suggested that different treatment strategies should be adopted in patients with NSCLC in Qujing.

DATA AVAILABILITY STATEMENT

The datasets presented in this study can be found in online repositories. The names of the repository/repositories and accession number(s) can be found in the article/ **Supplementary Material**.

ETHICS STATEMENT

This study was conducted with approval from the Institutional Review Board of Yunnan Cancer Hospital. Informed consent was waived because of the retrospective nature of this study, and the de-sensitized clinical data were collected.

AUTHOR CONTRIBUTIONS

YH, YZ, and HS conceived and designed the experiments. FG, YD, QL, JC, XL, YG, ZS, and LD collected the data. YZ, ZH, FY, and CZ analyzed the data and wrote the manuscript. All authors read and approved the final manuscript.

FUNDING

This study was partially supported by The National Natural Science Fund (No. 81860513, and No. 81960335).

SUPPLEMENTARY MATERIAL

The Supplementary Material for this article can be found online at: https://www.frontiersin.org/articles/10.3389/fonc.2021.644895/full#supplementary-material

Supplementary Figure 1 | Mutation frequencies of *EGFR*, *ALK*, *ROS1*, and *KRAS* in patients with lung adenocarcinoma from Qujing and non-Qujing areas.

Supplementary Figure 2 | Co-mutations of driver genes in patients with NSCLC from Qujing and non-Qujing areas.

REFERENCES

1. Torre LA, Bray F, Siegel RL, Ferlay J, Lortet-Tieulent J, Jemal A. Global cancer statistics, 2012. *CA Cancer J Clin* (2015) 65:87–108. doi: 10.3322/caac.21262
2. Ferlay J, Soerjomataram I, Dikshit R, Eser S, Mathers C, Rebelo M, et al. Cancer incidence and mortality worldwide: sources, methods and major patterns in GLOBOCAN 2012. *Int J Cancer* (2015) 136:E359–86. doi: 10.1002/ijc.29210
3. Xiao Y, Shao Y, Yu X, Zhou G. The epidemic status and risk factors of lung cancer in Xuanwei City, Yunnan Province, China. *Front Med* (2012) 6:388–94. doi: 10.1007/s11684-012-0233-3
4. Barone-Adesi F, Chapman RS, Silverman DT, He X, Hu W, Vermeulen R, et al. Risk of lung cancer associated with domestic use of coal in Xuanwei, China: retrospective cohort study. *BMJ* (2012) 345:e5414. doi: 10.1136/bmj.e5414
5. Lan Q, He X, Shen M, Tian L, Liu LZ, Lai H, et al. Variation in lung cancer risk by smoky coal subtype in Xuanwei, China. *Int J Cancer* (2008) 123:2164–9. doi: 10.1002/ijc.23748
6. Cai L, Wu X, Goyal A, Han Y, Cui W, Xiao X, et al. Patterns and socioeconomic influences of tobacco exposure in tobacco cultivating rural areas of Yunnan Province, China. *BMC Public Health* (2012) 12:842. doi: 10.1186/1471-2458-12-842
7. Shen M, Chapman RS, He X, Liu LZ, Lai H, Chen W, et al. Dietary factors, food contamination and lung cancer risk in Xuanwei, China. *Lung Cancer* (2008) 61:275–82. doi: 10.1016/j.lungcan.2007.12.024
8. Taylor PR, Qiao YL, Schatzkin A, Yao SX, Lubin J, Mao BL, et al. Relation of arsenic exposure to lung cancer among tin miners in Yunnan Province, China. *Br J Ind Med* (1989) 46:881–6. doi: 10.1136/oem.46.12.881
9. Hosgood HD3, Pao W, Rothman N, Hu W, Pan YH, Kuchinsky K, et al. Driver mutations among never smoking female lung cancer tissues in China identify unique EGFR and KRAS mutation pattern associated with household coal burning. *Respir Med* (2013) 107:1755–62. doi: 10.1016/j.rmed.2013.08.018
10. Keohavong P, Lan Q, Gao WM, Zheng KC, Mady HH, Melhem MF, et al. Detection of p53 and K-ras mutations in sputum of individuals exposed to smoky coal emissions in Xuan Wei County, China. *Carcinogenesis* (2005) 26:303–8. doi: 10.1093/carcin/bgh328
11. Keohavong P, Lan Q, Gao WM, DeMarini DM, Mass MJ, Li XM, et al. K-ras mutations in lung carcinomas from nonsmoking women exposed to unvented coal smoke in China. *Lung Cancer* (2003) 41:21–7. doi: 10.1016/s0169-5002(03)00125-9
12. Zhou Y, Yang Y, Yang C, Chen Y, Yang C, Du Y, et al. Epidermal growth factor receptor (EGFR) mutations in non-small cell lung cancer (NSCLC) of Yunnan in southwestern China. *Oncotarget* (2017) 8:15023–33. doi: 10.18632/oncotarget.14706
13. El-Deiry WS, Goldberg RM, Lenz HJ, Shields AF, Gibney GT, Tan AR, et al. The current state of molecular testing in the treatment of patients with solid tumors, 2019. *CA Cancer J Clin* (2019) 69:305–43. doi: 10.3322/caac.21560
14. Li J, Guo W, Ran J, Tang R, Lin H, Chen X, et al. Five-year lung cancer mortality risk analysis and topography in Xuan Wei: a spatiotemporal correlation analysis. *BMC Public Health* (2019) 19:173. doi: 10.1186/s12889-019-6490-1
15. Hosgood HD3, Sapkota AR, Rothman N, Rohan T, Hu W, Xu J, et al. The potential role of lung microbiota in lung cancer attributed to household coal burning exposures. *Environ Mol Mutagen* (2014) 55:643–51. doi: 10.1002/em.21878
16. Seow WJ, Hu W, Vermeulen R, Hosgood Iii HD, Downward GS, Chapman RS, et al. Household air pollution and lung cancer in China: a review of studies in Xuanwei. *Chin J Cancer* (2014) 33:471–5. doi: 10.5732/cjc.014.10132
17. Wong J, Downward GS, Hu W, Portengen L, Seow WJ, Silverman DT, et al. Lung cancer risk by geologic coal deposits: A case-control study of female never-smokers from Xuanwei and Fuyuan, China. *Int J Cancer* (2019) 144:2918–27. doi: 10.1002/ijc.32034
18. McCarthy CE, Duffney PF, Gelein R, Thatcher TH, Elder A, Phipps RP, et al. Dung biomass smoke activates inflammatory signaling pathways in human small airway epithelial cells. *Am J Physiol Lung Cell Mol Physiol* (2016) 311:L1222–1222L1233. doi: 10.1152/ajplung.00183.2016
19. Mehra D, Geraghty PM, Hardigan AA, Foronjy R. A comparison of the inflammatory and proteolytic effects of dung biomass and cigarette smoke exposure in the lung. *PloS One* (2012) 7:e52889. doi: 10.1371/journal.pone.0052889
20. Mondal NK, Saha H, Mukherjee B, Tyagi N, Ray MR. Inflammation, oxidative stress, and higher expression levels of Nrf2 and NQO1 proteins in the airways of women chronically exposed to biomass fuel smoke. *Mol Cell Biochem* (2018) 447:63–76. doi: 10.1007/s11010-018-3293-0
21. Liu SY, Mok T, Wu YL. Novel targeted agents for the treatment of lung cancer in China. *Cancer* (2015) 121 Suppl 17:3089–96. doi: 10.1002/cncr.29522
22. Kris MG, Johnson BE, Berry LD, Kwiatkowski DJ, Iafrate AJ, Wistuba II, et al. Using multiplexed assays of oncogenic drivers in lung cancers to select targeted drugs. *JAMA* (2014) 311:1998–2006. doi: 10.1001/jama.2014.3741
23. Midha A, Dearden S, McCormack R. EGFR mutation incidence in non-small-cell lung cancer of adenocarcinoma histology: a systematic review and global map by ethnicity (mutMapII). *Am J Cancer Res* (2015) 5:2892–911. doi: 10.18632/oncotarget.12587
24. Chen Y, Ye L, Stanford RR, Zhang D, Zhang X, Wei W. Distinct epithelial growth factor receptor mutation profile in non-small-cell lung cancer patients from the Xuanwei area of China. *Mol Clin Oncol* (2016) 4:749–55. doi: 10.3892/mco.2016.805
25. Gristina V, Malapelle U, Galvano A, Pisapia P, Pepe F, Rolfo C, et al. The significance of epidermal growth factor receptor uncommon mutations in non-small cell lung cancer: A systematic review and critical appraisal. *Cancer Treat Rev* (2020) 85:101994. doi: 10.1016/j.ctrv.2020.101994
26. Sato H, Offin M, Kubota D, Yu HA, Wilhelm C, Toyooka S, et al. Allele-specific role of ERBB2 in the oncogenic function of EGFR L861Q in EGFR-mutant lung cancers. *J Thorac Oncol* (2020) 16:113–26. doi: 10.1016/j.jtho.2020.09.019
27. Kutsuzawa N, Takahashi F, Tomomatsu K, Obayashi S, Takeuchi T, Takihara T, et al. Successful Treatment of a Patient with Lung Adenocarcinoma Harboring Compound EGFR Gene Mutations, G719X and S768I, with Afatinib. *Tokai J Exp Clin Med* (2020) 45:113–6.
28. Yang CS, Pan XY, Feng Q, Wang YY, Xu WM, Jiang T, et al. [Mutation status of epidermal growth factor receptor and KRAS gene in non-small cell lung

cancers at Xuanwei regions of Yunnan Province]. *Zhonghua Bing Li Xue Za Zhi* (2016) 45:226–30. doi: 10.3760/cma.j.issn.0529-5807.2016.04.003
29. DeMarini DM, Landi S, Tian D, Hanley NM, Li X, Hu F, et al. and TP53 mutations in nonsmokers reflect exposure to PAH-rich coal combustion emissions. *Cancer Res* (2001) 61:6679–81. doi: 10.1016/S0140-6701(02)86513-4
30. Biernacka A, Tsongalis PD, Peterson JD, de Abreu FB, Black CC, Gutmann EJ, et al. The potential utility of re-mining results of somatic mutation testing: KRAS status in lung adenocarcinoma. *Cancer Genet* (2016) 209:195–8. doi: 10.1016/j.cancergen.2016.03.001
31. Jia Y, Jiang T, Li X, Zhao C, Zhang L, Zhao S, et al. Characterization of distinct types of KRAS mutation and its impact on first-line platinum-based chemotherapy in Chinese patients with advanced non-small cell lung cancer. *Oncol Lett* (2017) 14:6525–32. doi: 10.3892/ol.2017.7016
32. Liu SY, Sun H, Zhou JY, Jie GL, Xie Z, Shao Y, et al. Clinical characteristics and prognostic value of the KRAS G12C mutation in Chinese non-small cell lung cancer patients. *Biomark Res* (2020) 8:22. doi: 10.1186/s40364-020-00199-z
33. Yu XJ, Yang MJ, Zhou B, Wang GZ, Huang YC, Wu LC, et al. Characterization of Somatic Mutations in Air Pollution-Related Lung Cancer. *EBioMedicine* (2015) 2:583–90. doi: 10.1016/j.ebiom.2015.04.003
34. Ma Y, Li Q, Du Y, Chen W, Zhao G, Liu X, et al. Oncogenic Genetic Alterations in Non-Small-Cell Lung Cancer (NSCLC) in Southwestern China. *Cancer Manag Res* (2020) 12:10861–74. doi: 10.2147/CMAR.S266069
35. Zhou Y, Ma Y, Shi H, Du Y, Huang Y. Epidermal growth factor receptor T790M mutations in non-small cell lung cancer (NSCLC) of Yunnan in southwestern China. *Sci Rep* (2018) 8:15426. doi: 10.1038/s41598-018-33816-x
36. Lv L, Liu Z, Liu Y, Zhang W, Jiang L, Li T, et al. Distinct EGFR Mutation Pattern in Patients With Non-Small Cell Lung Cancer in Xuanwei Region of China: A Systematic Review and Meta-Analysis. *Front Oncol* (2020) 10:519073. doi: 10.3389/fonc.2020.519073
37. Wood K, Hensing T, Malik R, Salgia R. Prognostic and Predictive Value in KRAS in Non-Small-Cell Lung Cancer: A Review. *JAMA Oncol* (2016) 2:805–12. doi: 10.1001/jamaoncol.2016.0405
38. Tomasini P, Walia P, Labbe C, Jao K, Leighl NB. Targeting the KRAS Pathway in Non-Small Cell Lung Cancer. *Oncologist* (2016) 21:1450–60. doi: 10.1634/theoncologist.2015-0084
39. Canon J, Rex K, Saiki AY, Mohr C, Cooke K, Bagal D, et al. The clinical KRAS (G12C) inhibitor AMG 510 drives anti-tumour immunity. *Nature* (2019) 575:217–23. doi: 10.1038/s41586-019-1694-1
40. Liu C, Zheng S, Jin R, Wang X, Wang F, Zang R, et al. The superior efficacy of anti-PD-1/PD-L1 immunotherapy in KRAS-mutant non-small cell lung cancer that correlates with an inflammatory phenotype and increased immunogenicity. *Cancer Lett* (2020) 470:95–105. doi: 10.1016/j.canlet.2019.10.027

Conflict of Interest: ZH, FY, and CZ were employed by Amoy Diagnostics Co., Ltd.

The remaining authors declare that the research was conducted in the absence of any commercial or financial relationships that could be construed as a potential conflict of interest.

frontiers in Oncology

REVIEW
published: 13 April 2021
doi: 10.3389/fonc.2021.635329

Main N6-Methyladenosine Readers: YTH Family Proteins in Cancers

Xin-Yuan Dai[1†], Liang Shi[1†], Zhi Li[1†], Hai-Yan Yang[1], Ji-Fu Wei[2] and Qiang Ding[1*]*

[1] Jiangsu Breast Disease Center, The First Affiliated Hospital With Nanjing Medical University, Nanjing, China, [2] Research Division of Clinical Pharmacology, The First Affiliated Hospital With Nanjing Medical University, Nanjing, China

Among the over 150 RNA modifications, N6-methyladenosine (m6A) is the most abundant internal modification in eukaryotic RNAs, not only in messenger RNAs, but also in microRNAs and long non-coding RNAs. It is a dynamic and reversible process in mammalian cells, which is installed by "writers," consisting of METTL3, METTL14, WTAP, RBM15/15B, and KIAA1429 and removed by "erasers," including FTO and ALKBH5. Moreover, m6A modification is recognized by "readers," which play the key role in executing m6A functions. IYT521-B homology (YTH) family proteins are the first identified m6A reader proteins. They were reported to participate in cancer tumorigenesis and development through regulating the metabolism of targeted RNAs, including RNA splicing, RNA export, translation, and degradation. There are many reviews about function of m6A and its role in various diseases. However, reviews only focusing on m6A readers, especially YTH family proteins are few. In this review, we systematically summarize the recent advances in structure and biological function of YTH family proteins, and their roles in human cancer and potential application in cancer therapy.

Keywords: cancer, IYT521-B homology domain proteins, N6-methyladenosine, cancer therapy, RNA metabolism

OPEN ACCESS

Edited by:
Lorenzo Gerratana, University of Udine, Italy

Reviewed by:
Ping Yi, Third Affiliated Hospital of Chongqing Medical University, China
Ye Fu, Plaisance Capital Management, United States

***Correspondence:**
Qiang Ding
dingqiang@njmu.edu.cn
Ji-Fu Wei
weijifu@hotmail.com

[†]These authors have contributed equally to this work

Specialty section:
This article was submitted to Molecular and Cellular Oncology, a section of the journal Frontiers in Oncology

Received: *30 November 2020*
Accepted: *17 March 2021*
Published: *13 April 2021*

Citation:
Dai X-Y, Shi L, Li Z, Yang H-Y, Wei J-F and Ding Q (2021) Main N6-Methyladenosine Readers: YTH Family Proteins in Cancers. Front. Oncol. 11:635329. doi: 10.3389/fonc.2021.635329

INTRODUCTION

In recent years, post-transcriptional modification, which plays an important role in physiological and disease progression, has attracted more and more attention in molecular biology research. RNA modification is an emerging area of post-transcriptional modification. Among the over 150 RNA modifications, N6-methyladenosine (m6A) is identified as the most abundant and evolutionarily conserved internal RNA modification in eukaryotic RNAs, not only in messenger RNAs (mRNAs) (1), but also in microRNAs (2) and long non-coding RNAs (lncRNAs) (3). Although m6A was first discovered in the 1970s (1), the precise function of m6A residues in the regulation of gene expression has been identified until recent years with the advance of high-throughput sequencing technology, which mapped of m6A residues in the whole transcriptome (4, 5). Since then, numerous studies have carried out to verify the significance of m6A modification, which largely broadens the study in RNA fields (6, 7).

The m6A modification is mainly located in a consensus RNA motif of RRACH (R=A or G, H=A, U, or C) and particularly enriched in 3′ untranslated regions (3′ UTRs) and near stop codons (8). Similar to other epigenetic modifications like DNA and histone modification, m6A modification is dynamic and reversible. It is installed by "writers", which refer to m6A methylase complex consisting of methyltransferase-like 3 (METTL3), methyltransferase-like 14 (METTL14), Wilms tumor 1 associated protein (WTAP), RNA binding motif 15/15B (RBM15/15B), and

KIAA1429 (9–12). "Erasers" are m6A demethylases, including fat mass and obesity-associated protein (FTO) and AlkB homologue 5 (ALKBH5), which could remove m6A modification from RNAs and make m6A modification in a dynamic balance (13, 14). "Readers" refer to proteins that are capable to recognize and bind m6A modification, which mainly mediate the regulation of m6A modification in gene expression by affecting the fate of targeted RNAs (15). Reader proteins play the key role in executing m6A functions.

YT521-B homology (YTH) family proteins were the first identified m6A reader proteins. YTH family proteins can recognize m6A modification in a methylation-dependent manner through a specific YTH domain (16), which is recognized as a structured RNA binding domain and highly conserved among eukaryotes (17). By searching the human genome, there are five proteins in human genome carrying the YTH domain, which are divided into three categories: YTH m6A-binding protein (YTHDF) including YTHDF1-3, YTH domain-containing 1 (YTHDC1) and YTH domain-containing 2 (YTHDC2) (18). YTH family proteins are recruited by m6A and able to affect mRNA metabolism including mRNA splicing, nuclear export, translation, and mRNA degradation (6, 19). Accordingly, YTH family proteins are involved in many physiological processes, infection diseases and cancers. There are many reviews about the function of m6A and its role in various diseases (20, 21). However, reviews only focusing on m6A readers are few. In this review, we systematically introduce the main m6A readers YTH family proteins, summarize the structure features, the function of YTH family proteins in post-transcriptional gene regulation and their roles in tumorigenesis, cancer progression and potential application in cancer therapy. It may provide clues for the study of molecular mechanism of m6A readers in human cancers and exploring their clinical application in cancer treatment.

STRUCTURE FEATURES OF YTH DOMAIN

YTH domain was previously regarded was a structured RNA binding domain and highly conserved among eukaryotes (22). Subsequent studies proved that the ~150 amino acid YTH domain recognizes and binds RNAs in an m6A-dependent manner (16, 23). The structure of YTH family proteins have been understood until the crystal structures of the YTHDC1 YTH domain and YTHDC1–GG(m6A)CU complex were first studied, unveiling the molecular mechanism of m6A-YTH binding and sequence selectivity (16). The YTH domain adopts a conserved α/β fold containing 3α helices and 6β strands. 6β strands form a barrel fold and 3α helices are packed against the β strands to organize a hydrophobic core (16, 18). In the YTHDC1-GG(m6A)CU complex, the m6A is recognized by an aromatic cage consisting of 3 hydrophobic residues W377, W428, and L439. The aromatic cage of YTH domain forms a hydrophobic binding pocket that can recognize buried methyl groups with a cavity insertion mode. This complex structure provides the basis for specific m6A recognition by YTH domain. Compared to YTHDC1 YTH domain, other YTH family proteins have the similar cage structure. In YTHDC2, aromatic cage is composed of W1310, W1360 and L1365 (24); W411, W465 and W470 in YTHDF1 (25) and W432, W486 and W491 in YTHDF2 (26).

Despite conserved aromatic cages, YTH domain displays different sequence selectivity. The YTH domain of YTHDC1 favors a guanine nucleotide and disfavors an adenosine at the −1 position relative to the m6A. YTHDC1 shows preference to bind to the GG(m6A)C sequence. However, different from YTHDC1, YTHDF1, YTHDF2, and YTHDC2 YTH domains do not display sequence selectivity at the −1 position (25). The difference in sequence selectivity between YTHDC1 and other YTH family proteins may reflect the different m6A-binding requirement in the nucleus and cytoplasm (18). These structural data strongly support the proposal that YTH family proteins function as the reader for m6A.

Like most RNA binding domains which are surrounded by structured domains or low complexity regions with various functions (27), YTH domain is also flanked by several disordered regions. YTHDC1 is surrounded by regions rich in charged residues such as Glu-rich, Arg-rich segments, or in proline-rich (28). YTHDF family proteins are surrounded by Pro, Gln, and Asn-rich segments (26). Different from other YTH family proteins surrounded by low complexity regions, YTHDC2 is a multi-domain protein containing multiple helicase domains and two Ankyrin repeats. Consistent with its domain composition, YTHDC2 has ATPase and 3′→5′RNA helicase activities (29, 30). These unique features endow YTHDC2 with various functions, including recruiting and interacting with other protein complex members and exerting regulatory effects on RNA binding and RNA structure. These flanking regions are essential for YTH family proteins to exert functions in regulating fates of m6A-modified RNA by affecting the subcellular localization of YTH family proteins and their partners.

FUNCTIONS OF YTH FAMILY PROTEINS IN mRNA METABOLISM

mRNA metabolism refers to the entire mRNA life from birth to death that includes transcription, mRNA processing, mRNA nuclear exportation, mRNA translation and mRNA degradation. YTH family proteins play an essential role in regulating cellular fates of m6A-modified mRNAs. In 5 human YTH family proteins, YTHDC1 is the only nuclear protein involved in transcription (31), mRNA splicing (32) and nuclear export (33), whereas YTHDF1 (34, 35), YTHDF2 (36, 37), YTHDF3 (34, 38) and YTHDC2 (39) are cytoplasmic m6A readers mainly involved in mRNA translation and degradation. As shown in **Figure 1**, YTH family proteins are almost involved in every step of mRNA metabolism.

Regulation in mRNA Splicing and Nuclear Export

YTHDC1 is located in the nucleus and forms a novel compartment called YT bodies, which are adjacent to RNA

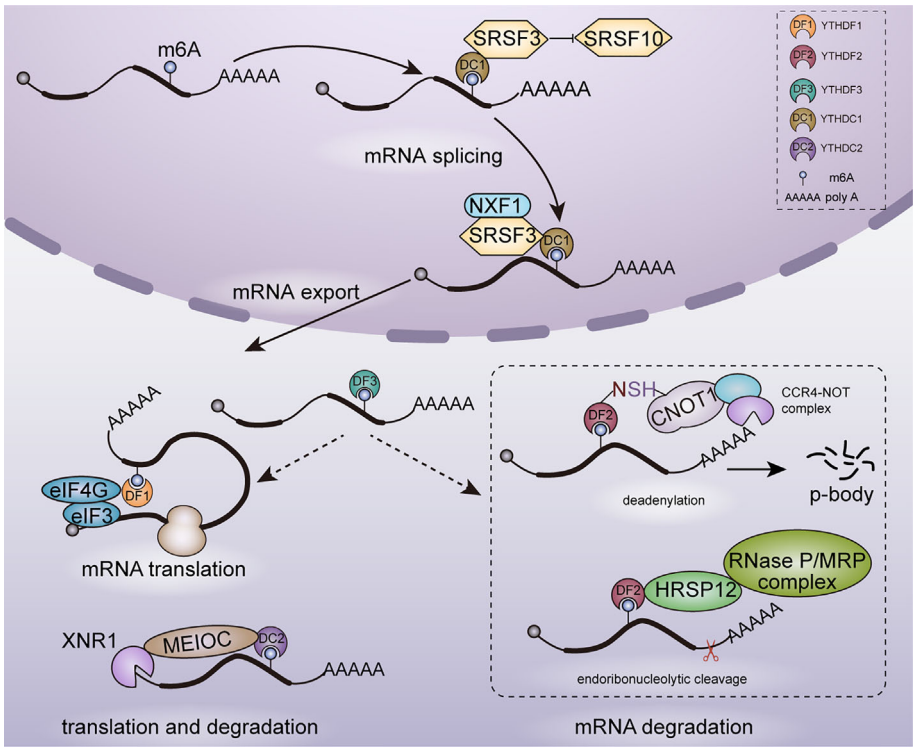

FIGURE 1 | Functions of YTH family proteins in mRNA metabolism. In nucleus, YTHDC1 participates in mRNA splicing and nuclear export. In cytoplasm, YTHDF1/2/3, YTHDC2 are involved in mRNAs translation and degradation.

processing speckles enriching mRNA splicing factors (28). This nuclear localization is consistent with that YTHDC1 interacts with several splicing regulators including SRSF3 (40), SAM68 (41) and SC35 (42). Role of YTHDC1 in regulating mRNA splicing was established in *Drosophila* sex determination and mouse embryogenesis. In *Drosophila*, YTHDC1 decoded m6A in the spliced intron of sex determination factor Sex lethal (Sxl) and facilitated the alternative splicing of Sxl pre-mRNA, which determines female physiognomy (43). In mouse oocytes, loss of YTHDC1 led to extensive alternative polyadenylation and massive defects in alternative splicing, which hindered oocyte maturation (33). Mechanically, YTHDC1 regulated mRNA splicing by recruiting pre-mRNA splicing factor SRSF3 to promote exon inclusion whiles blocking binding of SRSF10, which facilitated exon skipping (44).

Despite the essential role in alternative splicing, YTHDC1 was also reported to promote the export of methylated mRNA from nucleus to cytoplasm in HeLa cells. This process relied on the interaction with the splicing factor SRSF3 which functions as a key adaptor in nuclear RNA export factor 1 (NXF1) -dependent nuclear export pathway (33).

Regulation in mRNA Translation

Knockdown of YTHDF1 in HeLa cells led to reduced translation efficiency of its targeted transcripts and YTHDF1 was found to promote ribosome loading of targeted mRNAs, indicating the role of YTHDF1 in enhancing mRNA translation. With METTL3 depleted, the translation efficiency of YTHDF1 targeted transcripts was decreased completely. It confirmed that YTHDF1 promoted translation efficiency in an m6A-dependent manner. However, the underlying mechanism of YTHDF1 promoting translation efficiency is still unclear currently. It may rely on the interaction with eukaryotic initiation factor 3 (eIF3) and eIF4G-mediated loop formation (35). YTHDF3 shares numerous similar targets with YTHDF1 and YTHDF2: 58% of YTHDF3 targets are also recognized by YTHDF1 and 60% by YTHDF2, which indicates a potential coordination on common targets among YTHDF proteins. YTHDF3 was found to promote the translation of targeted mRNAs through interacting with YTHDF1 (34).

In YTHDC2–/– mouse testes, translation efficiency of YTHDC2 targets structural maintenance of chromosomes 3 (Smc3) and centrosomal protein 76 (Cep76) showed a significant decrease, whereas mRNA abundance showed an increase. Furthermore, YTHDC2 was observed in the 40–80S ribosome fraction, indicating that YTHDC2 may enhance translation efficiency by interacting with cellular machinery involved in translation initiation (39).

Regulation in mRNA Degradation

mRNA degradation plays key roles in gene expression regulation and mRNA quality control. YTHDF2 is the main m6A reader protein to promote the decay of m6A-containing mRNA (2, 36, 45). YTHDF2 selectively recognized m6A-containing mRNA through C-terminal of YTH domain, whereas its N-

terminal region localized the YTHDF2-m6A-mRNA complex from the translatable pool to mRNA decay sites such as processing bodies (P-bodies) for mRNA degradation (43). Furthermore, YTHDF2 triggered deadenylation and degradation of m6A-containing mRNAs by recruiting the carbon catabolite repression 4–negative on TATA-less (CCR4–NOT) deadenylase complex, with N-YTHDF2 interacting with the superfamily homology (SH) domain of CCR4–NOT transcription complex subunit 1 (CNOT1) (36). Despite CCR4-NOT complex-mediated deadenylation pathway, m6A RNAs bound by YTHDF2 can be degraded through another RNase P/MRP-mediated endoribonucleolytic pathway. An adaptor protein heat-responsive protein 12 (HRSP12) bridged YTHDF2 and RNase P/MRP, which aroused endoribonucleolytic cleavage of YTHDF2-binding m6A RNAs (45). Moreover, YTHDF3 was identified to accelerate the degradation of mRNAs through interacting with YTHDF2 (34).

In addition to YTHDF proteins, YTHDC2 also plays a role in affecting mRNA stability and promoting mRNA degradation. In a study on regulation of m6A on hepatic drug-metabolizing enzyme, YTHDC2 was identified to promote cytochrome P450 family 2 subfamily C member 8 (CYP2C8) mRNA degradation by recognizing the m6A-modified CYP2C8 mRNA and negatively regulated CYP2C8 expression (46). YTHDC2 is highly expressed in mouse testes and YTHDC2 plays an important role in facilitating proper spermatocyte development (39). YTHDC2 has ATPase and a 3′-5′ RNA helicase activity. It interacted with the meiosis-specific MEIOC protein as well as with 5′-3′ exoribonuclease XRN1 *via* the Ankyrin repeat insertion that is located within the helicase domain of YTHDC2 and then degraded m6A-containing transcripts (29). In contrast to YTHDF2, YTHDC2 regulates RNA stability in an RNA-independent manner through increasing the local concentration of the RNA decay machineries.

Regulation in RNA Phase Separation

The main mechanism by which YTHDF proteins target m6A-containing mRNAs to exact functions in various biological processes is through liquid-liquid phase separation (LLPS). Structurally, besides YTH domain at C-termini, all three YTHDF proteins have a low complexity domain at their N-termini, which seems to be Prion-like domain and has the potential to undergo phase separation. YTHDF proteins bound m6A-containing mRNA to undergo phase separation and formed RNA-protein droplets. These RNA-protein droplets partitioned into different endogenous phase-separated compartments, such as P-bodies, stress granules and other RNA-protein assemblies, where mRNAs could be stored or degraded (47–49). In addition, YTHDF proteins play an important role in promoting stress granule (SG) formation. They functioned as SG shell proteins and promoted SG formation by bringing together multiple SG core clusters to form large granules under oxidative stress (50).

Regulation in Transcription

Knockout of METTL3 or YTHDC1 in mouse embryonic stem cells was found to increase chromatin accessibility and activate transcription in an m6A-dependent manner. Mechanistically, nuclear reader YTHDC1 recognized m6A-modified chromosome-associated regulatory RNAs (carRNAs) deposited by METTL3 and promoted the decay of these RNAs through the NEXT-mediated nuclear degradation (31). Nuclear exosome targeting (NEXT) complex contains hMTR4, the Zn-knuckle protein ZCCHC8 and the putative RNA binding protein RBM7 (51). YTHDC1 was involved in nuclear degradation by interacting with the NEXT components RBM7 and ZCCHC8. However, whether these carRNAs play a role in various types of cancers warrants further studies. Currently, studies on m6A function mainly focus on post-transcription regulation, more precise mechanisms of m6A in regulating transcription are needed to be further investigated.

Dispute on Regulation of YTHDF Proteins in mRNA Metabolism

According to the prevailing mode for functions of YTHDF proteins in regulating mRNA metabolism, YTHDF1 enhances translation efficiency; YTHDF2 facilitates mRNA degradation; and YTHDF3 promotes translation and degradation by interacting with YTHDF1 and YTHDF2 (35, 43). Each YTHDF paralog controls various physiologic processes and diseases by targeting specific cohorts of m6A-containing mRNAs. However, other studies suggested that these three YTHDF proteins may have similar roles in mRNA degradation by recruiting the main mRNA deadenylation complex CCR4–NOT on m6A-containing mRNA (36, 52). In a recent study, Zaccara et al. proposed a novel unified model that all YTHDF paralogs bound to all m6A sites in a similar manner. The main effect of three YTHDF proteins was to facilitate the degradation of the same subset of mRNAs in a redundant manner, rather than enhance translation as previous studies suggested (53). Whether these three YTHDF proteins are functionally redundant and whether YTHDF proteins enhance mRNA translation are still disputed. Zaccara et al. thought that links between YTHDF proteins and mRNA translation presented by previous studies were affected by bioinformatic and technical issues, which may lead to the incorrect view that a major function of YTHDF proteins was to promote translation. So more independent studies with careful experimental design are needed to answer these questions in the future. In addition, interplay between these YTHDF proteins in impacting mRNA translation or degradation, and their interacting proteins involved in different cellular processes still warrant further research.

ROLES OF YTH FAMILY PROTEINS IN CANCERS

YTH family proteins play important roles in physiological processes through mediating metabolic process of targeted RNAs (54), such as sex determination (32, 55, 56), oocyte development (57), spermatogenesis (39), stem cell maintenance and differentiation (55, 56), and stress response (55, 56, 58).

Recently, the increasing evidences have shown that YTH family proteins exert effects on multiple human diseases. In this part, we focus on the roles of these YTH family proteins in various cancers (**Figure 2**, **Table 1**).

Hepatocellular Carcinoma (HCC)

Hepatocellular carcinoma is one of the most aggressive malignancies, which ranks as the fourth leading cause of cancer-related deaths worldwide. In 188 clinical HCC tissues, immunohistochemistry staining (IHC) results showed that the positive rate of YTHDF2 was 35.6% and nearly 83.9% in grade III HCC tissues, which revealed that YTHDF2 was closely associated with HCC (80). YTHDF2 was found to promote the liver cancer stem cell phenotype and cancer metastasis by enhancing OCT4 mRNA translation in a m6A-dependent manner (67). On the contrary, YTHDF2 was reported to function as a tumor suppressor in other studies, YTHDF2 inhibited the proliferation and growth of HCC cells *via* promoting the degradation of epidermal growth factor receptor (EGFR) mRNA, which is the upstream of the ERK/MAPK pathway (68). Moreover, silence of YTHDF2 escalated inflammation, vascular remodeling and metastasis of HCC. Mechanistically, YTHDF2 plays a suppressive role in HCC through promoting the degradation of inflammatory cytokines interleukin 11 (IL11) and serpin family E member 2 (SERPINE2) mRNAs (69).

YTHDF1 acts as an oncogene in HCC. YTHDF1 was overexpressed and positively correlated with pathology stage in HCC patients by analyzing TCGA data. Up-regulation of YTHDF1 was associated with poor prognosis in HCC patients (81, 82). Mechanistically, YTHDF1 promotes the epithelial mesenchymal transition (EMT) of HCC cells *via* promoting the translation of snail family transcriptional repressor 1 (Snail) mRNA (59). Similarly, YTHDF1 was also observed to promote HCC cell proliferation and metastasis by promoting the translational output of frizzled5 (FZD5) mRNA in an m6A-dependent manner and acts as an oncogene through activating the WNT/β-catenin pathway (60). Accordingly, YTHDF1 can be a potential biomarker for HCC diagnosis and prognosis.

Pancreatic Cancer

Pancreatic cancer is associated with extremely poor prognosis and remains a highly lethal disease due to difficulties in early diagnosis and metastasis. Interestingly, YTHDF2 plays the dual role in pancreatic cancer progression. It promoted the proliferation but suppressed migration and invasion of

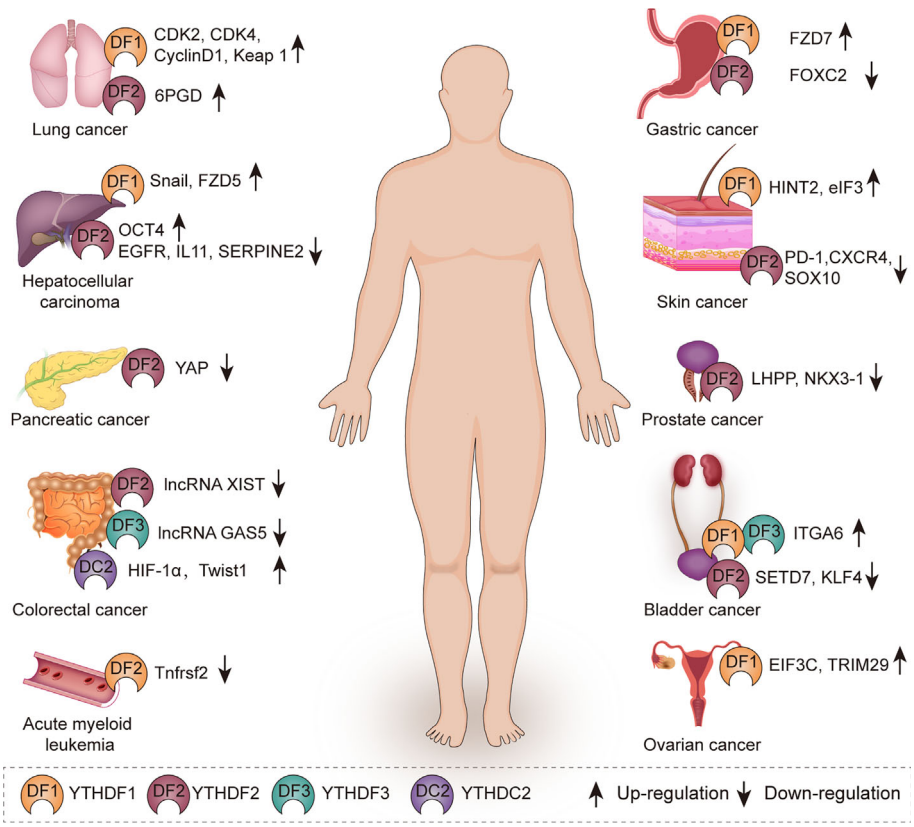

FIGURE 2 | The role of YTH family proteins in human cancers. YTH family proteins are associated with various kinds of cancers including lung cancer, hepatocellular carcinoma, pancreatic cancer, colorectal cancer, acute myeloid leukemia, gastric cancer, skin cancer, prostate cancer, bladder cancer, and ovarian cancer.

TABLE 1 | Multiple functions exerted by YTH family proteins in various cancers.

Molecule	Cancer type	Target	Effect on target	Role in cancer	Reference
YTHDF1	HCC	Snail	Translation	Promote EMT of HCC cells	(59)
	HCC	FZD5	Translation	Promote cell proliferation and metastasis	(60)
	Gastric cancer	FZD7	Translation	Promote cell proliferation	(61)
	Lung cancer	CDK2, CDK4, cyclin D1	Translation	Promote cell proliferation	(62)
	Ovarian cancer	EIF3C	Translation	Promote cell proliferation and metastasis	(63)
	Ovarian cancer	TRIM29	Translation	Enhance CSC-like characteristics	(64)
	Ocular melanoma	HINT2	Translation	Inhibit cell proliferation and migration	(65)
	MCC	eIF3	Translation	Promote cell proliferation	(66)
YTHDF2	HCC	OCT4	Translation	Promote CSC phenotype and metastasis	(67)
	HCC	EGFR	Degradation	Inhibit cell proliferation	(68)
	HCC	IL11, SERPINE2	Degradation	Inhibit inflammation, vascular remodeling and metastasis	(69)
	Pancreatic cancer	YAP	Expression	Promote cell proliferation but inhibit migration and invasion	(70)
	Gastric cancer	FOXC2	Expression	Inhibit cell proliferation, invasion and migration	(71)
	CRC	XIST	Degradation	Inhibit cell proliferation and metastasis	(72)
	Lung cancer	6PGD	Translation	Promote cell proliferation	(22)
	AML	Tnfrsf2	Stability	Promote LSC development and AML initiation	(73)
	Bladder cancer	SETD7, KLF4	Degradation	Promotes cell migration	(74)
	Prostate cancer	LHPP, NKX3–1	Degradation	Promote cell proliferation and migration	(75)
	Melanoma	PD-1, CXCR4, SOX10	Degradation	Inhibit cell proliferation and migration	(76)
YTHDF3	CRC	LncRNA GAS5	Degradation	Promote CRC progression	(77)
YTHDF1/3	Bladder cancer	ITGA6	Translation	Promote cell proliferation and migration	(78)
YTHDC2	CRC	HIF-1α,Twist1	Translation	Promote cell metastasis	(79)

HCC, hepatocellular carcinoma; CRC, colorectal cancer; MCC, Merkel cell carcinoma; AML, acute myeloid leukemia; EMT, epithelial mesenchymal transition; CSC, cancer stem cell; LSC, leukemic stem cell.

pancreatic cancer cells, which is so called "migration-proliferation dichotomy". Mechanistically, silence of YTHDF2 inhibited proliferation through Akt/GSK3b/CyclinD1 pathway and promoted EMT *via* up-regulation of yes-associated protein (YAP), YAP serves as the core components of the Hippo pathway, which can promote the proliferation and survival of epithelial cells (70).

Gastric Cancer

Gastric cancer is the fifth most common cancer and ranks third in cancer-related death worldwide. YTHDF1 acts as an oncogene in gastric cancer. High expression of YTHDF1 was associated with poor overall survival in gastric cancer patients. Suppression of YTHDF1 inhibited the proliferation and tumorigenesis of gastric cancer cells. Mechanistically, YTHDF1 recognizes m6A-modified frizzled7 (FZD7) mRNA and accelerates its translation. FZD7 is a key Wnt receptor and increased expression of FZD7 leads to hyper-activation of the Wnt/β-catenin pathway and promotion of gastric carcinogenesis (61). In addition, YTHDF2 is down-regulated in gastric cancer tissues and cells. Overexpression of YTHDF2 significantly inhibited the proliferation, invasion and migration of gastric cancer cells by negatively regulating forkhead box C2 (FOXC2), which acts as an oncogene in various cancers such as nasopharyngeal cancer, colorectal cancer and triple negative breast cancer (71, 83–85).

Colorectal Cancer

YTHDF1 acts as an oncogene in colorectal cancer (CRC) and is associated with poor prognosis in overall survival. Down-regulation of YTHDF1 inhibited CRC proliferation and increased sensitivity to the exposure of fluorouracil and oxaliplatin. Moreover, YTHDF1 is transcriptionally regulated by a well-known oncogenic transcription factor c-Myc in CRC (86). Mechanistically, knockdown of YTHDF1 significantly suppressed Wnt/β-catenin pathway activity in CRC. Wnt/β-catenin pathway is one of the best-characterized cancer drivers that can promote cancer progression and chemoresistance in various cancers (87). YTHDF1 plays an essential oncogenic role in CRC and is expected to be a therapeutic target for CRC.

YTHDC2 promotes the metastasis of colon cancer cells by facilitating the translation of hypoxia inducible factor 1 subunit alpha (HIF-1α) and twist family BHLH transcription factor 1 (Twist1) mRNA during hypoxia (79). In addition, METTL14 inhibits the malignancy of CRC by suppressing oncogenic long non-coding RNA XIST. YTHDF2 recognizes m6A-modified XIST and accelerated the decay of XIST (72). LncRNA GAS5 inhibits CRC progression *via* triggering phosphorylation and ubiquitin-mediated degradation of YAP. YTHDF3 is a target of YAP and furthermore plays a key role in YAP signaling by promoting m6A-modified lncRNA GAS5 decay (77).

Lung Cancer

Lung cancer is the leading cause of cancer-related death worldwide. YTHDF proteins play different roles in lung cancer progression by controlling the metabolism of different targets in a m6A-dependent manner. YTHDF2 is up-regulated in lung cancer tissues and functions as an oncogene in lung cancer. YTHDF2 promotes the proliferation of lung cancer cells and facilitates the pentose phosphate pathway (PPP) flux, which is critical in regulating cancer cell growth by supplying cells with ribose-5-phosphate and NADPH. Mechanistically, YTHDF2 directly binds to m6A-modified 6-phosphogluconate dehydrogenase (6PGD) mRNA and promotes 6PGD mRNA translation. 6PGD is upregulated in lung cancer and elevated

expression of 6PGD can promote lung cancer cell proliferation (22).

YTHDF1 promotes the proliferation of non-small cell lung cancer (NSCLC) cells by enhancing the translational efficiency of cell cycle regulators CDK2, CDK4 and cyclinD1. However, the clinical correlation analysis showed the adverse result. YTHDF1 high expression correlated with better clinical outcome in NSCLC and depletion of YTHDF1 rendered NSCLC cells resistant to cisplatin (DDP) treatment. Mechanistically, depletion of YTHDF1 can inhibit the translational efficiency of m6A-modified Keap1 mRNA in an oxidative stress state induced by DDP, and activated the antioxidant ROS clearance system (Nrf2-AKR1C1) in turn, leading to DDP resistance and a worse clinical outcome for NSCLC patients (62). According to above findings, it may provide a potential strategy to improve the clinical outcome of YTHDF1 low expressing NSCLC patients by using AKR1C1 specific inhibitors together with platinum based chemotherapy.

Acute Myeloid Leukemia (AML)

AML is a disorder characterized by a clonal proliferation derived from primitive hematopoietic stem cells (HSCs) or progenitor cells, resulting in blockade of myeloid differentiation and generation of self-renewing leukemic stem cells (LSCs). It is still a challenge to eliminate cancer stem cells while preserving hematopoiesis in leukemia treatment. YTHDF2 is up-regulated in AML and plays an essential role in leukemic stem cell (LSC) development and AML initiation by decreasing the half-life of tumor necrosis factor receptor TNF receptor superfamily member 2 (Tnfrsf2), which contributes to the overall integrity of LSC function. More importantly, YTHDF2 deficiency cannot derail hematopoiesis and can enhance HSC activity. So YTHDF2 is a unique therapeutic target in AML whose depletion selectively inhibits LSCs while accelerating HSC expansion (73).

Ovarian Cancer

Ovarian cancer ranks as the fifth leading cause of cancer-related death in women worldwide and has the highest mortality rate among gynecological cancers due to poor prognosis and high relapse rate. YTHDF1 is frequently overexpressed in ovarian cancer and up-regulation of YTHDF1 is associated with the adverse prognosis of ovarian cancer patients. Silence of YTHDF1 inhibited the growth and metastasis of ovarian cancer *in vitro* and *in vivo*. Mechanistically, YTHDF1 facilitates the malignancy by binding to m6A-modified eukaryotic translation initiation factor 3 subunit C (EIF3C) mRNA, which is a subunit of the protein translation initiation factor EIF3, and promotes the translation of EIF3C mRNA (63). In addition, cancer stem cells (CSCs) are a population of cells with stem-like characteristics that are able to cause chemoresistance and recurrence. YTHDF1 was found to enhance the CSC-like characteristics of the cisplatin-resistant ovarian cancer cells by binding to m6A-modified TRIM29 mRNA and promoting its translation (64). Thus, targeting YTHDF1 is expected to be a promising candidate for ovarian cancer therapy.

Bladder Cancer

In bladder cancer, three YTHDF proteins all act as oncogenes. YTHDF1/YTHDF3 promotes the tumor growth and progression by recognizing m6A-modified integrin subunit alpha 6 (ITGA6) mRNA and promoting its translation (78). YTHDF2 facilitates tumorigenesis through accelerating the degradation of tumor suppressors set domain containing 7 (SETD7) mRNA and Kruppel like actor 4 (KLF4) mRNA in bladder cancer (74).

Prostate Cancer

YTHDF2 was found frequently up-regulated in prostate cancer through immuno-histochemical (IHC) staining and chromogenic *in situ* hybridization (CISH). Knockdown of YTHDF2 inhibited the proliferation and migration of prostate cancer cells. MiR-493-3p was identified to be an upstream factor of YTHDF2, which suppressed prostate cancer by targeting YTHDF2 (88). Another study had the similar results, YTHDF2 mediated the degradation of tumor suppressors LHPP and NKX3–1 mRNA and indirectly induced AKT phosphorylation to promote prostate cancer progression in an m6A-dependent manner (75). Above results suggest that YTHDF2 acts as an oncogene in prostate cancer and YTHDF2 is expected to be a potential biomarker for diagnosis or targeted therapy of prostate cancer.

Skin Cancer

Melanoma is one of the most aggressive malignant skin tumors and its incidence has been increasing worldwide in recent decades. In melanoma, YTHDF2 suppresses the proliferation and migration of melanoma cells by promoting the decay of protumorigenic melanoma cell-intrinsic genes such as PD-1 (PDCD1), CXCR4 and SOX10 (76). In addition, YTHDF1 inhibits the growth and migration of ocular melanoma cells *via* facilitating the translation of histidine triad nucleotide binding protein 2 (HINT2) (65). Merkel cell carcinoma (MCC) is a kind of highly malignant skin cancer, of which 80% cases are mainly caused by the Merkel cell polyomavirus (MCPyV) (89). YTHDF1 is highly expressed in MCC, silence of YTHDF1 down-regulated the translational initiation factor eIF3, leading to the reduction of proliferative and clonogenic capacity in MCC cells (66).

POTENTIAL APPLICATION OF YTH FAMILY PROTEINS IN CANCER THERAPY

YTH family proteins serve as the potential therapeutic and prognostic targets in various cancers. For example, YTHDF2 is a critical regulator for acute myeloid leukemia (AML) initiation and propagation. Deficiency of YTHDF2 can limit leukemic stem cells activity while enhancing hematopoietic stem cells expansion and myeloid reconstitution. Thus, inhibition of YTHDF2 is expected to be a potential therapeutic strategy for AML treatment (73). In ovarian cancer, YTHDF1 acts as an oncogene. Up-regulation of YTHDF1 is associated with the poor prognosis of ovarian cancer patients and knockdown of YTHDF1 can inhibit the stem cell-like features of cisplatin-

resistant ovarian cancer cells. YTHDF1 may have strong potential as a therapeutic target for ovarian cancer (63, 64).

Nowadays, despite surgery, chemotherapy and radiotherapy, immunotherapy has become a promising method in cancer treatment. Immune check-point therapy based on cytotoxic T lymphocyte-associated antigen 4 (CTLA4), programmed death-1 (PD-1), and programmed death ligand-1 (PD-L1) inhibitors has a good effect in non–small-cell lung carcinoma and melanoma (90, 91). YTHDF1 deficiency was found to exert antitumor function by enhancing immunosurveillance. Loss of YTHDF1 facilitated the cross-presentation of tumor antigens on dendritic cells (DCs) and increased cross-priming of $CD8^+$ T cells. Mechanistically, YTHDF1 recognizes m6A-modified transcripts encoding lysosomal cathepsins in DCs and promotes their translation, which inhibits the cross-presentation of tumor neoantigens to achieve immune escape. In addition, YTHDF1 deficiency improves the therapeutic outcome of immune checkpoint inhibitor, which blocks the T cell inhibitor receptor PD1. Combined with immune checkpoint blockade, YTHDF1 can be a potential new target in cancer immunotherapy (92).

CONCLUSION AND PERSPECTIVES

YTH family proteins, as the main m6A reader proteins, participate in tumorigenesis, proliferation, invasion and metastasis of various cancers through regulating almost the entire process of targeted RNAs metabolism. According to the prevailing mode, the nuclear reader YTHDC1 is involved in mRNA splicing and nuclear export. YTHDF2 promotes mRNA degradation; YTHDF1 enhances translation; and YTHDF3 both accelerates translation and degradation through interacting with YTHDF1 and YTHDF2. However, whether three YTHDF proteins have distinct or redundant cellular functions has been disputed in recent studies. Considering that the expression of YTHDF2 is more highly than YTHDF1 and YTHDF3, effects of YTHDF1 or YTHDF3 deficiency may not be similar to YTHDF2 deficiency due to compensation. So silencing all three YTHDF proteins and then expressing one YTHDF protein exogenously may be a good way to detect their redundant functions. These disputes need to be settled through more careful experimental design in further studies.

YTH family proteins mainly act as oncogenes in different types of cancer with few exceptions. For example, YTHDF2 inhibits the progression of gastric cancer and melanoma. And YTHDF1 plays a suppressive role in ocular melanoma. The different roles of YTH family proteins act in various cancers may depend on their specific recognition of different m6A-mdified transcripts, which act as oncogenes or tumor suppressors. It is essential to identify more m6A-modified transcripts recognized by YTH family proteins, verify roles of these targets acted in cancer progression, and clarify the mechanism by which YTH family proteins achieve selectivity toward certain m6A-modified transcripts. In addition, different researchers presented the opposite role of the same YTH family protein acted even in the same cancer. Therefore, more large-scale and multi-center researches are needed to explore the functions and underlying mechanisms of YTH family proteins in various cancers, which provides basis for precise cancer treatment.

Studies on regulation of YTH family proteins in cancer progression are few. Recently, an additional function of non-coding RNAs in the control of YTH family proteins has been reported. In hepatocellular carcinoma (HCC), miR-145 modulates m6A levels by targeting the 3′-UTR of YTHDF2 mRNA and inhibits the progression of HCC cells (93). In prostate cancer, miR-493-3p is an upstream factor of YTHDF2 and exerts anti-tumor effects by targeting YTHDF2 (88). The profound mechanism by which interplay between YTH family proteins and non-coding RNA impacts cancer development needs to be further studied. In addition, post-translational modification plays an important role in regulating YTHDF family proteins. The SUMOylation of YTHDF2 at the major site of K571 significantly increases its binding affinity of m6A-modified mRNAs and results in deregulated gene expressions which accounts for cancer progression (94). Is there any other post-translational modification to regulate YTH family proteins and impact cancer progression? Whether there are external or internal stimuli leading to alteration of post-translational modification? These questions are worthy of further exploration.

The essential roles of m6A observed in various types of cancers suggest that they are potential therapeutic targets for cancer therapy. It has aroused great interest to develop small-molecule inhibitors targeting m6A writers or erasers. For example, meclofenamic acid (MA) and R-2-hydroxyglutarate (R-2HG), which can inhibit the activity of FTO, are applied to treat leukemia and glioma (95, 96). However, another approach that can be explored is to target YTH family proteins pharmacologically. Considering that YTH domain has a unique aromatic cage structure, the aromatic cage forms a hydrophobic binding pocket that is crucial for the specific recognition and binding of m6A. This site may be suitable for developing small molecule inhibitors that can compete with m6A-modified transcripts and counteract the effects of YTH family proteins. Besides small molecule inhibitors that target YTH family proteins directly, PROTAC (proteolysis targeting chimera)-based inhibitors which can selectively decay dysregulated m6A reader proteins may be a feasible method for cancer therapy. Development of small molecule inhibitors for targeting YTH family proteins could lead to a new way of cancer therapy in the future.

AUTHOR CONTRIBUTIONS

QD and J-FW designed the study. X-YD, LS, and ZL wrote the manuscript. H-YY revised the manuscript. All authors contributed to the article and approved the submitted version.

FUNDING

This work was supported by the National Natural Science Foundation of China (81972486, 81802748, 81802644), the Key Medical Talents of Jiangsu Province (ZDRCA2016029) and '333'

High-level Talents Training Project of Jiangsu Province (BRA2016505). Besides, the work was also funded by the International Cooperation Project of Jiangsu Provincial Science and Technology Department (BZ2018054) and the Priority Academic Program Development of Jiangsu Higher Education Institutions (PAPD).

REFERENCES

1. Desrosiers R, Friderici K, Rottman F. Identification of methylated nucleosides in messenger RNA from Novikoff hepatoma cells. *Proc Natl Acad Sci USA* (1974) 71(10):3971–5. doi: 10.1073/pnas.71.10.3971
2. Alarcón CR, Lee H, Goodarzi H, Halberg N, Tavazoie SF. N6-methyladenosine marks primary microRNAs for processing. *Nature* (2015) 519(7544):482–5. doi: 10.1038/nature14281
3. Patil DP, Chen CK, Pickering BF, Chow A, Jackson C, Guttman M, et al. m(6)A RNA methylation promotes XIST-mediated transcriptional repression. *Nature* (2016) 537(7620):369–73. doi: 10.1038/nature19342
4. Dominissini D, Moshitch-Moshkovitz S, Schwartz S, Salmon-Divon M, Ungar L, Osenberg S, et al. Topology of the human and mouse m6A RNA methylomes revealed by m6A-seq. *Nature* (2012) 485(7397):201–6. doi: 10.1038/nature11112
5. Linder B, Grozhik AV, Olarerin-George AO, Meydan C, Mason CE, Jaffrey SR. Single-nucleotide-resolution mapping of m6A and m6Am throughout the transcriptome. *Nat Methods* (2015) 12(8):767–72. doi: 10.1038/nmeth.3453
6. Zhao BS, Roundtree IA, He C. Post-transcriptional gene regulation by mRNA modifications. *Nat Rev Mol Cell Biol* (2017) 18(1):31–42. doi: 10.1038/nrm.2016.132
7. Dai D, Wang H, Zhu L, Jin H, Wang X. N6-methyladenosine links RNA metabolism to cancer progression. *Cell Death Dis* (2018) 9(2):124. doi: 10.1038/s41419-017-0129-x
8. Meyer KD, Saletore Y, Zumbo P, Elemento O, Mason CE, Jaffrey SR. Comprehensive analysis of mRNA methylation reveals enrichment in 3′ UTRs and near stop codons. *Cell* (2012) 149(7):1635–46. doi: 10.1016/j.cell.2012.05.003
9. Liu J, Yue Y, Han D, Wang X, Fu Y, Zhang L, et al. A METTL3-METTL14 complex mediates mammalian nuclear RNA N6-adenosine methylation. *Nat Chem Biol* (2014) 10(2):93–5. doi: 10.1038/nchembio.1432
10. Pan Y, Ma P, Liu Y, Li W, Shu Y. Multiple functions of m(6)A RNA methylation in cancer. *J Hematol Oncol* (2018) 11(1):48. doi: 10.1186/s13045-018-0590-8
11. Ping XL, Sun BF, Wang L, Xiao W, Yang X, Wang WJ, et al. Mammalian WTAP is a regulatory subunit of the RNA N6-methyladenosine methyltransferase. *Cell Res* (2014) 24(2):177–89. doi: 10.1038/cr.2014.3
12. Schumann U, Shafik A, Preiss T. METTL3 Gains R/W Access to the Epitranscriptome. *Mol Cell* (2016) 62(3):323–4. doi: 10.1016/j.molcel.2016.04.024
13. Jia G, Fu Y, Zhao X, Dai Q, Zheng G, Yang Y, et al. N6-methyladenosine in nuclear RNA is a major substrate of the obesity-associated FTO. *Nat Chem Biol* (2011) 7(12):885–7. doi: 10.1038/nchembio.687
14. Zheng G, Dahl JA, Niu Y, Fedorcsak P, Huang CM, Li CJ, et al. ALKBH5 is a mammalian RNA demethylase that impacts RNA metabolism and mouse fertility. *Mol Cell* (2013) 49(1):18–29. doi: 10.1016/j.molcel.2012.10.015
15. Patil DP, Pickering BF, Jaffrey SR. Reading m(6)A in the Transcriptome: m(6)A-Binding Proteins. *Trends Cell Biol* (2018) 28(2):113–27. doi: 10.1016/j.tcb.2017.10.001
16. Xu C, Wang X, Liu K, Roundtree IA, Tempel W, Li Y, et al. Structural basis for selective binding of m6A RNA by the YTHDC1 YTH domain. *Nat Chem Biol* (2014) 10(11):927–9. doi: 10.1038/nchembio.1654
17. Zhang Z, Theler D, Kaminska KH, Hiller M, de la Grange P, Pudimat R, et al. The YTH domain is a novel RNA binding domain. *J Biol Chem* (2010) 285 (19):14701–10. doi: 10.1074/jbc.M110.104711
18. Liao S, Sun H, Xu C. YTH Domain: A Family of N(6)-methyladenosine (m(6)A) Readers. *Genomics Proteomics Bioinformatics* (2018) 16(2):99–107. doi: 10.1016/j.gpb.2018.04.002
19. Nachtergaele S, He C. The emerging biology of RNA post-transcriptional modifications. *RNA Biol* (2017) 14(2):156–63. doi: 10.1080/15476286.2016.1267096
20. Deng X, Su R, Weng H, Huang H, Li Z, Chen J. RNA N-methyladenosine modification in cancers: current status and perspectives. *Cell Res* (2018) 28 (5):507–17. doi: 10.1038/s41422-018-0034-6
21. Chen M, Wong C-M. The emerging roles of N6-methyladenosine (m6A) deregulation in liver carcinogenesis. *Mol Cancer* (2020) 19(1):44. doi: 10.1186/s12943-020-01172-y
22. Sheng H, Li Z, Su S, Sun W, Zhang X, Li L, et al. YTH domain family 2 promotes lung cancer cell growth by facilitating 6-phosphogluconate dehydrogenase mRNA translation. *Carcinogenesis* (2020) 41(5):541–50.. doi: 10.1093/carcin/bgz152
23. Zhu T, Roundtree IA, Wang P, Wang X, Wang L, Sun C, et al. Crystal structure of the YTH domain of YTHDF2 reveals mechanism for recognition of N6-methyladenosine. *Cell Res* (2014) 24(12):1493–6. doi: 10.1038/cr.2014.152
24. Ma C, Liao S, Zhu Z. Crystal structure of human YTHDC2 YTH domain. *Biochem Biophys Res Commun* (2019) 518(4):678–84. doi: 10.1016/j.bbrc.2019.08.107
25. Xu C, Liu K, Ahmed H, Loppnau P, Schapira M, Min J. Structural Basis for the Discriminative Recognition of N6-Methyladenosine RNA by the Human YT521-B Homology Domain Family of Proteins. *J Biol Chem* (2015) 290 (41):24902–13. doi: 10.1074/jbc.M115.680389
26. Li F, Zhao D, Wu J, Shi Y. Structure of the YTH domain of human YTHDF2 in complex with an m(6)A mononucleotide reveals an aromatic cage for m(6)A recognition. *Cell Res* (2014) 24(12):1490–2. doi: 10.1038/cr.2014.153
27. Achsel T, Bagni C. Cooperativity in RNA-protein interactions: the complex is more than the sum of its partners. *Curr Opin Neurobiol* (2016) 39:146–51. doi: 10.1016/j.conb.2016.06.007
28. Nayler O, Hartmann AM, Stamm S. The ER repeat protein YT521-B localizes to a novel subnuclear compartment. *J Cell Biol* (2000) 150(5):949–62. doi: 10.1083/jcb.150.5.949
29. Wojtas MN, Pandey RR, Mendel M, Homolka D, Sachidanandam R, Pillai RS. Regulation of mA Transcripts by the 3′→5′ RNA Helicase YTHDC2 Is Essential for a Successful Meiotic Program in the Mammalian Germline. *Mol Cell* (2017) 68(2):374–87. doi: 10.1016/j.molcel.2017.09.021
30. Kretschmer J, Rao H, Hackert P, Sloan KE, Höbartner C, Bohnsack MT. The mA reader protein YTHDC2 interacts with the small ribosomal subunit and the 5′-3′ exoribonuclease XRN1. *RNA (New York NY)* (2018) 24(10):1339–50. doi: 10.1261/rna.064238.117
31. Liu J, Dou X, Chen C, Chen C, Liu C, Xu MM, et al. N6-methyladenosine of chromosome-associated regulatory RNA regulates chromatin state and transcription. *Science (New York NY)* (2020) 367(6477):580–6. doi: 10.1126/science.aay6018
32. Kasowitz SD, Ma J, Anderson SJ, Leu NA, Xu Y, Gregory BD, et al. Nuclear m6A reader YTHDC1 regulates alternative polyadenylation and splicing during mouse oocyte development. *PloS Genet* (2018) 14(5):e1007412. doi: 10.1371/journal.pgen.1007412
33. Roundtree IA, Luo GZ, Zhang Z, Wang X, Zhou T, Cui Y, et al. YTHDC1 mediates nuclear export of N(6)-methyladenosine methylated mRNAs. *eLife* (2017) 6. doi: 10.7554/eLife.31311
34. Shi H, Wang X, Lu Z, Zhao BS, Ma H, Hsu PJ, et al. YTHDF3 facilitates translation and decay of N(6)-methyladenosine-modified RNA. *Cell Res* (2017) 27(3):315–28. doi: 10.1038/cr.2017.15
35. Wang X, Zhao BS, Roundtree IA, Lu Z, Han D, Ma H, et al. N(6)-methyladenosine Modulates Messenger RNA Translation Efficiency. *Cell* (2015) 161(6):1388–99. doi: 10.1016/j.cell.2015.05.014
36. Du H, Zhao Y, He J, Zhang Y, Xi H, Liu M, et al. YTHDF2 destabilizes m(6)A-containing RNA through direct recruitment of the CCR4-NOT deadenylase complex. *Nat Commun* (2016) 7:12626. doi: 10.1038/ncomms12626
37. Lee Y, Choe J, Park OH, Kim YK. Molecular Mechanisms Driving mRNA Degradation by m(6)A Modification. *Trends Genet* (2020) 36(3):177–88. doi: 10.1016/j.tig.2019.12.007

38. Li A, Chen YS, Ping XL, Yang X, Xiao W, Yang Y, et al. Cytoplasmic m(6)A reader YTHDF3 promotes mRNA translation. *Cell Res* (2017) 27(3):444–7. doi: 10.1038/cr.2017.10
39. Hsu PJ, Zhu Y, Ma H, Guo Y, Shi X, Liu Y, et al. Ythdc2 is an N(6)-methyladenosine binding protein that regulates mammalian spermatogenesis. *Cell Res* (2017) 27(9):1115–27. doi: 10.1038/cr.2017.99
40. Liu N, Dai Q, Zheng G, He C, Parisien M, Pan T. N(6)-methyladenosine-dependent RNA structural switches regulate RNA-protein interactions. *Nature* (2015) 518(7540):560–4. doi: 10.1038/nature14234
41. Hartmann AM, Nayler O, Schwaiger FW, Obermeier A, Stamm S. The interaction and colocalization of Sam68 with the splicing-associated factor YT521-B in nuclear dots is regulated by the Src family kinase p59(fyn). *Mol Biol Cell* (1999) 10(11):3909–26. doi: 10.1091/mbc.10.11.3909
42. Imai Y, Matsuo N, Ogawa S, Tohyama M, Takagi T. Cloning of a gene, YT521, for a novel RNA splicing-related protein induced by hypoxia/reoxygenation. *Brain Res Mol Brain Res* (1998) 53(1-2):33–40. doi: 10.1016/S0169-328X(97)00262-3
43. Wang X, Lu Z, Gomez A, Hon GC, Yue Y, Han D, et al. N6-methyladenosine-dependent regulation of messenger RNA stability. *Nature* (2014) 505(7481):117–20. doi: 10.1038/nature12730
44. Xiao W, Adhikari S, Dahal U, Chen YS, Hao YJ, Sun BF, et al. Nuclear m(6)A Reader YTHDC1 Regulates mRNA Splicing. *Mol Cell* (2016) 61(4):507–19. doi: 10.1016/j.molcel.2016.01.012
45. Park OH, Ha H, Lee Y, Boo SH, Kwon DH, Song HK, et al. Endoribonucleolytic Cleavage of m(6)A-Containing RNAs by RNase P/MRP Complex. *Mol Cell* (2019) 74(3):494–507.e8. doi: 10.1016/j.molcel.2019.02.034
46. Nakano M, Ondo K, Takemoto S, Fukami T, Nakajima M. Methylation of adenosine at the N(6) position post-transcriptionally regulates hepatic P450s expression. *Biochem Pharmacol* (2020) 171:113697. doi: 10.1016/j.bcp.2019.113697
47. Wang J, Wang L, Diao J, Shi YG, Shi Y, Ma H, et al. Binding to mA RNA promotes YTHDF2-mediated phase separation. *Protein Cell* (2020) 11(4):304–7. doi: 10.1007/s13238-019-00660-2
48. Gao Y, Pei G, Li D, Li R, Shao Y, Zhang QC, et al. Multivalent mA motifs promote phase separation of YTHDF proteins. *Cell Res* (2019) 29(9):767–9. doi: 10.1038/s41422-019-0210-3
49. Ries RJ, Zaccara S, Klein P, Olarerin-George A, Namkoong S, Pickering BF, et al. mA enhances the phase separation potential of mRNA. *Nature* (2019) 571(7765):424–8. doi: 10.1038/s41586-019-1374-1
50. Fu Y, Zhuang X. mA-binding YTHDF proteins promote stress granule formation. *Nat Chem Biol* (2020) 16(9):955–63. doi: 10.1038/s41589-020-0524-y
51. Lubas M, Christensen MS, Kristiansen MS, Domanski M, Falkenby LG, Lykke-Andersen S, et al. Interaction profiling identifies the human nuclear exosome targeting complex. *Mol Cell* (2011) 43(4):624–37. doi: 10.1016/j.molcel.2011.06.028
52. Kennedy EM, Bogerd HP, Kornepati AVR, Kang D, Ghoshal D, Marshall JB, et al. Posttranscriptional m(6)A Editing of HIV-1 mRNAs Enhances Viral Gene Expression. *Cell Host Microbe* (2016) 19(5):675–85. doi: 10.1016/j.chom.2016.04.002
53. Zaccara S, Jaffrey SR. A Unified Model for the Function of YTHDF Proteins in Regulating mA-Modified mRNA. *Cell* (2020) 181(7):1582–95. doi: 10.1016/j.cell.2020.05.012
54. Berlivet S, Scutenaire J, Deragon JM, Bousquet-Antonelli C. Readers of the m(6)A epitranscriptomic code. *Biochim Biophys Acta Gene Regul Mech* (2019) 1862(3):329–42. doi: 10.1016/j.bbagrm.2018.12.008
55. Geula S, Moshitch-Moshkovitz S, Dominissini D, Mansour AA, Kol N, Salmon-Divon M, et al. Stem cells. m6A mRNA methylation facilitates resolution of naïve pluripotency toward differentiation. *Science (New York NY)* (2015) 347(6225):1002–6. doi: 10.1126/science.1261417
56. Zhang C, Chen Y, Sun B, Wang L, Yang Y, Ma D, et al. m(6)A modulates haematopoietic stem and progenitor cell specification. *Nature* (2017) 549(7671):273–6. doi: 10.1038/nature23883
57. Haussmann IU, Bodi Z, Sanchez-Moran E, Mongan NP, Archer N, Fray RG, et al. m(6)A potentiates Sxl alternative pre-mRNA splicing for robust Drosophila sex determination. *Nature* (2016) 540(7632):301–4. doi: 10.1038/nature20577
58. Zhou J, Wan J, Gao X, Zhang X, Jaffrey SR, Qian SB. Dynamic m(6)A mRNA methylation directs translational control of heat shock response. *Nature* (2015) 526(7574):591–4. doi: 10.1038/nature15377
59. Lin X, Chai G, Wu Y, Li J, Chen F, Liu J, et al. RNA m(6)A methylation regulates the epithelial mesenchymal transition of cancer cells and translation of Snail. *Nat Commun* (2019) 10(1):2065. doi: 10.1038/s41467-019-09865-9
60. Liu X, Qin J, Gao T, Li C, He B, Pan B, et al. YTHDF1 Facilitates the Progression of Hepatocellular Carcinoma by Promoting FZD5 mRNA Translation in an m6A-Dependent Manner. *Mol Ther Nucleic Acids* (2020) 22:750–65. doi: 10.1016/j.omtn.2020.09.036
61. Pi J, Wang W, Ji M, Wang X, Wei X, Jin J, et al. YTHDF1 promotes gastric carcinogenesis by controlling translation of FZD7. *Cancer Res* (2020). doi: 10.1158/0008-5472.CAN-20-0066
62. Shi Y, Fan S, Wu M, Zuo Z, Li X, Jiang L, et al. YTHDF1 links hypoxia adaptation and non-small cell lung cancer progression. *Nat Commun* (2019) 10(1):4892. doi: 10.1038/s41467-019-12801-6
63. Liu T, Wei Q, Jin J, Luo Q, Liu Y, Yang Y, et al. The m6A reader YTHDF1 promotes ovarian cancer progression via augmenting EIF3C translation. *Nucleic Acids Res* (2020) 48(7):3816–31. doi: 10.1093/nar/gkaa048
64. Hao L, Wang J-M, Liu B-Q, Yan J, Li C, Jiang J-Y, et al. m6A-YTHDF1-mediated TRIM29 upregulation facilitates the stem cell-like phenotype of cisplatin-resistant ovarian cancer cells. *Biochim Biophys Acta Mol Cell Res* (2021) 1868(1):118878. doi: 10.1016/j.bbamcr.2020.118878
65. Jia R, Chai P, Wang S, Sun B, Xu Y, Yang Y, et al. m(6)A modification suppresses ocular melanoma through modulating HINT2 mRNA translation. *Mol Cancer* (2019) 18(1):161. doi: 10.1186/s12943-019-1088-x
66. Orouji E, Peitsch WK, Orouji A, Houben R, Utikal J. Oncogenic Role of an Epigenetic Reader of m(6)A RNA Modification: YTHDF1 in Merkel Cell Carcinoma. *Cancers* (2020) 12(1):202. doi: 10.3390/cancers12010202
67. Zhang C, Huang S, Zhuang H, Ruan S, Zhou Z, Huang K, et al. YTHDF2 promotes the liver cancer stem cell phenotype and cancer metastasis by regulating OCT4 expression via m6A RNA methylation. *Oncogene* (2020) 39(23):4507–18. doi: 10.1038/s41388-020-1303-7
68. Zhong L, Liao D, Zhang M, Zeng C, Li X, Zhang R, et al. YTHDF2 suppresses cell proliferation and growth via destabilizing the EGFR mRNA in hepatocellular carcinoma. *Cancer Lett* (2019) 442:252–61. doi: 10.1016/j.canlet.2018.11.006
69. Hou J, Zhang H, Liu J, Zhao Z, Wang J, Lu Z, et al. YTHDF2 reduction fuels inflammation and vascular abnormalization in hepatocellular carcinoma. *Mol Cancer* (2019) 18(1):163. doi: 10.1186/s12943-019-1082-3
70. Chen J, Sun Y, Xu X, Wang D, He J, Zhou H, et al. YTH domain family 2 orchestrates epithelial-mesenchymal transition/proliferation dichotomy in pancreatic cancer cells. *Cell Cycle (Georgetown Tex)* (2017) 16(23):2259–71. doi: 10.1080/15384101.2017.1380125
71. Shen X, Zhao K, Xu L, Cheng G, Zhu J, Gan L, et al. YTHDF2 Inhibits Gastric Cancer Cell Growth by Regulating FOXC2 Signaling Pathway. *Front Genet* (2020) 11:592042. doi: 10.3389/fgene.2020.592042
72. Yang X, Zhang S, He C, Xue P, Zhang L, He Z, et al. METTL14 suppresses proliferation and metastasis of colorectal cancer by down-regulating oncogenic long non-coding RNA XIST. *Mol Cancer* (2020) 19(1):46. doi: 10.1186/s12943-020-1146-4
73. Paris J, Morgan M, Campos J, Spencer GJ, Shmakova A, Ivanova I, et al. Targeting the RNA m(6)A Reader YTHDF2 Selectively Compromises Cancer Stem Cells in Acute Myeloid Leukemia. *Cell Stem Cell* (2019) 25(1):137–48.e6. doi: 10.1016/j.stem.2019.03.021
74. Xie H, Li J, Ying Y, Yan H, Jin K, Ma X, et al. METTL3/YTHDF2 m(6) A axis promotes tumorigenesis by degrading SETD7 and KLF4 mRNAs in bladder cancer. *J Cell Mol Med* (2020) 24(7):4092–104. doi: 10.1111/jcmm.15063
75. Li J, Xie H, Ying Y, Chen H, Yan H, He L, et al. YTHDF2 mediates the mRNA degradation of the tumor suppressors to induce AKT phosphorylation in N6-methyladenosine-dependent way in prostate cancer. *Mol Cancer* (2020) 19(1):152. doi: 10.1186/s12943-020-01267-6
76. Yang S, Wei J, Cui YH, Park G, Shah P, Deng Y, et al. m(6)A mRNA demethylase FTO regulates melanoma tumorigenicity and response to anti-PD-1 blockade. *Nat Commun* (2019) 10(1):2782. doi: 10.1038/s41467-019-10669-0
77. Ni W, Yao S, Zhou Y, Liu Y, Huang P, Zhou A, et al. Long noncoding RNA GAS5 inhibits progression of colorectal cancer by interacting with and

triggering YAP phosphorylation and degradation and is negatively regulated by the m(6)A reader YTHDF3. *Mol Cancer* (2019) 18(1):143. doi: 10.1186/s12943-019-1079-y
78. Jin H, Ying X, Que B, Wang X, Chao Y, Zhang H, et al. N(6)-methyladenosine modification of ITGA6 mRNA promotes the development and progression of bladder cancer. *EBioMedicine* (2019) 47:195–207. doi: 10.1016/j.ebiom.2019.07.068
79. Tanabe A, Tanikawa K, Tsunetomi M, Takai K, Ikeda H, Konno J, et al. RNA helicase YTHDC2 promotes cancer metastasis via the enhancement of the efficiency by which HIF-1α mRNA is translated. *Cancer Lett* (2016) 376 (1):34–42. doi: 10.1016/j.canlet.2016.02.022
80. Yang Z, Li J, Feng G, Gao S, Wang Y, Zhang S, et al. MicroRNA-145 Modulates N(6)-Methyladenosine Levels by Targeting the 3′-Untranslated mRNA Region of the N(6)-Methyladenosine Binding YTH Domain Family 2 Protein. *J Biol Chem* (2017) 292(9):3614–23. doi: 10.1074/jbc.M116.749689
81. Zhao X, Chen Y, Mao Q, Jiang X, Jiang W, Chen J, et al. Overexpression of YTHDF1 is associated with poor prognosis in patients with hepatocellular carcinoma. *Cancer Biomark* (2018) 21(4):859–68. doi: 10.3233/cbm-170791
82. Zhou Y, Yin Z, Hou B, Yu M, Chen R, Jin H, et al. Expression profiles and prognostic significance of RNA N6-methyladenosine-related genes in patients with hepatocellular carcinoma: evidence from independent datasets. *Cancer Manage Res* (2019) 11:3921–31. doi: 10.2147/cmar.S191565
83. Chen Y, Deng G, Fu Y, Han Y, Guo C, Yin L, et al. FOXC2 Promotes Oxaliplatin Resistance by Inducing Epithelial-Mesenchymal Transition via MAPK/ERK Signaling in Colorectal Cancer. *Onco Targets Ther* (2020) 13:1625–35. doi: 10.2147/OTT.S241367
84. Song L, Tang H, Liao W, Luo X, Li Y, Chen T, et al. FOXC2 positively regulates YAP signaling and promotes the glycolysis of nasopharyngeal carcinoma. *Exp Cell Res* (2017) 357(1):17–24. doi: 10.1016/j.yexcr.2017.04.019
85. Cai J, Tian A-X, Wang Q-S, Kong P-Z, Du X, Li X-Q, et al. FOXF2 suppresses the FOXC2-mediated epithelial-mesenchymal transition and multidrug resistance of basal-like breast cancer. *Cancer Lett* (2015) 367(2):129–37. doi: 10.1016/j.canlet.2015.07.001
86. Nishizawa Y, Konno M, Asai A, Koseki J, Kawamoto K, Miyoshi N, et al. Oncogene c-Myc promotes epitranscriptome m(6)A reader YTHDF1 expression in colorectal cancer. *Oncotarget* (2018) 9(7):7476–86. doi: 10.18632/oncotarget.23554
87. Bai Y, Yang C, Wu R, Huang L, Song S, Li W, et al. YTHDF1 Regulates Tumorigenicity and Cancer Stem Cell-Like Activity in Human Colorectal Carcinoma. *Front Oncol* (2019) 9:332. doi: 10.3389/fonc.2019.00332
88. Li J, Meng S, Xu M, Wang S, He L, Xu X, et al. Downregulation of N(6)-methyladenosine binding YTHDF2 protein mediated by miR-493-3p suppresses prostate cancer by elevating N(6)-methyladenosine levels. *Oncotarget* (2018) 9(3):3752–64. doi: 10.18632/oncotarget.23365
89. Feng H, Shuda M, Chang Y, Moore PS. Clonal integration of a polyomavirus in human Merkel cell carcinoma. *Science (New York NY)* (2008) 319 (5866):1096–100. doi: 10.1126/science.1152586
90. Brahmer JR, Govindan R, Anders RA, Antonia SJ, Sagorsky S, Davies MJ, et al. The Society for Immunotherapy of Cancer consensus statement on immunotherapy for the treatment of non-small cell lung cancer (NSCLC). *J Immunother Cancer* (2018) 6(1):75. doi: 10.1186/s40425-018-0382-2
91. Werner J-M, Schweinsberg V, Schroeter M, von Reutern B, Malter MP, Schlaak M, et al. Successful Treatment of Myasthenia Gravis Following PD-1/CTLA-4 Combination Checkpoint Blockade in a Patient With Metastatic Melanoma. *Front Oncol* (2019) 9:84. doi: 10.3389/fonc.2019.00084
92. Han D, Liu J, Chen C, Dong L, Liu Y, Chang R, et al. Anti-tumour immunity controlled through mRNA m(6)A methylation and YTHDF1 in dendritic cells. *Nature* (2019) 566(7743):270–4. doi: 10.1038/s41586-019-0916-x
93. Yang Z, Li J, Feng G, Gao S, Wang Y, Zhang S, et al. MicroRNA-145 Modulates -Methyladenosine Levels by Targeting the 3′-Untranslated mRNA Region of the -Methyladenosine Binding YTH Domain Family 2 Protein. *J Biol Chem* (2017) 292(9):3614–23. doi: 10.1074/jbc.M116.749689
94. Hou G, Zhao X, Li L, Yang Q, Liu X, Huang C, et al. SUMOylation of YTHDF2 promotes mRNA degradation and cancer progression by increasing its binding affinity with m6A-modified mRNAs. *Nucleic Acids Res* (2021) 49 (5):2859–77. doi: 10.1093/nar/gkab065
95. Chen B, Ye F, Yu L, Jia G, Huang X, Zhang X, et al. Development of cell-active N6-methyladenosine RNA demethylase FTO inhibitor. *J Am Chem Soc* (2012) 134(43):17963–71. doi: 10.1021/ja3064149
96. Huang Y, Yan J, Li Q, Li J, Gong S, Zhou H, et al. Meclofenamic acid selectively inhibits FTO demethylation of m6A over ALKBH5. *Nucleic Acids Res* (2015) 43(1):373–84. doi: 10.1093/nar/gku1276

Conflict of Interest: The authors declare that the research was conducted in the absence of any commercial or financial relationships that could be construed as a potential conflict of interest.

frontiers in Oncology

REVIEW
published: 21 April 2021
doi: 10.3389/fonc.2021.659661

SUMOylation Wrestles With the Occurrence and Development of Breast Cancer

Yuanyuan Qin†, Hong Yuan†, Xu Chen†, Xinyi Yang, Zhengcao Xing, Yajie Shen, Wanying Dong, Siming An, Yitao Qi and Hongmei Wu**

Key Laboratory of the Ministry of Education for Medicinal Resources and Natural Pharmaceutical Chemistry, National Engineering Laboratory for Resource Developing of Endangered Chinese Crude Drugs in Northwest of China, College of Life Sciences, Shaanxi Normal University, Xi'an, China

Breast cancer has the highest incidence among cancers and is the most frequent cause of death in women worldwide. The detailed mechanism of the pathogenesis of breast cancer has not been fully elucidated, and there remains a lack of effective treatment methods for the disease. SUMOylation covalently conjugates a large amount of cellular proteins, and affects their cellular localization and biological activity to participate in numerous cellular processes. SUMOylation is an important process and imbalance of SUMOylation results in the progression of human diseases. Increasing evidence shows that numerous SUMOylated proteins are involved in the occurrence and development of breast cancer. This review summarizes a series of studies on protein SUMOylation in breast cancer in recent years. The study of SUMOylated proteins provides a comprehensive understanding of the pathophysiology of breast cancer and provides evolving therapeutic strategies for the treatment of breast cancer.

Keywords: SUMOylation, sentrin-specific protease, ubiquitin-proteasome system, breast cancer, cancer progression

OPEN ACCESS

Edited by:
Andrew Davis, Washington University in St. Louis, United States

Reviewed by:
Jian Zhu, Shandong University, China
Stefania Marsico, University of Calabria, Italy

****Correspondence:***
Yitao Qi
qiyitao@snnu.edu.cn
Hongmei Wu
hq8479@snnu.edu.cn

†These authors have contributed equally to this work

Specialty section:
This article was submitted to Molecular and Cellular Oncology, a section of the journal Frontiers in Oncology

Received: *28 January 2021*
Accepted: *02 March 2021*
Published: *21 April 2021*

Citation:
Qin Y, Yuan H, Chen X, Yang X, Xing Z, Shen Y, Dong W, An S, Qi Y and Wu H (2021) SUMOylation Wrestles With the Occurrence and Development of Breast Cancer. Front. Oncol. 11:659661. doi: 10.3389/fonc.2021.659661

INTRODUCTION

Breast Cancer

Breast cancer is the most common type of cancer (1). Approximately 1.2 million women worldwide suffer from breast cancer every year in the world, and about one-half of these patients die within 10 years of diagnosis (2). According to the latest cancer data released by the National Cancer Center of China and the American Cancer Society in 2019, breast cancer ranks first among all new cancer diagnoses in women and second in terms of mortality, accounting for 15-30% of deaths from newly diagnosed cancers (3–5). It is estimated that the incidence and mortality of breast cancer will increase over the next 5-10 years (6). Furthermore, the morbidity of breast cancer is highest in Europe, North America, New Zealand, and Australia, and its mortality is highest in sub-Saharan Africa and some Asian countries (1, 7). These data suggest that breast cancer is still a global public health problem.

Breast cancer is a heterogeneous disease that can be classified into four subtypes according to histological features, including luminal A, luminal B, human epidermal growth factor receptor 2 (HER2)-positive and triple-negative breast cancer (TNBC). Luminal A and luminal B tumors are mostly ER-positive, and the difference between them is that luminal A tumors are low grade tumors, while

luminal B tumors are high grade tumors. HER2-positive tumors exhibit overexpression of ERBB2 genes (1, 8). TNBC is a heterogeneous and aggressive form of breast cancer in which the cells do not express estrogen receptor α (ERα), progesterone receptor (PR), or HER2. TNBC accounts for 15% of breast carcinomas and 70-80% of basal-like breast cancers, and it is refractory to therapy (9, 10). Breast cancer is often accompanied with gene mutations, which are mainly divided into two types-functional gain mutations of oncogenes and functional loss mutations of tumor suppressor genes. BRCA1 and BRCA2 mutation play an important role in genetic susceptibility of breast cancer progression. Exon 4 and intron 3 of TP53 gene are frequently mutated in breast cancer, especially in TNBC. Most breast cancer cases have nothing to do with high penetrance mutations such as BRCA1, BRCA2, and TP53. Genes with low penetrance such as androgen receptor (AR), checkpoint kinase 2 (CHEK2), E-cadherin, Nijmegen breakage syndrome 1 (NBS1), RAD50, BRCA1 interacting protein C-terminal helicase 1 (BRIP1), and partner and localizer of BRCA2 (PALB2) are frequently mutated in the general population and play an important roles in the occurrence of breast cancer (11).

At present, the therapeutics of breast cancer mainly focus on surgery (12), radiation therapy (13), chemotherapy (14), endocrine therapy (15) and targeted therapy (16). Surgery is the most significant treatment (17), and remains the most accurate staging method for non-metastatic malignancies (12). Radiation therapy reduces local recurrence and breast cancer mortality after breast conservation after mastectomy (18), and radiation therapy after mastectomy is the standard of care for advanced breast cancer (13, 17). Chemotherapy is one of the main methods to improve survival and prognosis of patients through destroy cancer cells that have spread to various parts of the body. Current chemotherapeutic agents for breast cancer include alkylating agent cyclophosphamide (19), antimetabolic agent gemcitabine (14), anthracycline agent doxorubicin and paclitaxel agent paclitaxel (20). The advantage of endocrine therapy is that there are fewer adverse reactions and long drug maintenance. At the same time, endocrine therapy generally results in drug resistance, which is an urgent problem that needs to be solved. Targeted therapy can kill tumor cells efficiently and selectively with less adverse effects than chemotherapy. The drugs currently used in breast cancer include receptor tyrosine kinase inhibitor lapatinib, HER2 monoclonal antibody trastuzumab, mTOR inhibitor everolimus and the CDK4/6 inhibitor palbociclib (16). Although there are numerous studies on the treatment of breast cancer, many problems still need to be resolved.

SUMOylation

SUMO proteins, including SUMO1, SUMO2 and SUMO3, constitute a class of proteins with a molecular weight of approximately 11 KD that have similar structure with ubiquitin. The mature SUMO proteins are activated by E1, which is composed of two subunits, SAE1/Aos1 and SAE2/Uba2. Subsequently, SUMOs are transferred to the Ubc9, the single E2, and finally conjugated to the specific lysine residues of the substrate protein with the help of E3 ligases, which includes members of the protein inhibitor of activated STAT (PIAS) family, Ran binding protein 2 (RanBP2), and a few other E3 ligases. SUMOylation is a dynamic and reversible process, and the modification is reversible because of the regulation of SUMO/sentrin-specific protease (SENP), which deconjugates attached molecules from substrates and is required for the maturation of SUMO proteins (**Figure 1**). The well-known protease families include Ulp1 and Ulp2 in yeast and SENPs (SENP1-3 and SENP5-7) in mammals, and they are involved in embryonic development and human diseases (21, 22). SUMOylation regulates a variety of biological processes including cell division, DNA replication and repair, signal transduction and cell metabolism (23). Typical SUMOylation is observed during cellular activities because a rapid modification of even a small portion of targets is sufficient to produce significant functional changes (24).

In recent years, additional studies have shown that SUMOylation and its pathways are associated with human diseases (25–28). Various types of stress induce the upregulated SUMOylation, making SUMOylation a critical mechanism to protect cells from stress-induced apoptosis or cell death (29, 30). The low survival rate of patients with hepatocellular carcinoma is reported to be related to the overexpression of SUMO2 and E1 enzyme Uba2 subunits (31). The overexpression of E2 enzyme Ubc9 was found in human lung and neck cancers (32). The E3 enzyme PIAS3 was overexpressed in prostate, lung, colon, brain and breast cancers (33). Many recent reports have shown that SENPs and other SUMO-related proteins regulate the occurrence and development of breast cancer by modulating protein modifications (23). This suggests that SUMOylation is likely to play an important role in regulating breast cancer. In this review, we focus on the linkage between breast cancer and SUMOylation pathway to explore the role of SUMOylation in the occurrence and development of breast cancer.

SUMOylation ENZYMES AND BREAST CANCER

SAE2

SAE2 is a SUMO-activating enzyme (E1) in mammals (23). It was found that the global SUMO-2/3 modification was increased, but the SUMO2/3 modification of SAE2 was decreased in highly metastatic breast cancer cells (34). These two seemingly contradictory conclusions can be explained as follows: SAE2 can be SUMOylated at the K236 site, which alters its enzymatic activity and inhibits SUMO transfer from E1 to Ubc9; as a result, the decrease in SAE2 SUMOylation enhances global SUMOylation to some extent (35). Furthermore, SAE2 is required for Myc-dependent tumor growth in mice, and the analysis of gene expression in Myc-high human breast cancer suggests that low expression levels of SAE1 and SAE2 are correlated with longer metastasis-free survival of breast cancer patients (36). These results indicated that SAE1 and SAE2 may inhibit the development of tumor metastasis in breast cancer with high Myc expression (**Table 1**).

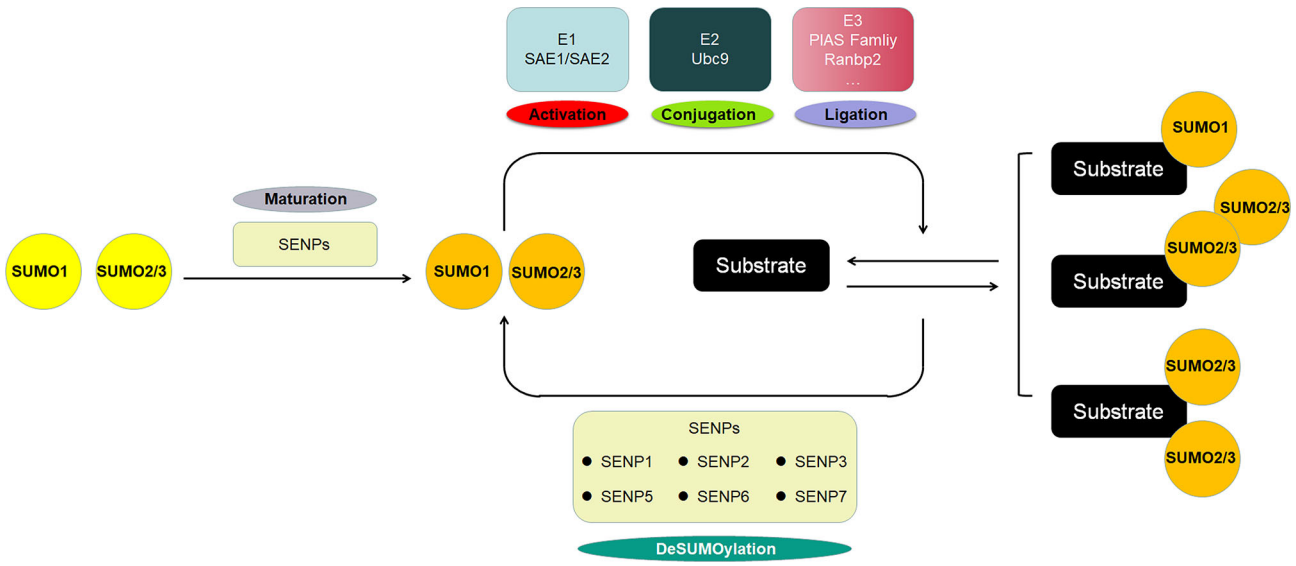

FIGURE 1 | The scheme of SUMOylation pathway. The SUMO protein precursor is cleaved and matured by SENP, then activated by E1, transferred to E2, and ultimately ligated to the target protein by E3. SUMO1 modification is usually conjugated as a monomer, whereas SUMO2/3 modification is often form poly-chain. The SENP family deconjugates the SUMO protein from the substrate to deSUMOylate target protein.

Ubc9

Ubc9 is the only SUMO-conjugating enzyme (23). It was observed that the expression of Ubc9 is 5.7-fold higher in breast cancer tissues, and ectopic expression of Ubc9 promotes tumor growth and invasion in an animal model (51, 52). In addition, it was found that Ubc9 positively regulates Bcl2, a well-known tumor promoter, indicating that Ubc9 may play a tumor promoter role in breast cancer development (53). Additional results showed that Ubc9 was downregulated by the tumor suppressor miR-30e and upregulated by cell division cycle 2 (Cdc2) in breast cancer (51, 54). Moreover, Ubc9 gene variants have been shown to be associated with the risk of grade 1 breast cancer (55). Recently, it was shown that the expression and activity of Ubc9 played a critical role in breast tumorigenesis and responded to anticancer drugs. It was reported that ERα and NF-Y bound directly to the proximal promoter of Ubc9 and were essential for the *in vivo* expression of Ubc9 through transcriptional regulation (41, 56), and the overexpression of Ubc9 increased ERα-mediated transcriptional activity *via* enhanced SUMOylation in MCF-7 breast cancer cells, suggesting a possible synergy between Ubc9 and the promoting factor during breast cancer development (57). These findings contribute to a better understanding of Ubc9 regulation in breast cancer cells and indicate that Ubc9 is a potential therapeutic target in breast cancer.

PIAS1

PIAS1 is a SUMO-ligating enzyme (58). Some reports have shown that PIAS1 is highly expressed in breast cancer and regulates breast cancer tumorigenesis (59). It was found that PIAS1 can enhance the expression of breast cancer signature genes, including ESR1 and CCND2, and the oncogene AIB1 (59, 60). However, PIAS1 can also cooperate with TNFγ to regulate SnoN SUMOylation and suppress the EMT, inhibiting the growth and invasion of MDA-MB-231 cell-derived organoids (44, 61). The role of PIAS1 in breast cancer may be a double-edged sword, and further investigations are required to clarify its regulatory mechanism.

SENP FAMILY MEMBERS AND BREAST CANCER

SENP1

Previous studies showed that SENP1 is highly expressed in human prostate cancer cells (62), lung cancer and colon cancer tissues (63, 64). SENP1 is also upregulated in TNBC tissues, and depletion of SENP1 attenuates TNBC cell proliferation and migration, tumor growth and metastasis (65). SENP1 may function by deSUMOylating related substrates. For example, a study found that SENP1 can deSUMOylate HIF-1α to enhance HIF-1α stabilization and ultimately promote breast cancer metastasis (66). Furthermore, SENP1 can deSUMOylate and regulate the protein activity and oncogenic function of the isomerase Pin1, which is an important regulator of cellular processes involving Pro-directed phosphorylation in breast cancer (67). These results suggest a critical role for SENP1 in TNBC cell proliferation, breast cancer formation and migration.

SENP2

SENP2 plays important roles in embryonic development (21) and myogenesis (22), and reversing SUMOylation of potassium channels may present a novel approach for treating SUDEP

TABLE 1 | Effects of SUMOylation of protein substrates in breast cancer.

SUMO substrates	Biophysical function	Test models	Biophysical and biological effects of SUMOylation
α-catenin	An essential protein in adherent junctions, and is critical for maintaining intercellular adhesion and cellular polarity.	4T1, HEK293T, MCF-7, MDA-MB-231, MD-MBA-157, and T47D cells; nude mice	SUMOylation of α-catenin plays a key role in the suppression of the NF-κB pathway, inhibiting breast cancer tumor growth and migration (37).
β-catenin	Maintains cell-cell adhesion at the membrane and initiate gene transcription upon nuclear translocation.	MCF10-2A and MCF7 cells	SUMOylated β-catenin transports to the nucleus and promotes transcription of oncogenes, ultimately promotes metastasis and invasion of breast cancer (38).
AMPK	An anabolic pathway inhibitor found in all eukaryotes, controlling fatty sugar and lipid metabolism process.	BT-474, BT-549, MDA-MB-231, MDA-MB-453, MDA-MB-468, and SKBR3 cells	SUMOylation of AMPK inhibits the response of AMPK towards mTORC1 signaling, and inhibits breast cancer growth (39).
FOXM1B	A well-known master regulator in controlling cell cycle and cell proliferation.	MCF-7 and H1299 cells	SUMOylation of FOXM1B promotes the expression of JNK1, and represses the expression of MiR-200b/c and p21, ultimately promotes MCF-7 cell proliferation (40).
FOXP3	A tumor suppressor.	MCF-7 cells	FOXP3 acts as a novel transcriptional activator of UBC9 gene, and regulates the global SUMOylation (41).
NEMO	Plays a regulatory role in NF-κB signaling through activating the degradation of NFκ-light polypeptide gene enhancer in IκBα.	MCF-7 and MDA-MB-231 cells	The inhibition of NEMO SUMOylation leads to inhibition of IκBα degradation and consequently a reduction of NF-κB activity, leading to the downregulation of metastasis related genes (42).
PES1	Involved in the synthesis and maturation of ribosome and chromatin stretch.	COS-7, MCF-7 and T47D cells; nude mice	SUMOylation stabilizes PES1 by inhibiting its ubiquitination (43).
PIAS1	SUMO E3 ligase enzyme.	MDA-MB-231 cells and nude mice	PIAS1 SUMOylation regulates the invasive and metastatic potential of malignant breast cancer cells (44, 45).
PML	Plays a critical role in tumorigenesis and metastasis.	MDA-MB-231and MDA-MB-468 cells	Upregulation of PML SUMOylation is associated with increased assembly of PML-NBs in metastatic cells (34).
SAE1/2	SUMO E1 activation enzyme.	MCF-7, MDA-MB-231, SKBR3, and SUM159 cells; nude mice	Required to support Myc-dependent human breast cancer cells *in vitro* and in mice (36).
Smurf2	The ubiquitin E3 ligase, suppresses TGFβ-induced EMT in non-transformed mammary epithelial cells.	MDA-MB-231 cells	Smurf2 function in the control of EMT is regulated by PIAS3, which associates with and triggers Smurf2 SUMOylation (46).
STAT5	Continuously activated in many human cancers, and related to dysregulated cell proliferation and apoptosis.	MDA-MB-231 cells	DeSUMOylation of STAT5 results in phosphorylation of STAT5, leading to inhibition of breast cancer cell growth and migration (47).
TGFβRI	Governing metastasis and prognosis in breast cancer through TGFβ signaling.	MCF-7, MDA-MB-231, MDA-MB-436, and T47D cells	TGFβRI SUMOylation regulates TGFβ-MMP9 cascade and inhibits anchorage-independence growth, proliferation, migration and invasion in breast cancer cells (48).
TFAP2A	TFAP2A activates transcription and regulates cell proliferation and migration, and xenograft outgrowth.	HBL-100, MCF-7, MDA-MB-231, MDA-MB-468, and MDA-MB-453 cells	SUMOylation of TFAP2A is necessary to maintain basal breast cancer phenotypes (49).
TP53	TP53 regulates the expression of numerous target genes to induce cell cycle arrest, apoptosis, senescence, and other anti-proliferative outcomes.	TNBC cells	SUMOylation of p53 inhibits breast cancer cell proliferation (50).

(sudden unexplained death in epilepsy) patients (25–27). SENP2 has been reported to play a crucial role in hepatocellular carcinoma (HCC) cell growth by modulating β-catenin stability (68). Moreover, SENP2 functions as a suppressor in bladder cancer metastasis partially by inhibiting the expression of MMP13 (69). Considering these reports, some studies have focused on the correlation between SENP2 and breast cancer. One study showed that SENP2 significantly represses estrogen-dependent and estrogen-independent proliferation of MCF-7 cells and revealed a novel property of SENP2 as a typical transcription coregulator (70). The polymorphic SENP2 genes examined to date cannot be used as independent markers of breast cancer, but studies using these forms may be useful in identifying a set of clinical markers helpful for breast cancer diagnosis and treatment (71). However, no in-depth studies on the specific role and mechanism of SENP2 in the development and progression of breast cancer have been reported, and further studies need to be performed to determine the critical role of SENP2 in breast cancer.

SENP5

Several studies have focused on the relationship between SENP5 and the development of breast cancer. One study showed that SENP5 silencing inhibits breast cancer cell growth, proliferation, migration and invasion by regulating the expression level of TGFβRI (48). Recently, another study showed that the expression levels of SENP5 were negatively correlated with the survival of breast cancer patients, and suggested SENP5 as a unique prognostic biomarker (72). These results were consistent with other findings demonstrating that SENP5 silencing reduced cell migration and invasion and indicating some interplay between TGFβRI and SENP5 (48). These results suggest that SENP5 acts as a tumor promoter in breast cancer development.

SENP7

Different SENP7 isoforms, including SENP7S and SENP7L, have a different subcellular localizations and biological functions (73). SENP7S and SENP7L are two isoforms that have been intensively studied. SENP7S is mainly located in the cytoplasm and is highly expressed in mammary epithelia but expressed at low levels in precancerous ductal carcinoma and is lost in invasive breast cancer (73). Another study revealed that deletion of SENP7S can directly enhance the tumorigenicity of MCF-10-2A cells. Mechanistically, SENP7 loss enhances the SUMOylation of β-catenin, and SUMOylated β-catenin is transported to the nucleus and promotes the transcription of oncogenes, including c-Myc, cyclin D, and Aurora kinase, ultimately promoting metastasis and invasion of breast cancer (38).

In contrast, SENP7L is highly expressed, promotes aberrant proliferation and initiates the EMT and invasion of breast cancer (73). It was reported that the SUMOylation of HP1α promoted HP1α localization to promoters and subsequently silenced genes. SENP7L deSUMOylated HP1α to release the inhibition of downstream genes and ultimately promote the proliferation and invasion of breast cancer cells (74, 75). Breast cancer patients who express low SENP7L exhibit higher survival rates after chemotherapy than patients who express high SENP7L (74). These results indicated that SENP7S acts as a tumor suppressor but that SENP7L plays a tumor-promoting role in breast cancer.

SUMOylated PROTEINS AND BREAST CANCER

α-Catenin

α-Catenin is an essential protein in adherent junctions, critical for the maintenance of cellular adhesion and polarity (76, 77), and has been recognized as a novel tumor suppressor gene (37, 78). α-Catenin plays a role in two different ways. In the traditional way, loss of α-Catenin specifically causes the loss of intracellular adhesion in E-cadherin-expressing breast cancer cells and induces further resistance to anoikis (79, 80). Another way is the adherent junction-independent pathway in which α-catenin suppresses E-cadherin-negative basal-like breast cancer by inhibiting NF-κB signaling (81). It was reported that α-catenin is SUMOylated, and SUMOylation stabilizes its interaction with IκBα, inhibiting the expression of NF-κB target genes (37, 79). A survival analysis showed a significant association between abnormal α-catenin expression and poor survival of breast cancer patients (82). In conclusion, α-catenin plays a significant role in breast cancer development, and its abnormal expression is associated with severe symptoms of breast cancer.

AMPKα1

AMPK is an anabolic pathway inhibitor found in all eukaryotes that controls fatty sugar and lipid metabolism processes (39, 83). Furthermore, the expression levels of AMPK are upregulated in TNBC and can be regarded as biomarkers for TNBC (84). Many targets are regulated by AMPK. Phosphorylated AMPK inactivates the serine/threonine protein kinase Akt, which is involved in tumor progression, thereby inhibiting anoikis and impairing autophagy, ultimately inhibiting anchorage-independent growth and metastasis (85). Furthermore, some reports revealed that the LKB1-AMPK axis governs the mTORC1 pathway to regulate tumor growth (83). AMPKα1 can be SUMOylated, and its SUMOylation inhibits the response of AMPK towards mTORC1 signaling, suggesting that suppression of AMPKα1 SUMOylation can be applied to regulate AMPK activation and thus suppress breast cancer cell growth (39). These findings indicate that the SUMOylation of AMPKα1 can be a potential target for the treatment of breast cancer.

BRCA1

It was reported that women with BRCA1 germline mutations usually develop TNBC (86). Researchers have identified a consensus SUMO modification site localized in the amino-terminal region of BRCA1. In contrast to the SUMO mutation in this potential SUMO-acceptor site of the BRCA1 protein, the wild-type BRCA1 protein can bind to the unique SUMO E2 Ubc9 (87). It seems that BRCA1 may be SUMOylated; however, research has shown that SUMO1 binds to the SUMO-binding motifs in BRCA1 and represses BRCA1-mediated transcription by recruiting HDAC in a SUMO-independent manner (88). Taken together, these results indicate that BRCA1 SUMOylation needs further investigation and that BRCA1 may regulate breast cancer in a SUMO-dependent and SUMO-independent manner.

FOXM1B

The transcription factor FOXM1 (forkhead box protein M1) is a critical regulator governing cell cycle pathway essential for mitosis, DNA replication, and cell proliferation (40). There are three main subtypes of FOXM1, of which FOXM1B is closely related to tumor growth and metastasis (89). FOXM1B can be SUMOylated on the K463 residue, and SUMOylation of FOXM1B is mediated by PIASy, and this SUMOylation is deconjugated by SENP2. SUMOylation of FOXM1B is necessary for its transcriptional activity, thus promoting the expression of its target gene JNK1 and repressing the expression of its targets MiR-200b/c and p21, ultimately promoting MCF-7 cell proliferation (40). Therefore, follow-up studies can be initiated directed toward the regulatory action of the SUMOylation of FOXM1B to explore strategies for the treatment of breast cancer.

FOXP3

Forkhead box protein P3 (FOXP3) is involved in regulatory T (Treg) cell development and inhibits tumorigenicity by downregulating oncogenes such as HER2/ErbB2 in breast cancer (89). Tumor immunotherapy has been successfully applied in the clinic. The role of Treg cells in immune suppression is well defined, and FOXP3 is a pivotal marker of Treg cells with immunosuppressive functions. In TNBC, the increase in FOXP3-positive Treg cells is associated with an improved survival rate (90). Furthermore, FOXP3 is modified by phosphorylation and acetylation, and the removal of

phosphate and acetyl groups from FOXP3 results in the attenuated transcriptional activity of Ubc9 (41). Increasing evidence has shown that FOXP3 mainly binds to the FOX response element in the proximal promoter region to activate the transcription of the Ubc9 gene. These results suggested that FOXP3 may have physiological functions as a novel regulator in global SUMOylation and in other post-translational modification systems in breast cancer.

Myc

Myc is an oncogenic transcription factor and is frequently dysregulated in human cancers. The overexpression of Myc may contribute to the acquired drug resistance in ER-positive breast cancer. One of the possible mechanisms is that Myc can positively regulate HSP111, which is an estrogen-responsive gene and is associated with the poor prognosis for patients (91). It has been reported that Myc may be SUMOylated by SUMO1 and deSUMOylated by SENP1. Myc SUMOylation can regulate its stabilization. Furthermore, PIAS1 can enhance the stability of Myc and promote Myc-driven tumorigenesis by recruiting JNK1 to phosphorylate Myc at S62 (92). SAE2 inhibition switches the Myc transcriptional subprogram from promoting to suppressing activity. SAE2 is necessary for Myc-dependent tumor growth in mice, and a gene expression analysis of human breast cancer with high Myc showed that lower SAE1 and SAE2 abundance in tumors is associated with a longer survival period without metastasis (36). Therefore, suppression of SUMOylation may be worthy of study, and inhibition of Myc SUMOylation is a potential treatment for Myc-driven breast cancer.

NEMO

The NF-κB essential modulator (NEMO) is a key activator of NF-κB signaling and IL6 secretion (93, 94). Once the IL6 receptor is activated, its downstream protein STAT3 is phosphorylated, and phosphorylated STAT3 binds to the PML promoter to activate PML expression (94). Several studies have shown that NEMO is regulated by SUMOylation, and the inhibition of NEMO SUMOylation suppresses the activation of NF-κB signaling in cells (95). Doxorubicin is a chemical drug commonly used for the treatment of breast cancer. However, breast cancer often develops treatment resistance, which leads to the recurrence and poor prognosis of the disease. Researchers found that SENP2 overexpression sensitized drug-resistant breast cancer cells to doxorubicin therapy. Mechanistically, the overexpression of SENP2 deconjugates the SUMOs of NEMO and inhibits NF-kB activation, especially in drug-resistant breast cancer cells. More importantly, when treated with an NF-κB pathway activator, the SENP2 overexpression-induced sensitivity of drug-resistant breast cancer cells to doxorubicin was eliminated (42). Taken together, these results suggest SENP2 activators may be used to treat doxorubicin-sensitive breast cancer patients, although this finding needs to be confirmed in clinical trials.

PES1

PES1 is a component of the nucleolar PeBoW complex (consisting of Pes1, Bop1 and WDR12) and is highly expressed in several kinds of cancers, including breast cancer (43, 96). PES1 promotes breast cancer development through multiple pathways. PES1 can directly bind to telomerase reverse transcriptase (TRET) and promote the formation of the TRET and TR complex, resulting in enhanced telomerase activity and telomere elongation, and inhibited cell senescence (96). In addition, PES1 can increase the expression of tumor-promoting ERα and decrease the expression of tumor-suppressive ERβ (97). Some studies demonstrated that in breast cancer cells, PES1 can be SUMOylated on K517, stabilizing PES1, which then promotes ERα transcription and inhibits ERα ubiquitination (42). Hence, the ultimate effect of PES1 SUMOylation is the acceleration of cell proliferation and cell cycle progression.

PML

The promyelocytic leukemia (PML) protein is highly expressed in TNBC. A report showed that PML inhibition led to cell proliferation arrest and senescence by downregulating Myc and PIM1 kinase, followed by the subsequent accumulation of p27 (98). Another study found that PML can promote the expression of SOX9 and thus enable breast cancer cells to acquire cancer-initiating cells (CIC) properties (99). PML can be modified by SUMO1, SUMO2, and SUMO3 at K65, K160, and K490, respectively (100). Previous studies have shown that global SUMO2/3 modification is enhanced in metastatic breast cancer. Consistently, the upregulation of PML SUMO-2/3 modification has been observed in metastatic breast cancer cells (34). Hence, it is likely that the upregulation of the PML SUMO-2/3 modification may result in the increased metastatic capacity of breast cells, a supposition that requires further investigation.

Smurf2

Smurf2 (Smad ubiquitination regulatory factor 2) is a HECT (homology to E6 carboxy-terminus domain)-containing ubiquitin E3 ligase that mediates substrate proteins for ubiquitination and degradation *via* the proteasome pathway (101). Smurf2 is expressed at low levels in breast cancer, especially in TNBC, and acts as a tumor suppressor. Smurf2 is located in the nucleus in normal cells but exhibits significant cytoplasmic sequestration in breast cancer cells (102, 103). Smurf2 can be SUMOylated at K29 and K369, and its SUMOylation contributes to the downregulation of TGFβ signaling and inhibits the EMT in breast cancer cells. Mechanistic studies showed that the SUMO E3 ligase PIAS3 maintains breast cancer organoids through Smurf2 SUMOylation under noninvasive conditions (101). Collectively, these findings identify a novel role for PIAS3-mediated Smurf2 SUMOylation in the suppression of breast cancer cell invasion (46). These findings identify Smurf2 SUMOylation as a novel biomarker and suggest the regulation of Smurf2 SUMOylation as a targeted approach to breast cancer therapy.

STAT5

Signal transducer and transcriptional activator (STAT) proteins, in particular STAT3 and STAT5, are continuously activated in many human cancers and are related to dysregulated cell proliferation and apoptosis (104). Drug-targeted activation of

STAT3 and STAT5 has been an active subject of cancer studies. System XC-, a cysteine/glutamate antiporter, contributes to the redox balance and facilitates the adaptation of aggressive cancer cells to increased levels of ROS (reactive oxygen species) (105). Protein xCT is the main impact factor in system XC- (105), and insufficient xCT expression potentially blocks cancer cell proliferation and metastasis (106). Previous studies have shown that the acute blockade of STAT3 and STAT5 with SH-4-54, a small-molecule inhibitor targeting the SH2 domains of these two proteins, can increase xCT expression and thus improve system XC- activity in breast cancer cells. However, current studies have shown that the chronic treatment of SH-4-54 followed by the cloning and selection of resistant MDA-MB-231 cells leads to the opposite effects (107). In resistant MDA-MB-231 cells, chronic treatment with SH-4-54 downregulates constitutive STAT3 phosphorylation and thus increases intracellular ROS levels, resulting in the deSUMOylation of STAT5 and the subsequent phosphorylation of STAT5. Activated STAT5 leads to a reduction in xCT mRNA and protein, which eventually abrogates cell growth and migration (47). Further studies addressing the relationship between STAT3 and STAT5 SUMOylation and the development of breast cancer are still needed.

TFAP2A

Transcription factor activator protein-2 (TFAP-2) activates transcription through GC-rich DNA sequences (108) and is important for cell proliferation and migration and xenograft outgrowth (49). Many solid cancers have an amplified CD44+/CD24- cancer stem cell (CSC) population that is relatively chemically resistant and leads to recurrence and metastasis. A durable response requires the development of therapeutics specific to CSCs (109). Recent evidence suggests that inhibiting the SUMOylation pathway inhibits tumor growth and invasion. It has been reported that in basal breast cancer, the inhibition of the SUMO pathway suppresses the expression of MMP14 and CD44, accompanied by decreased cell invasiveness and loss of CSC function (110). Another report showed that TFAP2A mediates SUMO pathway inhibition in breast cancer, indicating that TFAP2A may act as an upstream regulator of the SUMO pathway to regulate global SUMO modification in tumor cells and thus influence the cellular phenotype (111). Another study showed that SUMOylation of TFAP2A is necessary to maintain basal breast cancer phenotypes (49), suggesting that there may be a mutual regulatory relationship between TFAP2A and the SUMO pathway.

TP53

TP53 (p53), a well-known tumor suppressor, is a critical transcription factor that regulates the expression of numerous target genes to induce cell cycle arrest, apoptosis, senescence, and other anti-proliferative outcomes (50). p53 is the most frequently mutated gene in breast cancer. The incidence of mutations depends on the molecular subtype of breast cancer, most

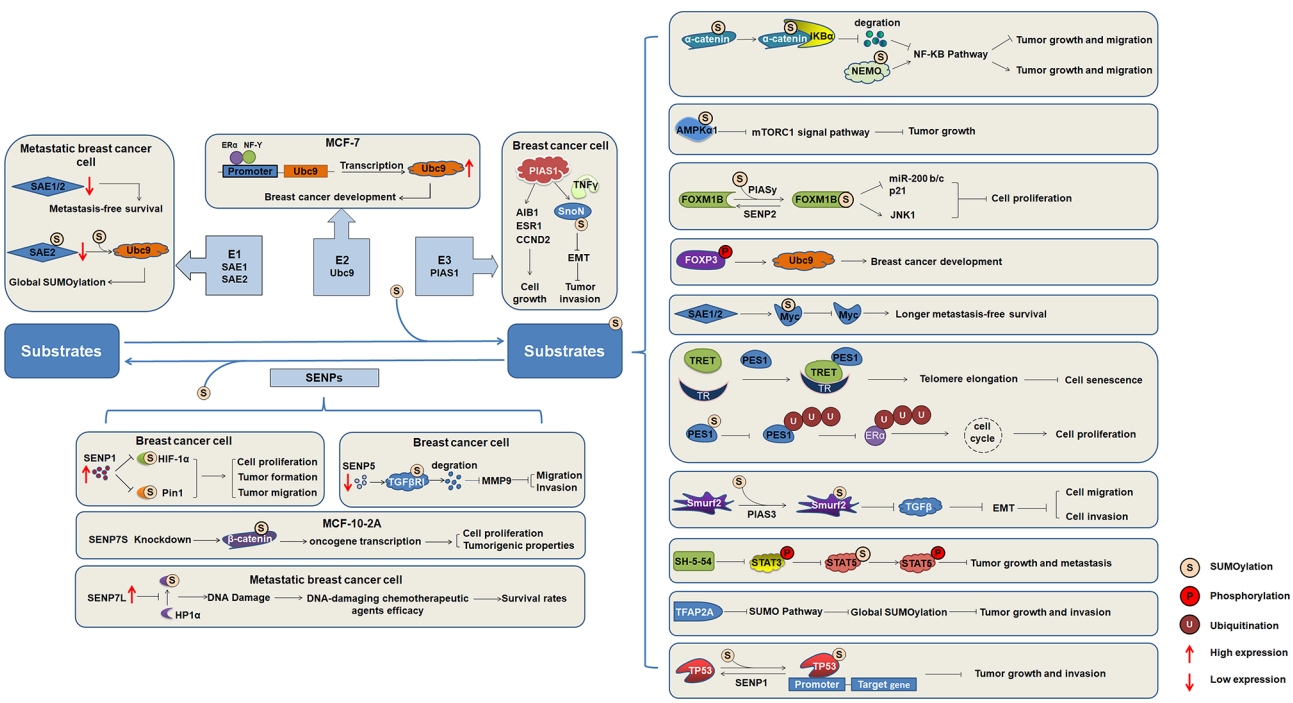

FIGURE 2 | The regulatory mechanism of substrates SUMOylation in the occurrence and development of breast cancer. SUMO activating enzymes E1, conjugating enzyme Ubc9, and ligating enzyme PIAS1, as well as SENP1, SENP5, and SENP7 regulate the progression of breast cancer. Increasing number of target proteins are SUMOylated, and SUMOylation of substrates regulate the function and involved in the occurrence and development of breast cancer.

common in the TN subtype and least in the Luminal A subtype (112). A research showed that p53 was SUMOylated by SUMO1 (50), another research found that p53 was conjugated with SUMO2/3 (113). Both SUMOylation promotes p53 bind to the target gene promoter, thereby enhances p53-mediated transcription. Meanwhile, it is found that SENP1 abolished SUMOylation of p53 and promotes cancer cell proliferation (50). These studies indicated that SUMO and SENP1 dynamically regulate the SUMOylation of p53, involving the progression of breast cancer.

CONCLUDING REMARKS AND PERSPECTIVES

SUMOylation has been studied since its discovery, and the understanding of its biochemistry and enzymological mechanisms has been advanced. SUMOylation is an important factor in the regulation of intracellular protein function, and the functional activity of other proteins can also be regulated by various other mechanisms. Abnormal SUMOylation levels lead to the occurrence and development of various human diseases. Numerous important transcription factors have been reported to be SUMOylated during the development of breast cancer (**Figure 2**), indicating that SUMOylation affects the occurrence and development of breast cancer.

Global SUMOylation is greatly upregulated in metastatic breast cancer cells compared with nonmetastatic control cells. Substrates identified with altered SUMOylation levels are involved in the cell cycle, migration, inflammation, and glycolysis, suggesting that perturbations of SUMOylation might contribute to cancer metastasis by affecting one or more of these biological processes (34). Dysregulation of SUMOylation plays a critical role in the metastasis of breast cancer. Although the molecular details of how SUMOylation affects breast cancer progression and metastasis are not well understood, accumulating evidence has suggested that targeting the SUMOylation pathway may be a strategy for targeting breast cancer. Therefore, further studies into the mechanism of SUMO modification in the process of gene transcription regulation are necessary for providing new ideas and methods for the prevention and treatment of breast cancer and important references for clarifying the pathogenesis of other nuclear receptor-related tumors.

AUTHOR CONTRIBUTIONS

YTQ and HW conceived the idea for the review. YYQ, HY, and XC performed the retrieval and collection of relevant literatures. ZX, XY, YS, WD, and SA provided suggestions. YYQ, HY, XC, YTQ, and HW wrote the paper. YYQ designed and prepared the figures. All authors contributed to the article and approved the submitted version.

FUNDING

This research was funded by the National Natural Science Foundation of China (81671294 and 81870241 to YTQ), and the Fundamental Research Funds for the Central Universities (GK201903066 to HW).

REFERENCES

1. Harbeck N, Gnant M. Breast cancer. *Lancet* (2017) 389(10074):1134–50. doi: 10.1016/S0140-6736(16)31891-8
2. Leyrer CM, Berriochoa CA, Agrawal S, Donaldson A, Calhoun BC, Shah C, et al. Predictive factors on outcomes in metaplastic breast cancer. *Breast Cancer Res Treat* (2017) 165(3):499–504. doi: 10.1007/s10549-017-4367-5
3. Chen WQ, Zheng RS, Baade PD, Zhang SW, Zeng HM, Bray F, et al. Cancer Statistics in China, 2015. *Ca-a Cancer J Clin* (2016) 66(2):115–32. doi: 10.3322/caac.21338
4. Siegel RL, Miller KD, Jemal A. Cancer statistics, 2019. *Ca-a Cancer J Clin* (2019) 69(1):7–34. doi: 10.3322/caac.21551
5. Medina MA, Oza G, Sharma A, Arriaga LG, Hernandez Hernandez JM, Rotello VM, et al. Triple-Negative Breast Cancer: A Review of Conventional and Advanced Therapeutic Strategies. *Int J Environ Res Public Health* (2020) 17(6):2078. doi: 10.3390/ijerph17062078
6. Anastasiadi Z, Lianos GD, Ignatiadou E, Harissis HV, Mitsis M. Breast cancer in young women: an overview. *Updates Surg* (2017) 69(3):313–7. doi: 10.1007/s13304-017-0424-1
7. Torre LA, Islami F, Siegel RL, Ward EM, Jemal A. Global Cancer in Women: Burden and Trends. *Cancer Epidemiol Biomarkers Prev* (2017) 26(4):444–57. doi: 10.1158/1055-9965.EPI-16-0858
8. Kennecke H, Yerushalmi R, Woods R, Cheang MC, Voduc D, Speers CH, et al. Metastatic behavior of breast cancer subtypes. *J Clin Oncol* (2010) 28 (20):3271–7. doi: 10.1200/JCO.2009.25.9820
9. Badve S, Dabbs DJ, Schnitt SJ, Baehner FL, Decker T, Eusebi V, et al. Basal-like and triple-negative breast cancers: a critical review with an emphasis on the implications for pathologists and oncologists. *Mod Pathol* (2011) 24 (2):157–67. doi: 10.1038/modpathol.2010.200
10. Brenton JD, Carey LA, Ahmed AA, Caldas C. Molecular classification and molecular forecasting of breast cancer: ready for clinical application? *J Clin Oncol* (2005) 23(29):7350–60. doi: 10.1200/JCO.2005.03.3845
11. Sheikh A, Hussain SA, Ghori Q, Naeem N, Fazil A, Giri S, et al. The spectrum of genetic mutations in breast cancer. *Asian Pac J Cancer Prev* (2015) 16(6):2177–85. doi: 10.7314/APJCP.2015.16.6.2177
12. Matsen CB, Neumayer LA. Breast cancer: a review for the general surgeon. *JAMA Surg* (2013) 148(10):971–9. doi: 10.1001/jamasurg.2013.3393
13. Castaneda SA, Strasser J. Updates in the Treatment of Breast Cancer with Radiotherapy. *Surg Oncol Clin N Am* (2017) 26(3):371–82. doi: 10.1016/j.soc.2017.01.013
14. Hassan MS, Ansari J, Spooner D, Hussain SA. Chemotherapy for breast cancer (Review). *Oncol Rep* (2010) 24(5):1121–31. doi: 10.3892/or_00000963
15. Zelnak AB, O'Regan RM. Optimizing Endocrine Therapy for Breast Cancer. *J Natl Compr Canc Netw* (2015) 13(8):e56–64. doi: 10.6004/jnccn.2015.0125
16. Gu G, Dustin D, Fuqua SA. Targeted therapy for breast cancer and molecular mechanisms of resistance to treatment. *Curr Opin Pharmacol* (2016) 31:97–103. doi: 10.1016/j.coph.2016.11.005
17. Veronesi U, Boyle P, Goldhirsch A, Orecchia R, Viale G. Breast cancer. *Lancet* (2005) 365(9472):1727–41. doi: 10.1016/S0140-6736(05)66546-4
18. Boyages J. Radiation therapy and early breast cancer: current controversies. *Med J Aust* (2017) 207(5):216–22. doi: 10.5694/mja16.01020
19. Bocci G, Tuccori M, Emmenegger U, Liguori V, Falcone A, Kerbel RS, et al. Cyclophosphamide-methotrexate 'metronomic' chemotherapy for the palliative treatment of metastatic breast cancer. A comparative

pharmacoeconomic evaluation. *Ann Oncol* (2005) 16(8):1243–52. doi: 10.1093/annonc/mdi240
20. McArthur HL, Hudis CA. Breast cancer chemotherapy. *Cancer J* (2007) 13 (3):141–7. doi: 10.1097/PPO.0b013e318074dc6f
21. Kang X, Qi Y, Zuo Y, Wang Q, Zou Y, Schwartz RJ, et al. SUMO-specific protease 2 is essential for suppression of polycomb group protein-mediated gene silencing during embryonic development. *Mol Cell* (2010) 38(2):191–201. doi: 10.1016/j.molcel.2010.03.005
22. Qi Y, Zuo Y, Yeh ET, Cheng J. An essential role of small ubiquitin-like modifier (SUMO)-specific Protease 2 in myostatin expression and myogenesis. *J Biol Chem* (2014) 289(6):3288–93. doi: 10.1074/jbc.M113.518282
23. Chang HM, Yeh ETH. SUMO: From Bench to Bedside. *Physiol Rev* (2020) 100(4):1599–619. doi: 10.1152/physrev.00025.2019
24. Kumar A, Zhang KY. Advances in the development of SUMO specific protease (SENP) inhibitors. *Comput Struct Biotechnol J* (2015) 13:204–11. doi: 10.1016/j.csbj.2015.03.001
25. Qi Y, Wang J, Bomben VC, Li DP, Chen SR, Sun H, et al. Hyper-SUMOylation of the Kv7 potassium channel diminishes the M-current leading to seizures and sudden death. *Neuron* (2014) 83(5):1159–71. doi: 10.1016/j.neuron.2014.07.042
26. Wu H, Chen X, Cheng J, Qi Y. SUMOylation and Potassium Channels: Links to Epilepsy and Sudden Death. *Adv Protein Chem Struct Biol* (2016) 103:295–321. doi: 10.1016/bs.apcsb.2015.11.009
27. Chen X, Zhang S, Huang J, Dong W, Xiao H, Shao H, et al. Hyper-SUMOylation of K(+) Channels in Sudden Unexplained Death in Epilepsy: Isolation and Primary Culture of Dissociated Hippocampal Neurons from Newborn Mice for Subcellular Localization. *Methods Mol Biol* (2018) 1684:63–71. doi: 10.1007/978-1-4939-7362-0_6
28. Zhao B, Zhang Z, Chen X, Shen Y, Qin Y, Yang X, et al. The important roles of protein SUMOylation in the occurrence and development of leukemia and clinical implications. *J Cell Physiol* (2021) 236(5):3466–80. doi: 10.1002/jcp.30143
29. Guo C, Hildick KL, Luo J, Dearden L, Wilkinson KA, Henley JM. SENP3-mediated deSUMOylation of dynamin-related protein 1 promotes cell death following ischaemia. *EMBO J* (2013) 32(11):1514–28. doi: 10.1038/emboj.2013.65
30. Saitoh H, Hinchey J. Functional heterogeneity of small ubiquitin-related protein modifiers SUMO-1 versus SUMO-2/3. *J Biol Chem* (2000) 275 (9):6252–8. doi: 10.1074/jbc.275.9.6252
31. Rabellino A, Andreani C, Scaglioni PP. The Role of PIAS SUMO E3-Ligases in Cancer. *Cancer Res* (2017) 77(7):1542–7. doi: 10.1158/0008-5472.CAN-16-2958
32. Bayer P, Arndt A, Metzger S, Mahajan R, Melchior F, Jaenicke R, et al. Structure determination of the small ubiquitin-related modifier SUMO-1. *J Mol Biol* (1998) 280(2):275–86. doi: 10.1006/jmbi.1998.1839
33. Wang L, Banerjee S. Differential PIAS3 expression in human malignancy. *Oncol Rep* (2004) 11(6):1319–24. doi: 10.3892/or.11.6.1319
34. Subramonian D, Raghunayakula S, Olsen JV, Beningo KA, Paschen W, Zhang XD. Analysis of changes in SUMO-2/3 modification during breast cancer progression and metastasis. *J Proteome Res* (2014) 13(9):3905–18. doi: 10.1021/pr500119a
35. Truong K, Lee TD, Chen Y. Small ubiquitin-like modifier (SUMO) modification of E1 Cys domain inhibits E1 Cys domain enzymatic activity. *J Biol Chem* (2012) 287(19):15154–63. doi: 10.1074/jbc.M112.353789
36. Kessler JD, Kahle KT, Sun TT, Meerbrey KL, Schlabach MR, Schmitt EM, et al. A SUMOylation-Dependent Transcriptional Subprogram Is Required for Myc-Driven Tumorigenesis. *Science* (2012) 335(6066):348–53 doi: 10.1126/science.1212728.
37. Chen H, Xu Z, Li X, Yang Y, Li B, Li Y, et al. alpha-catenin SUMOylation increases IkappaBalpha stability and inhibits breast cancer progression. *Oncogenesis* (2018) 7(3):28. doi: 10.1038/s41389-018-0037-7
38. Karami S, Lin FM, Kumar S, Bahnassy S, Thangavel H, Quttina M, et al. Novel SUMO-Protease SENP7S Regulates beta-catenin Signaling and Mammary Epithelial Cell Transformation. *Sci Rep* (2017) 7:46477. doi: 10.1038/srep46477
39. Yan Y, Ollila S, Wong IP, Vallenius T, Palvimo JJ, Vaahtomeri K, et al. SUMOylation of AMPKalpha1 by PIAS4 specifically regulates mTORC1 signalling. *Nat Commun* (2015) 6:8979. doi: 10.1038/ncomms9979
40. Wang CM, Liu R, Wang L, Nascimento L, Brennan VC, Yang WH. SUMOylation of FOXM1B alters its transcriptional activity on regulation of MiR-200 family and JNK1 in MCF7 human breast cancer cells. *Int J Mol Sci* (2014) 15(6):10233–51. doi: 10.3390/ijms150610233
41. Wang CM, Yang WH, Liu R, Wang L, Yang WH. FOXP3 Activates SUMO-Conjugating UBC9 Gene in MCF7 Breast Cancer Cells. *Int J Mol Sci* (2018) 19 (7):2036. doi: 10.3390/ijms19072036
42. Gao X, Wu Y, Qiao L, Feng X. SENP2 suppresses NF-kappaB activation and sensitizes breast cancer cells to doxorubicin. *Eur J Pharmacol* (2019) 854:179–86. doi: 10.1016/j.ejphar.2019.03.051
43. Li S, Wang M, Qu X, Xu Z, Yang Y, Su Q, et al. SUMOylation of PES1 upregulates its stability and function via inhibiting its ubiquitination. *Oncotarget* (2016) 7(31):50522–34. doi: 10.18632/oncotarget.10494
44. Chanda A, Chan A, Deng L, Kornaga EN, Enwere EK, Morris DG, et al. Identification of the SUMO E3 ligase PIAS1 as a potential survival biomarker in breast cancer. *PloS One* (2017) 12(5):e0177639. doi: 10.1371/journal.pone.0177639
45. Chanda A, Ikeuchi Y, Karve K, Sarkar A, Chandhoke AS, Deng L, et al. PIAS1 and TIF1gamma collaborate to promote SnoN SUMOylation and suppression of epithelial-mesenchymal transition. *Cell Death Differ* (2021) 28(1):267–82. doi: 10.1038/s41418-020-00611-z
46. Chandhoke AS, Chanda A, Karve K, Deng L, Bonni S. The PIAS3-Smurf2 sumoylation pathway suppresses breast cancer organoid invasiveness. *Oncotarget* (2017) 8(13):21001–14. doi: 10.18632/oncotarget.15471
47. Linher-Melville K, Nashed MG, Ungard RG, Haftchenary S, Rosa DA, Gunning PT, et al. Chronic Inhibition of STAT3/STAT5 in Treatment-Resistant Human Breast Cancer Cell Subtypes: Convergence on the ROS/SUMO Pathway and Its Effects on xCT Expression and System xc- Activity. *PloS One* (2016) 11(8):e0161202. doi: 10.1371/journal.pone.0161202
48. Cashman R, Cohen H, Ben-Hamo R, Zilberberg A, Efroni S. SENP5 mediates breast cancer invasion via a TGFbetaRI SUMOylation cascade. *Oncotarget* (2014) 5(4):1071–82. doi: 10.18632/oncotarget.1783
49. Bogachek MV, Chen Y, Kulak MV, Woodfield GW, Cyr AR, Park JM, et al. Sumoylation pathway is required to maintain the basal breast cancer subtype. *Cancer Cell* (2014) 25(6):748–61. doi: 10.1016/j.ccr.2014.04.008
50. Chauhan KM, Chen Y, Chen Y, Liu AT, Sun XX, Dai MS. The SUMO-specific protease SENP1 deSUMOylates p53 and regulates its activity. *J Cell Biochem* (2021) 122(2):189–97. doi: 10.1002/jcb.29838
51. Wu F, Zhu S, Ding Y, Beck WT, Mo YY. MicroRNA-mediated regulation of Ubc9 expression in cancer cells. *Clin Cancer Res* (2009) 15(5):1550–7. doi: 10.1158/1078-0432.CCR-08-0820
52. Zhu S, Sachdeva M, Wu F, Lu Z, Mo YY. Ubc9 promotes breast cell invasion and metastasis in a sumoylation-independent manner. *Oncogene* (2010) 29 (12):1763–72. doi: 10.1038/onc.2009.459
53. Mo YY, Yu Y, Theodosiou E, Ee PL, Beck WT. A role for Ubc9 in tumorigenesis. *Oncogene* (2005) 24(16):2677–83. doi: 10.1038/sj.onc.1208210
54. Tomasi ML, Tomasi I, Ramani K, Pascale RM, Xu J, Giordano P, et al. S-adenosyl methionine regulates ubiquitin-conjugating enzyme 9 protein expression and sumoylation in murine liver and human cancers. *Hepatology* (2012) 56(3):982–93. doi: 10.1002/hep.25701
55. Dunnebier T, Bermejo JL, Haas S, Fischer HP, Pierl CB, Justenhoven C, et al. Polymorphisms in the UBC9 and PIAS3 genes of the SUMO-conjugating system and breast cancer risk. *Breast Cancer Res Treat* (2010) 121(1):185–94. doi: 10.1007/s10549-009-0530-y
56. Ying S, Dunnebier T, Si J, Hamann U. Estrogen receptor alpha and nuclear factor Y coordinately regulate the transcription of the SUMO-conjugating UBC9 gene in MCF-7 breast cancer cells. *PloS One* (2013) 8(9):e75695. doi: 10.1371/journal.pone.0075695
57. Sentis S, Le Romancer M, Bianchin C, Rostan MC, Corbo L. Sumoylation of the estrogen receptor alpha hinge region regulates its transcriptional activity. *Mol Endocrinol* (2005) 19(11):2671–84. doi: 10.1210/me.2005-0042
58. Kahyo T, Nishida T, Yasuda H. Involvement of PIAS1 in the sumoylation of tumor suppressor p53. *Mol Cell* (2001) 8(3):713–8. doi: 10.1016/S1097-2765(01)00349-5
59. Liu B, Tahk S, Yee KM, Yang R, Yang Y, Mackie R, et al. PIAS1 regulates breast tumorigenesis through selective epigenetic gene silencing. *PloS One* (2014) 9(2):e89464. doi: 10.1371/journal.pone.0089464

60. Li S, Yang C, Hong Y, Bi H, Zhao F, Liu Y, et al. The transcriptional activity of co-activator AIB1 is regulated by the SUMO E3 ligase PIAS1. *Biol Cell* (2012) 104(5):287–96. doi: 10.1111/boc.201100116
61. Chanda A, Ikeuchi Y, Karve K, Sarkar A, Chandhoke AS, Deng L, et al. PIAS1 and TIF1gamma collaborate to promote SnoN SUMOylation and suppression of epithelial-mesenchymal transition. *Cell Death Differ* (2021) 28(1):267–82. doi: 10.1038/s41418-020-0599-8
62. Cheng J, Bawa T, Lee P, Gong L, Yeh ET. Role of desumoylation in the development of prostate cancer. *Neoplasia* (2006) 8(8):667–76. doi: 10.1593/neo.06445
63. Wang RT, Zhi XY, Zhang Y, Zhang J. Inhibition of SENP1 induces radiosensitization in lung cancer cells. *Exp Ther Med* (2013) 6(4):1054–8. doi: 10.3892/etm.2013.1259
64. Xu Y, Li J, Zuo Y, Deng J, Wang LS, Chen GQ. SUMO-specific protease 1 regulates the in vitro and in vivo growth of colon cancer cells with the upregulated expression of CDK inhibitors. *Cancer Lett* (2011) 309(1):78–84. doi: 10.1016/j.canlet.2011.05.019
65. Wang Z, Jin J, Zhang J, Wang L, Cao J. Depletion of SENP1 suppresses the proliferation and invasion of triple-negative breast cancer cells. *Oncol Rep* (2016) 36(4):2071–8. doi: 10.3892/or.2016.5036
66. Jia Y, Guo Y, Jin Q, Qu H, Qi D, Song P, et al. A SUMOylation-dependent HIF-1alpha/CLDN6 negative feedback mitigates hypoxia-induced breast cancer metastasis. *J Exp Clin Cancer Res* (2020) 39(1):42. doi: 10.1186/s13046-020-01547-5
67. Chen CH, Chang CC, Lee TH, Luo M, Huang P, Liao PH, et al. SENP1 deSUMOylates and regulates Pin1 protein activity and cellular function. *Cancer Res* (2013) 73(13):3951–62. doi: 10.1158/0008-5472.CAN-12-4360
68. Goeres J, Chan PK, Mukhopadhyay D, Zhang H, Raught B, Matunis MJ. The SUMO-specific isopeptidase SENP2 associates dynamically with nuclear pore complexes through interactions with karyopherins and the Nup107-160 nucleoporin subcomplex. *Mol Biol Cell* (2011) 22(24):4868–82. doi: 10.1091/mbc.e10-12-0953
69. Tan MY, Mu XY, Liu B, Wang Y, Bao ED, Qiu JX, et al. SUMO-specific protease 2 suppresses cell migration and invasion through inhibiting the expression of MMP13 in bladder cancer cells. *Cell Physiol Biochem* (2013) 32(3):542–8. doi: 10.1159/000354458
70. Nait Achour T, Sentis S, Teyssier C, Philippat A, Lucas A, Corbo L, et al. Transcriptional repression of estrogen receptor alpha signaling by SENP2 in breast cancer cells. *Mol Endocrinol* (2014) 28(2):183–96. doi: 10.1210/me.2013-1376
71. Mirecka A, Morawiec Z, Wozniak K. Genetic Polymorphism of SUMO-Specific Cysteine Proteases - SENP1 and SENP2 in Breast Cancer. *Pathol Oncol Res* (2016) 22(4):817–23. doi: 10.1007/s12253-016-0064-7
72. Jin ZL, Pei H, Xu YH, Yu J, Deng T. The SUMO-specific protease SENP5 controls DNA damage response and promotes tumorigenesis in hepatocellular carcinoma. *Eur Rev Med Pharmacol Sci* (2016) 20(17):3566–73.
73. Cai J, Wei X, Zhang G, Sui Y, Zhuang J, Liu Z, et al. Association of SENPs single-nucleotide polymorphism and breast cancer in Chinese population. *Med (Baltimore)* (2019) 98(6):e14168. doi: 10.1097/MD.0000000000014168
74. Lin FM, Kumar S, Ren J, Karami S, Bahnassy S, Li Y, et al. SUMOylation of HP1alpha supports association with ncRNA to define responsiveness of breast cancer cells to chemotherapy. *Oncotarget* (2016) 7(21):30336–49. doi: 10.18632/oncotarget.8733
75. Bawa-Khalfe T, Lu LS, Zuo Y, Huang C, Dere R, Lin FM, et al. Differential expression of SUMO-specific protease 7 variants regulates epithelial-mesenchymal transition. *Proc Natl Acad Sci USA* (2012) 109(43):17466–71. doi: 10.1073/pnas.1209378109
76. Buckley CD, Tan J, Anderson KL, Hanein D, Volkmann N, Weis WI, et al. Cell adhesion. The minimal cadherin-catenin complex binds to actin filaments under force. *Science* (2014) 346(6209):1254211. doi: 10.1126/science.1254211
77. Harris TJ, Tepass U. Adherens junctions: from molecules to morphogenesis. *Nat Rev Mol Cell Biol* (2010) 11(7):502–14. doi: 10.1038/nrm2927
78. Hollestelle A, Elstrodt F, Timmermans M, Sieuwerts AM, Klijn JG, Foekens JA, et al. Four human breast cancer cell lines with biallelic inactivating alpha-catenin gene mutations. *Breast Cancer Res Treat* (2010) 122(1):125–33. doi: 10.1007/s10549-009-0545-4
79. Piao HL, Yuan Y, Wang M, Sun Y, Liang H, Ma L. alpha-catenin acts as a tumour suppressor in E-cadherin-negative basal-like breast cancer by inhibiting NF-kappaB signalling. *Nat Cell Biol* (2014) 16(3):245–54. doi: 10.1038/ncb2909
80. de Groot JS, Ratze MA, van Amersfoort M, Eisemann T, Vlug EJ, Niklaas MT, et al. alphaE-catenin is a candidate tumor suppressor for the development of E-cadherin-expressing lobular-type breast cancer. *J Pathol* (2018) 245(4):456–67. doi: 10.1002/path.5099
81. Sun Y, Zhang J, Ma L. alpha-catenin. A tumor suppressor beyond adherens junctions. *Cell Cycle* (2014) 13(15):2334–9. doi: 10.4161/cc.29765
82. Nakopoulou L, Gakiopoulou-Givalou H, Karayiannakis AJ, Giannopoulou I, Keramopoulos A, Davaris P, et al. Abnormal alpha-catenin expression in invasive breast cancer correlates with poor patient survival. *Histopathology* (2002) 40(6):536–46. doi: 10.1046/j.1365-2559.2002.01392.x
83. Shackelford DB, Shaw RJ. The LKB1-AMPK pathway: metabolism and growth control in tumour suppression. *Nat Rev Cancer* (2009) 9(8):563–75. doi: 10.1038/nrc2676
84. Huang X, Li X, Xie X, Ye F, Chen B, Song C, et al. High expressions of LDHA and AMPK as prognostic biomarkers for breast cancer. *Breast* (2016) 30:39–46. doi: 10.1016/j.breast.2016.08.014
85. Saha M, Kumar S, Bukhari S, Balaji SA, Kumar P, Hindupur SK, et al. AMPK-Akt Double-Negative Feedback Loop in Breast Cancer Cells Regulates Their Adaptation to Matrix Deprivation. *Cancer Res* (2018) 78(6):1497–510. doi: 10.1158/0008-5472.CAN-17-2090
86. Roett MA, Evans P. Ovarian cancer: an overview. *Am Fam Physician* (2009) 80(6):609–16.
87. Xu J, Watkins T, Reddy A, Reddy ES, Rao VN. A novel mechanism whereby BRCA1/1a/1b fine tunes the dynamic complex interplay between SUMO-dependent/independent activities of Ubc9 on E2-induced ERalpha activation/repression and degradation in breast cancer cells. *Int J Oncol* (2009) 34(4):939–49. doi: 10.3892/ijo_00000220
88. Park MA, Seok YJ, Jeong G, Lee JS. SUMO1 negatively regulates BRCA1-mediated transcription, via modulation of promoter occupancy. *Nucleic Acids Res* (2008) 36(1):263–83. doi: 10.1093/nar/gkm969
89. Barger CJ, Branick C, Chee L, Karpf AR. Pan-Cancer Analyses Reveal Genomic Features of FOXM1 Overexpression in Cancer. *Cancers (Basel)* (2019) 11(2). doi: 10.3390/cancers11020251
90. Kalaw E, Lim M, Kutasovic JR, Sokolova A, Taege L, Johnstone K, et al. Metaplastic breast cancers frequently express immune checkpoint markers FOXP3 and PD-L1. *Br J Cancer* (2020) 123(11):1665–72. doi: 10.1038/s41416-020-01065-3
91. Fallah Y, Brundage J, Allegakoen P, Shajahan-Haq AN. MYC-Driven Pathways in Breast Cancer Subtypes. *Biomolecules* (2017) 7(3):53. doi: 10.3390/biom7030053
92. Chen Y, Sun XX, Sears RC, Dai MS. Writing and erasing MYC ubiquitination and SUMOylation. *Genes Dis* (2019) 6(4):359–71. doi: 10.1016/j.gendis.2019.05.006
93. Maubach G, Schmadicke AC, Naumann M. NEMO Links Nuclear Factor-kappaB to Human Diseases: (Trends Mol Med. 23, 1138-1155; 2017). *Trends Mol Med* (2018) 24(7):654. doi: 10.1016/j.molmed.2018.01.009
94. Elsarraj HS, Valdez KE, Hong Y, Grimm SL, Ricci LR, Fan F, et al. NEMO, a Transcriptional Target of Estrogen and Progesterone, Is Linked to Tumor Suppressor PML in Breast Cancer. *Cancer Res* (2017) 77(14):3802–13. doi: 10.1158/0008-5472.CAN-16-2794
95. Chen H, Xu Z, Li X, Yang Y, Li B, Li Y, et al. α-catenin SUMOylation increases IκBα stability and inhibits breast cancer progression. *Oncogenesis* (2018) 7(3):28. doi: 10.1038/s41389-018-0037-7
96. Cheng L, Yuan B, Ying S, Niu C, Mai H, Guan X, et al. PES1 is a critical component of telomerase assembly and regulates cellular senescence. *Sci Adv* (2019) 5(5):eaav1090. doi: 10.1126/sciadv.aav1090
97. Cheng L, Li J, Han Y, Lin J, Niu C, Zhou Z, et al. PES1 promotes breast cancer by differentially regulating ERalpha and ERbeta. *J Clin Invest* (2012) 122(8):2857–70. doi: 10.1172/JCI62676
98. Arreal L, Piva M, Fernandez S, Revandkar A, Schaub-Clerigue A, Villanueva J, et al. Targeting PML in triple negative breast cancer elicits growth suppression and senescence. *Cell Death Differ* (2020) 27(4):1186–99. doi: 10.1038/s41418-019-0407-5

99. Martin-Martin N, Piva M, Urosevic J, Aldaz P, Sutherland JD, Fernandez-Ruiz S, et al. Stratification and therapeutic potential of PML in metastatic breast cancer. *Nat Commun* (2016) 7:12595 doi: 10.1038/ncomms12595.
100. Maroui MA, Kheddache-Atmane S, El Asmi F, Dianoux L, Aubry M, Chelbi-Alix MK. Requirement of PML SUMO interacting motif for RNF4- or arsenic trioxide-induced degradation of nuclear PML isoforms. *PloS One* (2012) 7 (9):e44949. doi: 10.1371/journal.pone.0044949
101. Chandhoke AS, Karve K, Dadakhujaev S, Netherton S, Deng L, Bonni S. The ubiquitin ligase Smurf2 suppresses TGFbeta-induced epithelial-mesenchymal transition in a sumoylation-regulated manner. *Cell Death Differ* (2016) 23(5):876–88. doi: 10.1038/cdd.2015.152
102. Emanuelli A, Manikoth Ayyathan D, Koganti P, Shah PA, Apel-Sarid L, Paolini B, et al. Altered Expression and Localization of Tumor Suppressive E3 Ubiquitin Ligase SMURF2 in Human Prostate and Breast Cancer. *Cancers (Basel)* (2019) 11(4):506. doi: 10.3390/cancers 11040556
103. Liu X, Gu X, Sun L, Flowers AB, Rademaker AW, Zhou Y, et al. Downregulation of Smurf2, a tumor-suppressive ubiquitin ligase, in triple-negative breast cancers: involvement of the RB-microRNA axis. *BMC Cancer* (2014) 14:57. doi: 10.1186/1471-2407-14-57
104. Yu H, Jove R. The STATs of cancer–new molecular targets come of age. *Nat Rev Cancer* (2004) 4(2):97–105. doi: 10.1038/nrc1275
105. Ishimoto T, Nagano O, Yae T, Tamada M, Motohara T, Oshima H, et al. CD44 variant regulates redox status in cancer cells by stabilizing the xCT subunit of system xc(-) and thereby promotes tumor growth. *Cancer Cell* (2011) 19(3):387–400. doi: 10.1016/j.ccr.2011.01.038
106. Chen RS, Song YM, Zhou ZY, Tong T, Li Y, Fu M, et al. Disruption of xCT inhibits cancer cell metastasis via the caveolin-1/beta-catenin pathway. *Oncogene* (2009) 28(4):599–609. doi: 10.1038/onc.2008.414
107. Xiong A, Yang Z, Shen Y, Zhou J, Shen Q. Transcription Factor STAT3 as a Novel Molecular Target for Cancer Prevention. *Cancers (Basel)* (2014) 6 (2):926–57. doi: 10.3390/cancers6020926
108. Paonessa F, Foti D, Costa V, Chiefari E, Brunetti G, Leone F, et al. Activator protein-2 overexpression accounts for increased insulin receptor expression in human breast cancer. *Cancer Res* (2006) 66(10):5085–93. doi: 10.1158/0008-5472.CAN-05-3678
109. Bogachek MV, Park JM, De Andrade JP, Kulak MV, White JR, Wu T, et al. A novel animal model for locally advanced breast cancer. *Ann Surg Oncol* (2015) 22(3):866–73. doi: 10.1245/s10434-014-4174-8
110. Park SY, Lee HE, Li H, Shipitsin M, Gelman R, Polyak K. Heterogeneity for stem cell-related markers according to tumor subtype and histologic stage in breast cancer. *Clin Cancer Res* (2010) 16(3):876–87. doi: 10.1158/1078-0432.CCR-09-1532
111. Bogachek MV, Park JM, De Andrade JP, Lorenzen AW, Kulak MV, White JR, et al. Inhibiting the SUMO Pathway Represses the Cancer Stem Cell Population in Breast and Colorectal Carcinomas. *Stem Cell Rep* (2016) 7 (6):1140–51. doi: 10.1016/j.stemcr.2016.11.001
112. Duffy MJ, Synnott NC, Crown J. Mutant p53 in breast cancer: potential as a therapeutic target and biomarker. *Breast Cancer Res Treat* (2018) 170 (2):213–9. doi: 10.1007/s10549-018-4753-7
113. Stindt MH, Carter S, Vigneron AM, Ryan KM, Vousden KH. MDM2 promotes SUMO-2/3 modification of p53 to modulate transcriptional activity. *Cell Cycle* (2011) 10(18):3176–88. doi: 10.4161/cc.10.18.17436

Conflict of Interest: The authors declare that the research was conducted in the absence of any commercial or financial relationships that could be construed as a potential conflict of interest.

frontiers in Oncology

MINI REVIEW
published: 21 April 2021
doi: 10.3389/fonc.2021.617597

Communication Between Epithelial–Mesenchymal Plasticity and Cancer Stem Cells: New Insights Into Cancer Progression

Xiaobo Zheng[1], *Fuzhen Dai*[2], *Lei Feng*[3], *Hong Zou*[1,4], *Li Feng*[5] *and Mingqing Xu*[1,6]*

[1] *Department of Liver Surgery, West China Hospital, Sichuan University, Chengdu, China,* [2] *Department of General Surgery, The First People's Hospital of Longquanyi District, Chengdu, China,* [3] *Department of Biliary Surgery, West China Hospital, Sichuan University, Chengdu, China,* [4] *General Surgery Center of PLA, General Hospital of Western Theater Command, Chengdu, China,* [5] *Department of General Surgery, Hospital of Chengdu University of Traditional Chinese Medicine, Chengdu, China,* [6] *Department of Hepatopancreatobiliary Surgery, Meishan City People's Hospital, Meishan Hospital of West China Hospital, Sichuan University, Meishan, China*

The epithelial–mesenchymal transition (EMT) is closely associated with the acquisition of aggressive traits by carcinoma cells and is considered responsible for metastasis, relapse, and chemoresistance. Molecular links between the EMT and cancer stem cells (CSCs) have indicated that EMT processes play important roles in the expression of CSC-like properties. It is generally thought that EMT-related transcription factors (EMT-TFs) need to be downregulated to confer an epithelial phenotype to mesenchymal cells and increase cell proliferation, thereby promoting metastasis formation. However, the genetic and epigenetic mechanisms that regulate EMT and CSC activation are contradictory. Emerging evidence suggests that EMT need not be a binary model and instead a hybrid epithelial/mesenchymal state. This dynamic process correlates with epithelial–mesenchymal plasticity, which indicates a contradictory role of EMT during cancer progression. Recent studies have linked the epithelial–mesenchymal plasticity and stem cell-like traits, providing new insights into the conflicting relationship between EMT and CSCs. In this review, we examine the current knowledge about the interplay between epithelial–mesenchymal plasticity and CSCs in cancer biology and evaluate the controversies and future perspectives. Understanding the biology of epithelial–mesenchymal plasticity and CSCs and their implications in therapeutic treatment may provide new opportunities for targeted intervention.

Keywords: epithelial-mesenchymal plasticity, cancer stem cells, epithelial-mesenchymal transition, mesenchymal-epithelial transition, metastasis, stemness

OPEN ACCESS

Edited by:
Lorenzo Gerratana, University of Udine, Italy

Reviewed by:
Federico Bocci, University of California, Irvine, United States
Minal Garg, University of Lucknow, India

***Correspondence:**
Mingqing Xu
xumingqing0018@163.com

Specialty section:
This article was submitted to Molecular and Cellular Oncology, a section of the journal Frontiers in Oncology

Received: *15 October 2020*
Accepted: *23 February 2021*
Published: *21 April 2021*

Citation:
Zheng X, Dai F, Feng L, Zou H, Feng L and Xu M (2021) Communication Between Epithelial–Mesenchymal Plasticity and Cancer Stem Cells: New Insights Into Cancer Progression. Front. Oncol. 11:617597. doi: 10.3389/fonc.2021.617597

INTRODUCTION

Epithelial–mesenchymal transition (EMT) is the process through which epithelial cells alter their phenotype, enabling them to lose their main epithelial cell traits and convert into cells expressing mesenchymal cell markers (1, 2). Following the EMT, cells switch from polygonal to spindle-like fusiform shape, lose cell polarity, and gain increased resistance to apoptosis and the ability to migrate and invade (3–8). The EMT occurs in various physiological and pathological conditions, including embryonic processes essential for normal development, tissue morphogenesis and repair, tissue reconstruction, fibrogenesis, and tumorigenesis (9–12).

EMT has been associated with cancer stemness, characterized by an increase in the number of cancer stem cells (CSCs) (13–16). CSCs are subclone cells in the tumor tissue that obtain stem cell traits (17, 18). CSCs exhibit self-renewal, maintain tumor formation ability, and can differentiate into various cells to support the tumor; therefore, these cells are considered a source of tumorigenesis, metastasis, and relapse (19–21). In addition, CSCs are highly related to chemoresistance (22). Even if most tumor cells are eliminated by chemotherapy, if CSCs are not eradicated, relapse, metastasis, and chemoresistance still commonly occur (23). Similar to normal stem cells, most CSCs are quiescent and slow growing, which is why they are resistant to anticancer drugs (24).

Previous studies have suggested that cells undergoing EMT possess stem cell traits and that tumor cells retaining stemness express markers of the EMT (25). However, several studies have shown that stemness is coupled with the mesenchymal–epithelial transition (MET) rather than the EMT and that regulation of the EMT and stemness is distinct (26–30). Thus, the correlation between the EMT and stemness is not clear. Recently, the EMT was defined as a dynamic, hybrid epithelial/mesenchymal state (31–33). Of note, this hybrid state is a coexistence of epithelial and mesenchymal phenotypes, rather than the junction of separate phenotypes; epithelial–mesenchymal plasticity was used to describe this hybrid epithelial/mesenchymal state during EMT. Importantly, epithelial–mesenchymal plasticity is involved in cancer progression and associated with stem cell-like traits, which may help explain the conflicting relationship between EMT and CSCs (34, 35). In this review, we discuss the relationship between EMT/MET/epithelial–mesenchymal plasticity and CSCs.

EMT CONFERS TUMOR CELLS WITH TRAITS OF CSCS

Stemness acquired after the induction of the EMT provides cells with the traits of increased migratory ability and antitumor drug resistance and promotes tumor metastasis and recurrence (36–38). Dang et al. (39) found that the EMT induced by transforming growth factor (TGF) correlates with acquisition of tumor-initiating stem cells (TISCs) in breast cancer. SNAIL directly regulates the expression of Nanog in mesenchymal cells generated by the EMT. Deletion of SNAIL influences the growth but not the initial formation of the tumor. Kim et al. (40) found that $CD13^+$ liver CSCs can survive in a hypoxic environment after chemotherapy and that EMT enhances cell stemness by suppressing the activity of reactive oxygen species. Garg suggested that CSCs could be classified into two distinct functional transition states, one of which is cyclic CSCs with predominant epithelial phenotype that can self-renew and differentiate into mature cancer cells. The other subset is autophagic/non-cyclic CSCs with predominant mesenchymal phenotype that have the capacity to invade and metastasize and that are majorly responsible for cancer mortality (41). The EMT seems to work together with the microenvironment to promote proliferation and homing of CSCs. Cytokines are critical for regulating the microenvironment and are necessary for initiating the EMT (42). It was reported that the TGF-β/BMP signaling pathways regulate primary tumor and metastasis microenvironments in colorectal and breast cancer (43). Collectively, these studies point to the fact that CSCs can be induced by EMT and exhibit a mesenchymal phenotype with greater metastatic potential.

EMT and acquisition of CSC-like characteristics are key steps in the metastasis and recurrence of a tumor after radical resection. A study by Mani and colleagues (25) showed that EMT induction in immortalized human mammary epithelial cells led to increased mammosphere formation *in vitro* and tumorigenicity *in vivo*, suggesting that the EMT process can stimulate the acquisition of cell stemness. Moreover, the EMT confers stem cell-like properties, consistent with the migratory CSC concept. Several lines of evidence have supported the relationship between EMT and stemness. For example, Morel et al. (44) showed that $CD44^-CD24^+$ breast epithelial cells, which are non-tumorigenic, can induce the EMT after activating the RAS/mitogen-activated protein kinase pathway and acquire the $CD44^+CD24^-$ phenotype and stem cell traits. $CD24^+$ cells treated with TGF do undergo the EMT, as demonstrated by the downregulation of E-cadherin and the upregulation of vimentin, accompanied by acquisition of $CD24^-$ features. It is thus tempting to speculate that the EMT may be an important step in controlling the transition of $CD44^-CD24^+$ cells to $CD44^+CD24^-$ cells. In CSCs isolated from colorectal cancer surgery samples and analyzed using gene chips, Hwang et al. (45) found a high expression of CD44 and CD166, stem cell markers that regulate the EMT-associated transcription factor (TF) SNAIL. Subclones of basement-like breast cancer cells have a high proportion of $CD44^+CD24^-$ stem cell-like cells and overexpress EMT-correlated genes (46). Another study found that Fox2, an EMT-related TF, is highly expressed in breast cancer and is closely linked with basement-like subclones (47). Immunohistochemical analysis of 479 infiltrated breast cancer samples revealed that basement-like breast cancers express high levels of EMT-associated factors but low levels of E-cadherin (48). Taken together, these studies confirmed the fact that stemness and EMT are indeed intricately linked.

MET IN RECOVERING EPITHELIAL TRAITS FOR ENHANCING STEMNESS TO FACILITATE DISTAL COLONIZATION

Several results have linked the MET and stem cell-like traits, challenging the view on the relationship between the EMT and CSCs (31, 49–51). The general view suggests that EMT-related transcription factors (EMT-TFs) must be downregulated in order to convert mesenchymal cells into epithelial cells and to increase proliferation, thereby promoting tumor metastasis formation (52). In order to form clones, malignant tumor cells need to assume an epithelial phenotype and maintain a state of stemness (53). Interestingly, Padmanaban et al. revealed that the expression of E-cadherin needs to be rescued *via* the inhibition of TGFβ-receptor signaling during the detachment, systemic dissemination, and seeding phases of metastasis in invasive breast

ductal carcinomas (54). Fibroblasts must experience the MET to complete their progression to induced pluripotent stem cells (29). A study by Tsai et al. (27) clearly supported the role of the EMT in dissemination and the subsequent MET for colonization and macrometastasis. Additionally, a study by Ocaña et al. (28) also supported the role of the EMT in dissemination and the necessity of reversing the EMT for metastasis.

The mechanism underlying MET in recovering cancer cells stemness is still complicated. Several studies have reported that downregulation of traditional EMT-TFs cannot induce stemness because the regulation of stem cell properties is independent from that of epithelial plasticity (55). However, stem cell properties can be acquired through inhibition of Prrx1 (28, 56). Prrx1 and TWIST can both induce EMT properties alone; however, while deletion of Prrx1 induces lung metastasis, ablation of TWIST does not have the same effect. Intriguingly, deletion of Prrx1 in BT-549 cells enhances stemness, accompanied with increased mammosphere formation, self-renewal ability, and $CD24^{-}/CD44^{+}$ CSC proportion (28). Instead, downregulation of TWIST does not induce stemness, suggesting that downregulation of traditional EMT-TFs is not related to the occurrence of stemness and that regulation of the EMT and CSCs is distinct. In addition, Prrx1 expression predicts better prognosis and higher metastasis-free survival (57). Celià-Terrassa et al. (58) illustrated that the EMT can inhibit TISCs, suggesting that there are different subpopulations of EMT-TFs. In addition, the EMT must be reversed to allow growth and clonal expansion because invasive dedifferentiated tumor cells from the EMT were found to be quiescent, whereas proliferation was detected in redifferentiated metastatic tumor cells, suggesting that the EMT should reverse to the MET.

It has been reported that the mesenchymal state is related to early events in metastasis, such as dissemination, invasion, and intravascular infiltration. EMT-TFs initiate the invasion–metastasis cascade when aberrantly activated in tumors. A recent study showed that CSC formation is an early and frequent event in LSC progression (59). It has also been suggested that the epithelial state with stemness is correlated with later phases of metastasis (55). Moreover, the observations that CSC plasticity is elevated in advanced cancers and that regulation of the epithelial–mesenchymal states is increased are highly relevant (35). Mesenchymal state-associated invasion and dissemination are necessary, but not sufficient, to induce metastasis, and additional epithelial state with stemness is required to complete the full metastasis cascade (60). Therefore, epithelial–mesenchymal heterogeneity with stemness plasticity is involved in the entire process of invasion and metastasis.

EMERGENCE OF EPITHELIAL–MESENCHYMAL PLASTICITY

Recently, epithelial–mesenchymal plasticity was recommended as unified nomenclature by the EMT international association and was termed as the ability of cells to adopt mixed epithelial/mesenchymal (E/M) features and transit between EMT and MET states (50, 61). This epithelial–mesenchymal plasticity has been variably referred to as partial EMT, hybrid E/M status, intermediate EMT, a metastable EMT state, EMT continuum, and EMT spectrum, which were widely used in past studies (62). The cells undergoing epithelial–mesenchymal plasticity express a mixture of epithelial and mesenchymal features and express both epithelial and mesenchymal markers (63). Epithelial–mesenchymal plasticity also helps to account for the reversibility of the EMT process. Epithelial cells going through EMT give rise to cell populations that may enter reversibly into states with various proportions of epithelial and mesenchymal features (64, 65). Epithelial–mesenchymal plasticity is thought to provide cells with the fitness and flexibility to fulfill the diverse requirements during the course of either developmental or pathological processes. These cell transitions allow them to migrate from the primary tumor and invade the secondary site, playing a fundamental role in cancer metastasis. Epithelial–mesenchymal plasticity is associated with tumor cell migration, invasion, colonization, stemness, and drug resistance (66).

Epithelial–mesenchymal plasticity has been reported in many studies. The hybrid E/M phenotypes have been confirmed both *in vitro* and *in vivo*. Huang et al. systematically analyzed the protein levels of the epithelial and mesenchymal markers in 42 ovarian carcinoma cell lines. Among these 42 cell lines, 9 have been characterized as epithelial cells, 7 as mesenchymal cells, and the remaining 26 cell lines were characterized as hybrid E/M phenotypes (67). The existence of hybrid E/M states has also been observed in animal models. Pastushenko and colleagues screened a large panel of cell surface markers, such as EpCAM, vimentin, CD106, CD61, and CD51, in genetic mouse models of skin and mammary primary tumors. They identified the existence of multiple tumor subpopulations associated with different EMT stages: from completely epithelial to completely mesenchymal states, passing through intermediate hybrid states (68). The hybrid E/M phenotypes were also detected in clinical samples. Metastatic breast cancers were categorized as either having an epithelial or hybrid phenotype using a prediction algorithm, where the *VIM:CDH1* gene expression ratio was combined with the expression of *CLDN7* (69). A partial EMT process including the upregulation of mesenchymal genes in conjunction with the downregulation of certain epithelial genes was confirmed in a subset of HNSCC cells through single-cell RNA sequencing (70). Taken together, the epithelial–mesenchymal plasticity in cancer cells describes the presence of both epithelial and mesenchymal markers in the same cancer cells. It might reflect a stable state of cancer type or a transition phase of cancer cells while they are switching their phenotype. Its correlation with aggressiveness and metastasis further enforces the crucial role of epithelial–mesenchymal plasticity in cancer progression.

THE INTERPLAY BETWEEN EPITHELIAL–MESENCHYMAL PLASTICITY AND CSCS

Distal tumor subclone formation is thought to be a multistep and long-term process, which also explains why various subclones have distinct proliferative abilities (71). Stemness is also a

state of plasticity in tumor progression, allowing static and migratory CSCs to coexist (72). These ideas are consistent with the concept of epithelial–mesenchymal plasticity, a process that is thought to be a hybrid state during metastasis. The shift among the hybrid states of EMT may orchestrate the entire process of distant metastasis formation, from acquisition of invasive ability from primary tumor and dissemination *via* the bloodstream, to seeding in distant organs, stemness recovery for clonal expansion, and macrometastasis (73). Emerging evidence from theoretical and experimental studies has revealed the association of epithelial–mesenchymal plasticity with CSCs (74–77). Pastushenko et al. reported that the earliest EMT state already exhibits increased CSC frequency, and tumor stemness does not increase further in later hybrid epithelial–mesenchymal states (68). Francescangeli et al. reported that a pre-existing population of $ZEB2^{+}$ quiescent cells in colorectal cancer showed both stemness and mesenchymal features and dictated chemotherapy resistance (78). Co-expression of stem cell and both epithelial and mesenchymal characters was also observed in circulating tumor cells of bladder cancer patients (79). Epithelial–mesenchymal plasticity was associated with miRNA let-7, which was an important factor affecting the CSC phenotype in high-grade serous ovarian carcinoma samples and could be correlated with tumor growth and metastasis (80). Quan et al. reported that ∼60% of the leader CSCs in collective invasion co-existed with hybrid epithelial–mesenchymal states, indicating that CSCs with epithelial–mesenchymal plasticity play a key role in cancer cell collective invasion (81). Moreover, a previous study reported that in response to microenvironmental signals, lung cancer cells converted to CSC state through regulation of the balance between epithelial and mesenchymal transition (82). Collectively, the above results indicate that epithelial–mesenchymal plasticity confers cancer cells with the traits of stemness.

The mechanism underlying epithelial–mesenchymal plasticity and CSCs is still largely unknown. Recently, some factors that regulate the epithelial–mesenchymal plasticity and stemness of CSCs were reported. OvoL/Shavenbaby factors are a family of key epithelial stabilizers and are critical for adult stem cell homeostasis. Stemness and epithelial–mesenchymal plasticity could be regulated by interaction of EMT transcription factors and OvoL/Shavenbaby (83). A study reported that the non-coding RNAs expressed on the DLK1-DIO3 locus regulate the epithelial–mesenchymal plasticity in breast epithelial progenitor cells, providing evidence of the interplay of epithelial–mesenchymal plasticity and stemness (84). miRNAs, which are important factors in tumorigenesis and progression of cancers, are also involved in mediating interactions between epithelial–mesenchymal plasticity and CSCs (85–88). Jiang et al. reported that Prrx1 promotes epithelial–mesenchymal plasticity and activates cell dormancy in head and neck squamous cell carcinoma and that miR-642b-3p restoration rescues PRRX1-induced phenotype and cell dormancy (85). Furthermore, You et al. observed that miRNA-495 confers inhibitory effects on CSCs, as well as EMT, in oral squamous cell carcinoma through HOXC6-mediated TGF-β signaling pathway (86). The long non-coding RNA H19 mediates epithelial–mesenchymal plasticity by differentially sponging miR-200b/c and let-7b, wherein the latter is a CSC regulator in colon cancer (88, 89). Several studies have shown that cells with hybrid E/M states and CSC phenotypes are spatially segregated in the primary tumor (90). Bocci et al. observed through a mechanism-based dynamical model that the diffusion of EMT-inducing signals such as TGF-β, together with non-cell autonomous control of EMT and CSC decision-making *via* the Notch signaling pathway, can explain the experimentally observed disparate localization of subsets of CSCs with varying EMT phenotypes in the tumor (74). These results offer insights into the principles of spatiotemporal patterning in epithelial–mesenchymal plasticity and identify a relevant target during hybrid E/M states to alleviate multiple CSC subsets. Using a mechanism-based model, Bocci et al. explained how metformin can both inhibit EMT and blunt the aggressive potential of CSCs simultaneously by driving the cells out of a hybrid E/M stem-like state with enhanced Notch-Jagged signaling (91).

The expression levels of EMT-TFs, such as SNAIL and TWIST, in primary tumors are also fluctuant associated with cancer cell stemness. The consecutive expression of SNAIL, Prrx1, and TWIST also inhibits the formation of metastasis because EMT-TFs must be downregulated to facilitate stemness recovery and tumor formation (58). This is not contradictory, but simply reflects epithelial–mesenchymal plasticity and the dynamic process resembling the migration of embryonic cell populations to distant organs/sites. Thus, EMT-TFs are related to cell behavior rather than to cell fate, and hence, their expression is dynamic. Accordingly, as recommended by the EMT international association, EMT-TFs alone cannot be used as markers of differentiated cell populations, the equivalent of differentiated distant metastases (92). Further investigation of the downregulation of EMT-TFs in signaling pathways associated with the formation of CSCs is needed, particularly with regard to the interplay among the epithelial–mesenchymal plasticity, invasion of the primary tumor, and stemness recovery for tumor metastatic colonization. The complex interplay between epithelial–mesenchymal plasticity, CSCs, and tumor microenvironment gives rise to tumor heterogeneity that still represents the major challenge hampering therapy for metastasis and chemoresistance.

CONCLUSION AND PERSPECTIVES

This review suggests that epithelial–mesenchymal plasticity is involved in the process of CSC development. The coexistence of epithelial–mesenchymal plasticity and CSCs correlates with poor prognosis and resistance to therapy (93). Furthermore, emerging evidence has shown that targeting epithelial–mesenchymal plasticity-induced CSCs can effectively regulate tumor progression and drug resistance. Liu et al. reported that metformin inhibits prostate cancer resistant to enzalutamide by reducing the cells with hybrid E/M status and, thereby, restricting the formation of CSCs (94). Nevertheless, the mechanism underlying the relationship between epithelial–mesenchymal plasticity and CSCs still remains poorly understood. Additional

research is required at the molecular level to clarify, for example, how TWIST and Prrx1 interact, and how Prrx1 inhibits the induction of stemness while not inhibiting the EMT-promoting function of TWIST, as well as to elucidate the roles of other potential EMT-related factors, such as SNAIL and ZEB1. This will help to unveil the mechanisms underlying CSC initiation and tumor metastasis. In addition, it is plausible that non-CSCs can transition to CSCs during the dynamic process of epithelial–mesenchymal plasticity. Therefore, the plasticity of CSCs needs to be considered to explore therapeutic strategies aimed at overcoming tumor heterogeneity and chemoresistance by targeting CSCs. In all, understanding these molecular mechanisms can help improve the efficiency of the ongoing and planned therapeutic trials to control cancer progression, treatment resistance, and disease recurrence.

AUTHOR CONTRIBUTIONS

MX proposed the research. XZ, FD, and LeF collected the references. XZ, HZ, and LiF analyzed the references. XZ and MX wrote the paper. All authors contributed to the design and interpretation of the study and to the writing of the drafts.

FUNDING

This study was supported by the grants from the National Natural Science Foundation of China (No. 81803574), China Postdoctoral Science Foundation (2019M653430), and Post-Doctor Research Project, West China Hospital, Sichuan University (2018HXBH003)), and Key Technology Research and Development Program of the Sichuan Province (Nos. 2019YFS0208, 2021YFSY0009).

REFERENCES

1. Thiery JP, Acloque H, Huang RY, Nieto MA. Epithelial-mesenchymal transitions in development and disease. *Cell.* (2009) 139:871–90. doi: 10.1016/j.cell.2009.11.007
2. Kalluri R, Weinberg RA. The basics of epithelial-mesenchymal transition. *J Clin Invest.* (2009) 119:1420–8. doi: 10.1172/JCI39104
3. Abdullah A, Akhand SS, Paez JSP, Brown W, Pan L, Libring S. Epigenetic targeting of neuropilin-1 prevents bypass signaling in drug-resistant breast cancer. *Oncogene*. (2020) 40:322–33. doi: 10.1038/s41388-020-01530-6
4. Ji R, Zhu XJ, Wang ZR, Huang LQ. Cortactin in epithelial-mesenchymal transition. *Front Cell Dev Biol.* (2020) 8:585619. doi: 10.3389/fcell.2020.585619
5. Coban B, Bergonzini C, Zweemer AJM, Danen EHJ. Metastasis: crosstalk between tissue mechanics and tumour cell plasticity. *Br J Cancer*. (2020) 124:49–57. doi: 10.1038/s41416-020-01150-7
6. Babaei G, Aziz SG, Jaghi NZZ. EMT, cancer stem cells and autophagy; the three main axes of metastasis. *Biomed Pharmacotherap.* (2020) 133:110909. doi: 10.1016/j.biopha.2020.110909
7. Peyre L, Meyer M, Hofman P, Roux J. TRAIL receptor-induced features of epithelial-to-mesenchymal transition increase tumour phenotypic heterogeneity: potential cell survival mechanisms. *Br J Cancer*. (2020) 124:91–101. doi: 10.1038/s41416-020-01177-w
8. Sinha D, Saha P, Samanta A, Bishayee A. Emerging concepts of hybrid epithelial-to-mesenchymal transition in cancer progression. *Biomolecules*. (2020) 10:1561. doi: 10.3390/biom10111561
9. Brabletz T. EMT and MET in metastasis: where are the cancer stem cells? *Cancer Cell.* (2012) 22:699–701. doi: 10.1016/j.ccr.2012.11.009
10. Lamouille S, Xu J, Derynck R. Molecular mechanisms of epithelial-mesenchymal transition. *Nat Rev Mol Cell Biol.* (2014) 15:178–96. doi: 10.1038/nrm3758
11. De Craene B, Berx G. Regulatory networks defining EMT during cancer initiation and progression. *Nat Rev Cancer.* (2013) 13:97–110. doi: 10.1038/nrc3447
12. Kim DH, Xing T, Yang Z, Dudek R, Lu Q, Chen YH. Epithelial Mesenchymal transition in embryonic development, tissue repair and cancer: a comprehensive overview. *J Clin Med.* (2017) 7:1. doi: 10.3390/jcm7010001
13. Castagnoli L, Tagliabue E. Inhibition of the wnt signalling pathway: an avenue to control breast cancer aggressiveness. *Int J Mol Sci*. (2020) 21:9069. doi: 10.3390/ijms21239069
14. Dong X, Bai X. Exosomes and breast cancer drug resistance. *Cell Death Dis*. (2020) 11:987. doi: 10.1038/s41419-020-03189-z
15. Roy S, Sunkara RR, Parmar MY, Shaikh S, Waghmare SK. EMT imparts cancer stemness and plasticity: new perspectives and therapeutic potential. *Front Biosci.* (2021) 26:238–65. doi: 10.2741/4893
16. Tanabe S, Quader S, Cabral H, Ono R. Interplay of EMT and CSC in cancer and the potential therapeutic strategies. *Front Pharmacol.* (2020) 11:904. doi: 10.3389/fphar.2020.00904
17. Kreso A, Dick JE. Evolution of the cancer stem cell model. *Cell Stem Cell.* (2014) 14:275–91. doi: 10.1016/j.stem.2014.02.006
18. Chaffer CL, Weinberg RA. A perspective on cancer cell metastasis. *Science.* (2011) 331:1559–64. doi: 10.1126/science.1203543
19. Clevers H. The cancer stem cell: premises, promises and challenges. *Nat Med.* (2011) 17:313–9. doi: 10.1038/nm.2304
20. Eppert K, Takenaka K, Lechman ER, Waldron L, Nilsson B, van Galen P, et al. Stem cell gene expression programs influence clinical outcome in human leukemia. *Nat Med.* (2011) 17:1086–93. doi: 10.1038/nm.2415
21. Huang T, Song X, Xu D, Tiek D, Goenka A, Wu B, et al. Stem cell programs in cancer initiation, progression, and therapy resistance. *Theranostics.* (2020) 10:8721–43. doi: 10.7150/thno.41648
22. Singh SK, Clarke ID, Terasaki M, Bonn VE, Hawkins C, Squire J, et al. Identification of a cancer stem cell in human brain tumors. *Cancer Res.* (2003) 63:5821–8.
23. Xiang L, Semenza GL. Hypoxia-inducible factors promote breast cancer stem cell specification and maintenance in response to hypoxia or cytotoxic chemotherapy. *Adv Cancer Res.* (2019) 141:175–212. doi: 10.1016/bs.acr.2018.11.001
24. Visvader JE, Lindeman GJ. Cancer stem cells: current status and evolving complexities. *Cell Stem Cell.* (2012) 10:717–28. doi: 10.1016/j.stem.2012.05.007
25. Mani SA, Guo W, Liao MJ, Eaton EN, Ayyanan A, Zhou AY, et al. The epithelial-mesenchymal transition generates cells with properties of stem cells. *Cell.* (2008) 133:704–15. doi: 10.1016/j.cell.2008.03.027
26. Pinzani M. Epithelial-mesenchymal transition in chronic liver disease: fibrogenesis or escape from death? *J Hepatol.* (2011) 55:459–65. doi: 10.1016/j.jhep.2011.02.001
27. Tsai JH, Donaher JL, Murphy DA, Chau S, Yang J. Spatiotemporal regulation of epithelial-mesenchymal transition is essential for squamous cell carcinoma metastasis. *Cancer Cell.* (2012) 22:725–36. doi: 10.1016/j.ccr.2012.09.022
28. Ocaña OH, Córcoles R, Fabra A, Moreno-Bueno G, Acloque H, Vega S, et al. Metastatic colonization requires the repression of the epithelial-mesenchymal transition inducer Prrx1. *Cancer Cell.* (2012) 22:709–24. doi: 10.1016/j.ccr.2012.10.012
29. Li R, Liang J, Ni S, Zhou T, Qing X, Li H, et al. A mesenchymal-to-epithelial transition initiates and is required for the nuclear reprogramming of mouse fibroblasts. *Cell Stem Cell.* (2010) 7:51–63. doi: 10.1016/j.stem.2010.04.014
30. Sannino G, Marchetto A, Kirchner T, Grünewald TGP. Epithelial-to-mesenchymal and mesenchymal-to-epithelial transition in mesenchymal tumors: a paradox in sarcomas? *Cancer Res.* (2017) 77:4556–61. doi: 10.1158/0008-5472.CAN-17-0032

31. Williams ED, Gao D. Controversies around epithelial-mesenchymal plasticity in cancer metastasis. *Nat Rev Cancer*. (2019) 19:716–32. doi: 10.1038/s41568-019-0213-x
32. Genna A, Vanwynsberghe AM, Villard AV, Pottier C, Ancel J, Polette M, et al. EMT-associated heterogeneity in circulating tumor cells: sticky friends on the road to metastasis. *Cancers*. (2020) 12:1632. doi: 10.3390/cancers12061632
33. Jia D, Li X, Bocci F. Quantifying cancer epithelial-mesenchymal plasticity and its association with stemness and immune response. *J Clin Med*. (2019) 8:725. doi: 10.3390/jcm8050725
34. Santamaria PG, Moreno-Bueno G, Portillo F, Cano A. EMT: present and future in clinical oncology. *Mol Oncol*. (2017) 11:718–38. doi: 10.1002/1878-0261.12091
35. Liao TT, Yang MH. Revisiting epithelial-mesenchymal transition in cancer metastasis: the connection between epithelial plasticity and stemness. *Mol Oncol*. (2017) 11:792–804. doi: 10.1002/1878-0261.12096
36. Pradella D, Naro C, Sette C, Ghigna C. EMT and stemness: flexible processes tuned by alternative splicing in development and cancer progression. *Mol Cancer*. (2017) 16:8. doi: 10.1186/s12943-016-0579-2
37. Srivastava C, Irshad K, Dikshit B, Chattopadhyay P, Sarkar C, Gupta DK, et al. FAT1 modulates EMT and stemness genes expression in hypoxic glioblastoma. *Int J Cancer*. (2018) 142:805–12. doi: 10.1002/ijc.31092
38. Rodriguez-Aznar E, Wiesmüller L, Sainz B Jr, Hermann PC. EMT and stemness-key players in pancreatic cancer stem cells. *Cancers*. (2019) 11:1136. doi: 10.3390/cancers11081136
39. Dang H, Ding W, Emerson D, Rountree CB. Snail1 induces epithelial-to-mesenchymal transition and tumor initiating stem cell characteristics. *BMC Cancer*. (2011) 11:396. doi: 10.1186/1471-2407-11-396
40. Kim HM, Haraguchi N, Ishii H, Ohkuma M, Okano M, Mimori K, et al. Increased CD13 expression reduces reactive oxygen species, promoting survival of liver cancer stem cells via an epithelial-mesenchymal transition-like phenomenon. *Ann Surg Oncol*. (2012) 19(Suppl. 3):S539–48. doi: 10.1245/s10434-011-2040-5
41. Garg M. Epithelial plasticity, autophagy and metastasis: potential modifiers of the crosstalk to overcome therapeutic resistance. *Stem Cell Rev Rep*. (2020) 16:503–10. doi: 10.1007/s12015-019-09945-9
42. Weng YS, Tseng HY, Chen YA, Shen PC, Al Haq AT, Chen LM, et al. MCT-1/miR-34a/IL-6/IL-6R signaling axis promotes EMT progression, cancer stemness and M2 macrophage polarization in triple-negative breast cancer. *Mol Cancer*. (2019) 18:42. doi: 10.1186/s12943-019-0988-0
43. Shibue T, Brooks MW, Weinberg RA. An integrin-linked machinery of cytoskeletal regulation that enables experimental tumor initiation and metastatic colonization. *Cancer Cell*. (2013) 24:481–98. doi: 10.1016/j.ccr.2013.08.012
44. Morel AP, Lièvre M, Thomas C, Hinkal G, Ansieau S, Puisieux A. Generation of breast cancer stem cells through epithelial-mesenchymal transition. *PLoS ONE*. (2008) 3:e2888. doi: 10.1371/journal.pone.0002888
45. Hwang WL, Yang MH, Tsai ML, Lan HY, Su SH, Chang SC, et al. SNAIL regulates interleukin-8 expression, stem cell-like activity, and tumorigenicity of human colorectal carcinoma cells. *Gastroenterology*. (2011) 141:279–91:91.e1-5. doi: 10.1053/j.gastro.2011.04.008
46. Alkatout I, Wiedermann M, Bauer M, Wenners A, Jonat W, Klapper W. Transcription factors associated with epithelial-mesenchymal transition and cancer stem cells in the tumor centre and margin of invasive breast cancer. *Exp Mol Pathol*. (2013) 94:168–73. doi: 10.1016/j.yexmp.2012.09.003
47. Hollier BG, Tinnirello AA, Werden SJ, Evans KW, Taube JH, Sarkar TR, et al. FOXC2 expression links epithelial-mesenchymal transition and stem cell properties in breast cancer. *Cancer Res*. (2013) 73:1981–92. doi: 10.1158/0008-5472.CAN-12-2962
48. Sigurdsson V, Hilmarsdottir B, Sigmundsdottir H, Fridriksdottir AJ, Ringnér M, Villadsen R, et al. Endothelial induced EMT in breast epithelial cells with stem cell properties. *PLoS ONE*. (2011) 6:e23833. doi: 10.1371/journal.pone.0023833
49. Dongre A, Weinberg RA. New insights into the mechanisms of epithelial-mesenchymal transition and implications for cancer. *Nat Rev Mol Cell Biol*. (2019) 20:69–84. doi: 10.1038/s41580-018-0080-4
50. Lu W, Kang Y. Epithelial-mesenchymal plasticity in cancer progression and metastasis. *Dev Cell*. (2019) 49:361–74. doi: 10.1016/j.devcel.2019.04.010
51. Markopoulos GS, Roupakia E, Marcu KB, Kolettas E. Epigenetic regulation of inflammatory cytokine-induced epithelial-to-mesenchymal cell transition and cancer stem cell generation. *Cells*. (2019) 8:1143. doi: 10.3390/cells8101143
52. Ye X, Weinberg RA. Epithelial-mesenchymal plasticity: a central regulator of cancer progression. *Trends Cell Biol*. (2015) 25:675–86. doi: 10.1016/j.tcb.2015.07.012
53. van Denderen BJ, Thompson EW. Cancer: the to and fro of tumour spread. *Nature*. (2013) 493:487–8. doi: 10.1038/493487a
54. Padmanaban V, Krol I, Suhail Y, Szczerba BM, Aceto N, Bader JS, et al. E-cadherin is required for metastasis in multiple models of breast cancer. *Nature*. (2019) 573:439–44. doi: 10.1038/s41586-019-1526-3
55. Krebs AM, Mitschke J, Lasierra Losada M, Schmalhofer O, Boerries M, Busch H, et al. The EMT-activator Zeb1 is a key factor for cell plasticity and promotes metastasis in pancreatic cancer. *Nat Cell Biol*. (2017) 19:518–29. doi: 10.1038/ncb3513
56. Shi L, Tang X. A SIRT1-centered circuitry regulates breast cancer stemness and metastasis. *Oncogene*. (2018) 37:6299–315. doi: 10.1038/s41388-018-0370-5
57. Hirata H, Sugimachi K, Takahashi Y, Ueda M, Sakimura S, Uchi R, et al. Downregulation of PRRX1 confers cancer stem cell-like properties and predicts poor prognosis in hepatocellular carcinoma. *Ann Surg Oncol*. (2015) 22(Suppl. 3):S1402–9. doi: 10.1245/s10434-014-4242-0
58. Celià-Terrassa T, Meca-Cortés O, Mateo F, Martínez de Paz A, Rubio N, Arnal-Estapé A, et al. Epithelial-mesenchymal transition can suppress major attributes of human epithelial tumor-initiating cells. *J Clin Invest*. (2012) 122:1849–68. doi: 10.1172/JCI59218
59. Garg S, Reyes-Palomares A. Hepatic leukemia factor is a novel leukemic stem cell regulator in DNMT3A, NPM1, and FLT3-ITD triple-mutated AML. *Blood*. (2019) 134:263–76. doi: 10.1182/blood.2018862383
60. Castañón E, Soltermann A, López I, Román M, Ecay M, Collantes M, et al. The inhibitor of differentiation-1 (Id1) enables lung cancer liver colonization through activation of an EMT program in tumor cells and establishment of the pre-metastatic niche. *Cancer Lett*. (2017) 402:43–51. doi: 10.1016/j.canlet.2017.05.012
61. Hass R, von der Ohe J, Ungefroren H. The intimate relationship among EMT, MET and TME: A T(ransdifferentiation) E(nhancing) M(ix) to be exploited for therapeutic purposes. *Cancers*. (2020) 12:3674. doi: 10.3390/cancers12123674
62. Simeone P, Trerotola M, Franck J, Cardon T, Marchisio M, Fournier I, et al. The multiverse nature of epithelial to mesenchymal transition. *Semin Cancer Biol*. (2019) 58:1–10. doi: 10.1016/j.semcancer.2018.11.004
63. Zhang Y, Weinberg RA. Epithelial-to-mesenchymal transition in cancer: complexity and opportunities. *Front Med*. (2018) 12:361–73. doi: 10.1007/s11684-018-0656-6
64. Chen C, Zhao S, Karnad A, Freeman JW. The biology and role of CD44 in cancer progression: therapeutic implications. *J Hematol Oncol*. (2018) 11:64. doi: 10.1186/s13045-018-0605-5
65. Saitoh M. Involvement of partial EMT in cancer progression. *J Biochem*. (2018) 164:257–64. doi: 10.1093/jb/mvy047
66. Puré E, Hingorani SR. Mesenchymal cell plasticity and perfidy in epithelial malignancy. *Trends Cancer*. (2018) 4:273–7. doi: 10.1016/j.trecan.2018.02.007
67. Huang RY, Wong MK, Tan TZ, Kuay KT, Ng AH, Chung VY, et al. An EMT spectrum defines an anoikis-resistant and spheroidogenic intermediate mesenchymal state that is sensitive to e-cadherin restoration by a src-kinase inhibitor, saracatinib (AZD0530). *Cell Death Dis*. (2013) 4:e915. doi: 10.1038/cddis.2013.442
68. Pastushenko I, Brisebarre A, Sifrim A, Fioramonti M, Revenco T, Boumahdi S, et al. Identification of the tumour transition states occurring during EMT. *Nature*. (2018) 556:463–8. doi: 10.1038/s41586-018-0040-3
69. George JT, Jolly MK, Xu S, Somarelli JA, Levine H. Survival outcomes in cancer patients predicted by a partial EMT gene expression scoring metric. *Cancer Res*. (2017) 77:6415–28. doi: 10.1158/0008-5472.CAN-16-3521
70. Puram SV, Tirosh I, Parikh AS, Patel AP, Yizhak K, Gillespie S, et al. Single-cell transcriptomic analysis of primary and metastatic tumor ecosystems in head and neck cancer. *Cell*. (2017) 171:1611–24.e24. doi: 10.1016/j.cell.2017.10.044
71. Nguyen DX, Bos PD, Massagué J. Metastasis: from dissemination to organ-specific colonization. *Nat Rev Cancer*. (2009) 9:274–84. doi: 10.1038/nrc2622
72. Massagué J, Obenauf AC. Metastatic colonization by circulating tumour cells. *Nature*. (2016) 529:298–306. doi: 10.1038/nature17038

73. Steeg PS. Targeting metastasis. *Nat Rev Cancer.* (2016) 16:201–18. doi: 10.1038/nrc.2016.25
74. Bocci F, Gearhart-Serna L, Boareto M. Toward understanding cancer stem cell heterogeneity in the tumor microenvironment. *Proc. Natl Acad Sci USA.* (2019) 116:148–57. doi: 10.1073/pnas.1815345116
75. Shibue T, Weinberg RA. EMT, CSCs, and drug resistance: the mechanistic link and clinical implications. *Nat Rev Clin Oncol.* (2017) 14:611–29. doi: 10.1038/nrclinonc.2017.44
76. Varga J, Greten FR. Cell plasticity in epithelial homeostasis and tumorigenesis. *Nat Cell Biol.* (2017) 19:1133–41. doi: 10.1038/ncb3611
77. Garg M. Epithelial plasticity and cancer stem cells: Major mechanisms of cancer pathogenesis and therapy resistance. *World J Stem Cells.* (2017) 9:118–26. doi: 10.4252/wjsc.v9.i8.118
78. Francescangeli F, Contavalli P, De Angelis ML, Careccia S, Signore M, Haas TL, et al. A pre-existing population of ZEB2(+) quiescent cells with stemness and mesenchymal features dictate chemoresistance in colorectal cancer. *J Exp Clin Cancer Res.* (2020) 39:2. doi: 10.1186/s13046-019-1505-4
79. Zhang R, Xia J, Wang Y, Cao M, Jin D, Xue W, et al. Co-expression of stem cell and epithelial mesenchymal transition markers in circulating tumor cells of bladder cancer patients. *Onco Targets Ther.* (2020) 13:10739–48. doi: 10.2147/OTT.S259240
80. Chirshev E, Hojo N, Bertucci A, Sanderman L, Nguyen A, Wang H, et al. Epithelial/mesenchymal heterogeneity of high-grade serous ovarian carcinoma samples correlates with miRNA let-7 levels and predicts tumor growth and metastasis. *Mol Oncol.* (2020) 14:2796–813. doi: 10.1002/1878-0261.12762
81. Quan Q, Wang X, Lu C, Ma W, Wang Y, Xia G, et al. Cancer stem-like cells with hybrid epithelial/mesenchymal phenotype leading the collective invasion. *Cancer Sci.* (2020) 111:467–76. doi: 10.1111/cas.14285
82. Andriani F, Bertolini G, Facchinetti F, Baldoli E, Moro M, Casalini P, et al. Conversion to stem-cell state in response to microenvironmental cues is regulated by balance between epithelial and mesenchymal features in lung cancer cells. *Mol Oncol.* (2016) 10:253–71. doi: 10.1016/j.molonc.2015.10.002
83. Mancheno-Ferris A, Polesello C, Payre F. [OvoL factors: a family of key regulators of epithelium mesenchyme plasticity and stem cells]. *Med Sci.* (2020) 36 Hors série n° 1:61–6. doi: 10.1051/medsci/2020193
84. Budkova Z, Sigurdardottir AK, Briem E, Bergthorsson JT, Sigurdsson S, Magnusson MK, et al. Expression of ncRNAs on the DLK1-DIO3 locus is associated with basal and mesenchymal phenotype in breast epithelial progenitor cells. *Front Cell Dev Biol.* (2020) 8:461. doi: 10.3389/fcell.2020.00461
85. Jiang J, Zheng M, Zhang M, Yang X, Li L, Wang S-S, et al. PRRX1 regulates cellular phenotype plasticity and dormancy of head and neck squamous cell carcinoma through miR-642b-3p. *Neoplasia.* (2019) 21:216–29. doi: 10.1016/j.neo.2018.12.001
86. You X, Zhou Z, Chen W, Wei X, Zhou H, Luo W. MicroRNA-495 confers inhibitory effects on cancer stem cells in oral squamous cell carcinoma through the HOXC6-mediated TGF-β signaling pathway. *Stem Cell Res Therap.* (2020) 11:117. doi: 10.1186/s13287-020-1576-3
87. Selth LA, Das R, Townley SL, Coutinho I, Hanson AR, Centenera MM, et al. A ZEB1-miR-375-YAP1 pathway regulates epithelial plasticity in prostate cancer. *Oncogene.* (2017) 36:24–34. doi: 10.1038/onc.2016.185
88. Zhou W, Ye X-L, Xu J, Cao M-G, Fang Z-Y, Li L-Y, et al. The lncRNA H19 mediates breast cancer cell plasticity during EMT and MET plasticity by differentially sponging miR-200b/c and let-7b. *Sci Signal.* (2017) 10:eaak9557. doi: 10.1126/scisignal.aak9557
89. Cha ST, Tan CT, Chang CC, Chu CY, Lee WJ, Lin BZ, et al. G9a/RelB regulates self-renewal and function of colon-cancer-initiating cells by silencing Let-7b and activating the K-RAS/β-catenin pathway. *Nat Cell Biol.* (2016) 18:993–1005. doi: 10.1038/ncb3395
90. Liu S, Cong Y, Wang D, Sun Y, Deng L, Liu Y, et al. Breast cancer stem cells transition between epithelial and mesenchymal states reflective of their normal counterparts. *Stem Cell Rep.* (2014) 2:78–91. doi: 10.1016/j.stemcr.2013.11.009
91. Bocci F, Jolly MK, George JT, Levine H, Onuchic JN. A mechanism-based computational model to capture the interconnections among epithelial-mesenchymal transition, cancer stem cells and Notch-Jagged signaling. *Oncotarget.* (2018) 9:29906–20. doi: 10.18632/oncotarget.25692
92. Yang J, Antin P, Berx G, Blanpain C, Brabletz T, Bronner M, et al. Guidelines and definitions for research on epithelial-mesenchymal transition. *Nat Rev Mol Cell Biol.* (2020) 21:341–52. doi: 10.1038/s41580-020-0237-9
93. Jolly MK, Somarelli JA, Sheth M, Biddle A, Tripathi SC, Armstrong AJ, et al. Hybrid epithelial/mesenchymal phenotypes promote metastasis and therapy resistance across carcinomas. *Pharmacol Therap.* (2019) 194:161–84. doi: 10.1016/j.pharmthera.2018.09.007
94. Liu Q, Tong D, Liu G, Xu J, Do K, Geary K, et al. Metformin reverses prostate cancer resistance to enzalutamide by targeting TGF-β1/STAT3 axis-regulated EMT. *Cell Death Dis.* (2017) 8:e3007. doi: 10.1038/cddis.2017.417

Conflict of Interest: The authors declare that the research was conducted in the absence of any commercial or financial relationships that could be construed as a potential conflict of interest.

frontiers in Cell and Developmental Biology

ORIGINAL RESEARCH
published: 30 April 2021
doi: 10.3389/fcell.2021.665161

An EMT-Related Gene Signature for Predicting Response to Adjuvant Chemotherapy in Pancreatic Ductal Adenocarcinoma

Zengyu Feng[1,2,3], Kexian Li[1,2], Jianyao Lou[3], Yulian Wu[3] and Chenghong Peng[1,2]**

[1] Department of General Surgery, Pancreatic Disease Center, Ruijin Hospital, Shanghai Jiao Tong University School of Medicine, Shanghai, China, [2] Research Institute of Pancreatic Diseases, Shanghai Jiao Tong University School of Medicine, Shanghai, China, [3] Department of General Surgery, The Second Affiliated Hospital, School of Medicine, Zhejiang University, Hangzhou, China

Background: For pancreatic ductal adenocarcinoma (PDAC) patients, chemotherapy failure is the major reason for postoperative recurrence and poor outcomes. Establishment of novel biomarkers and models for predicting chemotherapeutic efficacy may provide survival benefits by tailoring treatments.

Methods: Univariate cox regression analysis was employed to identify EMT-related genes with prognostic potential for DFS. These genes were subsequently submitted to LASSO regression analysis and multivariate cox regression analysis to identify an optimal gene signature in TCGA training cohort. The predictive accuracy was assessed by Kaplan–Meier (K-M), receiver operating characteristic (ROC) and calibration curves and was validated in PACA-CA cohort and our local cohort. Pathway enrichment and function annotation analyses were conducted to illuminate the biological implication of this risk signature.

Results: LASSO and multivariate Cox regression analyses selected an 8-gene signature comprised DLX2, FGF9, IL6R, ITGB6, MYC, LGR5, S100A2, and TNFSF12. The signature had the capability to classify PDAC patients with different DFS, both in the training and validation cohorts. It provided improved DFS prediction compared with clinical indicators. This signature was associated with several cancer-related pathways. In addition, the signature could also predict the response to immune-checkpoint inhibitors (ICIs)-based immunotherapy.

Conclusion: We established a novel EMT-related gene signature that was capable of predicting therapeutic response to adjuvant chemotherapy and immunotherapy. This signature might facilitate individualized treatment and appropriate management of PDAC patients.

Keywords: PDAC, EMT, adjuvant chemotherapy, sensitivity, disease-free survival, risk score, prognostic signature

OPEN ACCESS

Edited by:
Andrew Davis, Washington University in St. Louis, United States

Reviewed by:
Ali M. Ardekani, Avicenna Research Institute (ARI), Iran
Taiping Zhang, Peking Union Medical College Hospital (CAMS), China

****Correspondence:***
Yulian Wu
yulianwu@zju.edu.cn
Chenghong Peng
chhpeng@yeah.net

Specialty section:
This article was submitted to Molecular and Cellular Oncology, a section of the journal Frontiers in Cell and Developmental Biology

Received: *07 February 2021*
Accepted: *13 April 2021*
Published: *30 April 2021*

Citation:
Feng Z, Li K, Lou J, Wu Y and Peng C (2021) An EMT-Related Gene Signature for Predicting Response to Adjuvant Chemotherapy in Pancreatic Ductal Adenocarcinoma. Front. Cell Dev. Biol. 9:665161. doi: 10.3389/fcell.2021.665161

Abbreviations: AUC, area under the curve; DFS, disease-free survival; EMT, epithelial to mesenchymal transition; GOm Gene Ontology; ICGC, International Cancer Genome Consortium; ICIs, Immune-checkpoint inhibitors; KEGG, Kyoto Encyclopedia of Genes and Genomes (KEGG); K-M, Kaplan-Meier; PDAC, pancreatic ductal adenocarcinoma; QRT-PCR, quantitative real time polymerase chain reaction; ROC, receiver operating characteristic; TCGA, The Cancer Genome Atlas; TNM, tumor, node, metastasis.

INTRODUCTION

Pancreatic ductal adenocarcinoma (PDAC) is a highly malignant and devastating disease with a 5 years survival rate not exceeding 10% and its incidence increases about 1% per year in the United States (Siegel et al., 2021). The dismal outcome of this malignancy is primarily due to a frequently late diagnosis, mostly at the metastatic and unresectable stage, and the notorious chemoresistance (Kamisawa et al., 2016). Surgery combined with adjuvant chemotherapy is the established therapy option for resectable PDAC patients (Mizrahi et al., 2020). Unfortunately, early postoperative recurrence in most patients caused by the inherent resistance to adjuvant chemotherapy limits the dramatic improvement of patient survival (Kleeff et al., 2016). Currently, adjuvant chemotherapy is administrated empirically, and individual survival benefit of this approach is still questionable. In PDAC patients, the clinical benefit response rates to regimens of chemotherapy are extremely low (Han et al., 2021). Non-responding patients are likely to suffer a variety of adverse events including asthenia and nausea (Phua et al., 2018). These intractable issues have motivated a number of groups to identify robust biomarkers that can predict therapeutic response to chemotherapy in PDAC patients (Kyrochristos et al., 2018).

As precision medicine has shown promising signs, *a priori* prediction of treatment response may facilitate individual management and maximize survival benefit of PDAC patients (Tu et al., 2016). Multiple studies have reported that a treatment-related decrease in serum CA19-9 can predict response to treatment (Xu et al., 2018; Aoki et al., 2019; Perri et al., 2020, 2021). Pre-clinical and clinical evidence demonstrates that patients with specific PDAC subtypes response differently to available treatments (Collisson et al., 2011; Aung et al., 2018). Several genes participating in drug uptake and metabolism have emerged as powerful predictors of drug sensitivity (Bird et al., 2017; Raffenne et al., 2019; Okamura et al., 2020). Recently, with the adventure of high throughput sequencing and bioinformatic technology, more and more gene expression signatures have been identified to evaluate drug sensitivity in PDAC (Kaissis et al., 2019; Clayton et al., 2020; Piquemal et al., 2020; Nicolle et al., 2021; Nishiwada et al., 2021).

Epithelial to mesenchymal transition (EMT) program is related to phenotypic conversion of epithelial cells into more aggressive mesenchymal-like cells and suppression of EMT results in enhanced gemcitabine sensitivity in PDAC mice (Zheng et al., 2015). Compelling evidence has proved a strong association between EMT-related gene expression and therapeutic resistance (Shibue and Weinberg, 2017). For instance, Byres et al. constructed a 76 gene signature based on EMT-related genes with satisfactory accuracy in predicting clinical response to EGFR and PI3K inhibitors for patients with non-small-cell lung carcinoma (Byers et al., 2013). These studies suggest EMT represents an under-explored source of credible biomarkers that could be used to predict drug response.

We purposed to establish a model for predicting response to adjuvant chemotherapy based on EMT-related genes in PDAC. We measured the association between EMT-related genes and disease-free survival (DFS), and established an 8-gene signature with excellent predictive performance in both training and validation datasets. Functionally, this signature is closely related to several pathways involved in drug response. Interestingly, we found that this signature also had potential to predict response to immune-checkpoint inhibitors (ICIs). These findings may facilitate personalized treatment and may potentially exempt patients from heavy finical burden and unnecessary adverse effects of overtreatment.

MATERIALS AND METHODS

PDAC Cohorts

Two public PDAC cohorts were included in this study. Among them, TCGA cohort was used as the training set, while PACA-CA cohort was used for external validation. Processed RNA-sequencing data and corresponding clinical data of TCGA cohort were downloaded from TCGA hub at UCSC Xena[1]. In the cases of PACA-CA cohort, normalized RNA-sequencing data and clinical information were retrieved and downloaded from the International Cancer Genome Consortium (ICGC)[2] database. In each cohort, the following criteria were used to exclude unqualified samples: (a) follow-up time < 1 month; (b) lack of survival and therapeutic data; (c) histopathological type is not PDAC. After a careful review, 99 samples in TCGA cohort and 105 samples in PACA-CA cohort were included in this study. All patients received adjuvant chemotherapy in both cohorts, and detail of chemotherapeutic drugs was only available in TCGA cohort. Patients whose response to chemotherapy is "clinical progressive disease" or "stable disease" were defined as chemotherapy-resistant, while patients whose response to chemotherapy is "complete response" or "partial response" were defined as chemotherapy-sensitive. Given the medium size of the cohorts we used, we additionally verified the EMT signature in our own cohort (Ruijin cohort). 48 PDAC frozen samples were collected as previously reported (Feng et al., 2020).

Construction of the EMT-Related Gene Signature for DFS Prediction

A total of 1,184 EMT-related genes were obtained from a previous article (Cai et al., 2020). In the TCGA training cohort, EMT-related genes that were significantly associated with DFS were screened using univariate cox regression analysis ($P < 0.01$). Subsequently, LASSO regression combined with multivariate cox regression analyses were used to determine the optimal risk model. The risk score was calculated as follows: Risk score = (coefficient 1 * expression value of gene 1) + (coefficient 2 * expression value of gene 2) + . + (coefficient X * expression value of gene X).

[1]https://tcga.xenahubs.net

[2]https://icgc.org/

Predictive Performance of the EMT-Related Gene Signature

Patients in each cohort were classified into low- and high-risk groups based on the medium value of risk scores. Kaplan–Meier (K-M) survival curves were employed to evaluate the DFS differences between low- and high-risk groups. Calibration plots comparing the predicted and observed survival probabilities were performed to assess the predictive accuracy. Receiver operating characteristic (ROC) curves were utilized to compare the efficiency of the signature with that of clinical predictors for DFS prediction. In addition, univariate and multivariate cox regression analyses were utilized to verify the independent prognostic role of the signature.

Functional Annotation and Pathway Enrichment

Aiming to clarify the biological function of the EMT signature, we conducted Pearson correlation analysis to identify genes whose expression levels were significantly ($P < 0.05$) correlated with risk scores in TCGA training cohort. Top 1,000 positively and negatively correlated genes were, respectively, submitted to Gene Ontology (GO) analysis and The Kyoto Encyclopedia of Genes

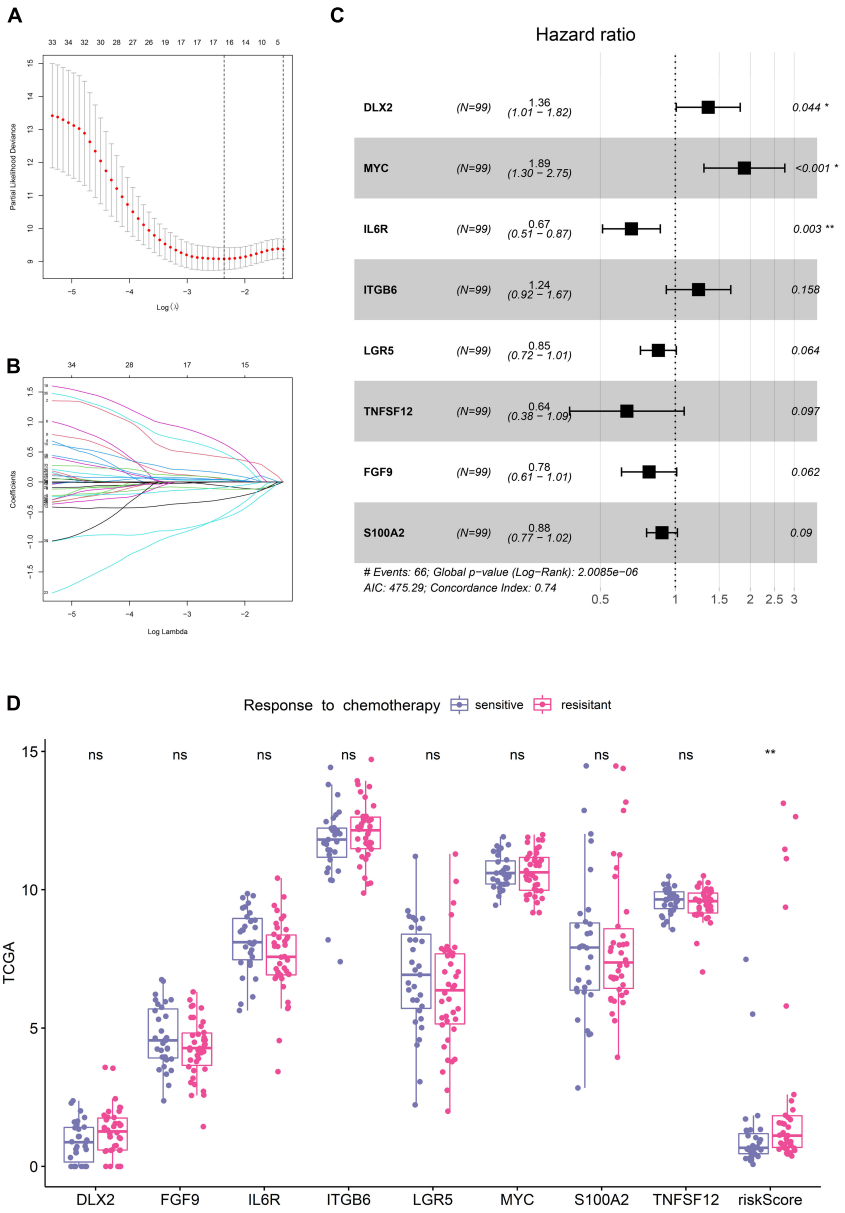

FIGURE 1 | Establishment of the EMT-related gene signature in TCGA training cohort. **(A)** Cross-validation for tuning parameter (lambda) screening in the LASSO regression model. **(B)** LASSO coefficient profiles of 35 prognostic EMT-related genes. **(C)** Forest plot of the eight EMT-related genes. **(D)** Distribution of the eight genes and risk scores in patients stratified by the chemotherapy sensitivity.

and Genomes (KEGG) pathway enrichment analysis on DAVID online website (Huang et al., 2007).

Quantitative Real Time Polymerase Chain Reaction (qRT-PCR)

Reverse transcription and qRT-PCR were performed as previously reported (Feng et al., 2020). The mRNA primer sequences are displayed in **Supplementary Table 1**.

Statistical Analysis

The statistical analysis and graphical work were done in the R environment (version 3.5.2). cox regression analyses were conducted by the "survival" package. K-M survival curves with log-rank tests were produced by the "survminer" package. LASSO regression analysis was done by the "glmnet" package. The ROC curves were plotted by the "survivalROC" package. Boxplots were depicted by the "ggpubr" package. Forest plot was derived

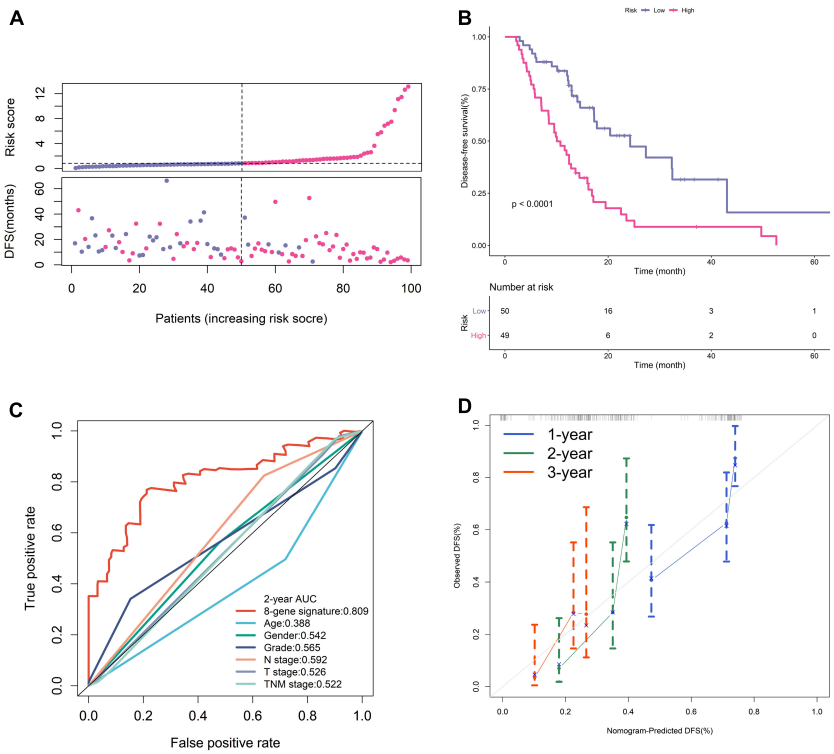

E

Variables	HR(95%CI)	P value
Univariate Cox regression		
Age(>65 vs ≤65)	0.81(0.50-1.31)	0.395
Gender(male vs female)	0.94(0.58-1.53)	0.804
Grade	1.32(0.89-1.98)	0.167
N stage(N1 vs N0)	1.50(0.81-2.75)	0.194
T stage	1.12(0.69-1.81)	0.660
TNM stage	1.09(0.58-2.04)	0.784
Risk score	1.34(1.23-1.46)	<0.001
Multivariate Cox regression		
Age(>65 vs ≤65)	0.79(0.48-1.31)	0.363
Gender(male vs female)	1.02(0.62-1.69)	0.934
Grade	1.12(0.74-1.70)	0.583
N stage(N1 vs N0)	1.38(0.73-2.62)	0.320
T stage	1.08(0.57-2.06)	0.804
TNM stage	1.35(0.61-2.96)	0.457
Risk score	1.35(1.23-1.49)	<0.001

FIGURE 2 | Prognostic performance of gene signature in TCGA training cohort. **(A)** From top to bottom are the risk score distribution and survival status distribution. **(B)** K-M survival curve for risk score. **(C)** ROC curve of the risk signature and clinical predictors. **(D)** Calibration curves for risk score. **(E)** Univariate and multivariate cox regression analyses of clinical parameters and gene signature for DFS.

from the "forestplot" package. Calibration curves were generated from the "rms" package. A two-sided log-rank $P < 0.05$ was considered significant.

RESULTS

Construction of the EMT-Related Gene Signature

With the selection criteria of $p < 0.01$, a total of 35 credibly prognostic EMT-related genes were identified through the univariate cox regression analysis in the TCGA training cohort. The LASSO regression algorithm was subsequently applied, and 16 candidate genes with most powerful predictive features were screened (**Figures 1A,B**). Then, multivariate cox regression analysis was performed on the 16 genes to avoid overfitting, and it finally determined an optimal 8-gene signature for DFS prediction (**Figure 1C**). Based on the expression levels and corresponding coefficients of these eight genes, we constructed a risk-score formula: Risk score = (0.30407 × expression value of DLX2) − (0.24245 × expression value of FGF9) − (0.40586 × expression value of IL6R) + (0.214597 × expression value of ITGB6) − (0.15683 × expression value of LGR5) + (0.638384 × expression value of MYC) − (0.12315 × expression value of S100A2) − (0.44785 × expression value of TNFSF12). K-M analysis illustrated that these eight individual genes adequately captured the DFS differences between low- and high-expression groups in the TCGA cohort (**Supplementary Figure 1**). In addition, the risk scores of chemotherapy-resistant patients were significantly

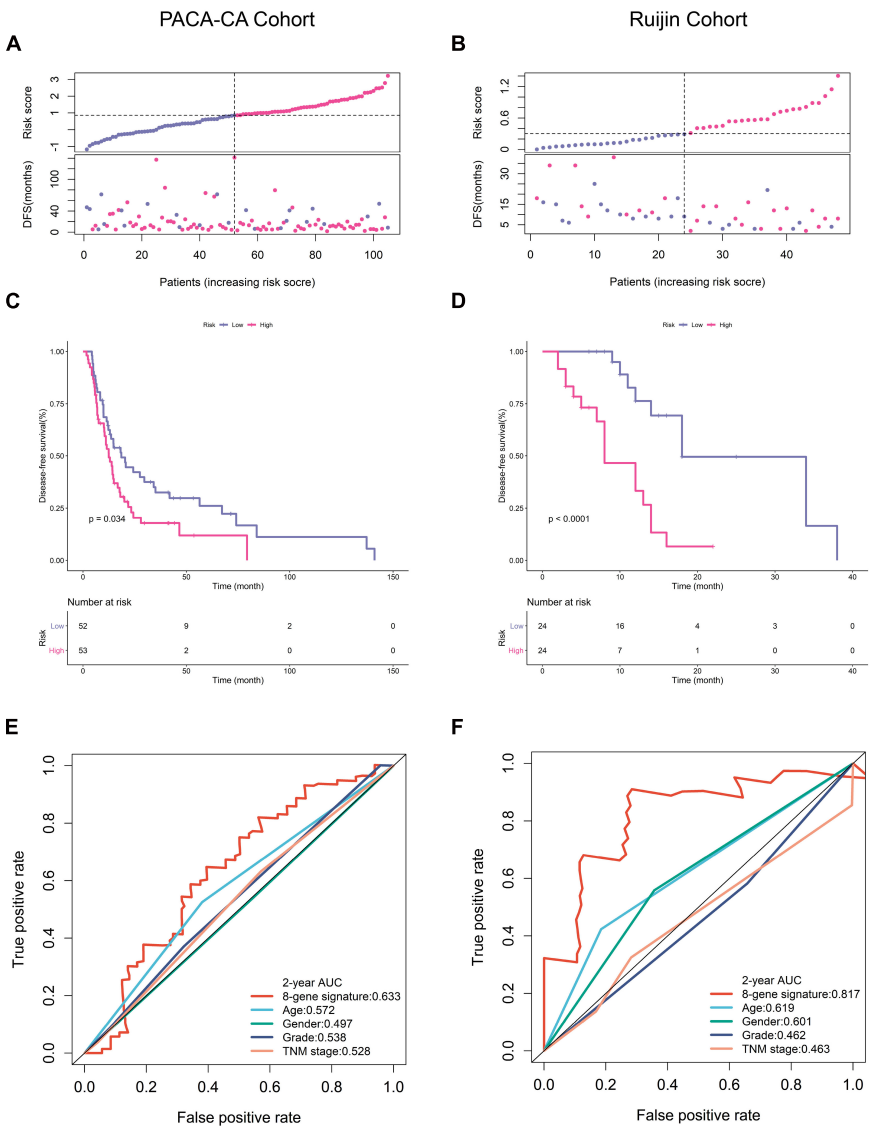

FIGURE 3 | Prognostic validation in PACA-CA and Ruijin cohorts. **(A,B)** Distribution of risk score and survival status in PACA-CA and Ruijin cohorts, respectively. **(C,D)** K-M survival curves estimating DFS difference in two cohorts. **(E,F)** ROC curves of risk signature and clinical indicators in two cohorts.

higher than those of chemotherapy-sensitive patients, indicating the hazardous role of the signature (**Figure 1D**).

Predictive Performance of the EMT-Related Gene Signature in TCGA Training Cohort

The distribution of the risk scores and survival status were shown in **Figure 2A**. The results suggested that patients in high-risk group had remarkably decreased DFS time.

K-M analysis illustrated that patients in the low-risk group had longer DFS (**Figure 2B**). ROC analysis demonstrated that this signature had high accuracy as the area under the curve (AUC) value was 0.809. What's more, the AUC value of this signature was high than that of clinical predictors including histological grade and TNM stage (**Figure 2C**).

The calibration curves proved the good agreement between predicted DFS and observed DFS (**Figure 2D**). In addition, both univariate and multivariate cox regression analyses certified that the proposed EMT signature was an independent risk factor for DFS (**Figure 2E**).

Predictive Performance of the EMT-Related Gene Signature in Two Validation Cohorts

We next verified the predictive accuracy of this signature in another public PDAC cohort (PACA-CA) and our own cohort (Ruijin). **Figures 3A,B** showed the distribution of the risk scores and survival status in these two cohorts. We observed that patients with a high-risk score had markedly increased recurrence rates. K-M survival curves estimated significantly

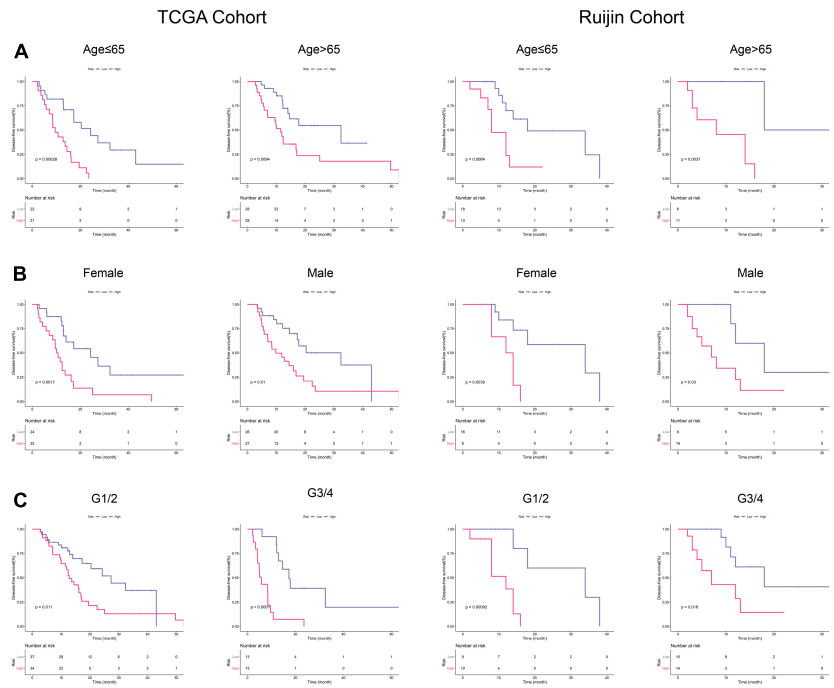

FIGURE 4 | Subgroup analyses in TCGA and Ruijin cohorts. **(A)** K-M curves for the risk signature in patients stratified by age. **(B)** Survival difference in high- and low-risk patients stratified by gender. **(C)** K–M curves evaluating the DFS between low- and high-risk patients stratified by histological grade.

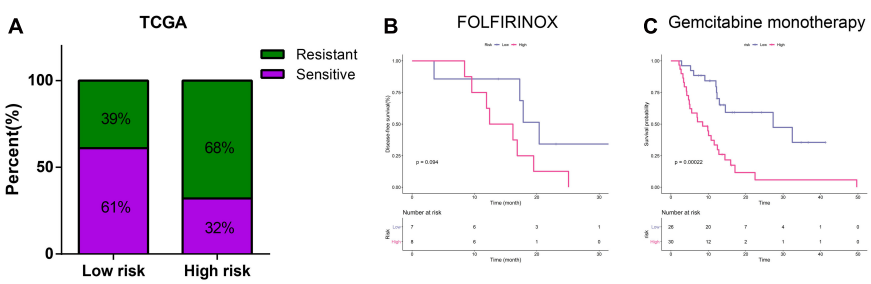

FIGURE 5 | Relationship between risk score and chemotherapeutic regimes. **(A)** Relationship of risk score and chemotherapy sensitivity. **(B)** K-M curves for the risk signature in patients receiving FOLFIRINOX. **(C)** K-M curves for the risk signature in patients receiving gemcitabine monotherapy.

decreased DFS of high-risk patients in both PACA-CA and Ruijin cohorts (**Figures 3C,D**). ROC curves demonstrated that this signature outperformed clinical indicators in predicting DFS (**Figures 3E,F**).

Subgroup Analyses of the EMT-Related Gene Signature

With the purpose to investigate the stability of this signature, we conducted subgroup analyses. As a small percentage of patients in PACA-CA cohort did not have clinical information regarding histological grade, we thus selected TCGA and Ruijin cohorts for further analyses. K-M curves showed that our signature had high-efficiency to distinguish patients with different DFS in every subgroup divided by age (**Figure 4A**), gender (**Figure 4B**), and histological grade (**Figure 4C**).

Relationship Between Risk Score and Response to Chemotherapeutic Regimes

Figure 5A illustrated that PDAC patients with a low-risk score had higher response rates to adjuvant chemotherapy than patients with a high-risk score in TCGA training cohort (61 vs. 32%, $p < 0.001$). Currently, adjuvant chemotherapy in PDAC is based on few regimes. Gemcitabine remains the most effective monotherapy and is often applied to patient who are ineligible for more aggressive treatments (Oba et al., 2020; Turpin et al., 2020). As for patients in good status, the polychemotherapy regimen including fluorouracil, leucovorin, irinotecan, and oxaliplatin (FOLFIRINOX) is preferentially recommended in the adjuvant settings (Marabelle et al., 2020). Among samples receiving FOLFIRINOX chemotherapy, we found that patients in low-risk group had a longer DFS, although the difference was not statistically significant probably due to the limited sample size (**Figure 5B**). For samples receiving gemcitabine monotherapy, patients with a low-risk score had a significantly longer DFS (**Figure 5C**).

Annotated Functions and Enriched Pathways Associated With the EMT-Related Gene Signature

As illustrated in **Figures 6A,B**, positively correlated genes with risk scores were mainly involved in pathways associated with response to treatment, such as DNA repair, DNA replication, cell cycle and mismatch repair. Genes negatively correlated with risk scores were closely associated with several immunological pathways like adaptive immune response, T cell costimulation, chemotaxis and chemokine signaling pathways (**Figures 6C,D**).

Relationship Between Risk Scores and Expression Levels of Immune Check Points

Above findings suggested that risk scores were inversely correlated with T cell co-stimulation and immune response, so

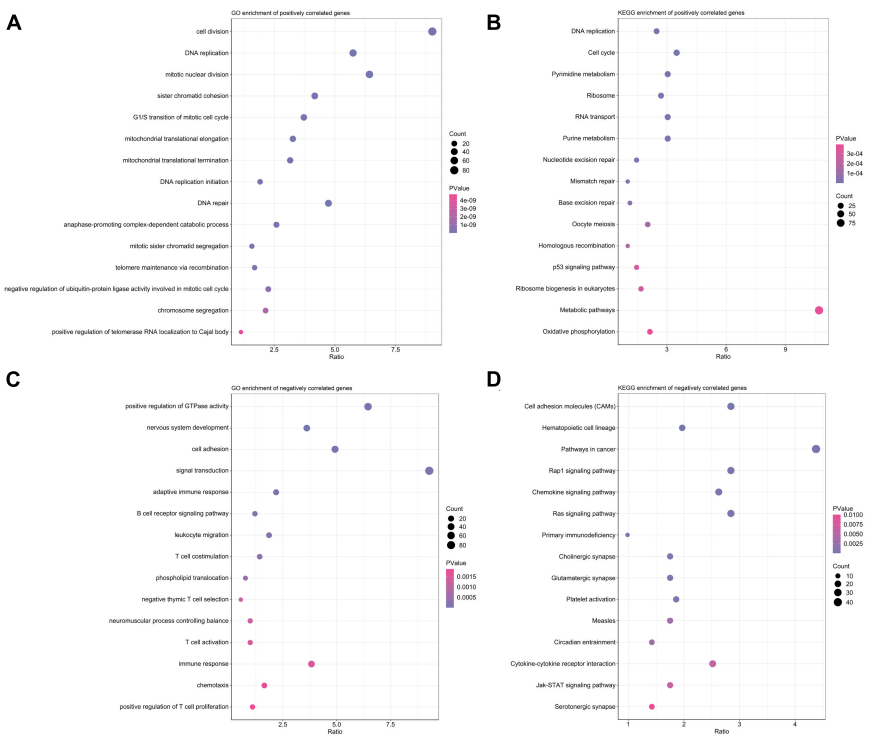

FIGURE 6 | Function annotation and pathway enrichment analyses in TCGA training cohort. **(A,B)** Top 15 enriched biological processes in GO analysis **(A)** and pathways in KEGG analysis **(B)** for genes positively correlated with risk scores. **(C,D)** Top 15 enriched biological processes in GO analysis **(C)** and pathways in KEGG analysis **(D)** for genes positively correlated with risk scores.

we wonder whether this signature could also predict response to ICIs. Recently, ICIs-based immunotherapy has drastically increased patient survival in certain cancers, but it is ineffective in the vast majority of patients with PDAC (Leinwand and Miller, 2020), biomarkers predicting response to ICIs thus are important for personalized oncology. As shown in **Figures 7A–F**, we observed that risk scores were negatively correlated with several common immune checkpoints, including CD28, CTLA4, PD1, TIGIT, TIM3, and VISTA. These findings indicated that PDAC patients who were not predicted to be sensitive to chemotherapy by our signature might be unsuitable for ICIs-based immunotherapy.

DISCUSSION

PDAC is a very devastating disease with extremely poor outcomes. As we all know, chemotherapy failure is one of the major problems to cure this disease and improve patient survival. PDAC features a notable intra- (Yachida and Iacobuzio-Donahue, 2013) and inter-tumoral (Cancer Genome Atlas Research Network, 2017) heterogeneity that drives chemoresistance. As cancer treatment has entered into the area of precision medicine, personalized therapy is a very attractive and laudable strategy. Determining the most effective drug to treat each patient with well balance between potential side events and expected survival benefits is definitely helpful to achieve the most favorable outcome. However, compared with other cancers, personalized treatments that translate the increased understanding of tumor molecular profiles into the clinical management are in their relative infancy for PDAC (Santofimia-Castaño and Iovanna, 2021).

Molecular characterization and subtyping of PDAC is providing a unique insight into predictive biomarkers for individualized treatments. The transcriptomic data has been a practical tool for PDAC subtyping and multiple stratification systems have been proposed to date by analyzing the transcriptional networks (Collisson et al., 2019). In addition, combining transcriptomic data with genomic sequencing, mutational landscape, immune infiltrate or genetic alteration can identify additional subtypes with clinical relevance (Bailey et al., 2016; Connor et al., 2017; Brunton et al., 2020; Rashid et al., 2020). More importantly than predicting patient prognosis and disease aggressiveness, recent studies find that transcriptomic data is also good at predicting chemotherapy sensitivity for PDAC (Deng et al., 2020; Nicolle et al., 2021; Nishiwada et al., 2021).

In this study, we initially analyzed the prognostic potential of EMT-related genes in predicting DFS through univariate cox regression analysis. Subsequently LASSO regression analysis and multivariate cox regression analysis identified an 8-gene signature for predicting response to adjuvant chemotherapy. K-M survival curves, ROC curves and calibration curves collectively proved the moderate accuracy

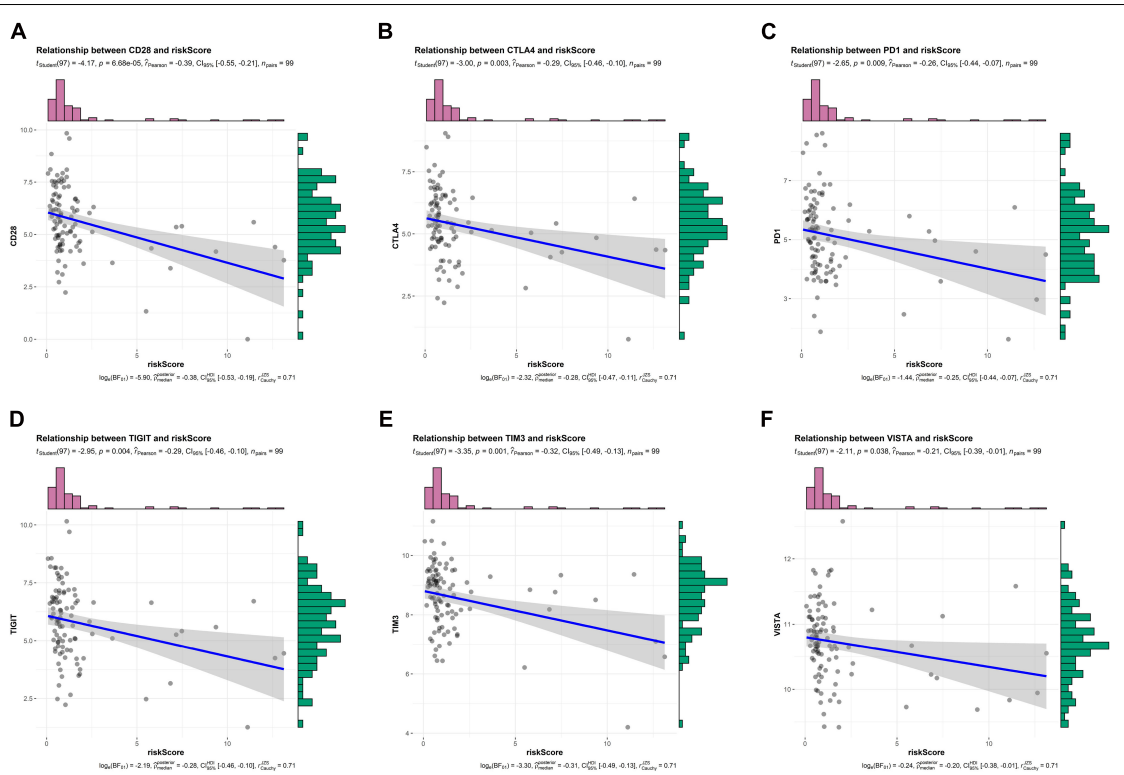

FIGURE 7 | Relationship between risk scores and expression levels of immune checkpoints in TCGA training cohort. **(A–F)** Relationship between risk scores and CD28, CTLA4, PD1, TIGIT, TIM3, and VISTA, respectively.

of the signature in predicting DFS. Functional analysis indicated that this signature was closely related to several cancer-related pathways. Subgroup analysis demonstrated the cross-clinicopathology stability. Intriguingly, except from chemotherapy, the signature also had great potential to predict response to ICIs. In other words, patients with a high-risk score predicted by our signature were very likely to be insensitive to neither chemotherapy nor ICIs-based immunotherapy. In this way, high-risk patients might be exempted from unnecessary drug toxicity and heavy finical burden.

The EMT program plays an indispensable role in therapeutic resistance in cancers. Mechanically, it inhibits multiple apoptotic signaling pathways, enhances drug efflux, and gives rise to cancer stem cells. These all contribute to cancer cells' increased resistance to anti-cancer drugs. In addition, EMT also upregulates several pathways that allow cancer cells to stave off the lethal effects of cytotoxic T cells, thus enhances resistance to immunotherapy (Huang et al., 2007). Transcriptional prognostic signatures based on EMT-related genes have been extensively reported recently (Cao et al., 2020; Zhang et al., 2020; Zhong et al., 2020; Cheng et al., 2021), but are rare in PDAC. Our study firstly constructed a robust response prediction model based on the eight EMT-related genes. We validated this signature in two public cohorts including American and Canadian populations, and our local cohort of Asian population, which enhanced the reliability and clinical applicability of this signature.

Despite explicit validation and considerable clinical relevance, this work is still based on retrospective data and has many limitations. Firstly, the cohorts used in this study are relatively small probably due to the low curative resection rates for PDAC patients.

Predictive efficiency needs to be verified in more prospective studies and larger cohorts. Second, owing to the limited sample size, some subgroup analyses cannot be implemented. For instance, 89 of 99 samples in TCGA cohorts are at stage II, subgroup analysis on tumor stage is thus meaningless. Third, detailed chemotherapy regimens are largely unknown in PACA-CA cohorts and incomplete in TCGA cohorts. Fourth, more *in vivo* and *in vitro* experiments are needed to elucidate biological function of eight genes in PDAC progression.

In conclusion, we proposed an EMT-related gene signature with satisfactory performance in predicting response to adjuvant chemotherapy. Functionally, it was associated with cell cycle, DNA repair and DNA replication. The signature outperformed clinical indicators in predictive chemotherapy sensitivity. After all, this signature was based on the retrospective cohorts and needed to be further validated in more prospective cohorts.

DATA AVAILABILITY STATEMENT

The original contributions presented in the study are included in the article/**Supplementary Material**, further inquiries can be directed to the corresponding author/s.

ETHICS STATEMENT

The studies involving human participants were reviewed and approved by the Ethics Committee of Ruijin Hospital affiliated with Shanghai Jiao Tong University. The patients/participants provided their written informed consent to participate in this study.

AUTHOR CONTRIBUTIONS

ZF and CP designed the study and wrote the manuscript. ZF, KL, and JL participated in data analysis, discussion, and language editing. YW reviewed the manuscript. All authors contributed to the article and approved the submitted version.

FUNDING

This work was supported by grants from the National Natural Science Foundation of China (81672325 and 81802316).

ACKNOWLEDGMENTS

We thank the National Natural Science Foundation of China for the grant funding. We also acknowledge the contributions from UCSC, TCGA, and ICGC databases.

SUPPLEMENTARY MATERIAL

The Supplementary Material for this article can be found online at: https://www.frontiersin.org/articles/10.3389/fcell.2021.665161/full#supplementary-material

REFERENCES

Aoki, S., Motoi, F., Murakami, Y., Sho, M., Satoi, S., Honda, G, et al. (2019). Decreased serum carbohydrate antigen 19-9 levels after neoadjuvant therapy predict a better prognosis for patients with pancreatic adenocarcinoma: a multicenter case-control study of 240 patients. *BMC Cancer* 19:252. doi: 10.1186/s12885-019-5460-4

Aung, KL., Fischer, SE., Denroche, RE., Jang, GH., Dodd, A., Creighton, S, et al. (2018). Genomics-driven precision medicine for advanced pancreatic cancer: early results from the COMPASS trial. *Clin. Cancer Res.* 24, 1344–1354. doi: 10.1158/1078-0432.Ccr-17-2994

Bailey, P., Chang, DK., Nones, K., Johns, AL., Patch, AM., Gingras, MC, et al. (2016). Genomic analyses identify molecular subtypes of pancreatic cancer. *Nature* 531, 47–52. doi: 10.1038/nature16965

Bird, NT., Elmasry, M., Jones, R., Psarelli, E., Dodd, J., Malik, H, et al. (2017). Immunohistochemical hENT1 expression as a prognostic biomarker in patients with resected pancreatic ductal adenocarcinoma undergoing adjuvant gemcitabine-based chemotherapy. *Br. J. Surg.* 104, 328–336. doi: 10.1002/bjs.10482

Brunton, H., Caligiuri, G., Cunningham, R., Upstill-Goddard, R., Bailey, UM., Garner, IM, et al. (2020). HNF4A and GATA6 loss reveals therapeutically actionable subtypes in pancreatic cancer. *Cell Rep.* 31:107625. doi: 10.1016/j.celrep.2020.107625

Byers, LA., Diao, L., Wang, J., Saintigny, P., Girard, L., Peyton, M, et al. (2013). An epithelial-mesenchymal transition gene signature predicts resistance to EGFR and PI3K inhibitors and identifies Axl as a therapeutic target for overcoming EGFR inhibitor resistance. *Clin. Cancer Res.* 19, 279–290. doi: 10.1158/1078-0432.Ccr-12-1558

Cai, L., Hu, C., Yu, S., Liu, L., Zhao, J., Zhao, Y, et al. (2020). Identification of EMT-related gene signatures to predict the prognosis of patients with endometrial cancer. *Front. Genet.* 11:582274. doi: 10.3389/fgene.2020.582274

Cancer Genome Atlas Research Network (2017). Integrated genomic characterization of pancreatic ductal adenocarcinoma. *Cancer Cell* 32, 185–203.e13. doi: 10.1016/j.ccell.2017.07.007

Cao, R., Yuan, L., Ma, B., Wang, G., Qiu, W., and Tian, Y. (2020). An EMT-related gene signature for the prognosis of human bladder cancer. *J. Cell Mol. Med.* 24, 605–617. doi: 10.1111/jcmm.14767

Cheng, YB., Li, S., Zhang, YP., Zhu, ZH., and Zhao, N. (2021). An epithelial-mesenchymal transition-related long non-coding RNA signature to predict overall survival and immune microenvironment in kidney renal clear cell carcinoma. *Bioengineered.* 12, 555–564. doi: 10.1080/21655979.2021.1880718

Clayton, EA., Pujol, TA., McDonald, JF., and Qiu, P. (2020). Leveraging TCGA gene expression data to build predictive models for cancer drug response. *BMC Bioinformatics* 21:364. doi: 10.1186/s12859-020-03690-4

Collisson, EA., Bailey, P., Chang, DK., and Biankin, AV. (2019). Molecular subtypes of pancreatic cancer. *Nat. Rev. Gastroenterol. Hepatol.* 16, 207–220. doi: 10.1038/s41575-019-0109-y

Collisson, EA., Sadanandam, A., Olson, P., Gibb, WJ., Truitt, M., Gu, S, et al. (2011). Subtypes of pancreatic ductal adenocarcinoma and their differing responses to therapy. *Nat. Med.* 17, 500–503. doi: 10.1038/nm.2344

Connor, AA., Denroche, RE., Jang, GH., Timms, L., Kalimuthu, SN., Selander, I, et al. (2017). Association of distinct mutational signatures with correlates of increased immune activity in pancreatic ductal adenocarcinoma. *JAMA Oncol.* 3, 774–783. doi: 10.1001/jamaoncol.2016.3916

Deng, Z., Li, X., Shi, Y., Lu, Y., Yao, W., and Wang, J. (2020). A novel autophagy-related incrnas signature for prognostic prediction and clinical value in patients with pancreatic cancer. *Front. Cell Dev. Biol.* 8:606817. doi: 10.3389/fcell.2020.606817

Feng, Z., Shi, M., Li, K., Ma, Y., Jiang, L., Chen, H, et al. (2020). Development and validation of a cancer stem cell-related signature for prognostic prediction in pancreatic ductal adenocarcinoma. *J. Transl. Med.* 18:360. doi: 10.1186/s12967-020-02527-1

Han, B., Kim, BJ., Kim, HS., Choi, DR., Shim, BY., Lee, KH, et al. (2021). A phase II study of gemcitabine, erlotinib and S-1 in patients with advanced pancreatic cancer. *J. Cancer* 12, 912–917. doi: 10.7150/jca.50514

Huang, DW., Sherman, BT., Tan, Q., Kir, J., Liu, D., Bryant, D, et al. (2007). DAVID bioinformatics resources: expanded annotation database and novel algorithms to better extract biology from large gene lists. *Nucleic Acids Res.* 35, W169–W175. doi: 10.1093/nar/gkm415

Kaissis, G., Ziegelmayer, S., Lohöfer, F., Steiger, K., Algül, H., Muckenhuber, A, et al. (2019). A machine learning algorithm predicts molecular subtypes in pancreatic ductal adenocarcinoma with differential response to gemcitabine-based versus FOLFIRINOX chemotherapy. *PLoS One* 14:e0218642. doi: 10.1371/journal.pone.0218642

Kamisawa, T., Wood, LD., Itoi, T., and Takaori, K. (2016). Pancreatic cancer. *Lancet* 388, 73–85. doi: 10.1016/s0140-6736(16)00141-0

Kleeff, J., Korc, M., Apte, M., La Vecchia, C., Johnson, CD., Biankin, AV, et al. (2016). Pancreatic cancer. *Nat. Rev. Dis. Primers.* 2:16022. doi: 10.1038/nrdp.2016.22

Kyrochristos, ID., Ziogas, DE., Glantzounis, GK., and Roukos, DH. (2018). Prediction of pancreatic cancer risk and therapeutic response with next-generation sequencing. *Biomark. Med.* 12, 5–8. doi: 10.2217/bmm-2017-0315

Leinwand, J., and Miller, G. (2020). Regulation and modulation of antitumor immunity in pancreatic cancer. *Nat. Immunol.* 21, 1152–1159. doi: 10.1038/s41590-020-0761-y

Marabelle, A., Le, DT., Ascierto, PA., Di Giacomo, AM., De Jesus-Acosta, A., Delord, JP, et al. (2020). Efficacy of pembrolizumab in patients with noncolorectal high microsatellite instability/mismatch repair-deficient cancer: results from the phase II KEYNOTE-158 study. *J. Clin. Oncol.* 38, 1–10. doi: 10.1200/jco.19.02105

Mizrahi, JD., Surana, R., Valle, JW., and Shroff, RT. (2020). Pancreatic cancer. *Lancet* 395, 2008–2020. doi: 10.1016/s0140-6736(20)30974-0

Nicolle, R., Gayet, O., Duconseil, P., Vanbrugghe, C., Roques, J., Bigonnet, M, et al. (2021). A transcriptomic signature to predict adjuvant gemcitabine sensitivity in pancreatic adenocarcinoma. *Ann. Oncol.* 32, 250–260. doi: 10.1016/j.annonc.2020.10.601

Nishiwada, S., Sho, M., Cui, Y., Yamamura, K., Akahori, T., Nakagawa, K, et al. (2021). A gene expression signature for predicting response to neoadjuvant chemoradiotherapy in pancreatic ductal adenocarcinoma. *Int. J. Cancer* 148, 769–779. doi: 10.1002/ijc.33284

Oba, A., Ho, F., Bao, QR., Al-Musawi, MH., Schulick, RD., and Del Chiaro, M. (2020). Neoadjuvant treatment in pancreatic cancer. *Front. Oncol.* 10:245. doi: 10.3389/fonc.2020.00245

Okamura, Y., Yasukawa, S., Narimatsu, H., Boku, N., Fukutomi, A., Konishi, M, et al. (2020). Human equilibrative nucleoside transporter-1 expression is a predictor in patients with resected pancreatic cancer treated with adjuvant S-1 chemotherapy. *Cancer Sci.* 111, 548–560. doi: 10.1111/cas.14258

Perri, G., Prakash, L., Qiao, W., Varadhachary, GR., Wolff, R., Fogelman, D, et al. (2020). Response and survival associated with first-line FOLFIRINOX vs Gemcitabine and nab-paclitaxel chemotherapy for localized pancreatic ductal adenocarcinoma. *JAMA Surg.* 155, 832–839. doi: 10.1001/jamasurg.2020.2286

Perri, G., Prakash, L., Wang, H., Bhosale, P., Varadhachary, GR., Wolff, R, et al. (2021). Radiographic and serologic predictors of pathologic major response to preoperative therapy for pancreatic cancer. *Ann. Surg.* 273, 806–813. doi: 10.1097/sla.0000000000003442

Phua, LC., Goh, S., Tai, DWM., Leow, WQ., Alkaff, SMF., Chan, CY, et al. (2018). Metabolomic prediction of treatment outcome in pancreatic ductal adenocarcinoma patients receiving gemcitabine. *Cancer Chemother. Pharmacol.* 81, 277–289. doi: 10.1007/s00280-017-3475-6

Piquemal, D., Noguier, F., Pierrat, F., Bruno, R., and Cros, J. (2020). Predictive values of blood-based rna signatures for the gemcitabine response in advanced pancreatic cancer. *Cancers (Basel)* 12:3204. doi: 10.3390/cancers12113204

Raffenne, J., Nicolle, R., Puleo, F., Le Corre, D., Boyez, C., Marechal, R, et al. (2019). hENT1 testing in pancreatic ductal adenocarcinoma: are we ready? a multimodal evaluation of hENT1 status. *Cancers (Basel)* 11:1808. doi: 10.3390/cancers11111808

Rashid, NU., Peng, XL., Jin, C., Moffitt, RA., Volmar, KE., Belt, BA, et al. (2020). Purity Independent Subtyping of Tumors (PurIST), a clinically robust, single-sample classifier for tumor subtyping in pancreatic cancer. *Clin. Cancer Res.* 26, 82–92. doi: 10.1158/1078-0432.Ccr-19-1467

Santofimia-Castaño, P., and Iovanna, J. (2021). Combating pancreatic cancer chemoresistance by triggering multiple cell death pathways. *Pancreatology* 21, 522–529. doi: 10.1016/j.pan.2021.01.010

Shibue, T., and Weinberg, RA. (2017). EMT, CSCs, and drug resistance: the mechanistic link and clinical implications. *Nat. Rev. Clin. Oncol.* 14, 611–629. doi: 10.1038/nrclinonc.2017.44

Siegel, RL., Miller, KD., Fuchs, HE., and Jemal, A. (2021). Cancer statistics, 2021. CA *Cancer J. Clin.* 71, 7–33. doi: 10.3322/caac.21654

Tu, SM., Bilen, MA., and Tannir, NM. (2016). Personalised cancer care: promises and challenges of targeted therapy. *J. R. Soc. Med.* 109, 98–105. doi: 10.1177/0141076816631154

Turpin, A., El Amrani, M., Bachet, JB., Pietrasz, D., Schwarz, L., and Hammel, P. (2020). Adjuvant pancreatic cancer management: towards new perspectives in 2021. *Cancers (Basel)* 12:3866. doi: 10.3390/cancers12123866

Xu, HX., Li, S., Wu, CT., Qi, ZH., Wang, WQ., Jin, W, et al. (2018). Postoperative serum CA19-9, CEA and CA125 predicts the response to adjuvant chemoradiotherapy following radical resection in pancreatic adenocarcinoma. *Pancreatology* 18, 671–677. doi: 10.1016/j.pan.2018.05.479

Yachida, S., and Iacobuzio-Donahue, CA. (2013). Evolution and dynamics of pancreatic cancer progression. *Oncogene* 32, 5253–5260. doi: 10.1038/onc.2013.29

Zhang, D., Zhou, S., and Liu, B. (2020). Identification and validation of an individualized EMT-related prognostic risk score formula in gastric

adenocarcinoma patients. *Biomed. Res. Int.* 2020:7082408. doi: 10.1155/2020/7082408

Zheng, X., Carstens, JL., Kim, J., Scheible, M., Kaye, J., Sugimoto, H, et al. (2015). Epithelial-to-mesenchymal transition is dispensable for metastasis but induces chemoresistance in pancreatic cancer. *Nature* 527, 525–530. doi: 10.1038/nature16064

Zhong, W., Zhang, F., Huang, C., Lin, Y., and Huang, J. (2020). Identification of epithelial-mesenchymal transition-related lncRNA with prognosis and molecular subtypes in clear cell renal cell carcinoma. *Front. Oncol.* 10:591254. doi: 10.3389/fonc.2020.591254

Conflict of Interest: The authors declare that the research was conducted in the absence of any commercial or financial relationships that could be construed as a potential conflict of interest.

frontiers in Oncology

ORIGINAL RESEARCH
published: 26 May 2021
doi: 10.3389/fonc.2021.667920

Autophagy-Mediated Clearance of Free Genomic DNA in the Cytoplasm Protects the Growth and Survival of Cancer Cells

*Mengfei Yao[1], Yaqian Wu[1], Yanan Cao[1], Haijing Liu[1], Ningning Ma[1], Yijie Chai[1], Shuang Zhang[2], Hong Zhang[2], Lin Nong[2], Li Liang[2] and Bo Zhang[1]**

[1] Department of Pathology, School of Basic Medical Sciences, Peking University Health Science Center, Beijing, China, [2] Department of Pathology, Peking University First Hospital, Beijing, China

The cGAS (GMP-AMP synthase)-mediated senescence-associated secretory phenotype (SASP) and DNA-induced autophagy (DNA autophagy) have been extensively investigated in recent years. However, cGAS-mediated autophagy has not been elucidated in cancer cells. The described investigation revealed that active DNA autophagy but not SASP activity could be detected in the BT-549 breast cancer cell line with high micronucleus (MN) formation. DNA autophagy was identified as selective autophagy of free genomic DNA in the cytoplasm but not nucleophagy. The process of DNA autophagy in the cytosol could be initiate by cGAS and usually cooperates with SQSTM1-mediated autophagy of ubiquitinated histones. Cytoplasmic DNA, together with nuclear proteins such as histones, could be derived from DNA replication-induced nuclear damage and MN collapse. The inhibition of autophagy through chemical inhibitors as well as the genomic silencing of cGAS or SQSTM1 could suppress the growth and survival of cancer cells, and induced DNA damage could increase the sensitivity to these inhibitors. Furthermore, expanded observations of several other kinds of human cancer cells indicated that high relative DNA autophagy or enhancement of DNA damage could also increase or sensitize these cells to inhibition of DNA autophagy.

Keywords: autophagy, cGAS, Micronuclei, cytoplasmic DNA, breast cancer

OPEN ACCESS

Edited by:
Lorenzo Gerratana, University of Udine, Italy

Reviewed by:
Carola Anke Neumann, University of Pittsburgh, United States
Tobias Eisenberg, University of Graz, Austria

****Correspondence:***
Bo Zhang
zhangbo@bjmu.edu.cn

Specialty section:
This article was submitted to Molecular and Cellular Oncology, a section of the journal Frontiers in Oncology

Received: *15 February 2021*
Accepted: *06 May 2021*
Published: *26 May 2021*

Citation:
Yao M, Wu Y, Cao Y, Liu H, Ma N, Chai Y, Zhang S, Zhang H, Nong L, Liang L and Zhang B (2021) Autophagy-Mediated Clearance of Free Genomic DNA in the Cytoplasm Protects the Growth and Survival of Cancer Cells. Front. Oncol. 11:667920. doi: 10.3389/fonc.2021.667920

INTRODUCTION

cGAS is an enzyme that catalyzes GTP and ATP to form cyclic dinucleic 2′,3′-cGAMP to stimulate stimulator of interferon gene (STING) and activate the kinases TBK1 and IKK, inducing the production of proinflammatory factor type I interferon (1). cGAS-STING has been identified as an innate immune mechanism, but many recent studies have shown that cGAS-STING plays a major role in the activation of the senescence-associated secretory phenotype (SASP), in which senescent cells secrete many cytokines, growth factors, proteases and chemokines acting through either autocrine or paracrine mechanisms to promote inflammation (2–6). The SASP is a crucial biological factor involved in aging-related diseases such as chronic inflammation, tissue degeneration or organ retardation. More importantly, the SASP has been revealed to be responsible for preventing the growth of cancer cells through its role as a tumor

suppressor in the late stages of tumor progression *via* genomic instability of cancer cells and remodeling of the tumor microenvironment (7). More interestingly, recent studies have also demonstrated that cGAS-STING could induce autophagy upon binding to dsDNA through either the cGAS interaction with Beclin-1 or STING-mediated LC3 lipidation. Nevertheless, either SASP (proinflammatory) or autophagy is important in host innate defense (8). However, cGAS-STING-mediated SASP or autophagy have not been fully elucidated in cancer cells.

Activation of cGAS has been confirmed upon its binding to DNA, and *in vitro* analysis proved that DNA could effectively recruit cGAS through phase transition (9). In living cells, cytoplasmic DNA, which can be exogenous, such as that from pathogenic organisms, and endogenous DNA of host cells, is a trigger that activates cGAS. Micronuclei (MNs) are small nuclei separated from the main nucleus. Similar to the main nucleus, MNs are encapsulated by the nuclear membranes and contain DNA and related substances (10). MNs are prevalent in cancer cells and are believed to be a consequence of DNA damage and aberrations in mitosis (11, 12). Moreover, studies have suggested that the existence of cytosolic DNA is closely related to MNs (6). MNs have been identified as the major source of cytoplasmic DNA involved in the activation of the cGAS-STING machinery to promote cancer progression and metastasis (13–15). Moreover, free DNA derived from ecc rDNA (extrachromosomal circular rDNA) could also trigger cGAS-STING activity (16). In addition, endogenous cytoplasmic DNA could be derived from mitochondria, which are injured under many circumstances (17). Nevertheless, in contrast to its role in triggering the SASP phenotype by free DNA, cGAS-STING-mediated DNA autophagy in cancer cells has rarely been evaluated.

The mechanism by which the cGAS-STING pathway mediates either SASP or autophagy in response to exogenous pathogens could lead to their eradication. However, it is unclear how cGAS-STING makes decisions in response to endogenous DNA in cells. In the described investigation, we unexpectedly found that the BT-549 breast cancer cell line with a high frequency of MN formation presented a low SASP phenotype but high autophagic activity, and subsequent experiments showed that its high DNA autophagy mediated by cGAS and cytosol-free DNA was closely related to MN formation and DNA damage, and inhibition of DNA autophagy could suppress its growth and survival. Furthermore, expanded observations indicated that enhancement of DNA damage or cancer cells with high relative DNA autophagy could increase DNA autophagy and sensitize the cells to autophagic inhibitors. These results proved that SASP and autophagy were related to the extent of DNA damage and that severe DNA damage or deficient DNA damage repair could increase autophagy in cells. Our research also clarified the potential therapeutic role of autophagic inhibition in some kinds of cancer cells with extensive DNA damage.

MATERIALS AND METHODS

Reagents and Antibodies

The anti-Lamin B1 rabbit polyclonal antibody, anti-Beclin1 rabbit polyclonal antibody, anti-STING (TMEM173, EPR13130) rabbit monoclonal antibody, and anti-DNase2 rabbit monoclonal antibody were purchased from Abcam (Cambridge, UK). The Stat6 (D-1) mouse monoclonal antibody, Lamin B1 mouse monoclonal antibody and cGAS (D-9) were purchased from Santa Cruz Biotechnology, Inc. (CA, 95060, USA), and anti-phospho-histone γH2AX mouse monoclonal antibody (Ser139) and anti-RPA2 mouse monoclonal antibody were from Millipore (Billerica, MA, USA). The anti-Lamin A/C (R386) rabbit polyclonal antibody, anti-IRF3 rabbit polyclonal antibody and anti-LAMP2 rabbit polyclonal antibody were from Bioworld Technology, Inc. (MN, USA). Anti-SQSTM1 rabbit polyclonal antibody and anti-LC3 rabbit polyclonal antibody were purchased from MBL, Ltd. (Chiba, Japan). Anti-phospho-STING (Ser366) rabbit monoclonal antibody and phospho-IRF3 rabbit monoclonal antibody were purchased from Cell Signaling Technology (Danvers, MA, USA). The information about antibodies were summarized in **Supplementary Table 1**. Nuclear Fast Red Staining Solution (0.1%; G1320), LysoTracker staining kit (Lysotracker Red DND-99) (L8010) and DAPI (C0060) were purchased from Solarbio (Beijing, China). The full-length expression plasmids Flag-cGAS, Flag-SQSTM1 and Flag-Beclin-1 were purchased from YouBio, Inc. (Beijing, China). Bafilomycin A1 and H-151 were purchased from Selleck (Shanghai, China), and chloroquine (CQ) and 2,3'-cGAMP were purchased from Sigma Aldrich (St. Louis, MO, USA). The protein marker (PM2510) was purchased from SMOBIO (Taiwan).

Cell Culture and Treatment

MDA-231, MCF-7, BT-549, 786-0, DU145, PC-3M, HCT-116, and HeLa cancer cell lines were maintained in 1640 or Dulbecco's modified Eagle's medium with high glucose (Gibco, Life Technologies, Grand Island, NY, USA) supplemented with 10% fetal bovine serum. The cells were incubated in a humidified atmosphere with 5% CO_2 at 37°C.

Small Interfering RNA

RNAi was designed and synthesized by GenePharma (Suzhou, China). RNAi was performed by the transfection of siRNA oligos using Lipofectamine 2000 transfection reagent (Invitrogen) according to the manufacturer's instructions. The sequences are as follows: si-cGAS-1: Forward: 5'-GGCCUCUG CUUUGAUAACUTT-3', Reverse: 5'-AGUUAUCAAAGCA GAGGCCTT-3'; si-cGAS-2: Forward: 5'-GGCUAUCCUUCU CUCACAUTT-3'; Reverse: 5' –AUGUGAGAGAAG GAUAGCCTT-3'. si-LC3-1: Forward: 5'-GCUACAAGGG UGAGAAGCATT-3'; Reverse: 5'-UGCUUCUCACCCUUG UAGCTT-3'; si-LC3-2: Forward: 5'-GCGAGUUGGUC AAGAUCAU TT-3'; Reverse: 5'-AUGAUCUUGACCAA CUCGCTT-3'; si-LC3-3: Forward: 5' –GCUUCCUC UAUAUGGUCUATT-3'; Reverse: 5'-UAGACCAUAU AGAGGAAGCTT-3'. si-SQSTM1-1: Forward: 5'-AGAUUCGCCGCUUCAGCUUTT-3'; Reverse: 5'-AAGCUGAAGCGGCGAAUC UTT-3'; si-SQSTM1-2: Forward: 5'-CGCUCACCGUGAAGGCCUATT -3'; Reverse: 5'-UAGGC CUUCACGGUGAGCGTT-3'; si-SQSTM1-3: Forward: 5'-GCACUACCGCGAU GAGGACTT-3'; Reverse: 5'-GUCCUCAUCGCGGUAGUGCTT-3'; si-DNase II-1:

Forward: 5'-GGCAGCCU GUAGACUGGUUTT-3'; Reverse: 5' -AACCAGUCUACAGGCUGCCTT-3'; si-DNase II-2: Forward: 5'-GCAUACAGCUGGCCUCAUATT-3'; Reverse: 5'-UAUGAGGCCAGCUGUAUG CTT-3'. The control RNAi (siNC) was composed of scrambled sequences.

Western Blotting

Total cell lysates were obtained by incubating the cells in 2× SDS for 30 minutes at 4°C. After centrifugation at 10,000×g for 10 minutes at 4°C, the supernatant was collected and stored at -20°C for subsequent analysis. For cell fractions, cytoplasmic and nuclear proteins were extracted using nuclear and cytoplasmic protein extraction kits (Sangon Biotech Co., Shanghai, China), respectively. Equal amounts of cell proteins (20-40 μg/lane) were separated by SDS-PAGE in 10% gels and transferred to PVDF membranes (Millipore, Billerica, MA, USA) using a semidry transfer cell (Bio-Rad,Hercules, CA, USA) at 25 V for 60 minutes. The membranes were then blocked for 1 hour with TBS-T (20 mmol/L Tris-HCl pH 7.6, 137 mmol/L NaCl and 0.1% Tween-20) containing 5% nonfat dry milk (Cell Signaling Technology, Beverly, MA, USA) or with 1% BSA (Sigma Aldrich) and incubated overnight with primary antibodies. After the membranes were washed, they were incubated for 1 hour with peroxidase-conjugated goat anti-rabbit IgG or peroxidase-conjugated goat anti-mouse IgG. The proteins were visualized using an enhanced chemiluminescence kit (Bio-Rad, CA, USA). Band images of three independent experiments were quantified by optical density using Lab-Works 4.6 software (Bio-Rad, CA, USA). β-actin was used as an internal control for each protein. The antibodies included anti-LC3 (1:1000), anti-β-actin (1:1000), anti-cGAS (D-9) (1:500), anti-SQSTM1 (1:1000), anti-DNase2 (1:1000), anti-lamin A/C (R386) (1:500), anti-IRF3 (1:500), anti-TMEM173 (1:1000), and anti-LAMP2 (1:1000).

Immunofluorescence

Immunofluorescence staining was performed as described previously (18). The results were observed and recorded using a fluorescence microscope (Model CX51; Olympus, Tokyo, Japan), and Photoshop version 7.0 (Adobe Systems, Inc.) was used to analyze the results. The antibodies used included anti-LC3 (1:1000), anti-β-actin (1:1000), anti-cGAS (D-9) (1:500), anti-SQSTM1 (1:1000), anti-DNase II (1:1000), anti-lamin A/C (R386) (1:500), IRF3 (1:500), anti-STING (1:1000), and anti-LAMP2 (1:1000).

Senescence Associated-β-galactosidase Staining (SA-β-gal)

Cells were subjected to SA-β-gal staining using an SA-β-gal staining kit (GenMed, GenMed Scientifics, Inc., USA) according to the manufacturer's directions. Five hundred cells were counted in random fields and the percentage of SA-β-gal-positive cells was calculated and the mean was calculated from independently repeated experiments at least five times.

Electron Microscopy

Cells were fixed with 0.1 mol/L sodium phosphate buffer (4% paraformaldehyde and 0.1% glutaraldehyde) at 4°C overnight. The samples were embedded with Lowicryl K4M (BioChemika), and sections were prepared with the Leica EM UC7 ultramicrotome and then stained with saturated uranyl acetate. The sections were observed under a transmission electron microscope (JEOL-1230, Japan) and recorded. The autophagosomes or autolysosomes are double-membrane enclosed in EM observations with the treatment of autophagy inhibitors.

Co-Immunoprecipitation

A total of $1x10^7$ transfected cells were washed twice with PBS, 600 μl of precooled hypo-osmic buffer (25 mmol/L Tris, pH 7.4, 85 mmol/L KCl) was added, and the samples were incubated on ice for 30 minutes and centrifuged at 4°C at 12000 rpm for 10 minutes. The supernatant was saved and incubated with Flag antibody-conjugated agarose beads (MBL, Chiba, Japan) and gently shaken on a turntable overnight at 4°C. The beads were washed with hypo-osmic buffer containing protease inhibitor cocktail for 10 minutes; this process was repeated 4 times. Finally, the beads were dissolved in 1.5×SDS loading buffer, and 30 μl of supernatant was analyzed by Western blotting. The primary whole cytoplasmic supernatant was used as input.

IP-PCR

A total of $2×10^7$ transfected cells were washed with preheated PBS at 37°C 3 times, fixed with 1% formaldehyde in PBS in a 37°C incubator for 15 minutes, quickly washed with ice-cold PBS 5 times, scraped into an Ep tube, and centrifuged at 800 g at 4°C for 3 minutes. Then, the supernatant was discarded, and 500 μl of hypo-osmic buffer (25 mmol/L Tris, pH 7.4, 85 mmol/L KCl) was added to isolate the cytoplasmic protein. Part of the supernatant was saved as the input. The remaining part was used for IP experiments. An appropriate amount of 500 μl elution buffer (1% SDS, 0.1 mol/L sodium bicarbonate was used to elute the protein-DNA complex on the beads for 10 minutes at room temperature. Then, RNase A was added, the samples were heated at 37°C and shaken for 2 h, Proteinase K was added, and the samples were heated at 55°C and shaken for 2~3 h. Then, the samples were heated at 65°C and shaken overnight to isolate the protein-DNA complexes. Finally, the IP DNA was extracted by the phenol and chloroform method, and the results were analyzed by PCR.

Sucrose Density Gradient Centrifugation

Gradient concentrations of sucrose solution (5%-40%, the concentration interval was 5%) with protease inhibitor cocktail were established as described (19). The cytoplasmic proteins, extracted by hypo-osmic buffer as described above, were carefully dropped on the top layer and centrifuged at 40,000 rpm (Beckman, Brea, CA, USA) for 4 hours at 4°C. After centrifugation, the samples were carefully collected from a 500 μl aliquot of each fraction, and the aliquot of each fraction was analyzed by Western blot. Cytoplasmic DNA was extracted from 100 μl of each fraction and analyzed by PCR.

Acid Extraction of Cytoplasmic Histones

Cytoplasmic histones were isolated by acid extraction methods with some modifications (20). Briefly, cytoplasmic proteins

from 1×10^7 cells of each kind, extracted by hypo-osmic buffer as described above, were slowly added to 0.4 N H_2SO_4 (500 µl of H_2SO_4 to a 100 µl cytoplasmic solution) and incubated at 4°C with intermittent rotation for 2 hours. After centrifugation at 5500 rpm for 5 minutes, the supernatants were gently added to 150 µl of 100% TCA (final concentration of 20%) and kept on ice for at least 5 hours without agitation. After centrifugation, the pellets were washed with 500 µl of acetone+0.1% HCl, and the tubes were left open overnight to evaporate the acetone. The pelleted histones were resuspended in 20 µl of ddH_2O and subsequently analyzed by SDS-PAGE and Western blotting.

PCR Detection

DNA in nuclear or cytoplasmic were separately extracted. The cells were cultured in 10 cm dishes and counted. A total of 1×10^3 cells were treated with hypo-osmic buffer (25 mmol/L Tris pH 7.4, 85 mmol/L KCl) and centrifuged, and the supernatant (the cytoplasmic components) was saved. Then, the cytoplasmic DNA was extracted by the phenol and chloroform method. The sediment (nuclear DNA) was extracted by Tigen Kits (Beijing, China). PCR was performed with using Alu and rDNA primers: Alu: sense: 5'-CCTGAGGTCAGGAG TTCGAG-3'; antisense: 5'-CCCGAGTAGCTGGGATTACA-3' (115 bp); 5.8S rDNA: sense: 5'- GAGGCAACCCCCTC TCCTCTT-3'; antisense: 5'-GAGCCGAGTTCACCGCTA-3' (136 bp); 18S rDNA: sense: 5'-CG CCGCGCTCTACCTTA CCTA-3'; antisense: 5' -TAGGAGAGGAGCGAGCGACCA-3' (159 bp); 28S rDNA: sense: 5' -CTCCGAGACGCGACCT CAGAT-3'; antisense: 5'-CGGGTCTTCC GTACGCCACAT-3' (173 bp). Quantitative real-time RT-PCR was performed on a PCR system (Applied Biosystems, Inc., Carlsbad, CA, USA) using SYBR Premix. The results were evaluated as the ratio of cytoplasmic: nuclear DNA; cytoplasmic DNA was normalized to nuclear DNA. The results were analyzed by GraphPad Prism 8.0.

FISH

The Alu probes were as follows: Alu-1: 5'-CCTGAGGTCAGGA GTTCGAGACCAGCCT-3'; Alu-2: 5'-ACGCCTGTAATCCCA GCACTTTGGGAGG-3'; Alu-3: 5' –TCGCGCCACTGCACTC CAGCCTGGGCGA-3'. They were synthesized and conjugated with a single Quasar 570 molecule at the 5' end (Sango Biotech, Shanghai, China). Cells grown on cover slides were fixed in 3% paraformaldehyde (pH 7.4) containing 0.1% Triton-X 100 for 30 minutes and permeabilized in 0.1% Triton X-100 for 20 minutes. After denaturation at 95°C for 5 minutes, hybridization was performed in a mixture of probes (20 ng/per slide) and 35% deionized formamide, 10% dextran sulfate, 1× Dehart's, and 2× SSC for 20 hours at 42°C. The slides were washed for 40 minutes in 2×SSC with several changes. Nuclei were stained with Hoechst 34580 (Sigma Aldrich) for 10 minutes, and the results were observed and recorded using a fluorescence microscope (Model CX51, Olympus, Tokyo, Japan), and Photoshop version 7.0 (Adobe Systems, Inc. San Jose, CA, USA) was used to observe and analyze the results. At least 500 cells were evaluated, and the results were evaluated as the ratio of the intensity in cytoplasmic and nuclear DNA; cytoplasmic signals were normalized to those of the nuclei.

Comet Assay

The comet assay was performed using a comet assay kit according to the manufacturer's instructions. First, 1×10^5 cells were prepared. Neutral or alkaline electrophoresis was performed. The slides were viewed by epifluorescence microscopy using a FITC filter. The results were analyzed by Comet Score software (Version 2.0038).

The comet assay was performed using a comet assay kit (Abcam, Cambridge, UK) according to the manufacturer's instructions. First, 1×10^5 cells were prepared. Comet Agarose was pipetted onto the Comet Slide to form base layer cells, which were combined with Comet Agarose at 37°C. Cell samples were combined with Comet Agarose at a 1/10 ratio (v/v). We pipetted the agarose/cell mixture on top of the base layer. The cells were treated with lysis buffer and alkaline solution. Electrophoresis was performed under alkaline or neutral conditions. Voltage was applied to the chamber for 10-15 minutes at 1 volt/cm. The cells were stained with DNA dye. The slides were viewed by epifluorescence microscopy using a FITC filter. The results were analyzed by Comet Score software (Version 2.0038).

BrdU Incorporation Assay

BrdU incorporation assays were performed as described previously (18). Briefly, BrdU (10 µM) was added to the culture medium for 30 minutes before analysis, and then, the cells were fixed with 4% formaldehyde, permeabilized with 0.1% Triton X-100, and denatured with 20 mmol/L HCl in 150 mmol/L NaCl and 3 mmol/L KCl for 20 minutes at 25°C. The cells were then incubated with a primary antibody mixture composed of primary antibodies (BrdU and MCM7 or Lamin B1).

Trypan Blue Exclusion Assay

Cell growth was determined by Trypan blue exclusion assays with a Trypan Blue Staining Cell Viability Assay Kit (Beyotime, Shanghai, China). Cells (1×10^4 cells/per well) grown with or without treatment with CQ, bafilomycin A1, or H-151 in 96-well plates were harvested, and 50 µl of trypan blue was added to a 50 µl cell suspension according to the manufacturer's protocol. Viable cells were counted under a microscope with a hemocytometer. The assays were performed in triplicate and repeated at least three times.

Live/Dead Viability Assay

A live/dead assay was performed using a live/dead cell viability assay kit (Abcam, Cambridge, UK). A total of 1×10^5 cells were seeded in 12-well or 96-well plates and incubated for 24 hours. The cells were treated with CQ or bafilomycin A1 and incubated for the indicated times. Subsequently, the cells were rinsed twice with PBS before the fluorochromes were added and incubated for 45 minutes. Fluorescence images were then taken (Model CX51, Olympus, Tokyo, Japan), and live or dead cells were counted and calculated.

MTS Assay

MTS assays were performed using an MTS assay kit (Bestbio, Shanghai, China). A total of 1×10^4 cells were seeded in 96-well plates and incubated for 24 hours. The cells were treated with CQ

or bafilomycin A1 and incubated for the indicated times. Ten microliters of MTS solution was added to each well and incubated for 3 hours at 37°C. The absorbance was measured at 490 nm, and cell viability was analyzed.

Statistical Analysis

All analyses were performed using software GraphPad Prism 8 (CA, USA), SPSS 27.0 (IBM, Armonk) and Excel 2010 (WA, USA). Comparisons between groups were performed using Student's t-test and one-way ANOVA with Tukey *post-hoc* test and Dunnett *post-hoc test* to correct for multiple testing. The data were presented as mean ± SEM or mean ± SD. A P-value of less than 0.05 was considered significant. All statistical tests and P values were 2-sided, and the level of significance was set at <0.05 (*), <0.01 (**), <0.001 (***), or<0.0001 (****); ns indicates no significance.

RESULTS

Detection of the Autophagy Activity in Breast Cancer Cells

Recently, it has been revealed that MN formed in MDA-231 cells could trigger SASP activity to promote metastasis and progression (15). Like MDA-231, the BT-549 cells are also a triple negative breast cancer (21), and beyond we noted that the BT-549 cells usually present frequent spontaneous formation of MN. The fact provoked our interest about relationship between MN and SASP activity. We used the MDA-231 and BT-549 as well as MCF-7 cells, another classis type of breast cancer cell line (22), for analysis of spontaneous MN formation by immunofluorescent staining of Lamin B1 and NAT10 as described previously (18). The rate of spontaneous MNs in the MCF-7 cells was approximately 5%, that in the MDA-231 cells was approximately 15%, and that in the BT-549 cells was approximately 35% (**Figure 1A**). However, the MNs formed in three cell lines generally contained DNA and Lamin B1 or A/C, nuclear lamina proteins, and other nuclear envelope components, including LBR (Lamin B receptor), nuclear pore complex components (MAB414, nucleoporin 153), the nuclear basket protein TPR (translocated promoter region), and integral membrane components (Sun2 and nesprin2), suggesting that the nuclear membrane of MNs generally maintained structural components similar to the membrane of the main nuclei (**Supplementary Figure 1A**).

MNs are considered a major source of free DNA, which triggers the activation of the SASP through DNA binding to cGAS-STING pathway components (6). Therefore, the MDA-231, BT-549, and MCF-7 cells were analyzed by SA-β-gal staining, and the results indicated that the MCF-7 and MDA-231 cells showed 4% and 8% SA-β-gal positivity, while the BT-549 cells unexpectedly showed no SA-β-gal-positive cells even with repeated staining (**Figure 1B**).

Subsequent Western blotting analysis showed the expression of the STING, pSTING, IRF3, pIRF3, STAT6 in BT-549 cells is lower than that of MDA-231 or MCF-7 cells, indicating that the activity of SASP in BT-549 cell line was significantly lower than that in MDA-231 and MCF-7 cells (**Figure 1C**). The SA-β-gal staining also showed that after treatment with the STING antagonist H-151 (2 μmol/L) for 24 hours, the SA-β-gal positive cells markedly decreased, confirming that the SASP phenotype is mediated *via* cGAS-STING in the MDA-231 cells (**Supplementary Figure 1B**). However, treatment with the STING agonist cGAMP (1) and transfection with Flag-cGAS or Flag-STING did not induce SA-β-gal staining, indicating blockade of cGAS-STING signaling in the BT-549 cells.

Recently, the cGAS-STING pathway was shown to mediate DNA autophagy. Therefore, autophagic activity was first compared among the MCF-7, MDA-231 and BT-549 cells. Western blotting showed that the BT-549 cells presented high expression of LC3-II, SQSTM1, and LAMP2, which was not obvious in the MDA-MB-231 or MCF-7 cells, and notably, a high level of DNase II was detected in the BT-549 cells (**Figure 1D**). The BT-549 cells were treated with the autophagic inhibitors CQ (10 μmol/L) for 4 hours or bafilomycin A1 (10 nmol/L) for 24 hours, and the levels of LC3-II, SQSTM1 and LAMP2 were strongly increased, (**Figure 1E**), while not for MCF-7, MDA-231 cells under the treatment of CQ (10 μmol/L) (**Supplementary Figure 1C**), confirming the autophagic activity in the BT-549 cells. Moreover, the expression of DNase II was dose-dependently enhanced by CQ treatment (10 μmol/L) in the BT-549 cells (**Figure 1E**). Furthermore, the staining of LysoTracker, a fluorescent probe for lysosome (23), showed that lysosomes were more abundant in the BT-549 cells than in the MDA-231 cells (**Figure 1F**). The results suggested the involvement of DNA autophagy in the BT-549 cells.

To further confirm the autophagic activity, we also performed electron microscopy of the MDA-MB-231 and BT-549 cells after treatment with bafilomycin A1 (10 nmol/L) for 32 hours, and the results showed that there were many autophagic vesicles in the BT-549 cells but not the MDA-MB-231 cells (**Figure 1G**).

Therefore, the above results demonstrated that breast cancer cells with MNs could differentially present SASP and autophagy, and cells with a high frequency of MNs presented an autophagic phenotype.

Detection of Genomic DNA Autophagy in the Cytoplasm of Breast Cancer Cells

High autophagic activity and frequent MN formation, as well as DNase II expression, indicated the possibility of active DNA autophagy in the BT-549 cells. First, SQSTM1 and LC3, the core proteins of autophagy, were stained by immunofluorescence in the MCF-7, MDA-231 and BT-549 cells. The results showed that the BT-549 cells presented marked cytoplasmic SQSTM1-positive granules or vesicles (~60% cells) (**Figure 2A**), but only a few cells showed cytoplasmic staining for SQSTM1 in MCF-7 and MDA-231. All three kinds of cells presented SQSTM1 positive in occasional Lamin B1-outlined MNs (~5% MNs) (**Supplementary Figure 2A**). Similarly, the BT-549 cells also presented much more cytoplasmic LC3-positive vesicles than the MDA-231 or MCF-7 cells (**Figures 2A, B**). However, almost no

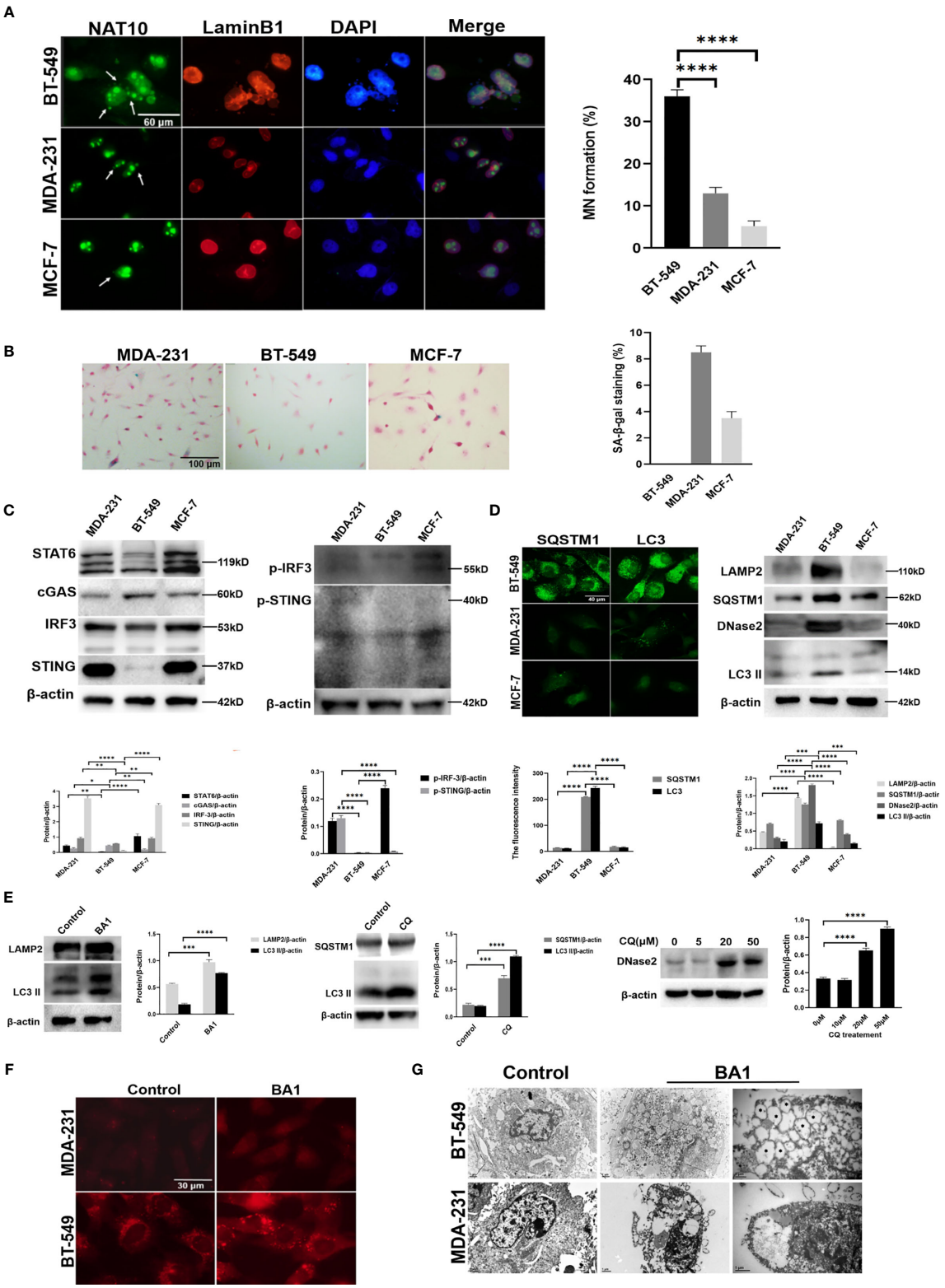

FIGURE 1 | Continued

FIGURE 1 | High frequency of MNs in breast cancer cells was associated with an autophagic phenotype. **(A)** MN formation in breast cancer cells. Left panels: MDA-231, BT-549 and MCF-7 cells were subjected to immunofluorescence staining for NAT10 and Lamin B1. Arrows indicate MNs. Right panel: the frequency of MNs in each kind of cell was counted and calculated as the percentage of total cells. The micronuclei outlined by LaminB1 and DAPI were counted and at each time 500 cells were measured. The experiments were repeated five times. The frequency of MN was calculated from independently repeated experiments. Data are presented as mean ± SEM. **(B)** Senescent phenotypes of breast cancer cells. Left panels: Representative images of SA-β-gal staining in the MDA-231, BT549 and MCF7 cells. Right panel: SA-β-gal-positive cells were counted and calculated as the percentage of total cells. The experiments were repeated five times. Data are presented as mean ± SEM. **(C)** The expression of SASP-related factors in breast cancer cells. The MDA-231, BT549 and MCF-7 cells were assessed by Western blotting. Left panels: the levels of STAT6, cGAS, STING, and IRF3. Right panels: p-STING and p-IRF3. The experiments were repeated three times. Data are presented as mean ± SD. **(D)** The expression of autophagy-related proteins in the MDA-231, BT-549 and MCF-7 cells. Left panels: The cells were subjected to immunofluorescence staining of SQSTM1 or LC3. Right panels: Total cell proteins were extracted, and LAMP2, SQSTM1, DNase II and LC3-II were measured by Western blotting. The experiments were repeated three times. Data are presented as mean ± SD. **(E)** The analysis of autophagic flow in the BT-549 cells. The BT-549 cells were treated with 50 μmol/L CQ for 4 hours or 10 nmol/L bafilomycin A1 for 24 hours or with the indicated concentrations of CQ for 4 hours, and total cell proteins were extracted and analyzed by Western blotting. Left panels: The levels of LAMP2 and LC3-II in the bafilomycin A1-treated cells. Middle panels: The levels of SQSTM1 and LC3-II in the CQ-treated cells. Right panels: The levels of DNase II in the indicated concentrations of CQ-treated cells. The experiments were repeated three times. Data are presented as mean ± SD. **(F)** The activity of lysosomes in the MDA-231 and BT-549 cells. After treatment with 10 nmol/L bafilomycin A1 BA1) for 24 hours, the cells were stained with LysoTracker staining kit Solarbio, Beijing, China) according to the manufacturer's instructions. The experiments were repeated three times. **(G)** Electron microscopy of the autophagic activity in the MDA-231 and BT-549 cells. After treatment with bafilomycin A1 BA1) for 32 hours, the cells were subjected to transmission electron microscopy. The double-membrane enclosed autophagosomes or autolysosomes are labelled by stars. The experiments were repeated twice. β-actin was used as an internal standard in Western blotting. The level of statistical significance was <0.05 *), <0.01 **), < 0.001 ***) and < 0.0001 ****). The images are representative of repeated experiments.

LC3 was detected in the MNs of the three kinds of cells (**Supplementary Figure 2B**).

Interestingly, the distribution of cGAS was shown to be similar to that of SQSTM1 or LC3. The BT-549 cells presented accumulation of cytoplasmic cGAS granules that colocalized with SQSTM1 (~50%) and cytoplasmic LC3 (~40% cells), while the MCF-7 and MDA-231 cells were faintly stained for cGAS (**Figures 2A, B**). All three kinds of cells showed staining for cGAS in occasional MNs (3%-5%) (**Supplementary Figure 2C**). In addition, only a few cGAS-positive MNs (~3%) were positive for SQSTM1 but not LC3 (**Figures 2B, C**). STING staining showed that a few cytoplasmic puncta were detected in the MCF-7 and MDA-231 cells but were distributed in the Golgi apparatus in the BT-549 cells (~30%), while the staining was generally weak (see **Supplementary Figure 3C**).

Further, Beclin-1, another autophagy mediator, was stained in breast cancer cells, but few cytoplasmic positive vesicles were detected and only occasional staining in cGAS positive MN (**Supplementary Figures 2D, E**).

To further confirm the autophagic activity, we treated the MDA-MB-231 and BT-549 cells with CQ (10 μmol/L) or bafilomycin A1 (10 nmol/L) for 24 hours, and the results showed that the BT-549 cells presented marked increases in cytoplasmic cGAS, SQSTM1 and LC3, while the MDA-231 and MCF-7 cells only showed slight increases in a few cells (**Figures 2A, B**). However, the MNs in the three kinds of cells presented no significant increase in positive staining of cGAS, SQSTM1, LC3 or Beclin-1 (data not shown). As expected, treatment with bafilomycin A1 markedly increased not only the levels of SQSTM1, LC3-II, and LAMP2 but also cGAS and STING in the BT-549 cells (**Figure 2D**).

The colocalization and accumulation of SQSTM1, cGAS and LC3 in the cytoplasm suggested the possibility of selective cytoplasmic DNA autophagy. To directly verify the genomic DNA in the cytoplasm, we independently isolated cytoplasmic DNA from the MCF-7, MDA-231 and BT-549 cells and the existence of genomic DNA was determined by PCR detection of Alu- or rDNA (5.8S, 18S and 28S) repeated sequences. The gel electrophoresis results showed that the cytoplasmic abundance of Alu in the BT-549 cells was significantly higher than that in the MDA-231 and MCF-7 cells (**Figure 2E**). Moreover, real-time PCR confirmed the greater cytoplasmic abundance of Alu and rDNA (5.8S, 18S and 28S) in the BT-549 cells than in the MCF-7 and MDA-231 cells (**Figure 2E**).

To explore the potential interaction between cGAS or SQSTM1 and genomic DNA in the cytoplasm, co-immunoprecipitation was carried out. Flag-SQSTM1 and Flag-cGAS were transfected into the MDA-231 and BT-549 cells, and the cytoplasmic fractions of Flag-SQSTM1 and Flag-cGAS were immunoprecipitated. The sequences of Alu- or 5.8S rDNA could be detected in either precipitated Flag-SQSTM1 or Flag-cGAS and were more abundantly detected in the BT-549 cells than in the MDA-231 cells (**Figure 2F**). Moreover, the sequences of Alu DNA in the cytoplasm showed greater detection in the BT-549 cells than in the MDA-231 cells by FISH, and following treatment with CQ and bafilomycin A1, the cytoplasmic signals were enhanced in the BT-549 cells (**Supplementary Figure 2G**), but the level of the LaminA/C or LBR in all three kind of cells were not changed in the presence of CQ (50 μmol/L) for 36 hours, (**Supplementary Figure 2F**).

Taken together, these data indicated that DNA autophagy in breast cancer cells could be selective autophagy of cytoplasmic free DNA but not nucleophagy and possibly involved cGAS, SQSTM1 and LC3.

DNA Autophagy in the Cytoplasm Was Involved in the Coordination of cGAS and SQSTM1

To explore the autophagic flux in DNA autophagy, we investigated the relationship between cGAS and SQSTM1 or LC3. After knockdown of either *LC3* or *SQSTM1* by siRNA, the level of cGAS was obviously increased in the BT-549 cells, as shown by Western blotting (**Figures 3A, B**, left panels), and in immunofluorescent staining (**Figures 3A, B**, right panels). Moreover, depletion of *LC3* increased the SQSTM1 levels (**Figure 3A**, left panels). In contrast, after knockdown of *cGAS*

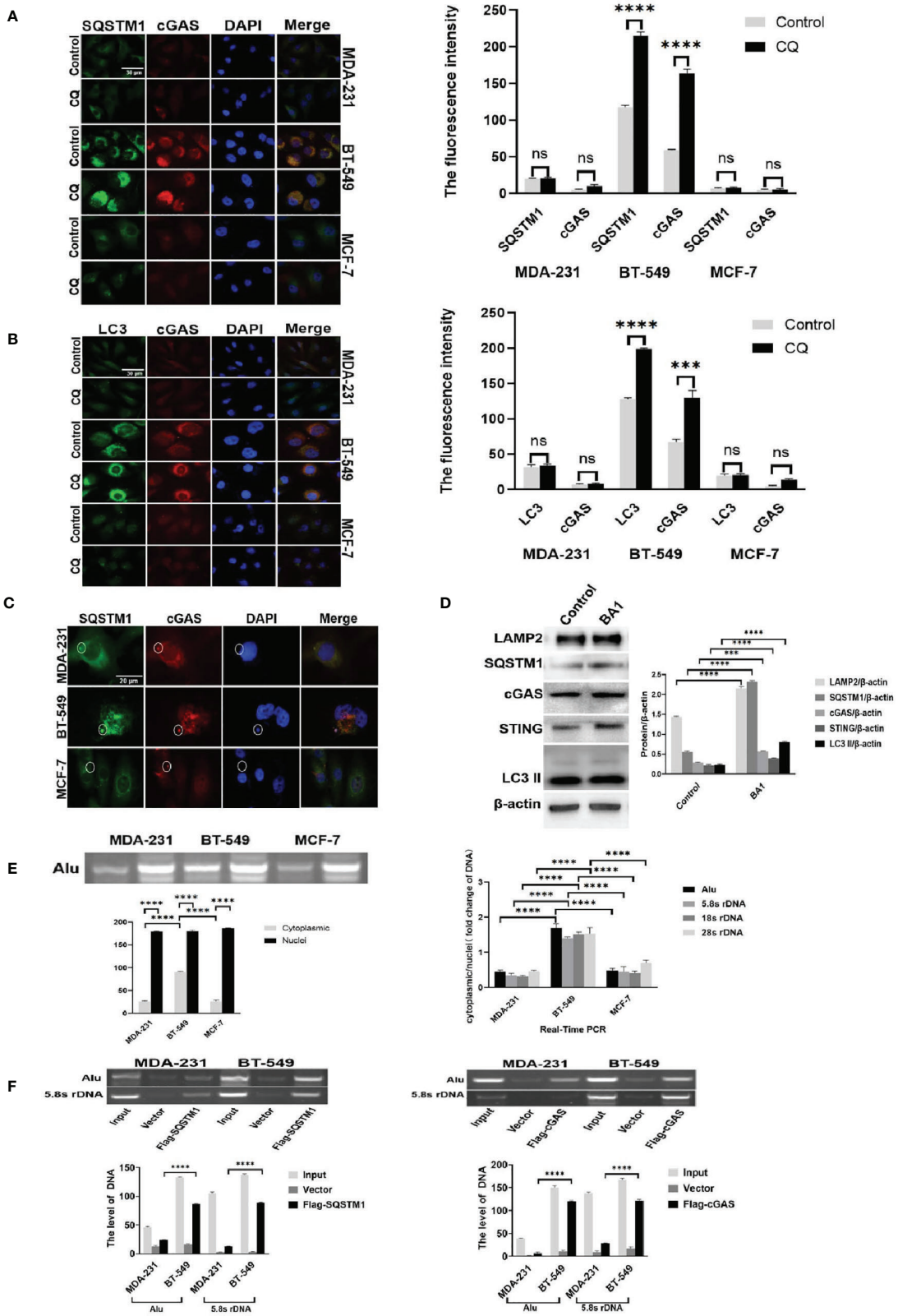

FIGURE 2 | Continued

FIGURE 2 | Detection of genomic DNA autophagy in the cytoplasm of breast cancer cells. **(A)** The effects of autophagic inhibition on the expression and distribution of SQSTM1 and cGAS in breast cancer cells. MDA-231 and BT-549 cells were treated with CQ 10 μmol/L) for 4 hours and subjected to double immunofluorescence staining of SQSTM1 green) and cGAS red). The experiments were repeated three times. Data are presented as mean ± SD. **(B)** The effects of autophagic inhibition on the expression and distribution of LC3 and cGAS in breast cancer cells. The MDA-231 and BT-549 cells were treated with CQ 10 μmol/L) for 4 hours and subjected to double immunofluorescence staining for LC3 green) and cGAS red). The experiments were repeated three times. Data are presented as mean ± SD. **(C)** Detection of SQSTM1 and cGAS in the MNs of breast cancer cells. The MDA-231, BT-549 and MCF-7 cells were doubly stained for SQSTM1 green) and cGAS red) by immunofluorescence, and MN colocalization is labeled with circles. The experiments were repeated three times. **(D)** Autophagic inhibition increased the level of cGAS in the BT-549 cells. The BT-549 cells were treated with bafilomycin A1 BA1, 10 nmol/L) for 24 hours, and the levels of cGAS, SQSTM1, STING, LAMP2, and LC3-II were measured by Western blotting. Data are presented as mean ± SD. **(E)** Analysis of cytoplasmic DNA in breast cancer cells. The cytoplasmic or nuclear DNA of the MDA-231, BT-549 and MCF-7 cells was independently isolated, and Alu and rDNA 5.8S, 18S and 28S) were individually detected by PCR from cytoplasmic or nuclear DNA, respectively, as described in the Materials and Methods. Left panels: The amplified Alu products are displayed by gel electrophoresis. The experiment repeated three times. Data are presented as mean ± SD. Right panel: The summarized results of rDNA 5.8S, 18S and 28S) in real-time PCR. The experiments were repeated three times. Results are expressed as mean ± SEM. **(F)** Immunoprecipitation analysis of genomic DNA and cGAS or SQSTM1 in the cytoplasm. The BT-549 cells and the MDA-231 cells were transfected with Flag-cGAS or Flag-SQSTM1 or vector) for 36 hours. After fixation with 1% formalin for 10 minutes, cytoplasmic extracts were isolated as described in the Materials and Methods. The genomic DNA was measured by PCR amplification of Alu- and 5.8S rDNA. Left panels: Flag-SQSTM1. Right panels: Flag-cGAS. β-actin was used as an internal standard in Western blotting. The experiments were repeated three times. Data are presented as mean ± SD. The level of statistical significance was <0.001 ***) and < 0.0001 ****). ns, no significance. All experiments were repeated three times independently, and the images are representative of repeated experiments.

by siRNA, the levels of either LC3-II or SQSTM1 were decreased in the BT-549 cells, as shown by immunofluorescence and Western blotting (**Figure 3C**).

After knockdown of *cGAS* by interfering RNAs, gel electrophoresis showed that the levels of cytoplasmic Alu- and rDNA sequences increased obviously in the BT-549 cell lines but not in the MCF-7 or MDA-231 cell lines (**Figure 3D**). Similarly, knockdown of *LC3* also resulted in the same findings (**Figure 3D**).

To explore the potential autophagic complex of SQSTM1, we further analyzed cGAS, LC3 and free DNA through cytoplasmic fractioning in a density gradient fraction assay, in which the detection of SQSTM1 partly overlapped in fractions containing cGAS, LC3 and free DNA (**Figure 3E**). Moreover, a coprecipitation analysis showed that genomic DNA could be detected in the MDA-231 and BT-549 cells transfected with either Flag-SQSTM1 or Flag-cGAS (**Figure 2F**). In addition, endogenous cGAS in the BT-549 cells coprecipitated with transfected Flag-SQSTM1 (**Supplementary Figure 3A**, upper panel).

However, so far there are no evidences on the direct interaction of SQSTM1 with either cGAS or DNA, and how SQSTM1 participates in DNA autophagy needs to be addressed. Generally, SQSTM1 recognizes ubiquitinated substances during autophagy, and it has been reported that cGAS undergoes K48-linked ubiquitination at K414, leading to SQSTM1-dependent selective autophagic degradation (24). Thus, Flag-SQSTM1 was transfected into the BT-549 cells, but K48-ubiquitinated cGAS could not be detected by Western blotting (**Supplementary Figure 3A**, lower panel).

Since DNA is usually coated with histones or other chromatin-binding proteins, cytoplasmic free DNA was also assumed to be bound to histones. To clarify this, we isolated cytoplasmic histones from the BT-549 or MDA-231 cells by acid-based extraction (20). Western blotting showed that cytoplasmic histones could be detected in both the BT-549 and MDA-231 cells, but the BT-549 cells presented more cytoplasmic histones than the MDA-231 cells (**Figure 3F**); these structures could be detected by anti-K48 ubiquitin and FK2 antibodies (against poly- or monoubiquitinated proteins) (**Figure 3F**). Moreover, immunofluorescence staining showed that more intensive staining of FK2 could be detected in the cytoplasm of the BT-549 cells than in that of the MDA-231 cells (**Supplementary Figure 3B**).

Taken together, the results suggested that free cytoplasmic DNA autophagy could be mediated in a complicated process, assumedly involving cGAS binding to DNA and recognition of ubiquitinated histones by SQSTM1, respectively.

Genomic DNA in the Cytoplasm Could be Derived From Either Damaged Nuclei or MNs

Since the cytoplasmic DNA undergoing autophagy was genomic DNA from the nuclei and nuclear membrane in the breast cancer cells were not generally broken (**Supplementary Figure 1A**), DNA damage was assumed to be involved. The level of DNA damage in the BT-549, MCF-7 and MDA-231 cells was analyzed by comet assays. **Table 1** shows that the tail length of the BT-549 cells was substantially longer than that of the MDA-231 (76.83, P<0.0001) and MCF-7 cells (70.59, P<0.0001), the tail intensity of the BT-549 cells was greater than that of the MDA-231 (70319, P<0.01), and MCF-7 cells (75513, P<0.0001), and the tail movement of the BT-549 cells was also obviously higher than that of the MDA-231 (13.09, P<0.0001) and MCF-7 cells (15.66, P<0.0001). These results indicated that the DNA damage was the most severe in the BT-549 cells (**Table 1** and **Figure 4A**).

Following bafilomycin A1 treatment, the length, intensity and movement of the tails in the BT-549 cells, but not in the MCF-7 and MDA-231 cells, increased significantly (182.47 (P=0.0008), 321391.66 (P=0.0002), and 60.12 (P=0.0024), respectively) (**Table 1** and **Figure 4A**). Similarly, knocking down *cGAS* and *LC3* in BT-549 cells by siRNA also increased the tail values in the comet assay (**Table 1**, P<0.001) (**Table 1** and **Figure 4A**). These results indicated that inhibition of autophagy could influence the status of DNA damage.

Moreover, TUNEL assays were performed to directly measure DNA breaks in breast cancer cells. BT-549 cells presented more TUNEL-positive cells than those of MCF-7, MDA-231, and the percentage of TUNEL-positive BT-549 cells was approximately

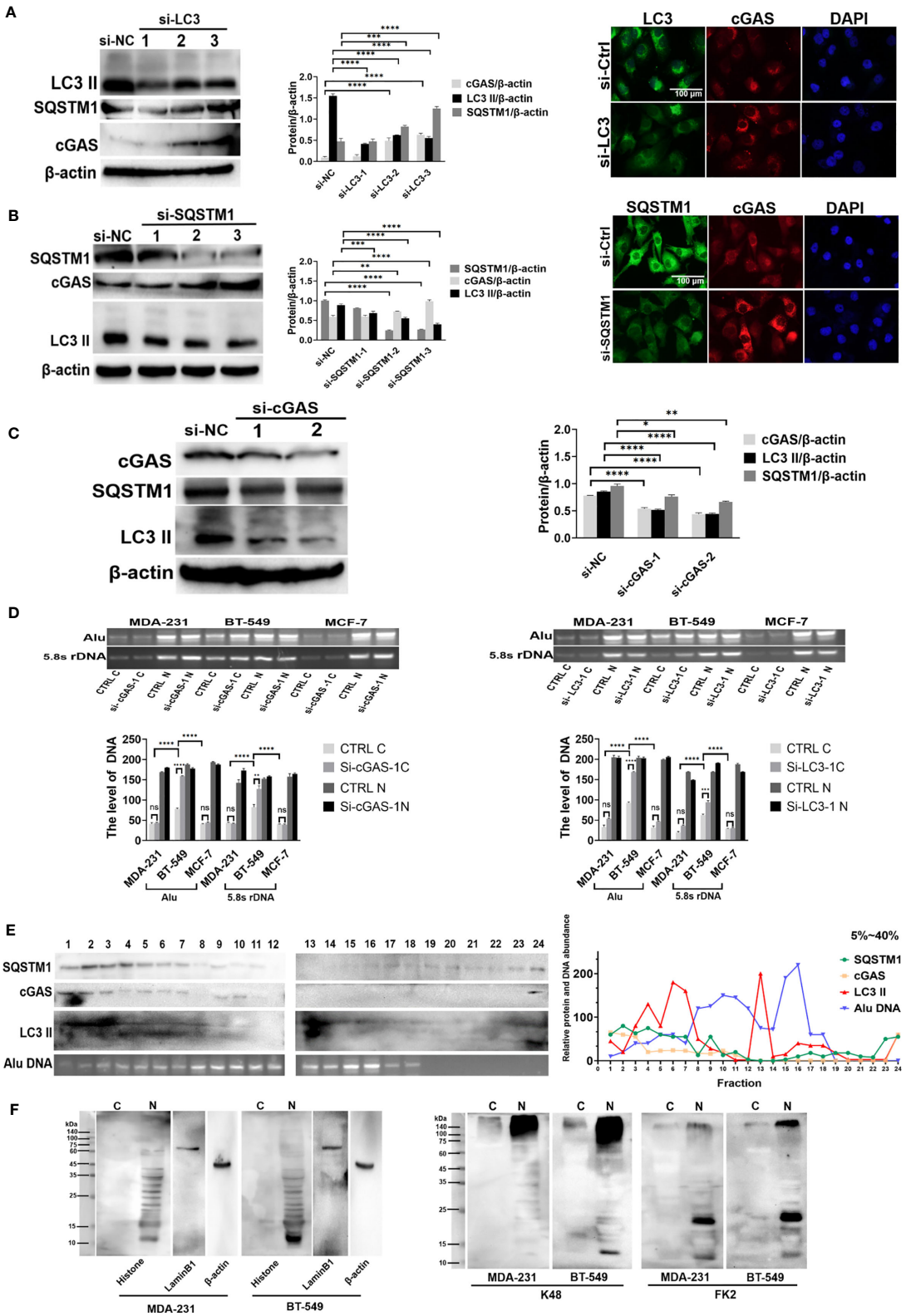

FIGURE 3 | Continued

FIGURE 3 | DNA autophagy in the cytoplasm was involved in the coordination of cGAS and SQSTM1. **(A)** The depletion of *LC3* increased the level of cGAS. After knockdown by *LC3* siRNA 1, 2, 3 in BT-549 cells, the level of cGAS was measured by Western blotting left panels), while the cellular distribution of LC3 (green) and cGAS (red) in the *LC3* siRNA 3-transfected cells was analyzed by immunofluorescence staining right panels). siNC: control iRNA. The experiments were repeated three times. Data are presented as mean ± SD. **(B)** The depletion of *SQSTM1* increased the level of cGAS but decreased LC3-II. After knockdown of *SQSTM1* by siRNA 1, 2, 3) in BT-549 cells, the levels of cGAS or LC3-II were measured by Western blotting left panels), and the c ellular distribution of cGAS and LC3 in the *SQSTM1* siRNA 3-transfected cells was analyzed by immunofluorescence staining right panels). siNC: control iRNA. The experiment repeated three times. Data are presented as mean ± SD. **(C)** The depletion of *cGAS* decreased the level of LC3-II. After knockdown by *cGAS* siRNA 1, 2 in BT-549 cells, the levels of LC3-II or SQSTM1 were measured by Western blotting. siNC: control iRNA. The experiment repeated three times. Data are presented as mean ± SD. **(D)** The silencing of autophagic genes increased the level of cytoplasmic DNA. Cytoplasmic or nuclear DNA was extracted from the MCF-7, MDA-231 and BT-549 cells or their corresponding cells with knockdown of *SQSTM1* or *LC3* by siRNA. The levels of cytoplasmic C) or nuclear N) DNA were measured by PCR amplification of Alu and 5.8S rDNA sequences, and the quantitative analysis was performed with the results of gel electrophoresis. The experiments were repeated three times. Data are presented as mean ± SD. **(E)** Sucrose density gradient analysis of the cytoplasmic fractions of the BT-549 cells. Cytoplasmic extracts from the BT-549 cells were isolated and fractioned through sucrose gradient centrifugation, and SQSTM1, cGAS, and LC3 II in each fraction were measured by Western blotting. Cytoplasmic genomic DNA in selected fractions was analyzed by Alu-based PCR amplification and gel electrophoresis. The amounts of the indicated proteins were quantified using ImageJ and plotted. The experiments were repeated three times. **(F)** Analysis of cytoplasmic histones and ubiquitination in breast cancer cells. Cytoplasmic or nuclear extracts from the MDA-231 or BT-549 cells were independently isolated by acid extraction and analyzed by Western blotting. Left panels: Core histone; middle panels: K48 antibody detection; right panels: FK2 antibody detection of mono- or polyubiquitinated proteins. The arrows indicate the putative histones. C, cytoplasmic; N, nuclear. The level of statistical significance was <0.05 *), <0.01 **), < 0.001 ***) and < 0.0001 ****). ns, no significance. The experiments were repeated three times, and the images are representative of repeated experiments.

TABLE 1 | The results of the Comet assay.

Cell lines		Tail length		Tail intensity		Tail movement	
		Mean	SD	Mean	SD	Mean	SD
MDA-231	Control	76.83	45.00	70319.47	59133.3	13.09	14.16
	Bafilomycin A1	87.43	43.28	69149.58	61988.6	16.14	20.33
	NC	78.88	46.56	69820.57	59621.2	12.78	13.21
	si-LC3	66.26	37.16	94829.15	116894	19.06	28.14
	si-cGAS	74.13	61.62	72505.77	72552.6	13.19	11.86
BT-549	Control	109.94(****)	39.37	185572.14(****)	139055	42.63(****)	25.33
	Bafilomycin A1	182.468(****)	71.71	321391.656(***)	183954	60.123(*)	51.03
	NC	100.67	45.72	189102.12	139234	45.22	25.43
	si-LC3	190.637(****)	81.25	484393.68(****)	136164	95.130(**)	35.25
	si-cGAS	163.324(****)	68.48	392065.161(***)	111780	70.662(**)	47.03
MCF-7	Control	70.59	41.03	75513.63	102705	15.66	21.45
	Bafilomycin A1	69.48	38.46	84516.05	114563	15.93	20.43
	NC	68.23	40.92	79333.41	99012.3	16.01	21.22
	si-LC3	59.94	30.88	95231.169(*)	100438	15.09	21.39
	si-cGAS	77.88	55.12	87188.13	93316.8	15.54	21.37

*Results are expressed as mean ± SD. (*p < 0.05, **p < 0.01, ***p < 0.001, ****p < 0.0001).*

35%, and the percentage of MDA-231 cells was 5% (P<0.05) (**Figure 4B**). Furthermore, the expression of ATM, ATR, and γ-H2AX in the MDA-231 and BT-549 cells further confirmed that the BT-549 cells generally had lower levels of ATM, ATR, and γ-H2AX, indicating a failure in the DNA damage response (**Figure 4C**).

Interestingly, the TUNEL assay also showed that the BT-549 cells presented TUNEL positivity not only in the nuclei but also in 30% of the MNs (**Figure 4B**), while there were no differences in 53BP1 or γ-H2AX staining in the MNs among the BT-549, MDA-231 and/or MCF-7 cells (**Supplementary Figure 4A**). However, in further DNA damage analysis, RPA2 (replication protein A2) and PICH (PLK1-interacting checkpoint helicase), the factors involved in DNA replication, were stained in breast cancer cells. Some MNs in the BT-549 cells, but not MDA-231 and/or MCF-7 cells, exhibited bright foci with RPA2 or PICH staining (**Figures 4D, E**), indicating DNA single or double breaks owing to DNA replication. Some MNs could be separately labeled by BrdU, indicating unscheduled DNA replication in the MNs (**Figure 4F**). More interestingly, immunofluorescence staining of pHH3 (phosphorylated histone 3), a marker of chromatin condensation, could be detected in some MNs, especially in the BT-549 cells, similar to mitotic cells, and pHH3-stained MNs were usually Lamin B1 negative (**Figure 4G**), which indicated that this DNA damage might be caused by a process similar to apoptosis in the MNs (25). The results indicated that at least a portion of cytoplasmic DNA possibly came from the collapse or degradation of MNs.

Taken together, the results suggested that free cytoplasmic DNA was involved in the DNA damage response failure and its consequential MN formation, part of which underwent collapse owing to replication and DNA damage.

Inhibition of DNA Autophagy Induced Growth Arrest or Cell Death of Cancer Cells

The above results demonstrated that breast cancer cells presented high DNA autophagic activity, which raised the

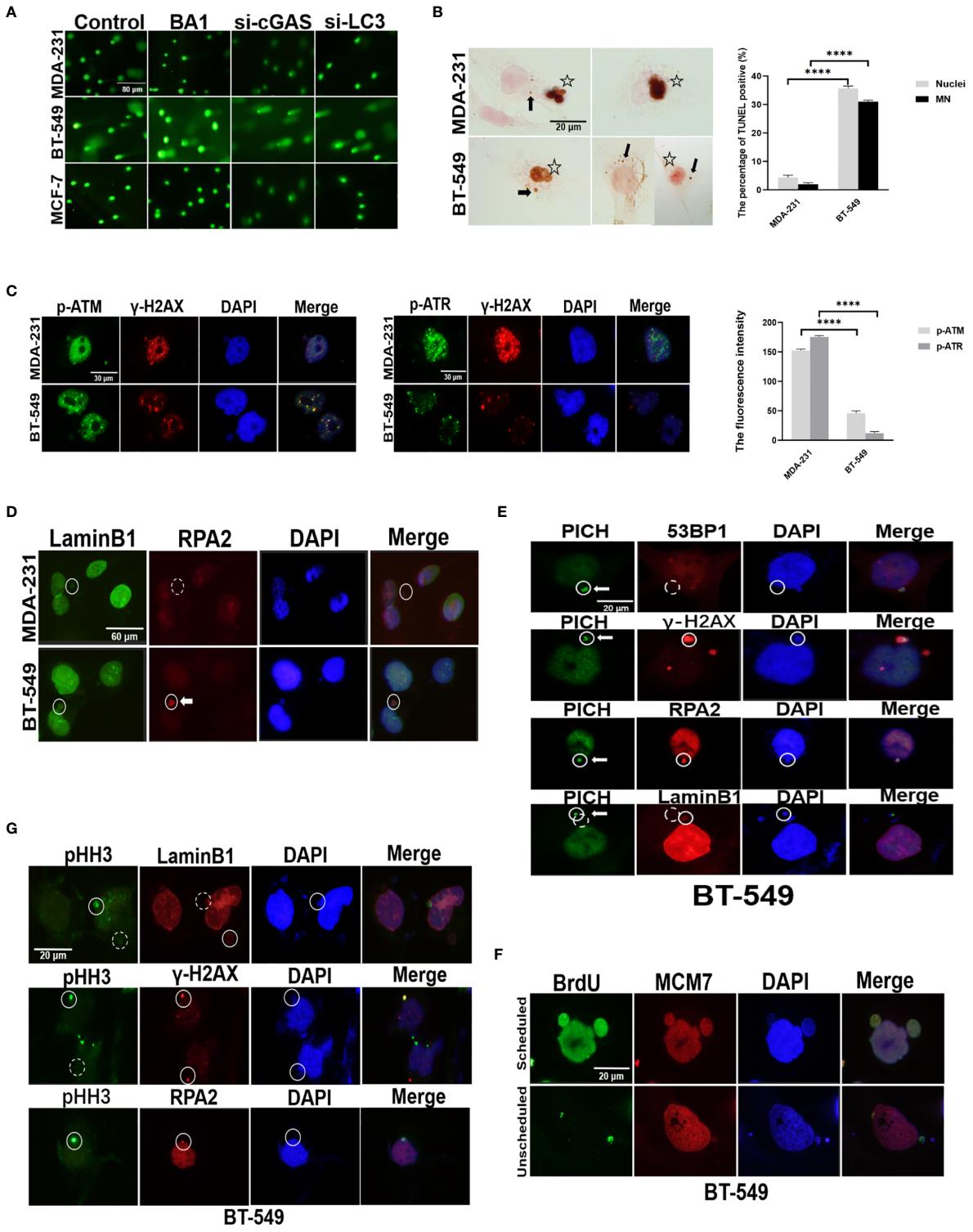

FIGURE 4 | Continued

FIGURE 4 | Genomic DNA in the cytoplasm could be derived from either damaged nuclei or MNs. **(A)** Comet assays of the status of DNA damage in breast cancer cells. The original MDA-231, BT-549 and MCF-7 cells, those in the presence of 10 nmol/L BAI bafilomycin A1) for 24 hours, or cells with silencing of cGAS or LC3 by transfection with either si-cGAS or si-LC3 for 48 hours were subjected to comet assays. Their more detailed data are summarized in **Table 1**. The experiments were repeated three times. **(B)** TUNEL analysis of breast cancer cells. A TUNEL assay was carried out on the MDA-231 and BT-549 cells, and positive staining in the nucleus and/or MNs was evaluated in whole slides and is presented as percentages. The experiments were repeated three times. Data are presented as mean ± SEM. Arrows indicate positive MNs, while stars label positive nuclei. **(C)** The status of DNA damage in breast cancer cells. The MDA-231 and BT-549 cells were stained for γ-H2AX and p-ATM or p-ATR, respectively left panels). The staining intensity was evaluated and plotted right panel). The experiments were repeated three times. Data are presented as mean ± SD. **(D)** Double staining of RPA2 and Lamin B1 was performed in the MDA-231 and BT-549 cells. Solid circles label positive staining, and dashed circles indicate weak or negative staining. Arrow indicates RPA2 foci in MNs. The experiments were repeated three times. **(E)** Double staining of PICH and RPA2 or 53BP-1 or γ-H2AX or Lamin B1 was performed in the BT-549 cells. Solid circles indicate positive staining, and dashed circles indicate weak or negative staining. Arrows indicate PICH foci in MNs. The experiments were repeated three times. **(F)** BrdU incorporation assays. After incubation with BrdU for 30 minutes, the BT-549 cells were doubly stained with BrdU and MCM7. Arrows indicate unscheduled replication in MNs. **(G)** Analysis of DNA damage in the MNs in breast cancers. Double staining of Lamin B1, RPA2 or γ-H2AX and pHH3 was performed in the BT-549 cells. Solid circles indicate highly stained MNs, and dashed circles indicate negative or weak staining of MNs. The experiment repeated three times. The level of statistical significance was < 0.0001 ****). The images are representative of repeated experiments.

question of whether autophagy influences the biological activity of this kind of cancer cell.

To further determine the role of autophagy in breast cancer cells, we grew MCF-7, MDA -231 and BT-549 cells in the presence of bafilomycin A1 at various concentrations (0 nmol/L, 1 nmol/L, 5 nmol/L, 10 nmol/L) for 72 hours, and the results showed that the growth of both the MDA-231 and BT-549 cells was inhibited in a dose-dependent manner (**Figure 5A**). However, the BT-549 cells showed cytotoxicity in the presence of 10 nmol/L bafilomycin A1. This finding was confirmed by time course analysis, in which the BT-549 cells with high autophagic activity died after treatment with 10 nmol/L bafilomycin A1 for 72 hours, while the MDA-231 cells only showed growth inhibition (**Figure 5A**).

Similarly, after further treatment of the MCF-7, MDA-231 and BT-549 cells with different concentrations of CQ (0 μmol/L, 5 μmol/L, 50 μmol/L, 100 μmol/L) for 72 hours, cell survival and growth were evaluated (**Figure 5B**).

The effects of cGAS or SQSTM1 expression on cell growth and survival of breast cancer cells were also clarified through silencing of either cGAS or SQSTM1 in the MCF-7, MDA-231 and BT-549 cells. The viability of the BT-549 cells was markedly reduced after either si-cGAS or si-SQSTM1 silencing. However, the MCF-7, MDA-231 and HeLa cells were not affected significantly (**Figure 5C**). Similarly, the BT-549 cells, but not MDA-231 cells, were inhibited by treatment with the STING antagonist H-151 (2 μmol/L, 10 μmol/L, 20 μmol/L) for 24 hours (**Supplementary Figure 5A**).

To further clarify inhibition of autophagy to DNA autophagy under enhanced DNA damage, MCF-7, MDA-231, HeLa cells treated with Hydroxyurea (26) (0.5mmol/L) or Aphidicolin (27) (1μmol/L), which could not only induce cytoplasmic accumulation of cGAS/SQSTM1, but also became sensitive to the inhibitors of CQ (50 μmol/L) or bafilomycinA1 (10 nmol/L) (**Figure 5D** and **Supplementary Figures 5B–D**).

To further expand the observation of DNA autophagic inhibition to cell activity, we screened a series of human cancer cells with immunofluorescence double-staining of cGAS and SQSTM1, and HCT116, 786-0, PC3M, and DU145 cells were screened. Three categories of cancer cells—cells with high cGAS and SQSTM1 (786-0 and PC3M), low cGAS and SQSTM1 (HeLa and HCT116), and high SQSTM1 but low cGAS (DU145)—were selected (**Figure 5E**). In further analysis, the survival of 786-0 cells with strong cGAS and SQSTM1 expression was reversely to the treatment of CQ or bafilomycin A1 in a dose-dependent way (**Figure 5F**), and the PC3M cells were also reduced significantly in the treatment of CQ (50 μmol/L) or bafilomycin A1 (10 nmol/L) (**Figure 5G**). In contrast, HCT116 cells with low levels of cGAS and SQSTM1 were not significantly affected with the treatment of CQ (50 μmol/L) or bafilomycin A1 (10 nmol/L) (**Figure 5G**). In similar, DU145 cells with high SQSTM1 but low cGAS levels were not affected in above treatments (**Figure 5G**). The results implied that the growth or survival of cancer cells with high DNA autophagy was sensitive to autophagic inhibition.

To explore the cell death induced by DNA autophagic inhibition, we analyzed the CQ- or bafilomycin A1-treated MCF-7, MDA-231 and BT-549 cells, and the active form of caspase-3 was not detected by staining (**Figure 5H**). Therefore, caspase-independent cell death (CICD) was investigated. Autophagy-related CICD could be achieved through lysosomal membrane permeabilization (LMP), but because CQ is an LMP inducer and bafilomycin A1 is an LMP inhibitor, LMP-induced cell death could be ruled out. Alternatively, CICD is usually mediated by increasing ROS (reactive oxygen species) owing to mitochondrial outer-membrane permeabilization (MOMP). The production of ROS was measured in the presence of CQ and bafilomycin A1 by dihydroethidium (1 mmol/L), and the results showed that either CQ or bafilomycin A1 could increase ethidium-stained BT-549 cells but only slightly affected the MDA-231 or MCF-7 cells (**Figure 5I**), confirming that CQ or bafilomycin A1 treatment could induce caspase-independent cell death in the BT-549 cells.

The results demonstrated that DNA autophagy could be necessary for the survival of cancer cells by clearing cytoplasmic free DNA to protect against cell death.

DISCUSSION

Autophagy is an important adaptive process to recycle substances or clear damaged organelles. For decades, autophagy has been thoroughly elucidated in terms of its process, forms, regulation and biological roles (28). DNA autophagy has also been identified,

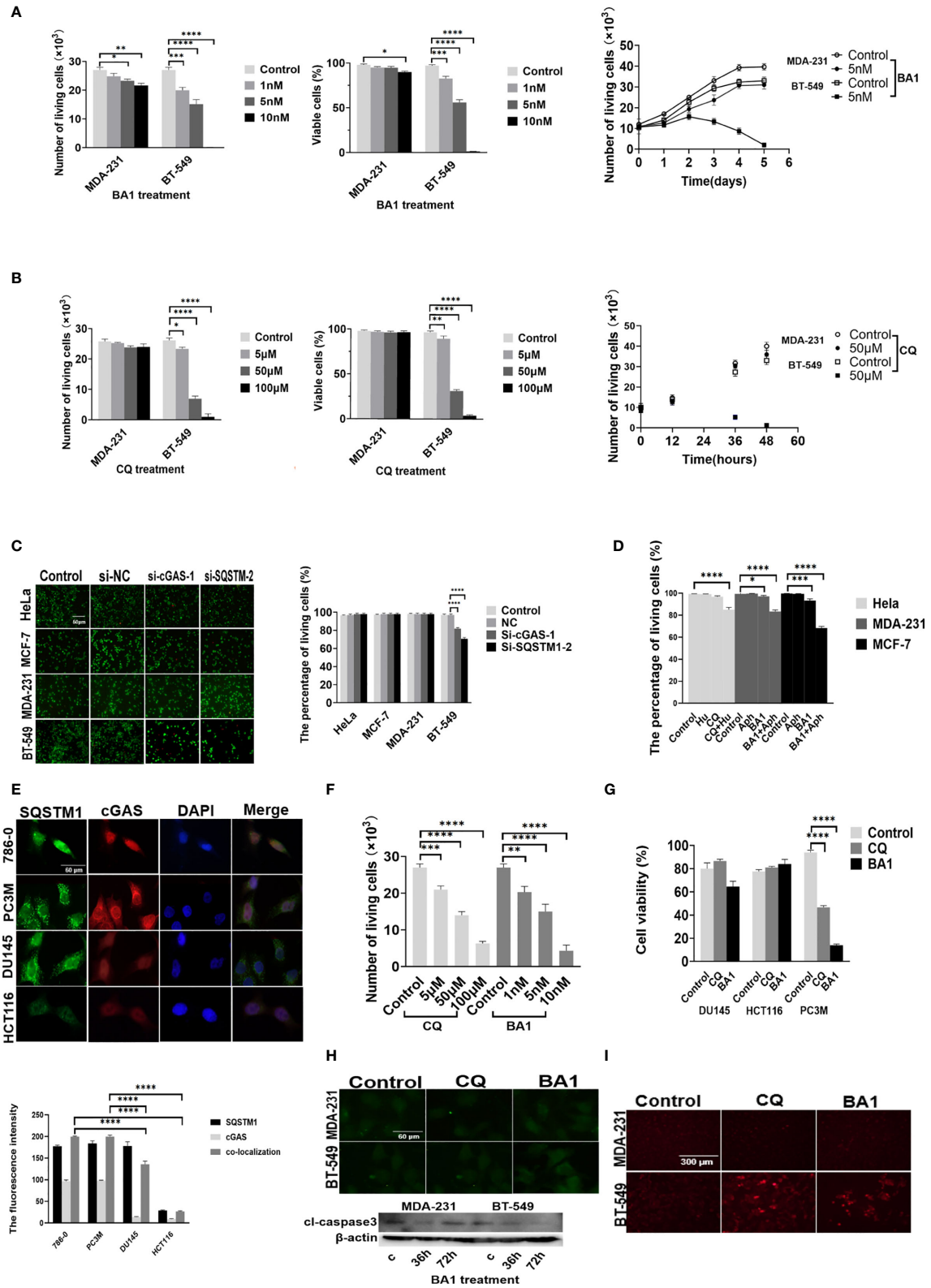

FIGURE 5 | Continued

FIGURE 5 | Inhibition of DNA autophagy induced growth arrest or cell death of cancer cells. **(A, B)** The effects of autophagic inhibition on the survival and growth of breast cancer cells. Left: MDA-231 and BT-549 cells were treated with the indicated concentrations of BA1 bafilomycin A1) or CQ for 36 hours, and cell viability was measured. Right: The growth of the MDA-231 and BT-549 cells was analyzed in the presence of 10 nmol/L BA1 or 50 μmol/L CQ for the indicated days. Cell viability was measured by Trypan blue exclusion assays. **(C)** The effects of downregulation of either cGAS or SQSTM1 on the survival of cancer cells. The MDA-231, BT-549, MCF-7 and HeLa cells were transfected with si-cGAS and si-SQSTM1 for 48 hours, and the post-transfection cell viability was analyzed by live and dead assays. **(D)** Enhancement of DNA damage sensitized cancer cells to autophagic inhibitors. The MCF-7, MDA-231, and HeLa cells were treated with hydroxyurea 0.5 mmol/L) or aphidicolin 1 μmol/L) for 4 hours and then further incubated in the presence of CQ 50 μmol/L) or bafilomycin A1 10 nmol/L) for 36 hours. Cell viability was analyzed by live and dead assays. **(E)** Upper panel: Double staining of SQSTM1 green) and cGAS red) was performed in the 786-0, HCT116, DU145 and PC3M cells. Lower panel: The quantification of immunofluorescence co-localization in three cells. **(F)** The 786-0 cells were treated with the indicated concentrations of CQ or BA1 for 36 hours. Cell viability was measured by live and dead assays. **(G)** The effects of autophagic inhibition on the survival of cancer cells. The HCT116, DU145 and PC3M cells were treated with CQ 50 μmol/L) or bafilomycin A1 BA110 nmol/L) for 36 hours, and cell viability was measured by MTS assays. **(H)** Detection of the active form of caspase-3 in the autophagy-inhibited breast cancer cells. The MDA-231 and BT-549 cells were treated with either CQ 50 μmol/L) or BA1 bafilomycin A1, 10 nmol/L) for 36 hours, stained for cl-caspase3 by immunofluorescence upper) and measured by Western blotting lower). **(I)** The inhibition of autophagy induced caspase-independent cell death in the BT-549 cells. After treatment with either CQ 50 μmol/L) or BA1 bafilomycin A1, 10 nmol/L) for 36 hours, the BT-549 cells were incubated *in vivo* with dihydroethidium 1 mmol/L) for 30 minutes, and ethidium-stained cells were counted in a total of 500 cells. The images are representative of repeated experiments. The level of statistical significance was <0.05*), < 0.01 **), < 0.001 ***), and < 0.0001 ****). Each of experiments was performed in triplicate, and all experiments were independently repeated at least three times. The images are representative of repeated experiments. Results are expressed as mean ± SEM.

especially as a mechanism against exogenous invasion of organisms, and is considered an innate immune mechanism (29) However, apparently, unlike that of other substances, autophagy of genomic DNA, the cellular genetic materials, is difficult to be considered for multicellular organisms. Nevertheless, in unicellular lower eukaryotes such as yeasts, DNA autophagy, in which cell nuclei can undergo autophagy by well-established regulatory pathways for nucleophagy through either piecemeal microautophagy of the nucleus (PMN) or late nucleophagy, has been identified (29). Even entire nuclei could be degraded by macroautophagy in filamentous fungi. For mammalian cells, MN-related nucleophagy has been described occasionally, but mechanistically, its detailed process is still elusive. Mammalian cells have a nuclear lamina structure, which is different from that of lower eukaryotes, such as yeasts, with no comparable lamins or a fibrous nuclear envelope scaffold (29). Nevertheless, nucleophagy is considered to play an important role in maintaining cellular genomic stability, detecting DNA damage, and regulating cellular apoptosis, as well as cellular senescence (30, 31). MN assays showed increased MN frequencies in breast cancer lymphocytes, which were correlated with the progression of breast cancer (32). MNs are abnormal components that exists in the cytoplasm, independent of the nuclear nucleus. Autophagy also contributes to the elimination of MN (29). However, for most cancer cells, MNs can persist, arguing the general elimination of MNs by nucleophagy. In addition, similar to other studies, our investigations showed that cGAS and/or SQSTM1 could be detected in some MNs. However, the percentage of MNs with colocalization was low even in the highly abundant MNs in the BT-549 cells. Nucleophagy was not a prevalent event in cancer cells. A previous report showed the interaction between Lamin B1 and LC3 and suggesting that it is a nucleophagic mechanism (25). However, we still did not observe such interactions in our experiments, for instance, in BT-549, MDA-231 or 786-0 cells, all of which usually showed a relatively high frequency of MN formation. Another possibility could not be ruled out: MNs undergoing nucleophagy could directly fuse with lysozyme, but this hypothesis needs to be further explored.

Selective DNA autophagy (33) has been well clarified in mammalian cells. It has been demonstrated that free DNA or RNA could directly mediate microautophagy *via* LAMP2 (lysosome-associated membrane protein 2) without the need for LC3 or other autophagic factors, but the nucleic acid transporter SIDT2 (SID1 transmembrane family member 2, SIDT2) is an integral lysosomal membrane protein for translocation into the lysosomal lumen (34). Nevertheless, specific DNA sensors, such as cGAS-STING, have also been revealed to participate in DNA autophagic initiation. cGAS binds to DNA (in MNs or free) and recruits Beclin-1 and STING, promoting autophagy. cGAS generates cGAMP and stimulates the STING-Golgi apparatus, but some studies have also shown that STING itself could mediate autophagy after its binding to DNA, and the intrinsic domains of STING could directly interact with LC3 (8). In a recent report, exogenous plasmids were first recognized by DAI/ZBP1 (DNA-dependent activator of interferon regulatory factors/Z-DNA binding protein 1) but not cGAS (35). However, in our study, upon introducing genomic DNA into the MCF-7, MDA-231 or BT-549 cells, we found that cytosolic inclusions of various sizes were positive for cGAS, LC3 and lysosomes, confirming DNA autophagy (**Supplementary Figure 6**). However, few inclusions were Beclin-1 positive (**Supplementary Figure 6**). Therefore, it seemed that cytoplasmic DNA autophagy might involve different forms owing to the source of DNA and especially the DNA status and its level, nucleophagy, and selective autophagy. Apparently, the molecular mechanism could be diverse, such as LC3-dependent or LC3-independent DNA sensors. In actual conditions, free DNA is not naked but is instead usually bound to nuclear proteins. Therefore, genomic DNA from MN collapse or nuclear release might trigger a more complicated autophagic reaction to both DNA and proteins, especially ubiquitination (see below).

In recent years, extensive research has demonstrated that SASP is activated by the cGAS-STING pathway, and its proinflammatory role has been demonstrated to be crucial for the occurrence of autoinflammatory disorders, age-related diseases

and even cancer progression (8). However, either cGAS or STING alone or their combination could mediate DNA autophagy (8). The described data also indicated that cGAS could play an important role in autophagy. These findings raise an important question of how the decision to choose SASP or autophagy is made in cells. Our research showed that autophagy was usually found in cells with profound DNA damage, while increased DNA damage could induce DNA autophagic activity, indicating that the extent of DNA damage could be a factor influencing this determination. cGAS-mediated SASP and autophagy could respond to DNA damage. Severe DNA damage should be cleared by autophagy, but relatively less severe damage triggers SASP. Apparently, the cellular ability of DNA damage repair could also be a factor. These findings raise the question of whether there is any difference between cGAS in mediating SASP and autophagy. The details of cGAS recognition of DNA to induce autophagy or SASP are still unclear. However, more importantly, released genomic DNA from the cytoplasm is not protein-free but is instead bound with histones or other nuclear proteins (36). The complex of DNA and protein could more easily activate autophagic activity since histones are usually ubiquitinated and generally recognizable by SQSTM1. To date, many studies have observed that SQSTM1 could be detected in the cell nucleus by either tagged SQSTM1 or immunohistochemistry (24). In fact, the nuclear localization signal of SQSTM1 has been revealed, and its nuclear translocation has been demonstrated to be involved in the DNA damage response (37, 38). Therefore, the cytoplasmic or nuclear distribution of SQSTM1 could be similar. Thus, it is more likely that with severe DNA damage or repair failure, a relative amount of genomic DNA with coated proteins is released into the cytoplasm to trigger an autophagy-mediated clearance response.

Recent reports suggest that activation of cGAS upon binding to DNA could trigger activation of STING, leading to either SASP or autophagy, and MCF-7, MDA-231 and BT-549 cells presented different endogenous levels of STING or phosphorylated STING, which was consistent with their SASP and autophagic phenotypes (**Figures 1B, C**). Moreover, endogenous or exogenous STING was present in a few cytoplasmic vesicles in the MCF-7 and MDA-231 cells but was distributed in the Golgi apparatus in the BT-549 cells and could be disrupted by brefeldin A (BFA) (**Supplementary Figure 3C**). In the BT-549 cells, the level of STING markedly increased in the presence of bafilomycin A1 (10 nmol/L) (**Figure 2D**) or with downregulation of *DNase II* (**Supplementary Figure 3D**). However, after treatment of the BT-549 cells with either the STING antagonist H-151 (2 μmol/L) or agonist cGAMP (300 nmol/L) for 24 hours, SQSTM1 or LC3 presented no change in immunofluorescence staining. Thus, degradation of STING may be involved in the autophagic process, while its activity in the regulation of autophagy in BT-549 cells requires further exploration.

Cytoplasmic DNA can easily be derived from mitochondria, organelles in the cytoplasm, but the mechanism by which genomic DNA accumulates in the cytoplasm is still unclear. MN formation is believed to be a major source since various reports have shown that MNs from some cancer cells are not intact in their nuclear lamina due to RB deficiency (39). Indeed, defects in nuclear membrane assembly, either aberrant nuclear pore complexes NPCs) or nuclear lamina defects owing to lamina gene mutations, have been shown to result in nuclear irregularity, lobulation or MN formation to cause cellular senescence and the SASP (6). More than 60% of MNs are disrupted, and then, damaged DNA is released (6, 39) However, in our investigation, as well as a previous report (18), MNs formed in a variety of cancer cell lines, including breast, colorectal, cervical and kidney cancer cell lines, generally had intact nuclear lamina proteins, such as Lamin A/C or B or their receptor LBR, nuclear pore complex Nup153), TPR blanked protein), and integral membrane proteins Sun2, nesprin2) (40). Nuclear rupture did not appear to be a prevalent event for cancer cells, and cytoplasmic DNA from MNs needs to be further explored. Similar to its main nucleus, MNs can undergo various activities, including replication, transcription and DNA damage. Chromothripsis has been demonstrated to be a consequence of DNA damage in MNs (10). This research also showed that unscheduled DNA replication and DNA damage could be detected in a portion of the MNs. Interestingly, some BT-549 cells with abundant MNs more frequently presented condensed focal staining of RPA2 or PICH, both of which participate in the DNA damage response; the former usually binds to single-stranded DNA, and the latter binds to double-stranded DNA (41, 42). More importantly, some MNs were frequently observed in pHH3-positive cells, similar to BT-549 cells (**Figure 4F**). It has been acknowledged that pHH3 is mainly found during chromatin condensation in mitosis and in apoptotic nuclei of cells (43, 44). For determination of whether pHH3-positive MNs undergo mitosis, cells were stained for Hec1 (45), a protein involved in kinetochore assembly. The results proved that no MNs were positive, but only mitotic and apoptotic cells were stained. In a cell-free apoptotic model, nuclear condensation could sequentially proceed with condensation, a nuclear necklace, collapse or disassembly (25, 35). Similarly, pHH3-stained MNs also presented these morphological changes (**Figure 4F**), indicating that MNs could undergo collapse owing to replication and damage. Accordingly, a portion of the MNs in the BT-549 cells showed positive staining of RPA2 and PICH, especially in the foci-staining pattern (**Figures 4D, E**), indicating severe DNA damage in these MNs. Apparently, the more MNs formed, the more frequently breakage was detected. In addition, the release of nuclear eccrDNA extrachromosomal circular rDNA) should be another source of cytoplasm see below).

Since MN formation can be generally induced by a variety of genotoxic agents, DNA damage is reasonably considered a key process, and aberrant mitosis is widely accepted (6, 12). However, recent studies have suggested that for cancer cells, DNA replication stress could be a likely common mechanism (41, 46–48). Oncogenic mutations induce accelerated DNA replication and trigger replication stress. The so-called common fragile sites in the genome, such as rDNA, are difficult to replicate, and stalled or collapsed replication forks usually induce the formation of UFBs ultrafine bridges) or lagging chromosomes to result in MN formation or to generate free DNA fragments, such as eccrDNA, which are hard to enclose in the late phase of mitosis during nuclear membrane assembly and are consequently released

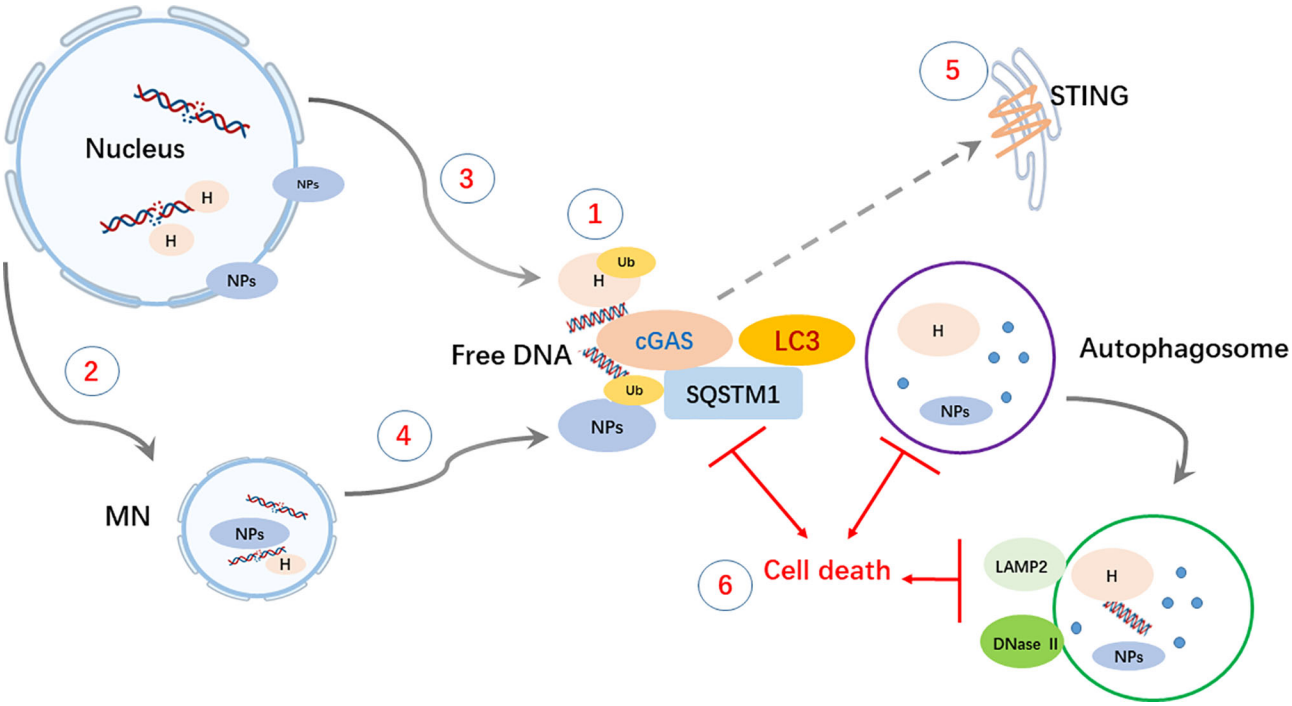

FIGURE 6 | Schematic summary of the main findings. Cytoplasmic DNA autophagy is initiated by the binding of cGAS to free DNA and may be coordinately accompanied by the recognition of ubiquitinated Ub) histones H) or nuclear proteins NPs) by SQSTM1. ① Cytoplasmic DNA and proteins) could be derived from either DNA replication-related nuclear damage ② and consequent MN formation ③, which would undergo collapse owing to its unscheduled replication ④. ⑤ The degradation of STING could be involved in autophagy and result in a failure to activate SASP activity, but the role of STING in DNA autophagy still needs further exploration. ⑥ Generally, in autophagy, free DNA and proteins are enclosed in autophagosomes *via* LC3 lipidation and degraded after fusion with LAMP2- and DNase II-containing lysosomes. The clearance of cytoplasmic DNA by autophagy could play a protective role in maintaining the growth and survival of cancer cells, and thus, disruption of the process could lead to caspase-independent cell death CICD).

to the cytoplasm (16, 42). In our investigation, in addition to MNs, cytoplasmic DNA from the genome, including Alu-repeated sequences and rDNA, was easily detected, indicating a replication stress-related mechanism. Moreover, intra-S phase checkpoints mediated by ATR and ATM kinases are crucial to replication stress, and their deficiency causes replication stress-related DNA damage (49). The BT-549 cells generally had low levels of pATM and pATR and high formation of MNs and cytoplasmic DNA as well as strong TUNEL staining, suggesting relationships between these factors.

Autophagy is a form of cellular activity that adapts to endogenous and environmental changes. Although gene mutations related to the regulation of autophagy have been clarified in tumorigenesis, for some kinds of cancer cells, inhibition of autophagy could promote their growth and survival, indicating that autophagic activity could be necessary for these cancer cell (50). However, how to determine the sensitivity of cancers to autophagic inhibition is still not established. Meanwhile, some studies have shown that the inhibition of autophagy can affect the viability of cancer cells (51). This investigation showed that inhibition of DNA autophagy could decrease cell viability, suggesting its potential therapeutic utility in cancer treatment, especially for cancer cells deficient in DNA repair. In recent years, DNA damage repair deficiency has been successfully used in cancer therapy; for instance, cancers with MSI microsatellite instability) can be treated with immune checkpoint blockade-based immunotherapies, while genomic mutations of BRCA1/2 or HRR homologous recombination repair) are targets of PARP inhibitors. DDR deficiency has been considered a promising anticancer target (52–54) Targeting autophagy could be another approach to treat DDR-deficient cancers.

In summary (**Figure 6**), our investigation revealed DNA autophagy in breast cancer cells with high MN formation. Autophagy of genomic DNA in the cytosol could be mediated by cGAS but is usually coordinated with other autophagic mediators. Cytoplasmic DNA could be derived from DNA replication-induced damage and MN collapse. The clearance of cytoplasmic DNA could be necessary for cancer cell growth and survival. Thus, autophagic inhibition could be a potential therapeutic approach for cancer cells with high DNA autophagic activity. Nevertheless, we acknowledged that our major evidences came from BT-549, there will be further work in BT-549 like breast or other cancer cells to solid our conclusions.

DATA AVAILABILITY STATEMENT

The original contributions presented in the study are included in the article/**Supplementary Material**. Further inquiries can be directed to the corresponding author.

AUTHOR CONTRIBUTIONS

MY and YW performed experiments and analyzed the data. YNC, NM, and YJC conducted the statistical analyses. BZ and MY designed the study and wrote the manuscript. YW and HL revised manuscript. HZ, SZ, LN, and LL assisted some experiments. All authors contributed to the article and approved the submitted version.

FUNDING

This project was supported by the National Natural Science Foundation of China No. 81872018) and the Key Project from the Chinese Ministry of Science and Technology No. 2017 FC0110200).

ACKNOWLEDGMENTS

We thank Dr. Dawei Xu and Cheng Liu for their kind suggestions to the manuscript and appreciate Mr. Hongquan Shao and Mr. Ning Li for helpful technique support.

SUPPLEMENTARY MATERIAL

The Supplementary Material for this article can be found online at: https://www.frontiersin.org/articles/10.3389/fonc.2021.667920/full#supplementary-material

REFERENCES

1. Ablasser A, Goldeck M, Cavlar T, Deimling T, Witte G, Röhl I, et al. cGAS Produces a 2'-5'-Linked Cyclic Dinucleotide Second Messenger That Activates STING. *Nature* (2013) 498(7454):380–4. doi: 10.1038/nature12306
2. Chen Q, Sun L, Chen ZJ. Regulation and Function of the cGAS-STING Pathway of Cytosolic DNA Sensing. *Nat Immunol* (2016) 17(10):1142–9. doi: 10.1038/ni.3558
3. Coppé JP, Patil CK, Rodier F, Sun Y, Muñoz DP, Goldstein J, et al. Senescence-associated Secretory Phenotypes Reveal Cell-Nonautonomous Functions of Oncogenic RAS and the p53 Tumor Suppressor. *PloS Biol* (2008) 6(12):2853–68. doi: 10.1371/journal.pbio.0060301
4. Sun L, Wu J, Du F, Chen X, Chen ZJ. Cyclic GMP-AMP Synthase is a Cytosolic DNA Sensor That Activates the Type I Interferon Pathway. *Sci New Y NY)* (2013) 339(6121):786–91. doi: 10.1126/science.1232458
5. Loo TM, Miyata K, Tanaka Y, Takahashi A. Cellular Senescence and Senescence-Associated Secretory Phenotype Via the cGAS-STING Signaling Pathway in Cancer. *Cancer Sci* (2020) 111(2):304–11. doi: 10.1111/cas.14266
6. Li T, Chen ZJ. The cGAS-cGAMP-STING Pathway Connects DNA Damage to Inflammation, Senescence, and Cancer. *J Exp Med* (2018) 215(5):1287–99. doi: 10.1084/jem.20180139
7. Hinds P, Pietruska J. Senescence and Tumor Suppression. *F1000Research* (2017) 6:2121. doi: 10.12688/f1000research.11671.1
8. Gui X, Yang H, Li T, Tan X, Shi P, Li M, et al. Autophagy Induction *Via* STING Trafficking is a Primordial Function of the cGAS Pathway. *Nature* (2019) 567(7747):262–6. doi: 10.1038/s41586-019-1006-9
9. Li X, Shu C, Yi G, Chaton CT, Shelton CL, Diao J, et al. Cyclic Gmp-AMP Synthase is Activated by Double-Stranded DNA-induced Oligomerization. *Immunity* (2013) 39(6):1019–31. doi: 10.1016/j.immuni.2013.10.019
10. Kisurina-Evgenieva OP, Sutiagina OI, Onishchenko GE. Biogenesis of Micronuclei. *Biochem Biokhimiia* (2016) 81(5):453–64. doi: 10.1016/j.immuni.2013.10.019
11. Jdey W, Thierry S, Popova T, Stern MH, Dutreix M. Micronuclei Frequency in Tumors is a Predictive Biomarker for Genetic Instability and Sensitivity to the DNA Repair Inhibitor Asidna. *Cancer Res* (2017) 77(16):4207–16. doi: 10.1158/0008-5472
12. Lewis CW, Golsteyn RM. Cancer Cells That Survive Checkpoint Adaptation Contain Micronuclei That Harbor Damaged DNA. *Cell Cycle Georgetown Tex)* (2016) 15(22):3131–45. doi: 10.1080/15384101.2016.1231287
13. Liu H, Zhang H, Wu X, Ma D, Wu J, Wang L, et al. Nuclear cGAS Suppresses DNA Repair and Promotes Tumorigenesis. *Nature* (2018) 563(7729):131–6. doi: 10.1080/15384101.2016.1231287
14. Mackenzie KJ, Carroll P, Martin CA, Murina O, Fluteau A, Simpson DJ, et al. cGAS Surveillance of Micronuclei Links Genome Instability to Innate Immunity. *Nature* (2017) 548(7668):461–5. doi: 10.1038/nature23449
15. Bakhoum SF, Ngo B, Laughney AM, Cavallo JA, Murphy CJ, Ly P, et al. Chromosomal Instability Drives Metastasis Through a Cytosolic DNA Response. *Nature* (2018) 553(7689):467–72. doi: 10.1038/nature25432
16. Liao Z, Jiang W, Ye L, Li T, Yu X, Liu L. Classification of Extrachromosomal Circular DNA With a Focus on the Role of Extrachromosomal DNA ecDNA) in Tumor Heterogeneity and Progression. *Biochim Biophys Acta Rev Cancer* (2020) 1874(1):188392. doi: 10.1016/j.bbcan.2020.188392
17. Banoth B, Cassel SL. Mitochondria in Innate Immune Signaling. *Trans Res: J Lab Clin Med* (2018) 202:52–68. doi: 10.1016/j.trsl.2018.07.014
18. Cao Y, Yao M, Wu Y, Ma N, Liu H, Zhang B. N-Acetyltransferase 10 Promotes Micronuclei Formation to Activate the Senescence-Associated Secretory Phenotype Machinery in Colorectal Cancer Cells. *Transl Oncol* (2020) 13(8):100783. doi: 10.1016/j.tranon.2020.100783
19. Fernandez-Martinez J, LaCava J, Rout MP. Density Gradient Ultracentrifugation to Isolate Endogenous Protein Complexes After Affinity Capture. *Cold Spring Harb Protoc* (2016) 2016(7):624–7. doi: 10.1101/pdb.prot087957
20. Murray K. The Acid Extraction of Histones From Calf Thymus Deoxyribonucleoprotein. *J Mol Biol* (1966) 15(2):409–19. doi: 10.1016/s0022-2836(66)80116-x
21. Kao J, Salari K, Bocanegra M, Choi YL, Girard L, Gandhi J, et al. Molecular Profiling of Breast Cancer Cell Line s Defines Relevant Tumor Models and Provides a Resource for Cancer Gene Discovery. *PloS One* (2009) 3;4(7):e6146. doi: 10.1371/journal.pone.0006146
22. Comşa Ş, Cîmpean AM, Raica M. The Story of MCF-7 Breast Cancer Cell Line: 40 Years of Experience in Research. *Anticancer Res* (2015) 35(6):3147–54.
23. Sundelin SP, Terman A. Different Effects of Chloroquine and Hydroxychloroquine on Lysosomal Function in Cultured Retinal Pigment Epithelial Cells. *APMIS: Acta Pathol Microbiol Immunol Scandinavica* (2002) 110(6):481–9. doi: 10.1034/j.16000463.2002.100606.x
24. Wang Y, Zhang N, Zhang L, Li R, Fu W, Ma K, et al. Autophagy Regulates Chromatin Ubiquitination in DNA Damage Response Through Elimination of SQSTM1/P62. *Mol Cell* (2016) 63(1):34–48. doi: 10.1016/j.molcel.2016.05.027
25. Toné S, Sugimoto K, Tanda K, Suda T, Uehira K, Kanouchi H, et al. Three Distinct Stages of Apoptotic Nuclear Condensation Revealed by Time-Lapse Imaging, Biochemical and Electron Microscopy Analysis of Cell-Free Apoptosis. *Exp Cell Res* (2007) 313(16):3635–44. doi: 10.1016/j.yexcr.2007.06.018
26. Kanu N, Cerone MA, Goh G, Zalmas LP, Bartkova J, Dietzen M, et al. DNA Replication Stress Mediates APOBEC3 Family Mutagenesis in Breast Cancer. *Genome Biol* (2016) 17(1):185. doi: 10.1186/s13059-016-1042-9
27. Oo ZY, Proctor M, Stevenson AJ, Nazareth D, Fernando M, Daignault SM, et al. Combined Use of Subclinical Hydroxyurea and CHK1 Inhibitor Effectively Controls Melanoma and Lung Cancer Progression, With Reduced Normal Tissue Toxicity Compared to Gemcitabine. *Mol Oncol* (2019) 13(7):1503–18. doi: 10.1002/1878-0261.12497

28. Yu L, Chen Y, Tooze SA. Autophagy Pathway: Cellular and Molecular Mechanisms. *Autophagy* (2018) 14(2):207–15. doi: 10.1080/15548627.2017.1378838
29. Mijaljica D, Devenish RJ. Nucleophagy at a Glance. *J Cell Sci* (2013) 126(Pt 19):4325–30. doi: 10.1080/15548627.2017.1378838
30. Bo Otto F, Thumm M. Nucleophagy-Implications for Microautophagy and Health. *Int J Mol Sci* (2020) 21(12):4506. doi: 10.3390/ijms21124506
31. Fu N, Yang X, Chen L. Nucleophagy Plays a Major Role in Human Diseases. *Curr Drug Targets* (2018) 19(15):1767–73. doi: 10.2174/1389450119666180518112350
32. Baeyens A. Chromosomal Radiosensitivity of Lymphocytes in South African Breast Cancer Patients of Different Ethnicity: An Indirect Measure of Cancer Susceptibility. *South Afr Med J Suid-Afrikaanse Tydskrif Vir Geneeskunde* (2015) 105(8):675–8.
33. Yim WW, Mizushima N. Lysosome Biology in Autophagy. *Cell Discov* (2020) 11:6. doi: 10.1038/s41421-020-0141-7
34. Chen X, Gu X, Zhang H. Sidt2 Regulates Hepatocellular Lipid Metabolism Through Autophagy. *J Lipid Res* (2018) 59(3):404–15. doi: 10.1194/jlr.M073817
35. Semenova N, Bosnjak M, Markelc B, Znidar K, Cemazar M, Heller L. Multiple Cytosolic DNA Sensors Bind Plasmid DNA After Transfection. *Nucleic Acids Res* (2019) 47(19):10235–46. doi: 10.1093/nar/gkz768
36. Giné E, Crespo M, Muntañola A, Calpe E, Baptista MJ, Villamor N, et al. Induction of Histone H1.2 Cytosolic Release in Chronic Lymphocytic Leukemia Cells After Genotoxic and non-Genotoxic Treatment. *Haematologica* (2008) 93(1):75–82. doi: 10.3324/haematol.11546
37. Kang C, Elledge SJ. How Autophagy Both Activates and Inhibits Cellular Senescence. *Autophagy* (2016) 12(5):898–9. doi: 10.1080/15548627.2015.1121361
38. Feng Y, Klionsky DJ. Autophagy Regulates DNA Repair Through SQSTM1/P62. *Autophagy* (2017) 13(6):995–6. doi: 10.1080/15548627.2017.1317427
39. Hatch EM, Fischer AH, Deerinck TJ, Hetzer MW. Catastrophic Nuclear Env Elope Collapse in Canc Er Cell Micronuclei. *Cell* (2013) 3;154(1):47–60. doi: 10.1016/j.cell.2013.06.007
40. Maass KK, Rosing F, Ronchi P, Willmund KV, Devens F, Hergt M, et al. Altered Nuclear Envelope Structure and Proteasome Function of Micronuclei. *Exp Cell Res* (2018) 371(2):353–63. doi: 10.1016/j.yexcr.2018.08.029
41. Gelot C, Magdalou I, Lopez BS. Replication Stress in Mammalian Cells and its Consequences for Mitosis. *Genes* (2015) 6(2):267–98. doi: 10.3390/genes6020267
42. Bjerregaard VA, Özer Ö, Hickson ID, Liu Y. The Detection and Analysis of Chromosome Fragile Sites. *Methods Mol Biol Clifton NJ)* (2018) 1672:471–82. doi: 10.3390/genes6020267
43. Webster PJ, Littlejohns AT, Gaunt HJ, Prasad KR, Beech DJ, Burke DA. AZD1775 Induces Toxicity Through Double-Stranded DNA Breaks Independently of Chemotherapeutic Agents in p53-mutated Colorectal Cancer Cells. *Cell Cycle Georgetown Tex)* (2017) 16(22):2176–82. doi: 10.1080/15384101.2017.1301329
44. Pérez-Cadahía B, Drobic B, Davie JR. H3 Phosphorylation: Dual Role in Mitosis and Interphase. *Biochem Cell Biol Biochim Biol Cellulaire* (2009) 87(5):695–709. doi: 10.1139/O09-053
45. Wimbish RT, DeLuca JG. Hec1/Ndc80 Tail Domain Function at the Kinetochore-Microtubule Interface. *Front Cell Dev Biol* (2020) 26:43. doi: 10.3389/fcell.2020.00043
46. Crowley LC, Marfell BJ, Waterhouse NJ. Analyzing Cell Death by Nuclear Staining With Hoechst 33342. *Cold Spring Harb Protoc* (2016) 2016(9):778–81. doi: 10.1101/pdb.prot087205
47. Wilhelm T, Olziersky AM, Harry D, De Sousa F, Vassal H, Eskat A, et al. Mild Replication Stress Causes Chromosome Mis-Segregation Via Premature Centriole Disengagement. *Nat Commun* (2019) 10(1):3585. doi: 10.1038/s41467-019-11584-0
48. Sabatinos SA, Ranatunga NS, Yuan JP, Green MD, Forsburg SL. Replication Stress in Early S Phase Generates Apparent Micronuclei and Chromosome Rearrangement in Fission Yeast. *Mol Biol Cell* (2015) 26(19):3439–50. doi: 10.1091 /mbc.E15-05-0318
49. Maréchal A, Zou L. DNA Damage Sensing by the ATM and ATR Kinases. *Cold Spring Harbor Perspect Biol* (2013) 5(9):a012716. doi: 10.1091/mbc.E15-05-0318
50. Kimmelman AC, White E. Autophagy and Tumor Metabolism. *Cell Metab* (2017) 25(5):1037–43. doi: 10.1016/j.cmet.2017.04.004
51. Guo W, Wang Y, Wang Z, Wang YP, Zheng H. Inhibiting Autophagy Increases Epirubicin's Cytotoxicity in Breast Cancer Cells. *Cancer Sci* (2016) 107(11):1610–21. doi: 10.1111/cas.13059
52. Hengel SR, Spies MA, Spies M. Small-Molecule Inhibitors Targeting DNA Repair and DNA Repair Deficiency in Research and Cancer Therapy. *Cell Chem Biol* (2017) 24(9):1101–19. doi: 10.1016/j.chembiol.2017.08.027
53. Goyal G, Fan T, Silberstein PT. Hereditary Cancer Syndromes: Utilizing DNA Repair Deficiency as Therapeutic Target. *Familial Cancer* (2016) 15(3):359–66. doi: 10.1007/s10689-016-9883-7
54. Dudley JC, Lin MT, Le DT, Eshleman JR. Microsatellite Instability as a Biomarker for PD-1 Blockade. *Clin Cancer Res: Off J Am Assoc Cancer Res* (2016) 22(4):813–20. doi: 10.1158/1078-0432.CCR-15-1678

Conflict of Interest: The authors declare that the research was conducted in the absence of any commercial or financial relationships that could be construed as a potential conflict of interest.

frontiers in Cell and Developmental Biology

ORIGINAL RESEARCH
published: 31 May 2021
doi: 10.3389/fcell.2021.661602

Exosomal miR-92b-3p Promotes Chemoresistance of Small Cell Lung Cancer Through the PTEN/AKT Pathway

Ming Li[1]†, Wulin Shan[1†], Yan Hua[1], Fengmei Chao[1], Yayun Cui[1], Lei Lv[1], Xiaoyan Dou[1], Xing Bian[2,3], Jinglu Zou[2,3], Hong Li[2,3] and Wenchu Lin[2,3]**

[1] Department of Laboratory Diagnostics, The First Affiliated Hospital of USTC, Division of Life Sciences and Medicine, University of Science and Technology of China, Hefei, China, [2] High Magnetic Field Laboratory, Hefei Institutes of Physical Science, Chinese Academy of Sciences, Hefei, China, [3] Key Laboratory of High Magnetic Field and Ion Beam Physical Biology, Hefei Institutes of Physical Science, Chinese Academy of Sciences, Hefei, China

OPEN ACCESS

Edited by:
Marco Mina,
Sophia Genetics, Switzerland

Reviewed by:
Bin Yuan,
George Washington University, United States
Avik Choudhuri,
Harvard University, United States

***Correspondence:**
Ming Li
liming19831002@163.com
Wenchu Lin
wenchu@hmfl.ac.cn

† These authors have contributed equally to this work and share first authorship

Specialty section:
This article was submitted to Molecular and Cellular Oncology, a section of the journal Frontiers in Cell and Developmental Biology

Received: 31 January 2021
Accepted: 19 April 2021
Published: 31 May 2021

Citation:
Li M, Shan W, Hua Y, Chao F, Cui Y, Lv L, Dou X, Bian X, Zou J, Li H and Lin W (2021) Exosomal miR-92b-3p Promotes Chemoresistance of Small Cell Lung Cancer Through the PTEN/AKT Pathway. Front. Cell Dev. Biol. 9:661602. doi: 10.3389/fcell.2021.661602

Resistance to first-line chemotherapy drugs has become an obstacle to improving the clinical prognosis of patients with small cell lung cancer (SCLC). Exosomal microRNAs have been shown to play pro- and anti-chemoresistant roles in various cancers, but their role in SCLC chemoresistance has never been explored. In this study, we observed that the expression of exosomal miR-92b-3p was significantly increased in patients who developed chemoresistance. Luciferase reporter analysis confirmed that PTEN was a target gene of miR-92b-3p. The PTEN/AKT regulatory network was related to miR-92b-3p-mediated cell migration and chemoresistance *in vitro* and *in vivo* in SCLC. Importantly, exosomes isolated from the conditioned medium of SBC-3 cells overexpressing miR-92b-3p could promote SCLC chemoresistance and cell migration. Furthermore, we found that plasma miR-92b-3p levels were significantly higher in patients with chemoresistant SCLC than in those with chemosensitive SCLC, but the levels were down-regulated in patients who achieved remission. Kaplan–Meier analysis showed that SCLC patients with high miR-92b-3p expression were associated with shorter progression-free survival. Overall, our results suggested that exosomal miR-92b-3p is a potential dynamic biomarker to monitor chemoresistance in SCLC and represents a promising therapeutic target for chemoresistant SCLC.

Keywords: exosome, miR-92b-3p, small cell lung cancer, chemoresistance, migration

INTRODUCTION

Lung cancer, one of the most common cancers worldwide, leads to high cancer-related death among both men and women (Siegel et al., 2019). Small cell lung cancer (SCLC) is a neuroendocrine tumor that accounts for approximately 15% of all lung cancers (Sun et al., 2017). SCLC is the most aggressive lung malignancy, exhibiting a strong proliferative capacity, early distant migration, and drug resistance, all of which lead to extremely poor outcomes for SCLC patients. The first line of treatment regimen for SCLC is platinum-based chemotherapy, usually in combination with the topoisomerase II inhibitor etoposide (William and Glisson, 2011; Borromeo et al., 2016).

The treatment regimen shows a good initial response in 60–80% SCLC patients, but almost all patients relapse within 6–12 months of treatment due to the development of multidrug resistance (MDR; Peng et al., 2016). The indicators currently used for monitoring SCLC chemoresistance are imaging data and traditional tumor markers, such as carcinoembryonic antigen, pro-gastrin-releasing peptide, and neuron-specific enolase. Owing to radiation hazards, imaging cannot be performed as a routine examination during chemotherapy. Most traditional tumor markers lack high sensitivity and specificity. Therefore, it is urgent to find reliable predictors and elucidate the molecular mechanism of SCLC chemoresistance.

MicroRNAs (miRNAs) are endogenously derived non-coding RNAs with 19–22 nucleotides. Numerous studies have revealed that miRNAs are involved in cell proliferation, apoptosis, drug resistance, cancer migration, and progression (Wei et al., 2017; Liu et al., 2019). The relationship between miR-92b-3p expression and cancer development remains controversial. Some reports suggest that miR-92b-3p expression is increased in most cancers, including colorectal cancer (Gong et al., 2018), esophageal squamous cell cancer (Wang et al., 2019), gastric cancer (Li C. et al., 2019), non-SCLC (NSCLC; Lei et al., 2014), and clear cell renal cell carcinoma (Wang et al., 2020). In contrast, miR-92b-3p is confirmed as a tumor suppressor miRNA in pancreatic cancer (Long et al., 2017) and triple-negative breast cancer (Li Y. Y. et al., 2019). However, the specific function of miR-92b-3p in SCLC is not yet understood.

Exosomes ranging from 30 to 150 nm in diameter are widely present in various bodily fluids. Exosomes can be produced by tumor, epithelial, T, B, and dendritic cells. Most studies have demonstrated that the exosomes secreted by tumor cells could migrate far away from their initial position and then transfer various types of functional effectors, including miRNAs, proteins, and lipids, to recipient cells. In addition, exosomal miRNAs have been considered as the most effective biomarkers for disease diagnosis and efficacy monitoring in the past few years (Joyce et al., 2016; Mao et al., 2020). However, the relationship between tumor-derived exosomal miRNAs and chemoresistance in SCLC has not been elucidated.

In the present study, we first isolated total RNA from plasma exosomes of two SCLC patients at the pre- and post-chemoresistant stages and used next-generation sequencing (NGS) to examine the differential expression of miRNAs. We found that the levels of miR-92b-3p in plasma exosomes were significantly increased in SCLC patients with chemoresistance compared with patients without chemoresistance. Hence, we focused on exosomal miR-92b-3p and studied its effect on SCLC chemoresistance. The data showed that miR-92b-3p could be transferred among cancer cells via exosomes to promote cell migration and chemoresistance through the PTEN/AKT pathway *in vitro* and *in vivo*. Additionally, miR-92b-3p was demonstrated to be significantly up-regulated in both the plasma and plasma exosomes of SCLC patients with chemoresistance. Our study reveals novel details elaborating the molecular mechanism of exosomal miR-92b-3p in SCLC chemoresistance and offers theoretical basis for identifying effective targets to improve the prognosis of SCLC chemoresistant patients.

MATERIALS AND METHODS

Cell Lines, Materials, and Antibodies

The human SCLC cell lines H82, SHP77, DMS273, and H69 were kept in our own laboratory. SBC-3 and H446 cells were purchased from the Cell Bank of Type Culture Collection of the Chinese Academy of Sciences (Shanghai, China). Cells were maintained in Roswell Park Memorial Institute (RPMI) 1640 medium (Life Technologies, CA, United States) supplemented with 10% fetal bovine serum (FBS; Gibco, Australia) and 1% penicillin/streptomycin in a humidified incubator at 37°C in 5% CO_2.

Cisplatin (DDP), adriamycin (ADM), and etoposide (VP16) were purchased from MCE (Concord, CA, United States), and stock solutions were prepared in dimethyl sulfoxide (Sigma-Aldrich, Saint Louis, Mo, United States) at a concentration of 1 mg/ml. Antibodies against CD63, TSG101, PTEN, phospho-AKT, and AKT were purchased from Cell Signaling Technology (Danvers, MA, United States). GAPDH antibody was purchased from TransBionovo (Beijing, China). The bicinchoninic acid (BCA) protein assay was purchased from Thermo Fisher Scientific (CA, United States).

MiR-92b-3p Transfection

SBC-3 and SHP77 cells were seeded 1 day before transfection. Lentivirus vectors containing the miR-92b-3p mimic (Lv3-miRNA-92b-3p mimics), miR-92b-3p inhibitor (Lv3-miRNA-92b-3p inhibitor sponge), or NC (Lv-NC) were amplified by GenePharma (Shanghai, China). All these plasmids and oligonucleotides were transfected into cells by Lipofectamine 3000 reagent (Invitrogen) following the manufacturer's instructions, and cells were continually incubated with puromycin (2.5 μg/ml, Sigma) to develop acquired resistance.

Western Blot and Immunohistochemistry Assays

For the western blot assay, total proteins were extracted using extraction buffer with a protease inhibitor cocktail (Thermo Scientific), and their concentration was quantified with the BCA assay. Protein of 50 μg was separated by sodium dodecyl sulfate (SDS)–polyacrylamide gel electrophoresis and then transferred to polyvinylidene fluoride membranes (Millipore). The membranes were blocked and probed overnight with primary antibodies, including CD63, TSG101, PTEN, and AKT (T/P). After incubation with secondary antibodies, the protein band intensity was quantified by densitometry using Image Lab software (Bio-Rad, Hercules, CA, United States).

For the immunohistochemistry (IHC) assay, tissue blocks were sectioned at a thickness of 4 μm, and the sections were deparaffinized. Briefly, the sections were incubated in xylene, followed by ethanol, and then washed with distilled water. For antigen retrieval, the sections were boiled in 10 mM of sodium citrate buffer for 10 min at 121°C. After being rinsed with distilled water, the sections were incubated in 3% peroxidase before they were washed with distilled water followed by buffer.

For staining, sections were exposed to primary antibody targeting PTEN or p-AKT (1:800) diluted in an antibody diluent. For antigen visualization, a peroxidase-labeled secondary antibody (EnVision/HRP system, DAKO, Carpinteria, CA, United States) was applied. Subsequently, the sections were rinsed in the buffer provided in the kit and immersed in a 3,3′-diaminobenzidine staining solution.

Quantitative Real-Time Polymerase Chain Reaction

Total RNA was isolated from cells using TRIzol. RNA from plasma or exosomes was isolated using the miRNeasy Micro Kit (Qiagen). cDNA was synthesized with the TaqMan® MiRNA Reverse Transcription Kit (Applied Biosystems). Aliquots of the reaction mixture were used for PCR on an LC480 PCR Detection System. All primers were synthesized by RiboBio (Guangzhou, China). All PCR experiments were performed in triplicate. The U6 RNA levels for cellular miR-92b-3p, miR-39 levels for plasma, and exosomal miR-92b-3p and GAPDH levels for mRNAs were used as respective internal controls for data normalization.

Exosome Purification and Identification

The isolation of SCLC supernatant exosomes was adapted from a previous study (Lobb et al., 2015). For exosome purification from cell culture supernatants, cells were cultured in medium containing 10% exosome-depleted FBS. In brief, culture supernatants were centrifuged at 300 × *g* for 10 min to remove living cells and 2,000 × *g* for 20 min to remove cell debris and dead cells. Microvesicles were pelleted after centrifugation at 16,500 × *g* for 45 min at 4°C (Beckman Coulter, J2-HS) and resuspended in phosphate-buffered saline (PBS). Supernatants filtered through a 0.22-μm membrane were then centrifuged at 100,000 × *g* for 2 h at 4°C (Beckman Coulter, Optima XPN-100). The pelleted exosomes were resuspended in PBS and collected by ultracentrifugation at 100,000 × *g* for 2 h. To isolate exosomes from the peripheral blood, samples were centrifuged at 2,000 × *g* for 10 min two times to separate the plasma, and exosomes were isolated via ultracentrifugation as described above.

Protein levels in exosomes were quantified by the BCA assay, and western blot analysis of exosome-related proteins CD63 and TSG101 was performed following standard procedures. Exosomes suspended in sucrose gradients were prepared as described above and resuspended in PBS. Sample aliquots of 4 ml were pipetted onto 200 mesh formvar/carbon grids (EMS), which had been subjected to glow discharge for 15 s. Samples were incubated on grids for 30 s and subsequently negatively stained with a 2% uranyl acetate solution. Data were acquired using a Philips CM200F electron microscope operating at 200 keV equipped with an UltraScan 1000 CCD camera (Gatan). Exosomes were quantified by a NanosightNS300 instrument (Malvern Instruments Ltd., United Kingdom) equipped with NTA 3.0 analytical software (Malvern Instruments Ltd., United Kingdom).

Cell Viability, Apoptosis, Migration, and Invasion Assays

For the cell viability assay, SCLC cells (1×10^4) were cultured in 96-well plates under the indicated experimental conditions. Cells were incubated with different concentrations of chemotherapy drugs, including DDP, ADM, and VP16. After 24 h, Cell Counting Kit 8 (CCK8, Dojindo, Japan) was used to detect cell viability. Then, the IC50 of each drug was calculated.

For the apoptosis assay, SCLC cells were treated with 3 μg/ml of DDP for 48 h and then collected. Annexin V/7-AAD (eBioscience, United States) was used according to the manufacturer's protocol.

Wound-healing analysis was performed to test cell migration. The artificial wounds were produced on aconfluent cell monolayer in FBS-free medium. Cell invasion was assessed using Transwell chambers according to the manufacturer's instructions. Briefly, SCLC cells (2×10^5 cells/well) were seeded in the upper chambers on a Matrigel-coated membrane in FBS-free medium. Meanwhile, the lower chambers were loaded with RPMI 1640 medium supplemented with 10% FBS. After incubation at 37°C for 48 h, cells remaining on the upper surface of the membrane were cleaned with a cotton swab. The lower chamber was washed with PBS, fixed with methyl alcohol, stained with 0.5% crystal violet, washed three times with water, and viewed under an inverted microscope.

Luciferase Reporter Assay

HEK 293T cells were co-transfected with miR-92b-3p mimics or with a non-specific control (NC; GenePharma) and wild-type or mutated PTEN 3′-untranslated region (3′-UTR) plasmids (constructed by GenePharma) using Lipofectamine 3000 (Invitrogen, United States). Luciferase activities were measured at 48 h post-transfection using a dual-luciferase analysis system (Promega, Madison, WI, United States). Luminescence readings were acquired using a FlexStation 3 Multiscan Spectrum (Molecular Devices, Sunnyvale, CA, United States).

Co-cultured Assays

To investigate the role of AKT, SCLC cells were cultured in 6-well or 96-well plates treated with the p-AKT inhibitor MK-2206 alone or in combination with DDP. After 48 h, cells were harvested and subjected to cell viability, migration, qRT-PCR, and western blot assays.

To investigate the potential transmission of chemoresistance, SCLC cells were seeded in 6-well plates and incubated with exosomes isolated from the culture supernatant of SCLC with miR-92b-3p overexpression (SCLC OE) cells in RPMI 1640 medium with 10% exosome-depleted FBS. Then, the cells were harvested for subsequent wound healing assays and measurement of miR-92b-3p and PTEN levels.

Exosome Uptake Assay

Exosomes were labeled with the red fluorescent dye PKH26 (Sigma-Aldrich) according to the manufacturer's protocol. Briefly, exosomes isolated from the culture supernatant of SBC-3 OE cells were resuspended in 0.5 ml of Diluent C. Then, 2 μl

of PKH26 was diluted in another 0.5 ml of Diluent C. The samples were mixed for 5 min, and then 5 ml of 1% bovine serum albumin was added to quench excess dye. Subsequently, the mixture was ultracentrifuged at 100,000 × *g* for 1 h, resuspended in PBS, and finally incubated with sensitive cells for 12 h at 37°C. Incorporation of exosomes into cells treated with DAPI was visualized by fluorescence microscopy (Carl Zeiss, Germany).

Animal Experiments

Animal experiments were approved by the Institutional Animal Care and Use Committees of Hefei Institutes of Physical Science, Chinese Academy of Sciences. 4-week-old female BALB/c nude mice were purchased from Beijing Vitong Lihua Laboratory Animal Technology Co., Ltd (Beijing, China).

To evaluate whether miR-92b-3p could promote SCLC tumor growth, SBC-3 NC, SBC-3 OE, and SBC-3 with miR-92b-3p knockdown (SBC-3 KD) cells (5×10^6 cells per point) were subcutaneously injected into the right upper and lower flanks of nude mice. Tumor growth was monitored two times per week. After 4 weeks, mice from each group were sacrificed, and their tumor samples were prepared for histological examination.

To evaluate whether exosomes isolated from the culture supernatant of SBC-3 OE cells could promote SCLC chemoresistance, SBC-3 cells (5×10^6 cells per mouse) were injected subcutaneously into the right upper and lower flanks of nude mice. 10 days later, when the tumors were approximately 100 mm^3 in size, purified exosomes (5 μg) or PBS was then injected intratumorally twice weekly with or without DDP (3.5 mg/kg). The tumor size was measured twice per week. Tumor volume (mm^3) was calculated as $0.5 \times width^2 \times length$.

Clinical Small Cell Lung Cancer Patient Samples

Fifty SCLC patients were enrolled in the Department of Respiratory Oncology of the Western Branch of the First Affiliated Hospital of University of Science and Technology of China (Hefei, China) from January 2016 to July 2019. The clinical and pathological characteristics of these patients are listed in **Table 1**. All patients received routine platinum agents combined with VP16 chemotherapy. The treatment response was divided into responder and non-responder groups. The responder group included patients who achieved a partial response (PR) or complete response (CR), and the non-responder group included patients with stable disease (SD) and progressive disease (PD). This study was approved by the Ethics Committee of the First Affiliated Hospital of University of Science and Technology of China.

Statistical Analysis

All statistical analyses were performed using GraphPad Prism software 8.5 (San Diego, CA, United States) and SPSS 21.0 (IBM Corporation, Armonk, NY, United States). The Mann–Whitney *U* test was performed to compare the levels of plasma and exosomal miR-92b-3p. The clinicopathological parameters were compared using Fisher's exact test. The statistical significance between two groups was analyzed using two-tailed unpaired Student's t test. Survival curves were constructed with the Kaplan–Meier method and compared by log-rank tests. $P < 0.05$ was considered statistically significant.

TABLE 1 | Univariate and multivariate prognostic analyses of SCLC.

Variables	Univariate analysis HR (95% CI)	*P* value	Multivariate analysis HR (95% CI)	*P* value
Sex male vs female	1.144 (0.621–2.108)	0.666		
Age < 64 vs ≥64	1.003 (0.981–1.026)	0.797		
Smoking yes vs no	0.759 (0.455–1.266)	0.291		
Stage LD vs ED	2.029 (1.108–3.716)	0.022	1.737 (0.928–3.251)	0.084
MiR-92b-3p high vs low	0.517 (0.341–0.851)	0.010	0.590 (0.353–0.988)	0.045

Note. SCLC, small cell lung cancer; LD, limited disease; ED, extensive disease.

RESULTS

MiR-92b-3p Is Aberrantly Up-Regulated in the Plasma Exosomes of Small Cell Lung Cancer Patients With Chemoresistance

Total RNA was isolated from plasma exosomes of two patients at the pre- and post-chemoresistant stages. MiRNA sequencing was performed to assess differential expression using NGS. The data showed that the levels of plasma exosomal miR-92b-3p were much higher in the post-chemoresistant stage than in the pre-chemoresistant stage (**Figure 1A**). To further explore the level of circulating miR-92b-3p in SCLC patients, another 20 plasma samples from SCLC patients at the pre- and post-chemoresistant stages was collected for exosome isolation. Consistent with the sequencing data, plasma exosomal miR-92b-3p levels were aberrantly increased after patients developed chemoresistance (**Figure 1B**).

To identify SCLC cell lines with differential responses to first-line chemotherapy drugs, a panel of six cell lines was screened using the CCK8 assay. As shown in **Figure 1C**, there was no significant difference in the IC50 of DDP among the SCLC cell lines, whereas the IC50 values of ADM and VP16 in SBC-3 and H446 cells were significantly lower than those of other cell lines, especially of SHP77 cells. The data indicated that SBC-3 and H446 cells were relatively sensitive to chemotherapy drugs, while SHP77 cells were resistant to these drugs. We further investigated miR-92b-3p expression in these six cell lines. Consistent with the data in plasma exosomes, miR-92b-3p expression was higher in chemoresistant SHP77 cells, whereas the lowest expression was observed in chemosensitive SBC-3 cells (**Figure 1D**). Our data implied

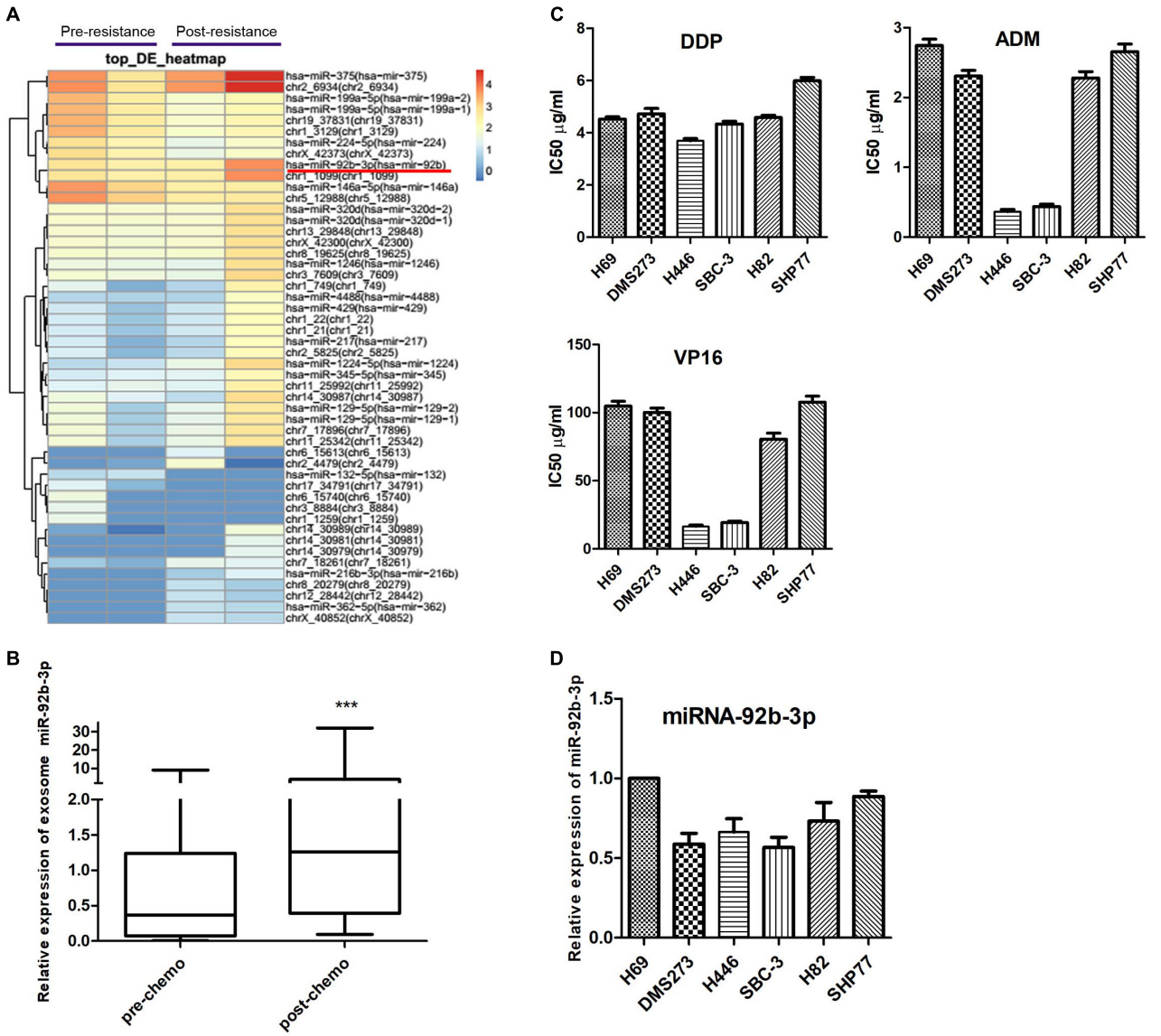

FIGURE 1 | Circulating miR-92b-3p is aberrantly up-regulated in SCLC chemoresistant patients. **(A)** The heatmap shows the top miRNAs with the largest changes (increased or decreased) in expression in plasma exosomes of two patients before and after developing chemoresistance. **(B)** The level of miR-92b-3p was higher in plasma exosomes from chemoresistant patients than from chemosensitive patients. ***$P < 0.001$. **(C)** IC50 values of DDP, ADM, and VP16 in SCLC cell lines. SBC-3 and H446 cells were relatively sensitive to chemotherapy drugs, while SHP77 cells were resistant to chemotherapy drugs. **(D)** MiR-92b-3p expression in SCLC cell lines. MiR-92b-3p expression was higher in chemoresistant SHP77 cells than in the other cell lines, whereas the lowest expression was observed in chemosensitive SBC-3 cells. **(B–D)** experiments were performed independently three times. SCLC, small cell lung cancer; miRNAs, microRNAs; DDP, cisplatin; ADM, adriamycin; and VP16, etoposide.

the potential importance of miR-92b-3p in promoting SCLC chemoresistance.

MiR-92b-3p Is Involved in Chemoresistance Regulation in Small Cell Lung Cancer Cells

We first used lentivirus transfection to construct SCLC cell lines with stable overexpression or knockdown of miR-92b-3p. After transfection, SCLC cells presented green fluorescence. The mimic and inhibitor fragments of miR-92b-3p are shown in **Figure 2A**. The expression of miR-92b-3p in SBC-3 OE and SHP77 OE cells was 8 and 2.54 times than that in the respective NC cells. Conversely, miR-92b-3p levels in SBC-3 KD and SHP77 KD cells were 30% and 50% of that in NC cells, respectively, (**Figure 2B**). After miR-92b-3p overexpression, the IC50 values of DDP, ADM, and VP16 were significantly increased in SBC-3 and SHP77 cells. Only the IC50 of DDP in SBC-3 KD cells was dramatically decreased, whereas the IC50 values of all the chemotherapy drugs were not observably changed in

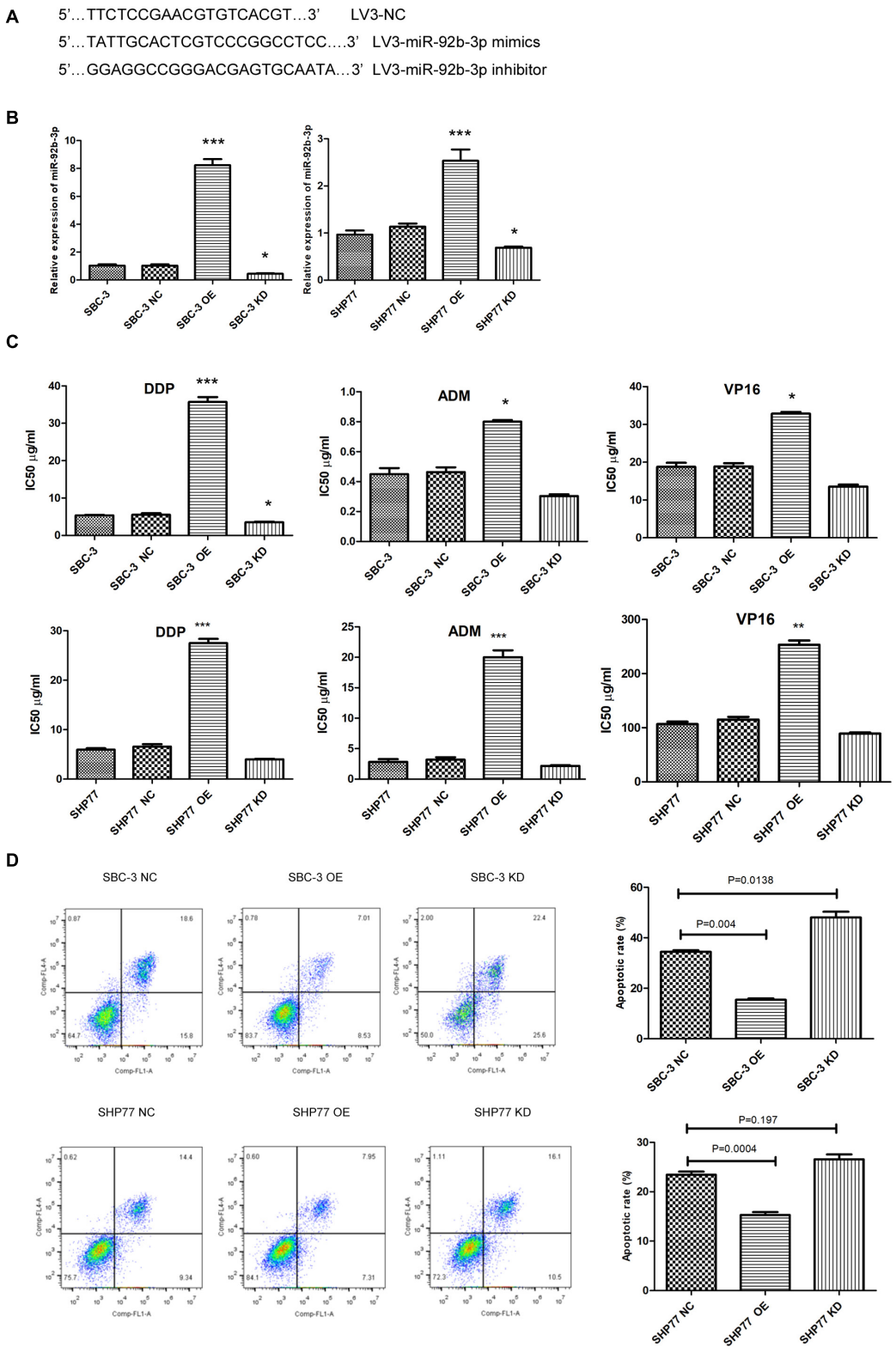

FIGURE 2 | MiR-92b-3p promotes chemoresistance and inhibits apoptosis in SCLC cells. **(A)** Primer sequences of lentiviral miR-92b-3p. **(B)** The miR-92b-3p levels were increased in SCLC OE cells and decreased in SCLC KD cells. **(C)** IC50 of DDP, ADM, and VP16 in SCLC cells. MiR-92b-3p promoted chemoresistance in SCLC cells. **(D)** MiR-92b-3p inhibited SCLC cell apoptosis. OE, miR-92b-3p overexpression; KD, miR-92b-3p knockdown. **(B–D)** analyses were performed in triplicate. SCLC, small cell lung cancer; DDP, cisplatin; ADM, adriamycin; and VP16, etoposide. $^{*}P < 0.05$, $^{**}P < 0.01$, $^{***}P < 0.001$.

SHP77 KD cells (**Figure 2C**). Moreover, after treatment with 3 μg/ml of DDP, the apoptosis rate was significantly decreased in SBC-3 OE cells and SHP77 OE cells. By contrast, the apoptosis rate was dramatically increased in SBC-3 KD cells, whereas the rate was not observably changed in SHP77 KD cells (**Figure 2D**). Wound healing and transwell assays demonstrated that SBC-3 KD cells showed significantly less migration and lower invasion ability, whereas the effects were reversed after miR-92b-3p overexpression (**Figures 3A,B**). The data shown above revealed that miR-92b-3p overexpression markedly enhanced chemoresistance in SCLC cells.

MiR-92b-3p Promotes Small Cell Lung Cancer Chemoresistance Through the PTEN/AKT Pathway *in vitro* and *in vivo*

We next explored the molecular mechanisms by which miR-92b-3p promoted SCLC chemoresistance. Bioinformatics

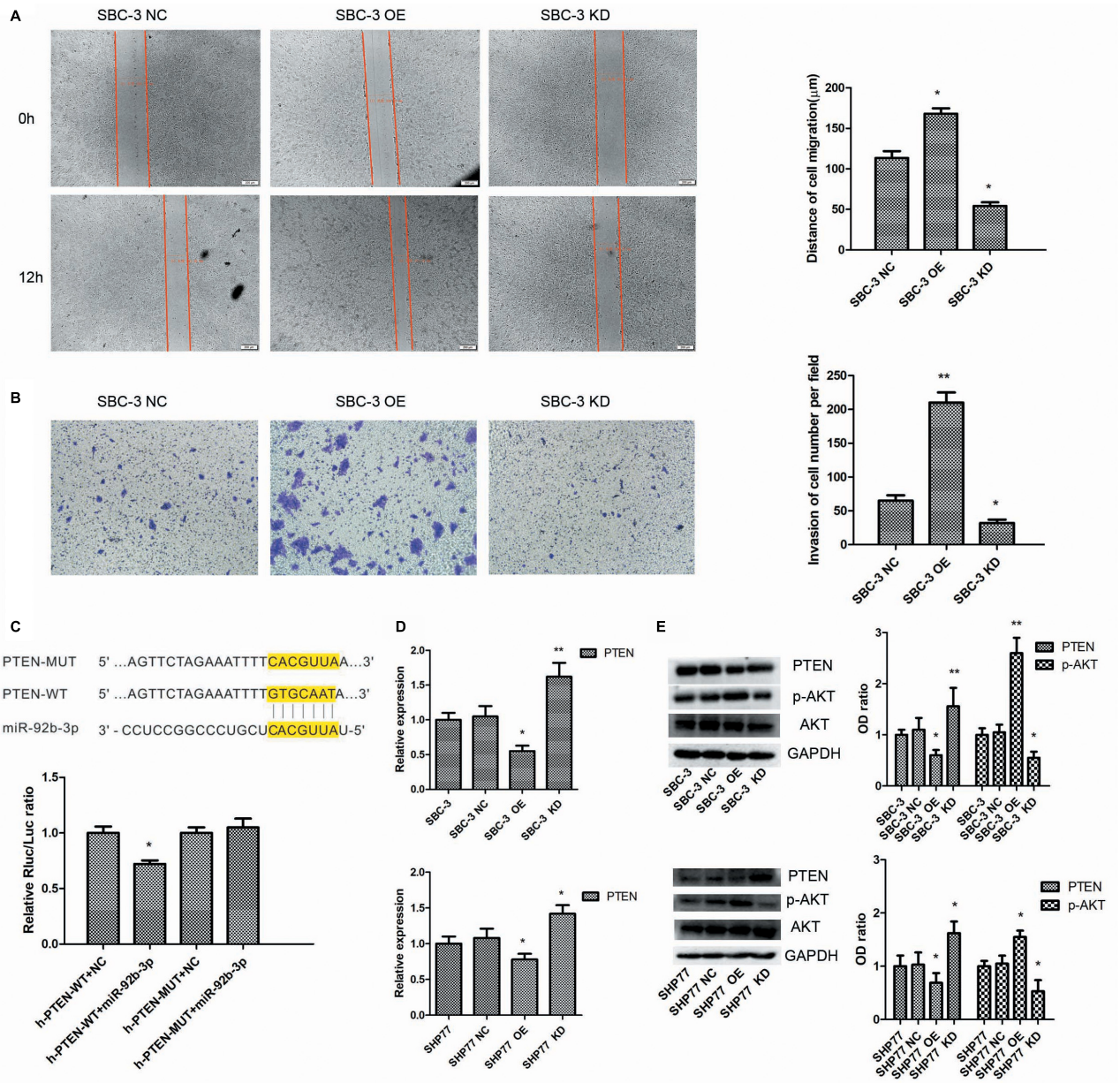

FIGURE 3 | MiR-92b-3p promotes SCLC chemoresistance by targeting the PTEN/AKT pathway. **(A,B)** MiR-92b-3p promotes SBC-3 cell migration and invasion. **(C)** The highly conserved miR-92b-3p binding motif in the 3′-UTR of PTEN. MiR-92b-3p only suppressed the luciferase activity in cells expressing the wild-type 3′-UTR of PTEN. **(D)** qRT-PCR data showed that PTEN expression was increased in SCLC KD cells but decreased in SCLC OE cells. **(E)** PTEN, AKT, and p-AKT levels were detected by western blot. The p-AKT level was significantly decreased in SCLC KD cells, whereas the PTEN level was increased in SCLC OE cells. **(A,B,D,E)** data points were determined three times. SCLC, small cell lung cancer. $^{*}P < 0.05$, $^{**}P < 0.01$.

analysis showed that the PTEN 3′-UTR contains sites complementary to miR-92b-3p (**Figure 3C**). To verify this prediction, we separately cloned fragments of the PTEN 3′-UTR that contained wild-type or mutated miR-92b-3p-binding sequences into psi-CHECK2 luciferase reporter plasmids. As shown in **Figure 3C**, the luciferase activities were significantly inhibited by miR-92b-3p in the plasmid carrying wild-type target sequences, whereas this inhibition was abrogated when the predicted sequences were mutated. Western blot and qRT-PCR data showed that the PTEN levels were increased in SBC-3 KD and SHP77 KD cells, and the levels were observably decreased in miR-92b-3p-overexpressing cells (**Figures 3D,E**). Additionally, we found that the p-AKT levels were significantly decreased in SBC-3 KD and SHP77 KD cells but were increased after miR-92b-3p overexpression (**Figure 3E**).

To further investigate the effects of PTEN/AKT pathway on SCLC cellular function and chemoresistance, we primarily reduced p-AKT expression using the p-AKT inhibitor MK-2206 in SCLC cells. After inhibition of p-AKT activity, SBC-3 OE and SBC-3 cells showed reduced migration ability (**Figure 4A**).

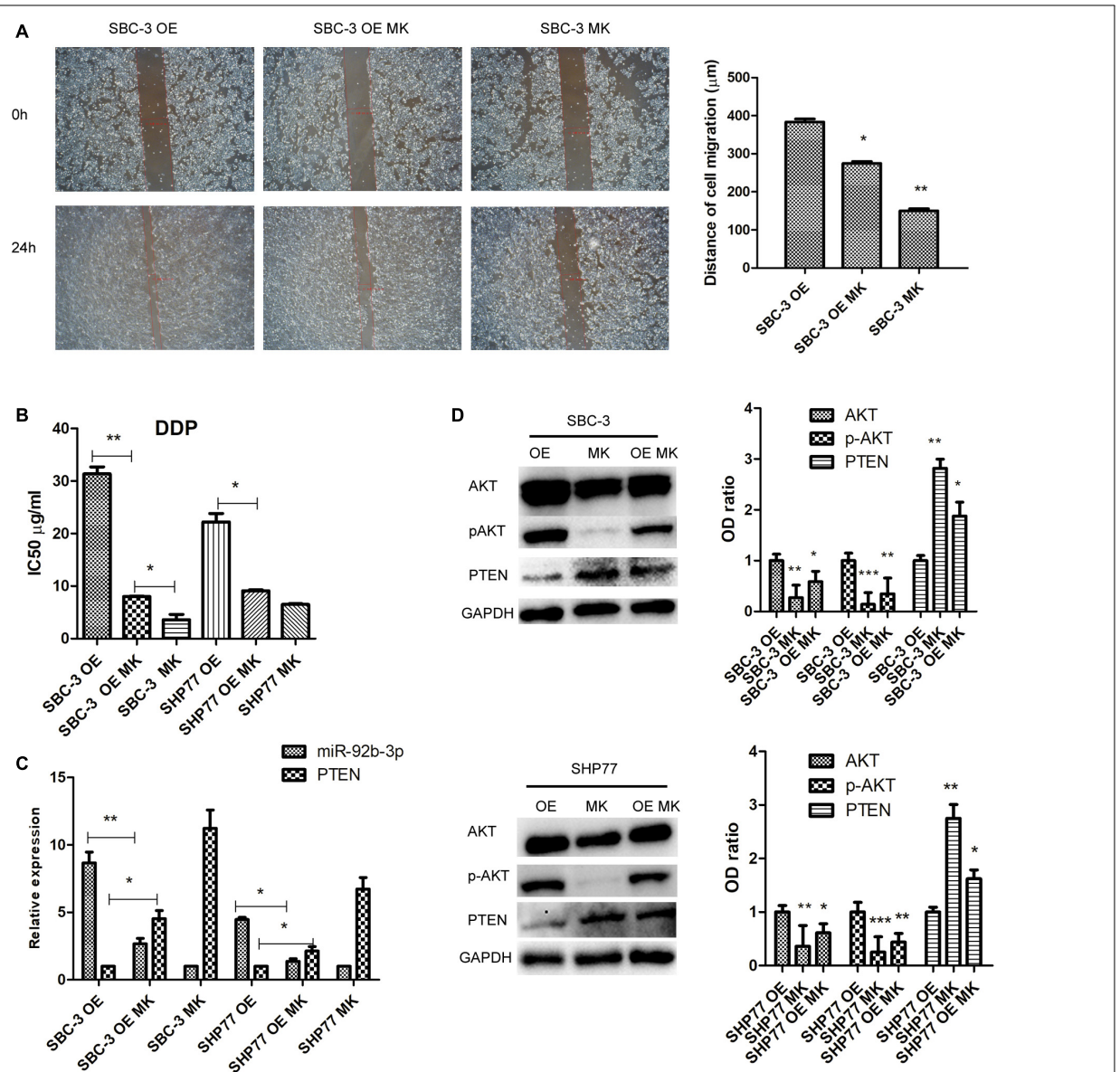

FIGURE 4 | p-AKT downregulation inhibited cell migration and chemoresistance of SCLC. **(A)** p-AKT downregulation inhibited SBC-3 OE and SBC-3 cell migration. **(B)** p-AKT downregulation decreased the IC50 value of DDP in SBC-3 and SHP77 cells, whereas this decrease was attenuated in SCLC OE cells. **(C)** MiR-92b-3p and PTEN levels as detected by qRT-PCR. p-AKT downregulation inhibited miR-92b-3p expression and enhanced PTEN levels in SCLC OE cells. **(D)** AKT, p-AKT, and PTEN levels as detected by western blot. p-AKT knockdown reduced p-AKT levels and increased PTEN levels in SCLC cells, but this was reversed by miR-92b-3p overexpression. All analyses were performed in triplicate. SCLC, small cell lung cancer and DDP, cisplatin. $^{*}P < 0.05$, $^{**}P < 0.01$, $^{***}P < 0.001$.

In addition, p-AKT downregulation observably decreased the IC50 values of DDP in SBC-3 and SHP77 cells, whereas this decrease was attenuated in SCLC cells overexpressing miR-92b-3p (**Figure 4B**). qRT-PCR data showed that p-AKT downregulation markedly inhibited miR-92b-3p expression and enhanced PTEN levels in SBC-3 OE and SHP77 OE cells (**Figure 4C**). p-AKT knockdown significantly reduced p-AKT levels in SBC-3 and SHP77 cells, whereas this reduction was attenuated in SBC-3 OE and SHP77 OE cells. Conversely, the PTEN levels in SCLC cells were enhanced after inhibiting p-AKT expression, whereas this increase was attenuated in SCLC OE cells (**Figure 4D**). These results indicated that p-AKT expression mediated cell migration, chemoresistance, and miR-92b-3p and PTEN levels in SCLC cells.

We finally studied the function of miR-92b-3p in SCLC *in vivo*. We performed a tumorigenesis assay by subcutaneously injecting cells (SBC-3 NC, SBC-3 OE, and SBC-3 KD) into the flanks of nude mice. The results showed that tumor growth was slowed by miR-92b-3p knockdown but was accelerated by miR-92b-3p overexpression (**Figures 5A,B**). The expression of PTEN and p-AKT was observed in the tumor tissue samples by IHC. The data confirmed that PTEN expression was down-regulated whereas p-AKT levels were increased in the SBC-3 OE group (**Figure 5C**). Conversely, these proteins showed an opposite trend in the SBC-3 KD group. Based on the above results, we concluded that miR-92b-3p promoted SCLC development and chemoresistance by regulating PTEN/AKT signaling.

MiR-92b-3p Is Transferred via Exosomes to Promote Cell Migration and Chemoresistance in Small Cell Lung Cancer

To determine the function of exosomal miR-92b-3p in SCLC development and chemoresistance, we conducted a series of experiments. First, exosomes from the supernatant of cultured SCLC cells were isolated. The isolated exosomes exhibited typical cup-shaped morphology and size (**Figures 6A,B**) and also positively expressed the protein markers CD63 and TSG101 (**Figure 6C**). The exosomes isolated from the conditioned medium of SBC-3 OE cells were labeled with PKH26 and co-cultured with SBC-3 cells for 24 h. Immunofluorescence was used

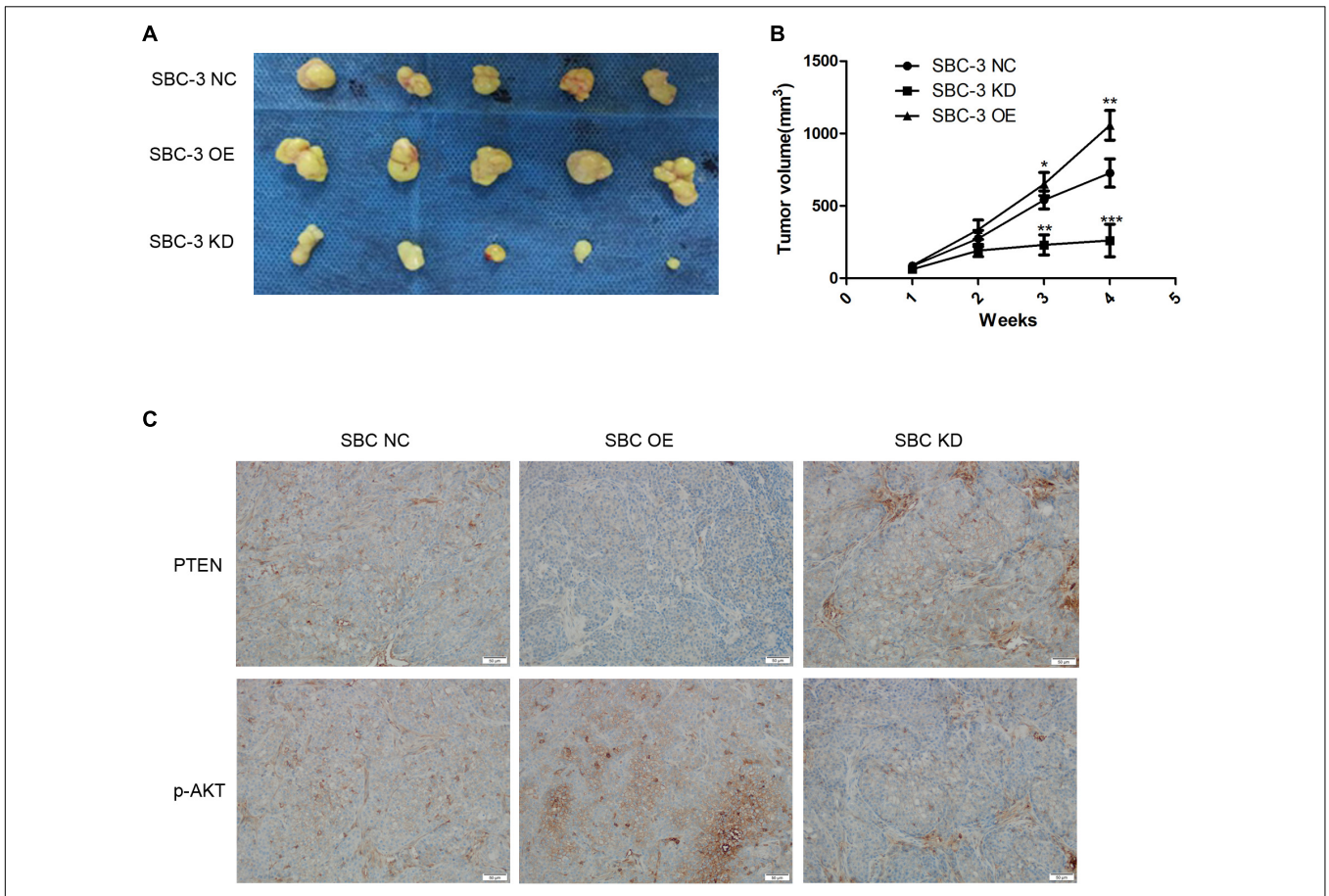

FIGURE 5 | MiR-92b-3p promotes SCLC development through the PTEN/AKT pathway *in vivo*. **(A,B)** The tumor-forming ability of SBC-3 cells with different miR-92b-3p expression levels. MiR-92b-3p promoted the tumor growth *in vivo*. Compared with SBC-3 NC group, $^{*}P < 0.05$, $^{**}P < 0.01$, and $^{***}P < 0.001$. **(C)** After miR-92b-3p overexpression, the IHC data confirmed that PTEN levels were down-regulated while p-AKT levels were up-regulated in tumor tissue. SCLC, small cell lung cancer and IHC, immunohistochemistry.

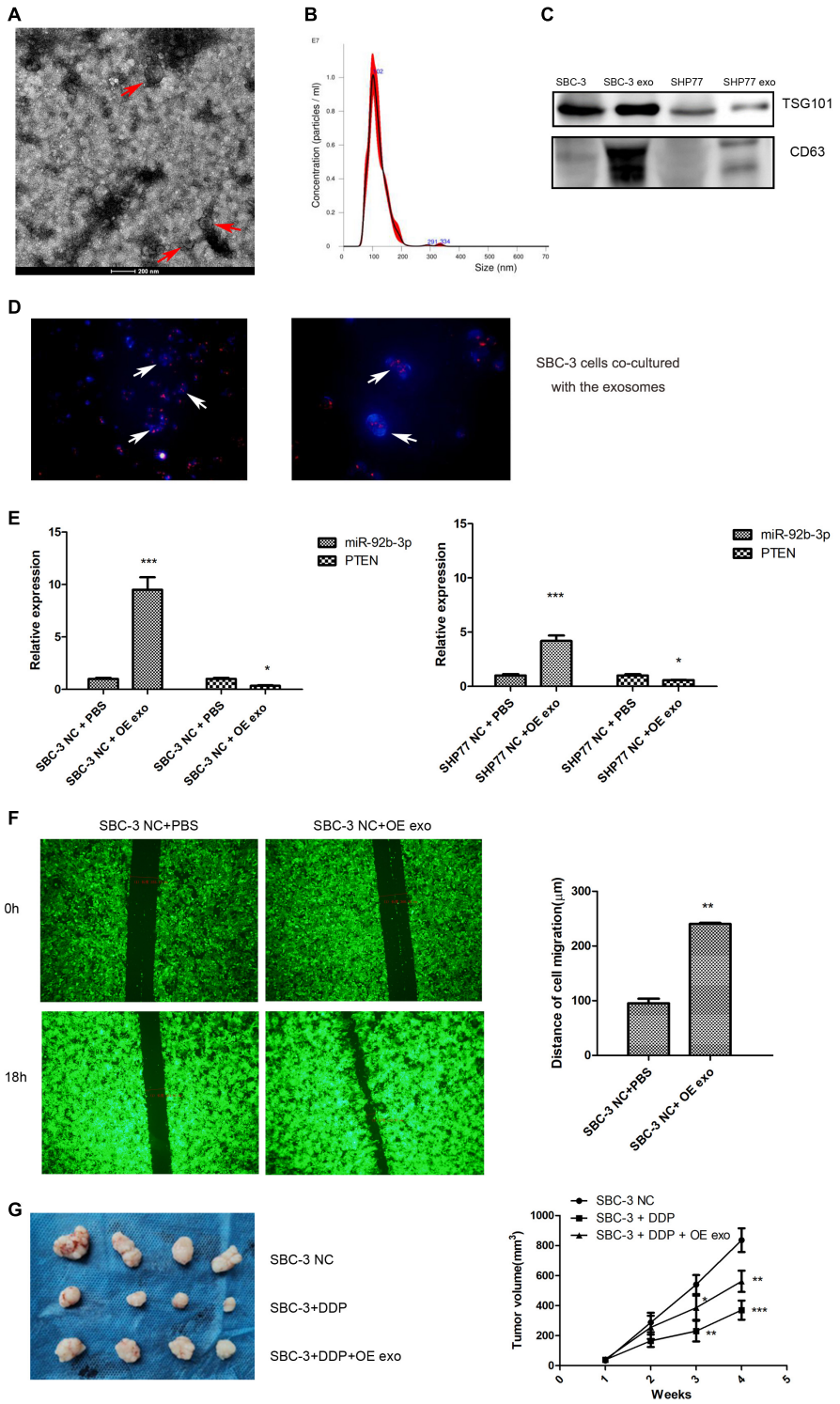

FIGURE 6 | Exosomes transfer miR-92b-3p to promote SCLC migration and chemoresistance. **(A)** TEM images of exosomes isolated from SCLC cells. **(B)** The size and quantitation of exosomes isolated from SCLC cells were examined by nanoparticle tracking analysis. **(C)** The levels of CD63 and TSG101 were detected by western blot. **(D)** Fluorescence microscopy images of SBC-3 cells after treatment with PKH26-labeled exosomes (green) stained with DAPI (blue). SBC-3 cells could effectively uptake the exosomes. **(E)** MiR-92b-3p and PTEN levels as detected by qRT-PCR. SCLC cells showed higher levels of miR-92b-3p and lower levels of PTEN after they were incubated with exosomes. **(F)** SCLC cells displayed higher migration ability after incubation with exosomes. **(G)** DDP treatment inhibited tumor growth, whereas this inhibition was reversed after combination therapy with exosomes. Compared with SBC-3 NC group, $^{*}P < 0.05$, $^{**}P < 0.01$, and $^{***}P < 0.001$. All experiments were performed independently three times. SCLC, small cell lung cancer and TEM, transmission electron microscopy.

to analyze the distribution of exosomes. As shown in **Figure 6D**, more PKH26-positive SBC-3 cells were observed, indicating that SBC-3 cells could effectively uptake these exosomes.

We measured miR-92b-3p and PTEN expression in SCLC cells after co-culturing with SCLC OE cell-derived exosomes and found that cells showed higher miR-92b-3p levels and lower PTEN levels (**Figure 6E**). We further assessed the effect of exosomes on cell migration. As expected, SBC-3 cells displayed high migration ability after incubation with SBC-3 OE cell exosomes (**Figure 6F**). To explore the role of the exosomes *in vivo*, we established a xenograft model. As shown in **Figure 6G**, DDP treatment inhibited tumor growth, whereas combination therapy with exosomes significantly reversed the antitumor effect of DDP. Taken together, these findings demonstrated that miR-92b-3p could be secreted by SCLC OE cells and then delivered via exosomes to promote cell migration and chemoresistance by mediating PTEN expression.

Plasma miR-92b-3p Expression Is Associated With Chemoresistance and Prognosis in Small Cell Lung Cancer Patients

To better understand the clinical value of miR-92b-3p in patients with SCLC, we measured the miR-92b-3p level in plasma samples. We found that plasma miR-92b-3p levels were significantly higher in patients with chemoresistant SCLC than in patients with chemosensitive SCLC (**Figure 7A**). Receiver operating characteristic (ROC) curves were plotted to determine the diagnostic efficacy of plasma miR-92b-3p for monitoring

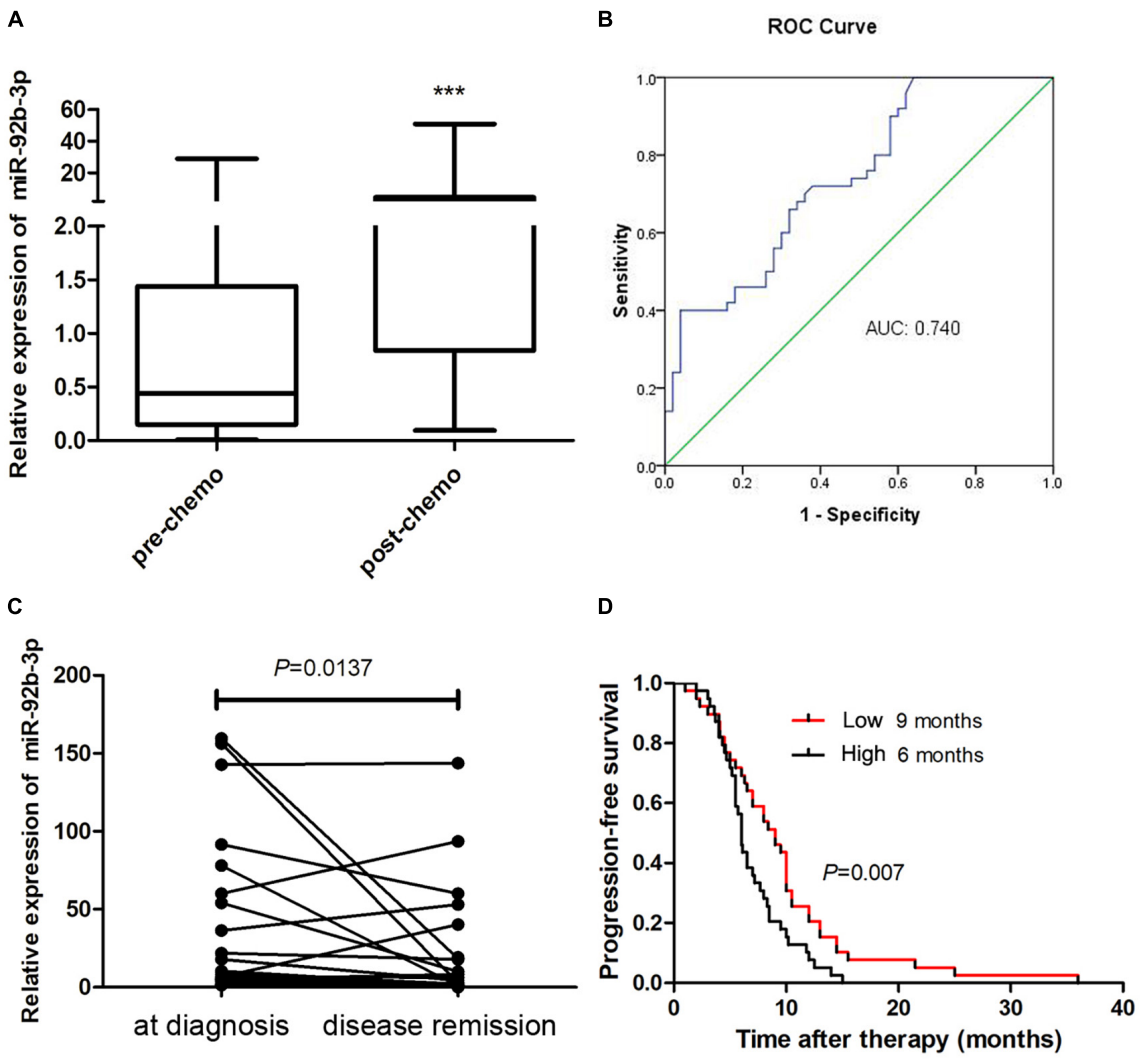

FIGURE 7 | MiR-92b-3p is a biomarker for monitoring the chemoresistance and prognosis of SCLC patients. **(A)** The expression of plasma miR-92b-3p in pre- and post-chemoresistant SCLC patients. **(B)** ROC curve analysis of plasma miR-92b-3p in pre- and post-chemoresistant SCLC patients. ***$P < 0.001$. **(C)** The level of circulating miR-92b-3p was particularly high in the plasma samples of SCLC patients who achieved disease remission. **(D)** Kaplan–Meier analysis showed that miR-92b-3p is a risk factor for the prognosis of SCLC patients. SCLC, small cell lung cancer and ROC, receiver operating characteristic.

chemoresistance in 50 SCLC patients. The area under the ROC curve (AUC) of miR-92b-3p was 0.74 (**Figure 7B**), indicating that miR-92b-3p was a potential biomarker that could distinguish pre- and post-chemoresistant SCLC patients. We next investigated whether miR-92b-3p could be used as a biomarker for monitoring the chemotherapy response in 25 SCLC patients. The relative levels of miR-92b-3p were significantly lower in the disease remission group than in the initial diagnosis group (**Figure 7C**), indicating that it has potential value for evaluating the chemotherapy response. We further conducted a prognostic Kaplan–Meier analysis of 78 SCLC patients. The progression-free survival (PFS) of SCLC patients with high miR-92b-3p expression was significantly shorter than that of patients with low miR-92b-3p expression (6 vs 9 months, $P = 0.007$, **Figure 7D**), indicating that miR-92b-3p was a risk factor for the prognosis of SCLC patients.

DISCUSSION

Multidrug resistance is an essential factor contributing to the high morbidity and mortality in SCLC. Therefore, it is important to explore possible targets to prevent the occurrence of chemoresistance (Huang et al., 2019; Peng et al., 2020). In recent years, numerous studies have shown that miRNAs play a key role in regulating the chemoresistance of cancer cells (Dong et al., 2019; Farhan et al., 2019; Yu et al., 2019). Both oncogenic and tumor-suppressive roles of different miRNAs have been reported in various cancers (Gong et al., 2018; Li C. et al., 2019; Wang et al., 2019). It is well recognized that several miRNAs, including miR-495 (Ye et al., 2017), miR-335 (Tang et al., 2016), miR-30a-5p (Yang et al., 2017), and miR-7 (Liu et al., 2015), are involved in SCLC chemoresistance. In the present study, we first analyzed the distribution of different miRNAs in plasma exosomes from SCLC patients at the pre- and post-chemoresistant stages. The data showed that miR-92b-3p levels were significantly increased in patients with chemoresistant SCLC. Similarly, miR-92b-3p expression was enhanced in chemoresistant SCLC cell lines. As expected, miR-92b-3p overexpression reversed the inhibitory effect of chemotherapy drugs on cell proliferation, migration, and invasion and reduced the rate of apoptosis. Moreover, miR-92b-3p overexpression promoted tumor growth in animal experiments. These results suggested that miR-92b-3p accelerated SCLC development and chemoresistance. However, the molecular mechanisms through which miR-92b-3p exerts these functions are still poorly understood.

MicroRNAs binding to the 3′-UTR of target mRNAs usually resulted in translational suppression or mRNA degradation of numerous target genes (Zhang et al., 2014). To gain insight into the molecular mechanisms through which miR-92b-3p regulates SCLC chemoresistance, bioinformatics was used to predict its possible target genes. As shown in the database, PTEN was found to be a target of miR-92b-3p. The PTEN/AKT pathway has been shown as an important target in remodeling of the nervous system. On the one hand, PTEN suppression reactivates the PI3K/AKT/mammalian target of rapamycin pathway, which leads to further neuron growth and protein synthesis (Goschzik et al., 2014). AKT phosphorylation can also suppress the activity of glycogen synthase kinase 3β and further modify microtubule or actin assembly within the axon, thereby contributing to axon regeneration (Liu et al., 2012; Berry et al., 2016). On the other hand, Godena and Ning (2017) demonstrated that PTEN downregulation could inhibit neuronal apoptosis through the AKT pathway. In addition, several studies have shown that the PTEN/PI3K/AKT pathway is involved in chemoresistance in various cancers. Zhao et al. revealed that miR-3142 regulated cell proliferation and chemoresistance through activating the PTEN/AKT pathway in CML (Zhao et al., 2017). Yu et al. (2008) demonstrated that the PI3K/AKT pathway played an important role in the chemoresistance of gastric cancer cells to etoposide and doxorubicin. Yang et al. (2020) reported that miR-1269b promoted DDP resistance in human NSCLC by modulating the PTEN/PI3K/AKT signaling pathway. Consistent with these findings, we predict that the PTEN/AKT pathway is involved in regulating SCLC chemoresistance. In our study, luciferase activity analysis confirmed that miR-92b-3p could directly target PTEN. We further observed that miR-92b-3p exerted the regulatory function by decreasing PTEN levels and consequently promoted phosphorylation of its downstream target, AKT, *in vitro* and *in vivo*. Additionally, p-AKT downregulation observably reduced cell migration and chemoresistance and promoted PTEN but reduced miR-92b-3p expression in SCLC cells. These data indicated that miR-92b-3p promoted SCLC chemoresistance through the PTEN/AKT pathway.

As secreted miRNAs, exosomal miRNAs appear to be appropriate as ideal biomarkers of cancers due to their non-invasive features. Tumor-derived exosomes contain multiple miRNAs involved in carcinogenesis, cell migration, invasion, and chemoresistance in various cancers (He et al., 2019). One probable explanation for these inconsistent effects may relate to the complex interactions among intercellular environmental factors, exosomes and recipient cells. Several serum exosomal miRNAs serve as predictive markers for chemoresistance in advanced colorectal cancer (Jin et al., 2019). Exosomes derived from gemcitabine-resistant cells can confer malignant phenotypes to target cells by delivering miRNA-222-3p (Wei et al., 2017). Li D. et al. (2020) reported that exosomal miR-613 could reverse resistance to DDP in NSCLC. Ma et al. (2019) showed that exosomes could transfer DDP-induced miR-425-3p to confer chemoresistance in NSCLC. However, few studies have identified the role of exosomal miRNAs in SCLC. In the present study, exosomes were extracted from the conditioned medium of SCLC cells overexpressing miR-92b-3p. Our results showed that these exosomes significantly promoted SBC-3 cell migration and chemoresistance *in vitro* and observably reduced the inhibitory effect of DDP on tumor growth *in vivo*. Moreover, SCLC cells incubated with exosomes showed lower PTEN levels and higher miR-92b-3p levels, indicating that miR-92b-3p could be transferred via exosomes and then target PTEN to confer chemoresistance in SCLC.

Since miRNAs are highly stable in plasma/serum, they have great potential as the biomarkers in cancer screening and monitoring (Mitchell et al., 2008). Serum levels of miR-21 and miR-92 have been reported to predict recurrence in colon cancer patients (Conev et al., 2015). Plasma miR-92a-2

is a potential biomarker for SCLC diagnosis (Yu et al., 2017). In our study, we found that plasma miR-92b-3p levels were significantly increased in chemoresistant SCLC patients, and the AUC was 0.74. Conversely, plasma miR-92b-3p expression was decreased in patients who achieved disease remission. Moreover, SCLC patients with high miR-92b-3p expression had shorter PFS. These data indicated that the plasma miR-92b-3p level has potential value for monitoring the chemoresistance, chemotherapy response, and prognosis of SCLC patients.

Certainly, our study possessed some limitations. First, our previous findings showed above indicated that circulating miR-92b and miR-375 might be ideal non-invasive biomarkers for monitoring the drug resistance during chemotherapy and evaluating the prognosis of the patients with SCLC (Li M. et al., 2020). The function and underlying molecular mechanism involved in miR-375-regulated the chemoresistance of SCLC remain unclear. Second, there are other potential target pathways for the miR-92b-3p associated with SCLC chemoresistance. Thus, more studies are needed to the unresolved areas in the future.

CONCLUSION

In summary, we investigated the involvement of the PTEN/AKT regulatory network in miR-92b-3p-mediated cell migration and chemoresistance *in vitro* and *in vivo*. In addition, our study verified that exosomes could transfer miR-92b-3p to promote the development of SCLC chemoresistance. Moreover, circulating miR-92b-3p might be a potential dynamic biomarker to monitor the chemoresistance, chemotherapy response, and prognosis of SCLC patients. Our data will provide new insights for the SCLC treatment and also lay a foundation for the clinical application of exosomal miRNAs.

DATA AVAILABILITY STATEMENT

The datasets presented in this study can be found in online repositories. The names of the repository/repositories and accession number(s) can be found below: Gene Expression Omnibus (GEO) database under accession number GSE168436.

ETHICS STATEMENT

The studies involving human participants were reviewed and approved by The Institutional Animal Care and Use Committee of The First Affiliated Hospital of University of Science and Technology of China. The patients/participants provided their written informed consent to participate in this study. The animal study was reviewed and approved by The Institutional Animal Care and Use Committee of The First Affiliated Hospital of University of Science and Technology of China.

AUTHOR CONTRIBUTIONS

WL and ML designed the project. YH, FC, YC, WS, LL, and XD collected samples and performed the clinical study. WS and ML designed the analysis and analyzed the data. WS wrote the manuscript. WL, ML, WS, LL, XB, JZ, and HL revised the manuscript. All authors contributed to the article and approved the submitted version.

FUNDING

This study was supported by the Natural Science Foundation of Anhui Province (grant number: 2008085MH288) and the National Natural Science Foundation of China (Grant Number: 81972191), Science and Technology Major Project of Anhui Province (Grant Number: 18030801140), the Fundamental Research Funds for Central University (grant numbers: WK9110000025, WK9110000072, and WK9110000071), and the National Cancer Center Climbing Funds (grant number: NCC201812B036). A portion of this work was supported by the High Magnetic Field Laboratory of Anhui Province.

REFERENCES

Berry, M., Ahmed, Z., Morgan-Warren, P., Fulton, D., and Logan, A. (2016). Prospects for mTOR-mediated functional repair after central nervous system trauma. *Neurobiol. Dis.* 85, 99–110. doi: 10.1016/j.nbd.2015.10.002

Borromeo, M. D., Savage, T. K., Kollipara, R. K., He, M., Augustyn, A., Osborne, J. K., et al. (2016). ASCL1 and NEUROD1 reveal heterogeneity in pulmonary neuroendocrine tumors and regulate distinct genetic programs. *Cell Rep.* 16, 1259–1272. doi: 10.1016/j.celrep.2016.06.081

Conev, N. V., Donev, I. S., Konsoulova-Kirova, A. A., Chervenkov, T. G., Kashlov, J. K., and Ivanov, K. D. (2015). Serum expression levels of miR-17, miR-21, and miR-92 as potential biomarkers for recurrence after adjuvant chemotherapy in colon cancer patients. *Biosci. Trends* 9, 393–401. doi: 10.5582/bst.2015.01170

Dong, C., Liu, X., Wang, H., Li, J., Dai, L., and Xu, Z. (2019). Hypoxic non-small-cell lung cancer cell-derived exosomal miR-21 promotes resistance of normoxic cell to cisplatin. *Oncol. Targets Ther.* 12, 1947–1956. doi: 10.2147/OTT.S186922

Farhan, M., Malik, A., Ullah, M. F., Afaq, S., Faisal, M., Farooqi, A. A., et al. (2019). Garcinol sensitizes NSCLC Cells to standard therapies by regulating EMT-modulating miRNAs. *Int. J. Mol. Sci.* 20, 800. doi: 10.3390/ijms20040800

Godena, V. K., and Ning, K. (2017). Phosphatase and tensin homologue: a therapeutic target for SMA. *Signal. Transduct. Target Ther.* 2:17038. doi: 10.1038/sigtrans.2017.38

Gong, L., Ren, M., Lv, Z., Yang, Y., and Wang, Z. (2018). miR-92b-3p promotes colorectal carcinoma cell proliferation, invasion, and migration by inhibiting FBXW7 in vitro and in vivo. *DNA Cell Biol.* 37, 501–511. doi: 10.1089/dna.2017.4080

Goschzik, T., Gessi, M., Denkhaus, D., and Pietsch, T. (2014). PTEN mutations and activation of the PI3K/Akt/mTOR signaling pathway in papillary tumors of the pineal region. *J. Neuropathol. Exp. Neurol.* 73, 747–751. doi: 10.1097/NEN.0000000000000093

He, S., Li, Z., Yu, Y., Zeng, Q., Cheng, Y., Ji, W., et al. (2019). Exosomal miR-499a-5p promotes cell proliferation, migration and EMT via mTOR signaling pathway in lung adenocarcinoma. *Exp. Cell Res.* 379, 203–213. doi: 10.1016/j.yexcr.2019.03.035

Huang, W. C., Kuo, K. T., Wang, C. H., Yeh, C. T., and Wang, Y. (2019). Cisplatin resistant lung cancer cells promoted M2 polarization of tumor-associated macrophages via the Src/CD155/MIF functional pathway. *J. Exp. Clin. Cancer Res.* 38:180. doi: 10.1186/s13046-019-1166-3

Jin, G., Liu, Y., Zhang, J., Bian, Z., Yao, S., Fei, B., et al. (2019). A panel of serum exosomal microRNAs as predictive markers for chemoresistance in advanced colorectal cancer. *Cancer Chemother. Pharmacol.* 84, 315–325. doi: 10.1007/s00280-019-03867-6

Joyce, D. P., Kerin, M. J., and Dwyer, R. M. (2016). Exosome-encapsulated microRNAs as circulating biomarkers for breast cancer. *Int. J. Cancer* 139, 1443–1448. doi: 10.1002/ijc.30179

Lei, L., Huang, Y., and Gong, W. (2014). Inhibition of miR-92b suppresses nonsmall cell lung cancer cells growth and motility by targeting RECK. *Mol. Cell. Biochem.* 387, 171–176. doi: 10.1007/s11010-013-1882-5

Li, C., Huo, B., Wang, Y., and Cheng, C. (2019). Downregulation of microRNA-92b-3p suppresses proliferation, migration, and invasion of gastric cancer SGC-7901 cells by targeting Homeobox D10. *J. Cell. Biochem.* 120, 17405–17412. doi: 10.1002/jcb.29005

Li, D., Meng, D., and Niu, R. (2020). Exosome-reversed chemoresistance to cisplatin in non-small lung cancer through transferring miR-613. *Cancer Manag. Res.* 12, 7961–7972. doi: 10.2147/CMAR.S254310

Li, M., Shan, W., Hong, B., Zou, J., Li, H., Han, D., et al. (2020). Circulating miR-92b and miR-375 for monitoring the chemoresistance and prognosis of small cell lung cancer. *Sci. Rep.* 10:12705. doi: 10.1038/s41598-020-69615-6

Li, Y. Y., Zheng, X. H., Deng, A. P., Wang, Y., Liu, J., Zhou, Q., et al. (2019). MiR-92b inhibited cells EMT by targeting Gabra3 and predicted prognosis of triple negative breast cancer patients. *Eur. Rev. Med. Pharmacol. Sci.* 23, 10433–10442. doi: 10.26355/eurrev_201912_19682

Liu, C. M., Hur, E. M., and Zhou, F. Q. (2012). Coordinating gene expression and axon assembly to control axon growth: potential role of GSK3 signaling. *Front. Mol. Neurosci.* 5:3. doi: 10.3389/fnmol.2012.00003

Liu, H., Huang, J., Peng, J., Wu, X., Zhang, Y., Zhu, W., et al. (2015). Upregulation of the inwardly rectifying potassium channel Kir2.1 (KCNJ2) modulates multidrug resistance of small-cell lung cancer under the regulation of miR-7 and the Ras/MAPK pathway. *Mol. Cancer* 14:59. doi: 10.1186/s12943-015-0298-0

Liu, T., Zhang, X., Du, L., Wang, Y., Liu, X., Tian, H., et al. (2019). Exosome-transmitted miR-128-3p increase chemosensitivity of oxaliplatin-resistant colorectal cancer. *Mol. Cancer* 18:43. doi: 10.1186/s12943-019-0981-7

Lobb, R. J., Becker, M., Wen, S. W., Wong, C. S., Wiegmans, A. P., Leimgruber, A., et al. (2015). Optimized exosome isolation protocol for cell culture supernatant and human plasma. *J. Extracell. Vesicles* 4, 27031. doi: 10.3402/jev.v4.27031

Long, M., Zhan, M., Xu, S., Yang, R., Chen, W., Zhang, S., et al. (2017). miR-92b-3p acts as a tumor suppressor by targeting Gabra3 in pancreatic cancer. *Mol. Cancer* 16:167. doi: 10.1186/s12943-017-0723-7

Ma, Y., Yuwen, D., Chen, J., Zheng, B., Gao, J., Fan, M., et al. (2019). Exosomal transfer of cisplatin-induced miR-425-3p confers cisplatin resistance in NSCLC through activating autophagy. *Int. J. Nanomed.* 14, 8121–8132. doi: 10.2147/IJN.S221383

Mao, S., Lu, Z., Zheng, S., Zhang, H., Zhang, G., Wang, F., et al. (2020). Exosomal miR-141 promotes tumor angiogenesis via KLF12 in small cell lung cancer. *J. Exp. Clin. Cancer Res.* 39:193. doi: 10.1186/s13046-020-01680-1

Mitchell, P. S., Parkin, R. K., Kroh, E. M., Fritz, B. R., Wyman, S. K., Pogosova-Agadjanyan, E. L., et al. (2008). Circulating microRNAs as stable blood-based markers for cancer detection. *Proc. Natl. Acad. Sci. U.S.A.* 105, 10513–10518. doi: 10.1073/pnas.0804549105

Peng, J., Wang, Q., Liu, H., Ye, M., Wu, X., and Guo, L. (2016). EPHA3 regulates the multidrug resistance of small cell lung cancer via the PI3K/BMX/STAT3 signaling pathway. *Tumour Biol.* 37, 11959–11971. doi: 10.1007/s13277-016-5048-4

Peng, L., Li, Y., Wei, S., Li, X., Dang, Y., Zhang, W., et al. (2020). LAMA4 activated by androgen receptor induces the cisplatin resistance in gastric cancer. *Biomed. Pharmacother.* 124:109667. doi: 10.1016/j.biopha.2019.109667

Siegel, R. L., Miller, K. D., and Jemal, A. (2019). Cancer statistics, 2019. *CA Cancer J. Clin.* 69, 7–34. doi: 10.3322/caac.21551

Sun, Y., Zhou, Y., Bai, Y., Wang, Q., Bao, J., Luo, Y., et al. (2017). A long non-coding RNA HOTTIP expression is associated with disease progression and predicts outcome in small cell lung cancer patients. *Mol. Cancer* 16:162. doi: 10.1186/s12943-017-0729-1

Tang, R., Lei, Y., Hu, B., Yang, J., Fang, S., Wang, Q., et al. (2016). WW domain binding protein 5 induces multidrug resistance of small cell lung cancer under the regulation of miR-335 through the Hippo pathway. *Br. J. Cancer* 115, 243–251. doi: 10.1038/bjc.2016.186

Wang, C., Uemura, M., Tomiyama, E., Matsushita, M., Koh, Y., Nakano, K., et al. (2020). MicroRNA-92b-3p is a prognostic oncomiR that targets TSC1 in clear cell renal cell carcinoma. *Cancer Sci.* 111, 1146–1155. doi: 10.1111/cas.14325

Wang, W., Fu, S., Lin, X., Zheng, J., Pu, J., Gu, Y., et al. (2019). miR-92b-3p functions as a key gene in esophageal squamous cell cancer as determined by co-expression analysis. *Onco Targets Ther.* 12, 8339–8353. doi: 10.2147/OTT.S220823

Wei, F., Ma, C., Zhou, T., Dong, X., Luo, Q., Geng, L., et al. (2017). Exosomes derived from gemcitabine-resistant cells transfer malignant phenotypic traits via delivery of miRNA-222-3p. *Mol. Cancer* 16:132. doi: 10.1186/s12943-017-0694-8

William, W. N. Jr., and Glisson, B. S. (2011). Novel strategies for the treatment of small-cell lung carcinoma. *Nat. Rev. Clin. Oncol.* 8, 611–619. doi: 10.1038/nrclinonc.2011.90

Yang, W., Xiao, W., Cai, Z., Jin, S., and Li, T. (2020). miR-1269b drives cisplatin resistance of human non-small cell lung cancer via modulating the PTEN/PI3K/AKT signaling pathway. *Onco Targets Ther.* 13, 109–118. doi: 10.2147/OTT.S225010

Yang, X., Bai, F., Xu, Y., Chen, Y., and Chen, L. (2017). Intensified beclin-1 mediated by low expression of Mir-30a-5p promotes chemoresistance in human small cell lung cancer. *Cell. Physiol. Biochem.* 43, 1126–1139. doi: 10.1159/000481754

Ye, M., Wei, T., Wang, Q., Sun, Y., Tang, R., Guo, L., et al. (2017). TSPAN12 promotes chemoresistance and proliferation of SCLC under the regulation of miR-495. *Biochem. Biophys. Res. Commun.* 486, 349–356. doi: 10.1016/j.bbrc.2017.03.044

Yu, C., Chen, D. Q., Liu, H. X., Li, W. B., Lu, J. W., and Feng, J. F. (2019). Rosmarinic acid reduces the resistance of gastric carcinoma cells to 5-fluorouracil by downregulating FOXO4-targeting miR-6785-5p. *Biomed. Pharmacother.* 109, 2327–2334. doi: 10.1016/j.biopha.2018.10.061

Yu, H. G., Ai, Y. W., Yu, L. L., Zhou, X. D., Liu, J., Li, J. H., et al. (2008). Phosphoinositide 3-kinase/Akt pathway plays an important role in chemoresistance of gastric cancer cells against etoposide and doxorubicin induced cell death. *Int. J. Cancer* 122, 433–443. doi: 10.1002/ijc.23049

Yu, Y., Zuo, J., Tan, Q., Zar Thin, K., Li, P., Zhu, M., et al. (2017). Plasma miR-92a-2 as a biomarker for small cell lung cancer. *Cancer Biomark.* 18, 319–327. doi: 10.3233/CBM-160254

Zhang, M., Luo, F., Zhang, Y., Wang, L., Lin, W., Yang, M., et al. (2014). *Pseudomonas aeruginosa* mannose-sensitive hemagglutinin promotes T-cell response via toll-like receptor 4-mediated dendritic cells to slow tumor progression in mice. *J. Pharmacol. Exp. Ther.* 349, 279–287. doi: 10.1124/jpet.113.212316

Zhao, L., Shan, Y., Liu, B., Li, Y., and Jia, L. (2017). Functional screen analysis reveals miR-3142 as central regulator in chemoresistance and proliferation through activation of the PTEN-AKT pathway in CML. *Cell Death Dis.* 8:e2830. doi: 10.1038/cddis.2017.223

Conflict of Interest: The authors declare that the research was conducted in the absence of any commercial or financial relationships that could be construed as a potential conflict of interest.

frontiers in Oncology

REVIEW
published: 10 June 2021
doi: 10.3389/fonc.2021.661620

Insights Into the Function and Clinical Application of HDAC5 in Cancer Management

Jun Yang[1†], Chaoju Gong[2†], Qinjian Ke[3], Zejun Fang[3], Xiaowen Chen[4], Ming Ye[5] and Xi Xu[6*]*

[1] Department of Orthopedic Surgery, Sanmen People's Hospital of Zhejiang Province, Sanmenwan Branch of the First Affiliated Hospital, College of Medicine, Zhejiang University, Sanmen, China, [2] Central Laboratory, The Municipal Affiliated Hospital of Xuzhou Medical University, Xuzhou, China, [3] Central Laboratory, Sanmen People's Hospital of Zhejiang Province, Sanmenwan Branch of the First Affiliated Hospital, College of Medicine, Zhejiang University, Sanmen, China, [4] Department of Pathophysiology, Zunyi Medical University, Zunyi, China, [5] Department of General Surgery, Sanmen People's Hospital of Zhejiang Province, Sanmenwan Branch of the First Affiliated Hospital, College of Medicine, Zhejiang University, Sanmen, China, [6] Department of Pathology, The Second Affiliated Hospital, Zhejiang University School of Medicine, Hangzhou, China

OPEN ACCESS

Edited by:
Lorenzo Gerratana, University of Udine, Italy

Reviewed by:
Jian Zhu, Shandong University, China
Viviana Moresi, National Research Council (CNR), Italy

***Correspondence:**
Xi Xu
zdxuxi@zju.edu.cn
Ming Ye
yemingsm@163.com

[†]These authors have contributed equally to this work

Specialty section:
This article was submitted to Molecular and Cellular Oncology, a section of the journal Frontiers in Oncology

Received: *31 January 2021*
Accepted: *18 May 2021*
Published: *10 June 2021*

Citation:
Yang J, Gong C, Ke Q, Fang Z, Chen X, Ye M and Xu X (2021) Insights Into the Function and Clinical Application of HDAC5 in Cancer Management. Front. Oncol. 11:661620. doi: 10.3389/fonc.2021.661620

Histone deacetylase 5 (HDAC5) is a class II HDAC. Aberrant expression of HDAC5 has been observed in multiple cancer types, and its functions in cell proliferation and invasion, the immune response, and maintenance of stemness have been widely studied. HDAC5 is considered as a reliable therapeutic target for anticancer drugs. In light of recent findings regarding the role of epigenetic reprogramming in tumorigenesis, in this review, we provide an overview of the expression, biological functions, regulatory mechanisms, and clinical significance of HDAC5 in cancer.

Keywords: HDAC5, cancer, biological function, clinical application, biomarker

INTRODUCTION

Covalent modification of chromatin regulates gene transcription during cell differentiation; this includes histone acetylation and deacetylation, which modulate the binding of transcription factors to DNA. Modifications can occur at various sites, including the N-terminal amino acid residues of histones H3 and H4, and the N- and C-terminal amino acid residues of histones H2A, H2B, and H1. Histone acetylation of the ϵ-amino group of lysine, one of the earliest and most common posttranslational modifications of histones, is regulated by histone acetyltransferases and histone deacetylases (HDACs) (1–5).

The HDAC family has 18 members that can be divided into 4 classess based on their structure and function (6, 7). Class I includes HDAC1-3 and 8; class II includes HDAC4-7, 9, and 10; and class III includes sirtuin enzymes (SIRT 1-7). These 3 classes constitute the classical HDACs. Class IV comprises only HDAC11, which is structurally distinct from the other HDACs. Class II HDACs are further divided into class IIa (HDAC4, 5, 7, and 9) and class IIb (HDAC6 and 10) based on their subcellular localization and expression pattern (8).

Class IIa HDACs have a high degree of homology to yeast hda1 (HDAC-1). In addition to the C-terminal catalytic core, all class IIa HDACs have a conserved N-terminal extension that can bind to transcription factors and the chaperone protein 14-3-3. For example, when phosphorylated by

calcium/calmodulin dependent protein kinase (CaMK) or protein kinase D (PKD), class IIa HDACs bind to 14-3-3, inducing its disaggregation from the transcription factor myocyte specific enhancer factor 2 (MEF2) and bringing about its shuttling from the nucleus to the cytoplasm (9).

As a class IIa HDAC, HDAC5 not only catalyzes the deacetylation of nuclear histones, but also deacetylates or forms complexes with other proteins in various physiologic contexts including nerve regeneration and neuronal apoptosis (10, 11), glucose metabolism (12), and insulin resistance (13). Cancer is one of the leading causes of death worldwide, and the identification of further specific molecular markers of cancer will be useful for early diagnosis, therapeutic targeting, and treatment response monitoring. This review highlights the current state of knowledge of the roles and clinical significance of HDAC5 in tumorigenesis.

STRUCTURE AND DISTRIBUTION OF HDAC5

Structure of HDAC5

HDAC5 was first identified in the mouse genome in 1999 (14). The gene encoding HDAC5 (also known as HD5 or NY-CO-9) in humans is located on chromosome 17q21 and spans 39,138 bp, comprising 26 exons. The protein consists of 1122 amino acids, has a molecular weight of 121.9 kDa, and has C-terminal deacetylase and N-terminal adapter domains. The former domain, which is also referred to as the HDAC domain, contains a nuclear export sequence(NES) and is highly conserved (80% homology) across class IIa HDACs; it is composed of 400-450 amino acids and shares 53% sequence similarity with yeast hda1 (15). The conserved 450-600 amino acid N-terminal adaptor domain has a nuclear localization sequence (NLS) and binds to transcription factors such as C-terminal-binding protein (CtBP), MEF2, and heterochromatin P1 (HP1) (3).

HDAC5 also has a flexible zinc-binding element outside the catalytic core. This element contains highly conserved cysteine and histidine residues that form a hydrophobic pocket near the substrate-binding channel. It may mediate substrate recognition and regulate enzymatic activity and interactions with other proteins (16). Moreover, HDAC5 also has a conserved histidine near the first zinc-binding site whose side chain turns outward and is far away from the catalytic active site (17). Thus, while HDAC5 by itself has no deacetylase activity, it can be induced by interaction with HDAC3 through the silencing mediator of retinoic acid and thyroid hormone receptor (SMRT)/nuclear receptor corepressor (NCoR) coinhibition complex (18). In other words, HDAC5 regulates gene expression by binding to transcription factors through its N terminal adapter domain and targeting the SMRT/NCoR-HDAC3 complex to a specific subcellular location through its C-terminal deacetylase domain.

Distribution of HDAC5

HDAC5 protein is expressed in lung, brain, myocardium, skeletal muscle, and placenta, and accumulating evidence indicates that it has variable expression and functions in different types of tumor: HDAC5 is overexpressed in breast cancer (19, 20), hepatocellular carcinoma (HCC) (21), lung cancer (22), pancreatic neuroendocrine cancer(pNET) (23) and colorectal cancer(CRC) (24). In contrast, although HDAC5 was shown to induce tissue invasion of gastric cancer cells (25), gene expression profiles of histone modifiers indicate that HDAC5 is downregulated in gastric cancer (26) (**Table 1**). These conflicting findings imply that HDAC5 exhibits dual functions in cancer development. Furthermore, HDAC5 mRNA and protein have been detected in the blood of patients with CRC (32, 33) and breast cancer (34), but not in that of healthy subjects or patients with nonrecurrent cancer, suggesting that circulating HDAC5 may serve as a potential biomarker for cancer diagnosis and prognosis.

REGULATION OF HDAC5

Posttranslational Modification of HDAC5

Proteomics analysis combined with phosphomutant screening has revealed that there are at least 17 phosphorylation sites in the HDAC5 functional domains (35), highlighting that HDAC5 can be phosphorylated at multiple conserved residues by a variety of protein kinases. For example, PKD, CaMK II, and AMPK phosphorylate Ser259 and Ser498 on both sides of the HDAC5

TABLE 1 | The expression of HDAC5 in various tumors.

Tumor types	Expression status	Detection methods	References
Breast cancer	Up-regulation	IHC	(20)
		IHC, qRT-PCR	(19)
Hepatocellular carcinoma	Up-regulation	IHC	(21)
Lung cancer	Up-regulation	Western Blot, qRT-PCR	(22)
		qRT-PCR	(27)
Melanoma	Up-regulation	IHC, Western Blot	(28)
Pancreatic neuroendocrine cancer	Up-regulation	IHC	(23)
Colorectal cancer	Up-regulation	qRT-PCR	(24)
Glioma	Up-regulation	Western Blot, qRT-PCR	(29)
Osteosarcoma	Up-regulation	Western Blot, qRT-PCR	(30)
Wilms' tumor	Up-regulation	Western Blot, qRT-PCR	(31)
Gastic cancer	Down-regulation	qRT-PCR	(26)

NLS, which promotes the binding of 14-3-3 to HDAC5 and its shuttling from the nucleus to the cytoplasm (36–38). In myocyte-like cells, cAMP signaling prevents 14-3-3 binding to HDAC5 by bringing about Ser498 hypophosphorylation (39). Protein kinase C-related kinase 1/2 (PRK1/2) phosphorylate HDAC5 at Thr292 in the NLS, promoting its binding to 14-3-3 and preventing HDAC5 nuclear entry (40). Additionally, minibrain-related kinase (Mirk) phosphorylates HDAC5 at Ser279, preventing its translocation from the cytoplasm to the nucleus (41) (**Figure 1**).

Non-Coding RNAs Modification to HDAC5

HDAC5 expression is regulated by miRNAs. miR-2861 was the first reported miRNA to directly regulate HDAC5, which it does by binding to the HDAC5 mRNA coding sequence (42). miR-9 suppresses HDAC5 activity (43) and inhibits the translation of HDAC5 transcript by binding to the 3′ untranslated region (44). Other miRNAs known to regulate HDAC5 are miR-124 (44, 45), miR-125a-5p (46), miR-589-5p (27), and miR-217 (47). Many miRNAs targeting HDAC5 have been identified using target prediction software (**Supplementary Table 1**), although most of these require experimental validation.

According to the competing endogenous RNA (ceRNA) hypothesis, long noncoding RNAs (lncRNAs) inhibit miRNA function by acting as endogenous miRNA sponges (48). The lncRNA SENEBLOC acts as a sponge regarding miR-3175, thereby upregulating HDAC5 (49). Additional studies investigating the role of lncRNAs in HDAC5 regulation are currently underway. The findings to date indicate that HDAC5 is epigenetically modified and regulated at the transcriptional level (**Figure 2**), providing new avenues for HDAC5-based cancer therapy.

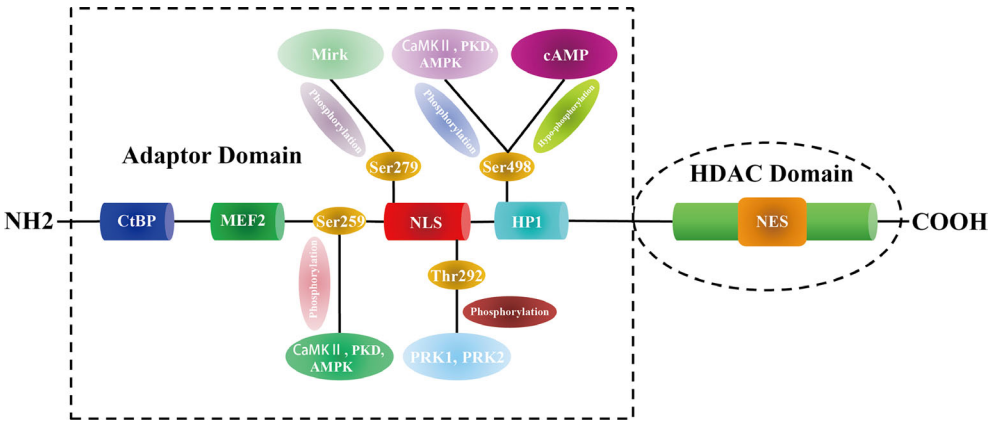

FIGURE 1 | The structure and modification sites of HDAC5.

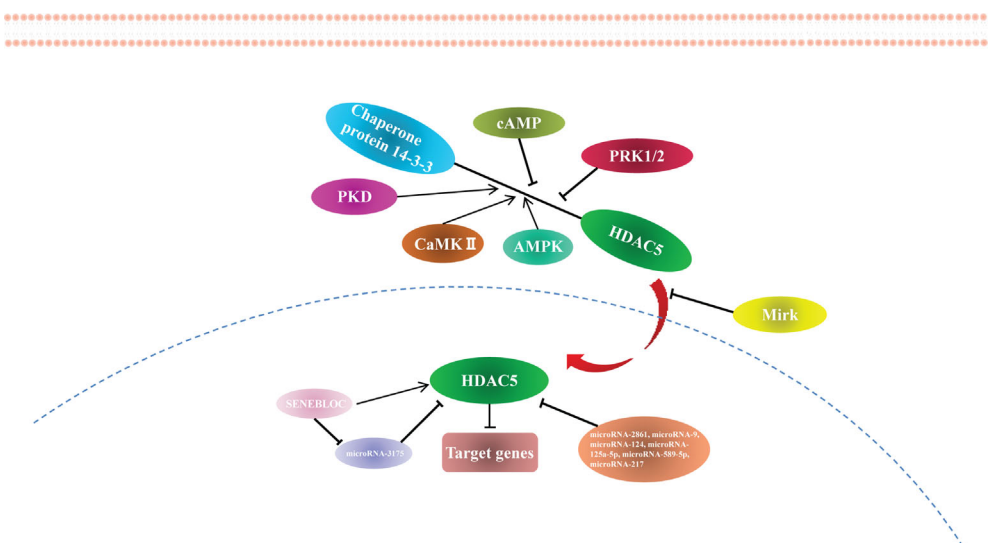

FIGURE 2 | The regulation of HDAC5.

HDAC5 IN CANCER

The functions of HDAC5 in tumorigenesis have been investigated in a variety of cancers. HDAC5 plays distinct roles in different cancer types. In this review, we summarize recent findings on the biological activities of HDAC5 in several common cancers and cancer-related processes (**Table 2**, **Figure 3**).

Role of HDAC5 in Cancer Metastasis and Invasion

PCR and immunohistochemical analyses have shown that HDAC5 was highly expressed in the cytoplasm of malignant epithelial cells, and HDAC5 expression was positively associated with distant metastasis and lymph node metastasis (65). HDAC5 expression was also found to be positively associated with

TABLE 2 | Multiple cellular processes of HDAC5 in cancer management.

Tumor type	Expression status	Target genes	Effect upon cell lines	References
Breast Cancer	Up-regulation	LSD1	Increase cell metastasis and invasion	(50)
	Up-regulation	p53	inhibit cell proliferation	(51)
	Up-regulation	RUNX3	increase cell stemness	(46)
	Up-regulation	SOX9	increase chemoresistance	(52)
	Up-regulation	miR-125a-5p, Sp1, survivin	increase chemoresistance	(53)
Neuroblastoma	Up-regulation	CD9	Increase cell metastasis and invasion	(54)
	Up-regulation	N-myc	promote cell proliferation	(55)
	Up-regulation	N-myc	block cell differentiation	(55)
Medulloblastoma	Up-regulation	caspase-3	inhibit cell apoptosis	(56)
Lung Cancer	Up-regulation	DLL4, Six1, Notch1, Twist1	promote cell proliferation	(22)
Colorectal Cancer	Up-regulation	DLL4	promote cell proliferation	(57)
Osteosarcoma	Up-regulation	Twist	promote cell proliferation	(30)
	Up-regulation	N/A	maintain long telomeres' length	(58)
Fibrosarcoma	Up-regulation	N/A	maintain long telomeres' length	(58)
Wilms' tumor	Up-regulation	c-Met	promote cell proliferation	(31)
Glioma	Up-regulation	Notch1	promote cell proliferation	(29)
Hepatocellular carcinoma	Up-regulation	Six1	promote cell proliferation	(59)
	Up-regulation	p21, cyclin D1, CDK2/4/6	promote cell cycle	(60)
	Up-regulation	p53, Bax, cyto C, caspase-3, Bcl-2	inhibit cell apoptosis	(60)
Urothelial Carcinoma	Down-regulation	TGF-β	hinder cell proliferation	(61)
Lymphoma	Up-regulation	TNF-α, MCP-1	induce pro-inflammatory function	(62)
Pancreatic Cancer	Up-regulation	Socs3, CCL2, TGF-β	promote macrophage recruitment	(63)
Ovarian Cancer	Up-regulation	YY1, miR-99a	increase cell stemness	(64)

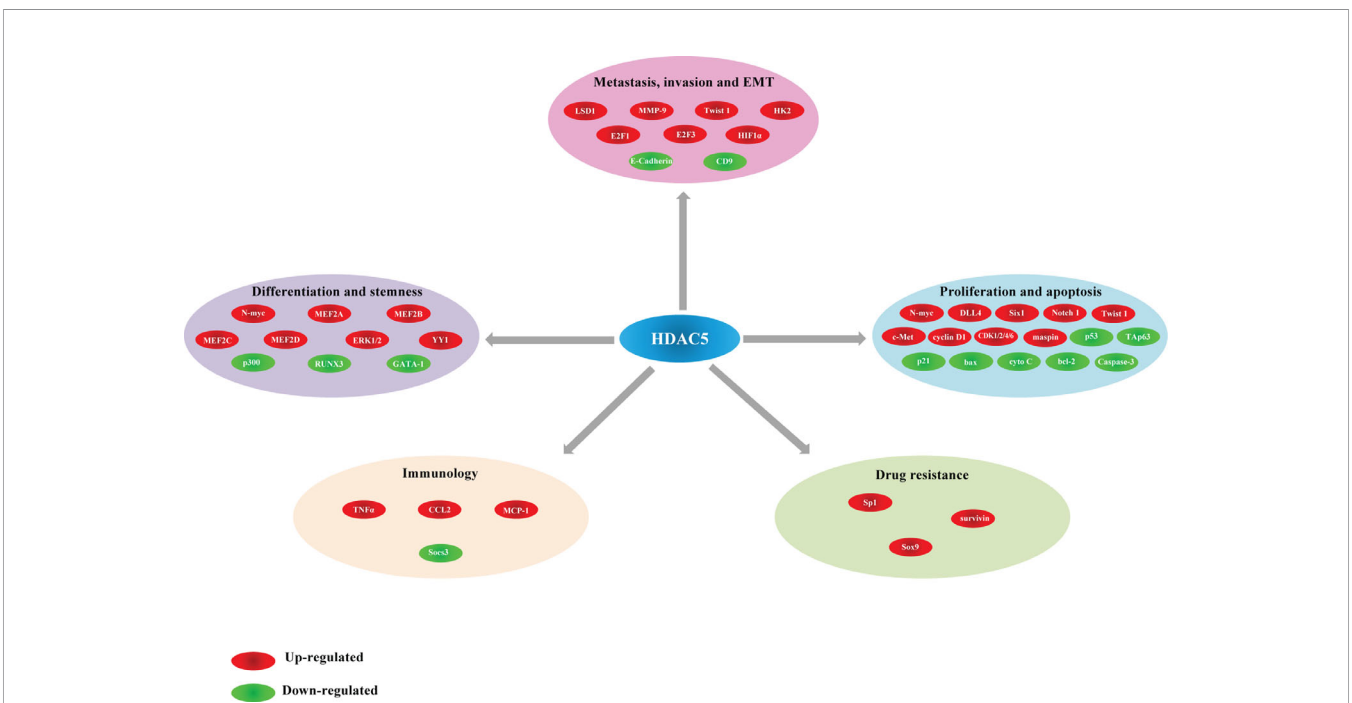

FIGURE 3 | Different actions of HDAC5 and their corresponding target genes in cancer.

intrahepatic metastasis and distant metastasis in HCC (21). In vitro and *in vivo* experiments have demonstrated that HDAC5 knockdown blocked metastasis of melanoma cells (28). Elevated HDAC5 expression is frequently observed in the luminal A and B subtypes of breast cancer, and HDAC5 silencing suppressed breast cancer cell motility and invasion (50). HDAC5 was also shown to promote cell invasion and metastasis in neuroblastoma (54), pancreatic cancer (66) and lung cancer (67).

In addition, HDAC5 enhanced the invasiveness of gastric cancer cell lines by stimulating protein kinase C (PKC)/matrix metalloproteinase 9 (MMP9) (25). Science MMP9 promotes tumor invasion and metastasis through extracellular matrix remodeling, regulation of cell adhesion, and degradation of vascular basement membrane and perivascular matrix during EMT (68, 69), the correlation between HDAC5 and EMT during tumorigenesis has drawn a great attention (**Table 3**).

In HCC, HDAC5 was shown to be involved in T-box 3 (Tbx3)-mediated EMT and metastasis, which was dependent on two HDAC5-interacting motifs (71). During HCC progression, application of the nonselective HDAC inhibitor (HDACi) panobinostat increased the expression of E-cadherin, an epithelial marker that is downregulated during EMT (74). HDAC5 was also found to promote doxorubicin-induced EMT in glioma cells, which could account for chemoresistance in glioma (73). On the other hand, it is worth noting that HDAC5 induced EMT but inhibited cell proliferation in urothelial carcinoma (UC) (61).

The basic helix-loop-helix transcription factor Twist1 can induce EMT by negatively regulating the transcription of E-cadherin (75). Twist1 is a downstream target of HDAC5 in osteosarcoma progression (30). In non-small cell lung cancer, HDAC5 activity was shown to induce the expression of EMT-related genes including the transcriptional regulators E2F1, E2F3, and Twist1 (27), providing evidence for its direct involvement in promoting EMT. As dysregulation of energy metabolism also contributes to EMT (76), it is possible that metabolic reprogramming is involved in HDAC5-mediated EMT. It was recently demonstrated that HDAC5 together with HDAC4 enhanced glycolysis by inducing the upregulation of hexokinase 2 (HK2), which was critical for EMT induced by hypoexpression of 5′ AMP-activated protein kinase (AMPK) in lung cancer (72).

Role of HDAC5 in Cancer Proliferation and Apoptosis

The contribution of HDAC5 to cancer cell proliferation has been investigated in many studies. For example, HDAC5 overexpression was shown to promote cell growth, while small interfering RNA (siRNA)-mediated silencing of HDAC5 caused cell cycle arrest at the G0 phase in medulloblastoma (56). In neuroblastoma, HDAC5 promoted cell proliferation but had little effect on cell death (55). Overexpression of HDAC5 increased the proliferation of lung cancer cells, possibly *via* upregulation of downstream target genes (22). HDAC5 also increased DLL4 expression in colorectal cancer (CRC) cells, thereby enhancing their proliferation (57). HDAC5 induced osteosarcoma cell proliferation in a Twist1-dependent manner, highlighting the varied functions of the HDAC5/Twist1 axis in tumor progression (30). HDAC5 also increased c-Met expression to promote Wilms' tumor cell proliferation (31). Notch1 signaling plays an important role in cancer cell proliferation (77, 78); HDAC5 was shown to promote Notch1 expression in glioma cells, leading to increased glioma cell proliferation (29). In HCC, HDAC5 activated cell proliferation by inducing Six1 expression, providing the first evidence for the oncogenic role of HDAC5 in HCC development and progression (59). However, HDAC5 also inhibits tumor cell proliferation. For example, elevated levels of HDAC5 in UC cells suppressed cell proliferation, an effect that may involve transforming growth factor β (TGF-β) (61).

Electron microscopy and immunohistochemical analyses of HDAC5 subcellular localization revealed that HDAC5 was associated with heterochromatin in S and G1 phases, suggesting a role in DNA replication and cell cycle progression (79). For example, HDAC5 silencing shielded cell-cycle of prostate cancer cells from RB-mediated repression (80). Knockdown of HDAC5 also induced G1 cell cycle arrest, which hindered breast cancer proliferation (50). Overexrpression of HDAC5 increased S phase of non-small cell lung cancer (NSCLC), which demonstrated that HDAC5 promote NSCLC proliferation through inducing DNA replication (27).

Cancer occurrence and progression are caused not only by abnormal cell proliferation and differentiation, but also by dysregulation of apoptosis. In fact, inducing cell apoptosis has become an important therapeutic strategy in cancer (81), and clarifying the role of cell apoptosis in cancer can provide insight into the molecular basis of tumorigenesis as well as a basis for the development of effective therapies. Recent studies have demonstrated the involvement of HDAC5 in cancer cell apoptosis. HDAC5 knockdown in medulloblastoma cell lines increased caspase-3 activity, which is important for apoptosis induction (56); and upregulation of apoptosis-related proteins and

TABLE 3 | The involvement of HDAC5 in epithelial-mesenchymal transition (EMT) processes.

Tumor Type	Up/down regulated	Target Genes	References
Hepatocellular carcinoma	Up	HIF1α	(70)
	Up	Tbx3	(71)
Gastric cancer	Up	MMP9	(25)
Lung cancer	Up	E2F1, E2F3, Twist1	(27)
	Up	HK2	(72)
	Up	E2F1, E2F3, Twist1, MMP2, MMP9, Vimentin	(27)
Glioma	Down	E-cadherin, Vimentin	(73)
Urothelial Carcinoma	Down	Cytokeratin 5, E-Cadherin, Vimentin	(61)

morphologic changes associated with apoptosis were observed in HeLa and MCF-7 cells transfected with a siRNA targeting HDAC5 (79). Overexpression of HDAC5 in HCC cells was correlated with reduced expression of p21 and hyperactivation of cyclin D1 and cyclin-dependent kinase 2/4/6 (CDK2/4/6), indicating that HDAC5 promotes cell cycle progression and blocks apoptosis in HCC tumorigenesis (60). However, in another study, overexpression of HDAC5 in MCF-7 breast cancer cells inhibited proliferation and promoted apoptosis in a p53-independent manner (51). Thus, HDAC5 may have opposite functions depending on the cellular context and interaction partner.

HDAC5 and Immuno-Oncology

Malignant cells can escape immune surveillance and rapidly proliferate to form a tumor. HDACs have been implicated in the immune response (82–84), and the regulation of HDACs in cellular immunity plays an important role in tumorigenesis. HDAC5 interacts with the immune system—including immune cells and inflammatory cytokines—in cancer occurrence or progression. HDAC5 was shown to be involved in macrophage differentiation in lymphoma U937 cells (85), and HDAC5 depletion in U937 cells reduced the levels of tumor necrosis factor α (TNF-α) and monocyte chemoattractant protein 1 (MCP-1) *via* stimulation of NF-κB activity, suggesting a regulatory function for HDAC5 in the proinflammatory response of macrophages (62). In vitro and *in vivo* experiments have shown that the suppressor function of regulatory T cells (Tregs) was attenuated in HDAC5$^{-/-}$ mice. Meanwhile, HDAC5 silencing suppressed the switch from CD4^{+} T cells to Tregs under polarizing conditions and inhibited interferon γ (IFN-γ) production by CD8^{+} T cells (86). Another study demonstrated that HDAC5 recruited macrophages to the tumor microenvironment through the Suppressor of cytokine signaling 3 (Socs3)/C-C motif chemokine ligand 2 (CCL2) axis and promoted pancreatic cancer *via* TGF-β-dependent paracrine signaling (63). These findings indicate that targeting HDAC5 is a promising cancer immunotherapy strategy.

HDAC5 in Cancer Cell Differentiation and Stemness

Aberrant differentiation plays an important role in tumorigenesis. Epigenetic modifications including histone deacetylation are involved in cell differentiation (87). As such, clarifying the role and mechanisms of HDAC5 in cellular differentiation may provide a basis for new therapeutic strategies in cancer.

HDAC5 overexpression inhibited murine embryonic kidney (MEK) cell differentiation through transcriptional repression of GATA-1 and prevented the colocalization of the 2 proteins during erythroid differentiation (88). HDAC5 was also observed to block N-myc-mediated differentiation in neuroblastoma cells (55). MEF2 family proteins, which are recruited by HDAC5, include MEF2A, MEF2B, MEF2C, and MEF2D (89). Alternative splicing of MEF2 genes can yield protein isoforms with distinct functions (90). MEF2Cα2 engaged in a weaker interaction with HDAC5 than MEF2Cα1 in rhabdomyosarcoma (RMS) cell lines, which nonetheless enhanced the ability of the MEF2Cα2 isoform to promote RMS differentiation (91).

Cancer stem cells play a key role in tumorigenesis and can significantly influence the response to tumor therapy (92). HDAC5 increased the stemness of human breast cancer stem cells through inhibiting the binding of the Runt-related transcription factor 3 (RUNX3)/p300 complex to the promoter of target genes (46). HDAC5 showed elevated expression in tumorspheres formed by H460 lung cancer cells. Application of the HDAC5 inhibitor LMK-235 reduced extracellular signal-regulated kinase 1/2 (ERK1/2) phosphorylation in a dose-dependent manner, demonstrating that the HDAC5-ERK1/2 axis plays an important role in maintaining the stemness of lung cancer stem cells (93). Additionally, during ovarian cancer (OC) progression, HDAC5 interacted with YY1 to promote OC cell stemness by deacetylating the promoter of the microRNA miR-99a (64). These results imply that HDAC5 regulates cancer cell differentiation and stemness through interaction with different cofactors.

HDAC5 and Drug Resistance

Drug resistance is a major reason for cancer treatment failure. The main mechanisms of resistance are enhanced anti-apoptotic capacity, hyperactivation of cell proliferation, DNA replication, and cell cycle progression (94). Given its important role in cell proliferation, cell cycling, and apoptosis, HDAC5 may play a key role in the development of therapeutic resistance.

HDAC5 knockdown was shown to increase the sensitivity of MCF-7 and HeLa cells to doxorubicin and cisplatin by inducing heterochromatin decondensation (79). HDAC5 was illustrated to be involved in sorafenib resistance of HCC as well (95). Tamoxifen is a first-line treatment for breast cancer, HDAC5 deacethylated SOX9 and made it localized in the nucleus, which was responsible for tamoxifen resistant in breast cancer (52). HDAC5 expression was also elevated in estrogen-independent breast cancer cells and induced tamoxifen resistance *via* the miR-125a-5p/specificity protein 1 (Sp1)/survivin axis (53). Additionally, formononetin inhibited HDAC5 expression to attenuate doxorubicin-induced EMT, thereby promoting doxorubicin sensitivity in glioma cells (73).

Telomeres are small DNA-protein complexes located at the end of linear chromosomes in eukaryotic cells that maintain chromosome integrity and are involved in cell cycle regulation (96). During tumorigenesis, telomerase stimulates the re-synthesis of telomeric DNA, allowing cancer cells to proliferate continuously, which reduces the efficacy of chemotherapy (97). Telomeres are subject to various epigenetic modifications (98–100). HDAC5 preferentially localized at long telomeres and maintains their length, and HDAC5 silencing was found to increase the sensitivity of osteosarcoma and fibrosarcoma cells with long telomeres to chemotherapy (58).

HDAC5 AND ONCOGENETIC SIGNALING PATHWAYS

Studies have indicated that HDAC5 participated in cancer progression through various oncogenetic signaling pathways, such as TAp63/maspin (21), HIPK2/HIF1α (70), and p65/NF-κB pathways (95)(**Figure 4**).

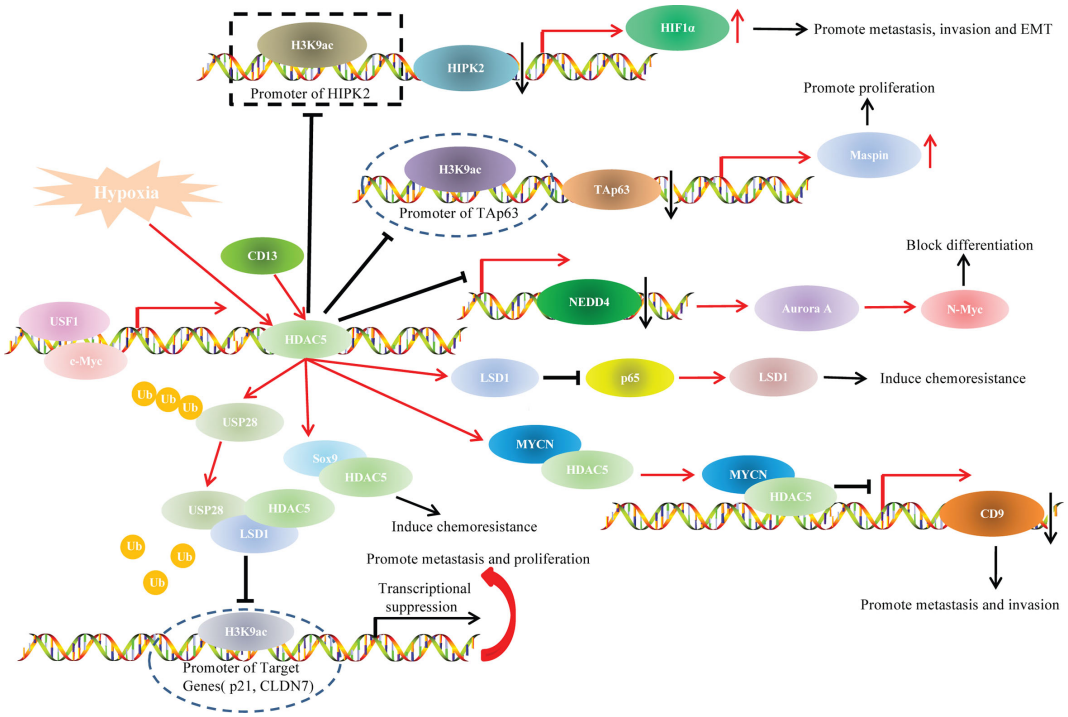

FIGURE 4 | DAC5 and oncogenic signaling pathways.

HDAC5 and TAp63/maspin Signaling

P63 is a new member of the p53 gene family. Although its structure is highly homologous to p53, p63 encodes a special C-terminal sequence, which contains sterile α group and a transcriptional inhibition domain. The C-terminus can bind to lipid membranes and inhibit transcription (101). Up to 14 p63 homologs have been identified, which are produced by transcription from different promoters and selective cleavage. The three p63 homologs that are produced through alternative splicing of mRNA transcribed from the promoter upstream of intron 1 are named TAp63α, TAp63β and TAp63γ because they contain a transcription domain (TA) (102). Many studies have demonstrated that these homologs are important transcriptional activators of mammary serine protease inhibitor (Maspin) (103, 104). Maspin (SERPINB5), a member of the serine protease inhibitor superfamily, is not only a serine protease inhibitor gene, but also a new soluble protein that is found in the cytoplasm. It can inhibit angiogenesis, increase cell adhesion, induce apoptosis and inhibit growth and metastasis of cancer cells (105, 106).

In our previous study, we explored the role of HDAC5 in HCC and found that HDAC5 overexpression induced HCC proliferation and tumorigenesis *in vitro*. We also knocked down HDAC5 in Hep3B (p53-null) and HepG2 (p53-WT) cells and investigated the expression levels of p53 family members. The results indicated that HDAC5 downregulated p53, TAp63, and p73 at both the mRNA and protein levels. In addition, TAp63 gradually decreased with HDAC5 overexpression in immortalized liver cell line (THLE-3 cells). Chromatin immunoprecipitation (ChIP) showed that HDAC5 knockdown increased the acetylation at the TAp63 promoter (i.e., at Lys9 of histone H3 [H3K9ac]), which indicated the suppressive effect of HDAC5 on TAp63 transcription. Rescue experiments showed that HDAC5 promoted proliferation and tumorigenesis *via* the Tap63/Maspin axis. In summary, our findings demonstrated that HDAC5 knockdown increased acetylation at the TAp63 promoter, resulting in TAp63 hyperactivation and Maspin overexpression, which blocked HCC cell proliferation and tumorigenesis (21).

HDAC5 and HIPK2/HIF1α Signaling

Hypoxia plays an important role in tumorigenesis and metastasis. Hypoxia inducible factor 1 (HIF1) is a key transcription factor that can transmit the hypoxia signal and mediate the effect of hypoxia. HIF1α is a functional subunit of HIF-1. Under hypoxia, HIF1α activates downstream target genes through interacting with hypoxia-response elements, which thereby regulate proliferation, apoptosis, invasion, metastasis, angiogenesis, energy metabolism, and chemoradiotherapy resistance of cancer cells (107).

Epithelial-to-mesenchymal transition (EMT) is a process that occurs under normal physiologic conditions such as embryonic development and wound healing. During EMT, epithelial cells lose their polarity and acquire mesenchymal-like features along with the capacity to migrate and invade other tissues (108). An increasing number of studies have reported that the change in the oxygen level in cancer microenvironments and the HIF1α-induced hypoxia signal transduction pathway acted as a vital

regulator of EMT, which played a key role in hypoxia-induced cancer invasion and metastasis (109, 110).

In our previous study, we illustrated that HDAC5 induced HCC migration, invasion and EMT only under hypoxia but not under normoxia. Although a dual luciferase reporter assay indicated increased transcription of HIF1α after ectopic HDAC5 expression under hypoxia, HDAC5 did not transactivate HIF1α directly even if under hypoxia. Further mechanistic analysis using ChIP assays unveiled that, under hypoxia, HDAC5 was recruited to the HIPK2 promoter; HDAC5 knockdown increased H3K9ac modification at this promoter, and the resultant upregulated HIPK2 bound to the HIF1α promoter to inhibit HIF1α expression. Our findings revealed that the HDAC5/HIPK2/HIF1α axis contributed to hypoxia-induced aggressiveness of HCC (70).

HDAC5 and LSD1 Signaling Pathways

Lysine-specific histone demethylase 1 (LSD1), also known as KDM1A or AOF2, is the first identified histone specific demethylase (111). LSD1 exhibits varying functions related to cancer progression in different cancer types, as the LSD1 protein is methylated in some cancer type and demethylated in others (112). HDAC5 was positively associated with LSD1 levels in breast cancer cells and tissue specimens. In vitro experiments unveiled that HDAC5 promoted invasion, metastasis and tumorigenic development *via* LSD1. Co-immunoprecipitation (Co-IP) and deletion mapping studies demonstrated that the NLS element was responsible for the HDAC5-LSD1 interaction. Protein ubiquitination assays indicated that HDAC5 stabilized LSD1 through blocking USP28 polyubiquitination. These results suggest an important role for the HDAC5/LSD1 axis in tumorigenesis (50).

In addition, HDAC5 also functioned as a downstream target gene of various upstream factors and participated in the regulatory pathways during cancer progression. For example, USF1 transactivated HDAC5 by physically binding to the HDAC5 promoter at −356 to −100 bp, thereby increasing the stability of LSD1 to induce chemoresistance of breast cancer (113).

HDAC5 and p65/NF-κB Signaling

NF-κB is a transcription factor involved in cell proliferation and transformation, apoptosis, immune responses and other important biological activities (114). NF-κB protein usually forms homodimer/heterodimer from p65 and p50, and is inactivated in cytoplasm due to the formation of trimer complex with inhibitor IKB (115). Therefore, the correlation between HDAC5 and p65/NF-κBsignaling during tumor progression has drawn researchers' attention. Hu et al. illustrated that CD13 promoted sorafenib resistance in HCC *via* indirectly increasing p65 protein stability. Co-IP indicated a strong interaction between CD13 and HDAC5. Truncation assays demonstrated that the N-terminal region of HDAC5 protein (amino acids 1-684), and the N-terminal cytoplasmic domain of CD13 (amino acids 2-8) accounted for the HDAC5-CD13 interaction. Hence, CD13 interacted with HDAC5 to increase the stabilization of LSD1, which demethylated p65 (50, 116) and thereby stabilized it and increased p65/NF-κB signaling; this resulted in sorafenib resistance and HCC progression (95).

HDAC5 and Myc Family

The Myc gene family is one of the most widely studied family of nuclear oncogenes. This family includes three main members: c-myc, N-myc and L-myc. N-myc protein can be stabilized with phosphorylated at serine 62 (Ser62) or be degraded with phosphorylated at threonine 58 (Thr58) (117). HDAC5 knockdown reduced N-myc at protein levels but had little effect on N-myc mRNA levels, so HDAC5 upregulated N-myc at the posttranscriptional level. HDAC5 overexpression significantly upregulated total N-myc protein in cells with Ser62 mutant N-myc but not in cells with Thr58-mutant N-myc. This indicated that HDAC5 upregulates N-myc protein by increasing N-Myc protein stability. Microarray and ChIP assays revealed that HDAC5 knockdown led to the transactivation of NEDD4 (an E3 ubiquitin–protein ligase). This illustrated that HDAC5 stabilized N-myc protein through suppressing the transcription of NEDD4 (55). Interestingly, HDAC5 was also shown to interact with N-myc protooncogene protein (MYCN), and the complex colocalized to the CD9 promoter and attenuated CD9 expression in neuroblastoma cells, leading to tumor cell invasion and metastasis (54).

In addition, C-myc transactivited HDAC5 though directly binding to the −200/+20 bp region upstream of the transcription start site of HDAC5, which contained C-myc-specific binding sequence (CACGTG). In turn, HDAC5 promoted SOX9 nuclear localization *via* interaction with its HMGB domain (amino acids 1–181) in estrogen receptor-positive breast cancer cells. These results indicated that the C-myc/HDAC5/SOX9 axis is a potential target for estrogen receptor-positive breast cancer therapy (52).

CLINICAL SIGNIFICANCE OF HDAC5 IN CANCER

HDAC5 and Cancer Diagnosis

Cancer cells release proteins into the peripheral blood during tumorigenesis. Thus, circulating proteins can serve as prognostic biomarkers for predicting disease recurrence and informing treatment decisions (118). Circulating HDAC5 is a potential marker for cancer diagnosis, given that it is detected at different levels in the peripheral blood of cancer patients as compared to healthy subjects or patients with nonrecurrent disease. One study found that the specificity of HDAC5 in distinguishing CRC patients from healthy subjects was 96.3%, indicating that it can be a diagnostic biomarker for CRC (32). Proteomic analysis with an antibody array identified proteins that were differentially expressed between breast cancer patients with and those without recurrence (34); moreover, HDAC5 was detected at a significantly higher level in the blood in patients with recurrent breast cancer than in those with recurrent triple-negative breast cancer.

Tumor antigens can provide insight into antitumor immune responses and the mechanisms of immune escape used by cancer

cells, which can aid cancer diagnosis and the establishment of immunotherapy strategies. An antibody reactivity screen revealed HDAC5 as the only serum antigen that differed between CRC patients and healthy subjects (33). Thus, serum HDAC5 has clinical utility as a diagnostic biomarker for cancer.

HDAC5 and Cancer Therapy

HDAC5 and HDAC Inhibitors

Molecular targeted therapies have specific antitumor effects, which limits their toxicity. Some studies demonstrated that HDAC5 is a potential therapeutic target for HDAC inhibitors (HDACis) as anticancer drugs (17, 25, 46, 73, 74, 119–123) (**Table 4**). HDACis can be divided into 4 groups according to their chemical structure—namely, hydroxamic acids, benzamides, cyclic peptides, and carboxylic acids. The basic structural features of HDACis are a hydroxamic acid complexed with Zn^{2+}, intermediate fatty chain linker, and lipophilic cap that engages in hydrophobic interaction with the binding pocket (127). HDACis could be divided into pan-HDACis and selective class IIA HDACis.

Trichostatin A (TSA)is the first identified pan-HDACis with an inhibitory activity depends on Zn^{2+}-dependent HDAC enzymes. The crystal structure of TSA and HDAC analogues showed that the conserved deacetylase active center were made up by a tubular bag, a zinc binding region and two ASP his (aspartate histidine) charge relay networks. The long fatty chain of TSA bound to the inner part of the tubular bag, and the hydroxime group at the end of the fatty chain showed connection with the zinc binding region through carbonyl and hydroxyl groups, which thereby inhibiting the ability of HDACs including recognizing substrate, regulating enzymatic activity and interacting with other proteins (128). TSA was illustrated to inhibit HDAC5 to block malignant behavior of cancer cells, including chemoresistance (120), proliferation (124) and invasion (25). Other HDACis such as belinostat, givenostat, panobinostat and dacinostat have the same mechanism with TSA as well. Among them, belinostat(PXD101) and panobinostat(LBH589) were US FDA-approved for cancer therapy (129, 130). Belinostat has been revealed to attenuate chemoresistance in estrogen receptor positive breast cancer *via* targeting class IIA HDACs including HDAC5 (119). Besides, HDAC3 and HDAC5 had copy number gain during HCC progression, panobinostat might inhibit HDAC3 and HDAC5 to decrease proliferation and induce apoptosis and autophagy of HCC, and this anticancer effect could be augmented by combination therapy with panobinostat and sorafenib (74).

Vorinostat(SAHA) is one of HDACis approved by FDA for cancer therapy. The hydroxime group of SAHA, also bound to Zn^{2+} in the way similar with TSA, but the fatty chain of SAHA showed less connection to the tubular bag than that of TSA, which indicated that the inhibitory activity of SAHA is lower than TSA (131). Hence, combination therapy with SAHA and other therapeutic drugs has drawn researchers' attention. Vasilatos et al. (122) explored the role of pargyline (an LSD1 inhibitor) and SAHA in breast cancer, the results demonstrated that both pargyline and SAHA suppressed cell proliferation and induced apoptosis through inhibiting HDAC5. Meanwhile, combination therapy with pargyline and SAHA led to superior anticancer effect. Interestingly, this anticancer effect was not found in non-TNBC counterparts or non-tumorigenic breast cells, which illustrated therapeutic efficacy of SAHA on breast cancer was subtype-dependent.

LMK-235, a selective HDACi showed preferable interactions with the catalytic zinc ion of class IIA HDACs, was illustrated to decrease phosphohistone H3 and Ki-67 levels in pancreatic neuroendocrine tumors (pNETs) while inducing pNET cell

TABLE 4 | Summary of HDAC5-targeted drugs in cancer therapy.

Agents	Anti-tumor properties	Reference
Trichostatin A (TSA)	Inhibit proliferation of gastric cancer	(25)
	Reduce chemoresistance of cancer	(120)
	Inhibit proliferation of breast cancer	(124)
	Induce apoptosis in breast cancer	(46)
Belinostat (PXD101)	Block chemoresistance in estrogen receptor positive breast cancer	(119)
Sodium butyrate	Inhibit migration and EMT in HCC	(71)
Panobinostat (LBH589)	Suppress invasion and metastasis in neuroblastoma	(54)
	Decrease cell viability and proliferation declined,and increase apoptosis and autophagy in HCC	(74)
Vorinostat	Reduce chemoresistance of cancer	(120)
Luotonin-A	Cause apoptosis and senescence in Hela cells	(17)
Formononetin	Prevent EMT in glioma	(73)
LMK-235	Reduce chemoresistance of cancer	(120)
	Induce apoptosis of pNET	(125)
	Induce apoptosis and reduce proliferation and migration of breast cancer	(20)
	Inhibit proliferation, metastasis and invasion of breast cancer	(65)
	Inhibit stemness of lung cancer	(93)
AR-42	Induce apoptosis in HCC	(121)
Vorinostat (SAHA)	Induce apoptosis in breast cancer	(122)
Ebselen	Decrease cell viability of cancer cells	(123)
Sulforaphane	Inhibit proferation of breast cancer	(113)
Simvastatin	Suppress proliferation of pancreatic cancer	(66)
	Inhibit proliferation of CRC	(126)

apoptosis and histone H3 acetylation, making it an effective targeted therapy for pNET that indirectly antagonizes the activity of HDAC4/5 (125). Similar findings were reported in breast (20, 65) and lung (93) cancers. However, LMK-235 induced HDAC5 expression in UC cells, indicating that HDAC5 is not a suitable therapeutic target in UC (132). Cao et al. (113) selected a series of HDACis including SAHA, TSA, LBH-589, PXD-101, MS-275, MC-1568, Romidepsin and Sulforaphane (SFN) to test their inhibitory effect towards HDAC5 expression on breast cancer cells. The results illustrated that SFN showed most significant inhibitory effect on HDAC5 expression at both mRNA level and protein level. Dual luciferase reporter assay indicated that SFN hindered the transcriptional activity of HDAC5 *via* affecting the region from −356 to −100 bp at HDAC5 promoter. In addition, USF1 could block the downregulation of HDAC5 mediated by SFN. These finding suggested SFN as a potential drug for breast cancer therapy.

HDAC5 and Metabolism Inhibitors

Hendrick et al. (133) demonstrated that knock down of HDAC5 induced cancer apoptosis through an iron-dependent reactive oxygen species (ROS) production. In addition, HDAC5-knock down cells adapted oxidative stress through glucose and glutamine metabolic reprogramming. Therefore, blocking glucose and glutamine metabolism in HDAC5-knock down cancer cells significantly induced cell death, which provided insight into a combination therapy with HDAC5 inhibitors and various inhibitors of metabolism as a new strategy for cancer treatment.

During tumorigenesis, cancer cells often undergone deregulated lipid metabolism (134). Statins, a class of 3-hydroxy-3-methylglutaryl coenzyme A (HMG-CoA) reductase inhibitors, can modulate the cell cycle, signal transduction pathways, and angiogenesis, and thus have therapeutic potential in cancer treatment (135–139). Simvastatin was shown to attenuate pancreatic cancer growth by inhibiting the oxysterol binding-related protein 5 (ORP5)/HDAC5 axis (66). Additionally, the combination of statins and other therapeutics was shown to prolong survival in cancer patients (140). For example, statins inhibited CRC cell proliferation by modulating the expression of enhancer of zeste homolog 2 (EZH2) and HDAC5, an effect that was enhanced in the presence of MC-1568, a class II HDACi. The underlying mechanism involved the upregulation of $p27^{(KIP1)}$ by statin *via* inhibition of EZH2; MC-1568 further increased $p27^{(KIP1)}$ expression by suppressing HDAC5, resulting in an antiproliferative effect in CRC (126).

Collectively, these findings highlight the clinical significance and utility of HDAC5 in targeted cancer therapy.

CONCLUSION

Accumulating evidence indicates that HDAC5 can serve as a biomarker for tumorigenesis in a variety of cancer types. HDAC5 expression is correlated with clinicopathologic features of cancer patients, highlighting its clinical value. Elucidating the targets and mechanisms of action of HDAC5 will enhance our understanding of the molecular basis of tumorigenesis and provide novel markers for early diagnosis, treatment response monitoring, and predicting disease prognosis, as well as an empirical basis for the development of effective cancer treatments.

AUTHOR CONTRIBUTIONS

XX and MY contributed to the study conception and design. XX edited the manuscript language. JY and CG wrote the main manuscript text and prepared the figures and tables. QK, ZF, and XC provided advice regarding the manuscript. All authors contributed to the article and approved the submitted version.

ACKNOWLEDGMENTS

This work was mainly supported by the Natural Science Foundation of Zhejiang Province (LQ21H160009), the Medical and Health Research Project of Zhejiang Province (2019RC175), Science and Technology Plan Project of Taizhou (1902KY193), The Applied Basic Research Plan of Xuzhou (KH17043) and 2016 Joint Funds of Zunyi city and school (E-214). We thank Charlesworth for the English language editing of the article.

SUPPLEMENTARY MATERIAL

The Supplementary Material for this article can be found online at: https://www.frontiersin.org/articles/10.3389/fonc.2021.661620/full#supplementary-material

Supplementary Table 1 | microRNAs predicted to regulate HDAC5.

REFERENCES

1. Allfrey VG, Faulkner R, Mirsky AE. Acetylation and Methylation Of Histones And Their Possible Role In the Regulation of RNA Synthesis. *Proc Natl Acad Sci U S A* (1964) 51:786–94. doi: 10.1073/pnas.51.5.786
2. Gray SG, Ekstrom TJ. The Human Histone Deacetylase Family. *Exp Cell Res* (2001) 262(2):75–83. doi: 10.1006/excr.2000.5080
3. Marks PA, Miller T, Richon VM. Histone Deacetylases. *Curr Opin Pharmacol* (2003) 3(4):344–51. doi: 10.1016/s1471-4892(03)00084-5
4. Marmorstein R, Roth SY. Histone Acetyltransferases: Function, Structure, and Catalysis. *Curr Opin Genet Dev* (2001) 11(2):155–61. doi: 10.1016/s0959-437x(00)00173-8
5. Roth SY, Denu JM, Allis CD. Histone Acetyltransferases. *Annu Rev Biochem* (2001) 70:81–120. doi: 10.1146/annurev.biochem.70.1.81
6. de Ruijter AJ, van Gennip AH, Caron HN, Kemp S, van Kuilenburg AB. Histone Deacetylases (HDACs): Characterization of the Classical HDAC Family. *Biochem J* (2003) 370(Pt 3):737–49. doi: 10.1042/BJ20021321
7. Gregoretti IV, Lee YM, Goodson HV. Molecular Evolution of the Histone Deacetylase Family: Functional Implications of Phylogenetic Analysis. *J Mol Biol* (2004) 338(1):17–31. doi: 10.1016/j.jmb.2004.02.006
8. Haberland M, Montgomery RL, Olson EN. The Many Roles of Histone Deacetylases in Development and Physiology: Implications for Disease and Therapy. *Nat Rev Genet* (2009) 10(1):32–42. doi: 10.1038/nrg2485

9. Lu J, McKinsey TA, Zhang CL, Olson EN. Regulation of Skeletal Myogenesis by Association of the MEF2 Transcription Factor With Class II Histone Deacetylases. *Mol Cell* (2000) 6(2):233–44. doi: 10.1016/s1097-2765(00)00025-3
10. Pita-Thomas W, Mahar M, Joshi A, Gan D, Cavalli V. HDAC5 Promotes Optic Nerve Regeneration by Activating the mTOR Pathway. *Exp Neurol* (2019) 317:271–83. doi: 10.1016/j.expneurol.2019.03.011
11. Wei JY, Lu QN, Li WM, He W. Intracellular Translocation of Histone Deacetylase 5 Regulates Neuronal Cell Apoptosis. *Brain Res* (2015) 1604:15–24. doi: 10.1016/j.brainres.2015.01.043
12. Seo WD, Lee JH, Jia Y, Wu C, Lee SJ. Saponarin Activates AMPK in a Calcium-Dependent Manner and Suppresses Gluconeogenesis and Increases Glucose Uptake Via Phosphorylation of CRTC2 and HDAC5. *Bioorg Medicinal Chem Lett* (2015) 25(22):5237–42. doi: 10.1016/j.bmcl.2015.09.057
13. Kain V, Kapadia B, Viswakarma N, Seshadri S, Prajapati B, Jena PK, et al. Co-Activator Binding Protein PIMT Mediates TNF-alpha Induced Insulin Resistance in Skeletal Muscle Via the Transcriptional Down-Regulation of MEF2A and GLUT4. *Sci Rep* (2015) 5:15197. doi: 10.1038/srep15197
14. Verdel A, Khochbin S. Identification of a New Family of Higher Eukaryotic Histone Deacetylases. Coordinate Expression of Differentiation-Dependent Chromatin Modifiers. *J Biol Chem* (1999) 274(4):2440–5. doi: 10.1074/jbc.274.4.2440
15. Johnstone RW. Histone-Deacetylase Inhibitors: Novel Drugs for the Treatment of Cancer. *Nat Rev Drug Discovery* (2002) 1(4):287–99. doi: 10.1038/nrd772
16. Lobera M, Madauss KP, Pohlhaus DT, Wright QG, Trocha M, Schmidt DR, et al. Selective Class IIa Histone Deacetylase Inhibition Via A Nonchelating Zinc-Binding Group. *Nat Chem Biol* (2013) 9(5):319–25. doi: 10.1038/nchembio.1223
17. Venkatesh R, Ramaiah MJ, Gaikwad HK, Janardhan S, Bantu R, Nagarapu L, et al. Luotonin-a Based Quinazolinones Cause Apoptosis and Senescence Via HDAC Inhibition and Activation of Tumor Suppressor Proteins in HeLa Cells. *Eur J Medicinal Chem* (2015) 94:87–101. doi: 10.1016/j.ejmech.2015.02.057
18. Fischle W, Dequiedt F, Hendzel MJ, Guenther MG, Lazar MA, Voelter W, et al. Enzymatic Activity Associated With Class II HDACs Is Dependent on a Multiprotein Complex Containing HDAC3 and SMRT/N-Cor. *Mol Cell* (2002) 9(1):45–57. doi: 10.1016/s1097-2765(01)00429-4
19. Patani N, Jiang WG, Newbold RF, Mokbel K. Histone-Modifier Gene Expression Profiles are Associated With Pathological and Clinical Outcomes in Human Breast Cancer. *Anticancer Res* (2011) 31(12):4115–25.
20. Oltra SS, Cejalvo JM, Tormo E, Albanell M, Ferrer A, Nacher M, et al. HDAC5 Inhibitors as a Potential Treatment in Breast Cancer Affecting Very Young Women. *Cancers* (2020) 12(2). doi: 10.3390/cancers12020412
21. Gu H, Fang Z, Cai X, Song R, Lin M, Ye J, et al. Highly Expressed Histone Deacetylase 5 Promotes the Growth of Hepatocellular Carcinoma Cells by Inhibiting the TAp63-maspin Pathway. *Am J Cancer Res* (2018) 8(3):462–75.
22. Zhong L, Sun S, Yao S, Han X, Gu M, Shi J. Histone Deacetylase 5 Promotes the Proliferation and Invasion of Lung Cancer Cells. *Oncol Rep* (2018) 40(4):2224–32. doi: 10.3892/or.2018.6591
23. Klieser E, Urbas R, Stattner S, Primavesi F, Jager T, Dinnewitzer A, et al. Comprehensive Immunohistochemical Analysis of Histone Deacetylases in Pancreatic Neuroendocrine Tumors: HDAC5 as a Predictor of Poor Clinical Outcome. *Hum Pathol* (2017) 65:41–52. doi: 10.1016/j.humpath.2017.02.009
24. Stypula-Cyrus Y, Damania D, Kunte DP, Cruz MD, Subramanian H, Roy HK, et al. HDAC Up-Regulation in Early Colon Field Carcinogenesis is Involved in Cell Tumorigenicity Through Regulation of Chromatin Structure. *PloS One* (2013) 8(5):e64600. doi: 10.1371/journal.pone.0064600
25. Lee KH, Choi EY, Kim MK, Kim KO, Jang BI, Kim SW, et al. Inhibition of Histone Deacetylase Activity Down-Regulates Urokinase Plasminogen Activator and Matrix Metalloproteinase-9 Expression in Gastric Cancer. *Mol Cell Biochem* (2010) 343(1-2):163–71. doi: 10.1007/s11010-010-0510-x
26. Orenay-Boyacioglu S, Kasap E, Gerceker E, Yuceyar H, Demirci U, Bilgic F, et al. Expression Profiles of Histone Modification Genes in Gastric Cancer Progression. *Mol Biol Rep* (2018) 45(6):2275–82. doi: 10.1007/s11033-018-4389-z
27. Liu C, Lv D, Li M, Zhang X, Sun G, Bai Y, et al. Hypermethylation of miRNA-589 Promoter Leads to Upregulation of HDAC5 Which Promotes Malignancy in Non-Small Cell Lung Cancer. *Int J Oncol* (2017) 50(6):2079–90. doi: 10.3892/ijo.2017.3967
28. Liu J, Gu J, Feng Z, Yang Y, Zhu N, Lu W, et al. Both HDAC5 and HDAC6 are Required for the Proliferation and Metastasis of Melanoma Cells. *J Trans Med* (2016) 14:7. doi: 10.1186/s12967-015-0753-0
29. Liu Q, Zheng JM, Chen JK, Yan XL, Chen HM, Nong WX, et al. Histone Deacetylase 5 Promotes the Proliferation of Glioma Cells by Upregulation of Notch 1. *Mol Med Rep* (2014) 10(4):2045–50. doi: 10.3892/mmr.2014.2395
30. Chen J, Xia J, Yu YL, Wang SQ, Wei YB, Chen FY, et al. HDAC5 Promotes Osteosarcoma Progression by Upregulation of Twist 1 Expression. *Tumour Biol J Int Soc Oncodevelop Biol Med* (2014) 35(2):1383–7. doi: 10.1007/s13277-013-1189-x
31. Cao X, Liu DH, Zhou Y, Yan XM, Yuan LQ, Pan J, et al. Histone Deacetylase 5 Promotes Wilms' Tumor Cell Proliferation Through the Upregulation of C-Met. *Mol Med Rep* (2016) 13(3):2745–50. doi: 10.3892/mmr.2016.4828
32. Chan CC, Fan CW, Kuo YB, Chen YH, Chang PY, Chen KT, et al. Multiple Serological Biomarkers for Colorectal Cancer Detection. *Int J Cancer* (2010) 126(7):1683–90. doi: 10.1002/ijc.24912
33. Scanlan MJ, Welt S, Gordon CM, Chen YT, Gure AO, Stockert E, et al. Cancer-Related Serological Recognition of Human Colon Cancer: Identification of Potential Diagnostic and Immunotherapeutic Targets. *Cancer Res* (2002) 62(14):4041–7.
34. Bera A, Russ E, Srinivasan M, Eidelman O, Eklund M, Hueman M, et al. Proteomic Analysis of Inflammatory Biomarkers Associated With Breast Cancer Recurrence. *Military Med* (2020) 185(Suppl 1):669–75. doi: 10.1093/milmed/usz254
35. Greco TM, Yu F, Guise AJ, Cristea IM. Nuclear Import of Histone Deacetylase 5 by Requisite Nuclear Localization Signal Phosphorylation. *Mol Cell Proteomics MCP* (2011) 10(2):M110 004317. doi: 10.1074/mcp.M110.004317
36. Haworth RS, Stathopoulou K, Candasamy AJ, Avkiran M. Neurohormonal Regulation of Cardiac Histone Deacetylase 5 Nuclear Localization by Phosphorylation-Dependent and Phosphorylation-Independent Mechanisms. *Circ Res* (2012) 110(12):1585–95. doi: 10.1161/CIRCRESAHA.111.263665
37. Mishra S, Gray CB, Miyamoto S, Bers DM, Brown JH. Location Matters: Clarifying the Concept of Nuclear and Cytosolic CaMKII Subtypes. *Circ Res* (2011) 109(12):1354–62. doi: 10.1161/CIRCRESAHA.111.248401
38. Fu X, Zhao JX, Liang J, Zhu MJ, Foretz M, Viollet B, et al. AMP-Activated Protein Kinase Mediates Myogenin Expression and Myogenesis Via Histone Deacetylase 5. *Am J Physiol Cell Physiol* (2013) 305(8):C887–95. doi: 10.1152/ajpcell.00124.2013
39. He T, Huang J, Chen L, Han G, Stanmore D, Krebs-Haupenthal J, et al. Cyclic AMP Represses Pathological MEF2 Activation by Myocyte-Specific Hypo-Phosphorylation of HDAC5. *J Mol Cell Cardiol* (2020) 145:88–98. doi: 10.1016/j.yjmcc.2020.05.018
40. Harrison BC, Huynh K, Lundgaard GL, Helmke SM, Perryman MB, McKinsey TA. Protein Kinase C-Related Kinase Targets Nuclear Localization Signals in a Subset of Class IIa Histone Deacetylases. *FEBS Lett* (2010) 584(6):1103–10. doi: 10.1016/j.febslet.2010.02.057
41. Deng X, Ewton DZ, Mercer SE, Friedman E. Mirk/dyrk1B Decreases the Nuclear Accumulation of Class II Histone Deacetylases During Skeletal Muscle Differentiation. *J Biol Chem* (2005) 280(6):4894–905. doi: 10.1074/jbc.M411894200
42. Li H, Xie H, Liu W, Hu R, Huang B, Tan YF, et al. A Novel microRNA Targeting HDAC5 Regulates Osteoblast Differentiation in Mice and Contributes to Primary Osteoporosis in Humans. *J Clin Invest* (2009) 119(12):3666–77. doi: 10.1172/JCI39832
43. Roccaro AM, Sacco A, Jia X, Azab AK, Maiso P, Ngo HT, et al. microRNA-dependent Modulation of Histone Acetylation in Waldenstrom Macroglobulinemia. *Blood* (2010) 116(9):1506–14. doi: 10.1182/blood-2010-01-265686
44. Gu X, Fu C, Lin L, Liu S, Su X, Li A, et al. miR-124 and miR-9 Mediated Downregulation of HDAC5 Promotes Neurite Development Through Activating MEF2C-GPM6A Pathway. *J Cell Physiol* (2018) 233(1):673–87. doi: 10.1002/jcp.25927
45. Dong N, Xu B, Shi H, Tang X. Baicalein Inhibits Amadori-Glycated Albumin-Induced MCP-1 Expression in Retinal Ganglion Cells Via a MicroRNA-124-Dependent Mechanism. *Invest Ophthalmol Visual Sci* (2015) 56(10):5844–53. doi: 10.1167/iovs.15-17444

46. Hsieh TH, Hsu CY, Tsai CF, Long CY, Wu CH, Wu DC, et al. HDAC Inhibitors Target HDAC5, Upregulate microRNA-125a-5p, and Induce Apoptosis in Breast Cancer Cells. *Mol Ther J Am Soc Gene Ther* (2015) 23 (4):656–66. doi: 10.1038/mt.2014.247
47. Shi L, Tian Z, Fu Q, Li H, Zhang L, Tian L, et al. Mir-217-Regulated MEF2D-HDAC5/ND6 Signaling Pathway Participates in the Oxidative Stress and Inflammatory Response After Cerebral Ischemia. *Brain Res* (2020) 1739:146835. doi: 10.1016/j.brainres.2020.146835
48. Salmena L, Poliseno L, Tay Y, Kats L, Pandolfi PP. A ceRNA Hypothesis: The Rosetta Stone of a Hidden RNA Language? *Cell* (2011) 146(3):353–8. doi: 10.1016/j.cell.2011.07.014
49. Xu CL, Sang B, Liu GZ, Li JM, Zhang XD, Liu LX, et al. SENEBLOC, a Long non-Coding RNA Suppresses Senescence Via p53-Dependent and Independent Mechanisms. *Nucleic Acids Res* (2020) 48(6):3089–102. doi: 10.1093/nar/gkaa063
50. Cao C, Vasilatos SN, Bhargava R, Fine JL, Oesterreich S, Davidson NE, et al. Functional Interaction of Histone Deacetylase 5 (HDAC5) and Lysine-Specific Demethylase 1 (LSD1) Promotes Breast Cancer Progression. *Oncogene* (2017) 36(1):133–45. doi: 10.1038/onc.2016.186
51. Huang Y, Tan M, Gosink M, Wang KK, Sun Y. Histone Deacetylase 5 is Not a p53 Target Gene, But its Overexpression Inhibits Tumor Cell Growth and Induces Apoptosis. *Cancer Res* (2002) 62(10):2913–22.
52. Xue Y, Lian W, Zhi J, Yang W, Li Q, Guo X, et al. HDAC5-Mediated Deacetylation and Nuclear Localisation of SOX9 is Critical for Tamoxifen Resistance in Breast Cancer. *Br J Cancer* (2019) 121(12):1039–49. doi: 10.1038/s41416-019-0625-0
53. Huang WT, Tsai YH, Chen SH, Kuo CW, Kuo YL, Lee KT, et al. HDAC2 and HDAC5 Up-Regulations Modulate Survivin and Mir-125a-5p Expressions and Promote Hormone Therapy Resistance in Estrogen Receptor Positive Breast Cancer Cells. *Front Pharmacol* (2017) 8:902. doi: 10.3389/fphar.2017.00902
54. Fabian J, Opitz D, Althoff K, Lodrini M, Hero B, Volland R, et al. MYCN and HDAC5 Transcriptionally Repress CD9 to Trigger Invasion and Metastasis in Neuroblastoma. *Oncotarget* (2016) 7(41):66344–59. doi: 10.18632/oncotarget.11662
55. Sun Y, Liu PY, Scarlett CJ, Malyukova A, Liu B, Marshall GM, et al. Histone Deacetylase 5 Blocks Neuroblastoma Cell Differentiation by Interacting With N-Myc. *Oncogene* (2014) 33(23):2987–94. doi: 10.1038/onc.2013.253
56. Milde T, Oehme I, Korshunov A, Kopp-Schneider A, Remke M, Northcott P, et al. HDAC5 and HDAC9 in Medulloblastoma: Novel Markers for Risk Stratification and Role in Tumor Cell Growth. *Clin Cancer Res an Off J Am Assoc Cancer Res* (2010) 16(12):3240–52. doi: 10.1158/1078-0432.CCR-10-0395
57. He P, Liang J, Shao T, Guo Y, Hou Y, Li Y. HDAC5 Promotes Colorectal Cancer Cell Proliferation by Up-Regulating DLL4 Expression. *Int J Clin Exp Med* (2015) 8(4):6510–6.
58. Novo CL, Polese C, Matheus N, Decottignies A, Londono-Vallejo A, Castronovo V, et al. A New Role for Histone Deacetylase 5 in the Maintenance of Long Telomeres. *FASEB J Off Publ Fed Am Societies Exp Biol* (2013) 27(9):3632–42. doi: 10.1096/fj.12-224204
59. Feng GW, Dong LD, Shang WJ, Pang XL, Li JF, Liu L, et al. HDAC5 Promotes Cell Proliferation in Human Hepatocellular Carcinoma by Up-Regulating Six1 Expression. *Eur Rev Med Pharmacol Sci* (2014) 18(6):811–6.
60. Fan J, Lou B, Chen W, Zhang J, Lin S, Lv FF, et al. Down-Regulation of HDAC5 Inhibits Growth of Human Hepatocellular Carcinoma by Induction of Apoptosis and Cell Cycle Arrest. *Tumour Biol J Int Soc Oncodevelop Biol Med* (2014) 35(11):11523–32. doi: 10.1007/s13277-014-2358-2
61. Jaguva Vasudevan AA, Hoffmann MJ, Beck MLC, Poschmann G, Petzsch P, Wiek C, et al. Hdac5 Expression in Urothelial Carcinoma Cell Lines Inhibits Long-Term Proliferation But Can Promote Epithelial-to-Mesenchymal Transition. *Int J Mol Sci* (2019) 20(9):2135. doi: 10.3390/ijms20092135
62. Poralla L, Stroh T, Erben U, Sittig M, Liebig S, Siegmund B, et al. Histone Deacetylase 5 Regulates the Inflammatory Response of Macrophages. *J Cell Mol Med* (2015) 19(9):2162–71. doi: 10.1111/jcmm.12595
63. Hou P, Kapoor A, Zhang Q, Li J, Wu CJ, Li J, et al. Tumor Microenvironment Remodeling Enables Bypass of Oncogenic KRAS Dependency in Pancreatic Cancer. *Cancer Discovery* (2020) 10(7):1058–77. doi: 10.1158/2159-8290.CD-19-0597
64. Qian S, Wang W, Li M. Transcriptional Factor Yin Yang 1 Facilitates the Stemness of Ovarian Cancer Via Suppressing miR-99a Activity Through Enhancing its Deacetylation Level. *Biomed Pharmacother = Biomed Pharmacother* (2020) 126:110085. doi: 10.1016/j.biopha.2020.110085
65. Li A, Liu Z, Li M, Zhou S, Xu Y, Xiao Y, et al. HDAC5, a Potential Therapeutic Target and Prognostic Biomarker, Promotes Proliferation, Invasion and Migration in Human Breast Cancer. *Oncotarget* (2016) 7 (25):37966–78. doi: 10.18632/oncotarget.9274
66. Ishikawa S, Nagai Y, Masuda T, Koga Y, Nakamura T, Imamura Y, et al. The Role of Oxysterol Binding Protein-Related Protein 5 in Pancreatic Cancer. *Cancer Sci* (2010) 101(4):898–905. doi: 10.1111/j.1349-7006.2009.01475.x
67. Gong S, Ying L, Fan Y, Sun Z. Fentanyl Inhibits Lung Cancer Viability and Invasion Via Upregulation of miR-331-3p and Repression of HDAC5. *OncoTargets Ther* (2020) 13:13131–41. doi: 10.2147/OTT.S281095
68. Huang H. Matrix Metalloproteinase-9 (MMP-9) as a Cancer Biomarker and MMP-9 Biosensors: Recent Advances. *Sensors* (2018) 18(10):3249. doi: 10.3390/s18103249
69. Scheau C, Badarau IA, Costache R, Caruntu C, Mihai GL, Didilescu AC, et al. The Role of Matrix Metalloproteinases in the Epithelial-Mesenchymal Transition of Hepatocellular Carcinoma. *Anal Cell Pathol* (2019) 2019:9423907. doi: 10.1155/2019/9423907
70. Ye M, Fang Z, Gu H, Song R, Ye J, Li H, et al. Histone Deacetylase 5 Promotes the Migration and Invasion of Hepatocellular Carcinoma Via Increasing the Transcription of Hypoxia-Inducible factor-1alpha Under Hypoxia Condition. *Tumour Biol J Int Soc Oncodevelop Biol Med* (2017) 39(6):1010428317705034. doi: 10.1177/1010428317705034
71. Dong L, Dong Q, Chen Y, Li Y, Zhang B, Zhou F, et al. Novel HDAC5-interacting Motifs of Tbx3 are Essential for the Suppression of E-cadherin Expression and for the Promotion of Metastasis in Hepatocellular Carcinoma. *Signal Transduct Targe Ther* (2018) 3:22. doi: 10.1038/s41392-018-0025-6
72. Feng S, Zhang L, Liu X, Li G, Zhang B, Wang Z, et al. Low Levels of AMPK Promote Epithelial-Mesenchymal Transition in Lung Cancer Primarily Through HDAC4- and HDAC5-mediated Metabolic Reprogramming. *J Cell Mol Med* (2020). 24(14):7789–7801. doi: 10.1111/jcmm.15410
73. Liu Q, Sun Y, Zheng JM, Yan XL, Chen HM, Chen JK, et al. Formononetin Sensitizes Glioma Cells to Doxorubicin Through Preventing EMT Via Inhibition of Histone Deacetylase 5. *Int J Clin Exp Pathol* (2015) 8 (6):6434–41.
74. Lachenmayer A, Toffanin S, Cabellos L, Alsinet C, Hoshida Y, Villanueva A, et al. Combination Therapy for Hepatocellular Carcinoma: Additive Preclinical Efficacy of the HDAC Inhibitor Panobinostat With Sorafenib. *J Hepatolo* (2012) 56(6):1343–50. doi: 10.1016/j.jhep.2012.01.009
75. Yang J, Mani SA, Donaher JL, Ramaswamy S, Itzykson RA, Come C, et al. Twist, a Master Regulator of Morphogenesis, Plays an Essential Role in Tumor Metastasis. *Cell* (2004) 117(7):927–39. doi: 10.1016/j.cell.2004.06.006
76. Lai X, Li Q, Wu F, Lin J, Chen J, Zheng H, et al. Epithelial-Mesenchymal Transition and Metabolic Switching in Cancer: Lessons From Somatic Cell Reprogramming. *Front Cell Dev Biol* (2020) 8:760. doi: 10.3389/fcell.2020.00760
77. Feng L, Wang K, Tang P, Chen S, Liu T, Lei J, et al. Deubiquitinase USP18 Promotes the Progression of Pancreatic Cancer Via Enhancing the Notch1-c-Myc Axis. *Aging* (2020) 12(19):19273–92. doi: 10.18632/aging.103760
78. Vinson KE, George DC, Fender AW, Bertrand FE, Sigounas G. The Notch Pathway in Colorectal Cancer. *Int J Cancer* (2016) 138(8):1835–42. doi: 10.1002/ijc.29800
79. Peixoto P, Castronovo V, Matheus N, Polese C, Peulen O, Gonzalez A, et al. HDAC5 is Required for Maintenance of Pericentric Heterochromatin, and Controls Cell-Cycle Progression and Survival of Human Cancer Cells. *Cell Death Differentiation* (2012) 19(7):1239–52. doi: 10.1038/cdd.2012.3
80. Zhou Y, Jin X, Ma J, Ding D, Huang Z, Sheng H, et al. HDAC5 Loss Impairs RB Repression of Pro-Oncogenic Genes and Confers Cdk4/6 Inhibitor Resistance in Cancer. *Cancer Res* (2021) 81(6):1486–99. doi: 10.1158/0008-5472.CAN-20-2828
81. Murray D, Mirzayans R. Cellular Responses to Platinum-Based Anticancer Drugs and UVC: Role of p53 and Implications for Cancer Therapy. *Int J Mol Sci* (2020) 21(16):5766. doi: 10.3390/ijms21165766
82. Dequiedt F, Kasler H, Fischle W, Kiermer V, Weinstein M, Herndier BG, et al. HDAC7, a Thymus-Specific Class II Histone Deacetylase, Regulates

Nur77 Transcription and TCR-mediated Apoptosis. *Immunity* (2003) 18 (5):687–98. doi: 10.1016/s1074-7613(03)00109-2
83. Barneda-Zahonero B, Roman-Gonzalez L, Collazo O, Rafati H, Islam AB, Bussmann LH, et al. HDAC7 is a Repressor of Myeloid Genes Whose Downregulation is Required for Transdifferentiation of Pre-B Cells Into Macrophages. *PloS Genet* (2013) 9(5):e1003503. doi: 10.1371/journal.pgen.1003503
84. de Zoeten EF, Wang L, Sai H, Dillmann WH, Hancock WW. Inhibition of HDAC9 Increases T Regulatory Cell Function and Prevents Colitis in Mice. *Gastroenterology* (2010) 138(2):583–94. doi: 10.1053/j.gastro.2009.10.037
85. Baek YS, Haas S, Hackstein H, Bein G, Hernandez-Santana M, Lehrach H, et al. Identification of Novel Transcriptional Regulators Involved in Macrophage Differentiation and Activation in U937 Cells. *BMC Immunol* (2009) 10:18. doi: 10.1186/1471-2172-10-18
86. Xiao H, Jiao J, Wang L, O'Brien S, Newick K, Wang LC, et al. HDAC5 Controls the Functions of Foxp3(+) T-Regulatory and CD8(+) T Cells. *Int J Cancer* (2016) 138(10):2477–86. doi: 10.1002/ijc.29979
87. Zhao M, Tao Y, Peng GH. The Role of Histone Acetyltransferases and Histone Deacetylases in Photoreceptor Differentiation and Degeneration. *Int J Med Sci* (2020) 17(10):1307–14. doi: 10.7150/ijms.43140
88. Watamoto K, Towatari M, Ozawa Y, Miyata Y, Okamoto M, Abe A, et al. Altered Interaction of HDAC5 With GATA-1 During MEL Cell Differentiation. *Oncogene* (2003) 22(57):9176–84. doi: 10.1038/sj.onc.1206902
89. Black BL, Olson EN. Transcriptional Control of Muscle Development by Myocyte Enhancer Factor-2 (MEF2) Proteins. *Annu Rev Cell Dev Biol* (1998) 14:167–96. doi: 10.1146/annurev.cellbio.14.1.167
90. Potthoff MJ, Olson EN. MEF2: A Central Regulator of Diverse Developmental Programs. *Development* (2007) 134(23):4131–40. doi: 10.1242/dev.008367
91. Zhang M, Zhu B, Davie J. Alternative Splicing of MEF2C pre-mRNA Controls its Activity in Normal Myogenesis and Promotes Tumorigenicity in Rhabdomyosarcoma Cells. *J Biol Chem* (2015) 290(1):310–24. doi: 10.1074/jbc.M114.606277
92. Vinogradov S, Wei X. Cancer Stem Cells and Drug Resistance: The Potential of Nanomedicine. *Nanomedicine* (2012) 7(4):597–615. doi: 10.2217/nnm.12.22
93. Zhao M, Li L, Zhou J, Cui X, Tian Q, Jin Y, et al. Mir-2861 Behaves as a Biomarker of Lung Cancer Stem Cells and Regulates the HDAC5-ERK System Genes. *Cell Reprogramming* (2018) 20(2):99–106. doi: 10.1089/cell.2017.0045
94. Longley DB, Johnston PG. Molecular Mechanisms of Drug Resistance. *J Pathol* (2005) 205(2):275–92. doi: 10.1002/path.1706
95. Hu B, Xu Y, Li YC, Huang JF, Cheng JW, Guo W, et al. CD13 Promotes Hepatocellular Carcinogenesis and Sorafenib Resistance by Activating HDAC5-LSD1-NF-kappaB Oncogenic Signaling. *Clin Trans Med* (2020) 10(8):e233. doi: 10.1002/ctm2.233
96. Gabet AS, Mortreux F, Charneau P, Riou P, Duc-Dodon M, Wu Y, et al. Inactivation of hTERT Transcription by Tax. *Oncogene* (2003) 22(24):3734–41. doi: 10.1038/sj.onc.1206468
97. Shammas MA, Koley H, Beer DG, Li C, Goyal RK, Munshi NC. Growth Arrest, Apoptosis, and Telomere Shortening of Barrett's-Associated Adenocarcinoma Cells by a Telomerase Inhibitor. *Gastroenterology* (2004) 126(5):1337–46. doi: 10.1053/j.gastro.2004.01.026
98. Garcia-Cao M, O'Sullivan R, Peters AH, Jenuwein T, Blasco MA. Epigenetic Regulation of Telomere Length in Mammalian Cells by the Suv39h1 and Suv39h2 Histone Methyltransferases. *Nat Genet* (2004) 36(1):94–9. doi: 10.1038/ng1278
99. Gonzalo S, Garcia-Cao M, Fraga MF, Schotta G, Peters AH, Cotter SE, et al. Role of the RB1 Family in Stabilizing Histone Methylation at Constitutive Heterochromatin. *Nat Cell Biol* (2005) 7(4):420–8. doi: 10.1038/ncb1235
100. Gonzalo S, Jaco I, Fraga MF, Chen T, Li E, Esteller M, et al. DNA Methyltransferases Control Telomere Length and Telomere Recombination in Mammalian Cells. *Nat Cell Biol* (2006) 8(4):416–24. doi: 10.1038/ncb1386
101. Sauer M, Bretz AC, Beinoraviciute-Kellner R, Beitzinger M, Burek C, Rosenwald A, et al. C-Terminal Diversity Within the p53 Family Accounts for Differences in DNA Binding and Transcriptional Activity. *Nucleic Acids Res* (2008) 36(6):1900–12. doi: 10.1093/nar/gkn044
102. Mangiulli M, Valletti A, Caratozzolo MF, Tullo A, Sbisa E, Pesole G, et al. Identification and Functional Characterization of Two New Transcriptional Variants of the Human p63 Gene. *Nucleic Acids Res* (2009) 37(18):6092–104. doi: 10.1093/nar/gkp674
103. Kim S, Han J, Kim J, Park C. Maspin Expression is Transactivated by p63 and is Critical for the Modulation of Lung Cancer Progression. *Cancer Res* (2004) 64(19):6900–5. doi: 10.1158/0008-5472.CAN-04-1657
104. Ito R, Nakayama H, Yoshida K, Oda N, Yasui W. Loss of Maspin Expression is Associated With Development and Progression of Gastric Carcinoma With p53 Abnormality. *Oncol Rep* (2004) 12(5):985–90. doi: 10.3892/or.12.5.985
105. Wang N, Chang LL. Maspin Suppresses Cell Invasion and Migration in Gastric Cancer Through Inhibiting EMT and Angiogenesis Via ITGB1/FAK Pathway. *Hum Cell* (2020) 33(3):663–75. doi: 10.1007/s13577-020-00345-7
106. Sun Q, Zhang K, Li H, Chen W, Liu L, Huang G, et al. The Overexpression of Maspin Increases the Sensitivity of Lung Adenocarcinoma Drug-Resistant Cells to Docetaxel *In Vitro* and *In Vivo*. *Ann Trans Med* (2020) 8(22):1522. doi: 10.21037/atm-20-7053
107. Akanji MA, Rotimi D, Adeyemi OS. Hypoxia-Inducible Factors as an Alternative Source of Treatment Strategy for Cancer. *Oxid Med Cell Longevity* (2019) 2019:8547846. doi: 10.1155/2019/8547846
108. Jonckheere S, Adams J, De Groote D, Campbell K, Berx G, Goossens S. Epithelial-Mesenchymal Transition (EMT) as a Therapeutic Target. *Cells Tissues Organs* (2021) 1–26. doi: 10.1159/000512218
109. Chatterjee R, Ghosh B, Mandal M, Nawn D, Banerjee S, Pal M, et al. Pathophysiological Relationship Between Hypoxia Associated Oxidative Stress, Epithelial-mesenchymal Transition, Stemness Acquisition and Alteration of Shh/ Gli-1 Axis During Oral Sub-Mucous Fibrosis and Oral Squamous Cell Carcinoma. *Eur J Cell Biol* (2020) 100(1):151146. doi: 10.1016/j.ejcb.2020.151146
110. Wang N, Muhetaer G, Zhang X, Yang B, Wang C, Zhang Y, et al. Sanguisorba Officinalis L. Suppresses Triple-Negative Breast Cancer Metastasis by Inhibiting Late-Phase Autophagy Via Hif-1alpha/Caveolin-1 Signaling. *Front Pharmacol* (2020) 11:591400. doi: 10.3389/fphar.2020.591400
111. Shi Y, Lan F, Matson C, Mulligan P, Whetstine JR, Cole PA, et al. Histone Demethylation Mediated by the Nuclear Amine Oxidase Homolog LSD1. *Cell* (2004) 119(7):941–53. doi: 10.1016/j.cell.2004.12.012
112. Wang GG, Allis CD, Chi P. Chromatin Remodeling and Cancer, Part I: Covalent Histone Modifications. *Trends Mol Med* (2007) 13(9):363–72. doi: 10.1016/j.molmed.2007.07.003
113. Cao C, Wu H, Vasilatos SN, Chandran U, Qin Y, Wan Y, et al. HDAC5-LSD1 Axis Regulates Antineoplastic Effect of Natural HDAC Inhibitor Sulforaphane in Human Breast Cancer Cells. *Int J Cancer* (2018) 143 (6):1388–401. doi: 10.1002/ijc.31419
114. Ramadass V, Vaiyapuri T, Tergaonkar V. Small Molecule NF-kappaB Pathway Inhibitors in Clinic. *Int J Mol Sci* (2020) 21(14):5164. doi: 10.3390/ijms21145164
115. Giridharan S, Srinivasan M. Mechanisms of NF-kappaB p65 and Strategies for Therapeutic Manipulation. *J Inflammation Res* (2018) 11:407–19. doi: 10.2147/JIR.S140188
116. Kim D, Nam HJ, Lee W, Yim HY, Ahn JY, Park SW, et al. PKCalpha-LSD1-NF-kappaB-Signaling Cascade Is Crucial for Epigenetic Control of the Inflammatory Response. *Mol Cell* (2018) 69(3):398–411 e6. doi: 10.1016/j.molcel.2018.01.002
117. Otto T, Horn S, Brockmann M, Eilers U, Schuttrumpf L, Popov N, et al. Stabilization of N-Myc Is a Critical Function of Aurora A in Human Neuroblastoma. *Cancer Cell* (2009) 15(1):67–78. doi: 10.1016/j.ccr.2008.12.005
118. Chen H, Werner S, Tao S, Zornig I, Brenner H. Blood Autoantibodies Against Tumor-Associated Antigens as Biomarkers in Early Detection of Colorectal Cancer. *Cancer Lett* (2014) 346(2):178–87. doi: 10.1016/j.canlet.2014.01.007
119. Chi F, Liu J, Brady SW, Cosgrove PA, Nath A, McQuerry JA, et al. A `One-Two Punch' Therapy Strategy to Target Chemoresistance in Estrogen Receptor Positive Breast Cancer. *Trans Oncol* (2021) 14(1):100946. doi: 10.1016/j.tranon.2020.100946
120. Marek L, Hamacher A, Hansen FK, Kuna K, Gohlke H, Kassack MU, et al. Histone Deacetylase (HDAC) Inhibitors With A Novel Connecting Unit

Linker Region Reveal a Selectivity Profile for HDAC4 and HDAC5 With Improved Activity Against Chemoresistant Cancer Cells. *J Medicinal Chem* (2013) 56(2):427–36. doi: 10.1021/jm301254q
121. Zhang M, Pan Y, Dorfman RG, Chen Z, Liu F, Zhou Q, et al. AR-42 Induces Apoptosis in Human Hepatocellular Carcinoma Cells *Via* HDAC5 Inhibition. *Oncotarget* (2016) 7(16):22285–94. doi: 10.18632/oncotarget.8077
122. Vasilatos SN, Katz TA, Oesterreich S, Wan Y, Davidson NE, Huang Y. Crosstalk Between Lysine-Specific Demethylase 1 (LSD1) and Histone Deacetylases Mediates Antineoplastic Efficacy of HDAC Inhibitors in Human Breast Cancer Cells. *Carcinogenesis* (2013) 34(6):1196–207. doi: 10.1093/carcin/bgt033
123. Wang Y, Wallach J, Duane S, Wang Y, Wu J, Wang J, et al. Developing Selective Histone Deacetylases (HDACs) Inhibitors Through Ebselen and Analogs. *Drug Design Dev Ther* (2017) 11:1369–82. doi: 10.2147/DDDT.S124977
124. Clarke CJ, Shamseddine AA, Jacob JJ, Khalife G, Burns TA, Hannun YA. ATRA Transcriptionally Induces nSMase2 Through CBP/p300-Mediated Histone Acetylation. *J Lipid Res* (2016) 57(5):868–81. doi: 10.1194/jlr.M067447
125. Wanek J, Gaisberger M, Beyreis M, Mayr C, Helm K, Primavesi F, et al. Pharmacological Inhibition of Class IIa HDACs by LMK-235 in Pancreatic Neuroendocrine Tumor Cells. *Int J Mol Sci* (2018) 19(10):3128. doi: 10.3390/ijms19103128
126. Ishikawa S, Hayashi H, Kinoshita K, Abe M, Kuroki H, Tokunaga R, et al. Statins Inhibit Tumor Progression *Via* An Enhancer of Zeste Homolog 2-Mediated Epigenetic Alteration in Colorectal Cancer. *Int J Cancer* (2014) 135 (11):2528–36. doi: 10.1002/ijc.28672
127. Marks PA, Xu WS. Histone Deacetylase Inhibitors: Potential in Cancer Therapy. *J Cell Biochem* (2009) 107(4):600–8. doi: 10.1002/jcb.22185
128. Woo SH, Frechette S, Abou Khalil E, Bouchain G, Vaisburg A, Bernstein N, et al. Structurally Simple Trichostatin A-Like Straight Chain Hydroxamates As Potent Histone Deacetylase Inhibitors. *J Medicinal Chem* (2002) 45 (13):2877–85. doi: 10.1021/jm020154k
129. Sawas A, Radeski D, O'Connor OA. Belinostat in Patients With Refractory or Relapsed Peripheral T-cell Lymphoma: A Perspective Review. *Ther Adv Hematol* (2015) 6(4):202–8. doi: 10.1177/2040620715592567
130. McDermott J, Jimeno A. Belinostat for the Treatment of Peripheral T-cell Lymphomas. *Drugs Today* (2014) 50(5):337–45. doi: 10.1358/dot.2014.50.5.2138703
131. Finnin MS, Donigian JR, Cohen A, Richon VM, Rifkind RA, Marks PA, et al. Structures of a Histone Deacetylase Homologue Bound to the TSA and SAHA Inhibitors. *Nature* (1999) 401(6749):188–93. doi: 10.1038/43710
132. Kaletsch A, Pinkerneil M, Hoffmann MJ, Jaguva Vasudevan AA, Wang C, Hansen FK, et al. Effects of Novel HDAC Inhibitors on Urothelial Carcinoma Cells. *Clin Epigenet* (2018) 10(1):100. doi: 10.1186/s13148-018-0531-y
133. Hendrick E, Peixoto P, Blomme A, Polese C, Matheus N, Cimino J, et al. Metabolic Inhibitors Accentuate the Anti-Tumoral Effect of HDAC5 Inhibition. *Oncogene* (2017) 36(34):4859–74. doi: 10.1038/onc.2017.103
134. Matsushita Y, Nakagawa H, Koike K. Lipid Metabolism in Oncology: Why It Matters, How to Research, and How to Treat. *Cancers* (2021) 13(3):474. doi: 10.3390/cancers13030474
135. Thibault A, Samid D, Tompkins AC, Figg WD, Cooper MR, Hohl RJ, et al. Phase I Study of Lovastatin, an Inhibitor of the Mevalonate Pathway, in Patients With Cancer. *Clin Cancer Res an Off J Am Assoc Cancer Res* (1996) 2(3):483–91.
136. Larner J, Jane J, Laws E, Packer R, Myers C, Shaffrey M. A Phase I-II Trial of Lovastatin for Anaplastic Astrocytoma and Glioblastoma Multiforme. *Am J Clin Oncol* (1998) 21(6):579–83. doi: 10.1097/00000421-199812000-00010
137. Kawata S, Yamasaki E, Nagase T, Inui Y, Ito N, Matsuda Y, et al. Effect of Pravastatin on Survival in Patients With Advanced Hepatocellular Carcinoma. A Randomized Controlled Trial. *Br J Cancer* (2001) 84 (7):886–91. doi: 10.1054/bjoc.2000.1716
138. Agarwal B, Bhendwal S, Halmos B, Moss SF, Ramey WG, Holt PR. Lovastatin Augments Apoptosis Induced by Chemotherapeutic Agents in Colon Cancer Cells. *Clin Cancer Res an Off J Am Assoc Cancer Res* (1999) 5(8):2223–9.
139. Mace AG, Gantt GA, Skacel M, Pai R, Hammel JP, Kalady MF. Statin Therapy is Associated With Improved Pathologic Response to Neoadjuvant Chemoradiation in Rectal Cancer. *Dis Colon Rectum* (2013) 56(11):1217–27. doi: 10.1097/DCR.0b013e3182a4b236
140. Lee J, Jung KH, Park YS, Ahn JB, Shin SJ, Im SA, et al. Simvastatin Plus Irinotecan, 5-Fluorouracil, and Leucovorin (FOLFIRI) As First-Line Chemotherapy in Metastatic Colorectal Patients: A Multicenter Phase II Study. *Cancer Chemother Pharmacol* (2009) 64(4):657–63. doi: 10.1007/s00280-008-0913-5

Conflict of Interest: The authors declare that the research was conducted in the absence of any commercial or financial relationships that could be construed as a potential conflict of interest.

frontiers in Cell and Developmental Biology

REVIEW
published: 21 June 2021
doi: 10.3389/fcell.2021.631486

Emerging Roles of Liquid–Liquid Phase Separation in Cancer: From Protein Aggregation to Immune-Associated Signaling

Jiahua Lu[1,2,3,4], Junjie Qian[2,3,4,5], Zhentian Xu[1,2,3,4], Shengyong Yin[2,3,4,5], Lin Zhou[2,3,4,5], Shusen Zheng[1,2,3,4,5,6] and Wu Zhang[5,6]**

[1] Division of Hepatobiliary and Pancreatic Surgery, Department of Surgery, First Affiliated Hospital, School of Medicine, Zhejiang University, Hangzhou, China, [2] NHC Key Laboratory of Combined Multi-Organ Transplantation, Hangzhou, China, [3] Key Laboratory of the Diagnosis and Treatment of Organ Transplantation, Research Unit of Collaborative Diagnosis and Treatment For Hepatobiliary and Pancreatic Cancer, Chinese Academy of Medical Sciences, Hangzhou, China, [4] Key Laboratory of Organ Transplantation, Research Center for Diagnosis and Treatment of Hepatobiliary Diseases, Hangzhou, China, [5] Organ Transplantation Institute, Zhejiang University, Hangzhou, China, [6] Shulan (Hangzhou) Hospital Affiliated to Shulan International Medical College, Zhejiang Shuren University, Hangzhou, China

OPEN ACCESS

Edited by:
Lorenzo Gerratana, University of Udine, Italy

Reviewed by:
Markus Zweckstetter, German Center for Neurodegeneratives, Helmholtz Association of German Research Centers (HZ), Germany
Mahdi Moosa, University at Buffalo, United States

***Correspondence:**
Wu Zhang
zhangwu516@zju.edu.cn
Shusen Zheng
shusenzheng@zju.edu.cn

Specialty section:
This article was submitted to Molecular and Cellular Oncology, a section of the journal Frontiers in Cell and Developmental Biology

Received: 20 November 2020
Accepted: 14 May 2021
Published: 21 June 2021

Citation:
Lu J, Qian J, Xu Z, Yin S, Zhou L, Zheng S and Zhang W (2021) Emerging Roles of Liquid–Liquid Phase Separation in Cancer: From Protein Aggregation to Immune-Associated Signaling. Front. Cell Dev. Biol. 9:631486. doi: 10.3389/fcell.2021.631486

Liquid–liquid Phase Separation (LLPS) of proteins and nucleic acids has emerged as a new paradigm in the study of cellular activities. It drives the formation of liquid-like condensates containing biomolecules in the absence of membrane structures in living cells. In addition, typical membrane-less condensates such as nuclear speckles, stress granules and cell signaling clusters play important roles in various cellular activities, including regulation of transcription, cellular stress response and signal transduction. Previous studies highlighted the biophysical and biochemical principles underlying the formation of these liquid condensates. The studies also showed how these principles determine the molecular properties, LLPS behavior, and composition of liquid condensates. While the basic rules driving LLPS are continuously being uncovered, their function in cellular activities is still unclear, especially within a pathological context. Therefore, the present review summarizes the recent progress made on the existing roles of LLPS in cancer, including cancer-related signaling pathways, transcription regulation and maintenance of genome stability. Additionally, the review briefly introduces the basic rules of LLPS, and cellular signaling that potentially plays a role in cancer, including pathways relevant to immune responses and autophagy.

Keywords: liquid–liquid phase separation, biomolecular condensate, cancer mechanism, protein aggregation, signaling transduction, genome stability

Abbreviations: ALS, amyotrophic lateral sclerosis; AD, Alzheimer disease; ATP, adenosine triphosphate; SV, synaptic vesicle; cGAMP, cyclic GMP-AMP; cGAS, cyclic GMP-AMP synthase; CRL3, cullin3-RING ligase; DAXX, death domain-associated protein; IDR, intrinsically disordered region; PTM, posttranslational modification; LAT, linker for the activation of T cells; LLPS, liquid–liquid phase separation; m^6A, N^6-methyladenosine; PAS, pre-autophagosomal structure; PML, promyelocytic leukemia; POZ, pox virus and zinc finger; RNP, ribonucleoprotein; SPOP, speckle-type POZ domain protein; CTD, carboxy-terminal domain; TCR, T cell antigen receptor; TF, transcription factor; APC, antigen-presenting cell; PRM, proline-rich motif; ATG, autophagy-related genes; PD-1, programmed cell death protein 1; CTLA-4, cytotoxic T lymphocyte antigen 4; TIM-3, T-cell immunoglobulin and mucin domain 3; TORC1, target of rapamycin complex 1; RBP, RNA-binding protein; DDR, DNA damage response; PARP1, Poly(ADP-ribose) polymerase 1; PARylation, poly(ADP-ribosyl)ation; ssDNA, single-strand DNA; 53BP1, p53-binding protein 1; DSB, DNA double-strand breaks; SH3, SRC homology 3; WASP, Wiskott–Aldrich syndrome protein; MATH, N-terminal meprin and TRAF-C homology.

INTRODUCTION

Intracellular components are compartmentalized, respectively, in living cells to facilitate the regulation of cellular activities in time and space. Apart from the traditional membrane-enclosed organelles, such as the mitochondria and endoplasmic reticulum, many organelles do not have membranous structures yet remain compartmentalized and can concentrate certain types of molecules (Handwerger and Gall, 2006; Mao et al., 2011a; Pederson, 2011). Such organelles include nuclear structures like nuclear paraspeckles, the nucleolus as well as Cajal bodies and cytoplasmic organelles such as the P-bodies, stress granules and centrosomes. Notably, membrane-less organelles such as the nucleolus, have been known since the 1830s when the structure of the cell nucleus was first described (Wagner and Barry, 1836; David, 1964). Additionally, these structures and organelles are usually composed of macromolecules such as proteins and RNA and are in many cases known as ribonucleoprotein (RNP) granules (Anderson and Kedersha, 2009). Moreover, the membrane-less compartments in the cytoplasm are involved in cellular signal transduction. For example, the Dvl protein family was initially assumed to transmit the Wnt signals in response to the binding of extracellular Wnt depending on membrane-bound vesicles. However, it was later shown that they were engaged without an enclosing membrane (Yanagawa et al., 1995; Schwarz-Romond et al., 2005; Kim W. et al., 2013).

These membrane-less organelles or structures exhibit significant liquid-like characteristics and are typically formed through a physicochemical process called liquid–liquid phase separation (LLPS) (Brangwynne et al., 2009). Given their liquid-like features, all the membrane-less intracellular organelles, structures and assemblies arising from LLPS are referred to as biomolecular condensates (Banani et al., 2017; Shin and Brangwynne, 2017). As with literal liquids, biomolecular condensates have a spherical shape and can fuse into a single large droplet upon contact with each other. Moreover, compartmentalized condensates are able to dynamically exchange components with the surrounding cytoplasm or nucleoplasm and this can selectively accelerate or inhibit biological reactions (Phair and Misteli, 2000; Snaar et al., 2000). Therefore, LLPS is increasingly being recognized as a fundamental process in the regulation of cellular activities in time and space.

Notably, earlier research on the aberrant LLPS process and formation of condensates, mainly focused on the molecular basis of specific neurodegenerative diseases such as the Alzheimer disease (AD) and amyotrophic lateral sclerosis (ALS) (Dormann et al., 2010; Wegmann et al., 2018). For instance, it was shown that ALS-derived mutations in RNA-binding proteins (RBPs), such as TIA1, HNRNPA1 and FUS, facilitate abnormal accumulation of the proteins in stress granules (which are cytoplasmic condensates) (Kim H. J. et al., 2013; Mackenzie et al., 2017). It was also suggested that this pathologic aggregation of proteins in ALS patients was associated with an altered LLPS process. In addition, *in vitro* experiments confirmed that these proteins had undergone phase separation and condensed into liquid-like droplets, and that over time they were converted into solid-like aggregates, which is the foundation of age-related diseases (Patel et al., 2015). Due to abundant proof that LLPS-derived protein aggregates are responsible for age-related diseases, the role of LLPS in cancer is also gaining increasing attention. For example, RNA N^6-methyladenosine (m^6A), one of the most prevalent epigenetic modifications on mRNAs, was reported to be associated with diverse cancer biological activities (Ma et al., 2019). Moreover, recent studies showed that m^6A-modified mRNAs can interact with its binding motifs and phase separate into compartmentalized condensates, leading to altered mRNA expression (Gao et al., 2019). Therefore, given the indispensable role of m^6A in cancer biology, it is likely that LLPS participates in m^6A-relavent tumor occurrence and development. In addition to participation in epigenetic modifications, LLPS is also involved in a wide range of cellular activities, such as transcriptional regulation, maintenance of genome stability, and signaling transduction, potentially contributing to tumorigenesis and tumor development.

Therefore, the current article gives a comprehensive review of existing research on LLPS, including a basic description of the process, its known role in cancer and the biological activities in which LLPS is involved that are potentially implicated in cancer. This review also gives a simplified description of the biophysics and biochemical mechanisms underlying LLPS, readers interested in details will be referred to the published literature (Alberti et al., 2019; Dignon et al., 2020).

MOLECULAR-LEVEL RULES AND COMPONENTS OF LLPS

Varying degrees of weak non-specific interactions between biomolecules are the driving forces behind phase separation at the molecular level (Shin and Brangwynne, 2017; Youn et al., 2019) (**Figure 1A**). In living cells, this interaction is represented by protein–protein or RNA–protein multivalency (Li et al., 2012). At a given temperature, phase separation occurs above a saturated concentration, beyond which weak transient interactions between biomolecules are stronger than the unfavorable entropy of demixing (Banani et al., 2017; Wang et al., 2018). Therefore, large biomolecules separate into two phases above this concentration threshold, one of which is dilute and the other is highly condensed. For biomolecules in cellular solutions, both phases are typically in a liquid state; thus, the process is termed LLPS (Youn et al., 2019). Furthermore, the probability of a solution to undergo LLPS is not only determined by its concentration and molecular multivalency, but also by environmental conditions such as temperature, salt, and pH (Riback et al., 2017). Additionally, the variety of physical determinants for LLPS further indicate that it can occur due to cellular stressors, like high temperature and hypoxia, which are common inducers for tumorigenesis (Riback et al., 2017).

Proteins and nucleic acids (RNA and DNA) are major components and mediators of LLPS. They can be altered by their biophysical properties as well as phase separation behaviors to form the highly multicomponent systems in condensates (Banani et al., 2016). The initially established multivalent interactions for

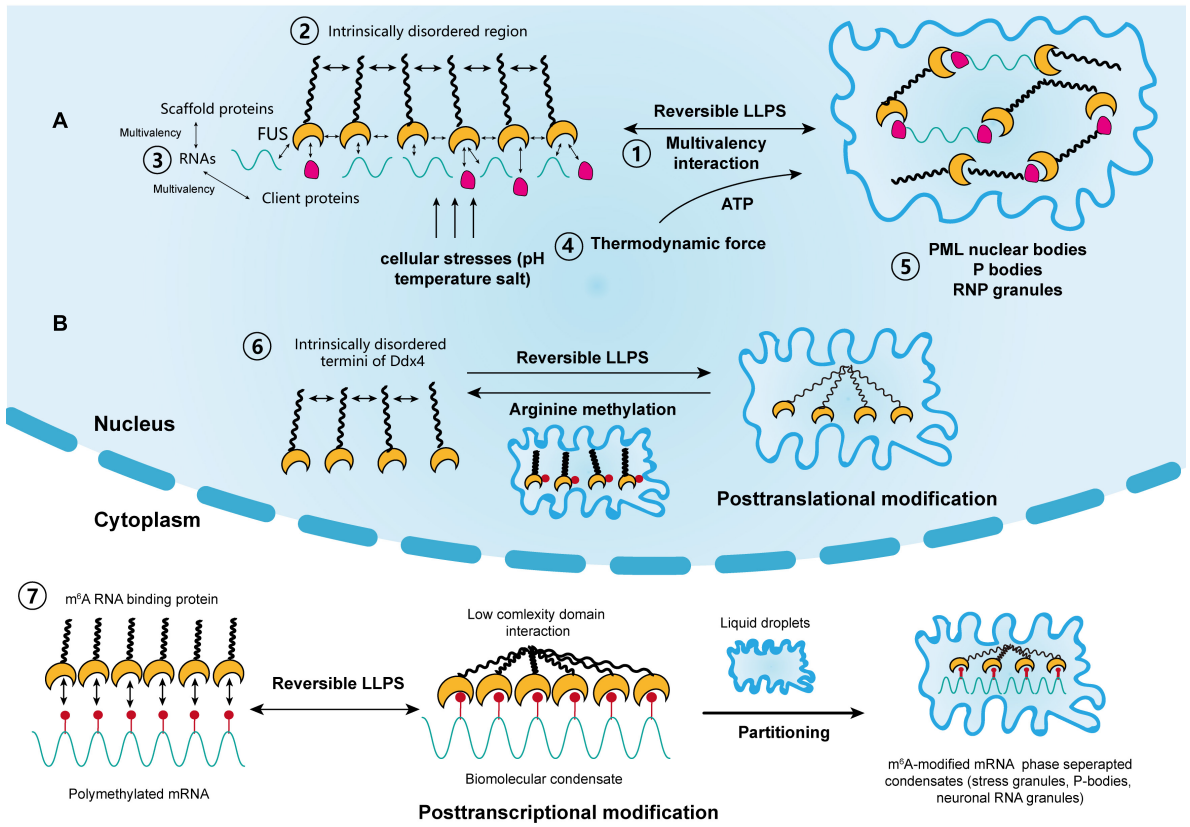

FIGURE 1 | The driving forces and regulation of liquid–liquid phase separation (LLPS) in cellular activity. **(A)** Scaffold proteins, such as FUS, concentrate low-valency client proteins through multivalent interactions, which is key for driving LLPS. The intrinsically disordered regions in some scaffolds also promote this process. Moreover, RNAs can further promote this process through interactions with RNA-binding regions. The thermodynamic force as well as cellular stressors, such as pH, temperature, and salt, may also support the reversible LLPS process. Classical nuclear structures formed by LLPS include PML bodies, P-bodies, and RNP granules. **(B)** LLPS is regulated by posttranslational and posttranscriptional modifications. Liquid condensates formed by Ddx4 are destabilized by its arginine methylation, whereas interactions between poly m^{6}A methylated mRNAs and m^{6}A binding proteins promote LLPS. Each step corresponds to its numbering.

phase behaviors occur between proteins containing repeats of the SRC homology 3 (SH3) domains and its binding proline-rich motifs (PRMs) (Li et al., 2012). In *in vitro* experiments, Li et al. (2012) demonstrated that these multi-valent, folded SH3/RPM domains are the drivers of phase separation. Additionally, the formation of liquid droplets was more evident at a higher SH3 concentration and valency (Li et al., 2012). Furthermore, Li et al. (2012) constructed a system containing nephrin, neural Wiskott–Aldrich syndrome protein (N-WASP) and NCK; they showed (*in vivo*) that the repeated SH2/SH3 domains from Nck and N-WASP, along with the phosphorylation of nephrin promoted the formation of liquid condensates through LLPS, which initiated the assembly of actins mediated by Arp2/3. Notably, nephrin plays a critical role in regulating the formation of glomerular filtration barrier, through actin assembly in kidney podocytes (Rohatgi et al., 2001; Jones et al., 2006). In addition, proteins that exhibit the same repetitive domains are often thought to be involved in the formation of signaling complexes, as in the case of T cell receptor (TCR) clusters in transmembrane signaling (Su et al., 2016). The process will be discussed in detail in subsequent paragraphs.

Proteins are the most common components of condensates, and can be classified into scaffolds and clients according to their functions (Banani et al., 2016). Scaffold proteins drive LLPS and maintain the integrity of condensates, whereas client proteins are low-valency molecules, which are concentrated by scaffolds during LLPS and dynamically exchange with the surrounding cytoplasm and nucleoplasm. Notably, members of the FUS family are typical scaffold proteins. They drive the accumulation of gel-like condensates, leading to the progression of ALS and age-related diseases (Crozat et al., 1993; Patel et al., 2015). Other scaffold proteins include HNRNPA1, HNRNPA2, TAF15, and ESWR1 (Lin et al., 2015; Ryan et al., 2018). In addition, scaffold proteins and RNP granules usually possess intrinsically disordered regions (IDRs). Typically, these regions are enriched with charged amino acids, which constitute the backbone of different kinds of charged interactions between RNA and proteins (Castello et al., 2012; Nott et al., 2015; Uversky, 2017). Moreover, compared with structured proteins with highly folded sequences, IDRs have low-sequence complexity domains (LCDs). These structural features make them energetically favorable and facilitate the occurrence of LLPS

(Burke et al., 2015; Elbaum-Garfinkle et al., 2015; Molliex et al., 2015; Conicella et al., 2016).

RNA is another significant component of condensates. It acts in concert with proteins to regulate LLPS in living cells (Zhang et al., 2015). Biomolecular condensates in the nucleus, such as the nucleolus, paraspeckles, and RNP granules all contain large amounts of both proteins and RNA as a result of LLPS (Berry et al., 2015). Additionally, RNA is an ideal scaffold element for its single-stranded, multivalent, and flexible structures. For example, a reduction in RNA concentration or a genetic depletion of RNA-binding in the nucleus accelerates LLPS, leading to the accumulation of cytotoxic gel-like FUS and TDP43 protein aggregates (Maharana et al., 2018). In contrast, a high RNA/protein ratio inhibits LLPS and the formation of biomolecular condensates. It was also suggested that RNA can buffer the aberrant protein aggregates arising from LLPS. Moreover, RBPs, such as RNA recognition motifs, were reported to play a role in RNA stability and metabolism. These proteins were shown to be responsible for interactions with RNAs during LLPS, which leads to the formation of nuclear RNP bodies, P-bodies, and stress granules (Clery et al., 2008). Furthermore, Molliex et al. (2015) reported that LLPS, mediated by a low-complexity sequence of HNRNPA1, was facilitated by RNA recognition motifs in the presence of RNA, during the persistent assembly of stress granules. This process was independent of IDRs and highlighted the significance of RNA in LLPS (Molliex et al., 2015). In most cases, proteins that contain both IDRs and RNA recognition motifs interact with RNAs to promote LLPS synergistically (Castello et al., 2012). This is now considered as an RNA-induced lowering of saturation concentration for LLPS, which is a prevalent effect on proteins (Lin et al., 2015; Molliex et al., 2015; Saha et al., 2016).

REGULATION OF LLPS IN CELLULAR ACTIVITIES

It remains unclear how the aging-related accumulation of protein aggregates, such as HNRNPA1 TIA1, and TAU progresses from liquid droplets into gel-like or solid-like particles and eventually nucleate into amyloid fibers. Mechanistically, the production of condensates by LLPS is reversible, although this reversibility is compromised over time within a pathological context (Lin et al., 2015; Zhang et al., 2015). Recent studies suggested that the solid-like state of these proteins is likely to be regulated by transcriptional activities that require the participation of energetic substances, such as adenosine triphosphate (ATP) (Jain et al., 2016; Mugler et al., 2016; Patel et al., 2017). Intriguingly, several studies have shown that nucleolar subcompartments and those within RNP granules have an apparent nucleolar viscosity, which is highly dependent on ATP, and that the fluidity of stress granules significantly decreases in the absence of ATP (Brangwynne et al., 2011; Feric et al., 2016; Jain et al., 2016). Moreover, it was reported that nucleoli undergo LLPS and preferentially assemble in the organizing regions of transcriptionally active rRNAs, in processes driven by thermodynamics (Berry et al., 2015). In addition, nucleolar components and structures show substantial changes after inhibiting transcription upon nucleolar condensation (Shav-Tal et al., 2005). Therefore, it is hypothesized that both the irreversible transformation of condensates and the changes in the viscosity of nucleolar subcompartments are driven by thermodynamic forces, which are modulated by transcriptional activities. The assumption is consistent with the findings from previous studies which showed that RNA can co-transcriptionally drive the assembly or nucleation of nuclear organelles such as the nucleolus, paraspeckles, and stress granules (Mao et al., 2011b; Shevtsov and Dundr, 2011). However, the thermodynamic parameters modulated by RNA transcription do not fundamentally alter the passive LLPS process. More specific experimental methods that include parameters such as temperature and pH could further elucidate the determinants of LLPS in biological activities. Furthermore, targeting specific RNA transcription or ATPase may be a new therapeutic strategy that can reverse the irreversible process of protein accumulation in cancer and aging diseases. Nonetheless, global ATP depletion or inhibition of transcription can influence normal cell function. Considering their multifaceted roles in cellular activities, targeted RNA interference or specific ATPase abrogation might be promising strategies for managing both diseases.

In addition, the metastability of biomolecular condensates highlights that these molecular structures, represented by proteins and RNAs, likely didn't reach thermodynamic equilibrium in most cases. Additionally, cells use functional modification as another regulatory mechanism to control the dynamics, composition and reversibility of phase separation, including posttranslational modification (PTM) and posttranscriptional modification (**Figure 1B**). Representatives of PTM in LLPS include phosphorylation and arginine methylation, which tend to facilitate or impair the formation of condensates by altering the valence of scaffold and client proteins. For example, it was reported that arginine methylation of Ddx4, whose IDRs condense to form condensates through LLPS, could destabilize the condensates and attenuate LLPS by altering its electrostatic interactions (Nott et al., 2015). Moreover, arginine methylation occurs within the nucleus of cervical cancer cells. In contrast, phosphorylation can either promote or impair the formation of condensates. For instance, synapsin, is a neurotransmitter-containing synaptic vesicle (SV) that forms through LLPS. It was previously shown to rapidly dissolve upon phosphorylation by Ca^{2+}/calmodulin-dependent kinase II to trigger the release of neurotransmitters (Milovanovic et al., 2018). Similar phenomena were observed in the low-sequence-complexity domains of FUS and other amyloid proteins (Monahan et al., 2017; Carpenter et al., 2018). Intriguingly, phosphorylation of the microtubule-binding domain of the tau protein instead altered its valency and facilitated the formation of liquid condensates, eventually leading to the aggregation of amyloid tangles (Ambadipudi et al., 2017). The modulatory effect of PTM on LLPS therefore shows its potential in cancer treatment, by tampering with the interaction between small molecules and target protein motifs.

Posttranscriptional modification is a newly identified mechanism of regulating LLPS and research has mainly focused on RNA m^6A (Gao et al., 2019; Ries et al., 2019; Liu et al., 2020;

Wang J. et al., 2020) (**Figure 1B**). m^6A methylation is the most prevalent epigenetic modification at the posttranscriptional level and is widely involved in numerous cellular processes. Ries et al. (2019) reported that LLPS is significantly facilitated by mRNAs containing multiple m^6A-modified domains through the regulation of m^6A readers. Moreover, polymethylated mRNA can serve as a multivalent scaffold for the binding of YTHDFs (the RBPs in the m^6A reader family), and simultaneously juxtapose their low-complexity domain to promote LLPS. Eventually, the mRNA–YTHDF combinants phase separate into compartmentalized droplets, forming liquid condensates such as stress granules and P-bodies, resulting in altered mRNA translation and degradation. Due to the prevalence of aberrant m^6A modification in tumor biology, therapies targeting m^6A to modulate LLPS and eventually, the expression of mRNA may have considerable potential (He et al., 2019).

THE EMERGING ROLE OF LLPS IN CANCER

Over the past decades, there has been great progress in understanding of the malignant behaviors of tumors, and this is represented by the proposal on the hallmarks of cancer (Hanahan and Weinberg, 2011). Notably, during the multistep development of tumors, cancer cells acquire six biological capabilities that allow them to evolve progressively to a malignant state. These include limitless proliferation, avoiding inhibition of growth, resistance to death, replicative immortality, induction of angiogenesis, invasiveness and distant metastasis, (Hanahan and Weinberg, 2000). It was confirmed that cancer mutations typically underpin the acquisition of these hallmarks, or they interfere with the functions of inhibitors of these hallmarks. However, it is still unclear why certain genetic mutations cause cancer. Therefore, the emergence of phase separation offers a new basis of interpreting and understanding cancer phenotypes, with potentially novel therapeutic avenues.

P53 Protein Aggregation: Question to Answer

As in the case of neurodegeneration, disease-linked genetic mutations in RBPs promoted the accumulation of their respective proteins, which forms membraneless-organelles in the cytoplasm or nucleus through reversible phase separation (Kim H. J. et al., 2013; Patel et al., 2015; Conicella et al., 2016; Mackenzie et al., 2017). A higher concentration of these proteins in condensates shifted the phase equilibrium toward a highly condensed state and simultaneously promoted the formation of irreversible protein aggregates (Patel et al., 2015; Wegmann et al., 2018). This irreversible liquid-to-solid transition corresponds to the formation of amyloid fibrils, which underlies the development of aging diseases (Shin and Brangwynne, 2017). However, the same mechanism is yet to be proven in cancer mutations. For instance, TP53, one of the most studied tumor suppressor genes, plays a critical role in maintaining genomic stability. It protects cells against tumorigenesis by inducing cell cycle arrest and binding to its target DNA sequence to initiate DNA repair or apoptosis (Silva et al., 2014; Eischen, 2016; Mantovani et al., 2019) (**Figure 2A**). Over 50% of human cancers exhibit TP53 gene mutations (Muller and Vousden, 2013). Previous studies reported that p53 can be uptaken into nuclear bodies such as the Cajal and PML bodies under conditions of stress responses (Fogal et al., 2000; Guo et al., 2000; Cioce and Lamond, 2005). In prostate cancer, p53, along with other proteins such as MYC and CDKN2D, accumulates within significantly enlarged cancer cell nucleoli (Dang and Lee, 1989; Wsierska-Gadek and Horky, 2003; Fischer et al., 2004; Pedrote et al., 2018). Moreover, mutant p53 protein is known to form amyloid-like aggregates, which abrogate its antitumor functions (Ghosh et al., 2017). It was also reported that mutant p53 aggregates faster than the wild-type, and the state transition is largely attributed to the p53 DNA binding domain, which has an amyloidogenic sequence and is likely to associate into solid-like fibrils (Lee et al., 2003; Ano Bom et al., 2012; Ghosh et al., 2017). Aggregated species of mutant p53, or in another word, oligomerization of p53 mutants, are highly expressed in cancer cells, and accumulate as amyloid oligomers, which are associated with malignant phenotypes such as chemoresistance and tumor growth (Melo Dos Santos et al., 2019; Pedrote et al., 2020; Zhang et al., 2020). Although oligomerization and phase separation are often coupled, they do represent distinct process, and can be experimentally separated. Therefore, notwithstanding the seemingly alike outcomes of aging-associated amyloidogenesis and p53 aggregation, the process they resulted from could be distinct.

Intriguingly, recent studies reported potential condensation-like behaviors of mutant p53 that exhibited a number of unique features, distinct from LLPS-originated liquid droplets. For instance, Yang et al. (2020) reported that p53 R248Q, one of the p53 mutants that strongly predicts poor outcomes in ovarian cancer patients, forms condensate-like clusters by destabilizing the structure of its core domain instead of interacting through its disordered regions. Moreover, the formed p53 R248Q clusters may lead to the misfolding and irreversible aggregation of p53 itself, and consequently amyloid fibrils. The condensate-like state was also observed in fluorescently tagged structural mutant p53 in osteosarcoma cells, and they were independent of PML or Cajal bodies (Lemos et al., 2020). Another study reported that p53 itself was found to form liquid-like droplets *in vitro*, at a neutral and slightly acidic pH environment, and at low salt concentrations (Kamagata et al., 2020). Although low-complexity domains that frequently being found in phase-separated proteins was not identified in p53, the multivalent electrostatic interactions between the C-terminal and N-terminal domains of p53 mutant were proven to be the key drivers for droplet formation (Kamagata et al., 2020). Additionally, this process was found to be regulated by molecular crowding agents, DNA, and PTM, while the effect of RNA on droplet formation is still unclear (Kamagata et al., 2020). Given the above studies, we presumed that the pathologic cancer-associated p53 aggregation may proceed via a functional step of LLPS, which explains why it shares similarities with LLPS yet exhibit distinguishable characteristics. Nevertheless, more studies are needed to ascertain the roles of p53 in cellular conditions, to determine its relationship with LLPS and amyloid formation,

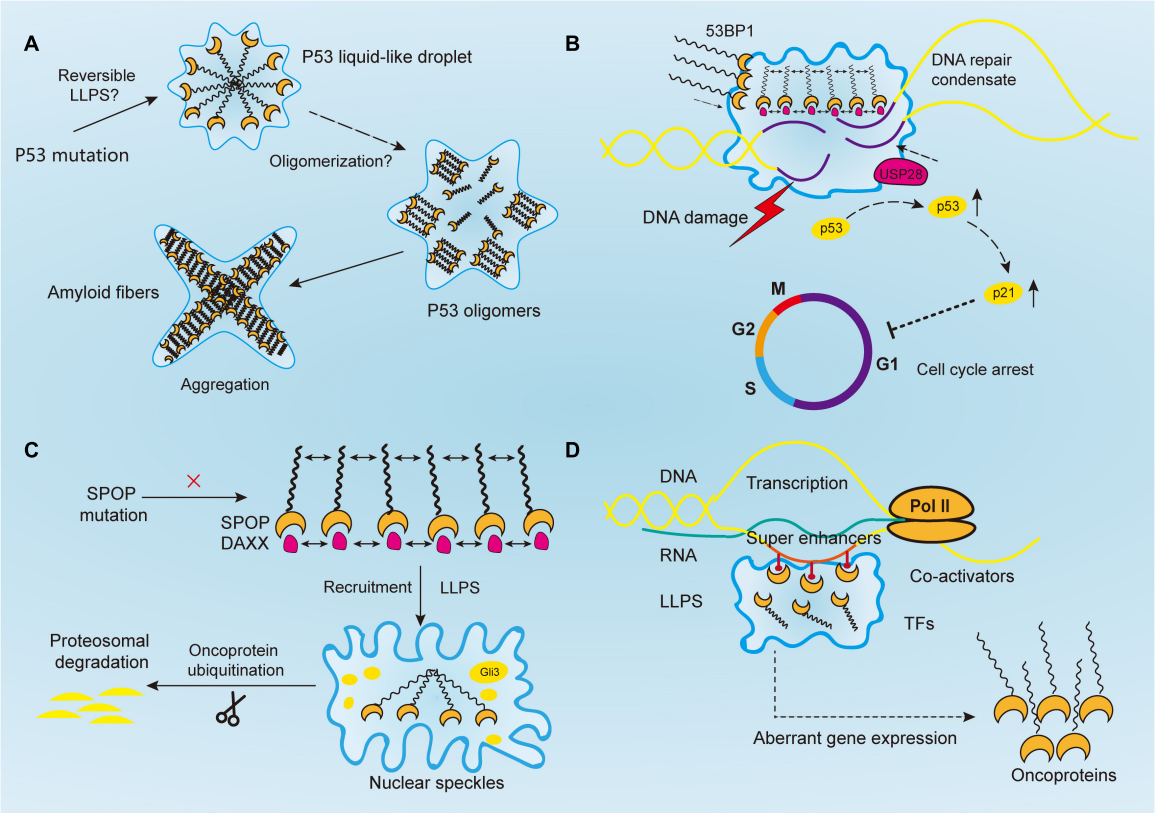

FIGURE 2 | Aberrantly regulated liquid–liquid phase separation (LLPS) in cancer. **(A)** Tumor suppressor p53 forms liquid-like droplet upon mutations, and it self-associates into oligomers through oligomerization. Consequently, p53 oligomers irreversibly aggregate into amyloid fibers. However, it is still unclear whether p53 undergoes reversible LLPS to form droplet. **(B)** Upon DNA damage, 53BP1 is recruited and assembles at the DNA damaged sites through phase separation. The phase separated 53BP1 condensates dynamically recruit and stabilize downstream proteins such as p53 and its co-activator USP28, leading to the overexpression of p53 target genes such as p21 and consequently arrest of cell cycle. **(C)** Highly ordered SPOP polymers and their binding protein substrates, such as DAXX, undergo LLPS and are recruited toward nuclear speckles, where SPOP oligomers facilitates the ubiquitination of substrates such as Gli3 and other oncoproteins to inhibit tumorigenesis. In cancers, this function is abrogated by SPOP mutation. **(D)** Transcriptional regulators, including super-enhancers, co-activators, transcription factors, and RNA polymerase II, all undergo a phase separation that promotes cancer transcriptional activities, resulting in the aberrant expression of oncogenes and facilitating tumor progression.

and to elucidate its possible involvement in the formation of membraneless organelles such as the Cajal and PML bodies.

Maintenance of Genome Stability

Genetic mutations are usually accompanied by the disruption of DNA damage response (DDR) and DNA repair, as exemplified in p53. Recent studies indicate that DDR can induce the formation of transient repair condensates at the sites of DNA damage to concentrate repair proteins and activate repair signaling (Jackson and Bartek, 2009; Kim et al., 2020). Poly(ADP-ribose) polymerase 1 (PARP1), the founding member of the PARP family, plays a crucial role in cancer biology, including chromatin remodeling, replication, transcription, and most importantly, DNA repair and genome maintenance (Ray Chaudhuri and Nussenzweig, 2017; Hanzlikova and Caldecott, 2019; Kim et al., 2020). Early studies also showed that it was overexpressed in a variety of cancers (Rouleau et al., 2010). PARPs, such as PARP1, that are capable of synthesizing negatively charged polymers of PAR chains are called "writers" of poly(ADP-ribosyl)ation (PARylation) (Kamaletdinova et al., 2019). PARylation is thought to regulate the biochemical properties, assembly and catalyzation of target proteins upon DNA damage in a spatio-temporal confined manner (Kim et al., 2020; Pahi et al., 2020). Recently, Altmeyer et al. (2015) demonstrated that the formation of PAR chains, its nucleic-acid like properties, and its multivalent anionic nature are prerequisite to trigger the assembly of proteins containing IDRs at the damaged DNA sites, and thereby initiate liquid demixing. Consequently, a transient and reversible intracellular compartmentalization is achieved in response to DNA damage, via selective recruitment of LCD-containing FET proteins such as FUS, TAF15, and EWS (Altmeyer et al., 2015). Moreover, the LLPS behavior driven by electrostatic interactions between the positively charged LCDs and negatively charged PARs is amplified by prion-like protein domains, facilitates DNA repair (Altmeyer et al., 2015). In fact, PARP inhibitors have been widely used in clinic as monotherapeutic agents to block single-strand DNA (ssDNA) repair thereby inducing the synthetic lethality in cancers including ovarian, breast, and

pancreatic cancer (Jiang et al., 2019; Slade, 2020; Zhu et al., 2020). With more functional complexity of PARPs revealed, such as its role in LLPS, higher efficacy of clinical medicine may be achieved through combinational treatment method targeting both LLPS and DNA DDR.

Following PAR signaling studies, p53-binding protein 1 (53BP1) has also received attention for its important role in maintaining genomic stability (**Figure 2B**). By binding with p53, 53BP1 directly regulates the stability of p53 and affects the expression of p53 target genes, and it has been reported to regulate tumor cell behaviors in a variety of malignancies such as esophageal, colorectal, and breast cancers (Misteli and Soutoglou, 2009; Bi et al., 2015; Mirza-Aghazadeh-Attari et al., 2019; Yang et al., 2019; Schochter et al., 2020). And reduction of 53BP1 expression was reported to be associated with cell cycle arrest in esophageal cancer cells (Yang et al., 2019). Previous studies have reported that 53BP1, as a regulator of the repair of DNA double-strand breaks (DSBs), facilitates formation of chromatin domains around the damaged DNA, where downstream effectors are simultaneously recruited to shield the DNA lesions against nucleolytic reactions (Panier and Boulton, 2014; Mirza-Aghazadeh-Attari et al., 2019). However, the mechanism of how repair proteins assemble in time and space at the DNA damaged sites was not revealed until recently. Kilic et al. (2019) confirmed the liquid droplet-like properties of 53BP1 assembly and proved their phase separated behaviors, which was mainly contributed by its C-terminal regions that highly enriched with tyrosine and arginine and oligomerization domains. Addition of chemical 1, 6-hexanediol, that disrupts hydrophobic interactions reversed LLPS processes and the assembly of 53BP1 (Kilic et al., 2019). Additionally, Pessina et al. (2019) demonstrated that long non-coding RNA synthesized at DSB can also drive the formation of 53BP1 assemblies through LLPS, and the process was halted upon transcription inhibition. Notably, the phase separated 53BP1 assemblies for repairing DNA damage dynamically recruit and stabilize downstream proteins such as p53 and its co-activator USP28 (Kilic et al., 2019). When the formation of assembly is damaged, p53 stability is consequently impaired, and so as its target gene p21, leading to cell cycle arrest (Kilic et al., 2019). Although corresponding inhibitors of 53BP1 has not been developed yet, its role in DNA damage repair by means of LLPS makes it promising target for inducing cancer cell death. Given their similar phase separated behaviors, 53BP1 might be used to sensitize chemoresistance cancer cells in combination with PARP inhibitors (D'Andrea, 2018).

SPOP

The speckle-type pox virus and zinc finger (POZ) domain protein (SPOP) is a substrate adaptor that pairs with the cullin3-RING ubiquitin ligase (CRL3). SPOP controls the ubiquitination and subsequent proteasomal degradation of various protein substrates such as the death domain-associated protein (DAXX), androgen receptor (AR), epigenetic regulators and hormone signaling effectors, therefore is involved in diverse cellular activities, including cell cycle control, epigenetic modification and hormone signaling (Mani, 2014). Mutation of SPOP and the resulting dysregulation of ubiquitin-proteasome pathways play an important role in the pathogenesis and progression of endometrial and prostate cancers, whereas its overexpression and mislocalization are correlated with kidney cancer (Li G. et al., 2014; Geng et al., 2017; Cuneo and Mittag, 2019; Wang Z. et al., 2020). SPOP is most frequently mutated in prostate cancer, and across 21 various types of cancers (Lawrence et al., 2014). In prostate cancer, SPOP mutation abrogates its interaction with the SRC-3 protein and subsequent regulation on AR transcription, leading to tumor progression and resistance to androgen deprivation therapies (Geng et al., 2013, 2017).

Human SPOP is mainly composed of three domains, in which the N-terminal meprin and TRAF-C homology (MATH) domain is the core domain responsible for recognizing protein substrates, while the other two synergistically promote the self-association of SPOP into linear, high-order oligomers (Marzahn et al., 2016). The size distribution of oligomers is highly dependent on SPOP concentration (Marzahn et al., 2016). Previous studies have proved that wild-type SPOP mainly localizes onto membraneless liquid nuclear speckles, where the interchromatin clusters are critically involved in mRNA maturation, DNA repair, RNA metabolism, and chromatin organization (**Figure 2C**) (Nagai et al., 1997; Galganski et al., 2017). The highly ordered SPOP oligomer can recruit substrates such as Gli3 and other oncoproteins to CRL3 for ubiquitination and subsequent proteasomal degradation, which mechanistically reduce tumorigenesis (Zhang et al., 2006, 2009; Cheng et al., 2018). However, the mechanism about how SPOP recruits oncogenic substrates to nuclear speckles remains elusive. Recently, Bouchard et al. (2018) reported that SPOP localizes onto liquid nuclear organelles through phase separation with DAXX, which contains multiple SPOP-binding motifs in intrinsically disordered domains. Moreover, they proved oligomerization of SPOP instead of its monomeric state can promote LLPS (Bouchard et al., 2018). In other words, the multivalent interactions between highly ordered SPOP oligomers and its binding substrate proteins can promote LLPS and their co-localization. Additionally, prostate cancer-associated SPOP mutants inhibit substrate ubiquitination by interfering with the LLPS process (Bouchard et al., 2018). Therefore, it is concluded that SPOP mutations can lead to the accumulation of oncogenic proteins, which in turn disrupts the formation of phase-separated condensates that regulate ubiquitin-dependent proteostasis. This may provide a theory basis for prostate cancer treatment that involves relocalizing SPOP to nuclear speckles by decreasing its saturation concentration or inventing substrate motifs compatible with SPOP, thereby restoring LLPS and the ubiquitination balance to inhibit tumor progression.

Transcription and Super-Enhancers

The development of cancer involves the aberrant regulation of downstream transcriptional networks, following the mutation of driver genes. A variety of cancer phenotypes including tumor growth, invasion, chemoresistance and distant metastasis, are driven by deregulated transcription activities (Bradner et al., 2017). Notably, RNA transcription requires the participation of RNA polymerases (Pol) and transcription factors (TFs), which

are both likely to be regulated by phase separation (**Figure 2D**). For instance, the carboxy-terminal domain (CTD) of RNA Pol II is a low-complexity domain with an IDR, which is vital for mRNA processing and transcription. It was previously observed that reducing the length of CTD led to a decrease in Pol II clustering and the recruitment of transcriptional apparatus, whereas extension of the CTD resulted in the opposite effect (Boehning et al., 2018). Mechanistically, CTD droplets can undergo phase separation to incorporate Pol II at gene promoters, and phosphorylation of CTD releases the Pol II from clusters for transcription elongation (Boehning et al., 2018). A similar process was shown to occur in TFs. Moreover, the activation domains from the TFs OCT4 and GCN4, when driven by weak multivalent interactions are phase separated into liquid droplets. Estrogen receptor, a ligand-dependent TF, also undergo LLPS for gene activation (Boija et al., 2018). Most activation domains on TFs contain intrinsically disordered low-complexity sequence domains. Additionally, the interactions between low-complexity sequence domains underlie LLPS and the subsequent stability of DNA binding, polymerase recruitment, and transcriptional activation (Chong et al., 2018). Moreover, phase separation of TFs has been reported to be implicated in the regulation of aberrant gene expression in cancers, as exemplified by EWS and FLI1 in Ewing's sarcoma, suggesting that disturbing the interactions of specific TF domains is a potential drug therapy (Chong et al., 2018).

Additionally, the emergence of LLPS provides a novel framework for understanding the molecular mechanisms of underlying dysregulated transcription, mediated by oncogenes such as MYC, whose regulatory basis is yet to be revealed. Recent researches have focused on a bunch of gene clusters called 'super-enhancers,' which are essential for regulating MYC expression levels in hematological tumors and colon cancer cells (Bahr et al., 2018; Scholz et al., 2019). Literally, super-enhancers are clusters of transcriptional enhancers or regulatory elements that mainly consist of master TFs and mediators (Hnisz et al., 2013; Whyte et al., 2013). Compared to conventional TFs, super-enhancers drive more robust expression of genes that prominently modulate cellular functions and determine cell identity. Therefore, they are expected to play an important role in cancer (Sengupta and George, 2017). Moreover, existing evidence shows that the high-density transcriptional apparatus of super-enhancers has the properties of biomolecular condensates, such as a sharp phase transition, the dynamic exchange of substances, and collapsing with the depletion of condensation, indicating the involvement of LLPS in the clustering of super-enhancers (Loven et al., 2013; Kwiatkowski et al., 2014; Hnisz et al., 2015; Proudhon et al., 2016; Sengupta and George, 2017). Recently, Sabari et al. (2018) reported that the transcriptional mediator co-activators BRD4 and MED1 are enriched by super-enhancers and can phase separate into compartmentalized condensates and concentrate the transcriptional apparatus to control gene expression. Therefore, we speculated that IDR-driven phase separation of super-enhancers or other transcriptional apparatus is a general mechanism for gene activation at the promoters by TFs.

With better understanding of the role of LLPS in transcriptional activities, Hnisz et al. (2017) proposed a phase separation model that can predict key determinants in transcriptional regulation. Upon epigenetic or chemical modifications, the components of enhancers, including multivalent proteins and nucleic acids (RNA and DNA), can form chain-like structures, and the residues could potentially interact with other chains, thus building cross-links (Hnisz et al., 2017). After a cascade of reactions, molecules within this system, such as master TFs, mediator co-activators, chromatin regulators, and RNA polymerases, can achieve a dynamic balance and phase separate into droplets, which cooperatively regulate transcriptional activities (Hnisz et al., 2017). Based on this theory, some mechanisms of transcriptional activities aberrantly regulated by enhancers in cancer can be partially explained. For instance, Mansour et al. (2014) demonstrated in T cell leukemias that the mutation of TAL1 oncogene enhancer can create binding motifs for master TF MYB, which recruits additional parts of the transcriptional apparatus, such as co-activator acetyltransferases CBP, as well as critical components of leukemic transcriptional complex, including GATA-3, RUNX1, and TAL1. Namely, the insertion of a single TF MYB has the potential to bind other co-factors at the transcriptional domain, leading to the initiation of super-enhancers upstream for the activation of TAL1 oncogene, and consequently promote leukemogenic progress (Mansour et al., 2014). From our perspective, the step-wise manner of the recruitment of TAL1 super-enhancer complex, and their spatio-temporal proximity on transcriptional domains correspond to certain characteristics of the formation of biomolecular condensates, indicating a potential role of LLPS in this process. In addition, the genetic deletion of enhancers within super-enhancers can reduce the recruitment of other co-factors, and lead to the collapse of the entire super-enhancer (Mansour et al., 2014). A reversible state of this process may further confirm the association between LLPS and transcriptional regulation in cancer. Thus, the LLPS model proposed by Hnisz et al. (2017) might be used for the prediction of potential enhancers aberrantly activated in cancers for downstream transcriptional regulation at promoters, and for therapies targeting specific driver genes such as MYB or MYC to block downstream gene expression and protein translation.

TRANSMEMBRANE SIGNALING TRANSDUCTION REGULATED BY LLPS: IMPLICATIONS IN CANCER

Cancer cells are continually exposed to aberrant external signals that are accepted by transmembrane receptors, which in turn initiate diverse intracellular signaling cascades, resulting in the malignant behaviors of cancer cells. Sustaining of proliferative signaling, for example, one of the most fundamental traits of cancer cells, is associated with classical cancerous signals such as the PI3K/Akt, JAK/STAT, and NF-κB signaling pathways, all of which involve membrane receptors assembling into two-dimensional clusters with transmitted molecules. Intriguingly, recent studies suggested that LLPS might be an essential mechanism for the high-order assembly of these receptors driven by weak, multivalent interactions. Therefore, we uncover two

relevant signaling pathways not only play important roles in tumorigenesis but also involve LLPS.

LLPS in Immune-Relevant Signaling Pathways

The assembly of signaling clusters on the membranes of immune cells has been observed for several decades. Previous studies reported that receptors on both T and B cells are assembled on membranes in response to external stimulation (Schumacher, 2002; Bankovich and Garcia, 2003; Gold and Reth, 2019). T cell antigen receptor (TCR) signaling is a well-studied system to elucidate the formation of transmembrane clusters (**Figure 3A**). Notably, linker for the activation of T cells (LAT) is a transmembrane adaptor protein that centrally modulates most downstream signals of the TCR at immune synapses [the interface between bound immune cells, such as when T cells bind with antigen-presenting cell (APC)] (Dustin and Choudhuri, 2016). Upon TCR activation, the tyrosine residues of LAT are phosphorylated by the membrane kinase ZAP70 (Zhang et al., 1998). These phosphorylated tyrosine residues are in turn necessary for attracting the multivalent Src Homology protein family members including Grb2, Gads and PLC-γ, and subsequent formation of membranous clusters and signal transduction (Samelson, 2002; Balagopalan et al., 2015). Thereafter, the PRMs of the adaptor proteins, such as Sos1 and SLP76, bind accordingly to the multivalent domains of Grb2 and Gads, and then initiate the recruitment of actin effectors such as WASP, Nck, and the Arp2/3 complex for the polymerization of actin filaments (Kumari et al., 2015; Huang et al., 2016). Consequently, these actin regulators and kinases induce TCR activation, calcium release, actin assembly and stimulation of MAPK signaling.

Bunnell et al. (2002) have reported that if TCR binds to stimulatory antibodies, clusters enriched with SLP-76, LAT, ZAP-70 and other signaling partners could form, leading to the generation of an immune synapse. Moreover, these clusters are formed without lipid membrane structures, and the components of clusters could be dynamically exchanged with the surroundings. However, it was not until 2016, that the role of

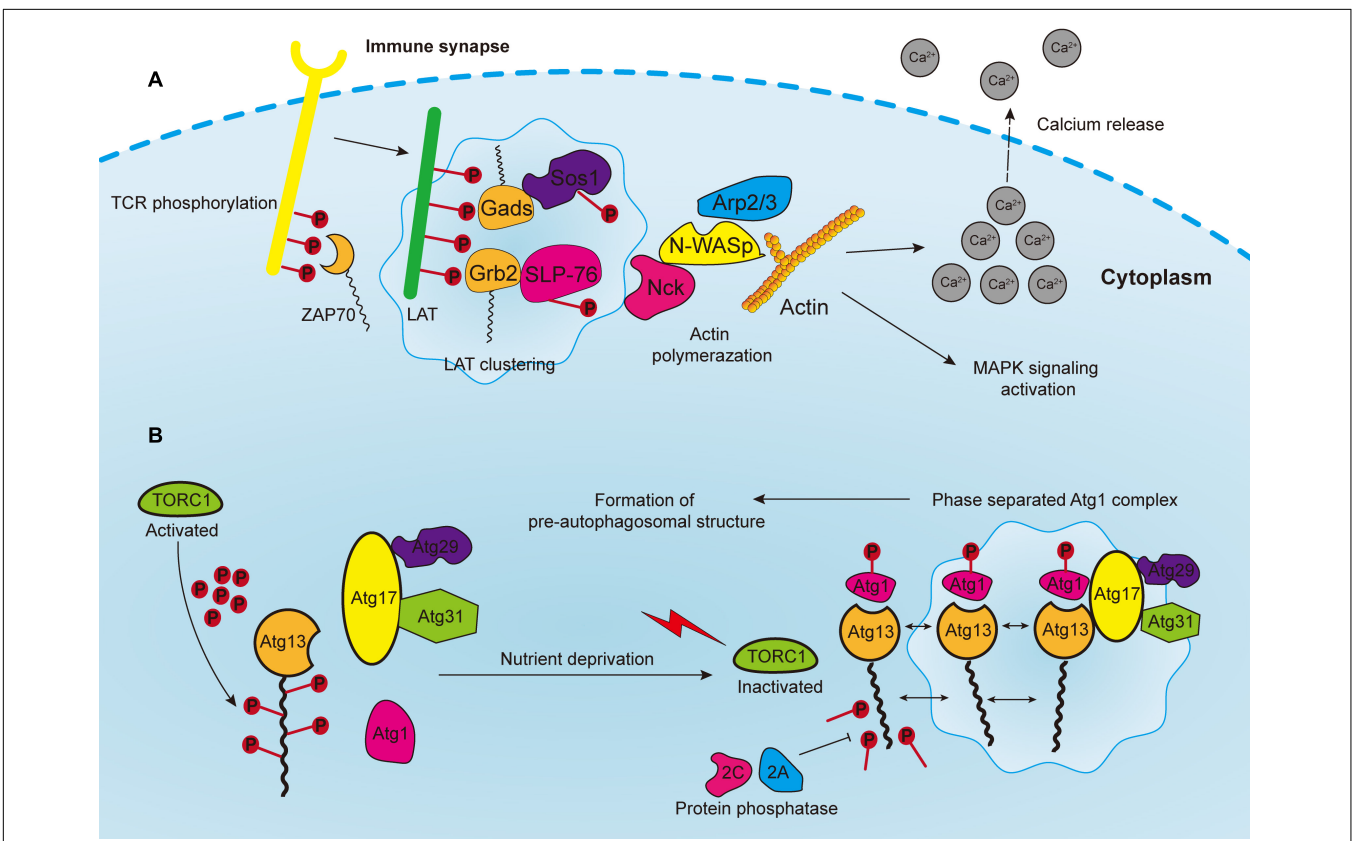

FIGURE 3 | (A) Phosphorylated T cell receptors (TCRs) recruit and activate cytoplasmic tyrosine kinase ZAP70, which in turn phosphorylates the linker for the activation of T cells (LAT). LAT drives the formation of clusters enriched with downstream proteins, such as Gads and Grb2, which recruit adaptor proteins, such as Sos1 and SLP76. Phosphorylated Sos1 and SLP76 initiate the recruitment of actin effectors such as WASP, Nck, and Arp2/3 complex for polymerization of actin filaments, consequently leading to calcium release, MAPK signaling activation, and the formation of an immune synapse. **(B)** In yeast cells, the Atg1 complex consists of five subunits including Atg1, Atg13, Atg17, Atg29, and Atg31, which are abundant with IDRs for subsequent phase separation. The Atg13 is highly phosphorylated by TORC1 under nutrient replete conditions, leading to the block of Atg1 complex formation. Upon nutrient deprivation, TORC1 is inactivated, and Atg13 is therefore dephosphorylated by protein phosphatases 2C and 2A, whereas Atg1 is auto-phosphorylated. Atg13 serves as a scaffold protein to bind with Atg1 and Atg17-Atg29-Atg31 to promote the phase separation of Atg1 complex, and consequently the formation of pre-autophagosomal structure.

LLPS in this process was uncovered (Balagopalan et al., 2015; Su et al., 2016). Su et al. (2016) biochemically reconstituted an *in vitro* TCR signaling system and revealed that the biochemical force-multivalency between molecules in LAT clusters interacted and resulted in phase separation. Additionally, CD45, one of the transmembrane phosphatases opposing TCR phosphorylation, was excluded from the LLPS-derived clusters, indicating that LLPS produces a specialized chemical environment by selectively concentrating molecules in clusters. Therefore, it is reasonable to speculate that other signaling pathways, or more specifically, the activation of other immune cells, employ the same mechanisms since clusters are prevalent on immune cell receptors.

Furthermore, it was assumed that a large proportion of biomolecules in the transmembrane signaling receptors on different T cells can phase separate into clusters to facilitate the transduction of signals and to regulate immune responses in cancers. Based on this assumption, therapies aimed at TCR and LLPS could be generalized to other co-inhibitory receptors on T cells, such as the programmed cell death protein 1 (PD-1), the cytotoxic T lymphocyte antigen 4 (CTLA-4), and T-cell immunoglobulin and mucin domain 3 (TIM-3) (Wei et al., 2018). For instance, CD28, is one of the co-stimulatory factors for T cells, and is mostly co-localized with PD1 clusters upon T cell activation (Hui et al., 2017). In addition, PD1 frequently recruits phosphatase Shp2, after being activated by its ligand PDL1, for the preferential dephosphorylation of CD28 in order to suppress T cell function (Hui et al., 2017). Therefore, T cells are selectively activated for the regulation of downstream signaling. It is also likely that the tumor-killing effects of immunotherapies may be enhanced by reducing the aberrantly clustered checkpoints binding to multivalent T cell adaptor proteins such as Grb2 or LAT through LLPS in ways such as tuning the biochemical multivalences between interactive domains (Brooks et al., 2004).

In addition to the membrane signaling pathways, LLPS also facilitates intracellular signaling transduction. Notably, cyclic GMP-AMP synthase (cGAS) is a cytoplasmic DNA sensor that catalyzes the generation of cyclic GMP-AMP (cGAMP) from guanosine triphosphate and ATP by binding to double-stranded DNA (dsDNA) (Gao et al., 2013; Sun et al., 2013; Ablasser and Chen, 2019). On the other hand, the secondary messenger cGAMP can activate the adaptor protein STING, which in turn induces type I interferon and consequently, an innate immune response. Du and Chen (2018) reported that double-stranded DNA binding with cGAS prominently promoted their phase separation and the formation of condensates, in which activated cGAS changed the multivalence of DNA. Mechanistically, the altered valence of the cGAS–DNA interaction and the increased protein and DNA concentration cooperatively lowered the saturation concentration. Therefore, the aberrant expression of cGAS or other secondary messengers could make them independent of ligands and constantly activate immune signaling pathways, which might be a viable therapeutic target.

Autophagy-Relevant Signaling Pathways

Autophagy is an evolutionarily conserved catabolic process that requires the formation of double-membrane vesicles known as autophagosomes to capture intracellular wastes, such as cytotoxic proteins and damaged organelles, and deliver it to the lysosome for degradation and recycling. Environmental stress, such as hypoxia and nutrient deprivation, activates autophagy-related genes (ATGs) in order to initiate and enhance intracellular autophagic degradation to fulfill the metabolic and energy demands of cancer cells. Moreover, autophagosome precursor, also known as the pre-autophagosomal structure (PAS) in yeast, is a transient structure modulated by nutrient signals and frequently forms on vacuoles upon starvation (Fujioka et al., 2020). Formation of PAS starts with the assembly of multiple Atg1/ULK complexes, which in turn recruit other ATG proteins by forming a scaffold (Yamamoto et al., 2016). In yeast cells, the Atg1 complex consists of five subunits, namely Atg1, Atg13, Atg17, Atg29, and Atg31, which are abundant with IDRs for subsequent phase separation (Yamamoto et al., 2016; Fujioka et al., 2020) (**Figure 3B**). Additionally, the activation of Atg1 requires the phosphorylation of its kinase domain at Thr226, which induces its clustering and makes it serve as a client protein. Whereas Atg13 is dephosphorylated by protein phosphatases 2A and 2C, then binds to the distinctive regions of Atg17 to form scaffold droplets, thus facilitating the LLPS of the Atg1 complex and the formation of autophagosome (Fujioka et al., 2014). Although the initiation of autophagy in mammalian and cancer cells remains unclear, important insights may be obtained from this mechanism in yeast cells. For instance, target of rapamycin complex 1 (TORC1), which covers most of the signaling pathways relevant to autophagy, inhibits the formation of autophagosome, and regulates cell metabolism as well as growth (Saxton and Sabatini, 2017; Murugan, 2019). The Atg1/ULK complex is highly phosphorylated by TORC1 under nutrient replete conditions, leading to the block of downstream signaling and inhibition of autophagy (Jung et al., 2010). In addition, rapamycin, which is one of the most widely used immunosuppressors, can effectively inhibit Atg1/ULK phosphorylation by targeting mTORC1 (Li J. et al., 2014). Moreover, rapamycin can block the PI3K/Akt/mTOR pathway to inhibit tumor growth (Dibble and Cantley, 2015). Since rapamycin can promote autophagy, one proposal is to develop synergistic small molecules to accelerate cell autophagy, and to cooperatively induce the autophagic death of cancer cells, thereby enhancing the tumor-killing effect of rapamycin (Kim and Guan, 2015). These small molecules will act as scaffold proteins binding to Atg1/ULK clusters to facilitate their LLPS process.

Additionally, recent studies showed that p62, one of the autophagic receptors targeting autophagosomal cargoes for degradation, can assemble into liquid condensates by binding with ubiquitinated proteins, and it is itself degraded through autophagy (Sun et al., 2018; Zaffagnini et al., 2018). Furthermore, the binding of p62 to the KEAP1 mutant and NRF2 stabilizes NRF2-regulated transcription, which alters cell metabolism and alleviates oxidative stress (Cloer et al., 2018). However, when the role of p62 in selective autophagy is impaired, it accumulates and regulates downstream signaling such as NRF2, mTORC1, and NF-κB. This in turn leads to imbalanced cellular oxidation, nutrition conditions and inflammatory responses, consequently enhancing the progression of cancer (Sanchez-Martin et al., 2019). Therefore, p62 is likely to play an important

role in autophagy-relevant cancer signaling, whereas detailed mechanism is needed to be determined in future experiments.

CONCLUSION

Tumorigenesis and cancer development are complex processes involving multiple steps, such as gene mutation, alteration of transcription, epigenetic modification, and abnormal protein expression. In addition, all the aberrations in each step collectively result in the occurrence and progression of cancer. Moreover, understanding the roles of LLPS in oncogenic activities, either individually or in combination with other mechanisms, can potentially promote the translation of fundamental research into novel cancer diagnosis and targeted therapies. The biophysical and biochemical interactions between every single biomolecule or their constituent structures underlies the basic principles of LLPS. Mechanistically, thermodynamic forces derived from various cellular activities, such as RNA transcription, PTM, and m^6A modification, cooperatively regulate phase separation. The maintenance of genome stability is also actively accompanied by LLPS. Since genetic mutations underlying the acquisition of cancer hallmarks are usually accompanied by genome instability, restoring LLPS may be helpful to inhibit tumorigenesis. Deregulated transcriptional activities might upregulate oncoproteins and lead to tumor onset, which is closely related with LLPS. Furthermore, master transcriptional regulators, such as super-enhancers, are crucial for the assembly of co-activators, a process in which LLPS has an important role. Therefore, it could be useful to interfere with the aberrant activation of transcription in cancers by targeting the biomolecules that trigger LLPS in condensates. Additionally, signal transduction, though not directly linked with cancer through LLPS, might be a potential target for cancer therapy. Existing evidence has not only demonstrated its regulatory effects on innate immune activation but also its significance in autophagy, both of which are key drivers for cancer progression. Overall, addressing the functionalities of intracellular biomolecules that are associated with higher-order organization, such as proteins, RNAs and DNAs, has deepened our understanding of the biological behavior of cancer. Nevertheless, more effort should be directed toward the functional exploration of LLPS in cancer because many problems remain unsolved.

AUTHOR CONTRIBUTIONS

JL wrote the first draft of the manuscript. JQ and ZX conceived the idea of the manuscript. LZ and SY designed the structure of the manuscript. SZ and WZ revised, read, and approved the submitted version. All authors read and approved the manuscript.

FUNDING

This research was funded by the National S&T Major Project of China (grants 2017ZX10203205 and 2018ZX10301201), the Research Unit Project of the Chinese Academy of Medical Sciences (2019-I2M-5-030), the Innovative Research Groups of the National Natural Science Foundation of China (grant 81721091), and the Grant from Health Commission of Zhejiang Province (JBZX-202004).

REFERENCES

Ablasser, A., and Chen, Z. J. (2019). cGAS in action: expanding roles in immunity and inflammation. *Science* 363:eaat8657. doi: 10.1126/science.aat8657

Alberti, S., Gladfelter, A., and Mittag, T. (2019). Considerations and challenges in studying liquid-liquid phase separation and biomolecular condensates. *Cell* 176, 419–434. doi: 10.1016/j.cell.2018.12.035

Altmeyer, M., Neelsen, K. J., Teloni, F., Pozdnyakova, I., Pellegrino, S., Grofte, M., et al. (2015). Liquid demixing of intrinsically disordered proteins is seeded by poly(ADP-ribose). *Nat. Commun.* 6:8088. doi: 10.1038/ncomms9088

Ambadipudi, S., Biernat, J., Riedel, D., Mandelkow, E., and Zweckstetter, M. (2017). Liquid-liquid phase separation of the microtubule-binding repeats of the Alzheimer-related protein Tau. *Nat. Commun.* 8:275. doi: 10.1038/s41467-017-00480-0

Anderson, P., and Kedersha, N. (2009). RNA granules: post-transcriptional and epigenetic modulators of gene expression. *Nat. Rev. Mol. Cell Biol.* 10, 430–436. doi: 10.1038/nrm2694

Ano Bom, A. P., Rangel, L. P., Costa, D. C., de Oliveira, G. A., Sanches, D., Braga, C. A., et al. (2012). Mutant p53 aggregates into prion-like amyloid oligomers and fibrils: implications for cancer. *J. Biol. Chem.* 287, 28152–28162. doi: 10.1074/jbc.M112.340638

Bahr, C., von Paleske, L., Uslu, V. V., Remeseiro, S., Takayama, N., Ng, S. W., et al. (2018). A Myc enhancer cluster regulates normal and leukaemic haematopoietic stem cell hierarchies. *Nature* 553, 515–520. doi: 10.1038/nature25193

Balagopalan, L., Kortum, R. L., Coussens, N. P., Barr, V. A., and Samelson, L. E. (2015). The linker for activation of T cells (LAT) signaling hub: from signaling complexes to microclusters. *J. Biol. Chem.* 290, 26422–26429. doi: 10.1074/jbc.R115.665869

Banani, S. F., Lee, H. O., Hyman, A. A., and Rosen, M. K. (2017). Biomolecular condensates: organizers of cellular biochemistry. *Nat. Rev. Mol. Cell Biol.* 18, 285–298. doi: 10.1038/nrm.2017.7

Banani, S. F., Rice, A. M., Peeples, W. B., Lin, Y., Jain, S., Parker, R., et al. (2016). Compositional control of phase-separated cellular bodies. *Cell* 166, 651–663. doi: 10.1016/j.cell.2016.06.010

Bankovich, A. J., and Garcia, K. C. (2003). Not just any T cell receptor will do. *Immunity* 18, 7–11. doi: 10.1016/s1074-7613(02)00517-4

Berry, J., Weber, S. C., Vaidya, N., Haataja, M., and Brangwynne, C. P. (2015). RNA transcription modulates phase transition-driven nuclear body assembly. *Proc. Natl. Acad. Sci. U S A.* 112, E5237–E5245. doi: 10.1073/pnas.1509317112

Bi, J., Huang, A., Liu, T., Zhang, T., and Ma, H. (2015). Expression of DNA damage checkpoint 53BP1 is correlated with prognosis, cell proliferation and apoptosis in colorectal cancer. *Int. J. Clin. Exp. Pathol.* 8, 6070–6082.

Boehning, M., Dugast-Darzacq, C., Rankovic, M., Hansen, A. S., Yu, T., Marie-Nelly, H., et al. (2018). RNA polymerase II clustering through carboxy-terminal domain phase separation. *Nat. Struct. Mol. Biol.* 25, 833–840. doi: 10.1038/s41594-018-0112-y

Boija, A., Klein, I. A., Sabari, B. R., Dall'Agnese, A., Coffey, E. L., Zamudio, A. V., et al. (2018). Transcription factors activate genes through the phase-separation capacity of their activation domains. *Cell* 175:e16. doi: 10.1016/j.cell.2018.10.042

Bouchard, J. J., Otero, J. H., Scott, D. C., Szulc, E., Martin, E. W., Sabri, N., et al. (2018). Cancer mutations of the tumor suppressor spop disrupt the formation of active, phase-separated compartments. *Mol. Cell* 72, 19–36.e8. doi: 10.1016/j.molcel.2018.08.027

Bradner, J. E., Hnisz, D., and Young, R. A. (2017). Transcriptional addiction in Cancer. *Cell* 168, 629–643. doi: 10.1016/j.cell.2016.12.013

Brangwynne, C. P., Eckmann, C. R., Courson, D. S., Rybarska, A., Hoege, C., Gharakhani, J., et al. (2009). Germline P granules are liquid droplets that localize by controlled dissolution/condensation. *Science* 324, 1729–1732. doi: 10.1126/science.1172046

Brangwynne, C. P., Mitchison, T. J., and Hyman, A. A. (2011). Active liquid-like behavior of nucleoli determines their size and shape in *Xenopus laevis* oocytes. *Proc. Natl. Acad. Sci. U S A.* 108, 4334–4339. doi: 10.1073/pnas.1017150108

Brooks, S. R., Kirkham, P. M., Freeberg, L., and Carter, R. H. (2004). Binding of cytoplasmic proteins to the CD19 intracellular domain is high affinity, competitive, and multimeric. *J. Immunol.* 172, 7556–7564. doi: 10.4049/jimmunol.172.12.7556

Bunnell, S. C., Hong, D. I., Kardon, J. R., Yamazaki, T., McGlade, C. J., Barr, V. A., et al. (2002). T cell receptor ligation induces the formation of dynamically regulated signaling assemblies. *J. Cell Biol.* 158, 1263–1275. doi: 10.1083/jcb.200203043

Burke, K. A., Janke, A. M., Rhine, C. L., and Fawzi, N. L. (2015). Residue-by-Residue view of in vitro FUS granules that bind the C-Terminal domain of RNA polymerase II. *Mol. Cell* 60, 231–241. doi: 10.1016/j.molcel.2015.09.006

Carpenter, K., Bell, R. B., Yunus, J., Amon, A., and Berchowitz, L. E. (2018). Phosphorylation-Mediated clearance of amyloid-like assemblies in meiosis. *Dev. Cell* 45:e6. doi: 10.1016/j.devcel.2018.04.001

Castello, A., Fischer, B., Eichelbaum, K., Horos, R., Beckmann, B. M., Strein, C., et al. (2012). Insights into RNA biology from an atlas of mammalian mRNA-binding proteins. *Cell* 149, 1393–1406. doi: 10.1016/j.cell.2012.04.031

Cheng, J., Guo, J., Wang, Z., North, B. J., Tao, K., Dai, X., et al. (2018). Functional analysis of Cullin 3 E3 ligases in tumorigenesis. *Biochim. Biophys. Acta Rev. Cancer* 1869, 11–28. doi: 10.1016/j.bbcan.2017.11.001

Chong, S., Dugast-Darzacq, C., Liu, Z., Dong, P., Dailey, G. M., Cattoglio, C., et al. (2018). Imaging dynamic and selective low-complexity domain interactions that control gene transcription. *Science* 361:eaar2555. doi: 10.1126/science.aar2555

Cioce, M., and Lamond, A. I. (2005). Cajal bodies: a long history of discovery. *Annu. Rev. Cell Dev. Biol.* 21, 105–131. doi: 10.1146/annurev.cellbio.20.010403.103738

Clery, A., Blatter, M., and Allain, F. H. (2008). RNA recognition motifs: boring? not quite. *Curr. Opin. Struct. Biol.* 18, 290–298. doi: 10.1016/j.sbi.2008.04.002

Cloer, E. W., Siesser, P. F., Cousins, E. M., Goldfarb, D., Mowrey, D. D., Harrison, J. S., et al. (2018). p62-Dependent phase separation of patient-derived KEAP1 mutations and NRF2. *Mol. Cell Biol.* 38:e00644-17. doi: 10.1128/MCB.00644-17

Conicella, A. E., Zerze, G. H., Mittal, J., and Fawzi, N. L. (2016). ALS mutations disrupt phase separation mediated by alpha-helical structure in the TDP-43 Low-complexity C-Terminal domain. *Structure* 24, 1537–1549. doi: 10.1016/j.str.2016.07.007

Crozat, A., Aman, P., Mandahl, N., and Ron, D. (1993). Fusion of CHOP to a novel RNA-binding protein in human myxoid liposarcoma. *Nature* 363, 640–644. doi: 10.1038/363640a0

Cuneo, M. J., and Mittag, T. (2019). The ubiquitin ligase adaptor SPOP in cancer. *FEBS J.* 286, 3946–3958. doi: 10.1111/febs.15056

D'Andrea, A. D. (2018). Mechanisms of PARP inhibitor sensitivity and resistance. *DNA Repair (Amst)* 71, 172–176. doi: 10.1016/j.dnarep.2018.08.021

Dang, C. V., and Lee, W. M. (1989). Nuclear and nucleolar targeting sequences of c-erb-A, c-myb. N-myc, p53, HSP70, and HIV tat proteins. *J. Biol. Chem.* 264, 18019–18023.

David, H. (1964). [Physiologic and pathologic modifications of the submicroscopic structure. I. karyoplasm. nuclear inclusions]. *Z Mikrosk Anat Forsch.* 71, 412–456.

Dibble, C. C., and Cantley, L. C. (2015). Regulation of mTORC1 by PI3K signaling. *Trends Cell Biol.* 25, 545–555. doi: 10.1016/j.tcb.2015.06.002

Dignon, G. L., Best, R. B., and Mittal, J. (2020). Biomolecular phase separation: from molecular driving forces to macroscopic properties. *Annu. Rev. Phys. Chem.* 71, 53–75. doi: 10.1146/annurev-physchem-071819-113553

Dormann, D., Rodde, R., Edbauer, D., Bentmann, E., Fischer, I., Hruscha, A., et al. (2010). ALS-associated fused in sarcoma (FUS) mutations disrupt Transportin-mediated nuclear import. *EMBO J.* 29, 2841–2857. doi: 10.1038/emboj.2010.143

Du, M., and Chen, Z. J. (2018). DNA-induced liquid phase condensation of cGAS activates innate immune signaling. *Science* 361, 704–709. doi: 10.1126/science.aat1022

Dustin, M. L., and Choudhuri, K. (2016). Signaling and polarized communication across the T Cell immunological synapse. *Annu. Rev. Cell Dev. Biol.* 32, 303–325. doi: 10.1146/annurev-cellbio-100814-125330

Eischen, C. M. (2016). Genome stability requires p53. *Cold Spring Harb. Perspect. Med.* 6:a026096. doi: 10.1101/cshperspect.a026096

Elbaum-Garfinkle, S., Kim, Y., Szczepaniak, K., Chen, C. C., Eckmann, C. R., Myong, S., et al. (2015). The disordered P granule protein LAF-1 drives phase separation into droplets with tunable viscosity and dynamics. *Proc. Natl. Acad. Sci. U S A.* 112, 7189–7194. doi: 10.1073/pnas.1504822112

Feric, M., Vaidya, N., Harmon, T. S., Mitrea, D. M., Zhu, L., Richardson, T. M., et al. (2016). Coexisting liquid phases underlie nucleolar subcompartments. *Cell* 165, 1686–1697. doi: 10.1016/j.cell.2016.04.047

Fischer, A. H., Bardarov, S. Jr., and Jiang, Z. (2004). Molecular aspects of diagnostic nucleolar and nuclear envelope changes in prostate cancer. *J. Cell Biochem.* 91, 170–184. doi: 10.1002/jcb.10735

Fogal, V., Gostissa, M., Sandy, P., Zacchi, P., Sternsdorf, T., Jensen, K., et al. (2000). Regulation of p53 activity in nuclear bodies by a specific PML isoform. *EMBO J.* 19, 6185–6195. doi: 10.1093/emboj/19.22.6185

Fujioka, Y., Alam, J. M., Noshiro, D., Mouri, K., Ando, T., Okada, Y., et al. (2020). Phase separation organizes the site of autophagosome formation. *Nature* 578, 301–305. doi: 10.1038/s41586-020-1977-6

Fujioka, Y., Suzuki, S. W., Yamamoto, H., Kondo-Kakuta, C., Kimura, Y., Hirano, H., et al. (2014). Structural basis of starvation-induced assembly of the autophagy initiation complex. *Nat. Struct. Mol Biol.* 21, 513–521. doi: 10.1038/nsmb.2822

Galganski, L., Urbanek, M. O., and Krzyzosiak, W. J. (2017). Nuclear speckles: molecular organization, biological function and role in disease. *Nucleic Acids Res.* 45, 10350–10368. doi: 10.1093/nar/gkx759

Gao, D., Wu, J., Wu, Y. T., Du, F., Aroh, C., Yan, N., et al. (2013). Cyclic GMP-AMP synthase is an innate immune sensor of HIV and other retroviruses. *Science* 341, 903–906. doi: 10.1126/science.1240933

Gao, Y., Pei, G., Li, D., Li, R., Shao, Y., Zhang, Q. C., et al. (2019). Multivalent m(6)A motifs promote phase separation of YTHDF proteins. *Cell Res.* 29, 767–769. doi: 10.1038/s41422-019-0210-3

Geng, C., He, B., Xu, L., Barbieri, C. E., Eedunuri, V. K., Chew, S. A., et al. (2013). Prostate cancer-associated mutations in speckle-type POZ protein (SPOP) regulate steroid receptor coactivator 3 protein turnover. *Proc. Natl. Acad. Sci. U S A.* 110, 6997–7002. doi: 10.1073/pnas.1304502110

Geng, C., Kaochar, S., Li, M., Rajapakshe, K., Fiskus, W., Dong, J., et al. (2017). SPOP regulates prostate epithelial cell proliferation and promotes ubiquitination and turnover of c-MYC oncoprotein. *Oncogene* 36, 4767–4777. doi: 10.1038/onc.2017.80

Ghosh, S., Salot, S., Sengupta, S., Navalkar, A., Ghosh, D., Jacob, R., et al. (2017). p53 amyloid formation leading to its loss of function: implications in cancer pathogenesis. *Cell Death Differ.* 24, 1784–1798. doi: 10.1038/cdd.2017.105

Gold, M. R., and Reth, M. G. (2019). Antigen receptor function in the context of the nanoscale organization of the B cell membrane. *Annu. Rev. Immunol.* 37, 97–123. doi: 10.1146/annurev-immunol-042718-041704

Guo, A., Salomoni, P., Luo, J., Shih, A., Zhong, S., Gu, W., et al. (2000). The function of PML in p53-dependent apoptosis. *Nat. Cell Biol.* 2, 730–736. doi: 10.1038/35036365

Hanahan, D., and Weinberg, R. A. (2000). The hallmarks of cancer. *Cell* 100, 57–70. doi: 10.1016/s0092-8674(00)81683-9

Hanahan, D., and Weinberg, R. A. (2011). Hallmarks of cancer: the next generation. *Cell.* 144, 646–674. doi: 10.1016/j.cell.2011.02.013

Handwerger, K. E., and Gall, J. G. (2006). Subnuclear organelles: new insights into form and function. *Trends Cell Biol.* 16, 19–26. doi: 10.1016/j.tcb.2005.11.005

Hanzlikova, H., and Caldecott, K. W. (2019). Perspectives on PARPs in S Phase. *Trends Genet.* 35, 412–422. doi: 10.1016/j.tig.2019.03.008

He, L., Li, H., Wu, A., Peng, Y., Shu, G., and Yin, G. (2019). Functions of N6-methyladenosine and its role in cancer. *Mol. Cancer* 18:176. doi: 10.1186/s12943-019-1109-9

Hnisz, D., Abraham, B. J., Lee, T. I., Lau, A., Saint-Andre, V., Sigova, A. A., et al. (2013). Super-enhancers in the control of cell identity and disease. *Cell* 155, 934–947. doi: 10.1016/j.cell.2013.09.053

Hnisz, D., Schuijers, J., Lin, C. Y., Weintraub, A. S., Abraham, B. J., Lee, T. I., et al. (2015). Convergence of developmental and oncogenic signaling pathways at

transcriptional super-enhancers. *Mol. Cell* 58, 362–370. doi: 10.1016/j.molcel.2015.02.014

Hnisz, D., Shrinivas, K., Young, R. A., Chakraborty, A. K., and Sharp, P. A. (2017). A phase separation model for transcriptional control. *Cell* 169, 13–23. doi: 10.1016/j.cell.2017.02.007

Huang, W. Y., Yan, Q., Lin, W. C., Chung, J. K., Hansen, S. D., Christensen, S. M., et al. (2016). Phosphotyrosine-mediated LAT assembly on membranes drives kinetic bifurcation in recruitment dynamics of the Ras activator SOS. *Proc. Natl. Acad. Sci. U S A.* 113, 8218–8223. doi: 10.1073/pnas.1602602113

Hui, E., Cheung, J., Zhu, J., Su, X., Taylor, M. J., Wallweber, H. A., et al. (2017). T cell costimulatory receptor CD28 is a primary target for PD-1-mediated inhibition. *Science* 355, 1428–1433. doi: 10.1126/science.aaf1292

Jackson, S. P., and Bartek, J. (2009). The DNA-damage response in human biology and disease. *Nature* 461, 1071–1078. doi: 10.1038/nature08467

Jain, S., Wheeler, J. R., Walters, R. W., Agrawal, A., Barsic, A., and Parker, R. (2016). ATPase-Modulated stress granules contain a diverse proteome and substructure. *Cell* 164, 487–498. doi: 10.1016/j.cell.2015.12.038

Jiang, X., Li, X., Li, W., Bai, H., and Zhang, Z. (2019). PARP inhibitors in ovarian cancer: sensitivity prediction and resistance mechanisms. *J. Cell Mol. Med.* 23, 2303–2313. doi: 10.1111/jcmm.14133

Jones, N., Blasutig, I. M., Eremina, V., Ruston, J. M., Bladt, F., Li, H., et al. (2006). Nck adaptor proteins link nephrin to the actin cytoskeleton of kidney podocytes. *Nature* 440, 818–823. doi: 10.1038/nature04662

Jung, C. H., Ro, S. H., Cao, J., Otto, N. M., and Kim, D. H. (2010). mTOR regulation of autophagy. *FEBS Lett.* 584, 1287–1295. doi: 10.1016/j.febslet.2010.01.017

Kamagata, K., Kanbayashi, S., Honda, M., Itoh, Y., Takahashi, H., Kameda, T., et al. (2020). Liquid-like droplet formation by tumor suppressor p53 induced by multivalent electrostatic interactions between two disordered domains. *Sci. Rep.* 10:580. doi: 10.1038/s41598-020-57521-w

Kamaletdinova, T., Fanaei-Kahrani, Z., and Wang, Z. Q. (2019). The enigmatic function of PARP1: from PARylation activity to PAR readers. *Cells* 8:1625. doi: 10.3390/cells8121625

Kilic, S., Lezaja, A., Gatti, M., Bianco, E., Michelena, J., Imhof, R., et al. (2019). Phase separation of 53BP1 determines liquid-like behavior of DNA repair compartments. *EMBO J.* 38:e101379. doi: 10.15252/embj.201810 1379

Kim, D. S., Challa, S., Jones, A., and Kraus, W. L. (2020). PARPs and ADP-ribosylation in RNA biology: from RNA expression and processing to protein translation and proteostasis. *Genes Dev.* 34, 302–320. doi: 10.1101/gad.334433.119

Kim, H. J., Kim, N. C., Wang, Y. D., Scarborough, E. A., Moore, J., Diaz, Z., et al. (2013). Mutations in prion-like domains in hnRNPA2B1 and hnRNPA1 cause multisystem proteinopathy and ALS. *Nature* 495, 467–473. doi: 10.1038/nature11922

Kim, W., Kim, M., and Jho, E. H. (2013). Wnt/beta-catenin signalling: from plasma membrane to nucleus. *Biochem. J.* 450, 9–21. doi: 10.1042/BJ20121284

Kim, Y. C., and Guan, K. L. (2015). mTOR: a pharmacologic target for autophagy regulation. *J. Clin. Invest.* 125, 25–32. doi: 10.1172/JCI73939

Kumari, S., Depoil, D., Martinelli, R., Judokusumo, E., Carmona, G., Gertler, F. B., et al. (2015). Actin foci facilitate activation of the phospholipase C-gamma in primary T lymphocytes via the WASP pathway. *eLife* 4:e04953. doi: 10.7554/eLife.04953

Kwiatkowski, N., Zhang, T., Rahl, P. B., Abraham, B. J., Reddy, J., Ficarro, S. B., et al. (2014). Targeting transcription regulation in cancer with a covalent CDK7 inhibitor. *Nature* 511, 616–620. doi: 10.1038/nature13393

Lawrence, M. S., Stojanov, P., Mermel, C. H., Robinson, J. T., Garraway, L. A., Golub, T. R., et al. (2014). Discovery and saturation analysis of cancer genes across 21 tumour types. *Nature* 505, 495–501. doi: 10.1038/nature12912

Lee, A. S., Galea, C., DiGiammarino, E. L., Jun, B., Murti, G., Ribeiro, R. C., et al. (2003). Reversible amyloid formation by the p53 tetramerization domain and a cancer-associated mutant. *J. Mol. Biol.* 327, 699–709. doi: 10.1016/s0022-2836(03)00175-x

Lemos, C., Schulze, L., Weiske, J., Meyer, H., Braeuer, N., Barak, N., et al. (2020). Identification of small molecules that modulate mutant p53 condensation. *iScience* 23:101517. doi: 10.1016/j.isci.2020.101517

Li, G., Ci, W., Karmakar, S., Chen, K., Dhar, R., Fan, Z., et al. (2014). SPOP promotes tumorigenesis by acting as a key regulatory hub in kidney cancer. *Cancer Cell* 25, 455–468. doi: 10.1016/j.ccr.2014.02.007

Li, J., Kim, S. G., and Blenis, J. (2014). Rapamycin: one drug, many effects. *Cell Metab.* 19, 373–379. doi: 10.1016/j.cmet.2014.01.001

Li, P., Banjade, S., Cheng, H. C., Kim, S., Chen, B., Guo, L., et al. (2012). Phase transitions in the assembly of multivalent signalling proteins. *Nature* 483, 336–340. doi: 10.1038/nature10879

Lin, Y., Protter, D. S., Rosen, M. K., and Parker, R. (2015). Formation and maturation of phase-separated liquid droplets by RNA-Binding proteins. *Mol. Cell* 60, 208–219. doi: 10.1016/j.molcel.2015.08.018

Liu, S. Y., Feng, Y., Wu, J. J., Zou, M. L., Sun, Z. L., Li, X., et al. (2020). m(6) A facilitates YTHDF-independent phase separation. *J. Cell Mol. Med.* 24, 2070–2072. doi: 10.1111/jcmm.14847

Loven, J., Hoke, H. A., Lin, C. Y., Lau, A., Orlando, D. A., Vakoc, C. R., et al. (2013). Selective inhibition of tumor oncogenes by disruption of super-enhancers. *Cell* 153, 320–334. doi: 10.1016/j.cell.2013.03.036

Ma, S., Chen, C., Ji, X., Liu, J., Zhou, Q., Wang, G., et al. (2019). The interplay between m6A RNA methylation and noncoding RNA in cancer. *J. Hematol. Oncol.* 12:121. doi: 10.1186/s13045-019-0805-7

Mackenzie, I. R., Nicholson, A. M., Sarkar, M., Messing, J., Purice, M. D., Pottier, C., et al. (2017). TIA1 mutations in amyotrophic lateral sclerosis and frontotemporal dementia promote phase separation and alter stress granule dynamics. *Neuron* 95:e9. doi: 10.1016/j.neuron.2017.07.025

Maharana, S., Wang, J., Papadopoulos, D. K., Richter, D., Pozniakovsky, A., Poser, I., et al. (2018). RNA buffers the phase separation behavior of prion-like RNA binding proteins. *Science* 360, 918–921. doi: 10.1126/science.aar7366

Mani, R. S. (2014). The emerging role of speckle-type POZ protein (SPOP) in cancer development. *Drug Discov Today* 19, 1498–1502. doi: 10.1016/j.drudis.2014.07.009

Mansour, M. R., Abraham, B. J., Anders, L., Berezovskaya, A., Gutierrez, A., Durbin, A. D., et al. (2014). Oncogene regulation. an oncogenic super-enhancer formed through somatic mutation of a noncoding intergenic element. *Science* 346, 1373–1377. doi: 10.1126/science.1259037

Mantovani, F., Collavin, L., and Del Sal, G. (2019). Mutant p53 as a guardian of the cancer cell. *Cell Death Differ.* 26, 199–212. doi: 10.1038/s41418-018-0246-9

Mao, Y. S., Sunwoo, H., Zhang, B., and Spector, D. L. (2011b). Direct visualization of the co-transcriptional assembly of a nuclear body by noncoding RNAs. *Nat. Cell Biol.* 13, 95–101. doi: 10.1038/ncb2140

Mao, Y. S., Zhang, B., and Spector, D. L. (2011a). Biogenesis and function of nuclear bodies. *Trends Genet.* 27, 295–306. doi: 10.1016/j.tig.2011.05.006

Marzahn, M. R., Marada, S., Lee, J., Nourse, A., Kenrick, S., Zhao, H., et al. (2016). Higher-order oligomerization promotes localization of SPOP to liquid nuclear speckles. *EMBO J.* 35, 1254–1275. doi: 10.15252/embj.201593169

Melo Dos, Santos, N., de Oliveira, G. A. P., Ramos Rocha, M., Pedrote, M. M., Diniz, et al. (2019). Loss of the p53 transactivation domain results in high amyloid aggregation of the Delta40p53 isoform in endometrial carcinoma cells. *J. Biol. Chem.* 294, 9430–9439. doi: 10.1074/jbc.RA119.007566

Milovanovic, D., Wu, Y., Bian, X., and De Camilli, P. (2018). A liquid phase of synapsin and lipid vesicles. *Science* 361, 604–607. doi: 10.1126/science.aat5671

Mirza-Aghazadeh-Attari, M., Mohammadzadeh, A., Yousefi, B., Mihanfar, A., Karimian, A., and Majidinia, M. (2019). 53BP1: a key player of DNA damage response with critical functions in cancer. *DNA Repair (Amst)* 73, 110–119. doi: 10.1016/j.dnarep.2018.11.008

Misteli, T., and Soutoglou, E. (2009). The emerging role of nuclear architecture in DNA repair and genome maintenance. *Nat. Rev. Mol. Cell Biol.* 10, 243–254. doi: 10.1038/nrm2651

Molliex, A., Temirov, J., Lee, J., Coughlin, M., Kanagaraj, A. P., Kim, H. J., et al. (2015). Phase separation by low complexity domains promotes stress granule assembly and drives pathological fibrillization. *Cell* 163, 123–133. doi: 10.1016/j.cell.2015.09.015

Monahan, Z., Ryan, V. H., Janke, A. M., Burke, K. A., Rhoads, S. N., Zerze, G. H., et al. (2017). Phosphorylation of the FUS low-complexity domain disrupts phase separation, aggregation, and toxicity. *EMBO J.* 36, 2951–2967. doi: 10.15252/embj.201696394

Mugler, C. F., Hondele, M., Heinrich, S., Sachdev, R., Vallotton, P., Koek, A. Y., et al. (2016). ATPase activity of the DEAD-box protein Dhh1 controls processing body formation. *eLife* 5:e18746. doi: 10.7554/eLife.18746

Muller, P. A., and Vousden, K. H. (2013). p53 mutations in cancer. *Nat. Cell Biol.* 15, 2–8. doi: 10.1038/ncb2641

Murugan, A. K. (2019). mTOR: role in cancer, metastasis and drug resistance. *Semin. Cancer Biol.* 59, 92–111. doi: 10.1016/j.semcancer.2019.07.003

Nagai, Y., Kojima, T., Muro, Y., Hachiya, T., Nishizawa, Y., Wakabayashi, T., et al. (1997). Identification of a novel nuclear speckle-type protein. SPOP. *FEBS Lett.* 418, 23–26. doi: 10.1016/s0014-5793(97)01340-9

Nott, T. J., Petsalaki, E., Farber, P., Jervis, D., Fussner, E., Plochowietz, A., et al. (2015). Phase transition of a disordered nuage protein generates environmentally responsive membraneless organelles. *Mol. Cell* 57, 936–947. doi: 10.1016/j.molcel.2015.01.013

Pahi, Z. G., Borsos, B. N., Pantazi, V., Ujfaludi, Z., and Pankotai, T. (2020). PARylation during transcription: insights into the fine-tuning mechanism and regulation. *Cancers (Basel)* 12:183. doi: 10.3390/cancers12010183

Panier, S., and Boulton, S. J. (2014). Double-strand break repair: 53BP1 comes into focus. *Nat. Rev. Mol. Cell Biol.* 15, 7–18. doi: 10.1038/nrm3719

Patel, A., Lee, H. O., Jawerth, L., Maharana, S., Jahnel, M., Hein, M. Y., et al. (2015). A liquid-to-solid phase transition of the ALS protein FUS accelerated by disease mutation. *Cell* 162, 1066–1077. doi: 10.1016/j.cell.2015.07.047

Patel, A., Malinovska, L., Saha, S., Wang, J., Alberti, S., Krishnan, Y., et al. (2017). ATP as a biological hydrotrope. *Science* 356, 753–756. doi: 10.1126/science.aaf6846

Pederson, T. (2011). The nucleolus. *Cold Spring Harb. Perspect. Biol.* 3:a000638. doi: 10.1101/cshperspect.a000638

Pedrote, M. M., de Oliveira, G. A. P., Felix, A. L., Mota, M. F., Marques, M. A., Soares, I. N., et al. (2018). Aggregation-primed molten globule conformers of the p53 core domain provide potential tools for studying p53C aggregation in cancer. *J. Biol. Chem.* 293, 11374–11387. doi: 10.1074/jbc.RA118.003285

Pedrote, M. M., Motta, M. F., Ferretti, G. D. S., Norberto, D. R., Spohr, T., Lima, F. R. S., et al. (2020). Oncogenic gain of function in glioblastoma is linked to mutant p53 amyloid oligomers. *iScience* 23:100820. doi: 10.1016/j.isci.2020.100820

Pessina, F., Giavazzi, F., Yin, Y., Gioia, U., Vitelli, V., Galbiati, A., et al. (2019). Functional transcription promoters at DNA double-strand breaks mediate RNA-driven phase separation of damage-response factors. *Nat. Cell Biol.* 21, 1286–1299. doi: 10.1038/s41556-019-0392-4

Phair, R. D., and Misteli, T. (2000). High mobility of proteins in the mammalian cell nucleus. *Nature* 404, 604–609. doi: 10.1038/35007077

Proudhon, C., Snetkova, V., Raviram, R., Lobry, C., Badri, S., Jiang, T., et al. (2016). Active and inactive enhancers cooperate to exert localized and long-range control of gene regulation. *Cell Rep.* 15, 2159–2169. doi: 10.1016/j.celrep.2016.04.087

Ray Chaudhuri, A., and Nussenzweig, A. (2017). The multifaceted roles of PARP1 in DNA repair and chromatin remodelling. *Nat. Rev. Mol. Cell Biol.* 18, 610–621. doi: 10.1038/nrm.2017.53

Riback, J. A., Katanski, C. D., Kear-Scott, J. L., Pilipenko, E. V., Rojek, A. E., Sosnick, T. R., et al. (2017). Stress-Triggered phase separation is an adaptive. *Evol. Tuned Response. Cell* 168:e19. doi: 10.1016/j.cell.2017.02.027

Ries, R. J., Zaccara, S., Klein, P., Olarerin-George, A., Namkoong, S., Pickering, B. F., et al. (2019). m(6)A enhances the phase separation potential of mRNA. *Nature* 571, 424–428. doi: 10.1038/s41586-019-1374-1

Rohatgi, R., Nollau, P., Ho, H. Y., Kirschner, M. W., and Mayer, B. J. (2001). Nck and phosphatidylinositol 4,5-bisphosphate synergistically activate actin polymerization through the N-WASP-Arp2/3 pathway. *J. Biol. Chem.* 276, 26448–26452. doi: 10.1074/jbc.M103856200

Rouleau, M., Patel, A., Hendzel, M. J., Kaufmann, S. H., and Poirier, G. G. (2010). PARP inhibition: PARP1 and beyond. *Nat. Rev. Cancer* 10, 293–301. doi: 10.1038/nrc2812

Ryan, V. H., Dignon, G. L., Zerze, G. H., Chabata, C. V., Silva, R., Conicella, A. E., et al. (2018). Mechanistic view of hnRNPA2 low-complexity domain structure. interactions, and phase separation altered by mutation and arginine methylation. *Mol. Cell* 69:e7. doi: 10.1016/j.molcel.2017.12.022

Sabari, B. R., Dall'Agnese, A., Boija, A., Klein, I. A., Coffey, E. L., Shrinivas, K., et al. (2018). Coactivator condensation at super-enhancers links phase separation and gene control. *Science* 361:eaar3958. doi: 10.1126/science.aar3958

Saha, S., Weber, C. A., Nousch, M., Adame-Arana, O., Hoege, C., Hein, M. Y., et al. (2016). Polar positioning of phase-separated liquid compartments in cells regulated by an mRNA competition mechanism. *Cell* 166:e16. doi: 10.1016/j.cell.2016.08.006

Samelson, L. E. (2002). Signal transduction mediated by the T cell antigen receptor: the role of adapter proteins. *Annu. Rev. Immunol.* 20, 371–394. doi: 10.1146/annurev.immunol.20.092601.111357

Sanchez-Martin, P., Saito, T., and Komatsu, M. (2019). p62/SQSTM1: 'Jack of all trades' in health and cancer. *FEBS J.* 286, 8–23. doi: 10.1111/febs.14712

Saxton, R. A., and Sabatini, D. M. (2017). mTOR Signaling in Growth. *Metab. Dis. Cell* 168, 960–976. doi: 10.1016/j.cell.2017.02.004

Schochter, F., Werner, K., Kostler, C., Faul, A., Tzschaschel, M., Alberter, B., et al. (2020). 53BP1 accumulation in circulating tumor cells identifies chemotherapy-responsive metastatic breast cancer patients. *Cancers (Basel)* 12:930. doi: 10.3390/cancers12040930

Scholz, B. A., Sumida, N., de Lima, C. D. M., Chachoua, I., Martino, M., Tzelepis, I., et al. (2019). WNT signaling and AHCTF1 promote oncogenic MYC expression through super-enhancer-mediated gene gating. *Nat. Genet.* 51, 1723–1731. doi: 10.1038/s41588-019-0535-3

Schumacher, T. N. (2002). T-cell-receptor gene therapy. *Nat. Rev. Immunol.* 2, 512–519. doi: 10.1038/nri841

Schwarz-Romond, T., Merrifield, C., Nichols, B. J., and Bienz, M. (2005). The Wnt signalling effector dishevelled forms dynamic protein assemblies rather than stable associations with cytoplasmic vesicles. *J. Cell Sci.* 118, 5269–5277. doi: 10.1242/jcs.02646

Sengupta, S., and George, R. E. (2017). Super-Enhancer-Driven transcriptional dependencies in cancer. *Trends Cancer* 3, 269–281. doi: 10.1016/j.trecan.2017.03.006

Shav-Tal, Y., Blechman, J., Darzacq, X., Montagna, C., Dye, B. T., Patton, J. G., et al. (2005). Dynamic sorting of nuclear components into distinct nucleolar caps during transcriptional inhibition. *Mol. Biol Cell.* 16, 2395–2413. doi: 10.1091/mbc.e04-11-0992

Shevtsov, S. P., and Dundr, M. (2011). Nucleation of nuclear bodies by RNA. *Nat. Cell Biol.* 13, 167–173. doi: 10.1038/ncb2157

Shin, Y., and Brangwynne, C. P. (2017). Liquid phase condensation in cell physiology and disease. *Science* 357:eaaf4382. doi: 10.1126/science.aaf4382

Silva, J. L., De Moura Gallo, C. V., Costa, D. C., and Rangel, L. P. (2014). Prion-like aggregation of mutant p53 in cancer. *Trends Biochem. Sci.* 39, 260–267. doi: 10.1016/j.tibs.2014.04.001

Slade, D. (2020). PARP and PARG inhibitors in cancer treatment. *Genes Dev.* 34, 360–394. doi: 10.1101/gad.334516.119

Snaar, S., Wiesmeijer, K., Jochemsen, A. G., Tanke, H. J., and Dirks, R. W. (2000). Mutational analysis of fibrillarin and its mobility in living human cells. *J. Cell Biol.* 151, 653–662. doi: 10.1083/jcb.151.3.653

Su, X., Ditlev, J. A., Hui, E., Xing, W., Banjade, S., Okrut, J., et al. (2016). Phase separation of signaling molecules promotes T cell receptor signal transduction. *Science* 352, 595–599. doi: 10.1126/science.aad9964

Sun, D., Wu, R., Zheng, J., Li, P., and Yu, L. (2018). Polyubiquitin chain-induced p62 phase separation drives autophagic cargo segregation. *Cell Res.* 28, 405–415. doi: 10.1038/s41422-018-0017-7

Sun, L., Wu, J., Du, F., Chen, X., and Chen, Z. J. (2013). Cyclic GMP-AMP synthase is a cytosolic DNA sensor that activates the type I interferon pathway. *Science* 339, 786–791. doi: 10.1126/science.1232458

Uversky, V. N. (2017). Intrinsically disordered proteins in overcrowded milieu: membrane-less organelles, phase separation, and intrinsic disorder. *Curr. Opin. Struct. Biol.* 44, 18–30. doi: 10.1016/j.sbi.2016.10.015

Wagner, R., and Barry, M. (1836). Some remarks and inquiries concerning the germinal vesicle (Vesicula Germinativa.). *Edinb. Med. Surg. J.* 45, 423–426.

Wang, J., Choi, J. M., Holehouse, A. S., Lee, H. O., Zhang, X., Jahnel, M., et al. (2018). A molecular grammar governing the driving forces for phase separation of prion-like RNA binding proteins. *Cell* 174:e16. doi: 10.1016/j.cell.2018.06.006

Wang, J., Wang, L., Diao, J., Shi, Y. G., Shi, Y., Ma, H., et al. (2020). Binding to m(6)A RNA promotes YTHDF2-mediated phase separation. *Protein Cell.* 11, 304–307. doi: 10.1007/s13238-019-00660-2

Wang, Z., Song, Y., Ye, M., Dai, X., Zhu, X., and Wei, W. (2020). The diverse roles of SPOP in prostate cancer and kidney cancer. *Nat. Rev. Urol.* 17, 339–350. doi: 10.1038/s41585-020-0314-z

Wegmann, S., Eftekharzadeh, B., Tepper, K., Zoltowska, K. M., Bennett, R. E., Dujardin, S., et al. (2018). Tau protein liquid-liquid phase separation

can initiate tau aggregation. *EMBO J.* 37:e98049. doi: 10.15252/embj.201798049

Wei, S. C., Duffy, C. R., and Allison, J. P. (2018). Fundamental mechanisms of immune checkpoint blockade therapy. *Cancer Discov.* 8, 1069–1086. doi: 10.1158/2159-8290.CD-18-0367

Whyte, W. A., Orlando, D. A., Hnisz, D., Abraham, B. J., Lin, C. Y., Kagey, M. H., et al. (2013). Master transcription factors and mediator establish super-enhancers at key cell identity genes. *Cell* 153, 307–319. doi: 10.1016/j.cell.2013.03.035

Wsierska-Gadek, J., and Horky, M. (2003). How the nucleolar sequestration of p53 protein or its interplayers contributes to its (re)-activation. *Ann. N Y Acad. Sci.* 1010, 266–272. doi: 10.1196/annals.1299.046

Yamamoto, H., Fujioka, Y., Suzuki, S. W., Noshiro, D., Suzuki, H., Kondo-Kakuta, C., et al. (2016). The intrinsically disordered protein Atg13 mediates supramolecular assembly of autophagy initiation complexes. *Dev. Cell* 38, 86–99. doi: 10.1016/j.devcel.2016.06.015

Yanagawa, S., van Leeuwen, F., Wodarz, A., Klingensmith, J., and Nusse, R. (1995). The dishevelled protein is modified by wingless signaling in Drosophila. *Genes Dev.* 9, 1087–1097. doi: 10.1101/gad.9.9.1087

Yang, D. S., Saeedi, A., Davtyan, A., Fathi, M., Safari, M. S., Klindziuk, A., et al. (2020). Mesoscopic liquid clusters represent a distinct condensate of mutant p53. *BioRxiv [Preprint]* doi: 10.1101/2020.02.04.931980

Yang, J., Jing, L., Liu, C. J., Bai, W. W., and Zhu, S. C. (2019). 53BP1 regulates cell cycle arrest in esophageal cancer model. *Eur. Rev. Med. Pharmacol. Sci.* 23, 604–612. doi: 10.26355/eurrev_201901_16874

Youn, J. Y., Dyakov, B. J. A., Zhang, J., Knight, J. D. R., Vernon, R. M., Forman-Kay, J. D., et al. (2019). Properties of stress granule and p-body proteomes. *Mol. Cell.* 76, 286–294. doi: 10.1016/j.molcel.2019.09.014

Zaffagnini, G., Savova, A., Danieli, A., Romanov, J., Tremel, S., Ebner, M., et al. (2018). p62 filaments capture and present ubiquitinated cargos for autophagy. *EMBO J.* 37:e98308. doi: 10.15252/embj.201798308

Zhang, H., Elbaum-Garfinkle, S., Langdon, E. M., Taylor, N., Occhipinti, P., Bridges, A. A., et al. (2015). RNA controls PolyQ protein phase transitions. *Mol. Cell* 60, 220–230. doi: 10.1016/j.molcel.2015.09.017

Zhang, Q., Shi, Q., Chen, Y., Yue, T., Li, S., Wang, B., et al. (2009). Multiple Ser/Thr-rich degrons mediate the degradation of Ci/Gli by the Cul3-HIB/SPOP E3 ubiquitin ligase. *Proc. Natl. Acad. Sci. U S A.* 106, 21191–21196. doi: 10.1073/pnas.0912008106

Zhang, Q., Zhang, L., Wang, B., Ou, C. Y., Chien, C. T., and Jiang, J. (2006). A hedgehog-induced BTB protein modulates hedgehog signaling by degrading Ci/Gli transcription factor. *Dev. Cell* 10, 719–729. doi: 10.1016/j.devcel.2006.05.004

Zhang, W., Sloan-Lancaster, J., Kitchen, J., Trible, R. P., and Samelson, L. E. (1998). LAT: the ZAP-70 tyrosine kinase substrate that links T cell receptor to cellular activation. *Cell* 92, 83–92. doi: 10.1016/s0092-8674(00)80901-0

Zhang, Y., Xu, L., Chang, Y., Li, Y., Butler, W., Jin, E., et al. (2020). Therapeutic potential of ReACp53 targeting mutant p53 protein in CRPC. *Prostate Cancer Prostatic Dis.* 23, 160–171. doi: 10.1038/s41391-019-0172-z

Zhu, H., Wei, M., Xu, J., Hua, J., Liang, C., Meng, Q., et al. (2020). PARP inhibitors in pancreatic cancer: molecular mechanisms and clinical applications. *Mol. Cancer* 19:49. doi: 10.1186/s12943-020-01167-9

Conflict of Interest: The authors declare that the research was conducted in the absence of any commercial or financial relationships that could be construed as a potential conflict of interest.

frontiers in Cell and Developmental Biology

ORIGINAL RESEARCH
published: 23 June 2021
doi: 10.3389/fcell.2021.643525

Andrographolide Suppresses the Growth and Metastasis of Luminal-Like Breast Cancer by Inhibiting the NF-κB/miR-21-5p/PDCD4 Signaling Pathway

Junchen Li[1†], Lixun Huang[1†], Zinan He[1], Minggui Chen[1], Yi Ding[1,2], Yuying Yao[1], Youfa Duan[1], Zixuan Li[1], Cuiling Qi[1,2], Lingyun Zheng[1,2], Jiangchao Li[1,2], Rongxin Zhang[1,2], Xiaoming Li[3], Jianwei Dai[4,5,6], Lijing Wang[1,2]* and Qian-Qian Zhang[1,2]**

[1] School of Life Sciences and Biopharmaceutics, Guangdong Pharmaceutical University, Guangzhou, China, [2] Guangdong Province Key Laboratory for Biotechnology Drug Candidates, Guangdong Pharmaceutical University, Guangzhou, China, [3] Department of Pathology, People's Hospital of Baoan District, Affiliated Baoan Hospital of Shenzhen, Southern Medical University, The Second Affiliated Hospital of Shenzhen University, Shenzhen, China, [4] Guangzhou Medical University-Guangzhou Institute of Biomedicine and Health (GMU-GIBH) Joint School of Life Sciences, Guangzhou Medical University, Guangzhou, China, [5] Key Laboratory for Major Obstetric Diseases of Guangdong Province, Key Laboratory of Reproduction and Genetics of Guangdong Higher Education Institutes, The Third Affiliated Hospital of Guangzhou Medical University, Guangzhou, China, [6] The State Key Lab of Respiratory Disease, Guangzhou Institute of Respiratory Disease, The First Affiliated Hospital, Guangzhou Medical University, Guangzhou, China

Tumor growth and metastasis are responsible for breast cancer-related mortality. Andrographolide (Andro) is a traditional anti-inflammatory drug used in the clinic that inhibits NF-κB activation. Recently, Andro has been found in the treatment of various cancers. Andro inhibits breast cell proliferation and invasion and induces apoptosis *via* activating various signaling pathways. Therefore, the underlying mechanisms with regard to the antitumor effects of Andro still need to be further confirmed. Herein, a MMTV-PyMT spontaneous luminal-like breast cancer lung metastatic transgenic tumor model was employed to estimate the antitumor effects of Andro on breast cancer *in vivo*. Andro significantly inhibited tumor growth and metastasis in MMTV-PyMT mice and suppressed the cell proliferation, migration, and invasion of MCF-7 breast cancer cells *in vitro*. Meanwhile, Andro significantly inhibited the expression of NF-κB, and the downregulated NF-κB reduced miR-21-5p expression. In addition, miR-21-5p dramatically inhibited the target gene expression of programmed cell death protein 4 (PDCD4). In the current study, we demonstrated the potential anticancer effects of Andro on luminal-like breast cancer and indicated that Andro inhibits the expression of miR-21-5p and further promotes PDCD4 *via* NF-κB suppression. Therefore, Andro could be an antitumor agent for the treatment of luminal-like breast cancer in the clinic.

Keywords: luminal-like breast cancer, andrographolide, growth, metastasis, NF-κB/miR-21-5p/PDCD4 signaling pathway

OPEN ACCESS

Edited by:
Lorenzo Gerratana, University of Udine, Italy

Reviewed by:
An Qin, Shanghai Ninth People's Hospital, China
Devesh Tewari, Lovely Professional University, India

***Correspondence:**
Qian-Qian Zhang
vinny223@126.com
Lijing Wang
wanglijing62@163.com
Jianwei Dai
daijw@gzhmu.edu.cn

[†] These authors have contributed equally to this work

Specialty section:
This article was submitted to Molecular and Cellular Oncology, a section of the journal Frontiers in Cell and Developmental Biology

Received: *18 December 2020*
Accepted: *14 May 2021*
Published: *23 June 2021*

Citation:
Li J, Huang L, He Z, Chen M, Ding Y, Yao Y, Duan Y, Li Z, Qi C, Zheng L, Li J, Zhang R, Li X, Dai J, Wang L and Zhang Q-Q (2021) Andrographolide Suppresses the Growth and Metastasis of Luminal-Like Breast Cancer by Inhibiting the NF-κB/miR-21-5p/PDCD4 Signaling Pathway. Front. Cell Dev. Biol. 9:643525. doi: 10.3389/fcell.2021.643525

INTRODUCTION

Breast cancer is the most common malignant tumor among women with a rising incidence rate. It is one of the important causes of female deaths worldwide (Siegel et al., 2020). According to the gene expression profile, breast cancer can be divided into five subtypes: luminal-like (A and B subtypes), HER-2^{+}, normal breast-like, and basal-like carcinomas (Sorlie et al., 2001, 2003). Luminal-like breast cancer accounts for more than 75% of the total incidence of breast cancer, and early luminal-like breast cancer is very sensitive to hormone endocrine therapy (Rosati et al., 2020). Luminal A and B breast cancers accounted for 37.1 and 8.6%, respectively, of patients with distant metastasis (Ihemelandu et al., 2008). Therefore, lumi-like breast cancer has a relatively high mortality rate due to distal metastasis. Monoclonal antibodies, tyrosine kinase inhibitors, and immunotherapy are commonly used to treat breast cancer in the clinic (Goldhirsch et al., 2011). However, there is no effective target therapy to treat metastatic luminal-like breast cancer. A recent study indicated that nuclear factor-kappa B (NF-κB) can be considered a valid drug target in cancers (Labbozzetta et al., 2020). The expression of NF-κB is highly correlated with the occurrence, late development, and metastasis of breast cancer (Yamamoto et al., 2013). Inhibition of NF-κB effectively prevents the growth and invasion of tumor cells (Liu et al., 2019). Therefore, whether NF-κB could be an effective therapeutic target in metastatic luminal-like breast cancer still needs to be further investigated.

Multiple cancer-related signaling pathways are involved in tumorigenesis and considered as new targets for breast cancer therapy (Li et al., 2017; Tewari et al., 2019, 2021). In recent years, traditional Chinese medicine has attracted increasing attention for anticancer therapy due to its potential to modulate multiple cancer-related signaling pathways (Yan et al., 2017). Andrographolide (Andro) is a diterpene lactone compound extracted from *Andrographis paniculata* and acts as an NF-κB inhibitor (Xia et al., 2004). *A. paniculata* is a classic Chinese herb with anti-inflammatory properties. It was demonstrated that Andro possesses anticancer activity by inducing tumor cell apoptosis, inhibiting tumor angiogenesis, affecting tumor cell cycle, and regulating autoimmune mechanisms (Zhang et al., 2014a,b). Recently *in vitro* studies indicated that Andro inhibits 12-*O*-tetradecanoylphorbol-13-acetate (TPA)-induced MCF-7 luminal-like breast cancer cell migration and invasion (Chao et al., 2013). Andro inactivates matrix metalloproteinase-9 (MMP9) *via* inhibition of the extracellular signal-regulated kinase (ERK) 1/2 and PI3K/Akt signaling that further suppresses the DNA binding activity of activator protein-1 (AP-1) and NF-κB (Chao et al., 2013). Meanwhile, Andro inhibits MDA-MB-231 triple-negative breast cancer cell proliferation and metastasis by suppressing MMP9 and induces apoptosis through arresting cell cycle progression by inducing changes in the Bax/Bcl-2 ratio (Zhai et al., 2015; Banerjee et al., 2016). However, *in vivo* research on the anti-breast cancer effects of Andro and the underlying mechanisms still needs to be further clarified.

MicroRNAs (miRNAs) have emerged as central posttranscriptional regulators of gene expression and further regulate tumor progression. It has been reported that miR-21-5p overexpression promotes tumor growth and metastasis in breast cancer (Zhang et al., 2014c; Petrovic, 2016). The tumor suppressor programmed cell death 4 (PDCD4) is downregulated in breast cancer and acts as a functional target of miR-21-5p in breast cancer cells (Chen et al., 2015; Tao et al., 2019). Furthermore, miR-21-5p/PDCD4 signaling has been reported to be involved in paclitaxel-resistant breast cancer cells (Tao et al., 2019). NF-κB binds to the promoter region of miR-21-5p and activates the transcription of miR-21-5p, further enhancing the survival of MDA-MB-231 cells (Polytarchou et al., 2011). In our previous report, we demonstrated that Andro inhibits miR-21-5p/TIMP3 signaling to suppress angiogenesis (Dai et al., 2017). However, whether the interplay between miR-21-5p and PDCD4 is involved in the Andro-induced inhibition of breast cancer growth and metastasis of luminal-like breast cancer remains undefined.

Here, we demonstrated that NF-κB promotes miR-21-5p expression and then further inhibits PDCD4 expression in luminal-like breast cancer. NF-κB/miR-21-5p/PDCD4 signaling promotes the tumor growth and metastasis of luminal-like breast cancer. Andro inhibits the tumor growth and metastasis of luminal-like breast cancer *in vitro* and *in vivo* mainly by targeting NF-κB/miR-21-5p/PDCD4 signaling.

MATERIALS AND METHODS

Reagents and Antibodies

Andro (365645) and ammonium pyrrolidinedithiocarbamate (APDC; NF-κB inhibitor, P8765) were obtained from Sigma-Aldrich (St. Louis, MO, United States) and were dissolved in dimethyl sulfoxide (DMSO). Cell Counting Kit-8 (CCK-8) was purchased from Beyotime (Shanghai, China). Rabbit anti-Ki67 (ab15580) was purchased from Abcam (Cambridge, MA, United States), rabbit anti-GAPDH (2118) was purchased from Cell Signaling Technology, Inc. (Danvers, MA, United States), rabbit anti-PDCD4 (BM5208) and rabbit anti-EGN (endoglin, BA2227) were both from Boster (Wuhan, China), and rabbit anti-NF-κB p65 (abs131170) and rabbit anti-phospho-NF-κB p65 (Ser536, abs130624) were purchased from Absin (Shanghai, China). All the miRNA mimics and inhibitors and the negative control (NC) RNAs were purchased from RiboBio Co., Ltd. (Guangzhou, China). All the primers were synthesized by Sangon Biotech Co., Ltd. (Shanghai, China).

Patients and Tissue Samples

A total of 12 cases of tumor tissues of female patients with luminal-like breast cancer, with a median age of 51.8 years (ranging from 40 to 66 years), and their matched non-tumorous breast tissues, as well as the corresponding clinical data, were collected from the Department of Pathology, People's Hospital of Baoan District. Pathologic diagnosis was performed by two independent pathologists based on the guidelines of the International Union Against Cancer (UICC). The study has been approved by the Institutional Ethics Committee of People's Hospital of Baoan District of Shenzhen (BYL20200902).

Animal Manipulations and Treatment

MMTV-PyMT mice (stock no. 002374) were purchased from the Jackson Laboratory (Bar Harbor, ME, United States) and housed in the Undergraduate Laboratory Animal Center of Guangdong Pharmaceutical University in an environmentally controlled condition with a 12:12-h light/dark cycle, temperature of 22 ± 2°C, and humidity of 60 ± 5%. All animal experiments were conducted according to the Guide for the Care and Use of Laboratory Animals by the National Academy of Sciences (NIH publication no. 80-23, revised 1996). The protocols were approved by the Undergraduate Laboratory Animal Center ethics committee of Guangdong Pharmaceutical University (gdpulac2020014). All possible efforts were made to minimize animal suffering.

MMTV-PyMT mice (9 weeks old, females) were randomly divided into two groups with intraperitoneal injection of Andro (5 μg/g) or DMSO twice a week for 4 weeks, in accordance with previous reports (Handa and Sharma, 1990; Zhang et al., 2014a,b; Peng et al., 2018). The length (L) and width (W) of tumors were measured with calipers, and the tumor volumes (V) were measured twice a week and calculated as follows: $V = (L \times W^2) \times 0.5236$. Mice were sacrificed after treatment, the tumors were peeled off and weighted, and the lung tissues were removed and fixed in Bouin's solution.

Cells

MCF-7 cells were kindly provided by the Stem Cell Bank, Chinese Academy of Sciences (Shanghai, China), and maintained in a humidified incubator with 5% CO_2 at 37°C. All cells were cultured in minimum essential medium (MEM; Invitrogen, Carlsbad, CA, United States) supplemented with 10% fetal bovine serum (FBS; Gibco, Waltham, MA, United States), 1% glutamax (Invitrogen), 1% non-essential amino acids (NECC; Invitrogen), 0.01 mg/ml human recombinant insulin (91077C, Sigma-Aldrich), 100 U/ml penicillin, and 100 μg/ml streptomycin (Gibco).

Cell Viability Assay

MCF-7 cells (1.5×10^3 cells/well) were seeded into 96-well plates and treated with the indicated concentrations of Andro and DMSO. Cell viability and proliferation were detected at the indicated time after treatment with Andro or DMSO using the CCK-8 reagent (Beyotime Institute Biotechnology, Shanghai, China). The CCK-8 reagent (10 μl) was added to each well and further incubated at 37°C for 3 h, and then the solution absorption was read at 450 nm by a spectrophotometer.

Cell Proliferation Assay

The colony formation assay was used to assess the cell proliferation ability. MCF-7 cells (3,000 cells/well) were seeded into six-well plates and then Andro (70 μM) or DMSO was added into the wells 24 h later. The colonies were fixed in 4% paraformaldehyde, stained with 0.1% crystal violet solution after 7 days, and the number of colonies was counted. The data shown were representative of three independent experiments, in which each treatment was assayed in duplicate.

Wound Healing Assay

MCF-7 cells were seeded into 12-well plates at a density of 5×10^5 cells per well. After 12 h, a scratch was created with a pipette tip in the center of the well and washed with phosphate buffer saline (PBS) to remove the scraped cells. Then, the cells were treated with Andro (70 μM) or DMSO and photographed at 0 and 12 h posttreatment. The migrated distances of cells from the wound edge since 0 h were measured.

Cell Migration and Invasion Assay

Transwell chambers (8 μM pores; Costar, Cambridge, MA, United States) uncoated or coated with 50 μl Matrigel (1:20 dilution with serum-free MEM; BD Biosciences, San Jose, CA, United States) were used to detect cell migration and invasion ability. The uncoated or coated chambers were placed in a 24-well plate at 37°C for 7 h. Then, the chambers were removed from the well of the 24-well plate with 600 μl MEM with 10% serum and the MCF-7 cells (2×10^5 cells) mixed with Andro (70 μM) or DMSO were added into the upper chambers. The membranes of the chambers were fixed with methanol and stained with 1% crystal violet after 20 h incubation, and then the cells on the upper membranes of the chambers were wiped. The membranes were photographed and the number of cells that migrated and invaded through the membranes was counted.

Real-Time Quantitative PCR Assay

Total RNAs from MCF-7 cells and the tumor tissue treated with Andro or DMSO were extracted using TRIzol reagent (Invitrogen). Briefly, total RNA (1,000 ng) was used for reverse transcription using a PrimeScript™ RT Reagent Kit (TaKaRa, Shiga, Japan). Then, real-time quantitative PCR was performed using the SYBR® Premix Ex Taq™ II (Tli RNaseH Plus) PCR Kit (TaKaRa, Japan) on a LightCycler® 96 PCR machine (Roche Diagnostics, Basel, Switzerland). All the experiments were carried out according to the manufacturers' instructions. All samples were tested in triplicate and repeated three times each. All the primers that were used for reverse transcription and PCR are presented in **Supplementary Table 1**.

Histological, Immunohistochemical, and Immunoblotting Analysis

The fixed lung tissues of Andro- or DMSO-treated MMTV-PyMT mice were embedded in paraffin, cut into 3-μM sections, and stained with hematoxylin and eosin (H&E) for histological analyses or incubated with ki67 antibodies for immunohistochemical (IHC) assay. The total proteins from the tumor tissues and MCF-7 cells were harvested by RIPA buffer and separated by 10% sodium dodecyl sulfate–polyacrylamide gel electrophoresis (SDS-PAGE). Then, the proteins were transferred onto polyvinylidene fluoride (PVDF) membranes and blocked with 10% non-fat milk in Tris-buffered saline containing 0.2% Tween 20 (TBST) for 1 h at room temperature. The blocked membranes were incubated with relevant primary antibodies and horseradish peroxidase (HRP)-conjugated secondary antibody. The bands

were visualized with an enhanced chemiluminescence (ECL) reagent. GAPDH served as a loading control.

Statistical Analysis

All data are represented as the mean ± standard deviation (SD). Student's two-sided *t*-test was used to analyze statistical differences between the two groups. The protein expression levels in the IHC slices were determined using IPP software (Media Cybernetics, Inc., Rockville, MD, United States) and those in the immunoblotting bands were analyzed using Quantity One software (Bio-Rad Laboratories, Inc., Hercules, CA, United States). The protein band intensities were quantified to those of GAPDH. $P < 0.05$ was considered the statistically significant difference between the two groups.

RESULTS

NF-κB Is Highly Expressed in Luminal-Like Breast Cancer Tissues

Previous reports indicated that Andro inhibits NF-κB activation in inflammation and cancers (Xia et al., 2004). Therefore,

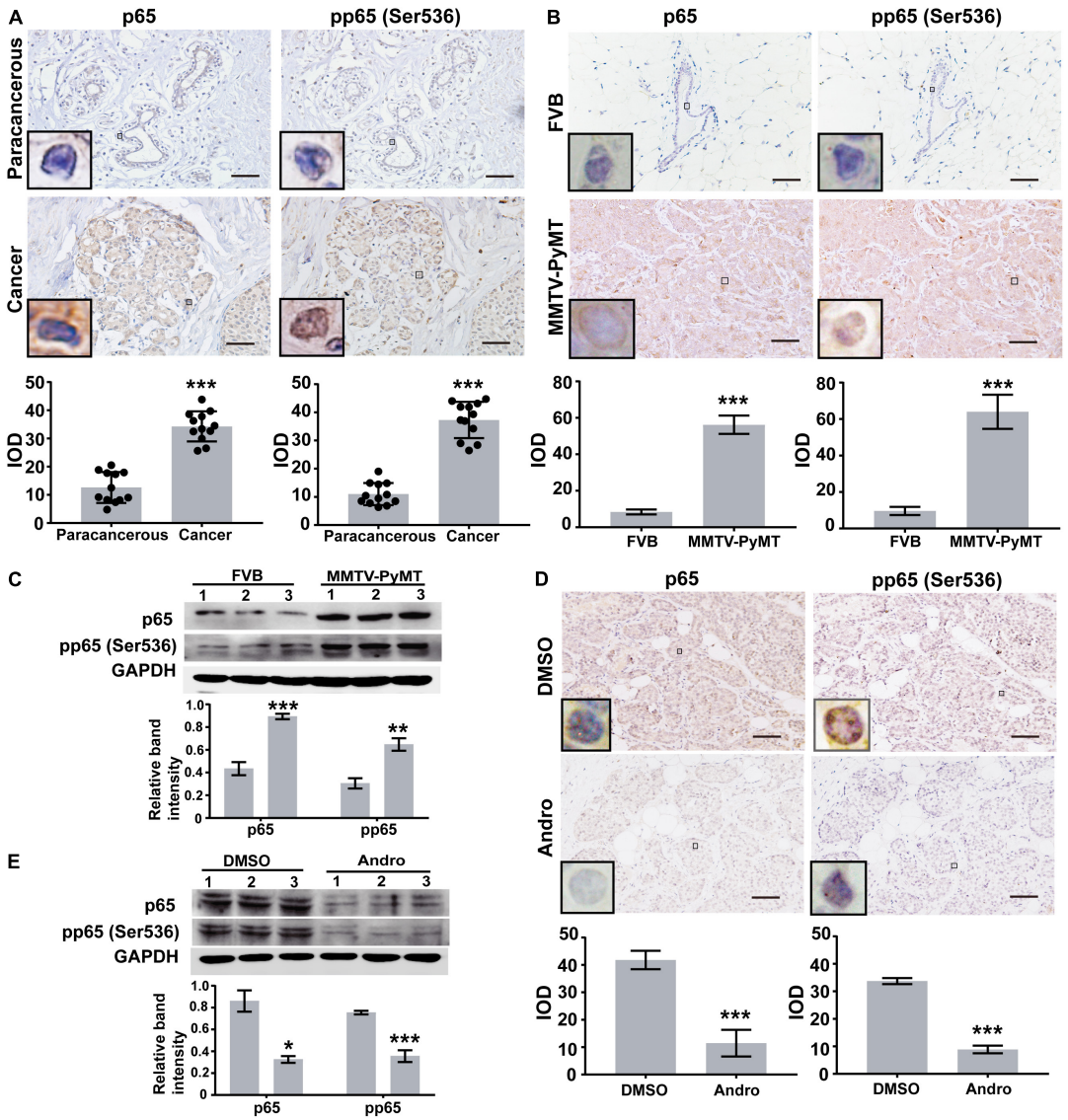

FIGURE 1 | Expression levels of NF-κB. Immunohistochemistry (IHC) assay analysis the expression levels of p65 and pp65(Ser536) in **(A)** human luminal-like breast cancer tissues and the matched surrounding non-cancerous breast tissues (paracancerous, $n = 12$) and **(B)** tumor tissues of spontaneous luminal-like breast cancer mice (MMTV-PyMT) and breast tissues of matched background mice (FVB, $n = 3$). **(C)** Immunoblotting analysis in mice breast tissue lysates. **(D)** Expressions of p65 and pp65 (Ser536) in the tumor tissues of dimethyl sulfoxide (DMSO)- or andrographolide (Andro)-treated MMTV-PyMT mice ($n = 3$). **(E)** Immunoblotting analysis of p65 and pp65 (Ser536) expression in MCF-7 cells. Quantitative data are expressed as the mean ± SD. Significant effect: $^{**}P < 0.01$; $^{***}P < 0.001$. *Scale bar*, 50 μM.

we first randomly selected 12 pairs of luminal-like breast cancer tissues and non-cancerous breast tissues (nine cases of luminal-like A type and three cases of luminal-like B type) to evaluate the expression of NF-κB in human luminal-like breast cancer by immunohistochemical staining. The expressions of p65 and phospho-p65 [pp65(Ser536)] in human luminal-like breast cancer were significantly higher than those of the matched non-cancerous breast tissues (**Figure 1A**). In addition, we found upregulated expressions of p65 and pp65(Ser536) in tumor tissues of MMTV-PyMT mice than in FVB mice (**Figures 1B,C**). Andro significantly inhibited the expressions of p65 and pp65 (Ser536) in the tumor tissues of MMTV-PyMT mice and MCF-7 cells (**Figures 1D,E**).

Andro Inhibits Tumor Growth of Luminal-Like Breast Cancer in MMTV-PyMT Mice

Female MMTV-PyMT mice were randomly divided into two groups and treated with Andro or DMSO twice a week for 4 weeks. The tumor volume was calculated twice a week. Andro significantly inhibited tumor growth after a 7-day treatment compared to DMSO (**Figure 2A**). After treatment, the tumor tissues were peeled off and weighed. The tumor weight of each mouse was markedly suppressed by Andro treatment compared to DMSO (**Figure 2B**). To explore the effect of Andro on luminal-like breast cancer development, a detailed histological analysis of the tumor tissues of DMSO- and Andro-treated MMTV-PyMT mice was performed. As shown in **Figure 2C**, Andro slowed down the pathological process of tumor tissues in MMTV-PyMT mice. Advanced-stage cancer invaded the tissues and extensive necrotic area were identified in the DMSO-treated mice. However, the structure of most of the tumor tissue basement membrane was complete in Andro-treated MMTV-PyMT mice. We further detected the cell proliferation index in the tumor tissues, and the results showed that cells expressing Ki67, a cell proliferation marker, were notably decreased in the Andro-treated group compared to the DMSO-treated group (**Figure 2D**). In our previous report, we demonstrated that Andro can inhibit angiogenesis, which can promote tumor growth and metastasis (Dai et al., 2017). EGN (CD105), a marker of angiogenic endothelial cells, is expressed specifically in tumor angiogenesis, including breast cancer (Minhajat et al., 2006). Therefore, we further examined the expression of EGN in tumor tissues and found that Andro can significantly inhibit the number of EGN-positive cells in tumor tissues. Furthermore, the vascular density in tumor tissues was significantly suppressed by Andro compared to treatment by DMSO (**Figure 2E**). Together, these results revealed that Andro inhibits the tumor growth of luminal-like breast cancer.

Andro Suppresses Tumor Metastasis of Luminal-Like Breast Cancer *in vivo*

The MMTV-PyMT transgenic mouse model is a widely used spontaneous luminal-like breast cancer mouse model with metastasis to the lungs (Fluck and Schaffhausen, 2009). Therefore, we further examined the anti-metastatic effect of

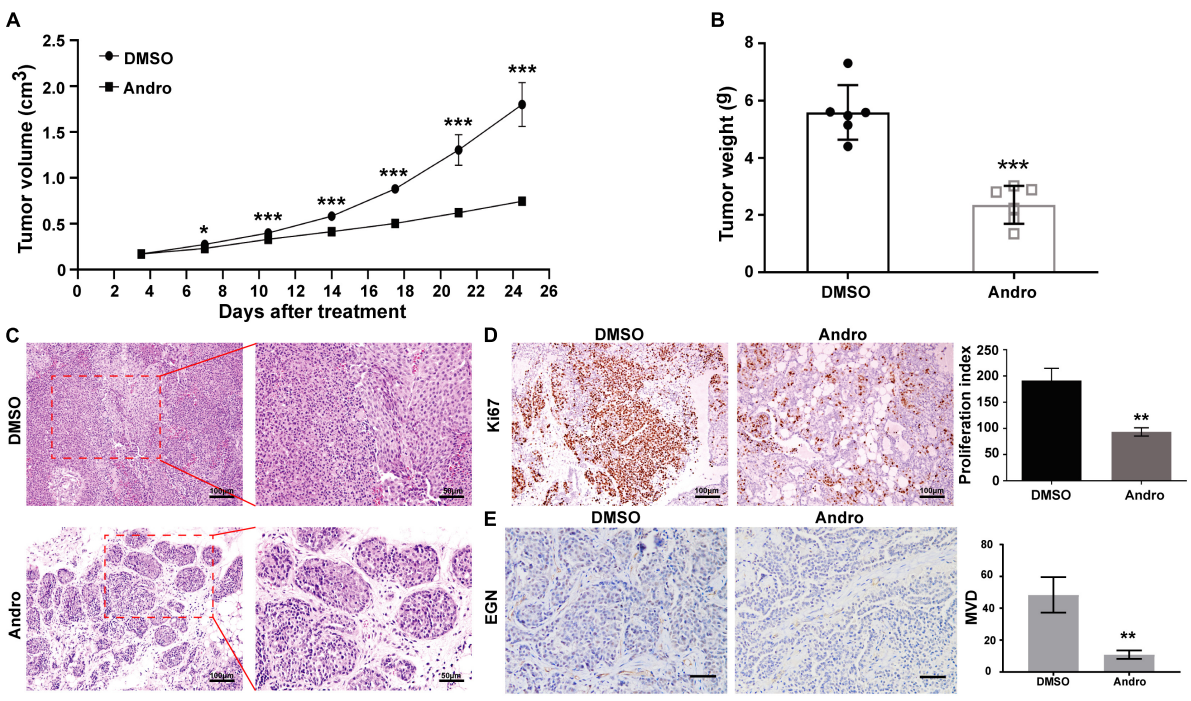

FIGURE 2 | Andrographolide (Andro) suppresses the tumor growth of MMTV-PyMT mice. **(A)** Tumor volume, **(B)** tumor weight, **(C)** tumor morphology, **(D)** Ki67, and **(E)** EGN expression detected in treatment with Andro or dimethyl sulfoxide (DMSO). Quantitative data are expressed as the mean ± SD (n = 6). Significant effect: $^{*}P < 0.05$; $^{**}P < 0.01$; $^{***}P < 0.001$.

Andro in luminal-like breast cancer. After treatment with Andro or DMSO, the lung tissues of mice were removed and fixed with Bouin's solution. Multiple large metastatic foci on the surface of the lung tissues were observed in DMSO-treated MMTV-PyMT mice, but not in the lung tissues of the Andro-treated mice (**Figure 3A**). Then, the numbers of metastatic foci on the surface of the lung tissues were counted; the results showed that Andro significantly inhibits tumor metastasis to the lungs compared to DMSO (**Figure 3B**). In addition, the lung tissues were embedded in paraffin and stained with H&E. The metastatic nodules on the tissue sections were larger in the DMSO-treated group than that in the Andro-treated group (**Figure 3C**). All of the data demonstrated that Andro inhibits the tumor metastasis of luminal-like breast cancer.

Andro Inhibits Cell Proliferation of MCF-7 Cells *in vitro*

MCF-7 luminal-like breast cancer cells were further employed to evaluate the inhibition effect of Andro on tumor cells *in vitro*. MCF-7 cells were treated with different concentrations of Andro. Andro significantly suppressed MCF-7 cell viability in a dose-dependent manner, with an IC_{50} of 70 μM for 48 h treatment (**Figure 4A**). In addition, the IC_{50} concentration of Andro inhibited cell viability in a time-dependent manner (**Figure 4B**). Next, colony formation assay was used to detect the long-term effect of Andro on cell proliferation. MCF-7 cells were seeded in a low density and treated with Andro (70 μM) or DMSO. After 7 days of treatment, Andro-treated colonies were smaller than the DMSO-treated ones (**Figure 4C**). Andro significantly decreased the number of colonies compared to DMSO (**Figure 4D**). All the results indicated that Andro could significantly inhibit the cell proliferation of MCF-7 luminal-like breast cancer cells in a dose- and time-dependent manner.

Andro Inhibits Cell Migration and Invasion of MCF-7 Cells *in vitro*

As shown in **Figure 5A**, the cell migration distances were markedly decreased at 12 h posttreatment with Andro compared to DMSO. In addition, the MCF-7 cell migration and invasion abilities were inhibited by Andro. The migrated and invaded cells through the Matrigel-uncoated or Matrigel-coated membranes of the chambers were less in

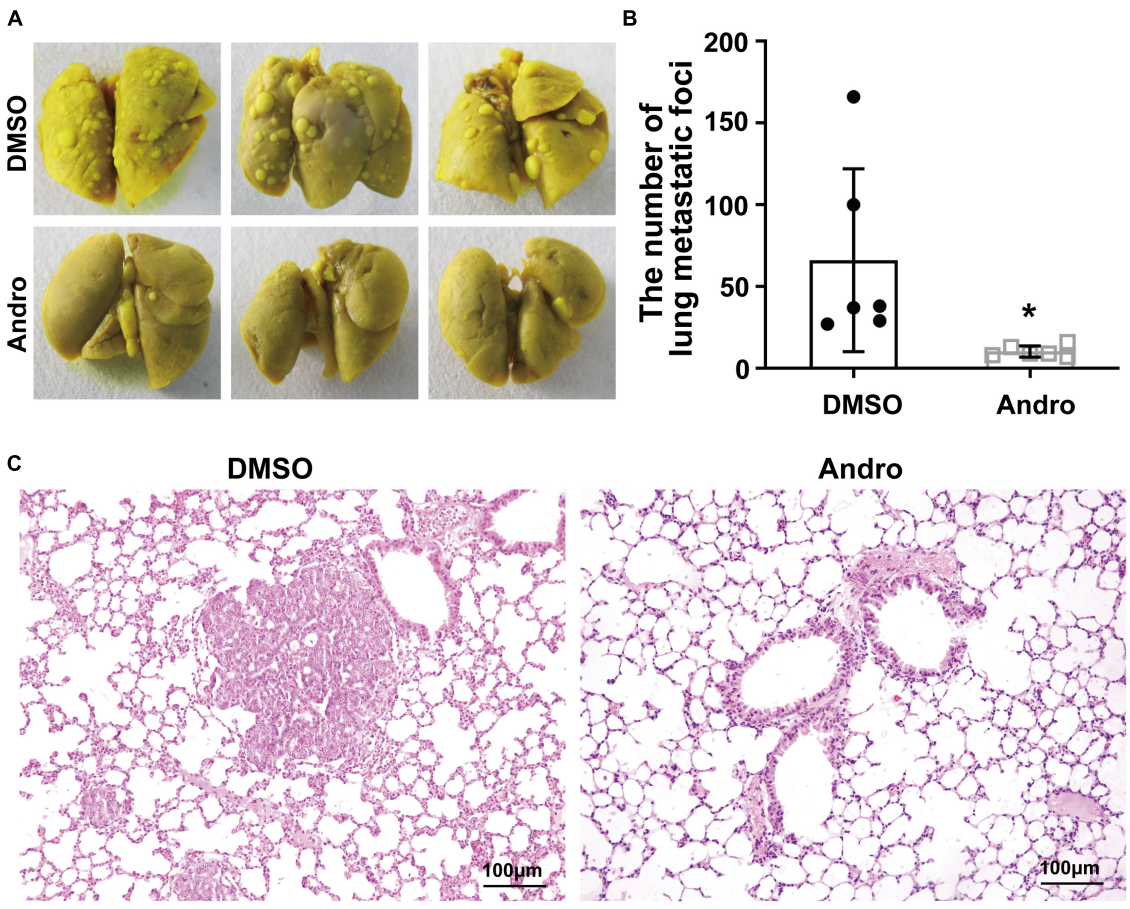

FIGURE 3 | Andrographolide (Andro) inhibits tumor metastasis to the lung in MMTV-PyMT mice. **(A)** Gross observation of metastatic foci on the surface of the lungs. **(B)** Quantification of metastatic foci. **(C)** Histological images of hematoxylin and eosin (H&E)-stained lung tissue sections. Quantitative data are expressed as the mean ± SD ($n = 6$). Significant effect: $^*P < 0.05$.

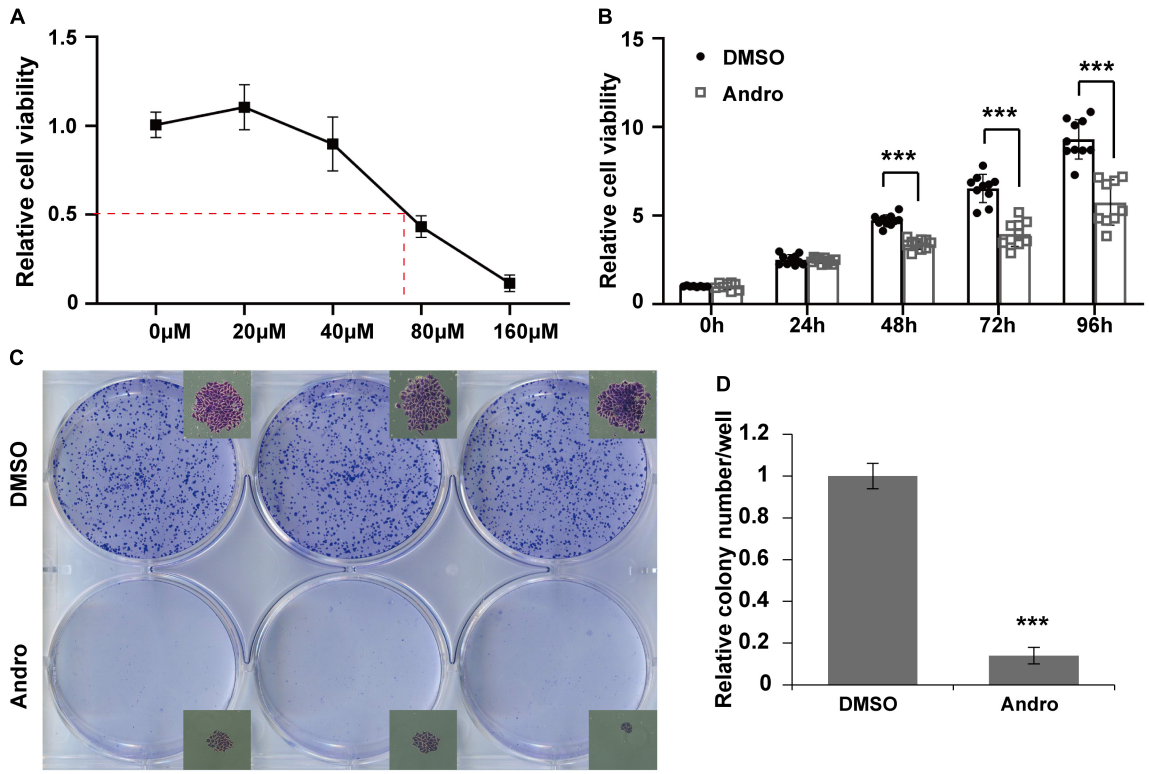

FIGURE 4 | Andrographolide (Andro) inhibits viability and proliferation of MCF-7 cells. **(A)** Dose-dependent effect of andrographolide (Andro) on MCF-7 cell viability at 48 h (IC_{50} = 70 μM). **(B)** Treatment duration effect of Andro (70 μM) on MCF-7 viability. **(C)** Colony formation assay. **(D)** Colony counts. Quantitative data are expressed as the mean ± SD (n = 3). Significant effect: ***P < 0.001.

the Andro-treated group than those in the DMSO-treated group (**Figures 5B,C**). These results demonstrated that Andro suppresses the migration and invasion of MCF-7 luminal-like breast cancer cells.

The NF-κB/miR-21-5p/PDCD4 Signaling Pathway Is Involved in Andro-Mediated Inhibition of MCF-7 Cell Proliferation, Migration, and Invasion

It has been reported that NF-κB regulates multiple miRNA expressions in various types of cancer cells (Shin et al., 2011; Wei et al., 2014). As shown in **Figure 6A**, miR-21-5p was significantly inhibited by the inactivation of NF-κB in MCF-7 cells. Previous studies have reported that NF-κB binding sites in the promoter of miR-21-5p transcription regulated the expression of miR-21-5p (Polytarchou et al., 2011; Yang et al., 2017). We demonstrated that Andro inhibits the expression of NF-κB in luminal-like breast cancer; however, whether Andro can inhibit miR-21-5p expression in luminal-like breast cancer still needs to be confirmed. In addition, we also found that the expression of miR-21-5p also decreased in MCF-7 cells and MMTV-PyMT mice treated with Andro compared with DMSO (**Figure 6B**). As shown in **Figure 6C**, inhibition of miR-21-5p significantly inhibited MCF-7 cell proliferation, migration, and invasion. Meanwhile, the overexpression of miR-21-5p in MCF-7 cells abolished the Andro-mediated inhibition of cell proliferation, migration, and invasion.

We further explored the target gene of miR-21-5p in breast cancer cells. In a previous study, we has confirmed that miR-21-5p directly binds to the 3′-UTR region of PDCD4 through dual-luciferase reporter assays (Yao et al., 2009). In this study, we demonstrated that Andro significantly upregulated the expression of PDCD4 in MMTV-PyMT mice and MCF-7 cells (**Figures 6D–F**). Andro treatment or miR-21-5p knockdown markedly upregulated PDCD4 expression compared to the control groups. Andro-induced PDCD4 expression in MCF-7 was abolished by miR-21-5p mimic treatment (**Figure 6F**). These results indicate that Andro inactivates NF-κB signaling to inhibit the expression of miR-21-5p, and the inhibition of miR-21-5p stimulates PDCD4 expression to inhibit luminal-like breast cancer growth, metastasis, and invasion.

DISCUSSION

Cost-effective drugs for luminal-like breast cancer treatment are still in high demand. In this study, we have demonstrated the promising therapeutic potential of Andro for luminal-like breast cancer and explored the underlying mechanisms (**Figure 6G**). We verify that NF-κB was expressed at a higher level in tumor tissues compared to that of matched non-cancerous tissues

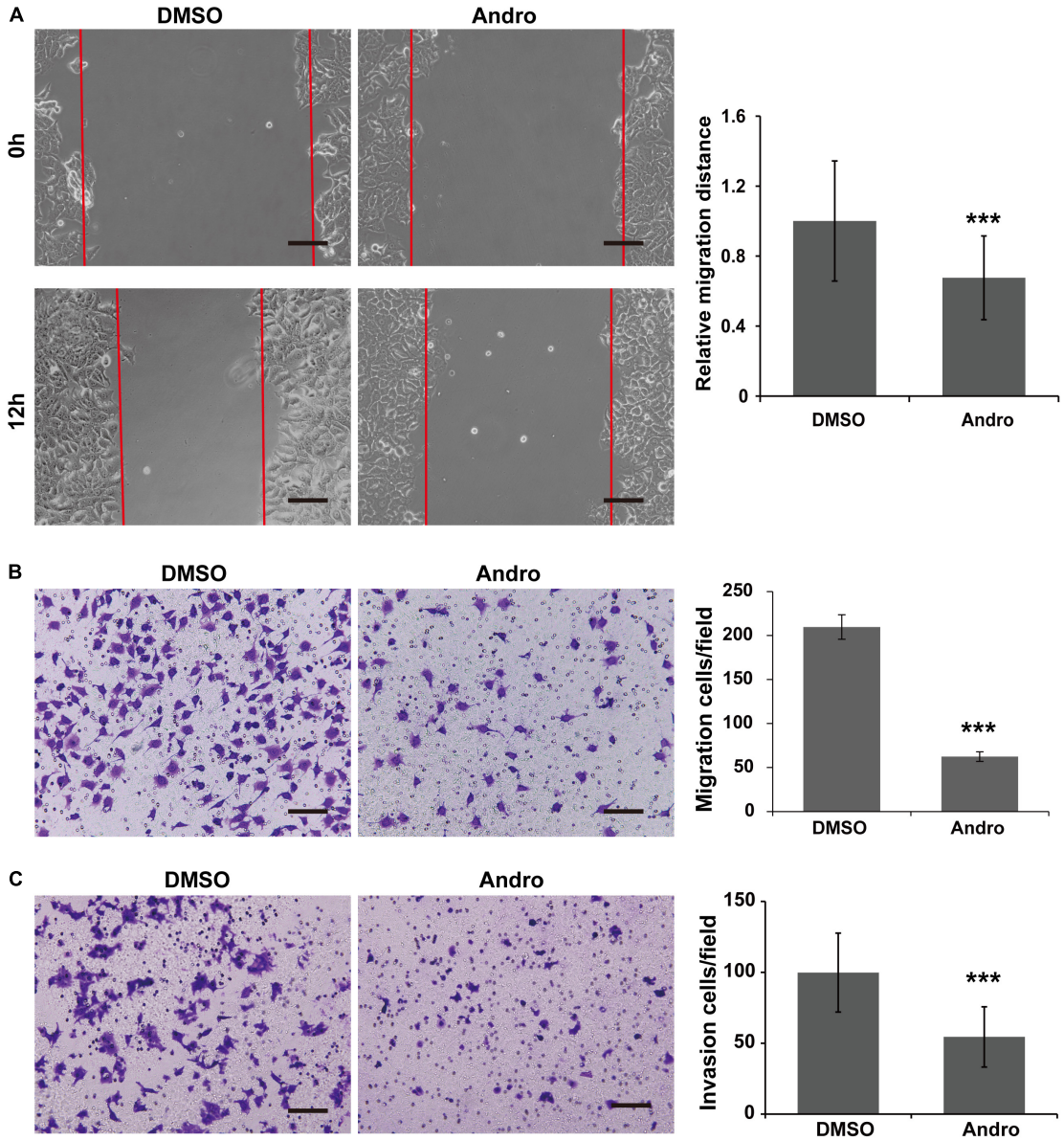

FIGURE 5 | Andrographolide (Andro) inhibits migration and invasion of MCF-7 cells. **(A)** Wound healing assay for MCF-7 cell migration. Transwell assay for the migration **(B)** and invasion **(C)** potential of MCF-7 cells. Quantitative data are expressed as the mean ± SD ($n = 3$). Significant effect: $^{***}P < 0.001$. *Scale bar*, 100 μM.

of luminal-like breast cancer. *In vivo* and *in vitro* studies demonstrated that Andro, a potent inhibitor of NF-κB, inhibits the tumor growth and metastasis of luminal-like breast cancer. Previous reports and our work further demonstrated that NF-κB inhibits PDCD4 expression in breast cancer cells *via* regulating miR-21-5p expression. These results indicate NF-κB/miR-21-5p/PDCD4 signaling was involve in the inhibition of tumor growth and metastasis by Andro in luminal-like breast cancer. Andro, a potent NF-κB inhibitor, which could be a possible drug to treat luminal-like breast cancer in the clinic.

Endocrine therapy is recommended as the first-line treatment in the clinic for luminal-like breast cancer, which is a type of hormone receptor-positive breast cancer (Cortes et al., 2020). More than half of luminal-like breast cancer patients exhibit treatment-related toxicity during chemotherapy, and some patients develop drug tolerance during endocrine therapy (Ignatiadis and Sotiriou, 2013). Both chemotherapy and endocrine therapy are not effective for metastasized luminal breast cancer (Kimbung et al., 2016). Therefore, this study aimed to explore a possible new molecular target for luminal-like breast cancer. A previous report has indicated NF-κB as a possible therapeutic target for various cancers (Labbozzetta et al., 2020). The tumor tissues of patients with luminal-like breast cancers and MMTV-PyMT mice showed NF-κB overexpression. These

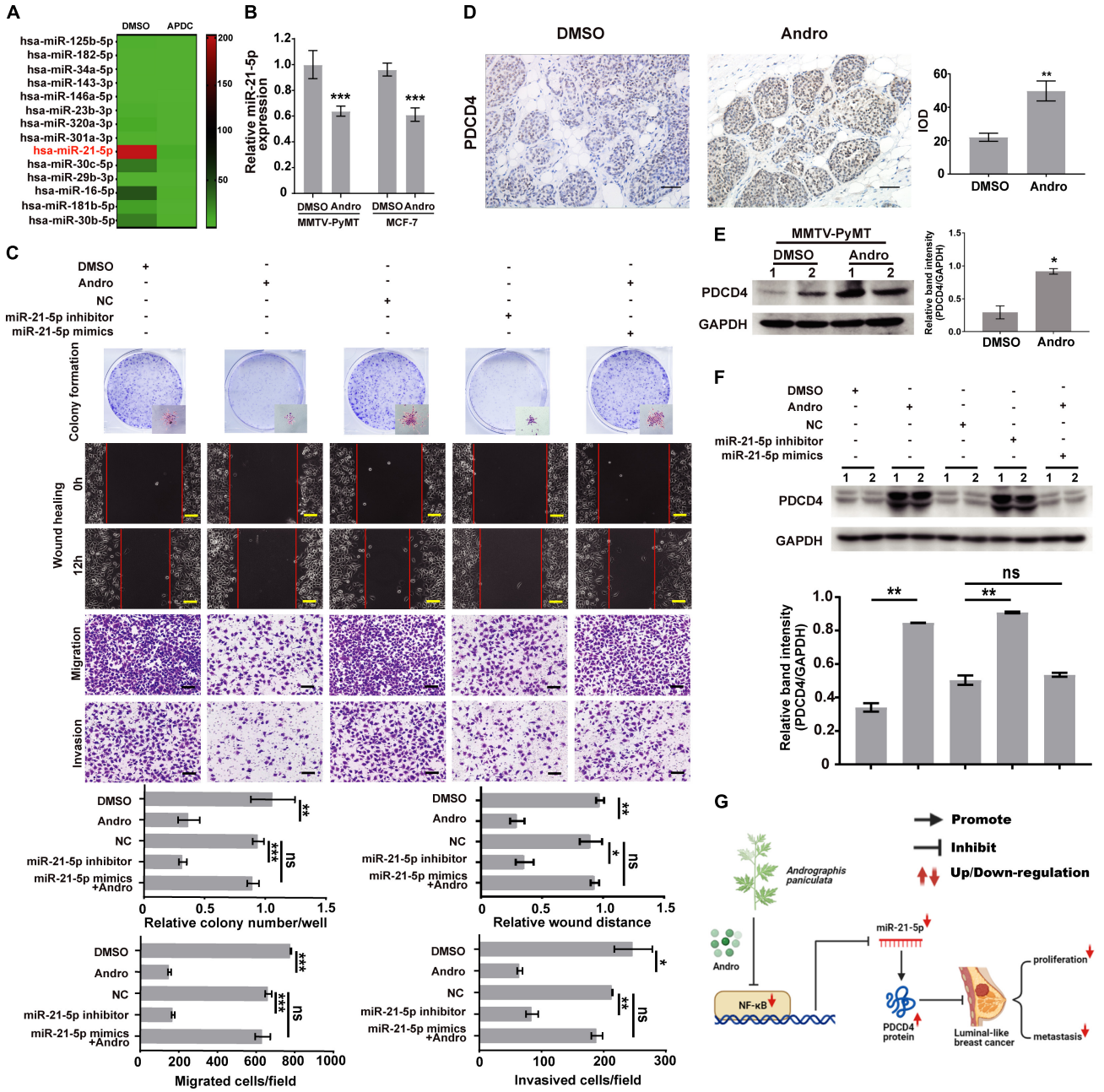

FIGURE 6 | Andrographolide (Andro) inhibits breast cancer cell proliferation, migration, and invasion *via* NF-κB/miR-21-5p/PDCD4 signaling. **(A)** Heat map of the qRT-PCR data of miRNA expression in MCF-7 cells with or without NF-κB inhibition. APDC: NF-κB inhibitor. **(B)** miR-21-5p expression in breast cancer tissue and MCF cells was also detected using qRT-PCR. miR-21-5p was markedly suppressed by Andro in MCF-7 cells and MMTV-PyMT mice. **(C)** Colony formation, wound healing, Transwell migration, and Matrigel invasion assay. Immunohistochemistry **(D)** and Immunoblotting assay **(E)** for PDCD4 expression in DMSO- and Andro-treated MMTV-PyMT mice. **(F)** Immunoblotting analysis for PDCD4 expression in MCF-7 cells. **(G)** Schematic of the mechanisms of Andro-mediated effect on luminal-like breast cancer growth and metastasis. Quantitative data are expressed as the mean ± SD, $n = 3$. Significant effect: $^{*}P < 0.05$, $^{**}P < 0.01$, $^{***}P < 0.005$. *ns*, no significant effect. *Scale bar*, 100 μM.

findings indicate NF-κB as a therapeutic target for luminal-like breast cancer.

A targeted therapy strategy based on molecular characteristics is well used for the treatment of hormone receptor- or HER2-positive breast cancer (Ithimakin et al., 2013). Luminal-like breast cancers, including the luminal A, luminal B HER2-negative, and luminal B HER2-positive subtypes, are often resistant to anti-hormone therapy (Santiago-Ortiz and Schaffer, 2016). Although anti-HER2 therapies have been shown to improve the outcomes of patients, these can only be used to treat

the luminal B HER2-positive subtype in luminal-like breast cancers (Tagliabue et al., 2010). *A. paniculata* Nees belongs to the family Acanthaceae and is an important traditional herbal medicine that is widely used in many Asian countries such as China, India, and others in Southeast Asia (Sun et al., 2019). Andrographolide (Andro), a diterpene lactone, is the major bioactive component extracted from *A. paniculata* Nees, which has been traditionally used for thousands of years to treat bacterial infections and inflammatory diseases (Zhang et al., 2020). In recent years, it has been demonstrated that Andro also possesses anticancer, antidiabetic, antimalarial, anti-HIV, and anti-angiogenic pharmacological effects (Sukardiman et al., 2007; Di Leva et al., 2014; Kang et al., 2018). Previous reports indicated that Andro inhibits cell growth, migration, and invasion and induces apoptosis in multiple types of breast cancer cells, including luminal-type (MCF-7 and TD-47) and triple-negative (MDA-MB-231 and 4T1) breast cancer cells, through various signaling pathways (Sukardiman et al., 2007; Chao et al., 2013; Zhai et al., 2015; Kang et al., 2018). It has been reported that Andro acts as an NF-κB inhibitor to suppress various cancers (Zhang et al., 2014a,b). Andro-mediated inhibition of NF-κB signaling has only been reported in MDA-MB-231 cells (Zhai et al., 2015). In this study, we further demonstrated that Andro inhibits the tumor growth and metastasis of luminal-like breast cancer by suppressing cell viability and cell migration and invasion *in vivo* and *in vitro*. Otherwise, our previous study demonstrated that Andro inhibits angiogenesis, which is essential for tumor growth and metastasis (Dai et al., 2017). We further confirmed that tumor angiogenesis is inhibit by Andro in the tumor tissues of MMTV-PyMT mice, which is consistent with our previous report indicated above. All of the data showed that Andro inhibits cancer development in luminal-like breast cancer, which may be through not only inhibiting tumor cell proliferation and invasion but also by suppressing angiogenesis.

Aberrant expressions of miRNAs are associated with breast cancer pathogenesis. Recent studies have indicated that miR-21-5p is an important oncogenic miRNA. miR-21-5p is consistently overexpressed in many solid tumors, including breast cancer (Zhang et al., 2014c). It has been shown that miR-21-5p specifically targets and inhibits tumor suppressor expression to promote cell proliferation, migration, and invasion in breast cancer (Wang et al., 2019). PDCD4 is a significant functional target of miR-21-5p in various types of cancers (Chen et al., 2015; Tao et al., 2019). *In vitro* studies indicated that miR-21-5p/PDCD4 signaling promotes cell proliferation in MCF-7 luminal-like breast cancer cells and induces the invasion and metastasis of MDA-MB-231 triple-negative breast cancer cells (Frankel et al., 2008; Zhu et al., 2008). Multiple miRNAs, including miR-21-5p, are validated as transcriptional targets of NF-κB (Polytarchou et al., 2011; Shin et al., 2011; Wei et al., 2014). In this study, NF-κB-inactivated luminal-like breast cancer cells demonstrated significant downregulation of miR-21-5p. In addition, NF-κB/miR-21-5p/PDCD4 signaling was involved in tumor growth and metastasis.

This study detected the crosstalk between NF-κB and miR-21-5p. Andro showed an inhibitory effect on luminal-like breast cancer growth and metastasis *via* the downregulation of NF-κB and miRNA-21-5p. Reports from the literature indicated that breast cancer development may be dependent on the crosstalk between NF-κB and other signaling pathways, including signal transducer and activator of transcription 3 (STAT3), glycogen synthase kinase 3 beta (GSK3-β), tumor suppressor p53, miRNAs, lncRNA, and the Wnt /β-catenin pathway (Moreau et al., 2011; Schneider and Kramer, 2011; Keklikoglou et al., 2012; Yu et al., 2014; Liu et al., 2015; Tewari et al., 2021). This is the first study to demonstrate the therapeutic effect of Andro on luminal-like breast cancer *via* targeting PDCD4 through the downregulation of NF-κB/miR-21-5p signaling. However, the interactions between NF-κB and other signaling pathways and that of miR-21-5p and its other targets involved in Andro-mediated tumor inhibition of luminal-like breast cancer need to be further explored.

DATA AVAILABILITY STATEMENT

The original contributions presented in the study are included in the article/**Supplementary Material**, further inquiries can be directed to the corresponding author/s.

ETHICS STATEMENT

The studies involving human participants were reviewed and approved by the Institutional Ethics Committee of People's Hospital of Baoan District of Shenzhen. The patients/participants provided their written informed consent to participate in this study. The animal study was reviewed and approved by the Undergraduate Laboratory Animal Center Ethics Committee of Guangdong Pharmaceutical University.

AUTHOR CONTRIBUTIONS

Q-QZ, JD, and LW conceptualized and supervised the study. CQ, LZ, JiL, and JD helped with the methodology. JuL, YY, ZH, MC, YDi, and ZL helped with the software. Q-QZ and JuL did the validation, wrote the manuscript—revised draft preparation, and contributed to the visualization. JuL, ZH, MC, YY, YDu, XL, and ZL did the formal analysis. JuL, LH, ZH, MC, YDi, YY, YDu, and ZL did the investigation. Q-QZ contributed to resources. Q-QZ, JuL, LH, YDu, and YY curated the data. Q-QZ, LW, JD, and RZ administered the project and helped with funding acquisition. All authors have read and agreed to the published version of the manuscript.

FUNDING

This work was supported by the National Natural Science Foundation of China (Grant No. 31771578), the Natural Science Foundation of Guangdong Province (Grant Nos. 2018A030313186 and 2021A1515010913), grant from the State Key Lab of Respiratory Disease, Guangzhou Medical University (Grant No. SKLRD-Z-202001), Innovation and University Promotion Project of Guangdong Pharmaceutical

University (Grant No. 2017KCXTD020), and the Key-Area Research and Development Program of Guangdong Province (Grant No. 2019B020234003).

ACKNOWLEDGMENTS

We thank Xiaodong He (Guangdong Pharmaceutical University) for technical assistance and Janak Pathak (Affiliated Stomatology Hospital of Guangzhou Medical University) for manuscript preparation.

SUPPLEMENTARY MATERIAL

The Supplementary Material for this article can be found online at: https://www.frontiersin.org/articles/10.3389/fcell.2021.643525/full#supplementary-material

REFERENCES

Banerjee, M., Chattopadhyay, S., Choudhuri, T., Bera, R., Kumar, S., Chakraborty, B., et al. (2016). Cytotoxicity and cell cycle arrest induced by andrographolide lead to programmed cell death of MDA-MB-231 breast cancer cell line. *J. Biomed. Sci.* 23:40. doi: 10.1186/s12929-016-0257-0

Chao, C. Y., Lii, C. K., Hsu, Y. T., Lu, C. Y., Liu, K. L., Li, C. C., et al. (2013). Induction of heme oxygenase-1 and inhibition of TPA-induced matrix metalloproteinase-9 expression by andrographolide in MCF-7 human breast cancer cells. *Carcinogenesis* 34, 1843–1851. doi: 10.1093/carcin/bgt131

Chen, Z., Yuan, Y. C., Wang, Y., Liu, Z., Chan, H. J., Chen, S., et al. (2015). Down-regulation of programmed cell death 4 (PDCD4) is associated with aromatase inhibitor resistance and a poor prognosis in estrogen receptor-positive breast cancer. *Breast Cancer Res. Treat.* 152, 29–39. doi: 10.1007/s10549-015-3446-8

Cortes, J., Ciruelos, E., Perez-Garcia, J., Albanell, J., García-Estévez, L., Ruiz-Borrego, M., et al. (2020). Contextualizing pertuzumab approval in the treatment of HER2-positive breast cancer patients. *Cancer Treat. Rev.* 83:101944. doi: 10.1016/j.ctrv.2019.101944

Dai, J., Lin, Y., Duan, Y., Li, Z., Zhou, D., Chen, W., et al. (2017). Andrographolide inhibits angiogenesis by inhibiting the Mir-21-5p/TIMP3 signaling pathway. *Int. J. Biol. Sci.* 13, 660–668. doi: 10.7150/ijbs.19194

Di Leva, G., Garofalo, M., and Croce, C. M. (2014). MicroRNAs in cancer. *Annu. Rev. Pathol.* 9, 287–314. doi: 10.1146/annurev-pathol-012513-104715

Fluck, M. M., and Schaffhausen, B. S. (2009). Lessons in signaling and tumorigenesis from polyomavirus middle T antigen. *Microbiol. Mol. Biol. Rev.* 73, 542–563. doi: 10.1128/MMBR.00009-09

Frankel, L. B., Christoffersen, N. R., Jacobsen, A., Lindow, M., Krogh, A., and Lund, A. H. (2008). Programmed cell death 4 (PDCD4) is an important functional target of the microRNA miR-21 in breast cancer cells. *J. Biol. Chem.* 283, 1026–1033. doi: 10.1074/jbc.M707224200

Goldhirsch, A., Wood, W. C., Coates, A. S., Gelber, R. D., Thürlimann, B., Senn, H. J., et al. (2011). Strategies for subtypes–dealing with the diversity of breast cancer: highlights of the St. gallen international expert consensus on the primary therapy of early breast cancer 2011. *Ann. Oncol.* 22, 1736–1747. doi: 10.1093/annonc/mdr304

Handa, S. S., and Sharma, A. (1990). Hepatoprotective activity of andrographolide from andrographis paniculata against carbontetrachloride. *Indian J. Med. Res.* 92, 276–283.

Ignatiadis, M., and Sotiriou, C. (2013). Luminal breast cancer: from biology to treatment. *Nat. Rev. Clin. Oncol.* 10, 494–506. doi: 10.1038/nrclinonc.2013.124

Ihemelandu, C. U., Naab, T. J., Mezghebe, H. M., Makambi, K. H., Siram, S. M., Leffall, L. D. Jr., et al. (2008). Basal cell-like (triple-negative) breast cancer, a predictor of distant metastasis in African American women. *Am. J. Surg.* 195, 153–158. doi: 10.1016/j.amjsurg.2007.09.033

Ithimakin, S., Day, K. C., Malik, F., Zen, Q., Dawsey, S. J., Bersano-Begey, T. F., et al. (2013). HER2 drives luminal breast cancer stem cells in the absence of HER2 amplification: implications for efficacy of adjuvant trastuzumab. *Cancer Res.* 73, 1635–1646. doi: 10.1158/0008-5472.CAN-12-3349

Kang, X., Zheng, Z., Liu, Z., Wang, H., Zhao, Y., Zhang, W., et al. (2018). Liposomal codelivery of doxorubicin and andrographolide inhibits breast cancer growth and metastasis. *Mol. Pharm.* 15, 1618–1626. doi: 10.1021/acs.molpharmaceut.7b01164

Keklikoglou, I., Koerner, C., Schmidt, C., Zhang, J. D., Heckmann, D., Shavinskaya, A., et al. (2012). MicroRNA-520/373 family functions as a tumor suppressor in estrogen receptor negative breast cancer by targeting NF-kappaB and TGF-beta signaling pathways. *Oncogene* 31, 4150–4163. doi: 10.1038/onc.2011.571

Kimbung, S., Johansson, I., Danielsson, A., Veerla, S., Egyhazi Brage, S., Frostvik Stolt, M., et al. (2016). Transcriptional profiling of breast cancer metastases identifies liver metastasis-selective genes associated with adverse outcome in luminal a primary breast cancer. *Clin. Cancer Res.* 22, 146–157. doi: 10.1158/1078-0432.CCR-15-0487

Labbozzetta, M., Notarbartolo, M., and Poma, P. (2020). Can NF-kappaB be considered a valid drug target in neoplastic diseases? Our point of view. *Int. J. Mol. Sci.* 21:3070. doi: 10.3390/ijms21093070

Li, L., Tang, P., Li, S., Qin, X., Yang, H., Wu, C., et al. (2017). Notch signaling pathway networks in cancer metastasis: a new target for cancer therapy. *Med. Oncol.* 34:180. doi: 10.1007/s12032-017-1039-6

Liu, B., Sun, L., Liu, Q., Gong, C., Yao, Y., Lv, X., et al. (2015). A cytoplasmic NF-kappaB interacting long noncoding RNA blocks IkappaB phosphorylation and suppresses breast cancer metastasis. *Cancer Cell* 27, 370–381. doi: 10.1016/j.ccell.2015.02.004

Liu, X., Sun, J., Yuan, P., Shou, K., Zhou, Y., Gao, W., et al. (2019). Mfn2 inhibits proliferation and cell-cycle in hela cells via Ras-NF-kappaB signal pathway. *Cancer Cell Int.* 19:197. doi: 10.1186/s12935-019-0916-9

Minhajat, R., Mori, D., Yamasaki, F., Sugita, Y., Satoh, T., and Tokunaga, O. (2006). Organ-specific endoglin (CD105) expression in the angiogenesis of human cancers. *Pathol. Int.* 56, 717–723. doi: 10.1111/j.1440-1827.2006.02037.x

Moreau, M., Mourah, S., and Dosquet, C. (2011). Beta-catenin and NF-kappaB cooperate to regulate the uPA/uPAR system in cancer cells. *Int. J. Cancer* 128, 1280–1292. doi: 10.1002/ijc.25455

Peng, Y., Wang, Y., Tang, N., Sun, D., Lan, Y., Yu, Z., et al. (2018). Andrographolide inhibits breast cancer through suppressing COX-2 expression and angiogenesis via inactivation of p300 signaling and VEGF pathway. *J. Exp. Clin. Cancer Res.* 37:248. doi: 10.1186/s13046-018-0926-9

Petrovic, N. (2016). miR-21 might be involved in breast cancer promotion and invasion rather than in initial events of breast cancer development. *Mol. Diagn. Ther.* 20, 97–110. doi: 10.1007/s40291-016-0186-3

Polytarchou, C., Iliopoulos, D., Hatziapostolou, M., Kottakis, F., Maroulakou, I., Struhl, K., et al. (2011). Akt2 regulates all akt isoforms and promotes resistance to hypoxia through induction of miR-21 upon oxygen deprivation. *Cancer Res.* 71, 4720–4731. doi: 10.1158/0008-5472.CAN-11-0365

Rosati, R., Oppat, K., Huang, Y., Kim, S., and Ratnam, M. (2020). Clinical association of progesterone receptor isoform a with breast cancer metastasis consistent with its unique mechanistic role in preclinical models. *BMC Cancer* 20:512. doi: 10.1186/s12885-020-07002-0

Santiago-Ortiz, J. L., and Schaffer, D. V. (2016). Adeno-associated virus (AAV) vectors in cancer gene therapy. *J. Control. Release* 240, 287–301. doi: 10.1016/j.jconrel.2016.01.001

Schneider, G., and Kramer, O. H. (2011). NFkappaB/p53 crosstalk-a promising new therapeutic target. *Biochim. Biophys. Acta* 1815, 90–103. doi: 10.1016/j.bbcan.2010.10.003

Shin, V. Y., Jin, H., Ng, E. K., Cheng, A. S., Chong, W. W., Wong, C. Y., et al. (2011). NF-kappaB targets miR-16 and miR-21 in gastric cancer: involvement of prostaglandin E receptors. *Carcinogenesis* 32, 240–245. doi: 10.1093/carcin/bgq240

Siegel, R. L., Miller, K. D., and Jemal, A. (2020). Cancer statistics, 2020. *CA Cancer J. Clin.* 70, 7–30. doi: 10.3322/caac.21590

Sorlie, T., Perou, C. M., Tibshirani, R., Aas, T., Geisler, S., Johnsen, H., et al. (2001). Gene expression patterns of breast carcinomas distinguish tumor subclasses

with clinical implications. *Proc. Natl. Acad. Sci. U.S.A.* 98, 10869–10874. doi: 10.1073/pnas.191367098

Sorlie, T., Tibshirani, R., Parker, J., Hastie, T., Marron, J. S., Nobel, A., et al. (2003). Repeated observation of breast tumor subtypes in independent gene expression data sets. *Proc. Natl. Acad. Sci. U.S.A.* 100, 8418–8423. doi: 10.1073/pnas.0932692100

Sukardiman, H., Widyawaruyanti, A., Sismindari, S., and Zaini, N. C. (2007). Apoptosis inducing effect of andrographolide on TD-47 human breast cancer cell line. *Afr. J. Tradit. Complement. Altern. Med.* 4, 345–351. doi: 10.4314/ajtcam.v4i3.31228

Sun, W., Leng, L., Yin, Q., Xu, M., Huang, M., Xu, Z., et al. (2019). The genome of the medicinal plant andrographis paniculata provides insight into the biosynthesis of the bioactive diterpenoid neoandrographolide. *Plant J.* 97, 841–857. doi: 10.1111/tpj.14162

Tagliabue, E., Balsari, A., Campiglio, M., and Pupa, S. M. (2010). HER2 as a target for breast cancer therapy. *Expert. Opin. Biol. Ther.* 10, 711–724. doi: 10.1517/14712591003689972

Tao, L., Wu, Y. Q., and Zhang, S. P. (2019). MiR-21-5p enhances the progression and paclitaxel resistance in drug-resistant breast cancer cell lines by targeting PDCD4. *Neoplasma* 66, 746–755. doi: 10.4149/neo_2018_181207N930

Tewari, D., Bawari, S., Sharma, S., DeLiberto, L. K., and Bishayee, A. (2021). Targeting the crosstalk between canonical Wnt/beta-catenin and inflammatory signaling cascades: a novel strategy for cancer prevention and therapy. *Pharmacol. Ther.* 6:107876. doi: 10.1016/j.pharmthera.2021.107876

Tewari, D., Patni, P., Bishayee, A., Sah, A. N., and Bishayee, A. (2019). Natural products targeting the PI3K-Akt-mTOR signaling pathway in cancer: a novel therapeutic strategy. *Semin. Cancer Biol.* S1044:30405. doi: 10.1016/j.semcancer.2019.12.008

Wang, H., Tan, Z., Hu, H., Liu, H., Wu, T., Zhen, C., et al. (2019). microRNA-21 promotes breast cancer proliferation and metastasis by targeting LZTFL1. *BMC Cancer* 19:738. doi: 10.1186/s12885-019-5951-3

Wei, C., Li, L., Kim, I. K., Sun, P., and Gupta, S. (2014). NF-kappaB mediated miR-21 regulation in cardiomyocytes apoptosis under oxidative stress. *Free Radic. Res.* 48, 282–291. doi: 10.3109/10715762.2013.865839

Xia, Y. F., Ye, B. Q., Li, Y. D., Wang, J. G., He, X. J., Lin, X., et al. (2004). Andrographolide attenuates inflammation by inhibition of NF-kappa B activation through covalent modification of reduced cysteine 62 of p50. *J. Immunol.* 173, 4207–4217. doi: 10.4049/jimmunol.173.6.4207

Yamamoto, M., Taguchi, Y., Ito-Kureha, T., Semba, K., Yamaguchi, N., Inoue, J., et al. (2013). NF-kappaB non-cell-autonomously regulates cancer stem cell populations in the basal-like breast cancer subtype. *Nat. Commun.* 4:2299. doi: 10.1038/ncomms3299

Yan, Z., Lai, Z., and Lin, J. (2017). Anticancer properties of traditional chinese medicine. *Comb. Chem. High Throughput Screen.* 20, 423–429. doi: 10.2174/1386207320666170116141818

Yang, Y., Weng, W., Peng, J., Hong, L., Yang, L., Toiyama, Y., et al. (2017). *Fusobacterium nucleatum* increases proliferation of colorectal cancer cells and tumor development in mice by activating toll-like receptor 4 signaling to nuclear factor-kappaB, and Up-regulating expression of MicroRNA-21. *Gastroenterology* 152, 851–866. doi: 10.1053/j.gastro.2016.11.018

Yao, Q., Xu, H., Zhang, Q. Q., Zhou, H., and HuQu, L. (2009). MicroRNA-21 promotes cell proliferation and down-regulates the expression of programmed cell death 4 (PDCD4) in hela cervical carcinoma cells. *Biochem. Biophys. Res. Commun.* 388, 539–542. doi: 10.1016/j.bbrc.2009.08.044

Yu, J., Wang, Y., Yan, F., Zhang, P., Li, H., Zhao, H., et al. (2014). Noncanonical NF-kappaB activation mediates STAT3-stimulated IDO upregulation in myeloid-derived suppressor cells in breast cancer. *J. Immunol.* 193, 2574–2586. doi: 10.4049/jimmunol.1400833

Zhai, Z., Qu, X., Li, H., Ouyang, Z., Yan, W., Liu, G., et al. (2015). Inhibition of MDA-MB-231 breast cancer cell migration and invasion activity by andrographolide via suppression of nuclear factor-kappaB-dependent matrix metalloproteinase-9 expression. *Mol. Med. Rep.* 11, 1139–1145. doi: 10.3892/mmr.2014.2872

Zhang, Q. Q., Ding, Y., Lei, Y., Qi, C. L., He, X. D., Lan, T., et al. (2014a). Andrographolide suppress tumor growth by inhibiting TLR4/NF-kappaB signaling activation in insulinoma. *Int. J. Biol. Sci.* 10, 404–414. doi: 10.7150/ijbs.7723

Zhang, Q. Q., Zhou, D. L., Ding, Y., Liu, H. Y., Lei, Y., Fang, H. Y., et al. (2014b). Andrographolide inhibits melanoma tumor growth by inactivating the TLR4/NF-kappaB signaling pathway. *Melanoma Res.* 24, 545–555. doi: 10.1097/CMR.0000000000000117

Zhang, S., Huang, F., Tian, W., Lai, L., Qian, L., Hong, W., et al. (2020). Andrographolide promotes pancreatic duct cells differentiation into insulin-producing cells by targeting PDX-1. *Biochem. Pharmacol.* 174:113785. doi: 10.1016/j.bcp.2019.113785

Zhang, W., Liu, J., and Wang, G. (2014c). The role of microRNAs in human breast cancer progression. *Tumour Biol.* 35, 6235–6244. doi: 10.1007/s13277-014-2202-8

Zhu, S., Wu, H., Wu, F., Nie, D., Sheng, S., and Mo, Y. (2008). MicroRNA-21 targets tumor suppressor genes in invasion and metastasis. *Cell Res.* 18, 350–359. doi: 10.1038/cr.2008.24

Conflict of Interest: The authors declare that the research was conducted in the absence of any commercial or financial relationships that could be construed as a potential conflict of interest.

frontiers in Genetics

ORIGINAL RESEARCH
published: 02 July 2021
doi: 10.3389/fgene.2021.672674

Four Prognosis-Associated lncRNAs Serve as Biomarkers in Ovarian Cancer

Jianfeng Zheng[1,2], *Jialu Guo*[3], *Huizhi Zhang*[3], *Benben Cao*[3], *Guomin Xu*[4], *Zhifen Zhang*[2] *and Jinyi Tong*[1,2*]

[1] Department of Obstetrics and Gynecology, Affiliated Hangzhou Hospital, Nanjing Medical University, Hangzhou, China, [2] Department of Obstetrics and Gynecology, Hangzhou Women's Hospital, Hangzhou, China, [3] Department of Fourth Clinical Medical College, Zhejiang Chinese Medical University, Hangzhou, China, [4] Department of Obstetrics and Gynecology, Haining Second People's Hospital, Haining, China

Long non-coding RNAs (lncRNAs) play crucial roles in ovarian cancer (OC) development. However, prognosis-associated lncRNAs (PALs) for OC have not been completely elucidated. Our study aimed to identify the PAL signature of OC. A total of 663 differentially expressed lncRNAs were identified in the databases. According to the weighted gene coexpression analysis, the highly correlated genes were clustered into seven modules related to the clinical phenotype of OC. A total of 25 lncRNAs that were significantly related to overall survival were screened based on univariate Cox regression analysis. The prognostic risk model constructed contained seven PALs based on the parameter λ_{min}, which could stratify OC patients into two risk groups. The results showed that the risk groups had different overall survival rates in both The Cancer Genome Atlas (TCGA) and two verified Gene Expression Omnibus (GEO) databases. Univariate and multivariate Cox regression analyses confirmed that the risk model was an independent risk factor for OC. Gene enrichment analysis revealed that the identified genes were involved in some pathways of malignancy. The competitive endogenous RNA (ceRNA) network included five PALs, of which four were selected for cell function assays. The four PALs were downregulated in 33 collected OC tissues and 3 OC cell lines relative to the control. They were shown to regulate the proliferative, migratory, and invasive potential of OC cells via Cell Counting Kit-8 (CCK-8) and transwell assays. Our study fills the gaps of the four PALs in OC, which are worthy of further study.

Keywords: ovarian cancer, lncRNA, weighted gene coexpression analysis, risk score model, cell function assays

OPEN ACCESS

Edited by:
Lorenzo Gerratana, University of Udine, Italy

Reviewed by:
Minghua Wang, Soochow University Medical College, China
Beifang Niu, Chinese Academy of Sciences (CAS), China

****Correspondence:***
Jinyi Tong
tongjinyi252@zju.edu.cn

Specialty section:
This article was submitted to Cancer Genetics, a section of the journal Frontiers in Genetics

Received: *26 February 2021*
Accepted: *31 May 2021*
Published: *02 July 2021*

Citation:
Zheng J, Guo J, Zhang H, Cao B, Xu G, Zhang Z and Tong J (2021) Four Prognosis-Associated lncRNAs Serve as Biomarkers in Ovarian Cancer. Front. Genet. 12:672674. doi: 10.3389/fgene.2021.672674

INTRODUCTION

Ovarian cancer (OC) is a gynecological malignancy with the highest morbidity and mortality rates worldwide (Stewart et al., 2019). Although the prognosis of patients in early cancer stages is better, most patients are already in the late stages of OC during the first diagnosis (Kaldawy et al., 2016; Eisenhauer, 2017). Thus, there is a need to identify novel biomarkers for predicting tumorigenesis and clinical diagnosis in earlier stages and to develop new therapeutic strategies and targets for OC.

Long non-coding RNAs (lncRNAs) are endogenous RNA transcripts more than 200 nucleotides in length that are not translated into polypeptides (Kopp and Mendell, 2018). Previous studies have found that lncRNAs could serve as strong prognostic biomarkers and play an important role in

different cell processes such as cell migration, growth, invasion, apoptosis, and differentiation in OC (Wang et al., 2019). For example, *SNHG9* was shown to serve as an anticancer biomarker by regulating *miR-214-5p* (Chen et al., 2021). *LINC01969* was confirmed to be a cancer-promoting biological marker via the *miR-144-5p*/*LARP1* axis (Chen et al., 2020).

The pathogenesis of most cancers, including OC, are caused by various genes rather than a single gene (Van Cott, 2020). The risk model can estimate a set of risk genes in any given cancer (Cintolo-Gonzalez et al., 2017; Tammemägi et al., 2019). Weighted correlation network analysis (WGCNA) is a combined method for analyzing clinical information and gene expression data (Sun et al., 2017). Through the analysis of gene modules with high correlation with clinical information, a series of key genes with high connectivity in the modules were obtained, which are potentially important for the occurrence and development of tumors (Tian et al., 2017). Previous studies have identified lncRNA-based signatures via WGCNA or by developing a risk model for OC (Li and Zhan, 2019; Zhao and Fan, 2019). However, these studies are still limited in their lack of cell function assays and constantly updated databases.

Thereby, the purpose of our research was to identify a prognosis-associated lncRNA (PAL) signature serving as a noteworthy prognostic biomarker in OC by using WGCNA and other comprehensive analyses. Two additional datasets from the GEO were used to check the accuracy of the model. A competitive endogenous RNA (ceRNA) network was established to explore the mechanisms of candidate PALs. Finally, four candidate PALs were selected for the *in vitro* assays.

MATERIALS AND METHODS

Data Extraction and Pre-treatment

The RNA data with corresponding clinical information were downloaded from TCGA TARGET GTEx (https://toil.xenahubs.net) (Goldman et al., 2020) and GEO (GSE32063 and GSE17260, https://www.ncbi.nlm.nih.gov/geo/) (Yoshihara et al., 2010, 2012). RNAs with expression levels >0 in 33% of the samples were identified as messenger RNAs (mRNAs) or lncRNAs based on annotation information from the GENCODE database (https://www.gencodegenes.org/) (Harrow et al., 2012). Differential gene analysis was based on linear regression and empirical Bayes using the limma package (http://www.bioconductor.org/packages/2.9/bioc/html/limma.html) (Ritchie et al., 2015). Meanwhile, we evaluated the differences in multiple and significance levels using Benjamini and Hochberg multiple comparisons ($P < 0.05$, $|\log FC| > 2$).

Screening Modules Related to Clinical Phenotype

WGCNA considers not only the coexpression patterns between two genes but also the overlap of neighboring genes (Langfelder and Horvath, 2008). A coexpression network between differentially expressed mRNAs and lncRNAs was established using WGCNA from the R package to identify modular genes closely related to the clinical phenotype. Clinical phenotypes in our study included age at initial pathological diagnosis, clinical stage (stage I, II, III, or IV), lymphatic invasion (no or yes), neoplasm histologic grade (grade I, II, III, or IV), tumor residual disease (no macroscopic disease, 1–10 mm, 11–20 mm, or >20 mm), venous invasion (no or yes), and vital status (dead or alive).

The WCGNA analysis should be subject to scale-free networks. Therefore, the applicable weight parameter β (SoftPower) of the gene coexpression matrix was supposed to conform to the scale-free distribution to the maximum extent. The correlation coefficients (R) of connectivity k and p(k) under each β were calculated, and then, β was selected when R^2 reached 0.85 for the first time. The highly correlated genes were clustered into modules based on clustering and dynamic pruning methods (minModuleSize = 30; MEDissThres = 0.3). Finally, the gene assembly modules closely related to the phenotype were identified via the correlation between the module and clinical phenotype.

Construction and Validation of Risk Model

The lncRNAs in the aforementioned modules were analyzed by univariate Cox regression analysis based on their expression values and overall survival (OS) of each OC sample ($P < 0.05$). Kaplan–Meier (K–M) analysis and log-rank test were performed using the R package to select the PALs ($P < 0.05$) for further analysis. Least absolute shrinkage and selection operator (Lasso) regression of the glmnet package (version 2.0-18) (Engebretsen and Bohlin, 2019) was carried out for further dimensionality reduction to screen the more significant PALs for risk model construction. According to multivariate Cox regression analysis, a prognostic risk model was generated based on the following formula:

$$\text{Risk score} = \sum \beta_{\text{lncRNA}} \times \text{Exp}_{\text{lncRNA}}$$

In the risk score (RS) formula, β_{lncRNA} represents the regression coefficient for PALs, and $\text{Exp}_{\text{lncRNA}}$ means the expression level of homologous PALs. OC patients in the study were divided into low- or high-risk groups according to the optimal cutoff point of RSs gained from Survminer (version 0.4.3) from the R package, and K–M survival analysis was performed between the two risk groups using the log-rank test. In addition, GSE32063 (40 OC samples) and GSE17260 (110 OC samples) were downloaded from National Center for Biotechnology Information (NCBI) GEO (Barrett et al., 2005) and used to develop a prognostic risk model using the same method.

Furthermore, the RSs of different clinical indicators, including age (age ≤60 years or >60 years), grade (grade II or III), and stage (stage III or IV) were compared. Several clinical indicators, such as age in GEO, grade I, grade IV, stage I, and stage II, were excluded due to insufficient sample size. Tumor mutational burden (TMB) scores were calculated for each OC patient from

Abbreviations: GEO, Gene Expression Omnibus; HR, hazard ratio; K–M, Kaplan–Meier; lncRNA, long non-coding RNA; OC, ovarian cancer; OS, overall survival; PAL, prognosis-associated lncRNA; ROC, receiver operating characteristic; TCGA, The Cancer Genome Atlas; WGCNA, weighted gene coexpression analysis.

TCGA, and the relationship between the risk model and TMB was also assessed.

Construction of ceRNA Network

The microRNAs (miRNAs) targeted by the corresponding PALs were speculated by the DIANA-LncBase v2 (Paraskevopoulou et al., 2016). The target mRNAs by the corresponding miRNAs were speculated using miRTarBase (Hsu et al., 2011). Subsequently, the ceRNA network based on the same miRNAs of PAL–miRNA and miRNA–mRNA was constructed and visualized using Cytoscape (Kohl et al., 2011).

Biofunctional Analysis

Kyoto Encyclopedia of Genes and Genomes (KEGG) analysis was performed on potential target mRNAs of clinical modules or PALs based on clusterProfiler of R package (version:3.8.1, pAdjustMethod = BH, pvalueCutoff = 0.05) (Yu et al., 2012).

In vitro Assays

With approval from the Ethics Committee, a total of 33 OC and 20 adjacent normal ovarian tissues were collected from surgery OC patients between May 2019 and January 2021 at the Affiliated Hangzhou Hospital of Nanjing Medical University (Hangzhou, China). The clinical features are shown in **Supplementary Table 1**. The OC cell line SKOV-3 was supplied by the Cell Bank of China Academic of Science (Shanghai, China). The IOSE-80, HO-8910, and A2780 cells were purchased from iCell Bioscience Inc. (Shanghai, China). SKOV-3 cells were cultured in McCoy's 5A medium supplemented with 10% fetal bovine serum (FBS) and 1% penicillin-streptomycin. IOSE-80, HO-8910, and A2780 cells were cultured in 90% Roswell Park Memorial Institute (RPMI) 1640 medium with 10% FBS and 1% penicillin-streptomycin. All cells were incubated in a 5% CO_2 incubator at 37°C.

After RNA extraction and reverse transcription, real-time quantitative PCR (qPCR) analysis was performed using an ABI 7500 instrument to evaluate the expression value of alternative PALs in cells and tissues based on the kit of Takara (Shiga, Japan). Primer sequences are listed in **Table 1**.

The plasmids used for the experiment were constructed by TSINGKE Biological Technology (Hangzhou, China) based on the known sequences of *TCL6*, *VLDLR-AS1*, *RP11-356I2.4*, and *LINC00893* from NCBI. SKOV-3 and HO-8910 cells were transfected with homologous plasmids (pcDNA-NC, pcDNA-TCL6, pcDNA-VLDLR-AS1, pcDNA-RP11-356I2.4, and pcDNA-LINC00893) using the jetPRIME transfection reagent (Polyplus Transfection, Shanghai, China), according to the manufacturer's instructions.

Subsequently, transfected SKOV-3 and HO-8910 cells were made into cell suspensions and then transferred to a 96-well plate or upper chamber (with or without Matrigel) of 24-well transwell inserts (8 μm pore size). For the Cell Counting Kit-8 (CCK-8) assays, the old culture media were removed, and 10 μl cell counting kit-8 solution (MedChemExpress, China) with 90 μl media was added to each well for an additional 2 h on days 1–4. At the wavelength of 450 nm, the OD value of each well was detected by a spectrophotometer (Thermo Scientific, Massachusetts, America). For the transwell assays, the lower chambers were added with 500 μl medium containing 30% FBS. The bottoms of the upper chamber were fixed with 4% paraformaldehyde and stained with crystal violet for 10 min on day 1. The number of cells that invaded through the membrane to the lower surface was counted using Image J software after photographing using a microscope.

The experiments were conducted in triplicate, and each experiment was repeated three times. Statistical analysis was performed using GraphPad Prism version 8.0.1. The data were analyzed by Student's *t*-test or one-way analysis of variance (ANOVA). $P < 0.05$ was considered statistically significant.

TABLE 1 | The primer sequences in PCR analysis.

Symbol	Sequences (5′-3′)
hGAPDH-F	GTCAACGGATTTGGTCTGTATT
hGAPDH-R	AGTCTTCTGGGTGGCAGTGAT
hTCL6-F	ACCATCCCAAAGCCAACG
hTCL6-R	AAGTCATAAGGAACGGCATAAA
hVLDLR-AS1-F	TCATCACAGCATCCTTCACAGCC
hVLDLR-AS1-R	AACAAGCCACACTGACAGACCAT
hRP11-356I2.4-F	AGCCTTGTTGCCACGGAGAC
hRP11-356I2.4-R	ACGCATGACGCACAGAAGAGT
hLINC00893-F	GCTGCTCCTCACTCTCACTCCT
hLINC00893-R	CCTCTCCTCATCCGACCACAGA

RESULTS

To facilitate the understanding of our entire study, we created a flowchart, which is shown in **Figure 1**.

Screening Modules Related to Clinical Phenotype

After the difference analysis, a total of 1,467 upregulated mRNAs and 1,431 downregulated mRNAs were extracted (**Figure 2A**), and 307 lncRNAs expressed at high levels and 356 lncRNAs expressed at low levels were obtained (**Figure 2B**).

WGCNA analysis was further conducted based on 3,560 differentially expressed genes to screen modules related to clinical phenotypes. We assigned the β value to 7 when R^2 was first ∼0.85, which ensured that the network connection was close to the scale-free distribution and was the minimum threshold for smoothing the curve (**Figures 2C,D**). The modules with correlation coefficients >0.7 (the divergence coefficient was <0.3) were consolidated after clustering (**Figure 2E**). A total of seven modules (M1-yellow, M2-black, M3-green, M4-brown, M5-blue, M6-turquoise, and M7-gray) were integrated, and the gray module could not be gathered into other modules; hence, the gray module would not be considered in subsequent analysis (**Figure 2F**).

Two further methods were used to mine the modules associated with clinical phenotypes. First, the correlation between each module feature vector gene and the clinical phenotype

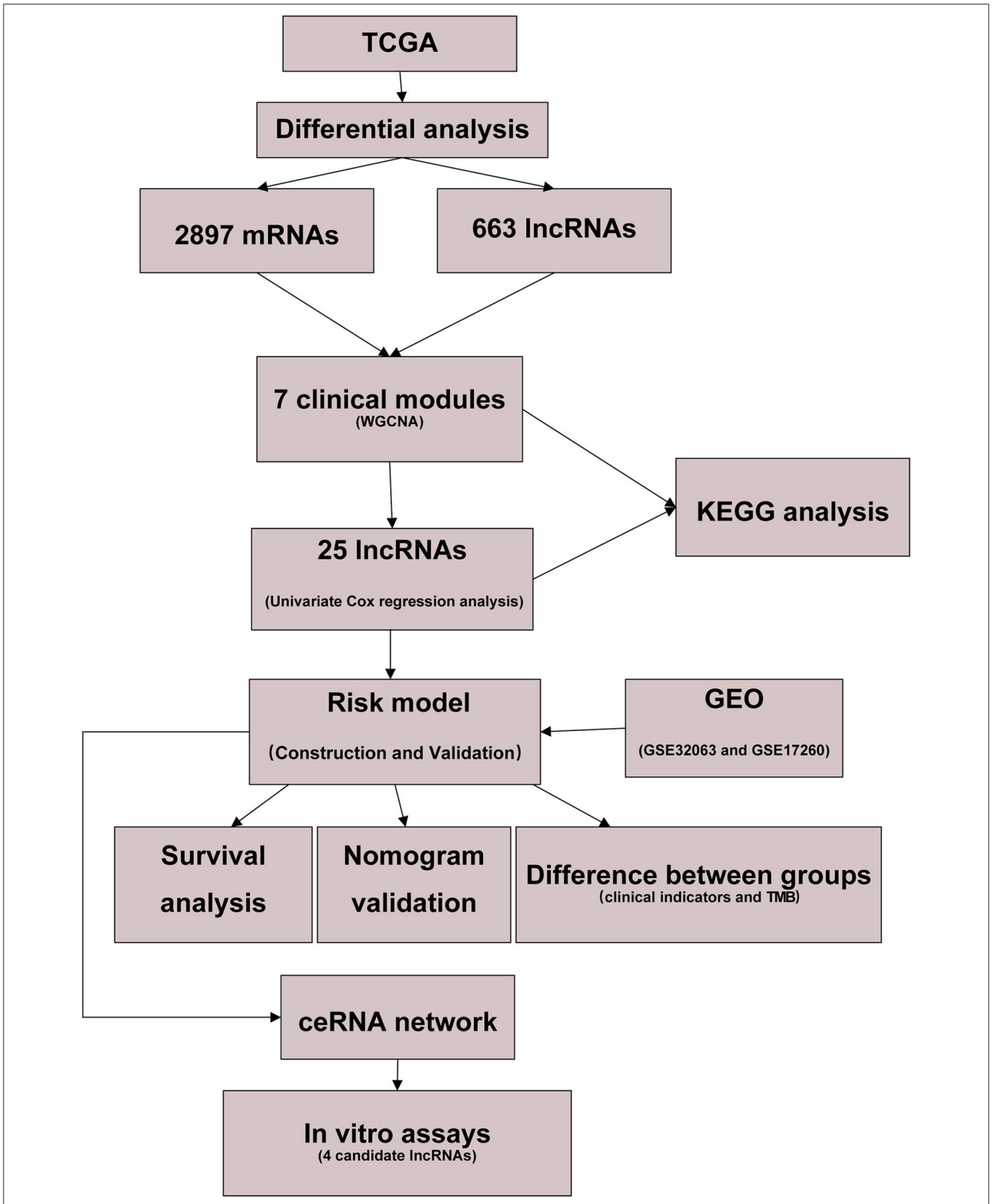

FIGURE 1 | Flow diagram of our study.

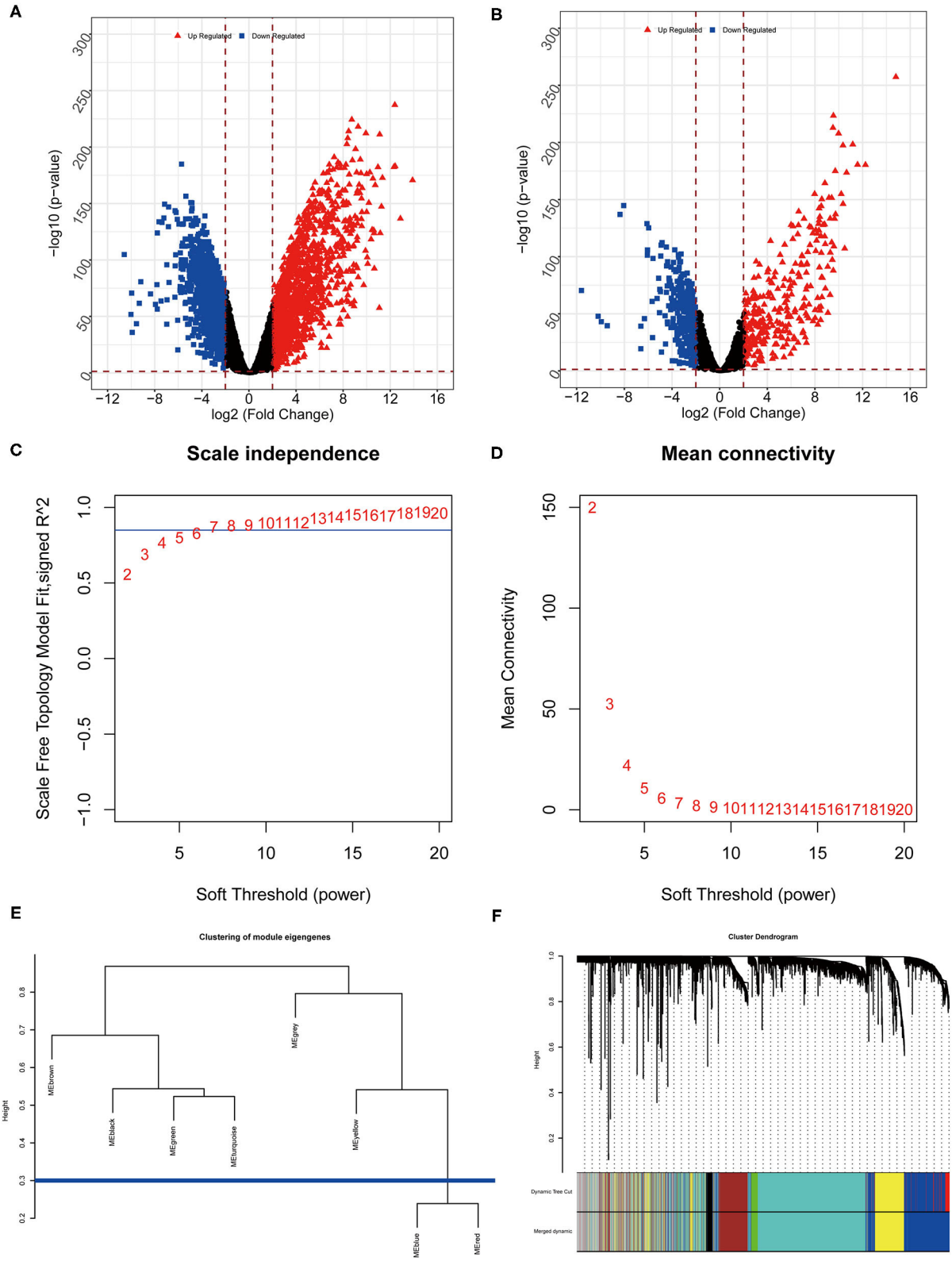

FIGURE 2 | Results of differential analysis and WGCNA. **(A)** Volcano map of differential mRNAs. **(B)** Volcano map of differential lncRNAs. **(C)** Selection graphs of β. **(D)** Schematic diagram of the mean connectivity. **(E)** The module clustering result diagram. The vertical axis represents the difference coefficient, and the blue line represents the difference coefficient of 0.3. **(F)** Systematic cluster tree of genes and gene modules generated by dynamic clipping method.

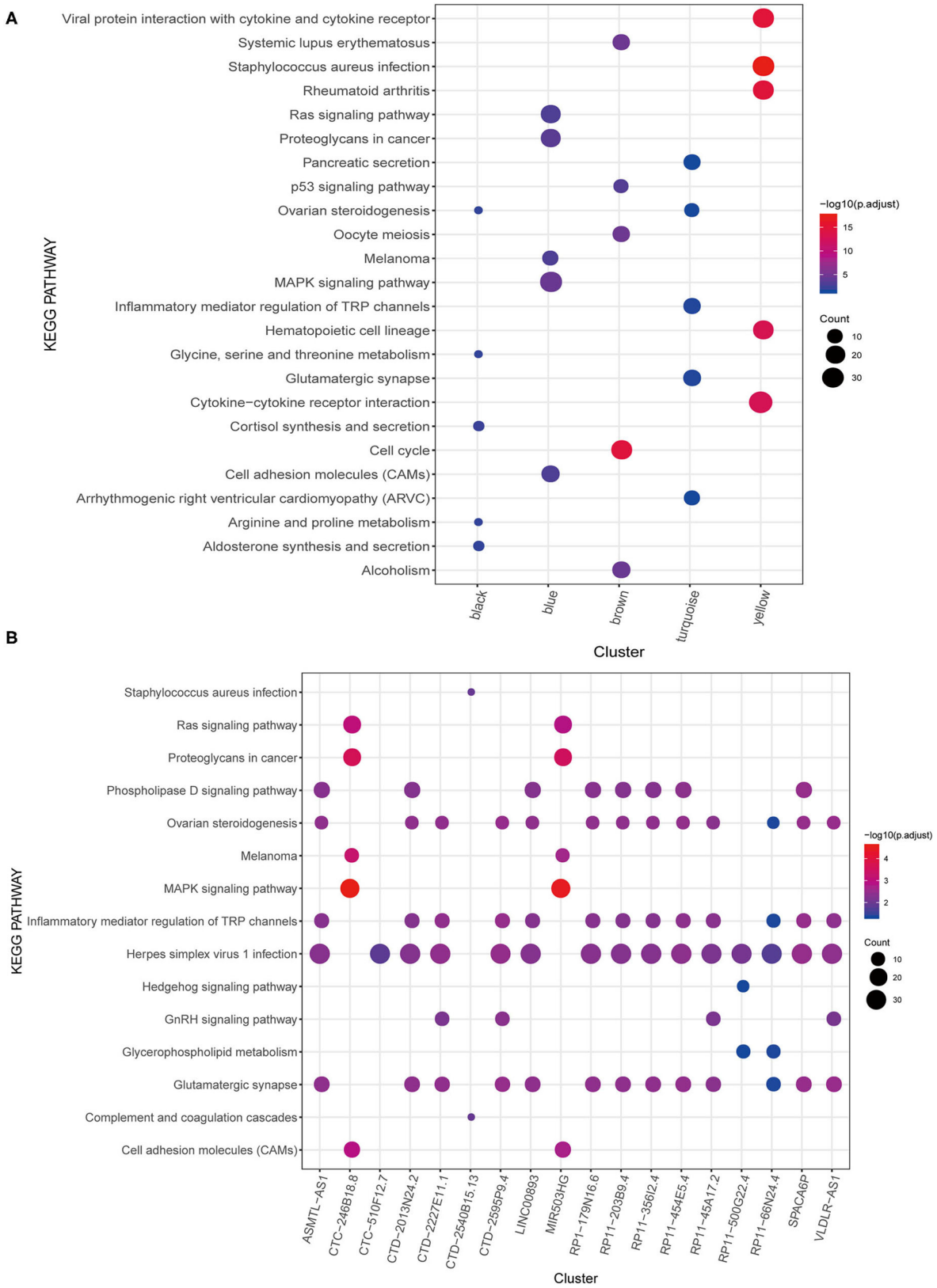

FIGURE 3 | KEGG pathway enrichment analysis. **(A)** WGCNA modules. **(B)** lncRNAs.

was calculated. The feature vector gene was the first principal component gene E of a specific module, which represents the overall level of gene expression in the module. Second, the absolute value of the correlation between gene expression in each module and the clinical phenotype was taken as the correlation between the module and the clinical phenotype (**Supplementary Figure 1**).

Furthermore, the mRNA in each module was subjected to KEGG pathway enrichment analysis, which showed that the black, blue, brown, turquoise, and yellow modules were significantly enriched in 13, 21, 11, 5, and 48 KEGG pathways. Nonetheless, no significant pathways were enriched in the green module. The KEGG pathway of each module was ranked according to the *P*-value, and the top five were selected for display (**Figure 3A**). Some of these modules are associated with important biological processes in tumor genesis and development, such as Ras signaling pathway and mitogen-activated protein kinase (MAPK) signaling pathway of the blue module, p53 signaling pathway of the brown module, and inflammatory mediator regulation of TRP channels in the turquoise module.

Construction and Validation of Risk Model

A total of 25 PALs that were significantly associated with OS were screened based on univariate Cox regression analysis, including one upregulated lncRNA (HR > 1) and 24 downregulated lncRNAs (HR < 1) (**Table 2**; **Supplementary Figure 2**). Among the 25 PALs, KEGG pathways were enriched to 19 lncRNAs, and the top five pathways were selected for display (**Figure 3B**). Some PALs were enriched in several classic signaling pathways of tumors, such as Ras signaling pathway, MAPK signaling pathway, Hedgehog signaling pathway, and so on. Interestingly, several lncRNAs were enriched in ovarian steroidogenesis or the GnRH signaling pathway (VLDLR-AS1, RP11-356I2.4, LINC00893, and so on) in OC.

Lasso regression was performed on the above 25 PALs to determine the optimal modeling parameter (λ) (**Figure 4A**). The two dashed lines indicate two special λ values: λ_{min} on the left and λ_{1se} on the right. The λ values between these two values was considered to be appropriate. The model constructed by λ_{1se} was the simplest, that is, it used a small number of genes, while λ_{min} had a higher accuracy rate and used a larger number of genes. Hence, λ_{min} was selected to build the model for accuracy in our study.

The final model contained seven PALs, namely, *CTD-2540B15.13*, *LINC00893*, *MIR503HG*, *RP11-356I2.4*, *RP11-386G11.10*, *TCL6*, and *VLDLR-AS1*. A total of 418 TCGA samples were divided into two risk groups, of which 201 were high risk (≥the optimal cut point) and 217 were low risk (<the optimal cutoff point). The results revealed that OS in the high-risk group was markedly lower than that in the low-risk

TABLE 2 | Kaplan–Meier survival analysis of 25 lncRNAs.

Gene	HR	Lower 0.95	Upper 0.95	*P*-value	Type	Moudle
CH507-254M2.2	0.89782612	0.84229443	0.95701896	0.00093768	down_lnc	brown
RP1-179N16.6	0.86639416	0.79455643	0.9447269	0.00116431	down_lnc	turquoise
CTD-2595P9.4	0.93999785	0.90293072	0.97858666	0.00257416	down_lnc	turquoise
RP11-386G11.10	0.92534363	0.87642424	0.97699356	0.00511256	down_lnc	blue
RP11-500G22.4	0.95173106	0.91827361	0.98640754	0.00673863	down_lnc	turquoise
RP11-356I2.4	0.86427736	0.77671338	0.96171302	0.0074451	down_lnc	turquoise
CTD-2227E11.1	0.9271007	0.87607788	0.98109509	0.00877255	down_lnc	turquoise
TCL6	0.94990532	0.9140781	0.98713678	0.0087936	down_lnc	brown
CTC-564N23.2	0.923453	0.8685364	0.98184193	0.01090358	down_lnc	yellow
LINC00893	0.89868222	0.82738124	0.97612767	0.01131416	down_lnc	turquoise
RP5-1180E21.5	0.96699305	0.94185858	0.99279825	0.0124944	down_lnc	turquoise
RP11-66N24.4	0.88211727	0.79714411	0.97614831	0.01522047	down_lnc	turquoise
RP11-454E5.4	0.87249941	0.78102511	0.97468725	0.01579247	down_lnc	turquoise
CTC-246B18.8	1.08022122	1.01397626	1.15079409	0.01685716	up_lnc	blue
MIR503HG	0.91727562	0.85356375	0.98574308	0.01872699	down_lnc	blue
CTD-2013N24.2	0.91086867	0.84264021	0.98462159	0.01876848	down_lnc	turquoise
RP13-39P12.3	0.91678305	0.85080369	0.98787908	0.02260895	down_lnc	turquoise
CTD-2540B15.13	0.89876543	0.81847421	0.9869331	0.02538823	down_lnc	yellow
CTC-510F12.7	0.90586195	0.83058035	0.98796687	0.02551983	down_lnc	turquoise
RP11-254F7.3	0.94196846	0.89291289	0.99371909	0.02846161	down_lnc	turquoise
VLDLR-AS1	0.92027511	0.85239314	0.99356299	0.03357438	down_lnc	turquoise
SPACA6P	0.88785293	0.79493949	0.9916262	0.03493912	down_lnc	turquoise
RP11-45A17.2	0.94046304	0.8881824	0.99582105	0.03542486	down_lnc	turquoise
RP11-203B9.4	0.88611018	0.79063991	0.99310854	0.03763039	down_lnc	turquoise
ASMTL-AS1	0.92770067	0.86065926	0.99996429	0.04989104	down_lnc	turquoise

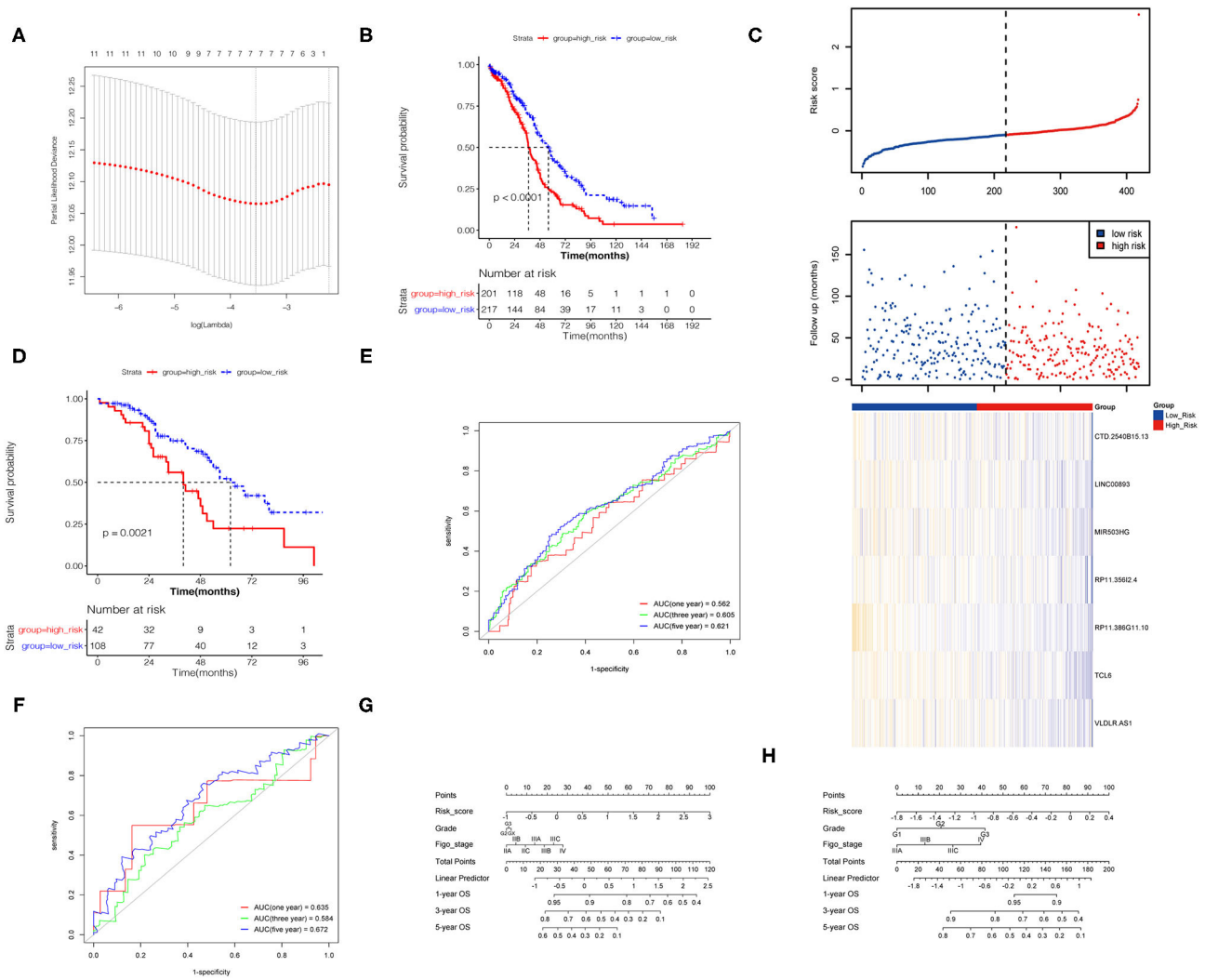

FIGURE 4 | Construction of the prognostic risk model. **(A)** The λ selection diagram in the Lasso model. **(B)** K–M survival curves of high- and low-risk groups for TCGA database. **(C)** Risk score distribution and lncRNA expression heat map for TCGA database. **(D)** K–M survival curves of high- and low-risk groups for GEO database. **(E,F)** Time-dependent receiver operating characteristic (ROC) curve for predicting OS of the risk model. **(G,H)** The nomogram based on the signature and clinical information.

TABLE 3 | Univariate and multivariate Cox analyses of risk signature in TCGA and GEO dataset.

Variables	Univariate			Multivariate		
	Coefficient	HR (95% CI)	*P*-value	Coefficient	HR (95% CI)	*P*-value
TCGA dataset						
Risk score	1.038	2.824 (1.98–4.026)	<0.001	0.887	2.427 (1.601–3.681)	<0.001
Age	0.023	1.023 (1.01–1.036)	0.001	0.024	1.024 (1.011–1.038)	<0.001
Grade	0.119	1.126 (0.786–1.614)	0.517	−0.011	0.989 (0.684–1.429)	0.952
Figo stage	0.178	1.195 (1.017–1.405)	0.031	0.169	1.184 (0.996–1.407)	0.056
GEO dataset						
Risk score	1.000	2.718 (1.173–6.3)	0.020	0.816	2.262 (0.96–5.328)	0.032
Grade	0.481	1.618 (1.122–2.335)	0.010	0.373	1.452 (0.987–2.136)	0.058
Figo stage	0.313	1.368 (0.953–1.963)	0.090	0.236	1.267 (0.859–1.868)	0.233

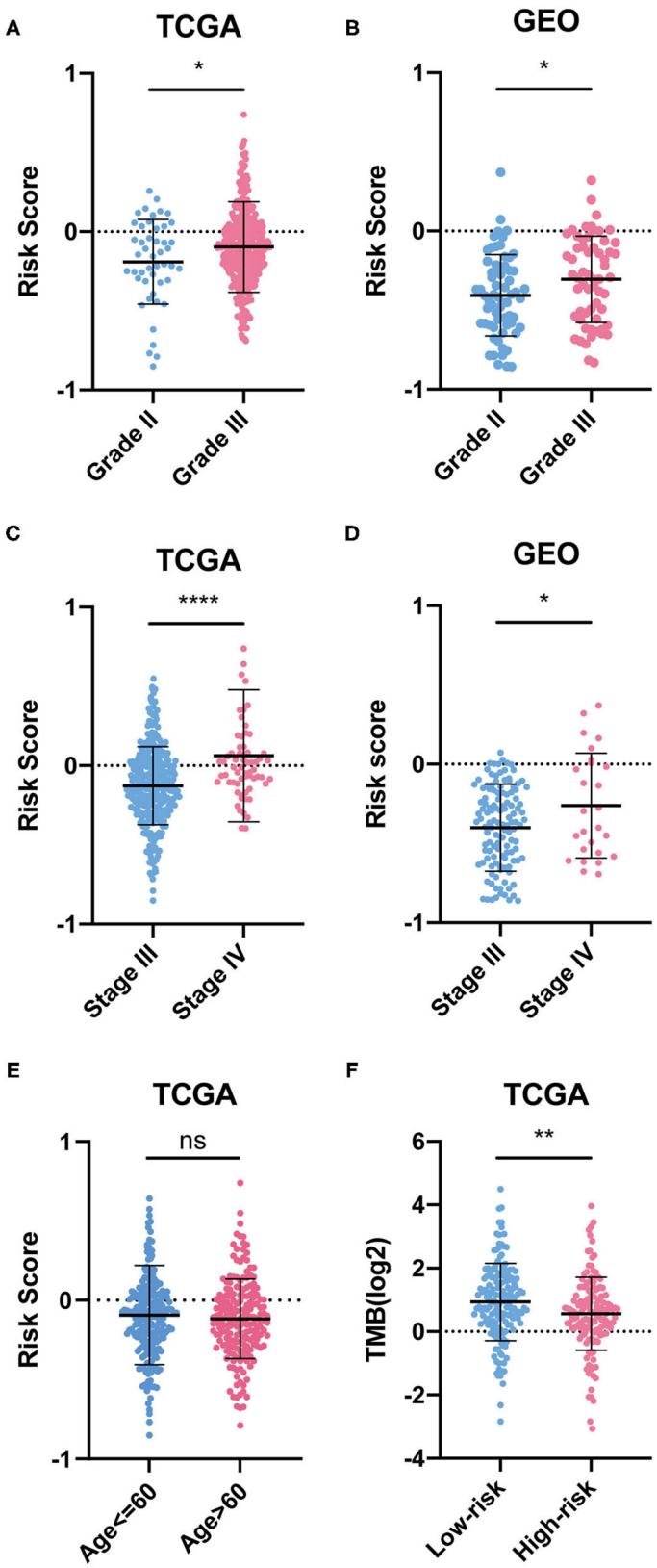

FIGURE 5 | Difference between groups. **(A–E)** Risk scores of clinical indicators. **(F)** TMB between risk groups.

group (**Figure 4B**). The heat map and RS distribution map of seven lncRNA expression values in each sample were drawn as shown in **Figure 4C**, which showed that the lower the expression level of the seven PALs, the higher the RS and the shorter survival time. Two GEO datasets were utilized to verify the risk model according to the same method described above, and the K–M curve proved the validity of the model constructed by the seven PALs in survival prediction (**Figure 4D**).

Univariate and multivariate Cox regression analyses of risk model, grade, Figo stage, and age for TCGA and GEO datasets demonstrated that the risk model was an independent risk factor for OC patients (**Table 3**). The 1-, 3-, and 5-year survival ROC curves predicted by the risk model were drawn (**Figures 4E,F**). To better predict prognosis at 1-, 3-, and 5-year OS of OC patients, we constructed a nomogram of variables such as the risk score, grade, and Figo stage (**Figures 4G,H**).

We also found that OC patients with grade III and stage IV OC had higher RSs, while RS was not related to age (**Figures 5A–E**). As for TMB, OC patients in the low-risk group had lower TMB scores, which indicated that they may be more likely to respond to immunotherapy (**Figure 5F**).

Construction of a PAL-Associated ceRNA Network

We predicted 19,630 miRNA–mRNA pairs and 129 PAL–miRNA relationship pairs. PALs and mRNAs that were regulated by the same miRNA were screened, and the positively coexpressed PAL–mRNA pairs were combined. Finally, 347 PAL–miRNA–mRNA relationship pairs were obtained, including 5 PALs (*TCL6*, *VLDLR-AS1*, *RP11-356I2.4*, *LINC00893*, and *MIR503HG*), 70 miRNAs, and 199 mRNAs (**Figure 6**). There were 71 PAL–miRNA relationship pairs, 341 miRNA–mRNA relationship pairs, and 242 PAL–mRNA coexpression relationships in the ceRNA network, which could be used to explore the molecular mechanisms involved in the development of OC.

In vitro Assays

Among the five PALs in the ceRNA network we constructed, the functions of lncRNA MIR503HG involved in OC have been investigated (Zhu et al., 2020); hence, the remaining four PALs were preliminarily selected as candidate molecules to perform cell function assays *in vitro*. Analysis of TCGA dataset (418 OC samples), GSE32063 (40 OC samples), GSE17260 (110 OC samples), and our cohort (33 OC samples) showed that the four PALs were evidently downregulated in OC tissues when compared with normal controls (**Figures 7A–P**). The expression of the four PALs in three OC cell lines (SKOV-3, HO8910, and A2780) and the normal ovarian epithelial cell line IOSE-80 was detected. As shown in **Figures 8A–D**, the expression of the four PALs was significantly lower in OC cells than in IOSE-80 cells ($p < 0.05$).

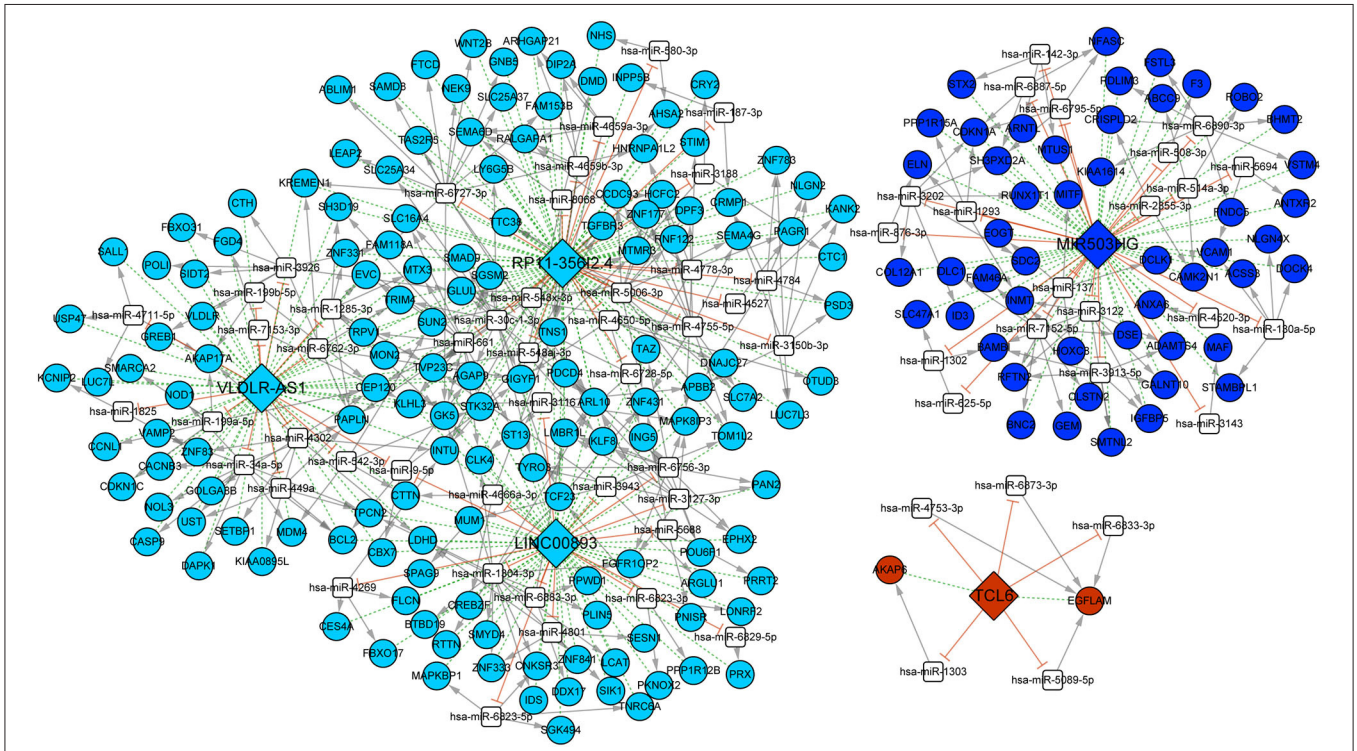

FIGURE 6 | ceRNA network of five PALs. Different colors represented different modules. Diamonds represented lncRNAs, circles represented mRNAs, and white squares represented predicted miRNAs. Dotted green lines represented coexpression of lncRNAs and mRNAs, gray arrows represented miRNA regulated mRNAs, and orange T-shaped lines represented competing binding mRNAs.

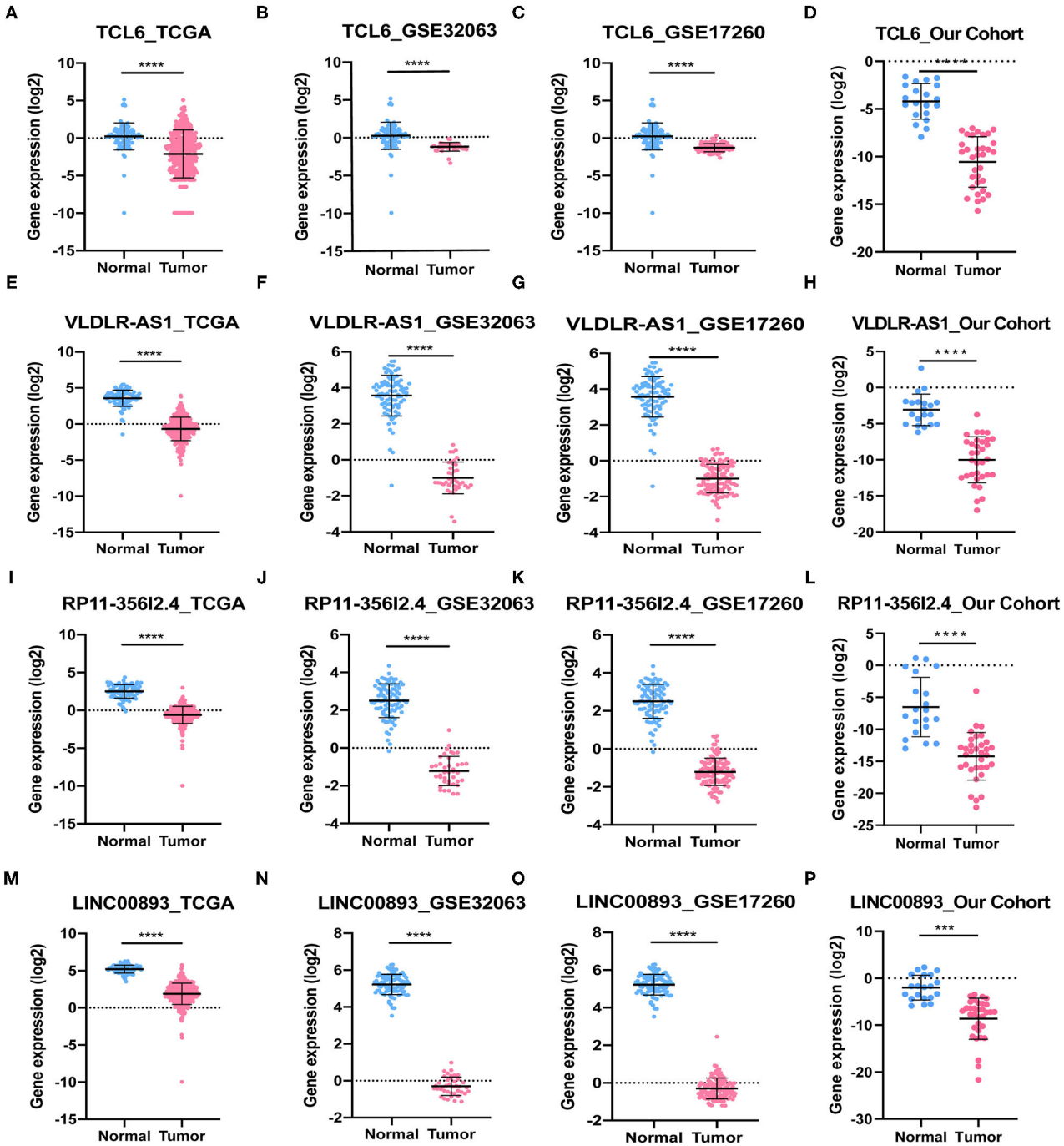

FIGURE 7 | The expression of four PALs in normal and OC samples. **(A–D)** TCL6. **(E–H)** VLDLR-AS1. **(I–L)** RP11-356I2.4. **(M–P)** LINC00893. ****$P < 0.0001$. ***$P < 0.001$.

The K–M survival curves confirmed that higher expression of the four PALs was associated with better OS, which indicated that they may serve as tumor suppressor genes for OC (**Supplementary Figure 2**). Subsequently, we confirmed that the expression levels of the four PALs increased following plasmid transfection in SKOV-3 and HO-8910 cells (**Figures 8E–H**). Later, data from the CCK-8 assay illustrated that overexpression of TCL6, RP11-356I2.4, and LINC00893 reduced the viability of OC cells (**Figures 9A,B**). Nevertheless, the proliferative abilities of SKOV-3 and HO-8910 cells increased after VLDLR-AS1 overexpression (**Figures 9A,B**). In addition, the number of migrated and invaded OC cells declined with

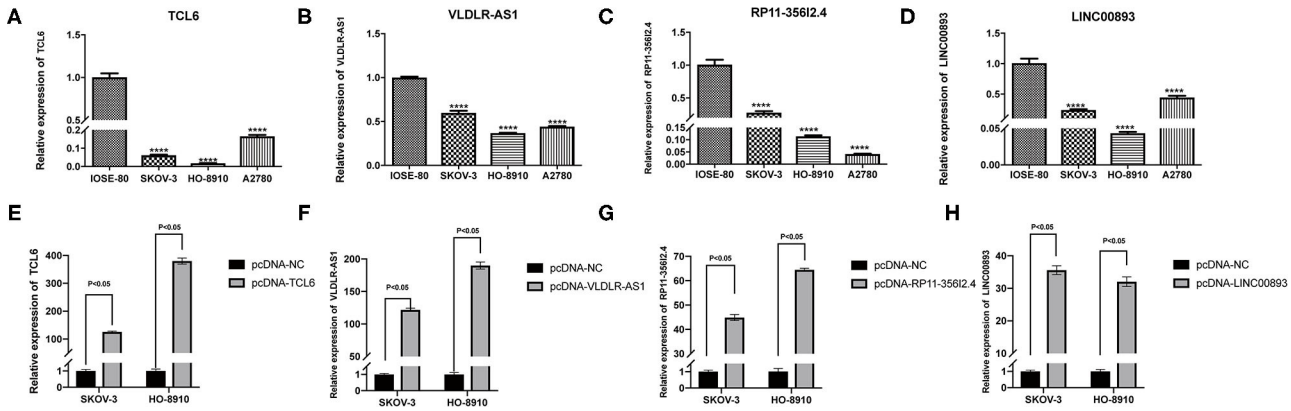

FIGURE 8 | (A–D) The expression of four candidate PALs in IOSE-80 and OC cells. **(E–H)** The expression level of four candidate PALs under SKOV-3 and HO-8910 transfection.

the overexpression of TCL6, RP11-356I2.4, and LINC00893, according to data from transwell assays (**Figures 9C–H**). On the contrary, overexpression of VLDLR-AS1 increased the invasive and metastatic abilities of SKOV-3 and HO-8910 cells (**Figures 9C–H**).

DISCUSSION

Recent studies have shown that lncRNAs play an important role in regulating the growth, division, metastasis, invasion, proliferation, and drug resistance of OC cells (Braga et al., 2020). Abnormal expression of some lncRNAs in OC may provide important reference information for the diagnosis, treatment, and prognosis of patients (Salamini-Montemurri et al., 2020). However, compared with miRNA, the study of lncRNAs for OC is still in its infancy (Razavi et al., 2021). Therefore, it is necessary to further study lncRNAs in OC. Previous studies have inspired us to explore potential prognosis-associated lncRNAs in OC.

WGCNA is the most representative systems biology algorithm based on transcriptome data to construct gene coexpression networks (Zhang and Horvath, 2005; Langfelder and Horvath, 2008). Using WGCNA, information on gene expression in biological systems can be analyzed quantitatively and at different levels. Although previous studies have applied WGCNA to established an lncRNA-associated signature in malignant tumors (Gong and Ning, 2020; Han P. et al., 2020; Li et al., 2020; Tian et al., 2021; Yuan et al., 2021), research on its application in OC is sparse. In our study, seven stable modules with highly correlated 3,560 genes and correlations with specific clinical factors were clustered. The prognostic risk model based on seven PALs could divide OC patients into two risk groups according to optimal cutoff point, which was validated using two datasets from GEO. After construction of the ceRNA network, four PALs (*TCL6*, *VLDLR-AS1*, *RP11-356I2.4*, and *LINC00893*) in the network were selected for further cell function assays. In the WGCNA analysis, *TCL6* was gathered into the brown module, and *VLDLR-AS1*, *RP11-356I2.4*, and *LINC00893* were gathered into the turquoise module. Therefore, *TCL6* may be related to the clinical stage and histological grade of OC. Meanwhile, *VLDLR-AS1*, *RP11-356I2.4*, and *LINC00893* may be associated with the clinical stage. The KEGG pathway of coexpression analysis showed that three PALs were enriched in several biological functions of OC, such as glutamatergic synapse, inflammatory mediator regulation of TRP channels, and ovarian steroidogenesis, which indicated their potential therapeutic targets.

A previous study revealed that lncRNA *miR503HG* was downregulated in OC, and downregulation of *miR503HG* predicted poor survival of OC patients (Zhu et al., 2020), which coincided with *miR503HG* in our prognostic risk model signature. Coincidentally, the expression of *MIR503HG* was decreased in colon cancer (Chuo et al., 2019; Han H. et al., 2020), triple-negative breast cancer (Fu et al., 2019; Tuluhong et al., 2020), non-small cell lung cancer (Lin et al., 2019; Dao et al., 2020; Xu et al., 2020), cervical squamous cell carcinoma (Zhao et al., 2020), bladder cancer (Qiu et al., 2019), and hepatocellular carcinoma (Wang et al., 2018). *MIR503HG* was also proved to serve as a tumor suppressor in *in vivo* experiment. *TCL6* had been demonstrated to be a potential tumor suppressor in breast cancer (Zhang et al., 2020), hepatocellular carcinoma (Luo et al., 2020), renal cell carcinoma (Yang et al., 2018; Kulkarni et al., 2021), and B-cell acute lymphoblastic leukemia (Cuadros et al., 2019). Overexpression of *TCL6* in corresponding cancer cell lines impairs their oncogenic functions, such as cell proliferation and migration/invasion. *RP11-356I2.4* (also known as *WAKMAR2*, *lnc-TNFAIP3*, or *LOC100130476*) has been shown to act as a tumor suppressor gene in esophageal cancer and gastric cardia adenocarcinoma. In addition, upregulation of *RP11-356I2.4* led to the inhibition of proliferation and invasiveness of cancer cells (Guo et al., 2016a,b). *LINC00893* was lowly expressed in thyroid carcinoma tissues and papillary thyroid cancer (PTC) cells. Furthermore, *LINC00893* overexpression abrogated the proliferation and migration abilities of PTC cells (Li et al., 2021). In our prognostic risk model signature, lncRNA *TCL6*,

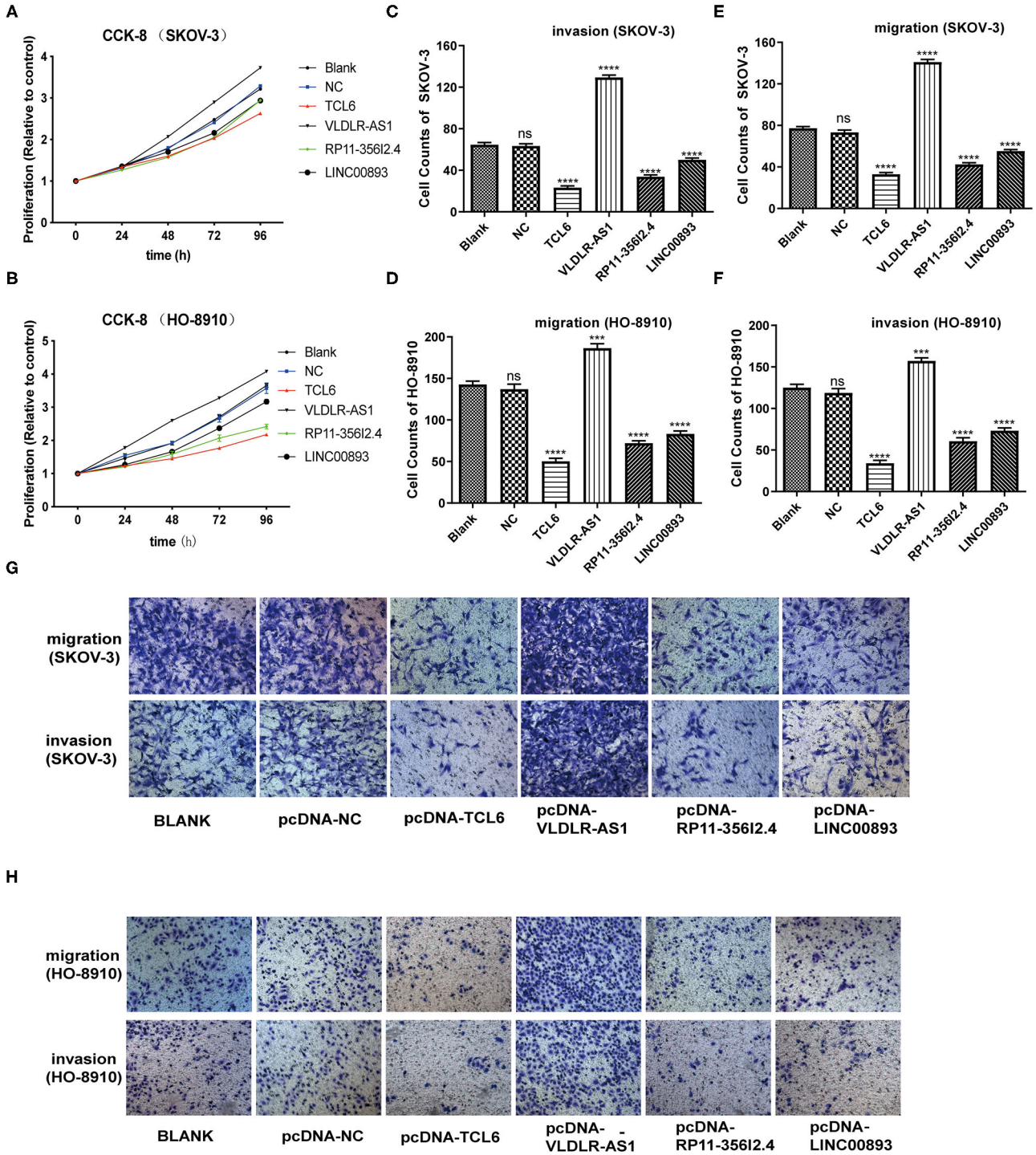

FIGURE 9 | CCK-8 and transwell assays. **(A)** CCK-8 assays of transfected SKOV-3. **(B)** CCK-8 assays of transfected HO-8910 cells. **(C–H)** Transwell assays of transfected SKOV-3 or HO-8910 cells.

RP11-356I2.4, and *LINC00893* were all downregulated in OC cells and tissues. In addition, downregulation of these genes indicated poor OS in patients with OC. Through gain-of-function assays, we determined that the overexpression of the three PALs restrained the proliferation and migration abilities of OC cells, which would fill the gap in their study in OC. Hence, these three molecules are also tumor suppressor genes for OC, suggesting their potential as biomarkers and therapeutic targets. Previous studies and our cell function assays further illustrate the accuracy of our risk score model. However,

more in-depth molecular mechanisms are yet to be studied by subsequent researchers.

Although lncRNA *VLDLR-AS1* was downregulated and downregulation of VLDLR-AS1 indicated poor survival in OC, *VLDLR-AS1* seemed to be an oncogene in terms of OC cellular function. Previous studies showed that *VLDLR-AS1* is highly expressed in esophageal squamous cell carcinoma (Chen et al., 2019) and hepatocellular carcinoma (HCC) (Yang et al., 2017). Knocking down the expression of *VLDLR-AS1* inhibited the proliferation of HCC cells, which was consistent with our cell function assays. The differences in *VLDLR-AS1* expression were not consistent with the cell function experiment in OC, which is worthy of further study by subsequent researchers.

There are some limitations to our study. First, there were only 33 OC patients without OS in our cohort; hence, more time and more samples are needed for follow-up. Second, the cell function assays of four candidate lncRNAs were preliminary, which requires further investigation to provide a better understanding.

CONCLUSIONS

In summary, we performed weighted gene coexpression analysis on differentially expressed genes obtained from datasets to screen for modules related to clinical phenotypes and established a seven-PAL-based signature with a prognostic value for OC, which could stratify OC patients into two risk groups with significant differences in prognosis. Two additional datasets were used to verify the accuracy of the model. Meanwhile, four candidate PALs were selected to perform cell function assays, which need further studies of subsequent researchers.

DATA AVAILABILITY STATEMENT

The datasets presented in this study can be found in online repositories. The names of the repository/repositories and accession number(s) can be found in the article/**Supplementary Material**.

ETHICS STATEMENT

The studies involving human participants were reviewed and approved by Affiliated Hangzhou Hospital of Nanjing Medical University. The patients/participants provided their written informed consent to participate in this study.

AUTHOR CONTRIBUTIONS

JT and ZZ conceived, designed, and supervised the study. JZ performed data analysis and drafted the manuscript. JG helped revise the manuscript. GX, HZ, and BC collected the data. All the authors reviewed and approved the final manuscript.

FUNDING

This work was supported by the Research Fund of China National Health Commission (grant number WKJ-ZJ-2010), Medical Scientific Research Foundation of Zhejiang Province (grant number 2019KY495), National Natural Science Foundation of China (grant number 31900922), and WU JIEPING MEDICAL FOUNDATION (grant number 320.6750.2020-04-13).

SUPPLEMENTARY MATERIAL

The Supplementary Material for this article can be found online at: https://www.frontiersin.org/articles/10.3389/fgene.2021.672674/full#supplementary-material

Supplementary Figure 1 | Correlation analysis results between WGCNA modules and clinical phenotypes. **(A)** The upper number represented the correlation coefficient, and the lower bracket number represented the significance *P*-value. The modules related to clinical phenotype were mined. **(B)** Age at initial pathologic diagnosis. **(C)** Clinical stage. **(D)** Lymphatic invasion. **(E)** Neoplasm histologic grade. **(F)** Tumor residual disease. **(G)** Venous invasion. **(H)** Vital status.

Supplementary Figure 2 | K-M survival curves of 24 lncRNAs.

Supplementary Table 1 | Baseline characteristic of patients with ovarian cancer.

REFERENCES

Barrett, T., Suzek, T. O., Troup, D. B., Wilhite, S. E., Ngau, W. C., Ledoux, P., et al. (2005). NCBI GEO: mining millions of expression profiles–database and tools. *Nucleic Acids Res.* 33, D562–D566. doi: 10.1093/nar/gki022

Braga, E. A., Fridman, M. V., Moscovtsev, A. A., Filippova, E. A., Dmitriev, A. A., and Kushlinskii, N. E. (2020). LncRNAs in ovarian cancer progression, metastasis, and main pathways: ceRNA and alternative mechanisms. *Int. J. Mol. Sci.* 21:8855. doi: 10.3390/ijms21228855

Chen, G. Y., Zhang, Z. S., Chen, Y., and Li, Y. (2021). Long non-coding RNA SNHG9 inhibits ovarian cancer progression by sponging microRNA-214-5p. *Oncol. Lett.* 21:80. doi: 10.3892/ol.2020.12341

Chen, J., Li, X., Yang, L., and Zhang, J. (2020). Long Non-coding RNA LINC01969 promotes ovarian cancer by regulating the miR-144-5p/LARP1 axis as a competing endogenous RNA. *Front. Cell Dev. Biol.* 8:625730. doi: 10.3389/fcell.2020.595585

Chen, Y., Liu, L., Li, J., Du, Y., Wang, J., and Liu, J. (2019). Effects of long noncoding RNA (linc-VLDLR) existing in extracellular vesicles on the occurrence and multidrug resistance of esophageal cancer cells. *Pathol. Res. Pract.* 215, 470–477. doi: 10.1016/j.prp.2018.12.033

Chuo, D., Liu, F., Chen, Y., and Yin, M. (2019). LncRNA MIR503HG is downregulated in Han Chinese with colorectal cancer and inhibits cell migration and invasion mediated by TGF-β2. *Gene* 713:143960. doi: 10.1016/j.gene.2019.143960

Cintolo-Gonzalez, J. A., Braun, D., Blackford, A. L., Mazzola, E., Acar, A., Plichta, J. K., et al. (2017). Breast cancer risk models: a comprehensive overview of existing models, validation, and clinical applications. *Breast Cancer Res. Treat.* 164, 263–284. doi: 10.1007/s10549-017-4247-z

Cuadros, M., Andrades, Á., Coira, I. F., Baliñas, C., Rodríguez, M. I., Álvarez-Pérez, J. C., et al. (2019). Expression of the long non-coding RNA TCL6 is associated with clinical outcome in pediatric B-cell acute lymphoblastic leukemia. *Blood Cancer J.* 9:93. doi: 10.1038/s41408-019-0258-9

Dao, R., Wudu, M., Hui, L., Jiang, J., Xu, Y., Ren, H., et al. (2020). Knockdown of lncRNA MIR503HG suppresses proliferation and promotes apoptosis of non-small cell lung cancer cells by regulating miR-489-3p and miR-625-5p. *Pathol. Res. Pract.* 216:152823. doi: 10.1016/j.prp.2020.152823

Eisenhauer, E. A. (2017). Real-world evidence in the treatment of ovarian cancer. *Ann. Oncol.* 28(Suppl. 8), viii61–viii65. doi: 10.1093/annonc/mdx443

Engebretsen, S., and Bohlin, J. (2019). Statistical predictions with glmnet. *Clin. Epigenetics* 11:123. doi: 10.1186/s13148-019-0730-1

Fu, J., Dong, G., Shi, H., Zhang, J., Ning, Z., Bao, X., et al. (2019). LncRNA MIR503HG inhibits cell migration and invasion via miR-103/OLFM4 axis in triple negative breast cancer. *J. Cell. Mol. Med.* 23, 4738–4745. doi: 10.1111/jcmm.14344

Goldman, M. J., Craft, B., Hastie, M., Repečka, K., McDade, F., Kamath, A., et al. (2020). Visualizing and interpreting cancer genomics data via the Xena platform. *Nat. Biotechnol.* 38, 675–678. doi: 10.1038/s41587-020-0546-8

Gong, X., and Ning, B. (2020). Five lncRNAs associated with prostate cancer prognosis identified by coexpression network analysis. *Technol. Cancer Res. Treat.* 19:1533033820963578. doi: 10.1177/1533033820963578

Guo, W., Dong, Z., Shi, Y., Liu, S., Liang, J., Guo, Y., et al. (2016a). Aberrant methylation-mediated downregulation of long noncoding RNA LOC100130476 correlates with malignant progression of esophageal squamous cell carcinoma. *Dig. Liver Dis.* 48, 961–969. doi: 10.1016/j.dld.2016.05.010

Guo, W., Dong, Z., Shi, Y., Liu, S., Liang, J., Guo, Y., et al. (2016b). Methylation-mediated downregulation of long noncoding RNA LOC100130476 in gastric cardia adenocarcinoma. *Clin. Exp. Metastasis* 33, 497–508. doi: 10.1007/s10585-016-9794-x

Han, H., Li, H., and Zhou, J. (2020). Long non-coding RNA MIR503HG inhibits the proliferation, migration, and invasion of colon cancer cells via miR-107/Par4 axis. *Exp. Cell Res.* 395:112205. doi: 10.1016/j.yexcr.2020.112205

Han, P., Yang, H., Li, X., Wu, J., Wang, P., Liu, D., et al. (2020). Identification of a novel cancer stemness-associated ceRNA axis in lung adenocarcinoma via stemness indices analysis. *Oncol. Res.* doi: 10.3727/096504020X16037124605559. [Epub ahead of print].

Harrow, J., Frankish, A., Gonzalez, J. M., Tapanari, E., Diekhans, M., Kokocinski, F., et al. (2012). GENCODE: the reference human genome annotation for The ENCODE Project. *Genome Res.* 22, 1760–1774. doi: 10.1101/gr.135350.111

Hsu, S. D., Lin, F. M., Wu, W. Y., Liang, C., Huang, W. C., Chan, W. L., et al. (2011). miRTarBase: a database curates experimentally validated microRNA-target interactions. *Nucleic Acids Res.* 39, D163–D169. doi: 10.1093/nar/gkq1107

Kaldawy, A., Segev, Y., Lavie, O., Auslender, R., Sopik, V., and Narod, S. A. (2016). Low-grade serous ovarian cancer: a review. *Gynecol. Oncol.* 143, 433–438. doi: 10.1016/j.ygyno.2016.08.320

Kohl, M., Wiese, S., and Warscheid, B. (2011). Cytoscape: software for visualization and analysis of biological networks. *Methods Mol. Biol.* 696, 291–303. doi: 10.1007/978-1-60761-987-1_18

Kopp, F., and Mendell, J. T. (2018). Functional classification and experimental dissection of long noncoding RNAs. *Cell* 172, 393–407. doi: 10.1016/j.cell.2018.01.011

Kulkarni, P., Dasgupta, P., Hashimoto, Y., Shiina, M., Shahryari, V., Tabatabai, Z. L., et al. (2021). A lncRNA TCL6-miR-155 interaction regulates the Src-Akt-EMT network to mediate kidney cancer progression and metastasis. *Cancer Res.* 81, 1500–1512. doi: 10.1158/0008-5472.CAN-20-0832

Langfelder, P., and Horvath, S. (2008). WGCNA: an R package for weighted correlation network analysis. *BMC Bioinformatics* 9:559. doi: 10.1186/1471-2105-9-559

Li, J., Zhou, J., Kai, S., Wang, C., Wang, D., and Jiang, J. (2020). Network-based coexpression analysis identifies functional and prognostic long noncoding RNAs in hepatocellular carcinoma. *Biomed Res. Int.* 2020:1371632. doi: 10.1155/2020/1371632

Li, N., and Zhan, X. (2019). Identification of clinical trait-related lncRNA and mRNA biomarkers with weighted gene co-expression network analysis as useful tool for personalized medicine in ovarian cancer. *EPMA J.* 10, 273–290. doi: 10.1007/s13167-019-00175-0

Li, S., Zhang, Y., Dong, J., Li, R., Yu, B., Zhao, W., et al. (2021). LINC00893 inhibits papillary thyroid cancer by suppressing AKT pathway via stabilizing PTEN. *Cancer Biomark.* 30, 277–286. doi: 10.3233/CBM-190543

Lin, H., Li, P., Zhang, N., Cao, L., Gao, Y. F., and Ping, F. (2019). Long non-coding RNA MIR503HG serves as a tumor suppressor in non-small cell lung cancer mediated by wnt1. *Eur. Rev. Med. Pharmacol. Sci.* 23, 10818–10826. doi: 10.26355/eurrev_201912_19785

Luo, L. H., Jin, M., Wang, L. Q., Xu, G. J., Lin, Z. Y., Yu, D. D., et al. (2020). Long noncoding RNA TCL6 binds to miR-106a-5p to regulate hepatocellular carcinoma cells through PI3K/AKT signaling pathway. *J. Cell. Physiol.* 235, 6154–6166. doi: 10.1002/jcp.29544

Paraskevopoulou, M. D., Vlachos, I. S., Karagkouni, D., Georgakilas, G., Kanellos, I., Vergoulis, T., et al. (2016). DIANA-LncBase v2: indexing microRNA targets on non-coding transcripts. *Nucleic Acids Res.* 44, D231–D238. doi: 10.1093/nar/gkv1270

Qiu, F., Zhang, M. R., Zhou, Z., Pu, J. X., and Zhao, X. J. (2019). lncRNA MIR503HG functioned as a tumor suppressor and inhibited cell proliferation, metastasis and epithelial-mesenchymal transition in bladder cancer. *J. Cell. Biochem.* 120, 10821–10829. doi: 10.1002/jcb.28373

Razavi, Z. S., Tajiknia, V., Majidi, S., Ghandali, M., Mirzaei, H. R., Rahimian, N., et al. (2021). Gynecologic cancers and non-coding RNAs: epigenetic regulators with emerging roles. *Crit. Rev. Oncol. Hematol.* 157:103192. doi: 10.1016/j.critrevonc.2020.103192

Ritchie, M. E., Phipson, B., Wu, D., Hu, Y., Law, C. W., Shi, W., et al. (2015). limma powers differential expression analyses for RNA-sequencing and microarray studies. *Nucleic Acids Res.* 43:e47. doi: 10.1093/nar/gkv007

Salamini-Montemurri, M., Lamas-Maceiras, M., Barreiro-Alonso, A., Vizoso-Vázquez, Á., Rodríguez-Belmonte, E., Quindós-Varela, M., et al. (2020). The challenges and opportunities of LncRNAs in ovarian cancer research and clinical use. *Cancers (Basel)* 12:1020. doi: 10.3390/cancers12041020

Stewart, C., Ralyea, C., and Lockwood, S. (2019). Ovarian cancer: an integrated review. *Semin. Oncol. Nurs.* 35, 151–156. doi: 10.1016/j.soncn.2019.02.001

Sun, Q., Zhao, H., Zhang, C., Hu, T., Wu, J., Lin, X., et al. (2017). Gene co-expression network reveals shared modules predictive of stage and grade in serous ovarian cancers. *Oncotarget* 8, 42983–42996. doi: 10.18632/oncotarget.17785

Tammemägi, M. C., Ten Haaf, K., Toumazis, I., Kong, C. Y., Han, S. S., Jeon, J., et al. (2019). Development and validation of a multivariable lung cancer risk prediction model that includes low-dose computed tomography screening results: a secondary analysis of data From the national lung screening trial. *JAMA Netw. Open* 2:e190204. doi: 10.1001/jamanetworkopen.2019.0204

Tian, F., Zhao, J., Fan, X., and Kang, Z. (2017). Weighted gene co-expression network analysis in identification of metastasis-related genes of lung squamous cell carcinoma based on the Cancer Genome Atlas database. *J. Thorac. Dis.* 9, 42–53. doi: 10.21037/jtd.2017.01.04

Tian, S., Zhang, M., and Ma, Z. (2021). An edge-based statistical analysis of long non-coding RNA expression profiles reveals a negative association between Parkinson's disease and colon cancer. *BMC Med. Genomics* 14:36. doi: 10.1186/s12920-021-00882-6

Tuluhong, D., Dunzhu, W., Wang, J., Chen, T., Li, H., Li, Q., et al. (2020). Prognostic value of differentially expressed lncrnas in triple-negative breast cancer: a systematic review and meta-analysis. *Crit. Rev. Eukaryot. Gene Expr.* 30, 447–456. doi: 10.1615/CritRevEukaryotGeneExpr.2020035836

Van Cott, C. (2020). Cancer genetics. *Surg. Clin. North Am.* 100, 483–498. doi: 10.1016/j.suc.2020.02.012

Wang, H., Liang, L., Dong, Q., Huan, L., He, J., Li, B., et al. (2018). Long noncoding RNA miR503HG, a prognostic indicator, inhibits tumor metastasis by regulating the HNRNPA2B1/NF-κB pathway in hepatocellular carcinoma. *Theranostics* 8, 2814–2829. doi: 10.7150/thno.23012

Wang, J. Y., Lu, A. Q., and Chen, L. J. (2019). LncRNAs in ovarian cancer. *Clin. Chim. Acta* 490, 17–27. doi: 10.1016/j.cca.2018.12.013

Xu, S., Zhai, S., Du, T., and Li, Z. (2020). LncRNA MIR503HG inhibits non-small cell lung cancer cell proliferation by inducing cell cycle arrest through the downregulation of cyclin D1. *Cancer Manag. Res.* 12, 1641–1647. doi: 10.2147/CMAR.S227348

Yang, K., Lu, X. F., Luo, P. C., and Zhang, J. (2018). Identification of six potentially long noncoding RNAs as biomarkers involved competitive endogenous RNA in clear cell renal cell carcinoma. *Biomed Res. Int.* 2018:9303486. doi: 10.1155/2018/9303486

Yang, N., Li, S., Li, G., Zhang, S., Tang, X., Ni, S., et al. (2017). The role of extracellular vesicles in mediating progression, metastasis and potential treatment of hepatocellular carcinoma. *Oncotarget* 8, 3683–3695. doi: 10.18632/oncotarget.12465

Yoshihara, K., Tajima, A., Yahata, T., Kodama, S., Fujiwara, H., Suzuki, M., et al. (2010). Gene expression profile for predicting survival in advanced-stage serous ovarian cancer across two independent datasets. *PLoS ONE* 5:e9615. doi: 10.1371/journal.pone.0009615

Yoshihara, K., Tsunoda, T., Shigemizu, D., Fujiwara, H., Hatae, M., Fujiwara, H., et al. (2012). High-risk ovarian cancer based on 126-gene expression signature is uniquely characterized by downregulation of antigen presentation pathway. *Clin. Cancer Res.* 18, 1374–1385. doi: 10.1158/1078-0432.CCR-11-2725

Yu, G., Wang, L. G., Han, Y., and He, Q. Y. (2012). clusterProfiler: an R package for comparing biological themes among gene clusters. *Omics* 16, 284–287. doi: 10.1089/omi.2011.0118

Yuan, C., Yuan, H., Chen, L., Sheng, M., and Tang, W. (2021). A novel three-long noncoding RNA risk score system for the prognostic prediction of triple-negative breast cancer. *Biomark. Med.* 15, 43–55. doi: 10.2217/bmm-2020-0505

Zhang, B., and Horvath, S. (2005). A general framework for weighted gene co-expression network analysis. *Stat. Appl. Genet. Mol. Biol.* 4:17. doi: 10.2202/1544-6115.1128

Zhang, Y., Li, Z., Chen, M., Chen, H., Zhong, Q., Liang, L., et al. (2020). lncRNA TCL6 correlates with immune cell infiltration and indicates worse survival in breast cancer. *Breast Cancer* 27, 573–585. doi: 10.1007/s12282-020-01048-5

Zhao, Q., and Fan, C. (2019). A novel risk score system for assessment of ovarian cancer based on co-expression network analysis and expression level of five lncRNAs. *BMC Med. Genet.* 20:103. doi: 10.1186/s12881-019-0832-9

Zhao, S., Yu, M., and Wang, L. (2020). LncRNA miR503HG regulates the drug resistance of recurrent cervical squamous cell carcinoma cells by regulating miR-155/Caspase-3. *Cancer Manag. Res.* 12, 1579–1585. doi: 10.2147/CMAR.S225489

Zhu, D., Huang, X., Liang, F., and Zhao, L. (2020). LncRNA miR503HG interacts with miR-31-5p through multiple ways to regulate cancer cell invasion and migration in ovarian cancer. *J. Ovarian Res.* 13:3. doi: 10.1186/s13048-019-0599-9

Conflict of Interest: The authors declare that the research was conducted in the absence of any commercial or financial relationships that could be construed as a potential conflict of interest.

frontiers in Oncology

ORIGINAL RESEARCH
published: 08 July 2021
doi: 10.3389/fonc.2021.636632

Long Noncoding RNA NONHSAT079852.2 Contributes to GBM Recurrence by Functioning as a ceRNA for has-mir-10401-3p to Facilitate HSPA1A Upregulation

Ningning Zhao[1], Jiajie Zhang[1], Lili Zhao[1], Xiaoni Fu[1], Qian Zhao[1], Min Chao[2], Haiyan Cao[2], Yang Jiao[2], Yaqin Hu[2], Chao Chen[1], Liang Wang[2]* and Huijuan Wang[1]**

[1] College of Life Sciences, Northwest University, Xian, China, [2] Department of Neurosurgery, Tangdu Hospital of Air Force Medical University, Xian, China

OPEN ACCESS

Edited by:
Marco Mina,
Sophia Genetics, Switzerland

Reviewed by:
Roopa Biswas,
Uniformed Services University of the Health Sciences, United States
Shengying Qin,
Shanghai Jiao Tong University, China

***Correspondence:**
Huijuan Wang
whj@nwu.edu.cn
Liang Wang
drwangliang@126.com
Chao Chen
cchen898@nwu.edu.cn

Specialty section:
This article was submitted to Cancer Genetics, a section of the journal Frontiers in Oncology

Received: 01 December 2020
Accepted: 22 March 2021
Published: 08 July 2021

Citation:
Zhao N, Zhang J, Zhao L, Fu X, Zhao Q, Chao M, Cao H, Jiao Y, Hu Y, Chen C, Wang L and Wang H (2021) Long Noncoding RNA NONHSAT079852.2 Contributes to GBM Recurrence by Functioning as a ceRNA for has-mir-10401-3p to Facilitate HSPA1A Upregulation. Front. Oncol. 11:636632. doi: 10.3389/fonc.2021.636632

Glioblastoma multiforme (GBM) is the most common brain malignancy and major cause of high mortality in patients with GBM, and its high recurrence rate is its most prominent feature. However, the pathobiological mechanisms involved in recurrent GBM remain largely unknown. Here, whole-transcriptome sequencing (RNA-sequencing, RNA-Seq) was used in characterizing the expression profile of recurrent GBM, and the aim was to identify crucial biomarkers that contribute to GBM relapse. Differentially expressed RNAs in three recurrent GBM tissues compared with three primary GBM tissues were identified through RNA-Seq. The function and mechanism of a candidate long noncoding RNA (lncRNA) in the progression and recurrence of GBM were elucidated by performing comprehensive bioinformatics analyses, such as functional enrichment analysis, protein–protein interaction prediction, and lncRNA–miRNA–mRNA regulatory network construction, and a series of *in vitro* assays. As the most significantly upregulated gene identified in recurrent GBM, HSPA1A is mainly related to antigen presentation and the MAPK signaling pathway, as indicated by functional enrichment analysis. HSPA1A was predicted as the target gene of the lncRNA NONHSAT079852.2. qRT-PCR revealed that NONHSAT079852.2 was significantly elevated in recurrent GBM relative to that in primary GBM, and high NONHSAT079852.2 expression was associated with the poor overall survival rates of patients with GBM. The knockdown of NONHSAT079852.2 successfully induced tumor cell apoptosis, inhibited the proliferation, migration, invasion and the expression level of HSPA1A in glioma cells. NONHSAT079852.2 was identified to be a sponge for hsa-miR-10401-3p through luciferase reporter assay. Moreover, HSPA1A was targeted and regulated by hsa-miR-10401-3p. Collectively, the results suggested that NONHSAT079852.2 acts as a sponge of hsa-mir-10401-3p and thereby enhances

HSPA1A expression, promotes tumor cell proliferation and invasion, and leads to the progression and recurrence of GBM. This study will provide new insight into the regulatory mechanisms of NONHSAT079852.2-mediated competing endogenous RNA in the pathogenesis of recurrent GBM and evidence of the potential of lncRNAs as diagnostic biomarkers or potential therapeutic targets.

Keywords: recurrent glioblastoma multiforme, RNA-sequencing, lncRNAs, HSPA1A, ceRNA

INTRODUCTION

Glioblastoma multiforme (GBM) is one of the most common and most aggressive primary adult brain tumors. Despite the availability of aggressive treatments, including surgical tumor removal and radiochemotherapy, GBM has a high recurrence rate, and the median survival time of patients with GBM is only 15 months (1–3). Recurrent tumors are less sensitive to chemotherapy than original tumors, and in most cases, a second surgical resection cannot be performed due to invaded functional brain areas. Currently, most research efforts are focused on exploring the pathogenesis of primary GBM, and few studies have emphasized the biology of recurrent GBM (4, 5). Understanding the mechanism of GBM recurrence is of great significance to the treatment of GBM.

Long noncoding RNAs (lncRNAs) are non-protein coding transcripts that are longer than 200 nucleotides in length and regulate gene expression during biological and pathological processes at the epigenetic, transcription, and post-transcription level (6, 7). Substantial evidence indicates lncRNAs play critical roles in tumor initiation and malignant progression. In particular, recent studies reported that lncRNA can interact with miRNAs as a competing endogenous RNA (ceRNA) to participate in expression regulation of target genes. This newly presented model for gene expression regulation may aid to identification of new targets for tumor treatment (8–10).

Recently, a number of lncRNAs have been implicated in the oncogenesis of gliomas and associated with cell proliferation and apoptosis of glioma and the prognosis of GBM patients. Some of them are increasingly being considered potential therapeutic targets (11, 12). Chen et al. reported that NEAT1 can promote GBM cell growth and invasion *via* the WNT/b-catenin pathway (1). Liu et al. confirmed that the lncRNA HOTAIR promotes glioma progression by acting as a competing endogenous RNA for miR-126-5p (13). Another study revealed that the expression level of the lncRNA SPRY4-IT1 in human glioma tissues and cell lines is upregulated and SPRY4-IT1 can suppress cell growth and metastasis; thus, SPRY4-IT1 may be used as a therapeutic target (14). Collectively, these lncRNAs are of great value as novel biomarkers to clinical applications. However, most current studies were performed using primary GBM clinical samples or cells, and the biological roles and functions of lncRNAs in recurrent GBM have not been fully explored.

Therefore, in this study, whole-transcriptome sequencing (RNA-sequencing, RNA-Seq) of recurrent and primary GBM specimens and subsequent comprehensive bioinformatics analyses were performed for the identification of key lncRNAs associated with glioma. Then, the functional characterization of the selected lncRNA in GBM pathogenesis was performed through a series of *in vitro* biological assays.

MATERIALS AND METHODS

Sample Preparation

Six fresh tumor specimens from three cases of primary GBM (two females and one male, sample serial numbers: 01, 02, and 03) and three cases of recurrent GBM (two females and one male, sample serial numbers: 04, 05, and 06) were obtained from the Department of Neurosurgery in Tangdu Hospital of Air Force Medical University. The patients with primary GBM were treatment-naïve before surgery and the patients with recurrent GBM had been treated with temozolomide plus radiotherapy before relapse. The resected specimens were histologically examined using hematoxylin and eosin (H&E) staining (**Supplementary Figure 1**). The patients and/or their family members understood the process of this study, and each patient signed an informed consent. This study was approved by the Medical Ethics Committee of Tangdu Hospital (TDLL-2017-172).

RNA Extraction, Library Construction, and RNA-Seq

Total RNA was extracted using TRIzol reagent in accordance with the manufacturer's instructions, then the concentration and purity of the RNA were measured with a NanoDrop ND-1000 spectrophotometer (NanoDrop Technologies, Wilmington, DE, USA). cDNA libraries were constructed using rRNA-depleted total RNAs as templates according to the protocol of the mRNA-Seq sample preparation kit (Illumina, San Diego, USA). The resulting libraries were sequenced on an Illumina Hiseq 2500 platform (Illumina San Diego CA, USA). More than 200 million paired-end reads were generated. We obtained three biological replicates to minimize experimental errors and the number of false positives.

Differential Expressed Genes

Differentially expressed genes (DEGs) in recurrent GBMs compared with primary GBMs were analyzed using the R software DEGseq (15). A fold change (FC) of ≥2 and false discovery rate (FDR) of <0.05 were considered as the criteria for DEG selection. According to the obtained DEGs, ggplot2 in R software was used in creating a volcano plot and heatmap for drawing DEGs.

Gene Function Annotation

The differentially expressed mRNAs (DEmRNAs) were functionally annotated through Gene Ontology (GO) and the Kyoto Encyclopedia of Genes and Genomes (KEGG) pathway enrichment analysis, which were performed using the R language version 3.4.4 cluster Profiler. A P value of <0.05 was used as the threshold value.

Protein–Protein Interaction Analysis

According to the DEG results and protein–protein interactions included in the STRING database (https://string-db.org/), protein–protein (PPI) pairs between DEmRNAs were obtained, and Cytoscape (Version 3.7.2) was used in visualizing the PPI network.

LncRNAs Target Gene Analysis

For a lncRNAs with a known gene symbol, the gene symbol was used in searching information related to target genes in a software database (starBase, http://starbase.sysu.edu.cn/index.php; ChIPBase, http://rna.sysu.edu.cn/chipbase/; and nonecode, http://www.noncode.org/). The correlation between the gene expression levels of differentially expressed lncRNAs (DElncRNAs) and DEmRNAs was evaluated using the Pearson correlation method. mRNAs with absolute value of correlation coefficients of >0.9 and P of <0.01 were considered potential targets of lncRNAs.

miRNA Target Gene Prediction

On the basis of miRNA and human gene sequence information, miRNAs targeting DEmRNAs were predicted using miRanda (http://www.mirbase.orgmiRBase) and targetscan (http://www.targetscan.org/), and miRNA–mRNA regulatory networks were obtained.

Analysis of the NONHSAT079852.2-Mediated Regulatory Network

LncRNA–miRNA and miRNA–mRNA relationships were established, and lncRNAs and mRNAs that had at least five co-bind miRNAs were defined as competitive RNAs, and ceRNA was established with Cytoscape.

Histopathological Examinations

For H&E staining, fresh GBM tissues were fixed in 4% paraformaldehyde for 24 h. Paraffin blocks were embedded and then cut into sections. The paraffin sections were stained with H&E. The rabbit anti-human HSPA1A (dilution fold; 1:100; cat. no. A12948) and CPS1 (dilution fold; 1:100; cat. no. 4214) antibodies were purchased from ABclonal Biotech Co., Ltd (Cambridge, USA).

Cell Lines and Reagents

A human U251 cell line with short tandem repeat (STR) analysis-based identification certificate was purchased from Wuhan Punosai Life Science and Technology Co., Ltd. GBM-W, a primary GBM cell line derived from a clinical GBM specimen, was obtained from Tangdu Hospital and identified through STR analysis (**Supplementary Figure 2**). The cells were cultured in DMEM (Wuhan Punosai Life Technology Co., Ltd.) supplemented with 10% fetal bovine serum and 1% penicillin. The shRNA plasmid used to knock down the expression of lncRNA NONHSAT079852.2 was purchased from Shanghai Jikai Gene Co., Ltd.

Cell Transfection

The U251 and GBM-W cells were divided into the control (without treatment), shGFP (transfected with a negative control plasmid against GFP), and shRNA (transfected with a shRNA plasmid against NONHSAT079852.2) groups. The plasmids were purchased from Shanghai Jikai Biotechnology Co., LTD. (Shanghai, China). Lipofectamine 2000 (Invitrogen Inc., Carlsbad, CA) was used for cell transfection according to the manufacturer's instructions. The shRNA targeting sequences for NONHSAT079852.2 were listed in **Supplementary Table 1**. Of three shRNA targeting sequences, shRNA-652 was validated for the most efficient interference of NONHSAT079852.2 by qRT-PCR and WB, and chosen for further study.

qRT-PCR Validation

Total RNA from the six GBM tissues and cells was isolated using a TRIzol reagent (Invitrogen, USA), which was reverse-transcribed to cDNA with EasyScript® All-in-One First-Strand cDNA Synthesis SuperMix for qPCR (TransGen Biotech, Beijing, China). The expression levels of selected mRNAs (HSPA1A, CPS1, CCL18, CCL8, and CCL5) and lncRNAs (MSTRG.224498.5, MSTRG.65777.2, and MSTRG.150858.14) were determined through qPCR analysis with a Vii7 QRT-PCR system (Thermo Fisher Scientific). Detailed primer sequences were shown in **Supplementary Table 2**.

Fluorescence *In Situ* Hybridization (RNA FISH) for NONHSAT079852.2

The subcellular location of the NONHSAT079852.2 was determined using an RNA fluorescence *in situ* hybridization kit (Shanghai GenePharma Co., Ltd.) according to the manufacturer's instructions. The GBM-W cells were washed with PBS and fixed in 4% paraformaldehyde for 15 min. A biotin-labeled probe was coupled with CY3 fluorescent dye was used, and the cells were incubated at 37°C for 37 min. Hybridization was performed at 37°C for 16 h, the slide was washed, and nuclei were stained with DAPI for 15 min. The images were examined through confocal microscopy with original magnification of 1200× (Leica TCS SP5; Leica Microsystems GmbH, Wetzlar, Germany). The probe sequences were listed in **Supplementary Table 3**.

Western Blot Analysis

Proteins were extracted from the U251 and GBM-W cells, and protein concentration was determined through the BCA method (Pierce, Rockford, IL). Approximately 40 μg of protein was separated using SDS-containing polyacrylamide gels and transferred onto a polyvinylidene fluoride membrane (Millipore, Billerica, MA, USA). A nonspecific antibody was incubated with 5% milk blocking solution for 2 h and then with primary antibody against HSPA1A (cat. no. A12948; ABclonal

Biotech; 1:1000) overnight at 4°C. The membranes were washed with TBST buffer and incubated with peroxidase-labeled secondary antibodies (cat. no. SA00001-1; Proteintech) for 2 h at room temperature. The membranes were rinsed with TBST buffer. Protein bands were exposed with an ECL luminescence solution and detected with a chemiluminescence apparatus (Bio-Rad Hercules, CA, USA).

CCK-8 and Colony-Formation Assays

The U251 or GBM-W Cells at 5×10^4 cells/well were seeded in 96-well plates. Cell proliferation was determined through Cell Counting Kit-8 assay (Dojindo Laboratories, Kumamoto, Japan) before transfection and 24, 48, and 72 h after transfection. For cell colony formation assay, cells at 2000 cells/cm^2 were seeded in six-well plates. After 2 weeks, cell colonies were stained using crystal violet and counted.

Cell Migration and Invasion Assays

The ratio between the matrix glue and basic medium was set at 1:4, and 50 µl of the mixture was added to each upper chamber. After 3 h, 50 µl of the medium containing 1% serum was added to the upper chamber to hydrate the basement membrane, and 100 µl of cell suspension containing 5×10^4 U251 or GBM-W cells were added. Exactly 400 µl of medium containing 10% serum was added to the lower chamber. After 36 h, the medium was discarded, the substrate glue in the upper chamber was erased, and the cells on the lower surface of the upper chamber were fixed with 4% paraformaldehyde. The cells were washed with PBS and stained with 0.2% crystal violet. The number of migratory/invaded cells from three different fields was determined through microscopy.

Wound Healing Assay

The U251 and GBM-W cells were seeded in six-well plates and transfected for 24 h. After the cells reached 80% confluence, a 0.5-mm-wide straight scratch was made on a monolayer of the subconfluent cells with a 200 µl sterile pipette-tip. Cell movement during wound closure was recorded through photography with a phase-contrast inverted microscope at three random fields and time points of 0, 24, and 48 h. Migration rate was calculated as follows: migration rate (%)= (original width−closure width)/original width×100%.

Flow Cytometry Analysis of Cell Cycle and Apoptosis

After the cells were transfected for 48 h, the cells were collected from the flow tube, and cell cycle (BD-Pharmingen Annexin V PE) and apoptosis (BD Pharmingen™ 7-AAD) were detected through flow cytometry (BD Biosciences, USA).

Luciferase Reporter Gene Assay

The binding sites of NONHSAT079852.2 and hsa-miR-10401-3p were predicted using the miRanda database, and wild-type NONHSAT079852.2-WT containing a binding site and NONHSAT079852.2-MUT luciferase plasmid containing a binding site mutation were constructed. The luciferase plasmids NONHSAT079852.2-WT and NONHSAT079852.2-MUT were co-transfected with hsa-miR-10401-3p mimics into U251 and GBM-W cells. After 48 h, the luciferase activities of the glioma cells were detected using a dual-luciferase reporter gene detection kit (Promega E1910) by Promega GloMax 20/20 Luminescence Detector (USA).

Statistical Analysis

Statistical analysis was performed using SPSS 20.0 (SPSS, Inc. Chicago, USA). Pearson correlation analysis was used in determining correlations between each pair of gene expression levels. A scatter diagram was used for the linear analysis of gene expression. The prognoses of patients with GBM were analyzed using Kaplan–Meier curves. Quantitative values were expressed as (mean ± SD). Each experiment was repeated at least three times. An independent sample *t* test was used for comparison between two groups. $P<0.05$ was considered statistically significant.

RESULTS

Identification of the DEGs Between Recurrent and Primary GBM

Through the comparison of the RNA-seq data of three cases of recurrent GBM and three cases of primary GBM, a total of 1025 DEGs were identified, of which 718 were lncRNAs (378 upregulated and 340 downregulated), 293 were mRNAs (204 upregulated and 89 downregulated), 11 were circRNAs (all upregulated), and three were miRNAs (two upregulated and one downregulated). **Figures 1A–D** shows in detail the volcano plots of DElncRNA, DEmRNA, DEcircRNA, and DEmiRNA expression profiles, respectively. Unsupervised clustering analysis shows the expression profiles of lncRNAs and DEmRNAs (**Figures 1E, F**).

HSPA1A Has Important Biological Functions and Is Upregulated in Recurrent GBM

GO enrichment analysis results showed that the DEmRNAs were markedly enriched in molecular functions, including antioxidant activity, receptor regulator activity, chemoattractant activity, and morphogen activity (**Figure 2A**). The DEmRNAs were significantly enriched in several KEGG signaling pathways, including tumor signaling pathways, immune response, and cytokine and receptor functions (**Figure 2B**). As the highest upregulated DEmRNA in recurrent GBMs (nine times that of primary GBM), HSPA1A, a member of the Hsp70 protein family (Hsp70-1), was mainly related to antigen presentation and MAPK signaling pathway regulation (**Figure 2C**). PPI analysis results showed that carbamoyl-phosphate synthase 1 (CPS1) and Hsp family member 13 (DNAJB3; a co-chaperone and member of the Hsp40 family) are HSPA1A-interacting proteins (**Figure 2D**). A significant correlative relationship was observed between HSPA1A and other proteins, including CPS1 (r=0.996, $P=0.002$), CCL18 (r=0.927, $P=0.008$), CCL8 (r=0.993, $P<0.001$), and CCL5 (r=0.919, $P=0.010$) (**Figure 2E**). Moreover, the expression level of HSPA1A determined by qRT-PCR was consistent with that obtained by RNA-seq (**Figure 2F**). IHC

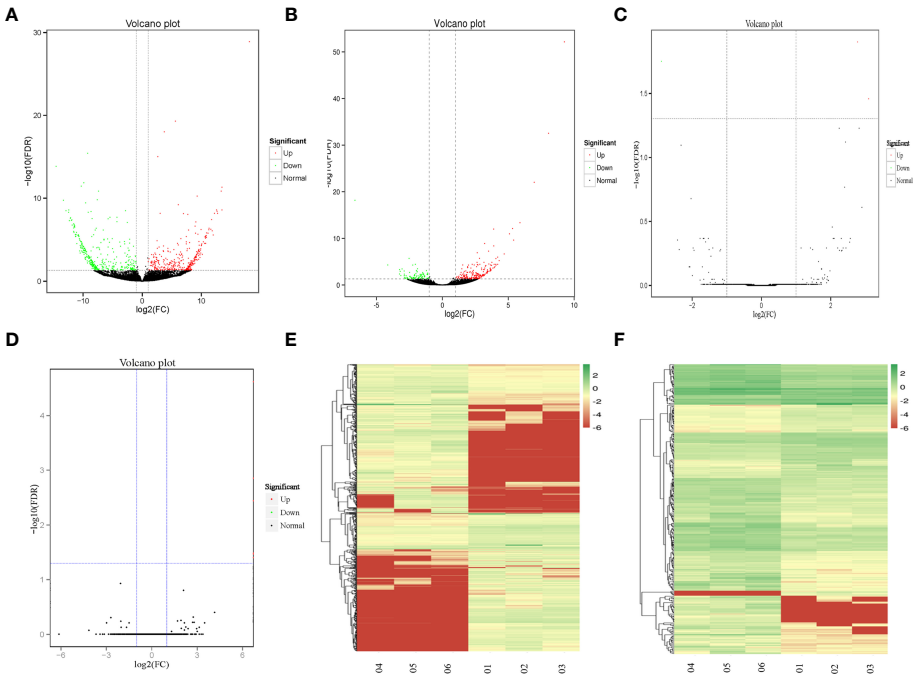

FIGURE 1 | The DEGs between recurrent and primary GBM. **(A–D)** Volcano map of DElncRNAs, DEmRNAs, DEcircRNAs, and DEmiRNAs, expression profiles between recurrent and primary GBMs. The x-axis represents an adjusted a log2FC and the y-axis represents the P-value. The green dots represent down-regulated DEGs, the red dots represent up-regulated DEGs, and the black dots represent non-differentially expressed RNAs. **(E, F)** Unsupervised clustering analysis showing expression profiles of lncRNAs and mRNAs between recurrent and primary GBMs. The color gradient from green to red shows a trend from low expression to high expression.

showed that the expression levels of HSPA1A and CPS1 in recurrent GBM were significantly higher than those of primary GBM (**Figures 2G, H**). Therefore, HSPA1A was selected as the target mRNA for screening key lncRNAs.

NONHSAT079852.2 Targets mRNA HSPA1A and Is Highly Expressed in Recurrent GBM

According to the results of the analysis of lncRNAs and miRNA target genes, 54 differentially expressed lncRNAs targeted HSPA1A, of which 16 lncRNAs competed with HSPA1A in a ceRNA mode. Meanwhile, 37 DEmiRNAs targeted HSPA1A, and 3761 miRNAs targeted 16 lncRNAs. The 16 lncRNAs, HSPA1A, and their co-targeted miRNAs formed a ceRNA network (**Figure 3A**). The differential expression levels of the 16 lncRNAs were validated by qRT-PCR, and three lncRNAs (MSTRG.224498.5, MSTRG.65777.2, and MSTRG.150858.14) showed results that were consistent with those of RNA-seq (**Figure 3B**). The lncRNA MSTRG224498.5 is also known as lncRNAs NONHSAT079852.2 and belongs to intergenic lncRNA. It is located on chromosome 20 with a length of 1657 bp. Lnclocator shows that lncRNAs NONHSAT079852.2 is located in the cytoplasm (0.113725065505), nucleus (0.0499335493761), ribosome (0.338593997721), cytosol (0.449439437366), and exosome (0.0483079500317) (16). FISH experiment showed that the subcellular location of the NONHSAT079852.2 is the cytosol (**Figure 3C**). Therefore, we selected NONHSAT079852.2 as the key lcnRNA for subsequent analysis.

NONHSAT079852.2 Can Promote the Proliferation, Invasion, and Migration of Glioma Cells

When the lncRNA MSTRG224498.5was knocked down by shRNA, the mRNA and protein expression levels of HSPA1A were reduced (**Figures 4A–C**). CCK-8 assay (**Figure 4 D1, D2**), colony-formation assay (**Figure 4E**), cell migration and invasion assay (**Figure 4F**), and wound healing assay (**Figure 4G**) showed that cell proliferation, invasion, and migration were inhibited.

NONHSAT079852.2 Can Modulate the Cell Cycle and Apoptosis of Glioma Cells

When NONHSAT079852.2 was knocked down by shRNA, flow cytometry assay showed that the number of glioma cells in the G_1/G_0 phase increased, whereas the number of glioma cells in the G_2/S phase decreased (**Figure 5A**). In addition, the apoptosis rate of glioma cancer cells increased (**Figure 5B**).

NONHSAT079852.2 Functions as a ceRNA for has-mir-10401-3p to Facilitate HSPA1A Expression

CeRNA network analysis showed that five miRNAs co-targeted lncRNA MSTRG224498.5 and HSPA1A, and two of them are

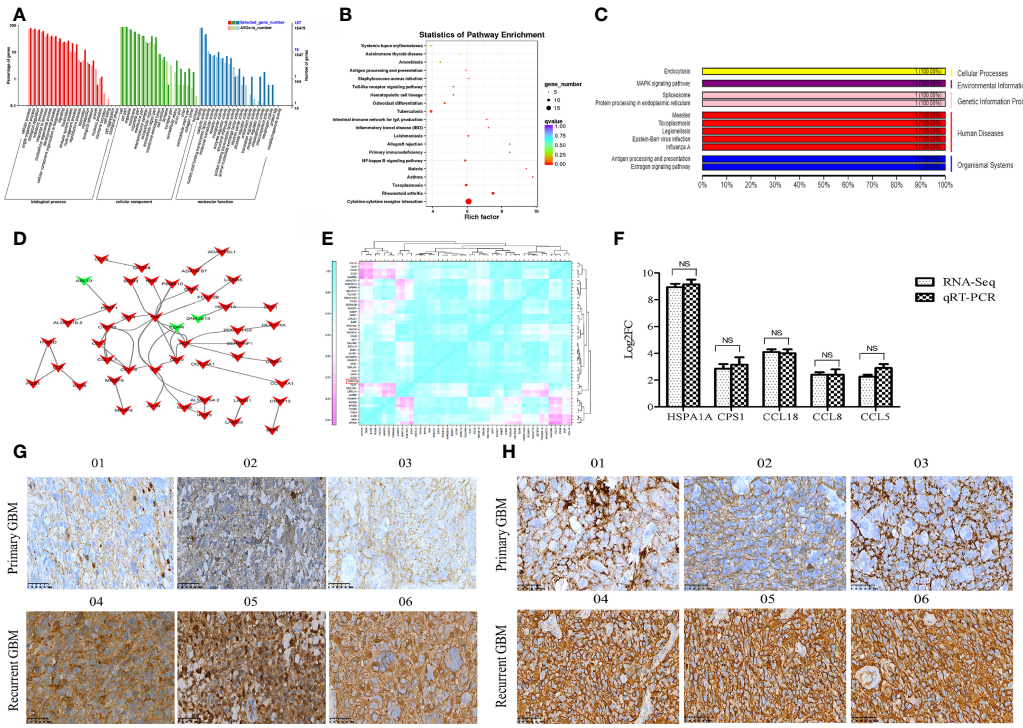

FIGURE 2 | Functional annotation of DEmRNAs and expression validation of selected genes by qRT-PCR and IHC**. (A)** GO classification map of DEmRNAs. **(B)** KEGG functional enrichment map of DEmRNAs. **(C)** KEGG functional classification map of mRNA HSPA1A. **(D)** The PPI map of DEGS mRNA. The DEGs mRNA was indicated by arrows. The up-regulated genes are indicated in red, while the down-regulated genes are indicated in green. **(E)** Correlation analysis of 47 DEmRNAs highly correlated to HSPA1A. **(F)** The differential expression of selected mRNAs was validated by qRT-PCR. **(G)** The IHC image of HSPA1A expression in GBM sample. **(H)** The IHC image of CPS1 expression in GBM specimens. 01-03 represents primary GBM,04-06 represents recurrent GBM.

known miRNAs (**Figures 6A, B**). The RegRNA2.0 database (http://regrna2.mbc.nctu.edu.tw/) showed that NONHSAT079852.2 can interact with miR_571 (novel), hsa-miR-7110-5p, miR_299(novel), miR_956 (novel), and hsa-miR-10401-3p through complementary base pairing. Therefore, NONHSAT079852.2 was speculated to regulate the function of glioma cells by acting as a ceRNA for these miRNAs. The binding ability of NONHSAT079852.2 for the two known miRNAs (hsa-miR-7110-5p and hsa-miR-10401-3p) was further confirmed in glioma cells through an immunofluorescence reporter assay, and the results showed that luciferase activity decreased in the glioma cells that were co-transfected with has-mir-10401-3p and NONHSAT079852.2 but was not reduced in cells containing hsa-miR-7110-5p, Therefore, has-mir-10401-3p was used as a candidate miRNA (**Figure 6C**). We constructed the fluorescent reporter enzyme plasmids NONHSAT079852.2-WT and NONHSAT079852.2-MUT, which contained has-mir-10401-3p binding sites. The upregulation of has-mir-10401-3p significantly reduced luciferase activity in glioma cells co-transfected with NONHSAT079852.2-WT, whereas the upregulation of has-mir-10401-3p had no effect on luciferase activity when the cells were co-transfected with NONHSAT079852.2-MUT. These results suggested that NONHSAT079852.2 bound directly to has-mir-10401-3p (**Figure 6D**). MiRanda and TargetsCAN were used in predicting the possible binding sites of miRNA target genes and regulatory networks, and the results showed the binding sites of has-mir-10401-3p that were co-targeted by lncRNA MSTRG224498.5 and mRNA HSPA1A (**Figure 6E**).

High NONHSAT079852.2 Expression Is Associated With the Poor Prognoses of Patients With GBM

Forty-four patients with primary GBM (19 females and 25 males) who underwent surgery were followed up for 1-24 months. The expression levels of NONHSAT079852.2 in the tumor tissues of 44 patients with GBM were detected through qRT-PCR, and the patients were divided into high- and the low-expression groups according to the median expression level (**Figure 7A**). Kaplan–Meier curves showed that the overall survival time of the high-expression group was significantly lower than that of the low-expression group (Log Rank P=0.000; **Figure 7B**).

DISCUSSION

To explore the role of lncRNAs in glioma recurrence, we detected the differential transcriptome expression profiles of the recurrent

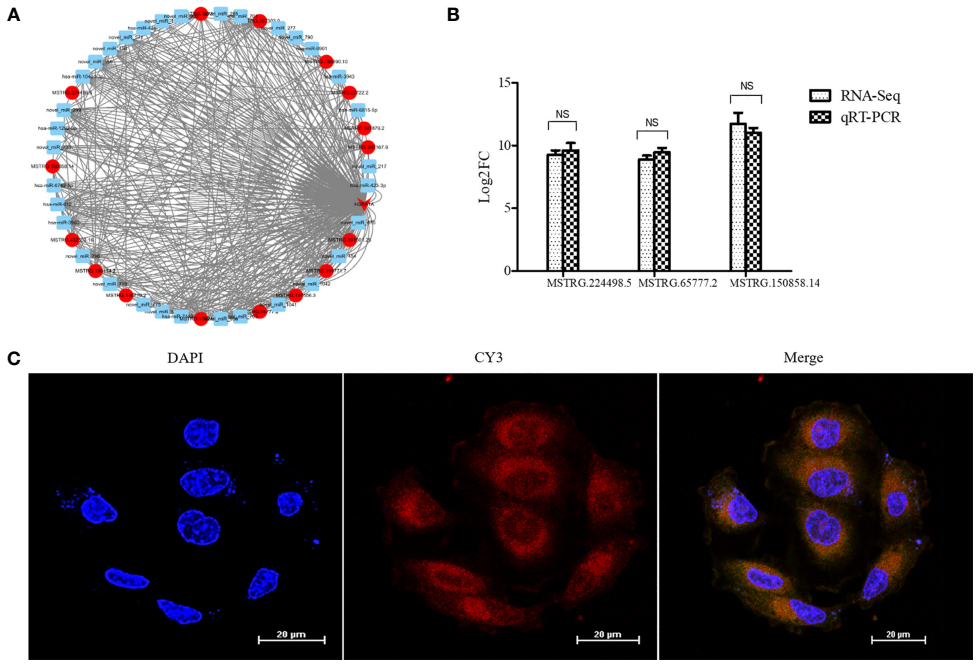

FIGURE 3 | LncRNAs NONHSAT079852.2 targets mRNA HSPA1A and is highly expressed in recurrent GBM and main located in Cytosol. **(A)** The ceRNA network construction of lncRNAs, miRNA and HSPA1A. lncRNAs is indicated by a circle. mRNA is indicated by an arrow. miRNA is indicated by a square. The up-regulated genes are indicated in red, while the genes with insignificant changes are indicated in blue. **(B)** The comparison of qRT-PCR and RNA-seq detection of lncRNAs expression levels in the recurrent GBM and primary GBM. **(C)** Fish experiment demonstrated that the LncRNA NONHSAT079852.2 was mainly distributed in the cytoplasm of glioma cells. The results are presented as mean ± SD. NS, not significant.

GBM tissues through RNA-seq. After performing lncRNA–mRNA–miRNA ceRNA network analysis, we selected NONHSAT079852.2, which was upregulated in the recurrent GBMs and associated with the poor prognoses of patients with GBM. Through comprehensive bioinformatic analysis and *in vitro* function assays, we found that NONHSAT079852.2 acts as a sponge for has-mir-10401-3p to increase HSPA1A expression and thereby promotes the proliferation, migration, and invasion of glioma cells. Thus, it may be involved in the progression and recurrence of GBM.

Although the functions of most lncRNAs remain unclear, lncRNAs play an important role in tumor initiation and progression by regulating gene expression through diverse mechanisms (17–19). Therefore, through the identification of DEGs and gene functional enrichment analysis, the target mRNA selected was found to be an important factor in tumor pathogenesis. Through mRNA–lncRNA network analysis, we selected interacted lncRNAs that play key roles in recurrent GBM. Using this strategy, we selected HSPA1A as the target mRNA. The major stress-inducible protein HSPA1A is a highly conserved protein of the heat-shock protein 70 (Hsp70) family and plays an important role in protein folding, signal transduction, and general response to stress factors (20–23). Strong evidence suggests that HSPA1A is overexpressed in various tumors, such as lung cancer, gastric cancer, and GBM, and promotes tumor proliferation, metastasis, and drug resistance (24–26). The correlation between increase in Hsp70 expression level and tumor development and progression has prompted scientists to consider Hsp70 as a target for cancer therapy (27–29). Recently, targeting Hsp70 in glioma cells with magnetic nanoparticles has been found to increase the retention of nanoparticles within tumor cells (30, 31). In our study, we found that HSPA1A interacts with CPS1 and DNAJB13, and its expression level was highly correlated with the expression levels of CPS1, CCL18, CCL8, and CCL5. CPS1, a key enzyme in the urea cycle, is highly expressed in different types of cancers and promotes cell proliferation and metastasis (32–34). DNAJB13, one of the HSP40 subfamily members, has a negative correlation with HSPA1A. Hsp40s are cofactors of HSP70s and are involved in various biological processes. The DNAJB1–Hsp70 complex is a potential valuable target for tumor treatment (35, 36). As chemokines, CCL8 and CCL5 are involved in tumor cell proliferation and metastasis (37–39). Basing on the description above, we selected HSPA1A as the target gene for the identification of lncRNAs associated with GBM recurrence.

The lncRNA–mRNA regulatory network showed that HSPA1A, a key gene in the development of GBM, is the targeting gene of NONHSAT079852.2 (lncRNA MSTRG224498.5). The expression of NONHSAT079852.2 significantly increased in recurrent GBM relative to that in primary GBM. Moreover, the knocking down of NONHSAT079852.2 inhibited the proliferation of glioma cells by downregulating HSPA1A expression. These results indicated that

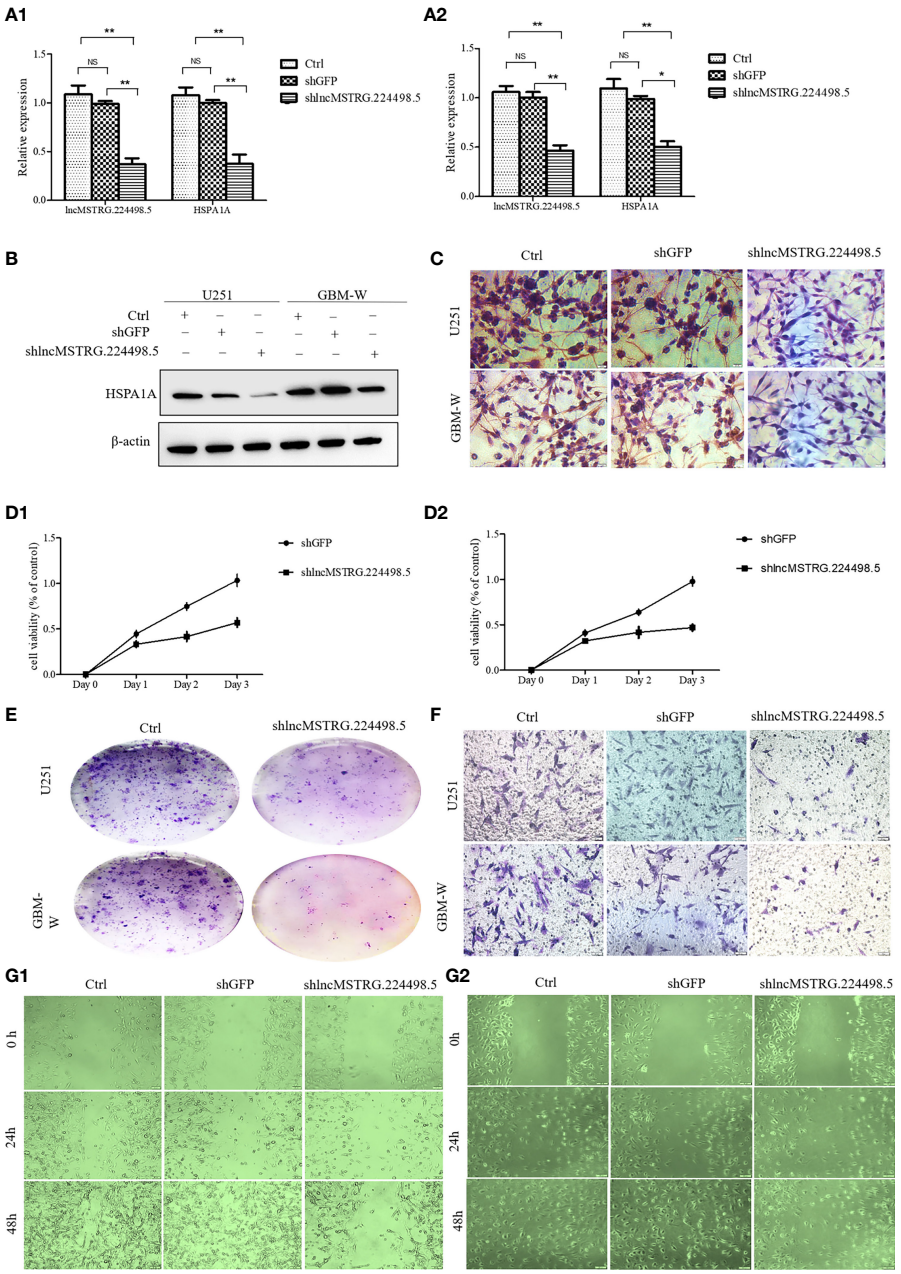

FIGURE 4 | LncRNAs NONHSAT079852.2 can promote the proliferation, invasion and migration of glioma cells. **(A)** qRT-PCR analysis of HSPA1A in U251(A1) or GBM-W(A2) cells after transfection for 48 hours. **(B)** Western blot analysis of HSPA1A in U251 or GBM-W cells after transfection for 48 hours. **(C)** IHC analysis of HSPA1A in U251 or GBM-W cells after transfection for 48 hours. **(D)** Growth curve of U251(D1) or GBM-W (D2) cells after transfection for 48 hours by CCK8 assay. **(E)** Proliferation of U251 or GBM-W cells after transfection for two weeks as determined by colony-formation assay. **(F)** Migration and invasion ability of U251 or GBM-W cells after transfection for 48 hours. **(G)** Migration of U251(G1) or GBM-W(G2) cells after transfection for 48 hours as detected by wound healing assay. Results were presented as mean ± SD. $^{*}p < 0.05$, $^{**}p < 0.01$, NS, not significant.

NONHSAT079852.2 contributes to GBM recurrence by upregulatimg HSPA1A. NONHSAT079852.2 belongs to intergenic lncRNA and is located on chromosome 20 with a length of 1657 bp. FISH experiment revealed that NONHSAT079852.2 was mainly distributed in the cytoplasm of glioma cells. Therefore, NONHSAT079852.2 might regulate the function of glioma cells through a ceRNA mechanism. Using bioinformatics and luciferase reporter gene assay, we confirmed that NONHSAT079852.2 competitively bound to hsa-miR-10401-3p and thus upregulated HSPA1A expression. In addition, we showed that the high expression of lncRNA MSTRG224498.5 in GBM was associated with poor prognosis. Therefore,

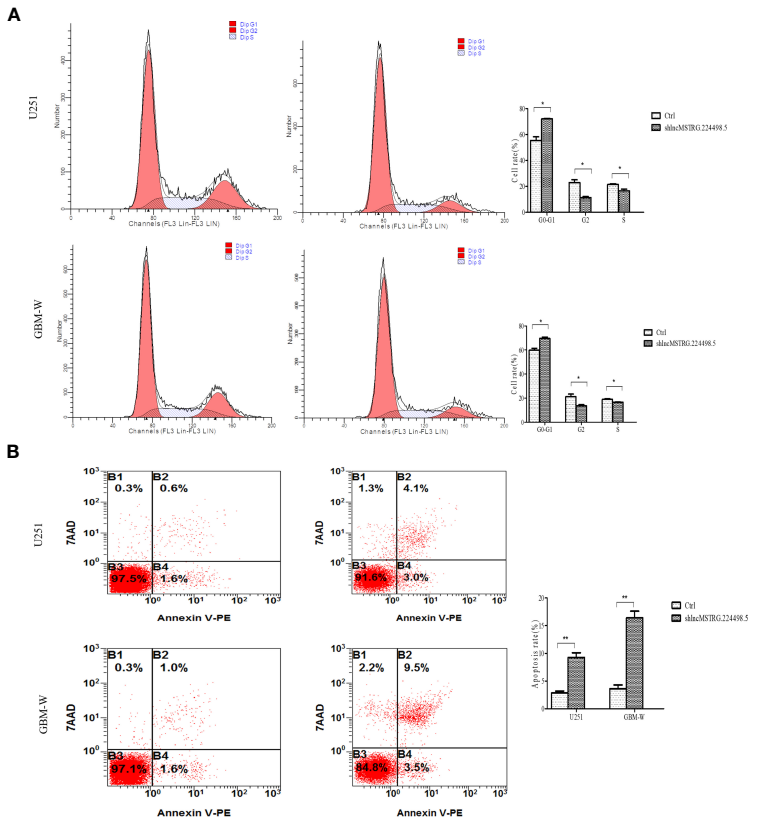

FIGURE 5 | LncRNAs MSTRG224498.5 can adjust the cell cycle and apoptosis of glioma cells. **(A)** Flow cytometry analysis of the cell cycle of U251 or GBM-W cells after transfection for 48 hours. **(B)** Flow cytometry analysis of the apoptosis rate of U251 or GBM-W cells after transfection for 48 hours. Results were presented as mean ± SD. $*p < 0.05$, $**p < 0.01$.

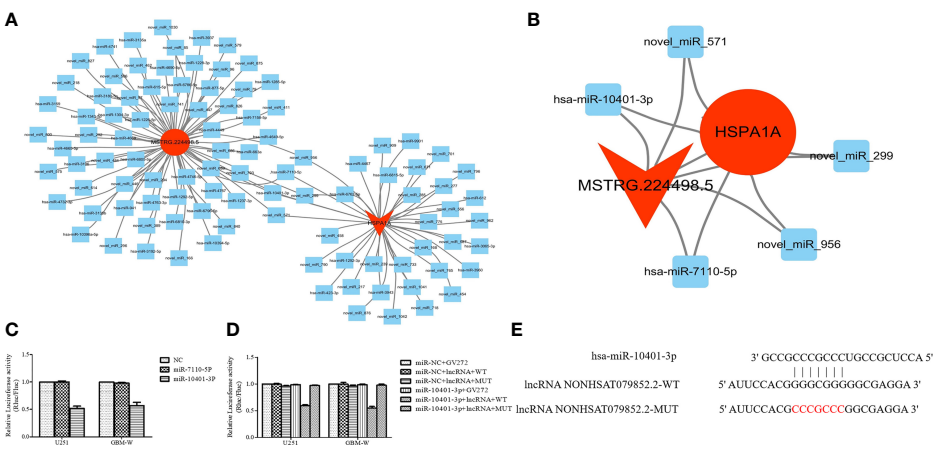

FIGURE 6 | LncRNAs NONHSAT079852.2 Functions as a ceRNA for has-mir-10401-3p to facilitate HSPA1A Expression. **(A)** miRNA targeting HSPA1A and lncRNA NONHSAT079852.2, respectively. **(B)** Co-targeting miRNAs of HSPA1A- lncRNA NONHSAT079852.2; LncRNAs is represented by a circle, miRNA is represented by a diamond, mRNA is represented by an arrow, The up-regulated expression gene is indicated by red, and the gene without significant change is indicated by blue. **(C)** Relative luciferase activity in U251 and GBM-W cells co-transfected with lncRNA MSTRG224498.5 reporter plasmid and candidate miRNAs. **(D)** Relative luciferase activity in glioma cells transfected with wild-type lncRNA NONHSAT079852.2 vector, mutant-type vector or empty vector. **(E)** has-mir-10401-3p and lncRNA NONHSAT079852.2 binding sequences and lncRNA NONHSAT079852.2 mutation sequences.

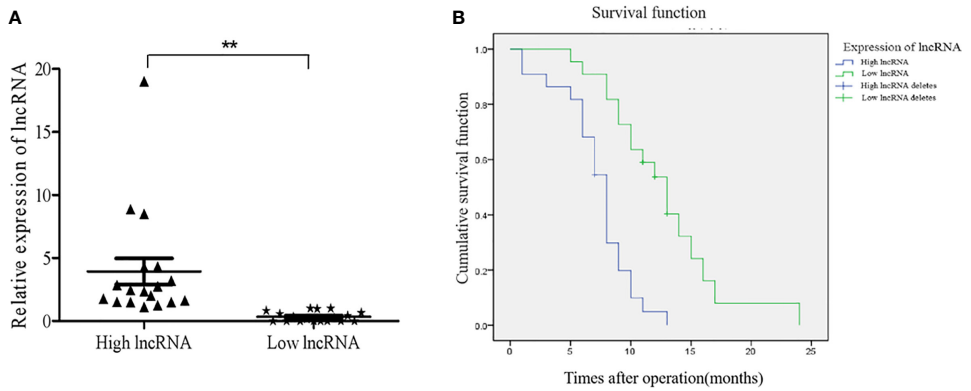

FIGURE 7 | The expression levels of lncRNAs NONHSAT079852.2 in GBM patients and its relationship with the prognosis of patients. **(A)** qRT-PCR analysis of lncRNA MSTRG224498.5 of GBM tissues. **(B)** High expression of lncRNA NONHSAT079852.2 correlates with poor prognosis in GBM patients. Results are presented as mean ± SD. $^{**}p < 0.01$.

MSTRG224498.5 might serve as a putative prognosis marker for patients with recurrent GBM.

This is the first study to characterize the role of the NONHSAT079852.2 in recurrent GBM. GBM clinical specimens were used for RNA-seq analysis. The heterogeneity of these specimens is strong, and this feature provides a reliable foundation for exploring GBM recurrence and drug resistance (40, 41). We established a GBM primary cell line, which maintained the heterogeneity of tumor cells and thus ensured the reliability of the research results (42, 43). In our next study, by using a larger sample size and performing *in vivo* experiments, we will conduct in-depth research and provide reliable evidence for clinical practice.

In summary, our study demonstrated that the NONHSAT079852.2 enhances recurrence and promotes the proliferation, invasion, and migration of glioma cells and these features are related to the poor prognoses of patients with GBM. The tumor-promoting effect of NONHSAT079852.2 may be attributed to its competitive binding to hsa-mir-10401-3p, and the resulting bond upregulates HSPA1A expression. Thus, the NONHSAT079852.2/hsa–mir-10401-3p–HSPA1A axis may be one of the potential mechanisms that promote GBM recurrence and is a potential therapeutic target for controlling and treating GBM.

DATA AVAILABILITY STATEMENT

The datasets presented in this study can be found in online repositories. The names of the repository/repositories and accession number(s) can be found in the article/**Supplementary Material**.

ETHICS STATEMENT

The studies involving human participants were reviewed and approved by Tangdu Ethics Committee Number TDLL-2017-172. The patients/participants provided their written informed consent to participate in this study.

AUTHOR CONTRIBUTIONS

NZ and JZ conducted all experiments and analyzed the data. LW, MC, HC, YJ and YH provided clinical samples. HW, CC, LW and NZ contributed to the conception and design of the study. LZ, XF, QZ collected clinical data. NZ and JZ wrote the manuscript. All authors contributed to the article and approved the submitted version.

FUNDING

This work was supported by the National Natural Science Foundation of China (Grant No. 81702483 and 81772661) and Natural Science Basic Research Program of Shaanxi (Program No. 2019JQ-207 and 2020JZ-30).

SUPPLEMENTARY MATERIAL

The Supplementary Material for this article can be found online at: https://www.frontiersin.org/articles/10.3389/fonc.2021.636632/full#supplementary-material

REFERENCES

1. Chen Q, Cai J, Wang Q, Wang Y, Liu M, Yang J, et al. Long non-Coding RNA NEAT1, Regulated by the EGFR Pathway, Contributes to Glioblastoma Progression Through the WNT/β-Catenin Pathway by Scaffolding EZH2. *Clin Cancer Res* (2017) 24(3):684–95. doi: 10.1158/1078-0432.CCR-17-0605
2. Kamran N, Calinescu A, Candolfi M, Chandran M, Mineharu Y, Assad AS, et al. Recent Advances and Future of Immunotherapy for Glioblastoma.

Expert Opin Biol Ther (2016) 16(10):1245–64. doi: 10.1080/14712598.2016.1212012
3. Delphine G, Brian M, Thomas K, Paul D, Ankit S, Bassam A, et al. Divergent Evolution of Temozolomide Resistance in Glioblastoma Stem Cells is Reflected in Extracellular Vesicles and Coupled With Radiosensitization. *Neuro Oncol* (2018) 2):2. doi: 10.1093/neuonc/nox142
4. Droop A, Bruns A, Tanner G, Rippaus N, Morton R, Harrison S, et al How to Analyse the Spatiotemporal Tumour Samples Needed to Investigate Cancer Evolution: A Case Study Using Paired Primary and Recurrent Glioblastoma. *Int J Cancer* (2018) 142(8):1620–6. doi: 10.1002/ijc.31184
5. Messaoudi K, Clavreul A, Lagarce F. Toward an Effective Strategy in Glioblastoma Treatment. Part II: RNA Interference as a Promising Way to Sensitize Glioblastomas to Temozolomide. *Drug Discov Today* (2015) 20 (6):772–9. doi: 10.1016/j.drudis.2015.02.014
6. Zheng Y-L, Li L, Jia Y-X, Zhang B-Z, Li J-C, Zhu Y-H. LINC01554-Mediated Glucose Metabolism Reprogramming Suppresses Tumorigenicity in Hepatocellular Carcinoma via Downregulating PKM2 Expression and Inhibiting Akt/mTOR Signaling Pathway. *Theranostics* (2019) 9(3):796–810. doi: 10.7150/thno.28992
7. Sheng SR, Wu JS, Tang YL, Liang XH. Long Noncoding RNAs: Emerging Regulators of Tumor Angiogenesis. *Future Oncol* (2017) 13(17):1551–62. doi: 10.2217/fon-2017-0149
8. Salmena L, Poliseno L, Tay Y, Kats L, Pandolfi PP. A ceRNA Hypothesis: The Rosetta Stone of a Hidden RNA Language? *Cell* (2011) 146(3):353–8. doi: 10.1016/j.cell.2011.07.014
9. Qu L, Ding J, Chen C, Wu ZJ, Liu B, Gao Y, et al. Exosome-Transmitted lncARSR Promotes Sunitinib Resistance in Renal Cancer by Acting as a Competing Endogenous RNA. *Cancer Cell* (2016) 29(5):653–68. doi: 10.1016/j.ccell.2016.03.004
10. Cesana M, Cacchiarelli D, Legnini I, Santini T, Sthandier O, Chinappi M, et al. A Long Noncoding RNA Controls Muscle Differentiation by Functioning as a Competing Endogenous RNA. *Cell* (2011) 147(2):358–69. doi: 10.1016/j.cell.2011.09.028
11. Ji J, Xu R, Ding K, Bao G, Wang J. Long Noncoding RNA SChLAP1 Forms a Growth Promoting Complex With HNRNPL in Human Glioblastoma Through Stabilization of ACTN4 and Activation of NF-κb Signaling. *Clin Cancer Res* (2019) 25(22):clincanres.0747.2019. doi: 10.1158/1078-0432.CCR-19-0747
12. Katsushima K, Natsume A, Ohka F, Shinjo K, Hatanaka A, Ichimura N, et al. Targeting the Notch-Regulated Non-Coding RNA TUG1 for Glioma Treatment. *Nat Commun* (2016) 7:13616. doi: 10.1038/ncomms13616
13. Liu L, Cui S, Wan T, Li X, Shi Y. Long Non-Coding RNA HOTAIR Acts as a Competing Endogenous RNA to Promote Glioma Progression by Sponging miR-126-5p. *J Cell Physiol* (2018) 233(5):6822–31. doi: 10.1002/jcp.26432
14. Liu H, Lv Z, Guo E. Knockdown of Long Noncoding RNA SPRY4-IT1 Suppresses Glioma Cell Proliferation, Metastasis and Epithelial-Mesenchymal Transition. *Int J Clin Exp Pathol* (2015) 8(8):9140–6.
15. Wang L, Feng Z, Wang X, Wang X, Zhang X. DEGseq: An R Package for Identifying Differentially Expressed Genes From RNA-Seq Data. *Bioinformatics* (2010) 26(1):136–8. doi: 10.1093/bioinformatics/btp612
16. Cao Z, Pan X, Yang Y, Huang Y, Shen HB. The Lnclocator: A Subcellular Localization Predictor for Long Non-Coding RNAs Based on a Stacked Ensemble Classifier. *Bioinformatics* (2018) 34(13):2185–94. doi: 10.1093/bioinformatics/bty085
17. Liu S, Mitra R, Zhao M-M, Fan W-H, Eischen C, Yin F, et al. The Potential Roles of Long Noncoding RNAs (lncRNA) in Glioblastoma Development. *Mol Cancer Ther* (2016) 15(12):2977–86. doi: 10.1158/1535-7163.MCT-16-0320
18. Kraus T, Greiner A, Guibourt V, Lisec KA, Kretzschmar H. Identification of Stably Expressed lncRNAs as Valid Endogenous Controls for Profiling of Human Glioma. *J Cancer* (2015) 6(2):111–9. doi: 10.7150/jca.10867
19. Rinn JL, Kertesz M, Wang JK, Squazzo SL, Xu X, Brugmann SA, et al. Functional Demarcation of Active and Silent Chromatin Domains in Human HOX Loci by Noncoding RNAs. *Cell* (2007) 129(7):1311–23. doi: 10.1016/j.cell.2007.05.022
20. Chen D, Bhat-Nakshatri P, Goswami C, Badve S, Nakshatri H. ANTXR1, a Stem Cell-Enriched Functional Biomarker, Connects Collagen Signaling to Cancer Stem-Like Cells and Metastasis in Breast Cancer. *Cancer Res Off Organ Am Assoc Cancer Res Inc* (2013) 73(18):5821–33. doi: 10.1158/0008-5472.CAN-13-1080
21. Frezzato F, Raggi F, Martini V, Severin F, Trimarco V, Visentin A, et al. HSP70/HSF1 Axis, Regulated via a PI3K/AKT Pathway, Is a Druggable Target in Chronic Lymphocytic Leukemia. *Int J Cancer* (2019) 145(11):3089–100. doi: 10.1002/ijc.32383
22. Kita K, Shiota M, Tanaka M, Otsuka A, Tomita S. Hsp70 Inhibitors Suppress Androgen Receptor Expression in LNCaP95 Prostate Cancer Cells. *Cancer ence* (2017) 108(9):1820–27. doi: 10.1002/ijc.32383
23. Dimas DTh, Perlepe CD, Sergentanis TN, Misitzis L, Kontzoglou K, Patsouris E, et al. The Prognostic Significance of Hsp70/Hsp90 Expression in Breast Cancer: A Systematic Review and Meta-Analysis. *Anticancer Res Int J Cancer Res Treat* (2018) 38(3):1551–62. doi: 10.21873/anticanres.12384
24. Lee JH, Han YS, Yoon YM, Yun CW, Yun SP, Kim SM, et al. Role of HSPA1L as a Cellular Prion Protein Stabilizer in Tumor Progression *via* HIF-1α/GP78 Axis. *Oncogene* (2017) 36(47):6555–67. doi: 10.1038/onc.2017.263
25. Sheng L, Tang T, Liu Y, Ma Y, Wang Z, Tao H, et al. Inducible HSP70 Antagonizes Cisplatin?Induced Cell Apoptosis Through Inhibition of the MAPK Signaling Pathway in HGC-27 Cells. *Int J Mol Med* (2018) 42(4):2089–97. doi: 10.3892/ijmm.2018.3789
26. Zhang S, Wang B, Xiao H, Dong J, Li Y, Zhu C, et al. LncRNA HOTAIR Enhances Breast Cancer Radioresistance Through Facilitating HSPA1A Expression via Sequestering miR-449b-5p. *Thoracic Cancer* (2020) 11 (7):1801–16. doi: 10.1111/1759-7714.13450
27. Zhe Y, Li Y, Liu D, Su DM, Liu JG, Li HY. Extracellular HSP70-Peptide Complexes Promote the Proliferation of Hepatocellular Carcinoma Cells *via* TLR2/4/JNK1/2MAPK Pathway. *Tumor Biol* (2016) 37(10):13951–9. doi: 10.1007/s13277-016-5189-5
28. Wu FH, Yuan Y, Li D, Liao SJ, Yan B, Wei JJ, et al. Extracellular HSPA1A Promotes the Growth of Hepatocarcinoma by Augmenting Tumor Cell Proliferation and Apoptosis-Resistance. *Cancer Lett* (2012) 317(2):157–64. doi: 10.1016/j.canlet.2011.11.020
29. Zongguo Y, Liping Z, Peter S, Li W, Hua S, Yunfei L, et al. Upregulation of Heat Shock Proteins (HSPA12A, HSP90B1, HSPA4, HSPA5 and HSPA6) in Tumour Tissues is Associated With Poor Outcomes From HBV-Related Early-Stage Hepatocellular Carcinoma. *Int J Med ences* (2015) 12(3):256–63. doi: 10.7150/ijms.10735
30. Shevtsov M, Nikolaev B, Ryzhov V, Yakovleva L, Marchenko Y, Parr M, et al. Ionizing Radiation Improves Glioma-Specific Targeting of Superparamagnetic Iron Oxide Nanoparticles Conjugated With cmHsp70.1 Monoclonal Antibodies (SPION-cmHsp70.1). *Nanoscale* (2015) 7(48):20652–l64. doi: 10.1039/c5nr06521f
31. Fellinger H, Stangl S, Schnelzer A, Schwab M, Genio T, Pieper M, et al. Time- and Dose-Dependent Effects of Ionizing Irradiation on the Membrane Expression of Hsp70 on Glioma Cells. (2020). doi: 10.3390/cells9040912
32. Kim J, Hu Z, Cai L, Li K, Choi E, Faubert B, et al. CPS1 Maintains Pyrimidine Pools and DNA Synthesis in KRAS/LKB1-Mutant Lung Cancer Cells. *Nature* (2017) 546(7656):168–72. doi: 10.1038/nature22359
33. Zhou X, Rao Y, Sun Q, Liu Y, Chen J, Bu W. Long Noncoding RNA CPS1-IT1 Suppresses Melanoma Cell Metastasis Through Inhibiting Cyr61 *via* Competitively Binding to BRG1. *J Cell Physiol* (2019) 234(12):22017–27. doi: 10.1002/jcp.28764
34. Zhang W, Yuan W, Song J, Wang S, Gu X. LncRna CPS1-IT1 Suppresses Cell Proliferation, Invasion and Metastasis in Colorectal Cancer. *Cell Physiol Biochem* (2017) 44(2):567–80. doi: 10.1159/000485091
35. Takashima K, Oshiumi H, Matsumoto M, Seya T. DNAJB1/HSP40 Suppresses Melanoma Differentiation-Associated Gene 5-Mitochondrial Antiviral Signaling Protein Function in Conjunction With Hsp70. *J Innate Immun* (2017) 10(1):44–55. doi: 10.1159/000480740
36. Moses MA, Kim YS, Rivera-Marquez GM, Oshima N, Neckers LM. Targeting the Hsp40/Hsp70 Chaperone Axis as a Novel Strategy to Treat Castration-Resistant Prostate Cancer. *Cancer Res* (2018) 78(14):canres.3728.2017. doi: 10.1158/0008-5472.CAN-17-3728
37. Chen J, Yao Y, Gong C, Yu F, Su S, Chen J, et al. CCL18 From Tumor-Associated Macrophages Promotes Breast Cancer Metastasis *via* PITPNM3. *Cancer Cell* (2011) 19(4):541–55. doi: 10.1016/j.ccr.2011.02.006
38. Zhou Z, Peng Y, Wu X, Meng S, Yu W, Zhao J, et al. CCL18 Secreted From M2 Macrophages Promotes Migration and Invasion *via* the PI3K/Akt Pathway in

Gallbladder Cancer. *Cell Oncol* (2019) 42(1):81–92. doi: 10.1007/s13402-018-0410-8
39. Shen T, Yang Z, Cheng X, Xiao Y, Yu K, Cai X, et al. CXCL8 Induces Epithelial-Mesenchymal Transition in Colon Cancer Cells via the PI3K/Akt/NF-κB Signaling Pathway. *Oncol Rep* (2017). doi: 10.3892/or.2017.5453
40. Brown H, Tellez-Gabriel M, Cartron P-F, Vallette F-M, Heymann M-F, Heymann D, et al. Characterization of Circulating Tumor Cells as a Reflection of the Tumor Heterogeneity: Myth or Reality? *Drug Discov Today* (2018) 24(3):763–72. doi: 10.1016/j.drudis.2018.11.017
41. Razmara AM, Sollier E, Kisirkoi GN, Baker SW, Casey KM. Tumor Shedding and Metastatic Progression After Tumor Excision in Patient-Derived Orthotopic Xenograft Models of Triple-Negative Breast Cancer. *Clin Exp Metastasis* (2020) 37(1):413–24. doi: 10.1007/s10585-020-10033-3
42. Dutil J, Chen Z, Monteiro A, Teer J, Eschrich S. An Interactive Resource to Probe Genetic Diversity and Estimated Ancestry in Cancer Cell Lines. *Cancer Res* (2019) 79(7):1263–73. doi: 10.1158/0008-5472.CAN-18-2747
43. Hagemann J, Jacobi C, Hahn M, Schmid V, Welz C, Schwenk-Zieger S, et al. Spheroid-Based 3D Cell Cultures Enable Personalized Therapy Testing and Drug Discovery in Head and Neck Cancer. *Anticancer Res Int J Cancer Res Treat* (2017)37(5):2201–10. doi: 10.21873/anticanres.11555

Conflict of Interest: The authors declare that the research was conducted in the absence of any commercial or financial relationships that could be construed as a potential conflict of interest.

frontiers in Cell and Developmental Biology

ORIGINAL RESEARCH
published: 09 July 2021
doi: 10.3389/fcell.2021.619396

Comprehensive Analysis of the Clinical and Biological Significances of Endoplasmic Reticulum Stress in Diffuse Gliomas

Ruoyu Huang[1,2,3], Guanzhang Li[1,2,3], Kuanyu Wang[3,4], Zhiliang Wang[1,2,3], Fan Zeng[1,3], Huimin Hu[1,3] and Tao Jiang[1,2,3]**

[1] Department of Molecular Neuropathology, Beijing Neurosurgical Institute, Capital Medical University, Beijing, China, [2] Department of Neurosurgery, Beijing Tiantan Hospital, Capital Medical University, Beijing, China, [3] Chinese Glioma Cooperative Group (CGCG), Beijing, China, [4] Department of Gamma Knife Center, Beijing Neurosurgical Institute, Capital Medical University, Beijing, China

OPEN ACCESS

Edited by:
Lorenzo Gerratana, University of Udine, Italy

Reviewed by:
Rui Manuel Reis, Barretos Cancer Hospital, Brazil
Emiliano Dalla, University of Udine, Italy

****Correspondence:***
Huimin Hu
huhm_bjni@163.com
Tao Jiang
taojiang1964@163.com

Specialty section:
This article was submitted to Molecular and Cellular Oncology, a section of the journal Frontiers in Cell and Developmental Biology

Received: *20 October 2020*
Accepted: *21 June 2021*
Published: *09 July 2021*

Citation:
Huang R, Li G, Wang K, Wang Z, Zeng F, Hu H and Jiang T (2021) Comprehensive Analysis of the Clinical and Biological Significances of Endoplasmic Reticulum Stress in Diffuse Gliomas. Front. Cell Dev. Biol. 9:619396. doi: 10.3389/fcell.2021.619396

Background: As a critical organelle for protein and lipid synthesis, the dysfunction of endoplasmic reticulum has a significant impact on multiple biological processes of cells. Thus, in this study, we constructed an ER stress-related risk signature to investigate the functional roles of ER stress in gliomas.

Methods: A total of 626 samples from TCGA RNA-seq dataset (training cohort) and 310 samples from CGGA RNA-seq dataset (validation cohort) were enrolled in this study. Clinical information and genomic profiles were also obtained. The ER stress signature was developed by the LASSO regression model. The prognostic value of the risk signature was evaluated by Cox regression, Kaplan-Meier and ROC Curve analyses. Bioinformatics analysis and experiment *in vitro* were performed to explore the biological implication of this signature.

Results: We found that the ER stress-related signature was tightly associated with major clinicopathological features and genomic alterations of gliomas. Kaplan-Meier curve and Cox regression analysis indicated that ER stress activation was an independent prognostic factor for patients with glioma. Besides, we also constructed an individualized prognosis prediction model through Nomogram and ROC Curve analysis. Bioinformatics analysis suggested that ER stress activation also promoted the malignant progression of glioma and participated in the regulation of tumor immune microenvironment,especially the infiltration of macrophages in M2 phase. These results were further validated in IHC analysis and cell biology experiments.

Conclusion: The ER stress activation had a high prognostic value and could serve as a promising target for developing individualized treatment of glioma.

Keywords: glioma, ER stress, signature, prognosis, tumor immune environment

INTRODUCTION

Glioma is the most common and aggressive tumor in central nervous system (Wen and Kesari, 2008; Ricard et al., 2012; Jiang et al., 2016). Despite significant advances in conventional therapies including surgical resection with concomitant radiotherapy and chemotherapy, the clinical prognosis of patients with malignant glioma were still unsatisfied, with a five-year survival rate of 5–13% (Phillips et al., 2006; Nuno et al., 2013; Reifenberger et al., 2017). In past decades, researches were devoted to the targeted drugs and immunotherapy of gliomas and produced very limited success (Osuka and Van Meir, 2017; Cloughesy et al., 2019; Zhao et al., 2019). In order to develop more effective treatment strategies to improve the clinical prognosis of patients, a deeper understanding of the molecular mechanisms underlying the genesis and malignant progression of glioma is imperative. In this study, we focused on the functional roles and prognosis value of endoplasmic reticulum (ER) stress activation in gliomas.

Endoplasmic reticulum stress is imbalance of the ER homeostasis induced by accumulation of unfolded or misfolded proteins and alteration of the Ca^{+} concentration (Adamopoulos et al., 2014, 2016; Leprivier et al., 2015). As a crucial organelle, the dysfunction of ER has significant impact on multiple cellular processes (Gutierrez and Simmen, 2014). Relevant researches proved that ER stress participates in the genesis and malignant progression of multiple human cancers (Joo et al., 2007; Obacz et al., 2017). Besides, as a self-protective mechanism against the exogenous or endogenous stress, ER stress was involved in the proliferation of cancer cells in hypoxia environment and the resistance to radiotherapy or chemotherapy (Yao et al., 2020). However, excessive and sustained ER stress could also trigger programmed cell death or apoptosis. According to former research achievements, ER stress was tightly associated with drug-induced apoptosis in lung carcinoma and glioma cells (Joo et al., 2007; Chang et al., 2020). Moreover, cancer cells could acquire drug resistance and survive chemotherapies through ER stress mediated dormancy and immunosuppression (Hamanaka et al., 2005; Lee et al., 2014; Cubillos-Ruiz et al., 2017). These researches indicated that ER stress might be a valuable target for the treatment of malignant tumors. However, the association of ER stress with the biological characteristics and clinical prognosis of glioma remains unclear, which was worth to investigate thoroughly.

In this study, we divided patients into two subgroups based on the profile of ER stress related genes in The Cancer Genome Atlas (TCGA) and Chinese Glioma Genome Atlas (CGGA) datasets and found that there were significant differences in clinicopathological characteristics and prognosis between stratified patients. Then, we constructed a risk signature to evaluate the ER stress activation status and predict the clinical outcome of glioma patients in TCGA dataset. Kaplan-Meier (K-M) survival curve and Cox regression analysis suggested that the ER stress related signature was a valuable prognostic predictor. Besides, by applying nomogram plots, we developed an individualized prediction model which could accurately predict the 1-, 3- and 5-years survival for glioma patients. Bioinformatics analyses were performed to elucidate the functional roles of ER stress in glioma. Furthermore, the downregulation of ER stress could significantly inhibit the proliferation and migration of glioma cell lines *in vitro*. The IHC analysis also showed that the activation of ER stress was tightly associated with the infiltration of macrophages in M2 phase. The results indicated that the risk signature was tightly associated with malignant biological process and the regulation of tumor immune microenvironment in gliomas.

MATERIALS AND METHODS

Samples and Datasets

A total of 626 glioma samples (including 460 low-grade glioma and 166 GBM samples) with RNA sequencing data and clinical information from the Cancer Genome Atlas (TCGA) dataset[1] were used as discovery cohort. Similarly, 310 glioma samples (including 172 low-grade glioma and 138 GBM samples) with RNA sequencing data and clinical information were downloaded from CGGA dataset[2] as validation cohort (Zhao et al., 2017). The establishment and management of CGGA dataset was described in the previous study. The clinical characteristics of patients from TCGA and CGGA datasets were summarized in **Table 1**

[1]http://cancergenome.nih.gov/

[2]http://www.cgga.org.cn

TABLE 1 | Characteristics of patients in cluster 1 and cluster 2 in TCGA dataset.

Characteristic	*N*	Cluster 1	Cluster 2	*p* value
Total cases	626	324	302	
Gender				0.0933
Male	362	177	185	
Female	264	147	117	
Age (years)				< 0.0001
≤40	241	169	72	
>40	385	155	230	
Grade				< 0.0001
II	219	184	35	
III	241	139	102	
IV	166	1	165	
Subtype				< 0.0001
Classical	87	2	85	
Mesenchymal	99	2	97	
Proneural	224	165	59	
Neural	104	93	11	
IDH status				< 0.0001
Mutation	383	305	78	
Wildtype	234	18	216	
MGMT promoter				< 0.0001
Methylation	436	291	145	
Unmethylation	153	32	121	
1p19q				< 0.0001
Codel	152	144	8	
Intact	468	180	288	

and **Supplementary Table 1**, respectively. Besides, 270 GBM samples with RNA sequencing data and specific tumor anatomic structure information from Ivy Glioblastoma Atlas Project[3] were also enrolled in this study (Puchalski et al., 2018). All the RNA sequencing data were log2-transformed for further analysis. This study was approved by Institutional Review Board (IRB) of Beijing Tiantan Hospital Affiliated to Capital Medical University.

Consensus Clustering and Construction of Signature

Two ER stress-related gene sets (GO RESPONSE TO ENDOPLASMIC RETICULUM STRESS and GO REGULATION OF RESPONSE TO ENDOPLASMIC RETICULUM STRESS) were downloaded from Molecular Signature Database v7.0 (MSigDB, [4]). Overlapped genes were removed and the acquired ER stress-related gene set contained 272 genes. Among them, 256 genes could be found in TCGA dataset (**Supplementary Table 2**). Then, we performed univariate Cox analysis with these genes in all glioma patients from TCGA dataset and found that there were 208 genes within the list have prognostic value in patients with gliomas (**Supplementary Table 3**). The least absolute shrinkage and selection operator (LASSO) analysis was employed to identify the most valuable predictive genes (Bovelstad et al., 2007; Hu et al., 2017). The genes and their coefficients were determined by the best penalty parameter λ associated with the smallest 10-fold cross validation (Tibshirani, 1997; Bovelstad et al., 2007). Then, these obtained genes were employed to construct an optimal risk signature that was determined by a linear combination of their expression levels weighted with regression coefficients from LASSO analysis. The risk score for each sample was calculated as following formula: $Risk\ score = \sum_{i=1}^{n} \beta i x i$. In this formula, xi is the relative expression value of each selected gene and βi is the coefficient obtained from LASSO analysis. For validation, the same genes, regression coefficients and formula were applied in CGGA dataset to calculate the risk score.

Immunohistochemistry

In this study, we performed immunohistochemical (IHC) staining of the protein encoded by signature genes *PDIA4* (Protein disulfide-isomerase A4) and *P4HB* (prolyl 4-hydroxylase, β polypeptide), which were considered as the important biomarker of ER stress. In brief, the sections of glioma tissues were deparaffinized and boiled with ethylenediaminetetraacetic acid (EDTA) antigen retrieval buffer. Then, the sections were incubated with specific primary antibodies overnight at 4°C (anti-*PDIA4*, 1:500 dilutions; anti-*P4HB*, 1:1,000; anti-*CD163*, 1:500; anti-*IBA1*, 1:2,000; Abcam, Cambridge, United Kingdom). All the sections were then incubated with secondary antibodies (ZSGB-Bio, China) at room temperature for 1 h. Finally, the expression levels of each protein in glioma tissues were defined as the portion of positively stained cells against total counted cells in each scan field. IHC staining was quantified by analysis of images from at least five high-power fields. The measure was repeated three times for each section and performed by two experienced pathologists, respectively. Besides, to further validate the results of bioinformatics analysis, IHC staining was also performed to analysis the expression level of the biomarkers of macrophages, *CD163* and *IBA1* (van den Heuvel et al., 1999; Ohsawa et al., 2000). Patients were divided into "low-risk" and "high-risk" groups according to the median risk score in CGGA dataset. The positive expression rates of IHC were compared among glioma patients in the low- and high-risk score groups with a non-parametric test.

Cell Culture and Transfection

Human glioma cell line U-87MG (U87, RRID:CVCL_0022) and LN229 (RRID:CVCL_0393) were purchased from the Institute of Biochemistry and Cell Biology, Chinese Academy of Sciences. Both of the cell lines were cultured in DMEM medium (Gibco; Thermo Fisher Scientific, United States) supplemented with 10% fetal bovine serum (FBS, Gibco; Thermo Fisher Scientific) at 37°C in a humidified atmosphere of 5% CO_2. The *P4HB* and *PDIA4* small interference RNA (siRNA) and negative control (NC) were synthesized by RiboBio Co., Ltd. (Guangzhou, China). When the cell density reached 30–50%, LN229 or U87 cell lines was transfected with siRNA or NC (50 nM) at 37°C using the transfection reagent (Polyplus-transfection Co., Ltd., France). After 48 h, fresh medium without siRNA was added to the cells. The sequences for *PDIA4* and *P4HB* siRNA are as follows: *PDIA4* siRNA1 5′-GAGCAAGTTTATAGAAGAA-3′; *PDIA4* siRNA2 5′-GGAAGGCCTTATGACTACA-3′; *PDIA4* siRNA3 5′-GAGTCTTGGTCCTAAATGA-3′. P4HB siRNA1 5′-GTCTGACTATGACGGCAAA-3′; *P4HB* siRNA2 5′-GGCCATCGATGACATACCA-3′; *P4HB* siRNA3 5′-CCATCAAGTTCTTCAGGAA-3′. In this study, all experiments were performed with mycoplasma-free cells and all glioma cell lines have been authenticated using STR profiling.

Quantitative PCR and Western Blot

Quantitative PCR (qPCR) was performed using the SYBR SuperMix kit (Bio-Rad Laboratories, Inc.) in the 7,500 Fast Real-Time PCR system (Applied Biosystems, United States) according to the manufacturer's protocols. The relative mRNA expression levels of *PDIA4* and *P4HB* were normalized to *GAPDH* and were calculated using the $2^{-\Delta\Delta Cq}$ method. The primer sequences of *PDIA4*, *P4HB* and *GAPDH* were synthesized by GENEWIZ Co. (Beijing, China). The primer sequences were as follows: *PDIA4*, forward 5′-GGCAGGCTGTAGACTACGAG-3′, and reverse 5′-TTGGTCAACACAAGCGTGAC-3′; *P4HB*, forward 5′-GGTGCTGCGGAAAAGCAAC-3′, and reverse 5′-ACCTGATCTCGGAACCTTCTG-3′; and *GAPDH*, forward 5′-GGAGCGAGATCCCTCCAAAAT-3′, and reverse 5′-GGCTGTTGTCATACTTCTCATGG-3′. Western blot (WB) analysis was performed with rabbit anti-*PDIA4* and anti-*P4HB* polyclonal antibody (1:1,000 and 1:2,000, respectively, Abcam). Mouse anti-*GAPDH* antibody (1:5,000, Abcam) was used for loading control and goat anti-rabbit IgG-HRP (1:5,000, ZSGB-Bio, China) was used as secondary antibodies.

[3]http://glioblastoma.alleninstitute.org/

[4]http://www.broad.mit.edu/gsea/msigdb/

Cell Migration Assays

After transfection with *PDIA4* siRNA, *P4HB* siRNA or NC siRNA, 1×10^5 cells were seeded into upper chambers of a 24-well transwell chambers (Corning, United States) with 150 μl serum-free medium, while 600 μl medium contained 10% FBS was added into the lower chamber. After that, the mentioned U87 and LN229 cells were incubated at 37°C for 2 or 4 h, respectively. Then, cells on the upper surface of filters were removed with cotton swabs and cells at the bottom surface were fixed and stained with 0.5% crystal violet. Finally, the stained cells were observed using the ×1 and ×10 objectives and measured with × 20 objective.

Cell Scratch Assays

LN229 and U87 cells were seeded in 6-well plates (1×10^5 cells per well) and incubated at 37°C. After adherence, cells were transfected with specific siRNA for 48 h. Then, the cell monolayer was scraped with a sterile 200-μL pipette tip. After that, the medium in each well were replaced with fresh medium without serum and the "zero point" of migration in each well was photographed under computer-assisted microscopy (ZEISS, Germany). At the end of 48 h incubation, the same scratch area of each well was photographed again.

Cell Proliferation Assay

Cell proliferation *in vitro* was studied by cell counting kit-8 (CCK-8, Dojindo Laboratories, Japan). After the transfection with specific siRNA, LN229 and U87 cells were plated in 96-well plates and cultured at 37°C for 1–5 days (1×10^3 cells per well). At the same time of each day, 100 μl fresh culture medium and 10 μl CCK-8 reagent were thoroughly mixed and added to each well. After 2 h incubation at 37°C, the absorbances at 450 nm of the medium were measured for further analysis. The measures were performed in triplicate.

Clonogenic Assays

After transfection with specific siRNA, LN229 and U87 cells were digested and seeded into a 6-well culture plate (400 cells per well). Plates were maintained in a 37°C, 5% CO2 incubator for 12 days. To maintain a low-level of *PDIA4* and *P4HB* in the whole assay, siRNA transfection was repeated at the 6th day. After the 12 days of incubation, cell colonies were stained with crystal violet and photographed for further analysis.

Bioinformatic Analysis

In this study, we developed a nomogram prediction model to predict the 1-, 3- and 5-year survival rate of glioma patients using package "rms" in R Language. PCA was performed to explore the transcriptomic differences within groups using R package "princomp" (David and Jacobs, 2014). In TCGA and CGGA datasets, the genes which were tightly correlated with the risk signature (Pearson correlation analysis, $|R| > 0.5$) were uploaded on DAVID website[5]. Then, Gene Ontology (GO) analysis and Kyoto Encyclopedia of Genes and Genomes (KEGG) pathway analysis were carried out to identified the biological processes tightly related to the risk signature. Gene-set enrichment analysis (GSEA) was applied to further identify biological functions of statistical difference between high-risk and low-risk groups by using the GSEA v3 software[6] (Subramanian et al., 2005). CIBERSORT was also enrolled in this study to estimate the abundances of immune cells infiltrated in glioma tissue. In CIBERSORT analysis, a matrix of reference gene expression signatures (proposed by Newman et al.) was uploaded on the public website[7] to estimate the relative proportions of each cell type (Newman et al., 2015, 2019).

Statistical Analysis

The statistical analyses were mainly conducted using R language (version 3.6.2) and SPSS (version 16.0). Student's *t*-test and One-way ANOVA were performed to compare differences among groups. The Kaplan-Meier (K-M) survival curves analysis was conducted to estimate survival distributions. Cox regression analysis, nomogram model and time ROC curve analysis were used to evaluate the prognostic value of the ER stress related signature (Robin et al., 2011). In this study, $p < 0.05$ was regarded as statistically significant.

RESULTS

Cluster Model of ER Stress in Glioma Based on Consensus Clustering Analysis

In order to explore the association of ER stress status with the clinical characteristics and prognosis of patients with diffuse gliomas, consensus clustering analyses were performed with ER stress related genes in TCGA and CGGA RNA sequencing datasets. The results of consensus clustering suggested that patients could be grouped into two robust clusters and the optimal number of clusters ($k = 2$) was determined by cumulative distribution function (CDF) curves and consensus matrices (**Supplementary Figures 1A,B**). The heat map also showed that there were significant differences in the expression of ER stress related genes between these two clusters (**Supplementary Figures 1C,D**). Besides, we further explored the difference of clinical features between patients in different clusters through Chi-square test. As shown in **Table 1**, in TCGA dataset, patients in cluster 1 were mainly with younger age, lower grade of glioma, *IDH* mutated, *MGMT* promoter methylated, 1p/19q co-deleted and enriched in Neural and Proneural subtypes. Meanwhile, the clinicopathological characteristics of patients in cluster 2 were completely opposite. Consistent results were also obtained in CGGA dataset, with the exception of the MGMT Promoter status (**Supplementary Table 1**). Survival analysis suggested that the prognosis of patients in cluster 1 was much better than those in cluster 2 (**Supplementary Figures 1E,F**). Besides, considering the unique clinicopathological characteristics of IDH wildtype GBM samples, we also performed similar analysis in

[5]http://david.ncifcrf.gov/

[6]http://www.broadinstitute.org/gsea/index.jsp

[7]https://cibersort.stanford.edu/

these samples. After dividing these samples into two clusters based on the expression level of ER stress related genes, the survival analysis show the prognosis of IDH wildtype GBM patients in two clusters tend to be different although the difference was not statistically significant in TCGA dataset (**Supplementary Figures 1G,H**, $P = 0.13$ and $P = 0.03$ for TCGA and CGGA dataset, respectively). In addition, the prognosis of IDH wildtype GBM patients is generally very poor, which leads to the classification and prognostic value of ER stress status were limited in these patients. In brief, these results indicated that the ER stress may participate in the malignant progression of glioma and have a significant impact on the prognosis of patients.

Construction of ER Stress Related Signature in Diffuse Glioma

Considering the prognostic value of ER stress in patients with gliomas, we proposed to construct a risk score model to evaluate the ER stress status of glioma samples more accurately. First, we performed univariate Cox regression analysis with the 256 ER stress related genes and screened out 208 genes that were significantly associated with the prognosis of glioma patients in TCGA dataset ($p < 0.05$). After that, these 205 genes were introduced into the LASSO Cox regression algorithm to select the most valuable predictive genes with non-zero regression coefficients and a six-gene risk signature was constructed (**Figures 1A–C**). In TCGA and CGGA datasets, the risk score of each patient was calculated by the formula "*Risk score*" mentioned in Materials and Methods section. We found that the clinical features of patients in the low-risk group and the high-risk group were highly consistent with those of cluster 1 and cluster 2, respectively (**Figure 1D**). Besides, the heatmaps exhibited an overview of association between ER stress-related genes and clinical characteristics, as the samples were ranked according to their risk scores (**Figure 1E**). Furthermore, we performed IHC staining of glioma samples from the CGGA dataset to evaluate the association of the expression level of ER stress biomarkers with risk score and WHO grade. Considering the significant difference of pathological characteristics between lower-grade glioma (LGG, WHO Grade II and III) and GBM, the IHC analysis was performed in LGG and GBM, respectively. The results suggested that the expression level of *PDIA4* and *P4HB* were higher in samples from high-risk group (**Figures 1F,1G**). Besides, we also found that the expression level of PDIA4 and P4HB in GBM samples was higher than that in LGG samples (**Figure 1H**).

Association of the Risk Signature With Clinicopathologic Features and Genomic Alterations in Glioma

Considering the histopathological heterogeneity of glioma, we further investigate the association between risk score and clinicopathologic characteristics of patients in TCGA and CGGA datasets. We found that risk score was positively correlated with WHO grade of glioma (**Figure 2A**). Besides, we also found that the risk score of *IDH* wild-type glioma was higher than *IDH* mutation glioma (**Figure 2B**). The higher risk score was also detected in glioma samples with the molecular features of *MGMT* promoter unmethylated or 1p/19q non-codeleted (**Figures 2C,D**), which were generally thought to play a key role in the progression of glioma. Additionally, among various histopathologic types of glioma, GBM had the highest risk score (**Figure 2E**). Furthermore, we comprehensively analyzed RNA sequencing data for specific tumor anatomic structure in Ivy Glioblastoma Atlas Project dataset. The results suggested that glioma samples with high-risk score were mainly enriched in the leading edge, hyperplastic blood vessels and microvascular proliferation (**Figure 2F**), which are involved in the infiltration and proliferation of glioma. The four molecular subtypes of glioma defined by TCGA network have completely different molecular biological features. In this study, we found that the risk score was dramatically upregulated in gliomas of Mesenchymal subtype, which is generally associated with poor prognosis (**Figures 2G,H**). The ROC curve analysis also suggested that the risk signature could serve as a biomarker for the Mesenchymal subtype (**Figures 2G,H**). The association between the risk score and Mesenchymal subtype was also validated in the GBM samples (**Figures 2I,J**). In brief, these results indicated that ER stress might play an essential role in the malignant progression of gliomas.

Genomic instability including somatic mutations and copy number alterations (CNAs) drives the origin and development of gliomas. To further explore the molecular mechanisms influencing ER stress in gliomas, samples with available mutation and CNA information from TCGA dataset were analyzed. After dividing cases into four groups according to the order of increasing risk score. We found that higher incidence of 1p/19q codeletion and mutations in *IDH1*, *CIC*, *ATRX*, and *FUBP1* were observed in low-risk group (**Figures 3A,B**). Meanwhile, mutations in *EGFR*, *PTEN*, *NF1*, and *SPTA1* were mainly observed in high-risk group (**Figures 3A,B**). Besides, the results also showed that the mutations in *TTN*, *MUC16*, and *RYR2* tended to be different between low-risk and high-risk group. However, there was no significant difference in *TP53* mutation between patients stratified by risk score (**Figures 3A,B**). Furthermore, we also investigated the CNAs between cases in low-risk and high-risk group. The results suggested that 1p/19q codeletion, as a genomic hallmark of oligodendroglioma, tended to be enriched in low-risk group (**Figures 3C,D**). However, as a representative genomic alteration in GBM, chromosome 7 amplification accompanied chromosome 10 loss was mainly observed in the high-risk group (**Figures 3C,D**). Besides, it is worth mentioning that 7p11.2, which contains *EGFR* was one of the most commonly amplified genomic regions in high-risk group (**Figure 3D**). Meanwhile, the most frequently deleted region associated with high-risk score was 10q23.3, which contains the *PTEN* locus (**Figure 3D**).

Prognostic Value of the ER Stress-Related Signature

Since the ER stress-related signature was tightly associated with malignant progression of glioma, we further investigate the prognostic value of the risk signature. As the survival

overview shown in **Figures 4A,B**, the prognosis of glioma patients deteriorated significantly as the risk score increases. The K-M survival analysis also suggested that patients in high-risk group experienced a shorter overall survival (OS) time in whole grade gliomas. Furthermore, similar results were also obtained in glioma patients of WHO grade II, WHO grade III and WHO grade IV in both CGGA and TCGA datasets (**Figures 4C,D**). K-M survival analyses were also performed in patients stratified by *IDH* mutant, *MGMT* promoter methylation or 1p/19q codeletion status. The results indicated that patients with higher risk score had inferior outcome in each subgroup (**Supplementary Figure 2**). In IDH-wild-type GBM patients, due to the limitation of sample size, the difference is not statistically significant, but it can still be found that patients in the low-risk group tend to have a better prognosis (**Supplementary Figure 2**). Besides, ROC curve analysis was performed to estimate the predictive value of risk signature for the survival rate. The results revealed

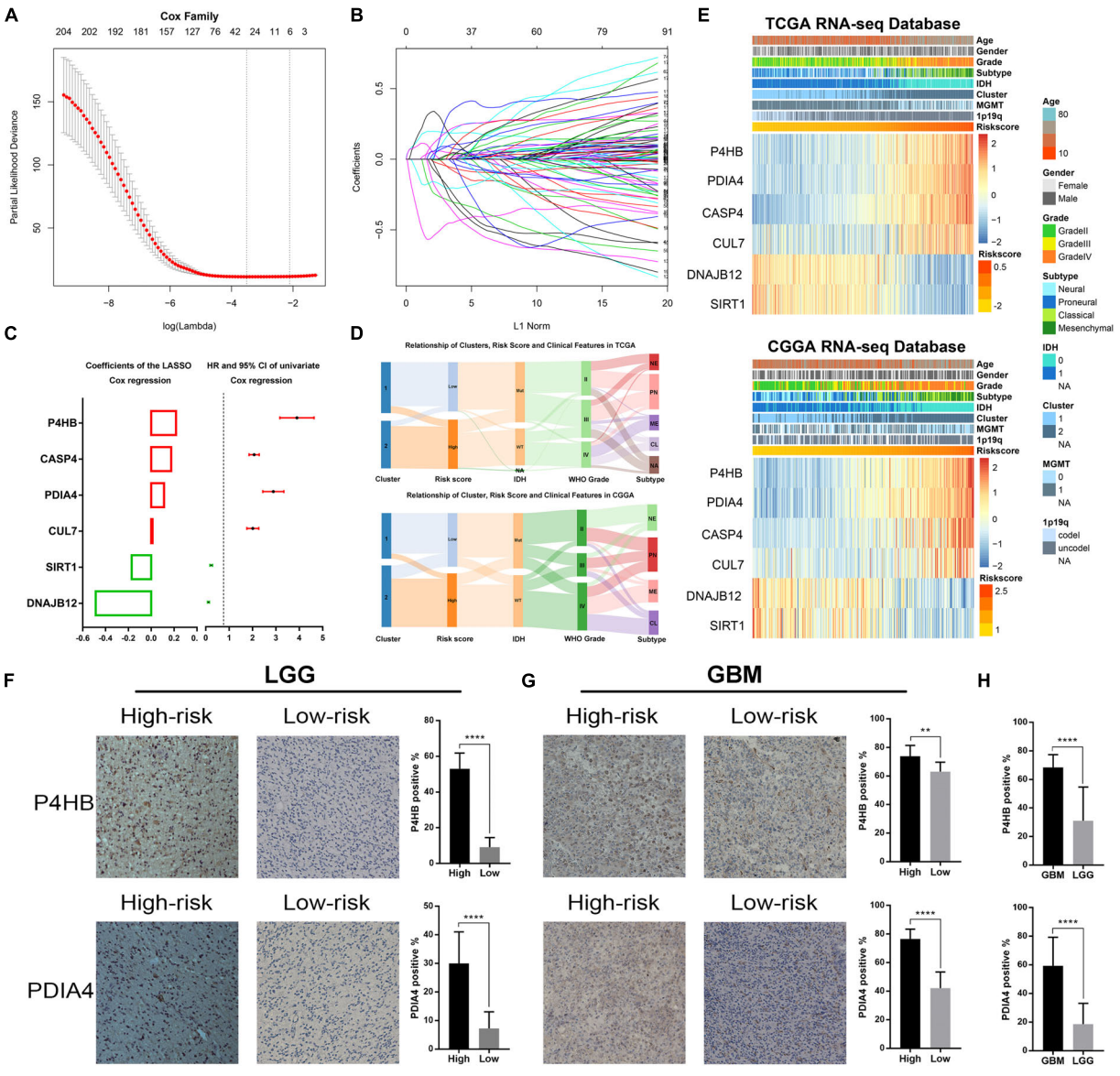

FIGURE 1 | Identification of the ER stress-related signature. **(A)** Cross-validation for tuning parameter screening in the LASSO regression model. **(B)** The coefficient profiles of the LASSO regression model. **(C)** The six genes' hazard ratios (HRs) and 95% confidence intervals (CIs) by univariate Cox regression analysis (right) and the coefficients by multivariate Cox regression analysis using LASSO (left). **(D)** Sankey diagram exhibiting the association among cluster, risk score and clinical features of glioma samples in TCGA and CGGA datasets. **(E)** Heat maps of six genes in the risk signature based on the risk score in TCGA and CGGA datasets. **(F)** IHC staining and positive rate statistics of *PDIA4* and *P4HB* in LGG samples from the CGGA dataset. **(G)** IHC staining and positive rate statistics of *PDIA4* and *P4HB* in GBM samples from the CGGA dataset. **(H)** Positive rate statistics of *PDIA4* and *P4HB* between LGG and GBM samples from the CGGA dataset. $^{**}p < 0.01$, $^{****}p < 0.0001$.

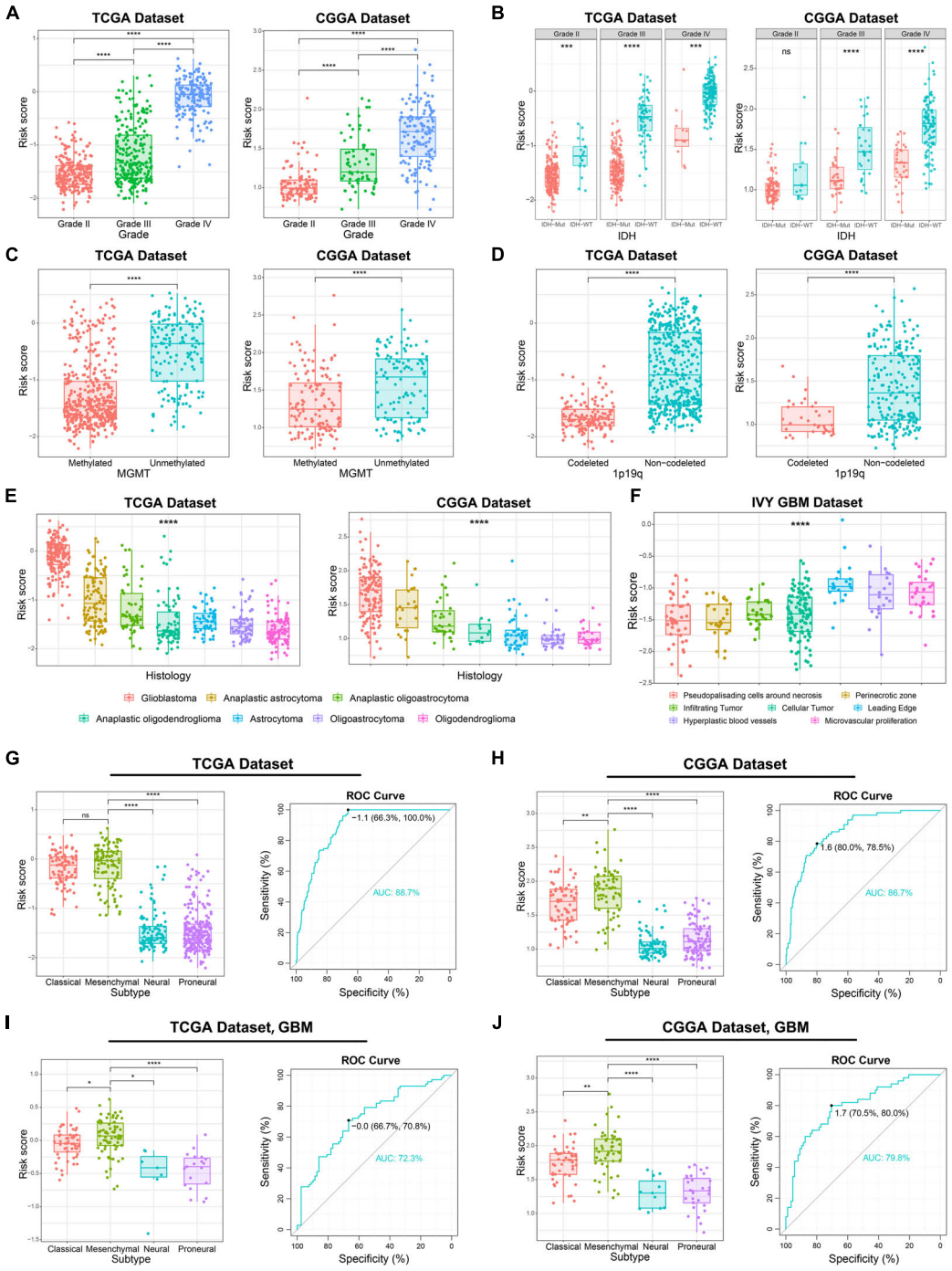

FIGURE 2 | Association between the ER stress-related signature and clinicopathologic features in TCGA and CGGA datasets. **(A–E)** The association between risk score and WHO grade **(A)**, IDH mutation status **(B)**, *MGMT* promoter methylation **(C)**, 1p/19q co-deletion status **(D)** and histopathologic classification **(E)** of glioma patients. **(F)** The distribution of risk score in the different location of GBM in IVY GBM dataset. **(G,H)** In glioma samples, the Mesenchymal subtype had the highest risk score among four molecular subtypes. ROC curves predicted ER stress activation as a biomarker of Mesenchymal subtype glioma. **(I,J)** In GBM samples, the Mesenchymal subtype had the highest risk score among four molecular subtypes. ROC curves predicted ER stress activation as a biomarker of Mesenchymal subtype glioma. *$p < 0.05$, **$p < 0.01$, ***$p < 0.001$, ****$p < 0.0001$, ns: no statistically significant.

that the risk signature had a favorable prognostic value with high time-dependent AUC for 1−, 3− and 5−year survival rate in both TCGA (86.61, 91.51, and 85.77%, respectively) and CGGA (81.94, 90.01, and 95.15%, respectively) datasets (**Figures 4E,F**). Considering that many clinicopathological factors have influence on the prognosis of glioma patients,

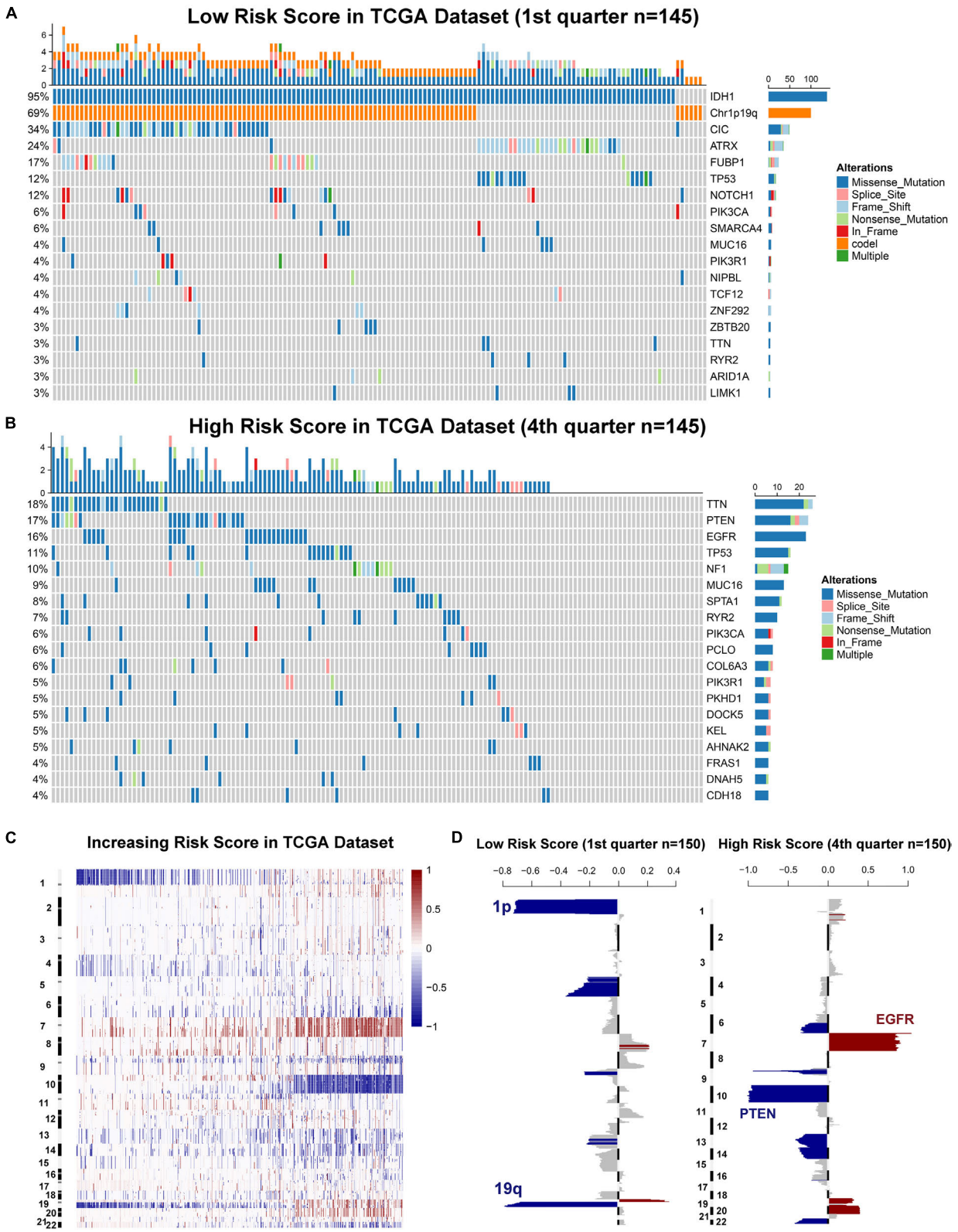

FIGURE 3 | Gliomas with different ER stress activation status have distinct genomic profiles. **(A,B)** Distinct somatic mutations identified by comparing gliomas with low- and high-risk score. **(C)** CNV profiles with increasing order of the risk score of ER stress-related signature. **(D)** A distinct CNV spectrum defined by risk scores of ER stress-related signature. The amplification (red) and deletion (blue) of chromosome segment are presented.

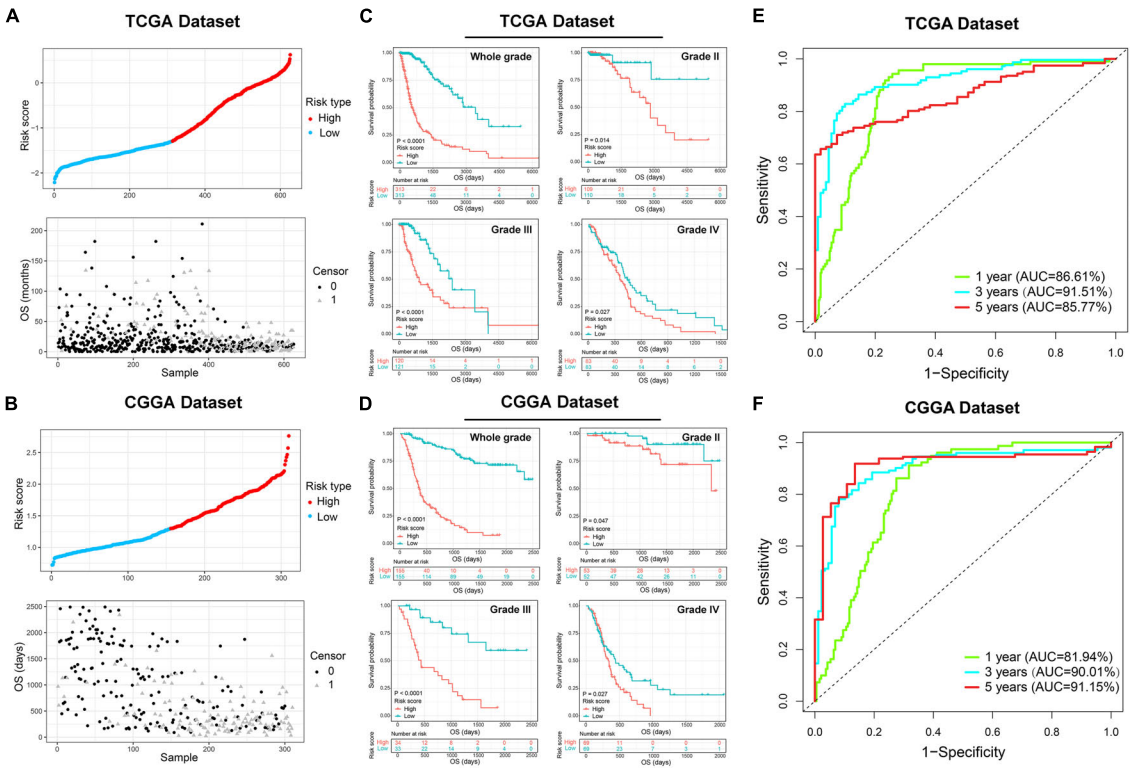

FIGURE 4 | The prognostic value of the ER stress-related signature in TCGA and CGGA datasets. **(A,B)** The distribution of the risk score and survival overview of patients with gliomas. **(C,D)** K-M survival analyses of the risk signature in glioma patients stratified by WHO grade. **(E,F)** The time ROC curve analyses were performed to predict 1−, 3−, and 5-year OS according to risk score.

Cox regression analysis was performed to further explore the clinical prognostic significance of the risk signature in gliomas. The univariate analysis showed that the risk score, age at diagnosis, WHO grade, TCGA subtypes, and the status of *IDH* mutation, *MGMT* promoter methylation and 1p/19q codeletion were significantly associated with OS in both TCGA and CGGA datasets (**Table 2** and **Supplementary Table 4**). After adjusting these factors in the multivariate analysis, we found that the risk signature was still a significant survival predictor in both datasets. These results suggested that the ER-stress related signature may serve as an independent predictor for the poor prognosis of gliomas.

In order to predict the survival rate of specific glioma patients more accurately, we constructed a nomogram model with the independent prognostic factors identified by multivariate COX analysis (**Supplementary Figure 3A**). Meanwhile, the calibration curves were performed to validate the accuracy of the nomogram model and the results showed a satisfactory concordance in the prediction of 1−, 3−, and 5-year OS in TCGA and CGGA datasets (**Supplementary Figures 3B,C**).

Biological Functions Related to the 6-Gene Signature

Considering the obvious difference in clinicopathological characteristics defined by distinct status of ER stress, principal components analysis (PCA) was performed based on the whole genome expression data to further explore the differences of gene expression pattern between patients in low− and high-risk group (**Figures 5A,B**). The results showed that cases in low− and high-risk group tended to distribute in different directions. To explore the biological functions associated with the risk signature in gliomas, A total of 4,975 and 2,572 genes which were tightly correlated with the risk signature were selected by

TABLE 2 | Univariate and multivariate analysis of OS in TCGA sequencing dataset.

Variables	Univariate analysis		Multivariate analysis	
	HR (95% CI)	*p* value	HR (95% CI)	*p* value
Risk score	5.999 (4.754–7.570)	<0.001	2.242 (1.310–3.839)	0.003
Age at Diagnosis	1.073 (1.061–1.085)	<0.001	1.056 (1.040–1.073)	<0.001
Gender	1.086 (0.818–1.440)	0.570	–	–
WHO Grade	4.862 (3.839–6.157)	<0.001	1.553 (1.059–2.276)	0.024
TCGA Subtype	2.022 (1.779–2.299)	<0.001	1.040 (0.823–1.313)	0.745
IDH mutation status	0.228 (0.158–0.329)	<0.001	0.996 (0.474–2.091)	0.991
MGMT methylation	0.320 (0.234–0.439)	<0.001	0.745 (0.496–1.118)	0.155
1p/19q co-deletion	0.227 (0.138–0.375)	<0.001	0.628 (0.337–1.170)	0.143

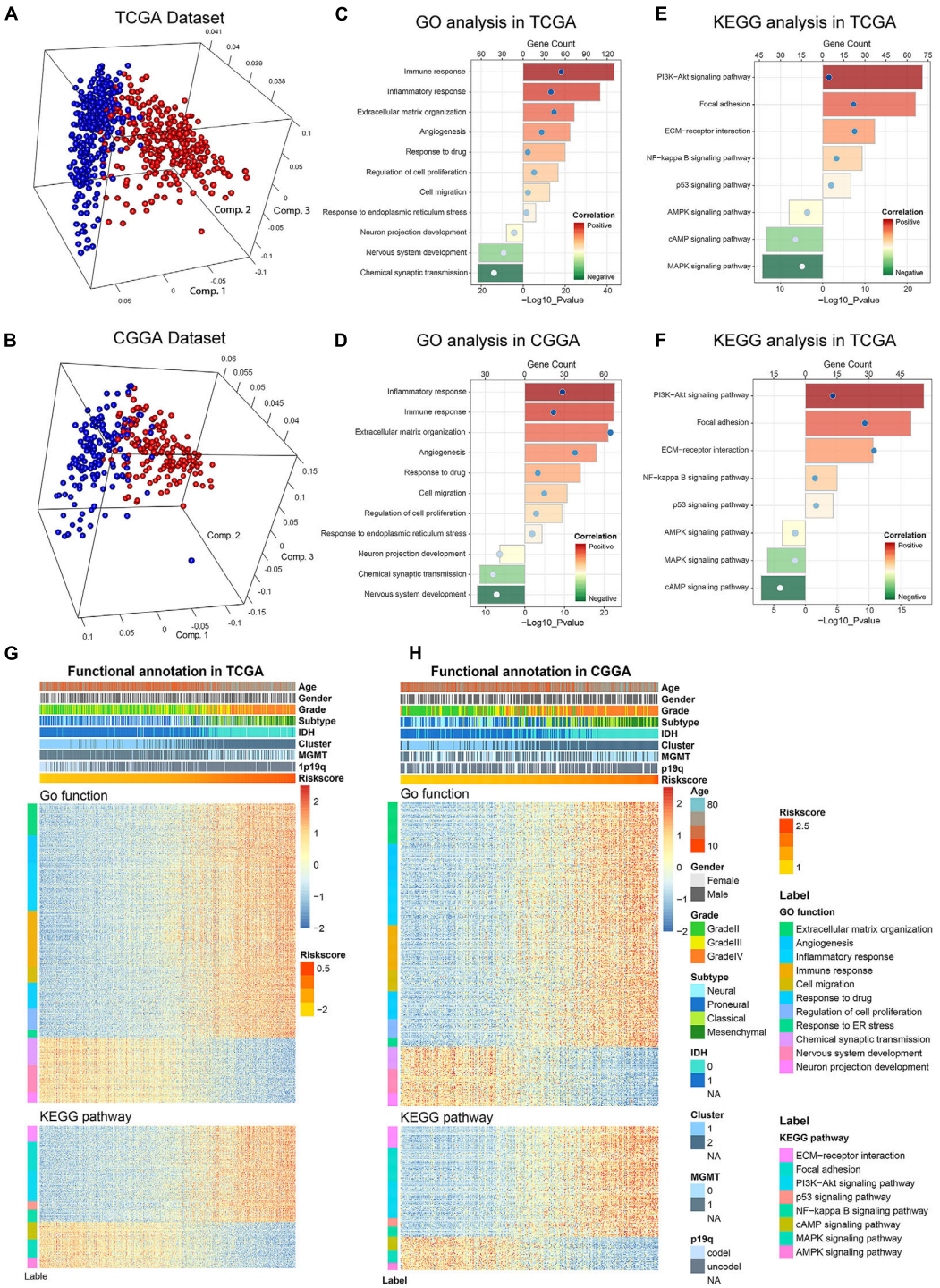

FIGURE 5 | Biological functions and pathways analyses of the ER stress-related signature in TCGA and CGGA datasets. **(A,B)** There is a significant separation between high-risk and low-risk groups in PCA analysis based on whole gene expression data. **(C,D)** GO analyses were performed to explore the biological processes tightly related to the risk signature. **(E,F)** KEGG pathway analyses were performed to explore the signaling pathways tightly related to the risk signature. **(G,H)** The heatmaps showed the association among risk score, clinicopathological features and ER stress-related biological functions and pathways.

performing Pearson correlation analysis ($|R| > 0.5$) in TCGA and CGGA datasets, respectively. Then, these genes were uploaded to DAVID website for GO analysis and KEGG pathway analysis. We found that the genes positively correlated with the risk score were mainly enriched in ER stress, inflammatory and immune response, cell migration, cell proliferation and angiogenesis in

CGGA and TCGA datasets (**Figures 5C,D**). While the negatively related genes were involved in normal biological processes such as nervous system development, and others (**Figures 5C,D**). Besides, KEGG pathway analysis showed that the risk signature was positively related to *PI3K-AKT* and *NF-kappaB* signaling pathway, which were thought to be involved in the malignant progression of multiple cancers (**Figures 5E,F**). In addition, the heat maps displayed the expression profiles of biological processes related to the risk signature in TCGA and CGGA datasets (**Figures 5G,H**). Meanwhile, we also performed GSEA to verify aforementioned results and obtained similar conclusions (**Supplementary Figure 4**). These findings suggested that the risk score was positively corelated to the malignant biological functions and signaling pathways in gliomas.

Association Between the Risk Signature and Immunologic Events

Previous studies reported that ER stress played an essential role in immune and inflammation response of multiple diseases (Engin, 2016; Feng et al., 2017; Gerakis and Hetz, 2018). This opinion was confirmed in glioma by our study. To further investigate the relationship between ER stress and immune response, several genes of immune checkpoints, such as *B7-H3*, *CTLA-4*, *TIM-3*, *PD-1,* and others were enrolled in this study. The results demonstrated that the risk signature was positively correlated to most of the immune checkpoints in CGGA and TCGA datasets, especially *B7-H3* (**Figure 6A** and **Supplementary Figure 5A**). It means that the excessive upregulation of ER stress may inhibit anti-tumor immune response in gliomas (Wang et al., 2016; Li et al., 2017). Besides, these results were also verified in lower-grade glioma (LGG) and GBM samples in two datasets (**Figures 6B,C** and **Supplementary Figures 5B,C**). In addition, we also selected several representative inflammatory genes to further investigate the association between ER stress and inflammation response. We found that the risk signature was positively correlated with *IL-6*, *CCL2,* and *HLA-A* (**Figures 6D–F** and **Supplementary Figures 5B,C**), suggesting T lymphocyte and macrophages mediated inflammatory response were involved in samples from high-risk group (Kolls and Linden, 2004; Germano et al., 2008). Considering that immune cell infiltration is an important component of tumor immune microenvironment (Gajewski et al., 2013; Gabrusiewicz et al., 2016), we further evaluated the proportion of various types of immune cell with CIBERSORT for CGGA and TCGA datasets. As samples were sorted by risk score in increasing order, the abundance of macrophages in M0 and M2 phase which had been reported to play an immunosuppressive role in cancers increased (Gabrusiewicz et al., 2016; **Figure 6G** and **Supplementary Figure 5G**). To verify these results, we also enrolled biomarkers of macrophages in different phases and found that the risk signature was significantly correlated to tumor-associated macrophage (TAM) and macrophages in M2 (**Figure 6H** and **Supplementary Figure 5H**). Besides, IHC staining was performed to further validate the infiltration of macrophages in tumor tissue from glioma patients stratified by risk score in CGGA dataset. We found that the expression levels of *CD163* and *IBA1* significantly increased in LGG and GBM samples from high-risk group, suggesting that the activation of ER stress could promote the infiltration of macrophages in M2 phase (**Figures 6I,J**). Besides, the results also suggested that *CD163* and *IBA1* were overexpressed in GBM (**Figure 6K**). These findings might provide a new insight into the suppression of anti-tumor immune response in gliomas.

ER Stress Inhibition Attenuated Glioma Progression *in vitro*

In this study, we performed experiments *in vitro* to further validate the results of bioinformatics analyses. First, LN229 and U87 cell lines were transfected with specific siRNA to knockdown the expression level of *P4HB* and *PDIA4*, which were considered as important biomarkers of ER stress activation (Joo et al., 2007; Kranz et al., 2017; Winship et al., 2017; Liu et al., 2019; Wang et al., 2020). WB and qPCR assays showed that both of the mRNA and protein expressions of *PDIA4* and *P4HB* could be significantly downregulated by specific siRNA (**Figures 7A–D**). Then, the transwell migration assays and cell scratch assays suggested that *PDIA4* or *P4HB* knockdown could significantly suppress cell migration of LN229 and U87 cells *in vitro* (**Figures 7E–H** and **Supplementary Figures 7A,B**). Besides, CCK-8 and clonogenic assays indicated that proliferative capacity and clonogenicity of glioma cell lines were attenuated after transfection with *PDIA4* or *P4HB* siRNA (**Figures 7I,J** and **Supplementary Figures 7C,D**). These results suggested that the activation of ER stress played an essential role in malignant progression of gliomas. Meanwhile, it is also indicated that anti-*PDIA4* and/or anti-*P4HB* therapy may be a novel approach for glioma treatments.

DISCUSSION

As the most malignant primary neoplasms in the central nervous system, the pathogenesis and progression of gliomas is a multi-factor and multi-step process (Ricard et al., 2012; Gusyatiner and Hegi, 2018). Due to the high invasiveness and heterogeneity of glioma cells, the efficacy of traditional treatment strategies was limited and the prognosis of glioma patients was dismal (Jiang et al., 2016; Reifenberger et al., 2017). Thus, novel therapeutic approaches and targets are urgently needed. In the past decade, ER stress becomes an increasingly eye-catching research field in various human cancers, which brings new hope for the improvement of individualized treatment of gliomas.

Endoplasmic reticulum is the most important organelle for protein synthesis and intracellular calcium storages, which is also involved in the regulation of multiple cellular signaling pathways (Tsai and Weissman, 2010; Schwarz and Blower, 2016). Upon the induction of intracellular and extracellular stress, the accumulation of unfolded or misfolded proteins can activate the unfolded protein response (UPR) to restore the homeostasis of ER (Namba, 2015). The *PERK/ATF4/CHOP*, *IRE-1/XBP1*, and *ATF6* signaling pathways have an essential role in regulating ER stress-induced physiological responses in cells (Lee, 2005; Luo and Lee, 2013). However, excessive and durable activation of

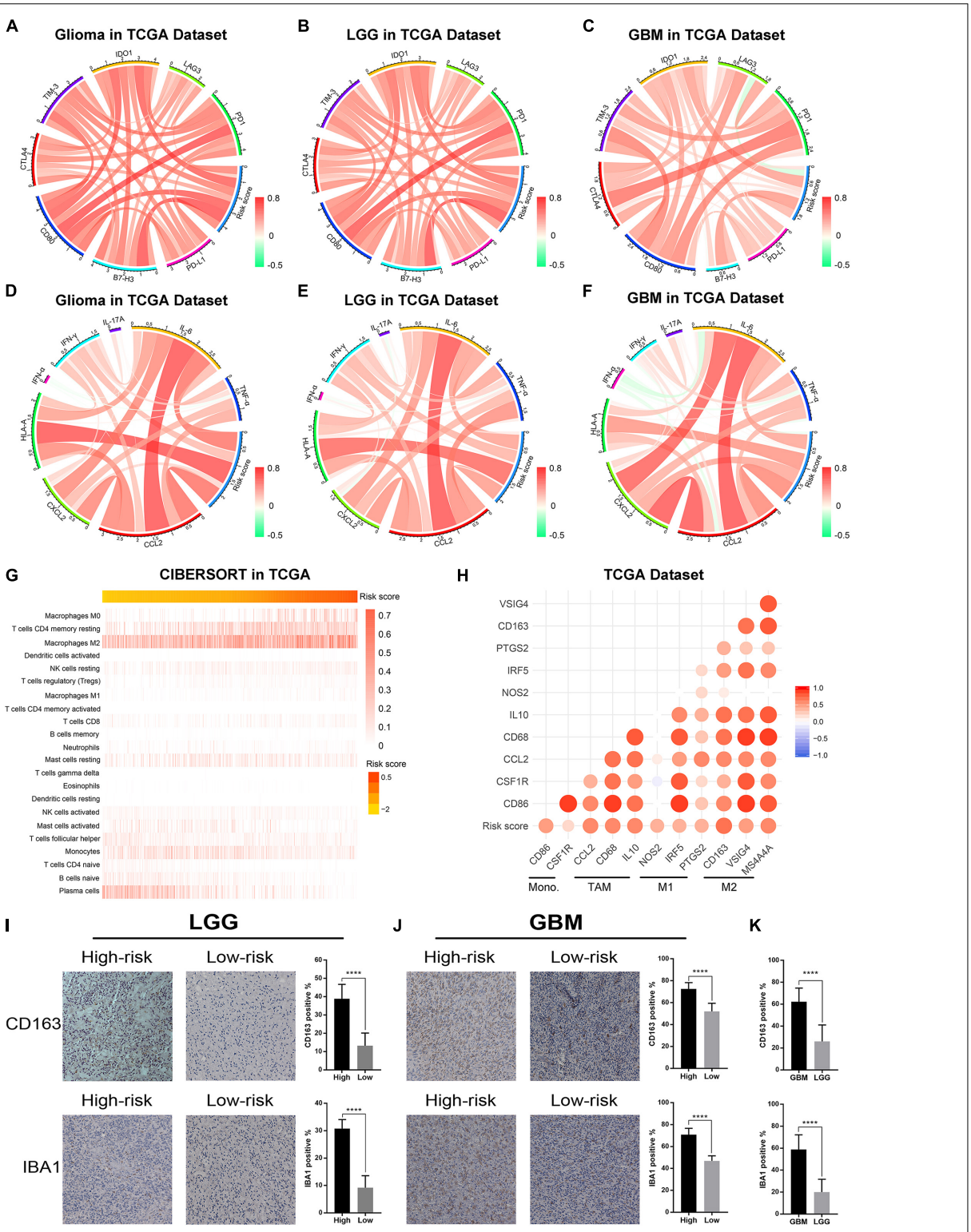

FIGURE 6 | The ER stress activation related immunologic events in glioma samples in TCGA dataset. **(A–C)** Correlation analysis between risk score and immune checkpoints in whole gliomas, low-grade gliomas and GBM, respectively. **(D–F)** Correlation analysis between risk score and inflammatory genes in whole gliomas, low-grade gliomas and GBM, respectively. **(G)** CIBERSORT was performed to evaluate the proportion of various types of immune cell infiltrated into glioma samples. **(H)** Correlation analysis between risk score and biomarkers of monocytes and macrophages. **(I)** IHC staining and positive rate statistics of *CD163* and *IBA1* in LGG samples from the CGGA dataset. **(J)** IHC staining and positive rate statistics of *CD163* and *IBA1* in GBM samples from the CGGA dataset. **(K)** Positive rate statistics of *CD163* and *IBA1* between LGG and GBM samples from the CGGA dataset. ****$p < 0.0001$.

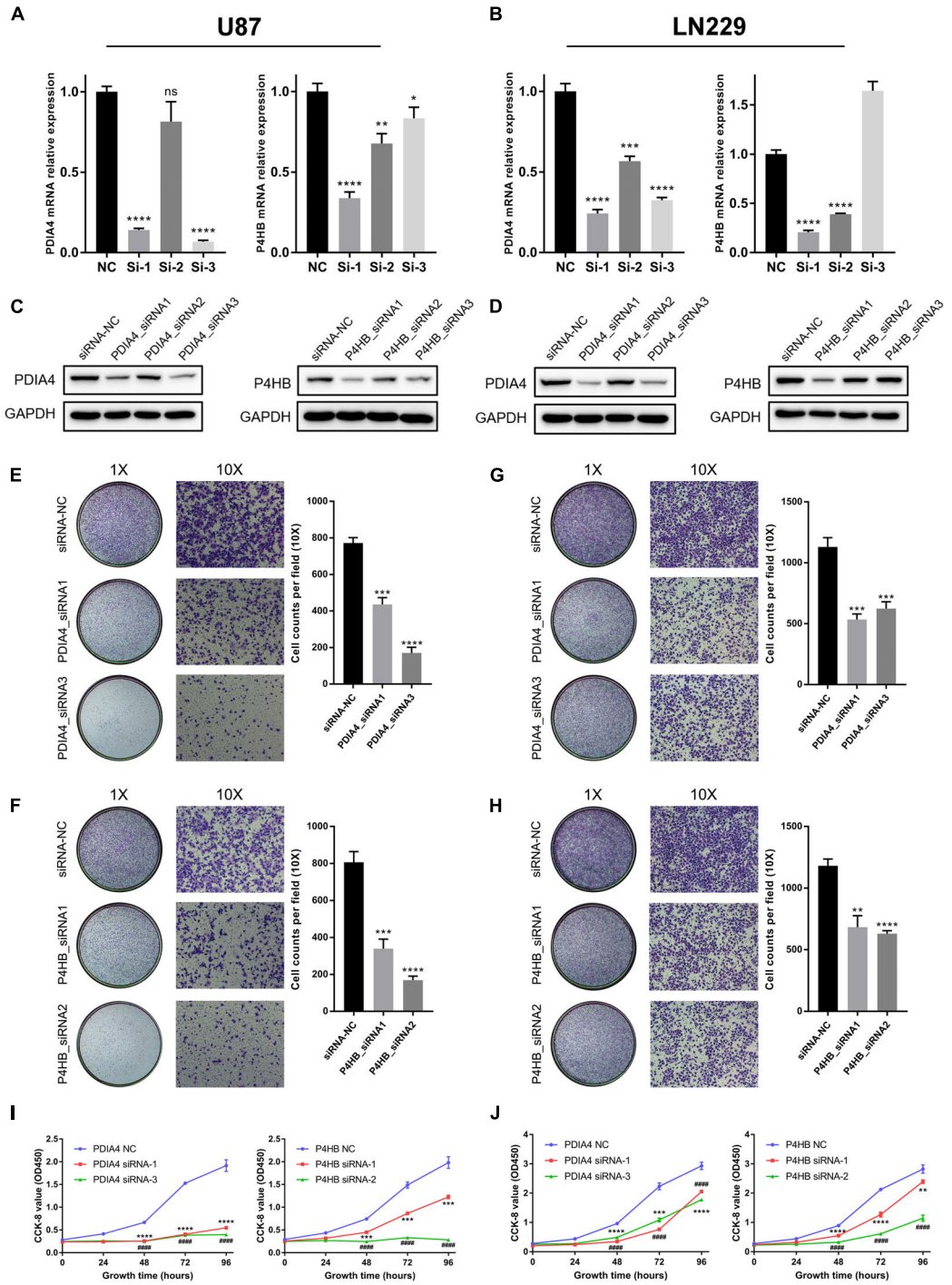

FIGURE 7 | ER stress activation promotes migration and proliferative capacity of glioma cell lines *in vitro*. **(A,B)** The real-time quantitative PCR (qPCR) assay of *PDIA4* and *P4HB* mRNA expression in LN229 and U87 cell lines after applying specific siRNA and negative control. **(C,D)** The western blot analysis of *PDIA4* and *P4HB* protein expression in LN229 **(C)** and U87 **(D)** cell lines after applying specific siRNA and negative control. **(E–H)** Transwell migration assay of LN229 **(E,F)** and U87 **(G,H)** cell lines treated with specific siRNA and negative control. **(I,J)** CCK-8 assay displaying proliferation of LN229 **(I)** and U87 **(J)** cell lines treated with specific siRNA and negative control. $^{*}p < 0.05$, $^{**}p < 0.01$, $^{***}p < 0.001$, $^{****}p < 0.0001$.

ER stress can also induce cell apoptosis (Szegezdi et al., 2006). ER stress is involved in the process of many diseases, such as Parkinson's disease (PD), Alzheimer's disease (AD), diabetes and tumors (Engin, 2016; Mercado et al., 2016; Gerakis and Hetz, 2018). The in-depth study of ER stress provides an important reference for the clinical treatment of these diseases.

In malignancy tissues, cancer cells which are constantly exposed to hypoxic tumor microenvironment and intracellular DNA damage stress have a high risk of ER stress activation. These mechanisms have been proved to participate in the malignant progression and drug resistance of many human cancers (Dasari and Tchounwou, 2014). The branch of *PERK-ATF4* can activate the epithelial-to-mesenchymal transition (EMT) response and promote the metastasis of breast cancer cells (Feng et al., 2017). In hepatocellular and prostate cancer, the transcription factors from UPR can bind and activate the promoter of *VEGF*, which resulting in the proliferation and migration of endothelial cells (Pereira et al., 2014; Ramakrishnan et al., 2014). Besides, the activation of ER stress can also induce the dormancy of cancer cells. Cellular dormancy can block the division and proliferation of cancer cells by arresting them in the G0/G1 phase of cell cycle (Aguirre-Ghiso, 2007; Vera-Ramirez and Hunter, 2017). The cancer cells which survive in a quiescent state are not sensitive to radiotherapy or chemotherapy, which eventually lead to tumor recurrence and poor prognosis of patients. Furthermore, relevant studies have proved that *IRE-1-XBP1* signaling pathway could inhibit anti-tumor immune responses and provide an opportunity for the formation of tumors (Cubillos-Ruiz et al., 2015). These results suggested that ER stress plays a key role in the remodeling of tumor immune microenvironment and h serving as a novel target of immunological therapy. Although serval studies have confirmed the therapeutic value of ER stress in glioma, the biological functions of ER stress in glioma have not been completely understood, especially the role of ER stress in the regulation tumor immune microenvironment (Chang et al., 2020).

In the present study, we constructed a risk signature to evaluate the ER stress activation of glioma samples from TCGA and CGGA datasets. Our findings showed that ER stress activation was tightly correlated to the malignant clinicopathological features and genomic alterations. These results revealed the significance of ER stress and the molecular mechanisms influencing ER stress activation in gliomas. It was interesting to note that the low-risk score was tightly associated with 1p/19q codeletion, suggesting the risk signature may server as a marker of oligodendrogliomas. Besides, K-M survival analysis and COX regression analysis suggested that this risk signature was an independent prognostic factor of patients with gliomas. Furthermore, both bioinformatics analysis and *in vitro* experiments indicated that ER stress activation can significantly promote the proliferation and migration of glioma cells. Besides, we also found that ER stress was tightly associated with the regulation of tumor immune microenvironment in glioma, especially the infiltration of macrophages in M2 phase. To further validated the results of bioinformatics analysis, IHC analysis and cell biology experiments were performed. The results suggested that ER stress activation promoted the malignant progression of glioma.

According to the previous researches, protein disulfide isomerase (PDI) family members play an essential role in ER stress activation (Hsu et al., 2019; Zhang et al., 2019). The *P4HB* (also known as *PDIA1*) and *PDIA4*, which were chosen from the six-gene signature, belong to the protein PDI protein family and have been proved to be related to ER stress activation in human cancers (Joo et al., 2007; Kranz et al., 2017; Winship et al., 2017; Liu et al., 2019; Wang et al., 2020), especially the PERK signaling pathway (Kranz et al., 2017, 2020). Serval recent researches has pointed out that *P4HB* and *PDIA4* correlated with the malignant progression of glioma, but these conclusions have not been sufficiently verified by *in vitro* experiments (Zou et al., 2018; Li et al., 2021). Besides, the *P4HB* and *PDIA4*, which have significant prognostic value in gliomas, were also the important components of the ER stress-related signature. Thus, in *in vitro* experiments, *P4HB* and *PDIA4* were selected as biomarkers of ER stress activation. We found that knockdown of the *P4HB* and *PDIA4* could significantly reduce the proliferation and migration of glioma cell lines *in vitro*. These findings indicated that *P4HB* and *PDIA4* may serve as promising target for glioma therapy. However, we also recognized that the current evidences were limited and future studies are necessary. Other four genes in the risk signature (*CASP4*, *CUL7*, *DNAJB12,* and *SIRT1*) were not directly participated in the three classic ER stress signaling pathway mentioned before. According to the findings in this study, we hypothesized that the other four genes may be involved in the regulation of ER stress activation through unknown molecular mechanisms, which is valuable for us to further investigate and discuss.

In this study, we have confirmed the importance of ER stress activation in the progression of glioma through sufficient bioinformatics analysis and *in vitro* experiments. Although, the prognostic value and biological functions of ER-stress in gliomas were fully discussed, the specific molecular mechanism underlying the interaction between ER stress and tumor immune microenvironment remains unclear. Thus, more in-depth exploration is needed. Taken together, our findings revealed the functional roles of ER stress in glioma and provided promising targets to enhance the individualized treatment of patients with glioma.

CONCLUSION

In this study, we constructed a risk signature to evaluated the ER stress activation status and prognosis of glioma patients. Functional analyses suggested that the ER stress activation was tightly correlated with cell migration and cell proliferation gliomas, which were further verified in the experiments *in vitro*. Besides, we also found that ER stress activation could promote the infiltration of macrophages in M2. *P4HB* and *PDIA4*, which played an essential role in the activation of ER stress, may serve as a novel potential target to enhance the anticancer therapies. Accordingly, these findings provided an important reference in personalized clinical treatment for glioma patients.

DATA AVAILABILITY STATEMENT

The datasets presented in this study can be found in online repositories. The names of the repository/repositories and accession number(s) can be found in the article/**Supplementary Material**.

ETHICS STATEMENT

The studies involving human participants were reviewed and approved by Institutional Review Board (IRB) of Beijing Tiantan Hospital Affiliated to Capital Medical University. The patients/participants provided their written informed consent to participate in this study.

AUTHOR CONTRIBUTIONS

RH, GL, and TJ: conception and design. RH, ZW, and HH: development of methodology. RH, GL, and KW: acquisition of data. RH, KW, and FZ: analysis and interpretation of data. RH and GL: writing, review and/or revision of the manuscript. TJ and HH: administrative, technical, or material support. TJ: study supervision. All authors read and approved the final manuscript.

FUNDING

This work was supported by grants from National Natural Science Foundation of China (81972816, 81702460, and 81802994).

ACKNOWLEDGMENTS

We would like to thank the contributions from the CGGA Network and TCGA Research Network.

SUPPLEMENTARY MATERIAL

The Supplementary Material for this article can be found online at: https://www.frontiersin.org/articles/10.3389/fcell.2021.619396/full#supplementary-material

Supplementary Figure 1 | Consensus clustering for ER stress-related genes in glioma patients from TCGA and CGGA dataset. **(A)** Consensus clustering CDF for $k = 2$ to $k = 10$. **(B)** Consensus clustering matrix of glioma samples from TCGA and CGGA dataset for $k = 2$, respectively. **(C,D)** Heatmap of two clusters identified by the top 50 variable expression genes. **(E,F)** K-M survival curve analyses of patients in two clusters. **(G,H)** By performing Consensus clustering analysis, IDH wildtype GBM patients were also divided into two clusters, K-M survival curve analyses was performed to evaluated the prognosis of IDH wildtype GBM patients in two clusters.

Supplementary Figure 2 | K-M survival analysis of the risk signature in glioma patients stratified by *IDH* mutation status, *MGMT* promoter methylation and 1p/19q co-deletion status in TCGA and CGGA datasets.

Supplementary Figure 3 | A nomogram model for predicting overall survival of patients with glioma. **(A)** A nomogram model was constructed by integrating the clinicopathologic features and risk score of patients in the TCGA dataset. **(B,C)** The calibration curve of nomogram for predicting OS at 1-, 3- and 5-years in the TCGA and CGGA datasets.

Supplementary Figure 4 | GSEA analysis was performed to investigate the biological functions and pathways that were tightly correlated with the ER stress activation.

Supplementary Figure 5 | The ER stress activation related immunologic events in glioma samples in CGGA dataset. **(A–C)** Correlation analysis between risk score signature and immune checkpoints in whole gliomas, low-grade gliomas and GBM, respectively. **(D–F)** Correlation analysis between risk score and inflammatory genes in whole grade of gliomas, low-grade gliomas and GBM, respectively. **(G)** CIBERSORT evaluating the proportion of various types of immune cell infiltrated into glioma samples. **(H)** Correlation analysis between risk score and biomarkers of monocytes and macrophages.

Supplementary Figure 6 | K-M survival analysis of each independent gene in the ER stress-related signature in TCGA and CGGA datasets.

Supplementary Figure 7 | ER stress activation promotes migration and proliferative capacity of glioma cell lines *in vitro*. **(A,B)** Cell scratch assay of U87 and LN229 cell lines treated with *PDIA4* siRNA, *P4HB* siRNA and negative control. **(C,D)** Clonogenic assay of U87 and LN229 cell lines treated with *PDIA4* siRNA, *P4HB* siRNA and negative control.

Supplementary Table 1 | Characteristics of patients in cluster 1 and cluster 2 in CGGA databset.

Supplementary Table 2 | ER stress related gene list.

Supplementary Table 3 | Univariate Cox analysis of ER stress-related genes.

Supplementary Table 4 | Univariate and multivariate analysis of OS in CGGA sequencing dataset.

REFERENCES

Adamopoulos, C., Farmaki, E., Spilioti, E., Kiaris, H., Piperi, C., and Papavassiliou, A. G. (2014). Advanced glycation end-products induce endoplasmic reticulum stress in human aortic endothelial cells. *Clin. Chem. Lab. Med.* 52, 151–160.

Adamopoulos, C., Mihailidou, C., Grivaki, C., Papavassiliou, K. A., Kiaris, H., Piperi, C., et al. (2016). Systemic effects of AGEs in ER stress induction in vivo. *Glycoconj. J.* 33, 537–544. doi: 10.1007/s10719-016-9680-4

Aguirre-Ghiso, J. A. (2007). Models, mechanisms and clinical evidence for cancer dormancy. *Nat. Rev. Cancer* 7, 834–846. doi: 10.1038/nrc2256

Bovelstad, H. M., Nygard, S., Storvold, H. L., Aldrin, M., Borgan, O., Frigessi, A., et al. (2007). Predicting survival from microarray data–a comparative study. *Bioinformatics* 23, 2080–2087. doi: 10.1093/bioinformatics/btm305

Chang, C. Y., Li, J. R., Wu, C. C., Wang, J. D., Liao, S. L., Chen, W. Y., et al. (2020). Endoplasmic reticulum stress contributes to indomethacin-induced glioma apoptosis. *Int. J. Mol. Sci.* 21:557. doi: 10.3390/ijms21020557

Cloughesy, T. F., Mochizuki, A. Y., Orpilla, J. R., Hugo, W., Lee, A. H., Davidson, T. B., et al. (2019). Neoadjuvant anti-PD-1 immunotherapy promotes a survival benefit with intratumoral and systemic immune responses in recurrent glioblastoma. *Nat. Med.* 25, 477–486. doi: 10.1038/s41591-018-0337-7

Cubillos-Ruiz, J. R., Bettigole, S. E., and Glimcher, L. H. (2017). Tumorigenic and immunosuppressive effects of endoplasmic reticulum stress in cancer. *Cell* 168, 692–706. doi: 10.1016/j.cell.2016.12.004

Cubillos-Ruiz, J. R., Silberman, P. C., Rutkowski, M. R., Chopra, S., Perales-Puchalt, A., Song, M., et al. (2015). ER stress sensor XBP1 controls anti-tumor immunity by disrupting dendritic cell homeostasis. *Cell* 161, 1527–1538. doi: 10.1016/j.cell.2015.05.025

Dasari, S., and Tchounwou, P. B. (2014). Cisplatin in cancer therapy: molecular mechanisms of action. *Eur. J. Pharmacol.* 740, 364–378. doi: 10.1016/j.ejphar.2014.07.025

David, C. C., and Jacobs, D. J. (2014). Principal component analysis: a method for determining the essential dynamics of proteins. *Methods Mol. Biol.* 1084, 193–226. doi: 10.1007/978-1-62703-658-0_11

Engin, F. (2016). ER stress and development of type 1 diabetes. *J. Investig. Med.* 64, 2–6. doi: 10.1097/jim.0000000000000229

Feng, Y. X., Jin, D. X., Sokol, E. S., Reinhardt, F., Miller, D. H., and Gupta, P. B. (2017). Cancer-specific PERK signaling drives invasion and metastasis through CREB3L1. *Nat. Commun.* 8:1079.

Gabrusiewicz, K., Rodriguez, B., Wei, J., Hashimoto, Y., Healy, L. M., Maiti, S. N., et al. (2016). Glioblastoma-infiltrated innate immune cells resemble M0 macrophage phenotype. *JCI Insight* 1:e85841.

Gajewski, T. F., Schreiber, H., and Fu, Y. X. (2013). Innate and adaptive immune cells in the tumor microenvironment. *Nat. Immunol.* 14, 1014–1022.

Gerakis, Y., and Hetz, C. (2018). Emerging roles of ER stress in the etiology and pathogenesis of Alzheimer's disease. *FEBS J.* 285, 995–1011. doi: 10.1111/febs.14332

Germano, G., Allavena, P., and Mantovani, A. (2008). Cytokines as a key component of cancer-related inflammation. *Cytokine* 43, 374–379. doi: 10.1016/j.cyto.2008.07.014

Gusyatiner, O., and Hegi, M. E. (2018). Glioma epigenetics: from subclassification to novel treatment options. *Semin. Cancer Biol.* 51, 50–58. doi: 10.1016/j.semcancer.2017.11.010

Gutierrez, T., and Simmen, T. (2014). Endoplasmic reticulum chaperones and oxidoreductases: critical regulators of tumor cell survival and immunorecognition. *Front. Oncol.* 4:291. doi: 10.3389/fonc.2014.00291

Hamanaka, R. B., Bennett, B. S., Cullinan, S. B., and Diehl, J. A. (2005). PERK and GCN2 contribute to eIF2alpha phosphorylation and cell cycle arrest after activation of the unfolded protein response pathway. *Mol. Biol. Cell* 16, 5493–5501. doi: 10.1091/mbc.e05-03-0268

Hsu, S. K., Chiu, C. C., Dahms, H. U., Chou, C. K., Cheng, C. M., Chang, W. T., et al. (2019). Unfolded Protein Response (UPR) in survival, dormancy, immunosuppression, metastasis, and treatments of cancer cells. *Int. J. Mol. Sci.* 20:2518. doi: 10.3390/ijms20102518

Hu, X., Martinez-Ledesma, E., Zheng, S., Kim, H., Barthel, F., Jiang, T., et al. (2017). Multigene signature for predicting prognosis of patients with 1p19q co-deletion diffuse glioma. *Neuro Oncol.* 19, 786–795. doi: 10.1093/neuonc/now285

Jiang, T., Mao, Y., Ma, W., Mao, Q., You, Y., Yang, X., et al. (2016). CGCG clinical practice guidelines for the management of adult diffuse gliomas. *Cancer Lett.* 375, 263–273.

Joo, J. H., Liao, G., Collins, J. B., Grissom, S. F., and Jetten, A. M. (2007). Farnesol-induced apoptosis in human lung carcinoma cells is coupled to the endoplasmic reticulum stress response. *Cancer Res.* 67, 7929–7936. doi: 10.1158/0008-5472.can-07-0931

Kolls, J. K., and Linden, A. (2004). Interleukin-17 family members and inflammation. *Immunity* 21, 467–476. doi: 10.1016/j.immuni.2004.08.018

Kranz, P., Neumann, F., Wolf, A., Classen, F., Pompsch, M., Ocklenburg, T., et al. (2017). PDI is an essential redox-sensitive activator of PERK during the unfolded protein response (UPR). *Cell Death Dis.* 8:e2986. doi: 10.1038/cddis.2017.369

Kranz, P., Sanger, C., Wolf, A., Baumann, J., Metzen, E., Baumann, M., et al. (2020). Tumor cells rely on the thiol oxidoreductase PDI for PERK signaling in order to survive ER stress. *Sci. Rep.* 10:15299.

Lee, A. S. (2005). The ER chaperone and signaling regulator GRP78/BiP as a monitor of endoplasmic reticulum stress. *Methods* 35, 373–381. doi: 10.1016/j.ymeth.2004.10.010

Lee, B. R., Chang, S. Y., Hong, E. H., Kwon, B. E., Kim, H. M., Kim, Y. J., et al. (2014). Elevated endoplasmic reticulum stress reinforced immunosuppression in the tumor microenvironment via myeloid-derived suppressor cells. *Oncotarget* 5, 12331–12345. doi: 10.18632/oncotarget.2589

Leprivier, G., Rotblat, B., Khan, D., Jan, E., and Sorensen, P. H. (2015). Stress-mediated translational control in cancer cells. *Biochim. Biophys. Acta* 1849, 845–860.

Li, G., Wang, Z., Zhang, C., Liu, X., Cai, J., Wang, Z., et al. (2017). Molecular and clinical characterization of TIM-3 in glioma through 1,024 samples. *Oncoimmunology* 6:e1328339. doi: 10.1080/2162402x.2017.1328339

Li, H., Liu, Q., Xiao, K., He, Z., Wu, C., Sun, J., et al. (2021). PDIA4 correlates with poor prognosis and is a potential biomarker in glioma. *Onco Targets Ther.* 14, 125–138. doi: 10.2147/ott.s287931

Liu, Y., Ji, W., Shergalis, A., Xu, J., Delaney, A. M., Calcaterra, A., et al. (2019). Activation of the unfolded protein response via inhibition of protein disulfide isomerase decreases the capacity for DNA repair to sensitize glioblastoma to radiotherapy. *Cancer Res.* 79, 2923–2932. doi: 10.1158/0008-5472.can-18-2540

Luo, B., and Lee, A. S. (2013). The critical roles of endoplasmic reticulum chaperones and unfolded protein response in tumorigenesis and anticancer therapies. *Oncogene* 32, 805–818. doi: 10.1038/onc.2012.130

Mercado, G., Castillo, V., Soto, P., and Sidhu, A. (2016). ER stress and Parkinson's disease: pathological inputs that converge into the secretory pathway. *Brain Res.* 1648(Pt B), 626–632. doi: 10.1016/j.brainres.2016.04.042

Namba, T. (2015). Regulation of endoplasmic reticulum functions. *Aging* 7, 901–902. doi: 10.18632/aging.100851

Newman, A. M., Liu, C. L., Green, M. R., Gentles, A. J., Feng, W., Xu, Y., et al. (2015). Robust enumeration of cell subsets from tissue expression profiles. *Nat. Methods* 12, 453–457. doi: 10.1038/nmeth.3337

Newman, A. M., Steen, C. B., Liu, C. L., Gentles, A. J., Chaudhuri, A. A., Scherer, F., et al. (2019). Determining cell type abundance and expression from bulk tissues with digital cytometry. *Nat. Biotechnol.* 37, 773–782. doi: 10.1038/s41587-019-0114-2

Nuno, M., Birch, K., Mukherjee, D., Sarmiento, J. M., Black, K. L., and Patil, C. G. (2013). Survival and prognostic factors of anaplastic gliomas. *Neurosurgery* 73, 458–465; quiz 65.

Obacz, J., Avril, T., Le Reste, P. J., Urra, H., Quillien, V., Hetz, C., et al. (2017). Endoplasmic reticulum proteostasis in glioblastoma-from molecular mechanisms to therapeutic perspectives. *Sci. Signal.* 10:eaal2323. doi: 10.1126/scisignal.aal2323

Ohsawa, K., Imai, Y., Kanazawa, H., Sasaki, Y., and Kohsaka, S. (2000). Involvement of Iba1 in membrane ruffling and phagocytosis of macrophages/microglia. *J. Cell Sci.* 113(Pt 17), 3073–3084. doi: 10.1242/jcs.113.17.3073

Osuka, S., and Van Meir, E. G. (2017). Overcoming therapeutic resistance in glioblastoma: the way forward. *J. Clin. Invest.* 127, 415–426. doi: 10.1172/jci89587

Pereira, E. R., Frudd, K., Awad, W., and Hendershot, L. M. (2014). Endoplasmic reticulum (ER) stress and hypoxia response pathways interact to potentiate hypoxia-inducible factor 1 (HIF-1) transcriptional activity on targets like vascular endothelial growth factor (VEGF). *J. Biol. Chem.* 289, 3352–3364. doi: 10.1074/jbc.m113.507194

Phillips, H. S., Kharbanda, S., Chen, R., Forrest, W. F., Soriano, R. H., Wu, T. D., et al. (2006). Molecular subclasses of high-grade glioma predict prognosis, delineate a pattern of disease progression, and resemble stages in neurogenesis. *Cancer Cell* 9, 157–173. doi: 10.1016/j.ccr.2006.02.019

Puchalski, R. B., Shah, N., Miller, J., Dalley, R., Nomura, S. R., Yoon, J. G., et al. (2018). An anatomic transcriptional atlas of human glioblastoma. *Science* 360, 660–663.

Ramakrishnan, S., Anand, V., and Roy, S. (2014). Vascular endothelial growth factor signaling in hypoxia and inflammation. *J. Neuroimmune Pharmacol.* 9, 142–160. doi: 10.1007/s11481-014-9531-7

Reifenberger, G., Wirsching, H. G., Knobbe-Thomsen, C. B., and Weller, M. (2017). Advances in the molecular genetics of gliomas - implications for classification and therapy. *Nat. Rev. Clin. Oncol.* 14, 434–452. doi: 10.1038/nrclinonc.2016.204

Ricard, D., Idbaih, A., Ducray, F., Lahutte, M., Hoang-Xuan, K., and Delattre, J. Y. (2012). Primary brain tumours in adults. *Lancet* 379, 1984–1996.

Robin, X., Turck, N., Hainard, A., Tiberti, N., Lisacek, F., Sanchez, J. C., et al. (2011). pROC: an open-source package for R and S+ to analyze and compare ROC curves. *BMC Bioinformatics* 12:77. doi: 10.1186/1471-2105-12-77

Schwarz, D. S., and Blower, M. D. (2016). The endoplasmic reticulum: structure, function and response to cellular signaling. *Cell. Mol. Life Sci. CMLS* 73, 79–94. doi: 10.1007/s00018-015-2052-6

Subramanian, A., Tamayo, P., Mootha, V. K., Mukherjee, S., Ebert, B. L., Gillette, M. A., et al. (2005). Gene set enrichment analysis: a knowledge-based approach for interpreting genome-wide expression profiles. *Proc. Natl. Acad. Sci. U.S.A.* 102, 15545–15550. doi: 10.1073/pnas.0506580102

Szegezdi, E., Logue, S. E., Gorman, A. M., and Samali, A. (2006). Mediators of endoplasmic reticulum stress-induced apoptosis. *EMBO Rep.* 7, 880–885. doi: 10.1038/sj.embor.7400779

Tibshirani, R. (1997). The lasso method for variable selection in the Cox model. *Stat. Med.* 16, 385–395. doi: 10.1002/(sici)1097-0258(19970228)16:4<385::aid-sim380>3.0.co;2-3

Tsai, Y. C., and Weissman, A. M. (2010). The unfolded protein response, degradation from endoplasmic reticulum and cancer. *Genes Cancer* 1, 764–778. doi: 10.1177/1947601910383011

van den Heuvel, M. M., Tensen, C. P., van As, J. H., van den Berg, T. K., Fluitsma, D. M., Dijkstra, C. D., et al. (1999). Regulation of CD 163 on

human macrophages: cross-linking of CD163 induces signaling and activation. *J. Leukoc. Biol.* 66, 858–866. doi: 10.1002/jlb.66.5.858

Vera-Ramirez, L., and Hunter, K. W. (2017). Tumor cell dormancy as an adaptive cell stress response mechanism. *F1000Research* 6:2134. doi: 10.12688/f1000research.12174.1

Wang, Z., Zhang, C., Liu, X., Wang, Z., Sun, L., Li, G., et al. (2016). Molecular and clinical characterization of PD-L1 expression at transcriptional level via 976 samples of brain glioma. *Oncoimmunology* 5:e1196310. doi: 10.1080/2162402x.2016.1196310

Wang, Z., Zhang, H., and Cheng, Q. (2020). PDIA4: the basic characteristics, functions and its potential connection with cancer. *Biomed. Pharmacother.* 122:109688. doi: 10.1016/j.biopha.2019.109688

Wen, P. Y., and Kesari, S. (2008). Malignant gliomas in adults. *N. Engl. J. Med.* 359, 492–507. doi: 10.1056/nejmra0708126

Winship, A. L., Sorby, K., Correia, J., Rainczuk, A., Yap, J., and Dimitriadis, E. (2017). Interleukin-11 up-regulates endoplasmic reticulum stress induced target, PDIA4 in human first trimester placenta and in vivo in mice. *Placenta* 53, 92–100. doi: 10.1016/j.placenta.2017.04.007

Yao, X., Tu, Y., Xu, Y., Guo, Y., Yao, F., and Zhang, X. (2020). Endoplasmic reticulum stress confers 5-fluorouracil resistance in breast cancer cell via the GRP78/OCT4/lncRNA MIAT/AKT pathway. *Am. J. Cancer Res.* 10, 838–855.

Zhang, Z., Zhang, L., Zhou, L., Lei, Y., Zhang, Y., and Huang, C. (2019). Redox signaling and unfolded protein response coordinate cell fate decisions under ER stress. *Redox Biol.* 25:101047. doi: 10.1016/j.redox.2018.11.005

Zhao, J., Chen, A. X., Gartrell, R. D., Silverman, A. M., Aparicio, L., Chu, T., et al. (2019). Immune and genomic correlates of response to anti-PD-1 immunotherapy in glioblastoma. *Nat. Med.* 25, 462–469.

Zhao, Z., Meng, F., Wang, W., Wang, Z., Zhang, C., and Jiang, T. (2017). Comprehensive RNA-seq transcriptomic profiling in the malignant progression of gliomas. *Sci. Data* 4:170024.

Zou, H., Wen, C., Peng, Z., Shao, Y., Hu, L., Li, S., et al. (2018). P4HB and PDIA3 are associated with tumor progression and therapeutic outcome of diffuse gliomas. *Oncol. Rep.* 39, 501–510.

Conflict of Interest: The authors declare that the research was conducted in the absence of any commercial or financial relationships that could be construed as a potential conflict of interest.

frontiers in Genetics

ORIGINAL RESEARCH
published: 12 July 2021
doi: 10.3389/fgene.2021.657658

Weighted Gene Co-expression Network Analysis Identified a Novel Thirteen-Gene Signature Associated With Progression, Prognosis, and Immune Microenvironment of Colon Adenocarcinoma Patients

*Cangang Zhang[1], Zhe Zhao[2], Haibo Liu[3], Shukun Yao[4,5] and Dongyan Zhao[4,5]**

[1] Department of Pathogenic Microbiology and Immunology, School of Basic Medical Sciences, Xi'an Jiaotong University, Xi'an, China, [2] Key Laboratory of Resource Biology and Biotechnology in Western China (Ministry of Education), College of Life Science, Northwest University, Xi'an, China, [3] Department of Hematology, The First Affiliated Hospital of Xi'an Jiaotong University, Xi'an, China, [4] Graduate School, Chinese Academy of Medical Sciences and Peking Union Medical College, Beijing, China, [5] Department of Gastroenterology, China-Japan Friendship Hospital, Beijing, China

OPEN ACCESS

Edited by:
Lorenzo Gerratana, University of Udine, Italy

Reviewed by:
Jyoti Sharma, Institute of Bioinformatics (IOB), India
Jinyan Huang, Zhejiang University, China

***Correspondence:**
Dongyan Zhao
zhaodongyanhappy@163.com

Specialty section:
This article was submitted to Cancer Genetics, a section of the journal Frontiers in Genetics

Received: *23 January 2021*
Accepted: *22 June 2021*
Published: *12 July 2021*

Citation:
Zhang C, Zhao Z, Liu H, Yao S and Zhao D (2021) Weighted Gene Co-expression Network Analysis Identified a Novel Thirteen-Gene Signature Associated With Progression, Prognosis, and Immune Microenvironment of Colon Adenocarcinoma Patients. Front. Genet. 12:657658. doi: 10.3389/fgene.2021.657658

Colon adenocarcinoma (COAD) is one of the most common malignant tumors and has high migration and invasion capacity. In this study, we attempted to establish a multigene signature for predicting the prognosis of COAD patients. Weighted gene co-expression network analysis and differential gene expression analysis methods were first applied to identify differentially co-expressed genes between COAD tissues and normal tissues from the Cancer Genome Atlas (TCGA)-COAD dataset and GSE39582 dataset, and a total of 309 overlapping genes were screened out. Then, our study employed TCGA-COAD cohort as the training dataset and an independent cohort by merging the GES39582 and GSE17536 datasets as the testing dataset. After univariate and multivariate Cox regression analyses were performed for these overlapping genes and overall survival (OS) of COAD patients in the training dataset, a 13-gene signature was constructed to divide COAD patients into high- and low-risk subgroups with significantly different OS. The testing dataset exhibited the same results utilizing the same predictive signature. The area under the curve of receiver operating characteristic analysis for predicting OS in the training and testing datasets were 0.789 and 0.868, respectively, which revealed the enhanced predictive power of the signature. Multivariate Cox regression analysis further suggested that the 13-gene signature could independently predict OS. Among the 13 prognostic genes, *NAT1* and *NAT2* were downregulated with deep deletions in tumor tissues in multiple COAD cohorts and exhibited significant correlations with poorer OS based on the GEPIA database. Notably, *NAT1* and *NAT2* expression levels were positively correlated with infiltrating levels of CD8+ T cells and dendritic cells, exhibiting a foundation for further research investigating the antitumor

immune roles played by *NAT1* and *NAT2* in COAD. Taken together, the results of our study showed that the 13-gene signature could efficiently predict OS and that *NAT1* and *NAT2* could function as biomarkers for prognosis and the immune response in COAD.

Keywords: colon adenocarcinoma, weighted gene co-expression network analysis, prognosis, *NAT1, NAT2*, immune infiltration

INTRODUCTION

Due to a number of factors including environmental exposure to carcinogens and genetic predisposition, the morbidity and mortality rates of colorectal cancer are increasing rapidly, and more than 2.2 million new cases are expected to be diagnosed, accounting for 1.1 million cancer-related deaths by 2030 (Arnold et al., 2017; Islami et al., 2018). Colon adenocarcinoma (COAD) is the most frequently diagnosed histological subtype of colorectal cancer, ranking fourth in terms of incidence and mortality among all kinds of malignant tumors in 2018 (Bray et al., 2018). Although considerable progress has been made in the early diagnosis strategies and multidisciplinary cancer management in recent decades, the invasion, migration, metastasis and recurrence of COAD have been bottlenecks for improving the long-term survival of patients, and these bottlenecks have kept the 5-year survival rate for patients diagnosed with COAD from exceeding 30% (Siegel et al., 2017; Watanabe et al., 2018; Li et al., 2019). Conventional methods utilizing the American Joint Committee on Cancer (AJCC) tumor node metastasis (TNM) classification system, vascular invasion and other parameters are widely employed to predict prognosis and guide treatment in COAD. However, considering the high genetic heterogeneity of COAD, disease metastasis, progression and clinical outcomes cannot be accurately predicted based on conventional staging methods (Weiser et al., 2011; Cancer Genome Atlas Network, 2012; Guinney et al., 2015). Although patients suffering from COAD may be in the same TNM stage, their clinical outcomes may differ considerably. Therefore, it is highly important to identify accurate prognostic biomarkers to understand the pathogenesis, predict clinical outcomes and devise personalized therapies in COAD.

Genome-sequencing technological development has strongly affected our understanding of the molecular mechanisms of colorectal carcinogenesis, and an increasing number of scientists have recognized the considerable potential of molecular signatures at the genetic level in predicting COAD prognosis. It has been reported that single genetic alterations, such as DNA mismatch repair (MMR) genes, *BRAF*, and *KRAS*, might represent as novel markers for predicting the prognosis of COAD (Punt et al., 2017). COAD is a molecularly complex disease that develops via the inactivation of tumor suppressor genes and the activation of oncogenes, suggesting that a single prognostic biomarker may differentiate COAD patients into different prognostic subgroups less reliably than a multiparameter molecular signature (Nguyen et al., 2020). Extensive studies have been conducted to investigate multigene-based signatures for the prediction of prognosis outcomes in COAD. For example, Ge et al. (2020) established a five-gene prognostic signature (*SMAD4*, *MUC16*, *COL6A3*, *FLG*, and *LRP1B*) that discriminates patients with stage III COAD into good- and poor-prognostic subgroups. Another study constructed a six-gene signature (*EPHA6*, *TIMP1*, *IRX6*, *ART5*, *HIST3H2BB*, and *FOXD1*) that accurately identified COAD patients at high risk of death (Zuo et al., 2019). However, few of these models have been widely applied in clinical practice, and a systematic study integrating gene expression profiling data from multiple source meta-analyses and improving statistical power for differentially expressed gene (DEG) identification are highly important for constructing more accurate and reproducible prognostic models. In addition, since a growing number of studies have identified hub genes that are increased in tumors tissues as compared with normal specimens, the tumor suppressor roles played by downregulated genes in tumors have largely been overlooked (Lv and Li, 2019; Yuan et al., 2020b). It is also important to explore the molecular mechanisms underlying hub genes that exhibit weak expression in tumors and are involved in the occurrence and development of COAD.

The overall goal of this study was to evaluate gene expression changes between COAD and normal samples and identify hub genes with prognostic value in COAD. Recently, considerable gene expression information regarding multiple carcinomas has been obtained from publicly available genomic datasets, such as The Cancer Genome Atlas Cancer Genome (TCGA) and Gene Expression Omnibus (GEO), and deep mining of both datasets has good application prospects in exploring cancer biology and identifying potential biomarkers for cancer diagnosis, treatment and prognosis (Chibon, 2013). In the current study, the transcriptomic expression data of the GEO GSE39582 dataset and TCGA-COAD dataset were downloaded and subjected to DEG analysis to evaluate gene expression changes between COAD and normal samples. Weighted gene co-expression network analysis (WGCNA) was employed to screen highly correlated gene clusters with COAD tumorigenesis. WGCNA, a powerful bioinformatic method, is widely used to detect potential modules of highly correlated genes and hub genes associated with clinical features on the basis of the theory that genes with similar functions or involved in common biological regulatory pathways may have similar co-expression patterns. Furthermore, univariate and multivariate Cox regression analyses were performed to select novel prognostic genes associated with the overall survival (OS) of COAD patients among the above genes and establish a stepwise 13-gene prognostic model. The prognostic performance of the 13-gene model was characterized by using the TCGA-COAD dataset and further validated in an independent dataset by merging the GSE39582 and GSE17536 datasets. Finally, in-depth

bioinformatic analyses were employed to identify the underlying regulatory mechanisms of the identified prognosis-related genes.

MATERIALS AND METHODS

Data Sources and Processing

A workflow of this study was depicted in **Figure 1**. Three independent human COAD datasets obtained from publicly available genomic datasets were included in this study: two expression microarray datasets (GSE39582 and GSE17536) and an RNA-sequencing dataset (TCGA-COAD). From the TCGA-COAD dataset[1], gene mRNA expression data and the corresponding clinical information from 480 tumor tissues and 41 paracancerous tissues were downloaded, in which the acquisition and application procedures aligned to the protocol. The mRNA-seq data were produced using the Illumina HiSeq 2000 platform and converted to the gene symbols based on the human reference genome hg38. For the expression microarray datasets, original Series Matrix Files of GSE39582 and GSE17536 were collected from the GEO database[2]. GSE39582 was submitted by Marisa et al. (2013) and contained 566 COAD tissues and 19 paracancerous tissues. GSE17536 was submitted by Smith et al. (2010) and consisted of 177 tumor tissues. Owing to the lack of normal tissues, GSE17536 dataset was not included in the next DEG analysis. Detailed information on these datasets is provided in **Supplementary Tables 1–3**. Standardized data were mapped to the corresponding genetic symbols based on the annotation file provided by the GPL570 platform (Affymetrix Human Genome U133 Plus 2.0 Array). The batch effect of the two-chip data was removed by using an SVA algorithm. Based on the requirement for data integration, data were processed according to the following criteria: (1) data from patients with incomplete information on clinicopathological variables, including survival status and survival time, were removed, and (2) duplicated samples were removed by the average expression values of all these genes.

[1]https://portal.gdc.cancer.gov/repository

[2]https://www.ncbi.nlm.nih.gov/geo/

Identification of Key Co-expression Modules Using WGCNA

Gene co-expression network analysis was specifically performed on the gene expression profiles of TCGA-COAD and GSE39582 using the "WGCNA" package. The analysis was conducted according to a previous study (Langfelder and Horvath, 2008).

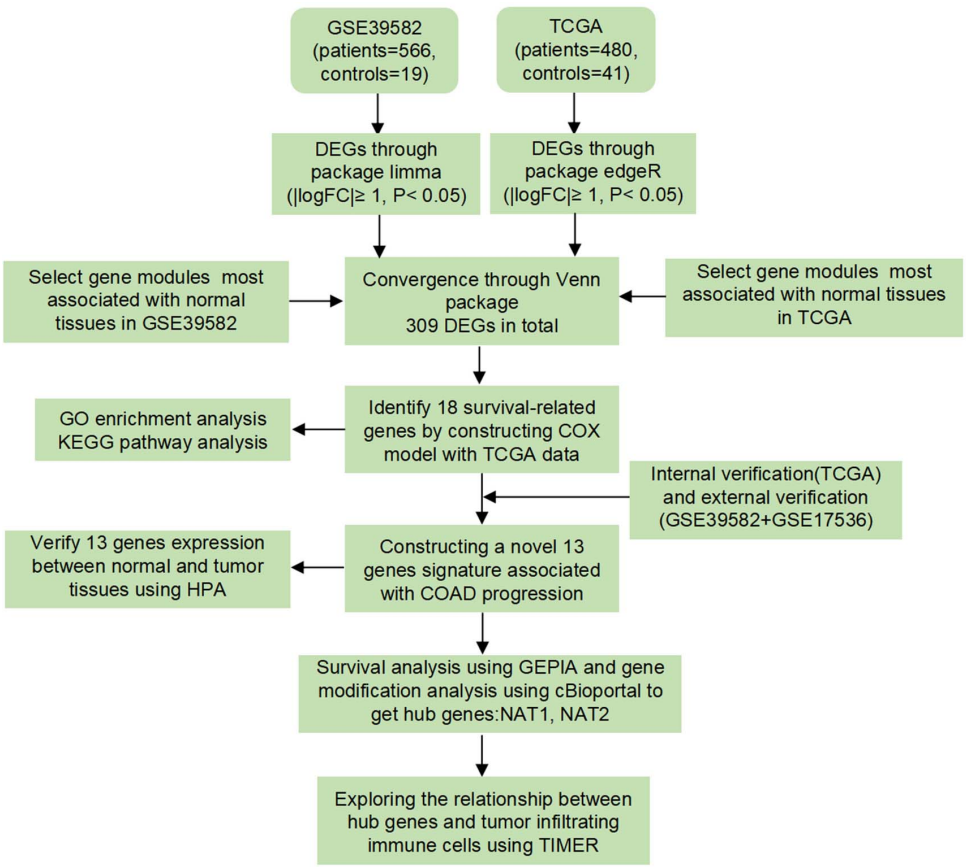

FIGURE 1 | Study design and workflow of this study.

First, co-expression analysis was performed for all pair-wise genes using Pearson's correlation matrices. Subsequently, the weighed adjacency matrix that described the correlation strength between each pair of nodes was constructed by using a power function $a_{mn} = |c_{mn}|^{\beta}$ (a_{mn} encoded the strength of the correlation between gene m and gene n; c_{mn} represented Pearson's correlation coefficient between gene m and gene n; β represented a soft-thresholding parameter). After selecting the optimal soft-thresholding power based on the pickSoftThreshold function in R language, the adjacency matrix was transformed into a topological overlap matrix (TOM), which could quantitatively describe the similarity in genes by comparing the weighted correlation between two genes and other genes. Next, hierarchical clustering was conducted to classify genes with similar expression profiles into different gene co-expression modules using the DynamicTreeCut algorithm based on TOM dissimilarity.

To identify candidate modules relevant to clinical traits, module eigengenes (MEs) were obtained using the moduleEigengenes function to indicate the principal component of each module, and the module-trait associations between MEs and clinical subtypes (normal and tumor) were calculated using linear regression. Modules with the highest correlation coefficient among all the selected modules were considered the key modules significantly associated with clinical subtypes of COAD and were subjected to further analysis.

Identification of DEGs

Screening of DEGs can identify the differences in gene expression levels between tumor tissues and matched normal tissues and identify the specific genes correlated with biological characteristics in tumors. We employed the "edgeR" package to analyze the differences between non-malignant samples and COAD tissues in the TCGA-COAD dataset. The analysis of DEGs in the GSE39582 dataset was conducted using the "limma" package in R software. DEGs including significantly downregulated and upregulated genes were selected for further study with the cut-off criteria of false discovery rate (FDR) < 0.05 and $|\log_2$ fold change (FC)$| > 1$ and visualized as volcano plots by using the "ggplot2" package. Afterward, the DEGs were intersected with the co-expression module genes that were extracted from the above mentioned analysis to obtain the overlapping candidate genes (OCGs). Finally, the OCGs were visualized as a Venn diagram using the "VennDiagram" package and subsequently applied to construct a predictive gene signature.

Construction of Prognostic Signature

The TCGA-COAD dataset served as a training cohort to establish a gene-based model for prognosis prediction of COAD. To determine the feasibility and reliability of survival-associated genes as prognostic markers in COAD, univariate Cox proportional hazards regression analysis was performed to evaluate the associations between the expression of OCGs and patient OS by using the "survival" package. Only those OCGs of the training set with P-values less than 0.05 were selected for stepwise multivariate Cox regression to build a prognostic predictive model. To elucidate the underlying biological mechanisms of survival-associated genes, pathway enrichment analysis including gene ontology (GO) terms and Kyoto Encyclopedia of Genes and Genomes (KEGG) pathways was performed using the "clusterProfiler" package and "org.Hs.eg.db" package. GO terms that consist of the three major classifications—biological process (BP), cellular component (CC), and molecular function (MF)—are able to provide a comprehensive understanding of the biological properties of gene sets for all organisms. The results of GO and KEGG pathway analyses were considered to indicate significance at a cut-off threshold of P-value < 0.05, and the "ggplot2" package was applied to visualize the enrichment results to help interpret the results.

Next, the risk score formula of each patient was constructed based on a linear combination of a regression coefficient (β) multiplied by the genetic expression level of significant OCG: The risk score = (β_{gene1} * expression level of gene1) + (β_{gene2} * expression level of gene2) + (β_{gene3} * expression level of gene3) + (β_{genen} * expression level of genen). In addition, univariate and multivariate analyses were performed to determine whether the prognostic value of the prognostic risk model was independent of other clinicopathological parameters including age, gender, stage, and TNM status in the TCGA-COAD dataset.

Evaluation of the Predictive Value of the Prognostic Signature

To validate the robustness and transferability of the prognostic risk model, the predictive power was validated on the testing cohort. To increase the sample sizes, we merged the GSE39582 and GSE17536 datasets as the testing cohort. With the median risk score as the cut-off value, patients were divided into high-risk and low-risk cohorts according to the gene-based risk score formula. Kaplan–Meier (KM) curves and log-rank tests were plotted to compare two groups' survival events. The ability of the signature to predict patient survival was further assessed by using receiver operating characteristic (ROC) curve methodology and calculating the area under the curve (AUC) with the R package "survival ROC." Otherwise, the prognostic risk model was visualized as a risk plot in the training and testing cohorts that comprised the distributions of the risk score, the survival status of each patient and the expression profiles of the screened OCGs.

Validation of Gene and Protein Expression of Prognostic Genes

Based on the data from the TCGA database, the gene expression levels of prognosis-related genes between COAD and normal tissues were normalized using the "edgeR" package and drawn as a box plot graph. The relationships among prognosis-related genes were analyzed using Pearson correlation analysis and plotted as co-expressed heatmaps in the COAD and normal tissues, respectively. Moreover, the Human Protein Atlas (HPA[3]) was utilized to validate the protein expression levels of prognosis-related genes by immunohistochemistry (IHC).

[3]http://www.proteinatlas.org

Genomic Alterations of Favorable Prognostic Genes by the cBioPortal Database

The cBioPortal Cancer Genomics Portal[4] is a web-based platform for performing multidimensional cancer genomics data exploration, analytics, and visualization (Gao et al., 2013). The gene alteration status of favorable prognostic genes derived from the prognostic risk model was analyzed using the cBioPortal tool regarding COAD. OncoPrint was constructed in cBioPortal (TCGA provisional) to directly provide an overview of genetic alterations in each gene.

Survival Analysis of Favorable Prognostic Genes Based on the GEPIA Database

The Gene Expression Profiling Interactive Analysis (GEPIA) database[5] is a web-based tool for analyzing RNA sequencing expression data and providing customizable functions such as patient survival analysis, which includes 9736 tumors and 8587 normal samples from the TCGA and Genotype-Tissue Expression databases (Tang et al., 2017). Survival curves were plotted using the online tool GEPIA to evaluate the relationship between OS and the expression of favorable prognostic genes in COAD patients.

Immune Infiltrate Analysis Based on the TIMER Database

TIMER[6] is a web-based data-mining platform that includes 10,897 samples across 32 cancer types and applies a deconvolution previously published statistical method to determine the relative levels of six immune infiltrates from their gene expression profiles (Li et al., 2017). The association of immune infiltration levels in COAD with somatic copy number alterations (SCNA) for prognostic genes was investigated by the "SCNA module" in the TIMER database. SCNAs in TIMER include deep deletions, arm-level deletions, diploid/normal alterations, arm-level gains and high amplifications. The distributions of each immune cell subset at each copy number status in COAD were plotted by box plots and a two-sided Wilcoxon rank sum test was utilized to compare the immune infiltration level in each SCNA category with that for normal samples. In addition, we further analyzed the correlation of *NAT1* and *NAT2* expression with tumor purity and levels of infiltrating CD8+ T cells and activated myeloid dendritic cells.

Statistical Analysis

R software (version 3.6.1) was employed to implement the statistical analyses in the study. *P*-values < 0.05 were considered to be significant unless otherwise specified.

[4]http://cbioportal.org

[5]http://gepia.cancer-pku.cn/

[6]https://cistrome.shinyapps.io/timer/

RESULTS

Construction of Weighted Co-expression Network and Identification of Key Modules

After data preprocessing and quality assessment, we obtained the expression matrices from the 521 samples in the TCGA-COAD dataset and the 585 samples in the GSE39582 dataset. Using the system biology method of WGCNA, co-expression modules in COAD patients were identified by constructing the co-expression networks from the TCGA-COAD and GSE39582 datasets. In the present study, a soft power $\beta = 5$ (**Figure 2A**) was chosen to build a scale-free network and 11 modules were generated through average linkage hierarchical clustering in the TCGA-COAD dataset (**Figure 2B**). Meanwhile, a total of 12 modules (**Figure 3B**) were obtained by selecting an appropriate soft-thresholding power = 5 in the GSE39582 dataset (**Figure 3A**). Furthermore, we analyzed the association of modules between each module and clinical subtypes (normal and tumor) to identify key modules and construct the heatmaps of module-trait relationships in **Figures 2C**, **3C**. MEyellow in the TCGA-COAD module ($r = 0.88$, $p < 0.001$) and MEbrown ($r = 0.69$, $p < 0.001$) in the GES39582 module that were found to have the highest association with normal tissues were selected as clinically significant modules.

Identification of DEGs and OCGs

Under the cut-off criteria of FDR < 0.05 and $|\log FC| \geq 1.0$, the "limma" algorithm identified 1461 DEGs in the GES39582 dataset (796 upregulated and 665 downregulated genes, **Figure 4B**). A total of 4021 DEGs in the TCGA-COAD dataset (1609 upregulated and 2412 downregulated genes, **Figure 4A**) were obtained by the "edgR" package. As plotted in **Figure 4C**, the brown module of the GES39582 dataset with 569 co-expression genes and the yellow module of the TCGA-COAD dataset with 818 co-expression genes intersected with the DEGs, and 309 genes were screened as the OCGs for further analyzed.

Identification of a Gene-Based Signature From the Training Dataset

All the OCGs in the training dataset (TCGA-COAD) were subjected to univariate Cox analysis and a total of 18 genes that were significantly associated with OS (**Figure 5**, $P < 0.05$) were considered to be prognostic genes for multivariate Cox regression analysis. To elucidate the underlying biological mechanisms of 18 survival-related genes, GO and KEGG pathway enrichment analyses were performed using the ClusterProfiler package, and the results demonstrated that 5 KEGG pathways and 241 GO terms were enriched for these prognostic genes (**Supplementary Tables 4, 5**). The top ten terms in the three functional groups (BP, CC, and MF) from the GO results are demonstrated in **Figure 6B**. Among the BPs, the prognostic genes were largely associated with metabolic biological processes, including xenobiotic, fatty acid, and icosanoid metabolic processes. For the CC results, it was demonstrated that the prognostic genes were primarily located at zymogen granules,

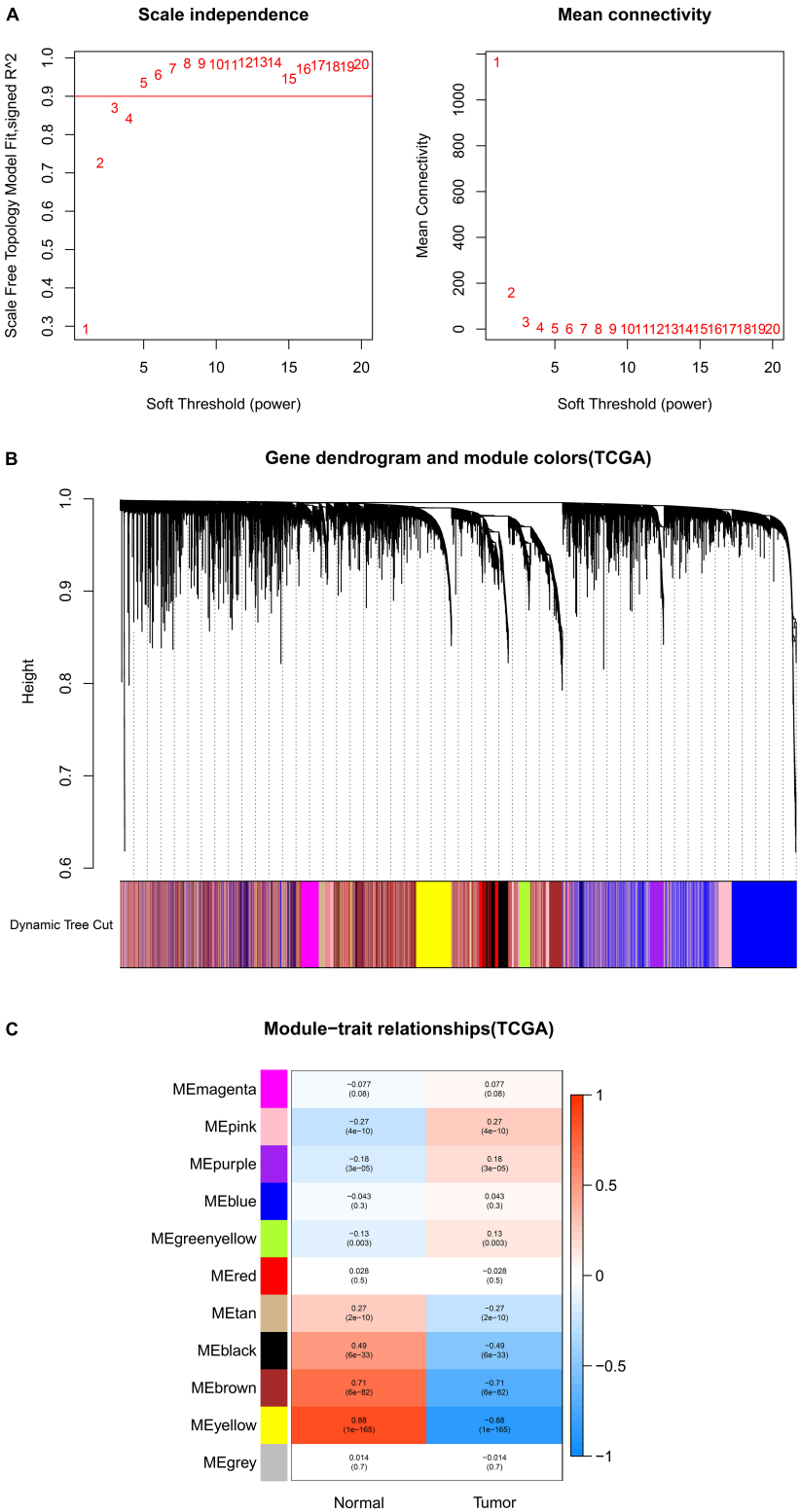

FIGURE 2 | Identification of modules associated with clinical information in the TCGA-COAD dataset. **(A)** Determination of soft-thresholding power in WGCNA analysis. **(B)** Gene cluster tree. Based on the adjacency-based dissimilarity of the hierarchical clustering gene clustering chart, dynamic tree cutting method was utilized to identify modules by dividing the tree diagram at significant branch points. Modules are assigned different colors in the horizontal bar immediately below the tree diagram. **(C)** Module-trait relationships for normal and tumor. Each row in the table corresponds to a color module, and each column to a clinical trait. Numbers in each cell reported the correlation coefficient between each module and clinical traits and the corresponding *p*-value.

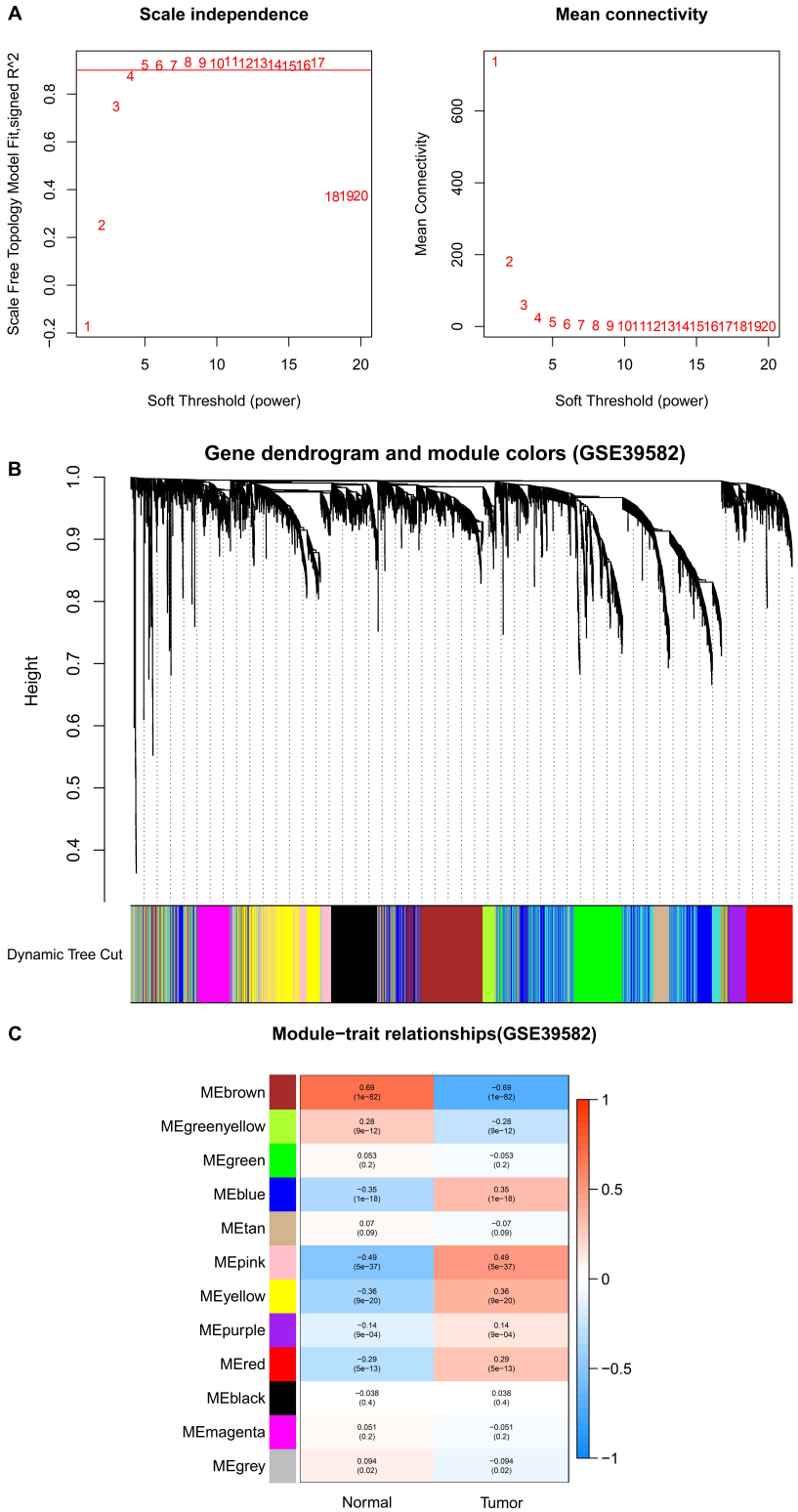

FIGURE 3 | Identification of modules associated with clinical information in the GSE39582 dataset. **(A)** Determination of soft-thresholding power in WGCNA analysis. **(B)** Gene cluster tree. Based on the adjacency-based dissimilarity of the hierarchical clustering gene clustering chart, dynamic tree cutting method was utilized to identify modules by dividing the tree diagram at significant branch points. Modules are assigned different colors in the horizontal bar immediately below the tree diagram. **(C)** Module-trait relationships for normal and tumor. Each row in the table corresponds to a module eigengene, and each column to a clinical characteristic. Numbers in each cell reported the correlation coefficient between each module and clinical traits and the corresponding *p*-value.

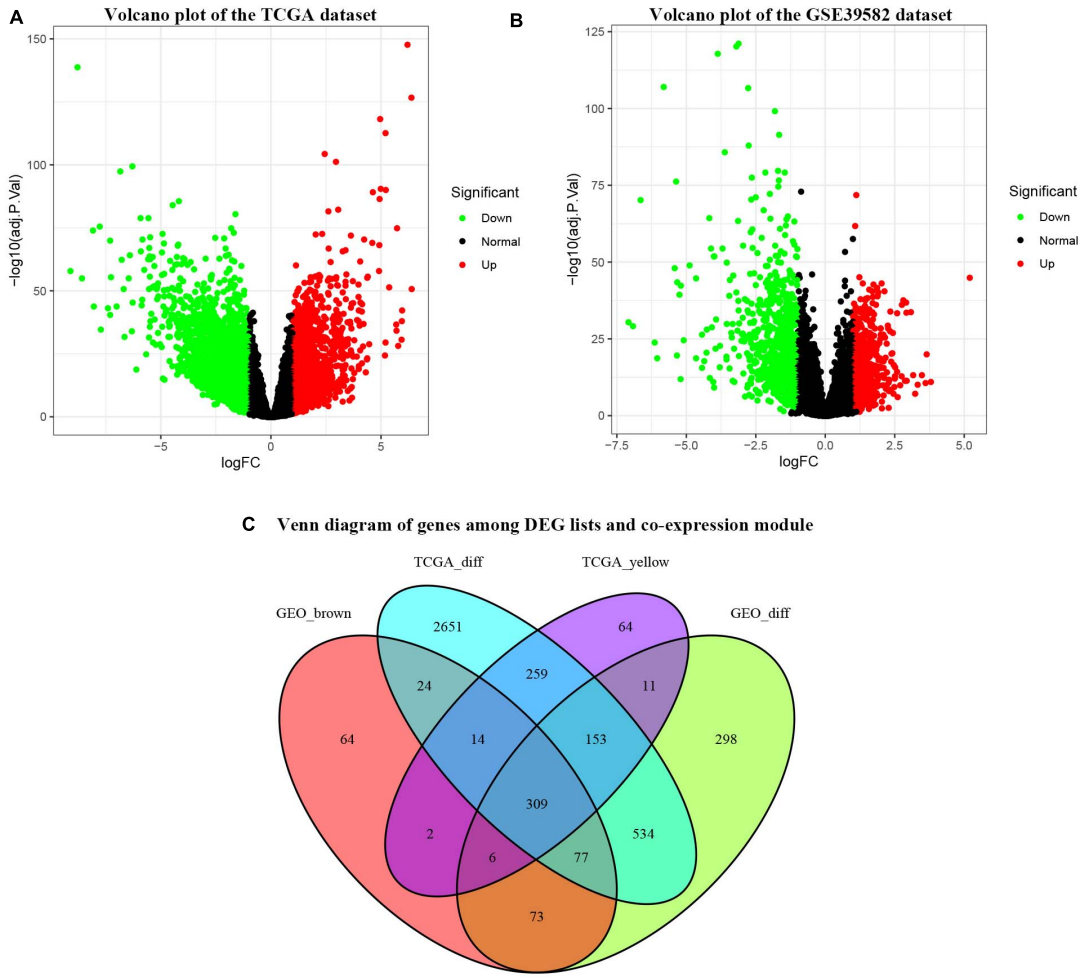

FIGURE 4 | Identification of consensus differentially expressed genes (DEGs) among the TCGA-COAD and GSE39582 datasets of COAD patients. **(A)** Volcano plot of DEGs in the TCGA-COAD dataset. **(B)** Volcano plot of DEGs in the GSE39582 dataset. **(C)** The Venn diagram showing the overlapping candidate genes among DEG lists and co-expression modules.

euchromatin, tricarboxylic acid cycle (TCA) enzyme complexes and peroxisomal matrices. Moreover, MF analysis indicated that these genes were primarily involved in regulating the biological functions of multiple enzymes and receptors, such as *N*-acetyltransferase, prostaglandin receptor, hydrolase and peroxisome proliferator activated receptor. According to KEGG analysis (**Figure 6A**), these genes were correlated with drug metabolism-other enzymes, chemical carcinogenesis and the TCA cycle, which modulated the metabolic biological processes to affect the tumorigenesis of COAD.

Next, 13 genes were further selected to establish a prognostic gene signature, of which four genes were independent prognostic factors associated with unfavorable overall survival (*FXYD3*, *FRMD3*, *LINC01133,* and *CHGA*), and nine genes were confirmed to be favorable prognostic factors for COAD (*TSPAN1*, *HRCT1*, *MIER3*, *NR3C2*, *SLC41A2*, *NAT1*, *NAT2*, *ZG16,* and *PPARGC1A*). The risk score formula for assessing the prognosis of each patient was calculated as follows: risk score = (−0.003) × (expression value of *TSPAN1*) + 0.002 × (expression value of *FXYD3*) + (−0.107) × (expression value of *HRCT1*) + 0.136 × (expression value of *FRMD3*) + (−0.039) × (expression value of *NR3C2*) + (−0.072) × (expression value of *SLC41A2*) + (−0.173) × (expression value of *NAT1*) + (−0.116) × (expression value of *NAT2*) + (−0.033) × (expression value of *MIER3*) + 0.076 × (expression value of *LINC01133*) + (−0.021) × (expression value of *ZG16*) + 0.016 × (expression value of *CHGA*) + (−0.074) × (expression value of *PPARGC1A*). Detailed information on the multivariate Cox regression is presented in **Table 1**.

Prognostic Role of the 13-Gene Signature

The 13-gene based risk score was calculated for each patient in the training and testing sets, and patients were stratified into the low-risk and the high-risk subgroups with the median

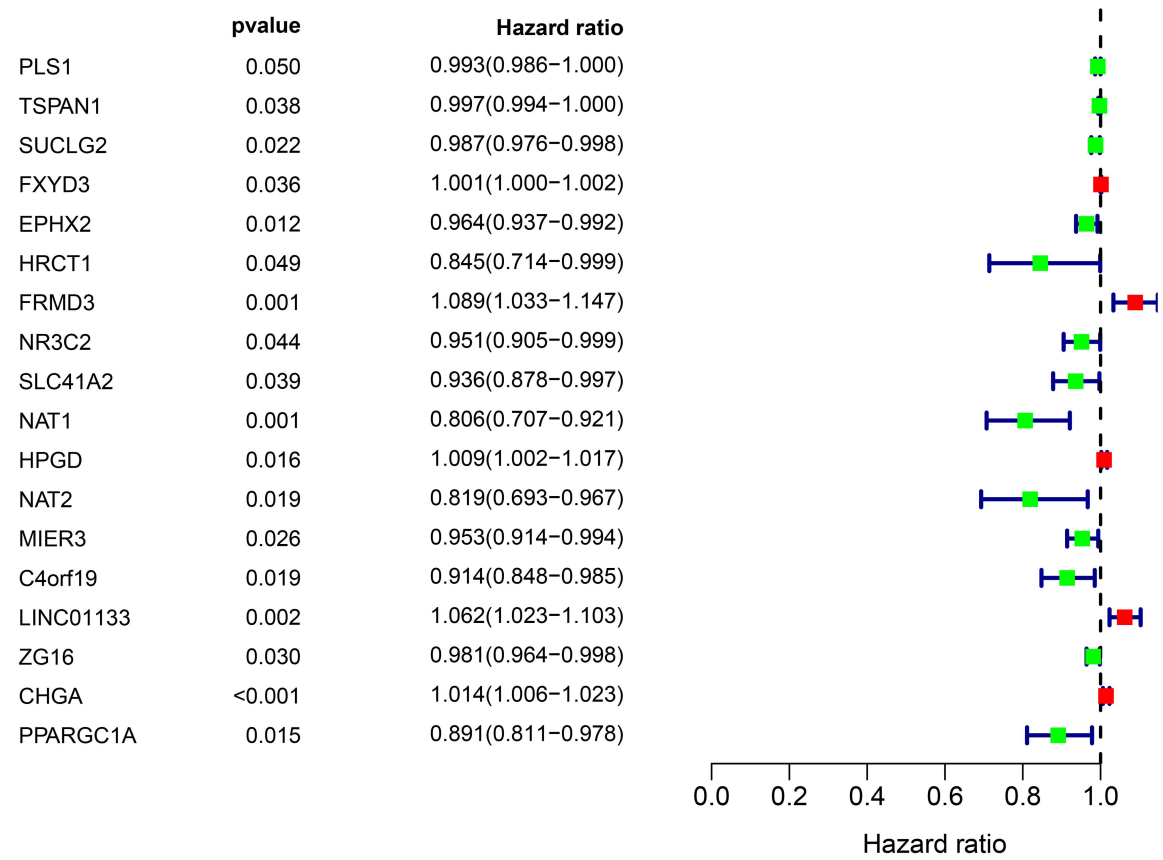

FIGURE 5 | Overall information of 18 prognostic DEGs screened out by univariate Cox proportional hazards regression in the TCGA-COAD dataset. Solid squares represent the hazard ratio (HR) of death, and close-ended horizontal lines represent the 95% confidence intervals (CI).

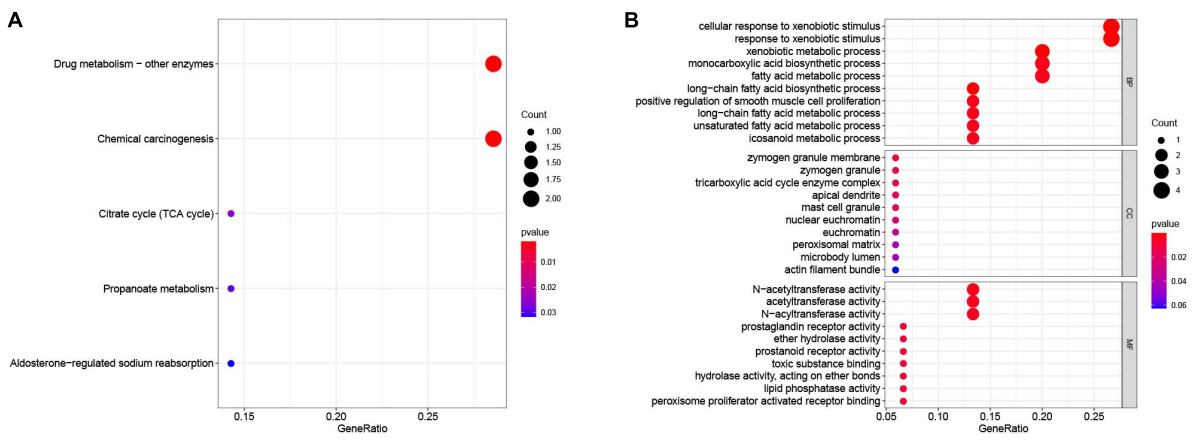

FIGURE 6 | Functional enrichment analysis of the 18 survival-associated genes. **(A)** KEGG pathways in enrichment analysis of the prognostic genes; **(B)** GO enrichment analysis results of the prognostic genes. Bubble color refers to the enrichment *P*-value, and the size of the bubble represents the gene number.

prognostic score of the training set serving as the cut-off point. Next, we used the KM plot and ROC curve to describe the performance of the 13-gene signature in predicting the survival risk of COAD patients. The distribution of the risk score along with the survival status of COAD patients and the heatmap of the 13 prognostic genes in the two datasets are displayed in **Figure 7** (left panel), which indicates that patients with low scores had lower mortality rates than did patients with high scores. Consistent with these results, the KM analyses showed that the high-risk group had a significantly shorter OS time than the

TABLE 1 | Coefficients of 13 genes constituting gene-based risk signature that were identified from multivariate Cox regression analysis.

Gene	Coefficient	HR	HR.95L	HR.95H	*P*-value
TSPAN1	−0.003	0.997	0.993	1.001	0.140
FXYD3	0.002	1.002	1.001	1.002	0.001
HRCT1	−0.107	0.899	0.768	1.054	0.189
FRMD3	0.136	1.146	1.070	1.227	0.001
NR3C2	−0.039	0.962	0.915	1.011	0.128
SLC41A2	−0.072	0.931	0.864	1.002	0.06
NAT1	−0.173	0.841	0.734	0.965	0.014
NAT2	−0.116	0.890	0.751	1.056	0.181
MIER3	−0.033	0.968	0.927	1.011	0.138
LINC01133	0.076	1.079	1.042	1.117	< 0.001
ZG16	−0.021	0.979	0.960	0.998	0.032
CHGA	0.016	1.016	1.008	1.023	< 0.001
PPARGC1A	−0.074	0.929	0.851	1.014	0.099

HR, Hazard ratio.

low-risk group (log-rank $p < 0.001$ in the training and testing sets, **Figure 7**, right panel). The AUCs for the 13-gene signature reached 0.789 and 0.868 in the training set and the testing set, respectively, indicating the enhanced power of the signature in predicting the survival outcomes of COAD patients (**Figure 7**, right panel). In addition, we included age as a continuous variable and gender and TNM stage as categorical variables for univariate and multivariable Cox regression analyses to further analyze the performance of our signature in the training set. The results of the multivariate Cox regression analyses showed that the 13-gene signature was an independent and unfavorable prognostic factor in terms of OS after adjusting for age, gender, and TNM stage (HR = 1.015, 95%CI = 1.008–1.022, $p < 0.001$, **Table 2**).

Verification of the Expression Patterns of the Prognostic Genes

To elucidate the role played by the prognostic genes derived from the predictive signature in COAD, we explored the gene expression levels of these genes among the patients of the TCGA database and verified the protein expression levels using the HPA database. As shown in the **Figure 8A**, all the gene expression levels of prognostic genes were significantly downregulated in COAD compared with non-tumor tissues (All *P*-values < 0.001). The characteristic IHC photos of prognostic genes in tumor and normal tissues are presented in **Figure 8B** and the results indicated that six of the prognostic genes showed significant downregulation in COAD compared with normal tissue, including *MIER3*, *CHGA*, *SLC41A2*, *NAT1*, *NAT2*, and *ZG16*. However, the HPA dataset did not provide the immunochemical profiles of *HRCT1*, *LINCO1133*, and *PPARGC1A*. Moreover, we employed Pearson correlation analysis to explore the correlation between the mRNA expressions of the 13 prognostic genes in the TCGA dataset. The co-expression pattern in the normal tissues (**Figure 8C**) was notably different from that in the tumor tissues (**Figure 8D**).

Somatic Mutation Landscape and Prognostic Values of Favorable Prognostic Genes

Nine genes showing negative coefficients in the prognostic signature were considered to be favorable prognostic genes. Since the tumor genome pattern is reportedly associated with tumorigenesis, we explored the somatic mutation for favorable prognostic genes contained in the prognostic signature by cBioPortal database analysis. **Figure 9A** illustrates the somatic mutation landscape of the nine favorable prognostic genes in COAD samples, with red and blue representing amplification and deep deletion, respectively. Gene alterations in *MIER3*, *NAT1*, and *NAT2* were observed to occur in 5% of the sequenced cases, and deep deletion accounted for the majority of alteration types. Approximately 3% of genetic alterations of *TSPAN1* were observed in COAD patients, including deep deletions and missense mutations with unknown significance. Moreover, copy number alterations (CNAs) were found in the most of COAD patients. In addition, OS analyses of the nine favorable prognostic genes were conducted by KM analyses based on the GEPIA database to further confirm the prognostic values of these genes in patients with COAD (**Figure 9B**). Among these genes, *NAT1*, *NAT2*, *NR3C2*, *ZG16*, and *PPARGC1A* showed significant positive correlations with OS and could be considered to be protective genes in COAD. From the above mentioned analyses, we found that only the two protective genes *NAT1* and *NAT2* underwent the deep deletion and tended to be downregulated in COAD tissues, suggesting that the two genes might play critical roles in cancer development and progression. Furthermore, we compared the differences in *NAT1* and *NAT2* among different subgroups in COAD (**Figure 10**). *NAT1* and *NAT2* were significantly differentially expressed in COAD patients with different AJCC stages. Lower *NAT1* and *NAT2* expression was associated with higher pathological stage.

Association of *NAT1* and *NAT2* Expression With Immune Infiltration

It is well-known that immune cells play an important anti-tumor surveillance role. Thus, to elucidate the potential regulatory mechanisms of *NAT1* and *NAT2* in the development of COAD, the relationships between the SCNAs of *NAT1* and *NAT2* and immune infiltrates in the COAD microenvironment were explored. Compared to the immune infiltrate levels of six cells, deletion of *NAT1* and *NAT2* was associated with substantially lower levels of four immune cell types, including B cells, CD8+ T cells, neutrophils, and dendritic cells, which indicated their influence on the tumor microenvironment (**Figure 11A**). Furthermore, we observed that *NAT1* and *NAT2* expression was significantly correlated with the infiltration levels of CD8+ T cells and dendritic cells (**Figure 11B**).

DISCUSSION

The molecular pathogenesis of COAD is multifaceted in nature and characterized by a variety of genomic instabilities,

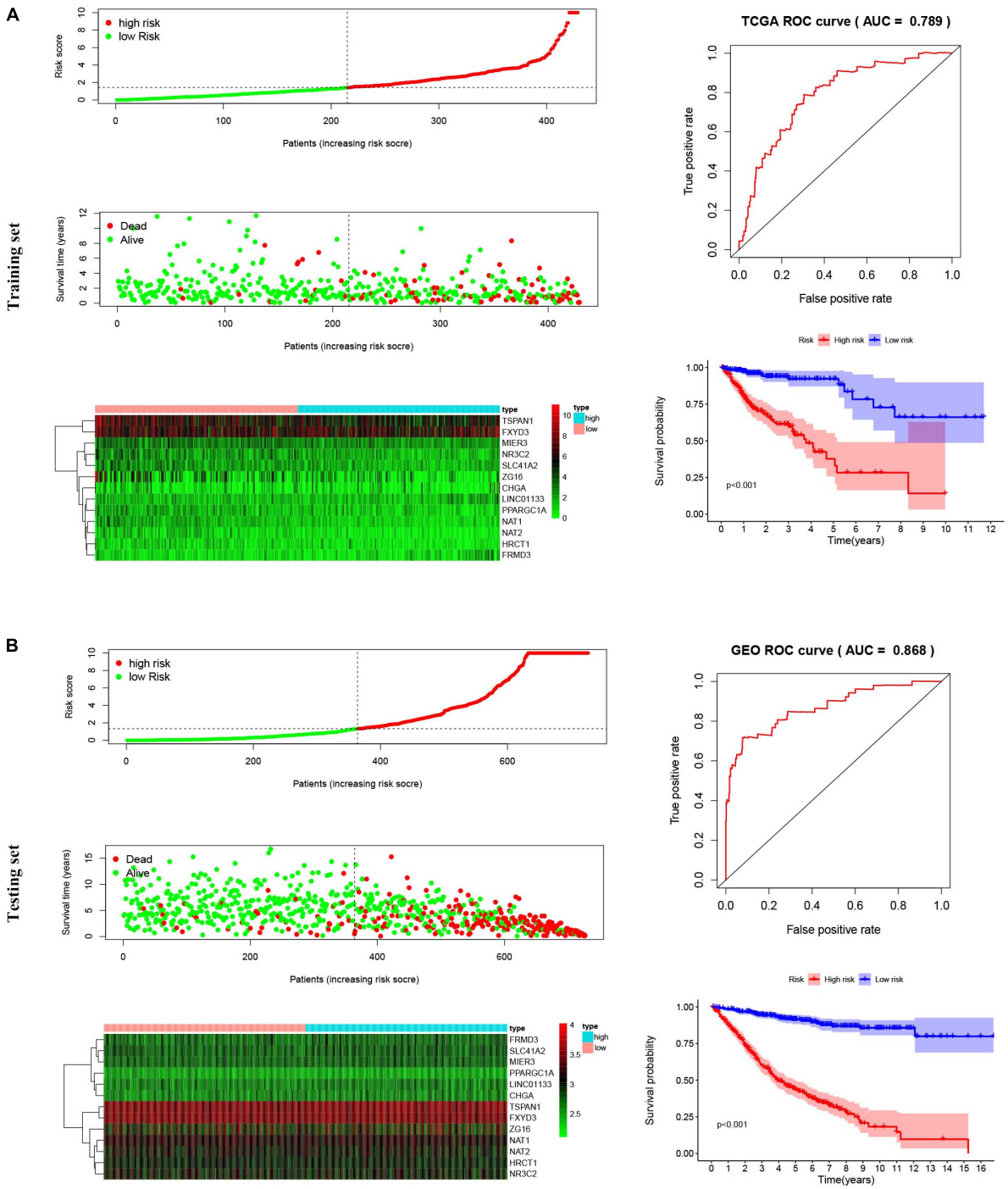

FIGURE 7 | Risk score analysis, Kaplan–Meier survival curves and ROC curves for the 13-gene signature in COAD. Our study employed TCGA-COAD cohort as the training dataset and an independent cohort by merging the GES39582 and GSE17536 datasets as the testing dataset. **(A)** The distributions of the risk score, survival status and expression profiles, Kaplan–Meier curve and ROC curve of the 13-gene signature in the training set. **(B)** The distributions of the risk score, survival status and expression profiles, Kaplan–Meier curve and ROC curve of the 13-gene signature in the testing set.

epigenomic alterations, gene expression dysregulation and chromosomal aberrations, which are not separate events but multiple cellular processes (Cancer Genome Atlas Network, 2012; Guinney et al., 2015). Although several advances focusing on diagnostic and therapeutic techniques have been identified to effectively reduce the mortality rates of COAD patients, there are still a number of challenges facing early diagnostic and therapeutic strategies, including a lack of the

TABLE 2 | Identifying the independent prognostic parameters in the TCGA-COAD dataset.

Variables	Univariable model			Multivariable model		
	HR	95%CI of HR	*P*-value	HR	95%CI of HR	*P*-value
13-gene risk score	1.016	1.009-1.023	< 0.001	1.015	1.008-1.022	< 0.001
Age	1.016	0.995-1.037	0.145	1.035	1.013-1.059	0.002
Gender	1.132	0.704-1.820	0.609	0.968	0.595-1.573	0.895
AJCC stage	3.883	2.309-6.530	< 0.001	1.993	0.595-1.573	0.047
ATCC T stage	7.330	1.791-29.996	0.006	3.163	0.743-13.475	0.119
AJCC N stage	4.512	2.790-7.294	< 0.001	2.788	1.590-4.888	< 0.001
AJCC M stage	3.721	2.300-6.019	< 0.001	1.598	0.903-2.829	0.108

HR, Hazard ratio; CI, confidence interval; AJCC, American Joint Committee on Cancer.

awareness of high-risk patients, a lack of clinically applicable biomarkers to identify high-risk patients, and the high cost of screening high-risk populations. Currently, genes can be utilized to construct a prognostic risk model that helps to assess tumor progression, prognosis and reaction to therapeutic strategies, and a number of studies have established gene signatures based on large-scale public datasets (Zuo et al., 2019; Yuan et al., 2020a). Therefore, to accurately predict survival time and identify high-risk patients, we conducted a comprehensive screening of DEGs from two independent datasets and subsequently constructed a 13-gene signature in prognosis prediction for COAD patients. We also performed validation analysis of the prognostic predictive signature and found that this signature was credible in predicting the OS of COAD patients.

Compared with the gene-based signatures constructed in the previous study (Zuo et al., 2019; Yuan et al., 2020a), our prognostic model was different. First, we adopted integrated bioinformatic methods, WGCNA and DEG analysis, to select significant DEGs related to the clinical traits from the GES39582 dataset and the TCGA-COAD dataset. Integrated bioinformatic analysis tends to be an effective method to identify tumor-specific genetic alterations associated with the occurrence and development of tumors and guide patients' personalized therapy. Although traditional DEGs analysis is a powerful analysis that can discover genetic alterations between control groups and experimental groups, then generating highly valuable information, only WGCNA, a data exploration tool, can be used to determine the interactions among genes and find modules of highly related genes that are significantly associated with clinical features and biological tumor behavior. Second, numerous studies have used WGCNA to select key modules associated with clinicopathological parameters in multiple cancers. For example, Xie and Xie (2019) identified genes significantly associated with pathological M stage based on WGCNA and constructed a 6-gene signature for the prognosis of non-small-cell lung cancer patients. A previous study defined one gene module related to tumor grades in colorectal cancer, and the putative representative biomarkers associated with prognosis were identified (Yuan et al., 2020b). Unlike traditional WGCNA, our study focused on the modules notably correlated with normal tissues in the two independent datasets and selected the module genes that might play an important role in maintaining physiological function. Thus, our study identified a brown module in the GES39582 dataset and a yellow module in the TCGA-COAD dataset, both of which were significantly related to normal tissues compared with tumor tissues. Furthermore, the 309 OCGs between DEGs and the co-expression module genes were obtained and subjected to univariate and multivariate Cox analyses for prognostic signature construction. Our study employed TCGA cohort as the training dataset and an independent cohort by merging the GES39582 and GSE17536 datasets as the testing dataset. Moreover, to minimize variability, an SVA algorithm was utilized to remove the batch effect of the two GEO datasets.

In this study, a total of 18 survival-related genes was firstly identified based on univariate Cox analysis in the TCGA-COAD dataset. Functional annotation analysis indicated that these genes were mainly involved in various metabolic processes, which might affect the development of cancer. The top activated pathway in the enrichment analysis was fatty acid metabolic process, an essential cellular process that reflects the function of mitochondria. Increased fatty acid synthesis is crucial for the proliferation and growth of cancer cells by new membrane biosynthesis and steroid hormone production, thereby promoting tumorigenesis and tumor progression (Röhrig and Schulze, 2016). Next, we constructed a novel gene-based signature consisting of 13 genes (*FXYD3*, *MIER3*, *LINC01133*, *CHGA*, *TSPAN1*, *HRCT1*, *FRMD3*, *NR3C2*, *SLC41A2*, *NAT1*, *NAT2*, *ZG16,* and *PPARGC1A*) for predicting the OS of COAD patients. Furthermore, the 13-gene signature could categorize COAD patients into low-risk and high-risk groups with statistically different survival outcomes, which was validated by the ROC analysis and KM curve analysis in both TCGA and the merged GEO datasets. Besides, to further clarify whether this signature is an independent factor in COAD, multivariate Cox regression analyses was performed and showed that it was able to predict the survival of COAD patients without consideration of other conventional clinicopathological variables, including age, gender, and AJCC stage. Taken together, these findings provide the evidence for translating the 13-gene signature into clinical practice.

In the 13-gene signature, most genes were regarded as favorable prognostic genes, while only *FXYD3*, *FRMD3*, *LINC01133,* and *CHGA* were found to do the opposite. As

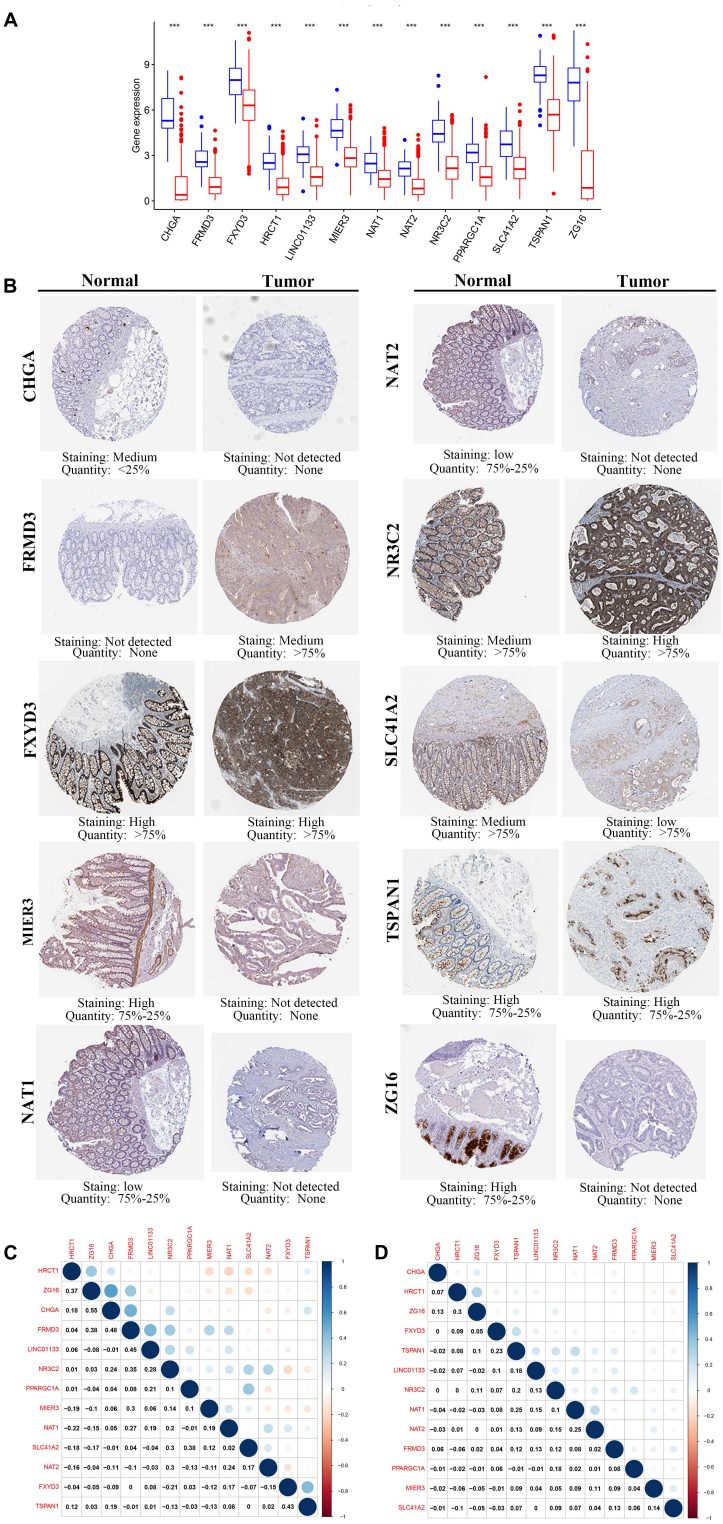

FIGURE 8 | The expression of the 13 prognostic genes in COAD. **(A)** The expression profiles of the 13 genes in the TCGA-COAD dataset. Wilcoxon rank-sum tests were conducted to compare the difference in the expression level of each gene between tumor and normal tissues. ***$p < 0.001$; N, normal tissues; T, tumor tissues. **(B)** Protein levels of the 13 genes in the COAD and normal tissues based on the Human Protein Atlas. **(C)** Transcription-level correlation analysis of the 13 prognostic genes in the normal tissues of TCGA-COAD dataset. **(D)** Transcription-level correlation analysis of the 13 prognostic genes in the tumor tissues of TCGA-COAD dataset. Pearson correlation analysis was performed to analyze the relationships among prognosis-related genes. Numbers in each cell reported the correlation coefficient between these genes.

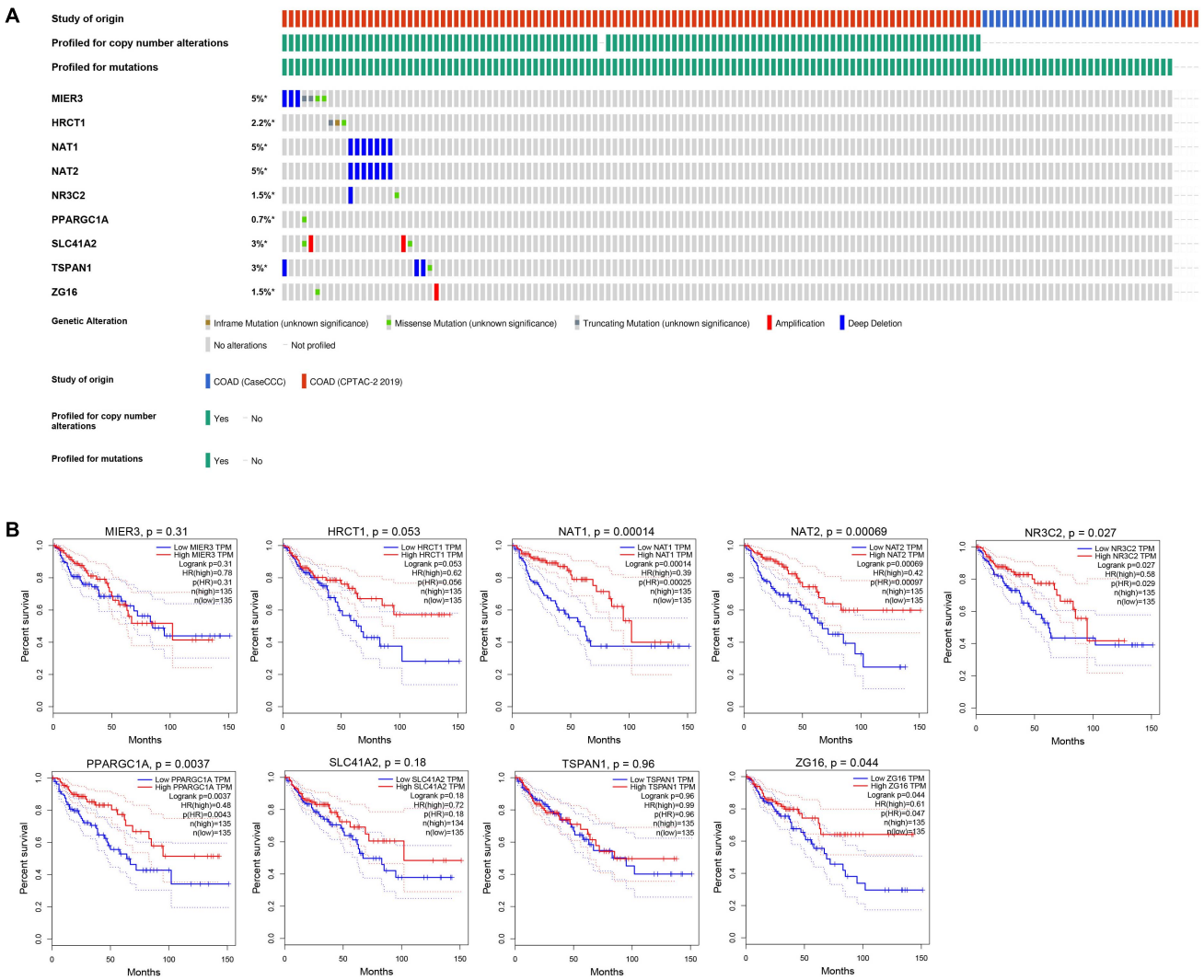

FIGURE 9 | The genomic mutations and prognostic values of the nine favorable prognostic genes in COAD. **(A)** The expression alteration profiles of the nine favorable prognostic genes based on the cBioPortal database. The genetic alterations of the favorable prognostic genes in COAD, including copy number amplification, deep deletion, amplification, and genomic mutation were assessed. The OncoPrint tab provides an overview of genetic alterations in each gene across a sample set. Each row refers to a gene, and each column refers to a tumor sample. **(B)** The overall survival analyses of the 9 favorable prognostic genes using the GEPIA online platform. Kaplan–Meier plotter was applied to evaluate the prognostic value of each gene. Hazard ratios (HRs) and log-rank p-values were calculated.

the survival time of cancer patients could be influenced by aberrant expression of genes, we confirmed the gene and protein expression patterns of the prognostic genes based on the TCGA database and HPA database. All 13 genes were determined to be downregulated at the genetic level in COAD tissues relative to normal samples, among which six genes were consistent with the IHC results in the HPA dataset and tended to be reduced at the protein level in tumor specimens, including *MIER3*, *CHGA*, *SLC41A2*, *NAT1*, *NAT2*, and *ZG16*, providing the vital function of favorable prognostic genes in COAD. However, unfavorable prognosis-related genes have also been reported to be involved in tumor proliferation. *FXYD3*, a new regulator of Na-K-ATPase, has been found to be expressed in normal colon tissues (Geering, 2006). A study on a total of 150 resected colorectal cancer specimens measured the protein levels of *FXYD3* by IHC staining and demonstrated an association of downregulated expression of *FXYD3* proteins with cancer progression defined by Dukes' staging (Widegren et al., 2009). Recent publications have revealed that *LINC01133* is significantly reduced in colorectal cancer and is considered as a potential tumor suppressor in cancer progression and metastasis (Kong et al., 2016; Zhang et al., 2017). *CHGA* has been approved as a powerful biomarker for the early detection of various digestive system carcinomas, including gastric cancer (Yang and Chung, 2008), pancreatic neuroendocrine tumors (Weisbrod et al., 2013), and colorectal cancer (Zhang et al., 2019). The current research mechanism of *FRMD3* in COAD has not been reported to date, but it has been reported that non-small cell lung carcinoma (NSCLC) is

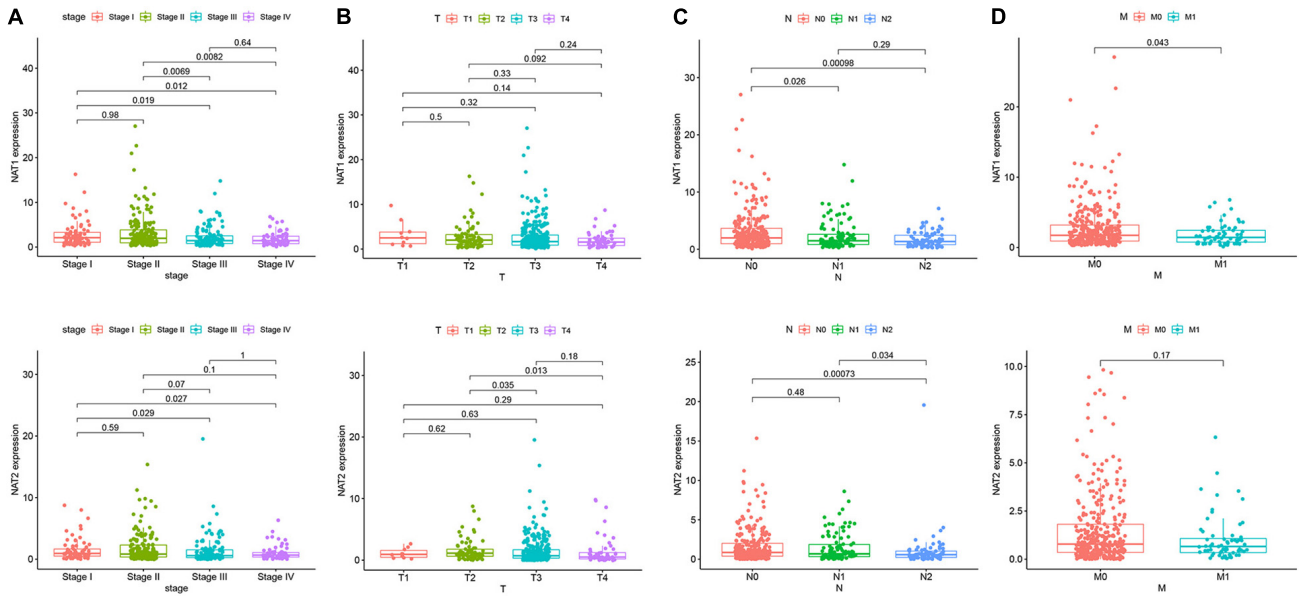

FIGURE 10 | *NAT1* and *NAT2* expression in subgroups of patients with COAD, stratified based on AJCC TNM stage. Wilcoxon rank sum tests were performed to compare the difference of NAT1 and NAT2 expression among different subgroups of clinicopathological variables. **(A)** Boxplot showing relative expression of *NAT1* and *NAT2* in COAD patients in stage 1, 2, 3, or 4. **(B)** Boxplot showing relative expression of *NAT1* and *NAT2* in COAD patients in T1, 2, 3, or 4. **(C)** Boxplot showing relative expression of *NAT1* and *NAT2* in COAD patients in N0, 1, or 2. **(D)** Boxplot showing relative expression of *NAT1* and *NAT2* in COAD patients in M0, or 1. The central mark is the median; the edges of the box are the 25th and 75th percentiles.

highly correlated with reduced *FRMD3* expression, which could induce apoptosis by regulating the activity of caspases in NSCLC. Therefore, further research is warranted to be carried out to characterize the role of *FRMD3* in COAD.

For the favorable prognostic genes, their genetic status was further analyzed by the cBioPortal tool. The results showed that deep deletion was the most common genetic alteration, which could result in gene expression downregulation in tumors, further indicating the credibility of our results. Various studies have suggested that these favorable prognostic genes might play important roles in tumor progression. A recent study showed that *MIER3* expression was significantly reduced in colorectal cancer at the mRNA and protein levels and was negatively correlated with aggressive tumors and poor clinical outcomes (Peng et al., 2017). Moreover, overexpression of *MIER3* could inhibit the aggressive behaviors of colorectal cancer *in vivo* and *in vitro* (Peng et al., 2017). In our study, the mRNA and protein levels of *MIER3* were significantly reduced in tumor tissues, and deep deletion was the most common type of *MIER3* mutation in COAD. However, no correlation was found between the gene expression of *MIER3* and the prognosis of COAD patients in our survival analysis. *TSPAN1*, a member of the transmembrane 4 superfamily, has been reported to be increased in various cancers at the mRNA level, including prostate cancer (Xu et al., 2000), gastric carcinoma (Chen et al., 2008), and COAD (Chen et al., 2009). A clinical study indicated that COAD patients with *TSPAN1* overexpression had a significantly shorter survival period than patients with weak expression, which was not consistent with our survival study (Chen et al., 2009). An *in vitro* study indicated that the downregulation of *TSPAN1* significantly inhibited the proliferation and invasion of colon cancer cells, suggesting that *TSPAN1* might be a valuable therapeutic target molecule in colon cancer (Chen et al., 2010). Thus, the molecular mechanisms governing *TSPAN1* in COAD still need to be further investigated. Zymogen granule protein 16 (*ZG16*) is primarily expressed in mucus-secreting cells, including goblet cells in the colon (Tateno et al., 2012). In a clinical study with a small sample size, *ZG16* expression was found to be sequentially downregulated from normal colon tissues and neoplastic precursor adenomatous polyps to COAD tissues (Meng et al., 2018). A recent study showed that the expression of *ZG16* was associated with distant metastasis and lymphatic invasion in colorectal cancer (Meng et al., 2020). In concordance with previous studies, our study found that the gene and protein expression levels of *ZG16* were significantly reduced in tumor tissues and correlated with poor prognosis, supporting the tumor suppressor role of *ZG16* in COAD progression. *PPARGC1A* is a transcriptional coactivator of the *PGC-1* gene family that modulates the process of energy metabolism and mitochondrial biogenesis (Seale, 2015). Based on the survival analysis in the GEPIA database, we found that patients with higher *PPARGC1A* expression had a better prognosis in COAD. However, the effect of *PPARGC1A* on the initiation and progression of colorectal cancer remains controversial. Accumulating studies have shown that *PPARGC1A* promoted tumor growth (Bhalla et al., 2011; Vellinga et al., 2015), whereas several studies have found that the lower expression of this gene in COAD is associated with an increased risk of cancer (Feilchenfeldt et al., 2004).

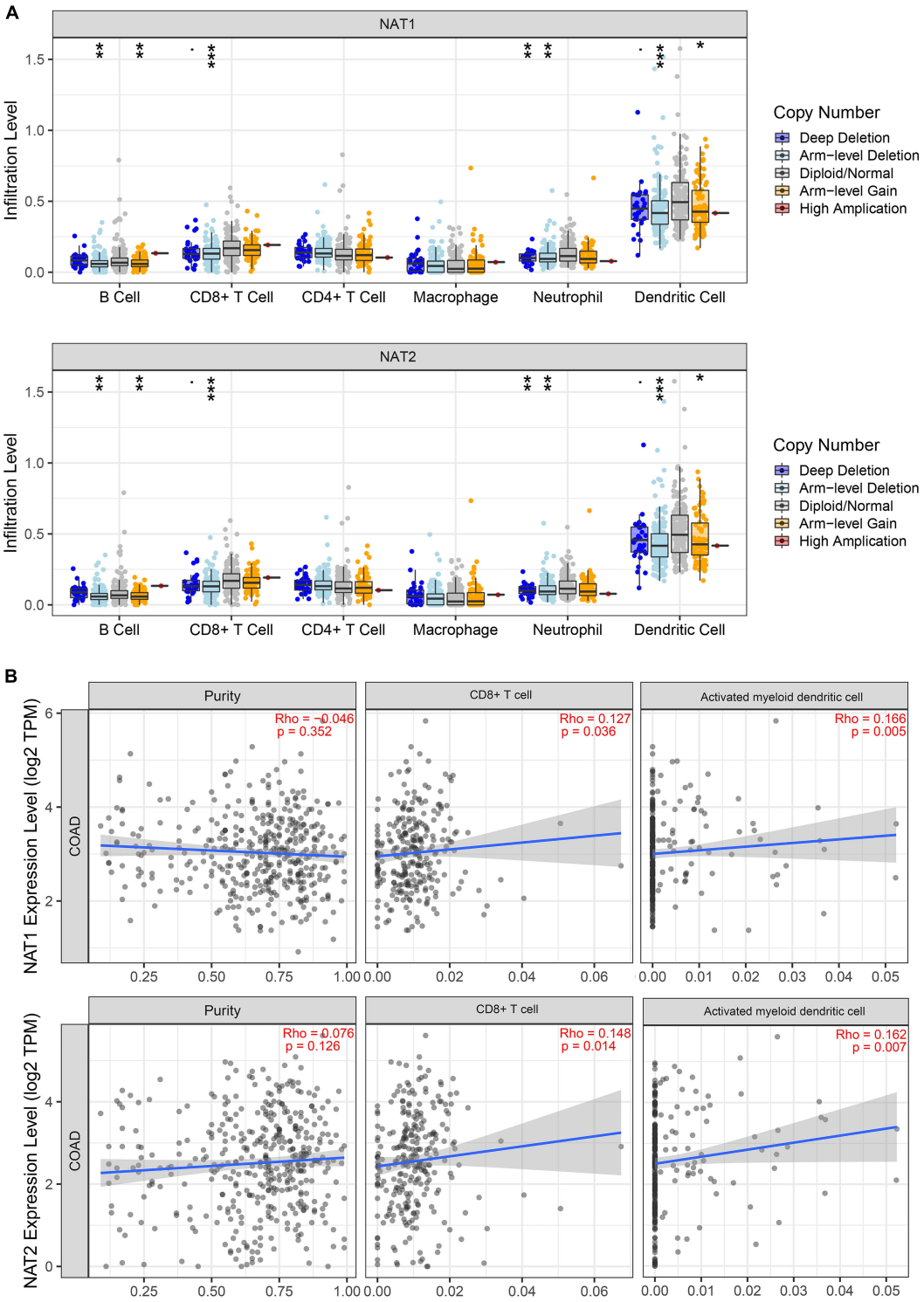

FIGURE 11 | TIMER analyses of *NAT1* and *NAT2*. **(A)** The associations of somatic copy number alterations (SCNAs) of *NAT1* and *NAT2* with immune infiltrates in COAD. The SCNAs in TIMER included deep deletions, arm-level deletions, diploid/normal alterations, arm-level gains and high amplifications. The SCNA categories of *NAT1* and *NAT2* were presented at the right bottom and the distributions of each immune cell subset at each mutation status were plotted by box plots. Two-sided Wilcoxon rank sum test with calculated *p*-value was utilized to compare the immune infiltration level in each category with that for normal samples. $^{*}P < 0.05$; $^{**}P < 0.01$; $^{***}P < 0.001$. **(B)** Correlation of *NAT1* and *NAT2* expression levels with tumor purity and infiltrating levels of CD8+ T cells and activated myeloid dendritic cells. The Spearman method was used to determine the correlation coefficient. *NAT1* and *NAT2* expression levels were plotted on the *y*-axis, while the abundance of immune infiltrating cells was plotted on the *x*-axis. Gene expression levels against tumor purity was displayed on the left-most panel.

In another study, genetic polymorphisms in *PPARGC1A* (*rs3774921*) increased the risk of colorectal cancer in individuals fed a highly inflammatory diet (Cho et al., 2017). *NR3C2* is a mineralocorticoid receptor gene encoding mineralocorticoid receptor (MR) that has been considered a tumor suppressor in colorectal cancer, which is consistent with our study (Tiberio et al., 2013). MR downregulation in colorectal cancer was correlated with increased expression of the *VEGF* receptor, indicating that *NR3C2* exerted specific role in decreasing angiogenesis in tumor (Tiberio et al., 2013). *HRCT1* and *SLC41A2* were not reported to be involved in the process of tumorigenesis. Further studies are needed to decipher the biological functions of *HRCT1* and *SLC41A2* in COAD.

NAT1 and *NAT2* are two members of the *N*-acetyltransferases (*NAT*) family that encode polymorphic enzymes catalyzing the metabolic activation of heterocyclic aromatic amines (HCAs), which have been considered established carcinogens in human colorectal cancer and urinary bladder cancer (Kadlubar et al., 1992; Cross and Sinha, 2004). GO enrichment analysis of the prognostic genes showed that these genes were closely related to *N*-acetyltransferase activity, which was consistent with the biological functions of *NAT1* and *NAT2*. Previous studies have shown that individuals with polymorphisms in *NAT1* or *NAT2* enzymes were susceptible to HCAs present in tobacco smoke and high-temperature cooked meat (Keku et al., 2003; Nöthlings et al., 2009). For example, *NAT1* and *NAT2* acetylator status might create predispositions to increased COAD risk with exposure to tobacco smoke and meat consumption (Lilla et al., 2006). Although most studies have focused on the role of *NAT1* and *NAT2* genetic polymorphisms in COAD risk, the potential role played by their aberrant expression in COAD has largely been ignored and whether *NAT1 and NAT2* expression influences cancer patient survival remains unknown. Liu et al. identified *NAT1* and *NAT2* as critical downregulated genes for CRC, but this study was limited by a small sample size (Liu et al., 2015). Consistent with the previous study, we found that the expressions of *NAT1* and *NAT2* was significantly reduced in tumor tissues at the mRNA and protein levels, possibly attributable to the highly frequent deep deletion of both genes in COAD, which was confirmed by cBioPortal analysis. Moreover, we used the online tool GEPIA to analyze the prognostic values of *NAT1 and NAT2* expression and found that lower levels of *NAT1 and NAT2* expression were correlated with poorer prognosis in COAD patients. These findings suggested that *NAT1 and NAT2* might play novel tumor suppressor roles in the development and metastasis of COAD and could be served as prognostic biomarkers in COAD.

Previous studies have shown that *NAT1* is expressed predominantly on T cells while *NAT2* is expressed in macrophages and natural killer cells, responsible for the adaptive and innate immune response (Salazar-González et al., 2014, 2018). The possible roles played by *NAT1* and *NAT2* in modulating the immune response in COAD have not been determined to date. Hence, we explored the relationship between *NAT1* and *NAT2* expression and the infiltration levels of immune cells and found that deletion of *NAT1* and *NAT2* was associated with substantially lower levels of immune cells, including B cells, CD8+ T cells, neutrophils, and dendritic cells. Moreover, positive relationships between *NAT1* and *NAT2* expression levels and infiltration levels of CD8+ T cells and dendritic cells were identified. It is well-known that neoantigens accumulating on tumor cells are initially recognized and presented by dendritic cells, subsequently promoting the production of CD8+ T cells, which are considered the main executors of cancer destruction, enhancing immune cell activities in the microenvironment, and thus preventing the development of cancer (Chen and Flies, 2013; Buoncervello et al., 2019). These results supported the notion that *NAT1* and *NAT2* downregulation might inhibit the antitumor immune response, enhancing tumor cell invasion and metastasis and thus decreasing the survival time of cancer patients. However, this hypothesis needs to be further validated.

Inevitably, there are several limitations in the present study. First, a major issue is that we did not collect patients diagnosed with COAD with adequate information in our own hospital to validate the predictive performance of the 13-gene based signature. A GEO cohort was used to confirm the robustness of this signature, which could make up for it slightly. Second, all of our samples and clinical data were based on the TCGA and GEO datasets, in which most patients were Western patients. Cohorts with larger sample sizes from other regions are warranted to extend our findings. Third, the prognostic risk model comprised too many genes, which might decrease the accuracy of the model and increase the expenses of laboratory testing, thereby limiting its clinical application. Moreover, although we performed a comprehensive bioinformatic analysis to build a prognostic risk model, the results of bioinformatic analysis can be biased to an extent when analyzing the data that have fewer non-tumor tissues than tumor tissues or addressing technical artifacts of WGCNA, which is similar to the limitations of other bioinformatic methods. Thus, large sample sizes of normal tissues will be important for reliable interpretation of data. In consideration of the credibility of the WGCNA results, TCGA data and IHC data from the HPA database were employed to confirm the gene and protein expression levels of the prognostic genes. However, due to the limitations of the HPA dataset, the IHC results of some prognostic genes in COAD patients were lacking. A series of experiments should be performed to clarify the underlying mechanism of the prognostic genes in the regulation of tumorigenesis in COAD.

In this study, we identified a 13-gene prognostic signature to predict the OS of COAD by using a series of bioinformatics analyses, which could accurately separate COAD patients with unfavorable prognoses from those with favorable prognoses. Moreover, the prognostic genes derived from the predictive signature have the potential to modulate the tumorigenesis and progression of COAD, especially *NAT1* and *NAT2*, which have been implicated in modulating antitumor immunity. Therefore, the results of the present study not only showed the value of the 13-gene signature as a promising classification tool for COAD prognosis but also provided new insights into the role of *NAT1* and *NAT2* in the tumorigenesis and progression of COAD.

DATA AVAILABILITY STATEMENT

Publicly available datasets were analyzed in this study. This data can be found here: TCGA repository (http://cancergenome.nih.gov/) and GEO (https://www.ncbi.nlm.nih.gov/geo/).

ETHICS STATEMENT

The studies involving human participants were reviewed and approved by China-Japan Friendship Hospital (No. 2018-116-K85-1). Written informed consent for participation was not required for this study in accordance with the national legislation and the institutional requirements.

AUTHOR CONTRIBUTIONS

CZ designed the study and performed the data analysis. ZZ and HL took part in analyzing the data. SY revised the manuscript. DZ designed the study and wrote the manuscript. All authors contributed to the article and approved the submitted version.

FUNDING

This study was supported by the National Key Development Plan for Precision Medicine Research (No. 2017YFC0910002).

SUPPLEMENTARY MATERIAL

The Supplementary Material for this article can be found online at: https://www.frontiersin.org/articles/10.3389/fgene.2021.657658/full#supplementary-material

REFERENCES

Arnold, M., Sierra, M. S., Laversanne, M., Soerjomataram, I., Jemal, A., and Bray, F. (2017). Global patterns and trends in colorectal cancer incidence and mortality. *Gut* 66, 683–691. doi: 10.1136/gutjnl-2015-310912

Bhalla, K., Hwang, B. J., Dewi, R. E., Ou, L., Twaddel, W., Fang, H. B., et al. (2011). PGC1α promotes tumor growth by inducing gene expression programs supporting lipogenesis. *Cancer Res.* 71, 6888–6898. doi: 10.1158/0008-5472.can-11-1011

Bray, F., Ferlay, J., Soerjomataram, I., Siegel, R. L., Torre, L. A., and Jemal, A. (2018). Global cancer statistics 2018: GLOBOCAN estimates of incidence and mortality worldwide for 36 cancers in 185 countries. *CA Cancer J. Clin.* 68, 394–424. doi: 10.3322/caac.21492

Buoncervello, M., Gabriele, L., and Toschi, E. (2019). The janus face of tumor microenvironment targeted by immunotherapy. *Int. J. Mol. Sci.* 20:4320. doi: 10.3390/ijms20174320

Cancer Genome Atlas Network (2012). Comprehensive molecular characterization of human colon and rectal cancer. *Nature* 487, 330–337. doi: 10.1038/nature11252

Chen, L., and Flies, D. B. (2013). Molecular mechanisms of T cell co-stimulation and co-inhibition. *Nat. Rev. Immunol.* 13, 227–242. doi: 10.1038/nri3405

Chen, L., Li, X., Wang, G. L., Wang, Y., Zhu, Y. Y., and Zhu, J. (2008). Clinicopathological significance of overexpression of TSPAN1, Ki67 and CD34 in gastric carcinoma. *Tumori* 94, 531–538. doi: 10.1177/030089160809400415

Chen, L., Yuan, D., Zhao, R., Li, H., and Zhu, J. (2010). Suppression of TSPAN1 by RNA interference inhibits proliferation and invasion of colon cancer cells in vitro. *Tumori* 96, 744–750. doi: 10.1177/030089161009600517

Chen, L., Zhu, Y. Y., Zhang, X. J., Wang, G. L., Li, X. Y., He, S., et al. (2009). TSPAN1 protein expression: a significant prognostic indicator for patients with colorectal adenocarcinoma. *World J. Gastroenterol.* 15, 2270–2276. doi: 10.3748/wjg.15.2270

Chibon, F. (2013). Cancer gene expression signatures - the rise and fall? *Eur. J. Cancer* 49, 2000–2009. doi: 10.1016/j.ejca.2013.02.021

Cho, Y. A., Lee, J., Oh, J. H., Chang, H. J., Sohn, D. K., Shin, A., et al. (2017). Genetic variation in PPARGC1A may affect the role of diet-associated inflammation in colorectal carcinogenesis. *Oncotarget* 8, 8550–8558. doi: 10.18632/oncotarget.14347

Cross, A. J., and Sinha, R. (2004). Meat-related mutagens/carcinogens in the etiology of colorectal cancer. *Environ. Mol. Mutagen.* 44, 44–55. doi: 10.1002/em.20030

Feilchenfeldt, J., Bründler, M. A., Soravia, C., Tötsch, M., and Meier, C. A. (2004). Peroxisome proliferator-activated receptors (PPARs) and associated transcription factors in colon cancer: reduced expression of PPARgamma-coactivator 1 (PGC-1). *Cancer Lett.* 203, 25–33. doi: 10.1016/j.canlet.2003.08.024

Gao, J., Aksoy, B. A., Dogrusoz, U., Dresdner, G., Gross, B., Sumer, S. O., et al. (2013). Integrative analysis of complex cancer genomics and clinical profiles using the cBioPortal. *Sci. Signal.* 6:l1.

Ge, W., Hu, H., Cai, W., Xu, J., Hu, W., Weng, X., et al. (2020). High-risk Stage III colon cancer patients identified by a novel five-gene mutational signature are characterized by upregulation of IL-23A and gut bacterial translocation of the tumor microenvironment. *Int. J. Cancer* 146, 2027–2035. doi: 10.1002/ijc.32775

Geering, K. (2006). FXYD proteins: new regulators of Na-K-ATPase. *Am. J. Physiol. Renal Physiol.* 290, F241–F250.

Guinney, J., Dienstmann, R., Wang, X., de Reyniès, A., Schlicker, A., Soneson, C., et al. (2015). The consensus molecular subtypes of colorectal cancer. *Nat. Med.* 21, 1350–1356.

Islami, F., Goding Sauer, A., Miller, K. D., Siegel, R. L., Fedewa, S. A., Jacobs, E. J., et al. (2018). Proportion and number of cancer cases and deaths attributable to potentially modifiable risk factors in the United States. *CA Cancer J. Clin.* 68, 31–54. doi: 10.3322/caac.21440

Kadlubar, F. F., Butler, M. A., Kaderlik, K. R., Chou, H. C., and Lang, N. P. (1992). Polymorphisms for aromatic amine metabolism in humans: relevance for human carcinogenesis. *Environ. Health Perspect* 98, 69–74. doi: 10.1289/ehp.929869

Keku, T. O., Millikan, R. C., Martin, C., Rahkra-Burris, T. K., and Sandler, R. S. (2003). Family history of colon cancer: what does it mean and how is it useful? *Am. J. Prev. Med.* 24, 170–176.

Kong, J., Sun, W., Li, C., Wan, L., Wang, S., Wu, Y., et al. (2016). Long non-coding RNA LINC01133 inhibits epithelial-mesenchymal transition and metastasis in colorectal cancer by interacting with SRSF6. *Cancer Lett.* 380, 476–484. doi: 10.1016/j.canlet.2016.07.015

Langfelder, P., and Horvath, S. (2008). WGCNA: an R package for weighted correlation network analysis. *BMC Bioinformatics* 9:559.

Li, T., Fan, J., Wang, B., Traugh, N., Chen, Q., Liu, J. S., et al. (2017). TIMER: a web server for comprehensive analysis of tumor-infiltrating immune cells. *Cancer Res.* 77, e108–e110.

Li, Y., He, M., Zhou, Y., Yang, C., Wei, S., Bian, X., et al. (2019). The prognostic and clinicopathological roles of PD-L1 expression in colorectal cancer: a systematic review and meta-analysis. *Front. Pharmacol.* 10:139.

Lilla, C., Verla-Tebit, E., Risch, A., Jäger, B., Hoffmeister, M., Brenner, H., et al. (2006). Effect of NAT1 and NAT2 genetic polymorphisms on colorectal cancer risk associated with exposure to tobacco smoke and meat consumption. *Cancer Epidemiol. Biomark. Prev.* 15, 99–107. doi: 10.1158/1055-9965.epi-05-0618

Liu, F., Ji, F., Ji, Y., Jiang, Y., Sun, X., Lu, Y., et al. (2015). In-depth analysis of the critical genes and pathways in colorectal cancer. *Int. J. Mol. Med.* 36, 923–930. doi: 10.3892/ijmm.2015.2298

Lv, J., and Li, L. (2019). Hub genes and key pathway identification in colorectal cancer based on bioinformatic analysis. *Biomed. Res. Int.* 2019:1545680.

Marisa, L., de Reyniès, A., Duval, A., Selves, J., Gaub, M. P., Vescovo, L., et al. (2013). Gene expression classification of colon cancer into molecular subtypes: characterization, validation, and prognostic value. *PLoS Med.* 10:e1001453. doi: 10.1371/journal.pmed.1001453

Meng, H., Ding, Y., Liu, E., Li, W., and Wang, L. (2020). ZG16 regulates PD-L1 expression and promotes local immunity in colon cancer. *Transl. Oncol.* 14:101003. doi: 10.1016/j.tranon.2020.101003

Meng, H., Li, W., Boardman, L. A., and Wang, L. (2018). Loss of ZG16 is associated with molecular and clinicopathological phenotypes of colorectal cancer. *BMC Cancer* 18:433.

Nguyen, L. H., Goel, A., and Chung, D. C. (2020). Pathways of colorectal carcinogenesis. *Gastroenterology* 158, 291–302. doi: 10.1053/j.gastro.2019.08.059

Nöthlings, U., Yamamoto, J. F., Wilkens, L. R., Murphy, S. P., Park, S. Y., Henderson, B. E., et al. (2009). Meat and heterocyclic amine intake, smoking, NAT1 and NAT2 polymorphisms, and colorectal cancer risk in the multiethnic cohort study. *Cancer Epidemiol. Biomark. Prev.* 18, 2098–2106. doi: 10.1158/1055-9965.epi-08-1218

Peng, M., Hu, Y., Song, W., Duan, S., Xu, Q., Ding, Y., et al. (2017). MIER3 suppresses colorectal cancer progression by down-regulating Sp1, inhibiting epithelial-mesenchymal transition. *Sci. Rep.* 7:11000.

Punt, C. J., Koopman, M., and Vermeulen, L. (2017). From tumour heterogeneity to advances in precision treatment of colorectal cancer. *Nat. Rev. Clin. Oncol.* 14, 235–246. doi: 10.1038/nrclinonc.2016.171

Röhrig, F., and Schulze, A. (2016). The multifaceted roles of fatty acid synthesis in cancer. *Nat. Rev. Cancer* 16, 732–749. doi: 10.1038/nrc.2016.89

Salazar-González, R. A., Turián-Espinoza, E., Hein, D. W., Niño-Moreno, P. C., Romano-Moreno, S., Milán-Segovia, R. C., et al. (2018). Arylamine N-acetyltransferase 1 in situ N-acetylation on CD3+ peripheral blood mononuclear cells correlate with NATb mRNA and NAT1 haplotype. *Arch. Toxicol.* 92, 661–668. doi: 10.1007/s00204-017-2082-y

Salazar-González, R., Gómez, R., Romano-Moreno, S., Medellín-Garibay, S., Núñez-Ruíz, A., Magaña-Aquino, M., et al. (2014). Expression of NAT2 in immune system cells and the relation of NAT2 gene polymorphisms in the anti-tuberculosis therapy in Mexican mestizo population. *Mol. Biol. Rep.* 41, 7833–7843. doi: 10.1007/s11033-014-3677-5

Seale, P. (2015). Transcriptional regulatory circuits controlling brown fat development and activation. *Diabetes Metab. Res. Rev.* 64, 2369–2375. doi: 10.2337/db15-0203

Siegel, R. L., Miller, K. D., and Jemal, A. (2017). Cancer statistics, 2017. *CA Cancer J. Clin.* 67, 7–30. doi: 10.3322/caac.21387

Smith, J. J., Deane, N. G., Wu, F., Merchant, N. B., Zhang, B., Jiang, A., et al. (2010). Experimentally derived metastasis gene expression profile predicts recurrence and death in patients with colon cancer. *Gastroenterology* 138, 958–968. doi: 10.1053/j.gastro.2009.11.005

Tang, Z., Li, C., Kang, B., Gao, G., Li, C., and Zhang, Z. (2017). GEPIA: a web server for cancer and normal gene expression profiling and interactive analyses. *Nucleic Acids Res.* 45, W98–W102.

Tateno, H., Yabe, R., Sato, T., Shibazaki, A., Shikanai, T., Gonoi, T., et al. (2012). Human ZG16p recognizes pathogenic fungi through non-self polyvalent mannose in the digestive system. *Glycobiology* 22, 210–220. doi: 10.1093/glycob/cwr130

Tiberio, L., Nascimbeni, R., Villanacci, V., Casella, C., Fra, A., Vezzoli, V., et al. (2013). The decrease of mineralcorticoid receptor drives angiogenic pathways in colorectal cancer. *PLoS One* 8:e59410. doi: 10.1371/journal.pone.0059410

Vellinga, T. T., Borovski, T., de Boer, V. C., Fatrai, S., van Schelven, S., Trumpi, K., et al. (2015). SIRT1/PGC1α-dependent increase in oxidative phosphorylation supports chemotherapy resistance of colon cancer. *Clin. Cancer Res.* 21, 2870–2879. doi: 10.1158/1078-0432.ccr-14-2290

Watanabe, T., Muro, K., Ajioka, Y., Hashiguchi, Y., Ito, Y., Saito, Y., et al. (2018). Japanese society for cancer of the colon and rectum (JSCCR) guidelines 2016 for the treatment of colorectal cancer. *Int. J. Clin. Oncol.* 23, 1–34.

Weisbrod, A. B., Zhang, L., Jain, M., Barak, S., Quezado, M. M., and Kebebew, E. (2013). Altered PTEN, ATRX, CHGA, CHGB, and TP53 expression are associated with aggressive VHL-associated pancreatic neuroendocrine tumors. *Horm Cancer* 4, 165–175. doi: 10.1007/s12672-013-0134-1

Weiser, M. R., Gönen, M., Chou, J. F., Kattan, M. W., and Schrag, D. (2011). Predicting survival after curative colectomy for cancer: individualizing colon cancer staging. *J. Clin. Oncol.* 29, 4796–4802. doi: 10.1200/jco.2011.36.5080

Widegren, E., Onnesjö, S., Arbman, G., Kayed, H., Zentgraf, H., Kleeff, J., et al. (2009). Expression of FXYD3 protein in relation to biological and clinicopathological variables in colorectal cancers. *Chemotherapy* 55, 407–413. doi: 10.1159/000263227

Xie, H., and Xie, C. (2019). A six-gene signature predicts survival of adenocarcinoma type of non-small-cell lung cancer patients: a comprehensive study based on integrated analysis and weighted gene coexpression network. *Biomed. Res. Int.* 2019:4250613.

Xu, J., Stolk, J. A., Zhang, X., Silva, S. J., Houghton, R. L., Matsumura, M., et al. (2000). Identification of differentially expressed genes in human prostate cancer using subtraction and microarray. *Cancer Res.* 60, 1677–1682.

Yang, S., and Chung, H. C. (2008). Novel biomarker candidates for gastric cancer. *Oncol. Rep.* 19, 675–680.

Yuan, Y., Chen, J., Wang, J., Xu, M., Zhang, Y., Sun, P., et al. (2020a). Development and clinical validation of a Novel 4-gene prognostic signature predicting survival in colorectal cancer. *Front. Oncol.* 10:595.

Yuan, Y., Chen, J., Wang, J., Xu, M., Zhang, Y., Sun, P., et al. (2020b). Identification hub genes in colorectal cancer by integrating weighted gene co-expression network analysis and clinical validation in vivo and vitro. *Front. Oncol.* 10:638.

Zhang, J. H., Li, A. Y., and Wei, N. (2017). Downregulation of long non-coding RNA LINC01133 is predictive of poor prognosis in colorectal cancer patients. *Eur. Rev. Med. Pharmacol. Sci.* 21, 2103–2107.

Zhang, X., Zhang, H., Shen, B., and Sun, X. F. (2019). Chromogranin-a expression as a novel biomarker for early diagnosis of colon cancer patients. *Int. J. Mol. Sci.* 20:2919. doi: 10.3390/ijms20122919

Zuo, S., Dai, G., and Ren, X. (2019). Identification of a 6-gene signature predicting prognosis for colorectal cancer. *Cancer Cell Int.* 19:6.

Conflict of Interest: The authors declare that the research was conducted in the absence of any commercial or financial relationships that could be construed as a potential conflict of interest.

frontiers in Genetics

ORIGINAL RESEARCH
published: 25 February 2022
doi: 10.3389/fgene.2022.648134

TIMP1 Indicates Poor Prognosis of Renal Cell Carcinoma and Accelerates Tumorigenesis *via* EMT Signaling Pathway

Yi Shou[1,2†], Yuenan Liu[1,2†], Jiaju Xu[1,2], Jingchong Liu[1,2], Tianbo Xu[1,2], Junwei Tong[1,2], Lilong Liu[1,2], Yaxin Hou[1,2], Di Liu[1,2], Hongmei Yang[1,2], Gong Cheng[1,2] and Xiaoping Zhang[1,2*]*

[1]Department of Urology, Union Hospital, Tongji Medical College, Huazhong University of Science and Technology, Wuhan, China, [2]Institute of Urologic Surgery, Tongji Medical College, Huazhong University of Science and Technology, Wuhan, China, [3]Department of Pathogenic Biology, School of Basic Medicine, Huazhong University of Science and Technology, Wuhan, China

OPEN ACCESS

Edited by:
Lorenzo Gerratana,
University of Udine, Italy

Reviewed by:
Reza Ghasemi,
Washington University School of Medicine in St. Louis, United States
Iman Mamdouh Talaat,
University of Sharjah, United Arab Emirates
Guohua Zeng,
First Affiliated Hospital of Guangzhou Medical University, China

***Correspondence:**
Gong Cheng
cg0178@qq.com
Xiaoping Zhang
xzhang@hust.edu.cn

[†]These authors have contributed equally to this work

Specialty section:
This article was submitted to Cancer Genetics, a section of the journal Frontiers in Genetics

Received: 31 December 2020
Accepted: 11 February 2022
Published: 25 February 2022

Citation:
Shou Y, Liu Y, Xu J, Liu J, Xu T, Tong J, Liu L, Hou Y, Liu D, Yang H, Cheng G and Zhang X (2022) TIMP1 Indicates Poor Prognosis of Renal Cell Carcinoma and Accelerates Tumorigenesis via EMT Signaling Pathway. Front. Genet. 13:648134. doi: 10.3389/fgene.2022.648134

Renal cell carcinoma (RCC) is one of the most common malignancies in the urinary system. The mortality of advanced RCC remains high despite advances in systemic therapy of RCC. Considering the misdiagnosis of early-stage RCC, the identification of effective biomarkers is of great importance. Tissue inhibitor matrix metalloproteinase 1 (TIMP1), which belongs to TIMP gene family, is a natural inhibitor of the matrix metalloproteinases (MMPs). In this study, we found TIMP1 was significantly up-regulated in cell lines and RCC tissues. Kaplan-Meier analysis revealed that high expression of TIMP1 indicated a poor prognosis. Multivariate analysis further indicated that TIMP1 overexpression was an independent prognostic factor of RCC patients. Furthermore, knockdown of TIMP1 *in vitro* suppressed the proliferation, migration, and invasion of RCC cells, while upregulating TIMP1 accelerated the proliferation, migration, and invasion of RCC cells. In addition, we also found that TIMP1 prompted the progression of RCC via epithelial-to-mesenchymal transition (EMT) signaling pathway. In conclusion, the present results suggested that TIMP1 indicated poor prognosis of renal cell carcinoma and could serve as a potential diagnostic and prognostic biomarker for RCC.

Keywords: TIMP1, renal cell carcinoma (RCC), tumorigenesis, biomarker, EMT-epithelial to mesenchymal transition

1 INTRODUCTION

Renal cell carcinoma (RCC) is one of the cancer types that originated from the renal epithelium, which accounts for most cancer-related deaths (Hsieh et al., 2017). The main histological subtypes of RCCs are clear cell (cc) RCC (~70% of RCCs), papillary (p) RCC (10%–15% of RCCs), and chromophobe (ch) RCC (~5% of RCCs) (Morris and Latif, 2017). Cancer-specific survival rates at 5 years for the above three types of RCC are 68.9%, 87.4%, and 86.7%, respectively (Cheville et al., 2003; Cinque et al., 2021). The five-year survival rate of early-stage RCC reaches 71%–88%. Still, the survival rate at 5 years of RCC plummets to only 12% when metastasis occurs according to the latest study (Leibovich et al., 2010; Cinque et al., 2021). Therefore, it is necessary to identify practical biomarkers for the early diagnosis of RCC.

Tissue inhibitor matrix metalloproteinase (TIMP) family comprises four paralogous genes (TIMP1, TIMP2, TIMP3, TIMP4) (Brew and Nagase, 2010). TIMPs participate in more

TABLE 1 | Clinical characteristics of 59 patients with renal cell carcinoma.

Characteristic	Data
Age, mean ± SEM (years)	52.3 ± 13.8
Gender, male/female	31/28
Tumor size, mean ± SEM (cm)	5.5 ± 3.1
Location, right/left	27/32
T stage, n (%)	
T1a	13 (22.03)
T1b	28 (47.46)
T2a	8 (13.56)
T2b	5 (8.47)
T3	2 (3.39)
T4	2 (3.39)
Unknown	1 (1.69)
N stage, n (%)	
N0	54 (91.53)
N1	5 (8.47)
M stage, n (%)	
M0	56 (94.92)
M1	3 (5.08)
Fuhrman grade, n (%)	
1	14 (23.73)
2	27 (45.76)
3	9 (15.25)
4	4 (6.78)
Unknown	5 (8.47)

protease-independent biological functions including anti-apoptosis, anti-angiogenesis, cell cycle regulation, and differentiation activities in epithelial or blood-derived cells (Seo et al., 2003; Cruz-Munoz et al., 2006; Jung et al., 2006; Taube et al., 2006; Grunwald et al., 2019). TIMP1 is a major member of the TIMP family with a molecular weight of 23 KDa, which consists of a two-domain structure possessing metalloproteinase-inhibitory and cytokine-like signaling activities (Grunwald et al., 2019). Previous studies showed that high expression of TIMP1 in tissue or blood suggested poor outcomes in various cancers (Holten-Andersen et al., 1999; Wang et al., 2013; Jackson et al., 2017). Song revealed that TIMP1 promoted tumor progression and suppressed apoptosis via FAK-PI3K/AKT and MAPK pathway in colon cancer (Song et al., 2016). Gong found that higher levels of TIMP1 expression were associated with poor prognosis in triple-negative breast cancer (Cheng et al., 2016). Hemmerlein investigated the expression of matrix metalloproteinases and their inhibitors in medulloblastomas and their prognostic relevance (Ozen et al., 2004). In the field of RCC, Kugler's study showed that the balance of MMP-2 and MMP-9 to TIMP-1 and TIMP-2 expression was an essential factor in the aggressiveness of RCC (Kugler et al., 1998). Kallakury pointed out that increased expression of TIMP1 correlated with poor prognostic variables in RCC (Kallakury et al., 2001). Hence, we aimed to explore the relationship between the expression of TIMP1 and clinicopathological factors in renal cancer. Furthermore, we investigated the functional roles of TIMP1 and the underlying biological signal pathway in renal cancer cells.

2 MATERIALS AND METHODS

2.1 RCC Tissue Samples

A total of 59 pairs of tumor and adjacent normal tissues were obtained from the Department of Urology, Union Hospital, Tongji Medical College (Wuhan, China) between January 2018 and January 2019. The normal kidney tissues were obtained from 2 cm away from the edge of lesions. The clinical information of these samples was presented in **Table 1**. The samples were divided into two groups. The first group was immediately stored in liquid nitrogen for RNA and protein extraction. The second group was fixed in formalin and embedded in paraffin, then used for immunohistochemistry assays. Among these samples, we randomly selected 8 pairs of tissues for protein detection, 20 pairs of samples for quantitative real-time PCR and 3 pairs of samples for immunohistochemistry. No patients received anticancer therapy before surgery. All patients gave written informed consent before inclusion in this study, and the study was approved by the Human Research Ethics Committee of Huazhong University of Science and Technology. The study complies with the guidelines of the Declaration of Helsinki.

2.2 Cell Culture

The human renal proximal tubular epithelial cell line HK-2, and 5 kinds of human renal cell carcinoma cell lines: 786-O, ACHN, A498, CAKI-1, and OSRC-2, were used in this study and were obtained from the American Type Culture Collection. These cell lines were used for RT-qPCR and western blotting. The cells were grown in Dulbecco's modified Eagles medium containing high glucose (4.5 g/L), fetal bovine serum (10%), and penicillin/streptomycin solution (1%). All cells were cultured under standard conditions: at 37°C in a 5% CO_2 atmosphere.

2.3 Immunohistochemical Staining Assays

The paired RCC tissues and adjacent normal tissues were first fixed in 4% formalin at room temperature for 12 h, dehydrated, and embedded in paraffin. Then the tissue sections were incubated with rabbit TIMP1 monoclonal antibody (Abcam, ab109125, 1:1,000) overnight at 4°C. Tissue sections were washed three times with phosphate-buffered saline and incubated with secondary antibodies that were conjugated to horseradish peroxidase at room temperature for 2 h. The sections were scanned by a NanoZoomer S360 (Hamamastu Corporation) and observed with NDP.view2 software (Hamamastu Corporation). Random fields were selected to interpret the expression of TIMP1 in tissue sections under 100x and 400x magnification.

2.4 RNA Extraction and RT-qPCR

Total RNA was isolated from tissues or cells using TRIzol® reagent (Thermo Fisher Scientific, Inc.). The concentration and purity of the RNA solution were detected using a NanoDrop 2000 spectrophotometer (NanoDrop Technologies; Thermo Fisher Scientific, Inc.). Total RNA was then reverse transcribed into cDNA using a Superscript II reverse

transcription kit (Takara Bio, Inc.) according to the manufacturer's protocols. All the experiments were repeated thrice for all the samples. The primers used to amplify TIMP1 and GAPDH were synthesized by TSINGKE Inc. The sequences of forward and reverse primers were as follows: TIMP1-forward: 5′-CGC AGC GAG GAG GTT TCT CAT-3'; TIMP1-reverse: 5′-GGC AGT GAT GTG CAA ATT TCC-3'. GAPDH-forward: 5′-CGT GGA AGG ACT CAT GAC CA-3'; GAPDH -reverse: 5′-GCC ATC ACG CCA CAG TTT C-3'.

2.5 Western Blot Assays

Total protein was extracted from RCC tissues and corresponding adjacent normal tissues of 12 patients using RIPA lysis buffer (Servicbio.Inc.) with protease inhibitor phenyl methane sulfonyl fluoride (PMSF, 1%), and then the concentration was measured with BCA protein assay kit (Beyotime Biotechnology, Jiangsu, China). Primary rabbit polyclonal antibody against primary antibodies (TIMP1 1:1,000, Abcam,Inc., ab109125; N-cadherin 1:5000, Abcam.Inc., ab76011; E-cadherin 1:10000, Abcam,Inc., ab40772) and β-actin (1:10000; Abclonal,Inc., cat.AC026) were incubated overnight at 4°C. All the procedures were performed according to the manufacturer's instructions.

2.6 Small Interfering RNA and Plasmids Construction, Transfections

Small interfering RNA (siRNA) oligonucleotide sequences specifically targeting TIMP1 (si-TIMP1) and negative control (si-NC) siRNA (cat. no. siBDM 1999A) were obtained from Guangzhou RiboBio Co., Ltd. The plasmids harboring TIMP1 (ov-TIMP1) and negative control (ov-NC) were constructed and supplied by Vigene Biology (Vigene, China). Cells were collected for subsequent experiments 48 h post transfection. The si-TIMP1 sequence was as follows: 5′-GCC AAT GTG ATG GTG GAC A-3'. The information about the plasmid that has been used for over expression of TIMP1 was provided in **Supplementary Figure S1**.

2.7 Cell Proliferation Assay

One thousand transfected cells were added to each hole in the 96-well plates. Cell proliferation was assessed by the CCK-8 assay (CCK8; Dojindo Molceular Technologies, Inc.) at 24, 48, 72, and 96 h following treatments, according to the manufacturer's instructions. Ten μl of CCK8 was added to each hole and incubated with cells for 2 h. Then the optical density values were measured by a spectrophotometer at 450 nm to estimate the number of living cells.

2.8 Cell Migration and Invasion Assays

We planted 1×10^4 cells into the upper chambers in serum-free medium for migration and 2×10^4 cells for invasion. Sixty μl Matrigel (Thermo Fisher Scientific; Waltham, USA) had been added into the upper chambers for invasion assays. The lower chambers were filled with 600 μl DMEM added with 10% FBS. After 24 h of incubation, the cells were fixed in 100% methanol, then stained with 0.05% crystal violet. Finally, the results were observed under a light microscope at 100x magnification, and the cells passed through the membrane were counted in 3 randomly chosen fields.

2.9 Bioinformatics Analysis

TIMP1, TIMP2, TIMP3, and TIMP4 mRNA expression and clinical information of The Cancer Genome Atlas (TCGA) clear cell renal cell carcinoma dataset (TCGA_KIRC) were downloaded from the Xena Functional Genomics Explorer of University of California Santa Cruz (https://xenabrowser.net/). Beroukhim renal, Jones renal, and Yusenko renal datasets (Jones et al., 2005; Beroukhim et al., 2009; Yusenko et al., 2009) were obtained from the Oncomine database (https://www.oncomine.org). The gene set enrichment analysis (GSEA) platform with the Kyoto Encylopedia of Genes and Genomes and Gene Ontology databases (c2.all.v6.2.symbols.gmt) was employed to find pathways enriched in the gene set, based on the pathway Enrichment Score (ES). STRING (Version11.0) was used to explore the protein-protein reaction and biological function of TIMP1(https://string-db.org/).

2.10 Statistical Analysis

All statistical analyses were processed by GraphPad Prism 7.0 (GraphPad Software, Inc., USA) and SPSS Statistics 22.0 software (IBM SPSS, Chicago, IL, United States). Data of paired cases were analyzed using a paired student t-test, while analysis of unpaired cases was performed using a one-way analysis of variance (ANOVA) or t-test. Pearson's χ2 test was applied to analyze the relationship between TIMP1 and TIMP3 expression and clinical parameters. The Kaplan-Meier analysis was used to estimate the correlation between TIMP1 and TIMP3 mRNA expression with overall survival (OS) and disease-free survival (DFS) times with the log-rank test. The TIMP1 mRNA levels downloaded from the TCGA_KIRC dataset were first divided into two groups according to different clinical parameters and then applied to draw receiver operating characteristic (ROC) curves and analyze the area under the curve (AUC) with GraphPad Prism 7.0. The diagnostic value of TIMP1 mRNA expression in RCC was evaluated by ROC curves and AUC. Finally, univariate and multivariate Cox proportional hazard regressions were applied to determine the prognostic significance of TIMP1 and TIMP3. All experiments were repeated thrice independently and all data were represented as mean ± SEM. A confidence threshold, $p < 0.05$, was considered to be statistically significant. *$p < 0.05$; **$p < 0.01$; ***$p < 0.001$; ****$p < 0.0001$.

3 RESULTS

3.1 TIMP1 Was Upregulated in RCC

To determine whether TIMP expression was related to the occurrence and progress of RCC, we downloaded the mRNA of 4 members in this family (TIMP1, TIMP2, TIMP3, and TIMP4) from TCGA_KIRC and drew a heatmap of them according to their mRNA expression. The result showed that TIMP1 was upregulated in RCC tissues (**Figure 1**). It was further verified that TIMP1 was found in higher expression levels in paired comparison (**Figure 2A**). To confirm these results, we compared the mRNA expression of TIMP1 in Oncomine datasets (Beroukhim, Jones, and Yusenko) and it was shown that TIMP1 was highly expressed in renal cancer samples (**Figure 2B**). All

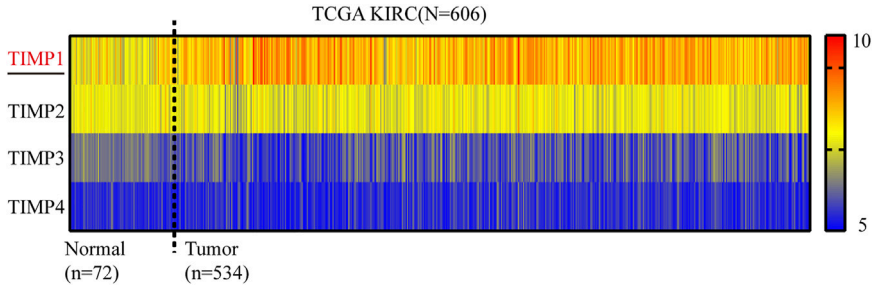

FIGURE 1 | Heatmap of mRNA expression levels of TIMP family obtained from TCGA_KIRC. Red represented high expression and blue represented low expression. TIMP, Tissue inhibitor matrix metalloproteinase; KIRC, kidney renal clear cell carcinoma; TCGA, The Cancer Genome Atlas.

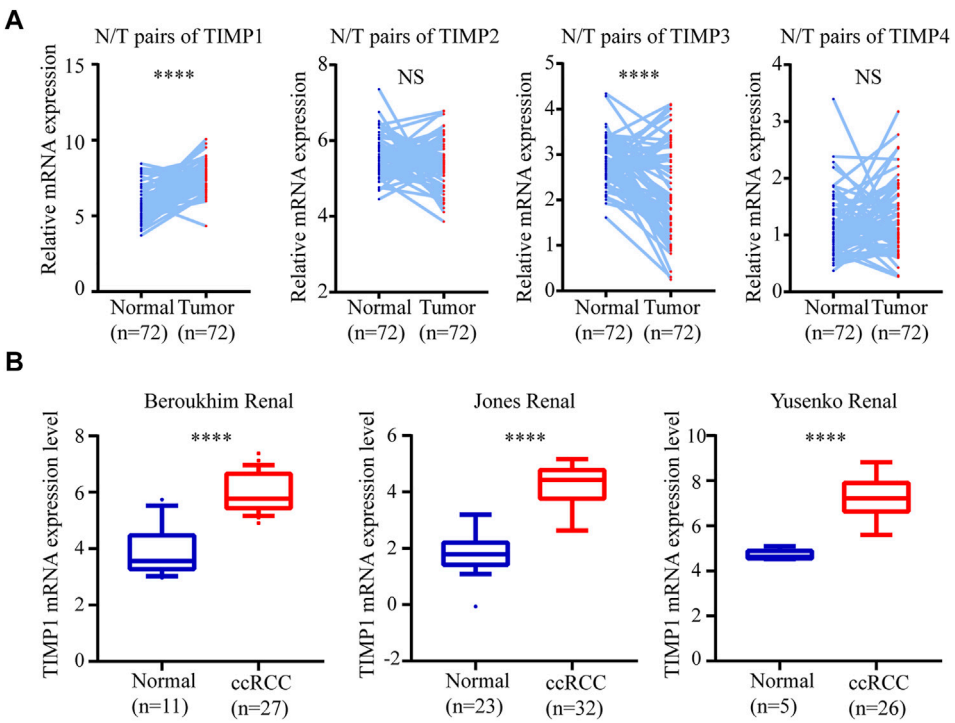

FIGURE 2 | TIMP1 was upregulated in RCC. The mRNA expression level and clinical parameters were downloaded from TCGA_KIRC. **(A)** mRNA levels of TIMP family proteins in RCC tissues and paired normal tissues. **(B)** TIMP1 was upregulated in three renal statistics downloaded from the Oncomine database, including Beroukhim, Jones, and Yusenko renal statistics. TIMP, Tissue inhibitor matrix metalloproteinase; TIMP1, Tissue inhibitor matrix metalloproteinase 1; RCC, clear cell renal cell carcinoma, TCGA, The Cancer Genome Atlas; KIRC, kidney renal clear cell carcinoma.

these results indicated that TIMP1 might play an important role in RCC progression, which raised our interest to further study.

3.2 High Level of TIMP1 Indicated a Poor Clinical Outcome in Subgroups of Patients With Different Clinical Parameters

Kaplan-Meier survival analysis and log-rank test were applied to determine the OS and DFS in patients with RCC. The result showed that patients with higher levels of TIMP1 had a poorer outcome (**Figure 3A**). Further Kaplan-Meier survival analysis for subgroups of patients with different clinical parameters demonstrated that TIMP1 was an ideal prognostic biomarker for patients with the following characteristics: T1+T2 stage (**Figure 3B**), N0 (**Figure 3C**), M0 (**Figure 3D**), G1+G2 stage (**Figure 3E**), age<60 (**Figure 3F**), age≥60 (**Figure 3G**), male (**Figure 3H**) and female (**Figure 3I**). The DFS survival analysis revealed that patients with higher TIMP1 had a shorter disease-free time (**Figure 4A**), and TIMP1 could act as a biomarker for patients with the following characteristics: T1+T2 (**Figure 4B**), N0 (**Figure 4C**), age≥60 (**Figure 4D**), and female (**Figure 4E**). Furthermore, we applied univariate and multivariate regression models to assess the integrated prognostic value of TIMP1. The results suggested that TIMP1 independently

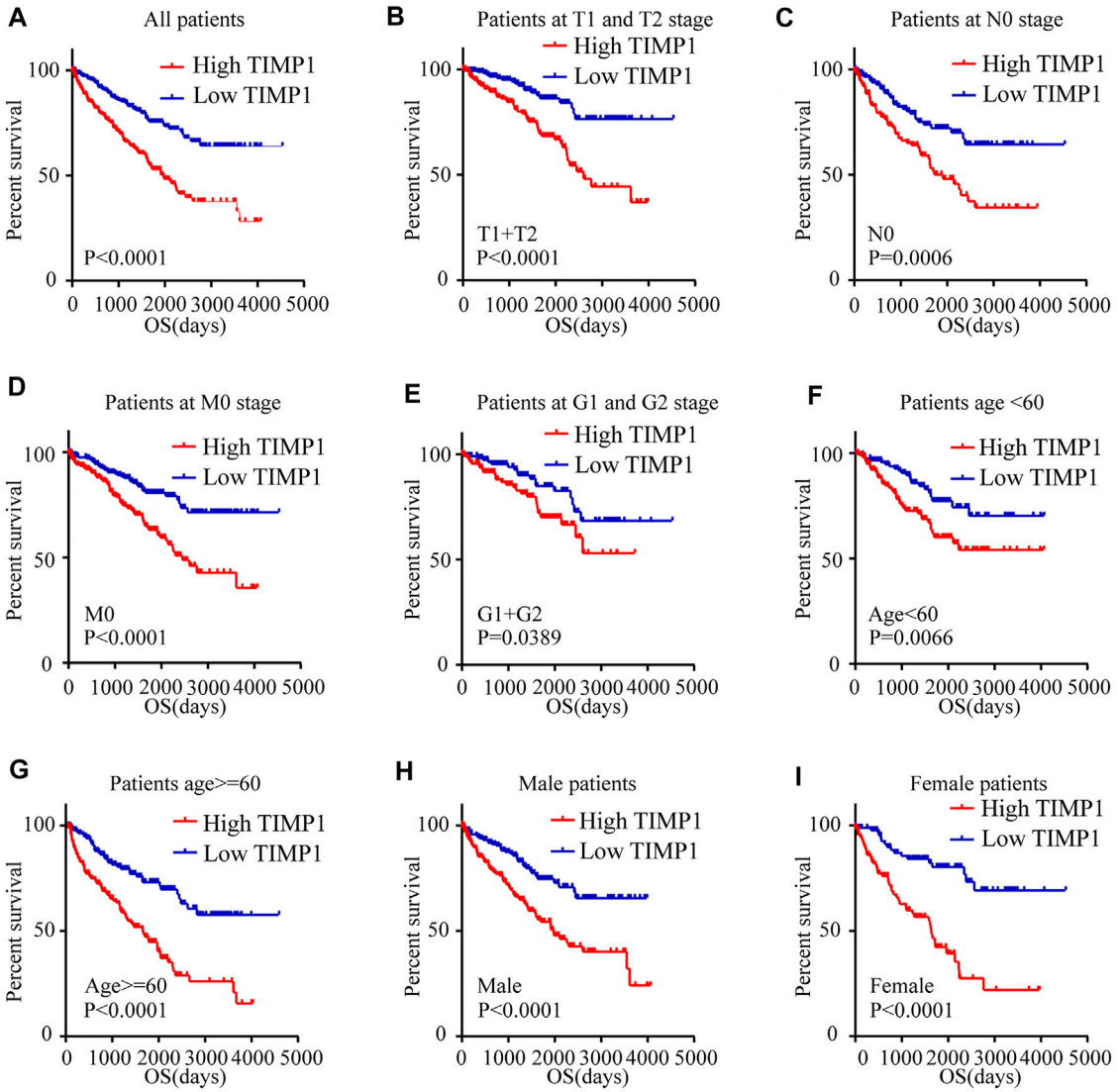

FIGURE 3 | High level of TIMP1 indicated poor OS of patients with RCC. Kaplan-Meier curves for overall survival (OS) were performed in patients with RCC based on the TCGA database. **(A)** OS was closely associated with TIMP1 levels. OS subanalysis was applied in patients with different clinical parameters. **(B)** Patients at T1 and T2 stage, **(C)** Patients at N0 stage, **(D)** Patients at M0 stage, **(E)** Patients at G1 and G2 stage, **(F)** Patient with age<60, **(G)** Patients with age≥60, **(H)** Male patients, **(I)** Female patients. TIMP1, Tissue inhibitor matrix metalloproteinase 1; RCC, renal cell carcinoma; TCGA, The Cancer Genome Atlas.

correlated with the OS and DFS status of RCC patients (**Tables 2**, **3**). In conclusion, the above results demonstrated that the high level of TIMP1 indicated a poor clinical outcome and TIMP1 could serve as an ideal prognostic biomarker for RCC.

3.3 TIMP1 Expression Level Was Associated With Different Clinicopathological Parameters

To clarify the expression pattern of TIMP1 in patients with different clinical parameters, the present study analyzed the TIMP1 expression levels of 522 cases from the TCGA database. The results confirmed that the high expression level of TIMP1 is associated with patients' gender, higher T stage, N stage, M stage, TNM stage, and histological grade (**Figures 5A–F**). Besides, patients with worse OS status and DFS status had a higher level of TIMP1 expression (**Figures 5G,H**). However, there were no obvious differences between patients aged ≥60 years and those aged <60 years (**Table 4**). These results demonstrated that TIMP1 was upregulated and closely related to gender, T stage, N stage, M stage, TNM stage, and histological grade in RCC.

3.4 The mRNA Expression Level of TIMP1 can Serve as a Biomarker for Clinical RCC Diagnosis

To access the value of TIMP1 mRNA expression level in the diagnosis of RCC, receiver operating characteristic (ROC)

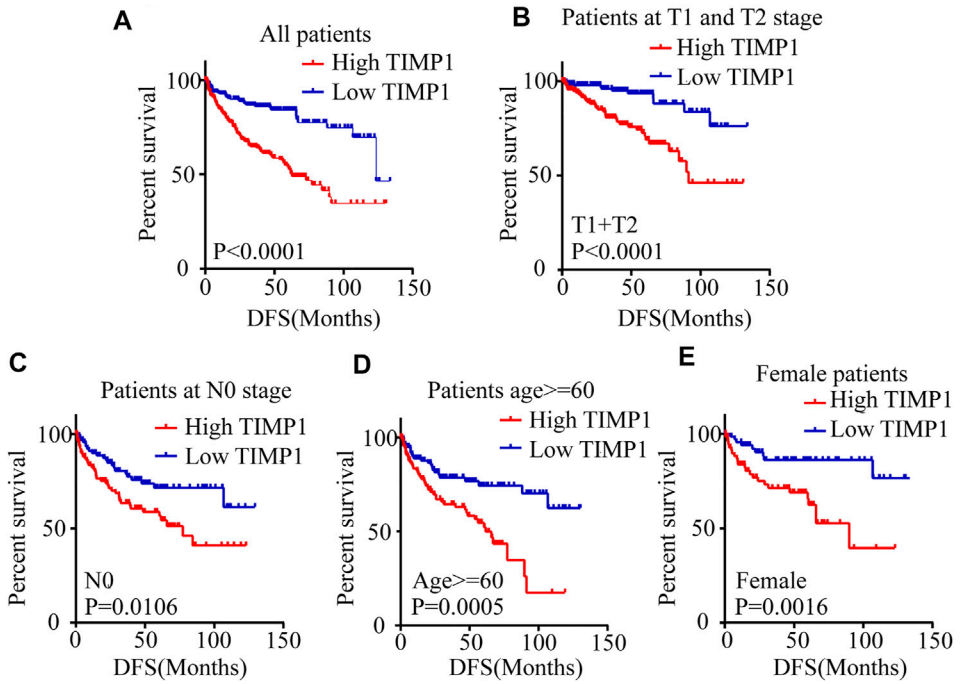

FIGURE 4 | High level of TIMP1 suggested poor DFS of patients with RCC. Kaplan-Meier curves for disease-free survival (DFS) were performed in patients with RCC. **(A)** High level of TIMP1 indicated poor DFS. Kaplan-Meier curves for DFS as determined by different clinical parameters in RCC. **(B)** Patients at T1 and T2 stage, **(C)** Patients at N0 stage, **(D)** Patients with age≥60, **(E)** Female patients. TIMP1, Tissue inhibitor matrix metalloproteinase 1; RCC, renal cell carcinoma; TCGA, The Cancer Genome Atlas.

TABLE 2 | Univariate and multivariate analyses of TIMP1 mRNA level and patient overall survival.

Variable	Univariate analysis			Multivariate analysis[a]		
	HR	95% CI	*p*-value	HR[b]	95% CI[c]	*p*-value
Overall survival (n = 522)						
TIMP1	2.375	1.724–3.271	<0.001	1.528	1.080–2.161	0.017
Age (years)	1.786	1.312–2.450	<0.001	1.600	1.159–2.209	0.004
Gender	0.933	0.683–1.275	0.663			
T stage	3.209	2.361–4.364	<0.001	1.572	1.089–2.270	0.016
N stage	3.944	2.135–7.285	<0.001	1.998	1.060–4.136	0.032
M stage	4.351	3.180–5.951	<0.001	2.521	1.766–3.599	<0.001
G grade	2.715	1.925–3.827	<0.001	1.477	1.009–2.162	0.045

[a]*Multivariate models were adjusted for TIMP1, T, N, M, G classification, and age.*
[b]*Hazard ratio, estimated from Cox proportional hazard regression model.*
[c]*Confidence interval of the estimated HR.*

curves were applied for patients with different clinicopathological variables. Area under curve (AUC) was used to evaluate the diagnostic efficiency. The results indicated that TIMP1 could adequately distinguish RCC patients with an AUC of 0.8858 ($p < 0.0001$; **Figure 6A**). Additionally, the TIMP1 expression level also exhibited diagnostic value for subgroups of patients with RCC as follows: T1+T2 vs. T3+T4 (AUC = 0.6414, $p < 0.0001$; **Figure 6B**), G1+G2 vs. G3+G4 (AUC = 0.6307, $p < 0.0001$; **Figure 6C**), M0 vs. M1 stage (AUC = 0.6375, $p = 0.0001$; **Figure 6D**), TNM I + II vs TNM III + IV stage (AUC = 0.6546, $p < 0.0001$; **Figure 6E**), OS good vs. OS poor (AUC = 0.6617, $p < 0.0001$; **Figure 6F**), DFS good vs DFS poor (AUC = 0.7056, $p < 0.0001$; **Figure 6G**) and male vs. female (AUC = 0.5875, $p = 0.001$; **Figure 6H**). Therefore, TIMP1 might act as a potential biomarker for RCC diagnosis.

3.5 TIMP1 Was Upregulated in RCC Cell Lines and Tissues

To further confirm the results from bioinformatics analysis, we performed a quantitative real-time polymerase chain reaction

TABLE 3 | Univariate and multivariate analyses of TIMP1 mRNA level and patient disease-free survival.

Variable	Univariate analysis			Multivariate analysis[a]		
	HR	95% CI	*p*-value	HR[b]	95% CI[c]	*p*-value
DFS (n = 428)						
TIMP1	2.999	2.024–4.442	<0.001	2.104	1.364–3.245	0.001
Age (years)	1.364	0.956–1.946	0.086			
Gender	1.421	0.957–2.112	0.082			
T stage	4.571	3.164–6.603	<0.001	1.954	1.275–2.996	0.002
N stage	6.024	3.024–11.997	<0.001	2.833	1.390–5.774	0.004
M stage	8.522	5.870–12.372	<0.001	4.999	3.317–7.681	<0.001
G grade	3.426	2.269–5.172	<0.001	2.124	1.363–3.309	0.001

[a]*Multivariate models were adjusted for TIMP1, T, N, M, G classification.*
[b]*Hazard ratio, estimated from Cox proportional hazard regression model.*
[c]*Confidence interval of the estimated HR.*

(qRT-PCR) analysis and western blot in RCC cell lines and tissues. We found a significantly higher level of TIMP1 mRNA in RCC cells (786-O, ACHN, A498, CAKI-1, OSRC-2) relative to HK-2 (**Figure 7A**). Western blot revealed that the expression level of TIMP1 in RCC was higher compared with HK-2 (**Figure 7B**). Then we studied the expression of TIMP1 mRNA and protein in tissues. We detected 20 pairs of RCC tissues and corresponding adjacent normal tissues for qRT-PCR and found TIMP1 over-expression in RCC in 17 pairs of tissues (**Figure 7C**). Western blot for tissues showed a similar result. TIMP1 expression was significantly higher in RCC compared with adjacent normal tissues (**Figure 7D**). Furthermore, IHC was conducted in 3 pairs of RCC tissues and adjacent normal tissues. TIMP1 was primarily located in the membranes and cytoplasm of cancer cells and renal tubular epithelial cells (**Figure 7E**). The results proved that the expression of TIMP1 was higher in RCC tissues again. These findings confirmed that TIMP1 was upregulated in RCC cells and tissues.

3.6 TIMP1 Promoted the Proliferation, Migration, and Invasion of RCC Cells

In order to elucidate the function of TIMP1 in RCC, TIMP1 was knocked down by TIMP1-siRNA and was overexpressed by transfecting plasmid into ACHN and 786-O cell lines. Then we used qRT-PCR and western blot to test the efficiency of transfection. The results showed that TIMP1-siRNA and plasmid carrying TIMP1 could raise corresponding effects on TIMP1 expression in cells (**Figures 8A,B**). CCK8 assays revealed that TIMP1 knockdown could significantly repress the proliferation rates of ACHN and 786-O, while overexpression of TIMP1 accelerated cell proliferation (**Figures 8C,D**). We applied transwell assays to detect the influence of TIMP1 on RCC cells' migration and invasion ability. The results showed that TIMP1 knockdown suppressed the migration and invasion ability of ACHN and 786-O, while TIMP1 overexpression promoted these features (**Figures 9E,F**). In conclusion, TIMP1 facilitated the progression of RCC by promoting the proliferation, migration, and invasion of RCC cells.

3.7 TIMP1 Was Involved in Multiple Biological Processes and Promoted RCC via the Epithelial-To-Mesenchymal Transition Pathway

To clarify the specific function of TIMP1 in RCC, GSEA based on the TCGA database was performed. Besides, we retrieved the biological process of TIMP1 in STRING (https://string-db.org/). The results of GSEA have shown that TIMP1 was closely related to tumorigenesis, metastasis, cell cycles, and epithelial-to-mesenchymal transition (**Figures 9A–F**). The protein-protein interaction network calculated by STRING displayed the proteins interacting with TIMP1 (**Figure 9G**). The major GO term included signaling transduction and cell migration (**Figure 9H**; **Table 5**). The KEGG pathways TIMP1 participated in involved PI3K-Akt and JAK-STAT signaling pathways (**Figure 9I**; **Table 6**). These results indicated that TIMP1 might play a key role in the metastasis of RCC and participate in extracellular signal transduction. According to the information above, we examined the EMT pathway which was proved to be critical in tumor metastasis by silencing TIMP1. The results revealed that TIMP1 silencing led to the downregulation of N-cadherin and upregulation of E-cadherin (**Figure 9J**). These findings illustrated that TIMP1 facilitated the progression of RCC *via* EMT transition.

4 DISCUSSION

RCC is one of the most common malignant tumors in the urinary system and accounts for 1.8% of deaths from cancers (Bray et al., 2018; Wan et al., 2019a; Wan et al., 2019b; Luo et al., 2019; Xu et al., 2019; Zhang et al., 2019; Zhou et al., 2019). So far, there is no effective systemic therapy. Due to the lack of effective tumor markers for early screening and the mild symptoms of early-stage RCC, 1/3 patients have ectopic metastases when diagnosed (Gong et al., 2016). For patients with distant metastases, first-line treatments mainly include surgical resections and TKI inhibitors such as sunitinib, pazopanib, and axitinib (Rini et al., 2011). There are also phase 3 clinical trials showing that everolimus (a mTOR inhibitor), compared with placebo, has a

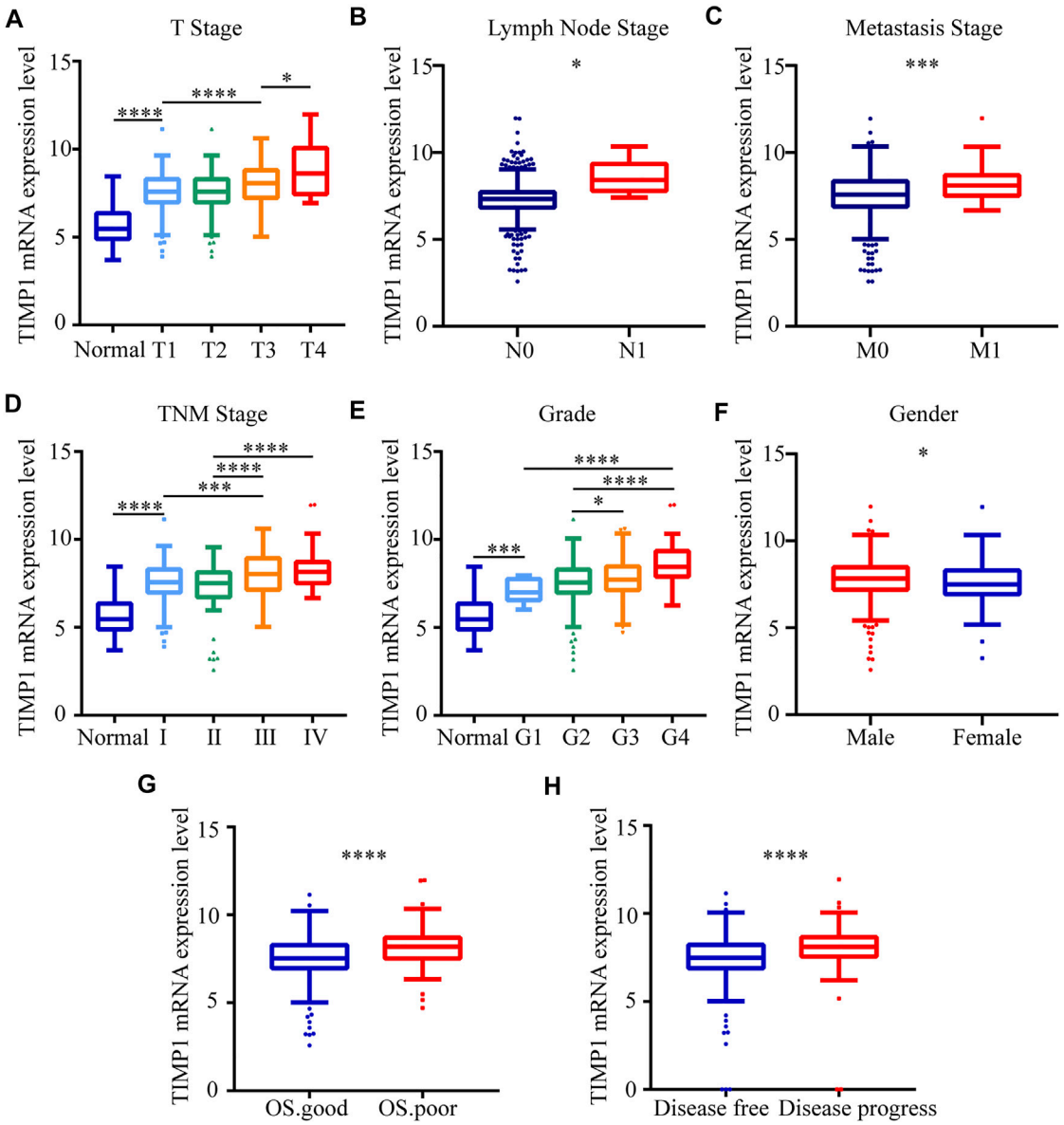

FIGURE 5 | TIMP1 expression level was associated with different clinicopathological parameters. The mRNA expression levels of TIMP1 were downloaded from the TCGA-KIRC database. TIMP1 was upregulated in **(A)** T stage, **(B)** lymph node metastasis, **(C)** distant metastases, **(D)** TNM stage, **(E)** G grade, **(F)** gender, **(G)** OS status, **(H)** DFS status. ****$p < 0.0001$; ***$p < 0.001$; *$p < 0.05$. TIMP1, Tissue inhibitor matrix metalloproteinase 1; RCC, clear cell renal cell carcinoma; KIRC, kidney renal clear cell carcinoma; TCGA, The Cancer Genome Atlas; TNM, Tumor-Node-Metastasis; OS, overall survival; DFS, disease-free survival.

longer disease-free survival (Choueiri et al., 2015; Motzer et al., 2015; Cella et al., 2016). However, the development of drug resistance leads to their failure and brings some adverse reactions such as liver toxicity, hand-foot syndrome, etc (Motzer et al., 2013). Thus, detecting RCC at early stage is of most importance for improving patients' survival by far.

Some most recent researches showed RAC2, LINC00160, IGFL2-AS1, AC023043.1 could serve as biomarkers for diagnosing RCC (Cheng et al., 2019; Liu et al., 2019; Cheng et al., 2020). In the present study, we selected the members of the TIMP family, which encoded the natural inhibitors for MMPs. We found an independent prognostic factor for RCC, TIMP1, by using bioinformatics analysis. We discovered that TIMP1 was significantly up-regulated in RCC and patients with a higher level of TIMP1 had worse clinical outcomes. ROC analysis revealed that TIMP1 could distinguish RCC patients from normal people. Meanwhile, TIMP1, as a secreted protein, could be detected in blood and other body fluid. So TIMP1 might be an ideal biomarker for RCC according to these findings.

Related research showed that TIMP1 could inhibit the proteolytic activity of matrix metalloproteinases (MMPs) by forming noncovalent 1:1 stoichiometric complex and regulate

TABLE 4 | Correlation between TIMP1 mRNA expression and clinicopathological parameters of ccRCC patients.

Parameter		Number	TIMP1 mRNA expression		*p* Value
			Low (*n* = 261)	High (*n* = 261)	
Age (years)	<60	244	119	125	0.599
	≥60	278	142	136	
Gender	Female	180	105	75	0.006[a]
	Male	342	156	186	
T stage	T1 or T2	335	190	145	<0.001[a]
	T3 or T4	187	71	116	
N stage	N0 or NX	507	258	249	0.018[a]
	N1	15	3	12	
M stage	M0 or MX	445	237	208	<0.001[a]
	M1	77	24	53	
G grade	G1 or G2 or Gx	245	146	99	<0.001[a]
	G3 or G4	277	115	162	
TNM stage	I + II	317	186	131	<0.001[a]
	III + IV	205	75	130	

[a]p < *0.05*.

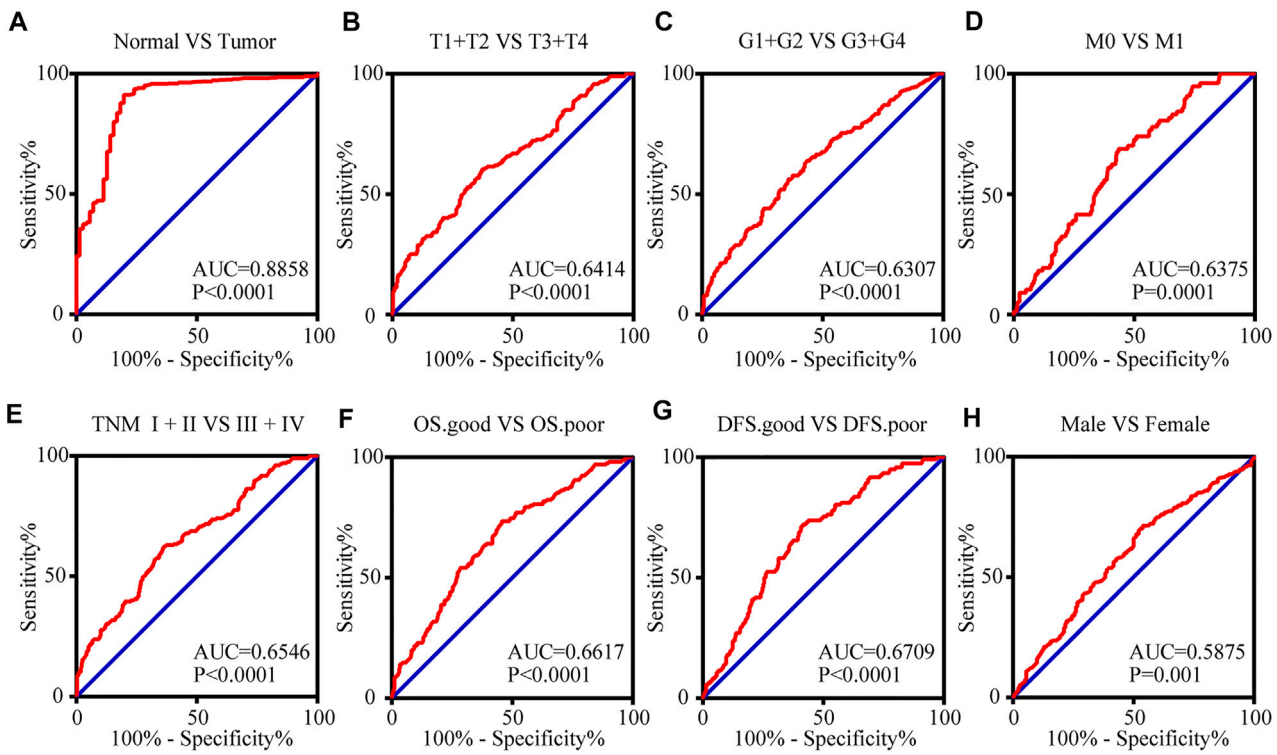

FIGURE 6 | The mRNA expression level of TIMP1 can serve as a biomarker for clinical RCC diagnosis. **(A)** TIMP1 could effectively distinguish RCC from normal tissues (AUC = 0.8858; $p < 0.0001$). ROC analysis was performed in the following subgroups of patients with RCC: **(B)** T grade, **(C)** G stage, **(D)** distant metastases, **(E)** TNM stage, **(F)** OS status, **(G)** DFS status and **(H)** gender. TIMP1, Tissue inhibitor matrix metalloproteinase 1; RCC, clear cell renal cell carcinoma; ROC, Receiver operating curve, AUC, area under the curve; OS, overall survival; DFS, disease-free survival.

the balance of matrix remodeling during degradation of extracellular matrix (Batra et al., 2012). However, the most recent studies revealed other important biological functions of TIMP1 including anti-apoptosis, anti-angiogenesis, cell cycle regulation, and differentiation activities. TIMP1 activated hepatic stellate cells via CD63 signaling to create a premetastatic niche in pancreatic cancer (Grunwald et al., 2016). Down-regulation of TIMP1 was found to enhance gemcitabine sensitivity and reverse chemoresistance in pancreatic cancer (Tan et al., 2020). TIMP1 was involved in

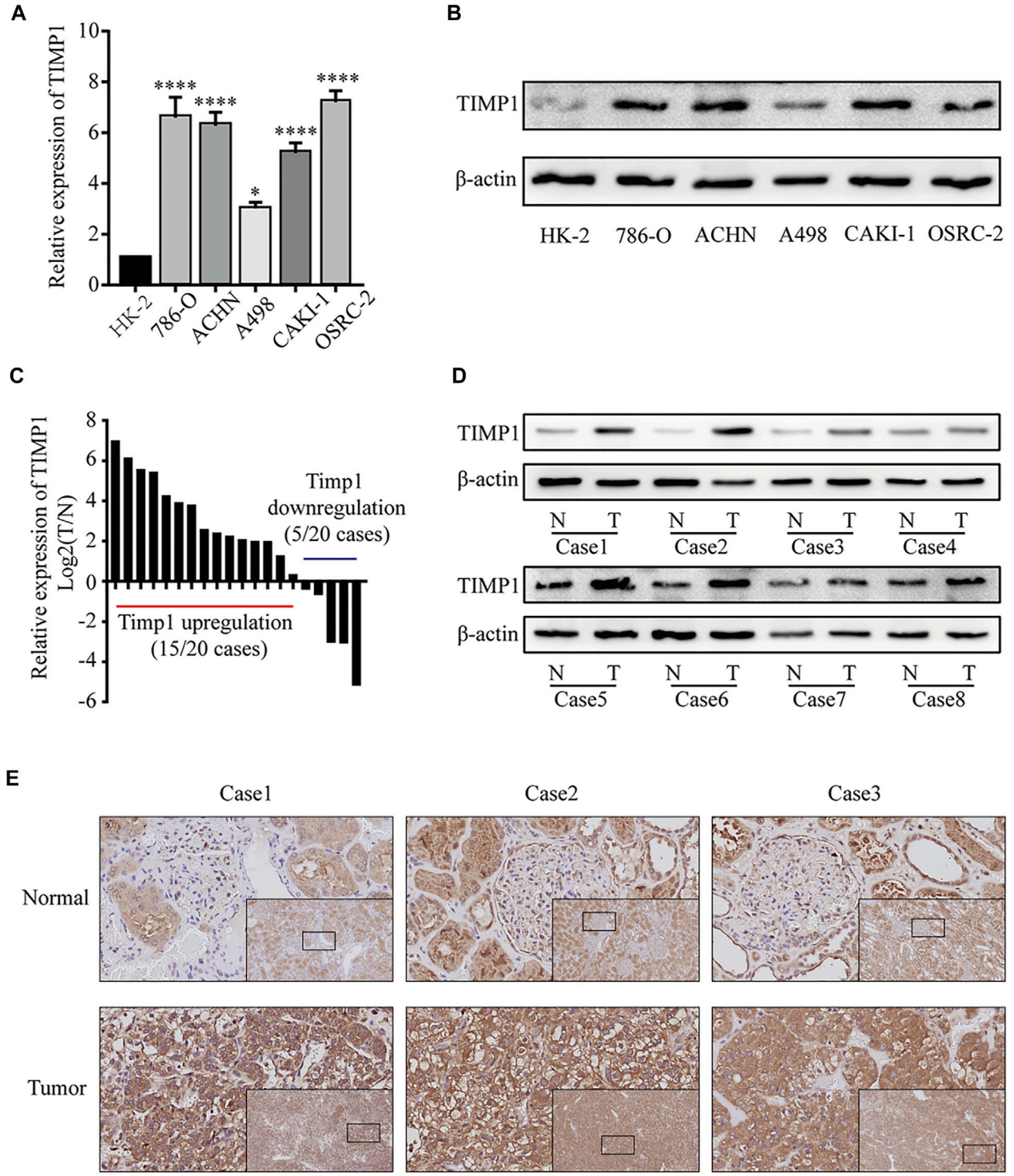

FIGURE 7 | TIMP1 was upregulated in RCC cell lines and tissues. **(A)** Levels of TIMP1 mRNA in 5 renal cancer cell lines (786-O, ACHN, A498, CAKI-1, OSRC-2) and a normal cell line (HK-2). **(B)** Levels of TIMP1 protein in 5 renal cancer cell lines (786-O, ACHN, A498, CAKI-1, OSRC-2) and a normal cell line (HK-2). **(C)** The mRNA levels of TIMP1 in 20 RCC tissues and adjacent nonmalignant tissues. **(D)** The protein levels of TIMP1 in RCC tissues and adjacent nonmalignant tissues. **(E)** Immunohistochemical (IHC) staining for TIMP1 in RCC tissues and adjacent nonmalignant tissues. The images are the lower magnification of the same tissue as that presented in the larger image of each set. Magnification, ×100 and ×400. TIMP1 expression was normalized to β-actin expression. ****$p < 0.0001$; *$p < 0.05$. TIMP1, Tissue inhibitor matrix metalloproteinase 1 RCC, clear cell renal cell carcinoma.

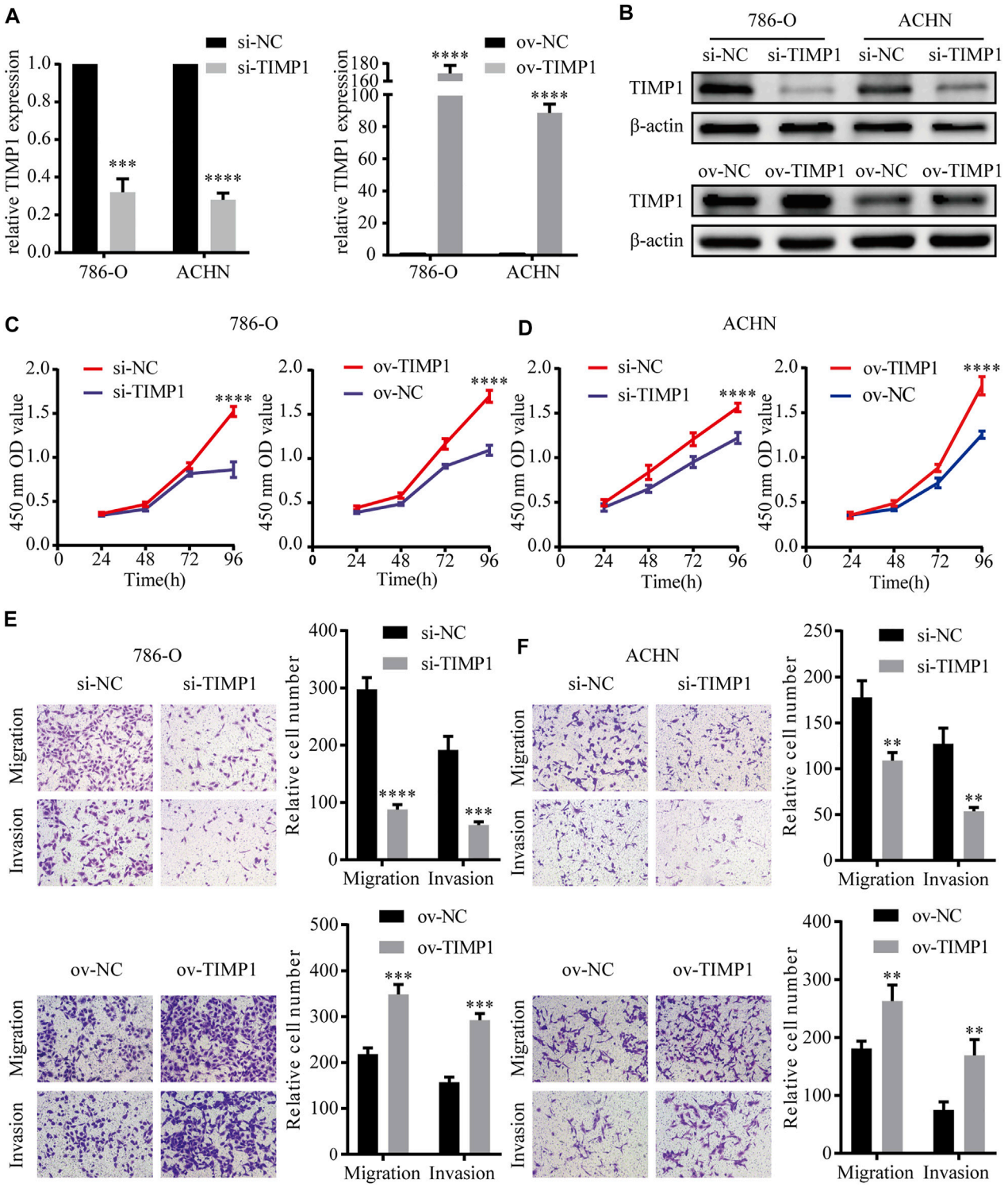

FIGURE 8 | TIMP1 promoted the proliferation, migration and invasion of RCC cells. **(A)** Verification of TIMP1 mRNA levels in transfected 786-O and ACHN cell lines. **(B)** Verification of TIMP1 protein levels in 786-O and ACHN cell lines after knocking down or overexpressing TIMP1. **(C,D)** Cell growth curves of CCK8 assays for transfected 786-O and ACHN cell lines to evaluate cell proliferation. **(E,F)** Transwell assays for transfected ACHN and 786-O cells to evaluate cell migration and invasion ability (Magnification: ×100). All results were plotted as the means ± SEM from three independent experiments. ****$p < 0.0001$, ***$p < 0.001$, **$p < 0.01$. TIMP1, Tissue inhibitor matrix metalloproteinase 1.

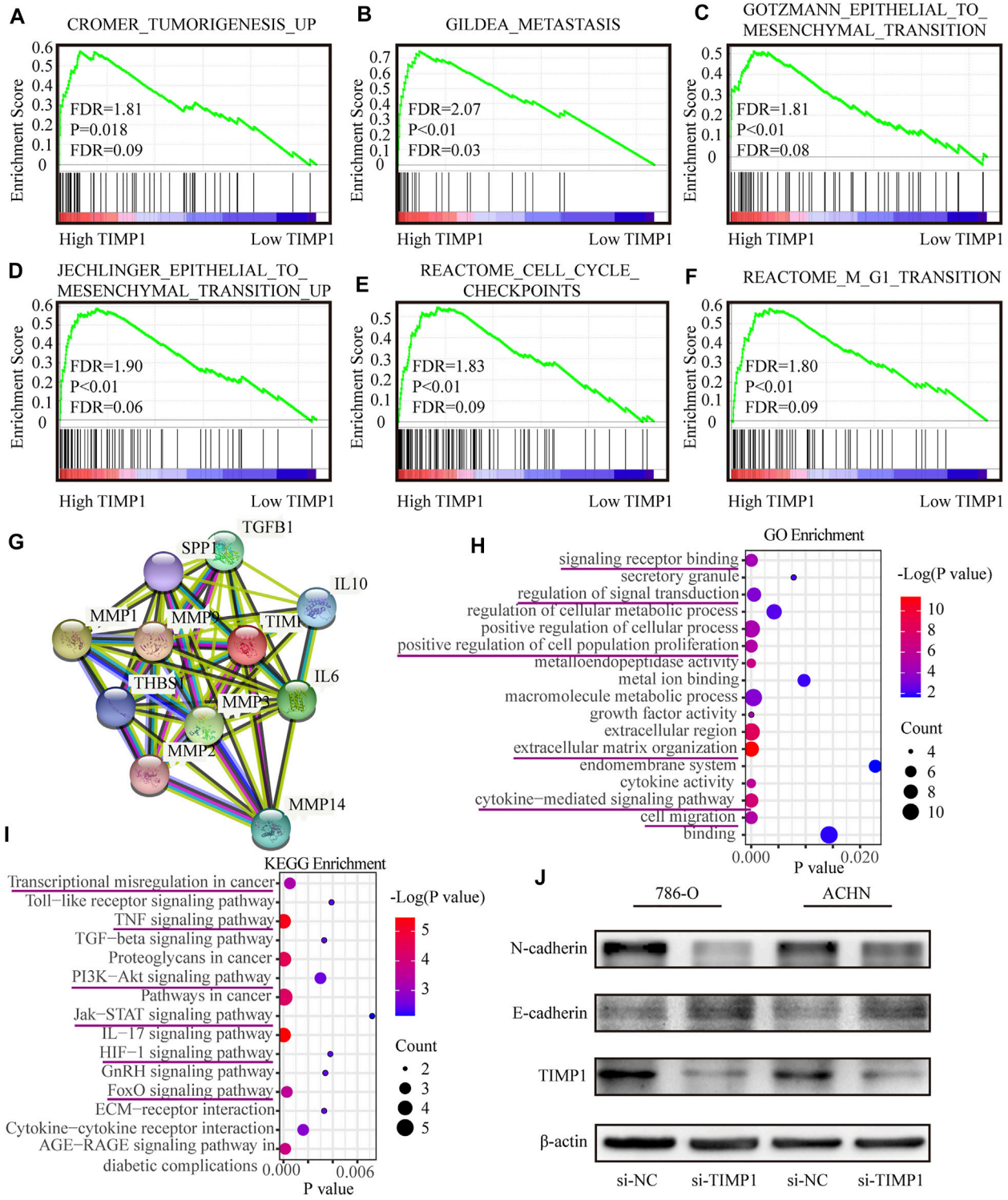

FIGURE 9 | TIMP1 was involved in multiple biological processes and promoted RCC via EMT pathway. **(A–F)** GSEA analysis for the correlations between the biological pathways with the levels of the TIMP1 mRNA based on TCGA database. FDR<25% and $p < 0.05$ were considered statistically significant. **(G)** The protein-protein interaction network of TIMP1. **(H,I)** Biological processes and KEGG pathways in STRING. **(J)** Verification of N-cadherin and E-cadherin protein changes after silencing TIMP1 in 786-O and ACHN. TIMP1, Tissue inhibitor matrix metalloproteinase 1, KEGG (Kyoto Encyclopedia of Genes and Genomes).

TABLE 5 | GO enrichment of TIMP1 retrieved from the STRING database.

Term ID	Term description	Observed gene count	Background gene count	FDR	Matching proteins
GO: 0030198	Extracellular matrix organization	7	296	4.32E-12	TIMP1, MMP2, TGFB1, THBS1, MMP3, MMP14, MMP1, MMP9, SPP1
GO: 0019221	Cytokine-mediated signaling pathway	11	655	5.25E-08	TIMP1, MMP2, TGFB1, MMP3, MMP1, MMP9, IL6, IL10
GO: 0016477	Cell migration	7	812	6.15E-06	TGFB1, THBS1, MMP14, MMP1, MMP9, IL6, IL10
GO: 0048522	Positive regulation of cellular process	11	4898	1.47E-05	TIMP1, MMP2, TGFB1, THBS1, MMP3, MMP14, MMP1, MMP9, SPP1, IL6, IL10
GO: 0008284	Positive regulation of cell population proliferation	8	878	7.74E-06	TIMP1, MMP2, TGFB1, THBS1, MMP9, IL6, IL10
GO: 0043170	Macromolecule metabolic process	9	7453	0.00039	TIMP1, MMP2, TGFB1, THBS1, MMP3, MMP14, MMP1, MMP9, SPP1, IL6, IL10
GO: 0009966	Regulation of signal transduction	11	3033	0.00052	TIMP1, TGFB1, THBS1, MMP14, MMP9, SPP1, IL6, IL10
GO: 0031323	Regulation of cellular metabolic process	8	6082	0.0042	TIMP1, TGFB1, THBS1, MMP3, MMP14, MMP9, SPP1, IL6, IL10
GO: 0005576	Extracellular region	9	2505	4.08E-09	TIMP1, MMP2, TGFB1, THBS1, MMP3, MMP14, MMP1, MMP9, SPP1, IL6, IL10
GO: 0012505	Endomembrane system	11	4347	0.0228	TIMP1, TGFB1, THBS1, MMP14, MMP9, SPP1, IL6
GO: 0004222	Metalloendopeptidase activity	7	110	2.39E-07	MMP2, MMP3, MMP14, MMP1, MMP9
GO: 0005125	Cytokine activity	5	216	1.31E-05	TIMP1, TGFB1, SPP1, IL6, IL10
GO: 0008083	Growth factor activity	4	160	1.77E-05	TIMP1, TGFB1, IL6, IL10
GO: 0046872	Metal ion binding	7	4087	0.0097	TIMP1, MMP2, THBS1, MMP3, MMP14, MMP1, MMP9
GO: 0005488	Binding	11	11878	0.0143	TIMP1, MMP2, TGFB1, THBS1, MMP3, MMP14, MMP1, MMP9, SPP1, IL6, IL10
GO: 0030141	Secretory granule	4	828	0.0078	TIMP1, TGFB1, THBS1, MMP9
GO: 0012505	Endomembrane system	7	4347	0.0228	TIMP1, TGFB1, THBS1, MMP14, MMP9, SPP1, IL6

GO, gene ontology; TIMP1, Tissue inhibitor matrix metalloproteinase 1; FDR, false discovery rate.

TABLE 6 | KEGG enrichment of TIMP1 retrieved from the STRING database.

Term ID	Term description	Observed gene count	Background gene count	FDR	Matching proteins
hsa04657	IL-17 signaling pathway	4	92	3.45E-06	MMP3, MMP1, MMP9, IL6
hsa04668	TNF signaling pathway	4	108	5.13E-06	MMP3, MMP14, MMP9, IL6
hsa05205	Proteoglycans in cancer	4	195	3.19E-05	MMP2, TGFB1, THBS1, MMP9
hsa05200	Pathways in cancer	5	515	4.61E-05	MMP2, TGFB1, MMP1, MMP9, IL6
hsa04068	Fofo signaling pathway	3	130	0.00027	TGFB1, IL6, IL10
hsa05202	Transcriptional misregulation in cancer	3	169	0.00052	MMP3, MMP9, IL6
hsa04060	Cytokine-cytokine receptor interaction	3	263	0.0016	TGFB1, IL6, IL10
hsa04151	PI3K-Act signaling pathway	3	348	0.003	THBS1, SPP1, IL6
hsa04350	TGF-beta signaling pathway	2	83	0.0033	TGFB1, THBS1
hsa04512	ECM-receptor interaction	2	81	0.0033	THBS1, SPP1
hsa04912	GnRH signaling pathway	2	88	0.0034	MMP2, MMP14
hsa04066	HIF-1 signaling pathway	2	98	0.0038	TIMP1, IL6
hsa04620	Toll-like receptor signaling pathway	2	102	0.0039	SPP1, IL6
hsa04630	Jak-STAT signaling pathway	2	160	0.0072	IL6, IL10
hsa04933	AGE-RAGE signaling pathway in diabetic complications	3	98	0.00014	MMP2, TGFB1, IL6

KEGG, kyoto encyclopedia of genes and genomes; TIMP1, Tissue inhibitor matrix metalloproteinase 1; FDR, false discovery rate.

angiogenesis in gastric cancer (Li et al., 2020). TIMP1 could even regulate the adipogenesis of adipose-derived stem cells via the WNT signaling pathway (Wang et al., 2020). Besides, TIMP1 was associated with fibrosis and suppression of programmed cell death of B Cells (Guedez et al., 1998; Arthur, 2000; LaRocca et al., 2017). The upregulation of TIMP1 was relative to poor prognosis of multiple cancers including colon cancer, breast cancer, gastric cancer, melanoma, papillary thyroid carcinoma, renal cell carcinoma, and so on (Hawthorn et al., 2004; Wang et al., 2013; Cheng et al., 2016; Song et al., 2016; Zurac et al., 2016).

To further investigate the function of TIMP1 in RCC, we applied qRT-PCR, WB, and IHC to confirm the upregulation of TIMP1 in RCC cells and tissues. Next, we researched the effect of TIMP1 on RCC cells by knocking down and overexpressing TIMP1. The results revealed that TIMP1 promoted proliferation, migration, and invasion of RCC cells. In order to figure out how TIMP1 facilitated RCC progression, we applied GSEA based on TCGA_KIRC and retrieved the biological functions of TIMP1 via STRING. The discovery showed that TIMP1 mainly participated in the regulation of extracellular matrix and closely associate with metastasis, EMT pathway, and some typical signal transduction pathways. Further study indicated that knockdown of TIMP1 led to up-regulation of E-cadherin and down-regulation of N-cadherin, which proved TIMP1 accelerated the progression of RCC via EMT pathway in a MMPs inhibitor-independent manner.

The EMT signal pathway was well known for its critical function in wound healing, tumor metastasis and malignant progression (Dongre and Weinberg, 2019; Brabletz et al., 2021). The cells developed into a quasi-mesenchymal state from the original epithelial state via the EMT pathway, which strengthens the metastatic potential of malignant cells (Kalluri and Weinberg, 2009; Nieto, 2009; Thiery et al., 2009; Nieto et al., 2016). Recent studies showed that TIMPs and MMPs were closely related to the EMT pathway, which supported our findings (Argote Camacho et al., 2021; Nayim et al., 2021). But studies involving the specific mutual effect between TIMP1 and the EMT pathway were rare.

Taking the above findings into consideration, it was reasonable to believe that the most critical function of TIMP1 was to enhance the metastatic ability of RCC cells via the EMT pathway, while the effect of TIMP1 on proliferation might be due to other minor functions of the EMT pathway. All these discoveries showed TIMP1 might be a potential diagnostic and prognostic biomarker for clear cell renal cell carcinoma that facilitated tumor progression. There were still some limitations in the present study. The effect of TIMP1 was not proved *in vivo*. Besides, the specific mechanism causing the abnormal regulation of TIMP1 was still unclear. Therefore, further study was required to solve these problems.

5 CONCLUSION

The present research proved that a high level of TIMP1 expression was associated with a poor clinical outcome. TIMP1 promoted the proliferation, migration, and invasion of RCC cells and facilitated the progression of RCC *via* the EMT pathway. We proved that the biological effects of TIMP1 mediated by signal transduction pathways were far more than those previously known as MMP inhibitors. The aforementioned results indicated that TIMP1 may be an ideal diagnostic and prognostic biomarker for RCC, and molecular targets for TIMP1 might provide a new choice for RCC treatment.

DATA AVAILABILITY STATEMENT

The datasets presented in this study can be found in online repositories. The names of the repository/repositories and accession number(s) can be found in the article/**Supplementary Material**.

ETHICS STATEMENT

The studies involving human participants were reviewed and approved by the Human Research Ethics Committee of Huazhong University of Science and Technology. The patients/participants provided their written informed consent to participate in this study.

AUTHOR CONTRIBUTIONS

YS and YL designed the study. YS, JL, JX, JL, TX, JT, LL, and YH carried out data acquisition and analysis. YS, YL, GC, and XZ wrote the manuscript. JX, YH, LL, and JT collected the clinical samples and managed the clinical data. HY and DL contributed to bioinformatics analysis. GC and XZ were involved in project management and contributed to preparing and making figures and tables. GC and XZ supervised the study. All authors read and approved the final manuscript.

FUNDING

Our study was supported by the Key Research and Development Plan in China (Grant No. 2017YFB1303100), the National Natural Science Foundation of China (Grant Nos. 82002704, 81927807, 81874090, 81672528, 81773282 & 81972630), and Individual Innovative Research Funding of Union Hospital (Grant No. 02.03.2019-156).

ACKNOWLEDGMENTS

We appreciated all involved in this study.

SUPPLEMENTARY MATERIAL

The Supplementary Material for this article can be found online at: https://www.frontiersin.org/articles/10.3389/fgene.2022.648134/full#supplementary-material

REFERENCES

Argote Camacho, A. X., González Ramírez, A. R., Pérez Alonso, A. J., Rejón García, J. D., Olivares Urbano, M. A., Torné Poyatos, P., et al. (2021). Metalloproteinases 1 and 3 as Potential Biomarkers in Breast Cancer Development. *Ijms* 22 (16), 9012. doi:10.3390/ijms22169012

Arthur, M. J. P. (2000). Fibrogenesis II. Metalloproteinases and Their Inhibitors in Liver Fibrosis. *Am. J. Physiology-Gastrointestinal Liver PhysiologyGastrointestinal Liver Physiol.* 279 (2), G245–G249. doi:10.1152/ajpgi.2000.279.2.g245

Batra, J., Robinson, J., Soares, A. S., Fields, A. P., Radisky, D. C., and Radisky, E. S. (2012). Matrix Metalloproteinase-10 (MMP-10) Interaction with Tissue Inhibitors of Metalloproteinases TIMP-1 and TIMP-2. *J. Biol. Chem.* 287 (19), 15935–15946. doi:10.1074/jbc.M112.341156

Beroukhim, R., Brunet, J.-P., Di Napoli, A., Mertz, K. D., Seeley, A., Pires, M. M., et al. (2009). Patterns of Gene Expression and Copy-Number Alterations in Von-Hippel Lindau Disease-Associated and Sporadic clear Cell Carcinoma of the Kidney. *Cancer Res.* 69 (11), 4674–4681. doi:10.1158/0008-5472.CAN-09-0146

Brabletz, S., Schuhwerk, H., Brabletz, T., and Stemmler, M. P. (2021). Dynamic EMT: a Multi-tool for Tumor Progression. *EMBO J.* 40 (18), e108647. doi:10.15252/embj.2021108647

Bray, F., Ferlay, J., Soerjomataram, I., Siegel, R. L., Torre, L. A., and Jemal, A. (2018). Global Cancer Statistics 2018: GLOBOCAN Estimates of Incidence and Mortality Worldwide for 36 Cancers in 185 Countries. *CA: a Cancer J. clinicians* 68 (6), 394–424. doi:10.3322/caac.21492

Brew, K., and Nagase, H. (2010). The Tissue Inhibitors of Metalloproteinases (TIMPs): an Ancient Family with Structural and Functional Diversity. *Biochim. Biophys. Acta (Bba) - Mol. Cel Res.* 1803 (1), 55–71. doi:10.1016/j.bbamcr.2010.01.003

Cella, D., Grünwald, V., Nathan, P., Doan, J., Dastani, H., Taylor, F., et al. (2016). Quality of Life in Patients with Advanced Renal Cell Carcinoma Given Nivolumab versus Everolimus in CheckMate 025: a Randomised, Open-Label, Phase 3 Trial. *Lancet OncolOncology* 17 (7), 994–1003. doi:10.1016/S1470-2045(16)30125-5

Cheng, G., Fan, X., Hao, M., Wang, J., Zhou, X., and Sun, X. (2016). Higher Levels of TIMP-1 Expression Are Associated with a Poor Prognosis in Triple-Negative Breast Cancer. *Mol. Cancer* 15 (1), 30. doi:10.1186/s12943-016-0515-5

Cheng, G., Liu, D., Liang, H., Yang, H., Chen, K., and Zhang, X. (2019). A Cluster of Long Non-coding RNAs Exhibit Diagnostic and Prognostic Values in Renal Cell Carcinoma. *Aging* 11 (21), 9597–9615. doi:10.18632/aging.102407

Cheng, G., Liu, Y., Liu, L., Ruan, H., Cao, Q., Song, Z., et al. (2020). LINC00160 Mediates Sunitinib Resistance in Renal Cell Carcinoma via SAA1 that Is Implicated in STAT3 Activation and Compound Transportation. *Aging* 12 (17), 17459–17479. doi:10.18632/aging.103755

Cheville, J. C., Lohse, C. M., Zincke, H., Weaver, A. L., and Blute, M. L. (2003). Comparisons of Outcome and Prognostic Features Among Histologic Subtypes of Renal Cell Carcinoma. *Am. J. Surg. Pathol.* 27 (5), 612–624. doi:10.1097/00000478-200305000-00005

Choueiri, T. K., Escudier, B., Powles, T., Mainwaring, P. N., Rini, B. I., Donskov, F., et al. (2015). Cabozantinib versus Everolimus in Advanced Renal-Cell Carcinoma. *N. Engl. J. Med.* 373 (19), 1814–1823. doi:10.1056/NEJMoa1510016

Cinque, A., Capasso, A., Vago, R., Lee, M. W., Floris, M., and Trevisani, F. (2021). The Role of Circulating Biomarkers in the Oncological Management of Metastatic Renal Cell Carcinoma: Where Do We Stand Now? *Biomedicines* 10 (1), 90. doi:10.3390/biomedicines10010090

Cruz-Muñoz, W., Kim, I., and Khokha, R. (2006). TIMP-3 Deficiency in the Host, but Not in the Tumor, Enhances Tumor Growth and Angiogenesis. *Oncogene* 25 (4), 650–655. doi:10.1038/sj.onc.1209104

Dongre, A., and Weinberg, R. A. (2019). New Insights into the Mechanisms of Epithelial-Mesenchymal Transition and Implications for Cancer. *Nat. Rev. Mol. Cel Biol* 20 (2), 69–84. doi:10.1038/s41580-018-0080-4

Gong, J., Maia, M. C., Dizman, N., Govindarajan, A., and Pal, S. K. (2016). Metastasis in Renal Cell Carcinoma: Biology and Implications for Therapy. *Asian J. Urol.* 3 (4), 286–292. doi:10.1016/j.ajur.2016.08.006

Grünwald, B., Harant, V., Schaten, S., Frühschütz, M., Spallek, R., Höchst, B., et al. (2016). Pancreatic Premalignant Lesions Secrete Tissue Inhibitor of Metalloproteinases-1, Which Activates Hepatic Stellate Cells via CD63 Signaling to Create a Premetastatic Niche in the Liver. *Gastroenterology* 151 (5), 1011–1024. doi:10.1053/j.gastro.2016.07.043

Grünwald, B., Schoeps, B., and Krüger, A. (2019). Recognizing the Molecular Multifunctionality and Interactome of TIMP-1. *Trends Cel Biol.* 29 (1), 6–19. doi:10.1016/j.tcb.2018.08.006

Guedez, L., Stetler-Stevenson, W. G., Wolff, L., Wang, J., Fukushima, P., Mansoor, A., et al. (1998). *In Vitro* suppression of Programmed Cell Death of B Cells by Tissue Inhibitor of Metalloproteinases-1. *J. Clin. Invest.* 102 (11), 2002–2010. doi:10.1172/jci2881

Hawthorn, L., Stein, L., Varma, R., Wiseman, S., Loree, T., and Tan, D. (2004). TIMP1 and SERPIN-A Overexpression and TFF3 and CRABP1 Underexpression as Biomarkers for Papillary Thyroid Carcinoma. *Head Neck* 26 (12), 1069–1083. doi:10.1002/hed.20099

Holten-Andersen, M. N., Murphy, G., Nielsen, H. J., Pedersen, A. N., Christensen, I. J., Høyer-Hansen, G., et al. (1999). Quantitation of TIMP-1 in Plasma of Healthy Blood Donors and Patients with Advanced Cancer. *Br. J. Cancer* 80 (3-4), 495–503. doi:10.1038/sj.bjc.6690384

Hsieh, J. J., Purdue, M. P., Signoretti, S., Swanton, C., Albiges, L., Schmidinger, M., et al. (2017). Renal Cell Carcinoma. *Nat. Rev. Dis. Primers* 3 (1), 2477–2490. doi:10.1038/nrdp.2017.9

Jackson, H. W., Defamie, V., Waterhouse, P., and Khokha, R. (2017). TIMPs: Versatile Extracellular Regulators in Cancer. *Nat. Rev. Cancer* 17 (1), 38–53. doi:10.1038/nrc.2016.115

Jones, J., Otu, H., Spentzos, D., Kolia, S., Inan, M., Beecken, W. D., et al. (2005). Gene Signatures of Progression and Metastasis in Renal Cell Cancer. *Clin. Cancer Res.* 11 (16), 5730–5739. doi:10.1158/1078-0432.CCR-04-2225

Jung, K.-K., Liu, X.-W., Chirco, R., Fridman, R., and Kim, H.-R. C. (2006). Identification of CD63 as a Tissue Inhibitor of Metalloproteinase-1 Interacting Cell Surface Protein. *EMBO J.* 25 (17), 3934–3942. doi:10.1038/sj.emboj.7601281

Kallakury, B. V., Karikehalli, S., Haholu, A., Sheehan, C. E., Azumi, N., and Ross, J. S. (2001). Increased Expression of Matrix Metalloproteinases 2 and 9 and Tissue Inhibitors of Metalloproteinases 1 and 2 Correlate with Poor Prognostic Variables in Renal Cell Carcinoma. *Clin. Cancer Res.* 7 (10), 3113–3119. doi:10.1093/carcin/22.10.1727

Kalluri, R., and Weinberg, R. A. (2009). The Basics of Epithelial-Mesenchymal Transition. *J. Clin. Invest.* 119 (6), 1420–1428. doi:10.1172/jci39104

Kugler, A., Hemmerlein, B., Thelen, P., Kallerhoff, M., Radzun, H.-J., and Ringert, R.-H. (1998). Expression of Metalloproteinase 2 and 9 and Their Inhibitors in Renal Cell Carcinoma. *J. Urol.* 160 (5), 1914–1918. doi:10.1097/00005392-199811000-00083

LaRocca, G., Aspelund, T., Greve, A. M., Eiriksdottir, G., Acharya, T., Thorgeirsson, G., et al. (2017). Fibrosis as Measured by the Biomarker, Tissue Inhibitor Metalloproteinase-1, Predicts Mortality in Age Gene Environment Susceptibility-Reykjavik (AGES-Reykjavik) Study. *Eur. Heart J.* 38 (46), 3423–3430. doi:10.1093/eurheartj/ehx510

Leibovich, B. C., Lohse, C. M., Crispen, P. L., Boorjian, S. A., Thompson, R. H., Blute, M. L., et al. (2010). Histological Subtype Is an Independent Predictor of Outcome for Patients with Renal Cell Carcinoma. *J. Urol.* 183 (4), 1309–1316. doi:10.1016/j.juro.2009.12.035

Li, X., Niu, N., Sun, J., Mou, Y., He, X., and Mei, L. (2020). IL35 Predicts Prognosis in Gastric Cancer and Is Associated with Angiogenesis by Altering TIMP1, PAI1 and IGFBP1. *FEBS Open Bio* 10, 2687–2701. doi:10.1002/2211-5463.13005

Liu, Y., Cheng, G., Song, Z., Xu, T., Ruan, H., Cao, Q., et al. (2019). RAC2 Acts as a Prognostic Biomarker and Promotes the Progression of clear Cell Renal Cell Carcinoma. *Int. J. Oncol.* 55 (3), 645–656. doi:10.3892/ijo.2019.4849

Luo, Y., Shen, D., Chen, L., Wang, G., Liu, X., Qian, K., et al. (2019). Identification of 9 Key Genes and Small Molecule Drugs in clear Cell Renal Cell Carcinoma. *Aging* 11 (16), 6029–6052. doi:10.18632/aging.102161

Morris, M. R., and Latif, F. (2017). The Epigenetic Landscape of Renal Cancer. *Nat. Rev. Nephrol.* 13 (1), 47–60. doi:10.1038/nrneph.2016.168

Motzer, R. J., Hutson, T. E., Cella, D., Reeves, J., Hawkins, R., Guo, J., et al. (2013). Pazopanib versus Sunitinib in Metastatic Renal-Cell Carcinoma. *N. Engl. J. Med.* 369 (8), 722–731. doi:10.1056/NEJMoa1303989

Motzer, R. J., Hutson, T. E., Glen, H., Michaelson, M. D., Molina, A., Eisen, T., et al. (2015). Lenvatinib, Everolimus, and the Combination in Patients with

Metastatic Renal Cell Carcinoma: a Randomised, Phase 2, Open-Label, Multicentre Trial. *Lancet Oncol.* 16 (15), 1473–1482. doi:10.1016/S1470-2045(15)00290-9

Nayim, P., Mbaveng, A. T., Sanjukta, M., Rikesh, J., Kuete, V., and Sudhir, K. (2021). CD24 Gene Inhibition and TIMP-4 Gene Upregulation by Imperata Cylindrica's Root Extract Prevents Metastasis of CaSki Cells via Inhibiting PI3K/Akt/snail Signaling Pathway and Blocking EMT. *J. Ethnopharmacology* 275, 114111. doi:10.1016/j.jep.2021.114111

Nieto, M. A. (2009). Epithelial-Mesenchymal Transitions in Development and Disease: Old Views and New Perspectives. *Int. J. Dev. Biol.* 53 (8-10), 1541–1547. doi:10.1387/ijdb.072410mn

Nieto, M. A., Huang, R. Y.-J., Jackson, R. A., and Thiery, J. P. (2016). EMT: 2016. *Cell* 166 (1), 21–45. doi:10.1016/j.cell.2016.06.028

Özen, Ö., Krebs, B., Hemmerlein, B., Pekrun, A., Kretzschmar, H., and Herms, J. (2004). Expression of Matrix Metalloproteinases and Their Inhibitors in Medulloblastomas and Their Prognostic Relevance. *Clin. Cancer Res.* 10 (14), 4746–4753. doi:10.1158/1078-0432.ccr-0625-03

Rini, B. I., Escudier, B., Tomczak, P., Kaprin, A., Szczylik, C., Hutson, T. E., et al. (2011). Comparative Effectiveness of Axitinib versus Sorafenib in Advanced Renal Cell Carcinoma (AXIS): a Randomised Phase 3 Trial. *The Lancet* 378 (9807), 1931–1939. doi:10.1016/S0140-6736(11)61613-9

Seo, D.-W., Li, H., Guedez, L., Wingfield, P. T., Diaz, T., Salloum, R., et al. (2003). TIMP-2 Mediated Inhibition of Angiogenesis. *Cell* 114 (2), 171–180. doi:10.1016/s0092-8674(03)00551-8

Song, G., Xu, S., Zhang, H., Wang, Y., Xiao, C., Jiang, T., et al. (2016). TIMP1 Is a Prognostic Marker for the Progression and Metastasis of colon Cancer through FAK-Pi3k/AKT and MAPK Pathway. *J. Exp. Clin. Cancer Res.* 35 (1), 148. doi:10.1186/s13046-016-0427-7

Tan, Y., Li, X., Tian, Z., Chen, S., Zou, J., Lian, G., et al. (2020). TIMP1 Down-Regulation Enhances Gemcitabine Sensitivity and Reverses Chemoresistance in Pancreatic Cancer. *Biochem. Pharmacol.* 189, 114085. doi:10.1016/j.bcp.2020.114085

Taube, M. E., Liu, X.-W., Fridman, R., and Kim, H.-R. C. (2006). TIMP-1 Regulation of Cell Cycle in Human Breast Epithelial Cells via Stabilization of p27KIP1 Protein. *Oncogene* 25 (21), 3041–3048. doi:10.1038/sj.onc.1209336

Thiery, J. P., Acloque, H., Huang, R. Y. J., and Nieto, M. A. (2009). Epithelial-mesenchymal Transitions in Development and Disease. *Cell* 139 (5), 871–890. doi:10.1016/j.cell.2009.11.007

Wan, B., Liu, B., Huang, Y., Yu, G., and Lv, C. (2019a). Prognostic Value of Immune-Related Genes in clear Cell Renal Cell Carcinoma. *Aging* 11 (23), 11474–11489. doi:10.18632/aging.102548

Wan, B., Liu, B., Yu, G., Huang, Y., and Lv, C. (2019b). Differentially Expressed Autophagy-Related Genes Are Potential Prognostic and Diagnostic Biomarkers in clear-cell Renal Cell Carcinoma. *Aging* 11 (20), 9025–9042. doi:10.18632/aging.102368

Wang, L., Zhang, C.-g., Jia, Y.-l., and Hu, L. (2020). Tissue Inhibitor of Metalloprotease-1 (TIMP-1) Regulates Adipogenesis of Adipose-Derived Stem Cells (ASCs) via the Wnt Signaling Pathway in an MMP-independent Manner. *Curr. Med. Sci.* 40 (5), 989–996. doi:10.1007/s11596-020-2265-2

Wang, Y.-Y., Li, L., Zhao, Z.-S., and Wang, H.-J. (2013). Clinical Utility of Measuring Expression Levels of KAP1, TIMP1 and STC2 in Peripheral Blood of Patients with Gastric Cancer. *World J. Surg. Onc* 11, 81. doi:10.1186/1477-7819-11-81

Xu, W.-H., Xu, Y., Wang, J., Wan, F.-N., Wang, H.-K., Cao, D.-L., et al. (2019). Prognostic Value and Immune Infiltration of Novel Signatures in clear Cell Renal Cell Carcinoma Microenvironment. *Aging* 11 (17), 6999–7020. doi:10.18632/aging.102233

Yusenko, M. V., Zubakov, D., and Kovacs, G. (2009). Gene Expression Profiling of Chromophobe Renal Cell Carcinomas and Renal Oncocytomas by Affymetrix GeneChip Using Pooled and Individual Tumours. *Int. J. Biol. Sci.* 5 (6), 517–527. doi:10.7150/ijbs.5.517

Zhang, C., He, H., Hu, X., Liu, A., Huang, D., Xu, Y., et al. (2019). Development and Validation of a Metastasis-Associated Prognostic Signature Based on Single-Cell RNA-Seq in clear Cell Renal Cell Carcinoma. *Aging* 11 (22), 10183–10202. doi:10.18632/aging.102434

Zhou, J., Wang, J., Hong, B., Ma, K., Xie, H., Li, L., et al. (2019). Gene Signatures and Prognostic Values of m6A Regulators in clear Cell Renal Cell Carcinoma - a Retrospective Study Using TCGA Database. *Aging* 11 (6), 1633–1647. doi:10.18632/aging.101856

Zurac, S., Neagu, M., Constantin, C., Cioplea, M., Nedelcu, R., Bastian, A., et al. (2016). Variations in the Expression of TIMP1, TIMP2 and TIMP3 in Cutaneous Melanoma with Regression and Their Possible Function as Prognostic Predictors. *Oncol. Lett.* 11 (5), 3354–3360. doi:10.3892/ol.2016.4391

Conflict of Interest: The authors declare that the research was conducted in the absence of any commercial or financial relationships that could be construed as a potential conflict of interest.

Publisher's Note: All claims expressed in this article are solely those of the authors and do not necessarily represent those of their affiliated organizations, or those of the publisher, the editors and the reviewers. Any product that may be evaluated in this article, or claim that may be made by its manufacturer, is not guaranteed or endorsed by the publisher.

Advantages of publishing in Frontiers

OPEN ACCESS
Articles are free to read for greatest visibility and readership

FAST PUBLICATION
Around 90 days from submission to decision

HIGH QUALITY PEER-REVIEW
Rigorous, collaborative, and constructive peer-review

TRANSPARENT PEER-REVIEW
Editors and reviewers acknowledged by name on published articles

Frontiers
Avenue du Tribunal-Fédéral 34
1005 Lausanne | Switzerland

Visit us: www.frontiersin.org
Contact us: frontiersin.org/about/contact

REPRODUCIBILITY OF RESEARCH
Support open data and methods to enhance research reproducibility

DIGITAL PUBLISHING
Articles designed for optimal readership across devices

FOLLOW US
@frontiersin

IMPACT METRICS
Advanced article metrics track visibility across digital media

EXTENSIVE PROMOTION
Marketing and promotion of impactful research

LOOP RESEARCH NETWORK
Our network increases your article's readership